2 Magnetic properties of rare earth elements, alloys and compounds

See Subvolume III/19d1

2.4 Compounds of rare earth elements and 3d elements

2.4.1 Introduction

2.4.1.1 General

The magnetic properties of binary and pseudo-binary intermetallic compounds between rare-earth (R) and 3d transition metals (M) have been extensively investigated. In addition to their interesting physical properties some from the above systems are suitable to be used in various technical applications as permanent magnets, magnetostrictive devices, hydrogen storage, etc. Some review papers [68 w 1, 71 t 1, 71 w 1, 72 r 1, 73 n 1, 73 t 1, 73 w 1, 75 b 1, 77 b 1, 78 k 1, 79 b 1, 79 c 1, 79 k 1, 79 s 1, 80 b 1, 80 b 2, 80 c 1, 82 b 1, 82 b 2, 82 g 1, 83 b 1, 86 b 1, 88 g 2, 88 k 1, 88 w 1, 88 y 1] have been published on the matter, evidencing the development of the field in different periods of time.

The interesting properties of RM_x compounds are the result of the presence in the same compound of both 4f and 3d atoms. The 4f shells of rare earths are enveloped by the 5s and 5p shells and thus their magnetic moments are well localized. Because of the influence of the metallic lattice, which results in crystal field effects or other influences, the theoretical magnetic moment of rare earth ions can differ sometimes from the experimental value. For example, crystal field and exchange field induce mixing of the excited levels ($J = 7/2, 9/2$) into the ground state ($J = 5/2$), accounting successfully for the magnetic properties of Sm^{3+} in some intermetallic compounds [84 A 11]. The magnetic interactions between R ions are weaker and take place through the conduction electrons. The magnetic moments of M atoms are rather sensitive to their environment, the electron concentration, as well as to the magnetic interactions in the system. Consequently, a large variety of magnetic behaviours in rare earth (yttrium) compounds is shown.

The strong correlation between the 3d electrons leads to a negative polarization of conduction electrons [73 B 3]. This polarization by a RKKY-type interaction [54 R 1, 56 K 1, 57 Y 1] between conduction electrons and those of the 4f shell, give rise to an antiparallel coupling between the spins of rare earths and those of M atoms. The sign of the coupling does not depend on the local surrounding, the interatomic distances and electron concentration. For R belonging to the first subgroup (Pr to Sm) $J = L - S$ and $L < S$, the negative coupling of spins leads to a parallel alignment of magnetic moments. In case of heavy rare earths (Gd to Tm) the negative coupling of spins leads to a ferrimagnetic ordering of R and M sublattices – Fig. 1.

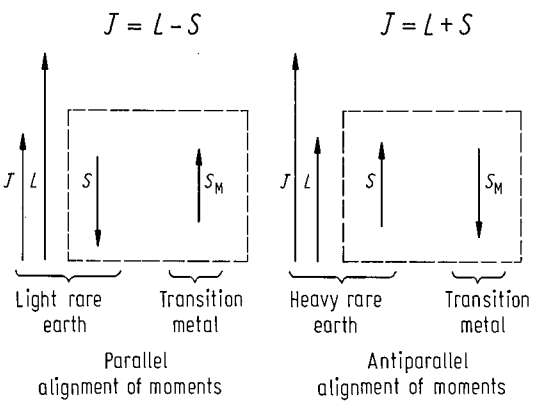

Fig. 1. Types of magnetic coupling between the rare earths and 3d transition metals.

In the present subsect. 2.4.1 we give a brief survey of the phase diagrams appearing in R-M systems, the compositions of the compounds, as well as their crystalline structures. Then an attempt for classification of the magnetic behaviour of binary and pseudobinary R-M compounds and the models used to describe their magnetic properties are given.

In subsect. 2.4.2, representative data on the magnetic properties of binary and pseudobinary R–M compounds are presented. In each chapter, the crystal structures of compounds and their hydrides are described at first. Some data on the lattice constants are also tabulated. In addition to the data obtained by magnetic measurements (mainly saturation magnetizations and Curie temperatures) the results of neutron diffraction studies, Mössbauer effect, NMR, FMR, EPR, anisotropy and magnetostriction, domain structure, magnetization processes, transport properties (electrical resistivity, specific heat, thermopower), optical studies, etc., are also given. These data allow a rather comprehensive description of the magnetic properties of R–M compounds.

When lattice parameters and magnetic moments are listed without specifying the temperature, these refer to room temperature and 4.2 K, respectively.

In the sections "See also", which provide additional references, studies performed on single crystals are indicated by asterisks, while theoretical papers are denoted by (T).

2.4.1.2 Phase diagrams. Crystal structure

When forming an alloy, at a microscopic scale, the order of the atoms is generally due to some factors such as: geometric, electronic, energetic as well as to the type of the chemical bonding. Consequently, it is very difficult to predict the stability of an atomic arrangement. However, some general features may be qualitatively interpreted as regards the chemical bonds between rare earths and some 3d transition metals. The main feature of these metallic bonds is the formation of closely packed structures which may be regarded as arrangement of hard spheres having different dimensions. The necessity of maximum packing – taking into account geometrical and energetical restrictions – leads to an ordered arrangement characteristic of the compounds with well defined stoichiometry, in which the atoms are distributed on specific crystallographic sites. The appearance of the atomic arrangements is favoured by the local environment effects resulting from the great difference between the electronegativity of M and R atoms.

For a given M element, the R–M phase diagrams show the presence of a number of compounds which due to similarities between chemical properties of rare earths may be observed (with some exceptions) for all rare earths.

A great volume of works was devoted to the study of R–M phase diagrams. Some examples are given below:

La–Co [67 B 3, 74 K 10, 74 R 2]; Ce–Co [66 E 1, 70 R 1, 73 R 2, 74 K 10, 74 R 2]; Pr–Co [70 R 1, 73 R 2, 74 R 2]; Nd–Co [70 R 1, 73 R 2, 74 R 2]; Sm–Co [69 L 3, 73 B 22, 74 K 7, 74 R 2, 74 W 2]; Gd–Co [61 N 2, 62 S 1, 69 B 3, 69 L 3, 73 B 22]; Dy–Co [64 W 7, 71 B 15]; Ho–Co [71 B 15]; Er–Co [71 B 15]; Yb–Co [72 B 16]; Y–Co [65 P 1, 71 B 15, 82 G 11];

La–Ni, Ce–Ni, Pr–Ni [47 V 1]; Gd–Ni [61 C 2]; Er–Ni [68 B 5]; Yb–Ni [72 B 16, 73 P 1];
Ce–Fe [70 B 14]; Sm–Fe [71 B 17]; Tb–Fe [76 D 1]; Dy–Fe [70 V 2]; Ho–Fe [70 R 2]; Er–Fe [69 B 5];
Ce–M [74 G 13]; R–M [75 H 2]; R–Fe–Co [86 L 3], etc.

Phase diagrams of R–M systems have been collected by many authors [58 h 1, 61 g 1, 62 s 1, 64 s 1, 65 e 1, 69 K 3, 69 s 1, 70 K 4, 71 B 15, 75 s 1, 78 m 1, 84 m 1].

To illustrate the above discussion and to show the compounds which appear in R–M systems, in Fig. 2, the phase diagrams of Sm–Mn [78 m 1], Sm–Fe [71 B 17], Sm–Co [73 N 1, 77 P 6], and Sm–Cu [75 K 6] are plotted. The phase diagrams of Ce–Fe [70 B 14], Ce–Co [74 G 13, 75 M 3], Ce–Ni [78 m 1], and Ce–Cu [74 G 13] systems are given in Fig. 3. The compounds appearing in Nd–Mn [78 m 1] and Tb–Mn [78 m 1] systems are plotted in Fig. 4, while those of Y–Co [84 m 1], La–Co [84 m 1] and Y–Ni [65 e 1] are given in Fig. 5.

In the present subsect. 2.4.1 we give a brief survey of the phase diagrams appearing in R-M systems, the compositions of the compounds, as well as their crystalline structures. Then an attempt for classification of the magnetic behaviour of binary and pseudobinary R-M compounds and the models used to describe their magnetic properties are given.

In subsect. 2.4.2, representative data on the magnetic properties of binary and pseudobinary R–M compounds are presented. In each chapter, the crystal structures of compounds and their hydrides are described at first. Some data on the lattice constants are also tabulated. In addition to the data obtained by magnetic measurements (mainly saturation magnetizations and Curie temperatures) the results of neutron diffraction studies, Mössbauer effect, NMR, FMR, EPR, anisotropy and magnetostriction, domain structure, magnetization processes, transport properties (electrical resistivity, specific heat, thermopower), optical studies, etc., are also given. These data allow a rather comprehensive description of the magnetic properties of R–M compounds.

When lattice parameters and magnetic moments are listed without specifying the temperature, these refer to room temperature and 4.2 K, respectively.

In the sections "See also", which provide additional references, studies performed on single crystals are indicated by asterisks, while theoretical papers are denoted by (T).

2.4.1.2 Phase diagrams. Crystal structure

When forming an alloy, at a microscopic scale, the order of the atoms is generally due to some factors such as: geometric, electronic, energetic as well as to the type of the chemical bonding. Consequently, it is very difficult to predict the stability of an atomic arrangement. However, some general features may be qualitatively interpreted as regards the chemical bonds between rare earths and some 3d transition metals. The main feature of these metallic bonds is the formation of closely packed structures which may be regarded as arrangement of hard spheres having different dimensions. The necessity of maximum packing – taking into account geometrical and energetical restrictions – leads to an ordered arrangement characteristic of the compounds with well defined stoichiometry, in which the atoms are distributed on specific crystallographic sites. The appearance of the atomic arrangements is favoured by the local environment effects resulting from the great difference between the electronegativity of M and R atoms.

For a given M element, the R–M phase diagrams show the presence of a number of compounds which due to similarities between chemical properties of rare earths may be observed (with some exceptions) for all rare earths.

A great volume of works was devoted to the study of R–M phase diagrams. Some examples are given below:

La–Co [67 B 3, 74 K 10, 74 R 2]; Ce–Co [66 E 1, 70 R 1, 73 R 2, 74 K 10, 74 R 2]; Pr–Co [70 R 1, 73 R 2, 74 R 2]; Nd–Co [70 R 1, 73 R 2, 74 R 2]; Sm–Co [69 L 3, 73 B 22, 74 K 7, 74 R 2, 74 W 2]; Gd–Co [61 N 2, 62 S 1, 69 B 3, 69 L 3, 73 B 22]; Dy–Co [64 W 7, 71 B 15]; Ho–Co [71 B 15]; Er–Co [71 B 15]; Yb–Co [72 B 16]; Y–Co [65 P 1, 71 B 15, 82 G 11];

La–Ni, Ce–Ni, Pr–Ni [47 V 1]; Gd–Ni [61 C 2]; Er–Ni [68 B 5]; Yb–Ni [72 B 16, 73 P 1];
Ce–Fe [70 B 14]; Sm–Fe [71 B 17]; Tb–Fe [76 D 1]; Dy–Fe [70 V 2]; Ho–Fe [70 R 2]; Er–Fe [69 B 5];
Ce–M [74 G 13]; R–M [75 H 2]; R–Fe–Co [86 L 3], etc.

Phase diagrams of R–M systems have been collected by many authors [58 h 1, 61 g 1, 62 s 1, 64 s 1, 65 e 1, 69 K 3, 69 s 1, 70 K 4, 71 B 15, 75 s 1, 78 m 1, 84 m 1].

To illustrate the above discussion and to show the compounds which appear in R–M systems, in Fig. 2, the phase diagrams of Sm–Mn [78 m 1], Sm–Fe [71 B 17], Sm–Co [73 N 1, 77 P 6], and Sm–Cu [75 K 6] are plotted. The phase diagrams of Ce–Fe [70 B 14], Ce–Co [74 G 13, 75 M 3], Ce–Ni [78 m 1], and Ce–Cu [74 G 13] systems are given in Fig. 3. The compounds appearing in Nd–Mn [78 m 1] and Tb–Mn [78 m 1] systems are plotted in Fig. 4, while those of Y–Co [84 m 1], La–Co [84 m 1] and Y–Ni [65 e 1] are given in Fig. 5.

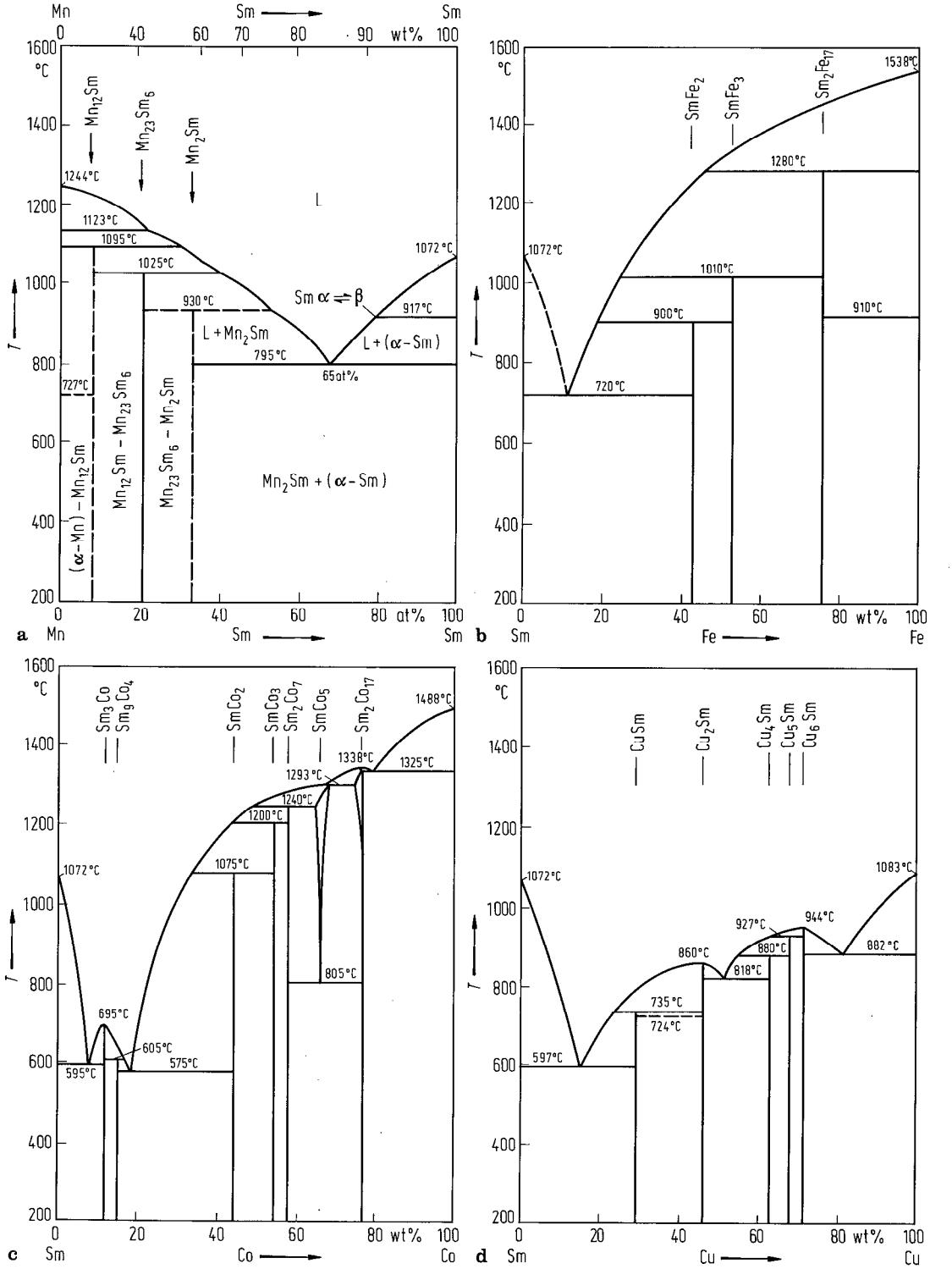

Fig. 2. Phase diagrams of (a) Sm–Mn [78 m 1], (b) Sm–Fe [71 B 17], (c) Sm–Co [73 N 1, 77 P 6] and (d) Sm–Cu [75 K 6] systems.

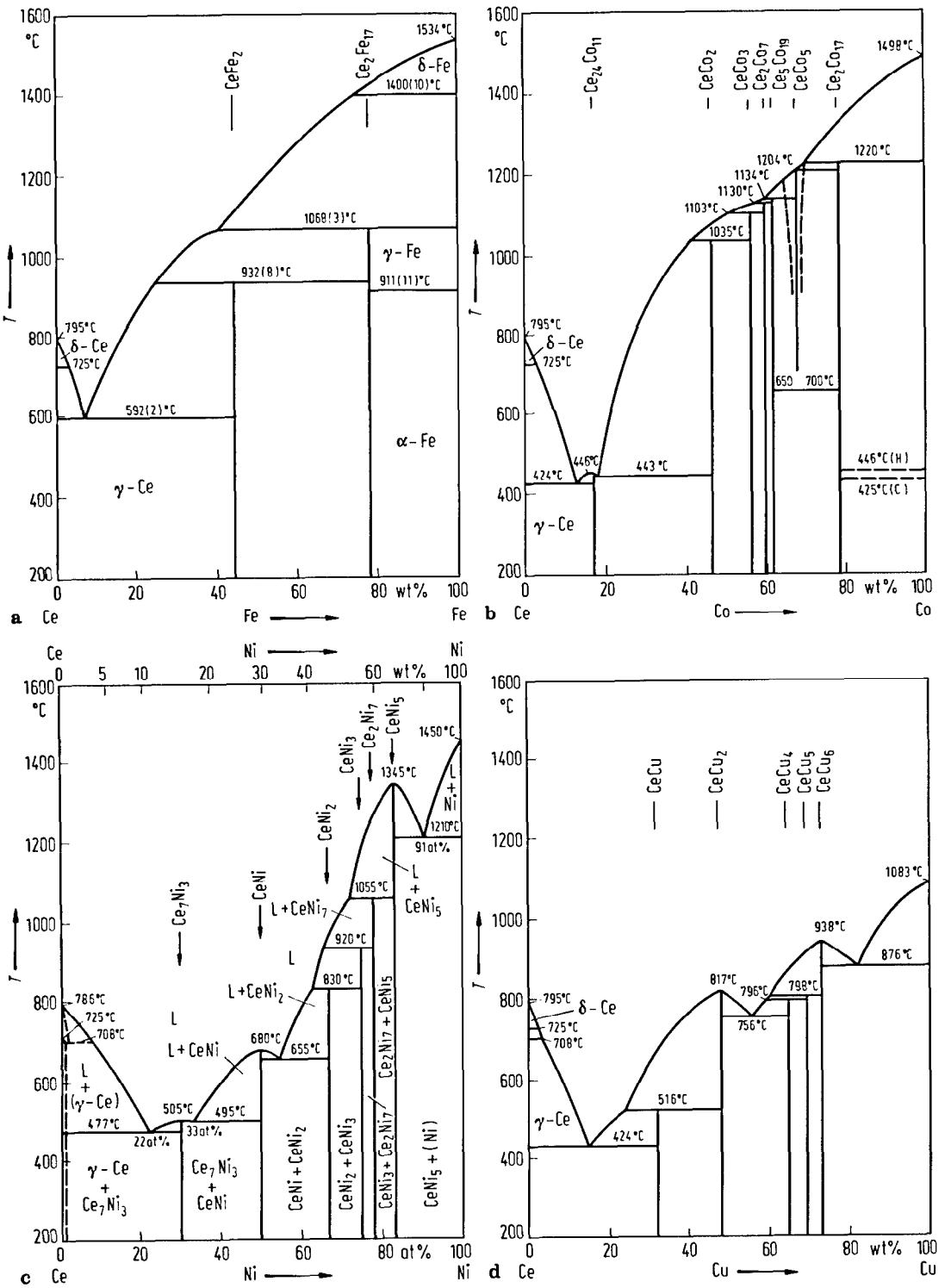

Fig. 3. Phase diagrams of (a) Ce–Fe [70 B 14], (b) Ce–Co [74 G 13, 75 M 3], (c) Ce–Ni [78 m 1] and (d) Ce–Cu [74 G 13] systems.

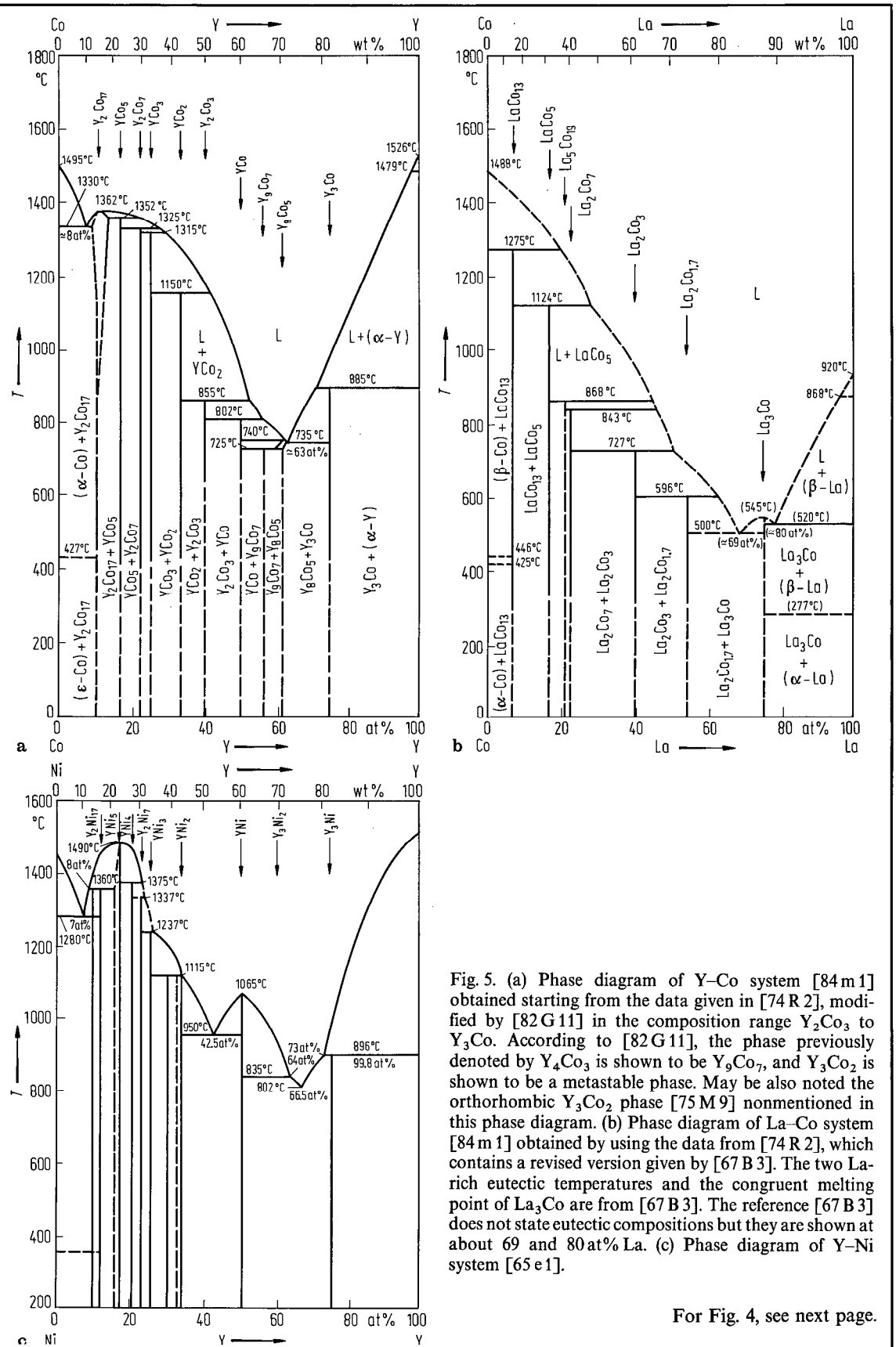

Fig. 5. (a) Phase diagram of Y–Co system [84 m 1] obtained starting from the data given in [74 R 2], modified by [82 G 11] in the composition range Y_2Co_3 to Y_3Co. According to [82 G 11], the phase previously denoted by Y_4Co_3 is shown to be Y_9Co_7, and Y_3Co_2 is shown to be a metastable phase. May be also noted the orthorhombic Y_3Co_2 phase [75 M 9] nonmentioned in this phase diagram. (b) Phase diagram of La–Co system [84 m 1] obtained by using the data from [74 R 2], which contains a revised version given by [67 B 3]. The two La-rich eutectic temperatures and the congruent melting point of La_3Co are from [67 B 3]. The reference [67 B 3] does not state eutectic compositions but they are shown at about 69 and 80 at% La. (c) Phase diagram of Y–Ni system [65 e 1].

For Fig. 4, see next page.

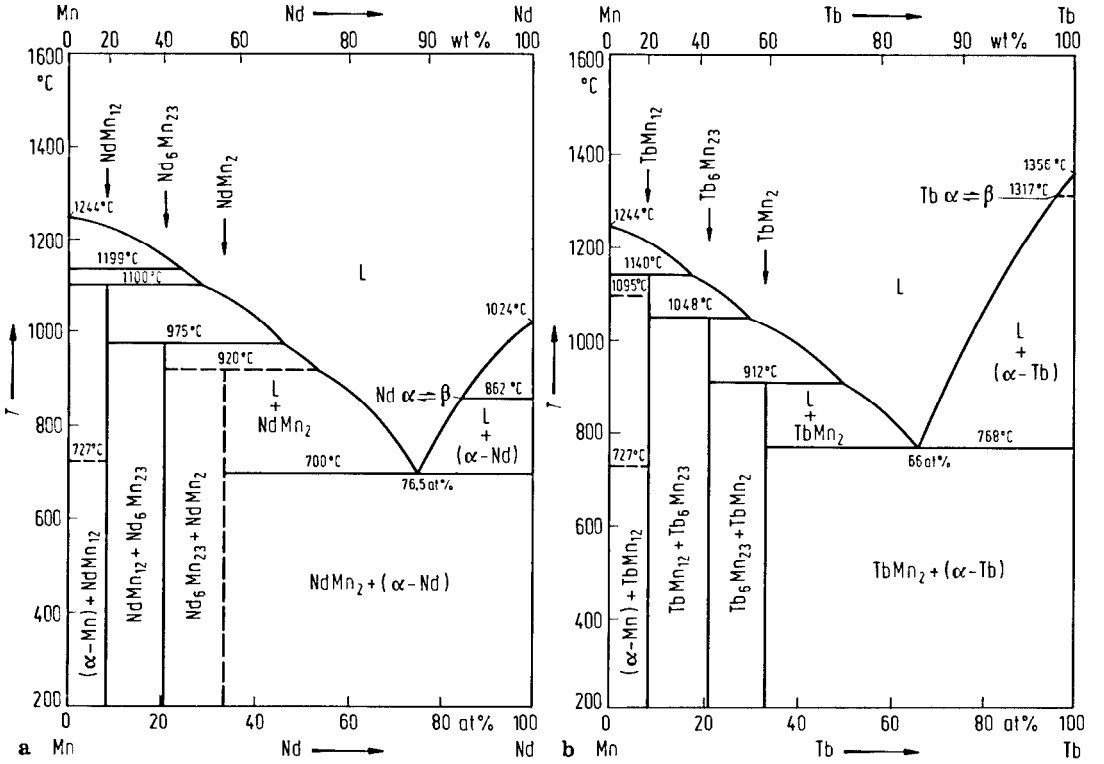

Fig. 4. Phase diagrams of (a) Nd–Mn and (b) Tb–Mn systems [78 m 1].

In the R–M phase diagrams there is at least an eutectic (in the composition range rich in rare earth), which has a low melting point and also intermetallic compounds having a very narrow composition range. The number of compounds appearing in the R–M systems increases from M = Mn to M = Ni. The compounds are generally formed by peritectic reactions. Some compounds present crystallographic modifications. In Table 1, the crystal structure of the compounds appearing in R–M systems are presented together with the sections of the review in which their properties are described.

Table 1. Compounds appearing in R–M systems and their crystal structures.

Sub-section	Compound	M at%	Crystal structure	R	M			
					Mn	Fe	Co	Ni
2.4.2.1	R_3M	25	orthorhombic: Pnma	R			×	×
2.4.2.2	R_5M_2	28.6	monoclinic: C2/c	Pr, Nd, Sm			×	
2.4.2.3	R_7M_3	30	hexagonal: $P6_3mc$	La, Ce, Pr, Nd				×
2.4.2.4	$R_{24}M_{11}$	31.4	hexagonal: $P6_3mc$	Ce			×	
2.4.2.5	$R_{12}M_7$	36.8	monoclinic: $P2_1/c$	Gd, Tb, Dy, Ho, Er			×	
2.4.2.6	R_8M_5	38.5	monoclinic: $P2_1/c$	Y			×	
2.4.2.7	R_3M_2	40	orthorhombic: Pnmm	Y			×	
			trigonal: $R\bar{3}$	Ho, Er				×
			monoclinic: C2/m	Tb, Dy, Ho				×
			tetragonal: $P4_12_12$	Y				×

Table 1 (continued)

Sub-section	Compound	M at%	Crystal structure	R	M			
					Mn	Fe	Co	Ni
2.4.2.8	$R_4M_3(R_9M_7)$	42.8 (43.8)	hexagonal: $P6_3/m$	Gd, Tb, Dy, Ho, Er, Tm, Lu, Y			×	
2.4.2.9	$RM_{0.85}(RM_{1-\varepsilon})$	45.9	hexagonal: $P6_3/mmc$	La, Pr, Nd			×	
2.4.2.10	RM	50	orthorhombic: Pnma	Tb				×
			monoclinic: $P2_1/m$	Tb				×
			orthorhombic: Pnma	Dy, Ho, Er, Tm, Yb, Lu				×
			monoclinic: $P2_1/c$	Y				×
2.4.2.11	R_2M_3	60	orthorhombic: Cmca	La			×	×
2.4.2.12	RM_2	66.6	cubic: Fd3m	R		×	×	×
				Gd, Tb, Dy, Ho, Y	×			
			hexagonal: $P6_3/mmc$	R = Pr, Nd, Sm, Ho, Er, Tm, Lu	×			
2.4.2.13	RM_3	75	trigonal: $R\bar{3}m$	Sm, Gd, Tb, Dy, Ho, Er, Tm, Y		×		
				Ce, Pr, Nd, Sm, Gd, Tb, Dy, Ho, Er, Tm, Yb, Lu, Y			×	
				La, Ce, Pr, Nd, Sm, Gd, Tb, Dy, Ho, Er, Tm, Yb, Y				×
			hexagonal: $P6_3/mmc$	Ce				×
2.4.2.14	R_2M_7	77.7	trigonal: $R\bar{3}m$	La, Ce, Pr, Nd, Sm, Gd			×	
				Pr, Nd, Sm, Gd, Tb, Dy, Ho, Er, Y				×
			hexagonal: $P6_3/mmc$	La, Ce, Pr, Nd, Sm, Gd, Tb, Dy				×
2.4.2.15	R_5M_{19}	79.2	trigonal: $R\bar{3}m$	La, Ce, Pr, Nd			×	
			hexagonal: $P6_3/mmc$	Sm			×	
2.4.2.16	R_6M_{23}	79.3	cubic: Fm3m	Nd, Sm, Gd, Tb, Dy, Ho, Er, Tm, Yb, Lu, Y	×			
				Gd, Tb, Dy, Ho, Er, Tm, Yb, Lu, Y		×		
2.4.2.17	RM_5	83.3	hexagonal: P6/mmm	R			×	×
2.4.2.18	R_2M_{17}	89.5	trigonal: $R\bar{3}m$	Ce, Pr, Nd, Sm, Gd, Tb, Y		×		
				Ce, Pr, Nd, Sm, Gd, Tb, Dy, Ho, Y			×	
			hexagonal: $P6_3/mmc$	Ce, Gd, Tb, Dy, Ho, Er, Tm, Yb, Lu, Y		×		
				Ce, Sm, Gd, Tb, Dy, Ho, Er, Tm, Yb, Lu, Y			×	
				R				×
2.4.2.19	RM_{12}	92.3	tetragonal: I_4/mmm	Nd, Gd, Tb, Dy, Ho, Er, Y	×			
2.4.2.20	RM_{13}	92.9	cubic: Fm3c	La			×	

The crystal structures of the R–M compounds may be classified into four groups. In the first one (A), the compounds rich in rare earths (generally more than 50 at % R) are included. In the second one (B) the compounds rich in 3d transition metals 66 at % < M < 90 at % are comprised. Between the above groups there are the compounds having strong directional bonds, such as $RCo_{1-\varepsilon}$ and R_2Co_3 (C) systems. In the last group (D) are included compounds having more than 90 at% M.

In the following the characteristic features and relationship between the crystal structures of the compounds having transition metal content smaller than 50 at % (A) and greater than 66 at % (B), respectively, are given.

(A) The structures of RM_x compounds with $x < 1$ may be grouped into those having exclusively trigonal prisms as coordination polyhedra (A1) and those with other polyhedra (A2) [77 P 1]. In the former case all M atoms are at the centres of trigonal prisms with one R atom at each corner. For the latter situation the M atoms are at the centres of trigonal prisms, squares, antiprisms, or truncated square antiprisms.

(A1) The crystal structures based on trigonal prisms can be correlated with trigonal prism linkage coefficient, LC, which is defined as the average number of M-centred prisms which share one R atom – Table 2. The LC value is related to the overall composition of the trigonal prism framework according to R_6M_{LC}. If there are no extra R atoms outside the trigonal prisms the formula of the compound is then equal to R_6M_{LC}. Two series of infinite chains of centred trigonal prisms have been recognized, $R_{2n+1}M_n$ and $R_{n+2}M_n$. The series $R_{2n+1}M_n$ includes the following structure types: R_3M (n = 1), R_5M_2 (n = 2), R_7M_3 (n = 3), and RM Pnma (n = ∞). The structures of R_3M, R_5M_2 and RM(Pnma) are comprised of infinite zig-zag chains of trigonal prisms, but the R_7M_3 structure type, although built up of trigonal prisms, has a different stacking. The series $R_{n+2}M_n$ includes the following structure types [77 P 1]: R_3M (n = 1), R_2M (n = 2), R_3M_2–C2/m (n = 4) and RM–Cmcm (n = ∞). All four structures are based on separate bands of infinite columns of trigonal prisms (Fig. 6). The number of columns of prisms which form each band is given by the number n. When different structures of the same formula are based on the same elementary unit of construction it is sometimes possible to transform one into the other, geometrically, by slicing one structure into blocks and stacking these blocks in a different way. In Fig. 7, the structures of Y_3Co_2 and Dy_3Ni_2 are shown in projection along one main symmetry axis. Starting from the Y_3Co_2 structure it is possible to imagine a slicing operation by which identical infinite slabs are formed. The shifting of slabs of equal heights in the same direction by equal amount leads to a new model representing the Dy_3Ni_2 structure [75 M 9]. Similar relationship may be evidenced in RM–Pnma, RM–Cmcm, TbNi(h)–Pnma and TbNi(l)–$P2_1/m$ structures [70 L 1].

Table 2. Structure types of rare earth – transition metal compounds where M atoms are at the centres of trigonal prisms, the kind of M–M linkage and the trigonal prism linkage coefficient [77 P 1].

Compound	Kind of M–M atom linkage	LC
R_3M	Isolated M atoms	2
R_5M_2	Isolated M atoms	$2\frac{2}{5}$
R_7M_3	Isolated M atoms	$2\frac{4}{7}$
R_8M_5	Pairs and group of 4M atoms	$3\frac{3}{4}$
R_3M_2:		
$Er_3Ni_2(R\bar{3})$	M atom pairs	$4\frac{1}{2}$ [1]
Dy_3Ni_2 (C2/m)	Chains of 4M atoms	4
Y_3Co_2 (Pnnm)	Chains of 4M atoms	4
Y_3Ni_2 ($P4_12_12$)	Group of 4M atoms	4
RM:		
CrB (Cmcm)	Infinite chains	6
FeB (Pnma)	Infinite chains	6
TbNi(h) (Pnma)	Infinite chains	6
TbNi(l) ($P2_1/m$)	Infinite chains	6

[1]) Not all R atoms participate in the formation of a trigonal prism.

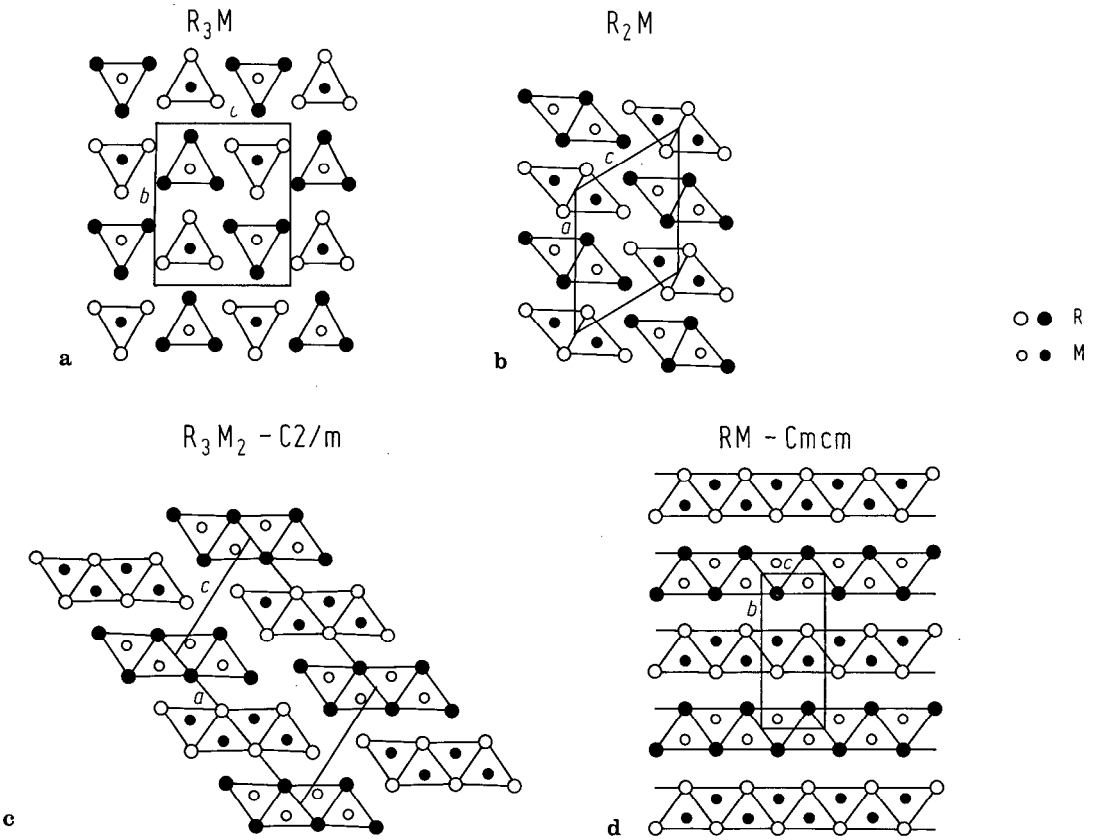

Fig. 6. Members of the $R_{n+2}M_n$ structure series having bands of trigonal prisms. The large circles are R atoms and the small circles correspond to M atoms. The open circles are at relative height zero, the solid ones at one half: (a) R_3M (n=1); (b) R_2M (n=2); (c) R_3M_2–C2/m (n=4); (d) RM–Cmcm (n=∞) [77 P 1].

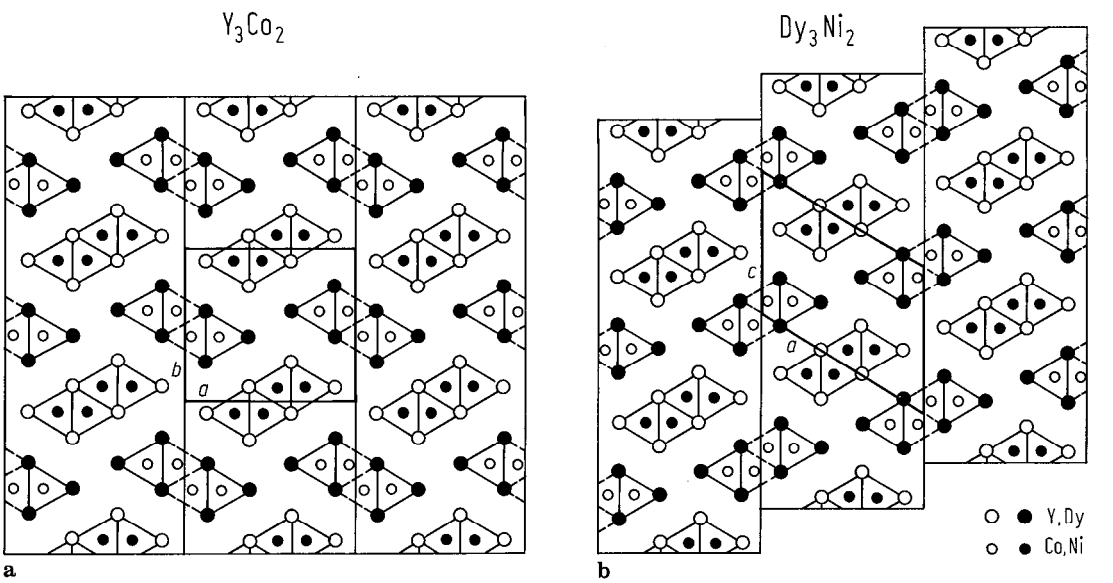

Fig. 7. Structures of (a) Y_3Co_2 and (b) Dy_3Ni_2 geometrically related by block stacking. The large circles are R atoms and the small circles correspond to M atoms. The white circles are the relative height zero, the black one at one-half [77 P 1].

The structures of R_3M, R_5M_2, R_7M_3, and RM -Pnma can be obtained from unit cell twinning of an ideal hexagonal close-packed structure. At least two of these structure types occur in R–Co or R–Ni systems. Unit cell twinning of a rare earth close-packed structure along particular planes leaves regular trigonal prism holes on the twinning planes. These planes are occupied by M atoms. The ratio between twinned and untwinned segments determines the overall composition of the compounds. In Fig. 8 it is shown how the R_3M, R_5M_2 and RM–Pnma structures can be derived in such a way from a hexagonal close-packed structure [77 P 1]. The same mechanism has been used to explain other equiatomic structures like RM–Cmcm, or the high (h)- and low (l)-temperature modifications of TbNi [76 P 1].

(A2) In case of structures with various coordination polyhedra, the situation is more complicated. The structures of all R-rich compounds in the R–Ni system are built up exclusively of trigonal prisms. This is perhaps related to the ideal size of the Ni atom which fits equally well into a trigonal rare earth prism formed by big La atoms or by small Lu atoms. But geometrical factors can only be of secondary importance. For instance, Co of nearly the same size as Ni, has a very different structural character as compared with the latter. Except for the R_3M phase, all rare-earth-rich compounds in the R–Co systems are different from the ones in the R–Ni systems. In particular, equiatomic RCo compounds do not exist and the structures often contain a mixture of coordination polyhedra. The structure of $R_{12}Co_7$ compounds [76 A 1], for example, is characterized by four Co-centred coordination polyhedra: two with coordination eight (a cube and a square antiprism) and two with coordination six (a prism and a square antiprism with two opposite corners through the centre missing). The latter can also be viewed as a pentagon with one corner replaced by pair of atoms in a direction perpendicular to the plane of the pentagon. An explanation of the reasons for the variety of coordination polyhedra is difficult [77 P 1].

(B) A relationship between the structures of the compounds having the M content $66\,at\% < M < 90\,at\%$ may be also considered [75 P 3]. Cromer and Larson [59 C 1] reported that the $CeNi_3$, $PuNi_3$, and Ce_2Ni_7 types can be obtained by alternate stacking of RM_2 and RM_5 layers. They also elaborated a description in which these structure types are based only on the hexagonal $CaCu_5$ structure type. By introducing ordered substitutions of R atoms in the twofold M positions of the RM_5 structure, followed by appropriate shifts of layers and small displacements of adjacent R atoms along the *c* axis, they could derive all the hexagonal and rhombohedral structure types. Lemaire [66 L 3] has also discussed this substitution scheme and formulated equations expressing the substitution mechanism for the different structure types.

Khan [74 K 9, 74 K 11] noted that the substitution scheme for the derivation of RM_x structure types appears very simple but the determination of the atomic positions for a particular structure type is quite laborious. He described a procedure by which the lattice parameters and atomic positions for any of the hexagonal and rhombohedral structure types could be easily calculated. Khan scheme [74 K 9, 74 K 11] reverts to the earlier [59 C 1] proposed sequence of RM_2 and RM_5 layers. The structures are considered to be divided into blocks of RM_2 as in the Laves phases and blocks of RM_5 as in the $CaCu_5$ type. The various structure types differ in the ratio of the number of RM_2 blocks to the number of RM_5 blocks.

A construction scheme rather complicated has been also proposed to show that the Zr_2Ni_7 structure may be derived from the $CaCu_5$ structure by removal of a layer of M atoms, collapse of the remaining structure, and shifts of atoms [72 E 2].

The hexagonal-rhombohedral series were discussed assuming a stacking of blocks of different size. The general formula in the composition range 66 to 83 at% M is RM_x with $x = (5n+4)(n+2)^{-1}$ and n being zero or any positive integer [74 K 9]. However, it was not possible to isolate a single-phase compound having the M concentration higher than that in the R_5M_{19} compound ($n = 3$). In the rhombohedral subseries, the stacking of R_2M_4 blocks is described only by the intraplanar translation $\boldsymbol{T}_{R_2M_4}$, while in the hexagonal subseries successive R_2M_4 blocks are derived from each other by translation followed by a 180° rotation.

For each structure type it is possible to formulate a mininum block sequence which leads to the complete structure after repeated stacking with the same orientation for the rhombohedral series, or alternate rotations of the R_2M_4 block for the hexagonal subseries. According to [75 P 3], these structure types are described by $R_{n+1}M_{5n-1}$ – Fig. 9. Here only contour lines of the structure blocks are shown. The RM_5 block is denoted by 15 and is represented by a rectangle and the R_2M_4 block is denoted by 24 and represented by a parallelogram. If the sum of the printed numbers in the minimum block sequence is formed, first ciphres separately from the second ciphres, the two totals correspond to the overall composition formula for the particular structure type.

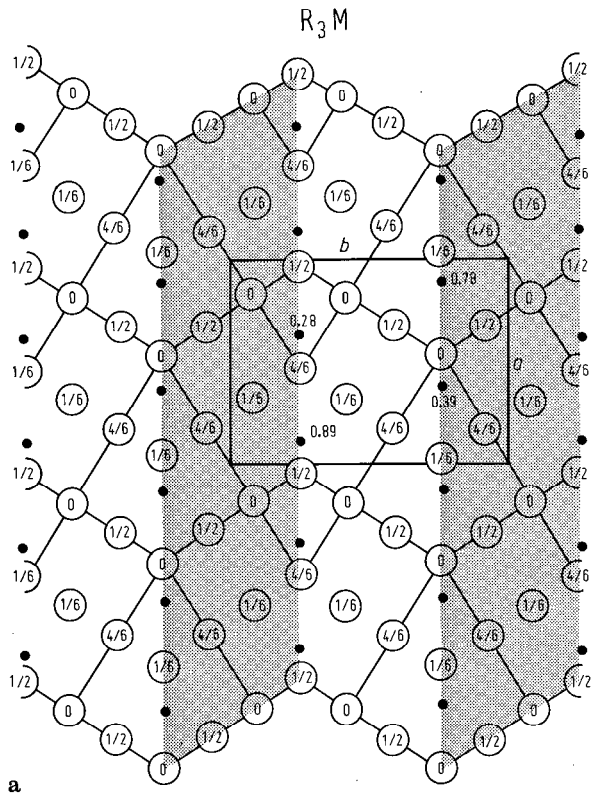

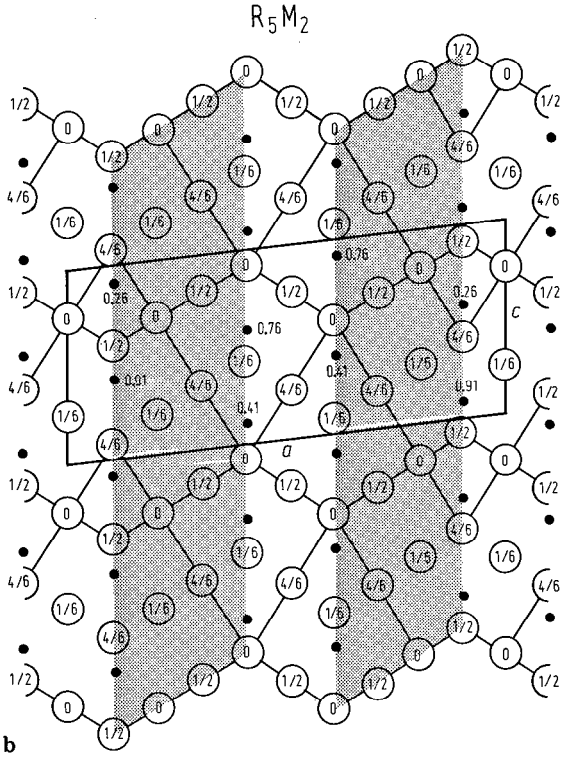

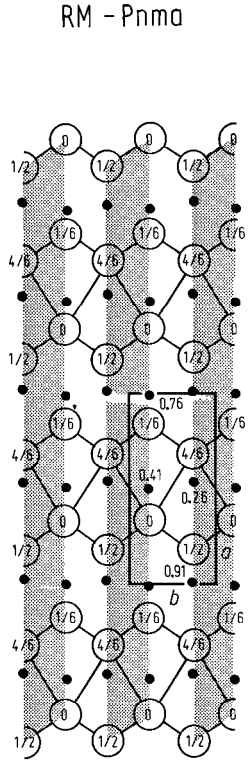

Fig. 8. (a) R_3M, (b) R_5M_2 and (c) RM–Pnma structure types interpreted from periodic unit cell twinning of a hexagonal close-packed base structure. The untwinned segments are alternately shaded and unshaded. The M sites, indicated by small black circles, are situated at the twin planes in the centres of the trigonal prismatic holes only [77 P 1].

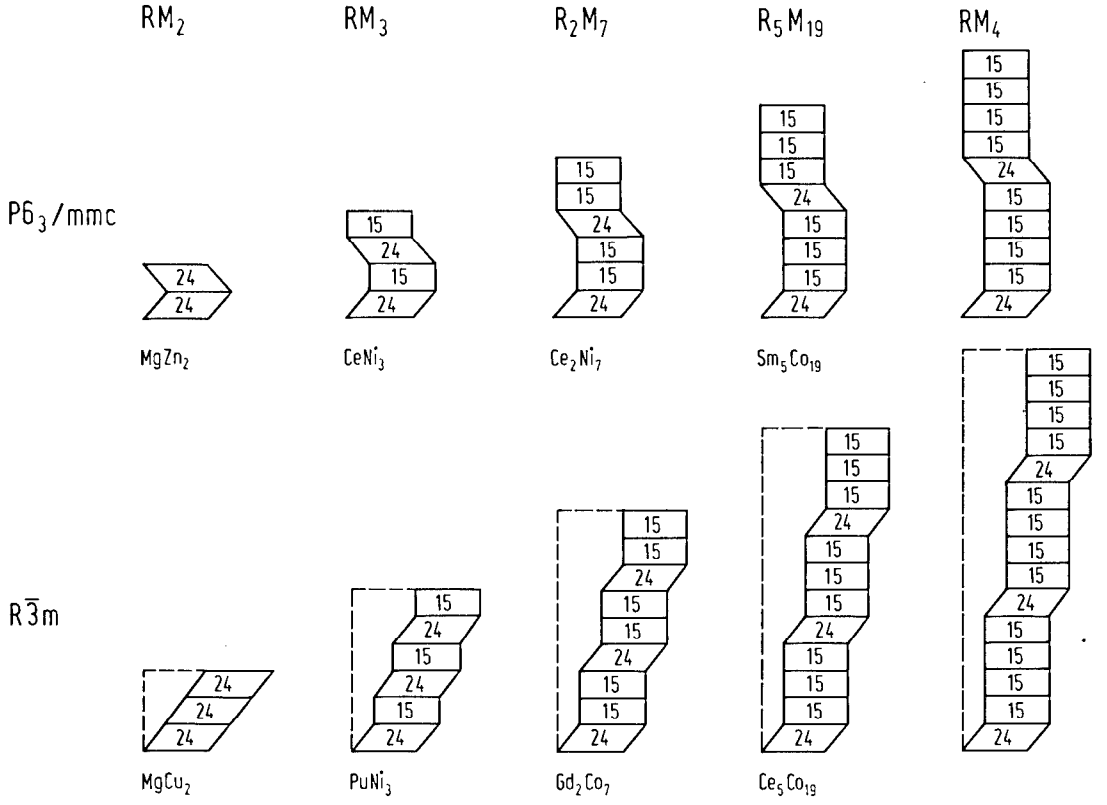

Fig. 9. Crystal types of the hexagonal-rhombohedral $R_{n+1}M_{5n-1}$ structure series described by stacking of R_2M_4 and RM_5 structure blocks (24 denotes the R_2M_4 block and 15 an RM_5 block) [75 P 3].

Other subseries can be constructed by assuming more complex stacking sequence of the R_2M_4 blocks.

The monoclinic subseries of the $R_{n+1}M_{5n+2}$ structure series were also analysed [75 P 3]. A study of the Zr_2Ni_7 and $PuNi_4$ structure types reveals that these two types belong to the monoclinic subseries of a new series involving R_2M_7 blocks and RM_5 blocks. The Zr_2Ni_7 type is the first member of this series and may be constructed by stacking R_2M_7 blocks alone. The block-stacking model for this structure type shows that it should be possible to describe this structure type with a unit-cell of half the volume of the one reported by [72 E 2]. The next member in the monoclinic subseries with $n=2$ has the crystal structure of $PuNi_4$. The block stacking of the hypothetical R_4M_{17} structure obtained with $n=3$ is described in [75 P 3].

The other series of the $R_{n+1}M_{5n+2}$ structure series may be generated [75 P 3]. Whereas in the monoclinic subseries the stacking of R_2M_7 blocks involves only $T_{R_2M_7}$ translation, new subseries are generated when successive blocks are not only translated by $T_{R_2M_7}$ but also rotated by 60°, 120° or 180°. At the present no structures of these subseries are known.

(C) The structures of the $LaCo_{1-\varepsilon}$ and La_2Co_3 compounds which show a strong directional order are described in subsects. 2.4.2.9 and 2.4.2.11.

(D) The structures of RM_{12} and RM_{13} compounds having very high M content are described in subsects. 2.4.2.19 and 2.4.2.20.

The formation and stability of RM_x binary intermetallic compounds was correlated by Miedema et al. [75 M 10, 76 M 11, 88 d 1] with the heat of formation, ΔH. The ΔH values for some RM_x compounds were tabulated [77 b 1, 88 d 1]. The analysis predicts an increase of the stability of RM_x compounds in the sequence M = Mn, Fe, Co, Ni and for R from La to Lu, in agreement with the observed behaviour.

2.4.1.3 General view on the magnetic behaviour of RM_x compounds

2.4.1.3.1 General

The magnetic properties of rare-earth-3d transition metals are rather complex. Depending on the magnetic contributions of M and R elements, several types of magnetic behaviours may be evidenced:

1. Compounds in which the 3d transition metal atoms do not carry a magnetic moment. Two situations are observed:

1.1. If the R atom is not magnetic, the compounds are Pauli paramagnets. As example we mention YCo_2, $LuCo_2$, YNi_5, YNi_2 compounds (subsect. 2.4.2.12, Fig. 118).

1.2. If the R atoms carry a magnetic moment, the compounds are ferromagnetic, antiferromagnetic, or show a complex magnetic structure.

2. Compounds in which the magnetization of M elements is driven by the 4f rare earth magnetic moment. The most representative class of compounds is the RCo_2 system. The compounds $LuCo_2$ or YCo_2 are Pauli paramagnets. Substituting Lu(Y) by a magnetic rare earth, a Co magnetic moment is induced (subsect. 2.4.2.12, Fig. 139). The Co magnetic moment may be also induced under the action of an external magnetic field (subsect. 2.4.2.12, Fig. 119).

3. Compounds with a strange magnetic behaviour. As example we mention that Y_9Co_7 at low temperatures is a superconductor and at higher ones is a ferromagnet (see subsect. 2.4.2.8).

4. Compounds in which M atoms have a magnetic moment sustained by the 3d band. This class contains the greatest number of RM_x compounds. Even in this case a fraction of M magnetic moments may be induced by magnetic interactions involving R atoms (subsect. 2.4.2.12, Fig. 139). These systems may be ordered ferromagnetically, ferrimagnetically, show a mictomagnetic or a more complex type of magnetic ordering.

In the following, some general features of the magnetic behaviour of ferromagnetic and ferrimagnetic RM_x compounds will be presented:

(1) The magnetic moments of R and M atoms are generally dependent on the lattice sites. By magnetic measurements only their mean contributions can be obtained. Because of the high symmetry of the crystalline cell, the Laves phase compounds, RM_2, are an exception, both R and M atoms being situated on one type of lattice site.

(2) The magnetic moments of 3d transition metals determined by neutron diffraction studies are somewhat greater than those obtained by saturation measurements. The last values include also the conduction electron polarization, negative at M site. As example, the Fe magnetic moment determined by saturation measurements in $LuFe_2$ is 1.45 μ_B [71 G 3], while from neutron diffraction studies a value of 1.74 μ_B was obtained [80 G 6]. The value of conduction electron polarization $p_{4s} = -0.29\ \mu_B$/Fe is close to that determined in iron metal, $p_{4s} = -0.25\ \mu_B$/Fe [62 S 2].

(3) In RM_x compounds with non-S state rare earth atoms, generally the saturation is hardly to be obtained because of the high anisotropy. Thus, even in high magnetic fields, reliable values of the saturation magnetization may be obtained only in single crystals along the easy axis of magnetization, or in polycrystalline compounds with gadolinium or a nonmagnetic rare earth atom (yttrium). To determine the magnetic contributions of M atoms, frequently it is supposed that the magnetic moment of R is given by the free-ion $g_J J$ values. Really, a reduction of the non-S state rare earth ionic magnetic moment by crystal field effects is sometimes observed. The above considerations may explain the differences in saturation magnetizations given by various authors as well as the estimated magnetic contributions of M atoms.

The thermal variations of spontaneous magnetization for some YFe_x ferromagnetic compounds are plotted in Fig. 10 [82 b 1]. As seen in the same figure, at temperatures higher than the Curie temperature T_C the reciprocal magnetic susceptibility follows a Curie-Weiss law.

The reduced spontaneous magnetizations, as function of reduced temperatures for $GdFe_x$ and $GdCo_x$ compounds are given in Fig. 11 [72 B 11, 82 b 1]. The Gd_3Co compound shows a metamagnetic behaviour, while other compounds are ferrimagnetic. According to the Néel classification [48 N 1] these are of Q-type for $GdFe_2$, $GdCo_2$ and $GdCo_3$, of N-type for $GdFe_3$ and Gd_2Co_7, and of P-type for $GdCo_5$ and Gd_2Co_{17}. As seen in Fig. 12, the thermal variations of the reciprocal magnetic susceptibilities for ferrimagnetic compounds are nonlinear.

The composition dependences of the mean Fe and Co magnetic moments, determined in yttrium, p_M^Y, and gadolinium, p_M^{Gd}, compounds are plotted in Fig. 10 [81 b 1]. The p_M values decrease by increasing yttrium (gadolinium) content. The transition metal magnetic moments are greater in gadolinium compounds than in corresponding yttrium ones. This fact is attributed to stronger exchange interactions in the gadolinium systems.

The effective 3d magnetic moments determined from the Curie constants are greater than the M magnetic moments obtained from saturation measurements. The ratio $r = n_p/n_s$ between the number of magnetic carriers per atom deduced from the Curie constants, n_p, and the number of carriers obtained from saturation data, n_s, give a measure of the localization of M magnetic moments. For a localized magnetic moment, we have $r = 1$. The r values obtained for the M atoms in rare earth (yttrium) compounds, as function of the Curie temperature, are plotted in Fig. 13 [78 B 12]. The points are approximately arranged on a unique curve. The degree of localization of the 3d transition metal magnetic moments is a function of the Curie temperature. This behaviour is similar to that observed for 3d transition metal alloys [62 W 3].

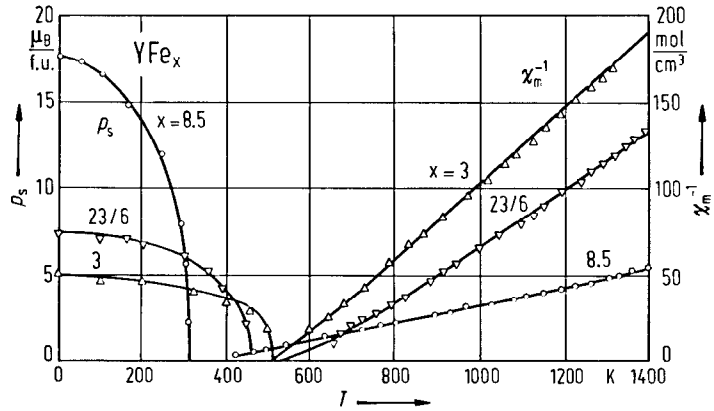

Fig. 10. Thermal variation of spontaneous magnetization and of reciprocal magnetic susceptibilities for YFe$_x$ (x = 3, 23/6, and 17/2) compounds [82 b 1].

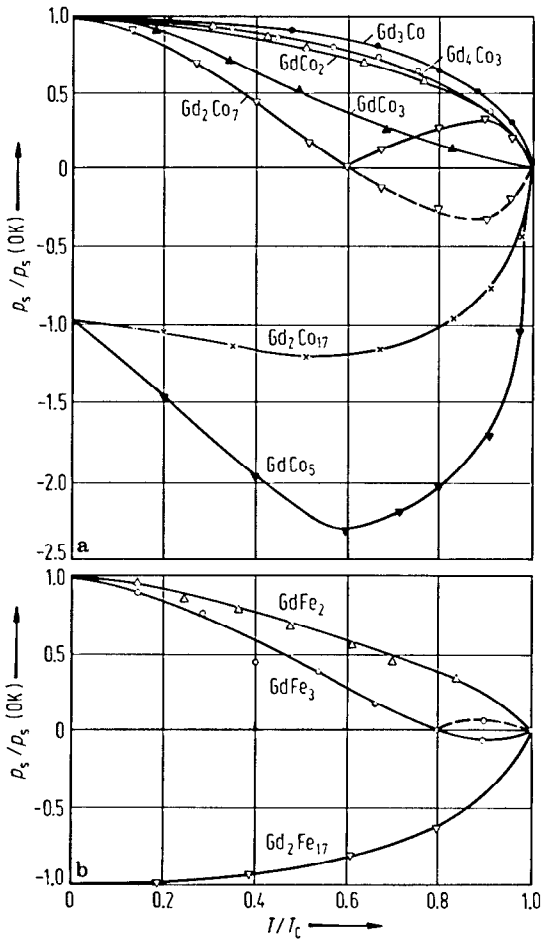

Fig. 11. Thermal variation of the reduced spontaneous magnetization as function of the reduced temperature in (a) Gd–Co and (b) Gd–Fe compounds [69 G 1, 72 B 11, 73 B 16].

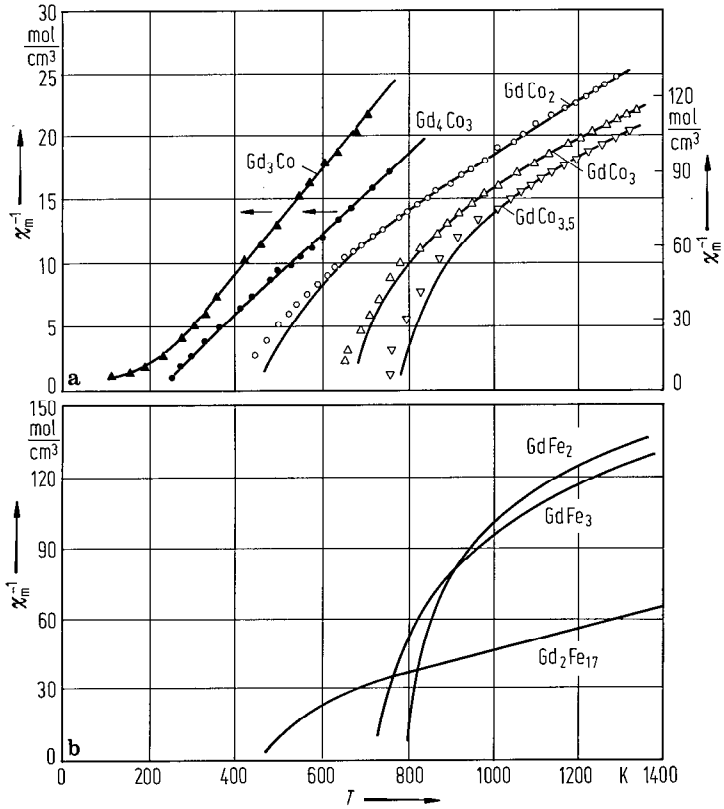

Fig. 12. Thermal variation of reciprocal magnetic susceptibilities for (a) Gd–Co and (b) Gd–Fe compounds [72 B 11, 73 B 16].

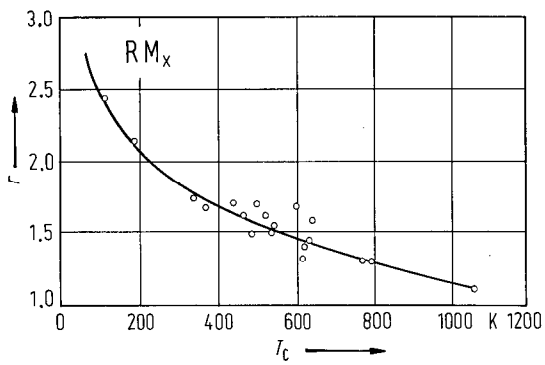

Fig. 13. Ratio r between the number of spins obtained from the Curie constant and saturation magnetization at 4.2 K, determined for M atoms in RM_x compounds, as function of Curie temperatures [78 B 12].

2.4.1.3.2 Magnetic interactions in RM_x compounds

The RM_x systems are generally characterized by the presence of magnetic interactions between rare earths (R–R), 3d transition metals (M–M), as well as between rare earths and 3d transition metals (R–M).

The interactions between rare earth ions (R–R) are the weakest ones and seem to be best described by the RKKY model [54 R 1, 56 K 1, 57 Y 1, 68 K 1, 71 R 7, 72 C 1, 81 b 1]. This type of magnetic coupling may be evidenced in RM_x compounds where the magnetic contribution of M elements is nil. A system of magnetic R ions with a localized moment $g_J J_n \mu_B$ situated at the site $\boldsymbol{R}_n$, induces at the site $\boldsymbol{r}$ a conduction electron polarization, $\sigma(\boldsymbol{r})$. Supposing that the exchange coupling, J_{sf}, is wavevector-independent, the electrons described by plane waves and a spherical Fermi surface, the polarization, $\sigma(\boldsymbol{r})$, is given by:

$$\sigma(\boldsymbol{r}) = \frac{9\pi}{4} z^2 \frac{J_{sf}(g_J-1)}{v^2 E_F} J_n F(2k_F|\boldsymbol{r}-\boldsymbol{R}_n|) \tag{1}$$

where ze is the ionic charge, v the atomic volume, E_F the Fermi energy and k_F the corresponding wavevector. The function $F(x)$ has the form

$$F(x) = \frac{x\cos x - \sin x}{x^4}. \tag{2}$$

The polarization of conduction electrons leads to an indirect exchange interaction between the magnetic R ions.

The paramagnetic Curie temperature is given by

$$\Theta = -\frac{3\pi}{4} z^2 \frac{J_{sf}^2(g_J-1)^2 J(J+1)}{v^2 E_F k_B} \sum_n F(2k_F \boldsymbol{R}_n). \tag{3}$$

For the same type of structure and supposing J_{sf} constant, the Curie temperatures are proportional to the De Gennes factor, $G=(g_J-1)^2 J(J+1)$ [58 D 1, 62 D 1]. The above prediction is fulfilled in RNi_2 compounds in which Ni is nonmagnetic (subsect. 2.4.2.12, Fig. 121). The reciprocal magnetic susceptibilities of these compounds follow a Curie-Weiss law. The determined effective magnetic moments of R ions are close to those of the free rare earth ions.

The dominant interactions between R and M ions seem to be those by indirect exchange and consequently may be described by the RKKY model (subsect. 2.4.1.1). Since the 4f electrons are well localized, only a small mixing with the 3d electron wave functions takes place. Supposing that the exchange interactions do not depend on $\boldsymbol{q}$, the difference between the wavevectors of electrons before and after scattering by the magnetic ions, the following exchange Hamiltonian has been obtained [71 B 18]

$$\mathcal{H}_{RM} = \left(\frac{3n}{N}\right)^2 \frac{2\pi}{E_F} J_R(0) J_M(0) \sum_{n,m} F(2k_F R_{nm}) \boldsymbol{J}_{R_n} \cdot \boldsymbol{S}_{M_m}. \tag{4}$$

where N is the number of lattice points and n is the number of conduction electrons. The summation over n and m involves all R–M distances $\boldsymbol{R}_{nm}$ present in the underlying structure. The quantities $J_R(0)$ and $J_M(0)$ are the effective s–f and s–d exchange integrals.

Analysing the magnetic properties of $R_2(Co_{1-x}M_x)_{17}$ with R = Sm, Y and M = Fe, Mn, or Cr [77 P 3] an indirect exchange propagated by s- and p-conduction states was considered. The exchange Hamiltonian has the form:

$$\mathcal{H}_{exch} = \sum_{ij} J(R_{ij}) \boldsymbol{S}_i \cdot (g_J-1) \boldsymbol{J}_j, \tag{5}$$

with

$$J(R_{ij}) = \frac{4me^2}{7\pi^3\hbar^2} \pi k_F^4 J_{sd} \langle r^2 \rangle (0.49 F(2k_F R_{ij}) + 0.266 k_F^2 F'(2k_F R_{ij})).$$

where m is the electron mass, k_F the Fermi wavevector, J_{sd} the s–d exchange integral, and $\langle r^2 \rangle$ the mean square of the 4f radius. $F(2k_F R)$ and $F'(2k_F R)$ are the RKKY-type functions corresponding to s- and p-type states, respectively.

The M–M-type interactions appearing in metallic systems are rather difficult to analyse. A large variety of models was used to describe their magnetic behaviour, covering the extreme descriptions: band and localized models.

In the following we mention only some models which take into account both localized and band features.

The concept of localization in the band model [61 F 2, 62 F 1, 66 L 2] was used to analyse the magnetic behaviour of Co in rare earth compounds [69 T 2, 71 B 18, 71 B 21, 72 B 10, 72 B 11].

Stearns [71 S 6, 73 S 7, 76 S 10] proposed an interaction model supposing that the ferromagnetism of metals is due to the indirect coupling of the localized d electrons by a small number of itinerant d electrons. The model suggests that in case of iron approximately 5% of d electrons are itinerant and 95% are in sufficiently narrow bands to be considered as localized. The model has been used to account for the magnetic behaviour of Fe in rare earth compounds [77 B 15, 78 B 12, 79 B 13, 80 B 13]. The ^{89}Y magnetic hyperfine fields in YFe_x compounds [73 O 9] are interpreted in terms of a long-range exchange polarization of the s-conduction electrons by means of the Fe magnetic moments according to Stearns' model. In the same model the Co magnetic hyperfine field in some RCo_5 compounds was analysed [75 H 1]. The high-pressure behaviour in R_2M_{17} compounds was discussed also in the above model [75 J 1].

2.4.1.3.3 Models used to analyse the magnetic properties of RM_x compounds

It is a difficult matter to analyse the magnetic properties of RM_x systems on a microscopic scale, having in view the complexity of the interactions. Therefore, for systems in which both R and M are magnetic, some simplified models were used in order to describe their magnetic behaviour.

At the beginning, the prediction of the molecular field model for ferrimagnetic RM_x systems, both in the supposition that the M atoms have at $T > T_C$ an intrinsic magnetic moment or an exchange-enhanced paramagnetism, are presented. The above situations were evidenced by neutron diffraction studies. An exchange-enhanced magnetic susceptibility was observed in RCo_2 (R = Ho, Tm) compounds at $T > T_C$ (subsect. 2.4.2.12, Fig. 164). On the other hand a magnetic moment of Fe of 1.0 μ_B was obtained, for example, in $CeFe_2$ above the Curie temperature [81 D 4]. This value is close to 1.15 μ_B determined at 4.2 K in the ferromagnetic state. Generally the value for p_M obtained at low temperatures by magnetic measurements is smaller than that determined from Curie constants, but the reason for this difference is not clear. Probably, the Curie constants need to be corrected for thermal variations of magnetic interactions [37 N 1]. On the other hand small quantities of phases with Curie temperatures higher than that of the phase studied may affect substantially the paramagnetic data. If the data are correct, the above difference gives a measure of the itinerancy degree of M moment (subsect. 2.4.1.3).

Admitting a two-sublattice model, corresponding to mean R and M magnetizations, the thermal variation of the resultant magnetic moment for ferrimagnetic compounds may be described by the Néel model [48 N 1]. At temperatures greater than the Curie temperature, the magnetic moments of R and M atoms are aligned under the action of the external and molecular fields,

$$\langle M_R \rangle = C_R T^{-1}(H + \lambda_{RR}\langle M_R \rangle + \lambda_{RM}\langle M_M \rangle), \tag{6}$$

$$\langle M_M \rangle = C_M T^{-1}(H + \lambda_{MM}\langle M_M \rangle + \lambda_{RM}\langle M_R \rangle), \tag{7}$$

where λ_{RR}, λ_{RM} and λ_{MM} are the molecular field coefficients characterizing the magnetic interactions inside and between magnetic sublattices.

The relation (7) may be written as

$$\langle M_M \rangle = A'(H + \lambda_{RM}\langle M_R \rangle) \tag{8}$$

with

$$A' = \frac{C_M T^{-1}}{1 - \lambda_{MM} C_M T^{-1}}. \tag{9}$$

The thermal variation of A' is of the form

$$A' = C_M (T - \Theta)^{-1}, \tag{10}$$

where $\Theta = C_M \lambda_{MM}$.

The temperature dependence of the reciprocal magnetic susceptibility of a two-sublattice ferrimagnet follows a Néel-type law [48 N 1]:

$$(\chi - \chi_P)^{-1} = \chi_0^{-1} + TC^{-1} - \sigma(T - \Theta')^{-1}, \tag{11}$$

where χ_P denotes a Pauli-type magnetic susceptibility. The parameters χ_0, C, σ and Θ' are related to the molecular field coefficients.

In the following we mention only some models which take into account both localized and band features.

The concept of localization in the band model [61 F 2, 62 F 1, 66 L 2] was used to analyse the magnetic behaviour of Co in rare earth compounds [69 T 2, 71 B 18, 71 B 21, 72 B 10, 72 B 11].

Stearns [71 S 6, 73 S 7, 76 S 10] proposed an interaction model supposing that the ferromagnetism of metals is due to the indirect coupling of the localized d electrons by a small number of itinerant d electrons. The model suggests that in case of iron approximately 5% of d electrons are itinerant and 95% are in sufficiently narrow bands to be considered as localized. The model has been used to account for the magnetic behaviour of Fe in rare earth compounds [77 B 15, 78 B 12, 79 B 13, 80 B 13]. The ^{89}Y magnetic hyperfine fields in YFe_x compounds [73 O 9] are interpreted in terms of a long-range exchange polarization of the s-conduction electrons by means of the Fe magnetic moments according to Stearns' model. In the same model the Co magnetic hyperfine field in some RCo_5 compounds was analysed [75 H 1]. The high-pressure behaviour in R_2M_{17} compounds was discussed also in the above model [75 J 1].

2.4.1.3.3 Models used to analyse the magnetic properties of RM_x compounds

It is a difficult matter to analyse the magnetic properties of RM_x systems on a microscopic scale, having in view the complexity of the interactions. Therefore, for systems in which both R and M are magnetic, some simplified models were used in order to describe their magnetic behaviour.

At the beginning, the prediction of the molecular field model for ferrimagnetic RM_x systems, both in the supposition that the M atoms have at $T > T_C$ an intrinsic magnetic moment or an exchange-enhanced paramagnetism, are presented. The above situations were evidenced by neutron diffraction studies. An exchange-enhanced magnetic susceptibility was observed in RCo_2 (R = Ho, Tm) compounds at $T > T_C$ (subsect. 2.4.2.12, Fig. 164). On the other hand a magnetic moment of Fe of 1.0 μ_B was obtained, for example, in $CeFe_2$ above the Curie temperature [81 D 4]. This value is close to 1.15 μ_B determined at 4.2 K in the ferromagnetic state. Generally the value for p_M obtained at low temperatures by magnetic measurements is smaller than that determined from Curie constants, but the reason for this difference is not clear. Probably, the Curie constants need to be corrected for thermal variations of magnetic interactions [37 N 1]. On the other hand small quantities of phases with Curie temperatures higher than that of the phase studied may affect substantially the paramagnetic data. If the data are correct, the above difference gives a measure of the itinerancy degree of M moment (subsect. 2.4.1.3).

Admitting a two-sublattice model, corresponding to mean R and M magnetizations, the thermal variation of the resultant magnetic moment for ferrimagnetic compounds may be described by the Néel model [48 N 1]. At temperatures greater than the Curie temperature, the magnetic moments of R and M atoms are aligned under the action of the external and molecular fields,

$$\langle M_R \rangle = C_R T^{-1}(H + \lambda_{RR}\langle M_R \rangle + \lambda_{RM}\langle M_M \rangle), \tag{6}$$

$$\langle M_M \rangle = C_M T^{-1}(H + \lambda_{MM}\langle M_M \rangle + \lambda_{RM}\langle M_R \rangle), \tag{7}$$

where λ_{RR}, λ_{RM} and λ_{MM} are the molecular field coefficients characterizing the magnetic interactions inside and between magnetic sublattices.

The relation (7) may be written as

$$\langle M_M \rangle = A'(H + \lambda_{RM}\langle M_R \rangle) \tag{8}$$

with

$$A' = \frac{C_M T^{-1}}{1 - \lambda_{MM} C_M T^{-1}}. \tag{9}$$

The thermal variation of A' is of the form

$$A' = C_M (T - \Theta)^{-1}, \tag{10}$$

where $\Theta = C_M \lambda_{MM}$.

The temperature dependence of the reciprocal magnetic susceptibility of a two-sublattice ferrimagnet follows a Néel-type law [48 N 1]:

$$(\chi - \chi_P)^{-1} = \chi_0^{-1} + TC^{-1} - \sigma(T - \Theta')^{-1}, \tag{11}$$

where χ_P denotes a Pauli-type magnetic susceptibility. The parameters χ_0, C, σ and Θ' are related to the molecular field coefficients.

The magnetic behaviour of a number of RM_x compounds was analysed by using the above model. We mention the RFe_2 compounds [73 B 18, 73 B 19, 73 H 3, 80 I 2], RCo_x-based compounds [73 B 18, 73 B 19, 75 T 2, 76 B 16], or RFe_x-based compounds [78 B 12, 78 H 5, 79 B 13].

Starting from a molecular field model, the high-temperature magnetic behaviour of systems with indirect exchange interactions was analysed [75 F 1]. The model describes correctly the Curie temperatures of RFe_2 compounds. The T_C values of the same system were also analysed by [76 R 1]. Considering a two-sublattice molecular field model, the T_C values are described with the following values of the exchange constants $J_{FeFe}=832\,K$, $J_{RFe}=-137\,K$ and $J_{RR}=98\,K$.

The molecular field model was used to analyse the dependence of M magnetic moments on the exchange interactions. As result of the substitution of magnetic M atoms by nonmagnetic ones or of the magnetic rare earths by La, Lu or Y, the exchange interactions appearing in the system are modified. This fact is reflected in the variation of M magnetic moments. As seen in Fig. 14, the induced M magnetic moments, Δp_M, scale linearly with the variation of exchange field [76 B 13]

$$\Delta p_M = V_M \Delta H_{exch}. \tag{12}$$

The proportionality constants in the above relation are $V_{Co}\cong(1/3)10^{-6}\,\mu_B/Oe$ and $V_{Fe}\cong(1/18)10^{-6}\,\mu_B/Oe$. V_M has the same dimension as the magnetic susceptibility and is supposed for $T>T_C$ to vary slowly with temperature. The Δp_M induced magnetic moments calculated with relation (12) are in good agreement with the experimental data [76 B 13, 76 B 17, 78 B 12, 79 B 13, 80 B 13, 81 B 10].

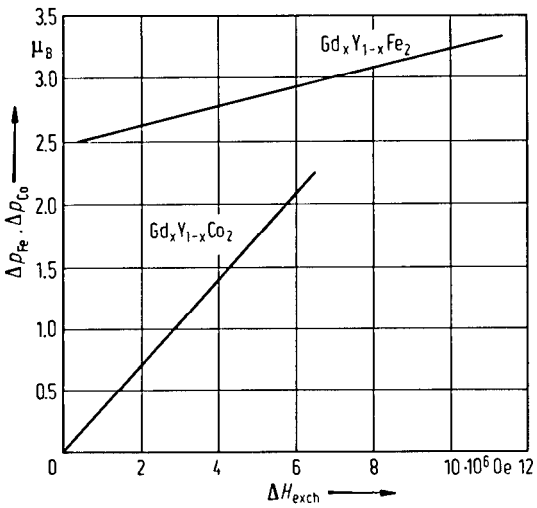

Fig. 14. Variation of Co and Fe induced magnetic moments in $Gd_xY_{1-x}M_2$ (M = Fe or Co) compounds as function of the variation of the exchange field [76 B 13]. $\Delta p_{Co}=(1/3)\cdot10^{-6}\,\Delta H_{exch}\,\mu_B/Oe$ and $\Delta p_{Fe}=(1/18)2))\cdot10^{-6}\,\Delta H_{exch}\,\mu_B/Oe$.

As mentioned above the Co magnetization in RCo_2 compounds is driven by the 4f magnetic moments. The $ErCo_2$, $HoCo_2$, and $DyCo_2$ compounds show first-order transitions between the ordered and the paramagnetic state [66 L 4, 72 B 10, 75 B 4]. In case of systems with light rare earth compounds, or in $TbCo_2$ and $GdCo_2$, a second-order phase transition is observed [72 B 10]. The possible existence of a first-order phase transition in $TmCo_2$ cannot be shown, because of the strong crystal field effects compared to the exchange interactions [76 G 4]. The analysis of the pressure dependence of T_C values in RCo_2 compounds [71 B 9] suggests that the type of phase transition may be connected with the Co band structure. Based on this observation a model has been proposed [70 B 4] in which, at $T>T_C$, only the rare earths have an intrinsic moment. The ordered Co magnetic moment, in this model, is induced in the 3d band, being associated with the Co paramagnetic

susceptibility, at $T > T_C$ supposed to be only weakly temperature-dependent. In this case, the C_M/T in relation (9) is replaced by $\chi_{M,0}$, the paramagnetic susceptibility of M metal when the magnetization of the R atoms is nil. The total magnetic susceptibility is the exchange-enhanced susceptibility

$$A' = \chi_y = \frac{\chi_{M,0}}{1 - \lambda_{MM}\chi_{M,0}}. \tag{13}$$

The total susceptibility of RM_2 (M = Co) samples is given by

$$\chi = \frac{C_R + \chi_y[T - (\lambda_{RR} - 2\lambda_{RM})C_R]}{T - \Theta}, \tag{14}$$

where

$$\Theta = (\lambda_{RR} + \chi_y \lambda_{RM}^2)C_R. \tag{15}$$

The spontaneous magnetization of Co atoms may be described by

$$M_M \cong \lambda_{RM}\chi_y M_R. \tag{16}$$

The above model [70 B 4] neglects the temperature dependence of the magnetic susceptibility associated with the Co 3d band. This was later considered [75 B 4] when the magnetic properties of RCo_2 compounds were correlated with those of YCo_2. The type of transition from ordered to paramagnetic state is connected with the Landau parameter $B(T)$. $B(T)$ is negative at low temperatures and becomes positive above 250 K. Thus, the presence of the first-order phase transition in $DyCo_2$, $HoCo_2$, and $ErCo_2$ ($T_C < 150$ K) and of the second-order phase transitions in $GdCo_2$ and $TbCo_2$ ($T_C > 250$ K) is associated with the sign of the Landau parameter B in the expression of the free energy of YCo_2 as function of magnetization.

The form of the thermal variation of the YCo_2 magnetic susceptibility, having a maximum at $T \cong 250$ K, may be understood when the Fermi level is situated near a minimum of the state density of the d-band. This supposition is not in agreement with the effect of impurities on T_C values [78 G 1]. The model [75 B 4] cannot be used to analyse the nonsymmetric behaviour of RCo_2 compounds with light rare earths which show a second-order phase transition, although T_C values of $PrCo_2$ and $NdCo_2$ are smaller than 100 K [66 L 4, 72 B 10]. The above data suggest that the state density at the Fermi level varies in the rare earth series.

The problem of RM_2 compounds was further theoretically analysed by Cyrot and Lavagna [79 C 8, 79 C 9]. The state density of YM_2 compounds was computed in tight-binding approximation by using the method of moments [75 D 1]. The matter is treated in two steps. The computing of the paramagnetic density of states is carried out self-consistently on the atomic level within Hartree-Fock approximation in order to take the charge transfer into account. Then, the magnetism of the compounds is accounted for by splitting up and down spin bands in the Stoner model. The substitution of Y by a magnetic rare earth increases the splitting energy by $J_0(g_J - 1)\langle J_z \rangle$, where in the molecular field approximation $J_0 = 2g_J \mu_B \lambda (g_J - 1)^{-1}$. Then, the mean magnetization is computed. The calculated Fe magnetic moments in RFe_2 compounds agree with the experimental data. In case of RNi_2 compounds, the density of states near the Fermi level is flat, the Ni magnetization is nil, being not affected by the band splitting. A more complicated situation is evidenced in RCo_2 compounds. If the temperature of the second-order phase transition, T_C', is greater than T_C corresponding to the first-order phase transition, the magnetization develops continuously by decreasing temperature, and thus a second-order phase transition takes place. When $T_C' < T_C$, the magnetization appears suddenly at T_C and the transition is of the first-order. By using this model, the calculated phase transition temperatures of $DyCo_2$, $HoCo_2$ and $ErCo_2$ agree with the experimental data. In case of RCo_2 compounds with light rare earths, a slight increase of the 5d atomic level across the rare earth series is expected. This probably leads to a state density at the Fermi level somewhat larger and thus a paramagnetic susceptibility greater than the critical value. Consequently, a second-order phase transition is expected.

This model has been also used to discuss the magnetic properties of compounds with complex crystalline structure where the transition metal atoms occupy M'- and M''-type of sites, as in $CaCu_5$-type structure (see subsect. 2.4.2.18) [81 G 6]. The local density of states of M' and M'' atoms is situated in a region of the high density of states when the number of rare earth neighbours is small. This is shown in Fig. 15. The M' atoms with lower R coordination show a permanent magnetic moment. The Stoner criterion is not fulfilled for the M'' atoms having a greater number of R nearest-neighbours. In this case, their magnetic susceptibility resembles that of YCo_2 (subsect. 2.4.2.12, Fig. 118). Under the action of the molecular field, the condition for the magnetism of M'' atoms is fulfilled. The magnetic properties of other RM_x were discussed in this model [80 G 4, 83 G 3].

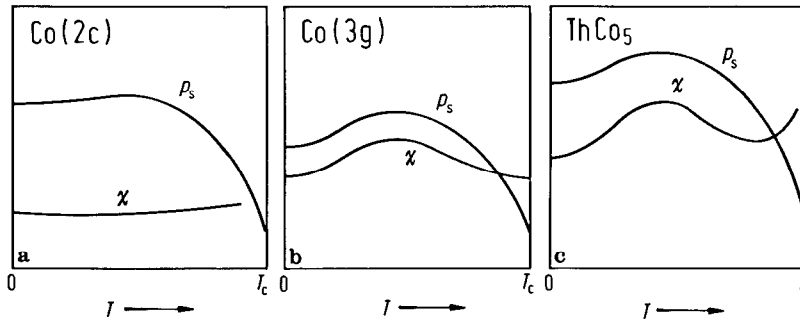

Fig. 15. Schematic plot of the magnetic behaviour of $ThCo_5$ compound. In (a) and (b) thermal variations of magnetizations and magnetic susceptibilities for Co(2c) and Co(3g) sites are given. In (c) the total magnetization and magnetic susceptibility of $ThCo_5$ compound is plotted [81 G 6].

Wohlfarth [79 W 4] extended the model of Bloch et al. [75 B 4] to analyse the magnetic behaviour of RCo_x ($x \geq 3$) compounds in which Co is already ferromagnetic. The composition dependence of the Curie temperatures shows the trend of those experimentally determined. The agreement with T_C values of $(Gd_xY_{1-x})Co_3$ compounds is also good, but not for $Gd(Co_xAl_{1-x})_3$ compounds [81 S 5].

Gomes and Guimaraes [74 G 9] analysed the magnetism of RM_x compounds when the M magnetic moment is driven by the localized f moments or is sustained by the d band. These two situations are discussed in terms of an effective s–d coupling and s–f exchange interaction.

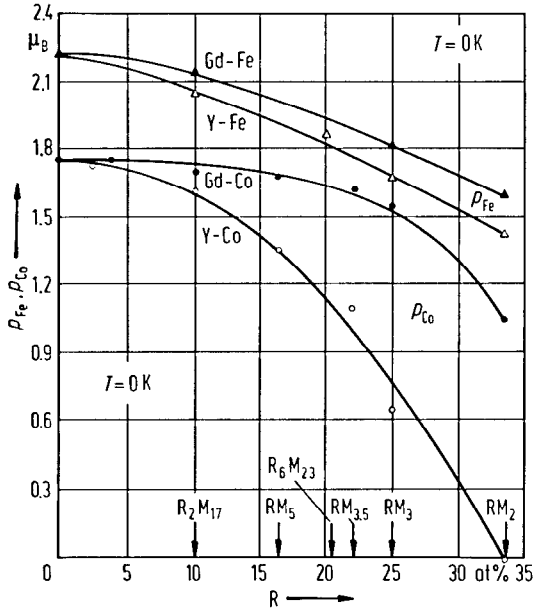

Fig. 16. Composition dependence of the mean magnetic moments at 0 K of Co and Fe atoms determined in Gd and Y compounds by saturation magnetization [73 B 18]. In all cases a decrease of the Fe and Co mean magnetic contributions is observed when increasing the R (R = Gd or Y) fraction in the compound.

Other band structure calculations have been performed on the RM_x systems. The complexity of the crystal structure of RM_x compounds means that some simplifying approximations are inevitable. The first self-consistent band structure calculation for a whole range of rare earth concentrations was realized by Szpunar [77 S 16, 77 S 17, 77 S 18]. The CPA theory when applied to RM_x compounds is only a very rough approximation. This model explained the decrease of the magnetic moment of the transition metals with increasing rare earth content, Fig. 16 [73 B 18], and also predicts the antiparallel coupling between R and M spins. For RM_5 compounds the self-consistent augmented-plane-wave method has also been used in band structure calculations with the simplifying assumption that the magnetic moments of the transition metals on

different sites are indistinguishable [77 M 4, 82 M 1]. By modifying CPA theory to the first four moments, the magnetic moment of Co in different sites has been calculated and is in satisfactory agreement with experimental data [82 S 25]. Then, the density of states of YCo_5 and Y_2Co_{17} has been computed in the tight-binding approximation using the continued fraction method [85 S 25]. The origin of antiparallel coupling between the spins of 3d electrons of the transition metals and spins of 4d electrons of the R metals has been explained. The calculated magnetic moments for different sites in YCo_5 and Y_2Co_{17} are in close agreement with the measured values.

The electronic structure of a number of Laves phase compounds, RM_2, has been also computed by the tight-binding approximation both for paramagnetic and ferromagnetic states [84 Y 1, 85 Y 1, 85 Y 3, 86 Y 1, 86 Y 2]. By using the spin-density-of-states curve in the paramagnetic range and taking into account the effect of spin fluctuations, the temperature dependence of the paramagnetic spin susceptibility of RFe_2 (R = Lu, Zr, Hf) is analysed [86 Y 1]. The same problem was discussed in case of RCo_2 compounds (R = Lu, Sc, Ti, Zr, Hf) [85 Y 3]. The energy band structure of $CeCo_2$ was calculated by using a self-consistent APW method [86 Y 4]. The local density of states at Ni and Y sites and the total density of states are computed for Y_2Ni_{17}, YNi_5, Y_2Ni_7 and YNi_3 in the recursion method. The occurrence of ferromagnetism in Y_2Ni_{17}, Y_2Ni_7 and YNi_3 is attributed to a peak in the density of states near the Fermi level [84 S 8].

The local band models [79 C 1, 79 M 17, 79 P 4, 84 B 8, 85 K 13] were used to describe the magnetic behaviour of 3d transition metals in rare earth compounds. In these cases a local mean field is assumed whose direction may vary in space and time. These directional fluctuations play the role of spin wave excitations. At and above the Curie temperature, only the average vector magnetization must vanish, so there may remain a local magnetization. Strong correlations are maintained above T_C, which can be regarded as a clustering of incompletely ordered magnetic moments. The magnitude of spins remains essentially constant for temperatures very much less than the Stoner temperature, but their directions become increasingly random. The above models, for example, may describe the magnetic behaviour of $CeFe_2$ [81 D 4]. The magnetic behaviour of $Y(Mn_{1-x}Al_x)_2$ compounds was analysed in the model developed by Moriya [79 M 17].

The maxima in $\chi(T)$ of exchange-enhanced paramagnets, as YCo_2 or $LuCo_2$ (see subsect. 2.4.2.12, Fig. 118) – if using a band description – involves a peculiar shape of the energy band. The state density curves which give a peak in the temperature dependence of the magnetic susceptibility have to be reflected in a corresponding peak in the electronic specific heat coefficient γ. The specific heat measurements on YCo_2 and YNi_2 [72 B 9] show that no anomalies are observed in the density of states as suggested by the maximum in the temperature dependence of the magnetic susceptibility. Consequently, the magnetic behaviour of RCo_2 exchange-enhanced paramagnets may be analysed in the spin fluctuation model. The electrical resistivity measurements in $Y(Fe_xCo_{1-x})_2$ [77 I 1] suggest that the fairly large temperature variation of the resistivity near composition x = 0 seems to be determined by the paramagnon scattering. The paramagnon scattering is suppressed by the substitutional Fe atoms. Analyses based on several theoretical models of the quenching of spin fluctuations by high magnetic fields suggest that the characteristic spin-fluctuation temperature is $T_{sf} \cong 20$ K for $ScCo_2$, $T_{sf} \cong 35$ K for YCo_2, and $T_{sf} \cong 16$ K for $LuCo_2$ [84 I 4].

The paramagnon picture of the low magnetic susceptibility of a nearly magnetic fermion system was generalized from a parabolic band to a band of itinerant fermions of arbitrary shape [80 B 3]. The model may account for the observed thermal variation of YCo_2 magnetic susceptibility. Analysing the magnetic properties associated with the onset of ferromagnetism in Y–Ni, Y–Co and Th–Co compounds [81 G 6], it was concluded that the paramagnon model accounts for the experimental data.

The magnetic properties of some RM_x compounds were analysed considering various descriptions based on the Fermi-liquid model [77 C 1, 80 B 3, 76 M 16, 80 N 2]. As example we mention CeNi [84 F 2], YCo_2, $LuCo_2$ [76 B 15, 76 M 16, 77 B 6, 78 M 12, 78 M 13], etc.

A number of other studies was devoted to the magnetic behaviour of 3d metals in rare earth compounds. For a longer time, the variation of the M magnetic moments in RM_x compounds was attributed to band-filling effects by the conduction electrons contributed by rare earths [71 t 1, 73 w 1]. Then, the effect of exchange interactions was emphasized [66 L 5, 74 B 12, 75 B 9]. The photoemission studies performed on RFe_x compounds suggest that the charge transfer as a dominant cause of the reduction of the Fe magnetic moment is excluded [79 A 6]. The same behaviour was observed in case of Gd–Fe amorphous alloys [76 G 13], $La(NiCu)_5$ compounds [82 W 2], etc. The variation of the Fe magnetic moment is attributed to the modification of the exchange splitting of the Fe 3d states. On the other hand it is difficult to consider band filling effects in pseudobinary systems, where the electron concentration is constant, as for example in $Gd(Co_xNi_{1-x})_2$ [74 B 12] or $Y(Fe_xCo_{1-x})_2$ [78 B 13, 80 Y 1] compounds. A different behaviour was suggested by the analysis of L_{III} absorption spectra in $Dy(MAl)_2$, M = Fe, Co compounds [82 S 20, 82 S 21, 84 S 14]. In these cases a charge transfer between 3d M and 5d Dy bands is considered. Chiu et al. [79 C 3] assumed that the susceptibility for band magnetization associated with Co is dependent on the magnitude of the Co magnetic moment, which in its turn depends on the Co concentration.

The exchange interactions are also dependent on the distances between the 3d transition metal atoms as previously evidenced by Néel [36 N 1] – Fig. 17. Thus, the variations in the distances between M atoms are to be reflected in their magnetic contributions. The first evidence for the Néel-Slater curve in case of rare-earth-transition metal compounds has been obtained by pressure studies [73 B 3] on RFe_x systems, although previously suggested [69 G 1, 71 B 12]. From the experimental results each compound can be placed on the curve – Fig. 17. The pressure studies on R_2M_{17} (M = Fe, Co or Ni) [75 J 1] can be also considered on the basis of the Néel-Slater curve. The Fe magnetic moments in RFe_2 compounds also exhibit the general feature of the above curve [81 S 11].

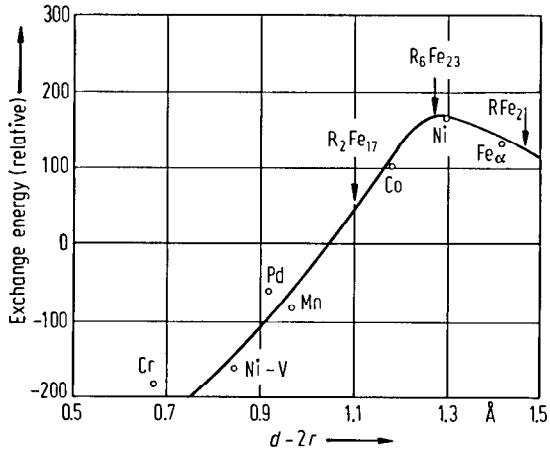

Fig. 17. Néel-Slater curve describing the dependence of the exchange interactions on the distance between 3d transition metal atoms [36 N 1, 73 B 3]. $2r$: atomic diameter.

Two mechanisms were considered to take into account the effect of the exchange interactions on the transition metal magnetic moments in rare earth compounds. The first is the collective electron metamagnetism [62 W 3] and was used to explain the magnetic properties of some RCo_x compounds [75 B 4, 81 G 6]. This involves the change of the number of electrons in the spin-up and spin-down subbands under the action of the exchange field. A second one considers the effect of the relative shifts of the majority spin subband relative to the minority spin subband and has been called induced magnetism or epamagnetism [78 B 11, 81 B 10]. These shifts are proportional to the exchange field (the sum of external and molecular fields) starting with a threshold value. The NMR measurements really show that the Co magnetic moment does not change continuously from nonmagnetic to magnetic state [79 H 7]. The formation of M magnetic moment takes place only on a local scale, as evidenced by NMR or neutron diffraction studies (see subsect. 2.4.2.12).

The local environment model [65 J 1, 74 B 12] is also strongly connected with the presence of exchange interactions. The model may describe the magnetic behaviour of some $R(M'_xM''_{1-x})_y$ compounds. In its simple form, the model supposes that the variation of the M′ mean magnetic moment may be ascribed to a loss of magnetic moments of those M′ atoms which have a smaller number of similar atoms as nearest neighbours than a critical value n_c. For a given concentration, x, the probability for a M′ atom to have n similar atoms as nearest neighbours from the maximum number of N is given by

$$P(x, n, N) = \frac{N!}{n!(N-n)!} x^n (1-x)^{N-n}. \tag{17}$$

The probability for a M′ atom to be surrounded by at least n_c M′ atoms as nearest neighbours is given by

$$P_{n_c}(x) = \sum_{n=n_c}^{N} P(x, n, N). \tag{18}$$

The mean magnetic moment of the alloy is

$$p_M(x) = x P_{n_c}(x) p_M(x=1). \tag{19}$$

If the short-range interactions dominate, the atoms situated only in the first coordination shell should be considered. This is the case of compounds with M′ = Co. By the solid line in Fig. 18 the calculated 3d transition metal magnetization is plotted according to the relation (19) in case of $Gd(Co_xNi_{1-x})_2$ compounds. The experimental data are correctly described by a critical number $n_c = 3$ for N = 8. If there are also long-range magnetic interactions, as in case of iron compounds, the atoms situated in more than one coordination shell may be considered [75 B 10, 77 B 10]. In addition, the transition metals can loose only a fraction of their magnetic moments.

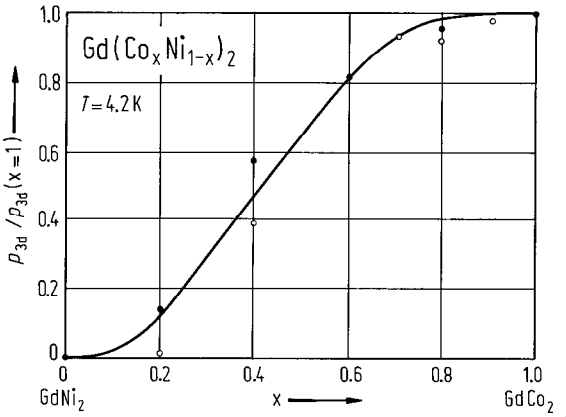

Fig. 18. Composition dependence of the 3d magnetic moments in $Gd(Co_xNi_{1-x})_2$ compounds at 4.2 K, normalized to the value of the Co magnetic moment in $GdCo_2$ [74 B 12]. Open circles are data from [69 T 1] and full circles are data from [74 B 12]. By the solid curve the relation (19) with $n_c = 3$ and N = 8 is plotted [74 B 12].

The above model was used to analyse the composition dependence of the magnetic moments of 3d transition metals in pseudobinary rare earth compounds as $Y_6(Fe_xAl_{1-x})_{23}$ [79 B 5], $Y(Fe_xCo_{1-x})_2$ [78 B 13, 80 Y 1], $Y(Co_xNi_{1-x})_5$ and $Y(Co_xCu_{1-x})_5$ [77 B 23], $Y(Mn_xCo_{1-x})_2$ [79 O 1], $Gd(Co_xAl_{1-x})_2$ [81 B 10], $Gd(Co_xNi_{1-x})_2$ [75 C 1], etc. The NMR studies show also local environment effects, as for example in $Y(Fe_xCo_{1-x})_2$ [76 O 9, 80 Y 1], $Gd(Co_xNi_{1-x})_2$ [80 T 3], $Gd(Fe_xCo_{1-x})_2$ [78 B 11] compounds.

Local environment effects were observed by the analysis of ^{57}Fe hyperfine field values in $Y(Fe_xMn_{1-x})_2$ and $Hf(Fe_xCo_{1-x})_2$ [79 V 2, 80 V 1]. The shape of the observed spectra indicates that the localized Fe magnetic moment is present, its value being sensitively dependent upon the number of and distances from the neighbouring Fe atoms. The effective hyperfine field at a Fe site surrounded by n and m nonmagnetic atoms in the first and second coordination shells, respectively, are

$$H_{hyp}(n, m) = H_{hyp}(0,0) - \sum_{i,j}^{n,m} \Delta H(i,j) \tag{20}$$

in which $\Delta H(n, m) = m\Delta H(n, 0)/3$ for $\Delta H(n, m) = H_{hyp}(0,0) - H_{hyp}(n, m)$.

Local environment effects on the ^{57}Fe hyperfine field has been also reported in $R(Fe_xCo_{1-x})_2$ [76 W 3, 79 M 16], $Y(Fe_xAl_{1-x})_2$ [77 V 4] compounds, etc.

At low temperatures the presence of spin waves is evidenced by using the inelastic neutron scattering [76 N 7, 77 R 1, 78 R 1] (see subsect. 2.4.2.12, Figs. 165 and 166). A nearest-neighbour interaction spin wave model was used to analyse the experimental data. The dispersion relation is given by solving

$$\hbar\omega(\boldsymbol{q}) S_i^+(\boldsymbol{q}) = -2 \sum_{j=1}^{6} [\langle S_{iz}\rangle J_{ij}(\boldsymbol{q}) S_j^+(\boldsymbol{q}) - \langle S_{jz}\rangle J_{ij}(0) S_i^+(\boldsymbol{q})] + \Delta S_i^+(\boldsymbol{q})(\delta_{i,1} + \delta_{i,2}), \tag{21}$$

where

$$J_{ij}(\boldsymbol{q}) = \sum_{n,m} J_{ij}^{nm} e^{i\boldsymbol{q}\cdot(\boldsymbol{r}_{ni} - \boldsymbol{r}_{mj})},$$

and Δ is the crystal field gap parameter. n, m and i, j, respectively, label the unit cells and the six atomic positions therein. For rare earth ions, i = 1, 2, the spin S is replaced by J. There are also six equivalent relations for S^-. The model fits well the experimental results.

The studies performed on pseudobinary compounds show in some cases the disappearance of long-range magnetic order and the presence of a mictomagnetic behaviour. The appearance of a percolation limit for the onset of long-range ferromagnetic order has been evidenced in $Y(Fe_xM_{1-x})_2$ (M = Al, Co, Rh) compounds [79 S 8]. The percolation limit depends strongly on the matrix magnetic susceptibility. Mictomagnetic behaviour can be deduced from magnetic, Mössbauer and neutron depolarization measurements for M = Co, Al below the percolation limit. For M = Rh a similar behaviour should occur as indicated by the dependence of the magnetic moment upon the magnetic pretreatment as well as by the magnetically split Mössbauer spectra, although no maxima of the low-field magnetization as a function of the temperature are observed. The mictomagnetic behaviour of $Y(Fe_xAl_{1-x})_2$ compounds was discussed also by other authors [82 H 5, 84 R 3]. The same behaviour was observed in pseudobinary Laves phase compounds [82 H 4], $La(Fe_{1-x}Ni_x)_5$ [87 L 1], or some hydrides.

The presentation of the models used to describe the magnetic properties of RM_x compounds is not exhaustive. This may give only a general view of the complexity of matter. References to other models will be made in subsect. 2.4.2 in connection with the experimental evidence.

For studies involving different types of structures see:

Crystal structure and lattice constants

RM_x [64 M 2, 69 K 2, 69 K 3, 73 B 17, 74 K 11, 79 i 1]; R = Nd, Sm [70 K 4]

RFe_x R = Sm [71 B 17]; R = Tb [76 D 1]; R = Dy [70 V 1, 70 V 2]; R = Ho [71 M 6]; R = Er [69 B 5]; R = Th [71 B 16]

RCo_x [66 B 5, 71 B 15, 75 P 3, 76 A 2, 77 A 4, 77 P 1];
R = La [67 B 3, 74 K 10]; R = Ce [73 R 2, 74 K 10]; R = Pr [73 R 2]; R = Nd [73 R 2]; R = Sm [69 L 3, 74 K 7, 78 Z 1, 79 L 8, 83 T 1]; R = Gd [62 S 1, 69 B 3, 69 B 6, 69 L 3, 70 B 6]; R = Er [68 B 7]; R = Yb [72 B 16]; R = Lu [71 G 1, 71 G 2]; R = Y [71 G 1, 71 G 2]; R = Th [71 B 16]

RNi_x [77 P 1]; R = La [72 B 17]; R = Sm [83 T 1, 88 H 3]; R = Er [68 B 5]; R = Yb [72 B 16, 73 P 1]

RM_xH_y [74 K 18]; YFe_xH_x [80 V 3]; $CeCo_xH_y$ [80 V 3]; $LaNi_xH_y$ [76 M 1, 76 O 5]; $CeNi_xH_y$ [80 V 3]; YNi_xH_y [80 V 3]; YCo_xH_y [80 V 3]

$(R'R'')M_x$ $(SmPr)Co_x$ [79 L 8]; $R(GaNi)_x$ [80 G 13]; $Ce(MnNi)_x$ [76 K 1]

$R(M'M'')_x$ $Dy(FeRe)_x$, $Dy(CoRe)_x$, $Dy(NiRe)_x$ [85 S 20]

Enthalpies of formation

RM_x R = Gd, Dy, Er, M = Co, Ni [86 S 9]; CeM_x [79 D 2]; $YbFe_x$, $YbCo_x$ [79 D 2]; YFe_x [85 S 24]; YCo_x [85 S 24]; $CeNi_x$ [86 C 8]; $GdNi_x$ [86 C 8, 87 C 4]; $YbNi_x$ [79 D 2]; YNi_x [87 C 4]

Thermal expansion

$SmCo_x$, $GdCo_x$ [74 B 14]

Hydrogen absorption and desorption

RM_xH_y [75 B 16, 76 G 9, 77 G 15, 78 B 21, 78 w 1, 79 B 18, 79 i 1, 84 b 1, 87 S 9, 88 f 1, 88 g 1, 88 p 1]

RMn_xH_y [76 V 3]

RFe_xH_y [76 V 3]; R = Ce [78 C 2]; R = Y [80 V 3]; R = Th [75 B 16]

RCo_xH_y R = Ce [78 C 2, 80 V 3]; R = Pr [75 C 4]; R = Th [75 B 16]

RNi_xH_y R = La [72 B 17, 76 M 1, 76 O 5, 77 B 17, 78 C 3]; R = Ce [78 C 2, 80 V 3]; R = Y [80 V 3]; R = Th [75 B 16]; $LaNi_xMn_yH_2$ [86 J 3]

Magnetic studies

RM_x [71 B 21, 73 B 16, 73 B 17, 73 B 19, 73 K 10, 74 B 8, 76 D 11, 79 b 2, 80 B 14, 84 K 5, 84 K 6, 85 K 6, 85 N 2];
R = Sm [72 S 2(T)]; R = Y [85 I 3(T), 87 S 11(T)]

RFe_x [69 G 1, 74 D 1, 84 I 6(T), 85 B 9, 86 P 7, 86 R 3, 87 B 8];
R = Gd [71 G 3, 76 B 17, 77 S 16(T), 77 S 17(T), 77 S 18(T), 78 L 2(T), 86 I 4]; R = Dy [70 V 1, 70 V 2, 79 S 11(T)]; R = Ho [71 M 6]; R = Er [69 B 5]; R = Lu [73 B 3]; R = Y [71 G 3, 73 B 3, 76 B 17, 78 L 3(T), 79 H 3, 79 S 11(T), 84 V 1, 85 I 3(T), 86 S 13(T), 87 S 11(T), 88 G 2, 88 I 1]; R = Th [71 B 16]

RCo_x [68 L 1, 71 B 15, 72 B 11, 73 B 18, 74 G 9(T), 79 W 4, 84 I 6(T), 85 B 9, 87 B 7];
R = La [87 G 3]; R = Ce [81 S 13]; R = Sm [78 Z 1]; R = Gd [59 N 1, 60 H 3, 66 B 5, 69 B 3, 70 B 6, 70 B 7, 73 B 15, 74 B 10, 76 B 17, 77 S 16(T), 77 S 17(T), 77 S 18(T), 78 L 1, 78 L 2(T), 81 K 2*, 85 S 17, 86 I 4, 87 B 1]; R = Dy [81 G 17]; R = Er [68 B 7]; R = Lu [71 G 1, 71 G 2]; R = Y [71 G 1, 71 G 2, 73 B 15, 76 B 17, 77 S 17(T), 78 L 3(T), 81 G 7, 82 B 14, 85 I 3(T), 85 P 3(T), 86 C 6, 86 S 13(T), 87 B 1, 87 S 11(T), 88 G 2]; R = Th [71 B 16, 81 G 7]

RNi_x [86 L 1, 83 J 1]; R = La [52 W 1]; R = Ce [81 S 13]; R = Gd [72 B 14, 77 S 17(T), 86 I 4]; R = Er [68 B 5]; R = Y [81 G 5, 81 G 7, 83 B 4, 84 S 8(T), 86 S 13(T), 87 G 3]

RM_xH_y [78 B 21, 78 W 1, 80 W 1]; RMn_xH_y, RFe_xH_y [78 W 3]

$R(M'M'')_x$ [85 W 2]; $Y(CoFe)_x$, $Y(CoNi)_x$ [71 P 2]

Neutron diffraction

RM_x [87 V 1]; YNi_x [81 G 5]

Nuclear γ-resonance

^{57}Fe RFe_x [82 S 13]; YFe_x [74 G 16]

^{155}Gd GdM_x [76 V 4, 85 D 5, 85 D 6]

^{161}Dy $DyCo_x$ [81 G 17, 82 B 14]

FMR and EPR studies

$GdNi_x$ [80 B 15]

Anisotropy

$GdCo_x$ [81 K 2*]; YCo_x [85 T 7]

Magnetoelastic effect

RM_x [79 G 4]; YFe_x [78 S 22]

Specific heat

RFe_x [74 D 1]; YFe_x [86 S 13]; YCo_x [85 M 6, 86 C 6, 86 S 13, 87 M 6]; YNi_x [86 S 13]

Resistivity studies

$CeNi_x$ [85 B 8]

Thermopower studies

YFe_x, YCo_x, YNi_x [86 S 13]; RNi_x [85 G 17]; $CeNi_x$ [84 L 7]

Magnetization processes

RM_x [76 D 11, 83 b 1]; RFe_x [86 R 3]; $GdFe_x$ [69 G 1]; YFe_x [69 G 1]; RCo_x [78 S 9]; $ErCo_x$ [68 B 7]; YNi_x [81 G 4]

Domain structure

$HoCo_x$ [79 K 6]; $ErCo_x$ [79 K 5]

2.4.2 Data

2.4.2.1 R_3M compounds

Crystal structure, lattice parameters

Table 3. Structural parameters of Ho_3Co compound [69 B 4].

Atom	Site	x	y	z
Ho(1)	4c	0.033	0.250	0.135
Co	4c	0.391	0.250	0.936
Ho(2)	8d	0.180	0.064	0.680

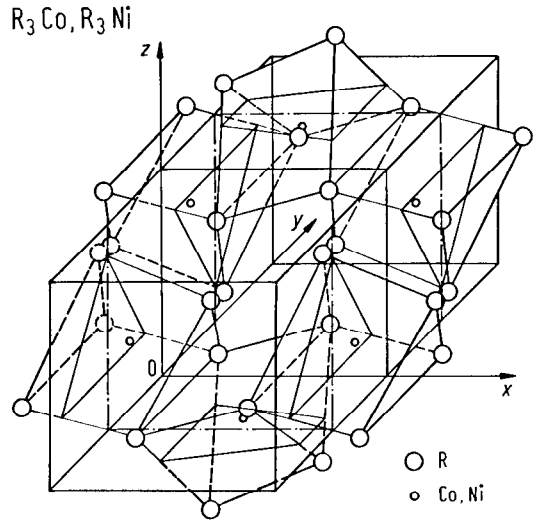

Fig. 19. Crystal structure of R_3M (M = Co, Ni) compounds. The positions of the atoms in R_3M lattice are given in Table 3.

Table 4b. Lattice parameters of R_3Ni compounds (Å) [67 L 2].

	a	b	c
La_3Ni	7.22	10.24	6.60
Pr_3Ni	7.07	9.96	6.49
Nd_3Ni	7.04	9.86	6.43
Sm_3Ni	6.99	9.72	6.37
Gd_3Ni	6.95	9.68	6.36
Tb_3Ni	6.88	9.61	6.29
Dy_3Ni	6.85	9.60	6.26
Ho_3Ni	6.83	9.54	6.25
Er_3Ni	6.79	9.45	6.23
Tm_3Ni	6.77	9.40	6.19
Y_3Ni	6.92	9.49	6.36

Table 4a. Lattice parameters of R_3Co compounds (Å).

	[61 C 3]			[68 G 1, 70 F 1, 73 G 1]			[69 B 4]		
	a	b	c	a	b	c	a	b	c
La_3Co	7.279	10.088	6.578	7.28	10.09	6.58	7.277	10.020	6.575
Pr_3Co				7.12	9.81	6.43	7.143	9.780	6.410
Nd_3Co				7.11	9.76	6.41	7.107	9.750	6.386
Sm_3Co				7.06	9.61	6.35	7.055	9.605	6.342
Gd_3Co				7.03	9.51	6.30	7.031	9.496	6.302
Tb_3Co				6.99	9.43	6.27	6.985	9.380	6.250
Dy_3Co				6.97	9.34	6.25	6.965	9.341	6.233
Ho_3Co				6.96	9.30	6.20	6.920	9.293	6.213
Er_3Co				6.90	9.19	6.19	6.902	9.191	6.189
Tm_3Co				6.91	9.12	6.19			
Lu_3Co				6.88	9.03	6.13			
Y_3Co				7.01	9.39	6.34	7.026	9.454	6.290

2.4.2 Data

2.4.2.1 R_3M compounds

Crystal structure, lattice parameters

Table 3. Structural parameters of Ho_3Co compound [69 B 4].

Atom	Site	x	y	z
Ho(1)	4c	0.033	0.250	0.135
Co	4c	0.391	0.250	0.936
Ho(2)	8d	0.180	0.064	0.680

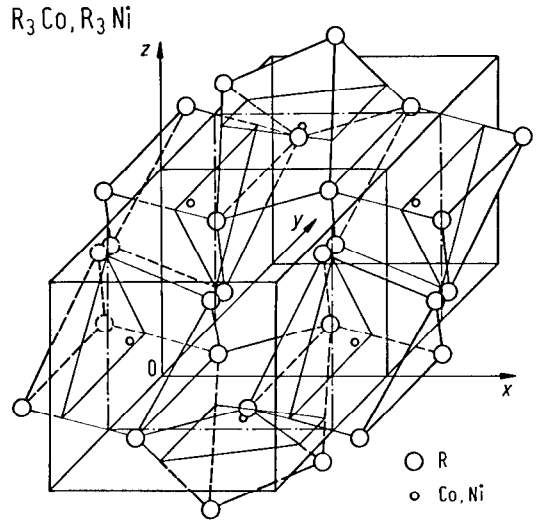

Fig. 19. Crystal structure of R_3M (M = Co, Ni) compounds. The positions of the atoms in R_3M lattice are given in Table 3.

Table 4b. Lattice parameters of R_3Ni compounds (Å) [67 L 2].

	a	b	c
La_3Ni	7.22	10.24	6.60
Pr_3Ni	7.07	9.96	6.49
Nd_3Ni	7.04	9.86	6.43
Sm_3Ni	6.99	9.72	6.37
Gd_3Ni	6.95	9.68	6.36
Tb_3Ni	6.88	9.61	6.29
Dy_3Ni	6.85	9.60	6.26
Ho_3Ni	6.83	9.54	6.25
Er_3Ni	6.79	9.45	6.23
Tm_3Ni	6.77	9.40	6.19
Y_3Ni	6.92	9.49	6.36

Table 4a. Lattice parameters of R_3Co compounds (Å).

	[61 C 3]			[68 G 1, 70 F 1, 73 G 1]			[69 B 4]		
	a	b	c	a	b	c	a	b	c
La_3Co	7.279	10.088	6.578	7.28	10.09	6.58	7.277	10.020	6.575
Pr_3Co				7.12	9.81	6.43	7.143	9.780	6.410
Nd_3Co				7.11	9.76	6.41	7.107	9.750	6.386
Sm_3Co				7.06	9.61	6.35	7.055	9.605	6.342
Gd_3Co				7.03	9.51	6.30	7.031	9.496	6.302
Tb_3Co				6.99	9.43	6.27	6.985	9.380	6.250
Dy_3Co				6.97	9.34	6.25	6.965	9.341	6.233
Ho_3Co				6.96	9.30	6.20	6.920	9.293	6.213
Er_3Co				6.90	9.19	6.19	6.902	9.191	6.189
Tm_3Co				6.91	9.12	6.19			
Lu_3Co				6.88	9.03	6.13			
Y_3Co				7.01	9.39	6.34	7.026	9.454	6.290

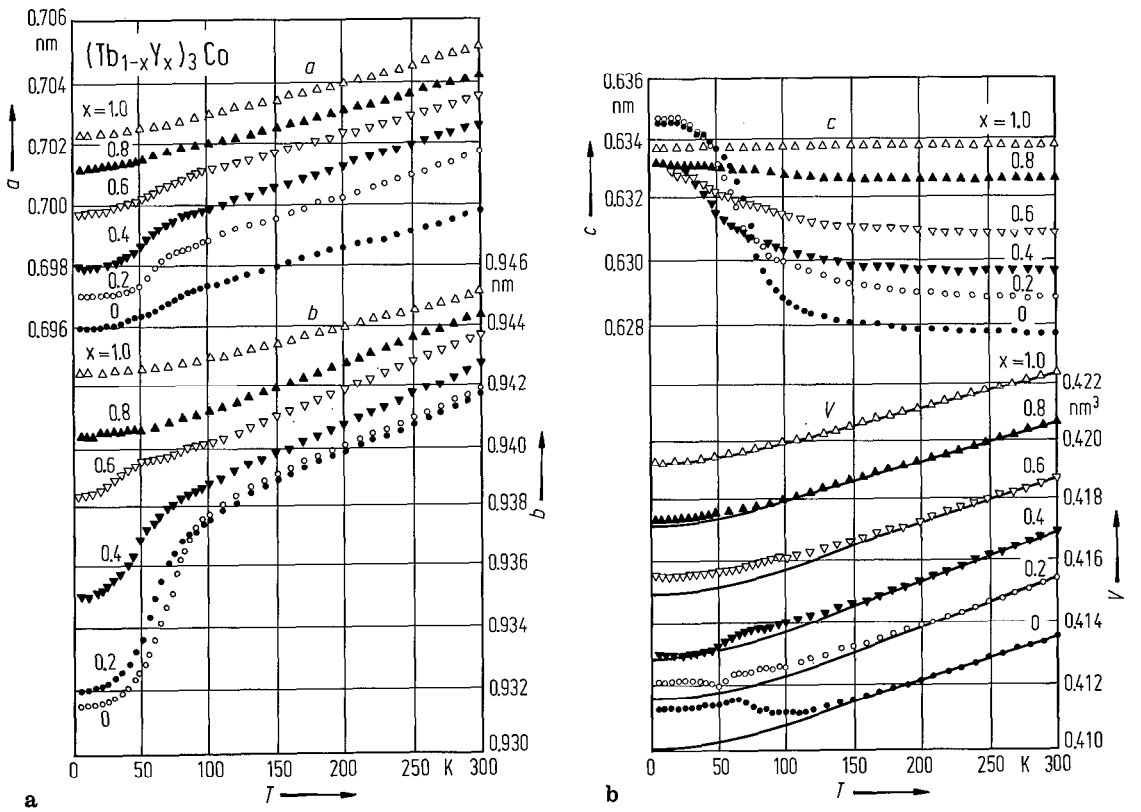

Fig. 20. Thermal variations of lattice parameters a and b (a), lattice parameters c and unit cell volume V (b) for $(Tb_{1-x}Y_x)_3Co$ single crystals. The above data suggest a change of the magnetic structure for $x \geqq 0.3$ [86 A 7].

For structure and lattice parameters, see also:

R_3Co [68 G 1, 70 B 10, 71 B 15, 73 G 1]; R = La, Pr, Nd, Sm, Gd, Tb, Dy, Ho, Er, Y [69 B 4]; R = Gd, Dy, Ho, Y [88 T 2*]; R = Gd [87 C 1]; R = Yb [86 T 6]; R = Dy [64 W 7]

R_3Ni [69 P 1]; R = La, Pr, Nd, Sm, Gd, Tb, Dy, Ho, Er, Tm, Y [67 L 2]; R = Pr, Nd, Gd, Tb, Dy, Ho, Er, Tm [68 F 1]; R = Ce, Pr, Nd, Gd, Tb, Dy, Ho, Er, Tm [70 B 2]; R = La [61 C 3]; R = Yb [86 T 6]

$(R'R'')_3M$ $(TbGd)_3Co$ [80 D 5, 83 S 5, 84 S 4*, 87 C 1]

$R_3(M'M'')$ $Gd_3(FeCo)$ [73 P 3]; $Gd_3(CoNi)$ [72 P 1, 73 P 3]

For thermal expansion see also

$(TbGd)_3Co$ [83 S 5]; $(TbY)_3Co$ [86 A 7]

Magnetization, Curie temperatures

Table 5a. Magnetic properties of R_3Co compounds.

	p_s (μ_B/R)			T_N (K)			T_C (K)	Θ (K)		p_{eff} (μ_B/R)		H_c (kOe) [6]	
	68 G 1 [1], 70 F 1	72 P 3 [2]	70 B 6 [3]	68 G 1, 70 F 1	70 B 6	72 P 3 [4]	68 G 1, 70 F 1	68 F 1	70 B 6	68 G 1, 73 G 1	70 B 6	72 P 3 [5]	68 G 1, 73 G 1
La_3Co		Pauli paramagnet [77 b 1, 73 G 1]			$\chi_p = 48.10^{-3}$ cm^3/mol [77 b 1]								
Pr_3Co	1.1	1.3					7	18		3.2			5
Nd_3Co	1.7			14		14		35		3.4		10	2; 20
Sm_3Co		Pauli paramagnet [68 G 1]											
Gd_3Co	7.3	8.1	7.2	127	130	143		159	160	8.1	8.05	9	4.7
Tb_3Co	5.3	8.0		82		76		85		10.1		63	10
Dy_3Co	5.4	6.4		45		45		65		10.3		52	
Ho_3Co	5.9	7.6		24		23		44		10.1		2	
Er_3Co	6.0	6.9				13	7	20		9.4		0	
Tm_3Co	3.5						5	0		7.4			
Y_3Co		Pauli paramagnet [68 G 1, 73 G 1]			$\chi_p = 6.5 \cdot 10^{-4}$ cm^3/mol								

[1]) At 4.2 K in fields of 60 kOe.
[2]) At 4.2 K in pulsed fields of 160 kOe.
[3]) At 4.2 K in fields of 30 kOe.
[4]) Temperature of the peak in initial susceptibility.
[5]) Determined in pulsed magnetic field.
[6]) At 4.2 K.

Table 5b. Magnetic properties of R_3Ni compounds.

	p_s (μ_B/R)			T_N (K)		T_C (K)	H_c (kOe)		Θ (K)	p_{eff} (μ_B/R)
	68 F 1 [1])	70 B 2 [2])	72 P 3 [3])	68 F 1	72 P 3 [4])	68 F 1	72 P 3 [5])	73 P 3	68 F 1	68 F 1
Pr_3Ni	0.64	0.72		2					−24	3.70
Nd_3Ni	0.50	0.70		15					0	3.60
Gd_3Ni	4.20	5.10	8.10	100	100		51	25(5)	60	8.10
Tb_3Ni	3.40	4.00	6.70	62	62		97		5	10.00
Dy_3Ni	2.80	3.70	5.70	33	33		76		29	10.60
Ho_3Ni	4.90	5.30	7.30	20	20		50		− 6	11.10
Er_3Ni	5.50	5.80	7.10	9	9		0		− 5	9.80
Tm_3Ni	3.60	3.70				12			0	7.40

[1]) At 4.2 K in fields of 60 kOe.
[2]) At 4.2 K in fields of 70 kOe.
[3]) At 4.2 K in pulsed field of 160 kOe.
[4]) Temperature of the peak in initial susceptibility.
[5]) In pulsed magnetic field.

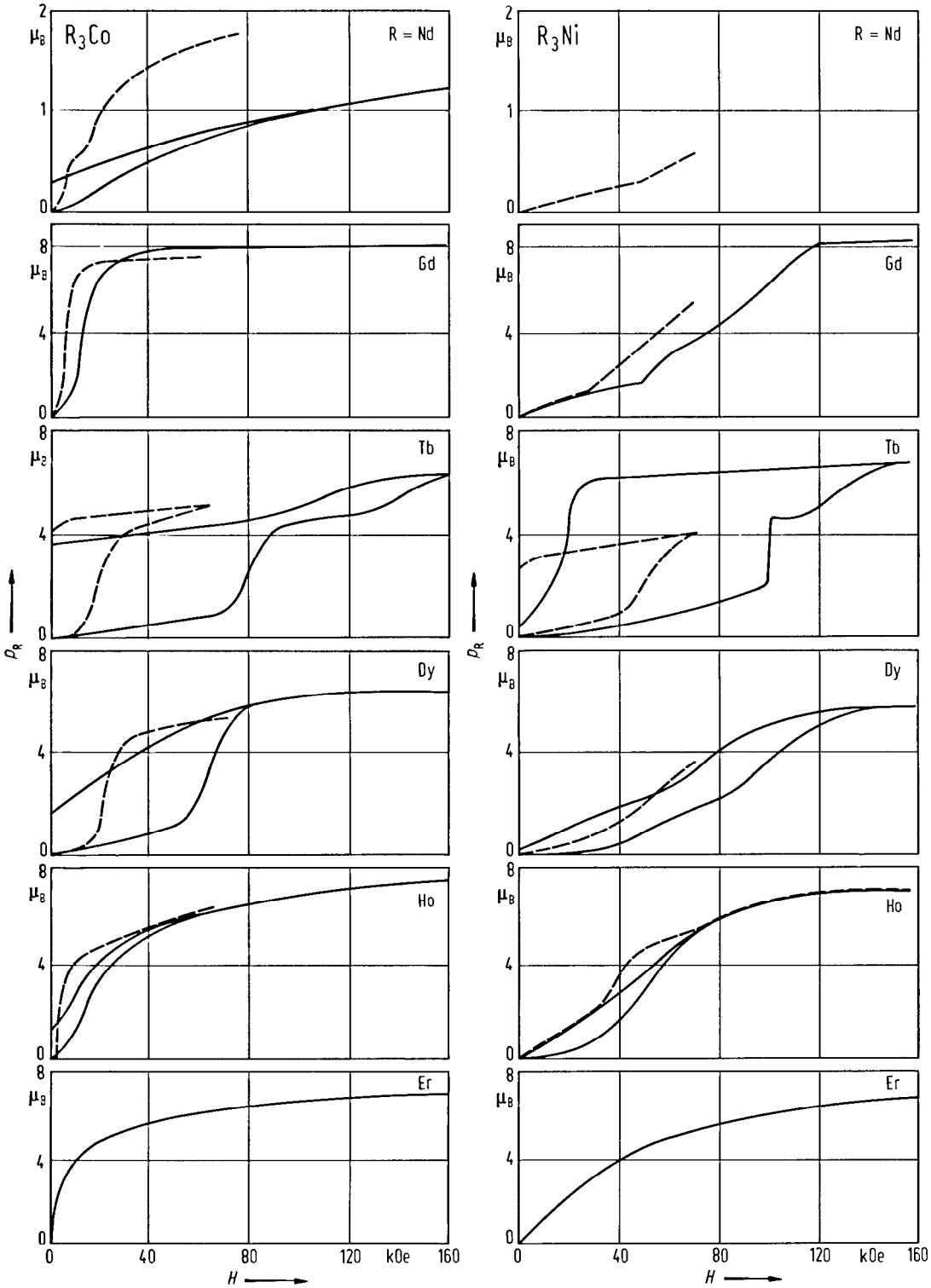

Fig. 21. Magnetic field dependence of the magnetization in R_3Co and R_3Ni compounds in pulsed magnetic fields [72 P 3]. By broken lines the data obtained in static magnetic field are plotted [68 F 1]. These show a field-induced phase transition in preponderantly antiferromagnetic compounds (R = Nd, Gd, Tb, Dy, Ho). The critical field strength in pulsed magnetic field is greater than that for static field, cf. Table 5.

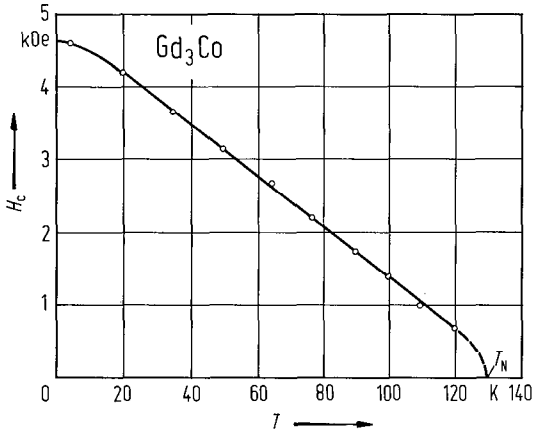

Fig. 22. Temperature dependence of the critical magnetic field in Gd_3Co compound [68 G 1].

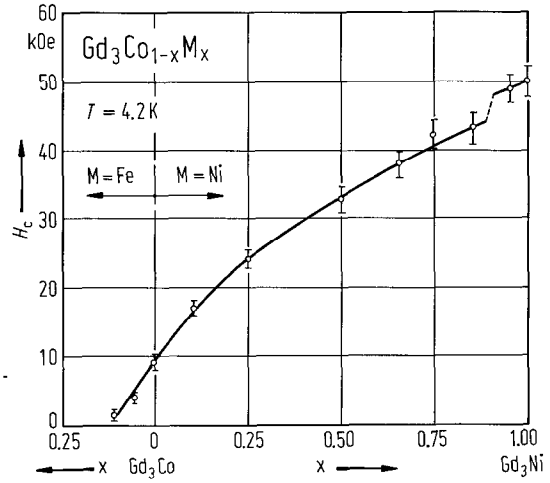

Fig. 23. Composition dependence of the critical magnetic field at 4.2 K in some pseudobinary $Gd_3Co_{1-x}M_x$ (M = Fe, Ni) compounds [73 P 3]. The field at which the transition takes place decreases continuously with increasing Co content for the Gd_3(Co, Ni) system and by extending the observations into the Gd_3(Fe, Co) system, a value $H_c \cong 0$ is obtained for a composition close to $Gd_3Fe_{0.1}Co_{0.9}$.

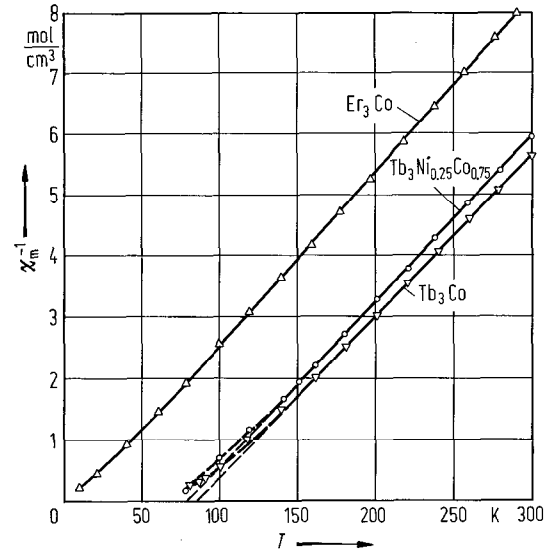

Fig. 24. Thermal variations of reciprocal magnetic susceptibilities for some R_3M-based compounds [73 G 1]. In all cases a Curie-Weiss behaviour is shown.

For magnetic properties see also

R_3Co [70 F 1]; R = Nd, Gd, Tb, Dy, Ho, Er [72 P 3]; R = Gd, Tb, Dy, Ho [71 T 3]; R = Gd [70 S 8, 87 C 1, 88 T 2*]; R = Tb [74 G 6]; R = Dy [80 B 1, 88 T 2*]; R = Ho [88 T 2*]

R_3Ni [69 P 1, 70 F 1]; R = Pr, Nd, Gd, Tb, Dy, Ho, Er, Tm [68 F 1]; R = Gd, Tb, Dy, Ho, Er [72 P 3]; R = Tb [82 G 4*]

$(R'R'')_3M$ $(TbGd)_3Co$ [80 D 5, 86 S 10, 87 C 1]; $(TbY)_3Co$ [72 T 2, 77 D 4, 86 B 5]

$R_3(M'M'')$ $Gd_3(CoFe)$ [72 P 1, 73 P 3]; $Gd_3(CoNi)$ [72 P 1, 73 P 3]

For magnetization processes see

R_3Co [68 G 1, 71 P 3]; R = Nd, Gd, Tb, Dy, Ho, Er [72 P 3]; R = Dy [72 T 3, 80 B 1]

R_3Ni R = Gd, Tb, Dy, Ho, Er [72 P 3]

$(R'R'')_3Co$ $(TbY)_3Co$ [72 T 2, 86 B 5]

$R_3(M'M'')$ $Gd_3(CoFe)$; $Gd_3(CoNi)$ [72 P 1, 73 P 3]

Neutron diffraction studies

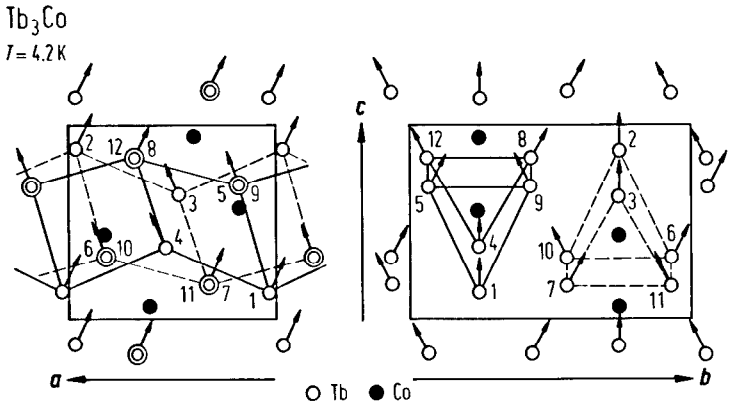

Fig. 25. Projection of the Tb_3Co magnetic structure, at 4.2 K on the (a,c) and (b,c) planes. The Tb magnetic moments are $p_{Tb}(4c) = p_{Tb}(8d) = 8.8\,\mu_B$, $\cos\alpha_x^{4c} = -0.44$, $\cos\alpha_z^{4c} = 0.90$, $\cos\alpha_x^{8d} = 0.31$, $\cos\alpha_y^{8d} = 0.44$ and $\cos\alpha_z^{8d} = 0.84$, and $p_{Co} \cong 0$. This magnetic structure reflects the strong anisotropic interactions. Such an anisotropy comes from crystal potential, low symmetry of the crystalline structures, and from the crystal field effect on the conduction band. In the magnetic lattice the resultant moment is parallel to the c axis having the mean magnetization $p_{Tb} = (8.8/2)\,(0.90 + 0.84)\,\mu_B = 7.6\,\mu_B$ [73 G 1].

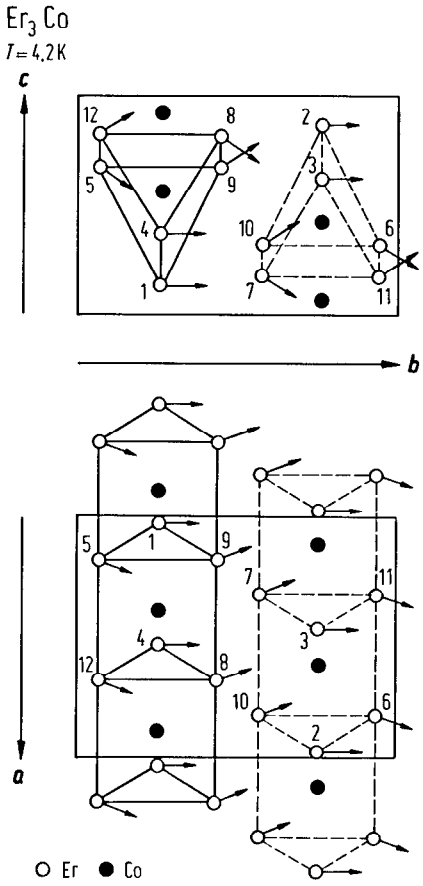

Fig. 26. Projection of the magnetic structure of Er_3Co at 4.2 K on the (a,b) and (b,c) planes determined by neutron diffraction measurements [73 G 1]. The Er magnetic moments on 4c and 8d sites are $p_{Er}(4c) = p_{Er}(8d) = 6.0(5)\,\mu_B$, with $\cos\alpha_y^{4c} = 1$, $\cos\alpha_x^{8d} = 0.28(1)$, $\cos\alpha_y^{8d} = 0.80(10)$ and $\cos\alpha_z^{8d} = -0.52(1)$. This structure shows a preponderantly ferromagnetic behaviour.

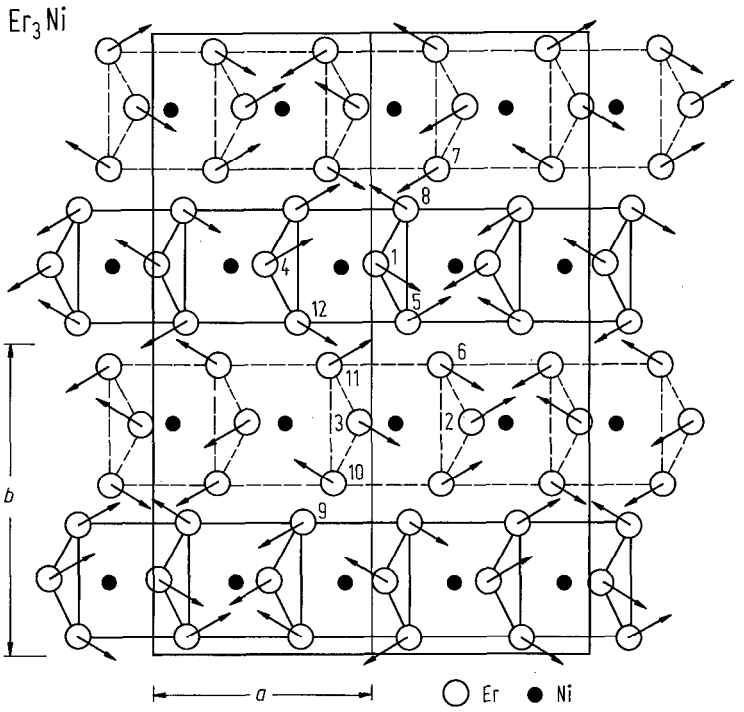

Fig. 27. Projection of the magnetic structure of Er_3Ni at 4.2 K on the (a, b) plane, which shows an antiferromagnetic arrangement of the Er moments. The magnetic structure belongs to P_c1 magnetic group. The magnetic lattice is four times that of chemical one with the parameters $2a$, $2b$, and c [73 G 1]. Ni has no magnetic moment.

For neutron diffraction studies see
Tb_3Co [74 G 6, 83 B 2]; Er_3Co [70 G 1]; Tb_3Ni [70 L 2, 82 G 4*]; Er_3Ni [70 B 2, 70 F 1, 70 G 1]
$(TbY)_3Co$ [86 A 7, 86 B 5]

Mössbauer effect

For nuclear γ-resonance see
^{57}Fe Dy_3Fe [82 Z 2]
^{161}Dy Dy_3Co [81 G 17]

Anisotropy, magnetostriction

For magnetostriction see
Dy_3Co [80 D 6]

For elastic properties see
Gd_3Co [84 B 1]

For anisotropy see
$(TbGd)_3Co$ [80 D 5]

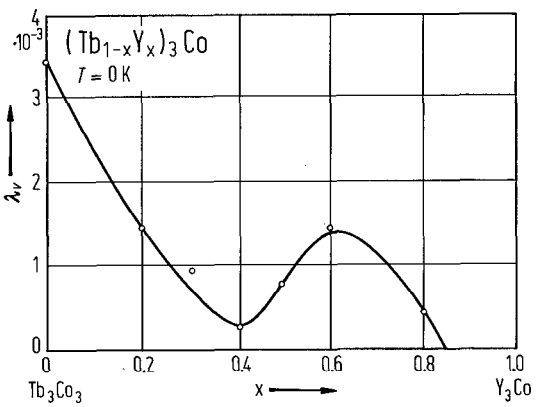

Fig. 28. Composition dependence of the volume magnetostriction of $(Tb_{1-x}Y_x)_3Co$ compounds at $T=0$ K [86 A 7]. These values may be analysed in correlation with the magnetic phase transitions.

Transport properties

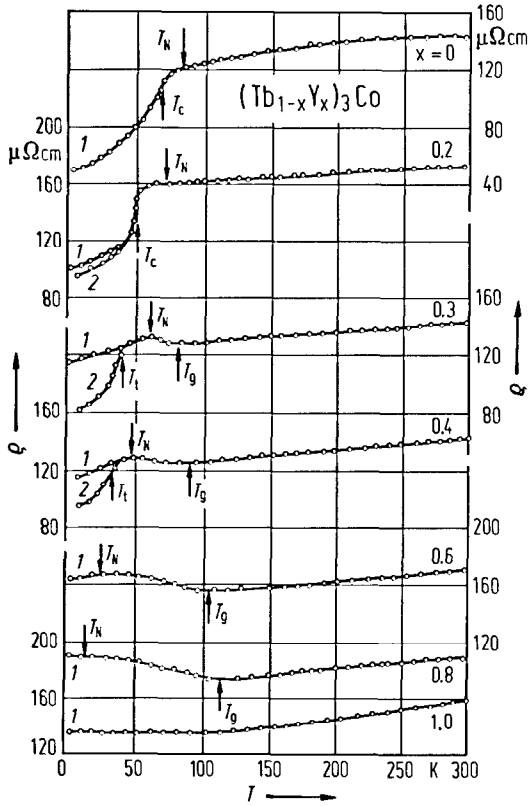

Fig. 29. Thermal variation of the electrical resistivity measured along the c axis of $(Tb_{1-x}Y_x)_3Co$ compounds. The data denoted by *1* were obtained on samples before the magnetic field was applied and by *2* after the samples were magnetized from 0 to 3.5 *T*. The Néel temperatures are indicated by arrows. T_g is the spin glass temperature and T_t the transition temperature from the field-induced magnetic state to the antiferromagnetic state [86 B 5].

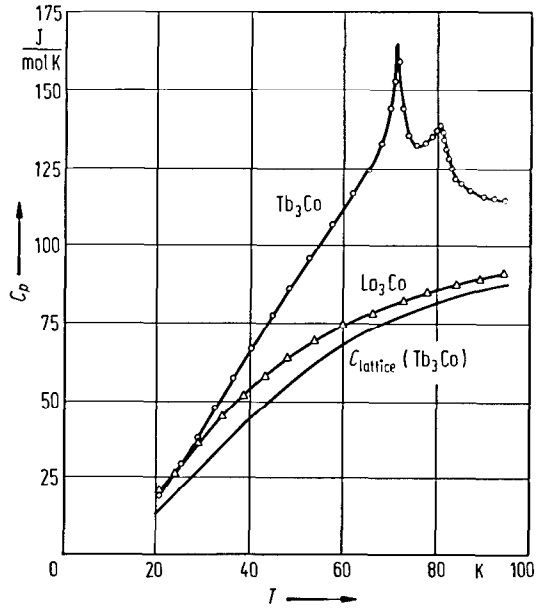

Fig. 30. Temperature dependence of the specific heat in La_3Co and Tb_3Co. The maximum observed at 81 K in Tb_3Co corresponds to the ordering temperature. The maximum evidenced at 71 K is due to the appearance of the spontaneous magnetization [73 G 1]. The La_3Co compound shows a Pauli-type paramagnetism.

For electrical resistivity studies see
R_3Co [82 D 5]; R = Gd, Dy, Ho, Y [88 T 2*]; R = Dy [80 D 6]
$(Tb, Y)_3Co$ [86 B 5]

2.4.2.2 R_5M_2 compounds

Crystal structure, lattice parameters

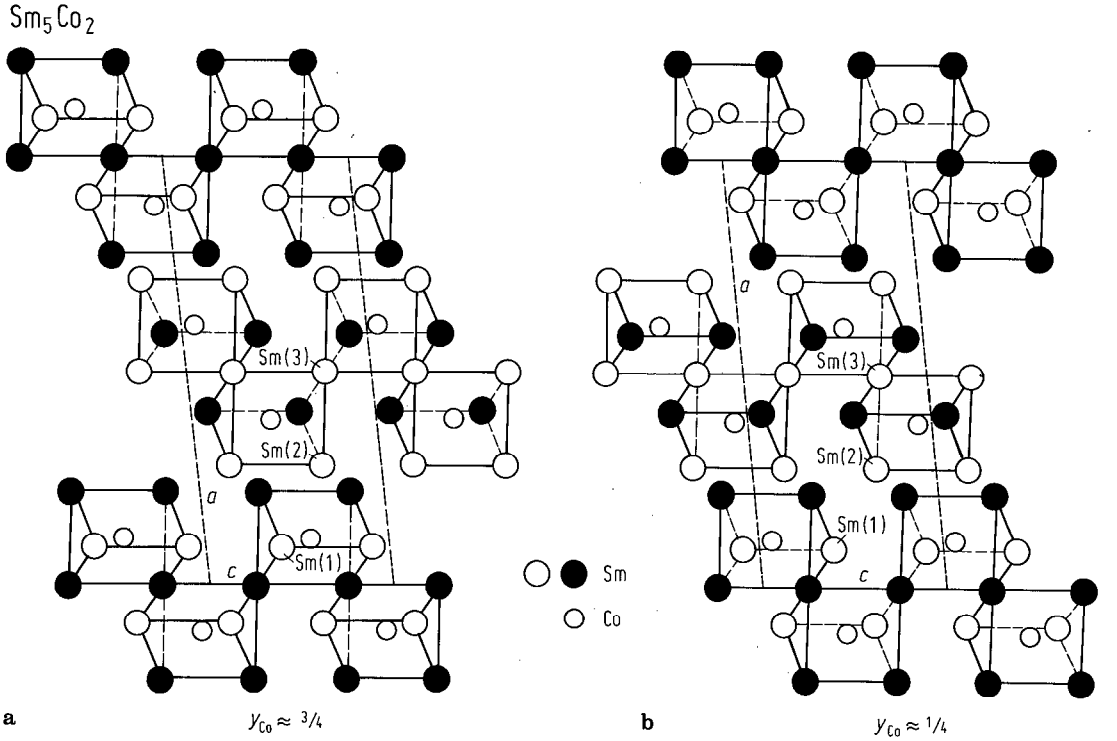

Fig. 31. Linkage of trigonal prisms in Sm_5Co_2 shown in projection down *b*. Large circles represent Sm atoms, small circles at the centres of the prisms, Co atoms. The number inscribed correspond to the numbers of the atoms given in Table 6. (a) Arrangement of prisms centred at Co atoms with $y_{Co} \cong 3/4$. White Sm atoms with $y \cong 1/2$ and black Sm atoms with $y \cong 1.0$. (b) Arrangement of prisms centred at Co atoms with $y_{Co} \cong 1/4$. White Sm atoms with $y \cong 1/2$ and black Sm atoms with $y \cong 0.0$ [76 M 18].

Table 6. Atomic positions in Sm_5Co_2 (space group C2/c) compound [76 M 18].

Atom	Site	*x*	*y*	*z*
Sm(1)	8f	0.0940(1)	0.1116(3)	0.4156(2)
Sm(2)	8f	0.2162(1)	0.5701(3)	0.3156(2)
Sm(3)	4e	0.00	0.5750(4)	0.2500
Co	8f	0.1107(3)	0.2901(7)	0.0738(6)

Table 7. Lattice parameters of R_5Co_2 compounds [76 M 18].

	a(Å)	*b*(Å)	*c*(Å)	*β*
Pr_5Co_2	16.540	6.480	7.100	98.6°
Nd_5Co_2	16.370	6.430	7.080	96.7°
Sm_5Co_2	16.282	6.392	7.061	96.61°

2.4.2.3 R_7M_3 compounds

Crystal structure, lattice parameters

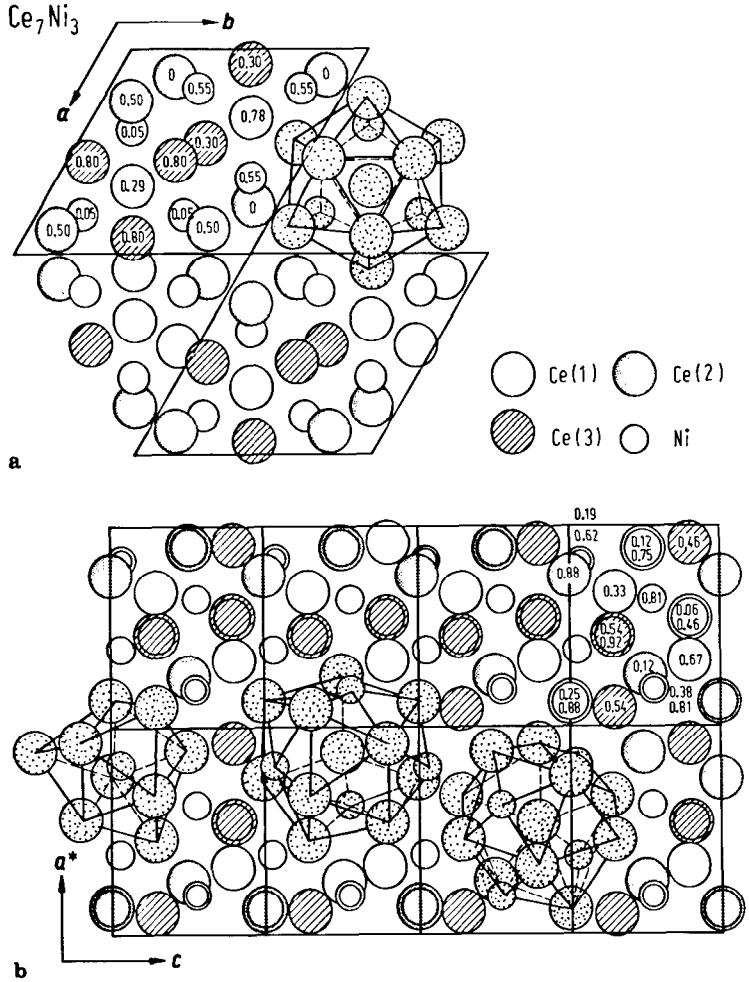

Fig. 32. Crystal structure of Ce_7Ni_3 compound. (a) The structure in projection down the *c* axis showing the polyhedron around Ce(1). (b) The structure in projection down the *b* axis showing from left to right the polyhedra around Ni, Ce(2) and Ce(3). The large open circles are Ce(1), the dotted circles are Ce(2), the lined circles are Ce(3) and the small open circles are Ni atoms. The *z* and *y* coordinates are also given in (a) and (b), respectively. The positions of the atoms in the lattice are presented in Table 8 [61 R 1].

Table 8. Atomic positions in Ce_7Ni_3-type structure (hexagonal having $P6_3mc$-space group) [61 R 1].

Atom	Site	*x*	*z*
Ce(1)	2b	1/3	0.7888(24)
Ce(2)	6c	0.1250(5)	0.0
Ce(3)	6c	0.5391(5)	0.8011(12)
Ni	6c	0.8118(11)	0.0496(26)

Table 9. Lattice parameters of R_7M_3 compounds (Å).

	56 F 1		61 R 1		69 P 1		73 O 8		78 B 18		78 F 6				76 O 3
	a	*c*	*a*	*c*	*a*	*c*	*a*	*c*	*a*	*c*	*a*	*c*	*a* [1]	*c* [1]	
La_7Ni_3					10.06	6.46	10.140	6.383	10.138(1)	6.471(1)	10.140(5)	6.475(3)	10.138(1)	6.471(1)	
Ce_7Ni_3			9.930(20)	6.330(20)			9.926	6.311			9.920(20)	6.330(20)			
Pr_7Ni_3					9.87	6.31	9.904	6.322							
Nd_7Ni_3					9.81	6.29	9.879	6.289							
Th_7Fe_3	9.850	6.150													
Th_7Co_3	9.830	6.170													
Th_7Ni_3	9.860	6.230													
$La_7Ni_3H_{21}$															amor-phous

[1]) Neutron diffraction study.

For lattice parameters see also
R_7Ni_3 [61 R 1, 73 O 8];
La_7Ni_3, $La_7Ni_3D_x$ [78 F 6, 78 F 7]. By hydriding
$La_7Ni_3D_x$ decomposes in $LaD_3 + LaNi_5$ [78 F 7], Ce_7Ni_3 [78 F 6]
$Th_7Co_3H_x$, $Th_7Ni_3H_x$ [80 M 1]
$Th_7M_3H_x$, M = Fe, Co, Ni [56 F 1, 82 S 11]

For hydrogen absorption in R_7M_3 compounds see
$La_7Ni_3H_{19.3}$, $Ce_7Ni_3H_{19.2}$ [78 B 18, 78 B 19]
$La_7Ni_3H_x$ [76 O 5, 77 B 17, 78 B 19, 78 F 7]; $La_7Ni_3H_x$, $Ce_7Ni_3H_x$ [78 B 18]

Magnetization, Curie temperatures

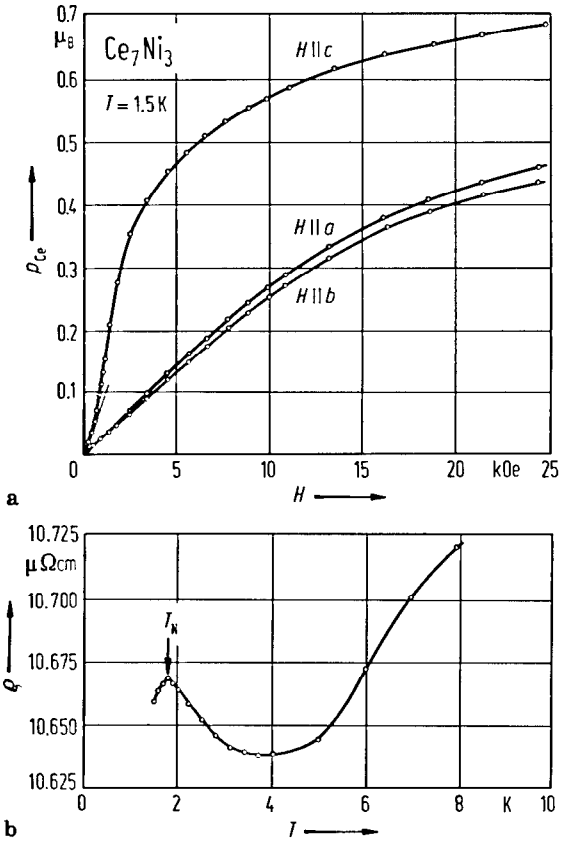

Fig. 33. (a) Magnetic field dependence of the Ce_7Ni_3 magnetizations measured at 1.5 K along the *a*, *b* and *c* axis of the orthohexagonal cell. (b) shows the thermal variation of the total electrical resistivity at low temperatures. In this compound Ce is close to the trivalent state and orders antiferromagnetically at 1.8 K. Although the magnetic structure is rather complex due to the low symmetry of the Ce sites, the magnetic susceptibility is the highest along the *c* axis. Along this direction the magnetic field dependence of magnetization exhibits a metamagnetic transition in low field. The minimum of the electrical resistivity observed around 4 K shows that Ce_7Ni_3 is a Kondo lattice system [85 G 6]. In case of $Ce_7Ni_3H_x$ no magnetic order was observed [76 O 5, 78 B 18].

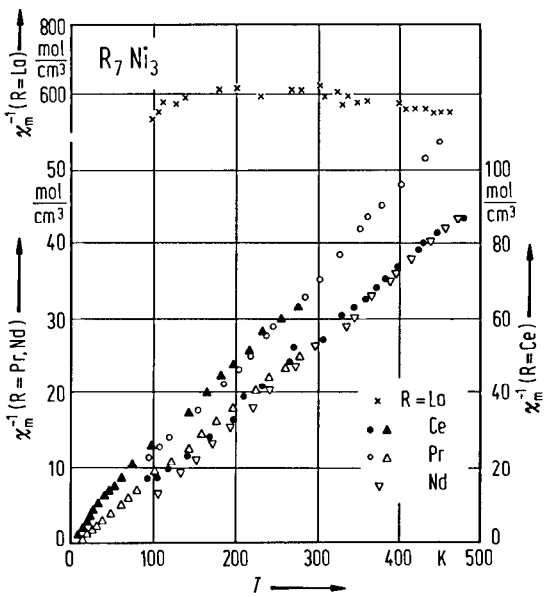

Fig. 34. Thermal variation of the reciprocal magnetic susceptibilities for R_7Ni_3 (R = La, Ce, Pr, Nd) compounds. Triangles [66 K 2], other symbols [73 O 8]. La_7Ni_3 shows a Pauli-type paramagnetism. For R = Pr, Nd and Ce ($T \gtrsim 60$ K) a Curie-Weiss behaviour is evidenced.

For magnetic properties see also
R_7Ni_3 [66 K 2, 73 O 8]; Ce_7Ni_3 [85 G 6]
$Ce_7Ni_3H_x$ [78 B 18, 78 F 6]; $Th_7Fe_3H_x$ [78 M 4, 78 W 3, 80 M 1, 82 S 11]; $Th_7Co_3H_x$ [80 M 1]
$Th_7Ni_3H_x$ [80 M 1]

Table 10. Magnetic properties of R_7M_3 compounds.

	T_C(K)		p_s(μ_B/f.u.)		p_{eff}(μ_B/R)			Θ(K)	
	85 G 6	78 M 4	78 B 18	78 M 4	66 K 2	73 O 8	78 B 18	66 K 2	73 O 8
La_7Ni_3							Pauli paramagnet $\chi_g = 0.70(5) \cdot 10^{-6}$ cm^{3}g^{-1}		
Ce_7Ni_3	1.8				2.41	2.16		−38	13
Pr_7Ni_3					3.60	3.55		− 2	23
Nd_7Ni_3						3.33			48
Th_7Fe_3 [1])		Pauli paramagnet							
$La_7Ni_3H_{19.3}$			Pauli paramagnet $\chi_g = 0.8(1) \cdot 10^{-6}$ cm^{3}g^{-1}						
$Th_7Fe_3H_x$				4.2					

[1]) Th_7Fe_3 is a superconductor below 1.86 K [78 M 4].

Mössbauer effect

^{57}Fe: Th_7Fe_3 [80 B 18]

Transport properties

For electrical resistivity of Ce_7Ni_3 see [85 G 17].

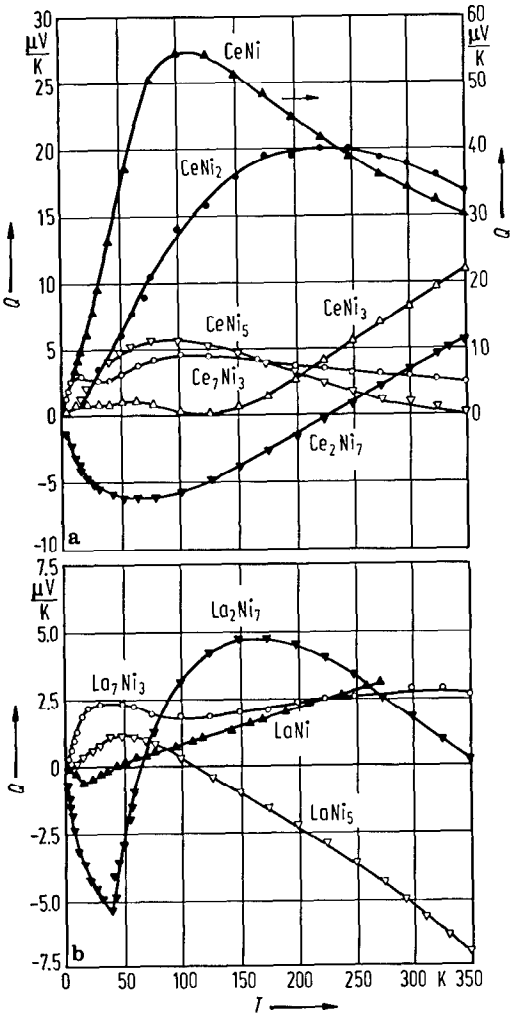

Fig. 35. Thermoelectric power (TEP) as function of temperature for $CeNi_x$ (a) and $LaNi_x$ (b) compounds [85 G 17]. For CeNi a maximum in $Q(T)$ of 55 μV/K, at $T = 110$ K, is observed. The peak decreases with increasing Ni concentration, and a more complex behaviour is observed at low temperatures. At low temperatures the TEP of $CeNi_2$, Ce_2Ni_7 and $CeNi_5$ is determined by scattering from Ni-derived 3d states [84 C 1]. Ce_7Ni_3 exhibits a double structure in $Q(T)$. Comparison with the results for the La_7Ni_3 suggests that the low-lying peak is due to phonon drag. After subtraction of the phonon drag contribution one is left with a negative diffusion TEP at low T, being characteristic of a Kondo lattice.

2.4.2.4 $R_{24}M_{11}$ compounds

Crystal structure, lattice parameters

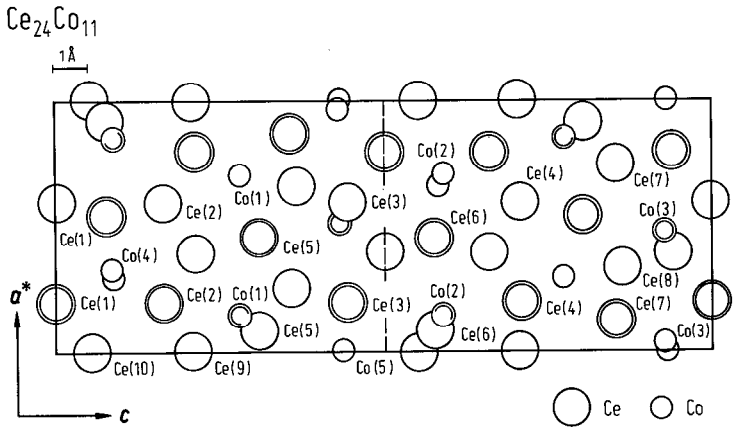

Fig. 36. Projection of the structure of $Ce_{24}Co_{11}$ on a plane normal to the *b* axis. The numbers inscribed correspond to the numbers of the atoms given in Table 11. The compound crystallizes in a hexagonal structure having the space group $P6_3mc$ [62 L 1].

Table 11. Atomic positions in $Ce_{24}Co_{11}$ compound [62 L 1].

Atoms	Site	*x*	*z*
Ce(1)	c	0.2011(7)	0.0
Ce(2)	c	0.2016(8)	0.1628(6)
Ce(3)	c	0.2029(6)	0.4414(6)
Ce(4)	c	0.2065(8)	0.7091(6)
Ce(5)	c	0.4580(6)	0.3057(6)
Ce(6)	c	0.4586(5)	0.5748(6)
Ce(7)	c	0.1245(6)	0.8542(6)
Ce(8)	b	1/3	0.8647(8)
Ce(9)	a	0	0.2070(10)
Ce(10)	a	0	0.0526(12)
Co(1)	c	0.1456(19)	0.2762(12)
Co(2)	c	0.1503(21)	0.5881(15)
Co(3)	c	0.4819(16)	0.9290(12)
Co(4)	b	1/3	0.0845(27)
Co(5)	a	0	0.4326(22)

Table 12. Lattice parameters of $Ce_{24}Co_{11}$ (space group $P6_3mc$) compound (Å).

	[62 L 1]		[84 O 3]	
	a	*c*	*a*	*c*
$Ce_{24}Co_{11}$	9.587(3)	21.825(10)	9.587(3)	21.840(10)

Magnetic properties

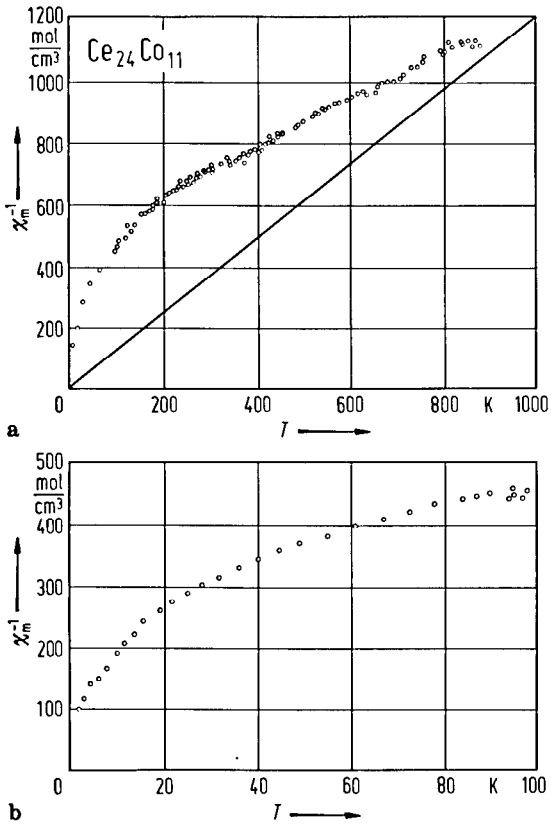

Fig. 37. Thermal variation of the reciprocal magnetic susceptibility for $Ce_{24}Co_{11}$ compound in the temperature range (a) 4.2···1000 K, and (b) 4.2···100 K. The Curie-Weiss law is not followed and no magnetic order occurs down to 4.2 K. A very small change in the thermal behaviour of the magnetic susceptibility appears above the melting point, $T_M = 750$ K. The abnormally low values of the magnetic susceptibility could be understood by assuming that Co is nonmagnetic and Ce is a temperature-dependent mixed-valence-state ion [84 O 3].

Photoemission studies

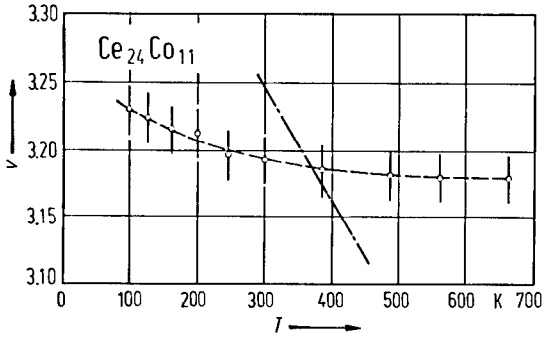

Fig. 38. Temperature dependence of the valence of Ce in $Ce_{24}Co_{11}$ deduced from XPS measurements (broken line). The dash-dotted line gives the slope one would obtain from the magnetic susceptibility by treating the Ce ion as isolated. The smooth but not negligible temperature dependence of the valence deduced from XPS is a strong and direct experimental support in favour of the importance of the interaction of Ce 4f with Bloch states. This interaction is the origin of the slower temperature dependence than expected for isolated ions [85 A 1].

2.4.2.5 $R_{12}M_7$ compounds

Crystal structure, lattice parameters

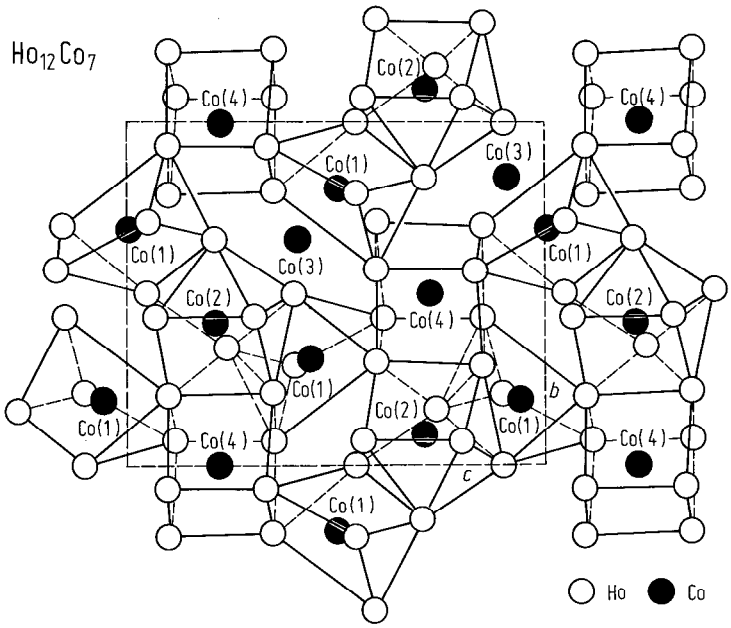

Fig. 39. Projection of the $Ho_{12}Co_7$ structure on the (100) plane showing three of the four different types of Co-centred rare-earth polyhedra. Co(1) is at the center of trigonal prism, Co(2) is surrounded by an Archimedian antiprism and Co(4) is at the center of a cube. For clarity of presentation the coordination figure around Co(3) has not been given. If 3.10 Å is to be considered the upper limit of the acceptable coordination distances, Co(3) is surrounded by six Ho atoms. The coordination can be described by two equivalent figures: either a truncated Archimedian antiprism with two opposite corners through the center of the antiprism missing or a pentagon with one corner being replaced by a pair of atoms along a direction perpendicular to the pentagon plane [76 A 1].

Table 13. Atomic sites in $Ho_{12}Co_7$ (space group $P2_1/c$) compound [76 A 1].

Atom	Site	x	y	z
Ho(1)	4e	0.8799(7)	0.5704(3)	0.8031(4)
Ho(2)	4e	0.5982(7)	0.2027(3)	0.1729(4)
Ho(3)	4e	0.9449(7)	0.5719(3)	0.5863(4)
Ho(4)	4e	0.6879(7)	0.2957(3)	0.4604(4)
Ho(5)	4e	0.8213(7)	0.8100(3)	0.6603(4)
Ho(6)	4e	0.5565(7)	0.0050(3)	0.3472(4)
Co(1)	4e	0.787(2)	0.694(1)	0.348(1)
Co(2)	4e	0.678(2)	0.089(1)	0.594(1)
Co(3)	4e	0.976(2)	0.836(1)	0.529(1)
Co(4)	2b	1/2	0	0

Table 14. Lattice parameters of $R_{12}Co_7$ compounds [76 A 1].

	a(Å)	b(Å)	c(Å)	β
$Gd_{12}Co_7$	8.410	11.390	14.020	138.8°
$Tb_{12}Co_7$	8.390	11.320	13.970	138.8°
$Dy_{12}Co_7$	8.360	11.250	13.920	138.8°
$Ho_{12}Co_7$	8.327	11.191	13.871	138.8°
$Er_{12}Co_7$	8.300	11.160	13.820	138.7°

2.4.2.6 R_8M_5 compounds

Crystal structure, lattice parameters

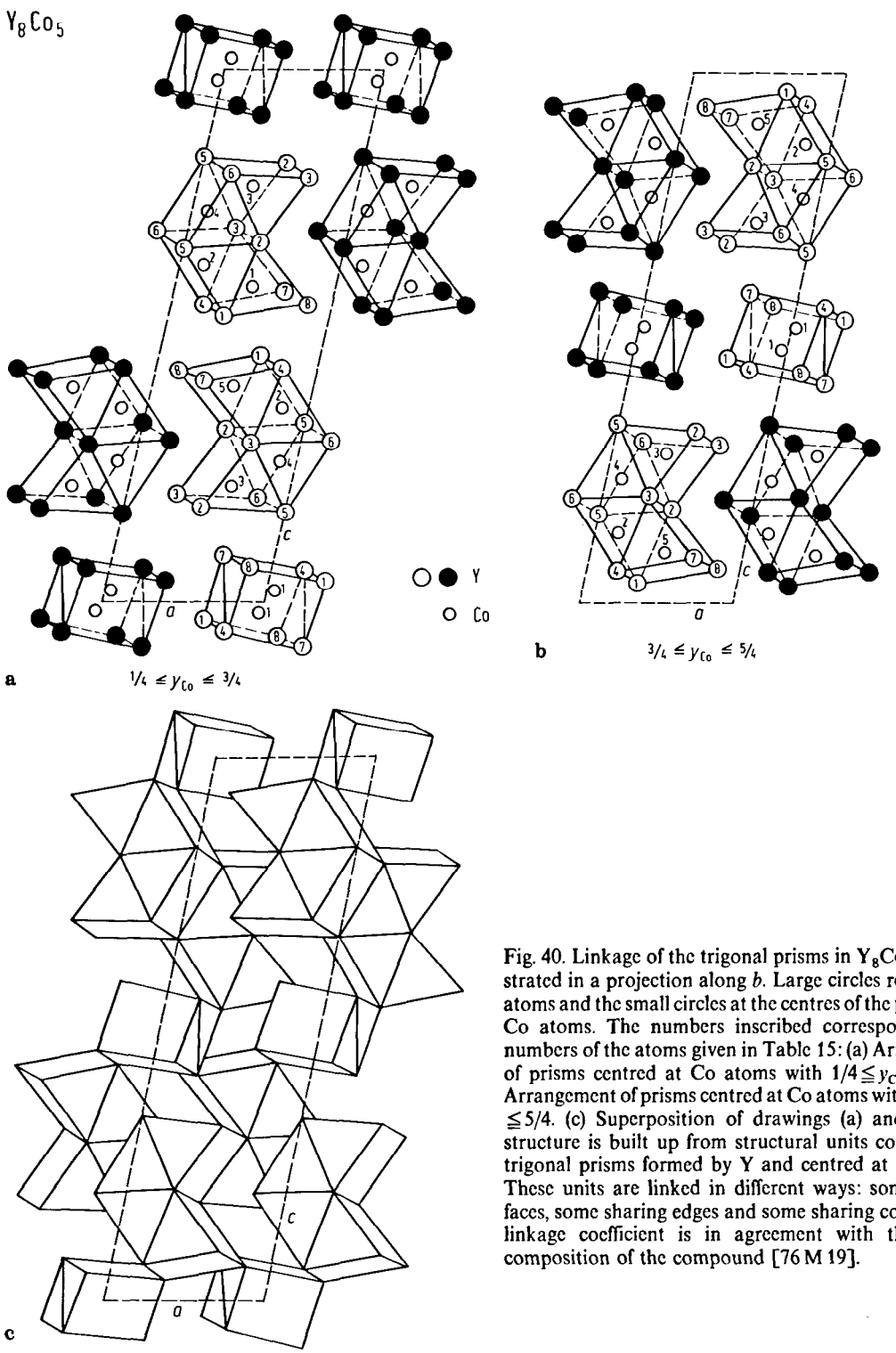

Fig. 40. Linkage of the trigonal prisms in Y_8Co_5 demonstrated in a projection along *b*. Large circles represent Y atoms and the small circles at the centres of the prisms, the Co atoms. The numbers inscribed correspond to the numbers of the atoms given in Table 15: (a) Arrangement of prisms centred at Co atoms with $1/4 \leqq y_{Co} \leqq 3/4$. (b) Arrangement of prisms centred at Co atoms with $3/4 \leqq y_{Co} \leqq 5/4$. (c) Superposition of drawings (a) and (b). The structure is built up from structural units consisting of trigonal prisms formed by Y and centred at Co atoms. These units are linked in different ways: some sharing faces, some sharing edges and some sharing corners. The linkage coefficient is in agreement with the overall composition of the compound [76 M 19].

Table 15. Positions and isotropic thermal parameter of the atoms in Y_8Co_5 compound [76 M 19].

Atom	x	y	z	$U(10^{-2}$ Å$^2)$
Y(1)	0.360(1)	0.185(1)	0.963(1)	1.2(2)
Y(2)	0.471(1)	0.173(1)	0.823(1)	1.2(2)
Y(3)	0.308(1)	0.815(1)	0.298(1)	1.1(2)
Y(4)	0.212(1)	0.835(1)	0.441(1)	1.3(2)
Y(5)	0.000(1)	0.181(1)	0.337(1)	1.2(2)
Y(6)	0.188(1)	0.182(1)	0.196(1)	1.0(2)
Y(7)	0.685(1)	0.956(1)	0.415(1)	0.9(2)
Y(8)	0.141(1)	0.976(1)	0.064(1)	1.5(2)
Co(1)	0.025(1)	0.142(1)	0.479(1)	1.6(3)
Co(2)	0.835(1)	0.028(1)	0.133(1)	1.1(3)
Co(3)	0.637(1)	0.029(1)	0.282(1)	1.6(3)
Co(4)	0.097(1)	0.030(1)	0.765(1)	1.3(3)
Co(5)	0.489(1)	0.884(1)	0.905(1)	1.5(3)

Table 16. Lattice parameters of Y_8Co_5 compound [76 M 19].

	a(Å)	b(Å)	c(Å)	β
Y_8Co_5	7.058(2)	7.286(2)	24.277(8)	102.11(7)°

Magnetic properties

Table 17. Physical properties of Y_8Co_5 compound determined in the temperature range 1.6 and 7 K [86 C 6].

	γ mJ mol^{-1} K^{-2}	Θ_D K	χ_m $\cdot 10^{-4}$ cm^3 mol^{-1}	$D_\chi(E_F)/D_\gamma(E_F)$ [1]
Y_8Co_5 [2]	4.6	221	6.7	4.8

[1]) Ratio between the electronic density of states at the Fermi level determined from magnetic susceptibility and specific heat measurements, respectively.

[2]) Superconducting transition temperature is 0.117 K.

2.4.2.7 R_3M_2 compounds

Crystal structure, lattice parameters

For the structure of Y_3Co_2 and Dy_3Ni_2 see Fig. 7.

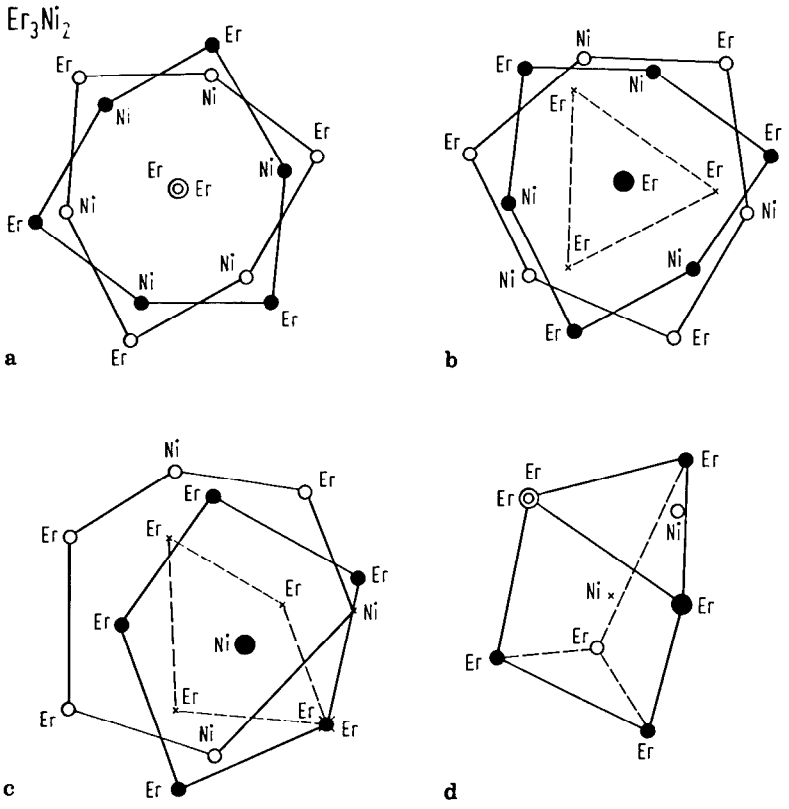

Fig. 41. Coordination polyhedra in projection along the c axis of Er_3Ni_2 structure. Thick lines: upper edges; thin lines: intermediate edges; dashed lines: lower edges. (a), (b) and (c) show, respectively, the Er(1)-, Er(2)- and Er(3)-centred coordination polyhedra. (d) Trigonal prism of Er atoms surrounding one Ni atom (x) with three outer atoms: 2Er + Ni [74 M 10].

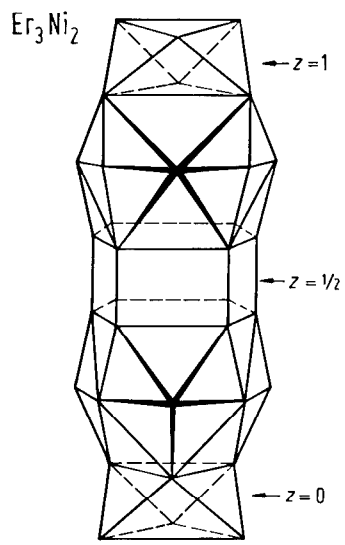

Fig. 42. Stacking of polyhedra along the c axis in one hexagonal cell of Er_3Ni_2. Successively, one regular octahedron of Er atoms centred at the origin ($z = 0$), the CN16 polyhedron centred at Er(2) as described in Fig. 41(b), and the CN14 polyhedron centred at Er(1) at $z = 1/2$ as described in Fig. 41a. The upper part ($1/2 < z < 1$) of the figure is related to the lower part ($0 < z < 1/2$) by a symmetry centre at $z = 1/2$ [74 M 10].

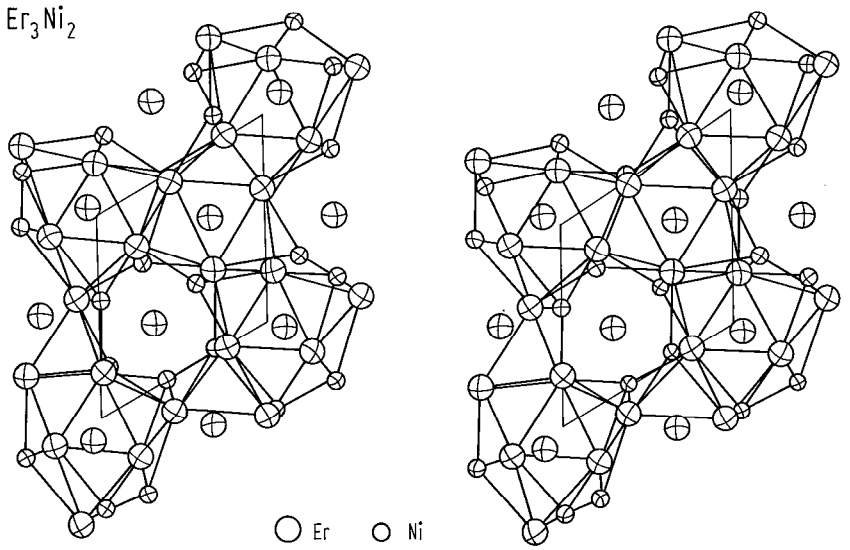

Fig. 43. Three-dimensional view along the c axis of two layers of Er and Ni atoms. Thin lines represent the unit cell. Ni atoms are shown smaller than the Er atoms. The Er_3Ni_2 structure can also be described by layers perpendicular to c axis since Er(3) and Ni atoms have very similar z parameters [74 M 10].

Table 18a. Atomic sites in Y_3Co_2 – Pnnm space group [75 M 9].

Atom	x	y	z
Y(1)	0.128(1)	0.193(1)	0
Y(2)	0.387(1)	0.373(2)	0
Y(3)	0.137(1)	0.574(2)	0
Co(1)	0.269(2)	0.860(2)	0
Co(2)	0.462(2)	0.883(3)	0

Table 18b. Atomic sites in Er_3Ni_2 – $R\bar{3}$ space group [74 M 10].

Atom	Site	x	y	z
Er(1)	3b	0	0	1/2
Er(2)	6c	0	0	0.2915(3)
Er(3)	18f	0.2357(3)	−0.0175(3)	0.0930(1)
Ni	18f	0.580(1)	−0.0229(9)	0.0630(4)

Table 18c. Atomic sites in Dy_3Ni_2 – C2/m space group [75 M 9].

Atom	x	y	z
Dy(1)	0.1322(2)	0	0.9972(2)
Dy(2)	0.4038(2)	0	0.3284(2)
Dy(3)	0.1442(2)	0	0.3696(2)
Ni(1)	0.5352(6)	0	0.1435(7)
Ni(2)	0.7439(4)	0	0.2266(7)

Table 18d. Atomic positions in Y_3Ni_2 – $P4_12_12$ space group [77 L 1].

Atom	Site	x	y	z
Y(1)	4a	0.966(2)	0.966(2)	0
Y(2)	4a	0.317(2)	0.317(2)	0
Y(3)	8b	0.808(2)	0.443(2)	0.0156(4)
Y(4)	8b	0.163(2)	0.659(2)	0.0680(4)
Y(5)	8b	0.645(2)	0.809(2)	0.0747(4)
Y(6)	8b	0.012(2)	0.163(2)	0.0891(4)
Y(7)	8b	0.514(2)	0.293(2)	0.0933(4)
Ni(1)	8b	0.310(3)	0.008(3)	0.0484(4)
Ni(2)	8b	0.630(3)	0.101(3)	0.0257(5)
Ni(3)	8b	0.840(3)	0.510(3)	0.1063(5)
Ni(4)	8b	0.322(3)	0.943(3)	0.1167(5)

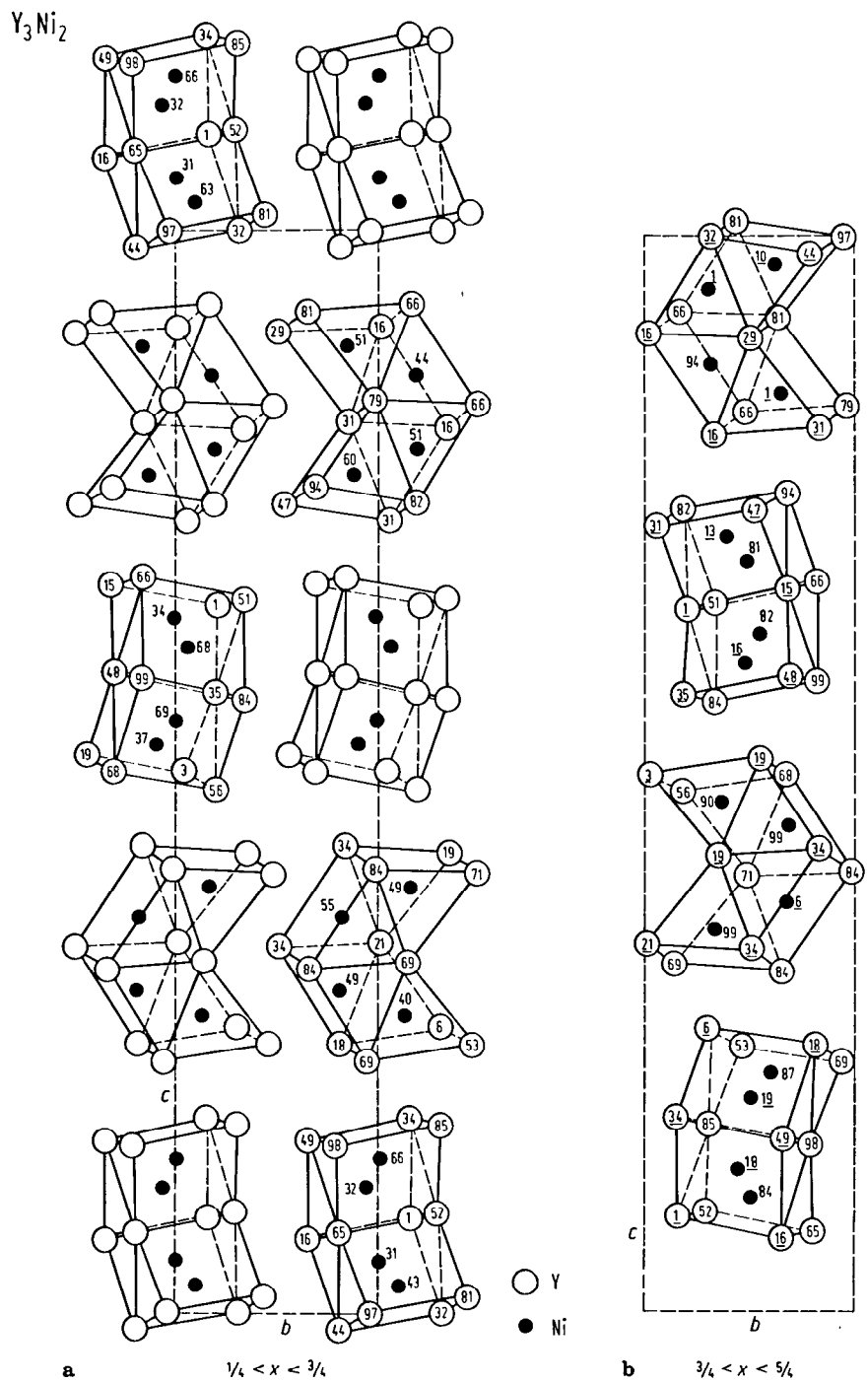

Fig. 44. Linkage of trigonal prisms in Y_3Ni_2 in projection down *a*. Large circles represent Y atoms, small circles in the centers of the prisms, the Ni atoms. The inscribed numbers correspond to the *x* parameters multiplied by 100. (a) Arrangement of prisms centred at Ni atoms with $1/4 < x < 3/4$. For crystal structure of Dy_3Co_2, see [64 W 7]. (b) Arrangement of prisms centred at Ni atoms with $3/4 < x < 5/4$. The drawing of the trigonal prisms becomes significant if 100 is added to the underlined inscribed values of $100x$ [77 L 1].

Table 19. Structure and lattice parameters of R_3M_2 compounds.

	Crystal structure	Space group	a(Å)	b(Å)	c(Å)	β	Ref.
Y_3Co_2	orthorhombic	Pnnm	12.278	9.389	3.975	–	75 M 9
Ho_3Ni_2(h) [1])	orthorhombic	$R\bar{3}$	8.520	–	15.750	–	74 M 11
Er_3Ni_2	orthorhombic	$R\bar{3}$	8.472	–	15.680	–	74 M 10
Tb_3Ni_2	monoclinic	C2/m	9.640	3.710	13.380	106.0°	74 M 11
Dy_3Ni_2	monoclinic	C2/m	9.512	3.662	13.321	105.72°	74 M 11
Ho_3Ni_2(l) [1])	monoclinic	C2/m	9.510	3.650	13.300	105.6°	75 M 11
Y_3Ni_2	tetragonal	$P4_12_12$	7.104	–	36.547	–	77 L 1

[1]) h indicates high-temperature modification and l low-temperature modification.

Magnetic properties

Table 20. Physical properties of Y_3Co_2 compound determined in the temperature range 1.6 and 7 K [86 C 6].

	γ mJ mol^{-1} K^{-2}	Θ_D K	χ_m 10^{-4} cm^3 mol^{-1}	$D_\chi(E_F)/D_\gamma(E_F)$ [1])
Y_3Co_2	5.5	221	2.4	1.55

[1]) The ratio between the electronic density of states at the Fermi level determined from susceptibility and specific heat measurements, respectively.

2.4.2.8 $R_4M_3(R_9M_7)$ compounds

Crystal structure, lattice parameters

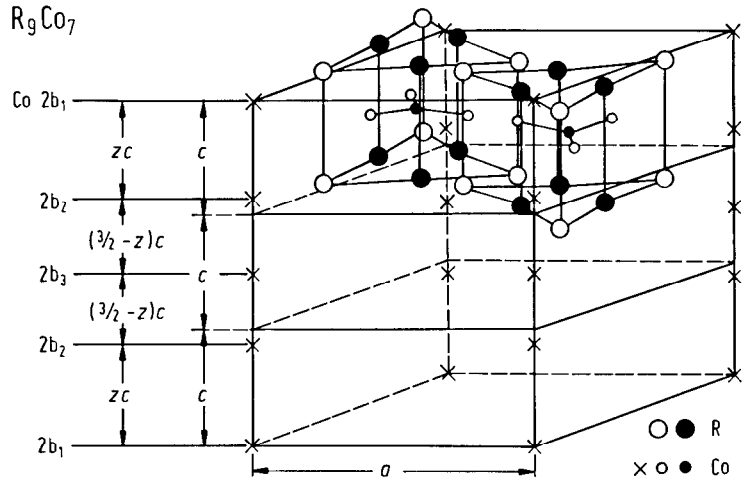

Fig. 45. Crystal structure of R_9Co_7 compounds. The presence of c axis Co sites with $z = 7/8$ were suggested in [82 G 11, 82 S 6, 83 Y 8]. 26 Y and 28 Co atoms of Y_9Co_7 are contained in the unit cell. The nonequivalent sites of Y and Co atoms are denoted by large solid ($6h_1$) and large open ($6h_2$) circles for Y, and by small solid circles (2d), small open circles (6h), and crosses ($2b_1$, $2b_2$, $2b_3$) for Co. Initially, the composition of these compounds has been considered to be R_4Co_3 [68 B 3, 69 B 3].

Table 21. Lattice parameters of R_4Co_3 compounds (Å).

	[68 B 3]		[70 B 10]		[71 G 2]		[86 S 4]	
	a	*c*	*a*	*c*	*a*	*c*	*a*	*c*
Gd_4Co_3	11.591(4)	4.054(2)	11.61	4.048				
Tb_4Co_3	11.514(4)	4.007(2)	11.49	4.005				
Dy_4Co_3	11.461(4)	4.005(2)	11.48	3.994				
Ho_4Co_3	11.410(4)	3.984(2)	11.40	3.980				
Er_4Co_3	11.352(4)	3.973(2)	11.32	3.967				
Tm_4Co_3	11.290(4)	3.952(2)						
Lu_4Co_3					11.21	3.92		
Y_4Co_3	11.529(4)	4.041(2)	11.48	4.04			11.45	4.04

For crystal structure and lattice parameters see
R_4M_3 Yb_4Mn_3 [83 T 7]
R_4Co_3 [68 B 3, 70 B 10, 71 B 15]; R = Gd, Tb, Dy, Ho, Er, Tm [69 L 2]; R = Ho [67 L 3]
Y_9Co_7 [82 G 11, 84 C 2, 87 K 9]

For thermal expansion see
Y_9Co_7 [84 O 4]

Magnetization, Curie temperatures

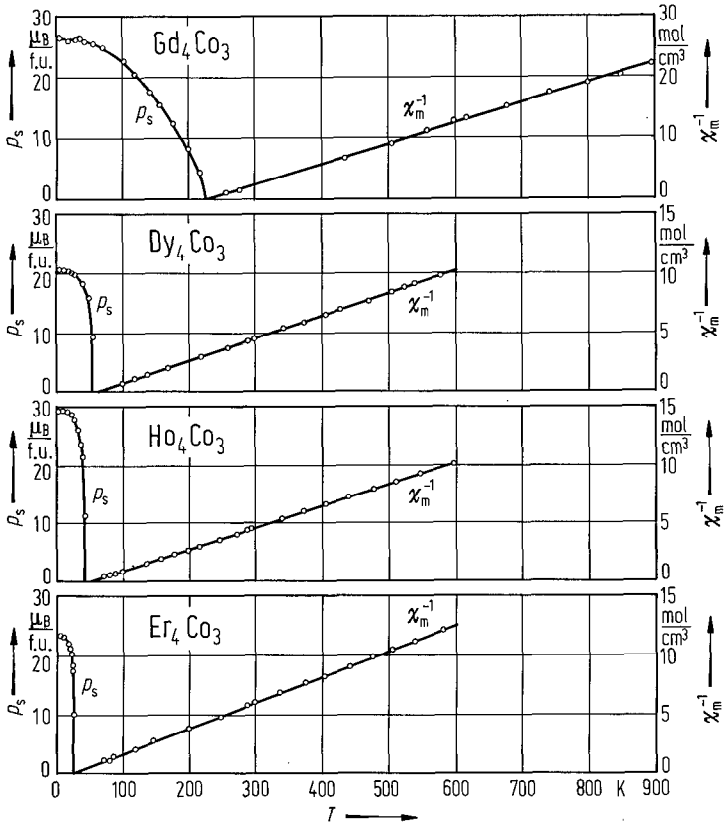

Fig. 46. Thermal variations of the spontaneous magnetizations and reciprocal magnetic susceptibilities for R_4Co_3 (R = Gd, Dy, Ho, Er) compounds [68 B 3].

For Fig. 47, see next page.

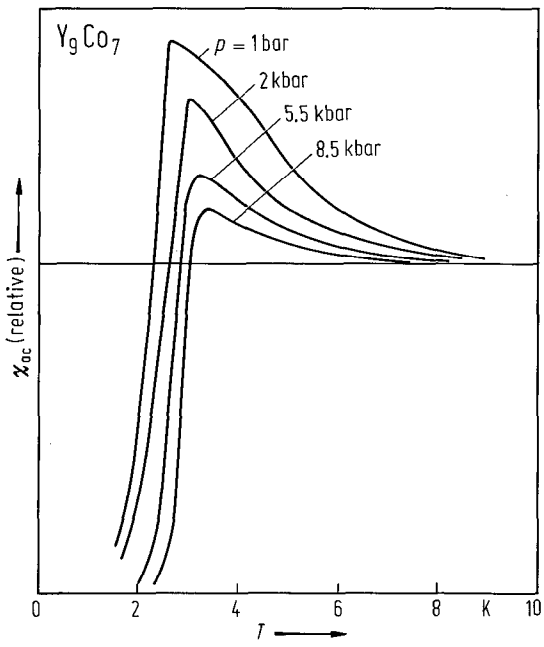

Fig. 48. Temperature dependence of the magnetic ac susceptibility for various applied pressures for Y_9Co_7. The superconductivity is enhanced under pressure [84 S 2].

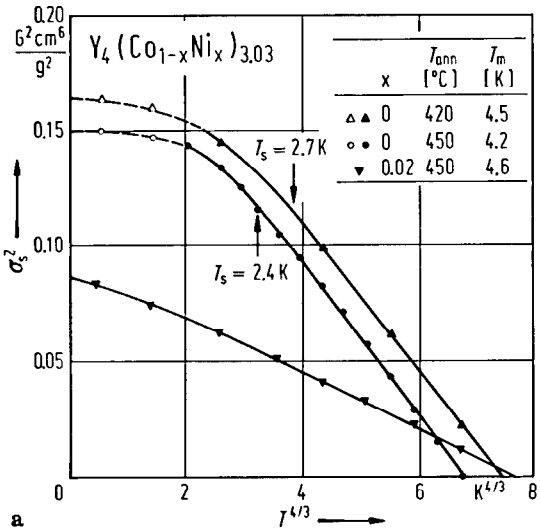

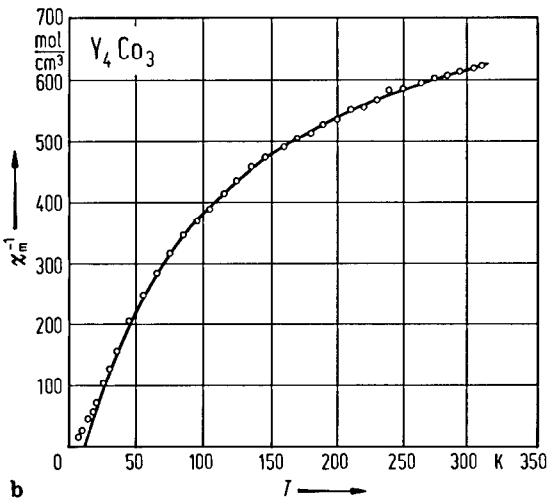

Fig. 47. (a) Temperature dependence of the zero-field magnetization deduced from Arrott plots for $Y_4Co_{3.03}$ and $Y_4(Co_{0.98}Ni_{0.02})_{3.03}$ samples. Open symbols mean that the values are speculative. Around the Curie points the magnetization follows the relation $M_s^2 \propto (T_C^{4/3} - T^{4/3})$ characteristic of weak itinerant-electron ferromagnet [83 Y 3]. The superconducting transition temperature is denoted by T_s, the magnetic phase transition temperature by T_m, T_{ann} is the annealing temperature. (b) Thermal variation of reciprocal magnetic susceptibilities for Y_4Co_3 compound [80 G 9]. This curve fits the relation $\chi_m = \chi_0 + C_m(T-\Theta)^{-1}$ with $C = 0.125\,cm^3\,K/mol$, $\Theta = 12\,K$ and $\chi_0 = 1.2 \cdot 10^{-3}\,cm^3/mol$. Similar data were obtained in [76 B 17, 84 Y 5].

Fig. 49. Low field behaviour of $\sigma - H$ curves in the neighbourhood of the superconducting transition temperature. A superconducting fraction of material of the order of 25% at $T = 1.14\,K$ is estimated from these data [81 G 12].

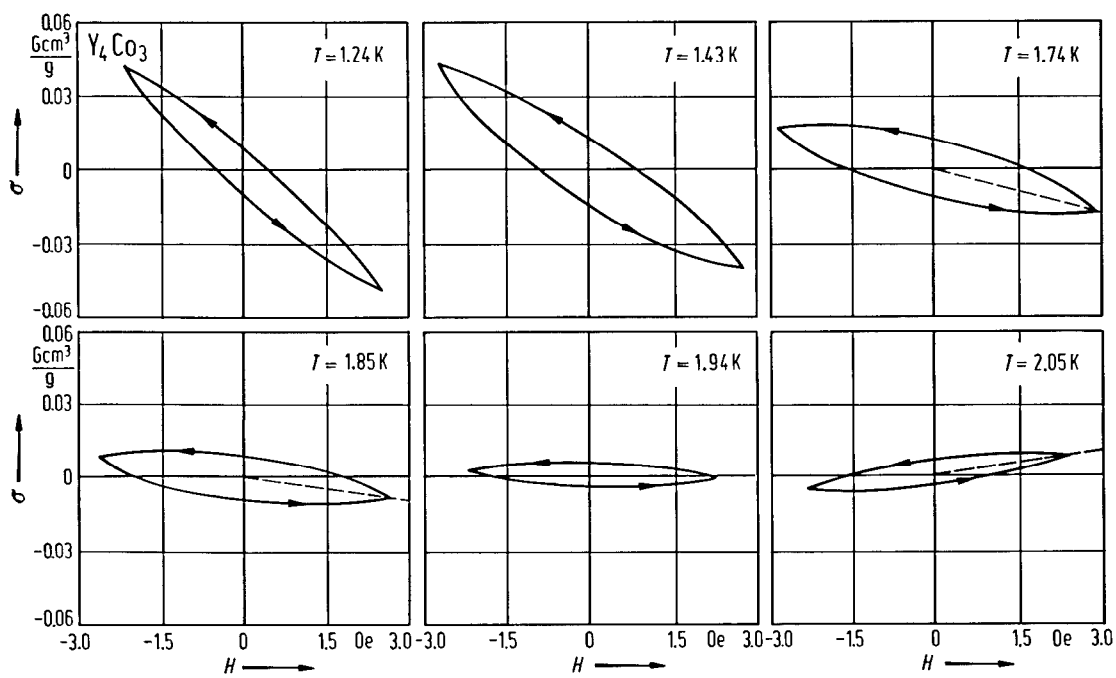

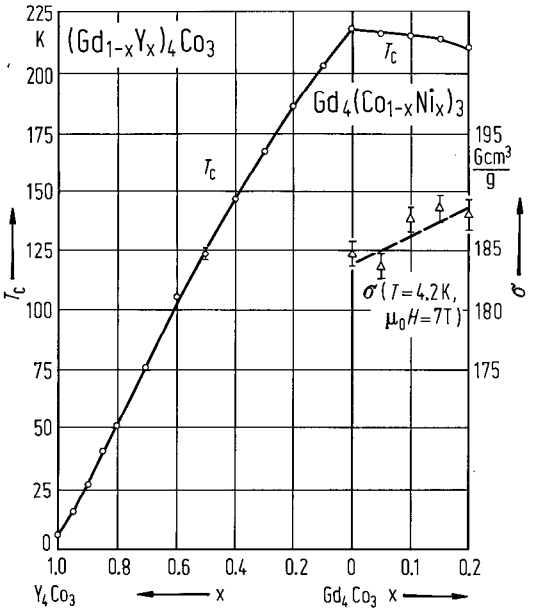

Fig. 50. Composition dependence of the Curie temperatures in $(Gd_{1-x}Y_x)_4Co_3$ and $Gd_4(Co_{1-x}Ni_x)_3$ ($0 \leqq x \leqq 0.2$), respectively, and of the magnetization of $Gd_4(Co_{1-x}Ni_x)_3$ at 4.2 K in a field of 7 T [82 G 8].

Table 22. Magnetic properties of R_4Co_3 compounds.

	p_m μ_B/f.u.	T_C K	Θ K	C_m $cm^3\,K\,mol^{-1}$	Ref.
Gd_4Co_3	26.3	230	242	31.4	68 B 3
Dy_4Co_3 [1])	20.9	55	62	56.1	68 B 3
Ho_4Co_3 [1])	20.6	44	50	55.7	68 B 3
Er_4Co_3 [1])	23.1	25	28	45.9	68 B 3
Lu_4Co_3		< 2			71 G 1
Y_4Co_3	0.11	13			68 B 3

[1]) A phase transition of metamagnetic type has been suggested at $T_t = 6$, 1.8, and 1.6 K for the Dy-, Ho-, and Er-compounds, respectively.

For magnetic properties see also:

R_4Co_3 [68 B 3]; R = Tb, Dy, Er, Tm [78 Y 1]; R = Y [80 G 9, 80 K 13, 81 G 12, 81 S 3, 82 C 6, 82 N 1, 82 V 2, 84 K 8];
Y_9Co_7 [82 S 3, 82 S 4, 82 S 5, 82 S 6, 83 G 13, 83 H 5, 83 K 3, 84 C 2, 84 K 7, 84 O 4, 84 S 1, 84 S 2, 84 Y 4, 84 Y 5, 85 K 8, 85 K 9, 85 K 11, 85 R 8, 85 S 4, 86 S 3, 86 S 4, 86 S 15(T), 87 K 8, 87 K 9]

$(R'R'')_4Co_3$ $(GdY)_4Co_3$ [80 G 8, 80 G 11]
$(RY)_9Co_7$, R = Zr, Sc, Lu [86 Y 3]; $(GdY)_9Co_7$ [83 G 13, 84 S 1]

$R_4(M'M'')_3$ $Y_4(CoNi)_3$ [83 Y 3]; $Y_4(CoSi)_3$ [83 Y 8]; $Gd_4(CoNi)_3$ [81 G 14, 82 G 8]
$Y_9(CoM)_7$, M = Ni, Mn [84 S 1]; $Y_9(CoNi)_7$ [82 S 3, 83 G 13]

Neutron diffraction

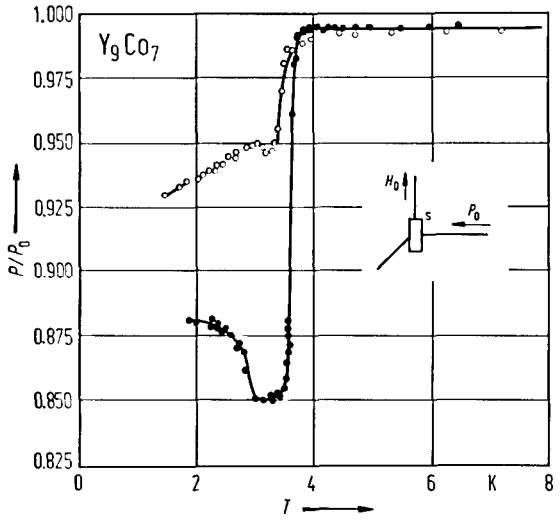

Fig. 51. Depolarization of polarized neutrons observed in field of 4.6 Oe applied perpendicular to the direction of polarized neutron spin (as indicated in inset) for two samples of Y_9Co_7. For $T>4$ K the depolarization is almost zero and this varies suddenly at $T\cong 4$ K. The depolarization seen by polarized neutrons describes a spatially inhomogeneous media. At $\cong 3$ K where the onset of superconductivity is observed, a reduction in P/P_0 is evidenced, suggesting a reduction in the magnetic correlations [87 S 4].

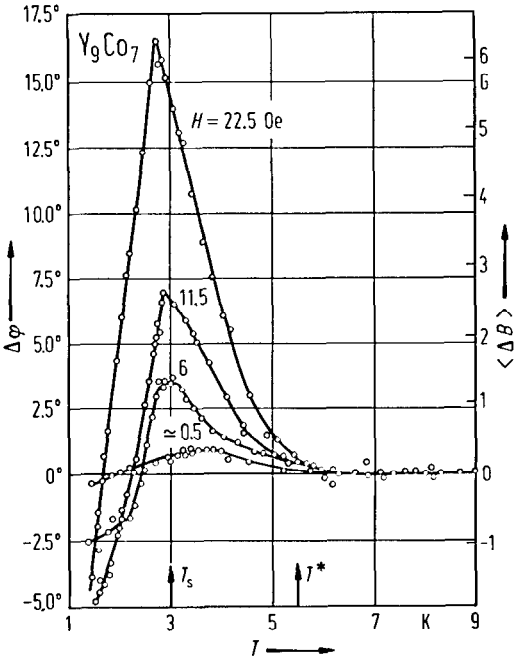

Fig. 52. Change in Larmor precession angle, $\Delta\varphi$, and the average local field $\langle \Delta B \rangle$ of Y_9Co_7 as function of temperature for different magnetic fields as determined by neutron spin echo and neutron spin depolarization studies. In zero field, the absence of spin rotation effects in both "hybrid" ($T_s < T < T^*$) and superconducting ($T \leqq T_s$) state is shown, whereas considerable field - induced effects have been observed in small fields. The "hybrid" state results show evidence for rapid fluctuation effects, and was associated with the c axis Co spin hopping in the two minima of the double-well potential. The presence of a field tends to affect the hopping by trapping some Co spins off their local positions, giving rise to localized spins which may coexist with the rest of the quasiparticles. This suggests that the observed neutron spin rotations are therefore associated with the spatially variable local fields and are due to field-induced localized c axis Co spins [87 S 4].

Table 23. Magnetic moments determined by neutron diffraction studies [78 Y 1]. [1])

	$p_{R(1)}$ μ_B	$p_{R(2)}$ μ_B	p_{Co} μ_B	Direction of moments
Er_4Co_3	8.7	8.1	−0.2(2)	$p_{R(1)} \parallel c$ axis $p_{R(2)} \perp c$ axis
Ho_4Co_3	8.7(5)	2.1(4)	−0.2(3)	$p_{R(1)}$, $p_{R(2)} \perp$ c axis

[1]) The crystal field parameters and direction of the rare earth magnetic moment for R_4Co_3 compounds were also calculated [78 Y 1].

For neutron depolarization see
Y_9Co_7 [82 S 3, 82 S 4, 85 S 5, 87 S 4]; $Y_9(Co_{0.97}Ni_{0.03})_7$ [85 S 5]

For muon spin rotation see
Y_9Co_7 [85 A 16]

Mössbauer effect

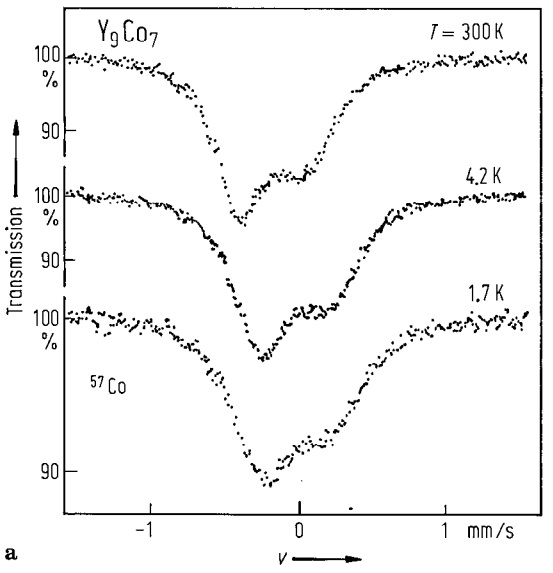

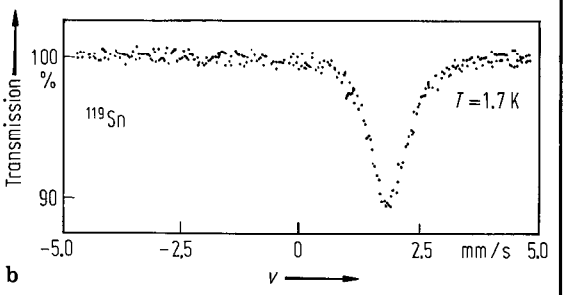

Fig. 53. Mössbauer spectra of (a) ^{57}Co and (b) ^{119}Sn in Y_9Co_7 at various temperatures [85 K 10]. The shape and asymmetry of the quadrupole spectra reveal the individual features of the h, d and b Co atoms in the Y_9Co_7 structure. Below the Curie temperature and in zero magnetic field an apparent broadening of the Mössbauer quadrupole spectra is observed. This may be evidence that the ferromagnetic ordering survives the appearance of the superconducting ordering in Y_9Co_7. For Mössbauer effect study of ^{161}Dy in Dy_4Co_3 see [81 G 17].

For Mössbauer effect see also
^{59}Co, ^{119}Sn in Y_9Co_7 [85 K 10]
^{161}Dy in Dy_4Co_3 [81 G 17]

NMR

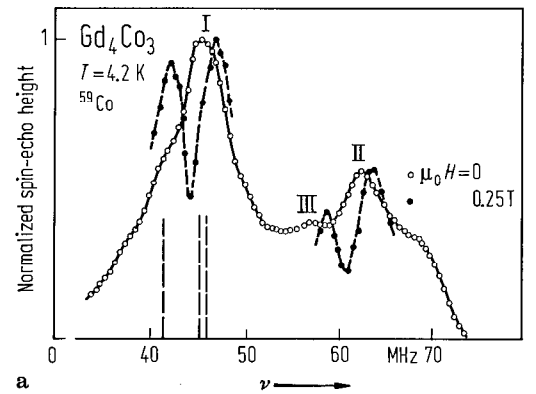

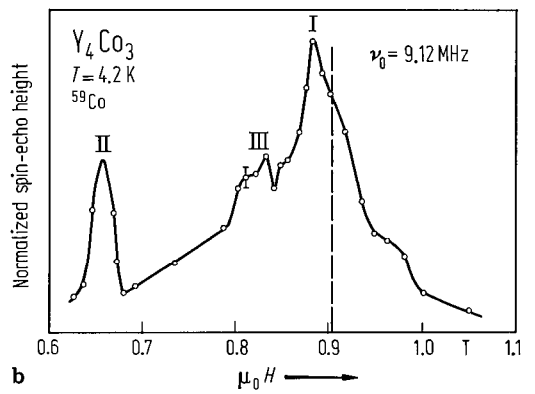

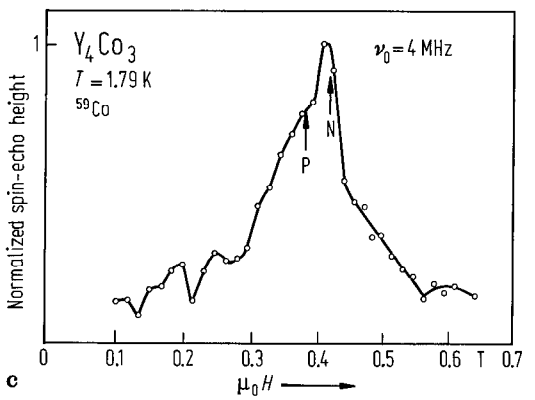

Fig. 54. (a) Frequency-dependent NMR spectrum of ^{59}Co in Gd_4Co_3 at 4.2 K for zero magnetic field and a field of 0.25 T. When applying an external magnetic field both the main lines (I, II) split into two due to antiparallel coupling between Gd and Co magnetic moments. (b) Field-dependent NMR spectrum of ^{59}Co in Y_4Co_3 compound at 4.2 K and for 9.12 MHz. The broken line represents the position of the paramagnetic resonance without Knight shift [81 F 4]. (c) ^{59}Co NMR spectrum of Y_4Co_3 at 1.79 K and for 4 MHz [83 L 2]. The first resonant line (P) with Knight shift $K = +2.5\%$ originates from Co atoms in h-type sites in the paramagnetic state and the second line ($K = -2\%$) denoted by N originates from the same atoms in the superconducting state.

Table 24. Magnetic moments of Co at 4.2 K determined by NMR in R_4Co_3 compounds (R = Y, Gd).

	p_{Co}(6h) μ_B	p_{Co}(2d) μ_B	p_{Co}(2b) μ_B	Ref.
Y_4Co_3 [1])	0	0.026	0.007	80 F 4, 81 F 4
Gd_4Co_3	0.51(1)	0.73(1)	0.58(1)	81 F 4

[1]) After Wada et al. [83 W 1] the 6h and 2d sites enclosed within Y prisms are almost nonmagnetic.

For NMR measurements see
^{59}Co Y_4Co_3 [80 F 4, 81 F 4, 83 K 1, 83 L 2, 83 T 2, 83 W 1]; Gd_4Co_3 [81 F 4]
Y_9Co_7 [83 K 3, 87 F 1]
$(GdY)_4Co_3$ [83 K 1, 85 F 1]

Transport properties

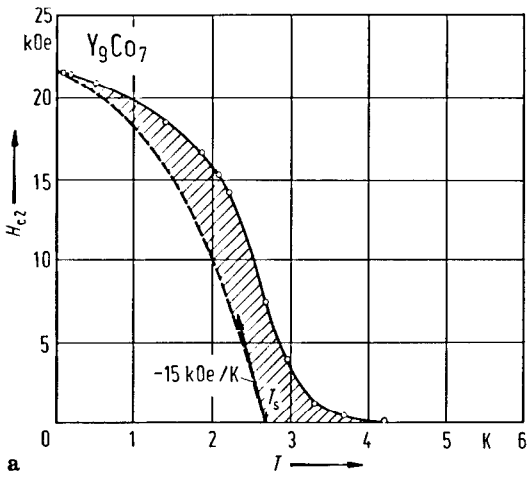

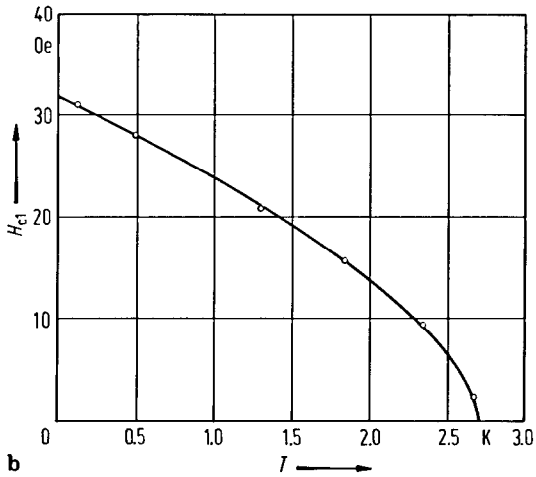

Fig. 55. (a) Upper critical field H_{c2} vs. temperature for Y_9Co_7 [86 S 4]. Assuming a conventional type-II superconductivity at $T=0$, the initial slope $(dH_{c2}/dT)_{T_s} \cong -15$ kOe/K was estimated. The behaviour of H_{c2} vs. T in absence of the "hybrid" state is shown by the dashed line. The shading depicts the coexistence region. (b) shows H_{c1} vs. T data below T_s.

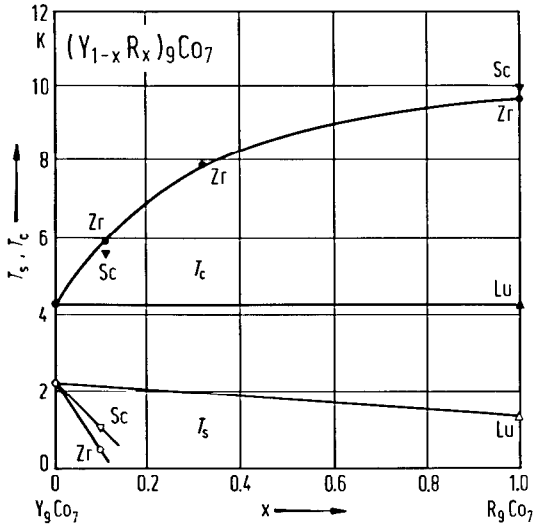

Fig. 56. Composition dependence of (solid symbols) the Curie temperature T_C and (open symbols) the superconducting transition temperature, T_s, in $(Y_{1-x}R_x)_9Co_7$. Zr and Sc strongly suppress the superconductivity and stabilize the magnetic state, while Lu scarcely affects these properties [86 Y 3]. Up to 10^3 ppm the substitution of 3d, 4d and 4f impurities smears out effects associated with the hybrid state of pure Y_9Co_7. Gd and Ni substitution at higher concentration push the system towards long-range magnetic order [83 G 13]. The sample with 3 at% Ni is an itinerant weak ferromagnet with $T_C = 6.3$ K and $T_s < 0.5$ K. The sample with 0.72 at% Mn is magnetic, while for 0.5 at% Gd long-range ferrimagnetic order is evidenced. These samples are not superconducting down to 70 mK.

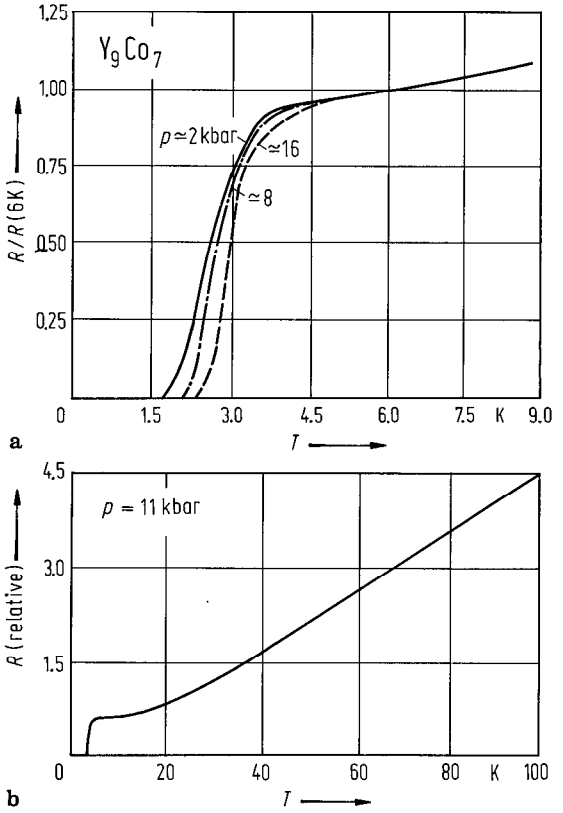

Fig. 57. Temperature dependence of the Y_9Co_7 electrical resistivity at various pressures [83 H 5]. As evidenced also in Fig. 48, the superconductivity is enhanced by pressure.

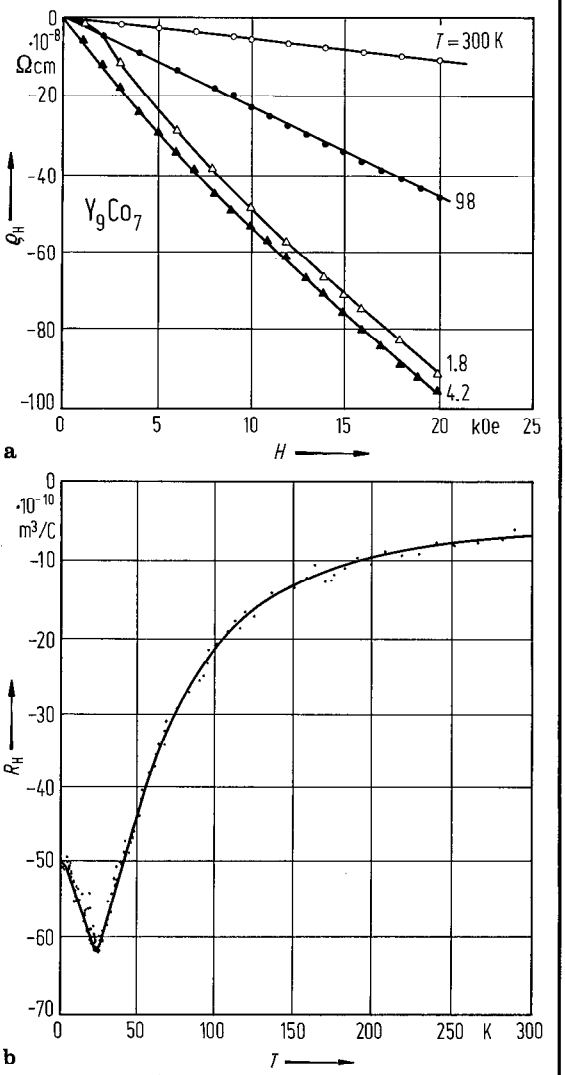

Fig. 58. (a) Hall resistivity ϱ_H of Y_9Co_7 as function of the magnetic field for some temperatures. A linear field dependence is observed at high temperatures, as expected for the ordinary Hall voltage caused by Lorentz force, and a nonlinear field dependence of ϱ_H at low temperatures is emphasized, associated with the extraordinary Hall voltage seen in materials with a magnetic moment. (b) Temperature dependence of the Hall coefficient R_H. (c) shows the low-temperature resistance R at two different magnetic fields. The $|R_H|$ values increase by decreasing temperature to a maximum at approximately 25 K. Below this temperature, $|R_H|$ decreases and finally tends to a constant value below 6 K. These features are associated with spin glass freezing below 25 K [87 A 5] in agreement with [85 R 8], which show the absence of long-range magnetic order.

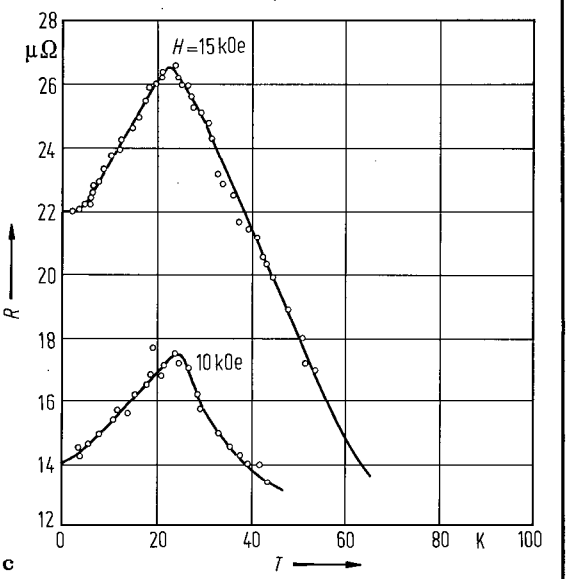

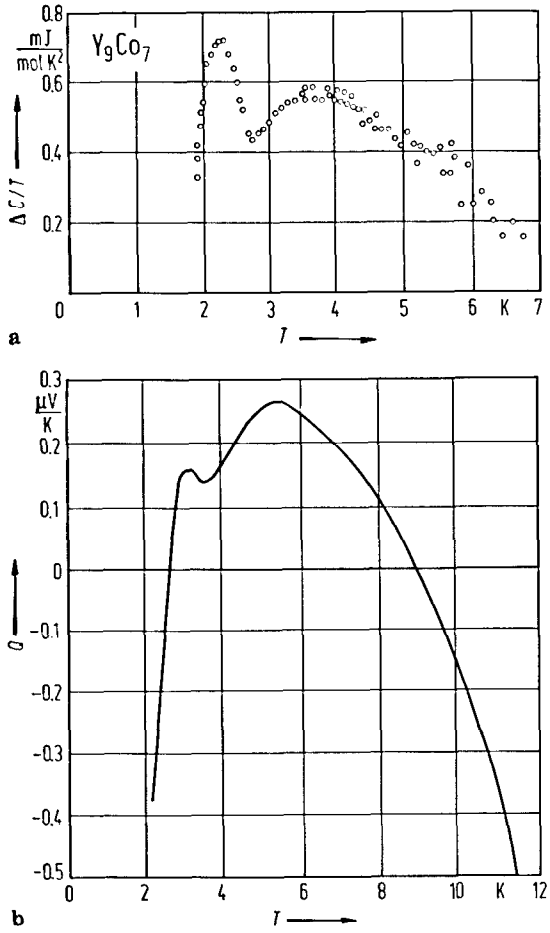

Fig. 59. (a) Temperature dependence of the excess heat capacity, $\Delta C/T$, of Y_9Co_7 after substracting lattice and electronic contributions. A broad hump in the magnetic region, followed by a peak at 2.5 K typical of superconductivity, is shown [82 S 3]. (b) shows the temperature dependence of the thermopower Q of Y_9Co_7. It is negative below ≅9 K and shows a maximum at ≅5 K which is compatible with the $\Delta C/T$ curve. The Q values reveal a superconducting transition temperature with a peak at ≅3 K which is followed by an abrupt drop of Q including a sign change [82 S 3].

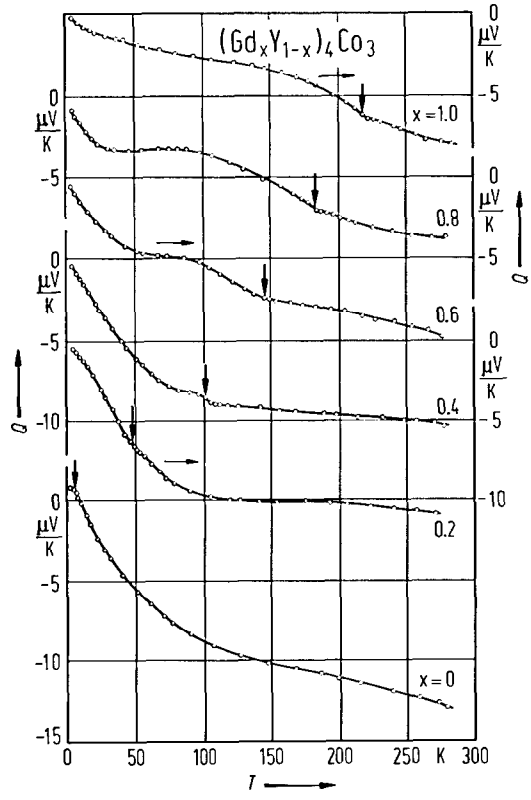

Fig. 60. Thermopower, Q, as function of temperature and Gd-concentration in $(Gd_xY_{1-x})_4Co_3$. The Curie temperatures are indicated by arrows [80 G 11]. A pronounced influence of the magnetic order is observed. In the high-Gd concentration range in particular, the Curie temperatures are manifested by a change in slopes of Q vs. T curves. It is suggested that the thermopower of these materials has contributions from the effect of the pure Co 3d matrix in Y_4Co_3 and from the admixture of the 4f moments which give an additive contribution arising from scattering processes of conduction electrons on these more or less perfectly ordered materials.

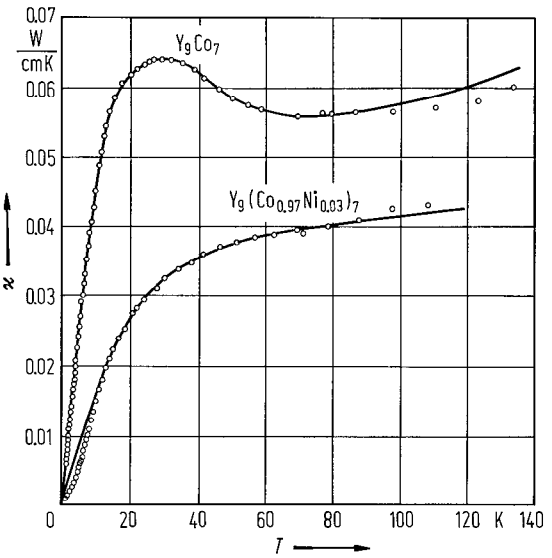

Fig. 61. Thermal conductivity $\varkappa$ of Y_9Co_7 and $Y_9(Co_{0.97}Ni_{0.03})_7$ samples. On cooling Y_9Co_7 from high temperatures, $\varkappa$ decreases and shows a minimum at $\cong 80$ K, before it passes through a maximum at $\cong 20$ K. This resembles the behaviour of $\varkappa$ in metallic superconductors and is strongly related to the high-T anomaly in $\varrho(T)$ and $Q(T)$ of Y_9Co_7. In Ni-doped specimen, the high-T anomaly of $\varkappa$ is much reduced and smeared out in comparison with Y_9Co_7 [86 S 5]. By solid lines are plotted the relation $\varkappa^{-1}=\alpha T^{-1}+\beta T^{-2}\cdot\exp[-(T_0/a_0T)^{1/2}]+\gamma T^{1/2}$, where α, β and γ are scattering parameters due to stacking faults, local modes and ordinary phonons, respectively. The a_0 is a parameter that characterises the dispersion in the frequency spectrum of the local modes, and T_0 is the effective characteristic temperature which determines the crossover between the region dominated by strong and weak temperature dependences.

For electrical resistivity see
Y_4Co_3 [80 G 9, 80 K 13, 82 V 2, 83 L 2, 83 S 25]
Y_9Co_7 [82 S 4, 83 H 5, 83 S 4, 84 K 7, 85 S 4, 86 S 3, 87 A 5]
$(GdY)_4Co_3$ [80 G 8, 80 G 11, 81 G 14]
$Gd_4(CoNi)_3$ [82 G 8]

For thermopower studies see
Y_4Co_3 [80 G 9, 81 G 10]; Gd_4Co_3 [81 G 10]; Y_9Co_7 [85 S 4, 86 S 3]
$(GdY)_4Co$ [80 G 11]; $Gd_4(CoNi)_3$ [82 G 8]

For superconducting properties see
Y_4Co_3 [81 G 12, 81 S 3, 82 C 6, 82 N 1]
Y_9Co_7 [82 S 3, 82 S 4, 82 S 5, 82 S 6, 83 G 13, 83 H 5, 84 C 2, 84 K 7, 84 N 1(T), 84 S 1, 84 S 2, 84 Y 4, 84 Y 5, 85 R 8, 86 S 4]
$(YR)_9Co_7$, R = Zr, Sc, Lu [86 Y 3]; $(YGd)_9Co_7$ [83 G 13, 84 S 1]
$Y_4(CoSi)_3$ [83 Y 8]; $Y_9(CoNi)_7$ [82 S 3, 83 G 13, 84 S 1]; $Y_9(CoMn)_7$ [84 S 1]

For thermal conductivity and specific heat
Y_4Co_3 [83 L 2]; Y_9Co_7 [83 K 3, 84 K 7, 84 O 4, 86 S 5]
$Y_9(Co_{0.97}Ni_{0.03})_7$ [86 S 5]

Magnetization processes

For magnetization processes see
Dy_4Co_3 [72 T 3]; Y_9Co_7 [86 R 5]

2.4.2.9 $RCo_{1-\varepsilon}(RCo_{0.85})$ compounds

Crystal structure

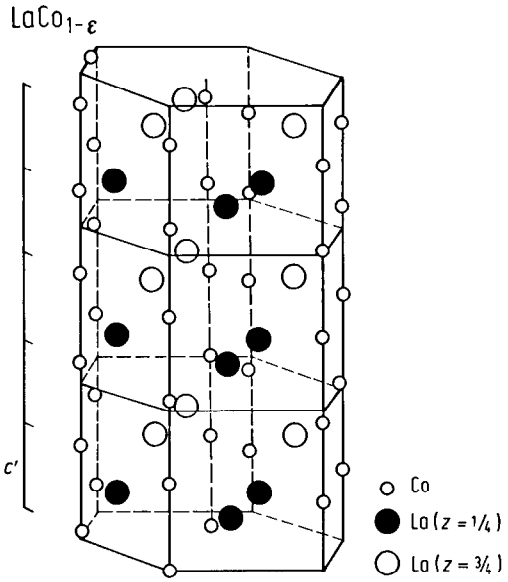

Fig. 62. Crystallographic structure of $LaCo_{1-\varepsilon}$ [86 B 4]. This consists of a skeleton of R ions forming an ABAB hexagonal packing and Co chains along the 6-fold axis. The smallest Co–Co distance, d_{CoCo}, in these chains is incommensurate with the c parameter of the R skeleton. Because of this peculiarity these compounds were denominated $RCo_{1-\varepsilon}$, where $1-\varepsilon$ is the half ratio of d_{CoCo} over c and depends on R ($(1-\varepsilon)=0.913$ with La and 0.863 with Nd) [87 B 5]. The distance between the chains is large compared to the Co–Co distance inside a chain and only weak correlations in the positions of Co atoms manifest themselves between these chains. Therefore Co has a quasi one-dimensional character.

Magnetic properties, neutron diffraction

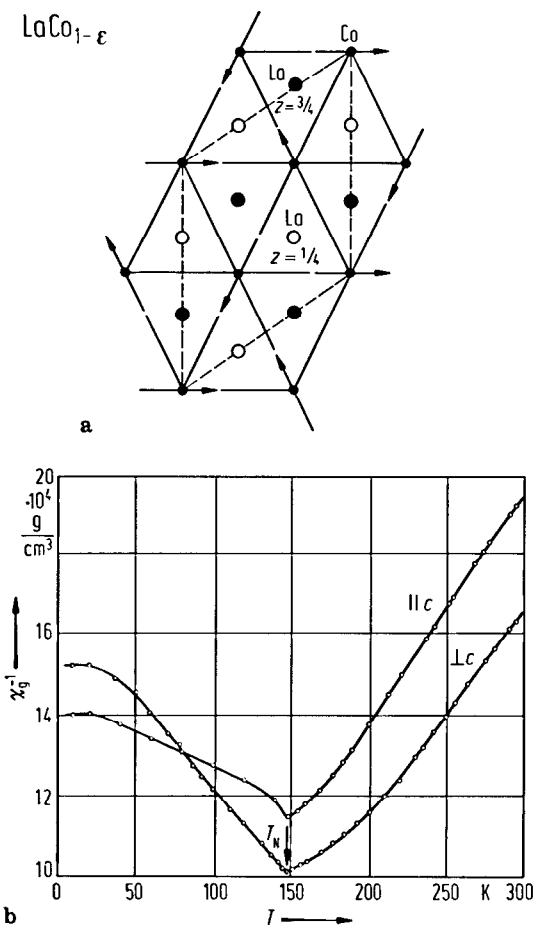

Fig. 63. (a) Magnetic structure of $LaCo_{1-\varepsilon}$ and (b) thermal variation of the reciprocal magnetic susceptibility, χ_g^{-1}, parallel and perpendicular to the chain axis (c axis) [85 G 10, 86 B 4, 87 B 1]. The compound is a basal-plane triangular antiferromagnet. The one-dimensional and compact arrangement of Co atoms is the origin of strong magnetic correlations which lead to ferromagnetism in the chains and the presence of Co magnetic moments. The triangular arrangement is ascribed to the frustration of negative exchange interactions between Co atoms of neighbouring chains. Because of the large interchain distances they originate from indirect Co–La–Co exchange through the 3d–5d hybridization. The χ_g^{-1} vs. T curves, at $T > T_N$, follow a Curie-Weiss behaviour, $\chi_g = \chi_0 + C_g(T-\Theta_{a,c})^{-1}$, with paramagnetic Curie temperatures along the a and c axes, $\Theta_a = -246$ K, $\Theta_c = -295$ K, respectively, and $\chi_0 = -2.2 \cdot 10^{-6}$ cm$^3 \cdot$ g^{-1}. At low temperatures the 6-fold axis appears as the easy-magnetization axis, but becomes a hard-magnetization axis at higher temperatures.

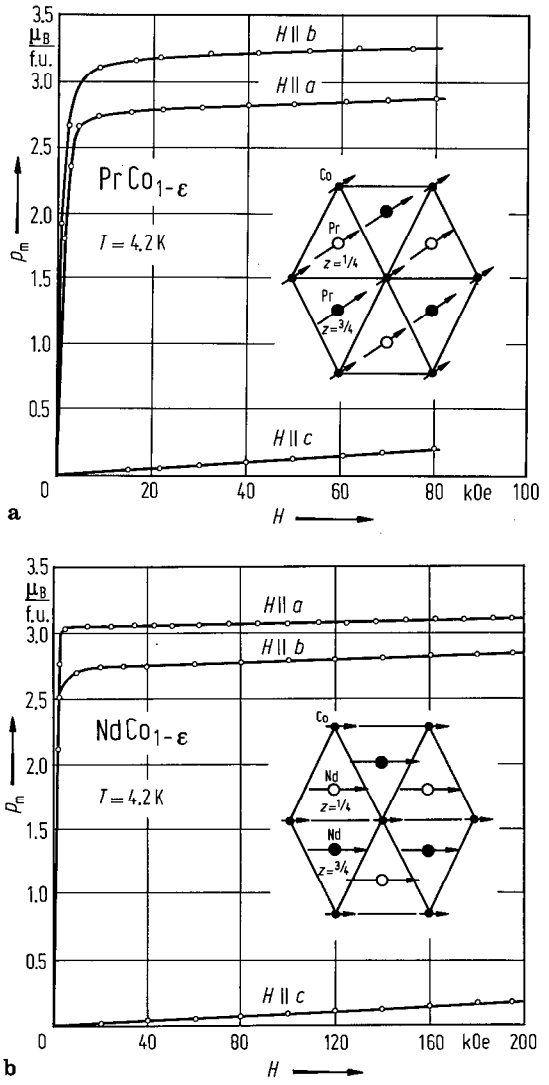

Fig. 64. Magnetization isotherms along the *a*, *b*, and *c* axes at 4.2 K and magnetic structures for $PrCo_{1-\varepsilon}$ (a) and $NdCo_{1-\varepsilon}$ (b) [86 B 4, 87 B 1]. Both compounds are collinear ferromagnets. The magnetic coupling between R (Pr, Nd) and Co is ferromagnetic and is responsible for parallel alignment of Co magnetic moments. High magnetocristalline anisotropy is evidenced between *c* axis and (*a*, *b*) plane, as well as in the (*a*, *b*) plane. The easy axes of magnetizations are the *b* and *a* axes for $PrCo_{1-\varepsilon}$ and $NdCo_{1-\varepsilon}$, respectively.

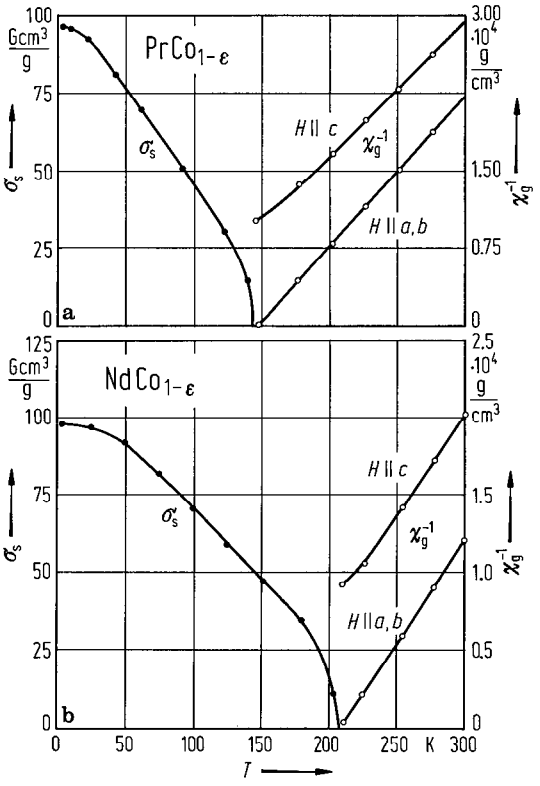

Fig. 65. Thermal variation of spontaneous magnetization and reciprocal magnetic susceptibility for $PrCo_{1-\varepsilon}$ (a) and $NdCo_{1-\varepsilon}$ (b) compounds. The anisotropy of the paramagnetic Curie temperature is 56 K for $PrCo_{1-\varepsilon}$ and 69 K for $NdCo_{1-\varepsilon}$ [87 B 1].

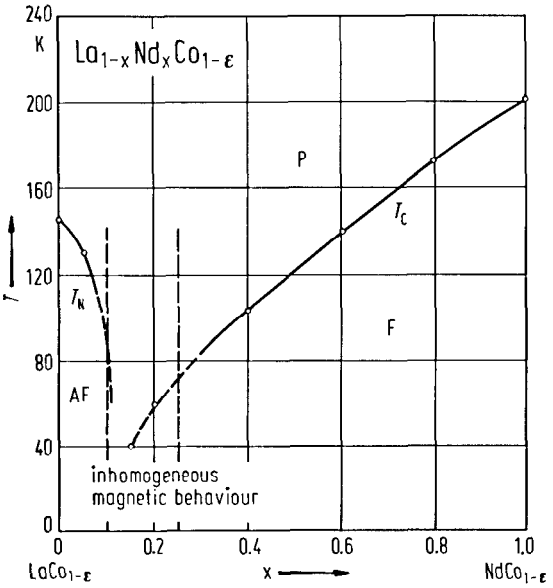

Fig. 66. Variation of the magnetic ordering temperature as function of Nd content in $La_{1-x}Nd_xCo_{1-\varepsilon}$ compounds [87 B 1]. The experimental results strongly suggest the occurrence of magnetic clusters in the composition range $0.10 \leqq x \leqq 0.25$.

Table 25. Physical properties of $RCo_{1-\varepsilon}$ compounds. Magnetic properties are from [85 G 10, 86 B 4, 87 B 1].

	[71 S 2]		[73 R 2]		[84 M 2, 85 G 10]						
	a Å	*c* Å	*a* Å	*c* Å	*a* Å	*c* Å	T_C K	T_N K	p_R [1] μ_B	p_{Co} [1] μ_B	p_{eff} μ_B/Co
$LaCo_{1-\varepsilon}$					4.890	4.312		146	–	0.7(1)	2.40
$PrCo_{1-\varepsilon}$	4.810	4.090	4.810(10)	4.090(20)			142		2.4(2)	0.7(2)	
$NdCo_{1-\varepsilon}$	4.790	4.070	4.795(2)	4.080(20)			202		2.8(2)	0.7(2)	

[1]) From neutron diffraction at $T = 4.2$ K.

Table 26. Crystal field parameters in the Hamiltonian $\mathcal{H}/k_B = 0.0672$ K/kOe $(H_{exch}+H)g_J\langle J\rangle + \sum_{nm} B_n^m O_n^m$ of $RCo_{1-\varepsilon}$ compounds [87 B 1].

	$PrCo_{1-\varepsilon}$	$NdCo_{1-\varepsilon}$
B_2^0 (K)	2.0	2.9
B_4^0 (K)	0.005	0.008
B_6^0 (K)	0.002	– 0.001
B_6^6 (K)	0.035	– 0.020
H_{exch} (kOe)	525	750

NMR

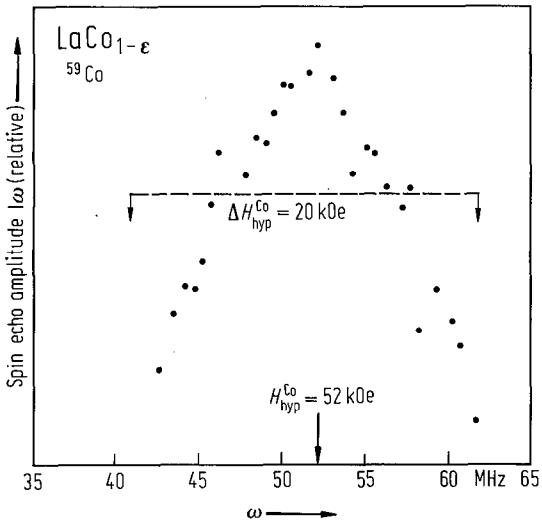

Fig. 67. ^{59}Co NMR spectrum in $LaCo_{1-\varepsilon}$ compound [87 B 1]. Because of the incommensurate structure, a large peak is shown. The relative spin and orbital contributions to the Co magnetic moment are estimated at 70% and 30%, respectively.

Table 27. Magnetic hyperfine fields at ^{59}Co in $RCo_{1-\varepsilon}$ compounds at $T=4.2$ K [87 B 1].

	H_{hyp} (kOe)
$LaCo_{1-\varepsilon}$	±52
$PrCo_{1-\varepsilon}$	3.5
$NdCo_{1-\varepsilon}$	8.7

Transport properties

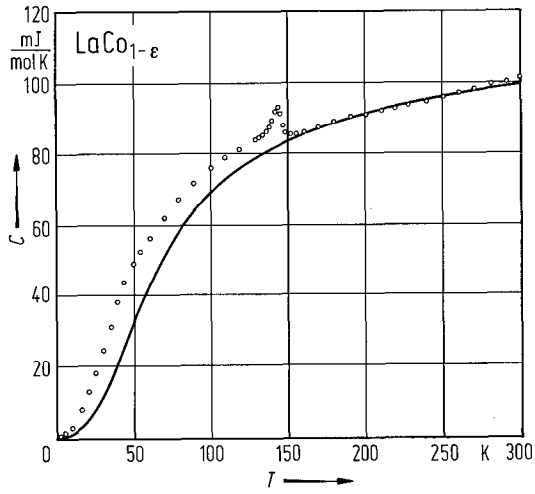

Fig. 68. Thermal variation of the specific heat in $LaCo_{1-\varepsilon}$ compound. By solid line the electronic and lattice contributions ($\gamma=35$ mJ mol^{-1} K^{-2} and $\Theta_D=270$ K) are plotted. A λ-type anomaly is evidenced at the Néel temperature, $T_N=146$ K. Below 150 K a large magnetic contribution to the specific heat is observed [84 M 2].

2.4.2.10 RNi compounds

Crystal structure, lattice parameters

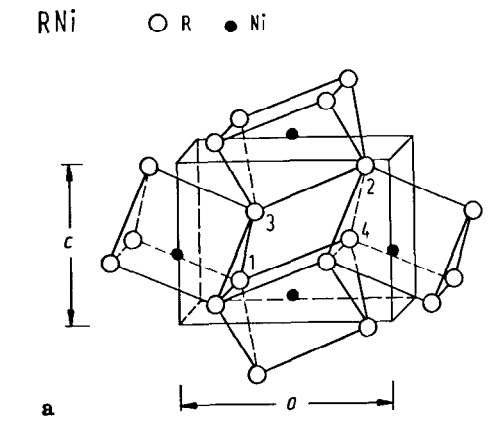

Fig. 69. (a) The crystal structure of RNi (R = Dy to Lu) compounds. This is orthorhombic of FeB-type, having Pnma space group [64 A 1]. There are four R and four Ni atoms in the unit cell, located in 4c-sites: 1: $(x, 1/4, z)$, 2: $(-x, -1/4, -z)$; 3: $(1/2-x, -1/4, 1/2+z)$ and 4: $(1/2+x, 1/4, 1/2-z)$. The RNi (R = La to Gd) compounds crystallize in a CrB-type structure (Cmcm-space group). TbNi shows dimorphism. The structure of the quenched sample, TbNi (h), is of Pnma-space group, while that of the annealed sample, TbNi(l), is of $P2_1/m$-space group. YNi crystallizes in orthorhombic structure having $P2_1/c$ space group. (b) The structure block relationship between the FeB, CrB and two TbNi structure types. The open circles are the R atoms. The solid circles are Ni atoms: (large circles) $-1/4$ sites; (small circles) $-3/4$ sites [74 G 3].

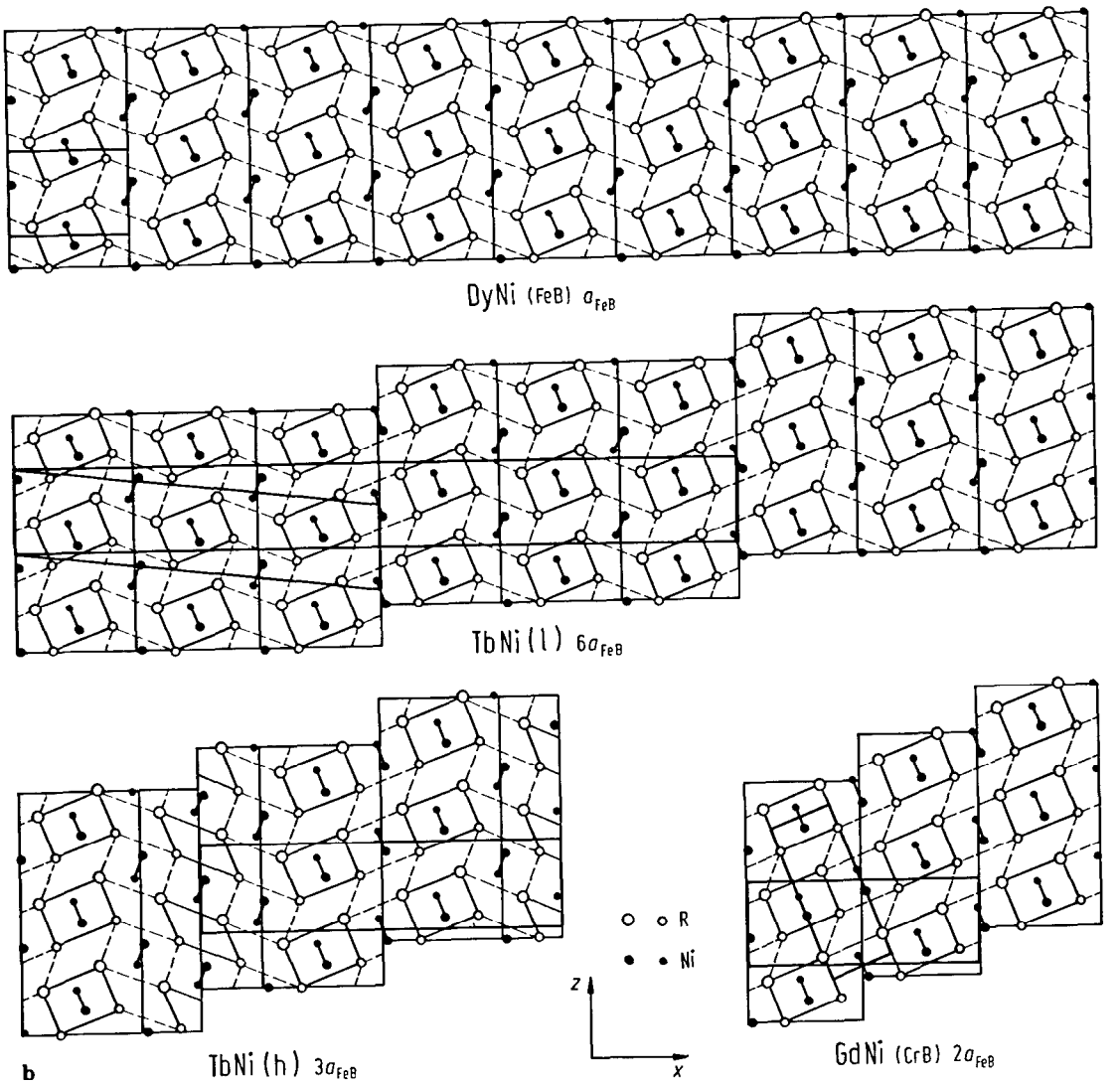

Table 28a. Lattice parameters of RNi compounds (Å), CrB-type structure (Cmcm-space group).

	64 A 1 [1]			64 W 3 [2]			65 D 2			69 P 1			86 G 6		
	a	*b*	*c*	*a*	*b*	*c*	*a*	*b*	*c*	*a*	*b*	*c*	*a*	*b*	*c*
LaNi	3.810(10)	10.62(3)	4.36(1)				3.907(1)	10.810(1)	4.396(1)	3.91	10.80	4.39	3.90	10.79	4.38
CeNi	3.733(8)	10.372(12)	4.286(8)	3.76	10.42	4.32	3.788(1)	10.556(1)	4.366(1)	3.77	10.54	4.36			
PrNi	3.817(3)	10.501(6)	4.347(4)	3.79	10.39	4.33	3.816(1)	10.503(1)	4.354(1)	3.81	10.51	4.35			
NdNi	3.801(3)	10.444(10)	4.338(4)	3.78	10.35	4.31	3.803(1)	10.461(1)	4.339(1)	3.80	10.47	4.34			
SmNi	3.772(1)	10.341(3)	4.270(2)	3.73	10.23	4.26	3.776(1)	10.358(1)	4.291(1)	3.77	10.37	4.28			
GdNi	3.764(1)	10.329(2)	4.242(1)	3.72	10.19	4.21	3.766(1)	10.316(1)	4.244(1)	3.76	10.30	4.24	3.81	10.32	4.21
TbNi	3.749(8)	10.260(2)	4.219(8)	3.70	10.10	4.19									

[1]) After [64 A 1] the RNi (R = Ho, Er, Tm, Y) crystallize also in a CrB-type structure. This fact has not been confirmed later [77 P 1].
[2]) Inaccuracy ±1%.

Table 28b. Lattice parameters of RNi compounds (Å), FeB-type structure (Pnma-space group).

	64 A 1			65 D 2 [1])			73 G 1			73 P 1		
	a	*b*	*c*	*a*	*b*	*c*	*a*	*b*	*c*	*a*	*b*	*c*
DyNi				7.043(1)	4.164(1)	5.451(1)	7.03	4.17	5.44			
HoNi	7.016(1)	4.143(1)	5.432(1)	7.022(1)	4.140(1)	5.435(1)	7.01	4.14	5.43			
ErNi	7.000(2)	4.118(1)	5.414(1)	6.991(1)	4.114(1)	5.418(1)	6.99	4.12	5.41			
TmNi	6.960(3)	4.100(2)	5.391(2)	6.959(1)	4.099(1)	5.398(1)	6.96	4.10	5.39			
YbNi										6.934	4.075	5.387
LuNi	6.910(2)	4.068(2)	5.362(6)	6.912(1)	4.073(1)	5.366(1)	6.91	4.07	5.36			

[1]) After [65 D 2] the YNi compound crystallizes also in a FeB-type structure. This statement is not in agreement with [77 P 1].

Table 28c. Lattice parameters of RNi compounds (Å), other structure types.

	Space group	73 G 1				65 S 1			
		a	*b*	*c*	*β*	*a*	*b*	*c*	*β*
TbNi(h)	Pnma	21.09	4.22	5.45					
TbNi(l)	$P2_1/m$	21.26	4.21	5.45	97°25′				
YNi	$P2_1/e$					4.114	7.140	5.501	90°

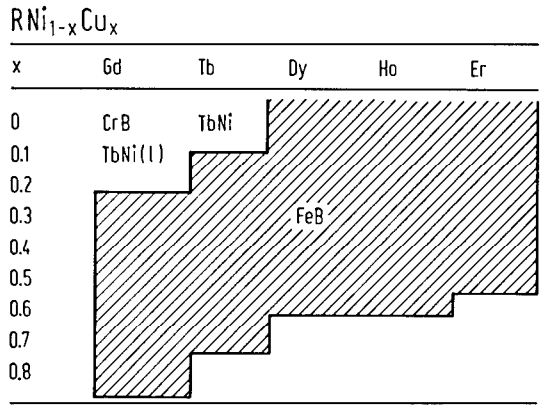

Fig. 70. Stability range of FeB-type structure in the $RNi_{1-x}Cu_x$ (R = Gd, Tb, Dy, Ho and Er) compounds [76 G 2]. The FeB-lattice is stabilized if 10 at% of Tb is replaced by smaller Y atoms or 10 at% of Ni atoms are substituted by greater Cu ones. For 65 at% Cu the diffraction lines become larger and for 85 at% Cu a CsCl-type structure appears (of TbCu-type).

For crystal structure and lattice parameters see

RNi [64 A 1, 69 P 1]; R = Ce, Pr, Nd, Sm, Gd, Tb, Dy, Ho, Er, Tm, Y [64 W 3]; R = Pr, Nd, Sm, Gd, Dy, Ho, Er, Tm, Lu, Y [65 D 2]; R = Tb, Dy, Ho, Er, Tm [73 G 2]; R = Ce [61 F 1]; R = Gd [72 U 1]; R = Tb [70 L 1, 76 P 1]; R = Y [65 S 1]

$RNiH_x$ R = La, Er, Yb [83 E 1]; R = La [78 B 18]

(R′R″)M (CeLa)Ni [86 I 5]; (GdDy)Ni [80 K 11]; (GdY)Ni [80 K 11]; (TbY)Ni [73 G 1]

R(M′M″) R(NiCu), R = Gd, Tb, Dy, Ho, Er [76 G 2]; R = Tb [73 G 1]; R = Yb [79 I 1]; La(NiPt) [84 G 1]; Ce(NiPt) [84 G 1, 87 G 4]

For thermal expansion see

RNi R = Ce [83 G 3a, 85 C 7, 86 C 10, 87 G 3, 87 G 5]; R = La [86 C 10, 87 G 5]

For hydrogen absorption and desorption see:

$RNiH_x$ R = La, Er, Yb [83 E 1]; R = La [78 B 18, 78 B 19]

Table 29. Magnetic properties of RNi compounds.

	T_C(K)				$p_s(\mu_B$/f.u.)				Θ(K)		$p_{eff}(\mu_B$/f.u.)		
	64 A 1	64 W 3	72 B 14	73 G 1	64 A 1 [3])	64 W 3 [1])	72 B 14	73 G 1	64 W 3	72 B 14	64 A 1	64 W 3	72 B 14
LaNi	Pauli paramagnet [64 A 1] $\chi_m = 1.5 \cdot 10^{-4}$ cm^3 mol^{-1} [86 G 6]												
CeNi	Pauli paramagnet [64 A 1, 64 W 3]												
PrNi	20	22			2.33	2.07			23		3.60	3.9	
NdNi	35	28		27	2.22	2.65			24		3.20	3.7	
SmNi	45	45			0.33	0.21							
GdNi	73	71	73		7.22	7.25	7.00		77	76	8.30	8.1	8.01
TbNi	50	52			8.00	6.49			40		9.74	9.7	
DyNi	48	62			7.80	8.54		6.3 [2])	64		10.75	10.7	
HoNi	31	37			9.30	8.32		6.9 [3])	36		10.60	10.7	
ErNi	10	13		13		7.58			13			9.8	
TmNi	4	8		7	5.30	4.72		4.1 [4])			7.60		
YbNi	Pauli paramagnet [64 A 1]												
LuNi	Pauli paramagnet [64 A 1]												
YNi	Pauli paramagnet [64 A 1]												

1) Saturation magnetic moment at 4.2 K in fields of 21 kOe.
2) Determined in a field of 21 kOe.
3) Determined in a field of 70 kOe.
4) At 1.5 K in a field of 20 kOe.

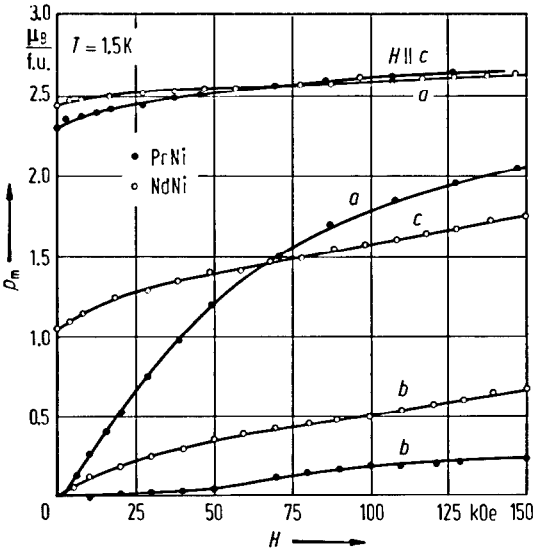

Fig. 71. Magnetization isotherms at 1.5 K for PrNi and NdNi single crystals for magnetic fields applied along the three principal crystallographic directions [84 F 2]. The easy direction of magnetization for PrNi is the *c* axis. For NdNi the spontaneous magnetization lies in the (*ac*) plane. At 1.5 K the magnetic moment for PrNi is 2.35 μ_B/f.u. For NdNi a value of 2.66 μ_B/f.u. was determined. The angle φ with the *a* direction is 23.5(5)°.

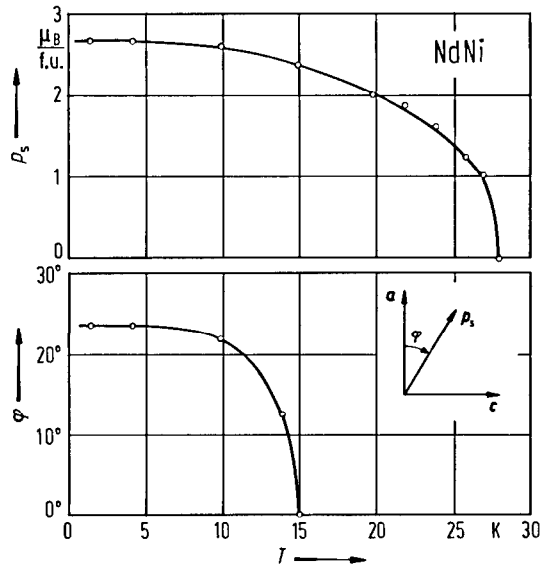

Fig. 72. Thermal variation of the spontaneous magnetization for a NdNi single crystal and of the angle φ of p_s with the *a* direction [84 F 2]. As temperature is increased, the spontaneous magnetization component along *c* decreases more rapidly than along *a* and disappears completely at 15 K, the *a* axis becoming the easy axis.

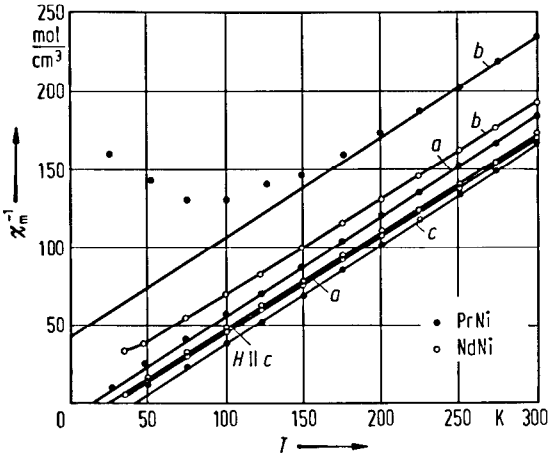

Fig. 73. Thermal variation of the reciprocal magnetic susceptibilities for PrNi and NdNi compounds along the three principal crystallographic directions [84 F 2]. For PrNi the susceptibility variations for fields applied along the *c* and *a* axis follow a Curie-Weiss law with identical slopes corresponding to the effective moment of the Pr^{3+} ion, $p_{eff} = 3.58\ \mu_B$/Pr. The χ_m^{-1} vs. *T* curve for fields applied along the *b* axis is not monotonous, but above 250 K this is linear having the same slope as previously mentioned. The paramagnetic Curie temperatures are $\Theta_c = 41$ K, $\Theta_a = 13$ K, and $\Theta_b = -67$ K. Similar χ^{-1} vs. *T* dependences are observed for the NdNi compound. The slopes of linear portions correspond to $p_{eff} = 3.62\ \mu_B$/Nd. The paramagnetic Curie temperatures are $\Theta_a = 27$ K, $\Theta_c = 25$ K, and $\Theta_b = -9$ K.

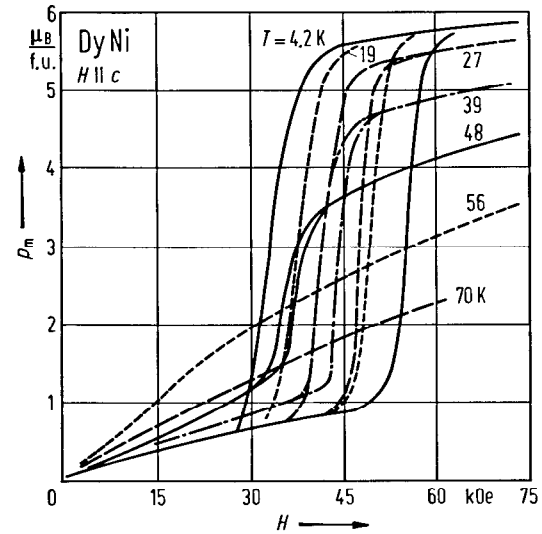

Fig. 74. Magnetization isotherms for a DyNi single crystal along the *c* axis. A drastic change at 4.2 K due to the spin flopping at about 50 kOe is observed [86 S 6]. For ErNi the critical field at 4.2 K is ≅ 5 kOe. The critical fields decrease by increasing temperature.

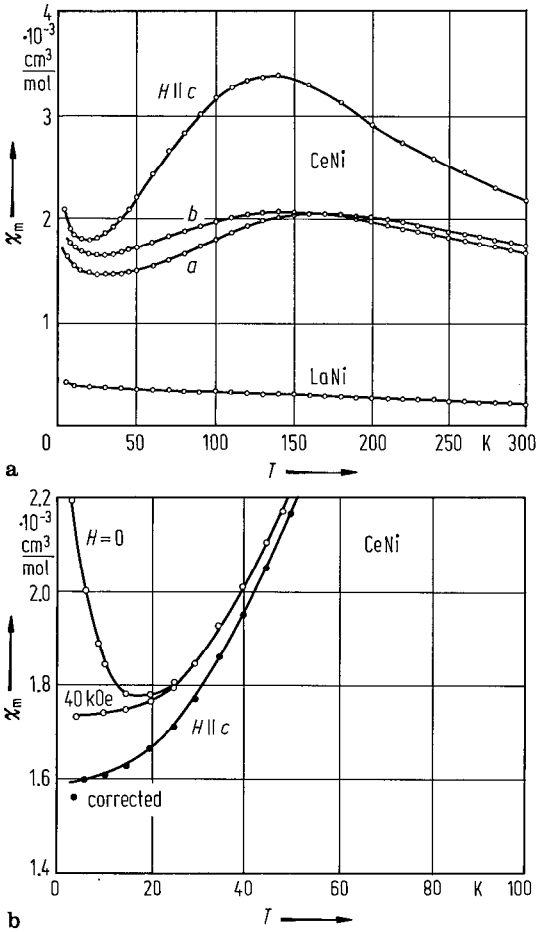

Fig. 75. (a) Thermal variations of the initial magnetic susceptibilities of a CeNi single crystal along the three principal crystallographic directions and of a LaNi polycrystalline sample. In(b) the variations at low temperatures of the CeNi differential c axis susceptibilities in zero magnetic field, in a field of 40 kOe, and corrected for a C/T term with $C = 2.3 \cdot 10^{-3}$ cm^3 K mol^{-1} [84 F 2, 87 G 5]. CeNi is an enhanced paramagnet in which the magnetic susceptibility passes through a maximum at about 140 K. This behaves as an anisotropic magnetic Fermi liquid in which the spin fluctuations are mainly longitudinal due to the crystal field effects. The magnetic susceptibility of LaNi is mainly independent of temperature.

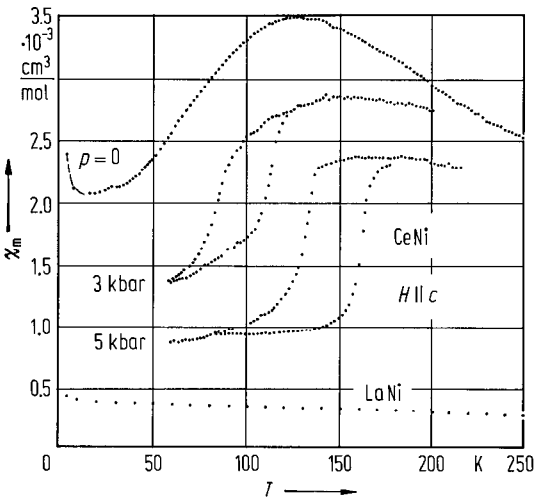

Fig. 76. Thermal variations of the magnetic susceptibility of CeNi measured along the c axis at ambient pressure and under 3 and 5 kbar, and thermal variation of the magnetic susceptibility of a polycrystalline sample of LaNi at ambient pressure [87 G 3]. Magnetization, electrical resistivity, and thermal expansion measurements under hydrostatic pressure show the existence of a first-order phase transition associated with a large decrease of the magnetic susceptibility, an increase of the electrical conductivity and a huge lattice change. This lattice change is, as for the other properties of this compound, strongly anisotropic and corresponds to a 4.6% decrease of the volume. The $p-T$ phase diagram of this transition shows that the variation of p at the transition is quadratic versus temperature and indicates the existence at 0 K of a critical pressure of 1.3 kbar. The strong anisotropy of the transition, on the lattice parameter, can be associated to the covalent character of the Ce–Ni hybridization responsible for the intermediate valence of Ce.

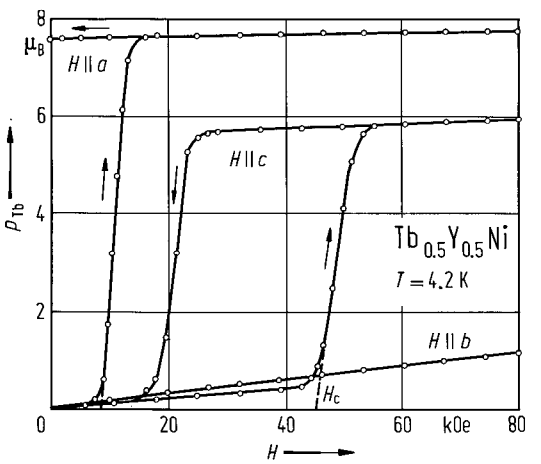

Fig. 77. Magnetization isotherm at 4.2 K along the a, b, and c axis in $Tb_{0.5}Y_{0.5}Ni$ single crystal [73 G 1, 74 G 3]. The field dependence of the magnetization along the a axis is typical of a metamagnetic behaviour (critical field $H_c = 45$ kOe). By decreasing the field, the transition shows a hysteresis, the critical field being 18.8 kOe. The magnetization along the b axis is linearly dependent on field up to $H = 8.8$ kOe and then a sudden increase occurs.

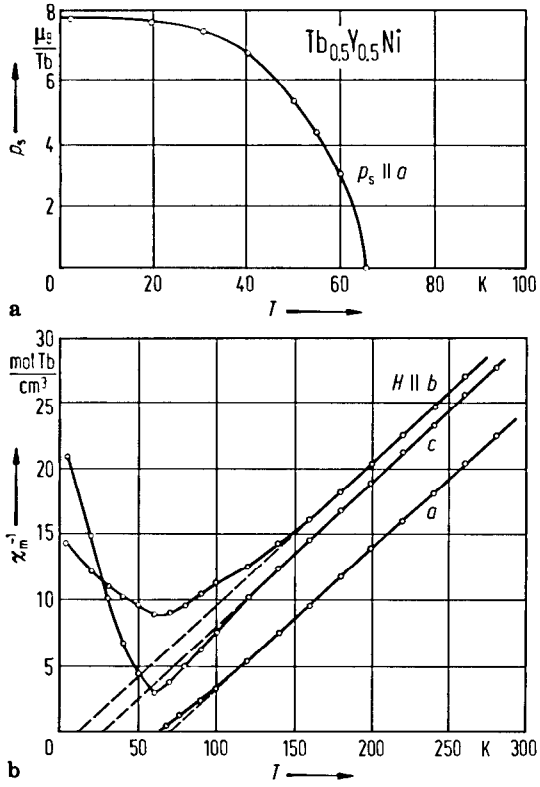

Fig. 78. Temperature dependences of (a) the spontaneous magnetization along the a axis and (b) the reciprocal magnetic susceptibilities χ_m^{-1} for a $Tb_{0.5}Y_{0.5}Ni$ single crystal. The χ_m^{-1} vs. T curves along the principal crystallographic axes are different due to great second-order anisotropy. The paramagnetic Curie temperatures are $\Theta_a = 70$ K, $\Theta_b = 11$ K, and $\Theta_c = 27$ K. The Curie temperature is $T_C = 66$ K [73 G 1, 74 G 3].

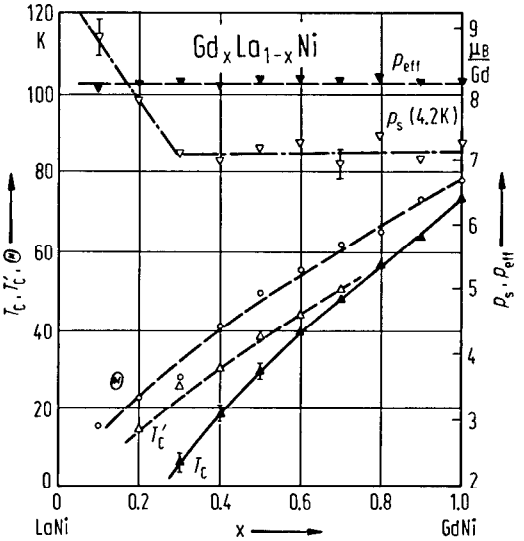

Fig. 79. Composition dependences of the Curie temperatures obtained from initial magnetic susceptibilities, T_C, and Arrott plots, T_C', paramagnetic Curie temperature, Θ, saturation magnetization, p_s, at 4.2 K (and $\mu_0 H = 7$ T) and the effective moment, p_{eff}, in $Gd_xLa_{1-x}Ni$ compounds [86 G 6]. Long-range ferromagnetic order exists for the composition range $0.3 \leqq x \leqq 1.0$.

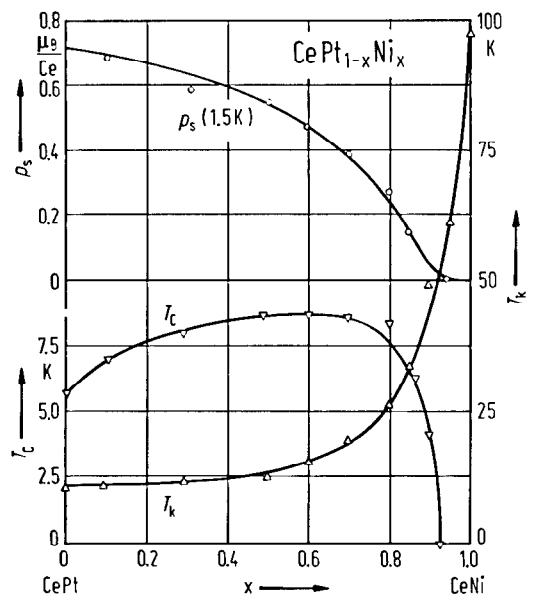

Fig. 80. Curie temperatures T_C, Kondo temperatures T_K and saturation magnetizations p_s extrapolated to zero internal magnetic field at 1.5 K in $CeNi_xPt_{1-x}$ compounds, as function of the Ni content [84 G 1, 85 G 6]. For $CeNi_{0.95}Pt_{0.05}$ and CeNi compounds, which are Pauli paramagnetic and intermediate valence compounds, it is not possible to define a Kondo temperature. In this case were reported half of the paramagnetic Curie temperatures, $\Theta/2$, which well extend the variation of T_C of the ferromagnetic compounds. The substitution of Ce by La in $CeNi_xPt_{1-x}$ leads to a decrease of the Curie temperature, T_C, and hence to an enhancement of the Kondo character in the thermal dependence of the electrical resistivity [87 G 4].

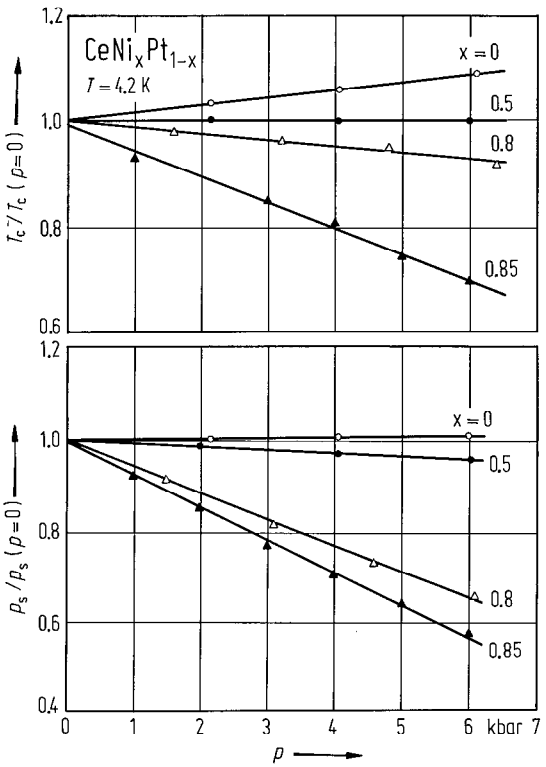

Fig. 81. Pressure dependence of the relative Curie temperatures and spontaneous magnetizations at 4.2 K for $CeNi_xPt_{1-x}$ compounds with $x \leqq 0.85$. The large pressure effects observed for ferromagnetic alloys ($x \leqq 0.9$) are consistent with the Kondo lattice model [86 G 2].

For magnetic properties see also:

RNi [69 P 1]; R = Ce, Pr, Nd, Sm, Gd, Tb, Dy, Ho, Er, Tm, Y [64 W 3]; R = Ce, Pr, Nd, Gd, Tb, Dy, Ho, Er, Tm [70 B 2]; R = Nd, Tb, Ho, [70 L 4]; R = Dy, Ho, Er, Tm [73 G 1, 74 G 3]; R = La [85 G 6, 85 G 9*, 87 G 5]; R = Ce [83 G 18, 84 F 2*, 85 C 7, 85 G 6, 85 G 7, 85 G 9*, 86 G 5, 87 G 3, 87 G 5]; R = Pr, Nd [84 F 2*]; R = Sm [85 I 7*]; R = Gd [80 S 1, 81 S 1*, 83 I 4*]; R = Dy [83 S 2, 86 S 6*]; R = Ho [81 M 12*, 82 S 7*, 82 S 8*, 83 S 3*]; R = Er [86 S 6*]; R = Tm [72 G 3*]

(R′R″)Ni (LaCe)Ni [86 I 5, 87 I 6]; (LaGd)Ni [86 G 6]; (GdY)Ni [78 C 1]; (TbY)Ni [73 G 1, 74 G 3, 74 G 5, 84 P 4]; (HoY)Ni [79 G 9]

R(M′M″) R(NiCu); R = Gd, Tb, Dy, Ho, Er [76 G 2]; R = Tb [71 B 5, 73 B 3, 73 G 1, 74 G 3]; R = Ho [79 G 8]; R = Yb [79 I 1]
La(NiPt) [84 G 1]; Ce(NiPt) [84 G 1, 85 G 6, 85 G 8, 86 G 2, 87 F 2, 87 G 4]; Gd(NiCo) [80 G 10]

$R(M'M'')H_x$ $Ce(NiCu)H_x$ [87 W 3]

Neutron diffraction

Table 30. Ferromagnetic moments of R atoms at 4.2 K determined by neutron diffraction in RNi compounds [74 G 3, 73 G 1].[1])

	p_s μ_B/R	φ [2]
NdNi	2.70(35)	25(5)°
DyNi	8.6(5)	29(2)°
HoNi	8.6(5)	25(2)°
ErNi	7.0(5)	61(2)°
TmNi	5.9(5)	52(2)°
$Tb_{0.5}Y_{0.5}Ni$	8.6	33°

[1]) The magnetic structures for ErNi and DyNi [73 G 1, 74 G 3] were confirmed [86 S 5]. In case of HoNi according to [82 S 7, 82 S 8, 83 S 3] in the temperature range $T_{c2}(15\,K) < T < T_{c1}(37\,K)$, the magnetic moments have ferromagnetic components along the *a* axis and antiferromagnetic components along the *c* axis. Below T_{c2} ferromagnetic components along the *b* axis occur and grow with decreasing temperature. At 4.2 K the direction of ferromagnetic components incline about 30° from the *a* axis in the (*ab*) plane. SmNi has a canted spin structure [85 I 7].

[2]) Angle between ferromagnetic moment and *a* axis.

Table 31. Magnetic structures and the magnetic moments in RNi compounds determined by neutron diffraction studies.

	T	Magnetic structure	Ref.
NdNi	4.2	The Nd moments ($p_{Nd}=2.70(35)\,\mu_B$) are parallel to (*a*, *c*) plane and make an angle $\varphi=25(5)°$ with *a* axis. The Ni moment is nil.	70 L 4
DyNi	4.2	Noncollinear magnetic structure. The ferromagnetic arrangement is of F_x-type and antiferromagnetic of C_z-type [1]). $p_{Ni}=0$ and $p_{Dy}=8.6(5)\,\mu_B$, the moments making an angle $\pm 29(2)$ with *a* axis.	74 G 3
HoNi	4.2	Noncollinear magnetic structure. The ferromagnetic arrangement is of F_x-type and antiferromagnetic of C_z-type. $p_{Ni}=0$ and $p_{Ho}=8.6(5)\,\mu_B$, the moments making an angle of $\pm 25(2)°$ with *a* axis.	74 G 3
HoNi	4.2	The magnetic arrangement is of $(F_xF_yC_z)$-type. $p_{Ni}=0$. The ferromagnetic components of Ho moments are $p_x=7.2\,\mu_B$, $p_y=4.2\,\mu_B$. The antiferromagnetic *z* component is $p_z=2.9\,\mu_B$. The angle with the (*a*, *b*) plane is 19.1°, and the angle of the projection in this plane with *a* axis is 30.7°.	84 I 7
	20	The magnetic arrangement is of (F_xC_z)-type. The *x* ferromagnetic component of Ho moment is $p_x=6.6\,\mu_B$ and the antiferromagnetic *z* component is $2.5\,\mu_B$. The angle with *a* axis is $\varphi_a=0$ and with (*a*, *b*) plane, $\varphi_{(a,b)}=20.8°$.	
ErNi	4.2	Noncollinear magnetic structure. The antiferromagnetic arrangement is parallel to *a* axis and may be described by C_x. The ferromagnetic component is parallel to *c* axis and shows a F_z arrangement. $p_{Ni}=0$, $p_{Er}=7.0(5)\,\mu_B$ and makes an angle of $\pm 61(2)°$ with *a* axis.	74 G 3
TmNi	1.3	Noncollinear magnetic structure. The antiferromagnetic arrangement is parallel to *a* axis and may be represented by C_x. The ferromagnetic component is parallel to *c* axis and shows a F_z arrangement. $p_{Ni}=0$, $p_{Tm}=5.9(5)\,\mu_B$ and makes an angle of $\pm 52(2)°$ with *a* axis.	74 G 3

[1]) The significations of F_x, F_z and C_z notations are $F_x=p_{1x}+p_{2x}+p_{3x}+p_{4x}$; $F_z=p_{1z}+p_{2z}+p_{3z}+p_{4z}$; $C_z=p_{1z}+p_{2z}-p_{3z}-p_{4z}$.

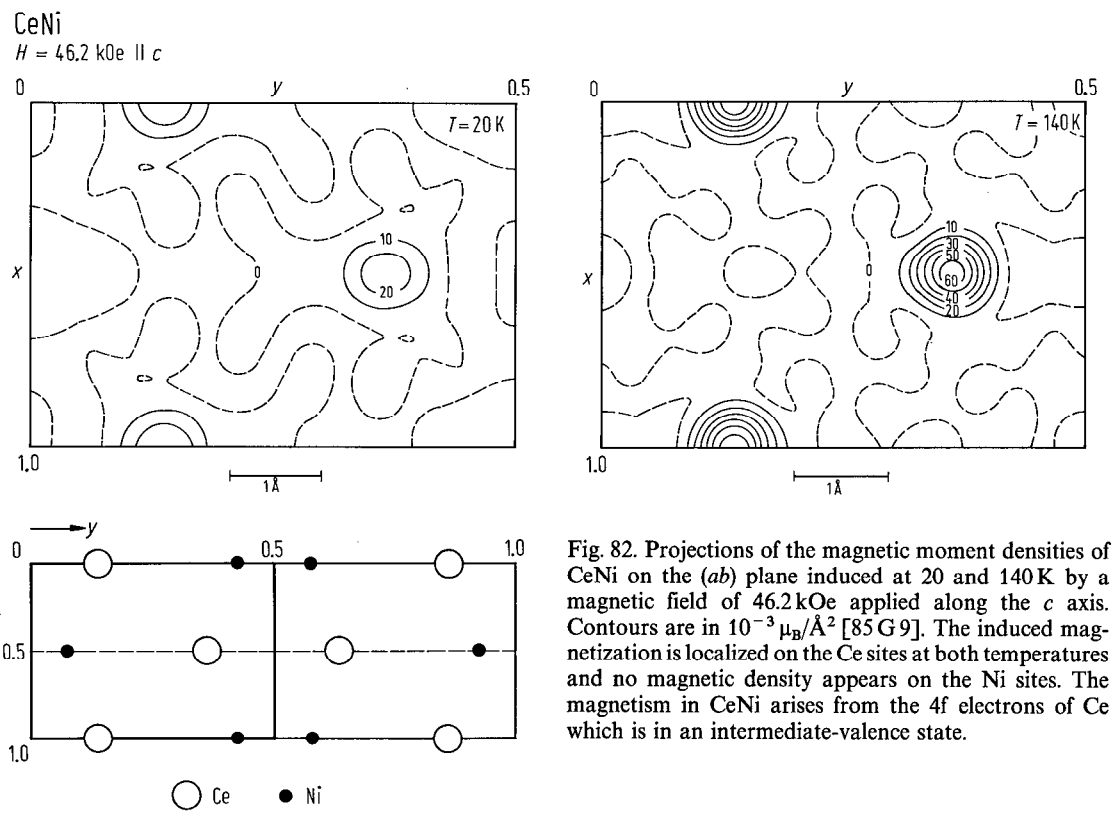

Fig. 82. Projections of the magnetic moment densities of CeNi on the (*ab*) plane induced at 20 and 140 K by a magnetic field of 46.2 kOe applied along the *c* axis. Contours are in $10^{-3}\,\mu_B/Å^2$ [85 G 9]. The induced magnetization is localized on the Ce sites at both temperatures and no magnetic density appears on the Ni sites. The magnetism in CeNi arises from the 4f electrons of Ce which is in an intermediate-valence state.

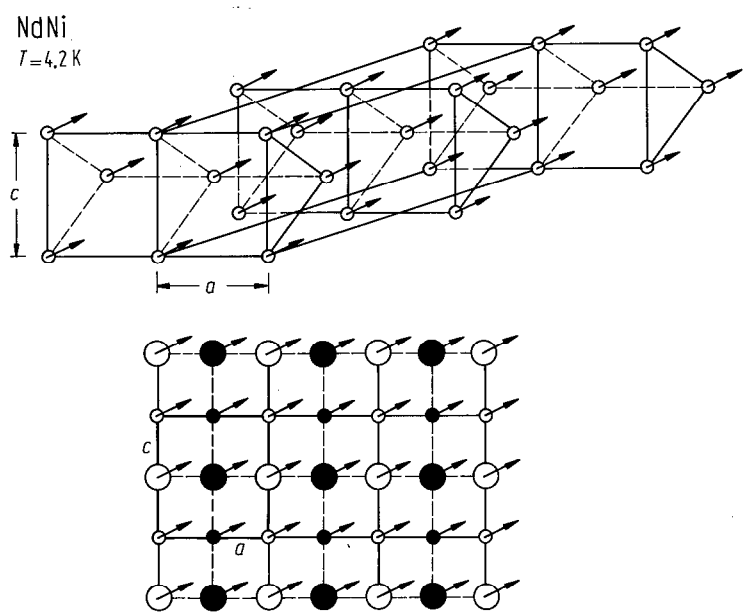

Fig. 83. Magnetic structure of NdNi at 4.2 K and projection on the (*ac*) plane. The magnetic moments of the given site are parallely oriented (see Table 32) [69 P 1, 70 L 4]. The large/small open and solid circles are Nd atoms in two successive prisms. The larger circles indicate atoms in the front planes of the prisms.

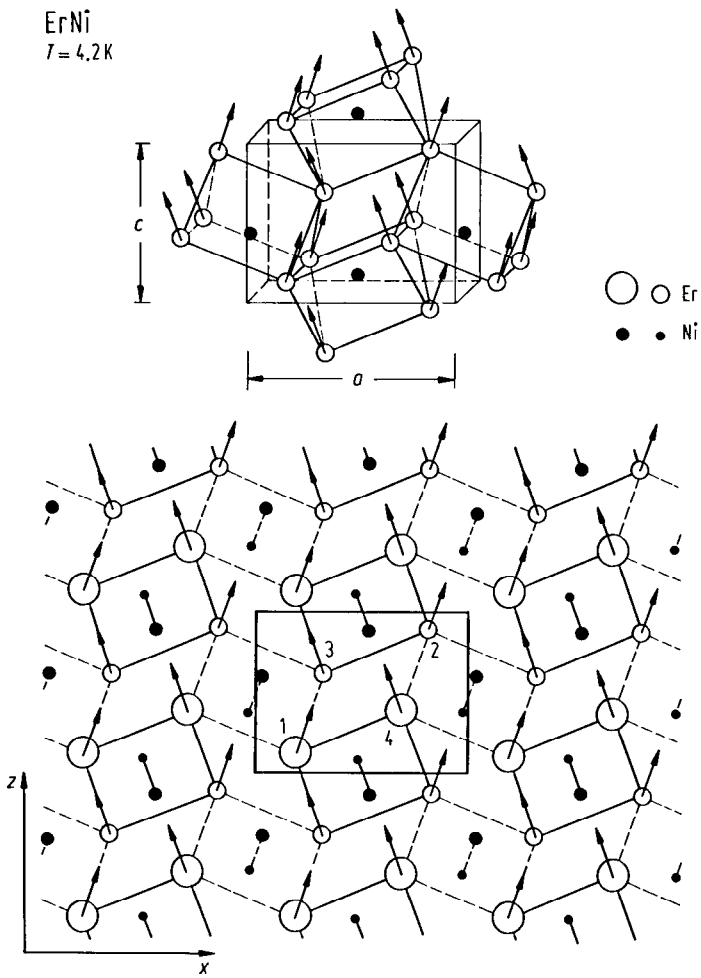

Fig. 84. Magnetic structure of ErNi at 4.2 K and projection on the (*ac*) plane. The structure belongs to Pnma space group. Large circles: 1/4 sites, small circles: 3/4 sites. Ni has no magnetic moment. The magnetic moment of Er atoms and their directions are given in Tables 30 and 31 [70 L 4, 73 G 1]

Table 32. Magnetic structures determined in some $RNi_{1-x}Cu_x$ compounds [74 G 3, 76 G 2].

	T K	Magnetic structure	Propagation vector	Periodicity Å	p_{max} μ_B	φ [1]
$TbNi_{0.6}Cu_{0.4}$	1.3	sinusoidal	$0.136b^*$	32.0	7.9(5)	38(2)°
$HoNi_{0.5}Cu_{0.5}$	1.3	sinusoidal	$0.254c^*$	21.1	8.8(5)	36(2)°
$ErNi_{0.6}Cu_{0.4}$	4.2	sinusoidal	$0.143b^*$	30.1	7.2(5)	44(2)°
$ErNi_{0.6}Cu_{0.4}$	1.3	antiphase	$0.143b^*$ $0.429b^*$	30.1	7.0(5)	44(2)°
$Tb_{0.5}Y_{0.5}Ni$	4.2	DyNi-type	–	–	9.0(5)	±33°

[1]) Angle between R magnetic moment and *a* axis.

Fig. 85. Magnetic structures of $ErNi_{0.6}Cu_{0.4}$ and $HoNi_{0.5}Cu_{0.5}$ at 4.2 K. For $ErNi_{0.6}Cu_{0.4}$ the propagation vector Q at 4.2 K is parallel to the b axis ($Q = 0.143b^*$). The magnetic cell is incommensurate with the crystallographic one, its periodicity in the b direction being $6.9b$. The magnetic arrangement is noncollinear; it has a ferromagnetic component parallel to c and an antiferromagnetic component parallel to a. From one cell to the other the magnetic moments have a sinusoidal variation with distance in the b direction. The maximum magnetic moment on the Er atoms is 7.2(4) μ_B. The angle φ_a between the moments and the a axis is 44(2)°. Below 1.5 K the modulated structure transforms into an antiphase structure, with periodicity $1/Q$. The arrangement in the chemical cell and the periodicity are the same as at 4.2 K, but all the moments have become equal. The magnetic moment on Er atoms is 7.0(5) μ_B and the angle φ_a is the same as at 4.2 K. In case of $HoNi_{0.5}Cu_{0.5}$ the propagation vector is parallel to c ($Q = 0.254c^*$). The magnetic structure is modulated, the periodicity in the c direction is $3.9c$. The magnetic arrangement is noncollinear; it has a ferromagnetic component parallel to a and an antiferromagnetic component parallel to c. The maximum magnetic moment on Ho atoms is 8.8(4) μ_B and makes an angle $\varphi_a = 36(8)°$ with the a axis. This modulated structure is stable at very low temperature. The noncollinearity of the structures results from the crystal field effects on the rare earths which lie in low-symmetry sites. The principal directions of the quadrupole surroundings are not parallel to the crystallographic axes. The R atoms are then divided into two sublattices with different easy directions of magnetization. Replacing Ni by Cu in RNi compounds, where magnetic interactions are strongly positive, introduces negative interactions. The competition between these interactions gives rise to the observed modulated structures. The thermal stability of the magnetic moment modulation depends on the nature of the R ion. In the compounds with Kramers rare-earth ions (as Er), the modulated structure is stable only in the vicinity of T_C and transforms at low temperature into an antiphase structure in order to decrease the entropy. In compounds with non-Kramers ions (as Ho), no entropy can be associated with the modulation of the p_R moment because of the low symmetry, the crystal field splits completely the multiplets, the ground state is a singlet. However, the exchange field induces a magnetic moment. The magnetic moment modulation results from a modulation of exchange field. Thus the observed modulation can remain stable down to 0 K [74 G 4, 76 G 2].

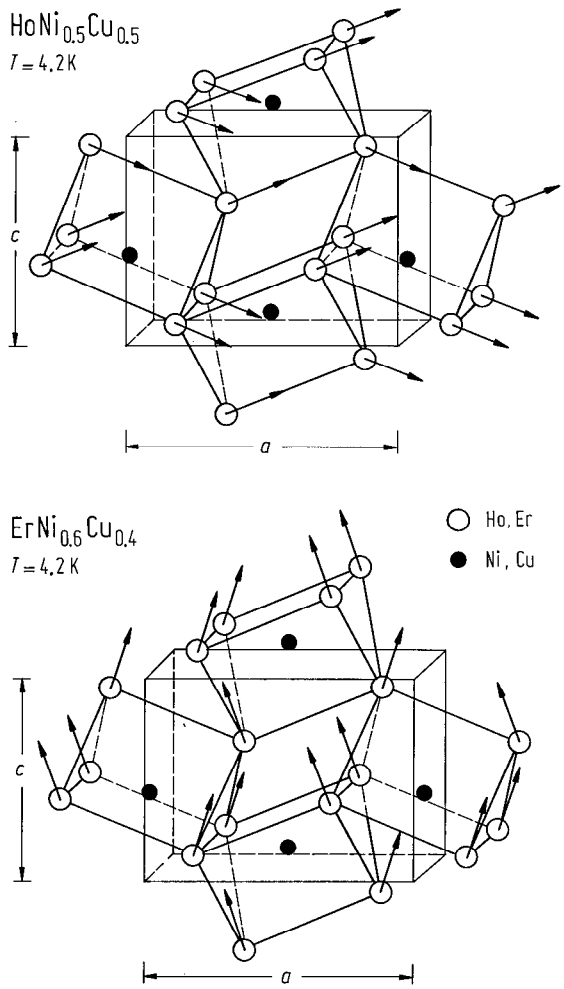

For neutron diffraction studies see also:

RNi [69 P 1]; R = Tb, Dy, Ho, Er, Tm [73 G 2]; R = La [85 G 9*]; R = Ce [85 G 9*]; R = Nd [70 L 4]; R = Dy [72 G 1, 73 B 3, 74 G 3]; R = Ho [70 B 2, 70 L 4, 74 G 3, 84 I 7*]; R = Er [70 B 2, 70 L 4, 74 G 3]; R = Tm [72 G 3*, 73 B 3, 74 G 3]

(R′R″)Ni (TbY)Ni [73 G 1, 74 G 3, 74 G 5]

R(NiCu) R = Gd, Tb, Dy, Ho, Er [76 G 2]; R = Tb [72 G 2, 73 B 3, 73 G 1, 74 G 3]; Er(NiCu) [74 G 4]

For inelastic neutron scattering see

CeNi [85 G 11]

Mössbauer effect

For nuclear γ-resonance studies ^{155}Gd see GdNi [85 D 5]. For ^{161}Dy in DyNi see also Table 59; ^{57}Fe in $TiFeH_x$ [80 B 8]

FMR, EPR

For EPR and FMR studies see Gd Ni [72 U 1, 80 B 15]

NMR

For NMR studies see ^{139}La in (GdLa)Ni [77 D 7]

Anisotropy, magnetostriction

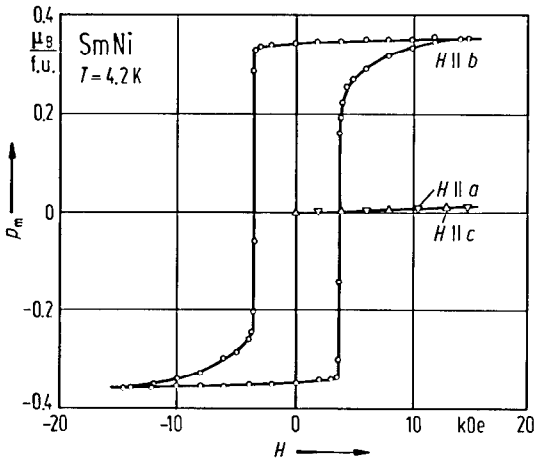

Fig. 86. Magnetization curves of SmNi at 4.2 K along the *a*, *b* and *c* axis. The anisotropy constant was estimated to be 10^7 erg cm^{-3} [85 I 7]. The anisotropy constants of GdNi at 4.2 K are $K_1 = 4.0 \cdot 10^6$ erg cm^{-3} and $K_3 = -2.7 \cdot 10^6$ erg cm^{-3} [81 S 1].

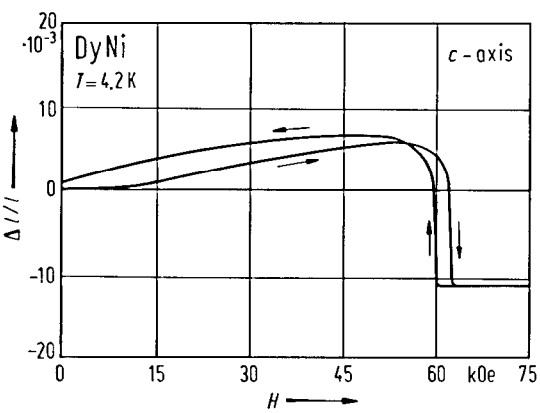

Fig. 87. Magnetic field dependence of the longitudinal magnetostriction at 4.2 K, along the *c* axis of a DyNi single crystal. Below about 50 kOe, Δl/l shows a positive and approximately linear field dependence with a slope of $12 \cdot 10^{-8}$ Oe^{-1}. A contraction due spin flopping is observed between about 50 and 62 kOe. Above 62 kOe, Δl/l values are constant and correspond to the saturation magnetization [86 S 6].

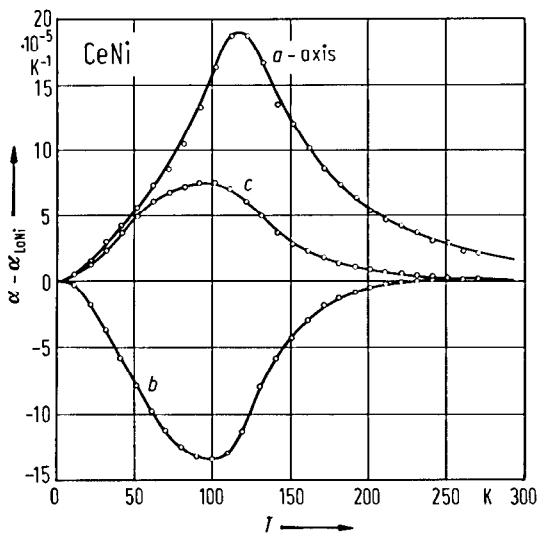

Fig. 88. Anomalous thermal expansion coefficients of CeNi in three crystallographic directions, obtained by subtracting the thermal expansion of LaNi [85 G 11]. The anisotropic dilatation of the lattice is correlated with the fact that the elastic constant c_{11} undergoes significant softening around 110 K, while c_{22} varies little with temperature.

For anisotropy see also:
CeNi [85 C 7]; GdNi [80 S 1*, 81 S 1*]; HoNi [81 M 12*, 82 S 8*]; Ce(NiPt) [87 F 2]

For spin reorientation see
HoNi [82 S 8*]; Ce(NiPd) [88 N 2]

For magnetostriction see also:
RNi CeNi [85 C 7, 86 C 10]; DyNi, ErNi [86 S 6*]

For elastic constants see
RNi CeNi [85 C 7, 85 G 11, 87 B 10]

Transport properties

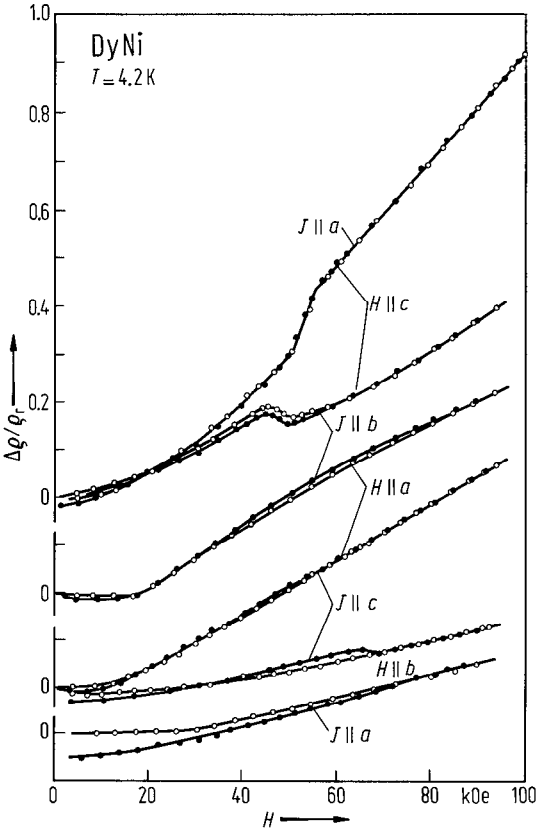

Fig. 89. Transverse magnetoresistance $\Delta\varrho/\varrho_r$ for DyNi single crystal at 4.2 K as function of applied field H for (open circles) increasing and (solid circles) decreasing H. The negative magnetoresistance was observed with a spin flopping of the magnetization along the c axis when the field was applied along the c axis and the current was parallel to the b axis. The negative magnetoresistance was not observed when the current was parallel to the a axis. The magnetoresistance increases monotonically with increasing magnetic induction. It was inferred that there are open orbits along the a and c axis [85 M 2].

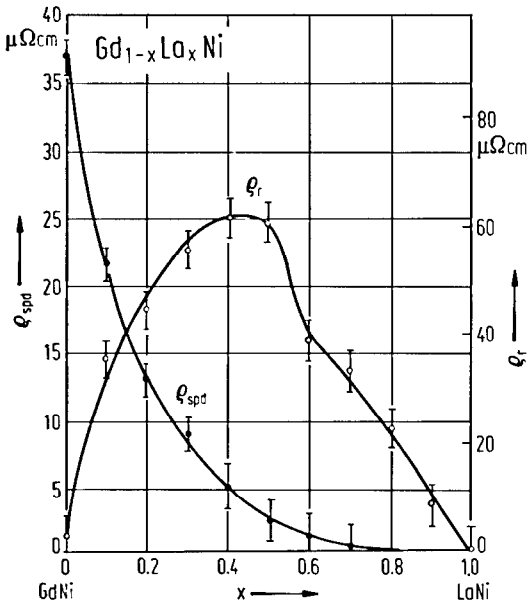

Fig. 90. Composition dependence of the residual electrical resistivity, ϱ_r, and spin-disorder electrical resistivity, ϱ_{spd}, in $Gd_{1-x}La_xNi$ compounds [80 G 10, 82 g 1]. The ϱ_{spd} values deviate from the parabolic shape predicted by Nordheim's rule. The asymmetrical shape indicates that additional spin-disorder scattering from domain walls contributed to the residual resistivity for increasing Gd concentration ($x \leq 0.6$). The magnetic contributions to the resistivity are given by the difference to the ϱ values of nonmagnetic isostructural LaNi.

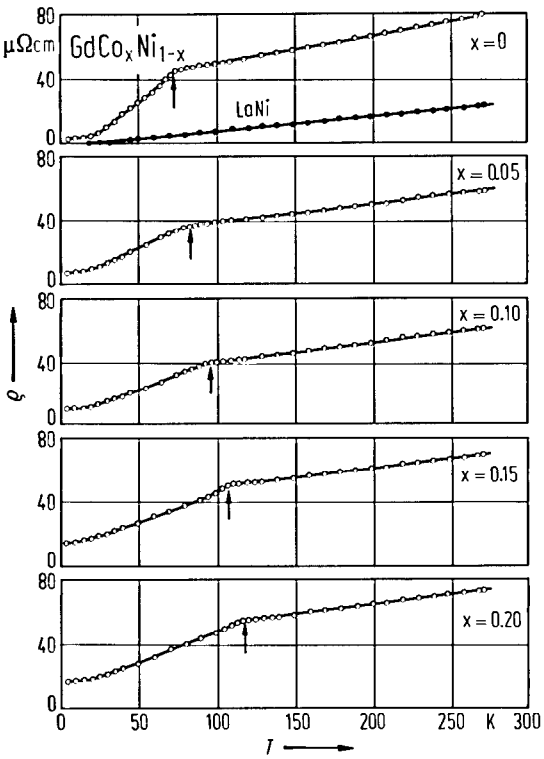

Fig. 91. Temperature dependence of the electrical resistivities in $GdCo_xNi_{1-x}$ system [80 G 10]. The ordering temperatures are indicated by arrows and increase with increasing Co content. The system is unstable for $x > 0.25$.

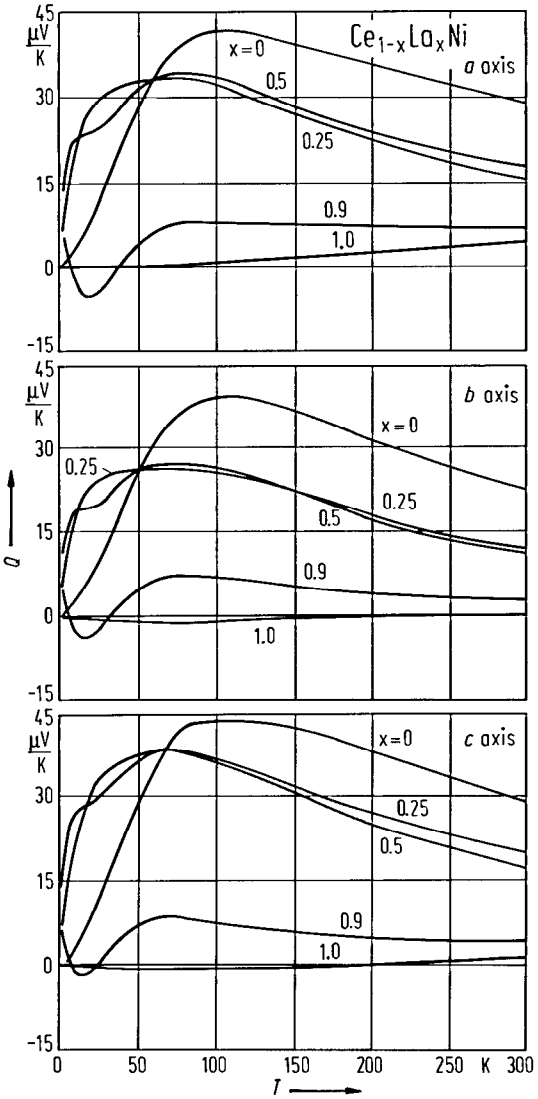

Fig. 92. Thermoelectric power, Q, of $Ce_{1-x}La_xNi$ samples along the a, b, and c axis as function of temperature. The huge peak of Q in CeNi, observed for the three directions around 100 K, gradually decreases with the change of the Ce 4f-electron state [87 O 2].

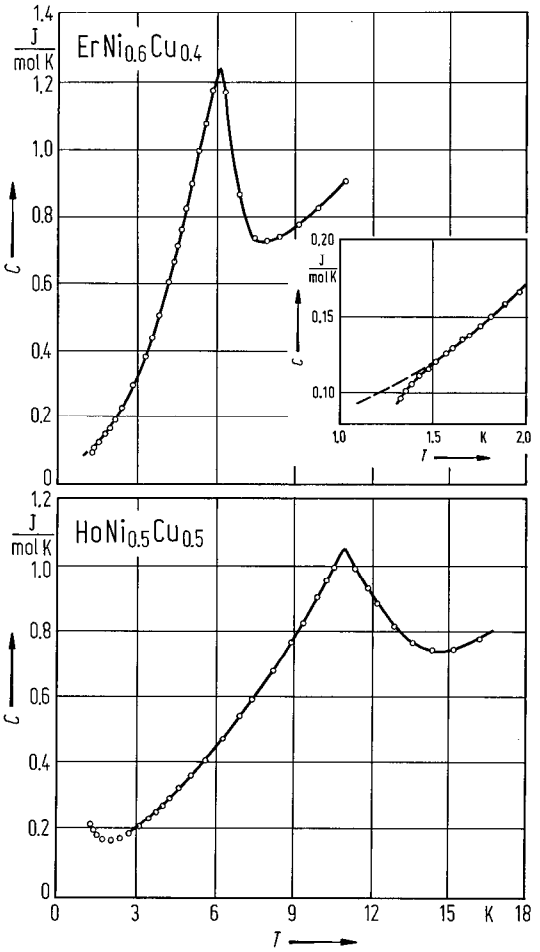

Fig. 93. Thermal variation of the specific heat of $ErNi_{0.6}Cu_{0.4}$ and $HoNi_{0.5}Cu_{0.5}$. In case of $ErNi_{0.6}Cu_{0.4}$ a λ-type anomaly at $T_N = 7$ K is observed. Below T_N the specific heat decreases with temperature. However, a quicker decrease appears near 1.5 K, as shown in the insert. This anomaly corresponds to a quicker decrease of the magnetic entropy and is attributed to the transformation of the modulated magnetic structure towards the antiphase magnetic structure. In case of $HoNi_{0.5}Cu_{0.5}$ a maximum in specific heat is observed at $T_N = 11$ K. Below 2.2 K, the specific heat increases with decreasing temperature because of the nuclear contribution [77 G 6].

For electrical resistivity and magnetoresistivity studies see:

RNi R = La [82 g 1, 87 O 2]; R = Ce [83 G 18, 85 G 6, 85 G 7, 87 S 3]; R = Gd [80 M 9*]; R = Ho [82 S 7*, 82 S 8*]; R = Er [84 M 3]

(R′R″)Ni (GdLa)Ni [86 G 6, 87 O 2*]

R(M′M″) La(NiPt) [84 G 1]; Ce(NiPt) [84 G 1, 85 G 6, 87 G 4]; Ce(NiPd) [88 N 2]; Gd(CoNi) [80 G 10, 82 g 1]

For specific heat measurements

ErNi [84 M 3]; (LaCe)Ni [87 I 6, 87 O 2*]; Ho(NiCu) [77 G 6]; Er(NiCu) [77 G 6]; Ce(NiPd) [88 N 2]

For thermopower studies see

LaNi [81 G 10]; CeNi [87 S 3]; GdNi [81 G 10]; (CeLa)Ni [87 S 2]

Magnetization processes

For magnetization processes see

RNi [70 B 2]; R = Gd [83 I 4*]; R = Dy [85 M 2*]

(R′R″)Ni (TbY)Ni [84 P 4]

R(M′M″) Tb(NiCu) [71 B 4, 71 B 5]

Spectroscopy

For spectroscopic studies see

L_{III} absorption spectra

CeNi [85 P 1]

X-ray absorption spectra

CeNi [86 H 4]

2.4.2.11 R_2M_3 compounds

Crystal structure, lattice parameters

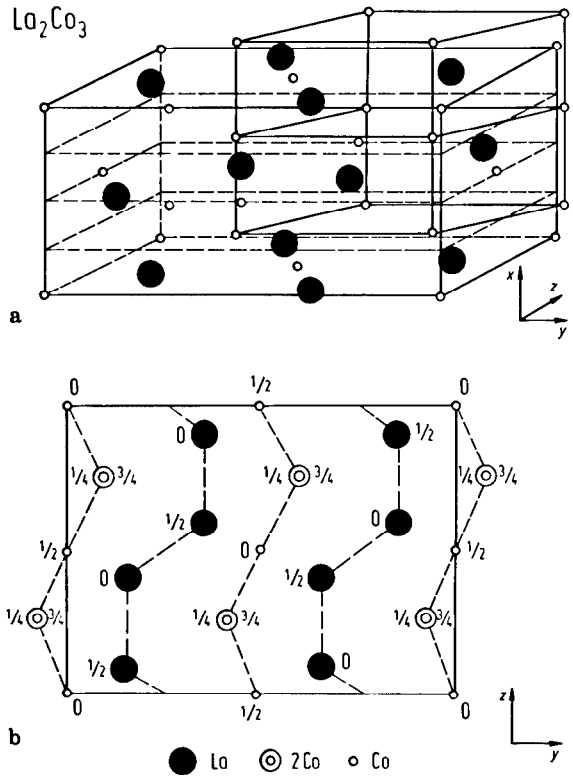

Fig. 94. (a) Crystal structure of La_2Co_3 compound and (b) projection of the crystal structure along the x axis. The structure is orthorhombic having the space group Cmca and can be described as a packing of alternative layers of Co and La along the b axis. Atoms of the same layer are connected in (b) by dashed lines. In a layer formed by Co atoms, the distances between nearest neighbours are small (2.43···2.47 Å), while the distances between the Co atoms of two successive layers are greater than 4.84 Å [84 M 2].

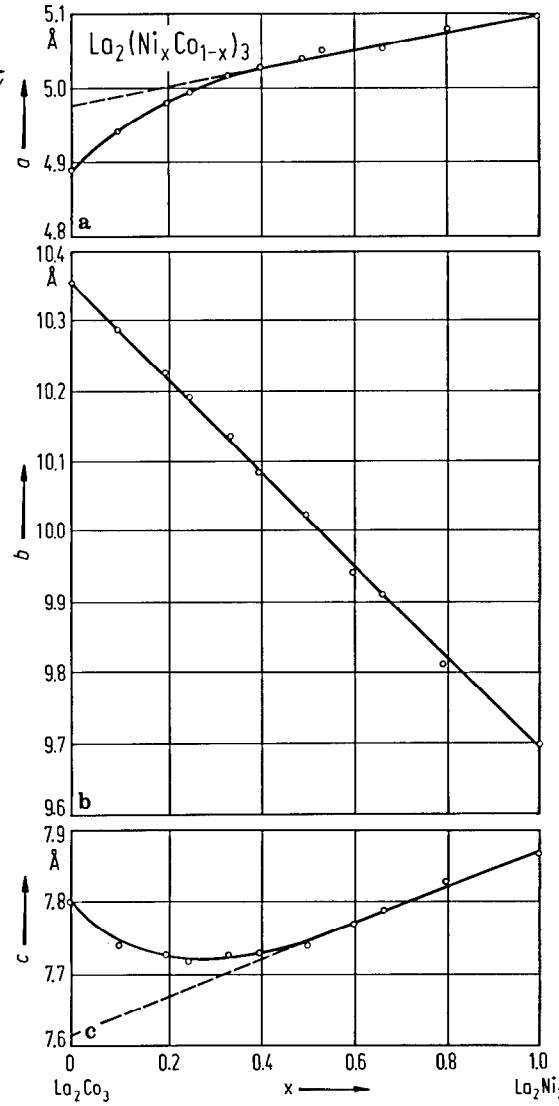

Fig. 95. Composition dependence of the lattice constants in $La_2(Ni_xCo_{1-x})_3$ compounds at room temperature. The abnormal behaviour of a and c parameters seems to be connected with the appearance of Co magnetic moments. The effects of crystal field on the magnetic orbitals are responsible for the observed deformations [84 M 2]. For La_2Ni_3 structure see [76 V 6].

Table 33. Atomic sites in La_2Co_3 compound (space group Cmca) [84 M 2].

Atom	Site	*x*	*y*	*z*
La	8f	0.0	0.1538(1)	0.4075(1)
Co(1)	8e	0.25	0.4117(2)	0.25
Co(2)	4a	0.0	0.0	0.0

Table 34. Lattice constants (Å) of R_2M_3 compounds (space group Cmca).

	a	*b*	*c*	Ref.
La_2Co_3	4.886(7)	10.340(10)	7.811(5)	67 B 3
La_2Co_3	4.853	10.350	7.801	85 G 10
La_2Co_3	4.895	10.350	7.799	84 M 2
Nd_2Co_3	4.963(4)	10.006(2)	7.549(4)	73 R 2
La_2Ni_3	5.101	9.697	7.866	84 M 2
La_2Ni_3	5.113	9.7316	7.9075	76 V 6

Magnetization, Curie temperatures

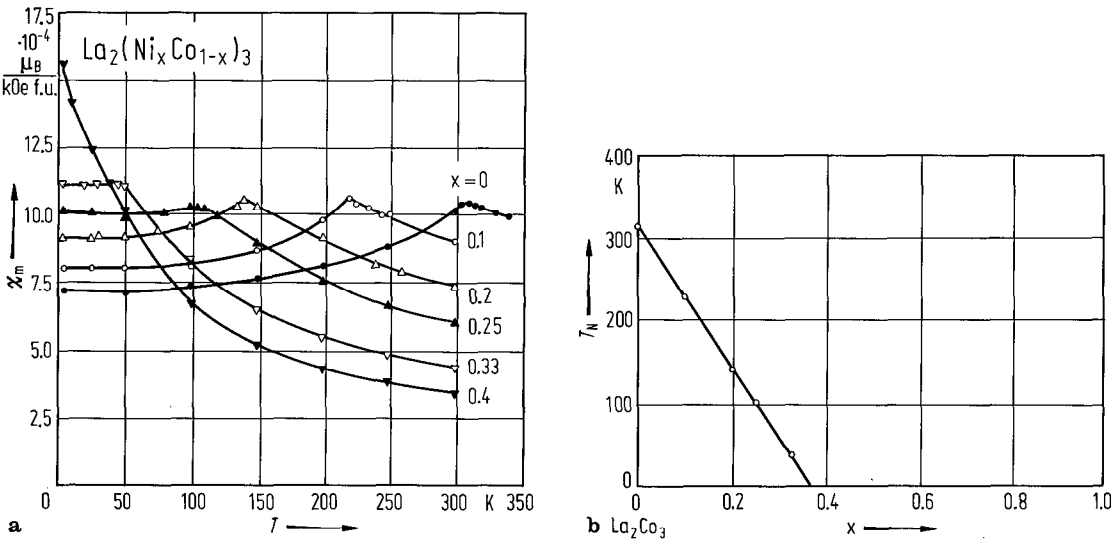

Fig. 96. (a) Thermal variation of initial magnetic susceptibilities for some $La_2(Ni_xCo_{1-x})_3$ compounds and (b) composition dependences of the Néel temperatures. For $x \leqq 0.35$ the compounds are antiferromagnetic. By increasing the Ni content, the antiferromagnetic interactions decrease and for $x \gtrsim 0.4$ the compounds are paramagnetic [84 M 2].

Neutron diffraction

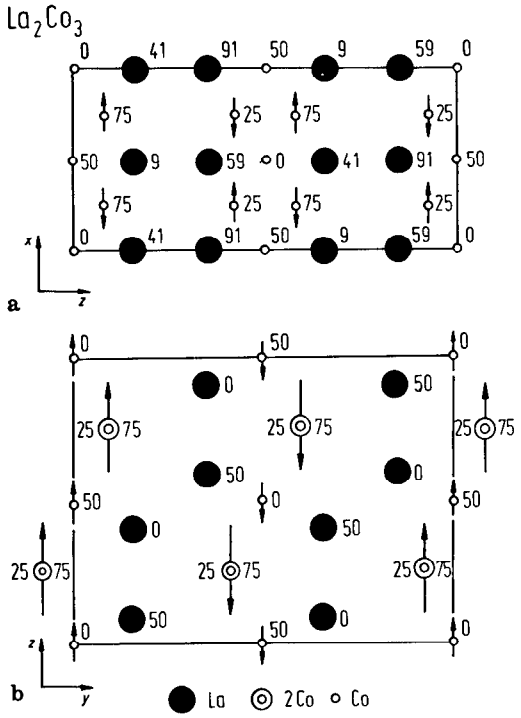

Fig. 97. Projections of La_2Co_3 magnetic structure on the (*ab*) and (*bc*) planes, respectively. The numbers give the values of the 100*z* and 100*x* coordinates, respectively, of the different atoms [84 M 2, 85 G 10]. The ferromagnetism inside the layers arises because of the small Co–Co distances. The antiferromagnetic interactions occur between Co atoms at around 5 Å separated by La atom zones. The negative interactions arise from an indirect Co–La–Co interaction through the 3d–5d hybridization and the negative polarisation of the spins of the 5d electrons by Co magnetic moments. These interactions are very similar to the superexchange interactions in the insulators.

Table 35. Magnetic moments of Co atoms in La_2Co_3 and $La_2(Co_{0.8}Ni_{0.2})_3$ determined by neutron diffraction studies at $T = 5$ K.

	Site	$p_x(\mu_B/M)$	$p_y(\mu_B/M)$	$p_z(\mu_B/M)$	$p_{Co}(\mu_B)$	Ref.
La_2Co_3	4a	0.0	0.0	0.35(5)	0.35(5)	84 M 2, 85 G 10
	8e	0.34	0.0	−0.85(5)	0.92(7)	
$La_2(Co_{0.8}Ni_{0.2})_3$	4a	0.0	0.0	0.09(5)	0.09(5)	84 M 2
	8e	0.27(5)	0.0	−0.56(5)	0.62(7)	

2.4.2.12 RM_2 compounds

Crystal structure, lattice parameters

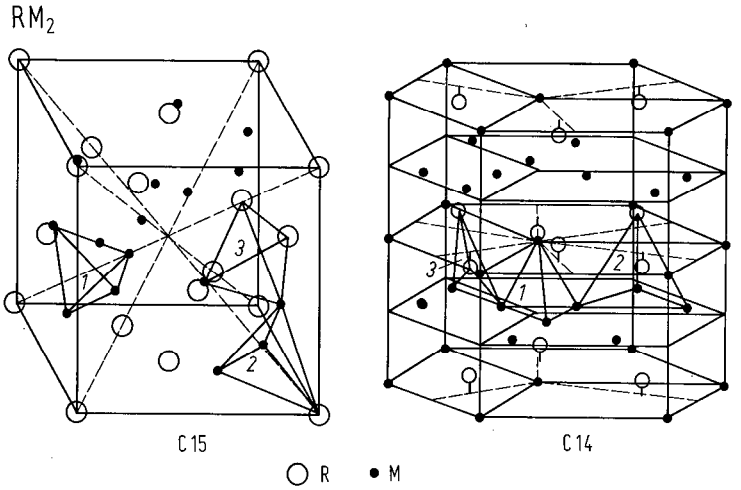

Fig. 98. Schematic drawings of cubic (C15) and hexagonal (C14) Laves phases in which RM_2 compounds crystallize. The R atoms are plotted as open circles and M atoms as solid circles. Three types of interstices are also shown: *1*: M_4 site; *2*: RM_3 site; *3*: R_2M_2 site [86 I 7]. The ideal C14 and C15 structures are in fact very similar, the only difference being a slightly different stacking arrangement [53 B 1, 80 K 6]. The R atoms in both cases are stacked as tetrahedra, joined alternatively point-to-point and base-to-base in the cubic structure and point-to-point in the hexagonal case.

Table 36. Metal and deuterium atom positions and occupancies of $ZrMn_2D_3$ (C14 structure having space group $P6_3/mmc$) as obtained by a profile analysis of the neutron diffraction pattern [1]). For comparison the metal position of $ZrMn_2$ are shown in parenthesis and the predicted D atom positions in brackets [79 D 8]. The number of formula units in the cell is $Z=4$.

Atom	Site	Coordinates		Neighbours	Occupancy
Zr	4f	$z=0.0661(8)$	(0.0635(1))		1.00
Mn(1)	2a	–	–		1.00
Mn(2)	6h	$x=0.8357(7)$	(0.8297(2))		1.00
				Zr_2Mn_2	
D(1)	24l	$x=0.042(2)$	[0.041]	1 Mn(1)	0.179(4)
				1 Mn(2)	
		$y=0.325(2)$	[0.330]	2 Zr	
		$z=0.562(1)$	[0.563]		
D(2)	12k	$x=0.456(1)$	[0.458]	2 Mn(2)	0.376(4)
				2 Zr	
		$z=0.632(1)$	[0.628]		
D(3)	6h	$x=0.463(2)$	[0.461]	2 Mn(2)	0.312(1)
				2 Zr	
D(4)	6h	$x=0.202(9)$	[0.206]	2 Mn(2)	0.052(2)
				2 Zr	
				Zr_1Mn_3	
D(5)	12k		$x=[0.132]$	1 Mn(1), 2 Mn(2)	
			$z=[0.138]$	1 Zr	
D(6)	4f		$z=[0.665]$	3 Mn(2), 1 Zr	
				Mn_4	
D(7)	4e		$z=[0.188]$	1 Mn(1), 3 Mn(2)	

[1]) The data show that D atoms occupy tetrahedral interstices of Zr_2M_2-type. The interstices are partially occupied and represent a 3-dimensional infinite network of diffusion paths for the D atoms. Each D atom site in this network is about 1.3 Å away from at least two other D atom sites. It is suggested that the positional disorder of the D atoms is thermally induced [79 D 8].

Table 37. Metal and tetrahedral sites in RM_2 compounds having C15-type structure (space group Fd3m), with the origin at the center of symmetry. The rhombohedral structure for a hydride model [79 S 6] having space group R$\bar{3}$m is also shown [1]).

	Cubic (Fd$\bar{3}$m)						Rhombohedral (R$\bar{3}$m)				
Atom	Site	Coordinates	Symmetry	Neighbours	Tetrahedron faces shared with	No. per RM_2	Site	Symmetry	Coordinates	Neighbours	No. per RM_2
R	8a	x, x, x $x=1/8$	$\bar{4}$3m				2c	3m			
M(1)	16d	$x=1/2$	$\bar{3}$m				1b	$\bar{3}$m			
M(2)							3e	2/m			
Tetrahedral sites	8b	x, x, x $x=3/8$	$\bar{4}$3m	4M	4(32e)	1	$2c_1$	3m	x, x, x $x=3/8$	1 M(1), 3 M(2)	1
	32e	x, x, x $x=9/32$	3m	1R3M	1(8b); 3(96g)	4	$2c_2$	3m	x, x, x $x=9/32$	1R, 3 M(2)	1
							$6h_1$	m	x, x, z $x=9/32$, $z=21/32$	1 R, 1 M(1), 2 M(2)	3
	96g	x, x, z $x=5/16$, $z=1/8$	m	2R2M	1(32e) 1(96g) 2(96g)		$6h_2$	m	x, x, z $x=1/8$, $z=1/2$	2 R, 2 M(2)	3
							$6h_3$	m	x, x, z $x=1/8$, $z=3/4$	2 R, 2 M(2)	3
							12i	1	x, y, z 3/4, 1/2, 1/8	2 R, 2 M(1)	6

[1]) The number of formula units in the cell is Z=8 for C15-type structure and Z=2 for rhombohedral structure.

Table 38a. Lattice constants of RMn_2 compounds at room temperature (Å). ▶

	Type structure	61 W 2		64 M 2		67 K 1		71 O 1		77 b 1	
		a	*c*	*a*	*c*	*a*	*c*	*a*	*c*	*a*	*c*
$PrMn_2$	C14										
$NdMn_2$	C14										
$SmMn_2$	C15										
	C14										
$GdMn_2$	C15			7.728		7.750					
$TbMn_2$	C15										
$DyMn_2$	C15			7.569		7.602					
$HoMn_2$	C15			7.507		7.592					
	C14					5.368	8.764				
$ErMn_2$	C14	5.281	8.621	5.281	8.621	5.307	8.702	5.321	8.719		
$TmMn_2$	C14	5.241	8.565								
$LuMn_2$	C14									5.227	8.537
YMn_2	C15			7.679		7.692					

Table 38b. Lattice constants of RFe_2 compounds at room temperature (Å).

	60 W 1	64 C 4	65 K 3	69 G 1	70 B 13	71 B 12	72 C 2	73 N 5	74 A 3	79 F 5
$CeFe_2$	7.303	7.304						7.250	7.301	
$PrFe_2$							7.467			
$NdFe_2$							7.452			
$SmFe_2$	7.415	7.411						7.450		
$GdFe_2$	7.394	7.389		7.390	7.396	7.389		7.400	7.3875	
$TbFe_2$		7.348			7.347	7.348				
$DyFe_2$	7.325	7.320			7.325	7.322		7.330		
$HoFe_2$	7.300	7.300			7.304	7.301		7.280		7.300
$ErFe_2$	7.274	7.280			7.283	7.276				7.280
$TmFe_2$						–				7.250
$YbFe_2$							7.239			
$LuFe_2$			7.217	7.227					7.233	
YFe_2				7.359	7.363	–		7.290		

Table 38c. Lattice constants of RCo_2 compounds at room temperature (Å).

	60 H 1	60 W 1	64 C 4	65 H 1	66 L 4	67 O 2	71 G 1	72 B 10	72 B 16	75 S 9	76 L 2	81 M 6
$CeCo_2$		7.161	7.162	7.1609								
$PrCo_2$		7.312	7.305	7.3061		7.287		7.309			7.307	
$NdCo_2$	7.300	7.300	7.300	7.2984	7.300			7.298			7.305	
$SmCo_2$		7.260	7.260	7.2625				7.263				
$GdCo_2$		7.255	7.258	7.2570	7.259			7.258			7.258	
$TbCo_2$		7.206	7.209	7.2100				7.206			7.200	
$DyCo_2$		7.187	7.188	7.1902				7.188			7.188	7.190
$HoCo_2$		7.168	7.168	7.1733	7.171			7.166		7.170	7.170	7.173
$ErCo_2$		7.144	7.151	7.1539				7.154			7.150	7.156
$TmCo_2$	7.121			7.1351								
$YbCo_2$									7.122			
$LuCo_2$							7.120					
YCo_2					7.217			7.215		7.220		7.220

Table 38a (continued)

81 M 1	82 H 1		83 G 1		83 M 1		85 T 1		86 O 2		
a	*a*	*c*	*a*	*c*	*a*	*c*	*a*	*c*	*a*	*c*	
							5.590	9.106	5.577	9.115	$PrMn_2$
							5.574	9.082	5.560	9.060	$NdMn_2$
									7.790		$SmMn_2$
							5.493	8.945	5.511	8.978	
7.724			7.748		7.750		7.758		7.740		$GdMn_2$
			7.648		7.640				7.626		$TbMn_2$
7.564			7.590		7.590				7.573		$DyMn_2$
7.507	7.518				7.530				7.520		$HoMn_2$
	5.282	8.660	5.330	8.600	5.320	8.680			5.282	8.622	
			5.255	8.695	5.280	8.620			5.280	8.620	$ErMn_2$
			5.238	8.660					5.241	8.565	$TmMn_2$
									5.215	8.550	$LuMn_2$
							7.687		7.681		YMn_2

Table 38d. Lattice constants of RNi_2 compounds at room temperature (Å).

	60 H 1	60 W 1 64 M 2	63 n 1	64 C 4	64 M 2	68 M 1	72 B 13	81 M 5	83 I 1
$LaNi_2$						7.3650			7.3612
$CeNi_2$		7.202		7.211		7.2240			7.2275
$PrNi_2$		7.285		7.286		7.2898	7.287		7.2857
$NdNi_2$		7.270		7.265		7.2709	7.267		7.2683
$SmNi_2$		7.226		7.230		7.2328	7.230		7.2247
$GdNi_2$		7.202		7.205		7.2082	7.205		7.2026
$TbNi_2$		7.160		7.178		7.1778	7.182		7.1770
$DyNi_2$		7.148		7.161		7.1637	7.155	7.160	7.1604
$HoNi_2$		7.136		7.142		7.1465	7.138	7.147	7.1397
$ErNi_2$		7.110		7.125		7.1321	7.125	7.127	7.1280
$TmNi_2$					7.088	7.1089	7.105		
$YbNi_2$	7.060								
$LuNi_2$			7.085						
YNi_2							7.188		7.1810

Table 39. Lattice distortions in RFe_2 compounds. The variation of the angle, α_4, between cube edges, $\alpha_4 = \pi/2 - \varepsilon$ in rad, at 300 and 0 K is tabulated. The 4f quadrupole, $\Delta E/A\varepsilon = \alpha_J \langle r^2 \rangle J(2J-1)$, is also given [77 B 4]. n.o.: not observed. ΔE is the CEF energy decrease due to the distortion and A is a constant.

	Type of distortion below T_C	$\Delta E/A\varepsilon$ Å^2	ε	
			$T = 300$ K	$T = 0$ K
$SmFe_2$	rhombohedral	0.10	−0.0023	n.o.
$TbFe_2$	rhombohedral	−0.14	0.0029	0.0045
$DyFe_2$	tetragonal	−0.13	n.o.	n.o.
$HoFe_2$	tetragonal	−0.05	n.o.	n.o.
$ErFe_2$	rhombohedral	0.04	n.o.	n.o.
$TmFe_2$	rhombohedral	0.12	n.o.	−0.0026

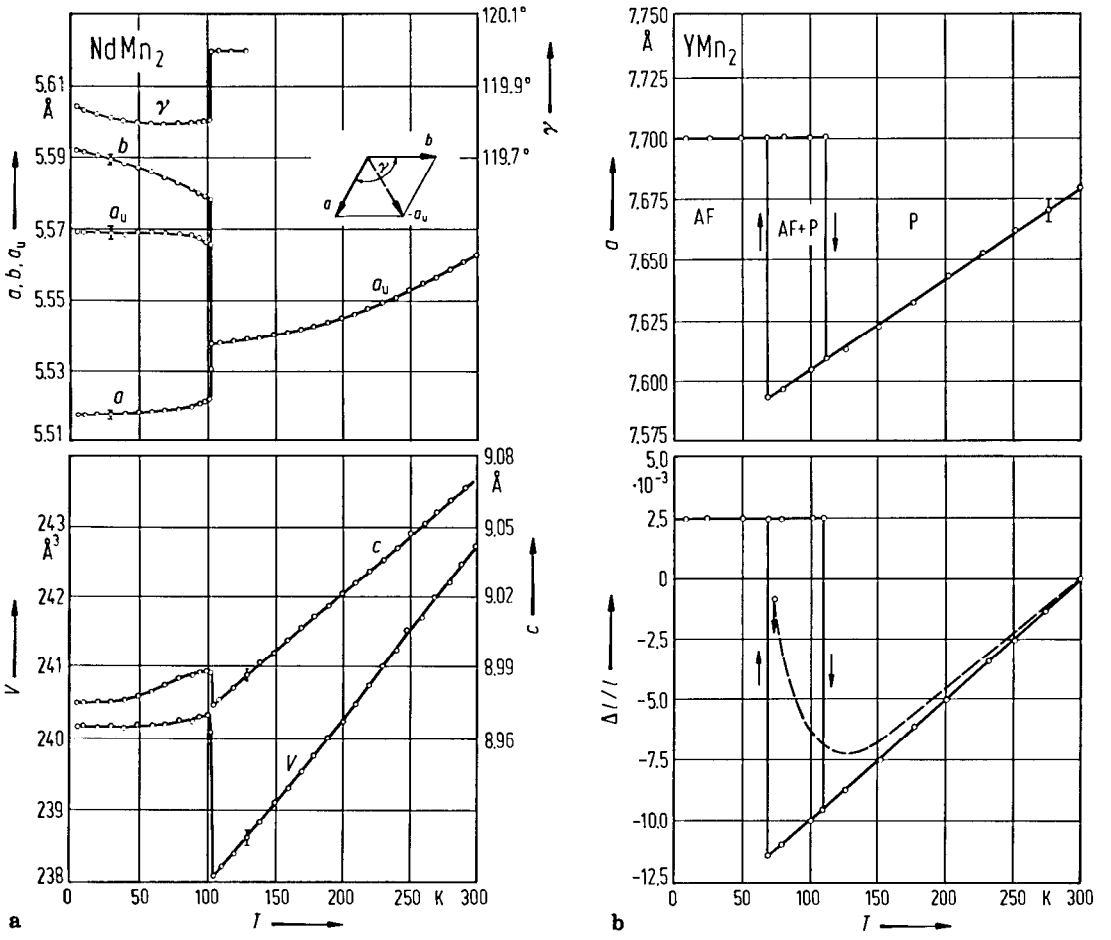

Fig. 99. (a) Thermal variation of lattice parameters for $NdMn_2$ compound, determined by X-ray diffraction studies. For temperatures higher than the Néel point ($T_N = 104$ K) the structure is hexagonal ($a_h = a_x = a_y = a_u$, c_h, and $\gamma = 120°$). The a and c lattice parameters as well as the volume increase with temperature. The thermal dilatation coefficients at 250 K are $\alpha_a = 3 \cdot 10^{-5}\,K^{-1}$, $\alpha_c = 4 \cdot 10^{-5}\,K^{-1}$ and $\beta_V = 10^{-4}\,K^{-1}$. For $T < T_N$ the structure is distorted to monoclinic one ($a = a_x$, $b = a_y$, $\gamma \cong 120°$). A great discontinuity in the volume, $\Delta V/V = 0.9\%$, is evidenced at T_N. The great anomalies in the dilatation are attributed to the distance dependence of the exchange energy between Mn atoms [86 O 2]. (b) Thermal variation of the lattice parameter a and of the linear dilatation coefficient, $\Delta l/l$, in YMn_2. In the paramagnetic state, the thermal dilatation coefficient is high (at 250 K, $\alpha_a = 5 \cdot 10^{-5}\,K^{-1}$, which corresponds to $\beta_V = 1.5 \cdot 10^{-4}\,K^{-1}$). In the antiferromagnetic phase ($T < 50$ K) the thermal variation of the lattice parameter is nil. The region of coexistence of the paramagnetic and antiferromagnetic phases (AF + P) depends on the sample preparation [86 O 2]. According to [83 N 3, 83 N 4, 85 N 2, 86 O 2] the structure in the antiferromagnetic phase is cubic. A small crystallographic, tetragonal [82 G 1] distortion has been also suggested. The arrow corresponds to the temperature at which the sample was crushed. Solid and dashed lines indicate results from neutron scattering and macroscopic measurements, respectively.

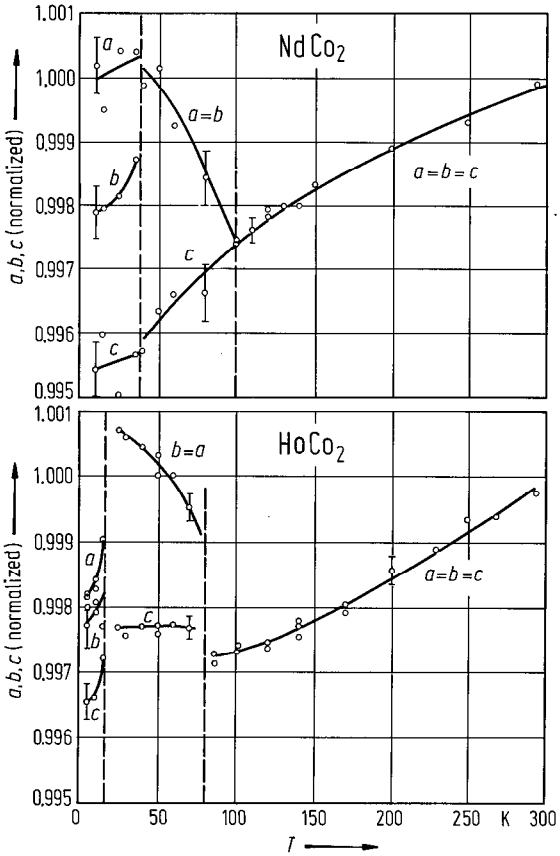

Fig. 100. Temperature dependence of the lattice parameters of $HoCo_2$ and $NdCo_2$ normalized to the respective RT values. A tetragonal distortion of the cubic $MgCu_2$-type structure has been shown to occur below the Curie temperature. A spin reorientation at 15 K in $HoCo_2$ and 43 K in $NdCo_2$ changes the distortion from tetragonal to orthorhombic [83 G 7].

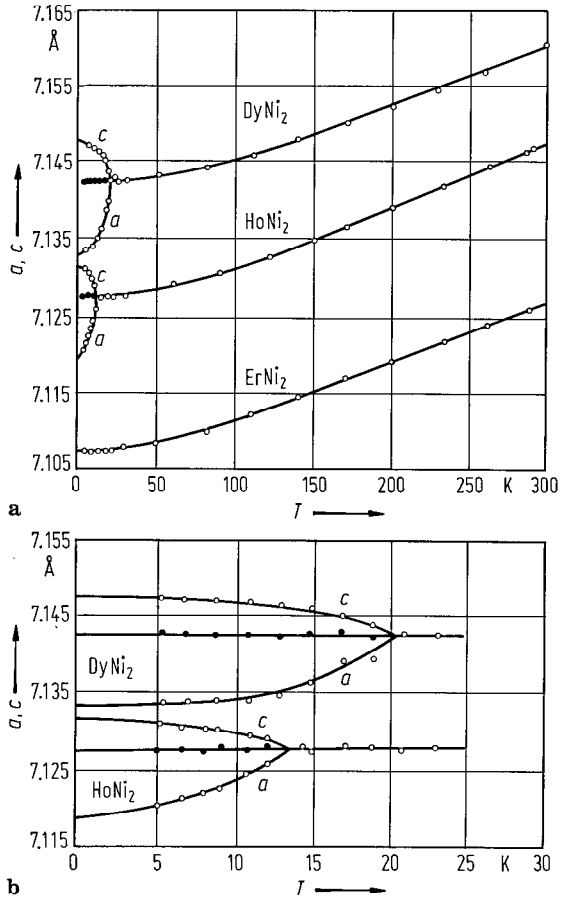

Fig. 101. Temperature dependence of the lattice parameters in $DyNi_2$, $HoNi_2$ and $ErNi_2$ between 5 and 290 K. A tetragonal distortion of the cubic $MgCu_2$-type structure has been shown to occur below the Curie temperature. The Curie temperature of $ErNi_2$ is below 5 K. The values $\sqrt[3]{ac^2}$ are plotted by full circles [81 M 5].

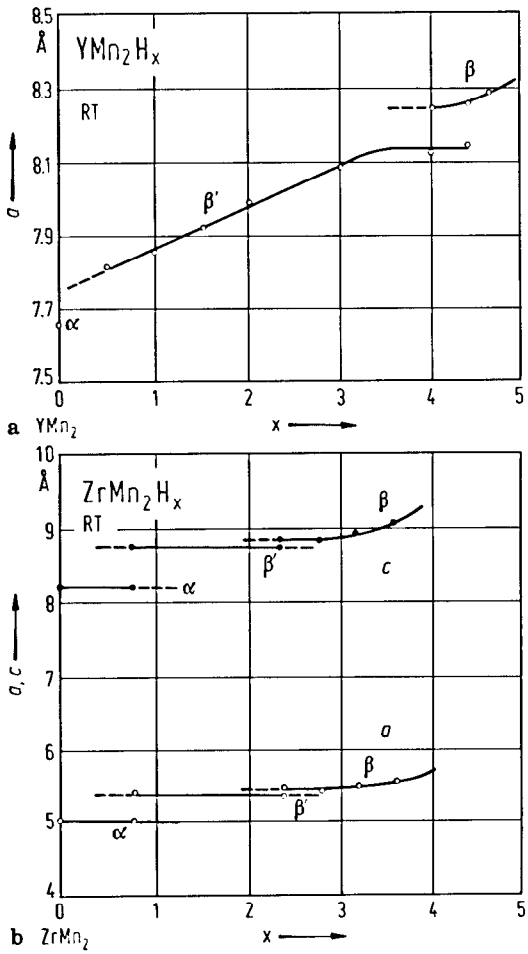

Fig. 102. Lattice constants as a function of hydrogen content in (a) YMn_2H_x and (b) $ZrMn_2H_x$ at room temperature. The intermediate metastable β' phases are observed between the α-phase and the fully charged β-phase in both hydrides. The β'-phase has the same crystal structure as in the hydrogen-free compound and the unit cell volume is smaller than in the β phase. In YMn_2H_x, the β' phase exists as a single phase for $0.5 < x < 3.5$ and the lattice constant expands continuously with increasing x, while it does not exist as a single phase in $ZrMn_2H_x$. There are two phases, the $\alpha + \beta'$ for $0 < x < 1.5$ and the $\beta' + \beta$ phases for $1.5 < x < 3.0$ and the lattice constants remain unchanged with increasing x in each phase [87 F 6].

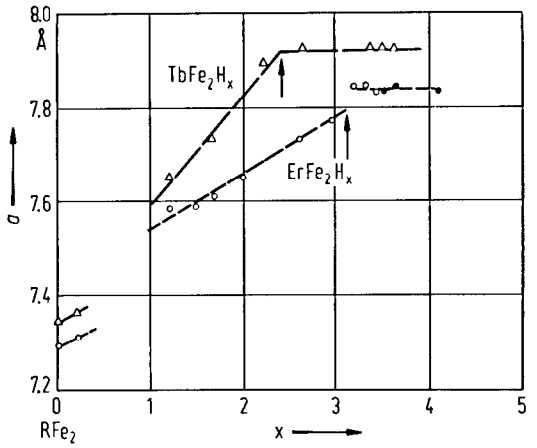

Fig. 103. Variation of the lattice parameter as a function of the hydrogen content x in $ErFe_2H_x$ and $TbFe_2H_x$ at room temperature [87 F 4]. Filled and half filled symbols correspond to [79 V 3, 79 V 4] and [76 G 10], respectively. The arrows indicate the critical hydrogen concentration for rhombohedral distortion. For $x < 1.2$ a two-phase region is observed corresponding to a broad equilibrium plateau. In range $1.2 < x < 2.5$ for Tb and $1.2 < x < 3.0$ for Er, the lattice constant a is quasi-linear with respect to x. This corresponds to a volume expansion $\Delta V/H$ of 3.2 Å^3 (H atom)$^{-1}$, a value which is very close to the mean value observed in metal hydrides [83 W 4, 83 W 5]. The rhombohedral distortion (present at higher hydrogen concentrations) appears at $x = 2.4$ for $TbFe_2H_x$ and $x = 3.2$ for $ErFe_2H_x$, with angular values of 91.3° and 91.2°, respectively. In case of Tb compounds, the lattice cell presents an expansion along [111] in the virgin alloy ($\gamma = 89.4°$) owing to a large magnetostriction and contraction along the same direction for $x > 2.5$ [87 F 4].

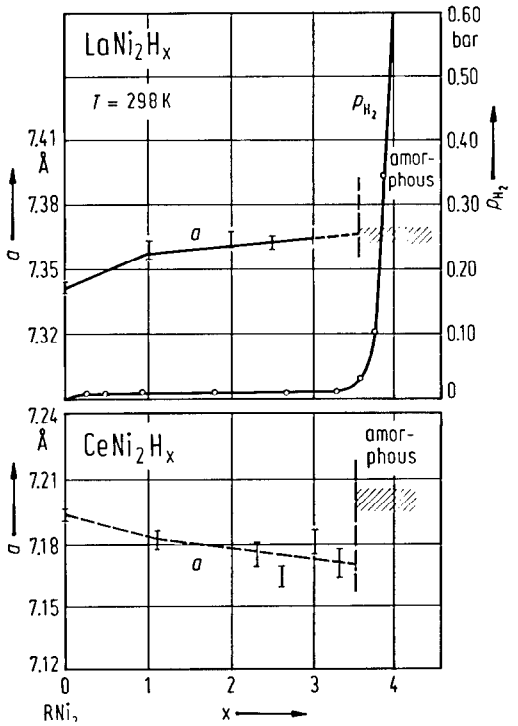

Fig. 104. Variation of the cell parameters a of $LaNi_2$ and $CeNi_2$ as function of the hydrogen content, at 298 K [87 P 2]. It is assumed that the crystalline phase corresponds to the α-phase and that the amorphous β-phase $LaNi_2H_4$ replaces it progressively. In case of hydrogenated samples, an increase in the cell parameter for $LaNi_2$ up to $LaNi_2H_1$ ($\Delta V/V = 1.4\%$) and decrease for $CeNi_2H_1$ ($\Delta V/V = -0.5\%$) is shown. Beyond $x = 1$, the cell parameter is almost constant. Above $x = 3.5$, the X-ray diffraction lines disappear completely. Also shown is the hydrogen content vs. hydrogen pressure.

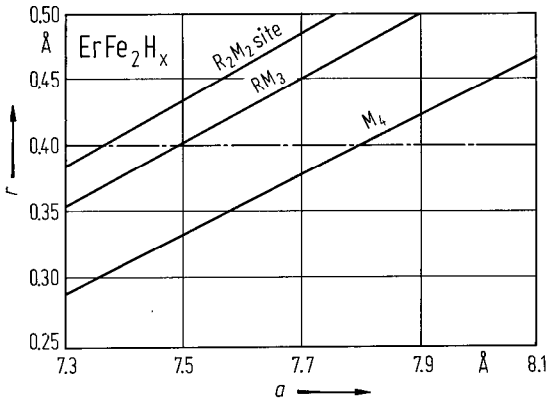

Fig. 105. Theoretical calculation of the interstitial site radii [83 W 4, 83 W 5] versus the cell parameter expansion for $ErFe_2H_x$ compound. The broken line corresponds to the critical radius (0.4 Å) for which a tetrahedron is either occupied or not occupied [87 F 4]. The same results are obtained for $TbFe_2$ if a scaling factor of approximately 1.3 is applied on the cell parameter axis. The data show clear evidence of preferential attraction of the R_2M_2 sites for hydrogen mainly in the low-concentration range, but a nonnegligible attractivity of the RM_3 sites for $x>3$. Owing to the threefold symmetry, the RM_3 occupancy probably drives the rhombohedral distortion observed at higher hydrogen concentration. The neutron diffraction measurements [87 F 5] have confirmed the occupation scheme predicted by the geometrical model. At this concentration, the rhombohedral symmetry introduces discrimination within the group of R_2M_2 and RM_3 sites. Thus, only RM_3 sites are selectively occupied inducing a cumulative presence of hydrogen atoms near the cell centre. The temperature dependence of the cell distortions measured by neutrons corresponds to a slight decrease in the rhombohedral distortion induced by hydrogen ($\gamma>90°$). A hydrogen diffusion process is seen by Mössbauer spectroscopy [85 D 4] up to 200 K, and this confirms the main role of local ordering imposed by hydrogen at low temperature on the physical properties.

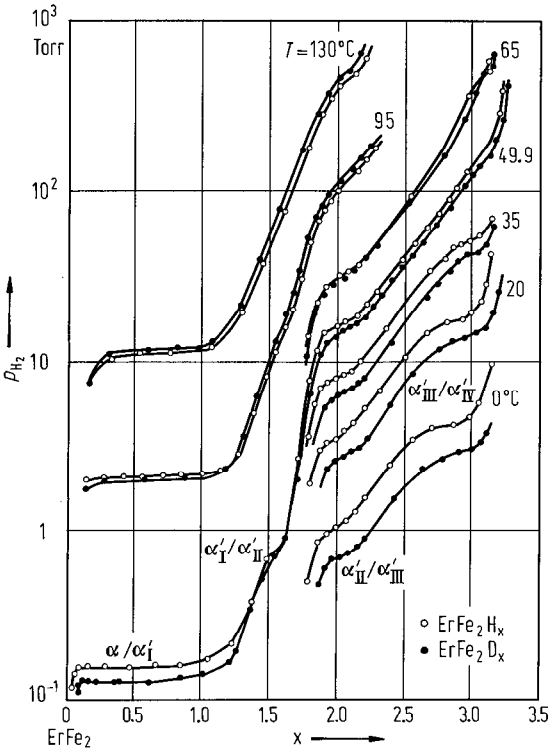

Fig. 106. Absorption isotherms of $ErFe_2$-hydrides [87 F 3]. The hydrogen isotherms are similar to those reported in [80 K 7] but extend here to higher temperatures. There are three plateaus in the range of contents investigated. Another plateau at $x\cong1.5$ has been reported [80 K 7] and there appears to be traces of a plateau here at the lowest temperature investigated (323.1 K), in all phases except the α-phase at $x=4$. Since $ErFe_2$ has the same structure, the phases have been labelled in order of increasing hydrogen contents as α, α'_I, α'_{II}, α'_{III}, α'_{IV} and β. In [80 K 7] five different solid phases were evidenced, but there were labelled by α, β, γ, δ, ε. Five two-solid phase coexistence regions are shown. For one the plateau pressure is not well defined over the temperature range investigated. The plateau pressure of the various two-phase regions must naturally increase with the average hydrogen content of the two-phase region. However, the enthalpies for hydride formation do not increase regularly with the plateau pressure. The D/H isotope effect is small and changes sign over the measured temperature range from 273 to 403 K.

Table 40a. Lattice parameters of some RM_2-hydrides (Å) at $T = 293$ K.

	x	Structure	a_0	c_0	a_x	c_x	$\Delta V/V$ (%)	Ref.
$DyMn_2H_x$	3.4	C15	7.587		8.270		29.5	80C8
$ErMn_2H_x$	4.0	C14	5.281	8.620	5.640	9.330	23	80V4
$ErMn_2H_x$	4.6	C14	5.281	8.620	5.810	9.530	34	80V4
$CeFe_2H_x$	3.7	C15	7.302	–	–			85D11
$SmFe_2H_x$	x	C15	7.417	–	8.090	–	29.8	77B18
$GdFe_2H_x$	x	C15	7.396	–	8.040	–	28.5	77B18
$TbFe_2H_x$	x	C15	7.347	–	7.970	–	27.7	77B18
$TbFe_2H_x$	3.0	C15	7.354	–	7.799	–	19.3	82P13
$DyFe_2H_x$	x	C15	7.325	–	7.940	–	27.4	77B18
$DyFe_2H_x$	3.4	C15	7.325	–	7.940	–	27.4	80C8
$DyFe_2H_x$	3.5	C15	7.320	–	7.940	–	27.6	82P13
$HoFe_2H_x$	x	C15	7.304	–	7.730	–	18.5	77B18
$HoFe_2H_x$	4.5	C15	7.284	–	7.880	–	26.6	76G10
$HoFe_2D_x$	3.5	C15	7.300	–	7.830	–	22.4	79F5
$ErFe_2H_x$	3.5	C15	7.283	–	7.810	–	23.3	81P4
$ErFe_2H_x$	x	C15	7.283	–	7.910	–	28.1	77B18
$ErFe_2H_x$	3.5	C15	7.280		7.830		24.4	79F5
$ErFe_2D_x$	3.5	C15	7.280	–	7.670	–	17.0	79F5
$ErFe_2H_x$	1.45	C15	7.292	–	7.574	–	12.1	85D4
	1.49	C15	7.292	–	7.581	–	12.4	85D4
	1.60	C15	7.292	–	7.590	–	12.8	85D4
	1.69	C15	7.292	–	7.615	–	13.9	85D4
	1.84	C15	7.292	–	7.621	–	14.2	85D4
	1.90	C15	7.292	–	7.633	–	14.7	85D4
	2.61	C15	7.292	–	7.733	–	19.3	85D4
	2.97	C15	7.292	–	7.770	–	21.0	85D4
	3.29	rhomb.	7.292	–	7.839	–	24.2	85D4
					$\alpha = 91.2°$			
	3.60	C15	7.292	–	7.886	–	26.5	85D4
	3.90	C15	7.292	–	7.828	–	23.7	85D4
$TmFe_2H_x$	3.5	C15	7.250	–	7.770	–	23.1	79F5
$LuFe_2H_x$	3.2	C15	7.223	–	7.698	–	21.1	85D11
YFe_2H_x	x	C15	7.363	–	7.840	–	20.7	77B18
$TbCo_2H_x$	3.2	C15	7.205	–	7.784	–	26.1	82P13
$TbCo_{1.4}Fe_{0.6}H_x$	2.0	C15	7.273	–	7.722	–	19.7	82P13
$DyCo_2H_x$	3.4	C15	7.175	–	7.721	–	24.6	80C8
$DyCo_2H_x$	3.3	C15	7.189	–	7.647	–	24.4	82P13
$DyCo_{1.4}Fe_{0.6}H_x$	3.1	C15	7.256	–	7.707	–	19.8	82P13
$HoCo_2H_x$	3.5	C15	7.166	–	7.763	–	27.1	81P4
$HoCo_{1.4}Fe_{0.6}H_x$	3.5	C15	7.227	–	7.668	–	19.5	81P4
$ErCo_2H_x$	3.5	C15	7.180	–	7.710	–	23.8	81P4
$ErCo_{1.4}Fe_{0.6}H_x$	3.5	C15	7.230	–	7.746	–	23.0	81P4
$ErCo_{0.66}Fe_{1.34}H_x$	3.5	C15	7.196	–	7.731	–	24.0	81P4

Table 40b. Lattice parameters of RFe_2-hydrides at $T = 293$ K.

	$GdFe_2H_x$		$HoFe_2H_x$		$ErFe_2H_x$		$TmFe_2H_x$		$LuFe_2H_x$
x	a [nm]	ε	a [nm]	ε	a [nm]	ε	a [nm]	ε	a [nm]
4	0.8029								
			0.7879	1°11′					
			0.7850	1°10′	0.7826	1°13′			
	0.7935	1°02′	0.7844	1°07′	0.7822	1°07′	0.7781	0°46′	
			0.7829	0°50′					
					0.7805	1°08′	0.7743		0.7698
3	0.7930		0.7804				0.7717		
	0.7895						0.7702		0.7642
			0.7761		0.7705				
					0.7657				
2			0.7724						
					0.7621				
									0.7500
					0.7561(70)		0.7533		
					0.7294(30)				
1			0.7555(80)		0.7561(45)				
			0.7300(20)		0.7294(55)				
							0.7520(50)		
							0.7256(50)		
0	0.7405		0.7296		0.7273		0.7241		0.7223

For hydrogen absorption and desorption in RM_2 compounds see also:

RM_2H_x [78 B 20, 79 S 6, 85 S 12]; GdM_2H_x, M = Mn, Fe, Co, Ni [79 J 1]

RMn_2H_x R = Y [87 F 6]; R = Zr [80 J 3, 82 W 1, 87 F 6]

RFe_2H_x [81 K 7, 87 F 5]; R = Gd, Ho, Er, Tm, Lu [84 D 4]; R = Ce [87 A 10]; R = Gd [76 B 21]; R = Dy [80 K 7]; R = Er [79 K 3, 80 K 7, 80 K 8, 80 S 6, 81 V 4, 83 F 5, 87 F 3]; R = Y [76 B 21]

RNi_2H_x R = La, Er, Yb [83 E 1]; R = La [78 K 10]; R = Gd [77 M 2]

RM_2H_x $ZrCr_2H_x$ [80 J 3]; $NiTi_2H_x$ [79 L 4]

$(R'R'')M_2H_x$ $(ZrCe)Mn_2H_x$ [83 P 16]; $(LaMg)Ni_2H_x$ [80 O 1]

$R(M'M'')_2H_x$ [81 F 6, 81 P 5]; $Zr(MnM)_2H_x$ [82 S 18]; $Zr(FeM)_2H_x$, $Zr(CoM)_2H_x$, M = V, Cr, Mn [77 S 8]; $Er(MnFe)_2H_x$ [77 G 12]; $Zr(MnFe)_2H_x$ [82 F 13, 83 S 16, 83 S 17, 86 W 2]; $Er(FeCo)_2H_x$ [77 G 12]; $Er(FeAl)_2H_x$ [77 G 12]; $Zr(FeAl)_2H_x$ [82 F 10]; $Er(CoNi)_2H_x$ [77 G 12]; $Zr(CoCr)_2H_x$ [83 H 2]; $Zr(FeCr)_2H_x$ [86 I 7]

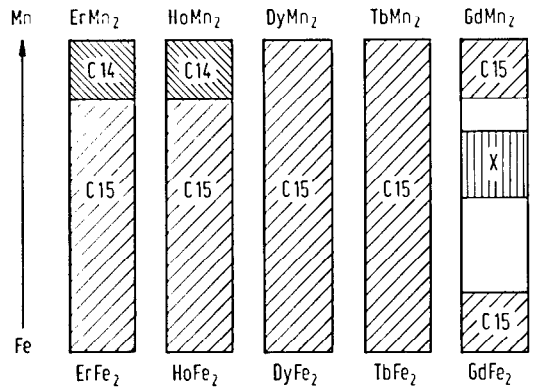

Fig. 107. Phase relationship for $R(Fe_{1-x}Mn_x)_2$ system. The region marked by X involves an unknown structure. The blank spaces represent two-phases regions involving the C15 and X structures [76 I 3].

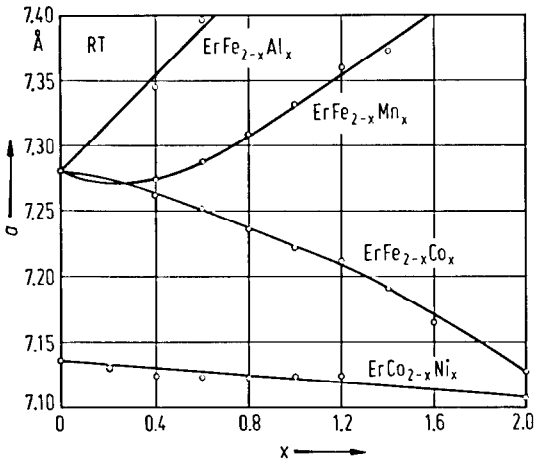

Fig. 109. Composition dependence of the lattice parameters in $ErFe_{2-x}M_x$, M = Co, Mn, Al, and $ErCo_{2-x}Ni_x$ compounds at room temperature [77 G 12]. In hydrogenated systems, Al substitution for Fe decreases the hydrogen capacity of $ErFe_2$. Mn substitution for Fe in $ErFe_2$ increases the hydrogen capacity considerably with a maximum hydride composition $ErFe_{0.8}Mn_{1.2}H_{4.6}$. Hydrogen concentration in this alloys exceeds $7 \cdot 10^{22}$ atoms cm^{-3}. Co substitution for Fe in $ErFe_2$ first increases and then decreases the hydrogen capacity, the maximum hydride composition being $ErFe_{1.2}Co_{0.8}H_{4.2}$. Ni substitution for Co in $ErCo_2$ has little effect on the hydrogen capacity of the alloy, although a large Ni concentration results in an increase in the equilibrium pressure. Lattice expansion is observed to correlate with the hydrogen concentration for the group of systems $ErFe_2H_y$, $ErFe_{2-x}Al_xH_y$ and $ErFe_{2-x}Mn_xH_y$. The maximum hydrogen capacity in the $ErFe_{2-x}Co_x$ system occurs at the same Co/Fe ratio which gives the maximum Fe magnetic moment.

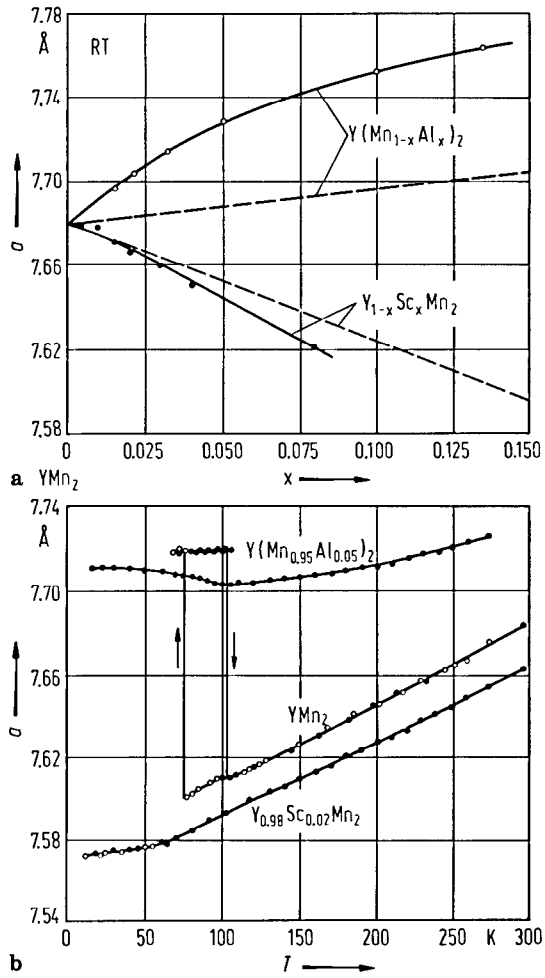

Fig. 108. (a) Composition dependence of the lattice parameters of $Y_{1-x}Sc_xMn_2$ and $Y(Mn_{1-x}Al_x)_2$, at room temperature. For $Y_{1-x}Sc_xMn_2$ the lattice parameters show a decrease with a small negative deviation from Vegard's law (dashed lines), while that of the Al system increases far more rapidly than Vegard's law with increasing x [87 W 2]. (b) Thermal expansion curves for $Y_{0.98}Sc_{0.02}Mn_2$, $Y(Mn_{0.95}Al_{0.05})_2$ and YMn_2 [87 W 2] on (open circles) cooling and (solid circles) heating. Both the volume change at T_N and thermal expansion coefficient above T_N are substantially reduced in $Y(Mn_{0.95}Al_{0.05})_2$. The $Y_{1-x}Sc_xMn_2$ system shows quite different thermal expansion from that of the Al system. First, the abrupt volume change for YMn_2 disappears by substitution of Y by a small amount of Sc. No anomaly was observed for x = 0.02. Below x = 0.02 two kind of phases with a difference in volume of about 5% at 4.2 K were observed, suggesting the coexistence of antiferromagnetic ordering with the same Mn magnetic moment as in YMn_2 and a nonmagnetic Mn state. Therefore, the transition from antiferromagnetic to nonmagnetic state is of the first order in $Y_{1-x}Sc_xMn_2$. The thermal expansion coefficient of $Y_{0.98}Sc_{0.02}Mn_2$ is fairly large and comparable to that of YMn_2 between 100 and 300 K. This suggests that the paramagnetic state of YMn_2 is stabilized down to liquid-helium temperature by substituting Y by a few percent of Sc.

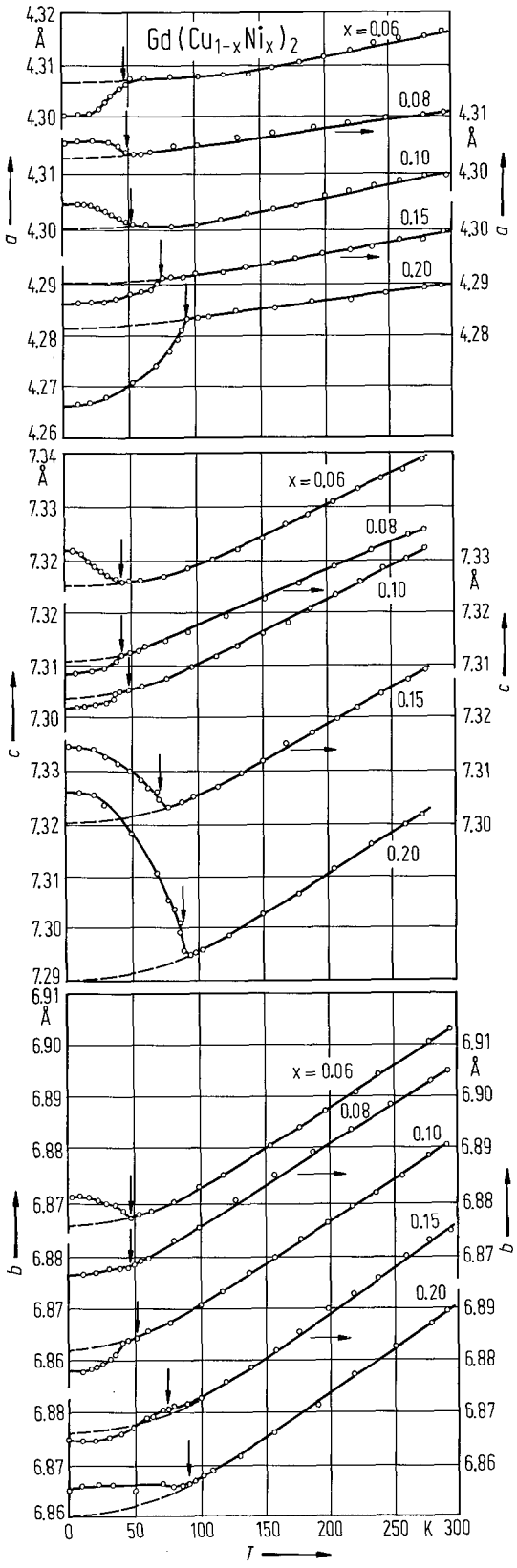

Fig. 110. Thermal variation of lattice parameters *a*, *b*, *c* of $Gd(Cu_{1-x}Ni_x)_2$ compounds having $x < 0.20$. These crystallize in a $CeCu_2$-type structure having space group D_{2h}^{28}. The Curie temperatures are indicated by arrows [87 B 12].

For structure and lattice constants see also:

RM_2 [67 H 1, 68 M 1, 68 M 2, 71 B 13]; R = Ce, Pr, Sm, Tb, Dy, Ho, Er, M = Fe, Co, Ni, Rh, Pt [64 C 4]

RMn_2 [67 K 1, 87 W 1]; R = Pr, Nd, Er, Tm, Lu [64 T 1]; R = Sm, Gd, Tb, Dy, Ho, Er, Yb, Y [72 E 1]; R = Gd [53 B 1, 61 B 1, 81 M 1, 85 G 2]; R = Tb [87 G 1]; R = Dy [61 B 1, 81 M 1]; R = Ho [81 M 1]; R = Er [61 W 2]; R = Tm [61 W 2]; R = Yb [83 T 7]; R = Y [61 D 1, 82 G 1, 87 M 7]; R = Th [52 F 1]; R = Sc [61 D 1]; R = Hf [61 W 2]

RFe_2 [65 K 3, 60 H 1, 68 R 1]; R = Sm, Gd, Dy, Ho, Y [60 N 1]; R = Ce, Sm, Gd, Dy, Ho, Er [60 W 1]; R = Gd, Tb, Dy, Ho, Er, Y [70 B 13]; R = Gd, Tb, Dy, Ho, Er, Tm, Y [71 B 12]; R = Ce, Sm, Gd, Tb, Dy, Ho, Er, Tm, Lu, Y, Zr [71 B 20]; R = Sm, Tb, Dy, Ho, Er, Tm [77 B 4]; R = Sc, Y [73 D 8]; R = Sm, Tb, Dy, Ho, Er, Lu [77 B 4]; R = Ce [55 J 1, 70 B 14, 74 A 3, 85 D 11]; R = Pr [72 C 2]; R = Nd [72 C 2]; R = Sm [61 S 2]; R = Gd [53 B 1, 61 B 1, 61 N 2, 61 S 2, 74 A 3, 78 C 7]; R = Dy [61 B 1, 82 B 1]; R = Ho [79 F 5]; R = Er [79 F 5]; R = Tm [79 F 5]; R = Yb [72 C 2, 85 T 5]; R = Lu [74 A 3, 81 G 15, 85 D 11]; R = Y [76 B 18]; R = Zr [53 B 1]

RCo_2 [65 K 3, 60 H 1, 65 H 1]; R = Ce, Sm, Gd, Dy, Ho, Y [60 N 1]; R = Ce, Pr, Sm, Gd, Tb, Dy, Ho, Y [60 W 1]; R = Ce, Pr, Nd, Sm, Gd, Tb, Dy, Ho, Er [64 R 1]; R = Nd, Gd, Ho, Y [66 L 4]; R = Nd, Pr, Sm, Gd, Tb, Dy, Ho, Er, Y [72 B 10]; R = La [72 R 2]; R = Pr [76 L 2, 82 G 10]; R = Nd [76 L 2]; R = Gd [53 B 1, 61 B 1, 61 N 2]; R = Tb [76 L 2]; R = Dy [61 B 1, 76 L 2]; R = Ho [76 L 2]; R = Er [76 L 2]; R = Tm [76 G 4]; R = Y [61 D 1]; R = Zr [53 B 1]; R = Ta [53 B 1]

RNi_2 [65 K 3, 60 H 1, 69 L 1, 72 B 13]; R = Ce, Sm, Gd, Dy, Ho, Y [60 N 1]; R = Ce, Pr, Nd, Sm, Gd, Tb, Dy, Ho, Er [60 W 1]; R = La, Ce, Pr, Nd, Sm, Gd, Tb, Dy, Ho, Er, Tm, Y [83 I 1]; R = Ce [53 B 1, 87 S 7]; R = Pr [53 B 1, 82 G 10]; R = Gd [61 B 1]; R = Dy [61 B 1, 81 M 5]; R = Ho [81 M 5]; R = Er [81 M 5]; R = Yb [60 H 1]; R = Sc [61 D 1]

RM_2H_x [77 B 21, 77 B 22, 79 S 6]

RMn_2H_x R = Er [80 V 4, 83 W 5]; R = Y [77 B 19, 87 F 6]; R = Zr [79 D 8, 83 W 5, 84 F 4, 87 F 6]

RFe_2H_x R = Ho, Er, Tm [79 F 5]; R = Gd, Ho, Er, Tm, Lu [84 D 4]; R = Ho, Er, Tm [76 G 10]; R = Ce, Sm, Gd, Tb, Dy, Ho, Er, Y [77 B 18]; R = Ce [76 B 18, 85 D 11, 87 A 10]; R = Tb [85 B 4, 87 F 4, 87 F 5]; R = Dy [80 P 6]; R = Er [84 A 12, 87 F 4, 87 F 5]; R = Lu [85 D 11]; R = Y [76 B 18];

RNi_2H_x R = La, Er, Yb [83 E 1]

$ZrCr_2H_x$, ZrV_2H_x [81 I 3]

$(R'R'')M_2$ [73 B 12]; $(PrGd)Mn_2$ [71 N 1]; $(PrTb)Mn_2$ [71 N 1]; $(DyHo)Mn_2$ [62 W 1]; $(GdY)Mn_2$ [86 O 2]; $(YLu)Mn_2$ [86 O 2]

$(CeGd)Fe_2$ [73 M 12, 75 M 8]; $(CeY)Fe_2$ [80 D 1]; $(PrSm)Fe_2$ [84 S 9, 85 S 15]; $(PrTb)Fe_2$ [85 S 15]; $(PrY)Fe_2$ [85 S 15]; $(NdSm)Fe_2$ [84 S 9]; $(SmEr)Fe_2$ [84 T 1]; $(SmY)Fe_2$ [84 K 9]; $(GdTh)Fe_2$ [73 M 12, 75 M 8]; $(TbDy)Fe_2$ [78 M 3]; $(TbY)Fe_2$ [75 P 9]

$(CeY)Co_2$ [85 A 9]; $(PrDy)Co_2$ [70 L 6, 70 L 7]; $(PrHo)Co_2$ [70 L 6, 70 L 7]; $(PrY)Co_2$ [74 K 12]; $(NdGd)Co_2$ [71 P 4]; $(GdEr)Co_2$ [69 H 1]; $(GdY)Co_2$ [76 B 16]; $(TbHo)Co_2$ [87 A 2]; $(TbY)Co_2$ [84 L 5]; $(ErY)Co_2$ [84 L 6]; $(HoY)Co_2$ [78 S 19]

$(LaY)Ni_2$ [87 S 19]; $(CeLa)Ni_2$ [85 S 3]; $(CeY)Ni_2$ [85 A 9, 87 S 19]; $(PrDy)Ni_2$ [70 L 6, 70 L 7]; $(PrHo)Ni_2$ [70 L 6, 70 L 7]; $(PrY)Ni_2$ [74 K 12]; $(PrY)(CoNi)_2$ [74 G 12]; $(PrY)(CoCu)_2$ [74 G 12]

$(R'R'')M_2H_x$ $(CeZr)Mn_2H_x$ [83 P 16]; $(YZr)Fe_2H_x$ [86 K 4]

$R(M'M'')_2$ [73 B 12]; $Gd(MnFe)_2$ [76 I 3, 86 N 1]; $Tb(MnFe)_2$ [76 I 3]; $Dy(MnFe)_2$ [62 W 1, 76 I 3]; $Ho(MnFe)_2$ [62 W 1, 76 I 2]; $Er(MnFe)_2$ [76 I 2, 77 G 12, 77 I 3]; $Y(MnFe)_2$ [86 Y 7]; $Y(MnCo)_2$ [86 Y 7]; $Gd(MnNi)_2$ [82 S 22]; $Tb(MCr)_2$, M = Mn, Fe, Co, Ni [85 G 2]; $Gd(MnAl)_2$ [78 S 16, 78 S 17, 80 S 13, 83 S 18]; $Tb(MnAl)_2$ [62 W 1, 72 O 3]; $Dy(MnAl)_2$ [62 W 1]; $Ho(MnAl)_2$ [62 W 1]; $Er(MnAl)_2$ [72 O 3]

$Ce(FeCo)_2$ [68 M 2, 75 L 2]; $Pr(FeCo)_2$ [68 M 2]; $Ho(FeCo)_2$ [81 P 4]; $Er(FeCo)_2$ [68 M 2, 77 G 12, 81 P 4, 85 A 15]; $Y(FeCo)_2$ [68 P 2, 82 K 3]; $R(FeM)_2$, M = Ni, Al, R = Y, Zr [77 M 12]; $Dy(Fe_{0.9}M_{0.1})_2$; M = Al, Ga, B [87 Z 1]; $Ce(FeNi)_2$, $Pr(FeNi)_2$, $Er(FeNi)_2$ [68 M 2]; $Dy(FeNi)_2$ [76 B 12, 78 B 12]; $Ho(FeNi)_2$ [78 B 12]; $R(MAl)_2$, R = Pr, Gd, Er, M = Mn, Fe, Co, Ni, Cu [74 O 2]; $R(FeAl)_2$ [68 D 2, 71 O 3, 73 Z 2]; R = Gd, Dy, Ho, Y [76 G 8]; R = Sc, Y, Lu [75 D 11]; R = Sc, Y, R [75 D 10]; $Pr(FeAl)_2$ [67 O 2]; $Gd(FeAl)_2$ [67 O 1, 79 B 6, 80 A 6]; $Tb(FeAl)_2$ [73 O 1]; $Dy(FeAl)_2$ [62 W 1, 72 O 4, 82 B 2]; $Ho(FeAl)_2$

[85 S 21]; $Er(FeAl)_2$ [71 O 5, 77 G 12]; $Lu(FeAl)_2$ [87 B 13]; $Y(FeAl)_2$ [75 B 12]; $R(FeCu)_2$ [85 T 4]; $Gd(FeCu)_2$ [86 T 7]; $Yb(FeCu)_2$ [86 T 7]; $Y(FeCu)_2$ [86 T 7]; $R(FeRu)_2$, R = Ho, Er [84 S 15]; $Y(FeRu)_2$ [74 R 1]

$Ce(CoNi)_2$ [68 M 2, 77 O 11, 83 D 1, 85 A 9]; $Pr(CoNi)_2$ [68 M 2]; $Gd(CoNi)_2$ [88 K 2]; $Er(CoNi)_2$ [68 M 2, 77 G 12]; $Y(CoNi)_2$ [74 K 12]; $Zr(CoCr)_2$ [83 H 2]; $Ce(CoAl)_2$ [68 M 2, 80 Z 2]; $Pr(CoAl)_2$ [67 O 2]; $Gd(CoAl)_2$ [67 O 1]; $Tb(CoAl)_2$ [73 O 1]; $Dy(CoAl)_2$ [62 W 1, 72 O 4, 80 S 13]; $Ho(CoAl)_2$ [73 O 1]; $Er(CoAl)_2$ [67 O 1, 70 O 2, 81 K 13]; $Lu(CoAl)_2$ [88 S 3]; $Y(CoAl)_2$ [73 Z 2, 86 I 6, 88 S 3]; $Sc(CoAl)_2$ [86 I 6, 88 S 3]; $Gd(MCu)_2$, M = Co, Ni, Al [87 B 12]; $Gd(CoCu)_2$ [86 B 12]; RCoGa, R = Ce, Pr, Nd, Sm, Y [83 R 7]; RCoSn [82 S 19]; $Gd(CoIr)_2$ [79 C 2, 79 C 3]; $R(CoRu)_2$, R = Ho, Er [84 S 15]; $Ce(CoRu)_2$ [71 S 5]; $Y(CoRu)_2$ [74 R 1]; $R(NiAl)_2$, R = Ce, Pr, Nd, Gd, Tb, Dy, Ho, Er [70 L 6, 70 L 7]; RNiAl [73 O 3, 82 R 5, 87 T 6]; $Gd(NiAl)_2$ [73 H 2]; $Ce(NiCu)_2$ [70 W 1, 85 M 11]; $Gd(NiCu)_2$ [70 W 1, 74 P 2, 86 B 11]; LaNiGa [86 Y 5]; $R(NiGe)_2$ [77 C 5]; RNiSn [83 D 8, 84 S 13, 85 R 10]; $R(NiRu)_2$, R = Ho, Er [84 S 15]; $Y(NiRu)_2$ [74 R 1]; $Mg(CuAl)_2$ [80 K 6]

$R(M'M'')_2H_x$ $Er(FeMn)_2H_x$ [78 S 2], $Zr(FeMn)_2H_x$ [83 S 17]; $Y(MnM)_2H_x$, M = Co, Ni, Al [88 F 3] $Ho(FeCo)_2H_x$ [81 P 4]; $Er(FeCo)_2H_x$ [81 P 4]; $Zr(FeCr)_2H_x$ [86 I 7]; $Zr(CrCo)_2H_x$ [83 H 2]; GdFeAlH_x [84 D 7]

GdNiAlH_x [84 D 7]

For thermal expansion of lattice parameters see

RMn_2 R = Gd, Tb, Dy, Ho [83 G 1]; R = Pr, Nd, Sm, Gd, Y [85 T 1]; R = Pr, Nd, Y, Th [86 O 2]; R = Tb [80 M 2]; R = Y [82 G 1, 88 G 1]; R = Th [87 D 7]

RFe_2 R = Ce, Hf, Ti, Sc [76 M 20]; R = Er, Y, Ti, Zr [73 B 23]; R = Tb [77 B 4, 77 I 4]

RCo_2 R = Nd, Gd, Tb, Dy, Ho, Er, Y [71 C 2]; R = Nd, Gd, Dy, Ho, Y [72 G 6]; R = Dy, Ho, Er [79 G 10]; R = Nd [83 G 7]; R = Gd [65 H 1, 82 L 4]; R = Tb [77 I 4, 80 G 7, 80 M 2, 83 Y 6]; R = Ho [83 G 7]; R = Y [82 L 5]

RNi_2 R = Dy, Ho, Er [81 M 5]; R = Gd [71 C 2]; R = Tb [80 M 2]; R = Ce [87 S 7]

RM_2H_x $HoFe_2H_x$ [82 A 11]; $ErFe_2H_x$ [82 A 11]

$(R'R'')M_2$ $(LaY)Mn_2$ [88 N 1]; $(YSc)Mn_2$ [87 W 2, 88 N 1]; $(TbDy)Fe_2$ [77 A 1]; $(TbHo)Fe_2$ [81 K 12]; $(ScTi)Fe_2$ [86 N 3]; $(TbHo)Co_2$ [83 I 3]; $(TbY)Co_2$ [84 L 5]; $(HoY)Co_2$ [78 S 19]; $(ErY)Co_2$ [84 L 6]

$R(M'M'')_2$ $Y(MnAl)_2$ [87 W 2, 88 S 1]; $Dy(FeAl)_2$ [85 K 3]; $Tb(CoNi)_2$ [82 M 2]; $Gd(CoAl)_2$ [84 B 5]; $Gd(NiAl)_2$ [85 K 1]

For thermal expansion see also

RMn_2 R = Gd, Tb, Ho, Er, Y [83 S 11]; R = Gd, Dy, Y [83 N 3]; R = Y [87 O 5, 88 N 1]; $ThMn_2$ [87 D 7]

RFe_2 R = Gd, Tb, Dy, Ho, Er, Tm, Y, Sc, Zr [83 G 12]

RCo_2 R = Nd, Tb, Dy, Ho, Y, Zr [83 G 12]

RNi_2 R = La, Nd, Sm, Tb, Dy, Ho, Er, Tm, Y [84 I 2]; R = Ce [87 S 7]

$(R'R'')M_2$ $(YLa)Mn_2$, $(YSc)Mn_2$ [88 N 1]; $(TbDy)Fe_2$ [86 S 7]; $(GdY)Co_2$ [83 M 7, 84 M 4, 84 M 5]

$R(M'M'')_2$ $Y(MnAl)_2$ [86 S 12, 87 S 8]; $Y(FeCo)_2$ [83 M 7]; $R(FeAl)_2$ [84 S 11]; $Gd(MCu)_2$, M = Co, Ni, Al [87 B 12]; $Ho(CoCu)_2$ [86 H 3]; $Er(CoCu)_2$ [88 D 3]; $Y(CoCu)_2$ [88 D 3]

For thermal decomposition see

$PrCo_2$, $NdCo_2$ [73 F 1]

For oxidation of RM_2 compounds see

R = Fe, Co, Ni [76 D 2, 76 L 1, 79 D 1]

For enthalpies of formation see

$GdFe_2$, $GdCo_2$, $GdNi_2$ [86 C 7]

For peretectic temperatures see

$Ce(CoNi)_2$ [85 D 1]

For crystal growing see

$HoFe_2$, $ErFe_2$ [76 M 14]; $(HoTb)Fe_2$ [74 M 7]

For texture see RCo_2 [77 H 3]

Magnetization, Curie temperatures

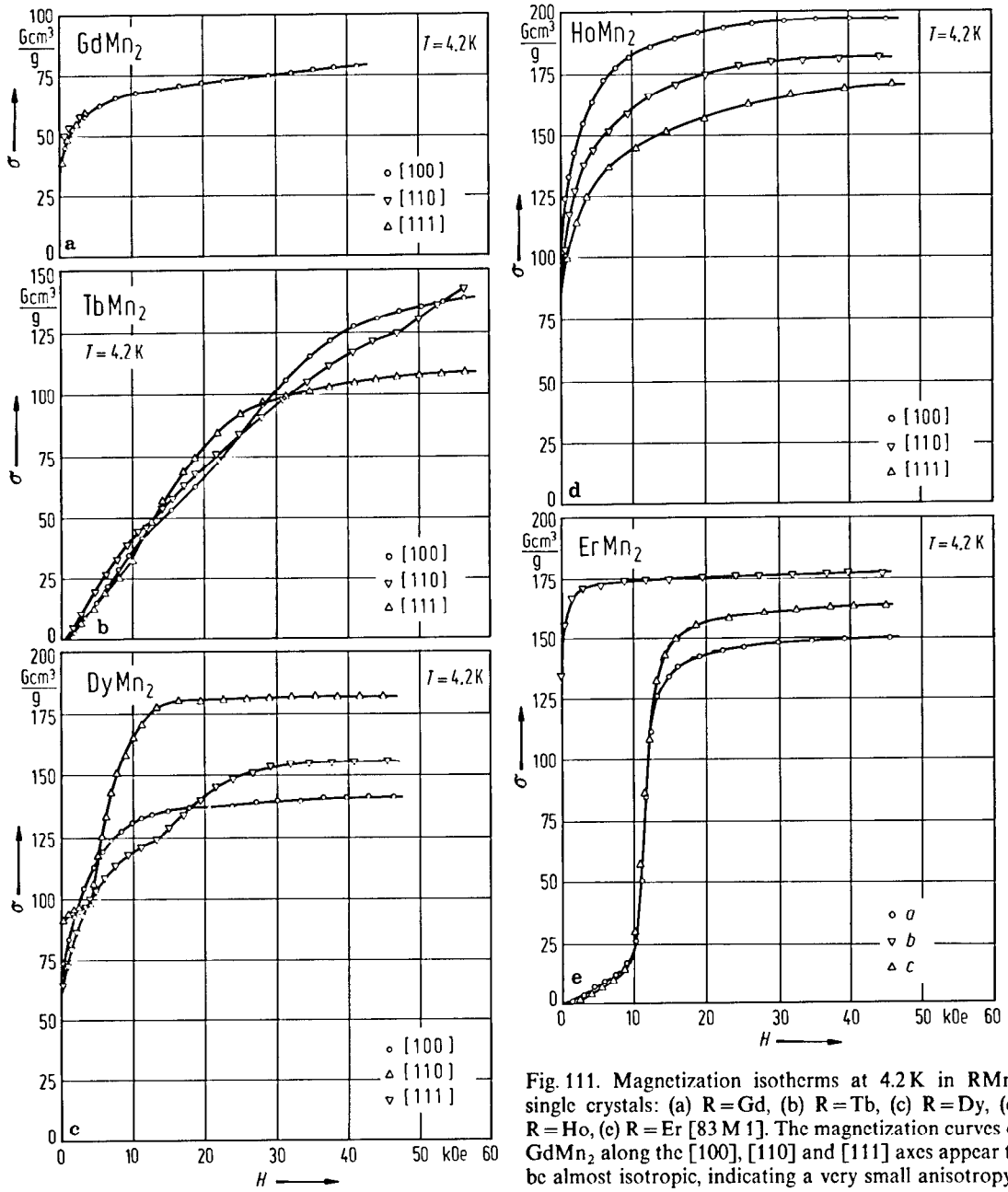

Fig. 111. Magnetization isotherms at 4.2 K in RMn_2 single crystals: (a) R = Gd, (b) R = Tb, (c) R = Dy, (d) R = Ho, (e) R = Er [83 M 1]. The magnetization curves of $GdMn_2$ along the [100], [110] and [111] axes appear to be almost isotropic, indicating a very small anisotropy.

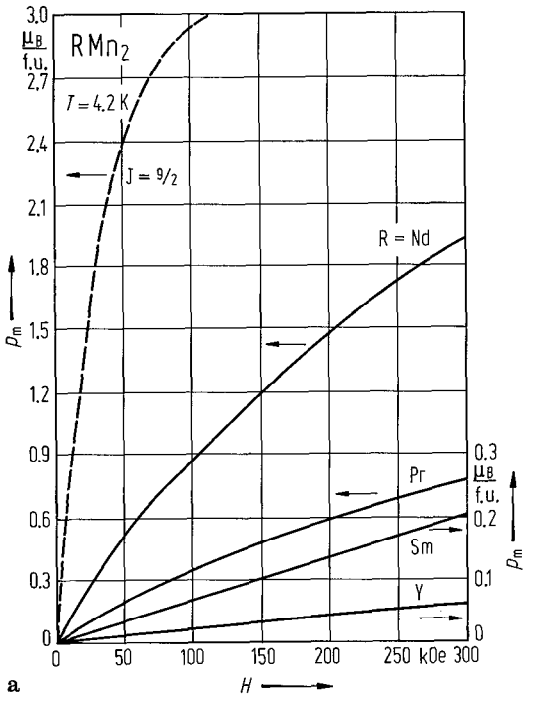

Fig. 112. (a) Magnetization isotherms of YMn_2, $PrMn_2$, $NdMn_2$ and $SmMn_2$ at 4.2 K in high fields. The dashed line shows a Brillouin function for $J = 9/2$ (Nd^{3+} ion). The magnetization of YMn_2 increases almost linearly with increasing the field. The magnetization isotherm is almost straight for $SmMn_2$ and slightly convex upward for $NdMn_2$ and $PrMn_2$. The values of the magnetizations at 300 kOe are 0.74 μ_B/f.u. for $PrMn_2$ and 0.19 μ_B/f.u. for $SmMn_2$. The magnetic moment of $NdMn_2$ is 1.88 μ_B/f.u. (b) Magnetization curves for $GdMn_2$, $TbMn_2$, $DyMn_2$, $HoMn_2$ and $ErMn_2$ at 4.2 K. The magnetizations show a trend of saturation in high fields [85 W 1].

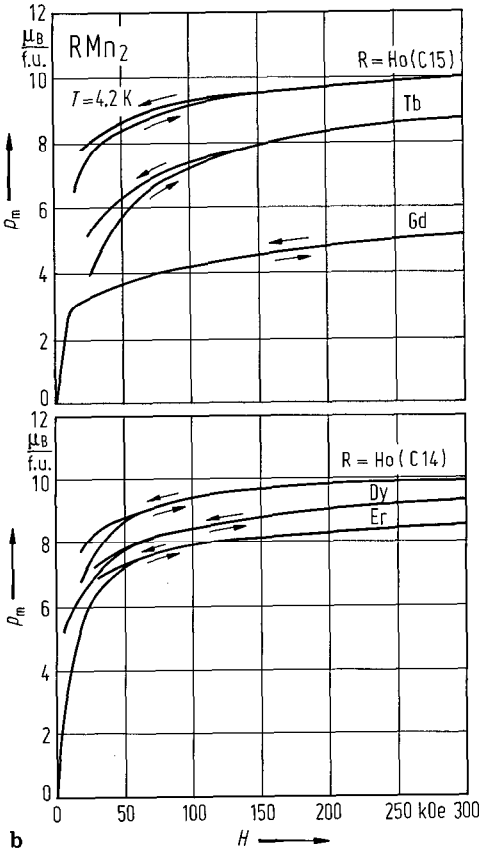

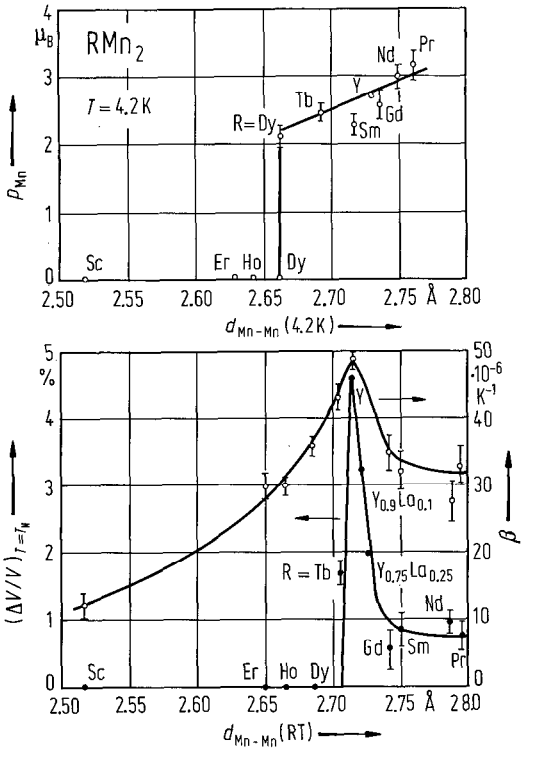

Fig. 113. Variations of Mn magnetic moment, volume change at T_N, and thermal volume expansion coefficient β with the interatomic distance d_{Mn-Mn} [87 W 1]: (a) Mn magnetic moment p_{Mn}, at 4.2 K in RMn_2 compounds [83 N 4, 84 Y 6, 86 Y 6], as a function of d_{Mn-Mn} at 4.2 K. (b) Volume change at T_N, $(\Delta V/V)_{T=T_N}$, and the average TEC between 200 and 300 K plotted against d_{Mn-Mn} at room temperature. The data suggest that the interatomic distance, d_{Mn-Mn}, is responsible for the onset of the ground-state Mn magnetic moment in RMn_2 compounds, and Mn magnetic moments collapse abruptly at a critical d_{Mn-Mn} value. $(\Delta V/V)_{T=T_N}$ disappears abruptly at a critical d_{Mn-Mn} distance, while its magnitude does not indicate the ground state Mn magnetic moment of each compound and has a maximum value for YMn_2. TEC is large in all RMn_2 compounds compared with that of $ScMn_2$, which is a Pauli paramagnet.

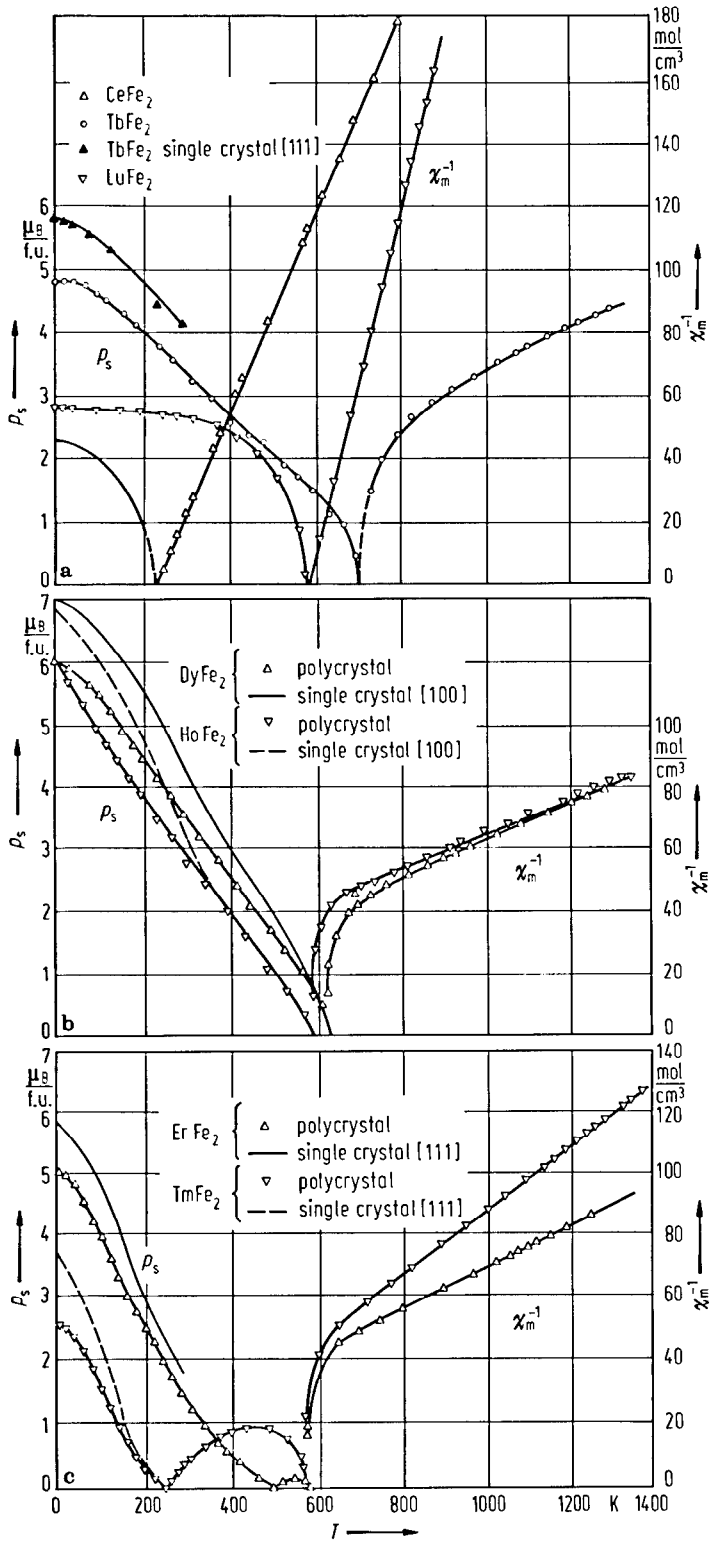

Fig. 114. (a) Thermal variations of the spontaneous magnetizations and reciprocal magnetic susceptibilities for $CeFe_2$ [81 D 4], $TbFe_2$ [71 B 12] and $LuFe_2$ [70 B 8, 71 G 3] polycrystalline compounds. The spontaneous magnetization vs. temperature for a $TbFe_2$ single crystal is also plotted [78 C 5]. (b) Thermal variations of the spontaneous magnetizations and reciprocal magnetic susceptibilities for $DyFe_2$ and $HoFe_2$ polycrystalline compounds [71 B 12]. The spontaneous magnetizations for $DyFe_2$ [78 C 5] and $HoFe_2$ [79 A 1] single-crystals are also plotted. (c) Thermal variations of the spontaneous magnetizations and reciprocal magnetic susceptibilities for $ErFe_2$ and $TmFe_2$ polycrystalline compounds [71 B 12]. The spontaneous magnetizations for $ErFe_2$ [74 C 2] and $TmFe_2$ [78 C 5] single-crystals are also plotted.

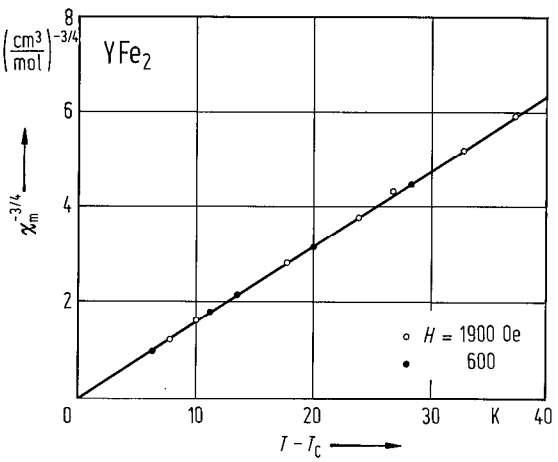

Fig. 115. Temperature dependence of the magnetic susceptibilities near T_C for YFe_2 [79 B 13]. The data fit the relation $\chi_m^{-1} = At^\gamma$, where $t = |T - T_C| T_C^{-1}$ and $\gamma \cong 1.34$.

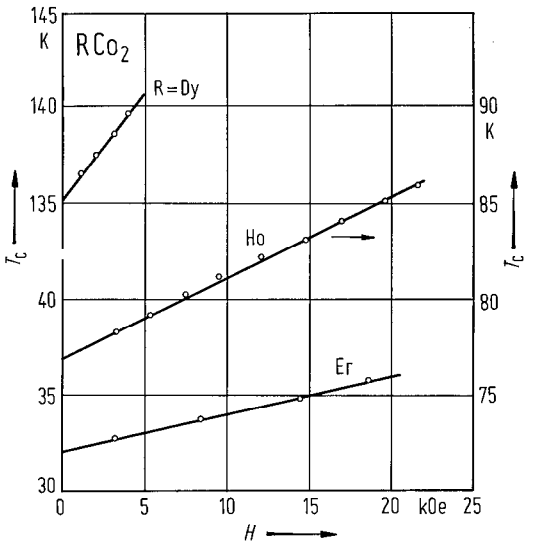

Fig. 116. Magnetic field dependence of the transition temperature in $DyCo_2$, $HoCo_2$ and $ErCo_2$ [72 G 5]. The observed behaviour is characteristic of a first-order phase transition. For RCo_2 (R = Pr, Nd, Sm, Gd, Tb) compounds a second-order phase transition is observed.

For Fig. 117, see next page.

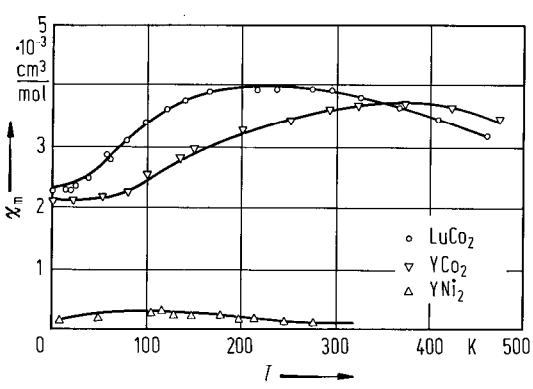

Fig. 118. Temperature dependence of the magnetic susceptibilities in $LuCo_2$ [71 B 9], YCo_2 [72 B 10] and YNi_2 [72 B 13]. These compounds show a Pauli-type behaviour.

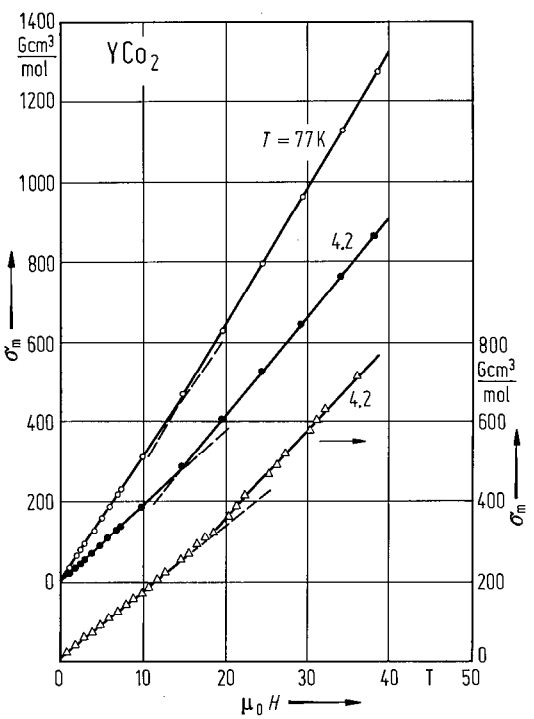

Fig. 119. Magnetization isotherms for YCo_2 [78 S 6]. Open and solid circles: sample 1 (77 and 4.2 K, respectively). Triangles: sample 2. The dashed straight lines only serve to guide the eye. In the presence of high fields, a magnetic moment is induced.

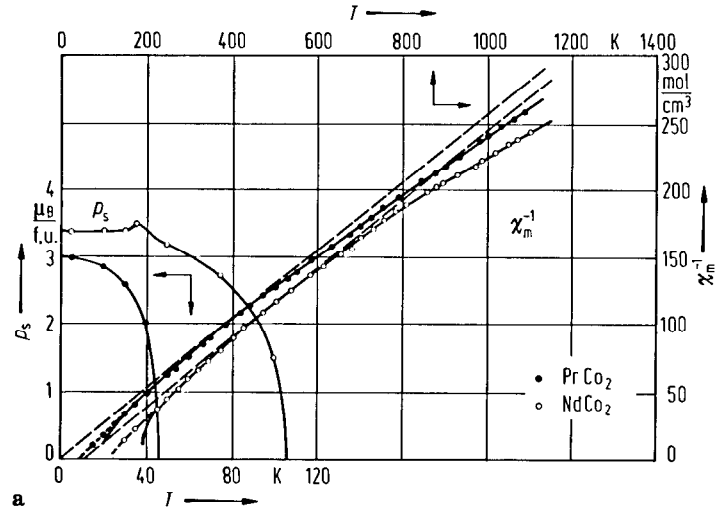
T
0 200 400 600 800 1000 1200 K 1400
300 mol/cm³ 250 200 150 100 50 0
χ_m^{-1}
4 μB/f.u. 3 2 1 0
p_s
p_s
χ_m^{-1}
• PrCo2
○ NdCo2
0 40 80 K 120
T
a

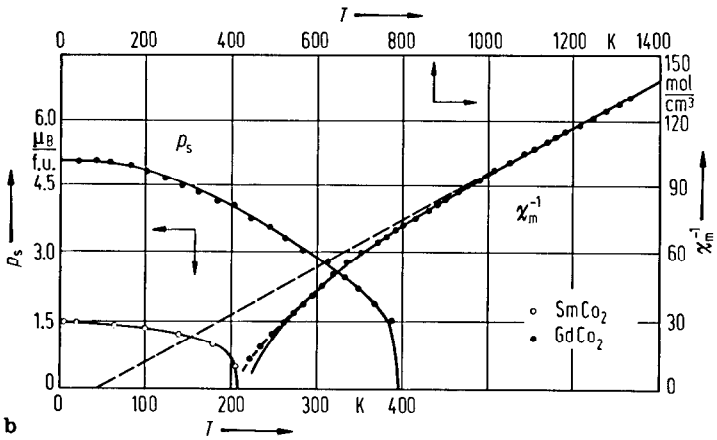
T
0 200 400 600 800 1000 1200 K 1400
150 mol/cm³ 120 90 60 30 0
χ_m^{-1}
6.0 μB/f.u. 4.5 3.0 1.5 0
p_s
p_s
χ_m^{-1}
○ SmCo2
• GdCo2
0 100 200 300 K 400
T
b

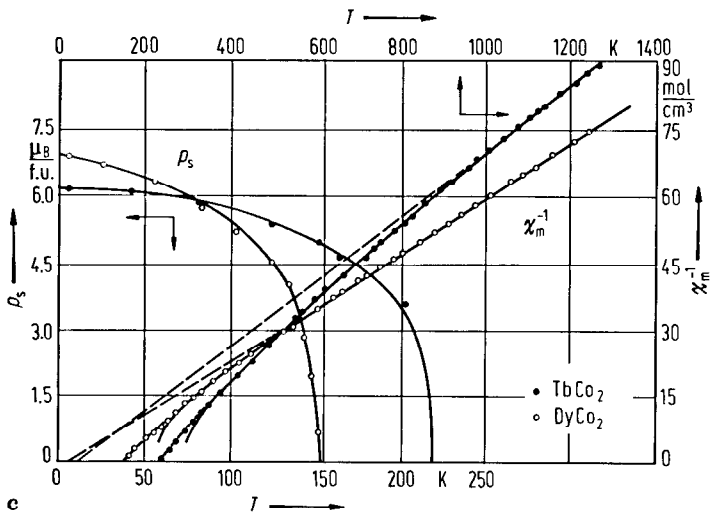
T
0 200 400 600 800 1000 1200 K 1400
90 mol/cm³ 75 60 45 30 15 0
χ_m^{-1}
7.5 μB/f.u. 6.0 4.5 3.0 1.5 0
p_s
p_s
χ_m^{-1}
• TbCo2
○ DyCo2
0 50 100 150 200 K 250
T
c

Fig. 117a–c.

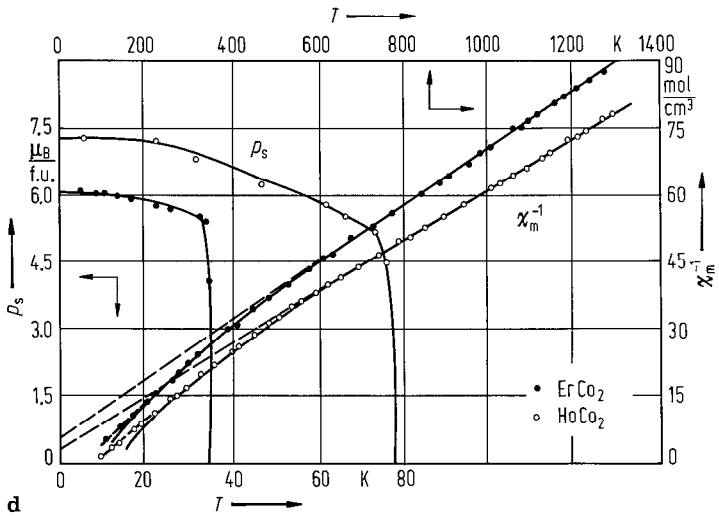

Fig. 117. Thermal variations of spontaneous magnetizations and of reciprocal susceptibilities for (a) $PrCo_2$ and $NdCo_2$, (b) $SmCo_2$ and $GdCo_2$, (c) $TbCo_2$ and $DyCo_2$, (d) $HoCo_2$ and $ErCo_2$ polycrystalline compounds [72 B 10].

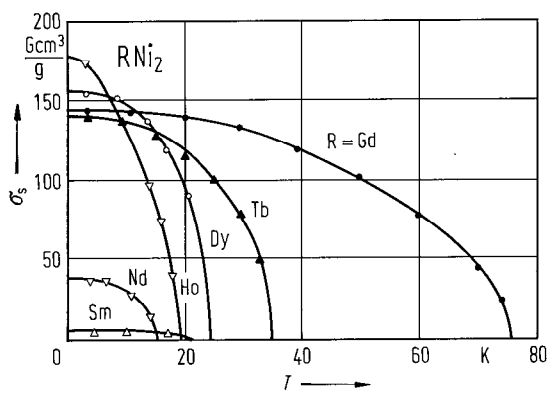

Fig. 120. Thermal variations of spontaneous magnetizations for some RNi_2 compounds [72 B 13].

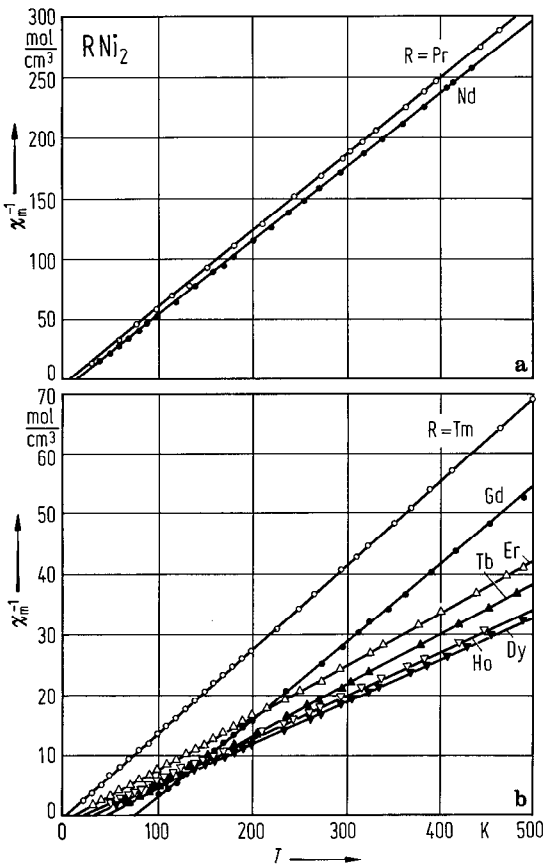

Fig. 121. Thermal variations of reciprocal susceptibilities for RNi_2: (a) R = Pr, Nd, (b) R = Gd, Tb, Dy, Ho, Er, Tm [72 B 13]. The effective magnetic moments are nearly the same as those of the R^{3+} free-ion values.

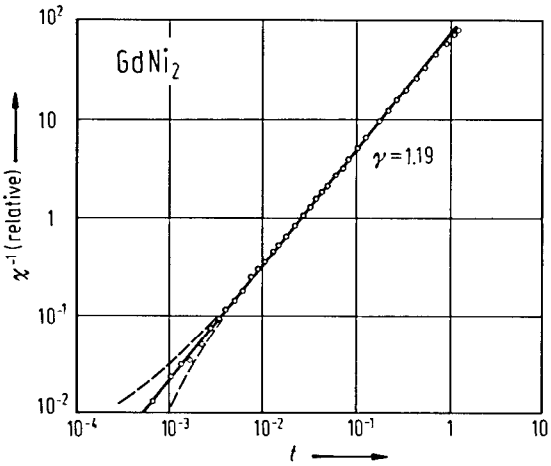

Fig. 122. Inverse magnetic susceptibility vs. reduced temperature for $GdNi_2$. The dashed lines represent a qualitative estimate of the uncertainty in $t=|T-T_C|T_C^{-1}$ due to an uncertainty in T_C of 30 mK. The experimental data fit the relation $\chi^{-1}=At^{\gamma}$ with $\gamma=1.19$ [74 H 8].

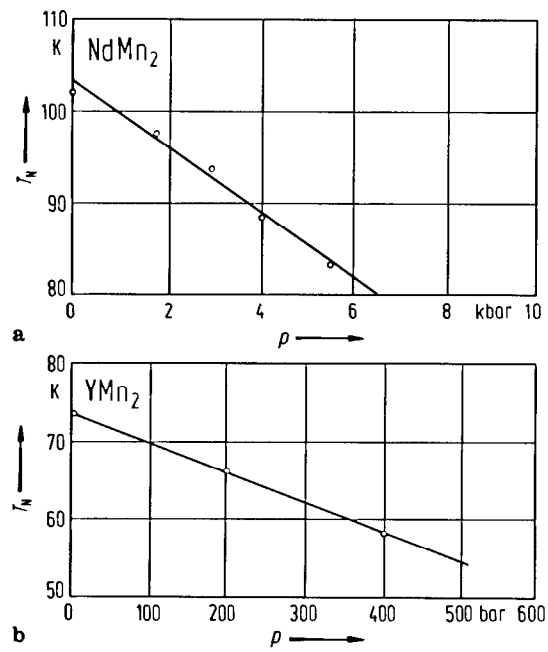

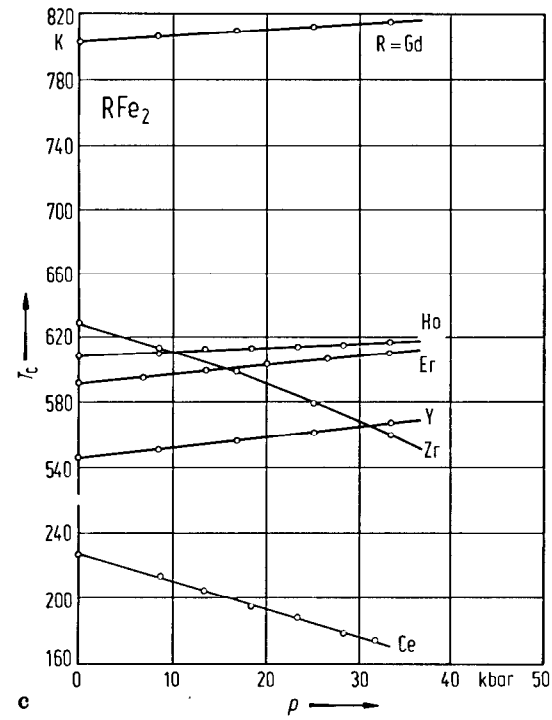

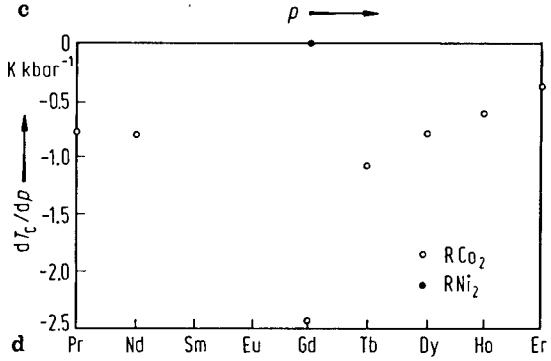

Fig. 123. Pressure dependence of the Néel temperature T_N in (a) $NdMn_2$ and (b) YMn_2 compounds. Values of $dT_N/dp=-3.5$ K/kbar and -35 K/kbar, respectively, are observed, evidencing the part played by the Mn-Mn interatomic distances on the Mn magnetic behaviour [86 O 2]. Pressure dependence of the Curie temperatures T_C in (c) RFe_2 [73 B 25] and (d) RCo_2 and RNi_2 [71 B 9] compounds. The observed behaviour in RFe_2 compounds is correlated with the distance between the transition metal atoms, as well as with the Fermi wavevector of the 3d band measured to the nearest band extremum. For $GdNi_2$, where Ni is nonmagnetic, the T_C value is not dependent on pressure.

Table 41a. Curie temperatures and saturation magnetizations of RMn_2 compounds. [1,2])

	T_C(K)				$p_s(\mu_B/f.u.)$					$p_{Mn}(\mu_B)$	
	65 F 1	81 M 1	83 G 1	83 M 1	85 T 1	81 M 1	83 G 1	83 M 1	85 W 1	83 G 1	83 M 1
$PrMn_2$					112				0.74 [5])		
$NdMn_2$					104						
$SmMn_2$					86				0.19 [5])		
$GdMn_2$			110	110	106	2.9	2.7	3.9	6.2 [6])	2.15	1.6
$TbMn_2$			26	48			$\cong$5.0 [4])	6.8 [3])	9.5 [6])	$\leqslant$2.0	
$DyMn_2$		38	49	36		7.2	7.1	8.9	10.0 [6])	$\leqslant$1.45	$\sim$0.6
$HoMn_2$		26	31	25		6.4	8.7	9.7	10.3 [6]) (C15) 10.2 [6]) (C14)	$\leqslant$0.65	0.2
$ErMn_2$	25			15				8.8	8.9 [6])		0.1
$TmMn_2$	12										
YMn_2					81 (cooling) 112 (heating)				[7])		

[1]) Because of the complex magnetic structure and/or lack of saturation, no reliable values of saturation magnetization, p_s, may be obtained. See figures 111 and 112.

[2]) For paramagnetic behaviour see [83 G 1, 83 M 1].

[3]) Value obtained in a field of 56 kOe for [111] direction.

[4]) Value obtained in a field of 55 kOe.

[5]) Values obtained in a field of 300 kOe.

[6]) Obtained from extrapolation of p_m to $1/H \rightarrow 0$, from fields up to 300 kOe.

[7]) The magnetization of YMn_2 increases linearly with the applied field.

Table 41b. Curie temperatures (K) of RFe_2 compounds.

	63 W 1 64 W 2	64 F 1	69 G 1 71 G 3	70 B 13	71 B 12	78 B 9	79 F 5	80 b 1	80 I 2	80 S 11 81 S 11	77 M 8 81 M 10
$CeFe_2$		235									
$PrFe_2$										525	543
$NdFe_2$										530	578
$SmFe_2$				676					674		
$GdFe_2$	790		798	785	793			789			
$TbFe_2$				711	697	693(3)		682	694		
$DyFe_2$	705			635	635	633(3)	612	633	630		
$HoFe_2$	614			612	597	593(3)	574	594	594		
$ErFe_2$	596			590	574		610	576	571		
$TmFe_2$	610				566			555	555		
$YbFe_2$											543
$LuFe_2$	610		583						562		
YFe_2	550		537	543	535			534	528		

Table 41c. Curie temperatures (K) of RCo_2 compounds.

	63 W 1	66 F 1	66 L 4	71 B 9	72 B 10	72 G 5	74 D 4	76 L 2	78 K 4	79 G 2	81 M 6
$CeCo_2$					Pauli paramagnet						
$PrCo_2$	50	50		54	46			40	34		
$NdCo_2$	126	116	99	98	98	99		99	98		
$SmCo_2$	232	259			211				204		
$GdCo_2$	408	410	404	395	395			395	398		
$TbCo_2$	245	256		228	228	228		230	230	240	
$DyCo_2$	169	159		135	135	135		133	135		138
$HoCo_2$	49	95	77.8	74	74	77		75	89		77.4
$ErCo_2$	48	86		33	33	32		32	30		32
$TmCo_2$	33	18				4.5	4...7 [1])		4		

[1]) Depending on preparation method.

Table 41d. Curie temperatures (K) of RNi_2 compounds.

	63 S 1	66 F 1	70 W 1	72 B 13	73 N 7	73 Z 3	75 G 2	77 G 2	81 M 5	83 I 1
$LaNi_2$				Pauli paramagnet						
$CeNi_2$				Pauli paramagnet						
$PrNi_2$	8									
$NdNi_2$	20	16		15.5						9
$SmNi_2$	77	21		21						22
$GdNi_2$	90	85	85	76		74.1				75
$TbNi_2$	46	45		35						40
$DyNi_2$	32	30		23				25	21	22
$HoNi_2$	23	22		18			13.4		13	16
$ErNi_2$	14	21		16					5	7
$TmNi_2$	14			13.5						
$YbNi_2$					5.7(4)					
$LuNi_2$				Pauli paramagnet						
YNi_2				Pauli paramagnet						

Table 41e. Saturation magnetization and paramagnetic behaviour of RFe_2 compounds.

	p_s (μ_B/f.u.)										Paramagnetic behaviour χ^{-1} vs. T
	63 W 1 71 w 1	64 F 1	69 G 1 71 G 3	70 B 13	71 B 12	75 D 8	79 B 6	80 b 1	80 c 1	80 S 11 81 S 11	
$CeFe_2$		2.38									
$PrFe_2$										4.7	
$NdFe_2$										4.6	
$SmFe_2$	2.50					2.90					
$GdFe_2$	3.35		3.78	2.80	3.75		3.90	3.70			nonlinear [70 B 8, 71 B 12, 80 I 2]
$TbFe_2$	3.68			4.72	5.00			5.60	5.81*		nonlinear [71 B 12, 80 I 2]
$DyFe_2$	4.91			5.50	6.00			5.60	6.87*		nonlinear [71 B 12, 80 I 2]
$HoFe_2$	5.11			5.50	6.00			6.00	6.70*		nonlinear [71 B 12, 80 I 2]
$ErFe_2$	4.75			4.80	5.00			5.00	5.79*		nonlinear [71 B 12, 80 I 2]
$TmFe_2$	2.52				2.70			3.10	3.72*		nonlinear [71 B 12, 80 I 2]
$YbFe_2$											
$LuFe_2$	2.97		2.88								C-W [70 B 8]
YFe_2	2.91		2.89	2.90				2.90			C-W [71 B 12, 70 B 8]

Table 41f. Saturation magnetization and paramagnetic behaviour of RCo_2 compounds. For measurements on single crystals see $GdCo_2$ [75 G 2*]; $HoCo_2$ [75 G 2*, 78 A 8*]; $TmCo_2$ [74 D 4*].

	p_s (μ_B/f.u.)							Paramagnetic behaviour
	63 W 1	66 F 1	66 L 4	72 B 10	74 D 4	75 G 2	79 G 2	χ^{-1} vs. T
$CeCo_2$	Pauli paramagnet							
$PrCo_2$	2.98	3.2		3.00				nonlinear [71 B 9, 72 B 10, 84 S 16]
$NdCo_2$	3.46	3.8	3.4 [1])	3.40				nonlinear [71 B 9, 72 B 10, 84 S 16]
$SmCo_2$	1.26	2.0		1.50				
$GdCo_2$	4.31	4.9	4.9	4.96		5.30		nonlinear [70 B 7, 71 B 9, 72 B 10, 72 B 11, 84 S 16]
$TbCo_2$	4.38	6.7		6.30			6.65	nonlinear [71 B 9, 72 B 10, 72 B 11, 84 S 16]
$DyCo_2$	6.72	7.6		6.80				nonlinear [71 B 9, 72 B 10, 72 B 11, 84 S 16]
$HoCo_2$	7.17	7.8		7.30		9.30		nonlinear [71 B 9, 72 B 10, 72 B 13, 84 S 16]
$ErCo_2$	5.87	7.0		6.20				nonlinear [71 B 9, 72 B 10, 72 B 11, 84 S 16]
$TmCo_2$	3.96	4.7			2.5(3)			nonlinear [74 D 4]
$YbCo_2$								
$LuCo_2$	Pauli paramagnet, see Fig. 118							
YCo_2	Pauli paramagnet, see Fig. 118							

[1]) Obtained from figure.

Table 41g. Saturation magnetization and paramagnetic behaviour of RNi_2 compounds. For measurements on RNi_2 single crystals see $DyNi_2^*$ [77 G 2], $HoNi_2^*$ [75 G 2], $ErNi_2^*$ [83 G 2].

	p_s (μ_B/f.u.)							Paramagnetic behaviour						
	63 S 1	66 F 1	69 K 1	72 B 13	75 G 2	77 G 2	83 G 2	χ^{-1} vs. T	Θ (K)				p_{eff} (μ_B/f.u.)	
									66 F 1	72 B 13	75 G 2	77 G 2	66 F 1	72 B 13
$LaNi_2$	Pauli paramagnet													
$CeNi_2$	Pauli paramagnet [66 F 1]													
$PrNi_2$	0.57	0.86						C-W	4	8			3.57	3.53
$NdNi_2$	1.62	1.80		1.75				C-W	10	16.5			3.74	3.61
$SmNi_2$		0.25		0.20				nonlinear						
$GdNi_2$	6.74	7.10	7.10	7.00				C-W	78	77			7.82	7.98
$TbNi_2$	5.84	7.80		6.90				C-W	35	44			9.82	9.71
$DyNi_2$	7.08	9.20		7.83		8.8		C-W	23	28		28	10.40	10.62
$HoNi_2$	7.04	8.40		8.90	7.55			C-W	12	18.5	16		10.50	10.64
$ErNi_2$	5.48	6.80		5.40			5.90	C-W	11	10			9.37	9.55
$TmNi_2$	2.48	3.20		3.34				C-W	0	2			7.28	7.56
$YbNi_2$	See [73 N 7]													
$LuNi_2$	Pauli paramagnet $\chi_m \cong 0.47 \cdot 10^{-3}\,cm^3\,mol^{-1}$ at 300 K [63 S 1]													
YNi_2	Pauli paramagnet [66 F 1, 72 B 13], see Fig. 118													

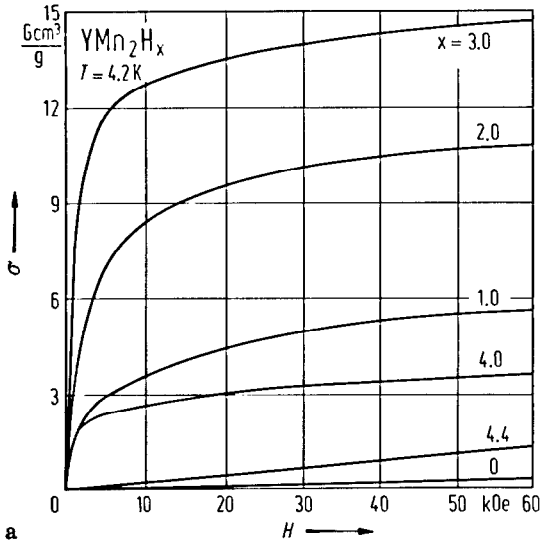

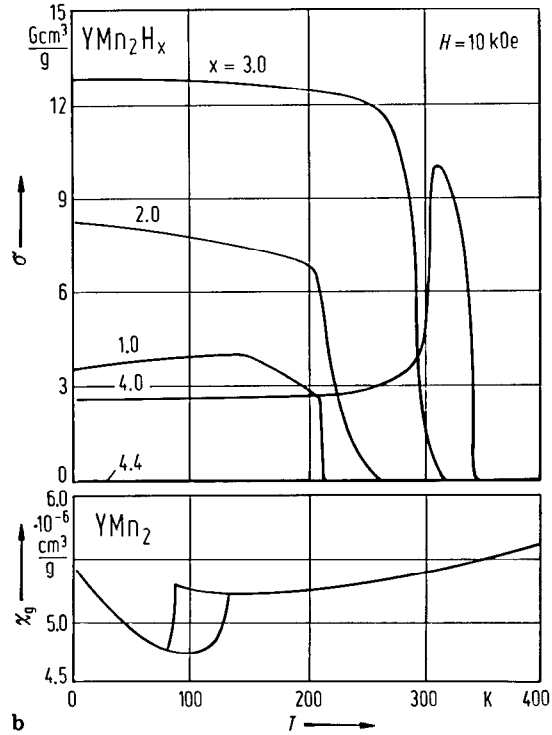

Fig. 124. (a) Magnetization isotherms at 4.2 K for some YMn_2H_x hydrides and (b) magnetization as function of temperature for the above samples in $H = 10$ kOe [87 F 6]. In the β' phase of YMn_2H_x with $0.5 \leqq x \leqq 3.0$ both the Curie temperature and the saturation moment increase by increasing x and reach the maxima of $T_C = 320$ K and $p_s = 0.60\,\mu_B$/f.u. for $YMn_2H_{3.0}$, respectively. In the more greatly charged YMn_2H_x with $x > 4.0$, the magnetization decreases drastically with increasing x and antiferromagnetism or paramagnetism becomes stable again, which is coincident with the appearance of the β phase. It should be noted that the $\sigma - H$ curve with $x = 4.0$ indicates an atypical behaviour. It looks similar to a cluster glass owing to the coexistence of the β'- and β-phases, but is not accompanied by any thermal history. This may be characteristic of diffusion of hydrogen at high temperatures. When hydrogeneration occurs the Mn–Mn distance exceeds the critical value [77 B 21, 85 I 3] and ferromagnetism is stabilized. If the Mn–Mn distance becomes too large, the Mn magnetic moment disappears again. In (b) the temperature dependence of the magnetic susceptibility of YMn_2 is also depicted.

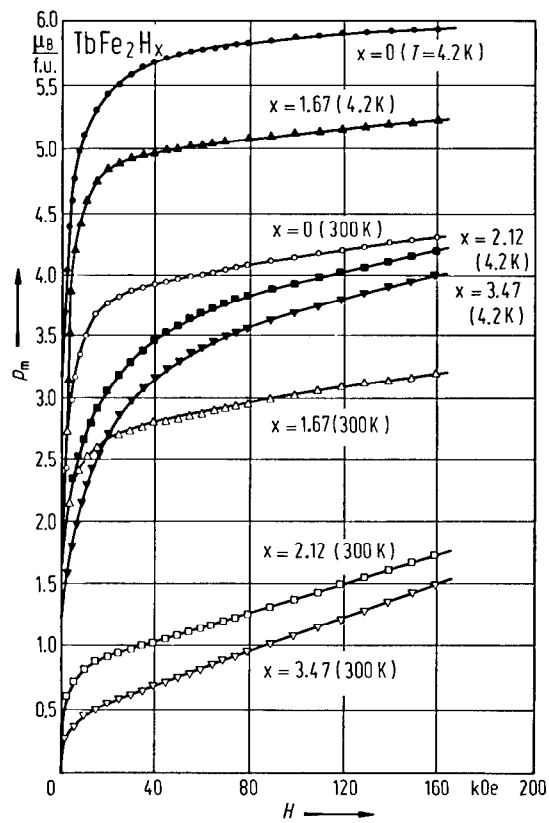

Fig. 125. Variation of the magnetization of $TbFe_2H_x$ versus applied magnetic field at 4.2 and 300 K for $x = 0$, 1.67, 2.12, and 3.47 [85 B 4]. The behaviour of the magnetization at 4.2 K for $x = 1.67$ is similar to that of the pure compound ($x = 0$). Nevertheless a decrease of $\cong 1\,\mu_B$ is observed for the saturation magnetic moment. This may be attributed to an enhanced Fe magnetic moment (by NMR studies the Tb magnetic moment is constant). For the highest values of x, the saturation is not complete at 4.2 K.

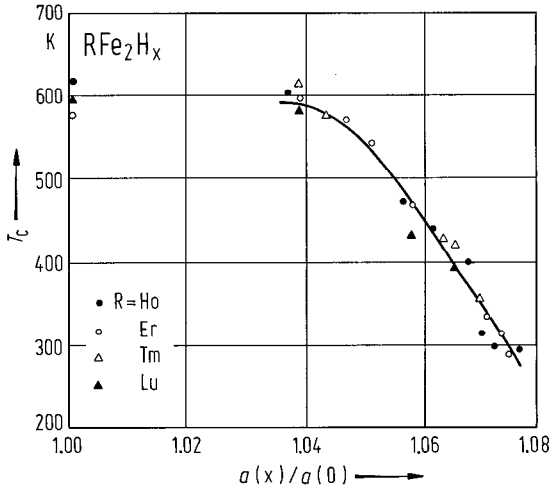

Fig. 126. Dependence of the Curie temperature T_C in RFe_2H_x hydrides on the relative variation of lattice parameters $a(x)/a(0)$ for R = Ho, Er, Tm, and Lu [84 D 4]. The T_C values decrease when increasing the lattice parameters. The same trend is observed for all compounds showing that Fe–Fe interactions determine mainly the T_C values.

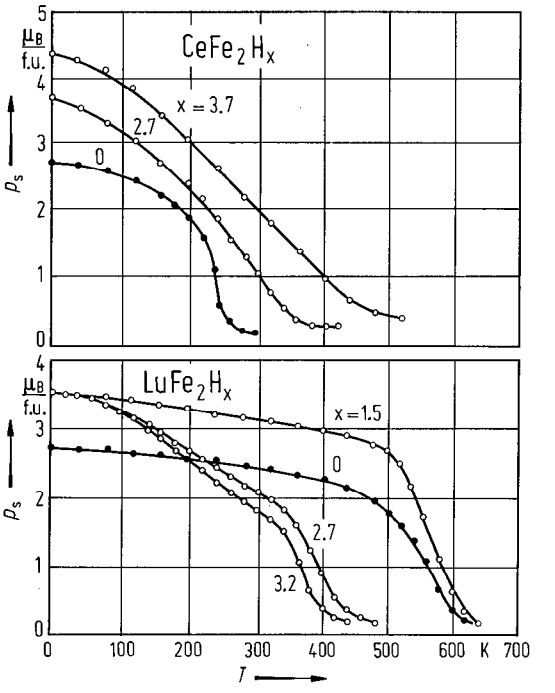

Fig. 127. Temperature dependence of the saturation magnetization in $CeFe_2H_x$ and $LuFe_2H_x$ hydrides. In case of $LuFe_2H_x$ hydrides, the magnetization increases from 2.8 μ_B for x = 0 to 3.5 μ_B for x = 1.5. These data are also in agreement with the Mössbauer effect measurements [85 D 11].

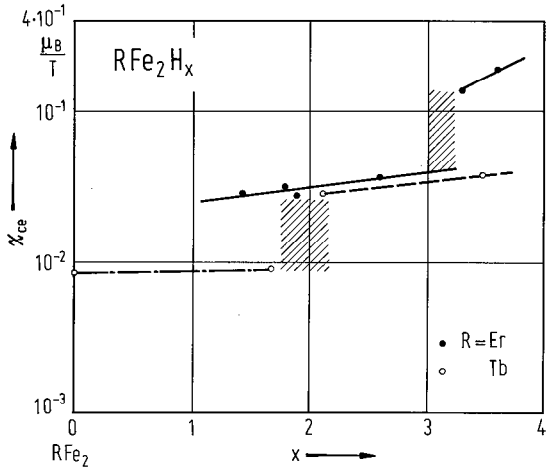

Fig. 128. Behaviour of the conduction electron magnetic susceptibility vs. hydride composition in RFe_2H_x (R = Er, Tb) systems. The shaded area corresponds to the structural distortion effect [87 F 4]. The conduction electron magnetization, which is superimposed on the localized magnetic moments, is dependent on the hydrogen content near the crystallographic transition (cubic (C)⇌rhombohedral (R)). The drop of this superimposed magnetic susceptibility occurs for x = 3.2 for Er, and x = 2.0 for the Tb system. This reflects the change in the crystal electric field as seen by the conduction electrons of 3d and 5d character. This change arises from the accumulation of electric charge on RM_3 interstitials sites which accompanies the C–R transition.

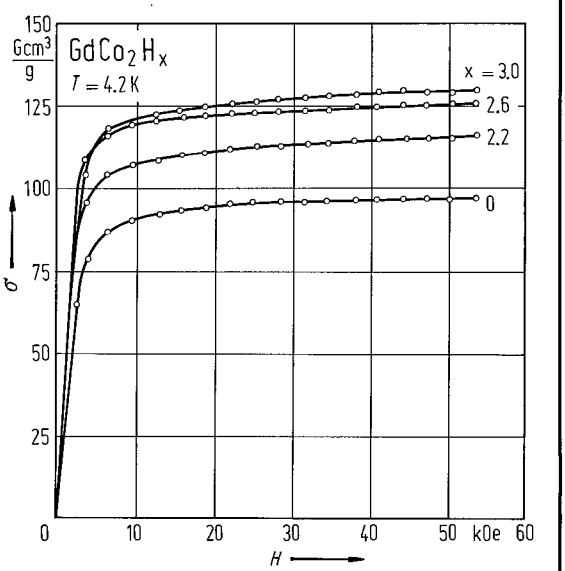

Fig. 129. Magnetization vs. applied magnetic field curves for the $GdCo_2$ compound and its hydrides $GdCo_2H_x$ (x = 2.2; 2.6 and 3.0) at 4.2 K [87 F 7]. The magnetization increases with the absorbed hydrogen content. The mean Co magnetic moment undergoes a drastic reduction by hydrogen absorption. This fact is ascribed to the reduction of exchange interactions.

Table 42. Magnetic properties of some RM_2-hydrides and parent compounds.

	Ordering temperature	p_s	p_R	p_M	Ref.
	K	μ_B/f.u.	μ_B		
$GdMn_2H_{4.6}$ (50 at)	< 4				80 O 2
YMn_2H_1 [1])	228				80 O 2
YMn_2H_x (0.1 at)	305	0.35			80 O 2
YMn_2H_x (4.5 at)	228				80 O 2
YMn_2H_x (6 at)	201				80 O 2
$Pr_{0.55}Er_{0.45}Mn_2H_{3.9}$	≅165				80 O 2
$CeFe_2$		2.66	0.50	1.08	85 D 11
$CeFe_2H_{3.7}$		4.43	–	2.22	85 D 11
$CeFe_2H_x$	358	4.80	–		77 B 18
$SmFe_2H_x$	333	3.20			77 B 18
$GdFe_2H_x$	388	4.00			77 B 18
$GdFe_2H_{3.6}$		2.60	7.00	2.21	84 D 4
$GdFe_2H_{4.0}$ [2])	388	4.10			76 B 21
$GdFe_2H_{4.1}$ (50 at)	338	5.39			80 O 2
$TbFe_2H_x$	303	4.60			77 B 18
$TbFe_2H_{3.0}$	>300	7.80 [3])			82 P 13
$DyFe_2H_x$	385	4.90			77 B 18
$DyFe_2H_{3.5}$	>300	7.60 [3])			82 P 13
$HoFe_2D_{3.5}$	295		5.30 [4])	1.90	79 F 5
$HoFe_2H_x$	298	5.50			77 B 18
$HoFe_2H_{4.5}$	285	2.35			76 G 10
$HoFe_2H_{3.5}$		3.30	6.80	1.74	84 D 4
$ErFe_2D_{3.5}$	440		4.30 [4])	1.60	79 F 5
$ErFe_2H_{3.5}$	450		4.90 [4])	1.50	79 F 5
$ErFe_2H_x$	265	5.20			77 B 18
$ErFe_2H_{3.5}$		1.50	5.10	1.80	84 D 4
$ErFe_2H_2$	>400		7.3	1.6	80 F 6
$ErFe_2H_2$	>400		9.00	1.7	79 V 4
$ErFe_2H_{3.65}$	450		4.0	1.6	80 F 6
$ErFe_2H_{3.56}$	450		8.5	1.9	79 V 4
$ErFe_2H_{4.1}$	≅ 2		6.5	0.2	79 V 4
$TmFe_2H_{3.1}$		0	3.60	1.81	84 D 4
$TmFe_2H_{3.5}$	305		3.80 [4])	– [5])	79 F 5
$LuFe_2$		2.83	0	1.41	85 D 11
$LuFe_2H_{3.2}$		3.52	0	1.76	85 D 11
$LuFe_2H_{3.2}$		3.50	0	1.75	84 D 4
YFe_2H_x	308	3.40		1.70	77 B 18
YFe_2H_4 [1])	308	3.66		1.83	76 B 21
YFe_2H_4	133	3.71			80 O 2

Table 42 (continued)

	Ordering temperature K	p_s μ_B/f.u.	p_R μ_B	p_M	Ref.
$ScFe_2$	542			1.15	81 N 2
$ScFe_2H_{1.7}$	>500			1.80	81 N 2
$ScFe_2H_{2.5}$	>500			1.90	81 N 2
$ScFe_2H_{3.2}$	>500			2.00	81 N 2
$GdCo_2H_{2.2}$		5.86		0.57	87 F 7
$GdCo_2H_{2.6}$		6.36		0.32	87 F 7
$GdCo_2H_{3.0}$		6.53		0.24	87 F 7
$GdCo_2H_{3.7}$ (amorphous)		6.15			80 O 2
$TbCo_2H_{3.2}$	50	4.15 [3])			82 P 13
$TbCo_{1.4}Fe_{0.6}$	590	5.55 [3])			82 P 13
$TbCo_{1.4}Fe_{0.6}H_2$	>300	5.80 [3])			82 P 13
$DyCo_2H_{3.3}$	40	4.70			82 P 13
$DyCo_{1.4}Fe_{0.6}$	545	6.50			82 P 13
$DyCo_{1.4}Fe_{0.6}H_{3.1}$	>300	3.80			82 P 13
$HoCo_2H_{3.5}$	40	4.70			81 P 4
$HoCo_{1.4}Fe_{0.6}$	545	6.50			81 P 4
$HoCo_{1.4}Fe_{0.6}H_{3.5}$	>300	3.80			81 P 4
$ErCo_2H_{3.5}$	25	4.35			81 P 4
$ErCo_{1.4}Fe_{0.6}$	510	4.85			81 P 4
$ErCo_{1.4}Fe_{0.6}H_{3.5}$	>300	3.80			81 P 4
$ErCo_{0.66}Fe_{1.34}$	670	4.65			81 P 4
$ErCo_{0.66}Fe_{1.34}H_{3.5}$	>300	2.90			81 P 4
$GdNi_2H_{3.9}$	8	4.20			77 M 2

[1]) Two-phase material.
[2]) At 4.2 K and in fields up to 18 kOe.
[3]) At 4.2 K and in fields up to 21 kOe.
[4]) The rare-earth spins in RFe_2 hydrides are not ordered in a unique direction. The random hydrogen site occupancy results in a variation in the direction of the local anisotropy field, such as found in amorphous alloys, which leads to a "fanning" of the individual rare-earth magnetic moments.
[5]) Not determined.

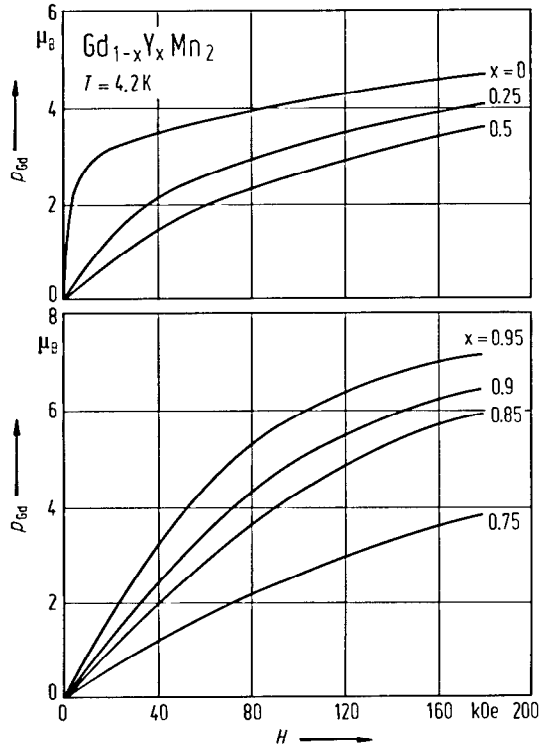

Fig. 130. Magnetization isotherms at 4.2 K in $Gd_{1-x}Y_xMn_2$ compounds. Even in a field of 150 kOe the magnetizations are lower than the expected values considering the contribution of Gd atoms. The magnetic structure of $GdMn_2$ seems to be stable up to $x = 0.5$. For higher Y content the observed curves may be attributed to the Gd magnetic moments situated in a nonzero molecular field due to Mn magnetic moments. The continuity of the form of the magnetization isotherms suggests that the arrangement of Mn magnetic moments is the same as in YMn_2 [86 O 2].

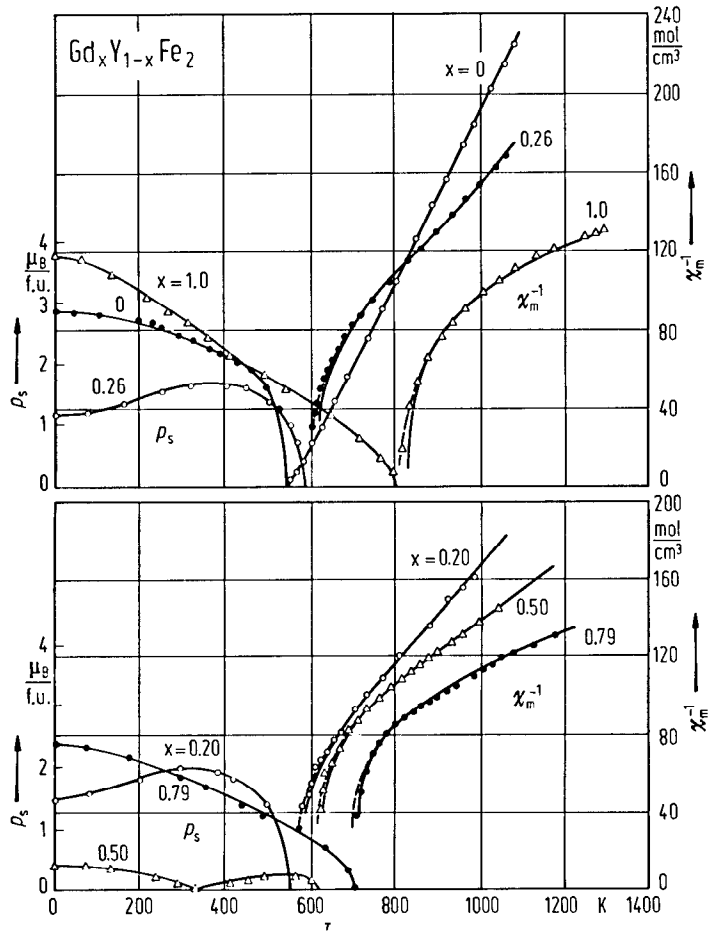

Fig. 131. Thermal variations of spontaneous magnetizations and reciprocal magnetic susceptibilities for some $Gd_xY_{1-x}Fe_2$ compounds [79 B 13]. Curves typical of ferrimagnetic ordering are observed at $T > T_C$ for $x > 0$.

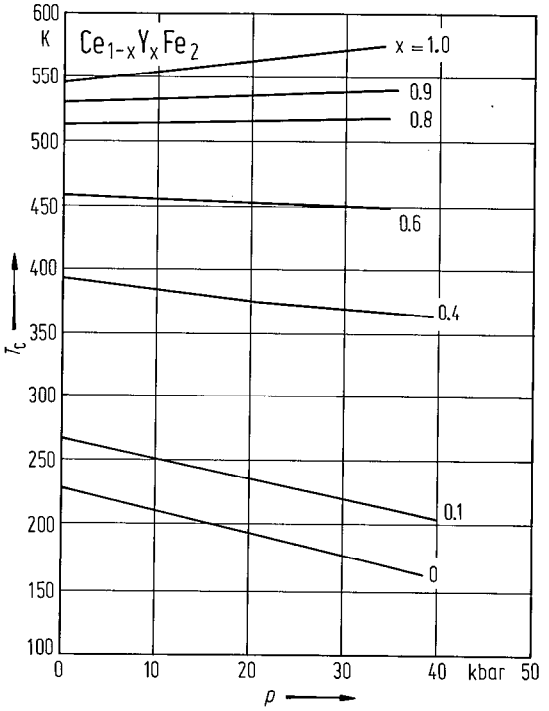

Fig. 132. Pressure dependence of the Curie temperatures T_C for several $Ce_{1-x}Y_xFe_2$ compounds. The prominent feature appearing in this system is a positive pressure derivative of T_C when T_C is large, shifting to negative value when T_C becomes smaller [77 B 23].

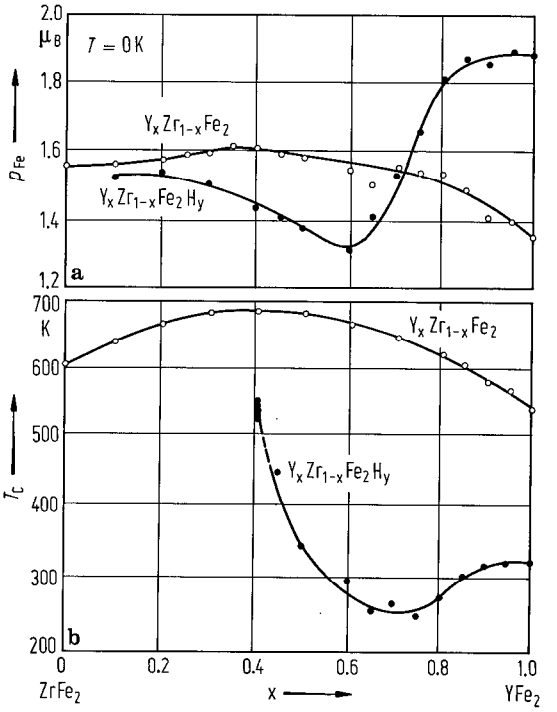

Fig. 133. (a) Magnetic moment of Fe in $Y_xZr_{1-x}Fe_2$ and $Y_xZr_{1-x}Fe_2H_y$, where Y and Zr are assumed to have no magnetic moment [86 K 4]. In $Y_xZr_{1-x}Fe_2$ the change of the magnetic moment is smooth with the maximum value at about $x = 0.35$. The hydrides have a different tendency with the boundary at $x = 0.6$. In the composition range $0.2 \leqq x \leqq 0.6$ the magnetic moments of hydrides decrease with x, while for $x \geqq 0.6$ they turn to increase. For $x \geqq 0.75$ they exceed those of the parent compounds and for $x \geqq 0.85$ the magnetic moment is almost constant. (b) Composition dependence of the Curie temperatures for $Y_xZr_{1-x}Fe_2$ and $Y_xZr_{1-x}Fe_2H_y$. In the composition range $0.2 \leqq x \leqq 0.65$, the Curie temperatures go down to 254 K at $Y_{0.65}Zr_{0.35}Fe_2H_{3.0}$, as the trend evidenced for the magnetic moments, and for $x \geqq 0.75$ they rise up to 320 K for $YFe_2H_{4.2}$. These two kinds of dependences suggest that the electronic state of the hydrides having the hydrogen content 0···3 is quite different from that of the hydrides with hydrogen content 3···4.

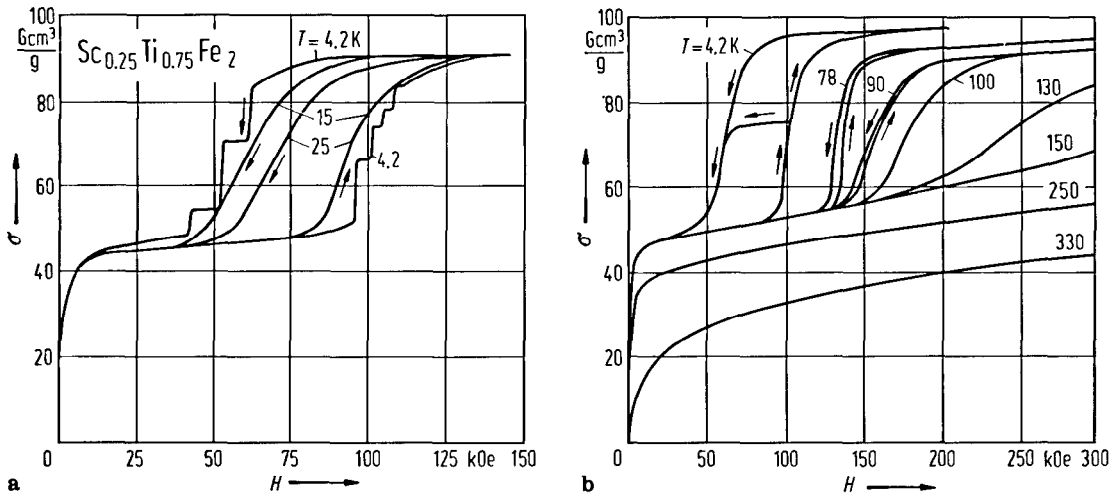

Fig. 134. Magnetization isotherms of $Sc_{0.25}Ti_{0.75}Fe_2$ at various temperatures obtained by (a) steady magnetic field and (b) pulsed magnetic field. The jumps become indistinct, at 4.2 K, in the pulsed-field measurements, but the width of hysteresis is almost the same as obtained by using the steady magnetic field. The hysteresis width decreases when increasing temperature, and disappears at approximately 100 K. A ferromagnetic⇌ferromagnetic transition is observed between states having different magnetic moments [87 K 7].

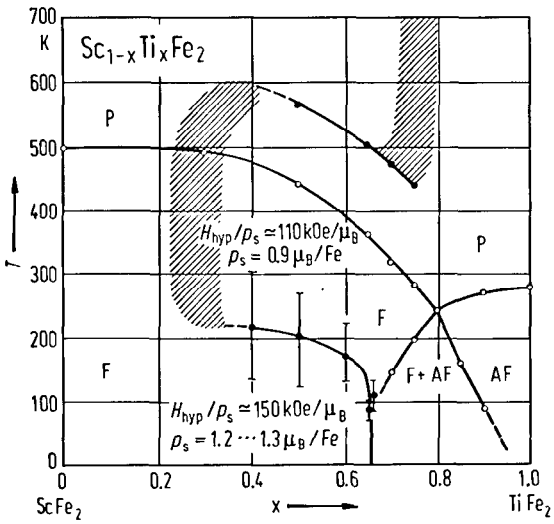

Fig. 135. Magnetic state of $Sc_{1-x}Ti_xFe_2$ [87 N 3]. Two ferromagnetic states with different degree of localization are observed. $ScFe_2$ is a ferromagnet with $T_C \cong 500$ K. By increasing Ti concentration above $x \cong 0.3$, the Curie temperatures start to decrease and another ferromagnetic state with a smaller ferromagnetic moment than $ScFe_2$ appears in the higher-temperature region. This ferromagnetic state continuously connects with the coexistent state of ferromagnetism and antiferromagnetism for $x \geqq 0.7$.

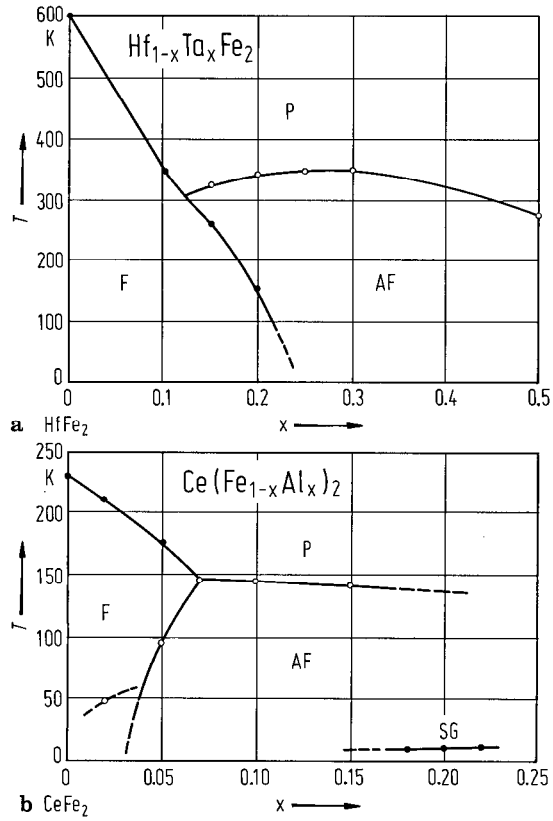

Fig. 136. Magnetic phase diagrams of $Hf_{1-x}Ta_xFe_2$ and $Ce(Fe_{1-x}Al_x)_2$ compounds [87 N 3]. The ferromagnetic state extends toward the antiferromagnetic region at low temperatures in $Hf_{1-x}Ta_xFe_2$. On the contrary, the antiferromagnetic state extends toward the ferromagnetic region in $Ce(Fe_{1-x}Al_x)_2$. The magnetic properties of $Ce(Fe_{1-x}Al_x)_2$ vary from the itinerant-electron type to the localized-moment type with increasing Al concentration. However, the spin glass state does not appear at the boundary of ferromagnetism and antiferromagnetism, but appears at the antiferromagnetic region with larger Al concentration. By increasing temperature, the transition from ferromagnetic to antiferromagnetic state takes place in $(Hf_{1-x}Ta_x)Fe_2$ and that from antiferromagnetic to ferromagnetic state in $Ce(Fe_{1-x}Al_x)_2$. It has been predicted theoretically that this type of first-order phase transition is induced by the temperature variation of the mean-square local amplitudes of spin fluctuations in itinerant-electron systems with competing ferromagnetism and antiferromagnetism [77 M 11]. The phase diagrams of $Hf_{0.8}Ta_{0.2}Fe_2$ and $Ce(Fe_{0.95}Al_{0.05})_2$ [86 K 3, 87 N 4] plotted in the external field versus temperature plane are qualitatively consistent with the theoretically obtained ones by spin fluctuation theory [77 M 11].

Fig. 137. Thermal variations of magnetization in $Gd_xY_{1-x}Co_2$ compounds ($x \leq 0.2$) in a magnetic field of 100 Oe. Solid curves are for zero-field-cooled samples and the dashed curves for the field-cooled samples [84 M 5]. Maxima are observed in zero-field-cooled samples for $0.075 \leq x \leq 0.175$. This behaviour suggests that magnetic cluster glasses are formed. The cluster magnetic moments may behave superparamagnetically at an intermediate temperature. Below a certain temperature corresponding to T_m, they may freeze in random directions.

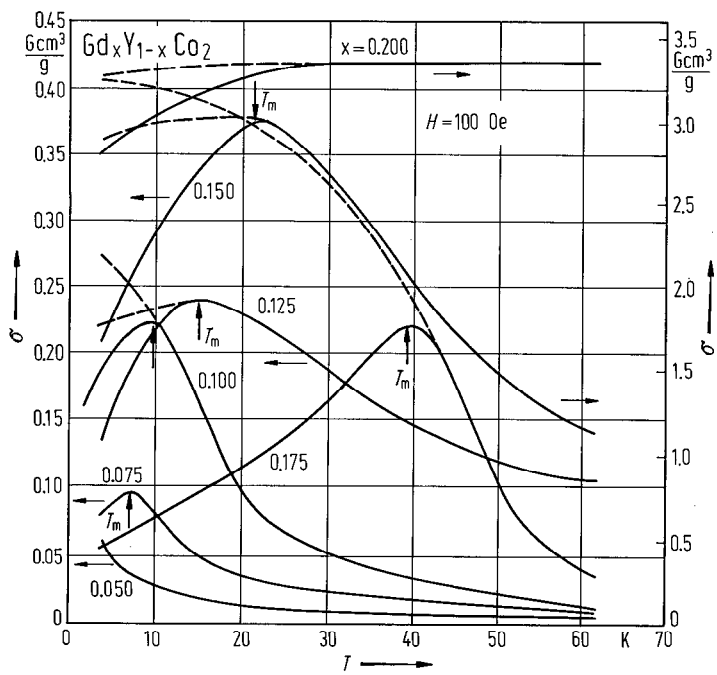

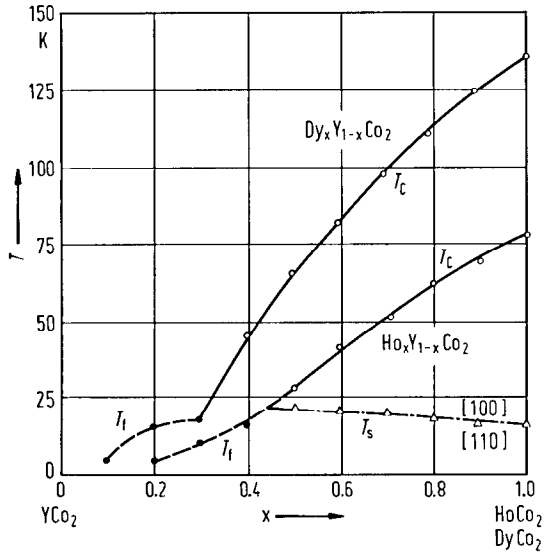

Fig. 138. Magnetic phase diagram of $Ho_xY_{1-x}Co_2$ and $Dy_xY_{1-x}Co_2$: Curie temperature T_C, spin-freezing temperature T_f and spin reorientation temperature T_s [87 P 5]. A spin reorientation (change of the easy axis of magnetization from [100] to [110]) was only observed in the $(Ho_xY_{1-x})Co_2$ system. The magnetic ordering temperature is reduced by diluting the magnetic R atoms by Y.

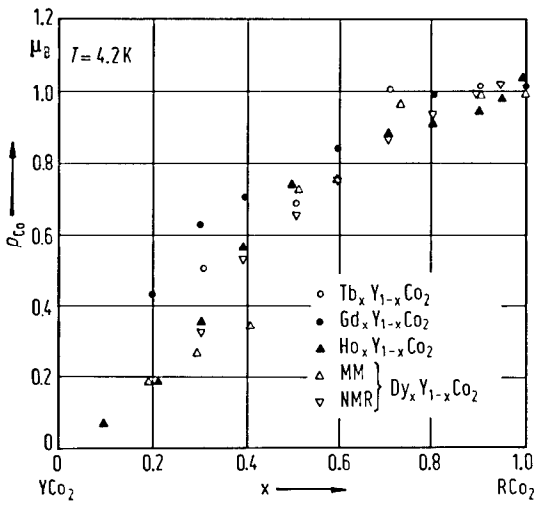

Fig. 139. Composition dependence of the mean Co magnetic moment at 4.2 K in $Gd_xY_{1-x}Co_2$ [73 V 5], $Ho_xY_{1-x}Co_2$ [78 S 19], $Tb_xY_{1-x}Co_2$ [83 F 6], $Dy_xY_{1-x}Co_2$ [84 Y 7]. The results of magnetic measurements are denoted by MM.

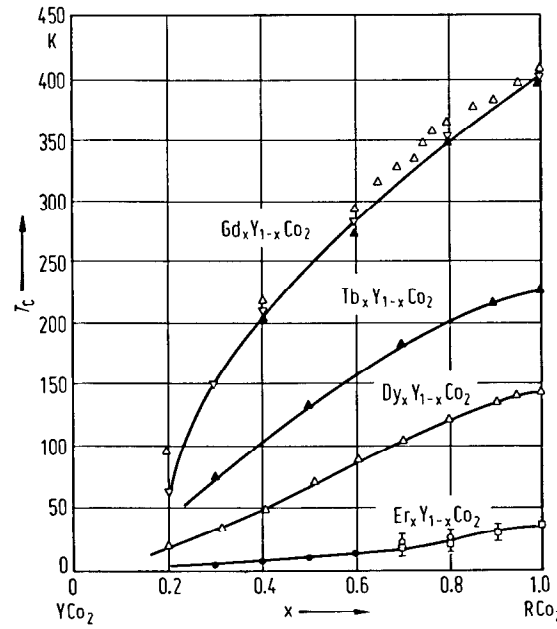

Fig. 140. Composition dependence of the Curie temperatures in $Gd_xY_{1-x}Co_2$, inverted open triangles [66 L 4], open triangles [75 T 2], solid triangles [76 B 16]; $Dy_xY_{1-x}Co_2$ [84 Y 7]; $Tb_xY_{1-x}Co_2$ [83 F 6]; $Er_xY_{1-x}Co_2$ [84 L 6]. The first-order and second-order-type transitions in $Er_xY_{1-x}Co_2$ are denoted by open and solid symbols, respectively.

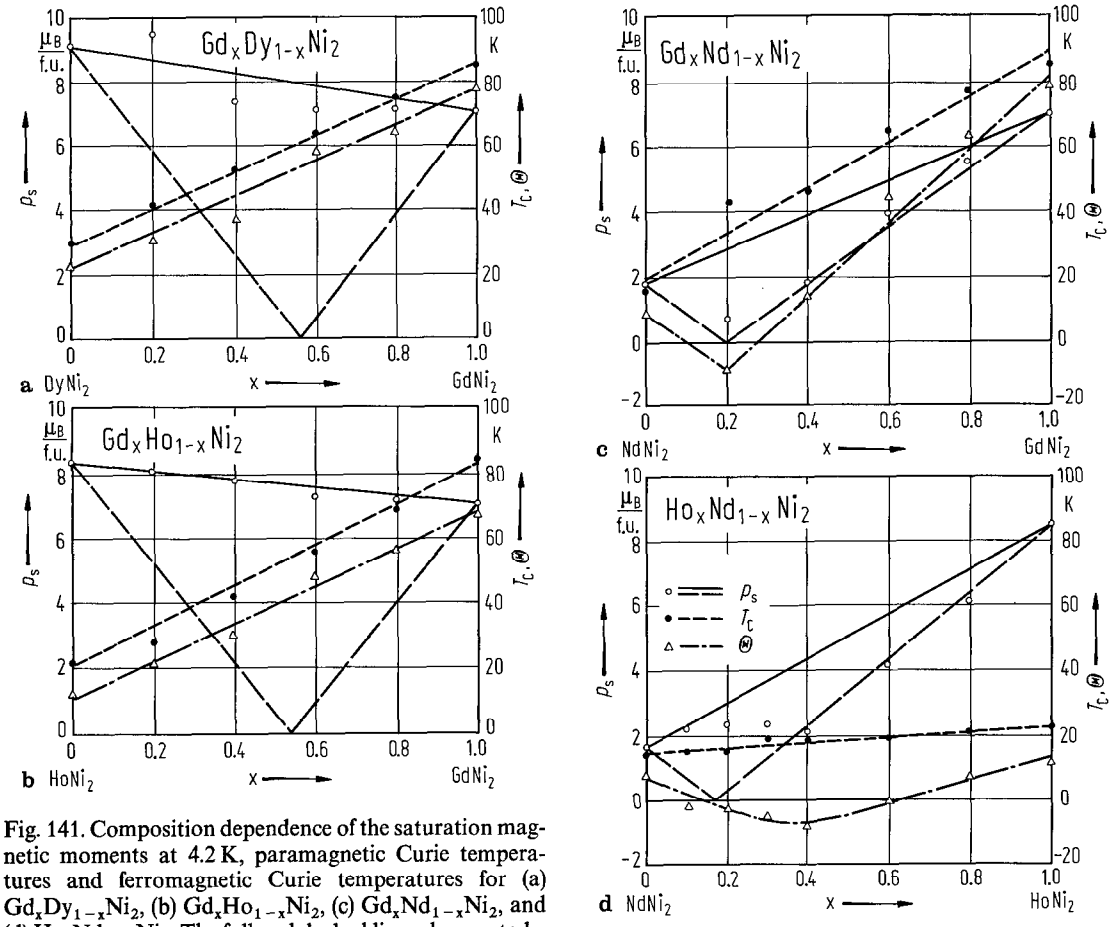

Fig. 141. Composition dependence of the saturation magnetic moments at 4.2 K, paramagnetic Curie temperatures and ferromagnetic Curie temperatures for (a) $Gd_xDy_{1-x}Ni_2$, (b) $Gd_xHo_{1-x}Ni_2$, (c) $Gd_xNd_{1-x}Ni_2$, and (d) $Ho_xNd_{1-x}Ni_2$. The full and dashed lines show p_s to be expected for ferromagnetic and antiferromagnetic coupling, respectively [69 W 1].

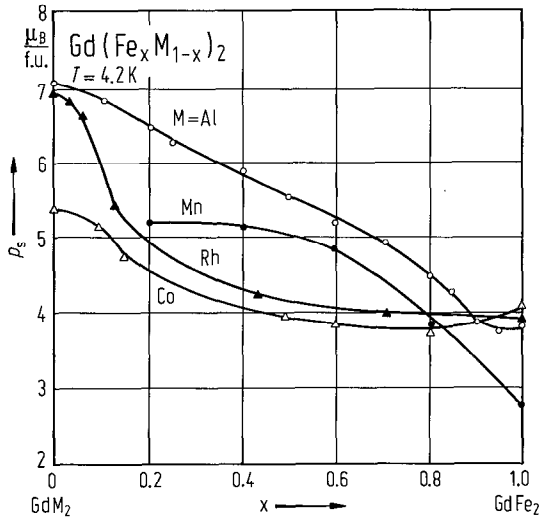

Fig. 142. Composition dependence of the saturation magnetization in $Gd(Fe_xM_{1-x})_2$ compounds at 4.2 K: M = Co [78 B 16], M = Al [79 B 6], M = Rh [82 T 2], M = Mn [76 M 10].

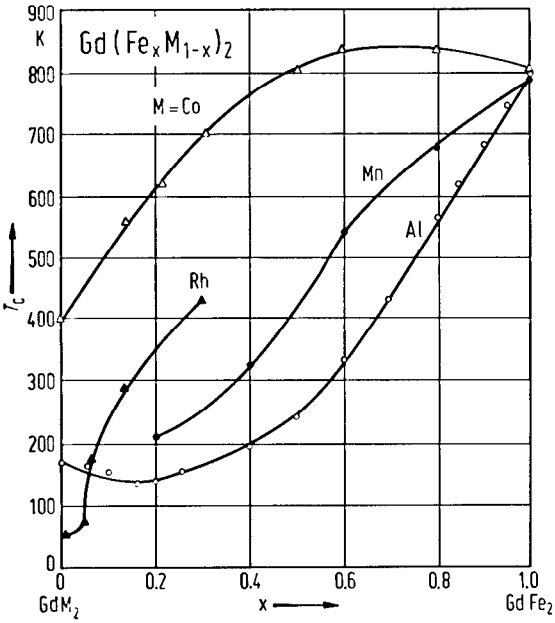

Fig. 143. Composition dependence of the Curie temperatures in $Gd(Fe_xM_{1-x})_2$ compounds: M = Co [78 B 16], M = Rh [82 T 2], M = Mn [76 M 10], M = Al [79 B 6].

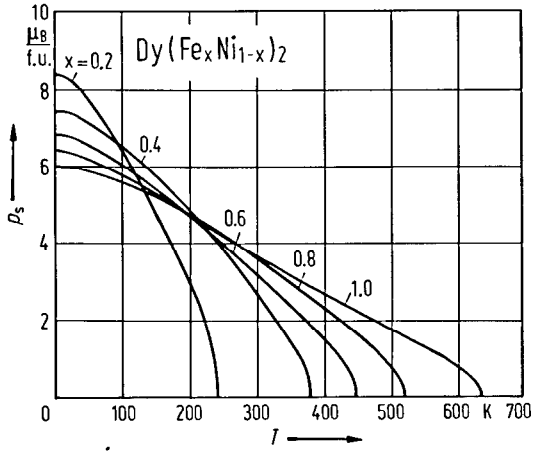

Fig. 144. Thermal variations of the spontaneous magnetizations for $Dy(Fe_xNi_{1-x})_2$ compounds [78 B 12].

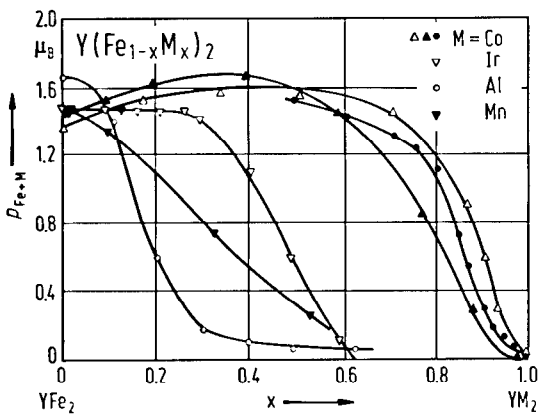

Fig. 145. Composition dependence of the mean transition metal magnetic moment in $Y(Fe_{1-x}M_x)_2$ at 4.2 K with M = Co, open triangles [78 B 13], solid circles [74 S 9], solid triangles [68 P 2]; M = Al [75 B 12]; M = Ir [79 V 2]; M = Mn [69 K 4].

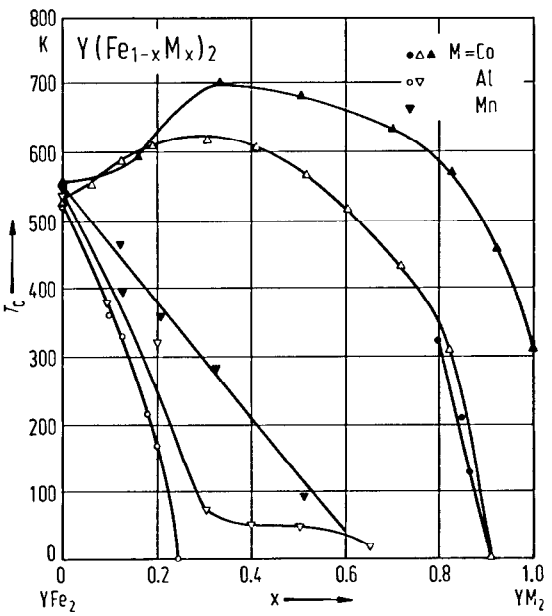

Fig. 146. Composition dependence of the Curie temperatures of $Y(Fe_{1-x}M_x)_2$ compounds M = Al, open triangles [75 B 12], open circles [80 S 15], M = Co, solid triangles [68 P 2], solid circles [74 S 9], open triangles [83 F 9]; M = Mn [69 K 4].

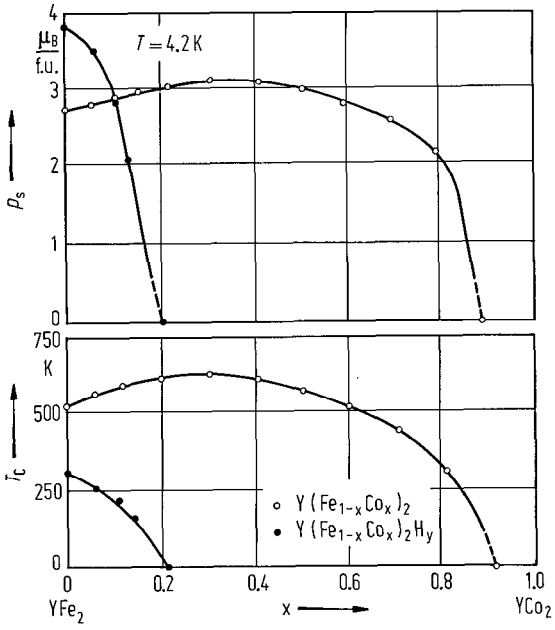

Fig. 147. Composition dependence of the saturation magnetizations at 4.2 K and the Curie temperatures for $Y(Fe_{1-x}Co_x)_2$ and their hydrides [83 F 9]. Both the saturation magnetic moment and the Curie temperature take a maximum around $x = 0.3$ for the nonhydrides. The saturation magnetic moment in the hydrides is larger than that in the corresponding host compounds for $x < 0.1$, but its value decreases sharply with x and ferromagnetism becomes unstable for $x \geqq 0.20$, beyond which a mictomagnetism is observed. The Curie temperature in the hydrides is much lower than that in the host compounds and its value drops rapidly with increasing x.

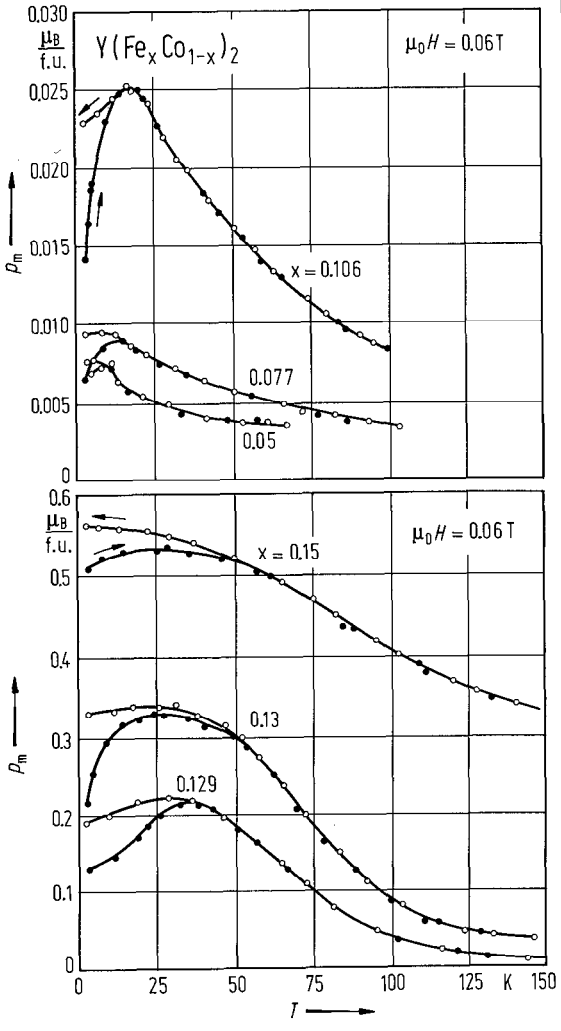

Fig. 148. Temperature dependence of the magnetization for some $Y(Fe_xCo_{1-x})_2$ samples cooled without any field to 4.2 K and measured in $\mu_0 H = 0.06$ T (solid circles) and field-cooled samples (open circles). The appearance of a maximum in the temperature dependence of the magnetization at T_m is observed for $0.05 \leqq x \leqq 0.15$, if, prior to the measurements, the samples are cooled to 4.2 K without an applied field. These maxima are shifted with increasing Fe concentration to higher temperatures. If the sample is cooled in the field, the temperature dependence of the magnetization coincides for $T > T_m$ with that of the zero-field-cooled sample, but appreciably higher values are obtained for $T < T_m$. A strong time dependence of the magnetization is observed at 4.2 K. From neutron depolarization measurements performed on $Y(Fe_{0.1}Co_{0.9})_2$ no depolarization is observed if the sample is cooled to 4.2 K without a field, whereas cooling in an applied field of 0.68 T, but measuring without a field leads to a depolarization of approximately 2% [79 S 8].

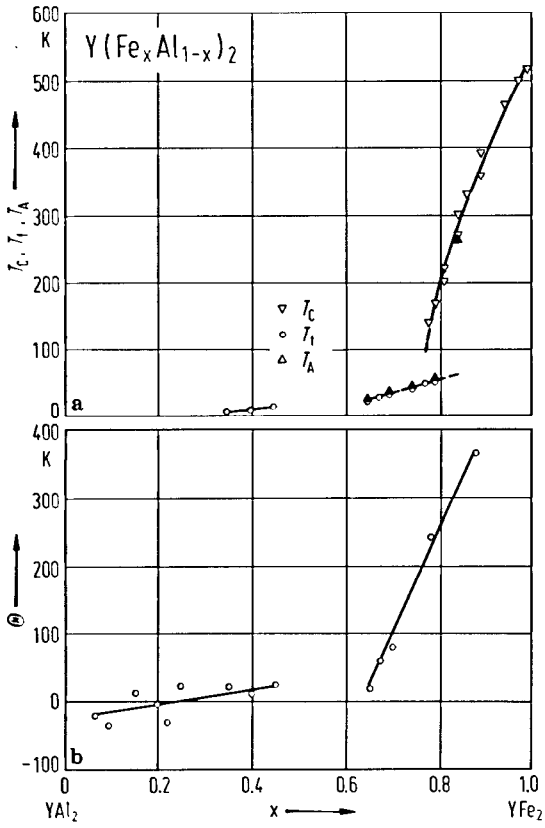

Fig. 149. (a) Composition dependence of the Curie temperature T_C, freezing temperature T_f, and temperature for vanishing magnetic hyperfine splitting, T_A, of $Y(Fe_xAl_{1-x})_2$ compounds [84 R 3]. In (b) the composition dependence of the paramagnetic Curie temperature Θ is plotted. In the intermediate Fe concentration range, a transition from a cubic C15-type structure to the hexagonal C14-type structure was evidenced. The mean spontaneous magnetic moment decreases rapidly and the long-range ferromagnetic order disappears at about $x = 0.78$. For lower Fe content, short-range magnetic order and freezing effects are observed, typical of mictomagnetism. The low-temperature data were analysed as the sum of a magnetic susceptibility and of a field-dependent magnetization caused by magnetic clusters originating from the statistical replacement of Al for Fe. These clusters exist throughout the whole Fe concentration range. The mean effective magnetic moment per Fe atom is only weakly dependent on Fe concentration.

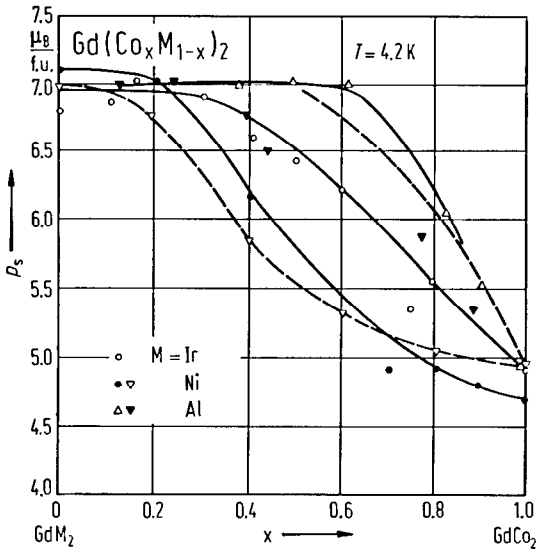

Fig. 150. Composition dependence of the saturation magnetization in $Gd(Co_xM_{1-x})_2$ compounds at 4.2 K: M = Ir [79 C 3]; M = Ni, inverted open triangles [74 B 12], solid circles [69 T 1] M = Al, triangles [67 O 1], inverted full triangles [81 B 10].

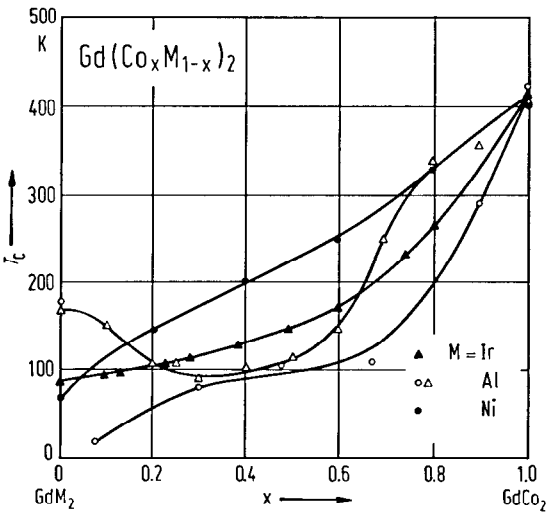

Fig. 151. Composition dependence of the Curie temperatures in $Gd(Co_xM_{1-x})_2$ compounds: M = Ir [79 C 3]; M = Ni [78 B 11]; M = Al, triangles [67 O 1], open circles [79 K 10].

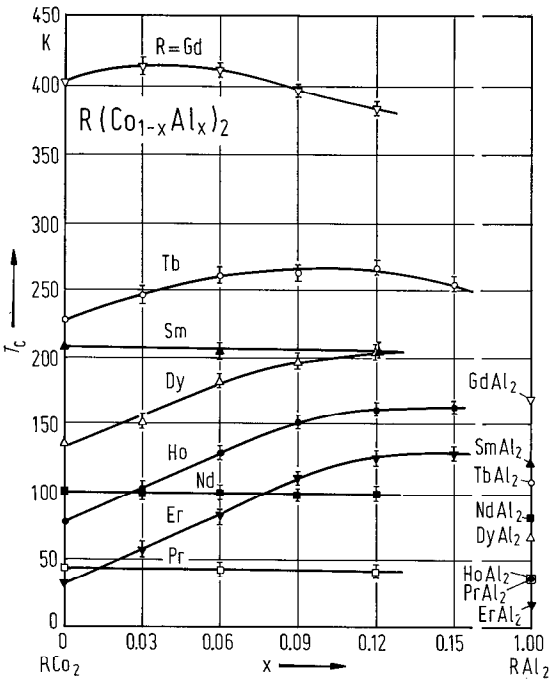

Fig. 152. Variation of the Curie temperatures of the $R(Co_{1-x}Al_x)_2$ compounds in the low-Al concentration range. When R = Nd, Pr or Sm, the Curie temperatures of $R(Co_{1-x}Al_x)_2$ compounds decrease steadily as x increases. For a small amount of Al, a large increase of T_C values for compounds with R = Gd, Tb, Dy, Ho and Er is observed. This suggests that the band structure must change through the series in agreement with the measured values of the electronic specific heat coefficients [78 G 1].

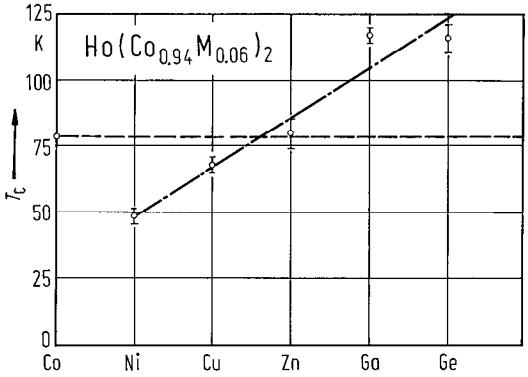

Fig. 153. Variation of the Curie temperatures of $Ho(Co_{0.94}M_{0.06})_2$ for M = Co, Ni, Cu, Zn, Ga, and Ge. The presence of a small amount of Al, Ga or Ge leads to a large increase of the magnetic energy. The replacement of Ni in $Ho(Co_{0.94}Ni_{0.06})_2$ by atoms with higher atomic number increase the T_C values. This fact is probably due to the increase of the number of conduction electrons leading to an increase of the exchange interactions [78 G 1].

For Fig. 154, see next page.

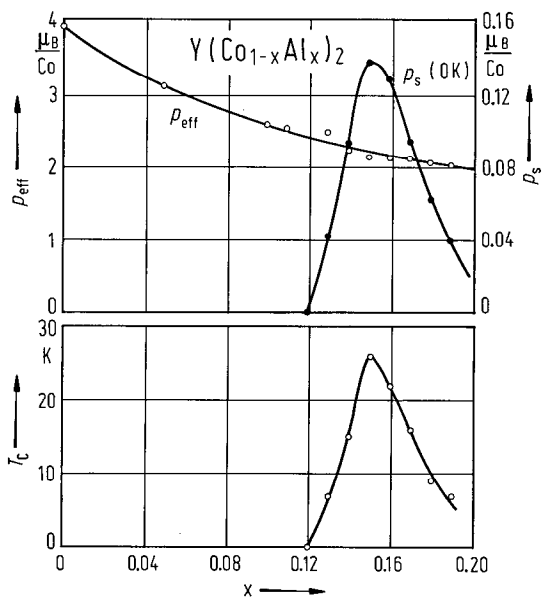

Fig. 155. Composition dependence of the Curie temperature T_C, effective Co magnetic moment p_{eff}, and saturation Co magnetic moment at 0 K, p_s, in $Y(Co_{1-x}Al_x)_2$ compounds [87 Y 11]. The Curie temperatures and the spontaneous magnetic moments at $T = 0$ are very small and are observed in the composition range $0.12 \leqq x \leqq 0.20$. The magnetic susceptibility obeys the Curie-Weiss law above 100 K. The effective paramagnetic moment determined from the Curie constant show large values. The paramagnetic Curie temperatures are higher than T_C by about 30% [87 Y 12]. Over a wide range of temperatures around T_C, both the square of the spontaneous magnetization and the reciprocal magnetic susceptibility are proportional to $|T^{4/3} - T_C^{4/3}|$ as expected from self-consistent renormalization theory of spin fluctuations.

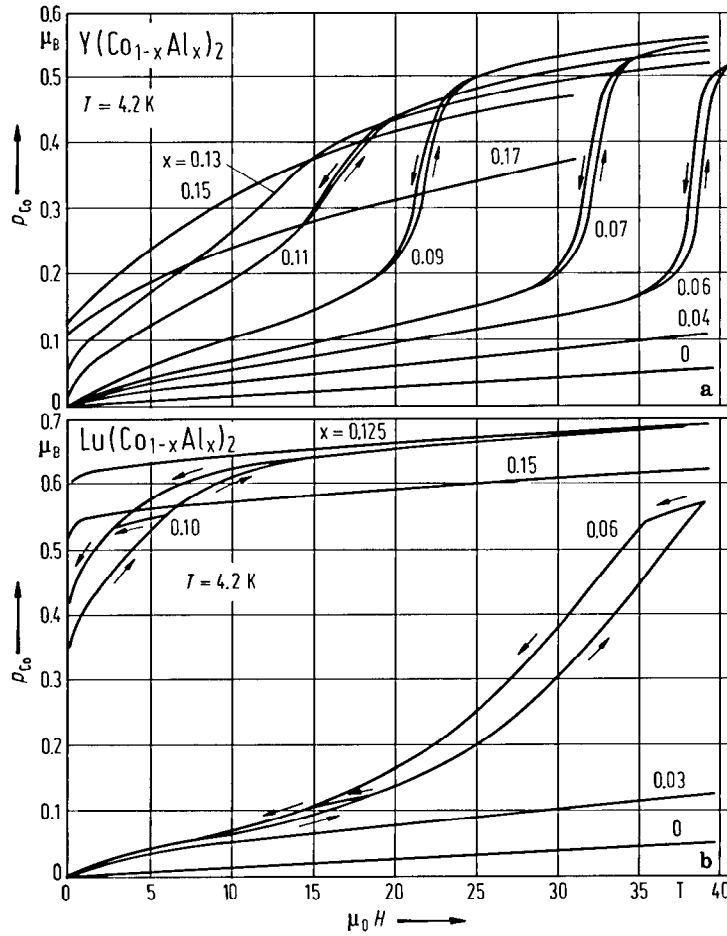

Fig. 154. Magnetization isotherms of (a) $Y(Co_{1-x}Al_x)_2$ and (b) $Lu(Co_{1-x}Al_x)_2$ at 4.2 K [87 S 1]. Clear metamagnetic transitions with small hysteresis are found in the region $0.06 \leqq x \leqq 0.11$ for R = Y, where the system is paramagnetic at zero magnetic field. The transition becomes sharper and the magnetization jump becomes larger with decreasing Al concentration. Above $x = 0.11$, the metamagnetic transition rapidly becomes broad and disappears upon the onset of weak ferromagnetism. It is noticed that the metamagnetically induced magnetic moment is much larger than the spontaneous magnetic moment of the weakly ferromagnetic phase. These facts strongly suggest that the predicted metamagnetic transition actually exists in YCo_2 and is the origin of the metamagnetism in $Y(Co_{1-x}Al_x)_2$. The sharpness of the transition in $Y(Co_{1-x}Al_x)_2$ may be related to the magnetically homogenous character of this system [85 Y 11]. Al substitution in $Lu(Co_{1-x}Al_x)_2$ induces also ferromagnetism. The critical concentration x_c for the onset of ferromagnetism is estimated at $x_c \cong 0.08$. The magnetic moment value in the ferromagnetic phase is apparently larger than that in $Y(Co_{1-x}Al_x)_2$. Moreover, the high-field magnetic susceptibility is much smaller than that in $Y(Co_{1-x}Al_x)_2$ indicating rather strong ferromagnetism in $Lu(Co_{1-x}Al_x)_2$. The transition with a large hysteresis occurs in a remarkably wide field range for $x = 0.06$, i.e., it starts at around 10 T and is not complete even at 40 T. The behaviour of the magnetization for $x = 0.10$ suggests the coexistence of ferromagnetism and metamagnetism. The data favour an inhomogeneous model and that the Co 3d-state is much localized in $Lu(Co_{1-x}Al_x)_2$ and affected by local environment.

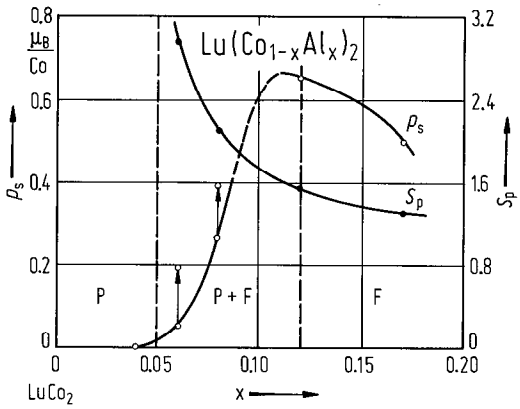

Fig. 156. Composition dependence of the spontaneous moment p_s and the number of spins S_p defined by $p_{eff}^2 = S_p(S_p+1)$ $(\mu_B/Co)^2$ in $Lu(Co_{1-x}Al_x)_2$ [87 E 4]. The NMR study shows that ferromagnetic and paramagnetic Co atoms coexist for $0.06 < x < 0.12$ and the increase in magnetization with increasing field is attributed to an increase in the number of ferromagnetic Co atoms. The value of the magnetic moment reaches $0.66\,\mu_B$. The magnetic moment in the region of two magnetic states (F + P) increases by increasing external field as indicated by arrows.

For magnetic properties of RM_2-based compounds see also

RM_2 R = Sm, Gd, Tb, Dy, Ho, Er, Y, M = Mn, Fe, Co, Ni [61 C 1]; R = Ce, Pr, Sm, Tb, Dy, Ho, Er, M = Fe, Co, Ni, Rh, Pt [64 C 4]; R = Pr, Gd, Dy, Er, M = Fe, Co, Ni [76 D 6]; R = Gd, Lu, Y, M = Mn, Fe, Co, Ni [85 S 9]; R = Gd, Y, M = Fe, Co, Ni [83 G 3]; M = Fe, Co, Ni [79 C 10(T)]; R = Sc, Ti, Zr, Nb, M = Cr, Mn, Fe, Co, Ni [88 A 1(T)]; R = Sc, Ti, Y, Zr, Nb, Lu, Hf, M = Mn, Fe, Co, Ni [88 Y 1(T)]; PrM_2, M = Fe, Co, Ni, Rh, Ru [74 Z 1(T)]; YM_2, M = Mn, Fe, Co, Ni [84 Y 1(T)]; RM_2, R = Y, Zr, M = Mn, Co, Ni, Cu [87 A 11(T)]

RMn_2 [63 N 1, 69 K 4, 81 M 1, 83 N 3, 83 N 4, 87 W 1, 88 S 1]; R = Gd, Tb, Dy, Ho [83 G 1]; R = Gd, Tb, Dy, Ho, Er [83 M 1]; R = Gd, Tb, Dy, Ho, Er [85 W 1]; R = Pr, Nd, Y, Th [86 O 2]; R = Y, Zr, M = Mn, Cr, Co, Ni [87 A 11(T)]; R = Gd [63 N 1, 66 K 1, 78 T 2, 81 M 1, 85 G 2, 87 Y 1(T)]; R = Tb [63 N 1, 80 M 2, 85 G 1, 87 G 1]; R = Dy [63 N 1, 66 K 1, 81 M 1]; R = Ho [63 N 1, 81 M 1]; R = Er [66 K 1]; R = Y [67 M 1, 77 B 19, 87 O 5, 87 Y 1(T), 88 F 2, 88 G 1, 88 N 1]

RFe_2 [72 G 9(T), 73 B 10, 73 N 5, 74 B 9, 75 F 1, 75 N 5, 76 B 13, 76 R 1, 77 B 15, 77 B 18, 79 B 2, 79 C 8(T), 79 L 2, 82 I 1, 88 R 1]; R = Sm, Tb, Ho, Er, Tm, Lu, Y [63 W 1, 79 I 2]; R = Sm, Tb, Ho, Er, Tm, Lu, Y [64 W 2]; R = Gd, Tb, Dy, Ho, Er, Y [70 B 13]; R = Gd, Tb, Dy, Ho, Er, Tm, Y [71 B 12]; R = Tb, Dy, Ho, Tm, Er [72 C 7]; R = Sm, Gd, Tb, Dy, Ho, Er, Tm, Lu, Y, Ce, Zr [71 B 20]; R = Gd, Tb, Dy, Ho, Er, Tm [73 H 3, 74 N 9]; R = Ce, Sm, Gd, Dy, Ho, Er, Tm [62 W 2]; R = Ce, Sm, Gd, Tb, Dy, Ho, Er, Tm, Lu, Y [80 I 2]; R = Dy, Er [74 C 2, 74 C 3]; R = Lu, Zr, Hf [86 Y 1(T)]; R = Mo, Hf, Ta, W [85 I 4(T)]; R = Ce [64 F 1, 72 B 15, 76 A 6, 76 B 18, 77 V 1, 79 M 9, 81 D 4, 81 M 7, 87 A 7]; R = Pr [80 S 11, 81 M 9, 81 M 10, 84 P 1(T)]; R = Nd [81 M 9, 81 M 10]; R = Sm [75 D 8, 76 A 6, 76 D 3]; R = Gd [62 H 1, 64 M 1, 78 V 1]; R = Tb [73 C 4, 74 B 10, 76 O 2, 78 C 5, 78 M 7, 79 N 5]; R = Dy [64 M 1, 74 B 10, 78 C 5, 78 M 7, 82 B 1, 83 P 11, 83 P 18]; R = Ho [79 A 1*]; R = Er [72 B 5, 73 B 9, 73 C 6]; R = Tm [78 A 1, 78 C 5, 82 B 9]; R = Yb [81 M 9, 81 M 10, 86 T 8]; R = Lu [70 B 8]; R = Y [67 M 1, 70 B 8, 73 B 2, 76 B 18, 84 V 1, 85 M 8(T), 86 A 8]; R = Zr [67 M 1, 72 B 15, 85 M 8(T), 86 A 8]; R = Ti [67 M 1, 68 N 1]; R = Sc [74 I 1, 76 S 2, 81 G 16, 85 I 5(T)]; R = Hf [70 N 1]

RCo_2 [70 B 4(T), 72 B 11, 72 G 9(T), 73 B 18, 73 V 5, 73 V 6, 74 B 9, 75 B 4(T), 76 B 1, 76 B 13, 77 B 15, 79 C 8(T), 80 W 4(T), 82 I 3, 84 S 16]; R = Ce, Pr, Nd, Gd, Dy [63 W 1]; R = Ce, Pr, Nd, Sm, Gd, Tb, Dy, Ho, Er [64 R 1]; R = Ce, Pr, Nd, Gd, Dy [64 W 2]; R = Nd, Tb, Ho, Er [65 M 1]; R = Ce, Pr, Nd, Sm, Gd, Tb, Dy, Ho, Er, Tm, Y [66 F 1]; R = Nd, Gd, Ho, Y [66 L 4]; R = Pr, Nd, Gd, Tb, Dy, Dy, Ho, Er, Lu [71 B 9]; R = Pr, Nd, Sm, Gd, Tb, Dy, Ho, Er, Y [72 B 10]; R = Nd, Tb, Dy, Ho, Er, Tm [72 G 5]; R = Nd, Gd, Tb, Dy, Ho, Er [72 V 2]; R = Gd, Tb, Dy [72 B 12]; R = Sc, Ti, Zr, Lu, Hf [85 Y 3(T)]; R = Nd, Tb, Dy, Ho, Er [71 V 1]; R = Dy, Ho, Er [79 C 9(T)]; R = Sc, Y, Lu [85 G 18]; R = Nb, Ta [86 Y 2(T)]; R = Sc, Y, Lu [84 I 4]; R = Ce [67 S 2, 85 Y 7(T), 86 C 6, 86 Y 4(T); R = Pr [81 D 3]; R = Nd [76 D 12]; R = Gd [70 B 9, 75 G 2*, 75 T 2, 76 B 14, 77 B 20, 77 S 9]; R = Tb [74 B 8, 79 G 5*, 80 M 2, 83 D 3]; R = Dy [77 H 6]; R = Ho [74 B 1, 75 G 2*, 77 G 4, 78 A 8*]; R = Er [68 P 1]; R = Tm [74 D 4, 77 G 4]; R = Lu [75 B 1, 76 B 15, 77 B 6, 78 M 12, 78 S 6, 85 M 3, 87 Y 2(T), 87 Y 4(T), 87 Y 9]; R = Y [75 B 1, 76 B 15, 77 B 6, 77 G 4, 78 M 12, 78 S 6, 80 W 5(T), 81 G 6, 84 S 5(T), 85 Y 1(T), 87 Y 2(T)]; R = Zr [86 C 6]; R = Sc [87 Y 2(T), 87 Y 4(T)]; R = Hf [73 A 3]

RNi_2 [72 B 13, 79 C 8(T)]; R = Ce, Pr, Nd, Sm, Gd, Tb, Dy, Ho, Er, Tm, Lu, Y [63 S 1]; R = Pr, Nd, Sm, Gd, Dy, Ho, Er, Tm [64 B 1(T)]; R = Ce, Pr, Nd, Sm, Gd, Tb, Dy, Ho, Er, Tm, Y [66 F 1]; R = Pr, Nd, Sm, Gd, Tb, Dy, Ho, Er, Tm [84 I 3]; R = Pr [80 M 10, 82 A 9, 82 G 9, 82 M 3, 82 M 5]; R = Sm [73 B 24, 74 B 16, 76 D 3]; R = Gd [71 C 1, 73 H 5(T), 74 B 16, 74 H 8, 75 P 4, 77 M 2, 77 M 3, 86 C 2, 86 J 1]; R = Tb [72 O 6, 80 M 2]; R = Dy [72 O 6, 77 G 2*, 86 C 2]; R = Ho [75 G 2*]; R = Er [83 G 2*]; R = Tm [86 D 2]; R = Y [75 P 4, 76 B 15, 81 G 6, 84 L 4]; R = Sc [85 Y 3(T)]; RM_2, M = Au, Ag [71 M 5]

RM_2H_x [78 B 20]

RMn_2H_x [77 B 21, 77 B 22]; R = Y [77 B 19, 78 B 22, 87 F 6]; R = Zr [80 J 2, 82 W 1, 87 F 6]; R = Sc [82 B 14]

RFe_2H_x [77 B 18, 79 W 1]; R = Tb, Er [87 F 4, 87 F 5]; R = Ho, Er, Tm [78 W 3, 79 F 5]; R = Gd, Ho, Er, Tm, Lu [84 D 4]; R = Er, Y, Sc [83 S 7]; R = Ce [76 B 18, 77 V 1, 78 B 22, 85 D 11, 87 A 10]; R = Gd [76 B 21, 82 N 2]; R = Tb [85 B 4]; R = Dy [80 P 6]; R = Ho [76 G 10]; R = Er [76 G 10, 82 S 12, 84 D 5, 85 D 4]; R = Tm [76 G 10, 82 N 2]; R = Lu [78 B 22, 85 D 11]; R = Y [76 B 18, 76 B 21, 78 B 22]

RCo_2H_x R = Pr [72 T 5, 80 M 7, 81 D 3]; R = Nd [72 T 5]; R = Gd [77 B 20, 78 B 22, 87 F 7]

RNi_2H_x R = Gd [77 M 2]

$(R'R'')M_2$ (LaY)Mn_2 [88 N 1]; (PrGd)Mn_2 [71 N 1]; (PrTb)Mn_2 [71 N 1]; (PrEr)Mn_2 [71 O 1]; (GdY)Mn_2 [86 O 2]; (GdHo)Mn_2 [81 T 3]; (LuY)Mn_2 [86 O 2]; (YSc)Mn_2 [88 N 1]

(RTb)Fe_2 [76 B 7]; (CeGd)Fe_2 [73 M 12, 75 M 8]; (CeY)Fe_2 [71 B 20, 80 D 1]; (PrSm)Fe_2 [83 S 12, 85 S 15]; (PrTb)Fe_2 [85 S 15]; (PrY)Fe_2 [85 S 15]; (SmDy)Fe_2 [78 B 6]; (SmHo)Fe_2 [78 B 6]; (SmEr)Fe_2 [84 T 1, 87 E 2]; (SmY)Fe_2 [84 K 9]; (GdY)Fe_2 [70 B 13, 71 B 20, 76 B 11, 79 B 13, 83 B 9, 84 B 9]; (GdTh)Fe_2 [73 M 12, 75 M 8]; (GdY)$(FeAl)_2$ [85 B 5]; (TbDy)Fe_2 [75 C 2, 76 A 6, 78 B 6, 78 C 5, 78 S 3, 80 S 3, 80 W 3*, 82 W 8, 84 A 14, 86 J 4, 86 S 7]; (TbHo)Fe_2 [75 N 4, 76 A 6, 81 K 12]; (TbY)Fe_2 [70 B 13, 75 N 9, 75 P 9, 83 S 23]; (DyEr)Fe_2 [76 A 6]; (DyY)Fe_2 [68 P 3]; (HoEr)Fe_2 [76 A 6]; (ErLu)Fe_2 [80 M 6]; (ErY)Fe_2 [71 B 20, 80 H 9, 80 M 6, 82 C 5]; (ErSc)Fe_2 [80 M 6]; (ScTi)Fe_2 [85 N 3, 85 N 4, 86 N 2, 87 K 7, 87 N 3]; (HfTa)Fe_2 [82 N 3, 83 N 7, 84 N 3, 87 N 3]; (ZrNb)Fe_2 [87 Y 5]

(LaY)Co_2 [87 Y 13]; (CeY)Co_2 [85 A 9]; (PrDy)Co_2 [70 L 6, 70 L 7]; (PrHo)Co_2 [70 L 6, 70 L 7]; (PrY)Co_2 [82 H 6]; (NdY)Co_2 [82 G 6, 83 B 1]; (NdGd)Co_2 [71 P 4]; (GdEr)Co_2 [69 H 1]; (GdY)Co_2 [66 L 4, 66 L 5, 66 T 1, 73 B 3, 75 B 9, 75 T 2, 76 B 16, 79 H 7, 80 I 3(T), 81 B 11, 83 B 9, 84 B 9, 84 M 5, 85 M 3]; (TbHo)Co_2 [83 I 3, 86 A 1, 87 A 2]; (TbY)Co_2 [83 F 6, 84 L 5, 86 B 7, 86 B 8, 86 K 7]; (DyY)Co_2 [84 Y 7, 85 D 14, 87 P 5]; (HoY)Co_2 [75 S 9, 78 S 18, 78 S 19, 82 G 6, 82 H 6, 87 P 5, 88 H 2]; (HoY)$(FeCo)_2$ [75 S 9]; (ErY)Co_2 [84 L 6, 88 D 4]

(CeLa)Ni_2 [85 S 3]; (CeY)Ni_2 [85 A 9]; (PrDy)Ni_2 [70 L 6, 70 L 7]; (PrHo)Ni_2 [70 L 6, 70 L 7]; (PrY)Ni_2 [68 W 1]; (NdHo)Ni_2 [69 W 1]; (GdNd)Ni_2 [69 W 1]; (GdDy)Ni_2 [69 W 1]; (GdHo)Ni_2 [69 W 1]; (GdY)Ni_2 [86 T 2]

$(R'R'')M_2H_x$ (YZr)Fe_2H_x [86 K 4]

$R(M'M'')_2$ [83 H 3(T)]; $R(FeM)_2$, R = Y, Zr, U, M = Mn, Co, Al [82 H 4]; $Tb(MCr)_2$, M = Mn, Fe, Co, Ni [85 G 2]; $R(FeMn)_2$ [69 K 4, 73 H 4]; R = Gd, Tb, Dy, Ho, Er [75 W 1, 76 M 10]; R = Gd [73 K 11, 86 N 1, 87 N 1]; R = Dy [85 N 1]; R = Ho [76 I 2]; R = Er [73 K 11, 76 I 2]; R = Y [68 K 2, 73 K 11, 77 G 9, 79 B 15, 79 H 6, 80 S 4, 82 B 8, 82 O 2, 85 W 3]; $Gd(MnCo)_2$ [86 O 1]; $Y(MnCo)_2$ [79 O 1, 82 O 1, 83 S 10, 87 I 4(T)]; $Gd(MnNi)_2$ [82 S 22, 87 N 2]; $Gd(MnAl)_2$ [78 S 16, 83 S 18]; $Tb(MnAl)_2$ [72 O 3]; $Er(MnAl)_2$ [72 O 3]; $Y(MnAl)_2$ [67 M 1, 86 M 4, 86 S 12, 87 S 8, 88 S 1]; $R(MSi)_2$, $R(MGe)_2$, R = La, Ce, Nd, Sm, Er, Gd [73 F 4]; M = Fe, Co, Ni,

$Gd(MRh)_2$, M = Mn, Fe, Co [82 T 2]; $R(FeCo)_2$ [71 S 4, 73 H 4]; R = Gd, Dy, Ho, Er, Y, Zr [75 W 1]; R = Ho, Er [81 P 4]; R = Ce [87 R 4, 88 P 2, 88 R 2, 88 W 4]; R = Gd [78 B 11, 78 B 16, 79 B 12, 81 B 11]; R = Er [85 A 15]; R = Y [68 A 1, 68 P 2, 74 S 9, 77 I 1, 78 B 13, 79 B 12, 80 S 16, 80 V 2, 83 T 4(T), 85 T 6(T), 87 S 23, 87 Y 3(T), 87 I 4(T), 87 Y 13]; R = Zr [77 G 9, 77 F 5, 83 H 2]; $Ce(FeNi)_2$ [87 R 4]; $Dy(FeNi)_2$ [74 B 11, 78 B 12]; $Ho(FeNi)_2$ [78 B 12]; $R(FeAl)_2$ [82 I 1, 84 S 11]; $R(MAl)_2$, R = Gd, Dy, Ho, Er, M = Fe, Co, Cu [81 G 13]; $R(FeM)_2$, R = Y, Zr, M = Ni, Al [77 M 12]; $R(FeM)_2$, M = Co, Al, Rh [78 S 8]; $R(FeM)_2$ [79 S 8]; $R(FeAl)_2$, R = Gd, Dy, Ho, Y [76 G 8]; $Ce(FeAl)_2$ [82 D 1, 85 F 2, 86 D 1, 87 N 3, 87 N 4, 87 R 11]; $Pr(FeAl)_2$ [67 O 2]; $Gd(FeAl)_2$ [67 O 1, 79 B 6, 80 B 13, 81 B 11, 82 V 1, 83 B 9, 84 B 9]; $Tb(FeAl)_2$ [71 O 4, 73 O 1, 76 P 6]; $Dy(FeAl)_2$ [72 O 4, 75 G 3, 82 B 2, 82 B 5, 83 S 15, 85 K 3]; $Ho(FeAl)_2$ [85 S 21]; $Er(FeAl)_2$ [71 O 5]; $Lu(FeAl)_2$ [87 B 13]; $Y(FeAl)_2$ [75 B 12, 77 B 10, 77 O 2, 78 B 4, 79 B 12, 79 B 16, 80 S 15, 82 H 5, 84 H 8, 84 R 3, 85 S 10, 87 S 23]; RFeAl, R = Gd, Tb, Dy, Ho, Er, Tm, Lu [77 O 3]; $Sc(FeAl)_2$ [76 S 1]; $Zr(FeAl)_2$ [82 H 5]; $Dy(Fe_{0.9}M_{0.1})_2$, M = Al, Ga, B [87 Z 1, 88 Z 2]; $Gd(FeCu)_2$ [86 T 7]; $Yb(FeCu)_2$ [86 T 7]; $Dy(FeGa)_2$ [82 M 7]; $SmFe_{0.67}Ge_{1.33}$ [72 F 1]; $R(FeRh)_2$, R = Gd, Dy, Ho, Y [79 H 10]; $Gd(FeRh)_2$ [80 T 4, 82 T 2]; $Tb(FeRh)_2$ [79 S 9, 83 S 23]; $Ho(FeRh)_2$ [83 S 23]; $Y(FeRh)_2$ [87 S 23]; $Gd(CoIr)_2$ [79 C 2, 79 C 3]; $Y(FeIr)_2$ [79 V 2, 80 V 2, 86 S 21, 87 S 23]; $Hf(FeIr)_2$ [80 V 2]; $Ce(FeRu)_2$ [88 R 3]; $Tb(FePt)_2$ [83 N 10]; $Ce(CoNi)_2$ [83 D 1, 84 S 6, 85 A 9]; $Gd(CoNi)_2$ [69 T 1, 70 C 2, 74 B 12, 75 C 1, 78 B 11, 79 B 12, 88 K 2]; $Tb(CoNi)_2$ [82 M 2]; $Dy(CoNi)_2$ [72 B 1, 72 T 4, 80 C 1]; $Ho(CoNi)_2$ [82 T 3, 82 T 4]; $Y(CoNi)_2$ [84 S 6]; $R(CoAl)_2$, R = Pr, Nd, Sm, Gd, Tb, Dy, Ho, Er [78 G 1]; $Pr(CoAl)_2$ [67 O 2]; $Gd(CoAl)_2$ [67 O 1, 81 B 10, 81 B 11, 83 B 9, 84 B 9]; $Tb(CoAl)_2$ [71 O 2, 71 O 6, 73 O 1, 88 L 1]; $Dy(CoAl)_2$ [72 O 4, 88 L 1]; $Ho(CoAl)_2$ [73 O 1]; $Er(CoAl)_2$ [67 O 1, 70 O 2, 71 O 6, 73 O 2, 81 K 13]; $Lu(CoAl)_2$ [87 S 1, 87 E 5, 88 S 3]; $Y(CoAl)_2$ [84 A 9, 85 A 6, 85 Y 11, 86 I 6, 86 S 2, 87 S 1, 87 T 1, 87 Y 11, 88 S 3, 88 Y 3]; $Sc(CoAl)_2$ [86 I 6, 87 E 5, 87 I 5, 87 T 1, 88 S 3]; $Gd(CoCu)_2$ [86 B 12]; $Ho(CoCu)_2$ [86 H 3]; $Dy(CoCu)_2$ [85 D 14]; $Er(CoCu)_2$ [88 D 3]; $Y(CoCu)_2$ [88 D 3]; RCoSn [82 S 19]; $Ce(CoRu)_2$ [71 S 5]; $Gd(CoRh)_2$ [82 T 2]

$R(NiAl)_2$, R = Gd, Tb, Ho, Er [71 L 1]; $Pr(NiAl)_2$ [67 O 2]; $Gd(NiAl)_2$ [73 H 2, 85 K 1]; RNiAl [82 R 5]; $R(NiCu)_2$ [85 S 19]; $Gd(NiCu)_2$ [74 P 2, 86 B 11]; $Ce(NiPt)_2$ [80 O 7]; RNiSn [84 S 13]

$R(M'M'')H_x$ $Zr(M'M'')_2H_x$ [81 F 6, 81 P 5]; $Zr(MnM)_2H_x$ [82 S 18]; $Er(MnFe)_2H_x$ [78 S 2]; $Y(MnFe)_2H_x$ [80 O 2, 82 O 2]; $Zr(MnFe)_2H_x$ [82 F 13]; $Y(MnCo)_2H_x$ [88 F 3]; $Y(MnNi)_2H_x$ [88 F 3]; $Y(MnAl)_2H_x$ [88 F 3]; $Tb(FeCo)_2H_x$ [82 P 13]; $Dy(FeCo)_2H_x$ [82 P 13]; $Ho(FeCo)_2H_x$ [81 P 4, 82 P 14]; $Er(FeCo)_2H_x$ [81 P 4, 82 P 14]; $Y(FeCo)_2H_x$ [83 F 9]; $Zr(FeCo)_2H_x$ [79 M 18]; $GdFeAlH_x$ [84 D 7]; $Zr(FeAl)_2H_x$ [82 F 10]; $Zr(CrCo)_2H_x$ [83 H 2]; $Zr(FeV)_2H_x$ [85 F 5]; $GdMAlH_x$, M = Fe, Ni [84 D 7]

Neutron diffraction

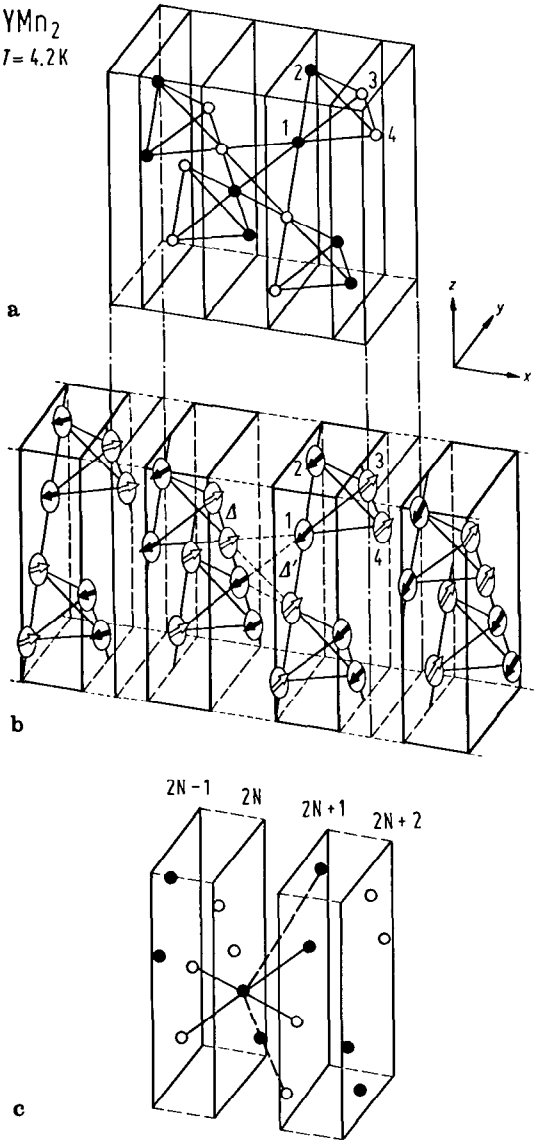

Fig. 157. Magnetic structure of YMn_2 at 4.2 K. Only the positions of the Mn atoms are shown. (a) Collinear antiferromagnetic structure proposed by [83 N 4]. Open and close circles represent Mn atoms with up and down spins, respectively. The propagation vector is $\boldsymbol{k}=[001]$. (b) Helimagnetic structure deduced from neutron diffraction studies using a long wavelength [87 B 6]. In the tetrahedron layers (solid lines) the antiferromagnetic arrangement is collinear as in (a). The propagation vector is $\boldsymbol{k}=[\tau 01]$ with $\tau=0.02$. Δ and Δ' are the two easy directions of Mn magnetic moments. (c) In both models, the Heisenberg exchange interactions do not cancel between pairs of atomic layers $2N-1$, $2N$, but do cancel between pairs of atomic layers $2N$, $2N+1$. The magnetic structures are then formed by highly correlated layers of tetrahedra with weak coupling between these layers.

Table 43a. Magnetic structure of some RMn_2 compounds.

	Crystal structure	T K	Magnetic structure	p_R μ_B	p_{Mn} μ_B	T_C K	Ref.
$PrMn_2$	C14 $P2_1m$	4.2	collinear	(4f) 2.6	(2a) 2.8 (2e) 2.8	115	86 O 2
		110	collinear	(4f) 1.8	(2a) 2.5 (2e) 2.5		
$PrMn_2$	C14 Pm	4.2	collinear	($2c_1$) 2.8 ($2c_2$) 2.4	(2c) 2.8 (1a) 2.8 (1b) 2.8	115	86 O 2
		110	collinear	($2c_1$) 2.1 ($2c_2$) 1.5	(2c) 2.5 (1a) 2.5 (1b) 2.5		
$NdMn_2$	C14 $P2_1/m$	4.2	see Fig. 159(b)	(4f) 2.9	(2a) 2.7 (2e) 2.7	104	86 O 2
		100	collinear	(4f) 1.9	(2a) 2.4 (2e) 2.4		
$NdMn_2$	C14 Pm	2	see Fig. 159(b)	($2c_1$) 2.9 ($2c_2$) 2.9	(2c) 2.7 (1a) 2.7 (1b) 2.7	104	86 O 2
		100	collinear	($2c_1$) 2.05 ($2c_2$) 1.70	(2c) 2.4 (1a) 2.4 (1b) 2.4		
$TbMn_2$	C15	4.2	modulated; spiral axis along [001]; ferrimagnetic spiral	8.0	2.5	40	64 C 3
$HoMn_2$	C15	4.2	ferrimagnetic	8.12	−0.84	26	82 H 1
	C14	4.2	ferrimagnetic	9.40	−0.64 (site a) −1.03 (site h)	26	
$HoMn_2$	C15	4.2	main component ferromagnetic	7.20		25	77 C 2
$ErMn_2$	C14	4.2	ferromagnetic along c axis	7.72	≅0	25	65 F 1
$TmMn_2$	C14	2.1	almost ferromagnetic along c axis	4.95(10)	≅0	12(2)	65 F 1
YMn_2 [1]	C15	2.0	helimagnetic, see Fig. 157		2.7(1)	110	87 B 6
YMn_2	C15	4.2	collinear type I antiferromagnet		2.7		83 N 4
$ThMn_2$	C14	5.0	below T_M one Mn atom (2a) in four remains nonmagnetic whilst the other order in a triangular configuration. See Fig. 159(a).		1.6(1) (6h)	115	87 D 7

[1]) YMn_2 is a helimagnet with a complex spin arrangement which has a very long period of modulation [87 B 6]. The magnetic moment per Mn atom is 2.7 μ_B at 2 K. Polarized neutron diffusion and polarization analysis [87 D 6] have been performed in the paramagnetic state up to $T = 3T_N$. These show that an effective magnetic moment persists above T_N, its magnitude being 1.60(10) μ_B at 120 K, 1.70(10) μ_B at 200 K, and 1.90(10) μ_B at 300 K. The reduction of the magnetic moment as compared to the ground state may be the origin of the large magnetovolume effects observed at T_N. The enhancement of the paramagnetic diffusion gives evidence for strong antiferromagnetic correlations which persist up to $T = 3T_N$.

Table 43b. Magnetic structures of some RFe_2, RCo_2 and RNi_2 compounds. n.d.: not determined, n.o.: not observed.

	Crystal structure	T K	Magnetic structure	p_R μ_B	p_M [1] μ_B	Ref.
$HoFe_2$	C15	4.2	ferri	n.d.	−1.70	71 M 6
$HoFe_2$	C15	4.2	ferri	9.15(10)	−1.88	79 F 6*
$HoFe_2$	C15	10	ferri	10.00	−1.70	79 F 5
$ErFe_2$	C15	10	ferri	8.80	−1.60	79 F 5
$ErFe_2$	C15	4.2	ferri	8.47	−1.97	71 B 6
$TmFe_2$	C15	10	ferri	7.00	n.d.	79 F 5
$YbFe_2$	C15	5	ferri	3.60	−1.50	86 T 8
$LuFe_2$	C15	4.2	ferro	–	1.67 [2]	80 G 6
$PrCo_2$	C15	4.2	ferro	2.70	+0.80	67 S 1
$PrCo_2$	C15	0 [3]	ferro	2.90(10)	+0.30(10)	78 H 4
$NdCo_2$	C15	4.2	ferro	2.60(20)	+0.80(20)	65 M 1
$NdCo_2$	C15	0 [3]	ferro	2.70(50)	+0.20(10)	78 H 4
$TbCo_2$	C15	4.2	ferri	8.80(20)	−1.00(20)	65 M 1
$TbCo_2$	C15	0 [3]	ferri	7.70(10)	−1.00(10)	78 H 4
$HoCo_2$	C15	4.2	ferri	8.80(20)	−1.00(20)	65 M 1
$HoCo_2$	C15	4.2	ferri	n.d.	−0.80	77 G 5
$HoCo_2$	C15	0 [3]	ferri	9.30(20)	−0.70(10)	78 H 4
$ErCo_2$	C15	4.2	ferri	8.90(20)	−1.00(20)	65 M 1
$TmCo_2$	C15	4.2	ferri	5.40(10)	−0.80(5)	76 G 4
$TbNi_2$	C15	4.2	ferro	7.20	n.o.	65 F 1

[1]) The signs + and − refer to parallel or antiparallel coupling to R magnetic moments, respectively.
[2]) Differences to the Fe magnetic moment determined by saturation measurements are due to the fact that the latter include the negative polarization of conduction electrons ($\cong -0.25\,\mu_B$/f.u.).
[3]) Extrapolated from 4.2 K.

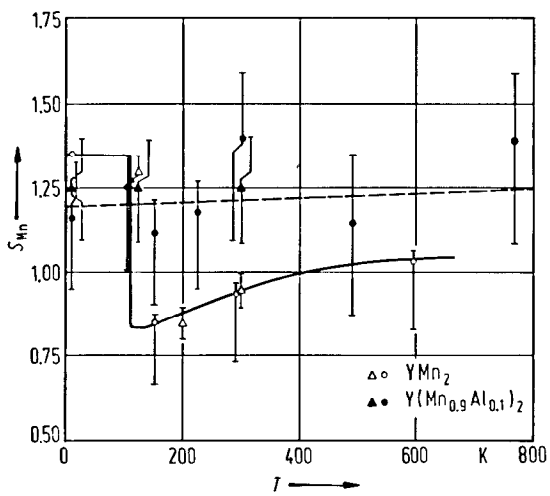

Fig. 158. Temperature variations of the local amplitude of spin fluctuations per Mn atom, S_{Mn}, for YMn_2 and $Y(Mn_{0.9}Al_{0.1})_2$. Triangles [87 D 5]; circles [88 F 2, 88 M 1]. In YMn_2 a change in the electronic state at T_N causes a collapse of the Mn magnetic moment. In the paramagnetic phase, strong antiferromagnetic correlations are observed at least up to $6T_N$. The local amplitude of spin fluctuations increases slightly with increasing temperature, as predicted by theoretical models [79 M 17]. Long-range antiferromagnetic order below T_N in YMn_2 has been shown to collapse by substituting only 5 at% Mn by Al. In the $Y(Mn_{1-x}Al_x)_2$ a spin glass transition has been evidenced. In $Y(Mn_{0.9}Al_{0.1})_2$, S_{Mn} does not depend on the temperature up to $\cong$760 K.

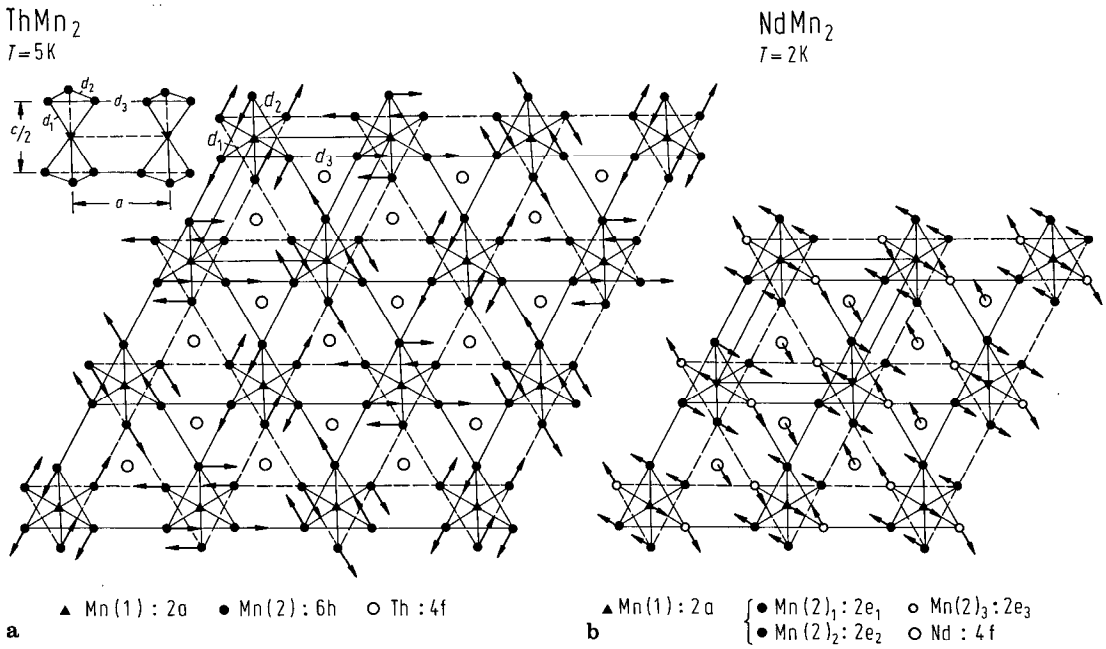

a b

Fig. 159. (a) Projection onto the basal plane of the $ThMn_2$ magnetic structure at 5 K. Only the Mn(6h) sites of the hexagonal Laves phase ($P6_3/mmc$) are magnetic [87 D 7]. The magnetic structure can be described as a stacking of magnetic atomic layers perpendicular to the c axis which are antiferromagnetically coupled. In each layer the magnetic arrangement shows two types of magnetic couplings: parallel alignment between Mn moments belonging to the same tetrahedron and triangular coupling between Mn moments belonging to the neighbouring chains. These properties enable the anomalous thermal expansion to be understood because of the strong dependence of the magnetic interaction with Mn–Mn distances [70 Y 1]. In the paramagnetic state the Mn tetrahedrons are regular so that all the Mn–Mn nearest neighbour distances are equal with a value of 2.75 Å at 120 K. Due to the presence of exchange rings involving odd numbers of Mn interatomic distances any antiferromagnetic ordering is frustrated. The nonmagnetic states of Mn (2a) atoms reduce this frustration without requiring any change of the Mn(2a)–Mn(6h) distance (noted by d_1). The anomalous decrease of the c parameter arises from the increase of the d_2 interatomic distance, between 6h atoms ($\Delta d_2/d_2 = -2\Delta c/c = 0.26\%$); such an increase reduces the negative interactions which are strongly frustrated because of the ferromagnetic coupling. The anomalous increase of the a parameter ($\Delta a/a = 0.09\%$) is less than $\Delta d_2/d_2 = 0.26\%$, since in order to improve the repartition of the frustrated energy in the 6h magnetic layers, the d_3 distance decreases ($\Delta a = \Delta d_1 = \Delta d_2$ and $\Delta d_3/d_3 = -0.06\%$) enhancing the negative interactions. As in YMn_2, such frustration should give rise to magnetic short-range ordering in the paramagnetic state. (b) Projection of the $NdMn_2$ magnetic structure parallel to the c axis at 2 K. Contrary to $ThMn_2$, a magnetic coupling between Nd and Mn atoms is present. The frustration is reduced by the great monoclinic distortion (Table 43a), 25% of the Mn atoms ($2e_3$) being magnetically decoupled from the other Mn atoms (2a, $2e_1$ and $2e_2$). Similar to the case of $ThMn_2$, the resultant effect of interactions on these sites by Mn nearest neighbours is nil. The $2e_3$ Mn atoms possess a magnetic moment due to the interactions involving Nd. At low temperatures, when the magnetocrystalline anisotropy is important, a reorientation of Nd magnetic moments is observed. This reorientation determines that of the $2e_3$ Mn atoms. The local symmetry of these Mn atoms does not involve a significant magnetocrystalline anisotropy. At low temperatures, the other Mn magnetic moments remain fixed on their directions. Thus, the atoms on the 2a sites of uniaxial symmetry have an important magnetocrystalline anisotropy, greater than the interaction energy with the Nd atoms. At higher temperature, an antiferromagnetic structure is observed – Table 43a [86 O 2].

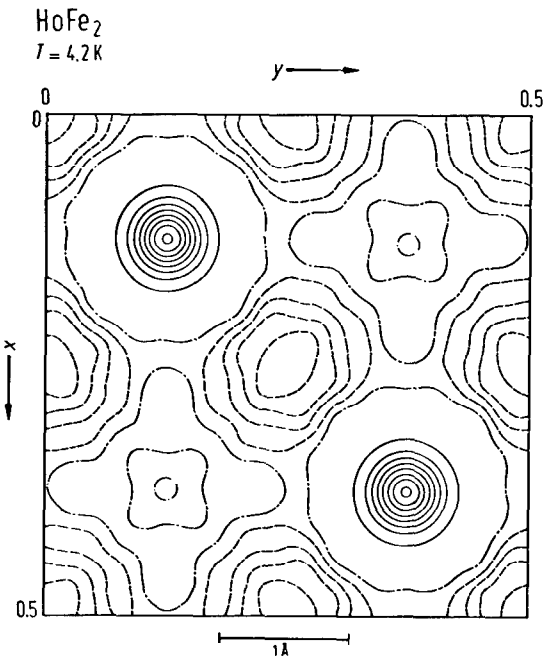

Fig. 160. Magnetization density projection of $HoFe_2$ at 4.2 K on (001) (solid lines): positive contours in steps of $5\,\mu_B/Å^2$, dashed lines: negative contours in steps of $0.5\,\mu_B/Å^2$ [79 F 6]. The Ho magnetization has a circular symmetry around the nucleus and a maximum of $41.4\,\mu_B/Å^2$. The magnetization on the Fe site is negative and reaches $-2.2\,\mu_B/Å^2$. Its shape, elongated perpendicular to the direction Fe–Ho, is an effect of the projection overlap with the Ho density. The Fe magnetic moment is $1.88(10)\,\mu_B$. In comparison with $LuFe_2$ results, $0.25\,\mu_B$ of the Fe magnetic moment is induced by interactions with Ho. Extrapolating the Ho magnetic amplitudes to $\sin\theta/\lambda = 0$, one finds a magnetic moment of $9.15(10)\,\mu_B$.

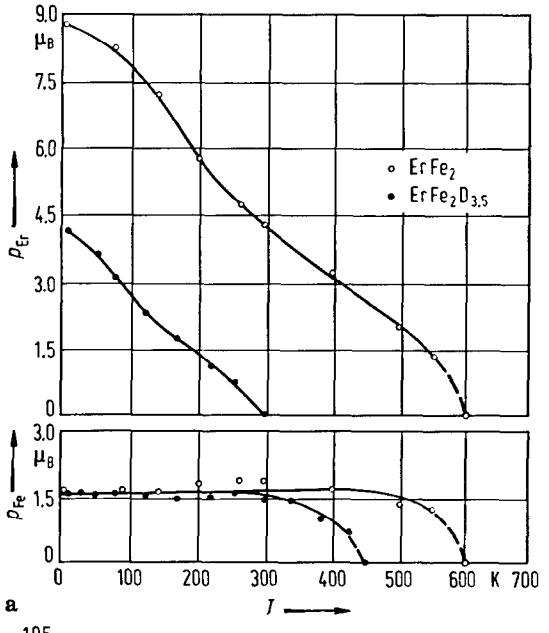

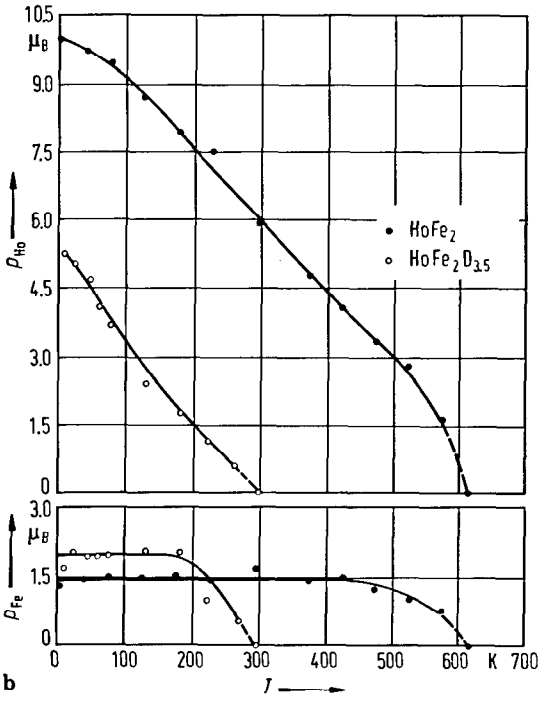

Fig. 161. Sublattice magnetization as a function of temperature as determined by neutron diffraction for (a) $ErFe_2$ and $ErFe_2D_{3.5}$, and (b) $HoFe_2$ and $HoFe_2D_{3.5}$. Curie temperatures were obtained from bulk magnetic susceptibility data [79 F 5].

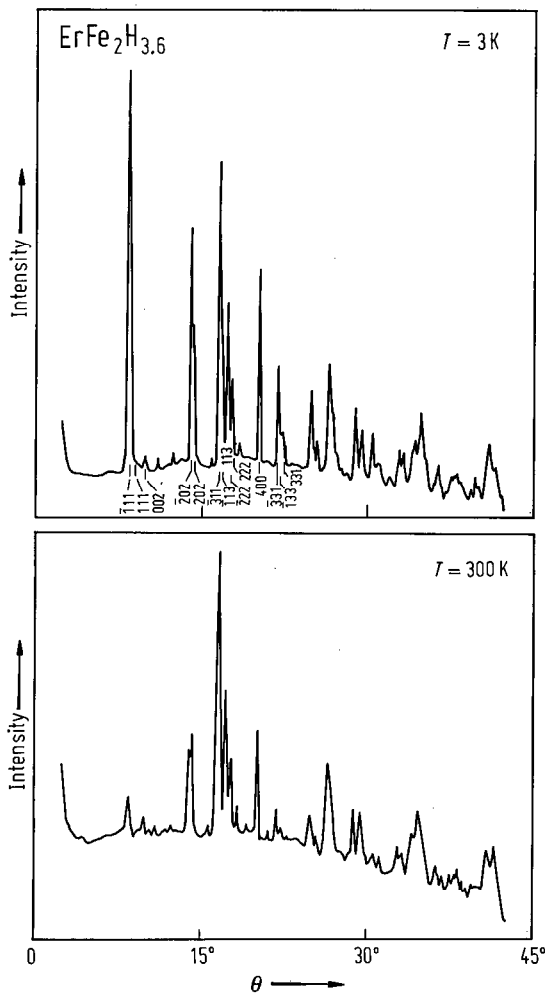

Fig. 162. Neutron diffraction pattern recorded at 300 K (paramagnetic state) and 3 K (ferrimagnetic state) of $ErFe_2H_{3.6}$ [87 F 4, 87 F 5]. The indices of the lines are evidence of the rhombohedral distortion. The weak broken lines come from a few percent of oxide impurity. The disappearance of the Er magnetic moment for $T > 200$ K is evidenced. In contrast to the $ErFe_2H_x$ ($x \leqq 3$) hydrides [79 F 5] the rhombohedral cell has a more complicated magnetic structure. Owing to the distortion, the four Fe sites do not have the same symmetry and according to the selective distribution of hydrogen on the interstitial sites, the Fe magnetic moments can be classified into two groups. Those having the shortest distance from hydrogen atoms (typically 1.6···2.2 Å) bear the smallest magnetic moment ($\cong 2.1\,\mu_B$) and those farthest from hydrogen (greater than 2.4 Å) exhibit the highest magnetic moment ($\cong 2.7\,\mu_B$) [87 F 4]. This discrimination effect agrees well with the results of Mössbauer effect measurements [85 A 4]. These may be correlated with the expansion or contraction of the structure due to the hydrogen presence. This fact influences also the 3d and 5d conduction electron magnetic susceptibility (see Fig. 128).

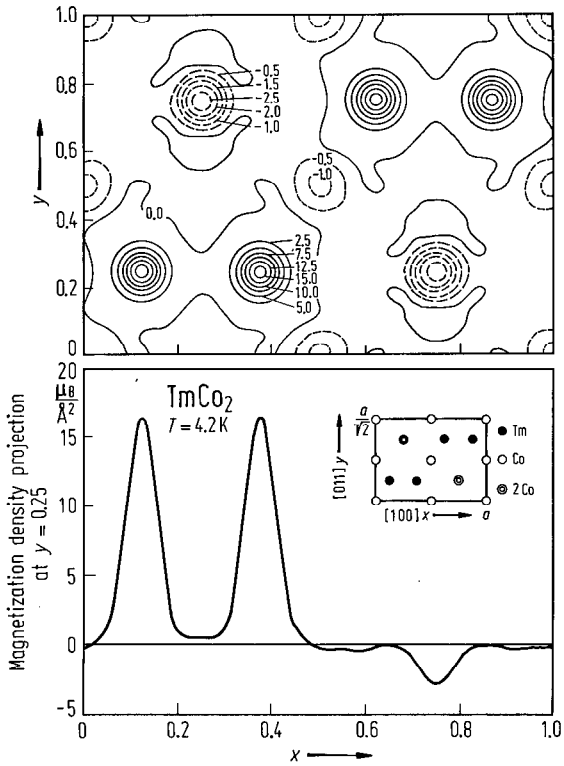

Fig. 163. Projection of the average magnetization density in $TmCo_2$ on the $(01\bar{1})$ plane at 4.2 K. Upper part: contour map. Numbers on contour lines give the magnetization density projection in units of $\mu_B/Å^2$. Thick lines are positive contours, thin lines zero contours, and dashed lines are negative contours. Lower part: projected density along the line y = 0.25 as shown on the sketch of corresponding atomic projection (insert). Values of Tm and Co magnetic moments, $p_{Tm} = 5.4(1)\,\mu_B$ and $p_{Co} = -0.80(5)\,\mu_B$, were determined [76 G 4].

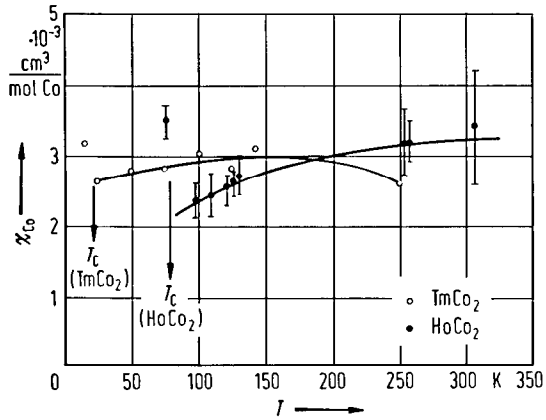

Fig. 164. Thermal variations of the Co magnetic susceptibility in $HoCo_2$ [77 G 5] and $TmCo_2$ [76 G 4] compounds determined by neutron diffraction. These show similar behaviour as observed in YCo_2 and $LuCo_2$ compounds. The Curie points of the $HoCo_2$ and $TmCo_2$ are also given.

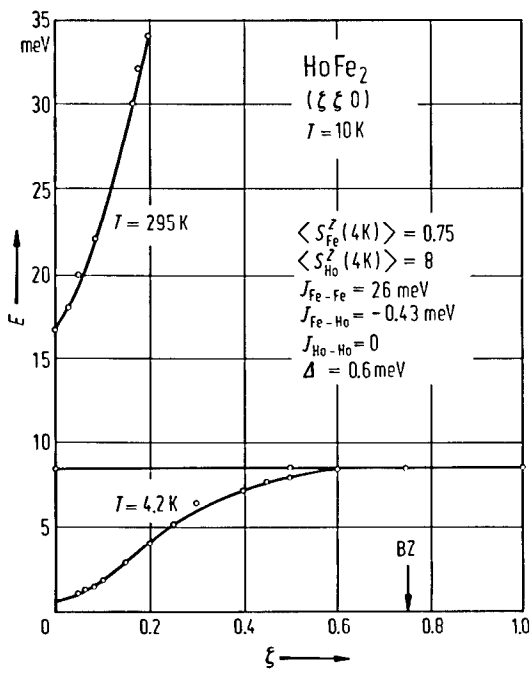

Fig. 165. Dispersion relations for spin waves propagating in the $(\zeta\zeta\zeta)$ direction in $HoFe_2$ [78 R 1, 87 R 8] at $T = 10$ K, which is representative at the ground-state excitation spectra found for other RFe_2 compounds. Measurements taken in $(\zeta\zeta\zeta)$ and $(\zeta 00)$ spin-wave propagation directions show similar behaviour with no evidence of anisotropy. The ground-state excitations consist of (1) an in-phase lowest-energy acoustic mode involving all spins with dispersion principally controlled by the R–M exchange interaction, (2) a flat dispersionless mode at 8.3 meV resulting from an out-of-phase mean-field excitation of the rare-earth spins, and (3) a highly dispersive upper mode which is an in-phase precession of the Fe spins and has dispersion, $E = Dq^2$, where $D \cong 200$ meV Å^2, which is comparable to that for pure Fe metal (280 meV Å^2). The remaining modes of the six expected from ground-state excitations, occur at very high energies (> 100 meV) as calculated from linear spin-wave theory [78 K 7] and do not have appreciable population at normal temperatures, nor are readily accessible to thermal neutron scattering energies. The extreme flatness of the rare earth optic mode is a consequence of the nearly vanishing exchange-coupling between rare-earth spins. The R–R coupling (calculated from the optic mode data to be less than 0.05 meV) is a result common to all the Laves phase Fe and Co compounds. The energy of this mode is given identically in both the mean-field theory and linear spin-wave theory by the Zeeman splitting energy of the rare-earth spin in the exchange field of Fe plus the contribution from the crystal field. The $q = 0$ gap of the Fe in-phase mode arises from the effect of the Fe–R exchange and can be expressed in the form [80 K 14, 81 K 14] $\Delta_2 = 12 J_{Fe-R}(\langle S_R\rangle - 2\langle S_{Fe}\rangle)$. The Fe branch in the figure is shown for 295 K (cf. 4.2 K for the other modes) and at low T the Fe mode gap at $E = 0$ is substantially larger due to the increased value of $\langle S_R\rangle$. The solid lines are the result of a linear spin-wave analysis (valid for low temperatures) [78 K 7, 80 K 14, 81 K 14] in which the spin wave energies are calculated from the Fourier transform of the equations of motion for the spin raising and lowering operators $S^{\pm}$ ($J^{\pm}$ of rare-earth site). The horizontal scale is in units of the reduced x component of the wavevector q.

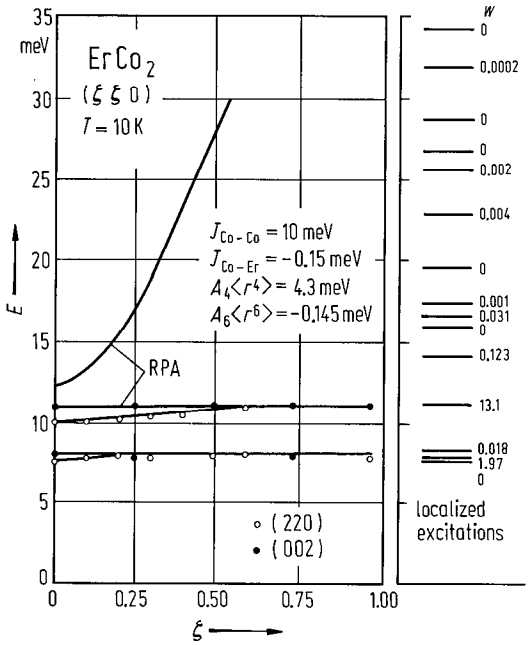

Fig. 166. Dispersion relations for spin waves propagating in the ($\zeta\zeta$0) direction in $ErCo_2$, measured near (220) and (002) reciprocal lattice points, open and solid circles, respectively [87 R 8]. The weaker R–M exchange in RCo_2 compounds compared to the Fe compounds allows transitions from the ground state to the states higher than the first excited state to have significant transition probability. This invalidates a linear spin-wave-theory analysis and requires a Green's function – RPA calculation [80 K 14, 81 K 14]. The Hamiltonian containing both exchange and crystal field terms is simplified by first separating out and directly diagonalizing the single-ion terms. The double-time Green's function can then be defined and solved by RPA. From this Green's function the scattered neutron intensity, which is proportional to the imaginary part of the generalized susceptibility, can be calculated from the transverse components of the total angular momentum. In the figure each transition involving rare-earth spins is double degenerate at the zone boundary and consists of both an in-phase component and an out-of phase component. The in-phase component is the mode exhibiting dispersion at low q. The other modes correspond to an out-of-phase spin precession of the two rare-earth spins in the primitive cell and give rise to dispersionless branches which have energies identical to mean-field excitations. The localized excitation energies, E, and transition probabilities, W, for the 16 states are shown, from which the lowest dispersionless mode may be identified with a transition from the ground state to the second excited state, and the second dispersionless mode with a transition from the ground state to the fourth excited state. The latter transition is found to be approximately six times as intense as the lower mode. The closely spaced in-phase and out-of-phase branches for each pair of modes were separated by making use of the selection properties of the dynamic structure factor. It should be noted that the Co–Co mode is calculated to have the dispersion shown but was not observable either in $ErCo_2$ or $HoCo_2$ [79 R 2] at any point in the zone. Castets et al. [80 C 2, 82 C 3] did observe a very weak Co mode in $HoCo_2$. For a summary and comparison of the exchange and cubic crystal field parameters in the RFe_2 and RCo_2 compounds see [80 K 15]. The horizontal scale is in units of the reduced x component of the wavevector q.

Table 44. Exchange and crystal-field parameters for some RM_2 compounds.

	J_{MM} meV	J_{RM} meV	J_{RR} meV	A_4^0 meV/a_0^4	A_6^0 meV/a_0^6	Method	Ref.
$TbFe_2$	26.0	−0.95				neutron inelastic	80 R 2
$HoFe_2$	26.0	−0.43		2.0	−0.075	neutron inelastic	78 R 1
$Ho_{0.88}Tb_{0.12}Fe_2$	23.5	−0.42		1.9	−0.087	neutron inelastic	76 N 7
$ErFe_2$	30.0	−0.32		3.2	−0.125	neutron inelastic	77 R 1, 78 K 7
$TbCo_2$		−0.18		10.0	−0.34	magnetization	79 G 2
$HoCo_2$		−0.22		4.3	−0.20	neutron inelastic	79 R 2
$HoCo_2$	37.3	−0.29	0.02	5.2	−0.16	magnetization	80 C 2
$ErCo_2$		−0.153	0.00(1)	4.3	−0.142	neutron inelastic	81 K 14
$TmCo_2$				13.3	−0.26	spin density	76 G 4, 77 G 3

For neutron diffraction studies see also

RMn_2 R = Pr [86 O 2, 88 B 2]; R = Nd [86 O 2, 88 B 2]; R = Tb [64 C 3]; R = Ho [77 C 2, 82 H 1]; R = Er [65 F 1]; R = Tm [65 F 1]; R = Y [87 B 6, 87 D 6, 88 F 2]; R = Th [86 O 2, 87 D 7]

RFe_2 [87 R 8]; R = Ce [81 D 4]; R = Tb [77 B 4]; R = Ho [70 M 5, 70 R 3, 79 F 5, 79 F 6*, 79 R 3, 80 F 6, 82 B 11]; R = Er [71 B 6, 71 W 4, 71 W 5, 79 F 5, 79 R 3, 80 F 6]; R = Tm [79 F 5, 79 R 3, 80 F 6]; R = Yb [86 T 8]; R = Lu [80 G 6]

RCo_2 R = Nd, Tb, Ho, Er [65 M 1]; R = Pr, Nd, Tb, Ho [78 H 4]; R = Pr [67 S 1]; R = Tb [79 G 2, 80 G 3]; R = Ho [77 G 3, 77 G 5]; R = Tm [76 G 4, 77 G 3, 77 G 4]

RNi_2 R = Tb [65 F 1, 76 G 6]

RM_2H_x RFe_2H_x, R = Er [78 R 2]; R = Ho, Er, Tm [79 F 5, 79 R 3, 80 F 6]; R = Tb, Er [87 F 4, 87 F 5]

$(R'R'')M_2$ $(TbHo)Fe_2$ [83 S 13]; $(TbY)Fe_2$ [81 S 12]

$R(M'M'')_2$ HoFeMn [77 C 2]; $Y(MnFe)_2$ [85 W 3]; $Tb(MnAl)_2$ [72 O 3]; $Er(MnAl)_2$ [72 O 3]; $Y(MnAl)_2$ [86 M 4, 87 D 5, 87 S 8]
$Tb(FeCo)_2$ [82 S 17]; $R(FeAl)_2$ [84 S 11]; $Tb(FeAl)_2$ [73 O 1]; $Dy(FeAl)_2$ [83 S 15]
$Tb(CoNi)_2$ [83 S 14]; $Tb(CoAl)_2$ [73 O 1]; $TbCo_{0.3}Al_{1.7}$ [71 O 2]; $Ho(CoAl)_2$ [73 O 1]; $Er(CoAl)_2$ [70 O 2]; $Gd(MCu)_2$, M = Co, Ni, Al [87 B 12]
$R(NiCu)_2$ [85 S 18]; $Tb(NiCu)_2$ [83 S 21, 84 S 10]; $Ho(NiCu)_2$ [83 S 21]

For inelastic neutron scattering see also

RMn_2 R = Y [87 M 7]

RFe_2 [80 K 15, 83 R 4]; R = Tb [80 R 2, 82 R 4]; R = Ho [78 M 15, 78 R 1, 82 R 4]; R = Er [77 R 1, 78 K 7, 80 K 14, 82 R 4]

RCo_2 [78 S 11(T), 80 K 15, 83 R 4]; R = Pr [82 G 10]; R = Ho [79 R 2, 80 C 2, 82 C 3, 82 R 4, 82 Y 1(T), 83 Y 2]; R = Er [79 K 8, 81 K 14, 82 R 4, 83 Y 2(T), 87 R 8]

RNi_2 R = Pr [82 A 9, 82 G 10, 82 M 3, 83 A 3, 83 A 4, 83 G 11]; R = Ho [82 C 4]; $PrAl_2$ [78 A 4]

$(R'R'')M_2$ $(HoTb)Fe_2$ [76 N 7]

$R(M'M'')_2$ $Y(MnAl)_2$ [87 D 5, 88 M 1]

EPR, FMR

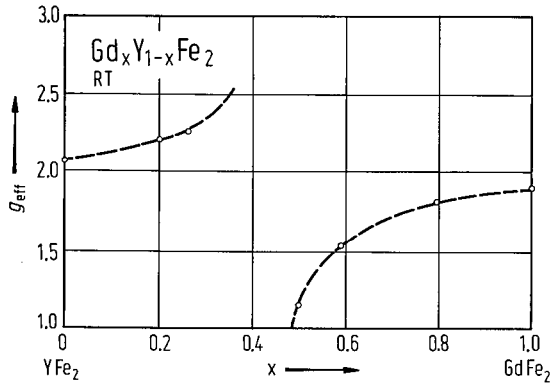

Fig. 167. Composition dependence of the effective spectroscopic splitting factor, g_{eff}, in the $Gd_xY_{1-x}Fe_2$ system at room temperature. By broken lines are plotted the relation $g_{eff}=(M_{Gd}-M_{Fe})(M_{Gd}/g_{Gd}-M_{Fe}/g_{Fe})^{-1}$ [56 W 1] with $g_{Gd}=2.00$ and $g_{Fe}=2.07$ [79 B 13].

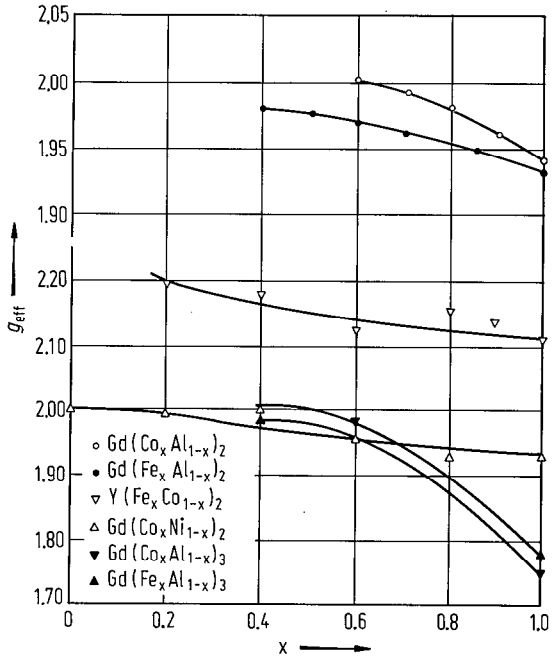

Fig. 168. Composition dependence of the effective spectroscopic splitting factors, g_{eff}, at 78 K in $Gd(Fe_xAl_{1-x})_2$, $Gd(Co_xAl_{1-x})_2$, $Gd(Co_xNi_{1-x})_2$, [83 U 2], $Y(Fe_xCo_{1-x})_2$ [78 B 14, 79 B 17], and $Gd(Fe_xAl_{1-x})_3$, $Gd(Co_xAl_{1-x})_3$ [83 U 2].

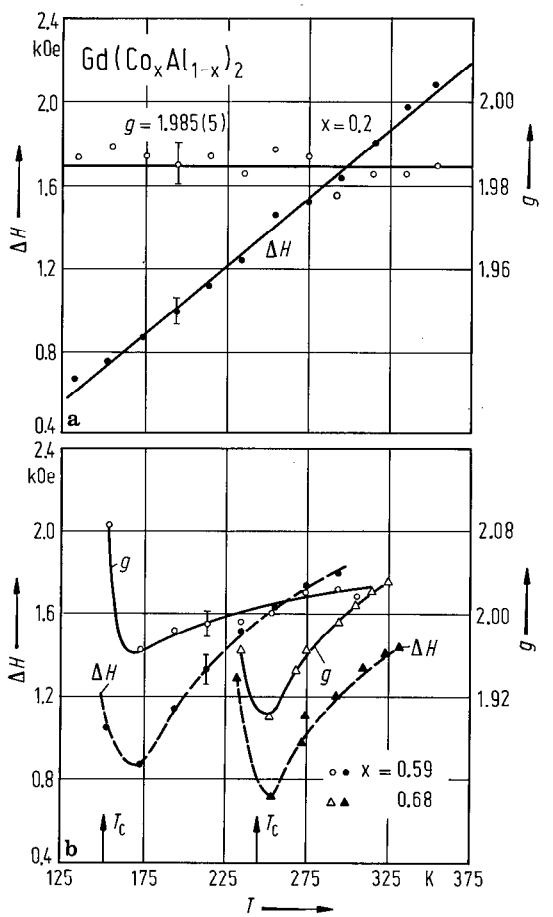

Fig. 169. Temperature dependence of the linewidth ΔH at $T > T_C$ and g values for $Gd(Co_xAl_{1-x})_2$ compounds. In compounds where Co is nonmagnetic a linear dependence of ΔH vs. T is shown (a). For ferrimagnetic compounds ΔH vs. T is nonlinear (b). By increasing the Co content a break in the bottleneck of the relaxation of conduction electron magnetization to the lattice is observed. (See also [67 P 2]). For compounds in which Co is nonmagnetic the g values are not dependent on temperature [81 B 10].

For FMR studies see also

RM_2 $GdFe_2$ [78 V 1]; YFe_2 [76 B 14]; $GdCo_2$ [76 B 14]

RM_2H_x $GdFe_2H_x$ [84 V 2]

$(R'R'')M_2$ $(GdY)Fe_2$ [77 B 16, 79 B 14]; (HoTbDy)Fe_2 [80 V 5]; $(GdY)Co_2$ [79 B 14, 81 B 11, 81 B 14]

$R(M'M'')_2$ $Y(FeMn)_2$ [79 B 15, 79 B 17]; $Gd(FeCo)_2$ [78 B 14, 79 B 12, 81 B 11]; $Y(FeCo)_2$ [78 B 14, 79 B 12, 84 B 10, 85 B 10]; $U(FeCo)_2$ [84 B 10]; $Gd(FeAl)_2$ [81 B 11, 83 U 2, 84 B 10]; $Y(FeAl)_2$ [79 B 17, 84 B 10, 85 B 10]; $U(FeAl)_2$ [79 B 17]; $Gd(CoNi)_2$ [79 B 12]; $Gd(CoAl)_2$ [81 B 10, 83 U 2, 84 B 10, 85 B 10]

For EPR measurements see also

RM_2 $GdCo_2$, $TbCo_2$ [71 B 11]; $GdCo_2$, $TbCo_2$, $DyCo_2$ [72 B 12]; $GdCo_2$ [72 B 10]; $GdNi_2$ [72 U 1, 72 B 13]; $ZrCo_2$, UCo_2 [66 G 1]

$(R'R'')M_2$ $(GdY)Co_2$ [80 B 2, 81 B 14]; $(GdY)Ni_2$ [80 B 2, 86 T 2]

$R(M'M'')_2$ $Gd(MnAl)_2$ [83 S 18]; $Gd(FeRh)_2$ [80 T 4]; $Gd(FeAl)_2$ [83 U 2, 85 B 10]; $Dy(FeAl)_2$ [85 K 3]; $GdFeAlH_x$, $GdNiAlH_x$ [84 D 7]; $Gd(CoNi)_2$ [78 B 15, 84 B 11]; $Gd(CoIr)_2$ [79 C 3]; $Gd(CoAl)_2$ [80 C 3, 81 B 10, 83 U 2, 85 B 10]

Gd in RNi_2, RCo_2, R = Sc, Y, Zr, Lu, Ce [81 D 9]; $Gd(NiAl)_2$ [85 K 1]; Gd in $PrNi_2$ [79 L 7]

Mössbauer effect, muon spin rotation, perturbed angular correlations

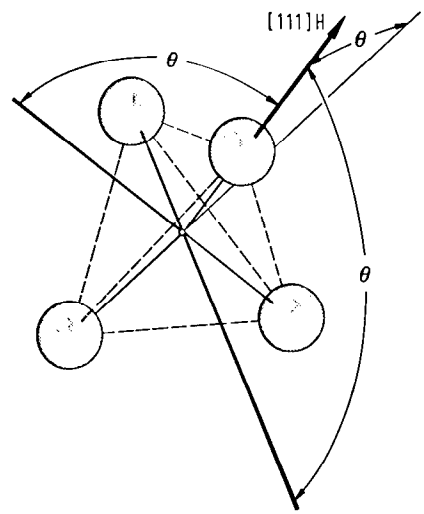

Fig. 170. Angular relationship between the direction of magnetization and axes of symmetry for one of the tetrahedra of Fe atoms of $MgCu_2$-type structure. The solid lines are the four three-fold symmetry axes which lie in [111] directions [64 W 6].

Table 45a. Easy directions of magnetizations at 4.2(78) K in RFe_2 compounds.

	YFe_2	$CeFe_2$	$PrFe_2$	$NdFe_2$	$SmFe_2$	$GdFe_2$ [1]			$TbFe_2$	$DyFe_2$ [2]	$HoFe_2$ [2]	$ErFe_2$	$TmFe_2$	$YbFe_2$	$LuFe_2$
Easy direction	[111]	[001] (78 K)	[001]	[011]	[011]	[001] (80 K)	[011]	non-major axis	[111]	[001]	[001]	[111]	[111] (78 K)	[100]	non-major axis
Ref.	73 B 1	71 G 6, 74 A 3	79 M 13, 80 S 11	79 M 13	74 R 4	74 A 3	76 M 17	68 B 4, 75 V 3, 79 M 15 81 G 2	68 B 4, 74 B 1, 78 C 5	68 B 4, 78 C 5	68 B 4, 74 B 1, 79 A 1	68 B 4, 74 C 2	64 W 6	77 M 8, 79 M 13	74 A 3

[1]) The effects on the easy direction of magnetization of the deviations from stoichiometry, heat-treatment, and impurities in Gd metal were analysed in [79 M 15, 78 C 7].

[2]) A small deviation of easy direction of magnetization from the [100] axis has been suggested [80 R 1].

Table 45b. Easy directions of magnetizations at 4.2 K in RCo_2 compounds.

	$PrCo_2$	$NdCo_2$	$SmCo_2$	$GdCo_2$	$TbCo_2$	$DyCo_2$	$HoCo_2$	$ErCo_2$	$TmCo_2$
Easy direction	[001]	[011]	[111]	[001]	[111]	[001]	[011]	[111]	[111]
Ref.	77 D 10	76 D 12	81 H 4	75 G 2	77 D 10	77 D 10	78 A 8	77 D 10	74 D 4

Table 45c. Easy directions of magnetizations at 4.2 K in RNi_2 compounds.

	$NdNi_2$	$SmNi_2$	$TbNi_2$	$DyNi_2$	$HoNi_2$	$ErNi_2$
Easy direction	[001]	[111]	[111]	[001]	[001]	[001]
Ref.	83 I 1	83 I 1	65 F 1, 83 I 1	77 G 2	75 G 2	83 G 2

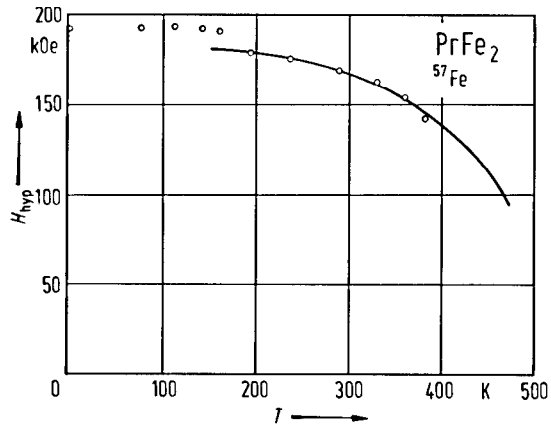

Fig. 171. Magnetic hyperfine field for ^{57}Fe in $PrFe_2$ as a function of temperature. The broken curve denotes a Brillouin function with $J=1/2$, $T_C=525$ K and $H_{hyp}(0\,K)=181$ kOe [80 S 11].

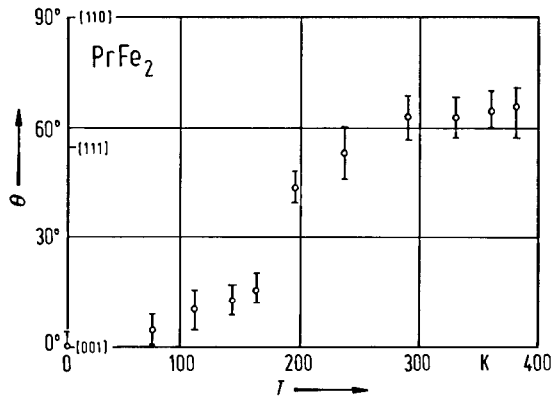

Fig. 172. Temperature dependence of the angle of inclination θ between the direction of the easy axis of magnetization and the [001] axis in $PrFe_2$ [80 S 11].

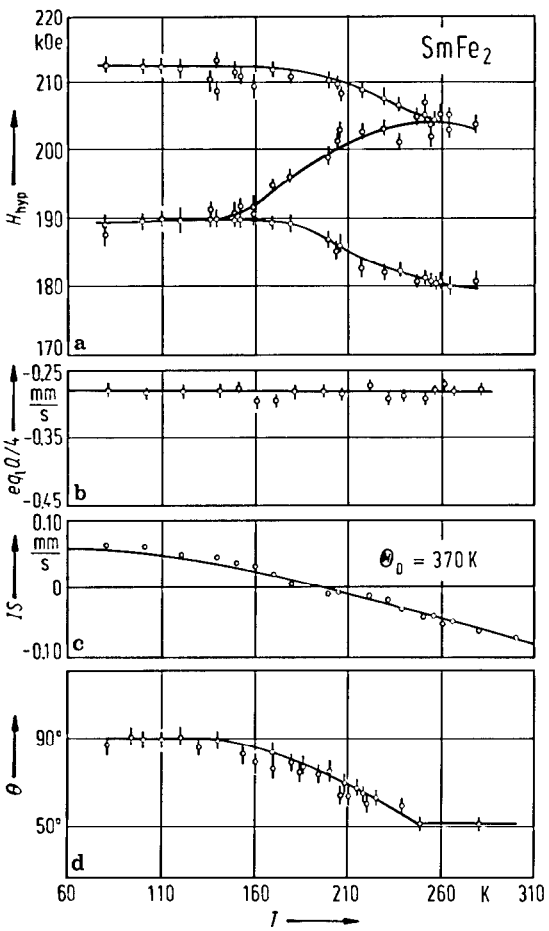

Fig. 173. (a) ^{57}Fe magnetic hyperfine fields, (b) electric quadrupole interactions (q_l: lattice electric field gradient), (c) isomer shifts relative to ^{57}Fe in Pd at room temperature and (d) direction of easy magnetization relative to major crystalline axes in $SmFe_2$ as function of temperature. A smooth curve has been drawn through the data points in (a), (b) and (d). The solid line in (c) describes the theoretical change of the isomer shift due to the second-order Doppler shift [81 B 2].

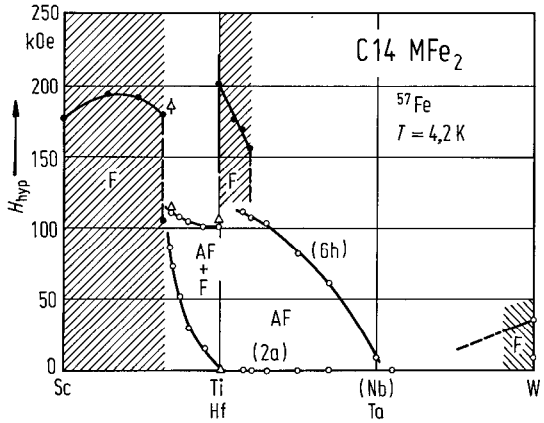

Fig. 174. Magnetic hyperfine fields of ^{57}Fe in MFe_2 with C14 structure at 4.2 K plotted against the difference in the d-electron number of the M atom and that of Sc [87 N 3]. In the Laves phase compounds with C14 structure, $ScFe_2$ [74 I 1] and $HfFe_2$ [70 N 1] exhibit ferromagnetism and $TiFe_2$ [68 N 1] antiferromagnetism. $NbFe_2$ and $TaFe_2$ are paramagnets [64 N 1]. The hyperfine magnetic field at ^{57}Fe varies with the change of M atoms. The ferromagnetic moment discontinuously decreases from 1.3 μ_B/Fe to 0.9 μ_B/Fe atom at $x \cong 0.65$ for $(Sc_{1-x}Ti_x)Fe_2$ and at $x \cong 0.35$ for $(Sc_{1-x}Nb_x)Fe_2$. In both systems, the critical concentration correspond to the difference in the d-electron number of $\cong 0.65$. Above these critical concentrations, the magnetic structure is a perpendicular superposition of ferromagnetic and antiferromagnetic spin densities [85 N 3]. In $(Hf_{1-x}Ta_x)Fe_2$ the ferromagnetic state changes into the antiferromagnetic one above $x \cong 0.15$ with increasing x [83 N 7]. WFe_2 with C14 structure stabilized by doping of Si exhibits a ferromagnetic behaviour at 4.2 K.

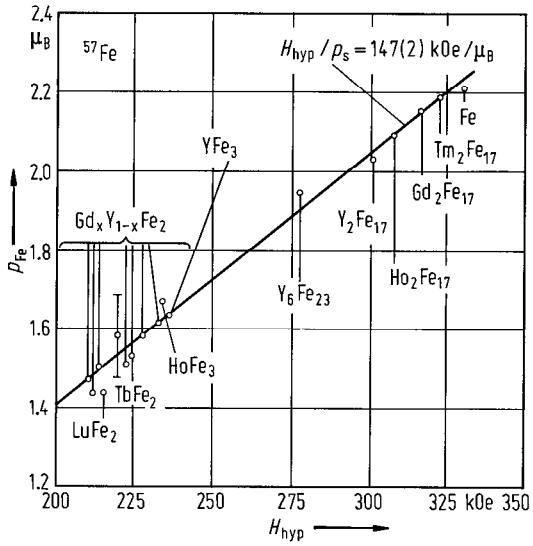

Fig. 175. Relationship between the mean ^{57}Fe magnetic hyperfine field and the mean Fe magnetic moment in some rare-earth compounds at low temperature [79 B 13]. Similar results were obtained in [77 b 1].

Fig. 176. Isomer shifts (*IS*) of ^{57}Fe relative to natural iron plotted against fractional volume change of Fe atoms in Laves phase compounds at 300 K [81 S 11]. The original plot [64 N 1] as supplemented with the data of Shimotomai et al. [81 S 11] (solid circles) and the data for $ErFe_2$, $DyFe_2$ and $HoFe_2$ [62 W 2], $LuFe_2$, $CeFe_2$ and $GdFe_2$ [64 W 1], $NpFe_2$ and $PuFe_2$ [70 B 5], $YbFe_2$ [77 M 8], and bcc-Fe and hcp-Fe [72 W 2]. The R atom exerts no first-order effect on *IS* except through its constraint on the volume available to the Fe atom. The change of the electron density at the Fe nucleus scales linearly with fractional volume up to 20%. The volume dependence of the *IS* in Laves phase compounds is associated with the close-packed arrangement of the constituent atoms.

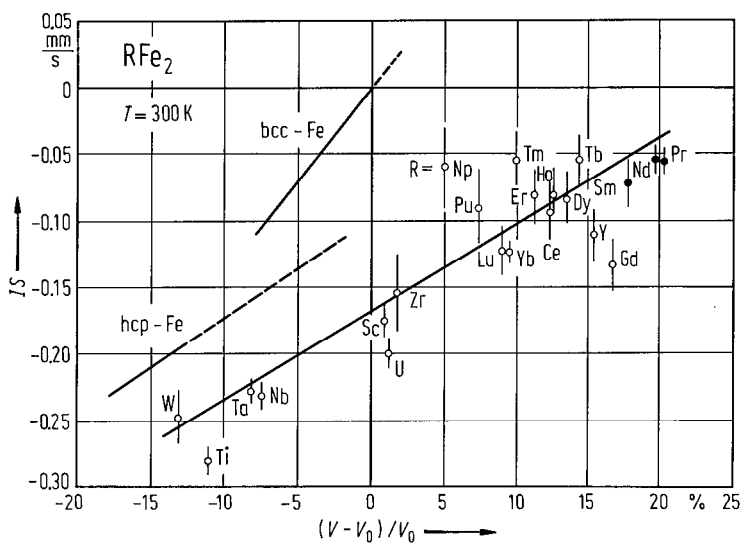

Table 46. Magnetic hyperfine fields at 4.2(80) K for Fe sites in RFe_2 compounds.

	T (K)	H_{hyp} [1] (kOe)		Ref.
		I	II	
$CeFe_2$	78	156		71 G 6
	80	156		74 A 3
	4.2	163		75 L 2
	4.2	174		78 G 5
$PrFe_2$	4.2	192.4		80 S 11
	4.2	190		79 M 13
$NdFe_2$	6	204 [2]	180 [2]	81 S 11
	4.2	203.1	176.4	81 M 10, 81 M 9
$SmFe_2$	78	216	190	71 G 6
	4.2	214	198	73 V 1
	78	214	190	73 A 5
$GdFe_2$	78	238	234	71 G 6
	78	225.6	–	74 A 3
$GdFe_2$	78	238	225	76 M 17
	4.2	237	229	74 B 1
	4.2	240	235	75 N 10
$TbFe_2$	78	226	197	71 G 6
	4.2	235	206	73 D 2
	4.2	225	195	74 B 1
$DyFe_2$ [3]	78	228		71 G 6
	78	222		82 B 2
	4.2	232		78 B 12
$HoFe_2$ [3]	78	221		71 G 6, 73 G 8
	20	228		74 V 2
	4.2	228		74 B 1, 78 B 12
$ErFe_2$	78	228	204	71 G 6
	4.2	232	201	73 D 2
	4.2	222	202	78 G 5
$TmFe_2$	78	216	202	64 W 6
	77	217	196	76 W 3
$YbFe_2$		205		79 M 13, 81 M 9
$LuFe_2$	78	207	203	71 G 6
	78	214.6	–	74 A 3
YFe_2	78	221	211	71 G 6, 73 G 8
	4.2	220	210	75 N 10
	4.2	218	200	76 M 17
	1.7	215	208	77 L 4
	4.2	215	208	78 G 5

[1]) The effective fields (I) and (II) are obtained for magnetically nonequivalent iron sites when the easy direction of magnetization is not the [001] axis.

[2]) Values obtained from figure in [80 S 11].

[3]) A small deviation of easy direction of magnetization from the [001] axis has been suggested [80 R 1].

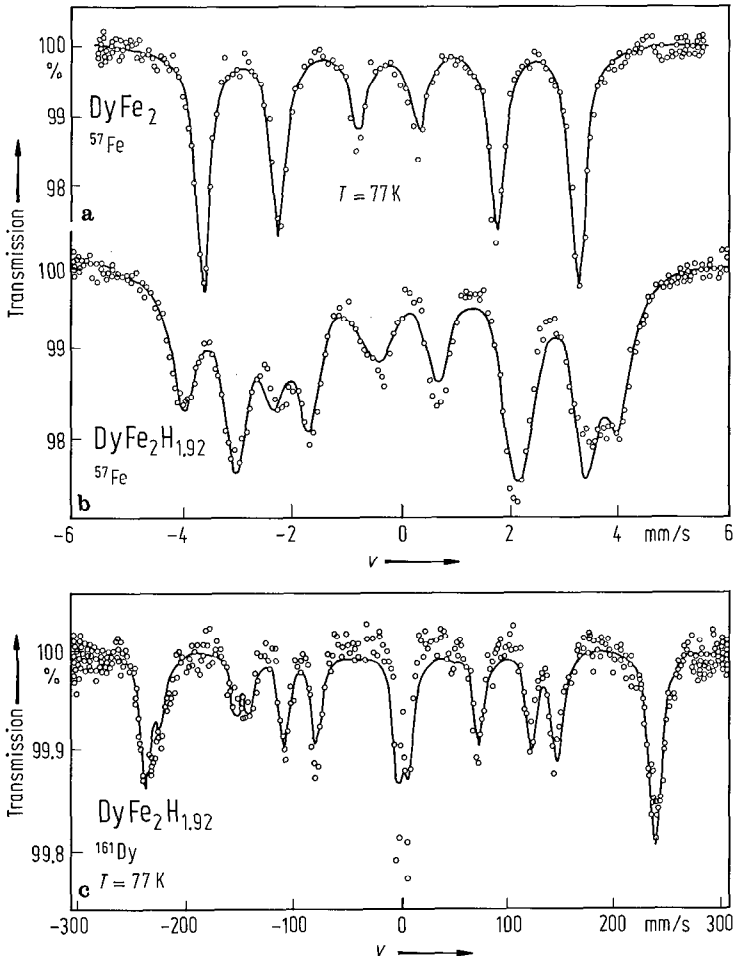

Fig. 177. Mössbauer spectra obtained at 77 K for (a) ^{57}Fe in $DyFe_2$, (b) ^{57}Fe in $DyFe_2H_{1.92}$ and (c) ^{161}Dy in $DyFe_2H_{1.92}$ [79 V 3]. In $DyFe_2$ only one magnetic hyperfine field at ^{57}Fe is observed corresponding to the single crystallographic (and magnetic) site. The spectrum for the hydride is more complex and shows resolved structure in spite of slightly broader resonances compared to $DyFe_2$, and was analysed as a superposition of two six-line magnetic hyperfine spectra. The different types of Fe sites in the hydride is associated with differences in the number and/or positions of surrounding hydrogen atoms. The two distinct sites for Fe indicate that the hydrogen forms an ordered structure at this composition. The measured hyperfine fields at 4.2 K are 195(4) kOe and 242(4) kOe, compared with the value 225(4) kOe obtained for $DyFe_2$. The isomer shifts are both positive relative to $DyFe_2$ by 0.28(2) mm s^{-1} and 0.08(2) mm s^{-1}, respectively, at 295 K. The ^{161}Dy spectrum at 4.2 K shows the presence of a single hyperfine field of 6050(50) kOe, which is close to the free-ion value (6200 kOe) but less than the value of 7080 kOe for $DyFe_2$ [65 O 1]. Hence, the saturated Dy magnetic moment in the hydride although somewhat reduced from the enhanced magnetic moment in $DyFe_2$ (due to conduction electron polarization) is still close to the free-ion value of 10 μ_B.

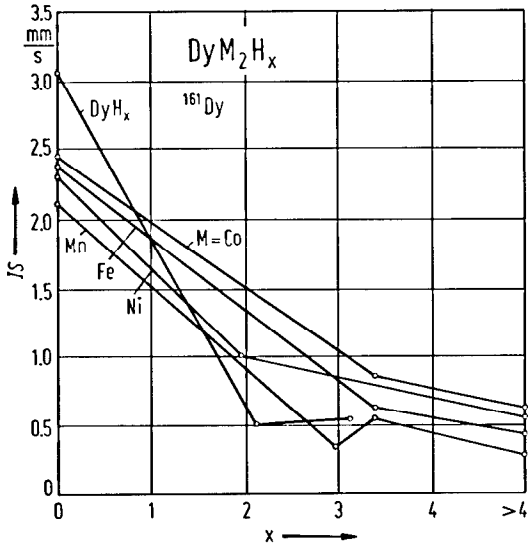

Fig. 178. Dependence of the isomer shift at ^{161}Dy on the hydrogen content in DyM_2H_x (M = Mn, Fe, Co, Ni) hydrides relative to $Gd_{0.5}Dy_{0.5}F_3$ source [80 C 8]. As the hydrogen is added to the lattice, the electron density at the Dy nucleus decreases, with the isomer shift approaching that of the hydride of dysprosium. The isomer shifts of the saturated hydrides (x > 4) are not identical but reflect the isomer shifts of the starting DyM_2 compounds.

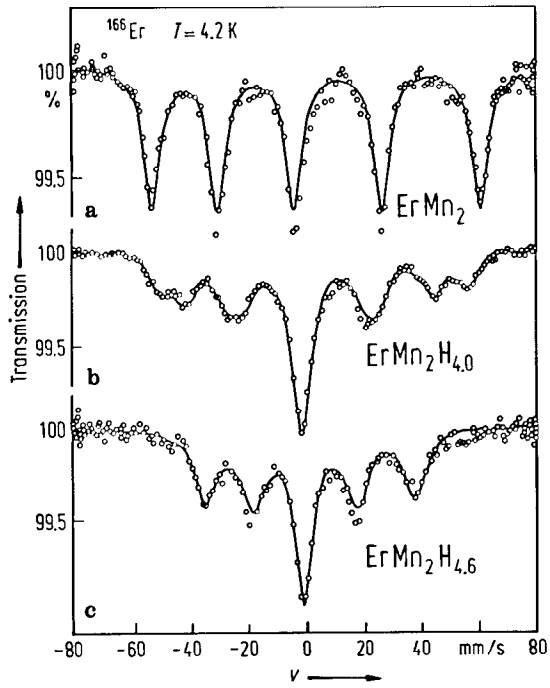

Fig. 179. ^{166}Er Mössbauer spectra at 4.2 K for $ErMn_2H_x$ samples having (a) x = 0, (b) x = 4.0, and (c) x = 4.6. The solid lines are the results of least-squares fits to the data [80 V 4]. The magnetic moment of Er in both hydride phases is below the value measured for $ErMn_2$. The ferromagnetic ordering present in $ErMn_2$ and $ErMn_2H_4$ is absent in $ErMn_2H_{4.6}$ down to 1.5 K. Two Er sites are detected in $ErMn_2H_4$ instead of the one expected for the C14 structure. The origins of these sites are attributed to the possible configurations of hydrogen site occupancy.

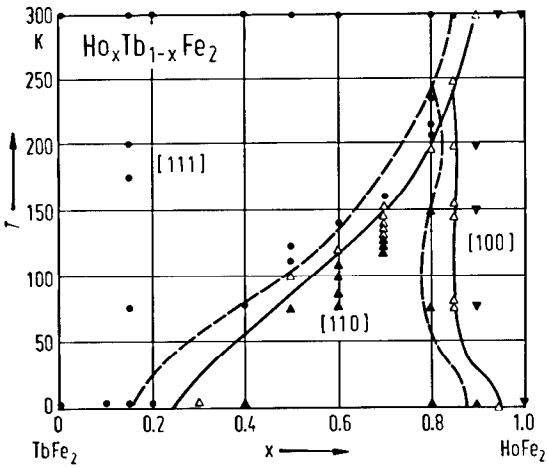

Fig. 180. Spin orientation diagram of the $Ho_xTb_{1-x}Fe_2$ system. Filled circles, filled triangles and inverted filled triangles correspond to experimentally determined Mössbauer spectra characteristic of the [111], [110] and [100] axes of magnetization, respectively. Open triangles correspond to intermediate types of spectra. The solid lines are experimentally determined boundaries of regions with different directions of magnetizations [73 A 6]. The dashed lines are the boundaries determined theoretically using the one-ion model [72 A 1].

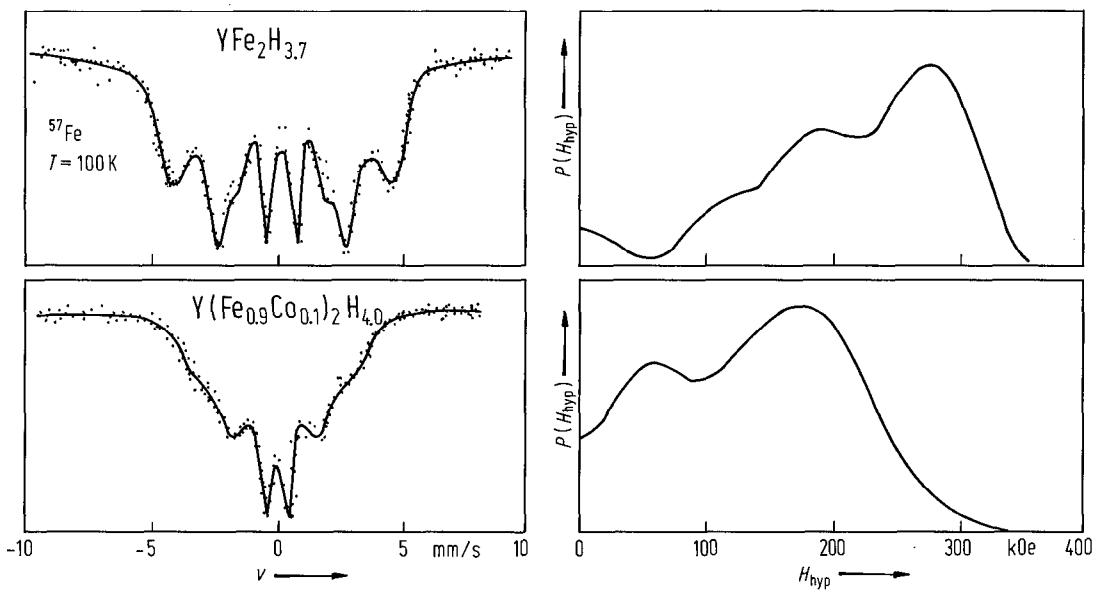

Fig. 181. Mössbauer spectra of ^{57}Fe in $YFe_2H_{3.7}$ and $Y(Fe_{0.9}Co_{0.1})_2H_{4.0}$ at 100 K [83 F 9]. The spectra are broad as compared to nonhydrogenated samples. The ^{57}Fe hyperfine field values in $Y(Fe_{1-x}Co_x)_2H_y$ become small upon hydrogenation for $x > 0.1$, leading to a decrease of the Fe magnetic moments. ^{59}Co NMR spectra indicate a serious reduction of the Co magnetic moments by hydrogenation. Both reductions are explained qualitatively in terms of loss in mutual contact between the 3d atoms upon H-uptake. The distribution functions $P(H_{hyp})$ of the hyperfine fields are also plotted.

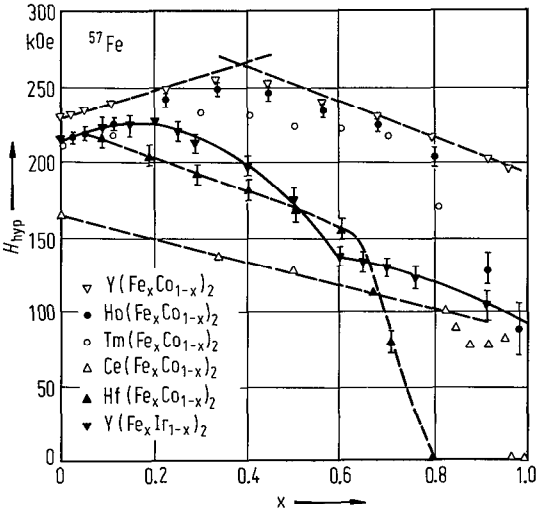

Fig. 182. Composition dependence of the mean hyperfine fields of ^{57}Fe in $Y(Fe_xCo_{1-x})_2$ at $T = 1.7$ K [77 L 4], $Ho(Fe_xCo_{1-x})_2$ at 20 K [74 V 2], $Tm(Fe_xCo_{1-x})_2$ at 77 K [76 W 3], $Ce(Fe_xCo_{1-x})_2$ at 4.2 K [75 L 2], $Y(Fe_xIr_{1-x})_2$ at 4.2 K [80 V 2] and $Hf(Fe_xCo_{1-x})$ at 4.2 K [80 V 2].

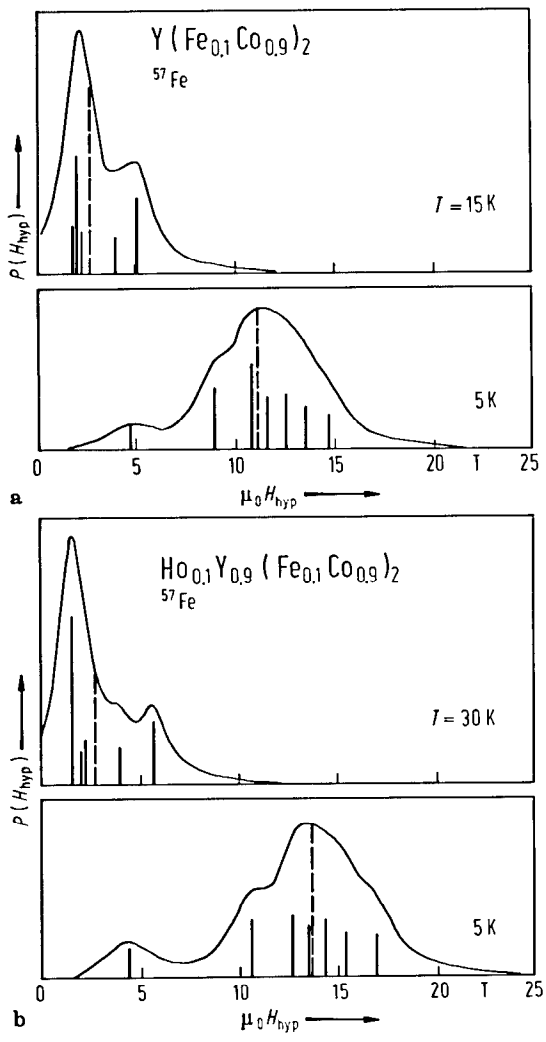

Fig. 183. Magnetic hyperfine field distribution, $P(H_{hyp})$, for (a) $Y(Fe_xCo_{1-x})_2$ and (b) $Ho_{0.1}Y_{0.9}(Fe_xCo_{1-x})_2$ compounds with $x = 0.1$. By broken lines are plotted the mean hyperfine fields [79 S 8]. Similar results were obtained for the composition range $0.05 \leqq x \leqq 0.2$. The width of the distribution increases with increasing x for $x \leqq 0.129$ and decreases for $x \geqq 0.15$. Corson et al. [77 C 6] reported magnetically split spectra for $x = 0.022$ at 0.15 K. This indicates the existence of Fe magnetic moments even at this low Fe concentration. It was concluded from extrapolation of the concentration dependence of the hyperfine field to vanishing Fe content, that a single Fe atom in a YCo_2 matrix still possesses a magnetic moment [77 L 4]. Later on [78 C 6] the spectrum recorded for $x = 0.022$ was analysed by means of a stochastic ferromagnetic relaxation model. Two nonequivalent Fe sites, with different T_C values (3.2 and 4.3 K, respectively) were obtained. However, the recorded spectra could not be explained completely by this treatment. The existence of Fe magnetic moments was tested for $Y(Fe_{0.1}Co_{0.9})_2$ by measurements in external field up to 1.72 T [79 S 8] at $T > T_A$, where T_A is determined by the vanishing of the magnetic hyperfine splitting. These show also that the Fe atoms possess a magnetic moment.

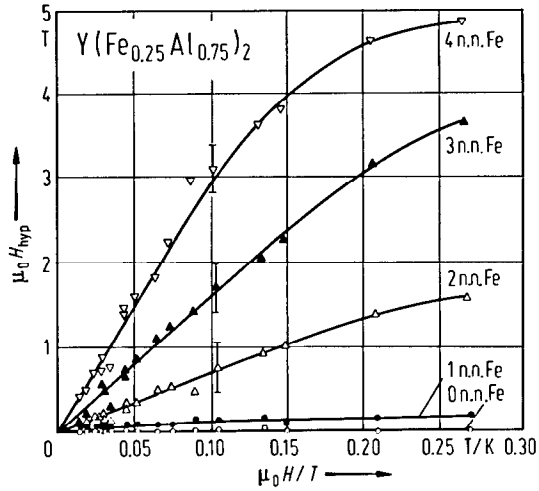

Fig. 184. Induced ^{57}Fe magnetic hyperfine fields, H_{hyp}, as function of H/T, where H is the external field, for $Y(Fe_{0.25}Al_{0.75})_2$ compound in the temperature range 50···300 K, for different nearest-neighbour Fe environment and fields up to 13.5 T. The lines are only guides for the eyes [87 R 6]. The temperatures studied are above the freezing temperatures. The data show the presence of magnetic clusters above T_C. Different H_{hyp} values are observed in the paramagnetic state for different Fe environments.

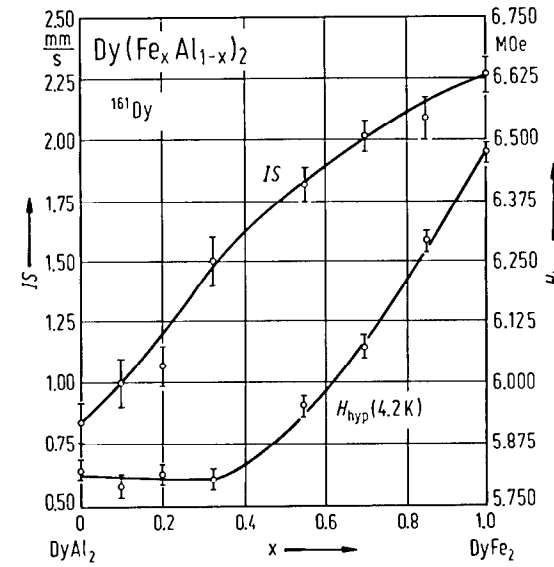

Fig. 185. Composition dependence of the magnetic hyperfine field at 4.2 K, H_{hyp}, and the isomer shift, IS, at ^{161}Dy nuclei in $Dy(Fe_xAl_{1-x})_2$ compounds [74 M 1].

Table 47. Magnetic hyperfine fields (experimental and conduction electron contribution) and exchange fields acting on rare-earth ions in RFe_2 and RCo_2 compounds.

	Probe	H_{hyp}(kOe)		Exchange field (K)	Ref.
		exp.	cond. el.		
$SmFe_2$	Eu^{3+}	−1090(20)	400(80)	105(10)	77Y4
$DyFe_2$	Dy^{3+}	7100(150)	870(150)	200	74B7
$TmFe_2$	Tm^{3+}	7650(180)	630(180)	165	64C1
$TmFe_2$	Yb^{3+}	4450(100)	350(100)	116(4)	75Y3
$SmCo_2$	Eu^{3+}	−1250(20)	210(80)	100(10)	77Y4
$DyCo_2$	Dy^{3+}	6500(150)	250(150)		66N1

For nuclear γ-resonance studies see also

^{57}Fe

RFe_2 [63W1, 71G6, 73B1, 74K14]; R=Ce, Sm, Gd, Tb, Dy, Ho, Er, Tm, Lu, Zr, Y [64W1]; R=Ce, Sm, Gd, Dy, Ho, Er, Tm [62W2]; R=Sm, Tb, Ho, Er, Tm, Lu, Y [64W2]; R=Nb, Sc, U, Zr, Ti, Sm, Gd, Er, Lu, Y [64N1]; R=Ce, Sm, Gd, Tb, Dy, Ho, Er, Y, Zr [68B4]; R=Dy, Ho [73B13]; R=Tb, Dy, Ho, Y [78B9]; R=Tb, Dy, Ho, Y [79F1]; R=Tb, Ho, Er [73T1]; R=Ce, Er, Y [78G5]; R=Ce [74A3, 77V1, 85D11]; R=Pr [79M13, 80M4, 80M5, 80S11, 81M9, 81M10, 81S11]; R=Nd [79M13, 80M4, 80M5, 81M9, 81M10, 81S11]; R=Sm [73A5, 73B4, 73V1, 74V1, 81S11]; R=Gd [74A3, 74B1, 75V3, 79M15, 81G2, 82B7]; R=Tb [74B1]; R=Dy [74S2, 76S8, 80J4, 80R1, 82B1]; R=Ho [74B1, 74S2, 80R1]; R=Er [77G14, 79R1]; R=Tm [64W6]; R=Yb [77M8, 79M12, 79M13, 80M4, 80M5, 81M9, 81M10]; R=Lu [74A3, 80B18, 85D11]; R=Y [61W1, 74M9, 76S8, 77G14, 82N4]; R=Sc [76S2, 80S14, 81G16, 81N2, 82S23]; R=Zr [64W6, 79R1]; R=U, Pu, Np [70B5]

$R(Co^{57}Fe)_2$ [77A8]; R=Pr [77D10]; R=Nd [76A8]; R=Gd [76A7]; R=Tb [77D10]; R=Dy [77D10]; R=Ho [76A8, 78A7]; R=Er [77D10]; R=Tm [82G14]

$R(Ni^{17}Fe)_2$ R=Gd, Tb, Dy, Ho, Er [77A7]

RFe_2H_x [84D4]; R=Ce [77V1, 85D11]; R=Gd [76B21, 82N2]; R=Tb [85A4]; R=Dy [79D10, 79V3]; R=Er [79D10, 79V4, 81V4, 85A4]; R=Tm [82N2]; R=Lu [80B18, 85D11]; R=Y [76B21, 78B22]; R=Sc [80S14, 81N2]

$R(Co^{57}Fe)_2H_x$ R=Ho, Y [83B11]

$(R'R'')M_2$ (CeY)Fe_2 [80D1]; (PrSm)Fe_2 [82S15, 83S12, 84S9]; (NdSm)Fe_2 [84S9]; (SmDy)Fe_2 [81B2]; (SmHo)Fe_2 [81B2]; (GdY)Fe_2 [76M17, 79B13]; (GdY)$(FeAl)_2$ [85B5]; (TbDy)Fe_2 [73A6, 77A10, 81S4]; (TbHo)Fe_2 [72A1, 73A6, 75D9, 81S4]; (TbY)Fe_2 [73D2, 73D3, 73M13, 75P9]; (TbDyEr)Fe_2 [85K4]; (DyEr)Fe_2 [73A6, 81S4]; (HoEr)Fe_2 [73A6, 75A8, 76R2, 81S4]; (HoTm)Fe_2 [73A6, 81S4]; (HoY)Fe_2 [61W1]; (HoY)$(FeCo)_2$ [80H1]; (ErY)Fe_2 [73D2, 73D3, 73M13]; (ZrHf)Fe_2 [61W1, 82A7]; (HfTa)Fe_2 [83N7]; (ScTi)Fe_2 [84N2, 85N3]; (ZrTi)Fe_2 [61W1]; (DyY)$(Co^{57}Fe)_2$ [87L8]

$R(M'M'')_2$ R(FeMn)$_2$, R=Gd, Tb, Dy, Ho, Er [75W1]; R=Gd [76I3]; R=Tb [76I3, 86I2]; R=Dy [76I3]; R=Ho [76I2]; R=Er [76I2, 86I1]; R=Y [80S4, 80V1]; R=Zr [83R3]; R(FeCo)$_2$, R=Gd, Dy, Ho, Er, Y, Zr [75W1]; Ce(FeCo)$_2$ [75L2, 88P2, 88P3]; Gd(FeCo)$_2$ [79M16]; Tb(FeCo)$_2$ [79F2]; Ho(FeCo)$_2$ [73G8, 74V2]; Tm(FeCo)$_2$ [76W3]; Y(FeCo)$_2$ [73G8, 77C6, 77L4, 77O13, 78C6, 79C7, 79M16, 80H1, 80S16]; Gd(FeNi)$_2$ [77B11]; Dy(FeNi)$_2$ [74B11, 75B10, 77C8, 78B12]; Ho(FeNi)$_2$ [75B10, 78B12]; R(FeM)$_2$, R=Y, Zr, M=Al, Ni [77M12]; R(FeAl)$_2$, R=Sc, Y, R [73D8, 75D10]; R(FeAl)$_2$, R=Sc, Y, Lu [75D11]; R(FeM)$_2$, M=Co, Al, Rh [78S8]; Gd(FeAl)$_2$ [80A6, 82V1]; Tb(FeAl)$_2$ [76P6]; Dy(FeAl)$_2$ [73G6, 74M1]; Y(FeAl)$_2$ [77V4, 78B4, 80S15, 82H5, 84R3, 86R6, 87R6, 88S5]; Ho(FeAl)$_2$ [85S21]; Zr(FeAl)$_2$ [82H5, 83R3]; Y(FeRu)$_2$ [87A8]; R(FeRh)$_2$, R=Gd, Dy, Ho, Y [82H12]; R=Tb [79S9]; Y(FeRh)$_2$ [83H4]; Y(FeIr)$_2$ [79V2, 86S21]

$R(M'M'')_2H_x$	$Zr(MnFe)_2H_x$ [83 R 3, 86 W 2]; $Ce(FeCo)_2H_x$ [88 W 4]; $Zr(FeAl)_2H_x$ [83 R 3]; $Y(FeCo)_2H_x$ [83 F 9]; $RFeAlH_x$, R = Sm, Gd, Dy, Ho, Er, Tm, Y [87 W 4]
^{61}Ni	$Dy(FeNi)_2$ [77 C 8]
^{119}Sn	$TmFe_2$ [85 D 9]; GdMnSi [85 D 10]
^{155}Gd	$GdMn_2$ [77 T 6]; $GdFe_2$ [77 T 6]; $GdCo_2$ [77 T 6, 86 C 9]; $GdNi_2$ [77 T 6] $(GdY)Fe_2$ [83 R 8]; $(GdY)Co_2$ [77 A 6]; $Ho_{0.03}Ce_xGd_{0.97-x}Fe_2$ [83 P 17]; $(GdCe)Fe_2$ [83 R 8]
^{155}Eu	SmM_2, M = Fe, Co, Ni [77 Y 4]
^{161}Dy	$DyMn_2$ [66 N 1, 80 C 8, 83 G 14]; $DyFe_2$ [65 O 1, 66 N 1, 68 o 1, 74 B 7, 82 B 1, 80 C 8, 83 P 18, 84 P 16, 85 P 11]; $DyCo_2$ [66 N 1, 66 O 1, 70 K 2, 74 B 7, 80 C 8]; $DyNi_2$ [66 N 1, 66 O 1, 70 K 2, 74 B 7, 80 C 8]; $DyMn_2H_x$ [80 C 8, 83 G 14]; $DyFe_2H_x$ [79 V 3, 80 C 8]; $DyCo_2H_x$ [80 C 8]; $DyNi_2H_x$ [80 C 8] $(DyY)Co_2$ [87 L 8]; (DyHo)Ni_2 [78 B 7]; $Dy(FeAl)_2$ [74 M 1, 82 B 2, 82 B 5]
^{166}Er	$ErCo_2$ [69 P 2]; $ErNi_2$ [69 P 2]; $ErMn_2H_x$ [80 V 4]; $ErFe_2H_x$ [79 V 4]; $Er(CoNi)_2$ [69 P 2, 71 Z 2]
^{169}Tm	$TmFe_2$ [64 C 1, 80 D 2, 82 B 9, 85 G 19]; $TmCo_2$ [80 D 2, 82 G 14, 85 G 19]; $TmNi_2$ [80 D 2, 85 G 19]; $TmFe_2H_x$ [82 N 2]
^{170}Yb	$YbFe_2$ [80 H 6]; $YbNi_2$ [73 N 7] $TmFe_2$ [74 H 7]; (TmHo)Fe_2 [75 Y 3]

For hyperfine field calculations in RFe_2, YMn_2 [87 A 12(T)]
For nuclear γ-resonance on ^{61}Ni, ^{155}Gd, and ^{161}Dy in RM_2 compounds see also Tables 60b, 60a, and 59.

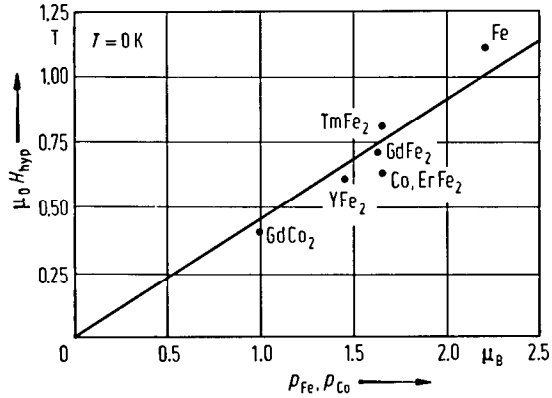

Fig. 186. Values of muon magnetic hyperfine fields extrapolated to $T = 0$, as function of the magnetic moment of transition metal atoms [86 B 6]. This shows that the main contribution to the hyperfine field at the muon site in RM_2 compounds comes from the 3d electrons of the transition metal partner.

For μSR studies see also
$GdFe_2$, YFe_2 [81 G 9]; $GdFe_2$, $ErFe_2$, $TmFe_2$, $GdCo_2$ [86 B 6]

For perturbed angular correlations studies see
^{44}Sc in $GdFe_2$ [75 C 5]
^{156}Gd in $ZrFe_2$ [80 Y 3]; $TbCo_2$, $TbFe_2$ [87 S 14, 87 S 15]
^{181}Ta in YFe_2 [83 A 2, 85 B 7, 88 S 4]; $LuFe_2$ [88 S 4]; $ZrFe_2$ [88 S 4]
(YHf)Fe_2 [84 A 6, 87 B 15, 88 B 4]; (ZrHf)Fe_2 [88 B 4]

NMR

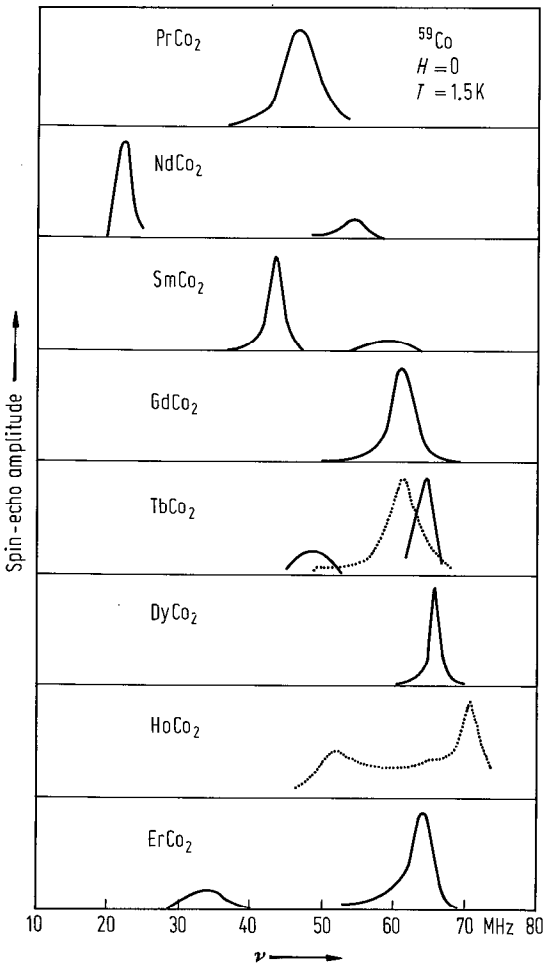

Fig. 187. Zero-field spin echo of ^{59}Co in RCo_2 compounds observed at 1.5 K. Solid lines indicate the spectra of ^{59}Co nuclei in magnetic domains and dotted lines those attributable to the nuclei in domain walls [81 H 4]. For the RCo_2 compounds with the easy direction of magnetization parallel to the [011] or [111] directions, the ^{59}Co hyperfine fields at two magnetically inequivalent Co sites are found to be antiparallel, revealing a large anisotropy in the ^{59}Co hyperfine field (see Table 48).

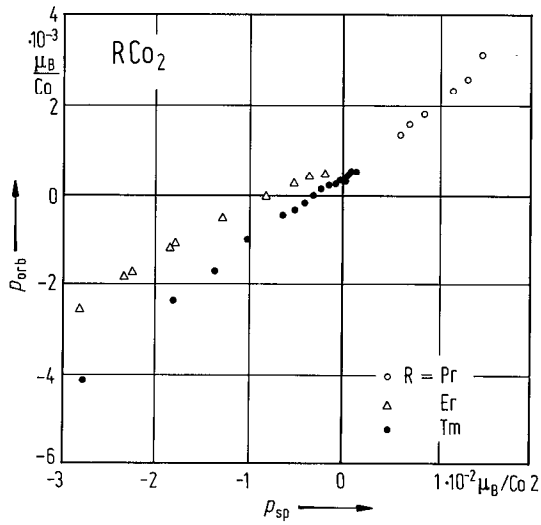

Fig. 188. Relation between spin and orbital magnetic moment of Co in the paramagnetic phase of RCo_2 (R = Pr, Er, Tm) compounds [82 H 8]. The positive direction is chosen to be parallel to the external field. The peculiar behaviour of the Knight shift which does not depend linearly on the magnetic susceptibility, is attributed to a change in fraction of the orbital magnetic moment induced by a resultant field, $H + H_{so}$, the sum of the external field, H, and of the effective field arising from the spin-orbit coupling, H_{so}.

Table 48. Spin and orbital Co magnetic moments (μ_B/Co) of RCo_2 compounds [81 H 4].

	p_{sp}	p_{orb}^{izo}	p_{orb}^{ax}
$PrCo_2$	0.37	0.13	–
$NdCo_2$	0.50	0.10	0.12
$SmCo_2$	0.46	0.04	0.12
$GdCo_2$	0.99	0.03	–
$TbCo_2$	1.04	0.10	0.11
$DyCo_2$	0.95	0.05	–
$HoCo_2$	0.76	0.04	0.07
$ErCo_2$	0.90	0.10	0.09
$TmCo_2$	0.41	0.07	0.02

Table 49. Magnetic hyperfine fields and estimated magnetic moments of Mn atom in RMn_2 compounds [81 S 10]. The nuclear g-factor of ^{55}Mn was taken 1.05 MHz/kOe.

	H_{hyp}(^{55}Mn) kOe	p_{Mn} μ_B
$GdMn_2$	130(3)	1.5
$TbMn_2$	104(2)	1.2
$DyMn_2$	70(1)	0.9
$HoMn_2$	24(1)	0.4
$ErMn_2$	19.0(5)	
$TmMn_2$	12.4(5)	

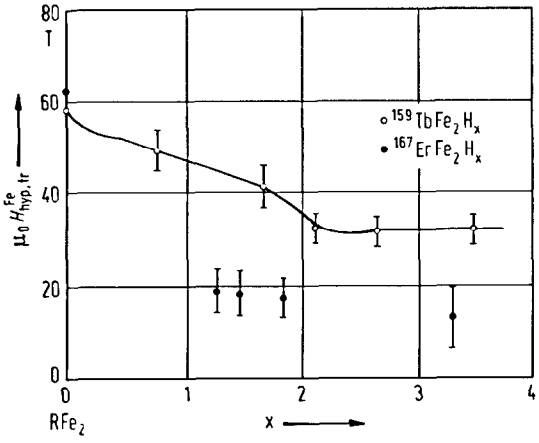

Fig. 189. Magnetic hyperfine field transferred from Fe to the rare-earth nuclei, $H^{Fe}_{hyp,tr}$, measured by zero-field NMR on ^{167}Er and ^{159}Tb in some RFe_2H_x compounds at low temperatures as function of x [85 B 4, 85 D 4]. The transferred hyperfine field values decrease as soon as the volume of the cell expands. This effect is due to the lowering of the R–Fe interaction as the Fe–R distance increases and it arises as soon as the R_2M_2 sites begin to be occupied. The values of the R magnetic moments, as deduced from NMR experiments, are independent of the concentration in Tb compounds, and decrease suddenly for $x > 3$ in Er compounds.

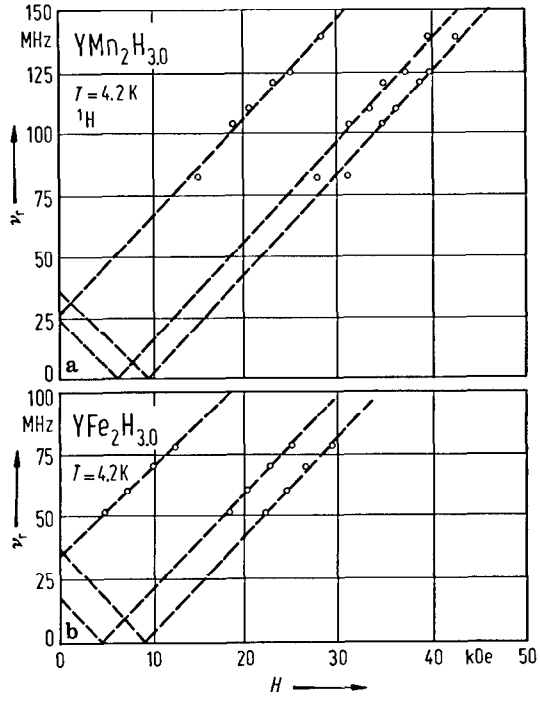

Fig. 190. Magnetic field dependence of the ^1H resonance frequency at 4.2 K of (a) $YMn_2H_{3.0}$ and (b) $YFe_2H_{3.0}$. Three dotted lines are drawn with slopes of $+\gamma$ and $-\gamma$, respectively, where γ is the gyromagnetic ratio of ^1H [87 F 8]. The ^1H hyperfine fields corresponding to these NMR signals can be analysed in terms of the magnetic dipole interaction between H nuclei and the localized magnetic moments of the Mn (or Fe) atoms surrounding the H atoms.

Table 50. Magnetic hyperfine fields (kOe) at ^{59}Co in $GdCo_2H_x$ hydrides [87 F 7].

	$GdCo_2$	$GdCo_2H_{2.2}$	$GdCo_2H_{2.6}$	$GdCo_2H_{3.0}$
$H_{hyp}(^{59}Co)$	61.4	50.3	49.8	48.5

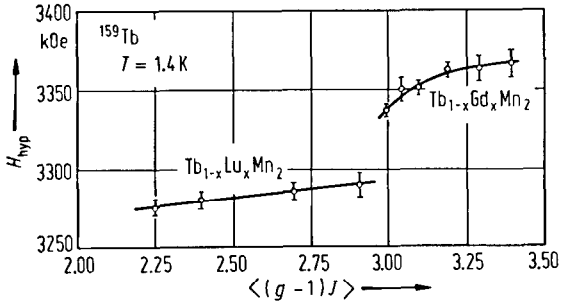

Fig. 191. Magnetic hyperfine field at ^{159}Tb in $Tb_{1-x}Gd_xMn_2$ and $Tb_{1-x}Lu_xMn_2$ at 1.4 K as a function of the mean rare-earth spin $\langle(g-1)J\rangle$. The solid lines are drawn as guide to the eyes [85 S 14]. From the above data, the positive hyperfine field transferred from the neighbouring rare-earth spins to the Tb site is about 20 kOe per rare-earth spin.

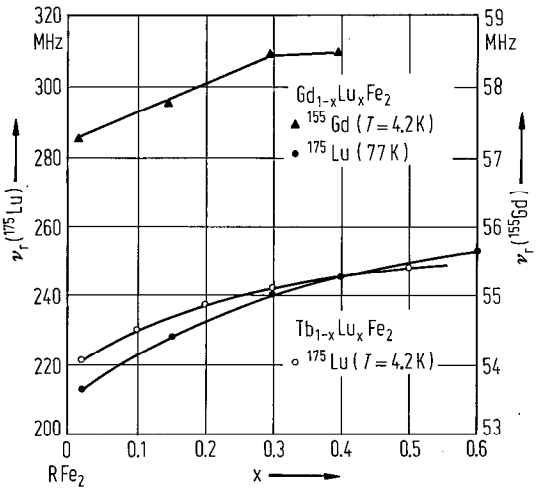

Fig. 192. Resonance frequencies of ^{155}Gd and ^{175}Lu in $Gd_{1-x}Lu_xFe_2$, and ^{175}Lu in $Tb_{1-x}Lu_xFe_2$ as function of Lu concentration [87 S 10]. The magnetic hyperfine field increases by increasing the Lu content.

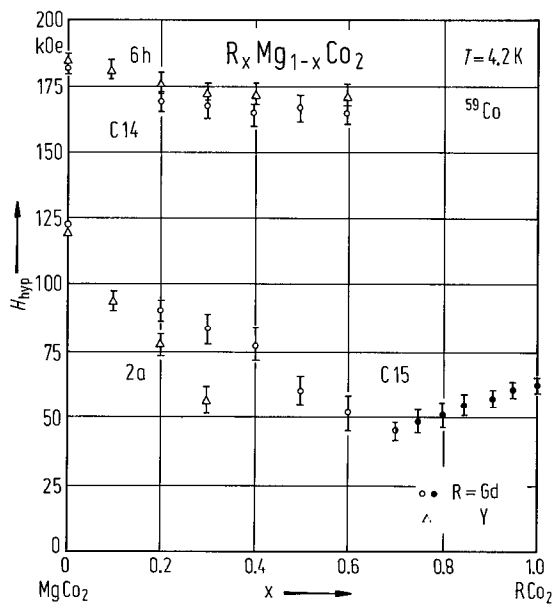

Fig. 194. Composition dependence of the ^{59}Co magnetic hyperfine fields at 4.2 K in $(R_xMg_{1-x})Co_2$ (R = Y, Gd) compounds for $0 \leqq x \leqq 1$ [87 I 2]. The hyperfine field at the 2a site decreases rapidly with increasing R concentration, while that at the 6h site is not dependent on R concentration. This means that the number of nearest neighbours Gd atoms at 2a site is larger than that of the 6h site.

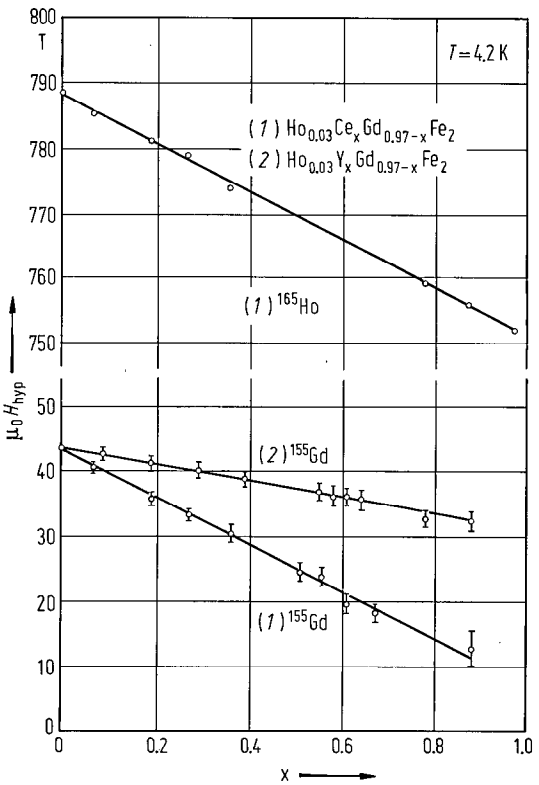

Fig. 193. Composition dependence of the total magnetic hyperfine field determined by Mössbauer effect and NMR at ^{155}Gd and ^{165}Ho in (*1*) $Ho_{0.03}Ce_xGd_{0.97-x}Fe_2$ and (*2*) $Ho_{0.03}Y_xGd_{0.97-x}Fe_2$ at 4.2 K [83 P 17]. A linear decrease with x of the hyperfine field is observed, the slope being three times greater than that found for ^{155}Gd in Ho(YGd)Fe_2 compounds. This is attributed to the influence of the increased conduction electron density when R^{3+} ions are replaced by Ce^{4+}.

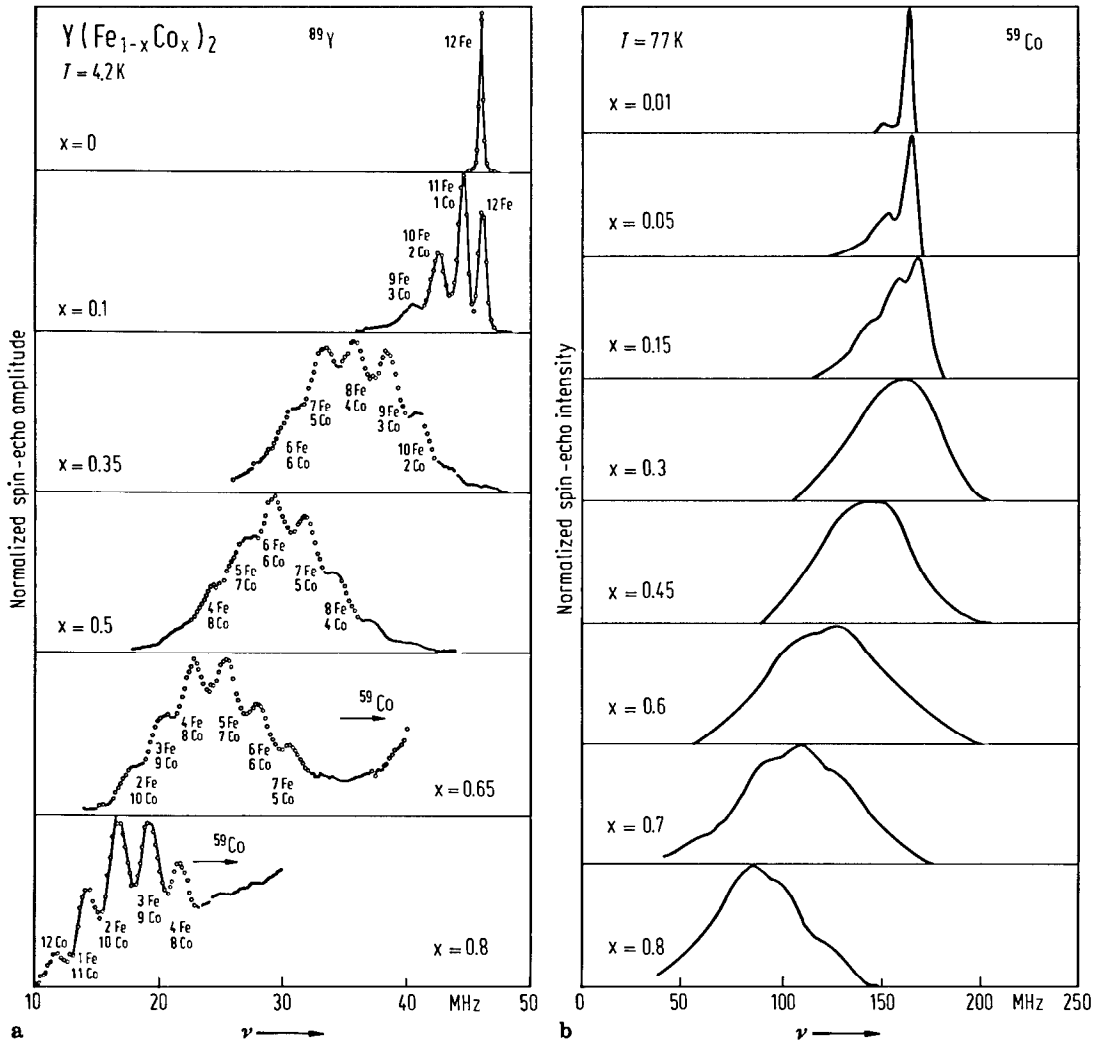

Fig. 195. (a) NMR spin-echo spectra of the ^{89}Y sites in $Y(Fe_{1-x}Co_x)_2$ ($0 \leqq x \leqq 0.8$) compounds at 4.2 K in zero external magnetic field [76 O 9]. Starting with the line at 46 MHz in pure YFe_2 (representing the situation with 12Fe neighbours atoms) and counting out the satellites, the different (Fe, Co) configurations have been assigned to these satellites as indicated. (b) Spin-echo spectra of ^{59}Co in $Y(Fe_{1-x}Co_x)_2$ at 77 K in zero external magnetic field [80 Y 1]. The substitution of Co for Fe gives rise to a developed satellite structure in the low Co concentration range.

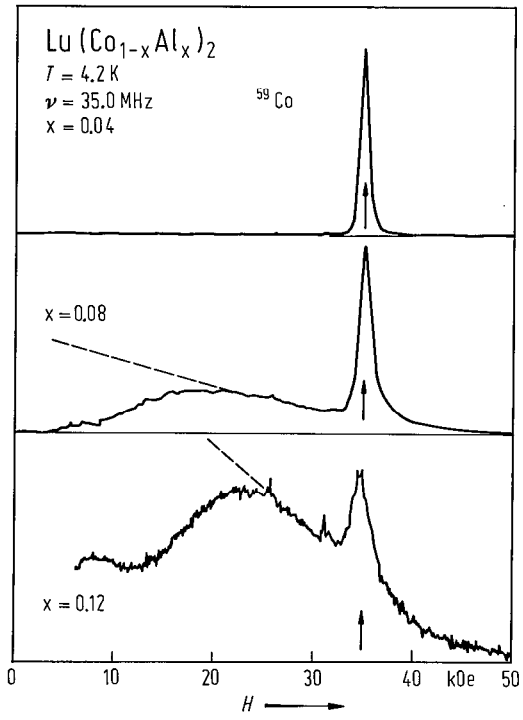

Fig. 196. Spin-echo spectra at 4.2 K and a fixed frequency of 35.0 MHz for $Lu(Co_{1-x}Al_x)_2$ compounds [87 S 13]. The arrows indicate the magnetic field corresponding to the zero Knight shift for ^{59}Co. In the sample with x = 0.04, only a sharp resonance line with a Knight shift of +1.4% was observed, corresponding to the majority of paramagnetic Co atoms in sample. In the ferromagnetic samples with x = 0.08 and 0.12, quite broad signals appeared at the lower-field side of sharp lines. These broad signals were characteristic of ferromagnetic samples. Their resonance fields correspond to large magnetic hyperfine fields and their intensities showed an enhancement effect due to magnetic domains, at low external fields. Thus, the spectra show that nonmagnetic and magnetic Co atoms coexist in the samples with x = 0.08 and 0.12. The relative intensity of the paramagnetic signal to the ferromagnetic one was greatly reduced for x = 0.12 compared with x = 0.08.

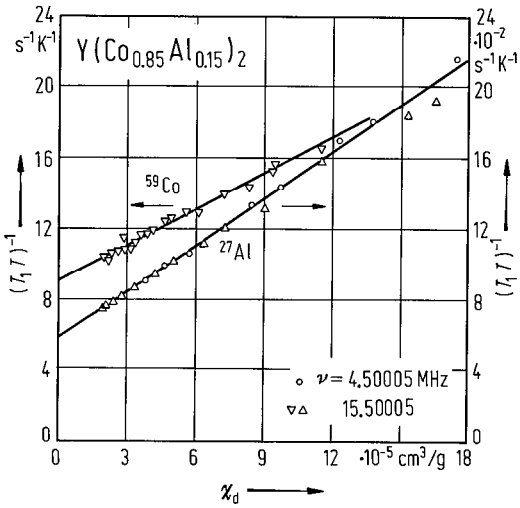

Fig. 197. Nuclear spin-lattice relaxation rates, $1/T_1$, of ^{59}Co and ^{27}Al nuclei in $Y(Co_{1-x}Al_x)_2$, showing a linear relation between $(T_1T)^{-1}$ and the 3d-spin magnetic susceptibility, χ_d, with temperature T as an implicit parameter [84 Y 8, 87 Y 12]. The relation $(T_1T)^{-1} \propto \chi_d$ holds in good agreement with self-consistent renormalization theory of spin fluctuations in weakly or nearly ferromagnetic metals.

For NMR studies see also:

^1H YMn_2H_x [87 F 8]; YFe_2H_x [87 F 8]
$Y(MnM)_2H_x$, M = Co, Al, Ni [88 F 3]; $Zr(MnFe)_2H_x$ [83 R 3]; $Zr(FeAl)_2H_x$ [83 R 3]

^{27}Al $Y(CoAl)_2$ [87 Y 11, 87 Y 12]; $Y(FeAl)_2$ [76 O 9, 85 I 1]; $Gd(CoAl)_2$ [87 I 1]

^{45}Sc $ScCo_2$ [84 I 8]; $(YSc)Mn_2$ [87 Y 10]; $Sc(FeCo)_2$ [77 O 12]; $Sc(CoNi)_2$ [66 B 1]

^{55}Mn RMn_2 [81 M 3, 81 N 1, 88 S 1]; R = Gd, Tb, Dy, Ho, Er, Tm [81 S 10]; R = Pr, Nd, Sm [84 Y 6]; R = Gd, Tb, Dy, Ho, Er, Tm [86 Y 6]; R = Sm, Gd, Y [83 N 3]; R = Dy, Ho [85 S 13]; R = Er [75 B 2]; R = Tm [75 B 2]; R = Y [83 Y 7, 88 N 1]
$(GdY)Mn_2$ [85 S 13]; $(GdEr)Mn_2$ [85 S 13]; $(TbLu)Mn_2$ [85 S 13]; $(YLa)Mn_2$ [88 N 1]; $(YSc)Mn_2$ [87 Y 10, 88 N 1]
$Gd(FeMn)_2$ [87 N 1]; $Zr(FeMn)_2$ [81 Y 1]; $Y(MnM)_2$, M = Fe, Co [86 Y 7]; $Y(MnAl)_2$ [88 S 1]; $Y(MnM)_2H_x$, M = Co, Ni, Al [88 F 3]; $Gd(MnCo)_2$ [87 I 1]

^{57}Fe RFe_2, R = Gd, Tb, Dy, Ho, Er, Tm, Lu, Y [81 V 1]; R = Y [81 B 5, 81 V 2, 81 V 3, 86 D 4]; R = Zr [86 D 4]; R = Ho, Y [87 D 11]; $(GdY)Fe_2$ [75 N 10]; $Gd(FeMn)_2$ [86 N 1]

^{59}Co RCo_2, R = Pr, Er, Tm, Y [82 H 9]; R = Nd, Gd, Tb, Ho [81 R 1]; R = Pr, Nd, Sm, Gd, Tb, Dy, Ho, Er, Tm [81 H 4, 82 H 8, 82 H 10]; R = Nd, Gd, Tb, Ho [81 R 1]; R = Ce, Pr, Nd, Er, Tm, Lu, Y, Zr, U [67 B 2]; R = Gd [71 B 10, 76 C 1, 85 B 2, 86 K 2]; R = Ho [86 G 8, 87 G 10]; R = Lu [87 Y 9]; R = Y [84 Y 8]; R = Sc [84 I 8]; $GdCo_2H_x$ [87 F 7]; $(PrY)Co_2$ [82 H 6]; $(GdDy)Co_2$ [69 T 2]; $(GdY)Co_2$ [69 T 2, 78 Y 4, 79 H 7]; $(GdY)(FeCo)_2$ [82 I 2]; $(TbDy)Co_2$ [82 H 7]; $(HoY)Co_2$ [82 H 6]; $(DyY)Co_2$ [84 Y 7]; $(MgR)Co_2$, R = Gd, Y [87 I 2]; $R(FeCo)_2$, R = Y, Zr, Sc [77 O 12]; $Gd(FeCo)_2$ [74 B 5, 76 B 8]; $Y(FeCo)_2$ [76 O 9, 80 Y 1]; $Zr(FeCo)_2$ [80 Y 1]; $Gd(CoNi)_2$ [69 T 2, 70 C 2, 80 T 3]; $Gd(CoAl)_2$ [83 G 15], $Lu(CoAl)_2$ [87 S 13, 88 S 3]; $Y(CoAl)_2$ [87 Y 11, 87 Y 12, 88 S 3, 88 Y 3]; $Sc(CoAl)_2$ [88 S 3]; $Gd(CoM)_2$, M = Mn, Fe, Ni, Al [87 I 1]

^{89}Y YFe_2 [73 O 9, 81 B 5, 81 V 3, 83 R 6*, 83 V 2, 85 R 9, 85 V 2, 86 D 4]; YFe_2H_x [86 V 1]
$(RY)Fe_2$, R = Tb, Dy, Ho [86 A 4]; $(GdY)Fe_2$ [78 B 2, 85 V 1]; $Y(FeM)_2$, M = V, Mn, Co, Ni, Al [83 I 2]; M = Co, Al, Pt [76 O 9]; $Y(FeMn)_2$ [83 N 1, 89 N 1]; $Y(FeCo)_2$ [77 B 23, 77 O 12, 80 Y 1]; $Y(FeAl)_2$ [85 I 1]; see also Table 61

^{91}Zr $ZrFe_2$ [86 D 4]
$Zr(FeMn)_2$ [81 Y 1]; $Zr(FeCo)_2$ [77 O 12]

^{93}Nb $(ZrNb)Fe_2$ [84 Y 2, 84 Y 3, 87 Y 5]; $(NbMo)Fe_2$ [85 Y 2]

^{139}La $(Gd_{0.9}La_{0.1})Ni_2$ [77 D 7]

^{143}Nd $NdFe_2$ [81 M 10]

^{155}Gd, ^{157}Gd $GdFe_2$, $GdMn_2$ [67 G 1]
$(GdLu)Fe_2$ [87 S 10]; $(GdY)Fe_2$ [73 V 4]; $Gd(FeMn)_2$ [86 N 1]; $Gd(MCo)_2$, M = Mn, Fe, Ni, Al [87 I 1]

^{159}Tb $TbMn_2$ [82 S 14]; $TbFe_2$ [81 D 7, 83 S 8, 85 B 4, 85 D 3, 87 S 5]; $TbNi_2$ [88 S 2]; $TbFe_2$ [81 B 7]; $TbFe_2H_x$ [85 B 4]
$(TbGd)Mn_2$ [85 S 14]; $(TbLu)Mn_2$ [85 S 14]; $(TbLu)Fe_2$ [87 S 10]; $(TbY)Fe_2$ [83 S 23, 86 S 14]; $(TbY)Co_2$ [86 B 7, 86 B 8]; $(TbGd)Ni_2$ [87 S 6]
$Tb(FeCo)_2$ [86 S 14]

^{163}Dy $DyMn_2$ [82 S 14]; $DyFe_2$ [81 B 7, 81 D 7, 85 B 3]; $(DyR)Al_2$, R = Y, Gd [77 B 9]

^{165}Ho $HoFe_2$ [85 B 3]
$(HoGd)Fe_2$ [71 M 2]; $(Ho_{0.03}Gd_xY_{0.97-x})Fe_2$ [84 A 7]
$(Ho_{0.03}Ce_xGd_{0.97-x})Fe_2$ [83 P 17]; $Ho_{0.03}Gd_{0.97}M_2$, M = Mn, Rh, Ir, Pt, Au [81 T 3]
$(Ho_{0.01}Gd_{0.99})M_2$ [78 T 2]; $(HoGd)Co_2$ [71 M 2]
$(Ho_{0.03}Gd_xY_{0.97-x})Co_2$ [75 A 3, 77 A 6]; $Ho_{0.01}Gd_xY_{1-x}Ni_2$ [79 T 1]; $Ho(CoNi)_2$ [82 T 3, 82 T 4]

^{167}Er $ErMn_2$ [82 S 14]; $ErFe_2$ [81 B 6, 81 B 7, 81 D 7, 85 B 3]; $ErFe_2H_x$ [85 D 4]; $Er_{0.9}La_{0.1}Fe_2$ [81 B 6]

^{169}Tm $TmFe_2$ [81 B 7]

^{175}Lu $(TbLu)Fe_2$ [87 S 10]; $(GdLu)Fe_2$ [87 S 10]

Anisotropy and magnetostriction

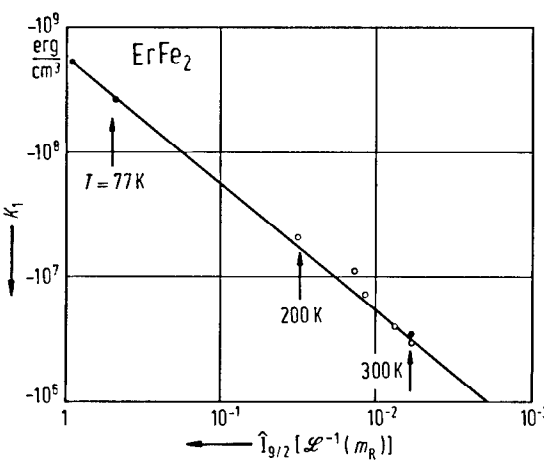

Fig. 198. Temperature dependence of the anisotropy constant K_1 of $ErFe_2$ plotted as function of the ratio of the hyperbolic Bessel function of order 9/2 to the hyperbolic Bessel function of the order 1/2. A linear relation is obtained, $K_1 = -5.4 \cdot 10^8 \hat{I}_{9/2}[\mathscr{L}^{-1}(m_R)]$ erg cm^{-3}, predicted by the single-ion theory [74 C 2]. $\mathscr{L}$ is the Langevin function and m_R is the reduced magnetization of Er sublattice. Solid circles: high-field magnetization data, open circles: magnetic torque data.

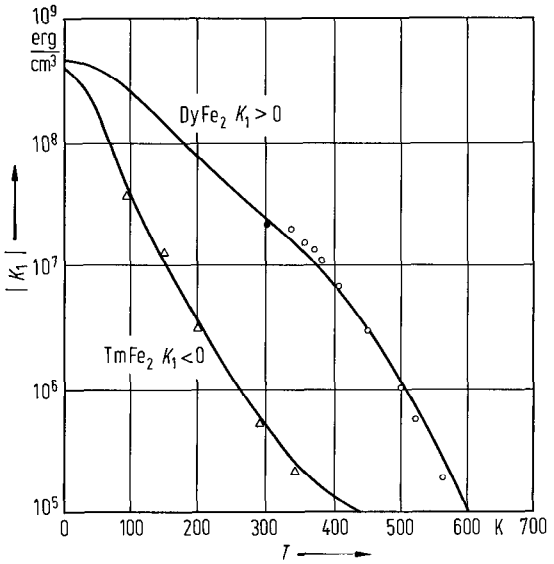

Fig. 199. Temperature dependence of the anisotropy constants K_1 of $DyFe_2$ and $TmFe_2$ [78 C 5]. The solid curves are the values calculated using single-ion theory.

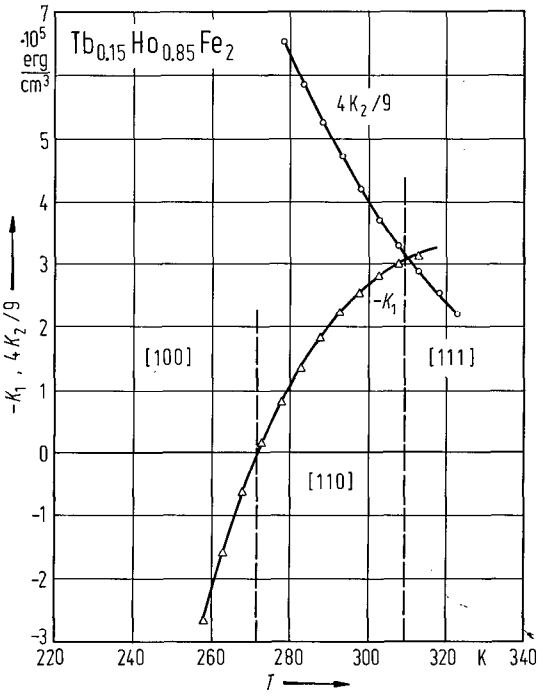

Fig. 200. Temperature dependence of K_1 and K_2 for a $Tb_{0.15}Ho_{0.85}Fe_2$ single crystal in the temperature range 238···325 K [75 W 3]. The easy axes of magnetization are indicated.

Table 51. Anisotropy constants (erg/cm³) of some RFe_2 compounds, K_1 and K_2 at 300 K, and intrinsic contributions, K_1^{int} at 300 and 0 K [80 c 1].

	K_1 10^{-4}	K_2 10^{-4}	K_1 [1] 10^{-4}	K_1^{int}(300 K) 10^{-4}	K_1^{int}(0 K) [2] 10^{-8}	Ref.
$SmFe_2$			− 970	−	−	
$TbFe_2$	−7600		−1330	−6300	−5.2	72 C 4, 75 C 3, 75 W 3
	−5800					
$DyFe_2$	2100		− 350	2450	4.7	72 C 4, 72 C 7
$HoFe_2$	580		− 7.5	590	2.7	75 W 3, 78 W 6, 79 A 1
	550					
$ErFe_2$	− 330		− 20	− 310	−5.4	73 C 6, 75 C 3
$TmFe_2$	− 53		− 9.7	− 43	−3.8	78 A 1
$Tb_{0.15}Ho_{1.85}Fe_2$	− 22	110				75 W 3

[1]) Calculated from $9c_{44}\lambda_{111}^2/2$ taking $c_{44} = 4.87 \cdot 10^{11}$ dyn cm^{-3} [77 R 2].
[2]) Extrapolated to 0 K using the single-ion theory.

For magnetic anisotropy and spin reorientation see also
RFe_2 [78 K 8, 79 L 2]; R = Tb, Dy, Ho, Er, Tm [72 C 7, 73 D 1]; R = Dy, Ho, Er [81 K 18]; R = Gd, Tb, Dy, Ho, Er, Tm, Lu [81 G 3]; R = Pr, Tb, Dy, Ho, Er, Tm, Yb [80 c 1]; R = Ce, Gd, Lu [74 A 3]; R = Ce [76 A 6]; R = Sm [73 V 1, 76 A 6]; R = Tb [75 C 3, 75 S 3, 78 C 5]; R = Dy [78 C 5]; R = Er [73 C 6, 75 C 3, 81 H 5]; R = Tm [78 A 1, 78 C 5]
$R(Co^{57}Fe)_2$ [77 A 8]; RCo_2 [76 A 7, 81 H 2, 82 H 13*]; R = Ho [78 D 2, 79 A 1*]

$(R'R'')M_2$, $(R'R'')Fe_2$ [81 C 5, 85 K 12]; $(PrSm)Fe_2$ [82 S 15, 84 S 9]; $(NdSm)Fe_2$ [84 S 9]; $(TbDy)Fe_2$ [73 A 6, 76 A 6, 78 C 5, 79 K 7, 80 W 3*, 81 H 2]; $(TbHo)Fe_2$ [72 A 1, 73 A 6, 73 R 5, 74 W 1, 75 D 9, 75 W 3, 76 A 6, 76 W 4, 78 K 8, 78 W 4, 78 W 5, 78 W 6(T), 80 K 12, 81 G 3, 81 K 12, 81 S 4], $(TbDyHo)Fe_2$ [77 W 2]; $(DyEr)Fe_2$ [73 A 6, 76 A 6]; $(HoEr)Fe_2$ [73 A 6, 75 A 8, 76 A 6, 76 R 2, 81 S 4]; $(HoTm)Fe_2$ [73 A 6, 81 S 4]

$R(M'M'')_2$ [81 K 4]; $Gd(MnNi)_2$ [82 S 22]; $Er((FeCo)_2$ [85 A 15]; $Sm(FeTi)_2$ [86 W 1]; $Tb(NiCu)_2$ [85 Y 12]

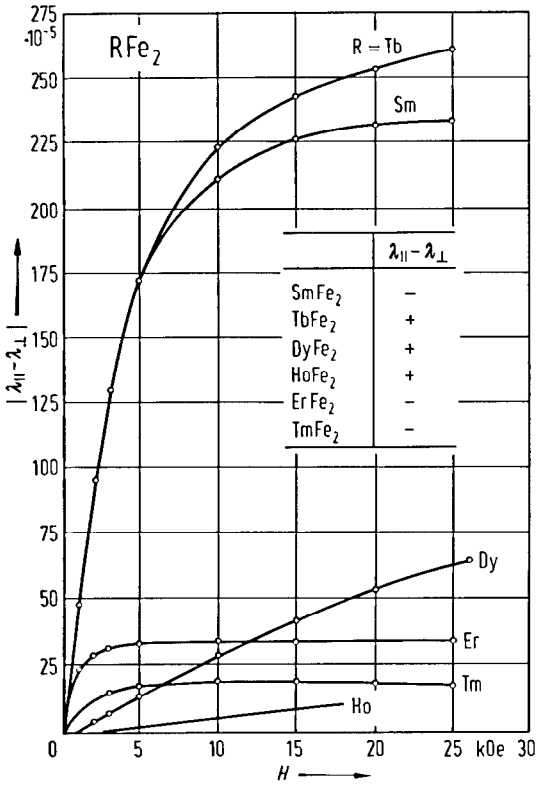

Fig. 201. Room temperature magnetostriction of polycrystalline RFe_2 compounds, $SmFe_2$, $TbFe_2$, $DyFe_2$, $ErFe_2$ and $TmFe_2$ [74 C 2] and $HoFe_2$ [74 K 17].

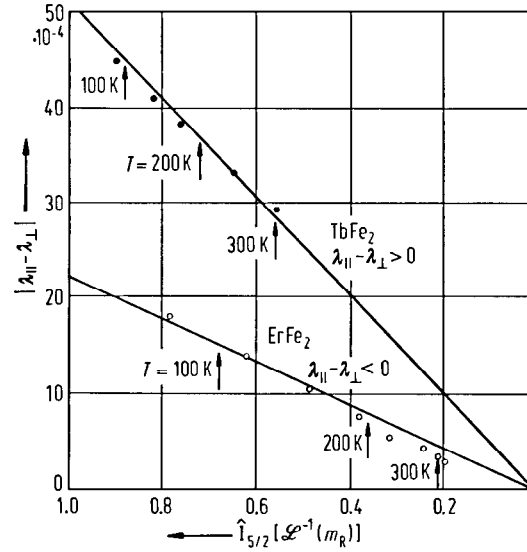

Fig. 202. Magnetostriction of $TbFe_2$ and $ErFe_2$ plotted against $\hat{I}_{5/2}[\mathcal{L}^{-1}(m_R)]$, the temperature dependence predicted by the one-ion model [72 C 4, 74 C 3, 80 c 1]. $\hat{I}_{5/2}$ is the normalized hyperbolic Bessel function, $\mathcal{L}^{-1}$ is the inverse Langevin function, and m_R is the reduced magnetization of the R sublattice.

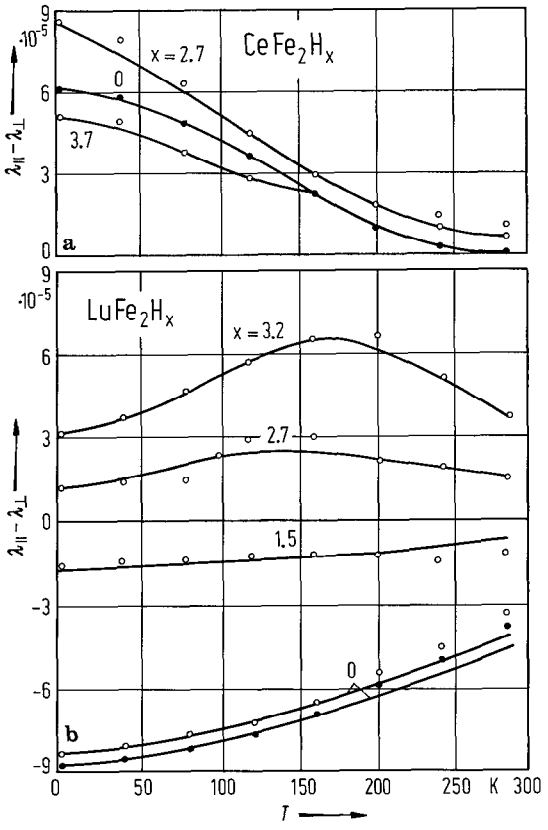

Fig. 203. Temperature dependence of the magnetostriction in (a) $CeFe_2H_x$, (b) $LuFe_2H_x$ hydrides. The upper of the two curves for x = 0 was obtained after dehydriding at 300 K the $LuFe_2H_{3.2}$ sample [85 D 11].

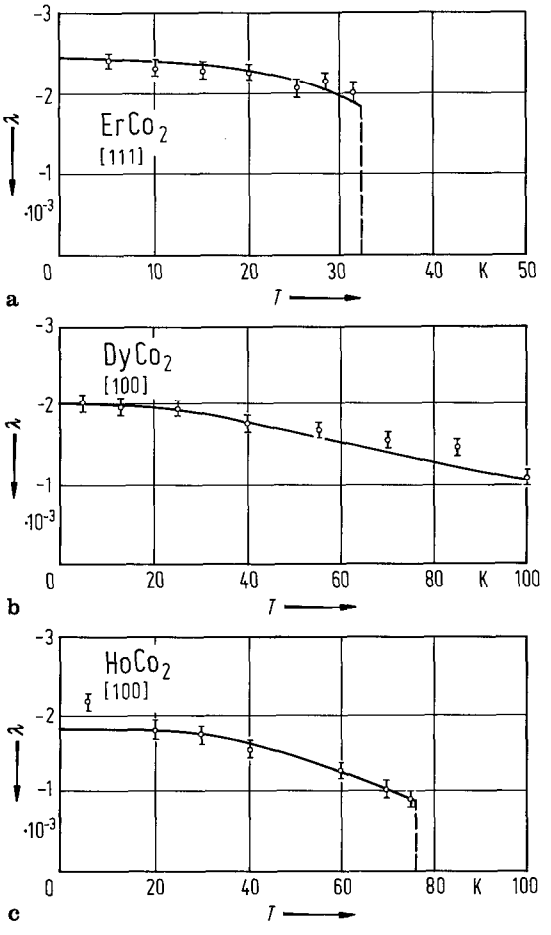

Fig. 204. Temperature dependence of the magnetostriction constants for (a) $ErCo_2$, (b) $DyCo_2$ and (c) $HoCo_2$. By solid lines are plotted the predictions of the one-ion model [81 M 6].

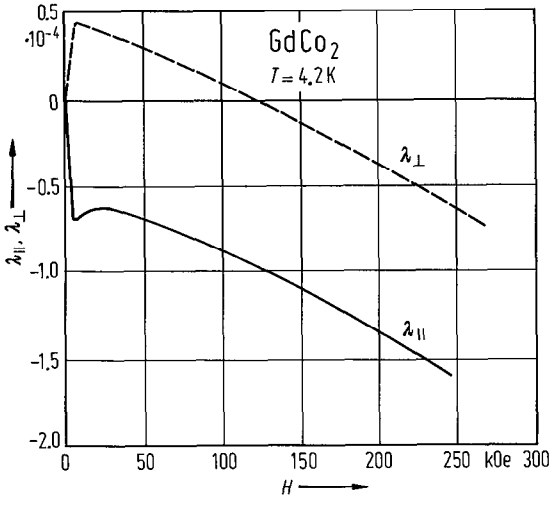

Fig. 205. Field dependence of the magnetostriction constants $\lambda_{\parallel}$ and $\lambda_{\perp}$ at 4.2 K in $GdCo_2$ compound [82 L 4, 83 B 5]. In high fields $-\partial\lambda_{\parallel}/\partial H = -\partial\lambda_{\perp}/\partial H$, which suggests that the magnetic moment of Co in this compound may be better described in the band model.

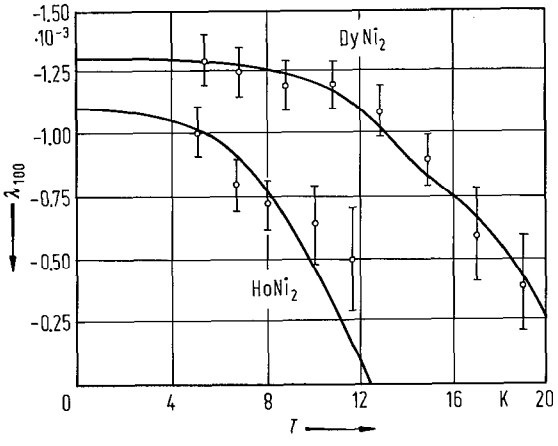

Fig. 206. Magnetostriction constants as function of temperature for $DyNi_2$ and $HoNi_2$ compounds. By solid lines are plotted the prediction of the one-ion model [81 M 5].

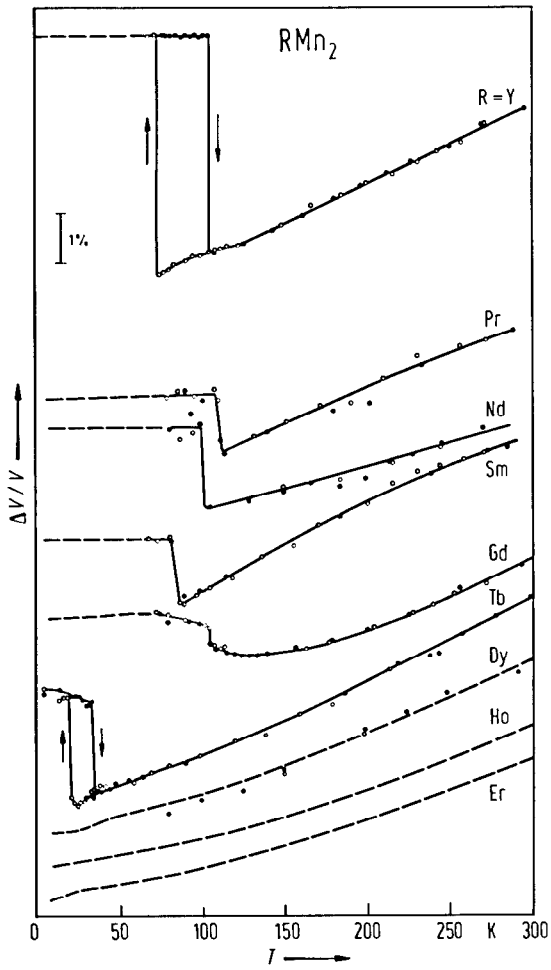

Fig. 207. Volume thermal expansion curves of RMn_2 compounds obtained by X-ray diffraction measurements (circles) and dilatometric measurements (dashed lines). Open and closed circles show the measurements with decreasing and increasing temperature, respectively. Solid lines are guides for the eyes [87 W 1]. Similarly to YMn_2, the RMn_2 (R = Pr, Nd, Sm, Gd and Tb) compounds show large volume changes at T_N. In these compounds large magnetic hyperfine fields of 100···150 kOe have been observed at Mn nuclei by NMR, which indicates the presence of large Mn magnetic moments [84 Y 6, 86 Y 6]. No distinct anomalies have been observed in thermal expansion curves of RMn_2 (R = Dy, Ho, Er), which suggests no or nearly zero Mn magnetic moments in these compounds. The absence of the Mn magnetic moment in $HoMn_2$ and $ErMn_2$ was also supported by small hyperfine fields of about 20 kOe at Mn nuclei, which are ascribed to the hyperfine fields transferred from R magnetic moments [84 Y 6, 86 Y 6].

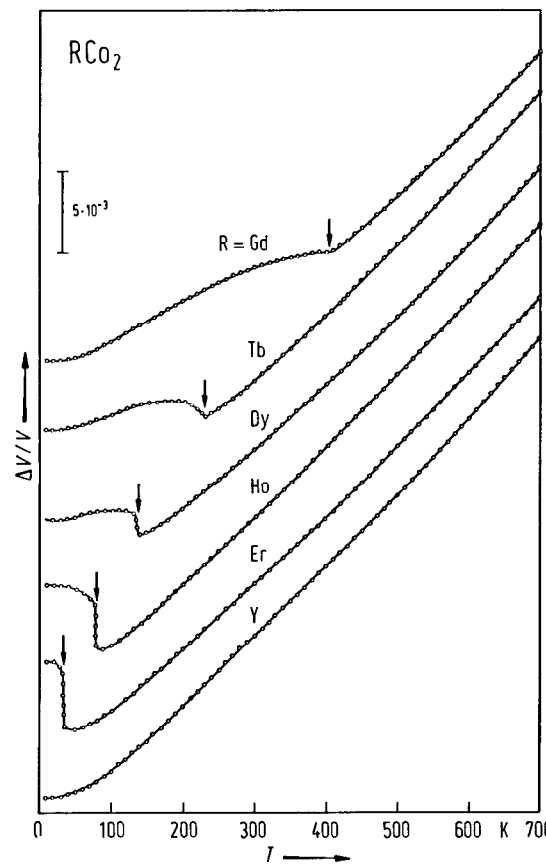

Fig. 208. Volume thermal expansion of RCo_2 compounds. The arrows indicate the Curie temperatures. A large thermal expansion anomaly is observed below the Curie temperatures for all the samples. Particularly, in the case of $DyCo_2$, $HoCo_2$ and $ErCo_2$, the volume change at the Curie temperature is almost discontinuous and the transition is considered to be of first order [76 M 15].

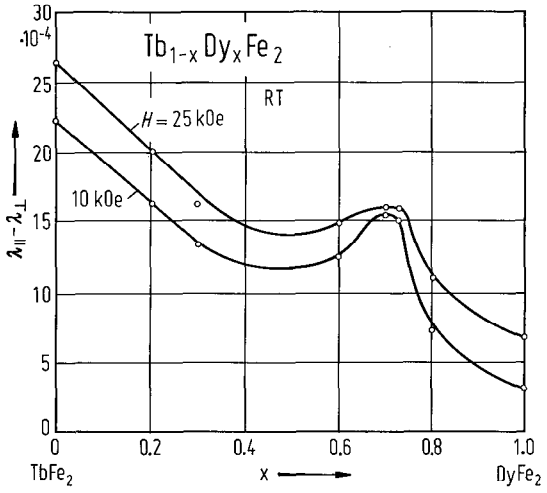

Fig. 209. Magnetostriction of $Tb_{1-x}Dy_xFe_2$ polycrystalline samples at room temperature [74 C 2] for external magnetic fields $H = 10$ kOe and $H = 25$ kOe. Near $x = 0.7$ the magnetostriction exhibits a peak, reflecting near zero magnetic anisotropy.

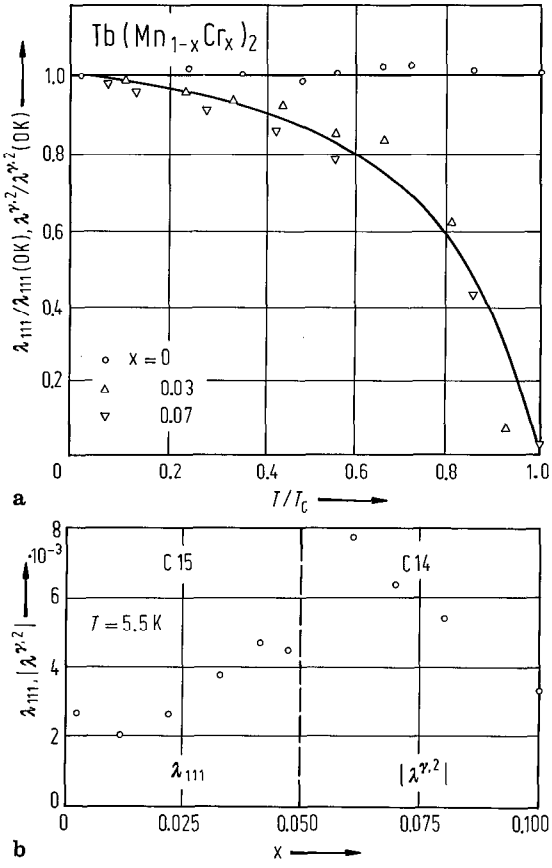

Fig. 211. (a) Reduced magnetostriction constants as function of reduced temperature for cubic phase, λ_{111}, and hexagonal phase, $\lambda^{\gamma,2}$ of $Tb(Mn_{1-x}Cr_x)_2$ compounds [85 G 2]. For a Cr content $x_c < 0.05$ the system crystallizes in a cubic lattice (C15-type) and for a greater Cr content in a C14 hexagonal structure. (b) Composition dependence of magnetostriction constants at 5.5 K.

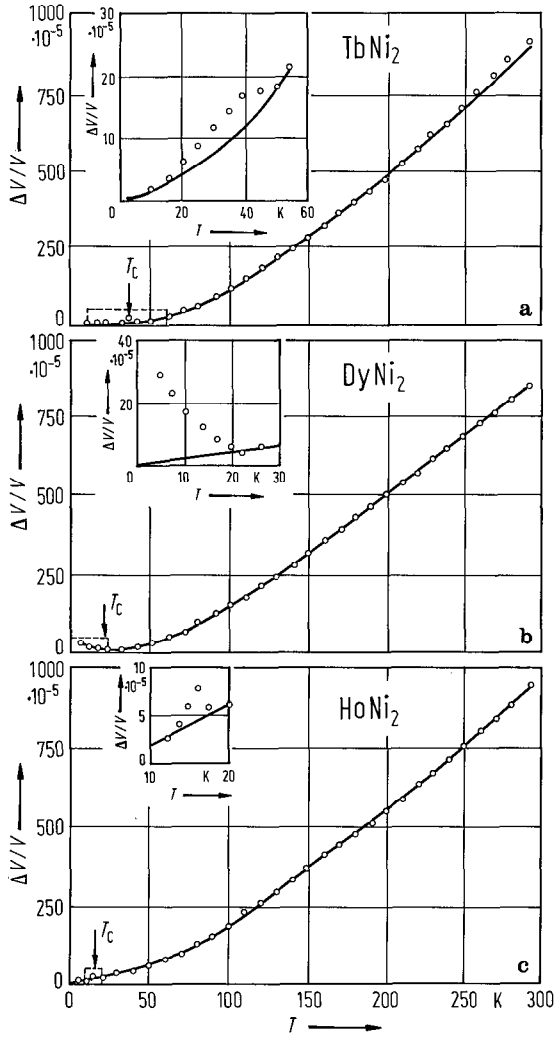

Fig. 210. Volume thermal expansion for (a) $TbNi_2$, (b) $DyNi_2$ and (c) $HoNi_2$. Circles: experimental data, solid lines: thermal expansion of nonmagnetic YNi_2 compound. In inserts the anomaly of the thermal expansion at T_C is shown [84 I 2].

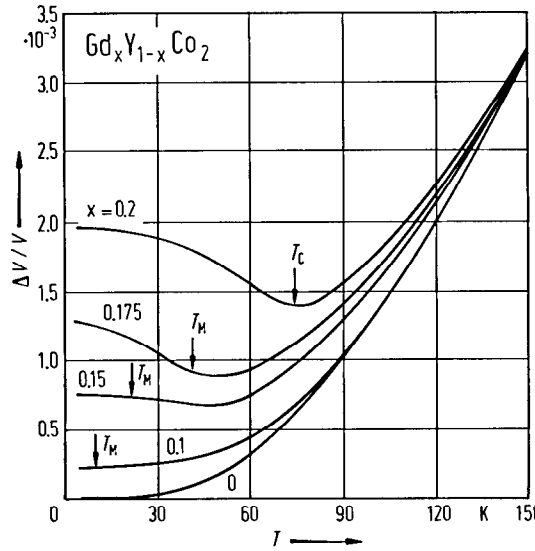

Fig. 212. Thermal expansion curves for $Gd_xY_{1-x}Co_2$ ($x \leqq 0.2$) compounds [84 M 5]. The spontaneous volume magnetostriction, $\omega_s(T)$, was evaluated as the difference between the observed curve and that of YCo_2. The $\omega_s(T)$ values change remarkably at T_C for $x = 0.2$. On the other hand for $x = 0.15$ and 0.1, $\omega_s(T)$ remains constant up to far above T_M and no remarkable change is observed at T_M. These data may be analysed considering a cluster model for volume magnetostriction.

For magnetostriction studies see also

RM_2 M = Fe, Co, Ni [77 C 9]

RMn_2 R = Gd [85 G 2]; R = Tb [80 M 2, 85 G 1]; R = Y [83 T 4(T)]

RFe_2 [76 C 3]; R = Tb, Dy, Er [76 C 4]; R = Ce, Sm, Tb, Dy, Ho, Er [76 A 6]; R = Sm, Tb, Dy, Ho, Er, Tm [77 B 3]; R = Pr, Sm, Tb, Dy, Ho, Er, Tm, Yb [78 C 11]; R = Ce, Sm, Gd, Tb, Dy, Ho, Er, Tm, Lu, Y [80 I 2]; R = Dy, Ho, Er [81 K 18]; R = Sm, Tb, Dy, Ho, Er, Tm [79 c 1]; R = Ce, Tb, Dy, Er [76 D 4]; R = Ce [79 M 9, 81 M 7]; R = Sm [74 C 2, 74 C 3, 81 N 3, 84 N 4], R = Tb [72 C 4, 72 C 5, 72 C 6, 74 C 2, 74 C 3, 75 C 3, 78 M 7, 79 N 5, 80 Z 1, 81 N 3, 83 N 9, 84 N 4, 85 C 6]; R = Dy [71 K 2, 72 C 4, 74 C 2, 78 M 7, 81 A 2]; R = Ho [71 K 2, 79 A 1*]; R = Er [71 K 2, 73 C 6, 74 C 2, 74 C 3, 74 N 9, 75 C 3, 81 A 2]; R = Tm [74 C 2, 74 C 3, 78 A 1]; R = Y [72 C 5]

RCo_2 [83 N 2]; R = Dy, Ho, Er [75 D 2]; R = Dy, Ho, Er, Y [81 M 6]; R = Gd, Tb, Dy, Ho, Er [76 M 15]; R = Dy, Ho, Er [78 P 2]; R = Tb, Dy, Er [84 A 8]; R = Gd, Tb, Dy, Ho, Er [78 S 10]; R = Gd [77 S 8, 82 L 4, 83 B 5]; R = Tb [79 G 5*, 79 P 3, 80 G 7, 80 M 2]; R = Ho [77 L 2]; R = Lu [85 M 3, 81 B 3(T)]; R = Y [83 B 5, 85 M 3]

RNi_2 [80 A 1, 85 D 7]; R = Dy, Ho, Er [81 M 5]; R = La, Ce, Pr, Nd, Sm, Gd, Tb, Dy, Ho, Er, Tm [83 I 1]; R = Pr, Nd, Sm, Tb, Dy, Ho, Er, Tm [84 I 1]; R = Gd [78 S 10]; R = Tb [80 M 2]

RM_2H_x $ErFe_2H_x$ [84 D 5]

$(R'R'')M_2$ $(RTb)Fe_2$ [77 B 8]; $(CePr)Fe_2$ [85 S 16]; $(PrSm)Fe_2$ [85 S 16]; $(PrY)Fe_2$ [85 S 16]; $(SmDy)Fe_2$ [82 A 1]; $(SmEr)Fe_2$ [84 T 1]; $(GdTb)Fe_2$ [76 C 4]; $(TbDy)Fe_2$ [74 C 2, 74 C 3, 75 S 2, 76 M 2, 77 A 1, 78 C 8, 78 C 9, 78 M 3, 79 K 7, 79 S 2, 81 N 3, 84 C 5, 84 N 4, 84 R 4, 85 C 6, 85 S 6, 86 J 4, 87 T 3, 88 C 1]; $(TbDyHo)Fe_2$ [79 S 2, 84 I 5]; $(TbHo)Fe_2$ [73 K 12, 74 K 17, 75 N 4, 76 T 1, 77 K 5]; $(TbY)Fe_2$ [75 B 3, 76 C 4]; $(HfTa)Fe_2$ [86 K 3]; $(ScTi)Fe_2$ [86 N 3]
$(GdY)Co_2$ [83 M 7, 83 M 8, 84 M 4, 84 M 5, 85 M 3]; $(TbDy)Co_2$ [84 A 8]; $(TbHo)Co_2$ [87 E 1]; $(DyEr)Co_2$ [84 A 8]

$R(M'M'')_2$ $Sm(FeCo)_2$ [81 L 4]; $Tb(FeCo)_2$ [75 B 3]; $Er(FeCo)_2$ [85 A 15]; $Y(FeCo)_2$ [83 M 7, 83 T 4(T)]; $Zr(FeCo)_2$ [80 M 12, 80 S 10, 83 T 4(T)]; $Ti(FeCo)_2$ [80 S 10]; $Dy(FeAl)_2$ [77 S 13]; $Tb(MCr)_2$, M = Mn, Fe, Co, Ni [85 G 2]; $Sm(FeV)_2$ [81 L 4]
$Gd(CoNi)_2$ [80 T 3]; $Tb(CoNi)_2$ [82 M 2]; $Gd(CoAl)_2$ [84 B 5]; $Tb(CoAl)_2$ [88 L 1]; $Dy(CoAl)_2$ [88 L 1]; $Y(CoAl)_2$ [88 W 1]

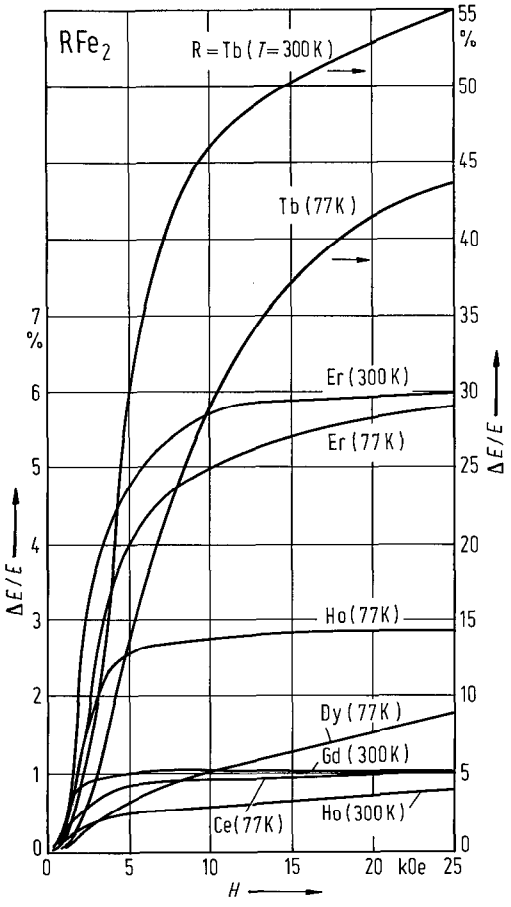

Fig. 213. Magnetic field dependence of the modulus change $\Delta E/E=(E_H-E_0)E_0^{-1}$ in RFe_2 compounds [74 K 16] where E_H and E_0 are the Young modulus in magnetized and unmagnetized samples, respectively. This is due to the variation of the magnetization direction in a magnetostrictive magnetic lattice. $\Delta E/E$ increases with the external magnetic field.

For elastic and magnetoelastic properties see also

RFe_2 [73 S 6(T), 78 C 11, 85 K 7]; R = Tb, Er, Y [73 C 5]; R = Ce, Sm, Tb, Dy, Ho, Er, Y [73 R 6]; R = Pr, Sm, Tb, Dy, Ho, Er, Tm, Yb [79 c 1]; R = Ce, Gd, Tb, Dy, Ho, Er, Y [74 K 16]; R = Sm [74 R 4, 81 N 3, 83 D 4, 84 D 6]; R = Tb [77 C 4, 78 C 5, 79 N 6, 80 K 4, 81 N 3, 84 D 6]; R = Dy [77 C 4, 78 C 5]; R = Tm [78 C 5]; R = Y [86 A 8]; R = Zr [86 A 8]

RCo_2 R = Pr, Nd, Tb, Dy, Ho, Er [76 L 2]; R = Pr, Nd, Gd, Tb, Dy, Ho, Er [76 L 3]; R = Pr, Nd, Sm, Gd, Tb, Dy, Ho, Er, Tm, Lu, Y [78 K 4, 79 K 4]; R = Gd [81 H 2]; R = Ho [82 B 16*]

$(R'R'')M_2$ $(CeTb)Fe_2$ [77 C 4]; $(PrTb)Fe_2$ [77 C 4]; $(SmDy)Fe_2$ [77 C 4, 78 B 6, 78 C 10, 78 S 4, 81 B 2]; $(SmHo)Fe_2$ [77 C 4, 78 B 6, 78 S 4, 81 B 2]; $(SmYb)Fe_2$ [77 C 4]; $(SmHoDy)Fe_2$ [78 S 4]; $(TbDy)Fe_2$ [75 C 2, 77 R 2, 77 S 5, 78 B 6, 78 C 9, 78 C 10, 78 R 4, 78 S 3, 78 S 5, 79 S 2, 81 N 3, 84 D 6, 87 G 9, 87 M 3]; $(TbHo)Fe_2$ [73 R 5, 76 T 2, 77 W 1, 80 K 12]; $(TbDyHo)Fe_2$ [77 S 5, 78 B 3, 79 S 2]; $(HoEr)Fe_2$ [76 R 2]; $(GdY)Co_2$ [83 M 8]

For ΔE effect see

RM_2 RFe_2 [74 K 16]; R = Tb, Er, Y [74 C 2, 74 C 3]; $HoCo_2$ [83 P 1]

$(R'R'')M_2$ $(TbDy)Fe_2$ [75 S 2, 78 C 5, 79 M 7, 81 H 2, 83 C 5, 84 K 2, 86 A 3, 87 G 9]; $(TbHo)Fe_2$ [73 R 5]; $(TbDyHo)Fe_2$ [78 B 3]; $(HoEr)Fe_2$ [76 R 2]

$R(M'M'')_2$ $Tb(FePt)_2$ [83 N 10]; $Gd(CoAl)_2$ [84 B 5]

Transport properties

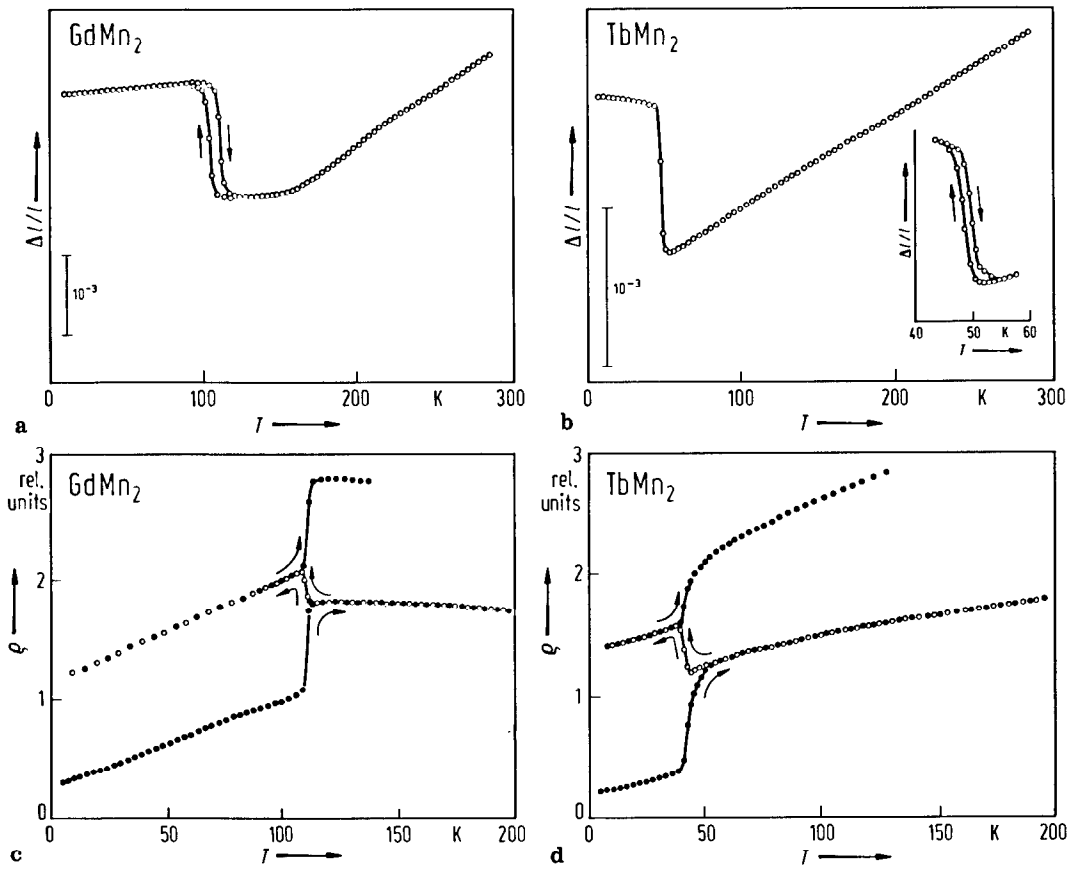

Fig. 214. Temperature dependence of the thermal expansion for (a) $GdMn_2$, (b) $TbMn_2$ and of electrical resistivity for (c) $GdMn_2$ and (d) $TbMn_2$ [83 M 1]. The open and closed circles in (c) and (d) indicate decreasing and increasing temperature, respectively. The anomalous change at T_C is also evidenced in the electrical resistivity versus temperature curves. The ϱ values exhibit a strong anomaly at a temperature T_t which depends strongly on the thermal history. This may be due to the appearance of some cracks in the crystal by a large axial distortion associated with the deformation of the crystal structure.

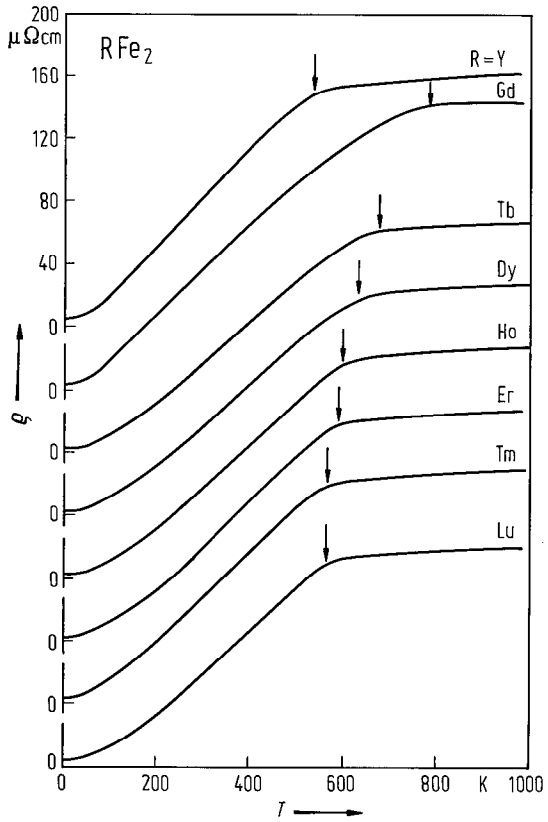

Fig. 215. Temperature dependence of the electrical resistivity of some RFe_2 compounds. Sharp kinks at the magnetic ordering temperatures (indicated by arrows), except for $GdFe_2$, are observed. The magnetic contributions to the resistivity show only a slight dependence on R magnetic moments, suggesting that these are mainly determined by the Fe 3d electrons [88 G 4].

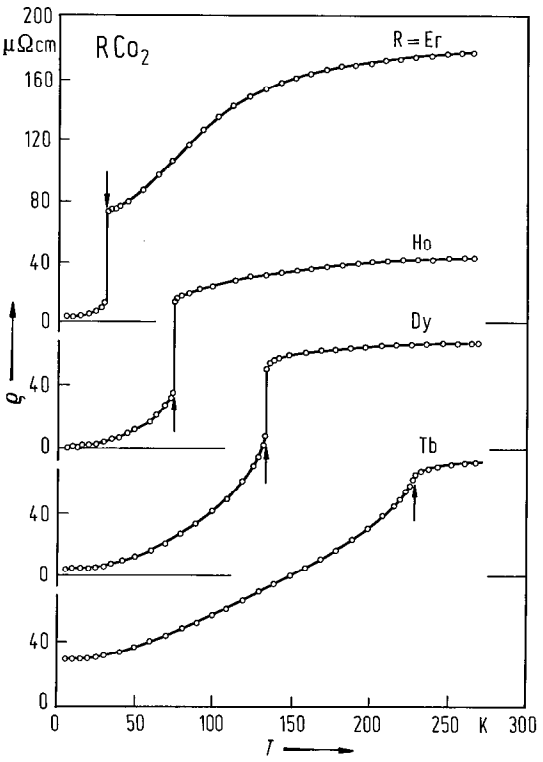

Fig. 216. Electrical resistivity as function of temperature for $ErCo_2$, $HoCo_2$, $DyCo_2$ and $TbCo_2$. A first-order magnetic transition is observed for $ErCo_2$, $HoCo_2$ and $DyCo_2$, while in case of $TbCo_2$ the transition is of second order [81 G 11].

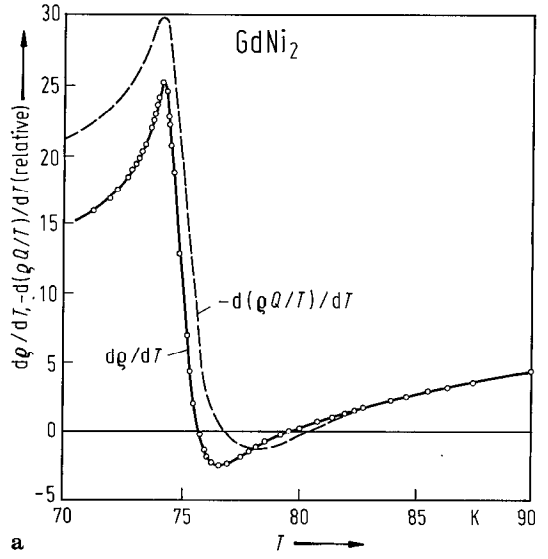

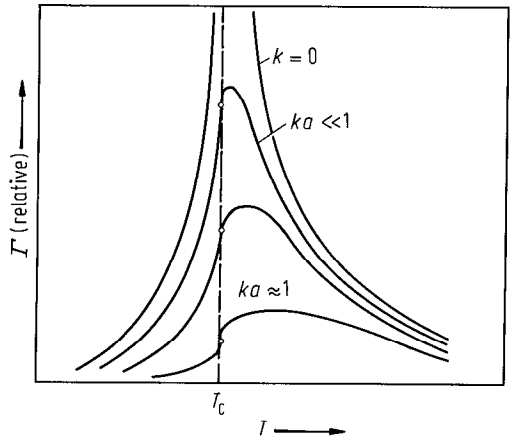

Fig. 217. (a) Temperature derivatives of the electrical resistivity, ϱ, and the quantity, $\varrho Q/T$, in $GdNi_2$, where Q is the thermopower. The curves have been arbitrarily normalized and arbitrarily shifted relative to each other in the vertical direction [73 Z 3]. The line through $d\varrho/dT$ data represents an eyeball fit. (b) shows expected form of spin-spin correlation function Γ in the vicinity of T_C [68 F 2].

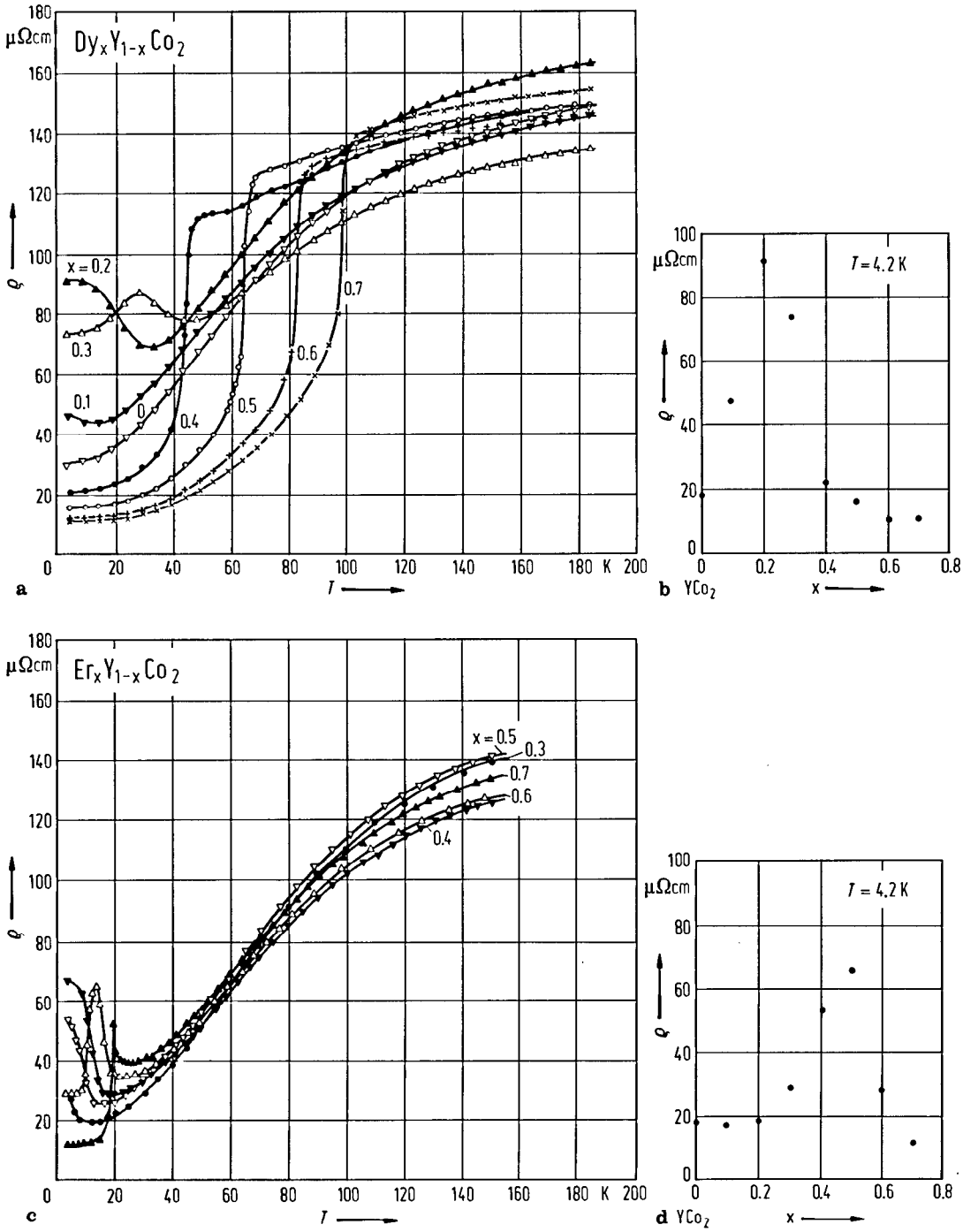

Fig. 218. (a) Temperature dependence of the electrical resistivity of $Dy_xY_{1-x}Co_2$ compounds ($0 \leqq x \leqq 0.7$). (b) shows the composition dependence of the electrical resistivity of $Dy_xY_{1-x}Co_2$ at 4.2 K [87 G 7]; (c) temperature dependence of the electrical resistivity of $Er_xY_{1-x}Co_2$ compounds ($0.3 \leqq x \leqq 0.7$). (d) shows the composition dependence of the electrical resistivity of $Er_xY_{1-x}Co_2$ at 4.2 K [87 G 7]. The R concentration regions where the compounds show long-range magnetic order are $0.4 \leqq x \leqq 1$ for R = Dy, $0.5 \leqq x \leqq 1$ for R = Ho, and $0.6 \leqq x \leqq 1$ for R = Er. For x values smaller than those mentioned above, freezing phenomena have been observed. Localized 4f-moments on the one hand and uniform spin fluctuations on the other hand give rise to spin-dependent scattering processes of the conduction electrons. The $\varrho(T)$ behaviour of the exchange-enhanced paramagnet YCo_2 shows a pronounced saturation tendency around 150 K and varies linearly in temperatures up to 1000 K [87 G 7]. This behaviour at high temperature together with a T^2 dependence at low temperatures [87 G 7] indicates the dominant contribution of spin fluctuations in YCo_2.

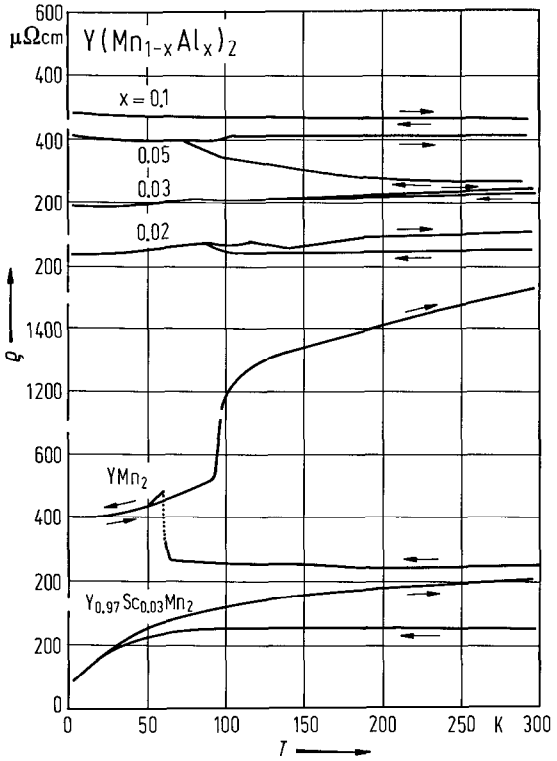

Fig. 219. Electrical resistivity ϱ of $Y(Mn_{1-x}Al_x)_2$ and $Y_{0.97}Sc_{0.03}Mn_2$ compounds as function of temperature. The scale of ϱ of YMn_2 in the heating run is cut at 100 K because of its huge increase [87 K 4]. In case of YMn_2 a sharp increase around 70 K on cooling, and at $T \cong 100$ K on heating is observed. Because of the thermal hysteresis, the transition is of first order. Since YMn_2 shows a large volume change ($\cong 5\%$) at the transition, the jump is considered to originate in microcracks introduced in a sample undergoing the transition in cooling as well as heating runs. Similar jumps of ϱ at the transition were observed for $Y(Mn_{1-x}Al_x)_2$ samples with $x = 0.02$ and 0.05. The sample having $x = 0.1$ has no more jump due to magnetic order but shows a monotonic increase with decreasing T.

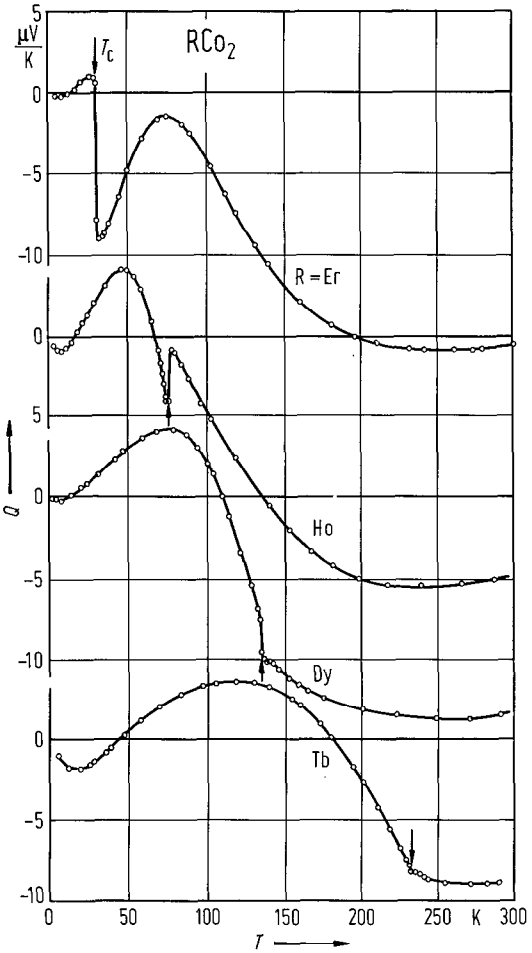

Fig. 220. Thermopower as function of temperature for $ErCo_2$, $HoCo_2$, $DyCo_2$ and $TbCo_2$. The discontinuities at T_C for $ErCo_2$, $HoCo_2$ and $DyCo_2$ are caused by magnetic first-order transitions. The results for $TbCo_2$ show a second-order magnetic transition [81 G 11].

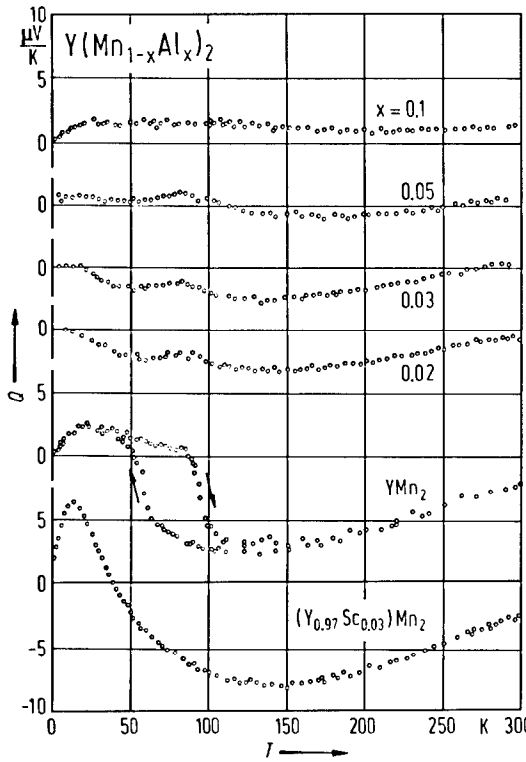

Fig. 221. Thermoelectric power Q of $Y(Mn_{1-x}Al_x)_2$ and of $Y_{0.97}Sc_{0.03}Mn_2$ as function of temperature. The thermal hysteresis was observed only for YMn_2 [87 K 4]. Since the value of Q is reproducible after the completition of the transition in a cooling or a heating process, the observed jump in Q has to be intrinsic. The thermoelectric power seems to be more insensitive to microcracks than the electrical resistivity. The temperature hysteresis of Q was not observed for other $Y(Mn_{1-x}Al_x)_2$ samples.

For electrical resistivity studies see also

RMn_2 R = Gd, Tb, Dy, Ho, Er [83 M 1]

RFe_2 R = Gd, Tb, Dy, Ho, Er, Tm, Lu [88 G 4]; R = Sc, Y, Ti, Zr, Hf, Nb, Ta [75 I 1]; R = Ce [81 T 2, 87 A 7]

RCo_2 [82 G 7]; R = Ti, Zr, Nb, Y [77 I 2]; R = Dy, Ho, Er [79 G 10]; R = Nd, Tb, Dy, Ho, Er [80 G 12]; R = Tb, Dy, Ho, Er, Y [81 G 11]; R = Ho, Y [87 G 6]; R = Ce [67 S 2] (superconductor with $T_C = 0.84(4)$ K); R = Gd [70 K 1]; R = Pr [82 G 10]

RNi_2 R = Gd [69 K 1, 70 K 1, 71 Z 3]; R = Pr [82 G 10]

RM_2H_x $PrCo_2H_x$ [72 T 5]; $NdCo_2H_x$ [72 T 5]; $NiTi_2H_x$ [79 L 4]

$(R'R'')M_2$ $(YSc)Mn_2$ [87 K 4]; (TbDyEr)Fe_2 [85 K 4]; $(CeY)Co_2$ [85 A 9]; $(PrY)Co_2$ [83 G 8]; $(NdY)Co_2$ [82 G 6, 83 B 1, 83 G 8]; $(DyY)Co_2$ [87 G 7]; $(HoY)Co_2$ [78 S 19, 82 G 6, 83 G 8]; $(ErY)Co_2$ [87 G 7, 88 D 4]; $(LaY)Ni_2$ [87 S 19]; $(CeY)Ni_2$ [85 A 9, 87 S 19]

$R(M'M'')_2$ $Gd(MnAl)_2$ [83 S 18]; $Ce(FeCo)_2$ [88 R 2]; $Y(FeCo)_2$ [77 I 1, 80 V 2]; $Hf(FeCo)_2$ [80 V 2]; $R(FeM)_2$, R = Y, Zr, U, M = Mn, Co, Al [82 H 4]; $R(MAl)_2$, R = Gd, Dy, Ho, Er, M = Fe, Co, Cu [81 G 13]; $R(FeAl)_2$ [84 S 11, 88 G 3]; $Ce(FeAl)_2$ [82 D 1, 82 T 1, 85 T 2, 86 D 1]; $Y(FeIr)_2$ [80 V 2]; $Ce(CoNi)_2$ [84 S 6, 85 A 9, 87 K 10]; $Y(CoNi)_2$ [84 S 6]; $Gd(NiCu)_2$ [77 G 10]; $Tb(NiCu)_2$ [78 P 1]

For thermopower studies see also

RM_2 RCo_2, R = Nd, Tb, Dy, Ho [80 G 12]; R = Tb, Dy, Ho, Er, Y [81 G 11]; R = Ho, Y [87 G 6]; $PrNi_2$ [82 M 3]

$(R'R'')M_2$ $(YSc)Mn_2$ [87 K 4]; $(ErY)Co_2$ [88 D 4]; $(CeLa)Ni_2$ [87 S 2, 88 K 4]

$R(M'M'')_2$ $Ce(FeCo)_2$ [88 R 2]; $Ce(CoNi)_2$ [87 K 10]

For Hall effect see

$(ErY)Fe_2$ [80 H 9]

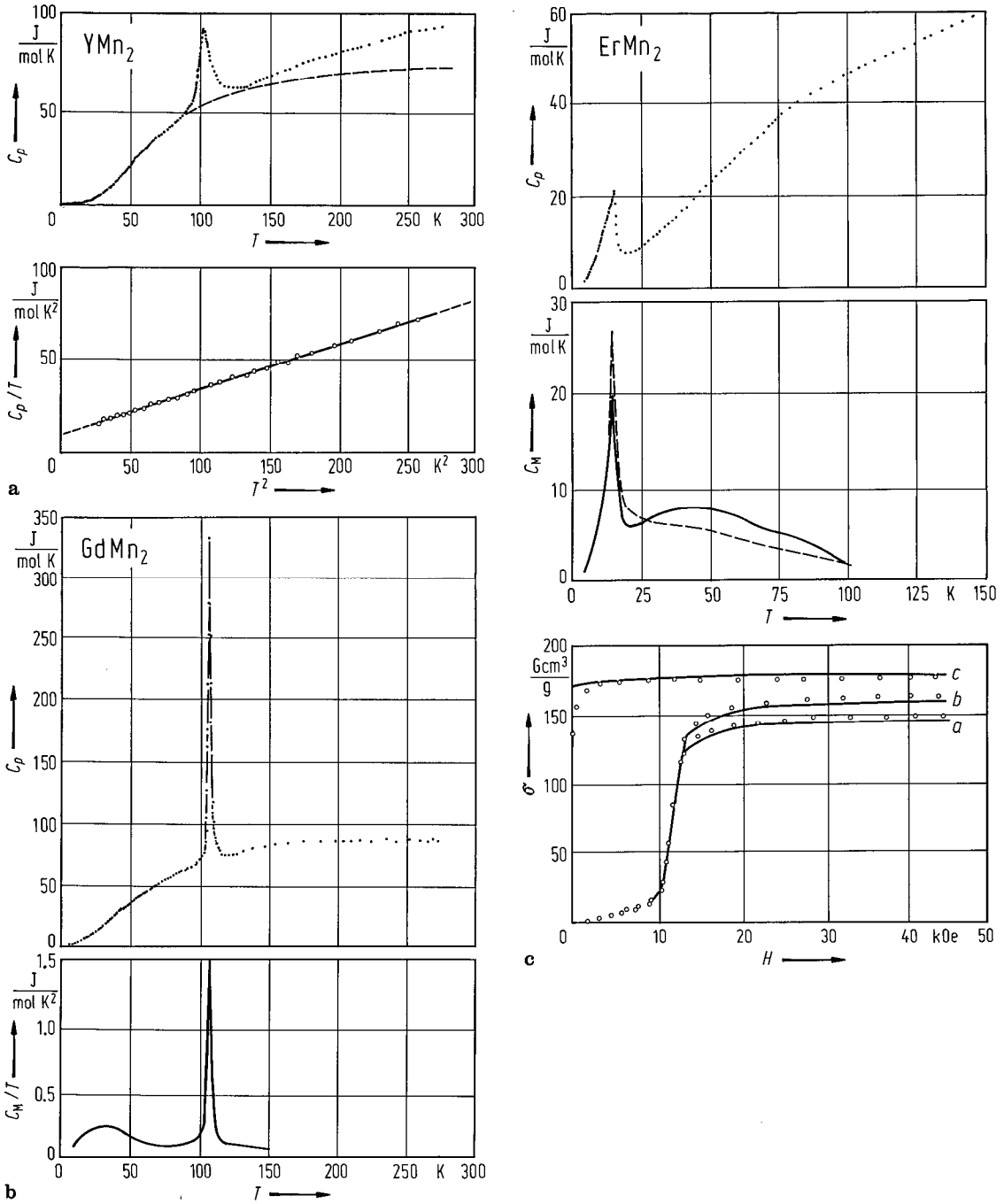

Fig. 222. Heat capacity of RMn_2 compounds as function of temperature for (a) R = Y, (b) R = Gd, (c) R = Er. In the lower part of (a) C_p/T vs. T^2 below 16 K is plotted, and in (b) the C_M/T vs. T curve is shown. The lower part of (c) shows the magnetization curves for $ErMn_2$ single crystal, while the figure in the middle shows C_M vs. T curves below 100 K; the solid and dashed lines indicate the experimental and calculated values, respectively [87 O 3]. The Mn magnetic moment in YMn_2 has an itinerant character and an additional C_M is observable even above T_N. In $GdMn_2$, the Gd magnetic moments are in disorder at T_N simultaneously with the Mn magnetic moments. The crystal electric field (CEF) contributions in $ErMn_2$ were calculated using a single-ion Hamiltonian. In case of YMn_2 a symmetric anomaly appears around T_N, indicating that the transition at T_N is of first order. A value $\Theta_D \cong 290$ K was estimated. The broken line in (a) represents the sum of the contributions from the lattice vibrations calculated using a Debye function and from the conduction electrons. Therefore the difference between the experimental points and the broken line gives the magnetic heat capacity of the Mn sublattice. The magnetic entropy associated with the Mn magnetic

moments around T_N is estimated at $\Delta S = 3.9\,J\,mol^{-1}\,K^{-1}$, which is much smaller than the value $2R\ln(2S+1) = 23\,J\,mol^{-1}\,K^{-1}$ expected from the disorder of localized spin $S = 3/2$, reflecting an itinerant character of the Mn magnetic moment. In case of $GdMn_2$ a sharp and symmetric peak is observed at $T_N = 110\,K$, but no clear anomaly occurs at 40 K where the magnetization in the M vs. H curve disappears. A value $\Theta_D \cong 245\,K$ was estimated [81 G 3]. The temperature dependence of C_M/T corresponding to the magnetic entropy, estimated by subtracting heat capacities due to the lattice and the conduction electrons from the total heat capacity, is plotted in the lower part of (b). The magnetic entropy below 50 K is $\cong 9.0\,J\,mol^{-1}\,K^{-1}$, which is much smaller than $R\ln(2S+1) = 17.3\,K\,mol^{-1}\,K^{-1}$ expected from disordering the Gd magnetic moments with $J = 7/2$. This indicates that the Gd magnetic moments are in disorder at $T_N = 110\,K$ simultaneously with the Mn magnetic moments. In case of $ErMn_2$, which is a c axis ferromagnet, a λ-type anomaly is observed at $T_C = 15\,K$ indicating a second-order transition. The magnetic and CEF contributions, C_M, are shown in the middle of (c). The lower part shows the magnetization isotherms along a, b and c axes, in which the solid lines indicate the magnetization calculated for CEF levels with $B_2^0 = 0.10\,K$, $B_4^0 = 0.72 \cdot 10^{-3}\,K$, $B_6^0 = 0.41 \cdot 10^{-5}\,K$, and $B_6^6 = 0.68 \cdot 10^{-5}\,K$. The CEF parameters thus obtained explain reasonably well C_M for $ErMn_2$ as shown by the dashed line in the C_M vs. T insert.

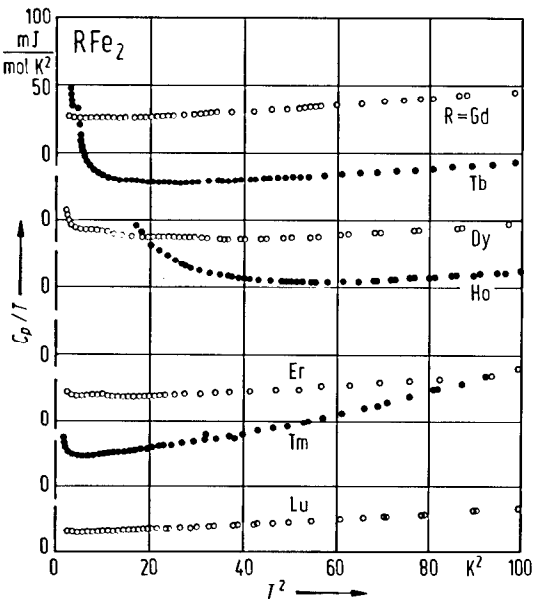

Fig. 223. Total heat capacity C_p in a C_p/T vs. T^2-plot in RFe_2 compounds [79 B 20]. The anomalies at $T < 5\,K$ are assumed to be due to magnetic rare-earth oxides. The apparent electronic heat capacity coefficients exhibit a cusp-like behaviour as the R atom is changed, with a maximum for $HoFe_2$.

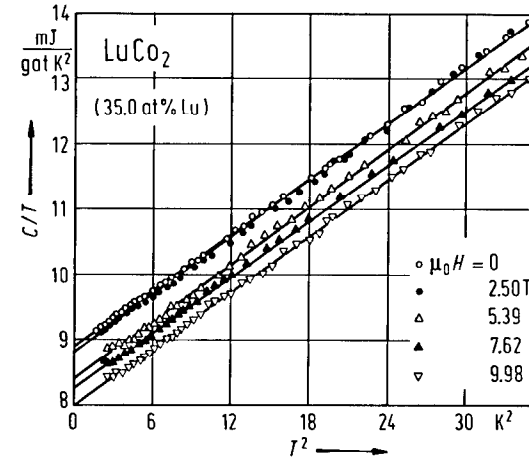

Fig. 224. Heat capacity of $LuCo_2$ in five magnetic fields. The solid lines are the results of a least-squares fitting of the data to the relation, $C/T = \gamma + \beta T^2$, where γ is the electronic specific-heat constant, $\beta = 1944/\Theta_D^3\,J\,mol^{-1}\,K^{-4}$, and Θ_D is the Debye temperature. Similar results were obtained for $ScCo_2$ and YCo_2. The electronic specific heat constant decreases with increasing field up to 10 T by 7% ($ScCo_2$), 4% (YCo_2) and 10% ($LuCo_2$). Analysis based on several theoretical models of the quenching of spin fluctuations by high magnetic fields suggests that the characteristic spin-fluctuation temperatures are $T_{sf}(ScCo_2) \cong 20\,K$, $T_{sf}(YCo_2) \cong 35\,K$ and $T_{sf}(LuCo_2) \cong 16\,K$ [84 I 4].

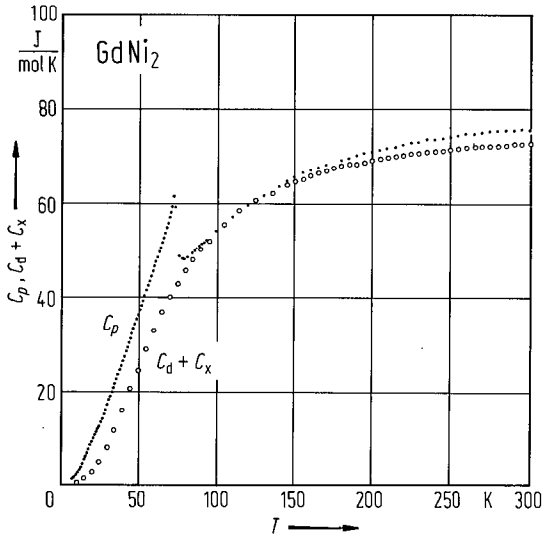

Fig. 225. Temperature dependence of the heat capacity of $GdNi_2$, C_p, and sum of lattice Debye ($\Theta_D = 266$ K), C_d, and linear temperature, C_x, corrections. The magnetic contribution, C_M, derived by subtracting $C_d + C_x$ from critical region C_p, obey an exponential law, $C_M \propto t^{-\alpha}$ for $T > T_C$, and $C_M \propto t^{-\alpha'}$ for $T < T_C$, with $t = |T - T_C|/T_C$, $\alpha \cong 0.36$, and $\alpha' \cong 0.026$ [73 C 1].

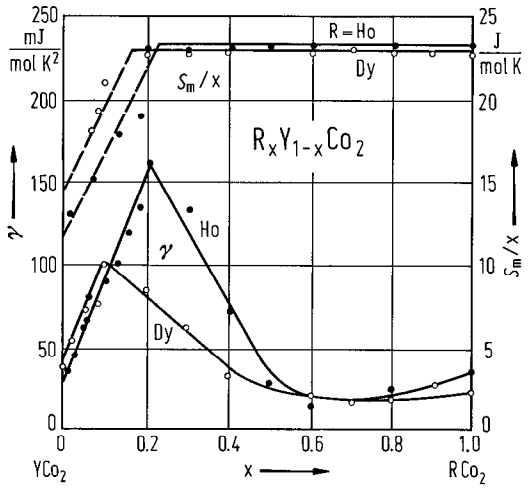

Fig. 226. Composition dependence of γ and S_m/x in $Ho_xY_{1-x}Co_2$ and $Dy_xY_{1-x}Co_2$ for $0 \leqq x \leqq 1$ [87 P 5]. The γ values increase with x in the dilute R concentration range from 35 mJ mol^{-1} K^{-2} to a maximum value of 160 and 100 mJ mol^{-1} K^{-2} at x = 0.2 and 0.1 for Ho and Dy compounds, respectively. The magnetic entropy per R atom, S_m/x, drops for $x < 0.2$, while for $x \geqq 0.2$, the theoretical value (derived from S_m/x), $R\ln(2J+1)$ of 23.5 J mol^{-1} K^{-1} for $Ho_xY_{1-x}Co_2$ and 23.05 J mol^{-1} K^{-1} for $Dy_xY_{1-x}Co_2$ is attained. In both systems, the magnetic entropy of the Co–3d magnetic moment corresponding to $S = 1/2$ (5.76 J mol^{-1} K^{-1}) cannot be observed above T_C.

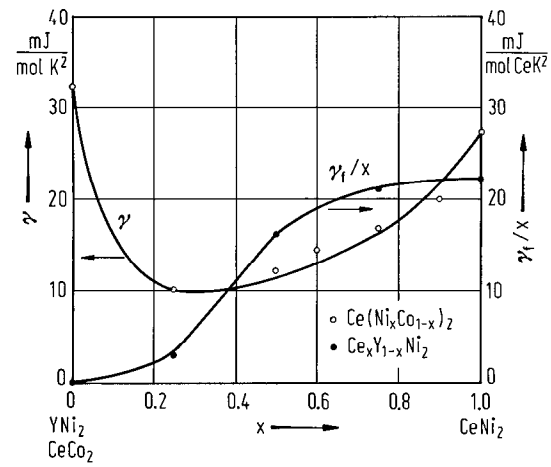

Fig. 227. Linear coefficient of specific heat, γ, of $Ce(Ni_xCo_{1-x})_2$, and γ_f/x, where $\gamma_f = \gamma_{Ce_xY_{1-x}Ni_2} - \gamma_{YNi_2}$, of $Ce_xY_{1-x}Ni_2$ compounds [85 A 9]. The drop of γ_f/x from 22 mJ (mol Ce)$^{-1}$ K^{-2} at $CeNi_2$ towards zero as one dilutes with Y is certainly suggestive that Ce is being driven toward the saturated or "tetravalent" state. The γ values for $Ce(Ni_xCo_{1-x})_2$ compounds first decrease from 27 mJ mol^{-1} K^{-2} for $CeNi_2$ to a minimum of 10 mJ mol^{-1} K^{-2} for $Ce(Co_{0.75}Ni_{0.25})_2$ and then rise to 32 mJ mol^{-1} K^{-2} for $CeCo_2$. The initial drop is probably associated with the increase of Ce valence towards the saturated value.

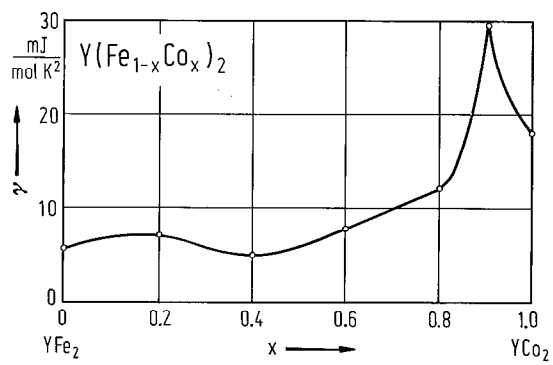

Fig. 228. Composition dependence of the electronic specific heat coefficient, γ, in $Y(Fe_{1-x}Co_x)_2$ system [77 M 13]. The observed extraordinarily high γ value for x = 0.9, which is near the critical concentration for the onset of ferromagnetism, is attributed to the spin fluctuations.

For heat capacity studies and Debye temperatures see also

RM_2 R = Pr, Gd, Dy, Er, M = Fe, Co, Ni [76 D 6]
RMn_2, R = Gd, Er, Y [87 O 3]
RFe_2, R = Gd, Tb, Dy, Ho, Er, Tm, Lu [79 B 20]; R = Ho, Er, Lu [79 G 1]
RCo_2 [73 V 5]; R = Lu, Y, Sc [82 G 12, 84 I 4, 85 G 18]; R = Ce [71 C 3, 86 C 6]; R = Pr [69 M 1, 72 D 1, 82 G 10]; R = Nd [72 D 1, 72 M 1]; R = Tb [74 V 4]; R = Ho [73 B 11, 74 V 4]; R = Lu [80 I 1, 81 B 3(T)]; R = Y [72 B 9]; R = Zr [68 J 2, 86 C 6]; R = Hf [68 J 2];
RNi_2 [67 D 1]; R = La [71 N 5, 82 S 1]; R = Ce [68 J 2, 70 W 2]; R = Pr [69 M 1, 70 W 2, 82 G 9, 82 G 10, 82 M 3, 82 M 5, 82 S 1]; R = Nd [70 W 2, 71 N 5]; R = Gd [73 C 1]; R = Tm [86 D 2]; R = Y [72 B 9, 82 M 6]

RM_2H_x $LuFe_2H_x$, $ErFe_2H_x$ [86 W 3]

$(R'R'')M_2$ $(YSc)Mn_2$ [87 W 2]; $(TbHo)Fe_2$ [81 G 3]; $(TbY)Fe_2$ [83 S 23]; $(CeY)Co_2$ [85 A 9]; $(TbY)Co_2$ [86 B 8, 86 K 7]; $(DyY)Co_2$ [87 P 5]; $(HoY)Co_2$ [87 P 5, 88 H 2]; $(ErY)Co_2$ [88 D 4, 88 P 4]; $(CeLa)Ni_2$ [85 S 3]; $(CeY)Ni_2$ [85 A 9]; $(PrLa)Ni_2$ [82 M 6]; $(GdY)Ni_2$ [86 T 2]

$R(M'M'')_2$ $Y(MnAl)_2$ [87 W 2]; $Ce(FeCo)_2$ [88 R 2]; $Y(FeCo)_2$ [77 M 13]; $Tb(FeRh)_2$ [83 S 23]; $Ho(FeRh)_2$ [83 S 23]; $Ce(CoNi)_2$ [85 A 9, 85 S 1]; $Dy(CoNi)_2$ [76 S 3, 76 S 4]; $Y(CoCu)_2$ [88 D 3]

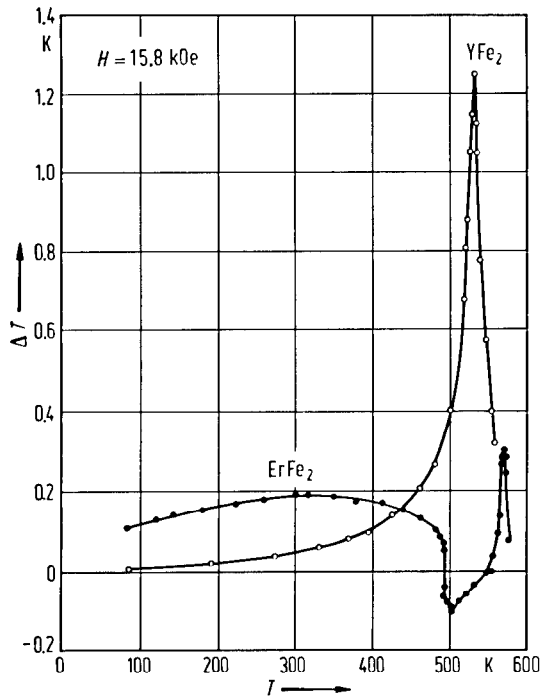

Fig. 229. Thermal variation of magnetocaloric effect, ΔT, in YFe_2 and $ErFe_2$ compounds in a magnetic field of 15.8 kOe [73 N 6]. For $HoFe_2$ a change in ΔT is observed at the compensation point, T_{comp}. From the behaviour of $\Delta T(H)$ the appearance of noncollinear magnetic structure near T_{comp} is evidenced.

For magnetocaloric effect see also
YFe_2, $ErFe_2$ [73 N 6]
$(TbDy)Fe_2$ [84 K 2]; $(TbY)Fe_2$ [75 N 9]

Spectral studies

Valence band spectra: $GdFe_2$ [79 A 6]; $CeCo_2$ [82 A 6]

L_{III} absorption and emission spectra
$Ce(M'M'')_2$ [81 B 1]; $Ce(NiCo)_2$ [84 S 6]; $Y(NiCo)_2$ [84 S 6]
$Dy(FeAl)_2$ [84 S 14]; $CeFe_2$, $CeNi_2$ [85 P 1]; RM_2, M = Fe, Co, Ni [87 S 18]

Photoemission spectra
$ErFe_2$ [82 L 2]; YFe_2 [85 H 2]; $ErFe_2H_x$ [79 L 3, 82 S 12]; $CeNi_2$ [81 K 15, 81 K 16]

X-ray absorption and emission spectra
RCo_2, R = Gd, Tb, Dy [80 H 7]; $Gd(MnAl)_2$ [79 S 7]; $Dy(CoAl)_2$ [82 S 20]; UMn_2, UFe_2 [84 L 3]; $Ce(NiAl)_2$ [85 M 11]
EXAPS: RNi_2, RNi_2H_x, R = La, Ce [87 P 2, 87 P 3]
XASCEELS: $CeCo_2$, $CeNi_2$ [86 H 4]

Magneto optical spectra:
RFe_2, R = Gd, Tb, Dy, Ho, Er [85 M 10]

SXS BIS spectra
$GdNi_2$, GdMnAl [82 S 21]

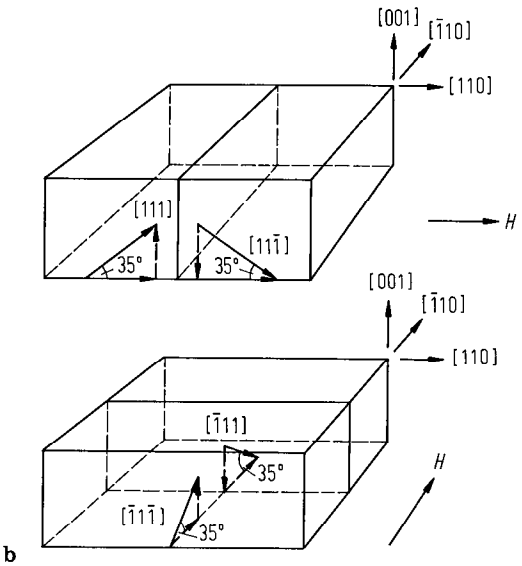

b

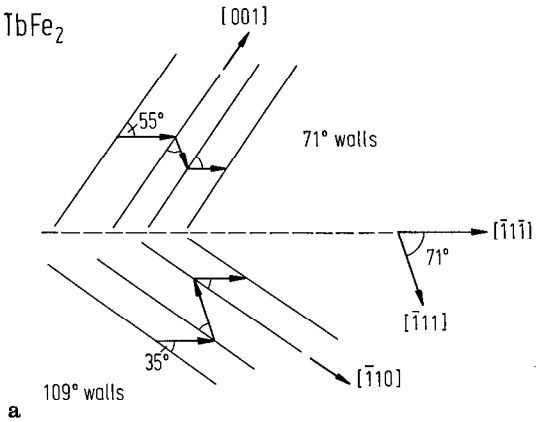

a

Fig. 230. (a) Model of 71°- and 109°-walls observed on (110) surfaces of $TbFe_2$ single crystals. (b) Model of 71°-walls observed in a $TbFe_2$ single crystal (100) surface [78 S 7]. In $TbFe_2$ single crystals 109°- and 71°-walls have been found by means of conventional microscopy using the Kerr effect and the Bitter solution technique. Polycrystalline patterns were more varied and domain width were an order of magnitude smaller than single crystal width. This is attributed to the large internal strains that take place when the temperature of a polycrystal is lowered through the Curie point. Domain widths were roughly 50 µm in the single crystals. In $TbFe_2$, the (100) surface domain widths were smaller than those seen on the (110) surface.

Domain structure, magnetization processes

For magnetization processes see
RM_2 RFe_2 [79 A 3, 79 L 2]; R = Pr, Sm, Tb, Dy, Ho, Er, Tm, Yb [79 c 1]; $DyCo_2$ [72 T 3, 77 H 6]
(R'R'')M_2 (TbDy)Fe_2 [82 C 11, 82 W 8]; (DyHo)Fe_2 [82 L 5*]; (HfTa)Fe_2 [86 K 3]
$R(M'M'')_2$ $Gd(MnAl)_2$ [80 S 13]; $Ce(FeCo)_2$ [88 R 2]; $R(FeAl)_2$, R = Gd, Dy, Ho, Y [76 G 8]; TbFeAl [71 O 4]; $Dy(FeAl)_2$ [72 O 4, 75 G 3]; $Dy(Fe_{0.9}M_{0.1})_2$, M = Al, Ga, B [87 Z 1, 88 Z 2]; $Dy(CoNi)_2$ [71 M 4, 71 T 2, 72 B 1, 72 T 4, 80 C 1]; $Tb(CoAl)_2$ [71 O 6]; $Dy(CoAl)_2$ [72 O 4, 80 S 13]; $Er(CoAl)_2$ [71 O 6, 72 O 2]; $Er(NiAl)_2$ [72 O 1]; $Tm(NiAl)_2$ [72 O 1]

For domain structure see also
RM_2 RFe_2 [74 K 2, 86 S 11]; R = Gd, Tb, Dy, Ho, Er [85 M 10]; R = Tb [78 S 7, 79 C 4, 79 K 1]; R = Dy [80 K 1, 83 P 11, 83 P 12]
(R'R'')M_2 (TbDy)Fe_2 [78 S 7, 79 C 4, 83 P 6, 85 S 6, 87 B 14, 87 J 1]

For after-effect and internal friction see
(TbDy)Fe_2 [84 K 2]; $Dy(CoNi)_2$ [72 B 2, 83 C 2]

2.4.2.13 RM_3 compounds

Crystal structure, lattice parameters

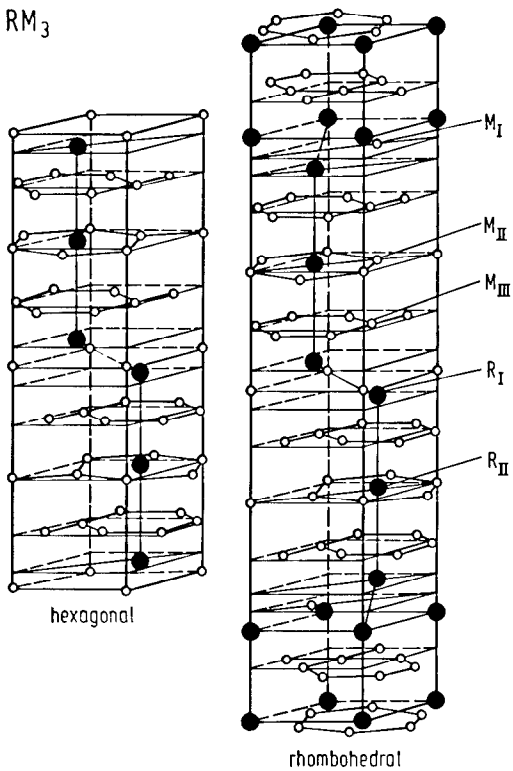

Fig. 231. Crystal structures of RM_3 compounds. These crystallize both in a hexagonal type ($P6_3/mmc$-space group) or in a rhombohedral type ($R\bar{3}m$-space group) [59 C 2]. The atomic sites are given in Table 52.

Table 52a. Atomic sites in RM_3 compounds, hexagonal $P6_3/mmc$-space group [69 P 1].

Atom	Site	Coordinates
R_I	2c	$\pm(1/3, 2/3, 1/4)$
R_{II}	4f	$\pm(1/3, 2/3, z; 2/3, 1/3, 1/2+z)$, $z=0.042$
M_I	2a	$(0,0,0; 0,0,1/2)$
M_{II}	2b	$\pm(0,0,1/4)$
M_{III}	2d	$\pm(1/3, 2/3, 3/4)$
M_{IV}	12k	$\pm(x, 2x, z; 2\bar{x}, \bar{x}, z; \bar{x}, 2\bar{x}, 1/2+z; 2x, x, 1/2+z; \bar{x}, x, 1/2+z)$, $x=0.833$, $z=0.127$

Table 52b. Atomic sites in RM_3 compounds, rhombohedral $R\bar{3}m$-space group [69 P 1].

Atom	Site	Coordinates
R_I	3a	$(0,0,0)$
R_{II}	6c	$\pm(0,0,z)$, $z=0.141$
M_I	3b	$(0,0,1/2)$
M_{II}	6c	$\pm(0,0,z)$, $z=0.333$
M_{III}	18h	$\pm(x, \bar{x}, z; x, 2x, z; 2\bar{x}, \bar{x}, z)$, $x=0.5$; $z=0.082$

The following translations are added (0, 0, 0; 2/3, 1/3, 1/3; 1/3, 2/3, 2/3).

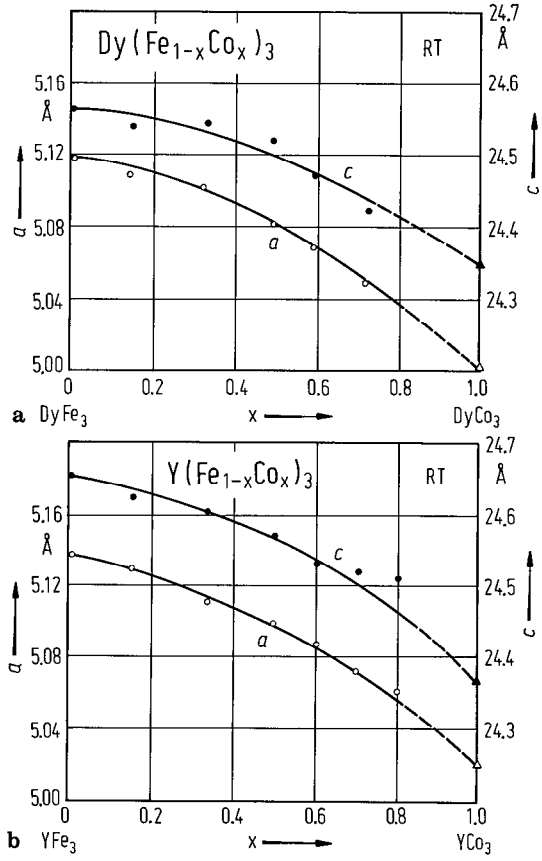

Fig. 232. Variations of the lattice parameters of (a) $Dy(Fe_{1-x}Co_x)_3$ and (b) $Y(Fe_{1-x}Co_x)_3$ at room temperature as function of Co content. Circles [75 A 5], triangles [65 B 1]. The lattice constants a and c do not vary linearly with composition (Vegard's law), positive deviations from the law being observed in both series.

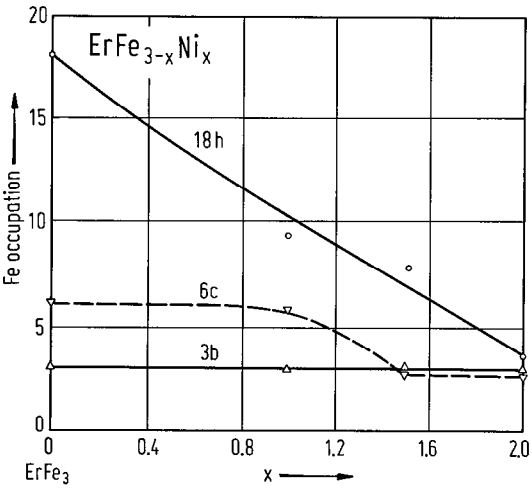

Fig. 233. Composition dependence of the occupation of crystallographic sites by Fe in $ErFe_{3-x}Ni_x$ compounds, as determined by neutron diffraction studies. The atomic ordering of Fe atoms is dominant at the 3b sites, while the 18h sites are preferred by Ni atoms [87 T 4].

Table 53a. Lattice parameters of RM_3 compounds (Å).

	69 G 1		70 V 1, 71 B 18		68 R 1		76 M 3		83 M 2	
	a	*c*	*a*	*c*	*a*	*c*	*a*	*c*	*a*	*c*
$SmFe_3$			5.187	24.91						
$GdFe_3$			5.166	24.76	5.166	24.71	5.167	24.71		
$TbFe_3$			5.145	24.63	5.160	24.58			5.140	24.590
$DyFe_3$	5.158	24.71	5.116	24.55	5.120	24.56	5.130	24.52		
$HoFe_3$			5.100	24.50	5.092	24.53	5.117	24.48		
$ErFe_3$			5.088	24.46	5.092	24.46			5.089	24.473
$TmFe_3$			5.077	24.43	5.074	24.43			5.063	24.621
$LuFe_3$					5.052	24.33				
YFe_3	5.140	24.59			5.137	24.61			5.137	24.610

Table 53b. Lattice parameters of RM_3 compounds (Å).

	65 B 1		71 G 1, 71 G 2		70 B 10, 77 b 1		76 I 1		80 P 5		81 M 2		85 Y 6	
	a	*c*	*a*	*c*	*a*	*c*	*a*	*c*	*a*	*c*	*a*	*c*	*a*	*c*
$CeCo_3$	4.952	24.73			4.955	24.75								
$PrCo_3$	5.068	24.79			5.062	24.81								
$NdCo_3$	5.067	24.76			5.060	24.78								
$SmCo_3$	5.053	24.61			5.050	24.59								
$GdCo_3$	5.043	24.51			5.039	24.52			5.040	24.53	5.038	24.66		
$TbCo_3$	5.019	24.42			5.011	24.38			5.012	24.38				
$DyCo_3$	5.004	24.35			4.995	24.36			4.995	24.34	4.987	24.36		
$HoCo_3$	4.992	24.30			4.981	24.29			4.980	24.28	4.981	24.30		
$ErCo_3$	4.979	24.25			4.972	24.18			4.970	24.20	4.979	24.28		
$TmCo_3$	4.969	24.16					4.986	24.16			4.973	24.17		
$YbCo_3$					4.952	24.19								
$LuCo_3$			4.95	24.00										
YCo_3	5.016	24.35	5.01	24.40	5.005	24.72							4.992	24.30

Table 53c. Lattice parameters of RFe_3 compounds (Å).

	69 P 1			70 B 12			74 N 4	
	a	c_{rh}	c_{hex}	a	c_{rh}	c_{hex}	a	c_{rh}
$LaNi_3$				5.083	25.09		5.10	25.04
$CeNi_3$	4.98		16.54	4.960		16.56		
$PrNi_3$	5.03	25.01		5.035	24.82			
$NdNi_3$	5.02	24.71		5.030	24.72			
$SmNi_3$	5.00	24.59		5.005	24.60			
$GdNi_3$	4.99	24.54		4.993	24.49			
$TbNi_3$	4.96	24.46		4.975	24.42			
$DyNi_3$				4.966	24.35		4.97	24.14
$HoNi_3$	4.95	24.19		4.951	24.31			
$ErNi_3$	4.94	24.21		4.941	24.25			
$TmNi_3$	4.93	24.25		4.930	24.25			
$YbNi_3$	4.91	24.27		4.920	24.16			
YNi_3	4.97	24.37		4.973	24.42			

Table 54. Physical properties of some RM_3 hydrides [1]).

	a Å	c Å	p_m μ_B/f.u.	T_{comp} K	T_C K	Ref.
$GdFe_3H_{3.1}$	5.387	27.01	1.38 [2])	170		78 W 3, 76 M 3
$DyFe_3H_{3.0}$	5.310	24.59	2.20 [3])	175		78 W 3, 76 M 3
$HoFe_3H_{3.6}$	5.316	24.39	2.53 [2])	112		78 W 3, 76 M 3
$ErFe_3H_{1.5}$	5.20	25.17				79 N 3
$ErFe_3H_{2.7}$	5.26	25.68				79 N 3
$ErFe_3H_{4.05}$	5.30	26.40				79 N 3
$TbFe_3H_{3.5}$	5.370	26.814	2.90		300	83 M 2
$ErFe_3H_{3.5}$	5.296	26.246	2.05		> 300	83 M 2
$TmFe_3H_3$			4.08		> 300	83 M 2
$YFe_3H_{3.5}$	5.375	24.460	5.70		545	83 M 2
$CeCo_3H_{4.0}$	4.956	32.69				80 V 3
$GdCo_3H_{4.6}$	5.314	27.14	3.92 [4])			81 M 2
$DyCo_3H_{4.3}$	5.224	26.37	3.81 [4])			81 M 2
$HoCo_3H_{4.2}$	5.250	26.32	1.26 [4])			81 M 2
$ErCo_3H_{4.3}$	5.217	26.03	1.04 [4])	170		81 M 2
$TmCo_3H_{4.3}$	5.2242	25.860	2.04 [4])	164	370	81 M 2
$CeNi_3H_3$	4.920	21.64				80 V 3
YNi_3H_4	5.267	24.57	Pauli paramagnet $\chi_g = 7 \cdot 10^{-6}$ cm^3 g^{-1}			79 B 19

[1]) As function of hydrogen content magnetic fields higher than ≅150 kOe are necessary to obtain saturation [85 Y 5], see Fig. 244, because of metamagnetic phase transitions.

[2]) Extrapolated from 21 kOe at 4.2 K to $H \rightarrow \infty$.

[3]) Value at 21 kOe, which is not close to saturation.

[4]) At 4.2 K in applied field of 21 kOe.

For crystal structure and lattice parameters see also:

RM_3 [65 V 1, 67 O 3]
RFe_3 [71 B 18, 71 B 19]; R = Tb, Er, Tm [83 M 2]; R = Dy [70 D 1, 74 N 4, 82 B 1, 84 P 14]; R = Y [76 B 18]
RCo_3 [65 B 1, 67 V 1, 70 B 10]; R = Ce, Pr, Nd, Gd, Tb, Dy, Ho, Er, Tm, Y [66 L 4]; R = Dy [74 N 4]; R = Ho [65 B 2]; R = Y [65 O 2, 69 K 5]
RNi_3 [65 V 1, 69 L 1, 69 V 1]; R = Pr, Nd, Sm, Gd, Tb, Dy, Ho, Er, Tm, Yb, Y [67 P 1]; R = La, Ce, Pr, Nd, Sm, Gd, Tb, Dy, Ho, Er, Y [70 B 12]; R = La [74 N 4]; R = Ce [59 C 2, 75 P 8]; R = Dy [74 N 4]; R = Y [79 B 19]

RM_3H_x RFe_3H_x, R = Gd, Dy, Ho [76 M 3, 78 G 2]; R = Tb, Er, Tm [83 M 2]; R = Dy [80 N 3]; R = Er [79 N 3]; R = Y [76 B 18]; RCo_3H_x, R = Er, Tm [81 M 2]; R = Gd, Dy, Ho, Er [78 M 5]; see Table 54.

$(R'R'')M_3$ $(R_{0.1}Th_{0.8})Fe_3$, R = La, Pr, Lu, Y, Sc [73 K 17]; $(RTh)Fe_3$, R = Ce, Pr, Dy, Lu, Y, Sc [73 K 19]; $(DyY)Fe_3$ [85 P 7]; $(DyTh)Fe_3$ [73 K 17]; $(LuTh)Fe_3$ [73 K 18]; $(YTh)Fe_3$ [73 K 18]; $(GdY)Co_3$ [81 S 5]; $(YZr)Co_{2.9}$ [87 K 5]

$R(M'M'')_3$ $Dy(FeCo)_3$ [75 A 5]; $Y(FeCo)_3$ [75 A 5, 75 T 1]; $Dy(FeNi)_3$ [73 T 2, 74 T 2, 76 A 5]; $Y(FeNi)_3$ [76 A 5, 78 M 16]; $Tb(FeAl)_3$ [75 O 1]; $Dy(FeAl)_3$ [85 P 8]; $Y(CoNi)_3$ [75 T 1]

$(R'R'')M_3H_x$ $(YZr)Co_{2.9}H_x$ [87 K 5]; $Ce(CoNi)_3H_x$ [87 P 4]; $Zr(CrFeHo_{0.8})H_x$, M = Fe, Co, Ni [84 H 7]

For thermal expansion see
$ErFe_3$ [73 B 23, 75 N 7]; YNi_3 [82 P 2]

For hydrogen absorption and desorption see

RM_3H_x [76 B 4, 85 S 12]; RFe_3H_x [78 G 2]; R = Gd, Dy, Ho [76 M 3]; R = Dy [80 K 10]; R = Er [79 N 3]; R = Y [76 B 18]
RCo_3H_x [76 T 1]; R = Ce, Pr, Tb, Dy, Er [79 B 11]; R = Gd, Dy, Ho [78 M 5]; R = Nd, Gd [81 K 11]; R = Ce [80 B 16]; R = Tb [81 K 10]; R = Dy [80 K 9]; R = Ho [81 K 8]; R = Er [81 K 9]; R = Tm [82 K 2]; R = Lu [84 K 4]; R = Y [81 K 10, 85 Y 6]; $CeNi_3H_x$ [80 B 16]
$Ce(CoNi)_3H_x$ [87 P 4]

Magnetization, Curie temperatures

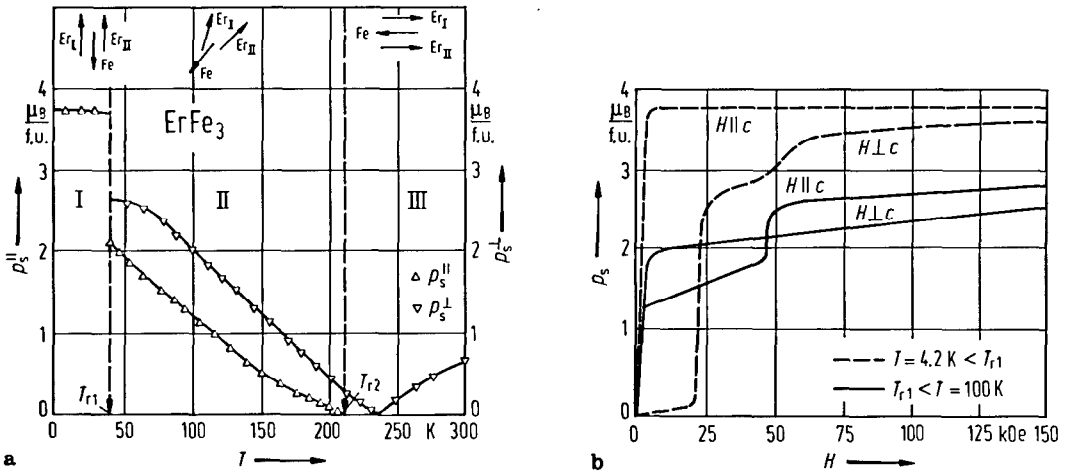

Fig. 234. (a) Thermal variation of the components of the spontaneous magnetization of $ErFe_3$ measured along and perpendicular to the c axis, respectively. A discontinuity of the two components is observed at $T_{r1} = 42$ K. The temperature range of the stability of the magnetic phases I, II and II is also shown. (b) Magnetization curves below T_{r1} (at 4.2 K) and above T_{r1} (100 K) are plotted [86 B 1]. The structure is collinear with the c axis below T_{r1}. In the temperature range $T_{r1} < T < T_{r2}$ ($T_{r2} \cong 220$ K), the structure is noncollinear. Above T_{r2} the structure is collinear and perpendicular to the c axis. The transition at T_{r1} is sharp and at T_{r2} it is smooth. In $ErCo_3$, the Co magnetic moments tend to be along the c axis. The transition between phases I and II is no more observed; it can only be induced by a magnetic field applied perpendicular to the c axis [75 G 1], see Fig. 239. These are a consequence of the local anisotropy of the sites.

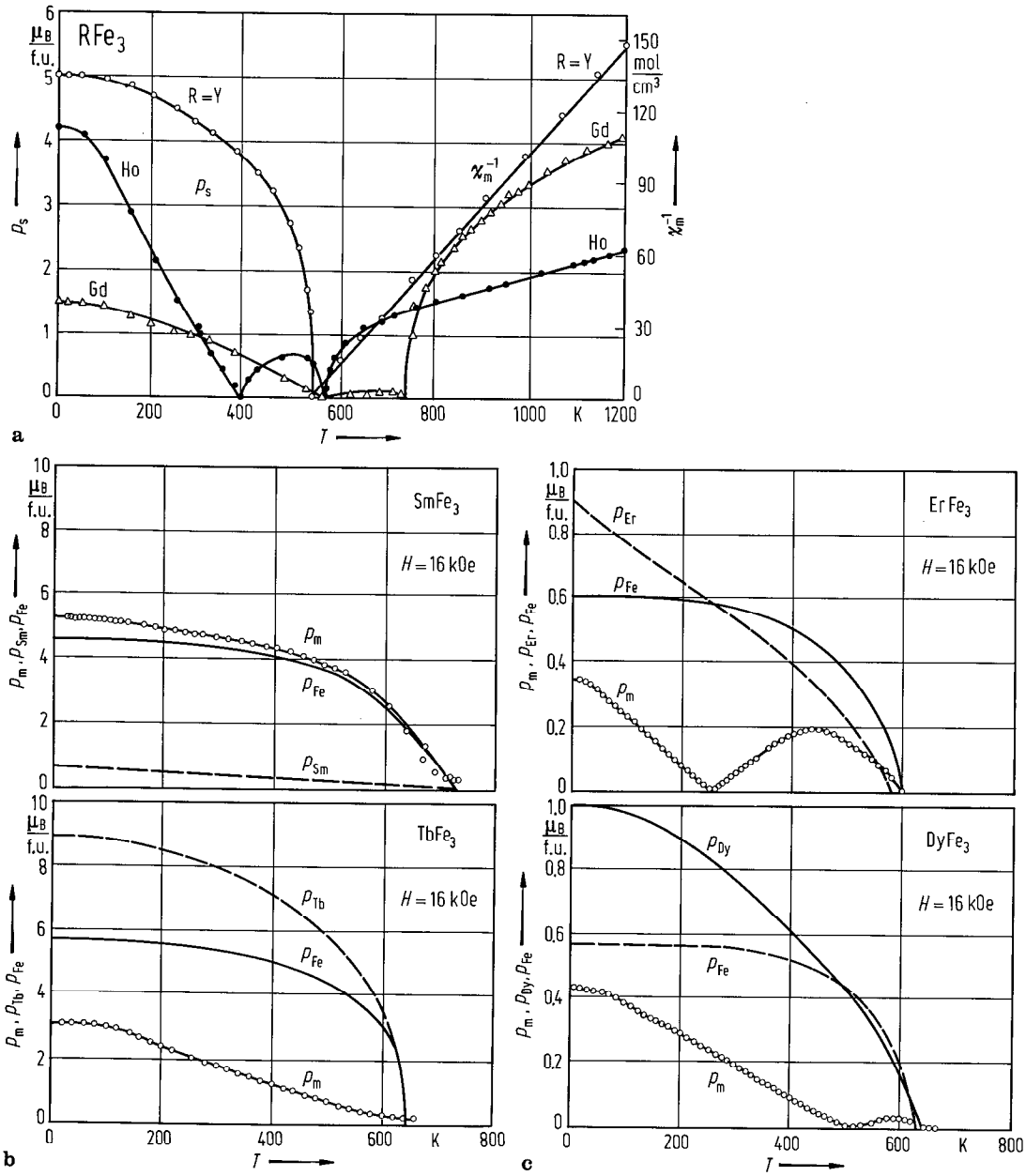

Fig. 235. (a) Temperature dependence of the spontaneous magnetizations for YFe_3, $GdFe_3$ [69 G 1], $HoFe_3$ [73 S 5] and reciprocal magnetic susceptibilities for YFe_3 [70 B 8], $GdFe_3$ [73 B 16] and $HoFe_3$ [73 S 5]. (b) Thermal variation of magnetizations at 16 kOe in $SmFe_3$ and $TbFe_3$ compounds [82 H 2]. The values of sublattice magnetizations calculated by using a two sublattices molecular field model are also plotted. (c) Thermal variation of magnetizations at 16 kOe in $DyFe_3$ and $ErFe_3$ compounds [82 H 2]. The values of sublattice magnetizations calculated by using a two-sublattices molecular field model are also plotted.

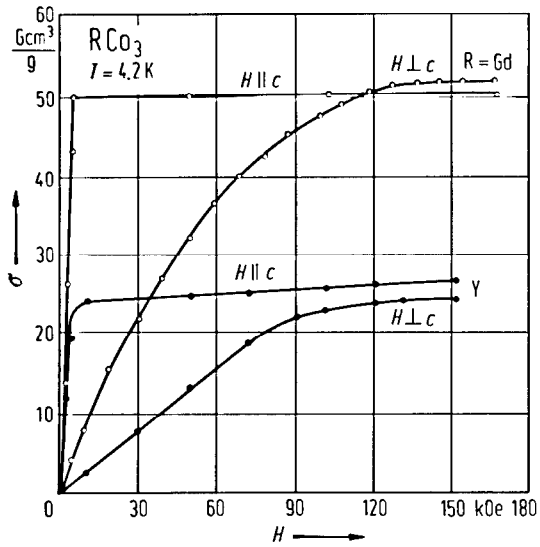

Fig. 236. Magnetization isotherms at 4.2 K for $GdCo_3$ and YCo_3 compounds. In both compounds the trigonal axis is the easy axis of magnetization. The anisotropy of YCo_3 magnetization is 8.6%. For $GdCo_3$, the saturation magnetization in the direction perpendicular to the trigonal axis is higher than that along this axis. The anisotropy of the magnetization as compared to Co (3.2%) is negative reflecting the ferrimagnetic ordering of this compound [87 B 1].

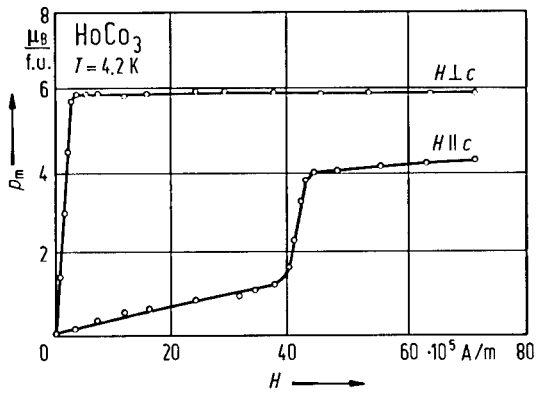

Fig. 237. Magnetization isotherms in $HoCo_3$ single crystal at 4.2 K [82 S 10].

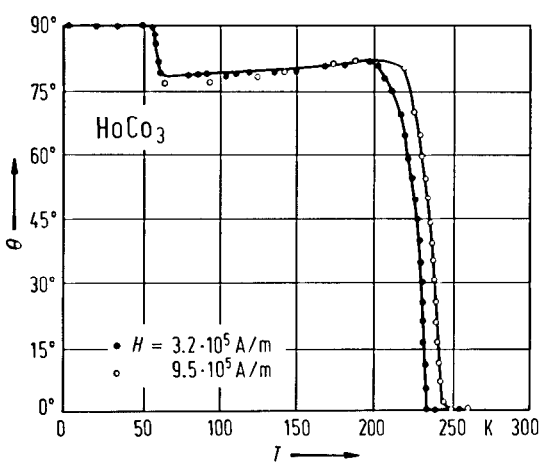

Fig. 238. Thermal variation of the angle between the easy axis of magnetization and the c axis of $HoCo_3$ single crystal in $H = 3.2 \cdot 10^5$ A m^{-1} (4 kOe) and $H = 9.5 \cdot 10^5$ A m^{-1} ($\cong$ 12 kOe) [82 S 10].

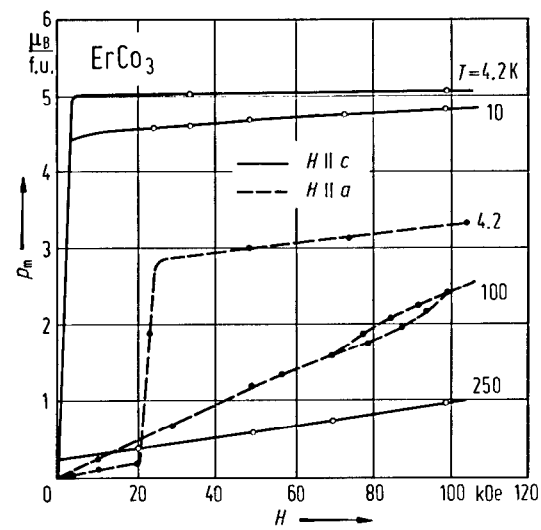

Fig. 239. Magnetization isotherms of $ErCo_3$ compound. Below T_C, the easy direction of magnetization is always along the c axis. A magnetic field applied in the basal plane induces a transition similar to that observed in $ErFe_3$. The critical field increases with temperature and a large hysteresis is associated with this transition [82 D 4].

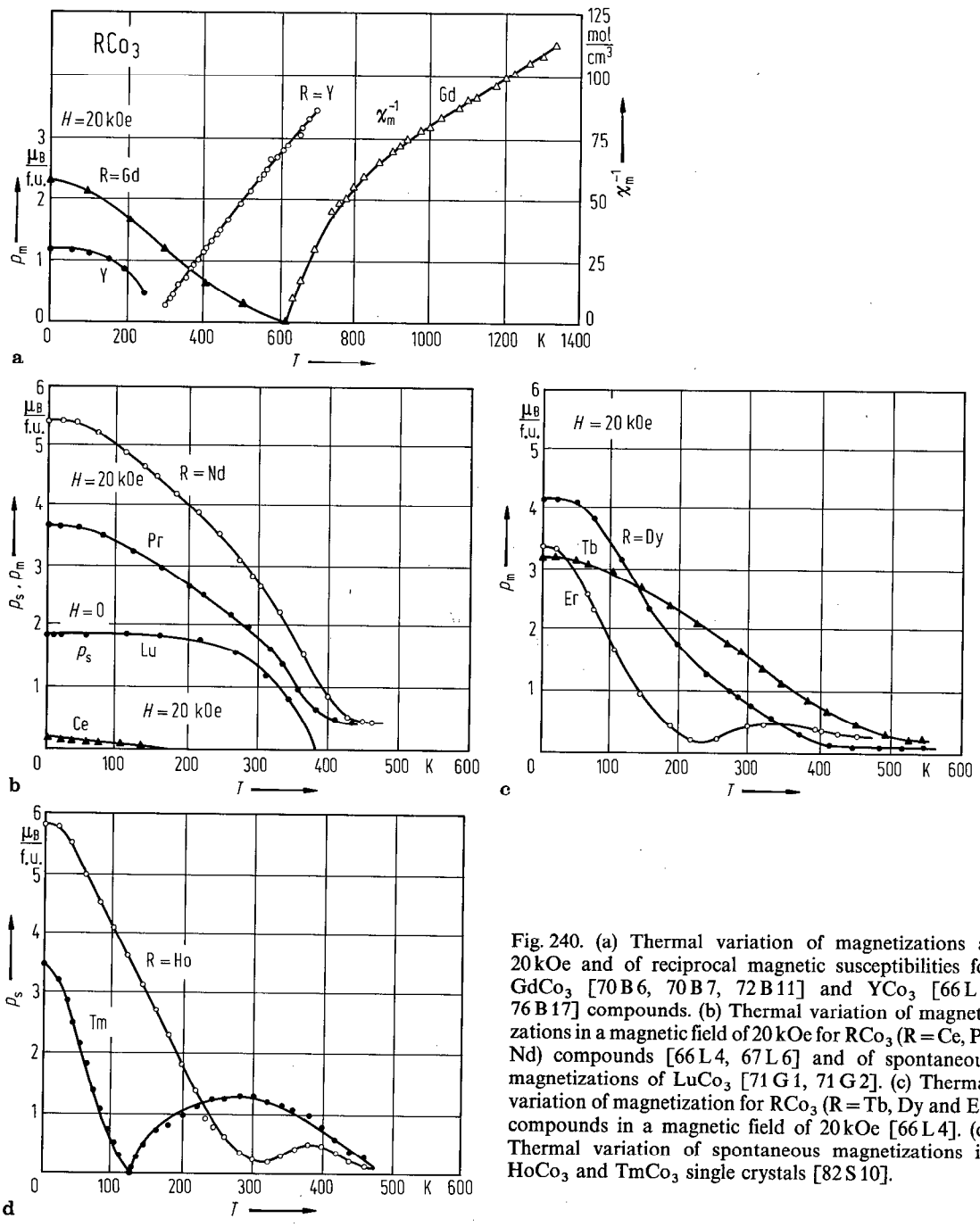

Fig. 240. (a) Thermal variation of magnetizations at 20 kOe and of reciprocal magnetic susceptibilities for $GdCo_3$ [70 B 6, 70 B 7, 72 B 11] and YCo_3 [66 L 4, 76 B 17] compounds. (b) Thermal variation of magnetizations in a magnetic field of 20 kOe for RCo_3 (R = Ce, Pr, Nd) compounds [66 L 4, 67 L 6] and of spontaneous magnetizations of $LuCo_3$ [71 G 1, 71 G 2]. (c) Thermal variation of magnetization for RCo_3 (R = Tb, Dy and Er) compounds in a magnetic field of 20 kOe [66 L 4]. (d) Thermal variation of spontaneous magnetizations in $HoCo_3$ and $TmCo_3$ single crystals [82 S 10].

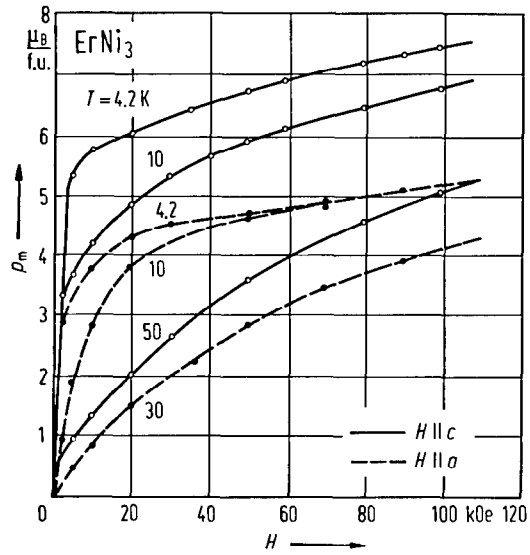

Fig. 241. Magnetization isotherms of $ErNi_3$ along the c and a axis. At 4.2 K a spontaneous magnetization is observed along c axis and in the basal plane. At zero field, the resultant magnetic moment is therefore in an intermediate direction between c axis and basal plane. At 10 K the magnetization is parallel to the c axis [82 D 4].

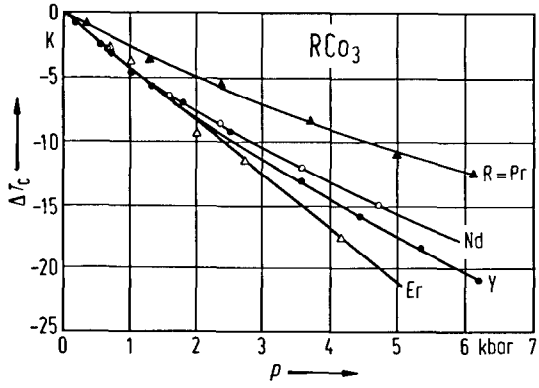

Fig. 243. Pressure dependence of the Curie temperatures for RCo_3 (R = Pr, Nd, Er and Y) compounds [69 B 2]. For $ErFe_3$ see [74 B 8]. For $GdNi_3$ and $TbNi_3$, values $dT_C/dp = -0.10$ K/kbar and -0.02, respectively, were obtained [75 P 4].

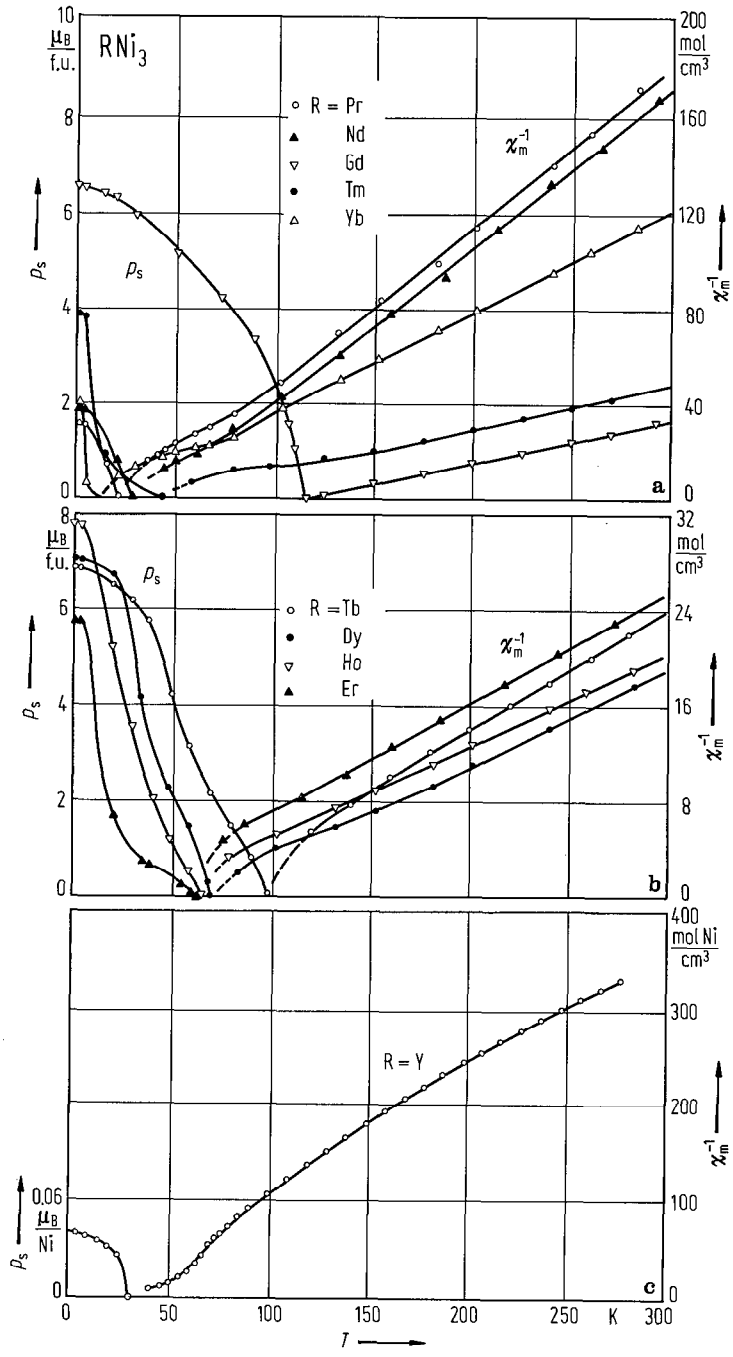

Fig. 242. (a) Thermal variation of spontaneous magnetizations and reciprocal magnetic susceptibilities for (a) $PrNi_3$, $NdNi_3$, $GdNi_3$, $TmNi_3$ and $YbNi_3$ [69 P 1]. (b) $TbNi_3$, $DyNi_3$, $HoNi_3$ and $ErNi_3$ [69 P 1]. (c) YNi_3 [80 G 5].

Table 55a. Magnetic properties of RFe_3 compounds.

	T_C(K)								p_s(μ_B/f.u.)					Paramagnetic behaviour
	71 B 18	71 G 3	73 B 6 72 B 5	73 N 3	73 K 17	74 N 8	75 A 6	82 H 2	71 G 3	73 B 6 72 B 5	73 N 3	82 H 2	83 P 14	70 B 8, 73 B 16 73 S 5
$SmFe_3$	650							655				5.32		
$GdFe_3$	725	733				728		728	2.0			1.62		χ^{-1} vs. T nonlinear
$TbFe_3$	655						643	648				3.19		
$DyFe_3$	605		631	612	609			602		4.6	4.08	4.29	4.25	
$HoFe_3$	575		570	565		570	577	565		4.4	4.30	4.59		χ^{-1} vs. T nonlinear
$ErFe_3$	555		546				533	552		2.8		3.42		
$TmFe_3$	535							542				1.47		
YFe_3		539				537	526	537	5.0	5.06		4.88		χ^{-1} vs. T C-W

Table 55c. Magnetic properties of RNi_3 compounds.

	T_C(K)					p_s(μ_B/f.u.)				Paramagnetic behaviour
	68 B 5	67 P 1	72 B 14	73 N 3	75 P 4	68 B 5	67 P 1	72 B 14	73 N 3	69 P 1, 72 B 14
$LaNi_3$										
$CeNi_3$										
$PrNi_3$		20					1.57			see Fig. 242(a)
$NdNi_3$		27					1.88			see Fig. 242(a)
$SmNi_3$		85					0.33			
$GdNi_3$		116	118		115		6.55	6.50		see Fig. 242(a)
$TbNi_3$		98			100		6.84			see Fig. 242(b)
$DyNi_3$		69		66			7.00		7.10	see Fig. 242(b)
$HoNi_3$		66		65			7.84		8.54	see Fig. 242(b)
$ErNi_3$	64	62				6.08	5.77			see Fig. 242(b)
$TmNi_3$		43					3.86			see Fig. 242(a)
$YbNi_3$		10					2.00			see Fig. 242(a)
YNi_3		33			33		0.16			see Fig. 242(c)

Table 55b. Magnetic properties of RCo_3 compounds.

	T_C(K)						p_s(μ_B/f.u.)								Par. beh.
	67 L 6	70 B 6	71 G 1, 71 G 2	73 N 3	77 b 1	82 S 10	67 L 6	70 B 6, 76 B 17	71 G 1, 71 G 2	73 N 3	77 b 1	81 M 2	82 S 10	85 Y 4	70 B 7, 72 B 11, 76 B 17
$CeCo_3$	78						0.2								
$PrCo_3$	349						3.8								
$NdCo_3$	395						5.6								
$SmCo_3$											3.1				
$GdCo_3$	612	611					2.2	2.3				2.85			χ^{-1} vs. T non-linear
$TbCo_3$	506						3.4								
$DyCo_3$	450			455			4.3			7.78		5.25			
$HoCo_3$	418			418		440	5.6			5.30		5.78	5.9		
$ErCo_3$	401					401	3.9					4.31			
$TmCo_3$	370						3.0						3.4		
$YbCo_3$					330							3.17			
$LuCo_3$			362						1.80						
YCo_3	301		310				1.4	2.10	1.62					2.28	χ^{-1} vs. T C-W

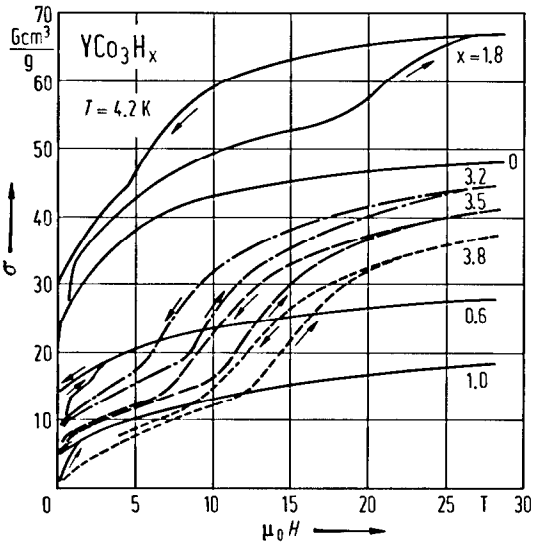

Fig. 244. Magnetization isotherms for YCo_3H_x at 4.2 K [86 G 4]. The shape of these curves is quite sensitive to hydrogen absorption. In the β- or γ-hydride a metamagnetic transition with hysteresis is observed. The magnetization abruptly increases at the critical field H_c in increasing fields and returns to the low value at H_c^* in decreasing fields.

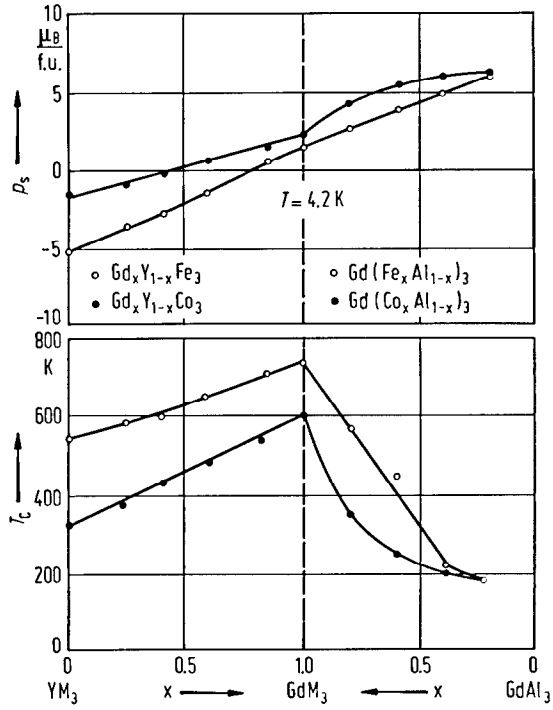

Fig. 245. Composition dependence of the saturation magnetization at 4.2 K and Curie temperatures in $Gd_xY_{1-x}Fe_3$ [82 B 12], $Gd_xY_{1-x}Co_3$ [81 B 13, 81 S 5], $Gd(Fe_xAl_{1-x})_3$ [82 B 12, 83 B 9] and $Gd(Co_xAl_{1-x})_3$ [82 B 13] compounds.

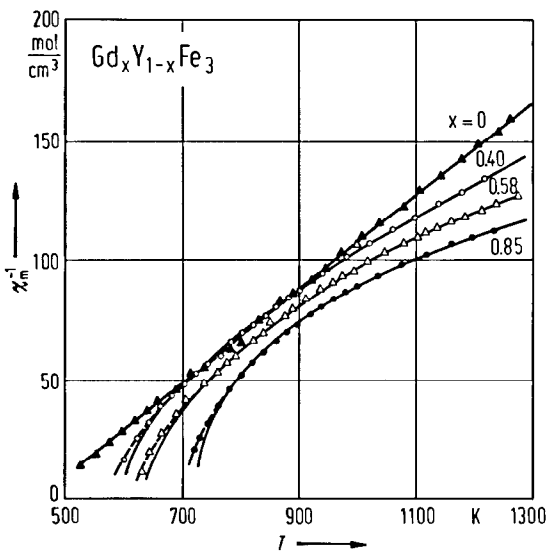

Fig. 246. Thermal variation of reciprocal magnetic susceptibilities for $Gd_xY_{1-x}Fe_3$ compounds [81 B 12, 82 B 12]. Similar dependences were obtained for $Gd(Fe_xAl_{1-x})_3$ [82 B 12, 83 B 9], $Gd_xY_{1-x}Co_3$ [81 B 13, 81 S 5] and $Gd(Co_xAl_{1-x})_3$ [82 B 13] compounds.

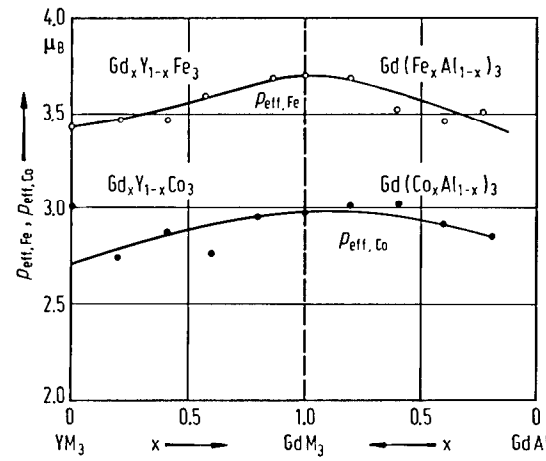

Fig. 247. Composition dependence of the effective Fe and Co magnetic moments determined in $Gd_xY_{1-x}Fe_3$ [82 B 12], $Gd_xY_{1-x}Co_3$ [81 B 13, 81 S 5], $Gd(Fe_xAl_{1-x})_3$ [82 B 12, 83 B 9] and $Gd(Co_xAl_{1-x})_3$ [82 B 13] compounds. These were obtained according to the addition law of magnetic susceptibilities, supposing that the Curie constants of R^{3+} ions are given by the free-ion values.

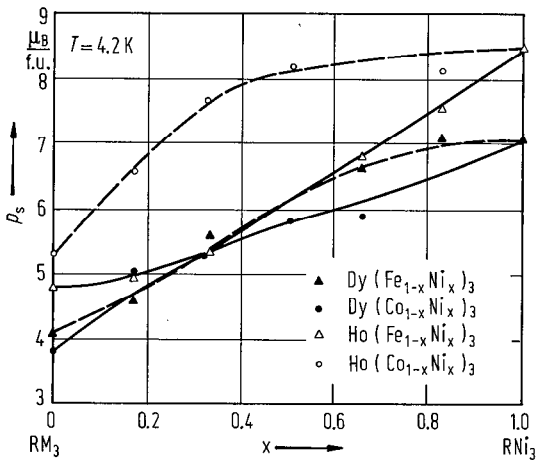

Fig. 248. Composition dependence of the saturation magnetization at 4.2 K in $R(Fe_{1-x}Ni_x)_3$ and $R(Co_{1-x}Ni_x)_3$ compounds with R = Dy and Ho [73 N 3].

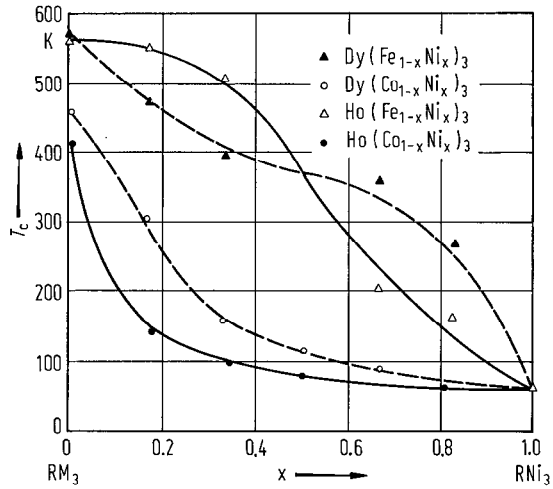

Fig. 249. Composition dependence of the Curie temperatures in $R(Fe_{1-x}Ni_x)_3$ and $R(Co_{1-x}Ni_x)_3$ compounds with R = Dy and Ho [73 N 3].

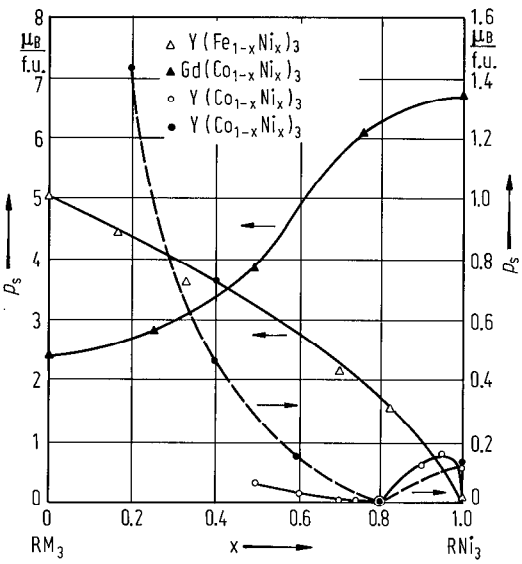

Fig. 250. Composition dependence of the saturation magnetizations at 4.2 K in $Gd(Co_{1-x}Ni_x)_3$ [77 E 3], $Y(Co_{1-x}Ni_x)_3$, open circles [80 H 8], $Y(Co_{1-x}Ni_x)_3$, solid circles [72 P 2], $Y(Fe_{1-x}Ni_x)_3$ [78 M 16], and for YFe_3 [71 G 3].

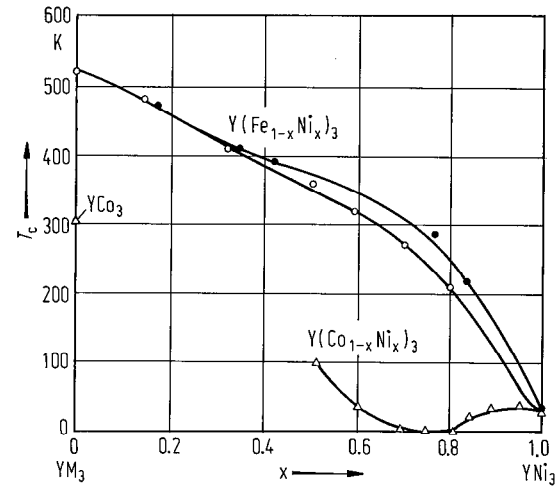

Fig. 251. Composition dependence of the Curie temperatures for $Y(Fe_{1-x}Ni_x)_3$, open circles [76 A 5], solid circles [78 M 16], and $Y(Co_{1-x}Ni_x)_3$ [80 H 8] compounds. The value determined for YCo_3 is also given [66 L 4].

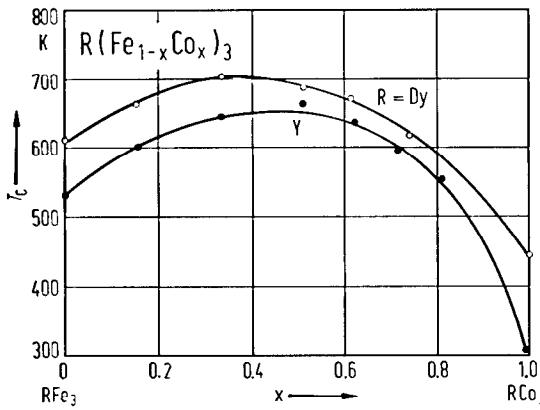

Fig. 252. Composition dependence of the Curie temperatures in $Dy(Fe_{1-x}Co_x)_3$ and $Y(Fe_{1-x}Co_x)_3$ compounds [75 A 5].

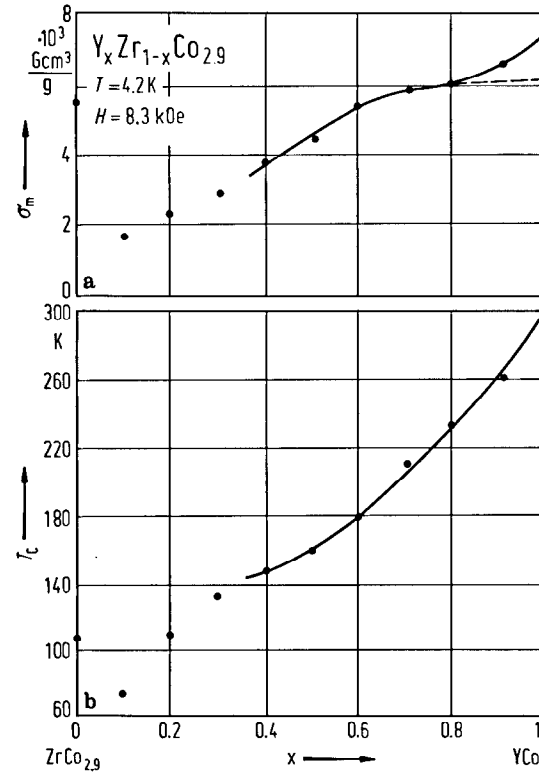

Fig. 253. Composition dependence of (a) the magnetizations at 4.2 K and 8.3 kOe. (b) Curie temperatures in $Y_xZr_{1-x}Co_{2.9}$ compounds [86 K 5]. The crystal structure is of rhombohedral ($R\bar{3}m$)-type for $x > 0.3$, four slabs hexagonal in the composition range $0.3 > x \geqq 0.1$, and cubic ($Fd3m$) at $x = 0$. The magnetizations and Curie temperatures decrease when decreasing Y content for $x > 0.1$. $ZrCo_{2.9}$ has a larger magnetic moment and higher Curie temperature than $Y_{0.1}Zr_{0.9}Co_{2.9}$ compound. The change of magnetic moments may be analysed in correlation with crystal structure formation (see subsect. 2.4.1.2).

For magnetic properties see also:

RM_3 M = Fe, Co, Ni [83 G 3]

RFe_3 [71 B 18, 71 B 19, 73 N 5, 75 F 2, 75 N 5, 79 B 2, 88 R 1]; R = Sm, Gd, Tb, Dy, Ho, Er, Tm, Y [82 H 2]; R = Dy, Ho, Er, Y [73 B 6]; R = Tb, Er, Tm [83 M 2]; R = Gd, Tb, Dy, Ho, Er, Tm [74 N 8]; R = Sm, Gd, Tb, Dy, Ho, Th [76 V 1]; R = Tb [76 O 2]; R = Dy [82 B 1, 83 P 14]; R = Ho [72 B 5, 73 B 9, 73 S 5, 81 L 2*]; R = Er [72 B 15, 73 B 9, 75 N 6, 77 B 14(T), 77 D 2, 81 K 5, 82 D 4, 86 B 1, 86 B 2]; R = Y [70 B 8, 76 B 18, 83 M 6(T), 84 V 1, 85 R 9]; R = Th [72 B 15]

RCo_3 [72 B 8]; R = Ce, Pr, Nd, Gd, Tb, Dy, Ho, Er, Tm, Y [66 L 4, 67 L 6, 70 S 2]; R = Pr, Nd, Er, Y [69 B 2]; R = Ho, Tm [82 S 10*]; R = Ce [80 B 16]; R = Er [75 G 1, 82 D 4, 86 B 2]; R = Y [83 M 6(T)]

RNi_3 [84 L 4]; R = Pr, Nd, Sm, Gd, Tb, Dy, Ho, Er, Tm, Yb [67 P 1]; R = Gd, Tb, Y [75 P 4]; R = Ce [80 B 16]; R = Gd [86 A 2]; R = Tb [87 H 1*]; R = Er [82 D 4, 86 B 2]; R = Y [79 B 19, 80 G 4, 80 G 5, 83 G 3, 85 L 3(T)]

RM_3H_x RFe_3H_x, R = Gd, Dy, Ho [76 M 3, 78 W 3]; R = Tb, Er, Tm [83 M 2]; R = Dy [80 N 3, 83 S 7]; R = Y [76 B 18]; R = Th [77 V 1]

RCo_3H_x, R = Er, Tm [81 M 2]; R = Y [85 Y 4, 85 Y 5, 85 Y 6, 86 G 4]; R = Ce [80 B 16]

RNi_3H_x, R = Y [79 B 19]; R = Ce [80 B 16]

$(R'R'')M_3$	$(R_{0.1}Th_{0.9})Fe_3$, R = La, Pr, Lu, Y [73 K 17]; (GdY)Fe_3 [78 K 14, 81 B 12, 82 B 12, 83 B 9, 84 B 9, 85 S 11]; (GdTh)Fe_3 [72 G 10]; (TbY)Fe_3 [86 S 16]; (DyY)Fe_3 [85 P 6, 85 P 7]; (DyTh)Fe_3 [73 K 17]; (ThLu)Fe_3 [73 K 16]; (ThY)Fe_3 [73 K 16, 76 N 5]; (ErTh)Fe_3 [78 N 2] (NdHo)Co_3 [72 N 1]; (GdY)Co_3 [81 B 13, 81 S 5, 83 B 9, 84 B 9, 85 S 11]; (TbY)Co_3 [84 B 2]; (HoY)Co_3 [86 S 8]; (YZr)$Co_{2.9}$ [87 K 5]; (GdY)Ni_3 [84 A 1]
$(R'R'')M_3H_x$	(YZr)$Co_{2.9}H_x$ [87 K 5]; (ErTh)Fe_3H_x [78 N 2]
$R(M'M'')_3$	$Dy(FeCo)_3$ [73 N 2, 75 A 5]; $Ho(FeCo)_3$ [73 N 2]; $Y(FeCo)_3$ [75 A 5, 75 T 1]; $Gd(FeNi)_3$ [71 G 5]; $Dy(FeNi)_3$ [73 N 3, 74 T 2]; $Ho(FeNi)_3$ [73 N 3]; $Y(FeNi)_3$ [78 M 16]; $Gd(FeAl)_3$ [82 B 12, 83 B 8, 83 B 9, 84 B 9, 85 S 11]; $Tb(FeAl)_3$ [73 O 6]; $Dy(FeAl)_3$ [77 O 1, 77 O 5, 83 P 13, 85 P 8] $Gd(CoNi)_3$ [71 G 5, 77 E 3]; $Dy(CoNi)_3$ [73 N 3]; $Ho(CoNi)_3$ [73 N 3]; $Y(CoNi)_3$ [72 P 2, 75 T 1, 80 H 8, 81 H 3]; $Gd(CoAl)_3$ [82 B 13, 83 B 8, 83 B 9, 84 B 9, 85 S 11]; $R(NiM)_3$, M = Fe, Co [31 N 2]
$R(M'M'')_3H_x$	$Zr(CrFeHo_{0.8})H_x$, M = Mn, Fe, Co, Ni [84 H 7]

Neutron diffraction

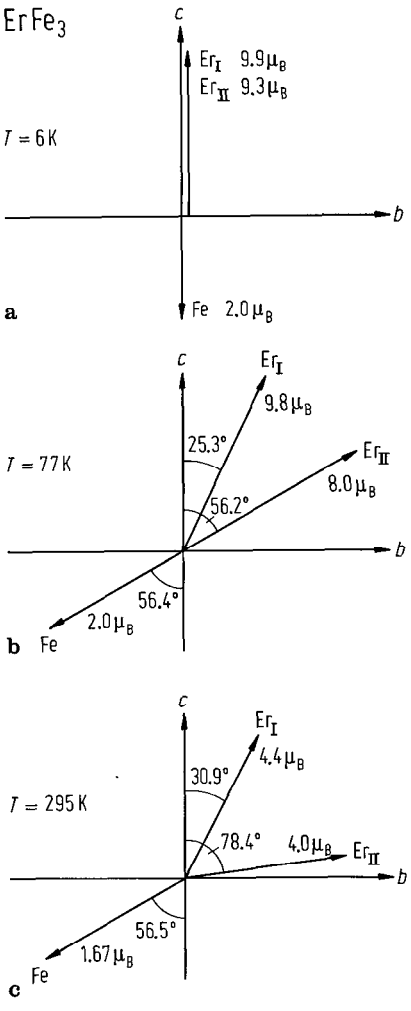

Fig. 254. Magnetic moments in $ErFe_3$, at 6, 77 and 295 K [77 D 1], see Table 56.

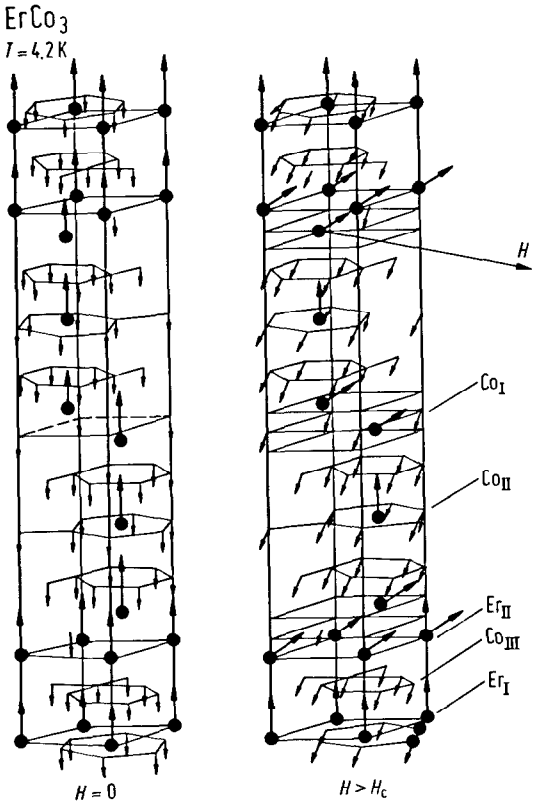

Fig. 255. Magnetic structure of $ErCo_3$ at 4.2 K with a magnetic field applied perpendicular to the c axis: (a) $H=0$, (b) $H>H_c$ [75 G 1].

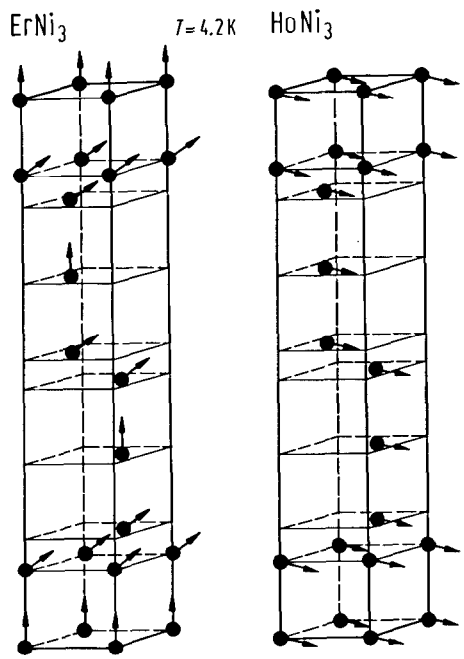

Fig. 256. Magnetic structure of $ErNi_3$ and $HoNi_3$ compounds at 4.2 K [71 P 1].

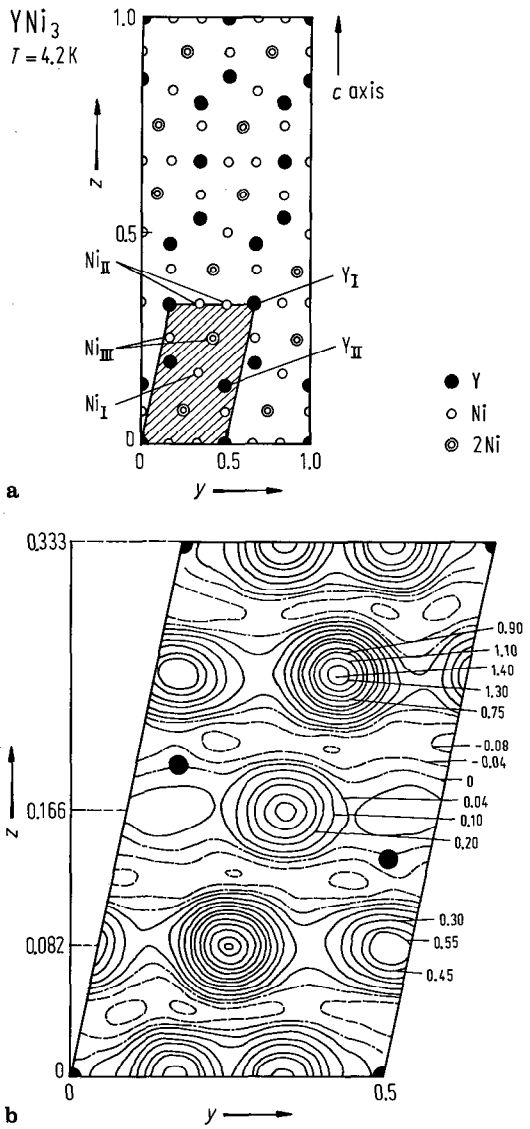

Fig. 257. Projection of the magnetic moment density of YNi_3 at 4.2 K in a plane perpendicular to the *a* axis of hexagonal cell: (a) schematic projection of the atoms of the orthohexagonal cell, (b) magnetic density map: representation of the unit cell of the magnetic density. Contours are in $10^{-1}\ \mu_B/Å^2$, full lines are positive contours, dashed lines are negative contours and the dot-dashed lines are zero contours [80 G 5, 81 G 5].

Table 56. Magnetic moments of R and M atoms in RM_3 compounds and the direction of moments determined by neutron diffraction measurements.

	T K	p_{RI} μ_B	φ_{RI} [1]	p_{RII} μ_B	φ_{RII} [1]	p_{MI} μ_B	p_{MII} μ_B	p_{MIII} μ_B	φ_M [1]	Ref.
$TbFe_3$	77	8.10	90°	7.58	90°	−1.49	−1.25	−1.85	90°	79 J 3
	295	6.55	90°	6.38	90°	−1.02	−1.32	−1.75	90°	
$DyFe_3$	4.2	9.8(2)	71.8(5)°	9.6(2)	51.5(5)°		−2.2(2)		253.6(5)°	86 J 2
	295	6.9(2)	83.9(5)°	6.5(2)	62.0(5)°		−1.9(2)		257.8(5)°	
$HoFe_3$	77	8.76	90°	9.01	90°	−1.88	−1.43	−1.61	90°	73 S 5
	297	5.07	90°	5.42	90°	−1.49	−1.12	−1.52	90°	
$ErFe_3$	6	9.9(10)	0°	9.3(5)	0°		−2.0(2)		0°	77 D 1
	77	9.8(15)	25.3(30)°	8.0(7)	56.2(35)°		−2.0(5)		56.4(80)°	
	295	4.4(11)	30.9(50)°	4.0(5)	78.4(60)°		−1.67(30)		56.5(110)°	
$ErFe_3$ [2]	300	3.6(2)	46°	4.1(2)	81°		−1.70(10)		62°	81 K 5
$ErFe_2Ni$	4.2	8.93	14(3)°	8.71	60(10)°	−2.45	−2.45	−2.45	180°	87 T 4
	77	8.03	7(1)°	6.44	22(3)°	−2.30	−2.30	−2.30	180°	
$ErFe_{1.5}Ni_{1.5}$	77	9.20	0°	6.20	0°	−2.21	−2.21	−2.21	180°	87 T 4
$ErFeNi_2$	77	8.57	0°	4.38	0°	−2.07	−2.07	−2.07	180°	87 T 4
$PrCo_3$	4.2	2.4(2)	0°	2.4(2)	0°	1.2(4)	0.9(2)	0.9(2)	0°	70 S 2,
	295	1.1(1)	0°	1.1(1)	0°	0.3(1)	0.5(1)	0.5(1)	0°	72 Y 3
$NdCo_3$	4.2	2.4(4)	0°	2.4(4)	0°	0.9(3)	1.2(2)	1.2(2)	0°	70 S 2,
	295	0.8(1)	90°	0.8(1)	90°	0.7(5)	0.7(2)	0.7(2)	90°	72 Y 3
$TbCo_3$	4.2	8.5(5)	90°	8.1(4)	90°	−1.9(6)	−0.9(4)	−1.2(3)	90°	70 S 2, 71 P 1
	295	5.7(2)	90°	4.8(2)	90°	−1.3(2)	−1.4(2)	−1.1(1)	90°	72 Y 3
$DyCo_3$	4.2	≅ 10.0 [3]	36.9°	≅ 10.0 [3]	36.9°		−1.2		211°	87 J 2
	295	6.4		6.4			−0.6		192.6°	
$DyCo_3$	80	6.6(3)	90°	6.0(4)	90°		−0.8(2)		90°	70 S 2,
	300	4.0(2)	90°	3.0(3)	90°		−0.7(2)		90°	75 Y 1
$HoCo_3$	4.2	10.0(4)	90°	9.6(3)	90°	−1.8(4)	−1.2(3)	−1.2(3)	90°	70 S 2,
	295	2.1(2)	0°	3.4(2)	0°	−0.4(2)	−1.5(3)	−0.6(1)	0°	72 Y 3
$ErCo_3$	4.2	8.2(8)	0°	7.5(6)	0°	−2.0(6)	−1.1(7)	−1.3(2)	0°	72 Y 3, 75 G 1
$TmCo_3$	4.2	6.7(3)	0°	6.2(4)	0°	−0.90(40)	−1.50(40)	−0.5(3)	0°	76 I 1
YCo_3	4.2	–	–	–	–	0.55(3)	0.79(4)	0.04(1)	0°	69 K 5

Table 56 (continued)

	T K	p_{RI} μ_B	φ_{RI} [1]	p_{RII} μ_B	φ_{RII} [1]	p_{MI} μ_B	p_{MII} μ_B	p_{MIII} μ_B	φ_M [1]	Ref.
$PrNi_3$	4.2	0.5(3)	0°	0.5(3)	0°					71 R 8
$NdNi_3$	4.2		57(3)°		20(3)°					71 R 8
$TbNi_3$	4.2		70(5)°		34(5)°					71 R 8
$DyNi_3$	4.2	9.8(5)	80(5)°	8.0(5)	30(5)°					71 R 8
$HoNi_3$	4.2	9.3(3)	90°	7.9(2)	90°					71 P 1, 71 R 8
$ErNi_3$	4.2	8.5(5)	10(4)°	7.5(5)	60(5)°					71 R 8
$ErNi_3$	4.2	8.5(8)	[4]	7.5(5)	[4]	$\cong 0$	$\cong 0$	$\cong 0$		82 D 4
$TmNi_3$	4.2		0°		0°					71 R 8
YNi_3	4.2	–	–	–	–	0.057(3)	0.073(3)	0.065(3)		80 G 5

[1]) φ is the angle between the direction of the magnetic moments and the c axis.
[2]) Determined in the supposition of noncollinearity of magnetic moments.
[3]) Close to free-ion value.
[4]) Noncollinear magnetic structure.

For neutron diffraction studies see also:
RFe_3 R = Tb [79 J 3]; R = Dy [85 J 1, 86 J 2]; R = Ho [73 S 5]; R = Er [77 D 1, 81 K 5, 82 D 4]
RCo_3 R = Pr, Nd, Ho, Tb, Er [70 S 2]; R = Pr, Nd, Tb, Ho, Er [72 Y 3]; R = Tb [76 Y 1, 84 K 3]; R = Dy [75 Y 2, 87 J 2]; R = Er [75 G 1]; R = Tm [76 I 1]; R = Y [69 K 5]
RNi_3 [72 Y 2]; R = Pr, Nd, Tb, Ho, Er, Tm [71 R 8]; R = Ho, Er [71 P 1]; R = Y [80 G 5, 81 G 5]
$R(M'M'')_3$ $Er(FeNi)_3$ [87 T 4]

EPR, FMR

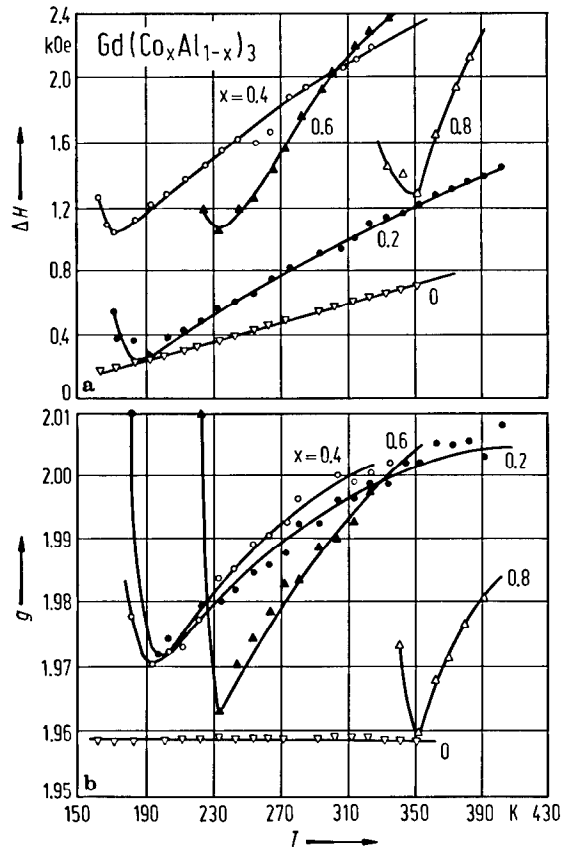

Fig. 258. Thermal variation of (a) the linewidth and (b) g values in some $Gd(Co_xAl_{1-x})_3$ compounds at temperatures greater than the Curie points. In compounds in which Co is nonmagnetic or in $GdAl_3$, the g values and the slope of the linewidth is not temperature-dependent [82 B 13]. A molecular field model was used to analyse the EPR behaviour of the ferrimagnetic compounds. The increase of the slope of the linewidth with transition metal content suggests the gradual opening of the relaxation of conduction electron magnetization to the lattice. The FMR measurements in some RM_3-based compounds show that the g values of Fe and Co are not sensitively modified as compared to those of the pure metals [82 b 1], cf. Fig. 168.

For FMR and EPR studies see also
YCo_3 [86 T 9, 87 T 7]; $GdNi_3$ [80 B 15]
$Gd(FeAl)_3$ [82 b 1, 83 U 2, 84 B 10, 85 B 10] see also Fig. 168
$Gd(CoAl)_3$ [82 b 1, 82 B 13, 83 U 2, 85 B 10]

Mössbauer effect, perturbed angular correlations

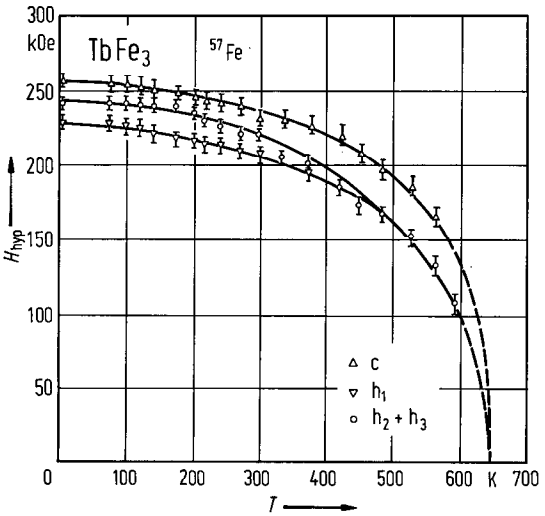

Fig. 259. Temperature dependence of the magnetic hyperfine fields, H_{hyp}, at ^{57}Fe in $TbFe_3$ compound [75 A 4, 75 A 5]. The behaviour of H_{hyp} values obtained for various lattice sites are plotted. The data suggest that the easy axis of magnetization is along the *b* axis at all temperatures.

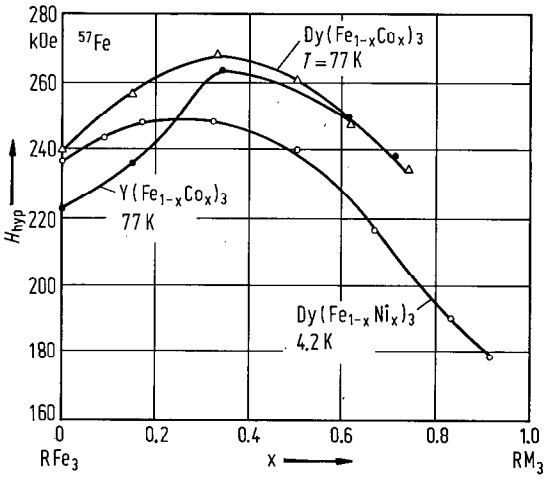

Fig. 260. Composition dependence of the mean magnetic hyperfine fields at ^{57}Fe in $Y(Fe_{1-x}Co_x)_3$, $Dy(Fe_{1-x}Co_x)_3$ at 77 K [75 A 5] and $Dy(Fe_{1-x}Ni_x)_3$ [74 T 2] compounds at 4.2 K.

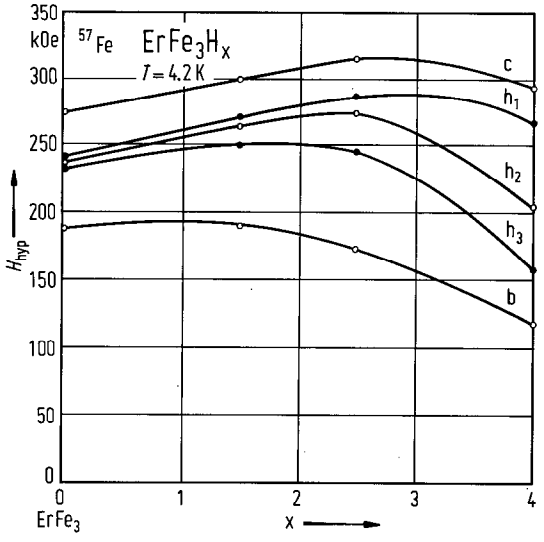

Fig. 261. Variation of the ^{57}Fe magnetic hyperfine fields at 4.2 K with the hydrogen content in $ErFe_3H_x$. An increase of the Fe magnetic moment on absorption of hydrogen up to x = 2.7 is evidenced [79 N 3].

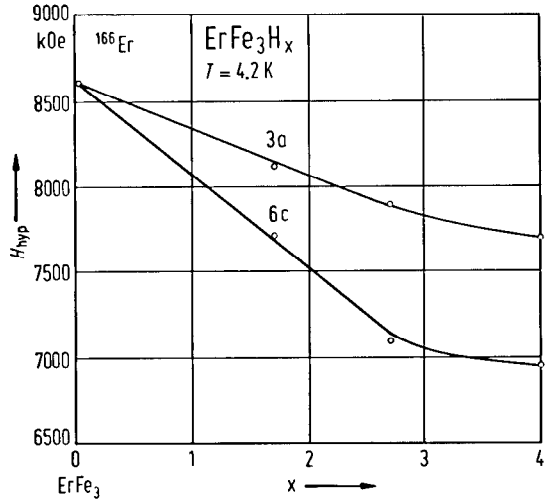

Fig. 262. Variation of the ^{166}Er magnetic hyperfine field H_{hyp} at 4.2 K with the hydrogen concentration in $ErFe_3H_x$ hydrides for positions 3a and 6c of the space group $R\bar{3}m$. The decrease of the H_{hyp} values may arise from changes in the contribution of conduction electron polarization and/or the decrease in the magnetic interaction relative to the crystal field interaction, as hydrogen is added [79 N 3].

Table 57. Magnetic hyperfine fields at ^{57}Fe in RFe_3 compounds.

	T K	H_{hyp} (kOe) at sites					Ref.
		h_1	h_2	h_3	c	b	
$SmFe_3$	393	202	202	202	226	149	76 V 1
$GdFe_3$	4.2	259	236	236	249	233	76 V 1
$TbFe_3$	77	242.5	242.5	228.5	245.5	245	75 A 6
$TbFe_3$	295	228	228	211	232	225	76 V 1
$DyFe_3$	77	237.5	233.5	234.5	245	249	75 A 6
$DyFe_3$	295	218	218	208	223	218	76 V 1
$HoFe_3$	77	237.5	224.5	224.5	246.5	253	75 A 6
$HoFe_3$	79	253	229	229	240	231	76 V 1
$HoFe_3$	138	235	235	226	242	238	76 V 1
$ErFe_3$ [1])	4.2	246	239	239	244	230	78 G 5
$ErFe_3$	77	235.5	235.5	235.5	227.5	253.5	75 A 6
YFe_3	4.2	229	235	235	242	222	78 G 5
YFe_3	77	227.6	227.7	227.5	219.5	229.5	75 A 6

[1]) Extrapolated hyperfine fields at $T=0$ K for *ab*-axis anisotropy of $ErFe_3$.

Table 58. Easy direction of magnetization of RFe_3 compounds determined by Mössbauer effect studies.

	$SmFe_3$	$GdFe_3$	$TbFe_3$	$DyFe_3$	$HoFe_3$	$ErFe_3$	YFe_3
Easy direction [76 V 1]	*c* axis	$T=4.2$ K *a* axis ——— basal plane	*b* axis	basal plane ——— $T=295$ K *b* axis	$T<100$ K *a* axis ——— $T>100$ K *b* axis	$T<50$ K *c* axis ——— $T>50$ K *b* axis	*b* axis
Easy direction [74 A 2, 75 A 6, 75 A 4]	–	–	*b* axis	$T=77$ K *ac* plane	$T<85$ K *a* axis ——— $T>85$ K *b* axis	*c* axis	*b* axis
Stevens factor α_j	+	0	–	–	–	+	0

Table 59. Hyperfine parameters at ^{161}Dy nuclei in Dy-3d transition metal compounds at 4.2 K.

	$IS\,h^{-1}$ MHz	$g_N\mu_N H_{hyp}h^{-1}$ MHz	$e^2qQ/4h$ MHz	Ref.
Dy	84(4) [2]	831(3)	642(5)	
$DyMn_2$	34.1 [3]	1.00(2)$H_{hyp,fi}$ [1]		66 N 1
$DyFe_2$	78.6(50) [2]	923.6(35)	697.8(75)	84 P 16
$DyFe_2$	78(4) [2]	926.6(40)	696.7(70)	74 B 7
$DyFe_2$	35.2 [3]	1.14(2)$H_{hyp,fi}$ [1]		66 N 1
$DyFe_3$	73.8(50) [2]	927.2(40)	695(7)	84 P 16
$DyFe_3$	79(5) [2]	918.9(45)	683.3(70)	74 B 7
Dy_2Fe_{17}	64.7(50) [2]	915.8(36)	685.4(120)	84 P 16
Dy_2Fe_{17}	65(5) [2]	911.5(65)	665(10)	74 B 7
$DyCo_2$	80(4) [2]	870.2(45)	698.3(70)	74 B 7
$DyCo_2$	35.2 [3]	1.04(2)$H_{hyp,fi}$ [1]	698.3	66 N 1
$DyCo_3$		883	677.6	75 Y 1
$DyCo_5$	10.3 [3]	1.05(2)$H_{hyp,fi}$ [1]		66 N 1
Dy_2Co_{17}	66(5) [2]	873.2(40)	679.6(80)	74 B 7
DyNi	30 [3]	1.02(2)$H_{hyp,fi}$ [1]		66 N 1
$DyNi_2$	93(4) [2]	836.5(40)	676.7(70)	74 B 7
$DyNi_2$	39.3 [3]	0.985(2)$H_{hyp,fi}$ [1]		66 N 1
$DyNi_5$	13.4 [3]			66 N 1
$DyAl_2$	49(4) [2]	844.5(40)	702.7	74 B 7

[1]) Hyperfine field of free Dy^{3+} ion, $H_{hyp,fi}$.
[2]) Relative to ^{161}Tb source obtained by irradiation of $^{160}GdFe_3$.
[3]) Relative to Gd_2O_3 neutron irradiated, containing 90% ^{160}Gd.

Table 60a. Results derived from ^{155}Gd Mössbauer spectra ($T = 4.2$ K). f_A: recoilless fraction, H_{hyp}: magnetic hyperfine field [1]), V_{zz}: electric field gradient, IS: isomer shift with respect to the ^{155}EuPd source, θ: angle between the direction of the hyperfine field and the local symmetry axis [2]). Standard deviations are given in parantheses [77 T 6].

	f_A	Local symmetry								Ref.
		(nearly) cubic				trigonal (hexagonal)				
	%	$\mu_0 H_{hyp}$ T	V_{zz} 10^{17} V cm^{-2}	IS μm s^{-1}	θ	$\mu_0 H_{hyp}$ T	V_{zz} 10^{17} V cm^{-2}	IS μm s^{-1}	θ	
$GdMn_2$	9.2(5)	(−)10.1(1)	–	107(2)	–					67 G 1
$GdFe_2$	11.0(5)	+43.48(6)	–	67(1)	–					67 G 1
$GdCo_2$	8.8(4)	+ 3.5(3)	–	43(2)	–					77 A 6
$GdNi_2$	8.5(4)	−12.0(5)	–	8(2)	–					77 T 6
$GdFe_3$	12.8(6)	(+)39.9(1)	−1.52(9)	67(2)	81(2)°	(+)22.4(2)	+ 8.31(6)	262(7)	90(2)°	77 T 6
$GdCo_3$	11.2(6)	(+)11.7(4)	−1.60(7)	70(2)	0(5)°	(+) 4.7(3)	+ 8.58(4)	222(3)	32(6)°	77 T 6
$GdNi_3$	11.1(6)	(−) 8.0(3)	−0.74(3)	62(2)	0(2)°	(−)13.8(2)	+10.59(3)	208(4)	22(2)°	77 T 6
$GdCo_5$	10.1(5)					(+) 4.3(1)	+ 8.18(1)	230(10)	0° (not varied)	77 T 6
$GdNi_5$	9.2(5)					−23.4(1)	+ 8.18(2)	256(3)	0(3)°	76 V 4
Gd_2Co_{17}	13.9(7)					(+) 8.0(1)	+ 4.26(1)	234(3)	62(2)°	77 T 6
		tetragonal symmetry								
Gd_6Mn_{23}	9.6(5)	(+)29.1(5)	+10.3(2)	140(5)	60(2)°					

[1]) Signs given without parenthesis have been determined experimentally. Signs indicated in parenthesis are hypotetical.

[2]) Values of θ given in the table are the results of least-squares fits when θ was varied independently for nonequivalent sites (with the exception of $GdCo_5$ where the determination of θ was not possible because of the small value of H_{hyp}). For $GdFe_3$ a good fit was obtained with the restriction $\theta = 90°$ for both sites, and for $GdCo_3$ with $\theta = 0°$ for both sites. For $GdNi_3$ such a constraint led to a significant increase of the χ^2 value.

Landolt-Börnstein New Series III/19d2

Table 60b. Results derived from ^{61}Ni Mössbauer spectra (T = 4.2 K). For definition of symbols see (a). Because of the small hyperfine splitting only average values for all sites can be obtained [77 T 6].

	f_A %	$\mu_0 H_{hyp}$ T	V_{zz}^{eff} 10^{17} V cm^{-2}	$\langle IS \rangle$ μm s^{-1}
$GdNi_2$	9(1)	2.41(5)	−2.0(3)	22(5)
$GdNi_3$	9(1)	1.67(4)	−0.4(4)	7(3)
$GdNi_5$	10(1)	1.32(10)	+1.6(8)	5(3)

For nuclear γ-resonance studies see also:

^{57}Fe RFe_3, R = Gd, Tb, Dy, Ho, Er [75 A 6]; R = Gd, Tb, Dy, Ho, Er, Th, Y [75 V 2]; R = Sm, Gd, Tb, Dy, Ho, Th [76 V 1]; R = Tb, Er, Y [75 A 4]; R = Er, Y, Th [78 G 5]; R = Dy [79 J 4, 82 B 1]; R = Ho [74 A 2]; R = Er [75 V 1, 77 G 14]; R = Y [73 F 6, 75 V 1, 76 O 10]
RFe_3H_x, R = Er [79 N 3, 81 D 1, 81 D 2]
$(ErGd)Fe_3$ [85 D 2]
$Dy(FeCo)_3$ [75 A 5]; $Er(FeCo)_3$ [79 G 13]; $Y(FeCo)_3$ [75 A 5]
$Dy(FeNi)_3$ [73 T 2, 74 T 2, 75 C 7, 76 A 5, 77 C 8]; $Y(FeNi)_3$ [76 A 5]

^{61}Ni $GdNi_3$ [77 T 6]; $Dy(FeNi)_3$ [77 C 8]

^{155}Gd GdM_3, M = Fe, Co, Ni [77 T 6]

^{161}Dy $DyFe_3$ [74 B 7, 82 B 1, 84 P 16, 85 P 11]; $DyCo_3$ [74 B 7, 75 Y 1, 76 C 2, 77 C 3]; $DyNi_3$ [71 Y 1]; $Dy(FeNi)_3$ [75 C 7]

^{169}Tm $TmCo_3$, $TmNi_3$ [83 N 6]

For perturbed angular correlations see

^{181}Ta in YFe_3 [86 B 10]

^{156}Gd in $TbFe_3$, $TbCo_3$ [87 S 14, 87 S 15]

NMR

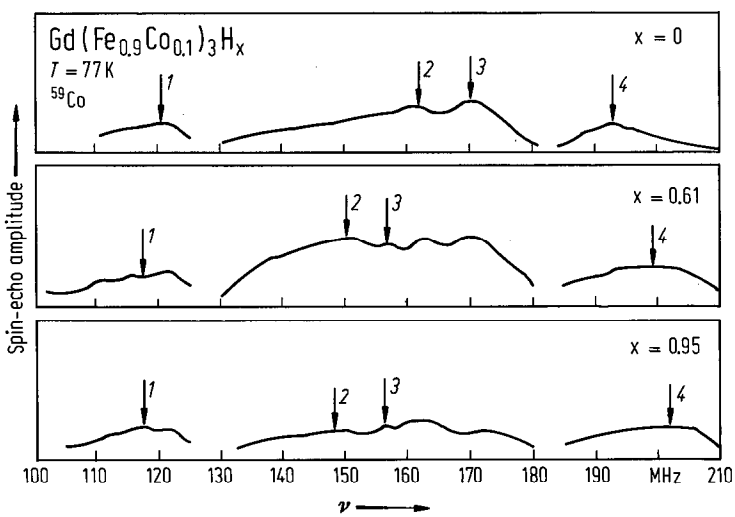

Fig. 263. ^{59}Co spectra (peaks are labelled) determined by NMR measurements at 77 K in $Gd(Fe_{0.9}Co_{0.1})_3H_x$. The magnetic hyperfine fields at ^{59}Co nuclei in Co_I (*1*) and Co_{III} (*2, 3*) sites decrease and the hyperfine field at ^{59}Co nuclei in Co_{II} (*4*) sites increases upon hydrogen absorption [83 F 10].

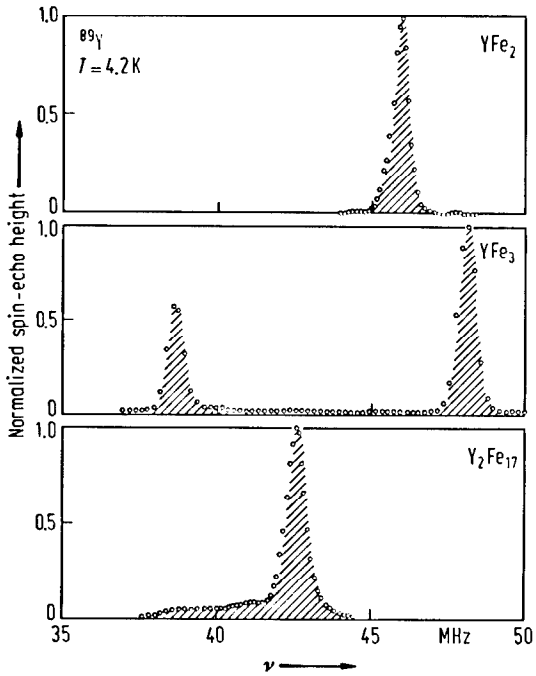

Fig. 264. ^{89}Y spin-echo spectra of YFe_2, YFe_3 and Y_2Fe_{17} compounds at 4.2 K [73 O 9]. The echo height factor has been corrected for the Boltzmann factor and the spectrometer sensitivity.

Table 61. Transferred hyperfine fields determined by ^{89}Y NMR at 4.2 K in Y–Fe and Y–Co compounds.

	Crystallographic site	H_{hyp} kOe	Ref.
YFe_2	8a	−220	73 O 9
		217	
YFe_3	3a	(−)185	73 O 9
	6c	−231	
Y_2Fe_{17}	6c	−204	73 O 9
YCo_3	3a	− 83.6	76 F 1
	6c	−112.2	
Y_2Co_7	$6c_1$	− 83.6	76 F 1
	$6c_2$	−111.8	
YCo_5	a	−101.7	76 F 1
Y_2Co_{17}	2b	− 89.8	76 F 1
	2d	− 99.8	
	6c	− 87.4	

For NMR studies see also:

^{1}H	$LaNi_3H_x$ [79 H 9, 80 H 10]
^{57}Fe	$GdFe_3$ [74 N 10]; YFe_3 [74 N 10, 83 V 2]
	$(GdY)Fe_3$ [75 N 8]
^{59}Co	$NdCo_3$ [75 S 10]; YCo_3 [77 F 3]; $Y(CoNi)_3$ [85 Y 10]
	$Gd(FeCo)_3H_x$, $Y(FeCo)_3H_x$ [83 F 10]
^{89}Y	YFe_3 [73 O 9, 83 R 6*, 83 V 2, 83 V 3, 85 R 9, 85 V 2]; YCo_3 [76 F 1, 77 F 3]
	$(GdY)Fe_3$ [75 N 8]; $Y(FeCo)_3$ [87 O 6]; $Y(FeAl)_3$ [87 O 6]
^{139}La	$(Gd_{0.9}La_{0.1})Ni_3$ [77 D 7]
^{143}Nd, ^{145}Nd	$NdCo_3$ [75 S 10, 77 S 14]
^{155}Gd, ^{157}Gd	$(GdY)Fe_3$ [75 N 8]
^{159}Tb	$TbFe_3$ [85 D 3]

Anisotropy, magnetostriction

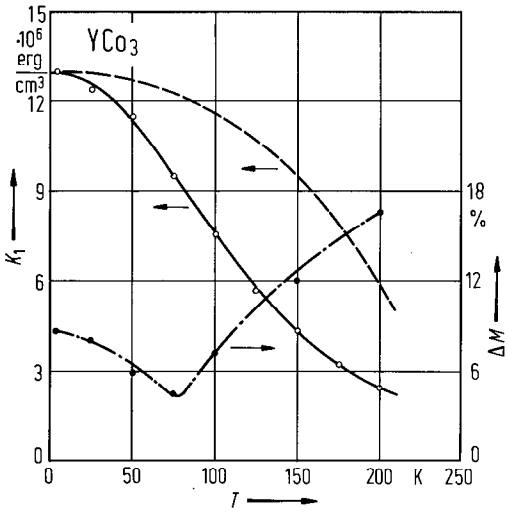

Fig. 265. Thermal variation of the anisotropy constant K_1 and of anisotropy of the magnetization, ΔM, for YCo_3. The K_1 values decrease more rapidly than the values predicted by the theoretical model [66 C 1] plotted by broken line. The thermal variation of the magnetization of this compound is due to both the transverse and longitudinal spin fluctuations, the latter being characteristic of itinerant magnetism close to the instability conditions. The anisotropy of the magnetization has a minimum at $T \cong 70$ K reflecting the effects of both contributions. The first contribution increases with temperature and it corresponds to the anisotropy of the transverse thermal fluctuations of the magnetization. The second contribution is intrinsic and is due to the spin-orbit coupling which induces an angular dependence of the opposed spin energy spectra shift. This shift is affected by the longitudinal fluctuations of magnetization, whose amplitude increases with temperature. Thus, the intrinsic contribution to the magnetization anisotropy decreases when increasing the temperature [87 B 1].

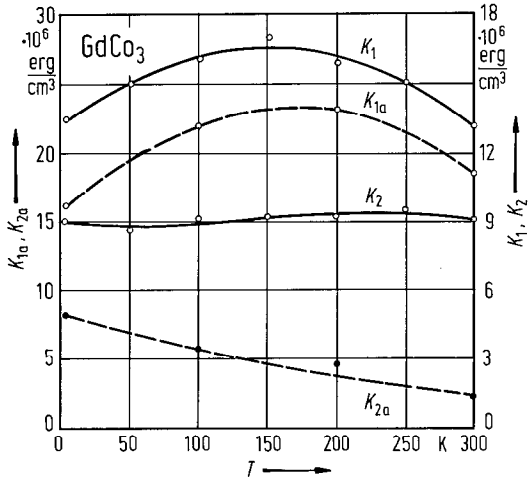

Fig. 266. Thermal variation of the anisotropy constants K_1 and K_2 for $GdCo_3$ compound. The K_1 values show a maximum at $T \cong 150$ K, while the K_2 (positive) ones are only weakly temperature-dependent. Considering the deformation of the ferrimagnetic configuration of $GdCo_3$ under the action of an external magnetic field, the K_{1a} and K_{2a} values of Co were also determined. The presence of Gd–Co exchange interactions deplaces the Co magnetic moments from the great instability conditions (characteristic of YCo_3), but the proportion of the unstable magnetic moments is important. A considerable fraction of the magnetization is induced by the exchange interactions. At low temperatures the K_{1a} values are reduced by the longitudinal fluctuations of the magnetization. The great K_2 values are due to the gradual quenching of these fluctuations by the magnetic field. By increasing the temperature, the effect of longitudinal fluctuations diminishes and the anisotropy constants have a thermal variation only due to transverse fluctuations of the magnetization [87 B 1].

For anisotropy see also

RFe_3 R = Ho [81 L 2*]; R = Er [86 B 2]; RCo_3, R = Tb, Dy [85 S 7]; R = Er [86 B 2]; R = Y [84 K 1, 86 T 9, 87 T 7]; RNi_3, R = Er [86 B 2]

$R(M'M'')_3$ [81 K 4]; $Er(FeNi)_3$ [87 T 4]; $Er(FeCo)_3$ [79 G 13]

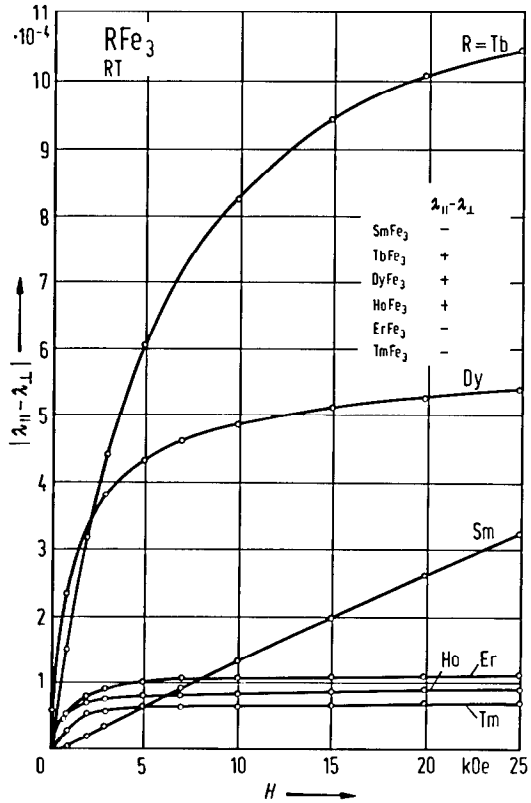

Fig. 267. Room-temperature magnetostriction of RFe_3 polycrystals as function of the external magnetic field [78 A 1, 80 c 1].

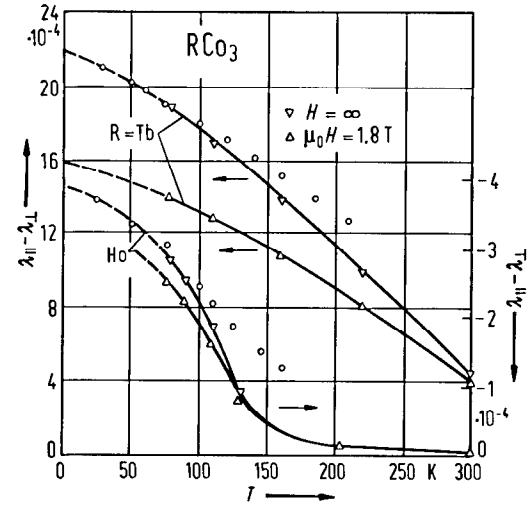

Fig. 268. Temperature variation of magnetostriction for $TbCo_3$ and $HoCo_3$. The dashed curves are extrapolations to 0 K. The predictions of the one-ion model, $\lambda(T) = \lambda(0)\hat{I}_{5/2}[\mathscr{L}^{-1}(m_R)]$, are also plotted [80 P 5]. The data suggest that the rare-earth ion is the main source of the magnetostriction in these compounds.

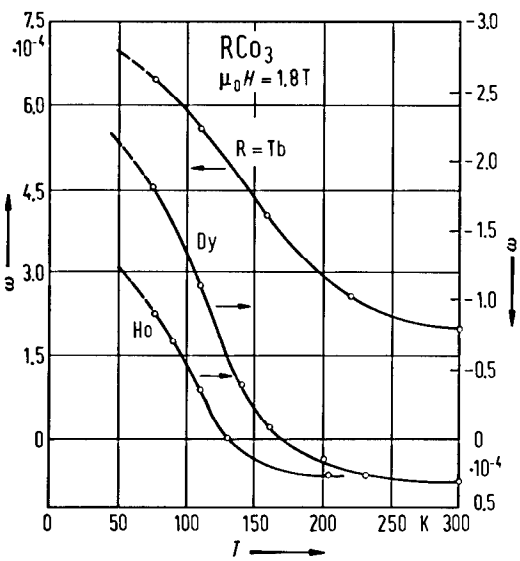

Fig. 269. Temperature dependence of volume strain ω for (a) $TbCo_3$, (b) $DyCo_3$ and (c) $HoCo_3$ at an applied field of 1.8 T [80 P 5]. Large volume strains are associated with the volume dependence of the magnetic anisotropy and are strongly temperature-dependent.

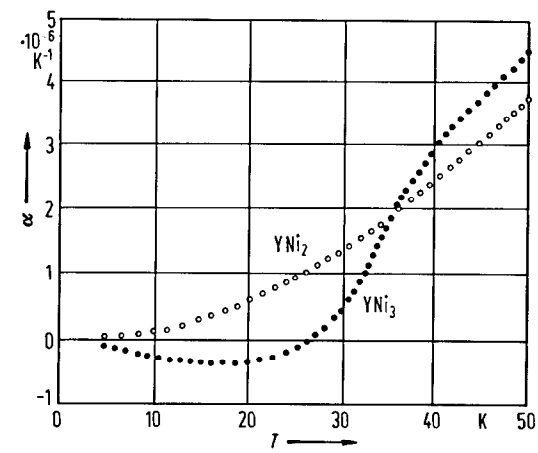

Fig. 270. Thermal expansion coefficients of YNi_3 and YNi_2 compounds [82 P 2]. YNi_2 has a smoothly increasing positive expansion typical of nonmagnetic metals. At low temperatures, YNi_3 exhibits a negative thermal expansion coefficient α. Near T_C, α becomes positive and it increases rapidly until, at above 40 K, it levels off to a normal nonmagnetic behaviour.

For magnetostriction see also
RFe_3 [80 c 1]; R = Tb [72 C 6, 74 C 2, 74 C 3]; RCo_3, R = Gd, Tb, Dy, Ho, Er [80 P 5]; R = Tb, Y [72 C 5]; RNi_3, R = Y [82 P 2]; $(GdY)Fe_3$ [78 K 14]

For ΔE effect see
$TbFe_3$ [74 C 2, 74 C 3]

Domain structure, magnetization processes

For magnetization processes see
$DyFe_3$ [84 P 14]; $DyCo_3$ [72 T 3]

For domain structure
$DyFe_3$ [83 P 14, 84 P 14]

Transport properties

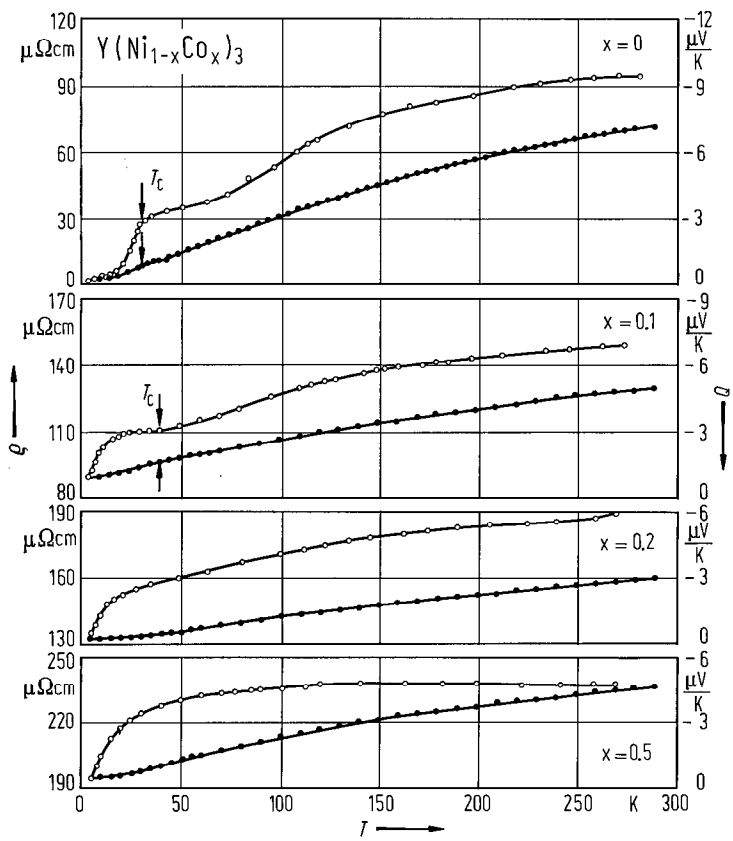

Fig. 271. Temperature dependence of the electrical resistivity (solid circles) and thermopower (open circles) in $Y(Ni_{1-x}Co_x)_3$ compounds. The Curie temperatures T_C are also evidenced [80 H 8].

For resistivity and thermopower studies see also
$(TbY)Co_3$ [84 B 2]; $(YTh)Fe_3$ [79 N 2]
$Y(CoNi)_3$ [80 H 8, 81 H 3]

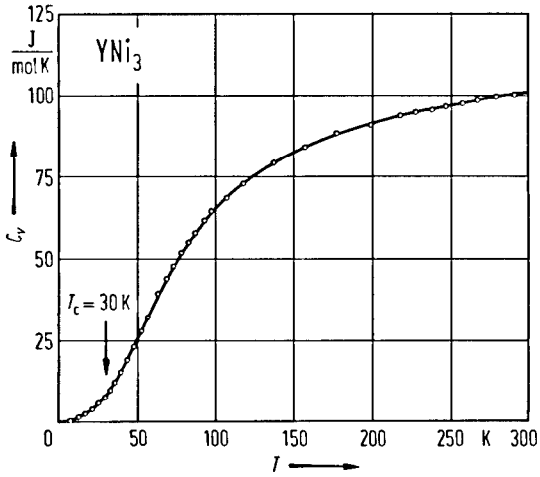

Fig. 272. Thermal variation of the specific heat of YNi_3. Circles are the experimental values. The full line corresponds to the electronic and lattice contributions. No anomaly is observed at the Curie temperature. $T_C = 30$ K. From these data a Debye temperature $\Theta_D = 335$ K and an electronic specific heat coefficient $\gamma = 31$ mJ mol^{-1} K^{-2} were obtained [80 G 5].

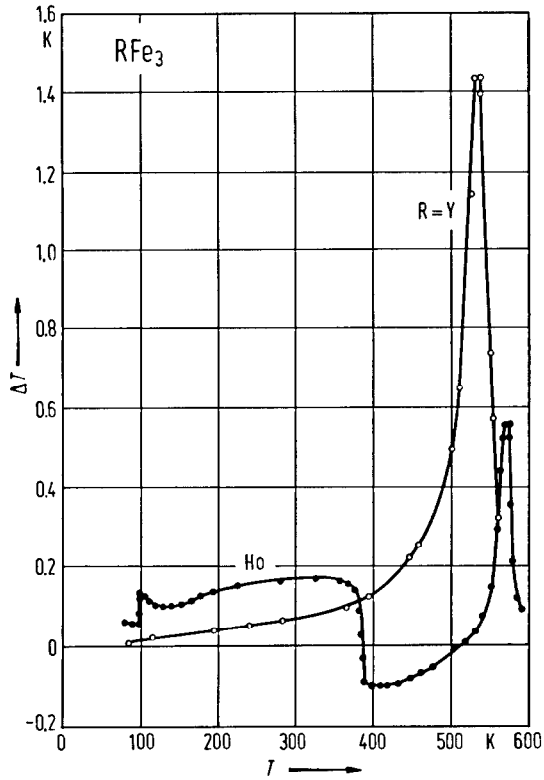

Fig. 273. Temperature dependence of the magnetocaloric effect in YFe_3 and $HoFe_3$ compounds in a magnetic field of 15.8 kOe. A change in sign of the magnetocaloric effect is observed around the compensation temperature of $HoFe_3$ [73 N 6].

For specific heat studies see also
DyM_3, M = Fe, Co, Ni [74 N 4]; $LaNi_3$ [74 N 4]; YNi_3 [80 G 5]
Y(Th)Fe_3 [75 K 7]
Y$(FeNi)_3$ [78 M 16]

For magnetocaloric effects see
RFe_3, R = Ho,Y [73 N 6, 74 N 9]

Spectral studies

X-ray absorption spectra
RCo_3, R = Gd, Tb, Dy [80 H 7]; R = Y [73 B 8]

Photoemission spectra
$GdFe_3$ [79 A 6]; YFe_3 [85 H 2]

L_{III} absorption
$CeNi_3$ [85 P 1]

2.4.2.14 R_2M_7 compounds

Crystal structure, lattice parameters

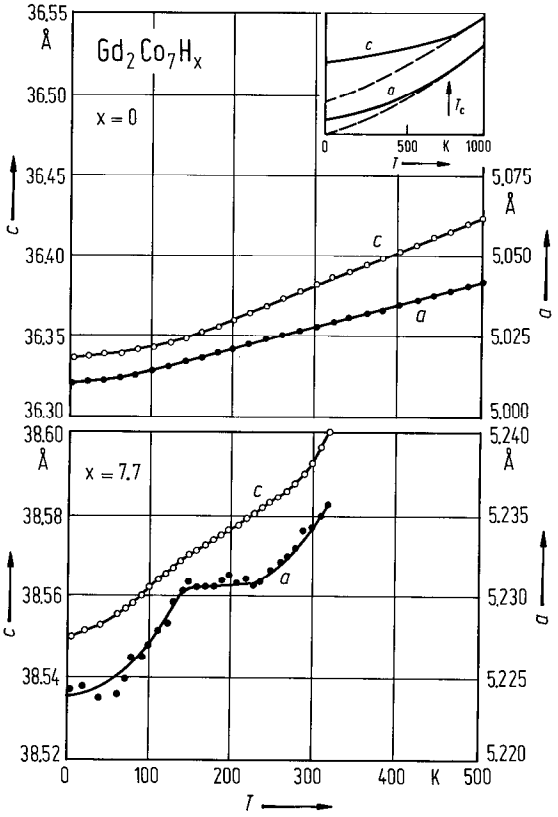

Fig. 275. Temperature dependence of the lattice parameters a and c for Gd_2Co_7 and $Gd_2Co_7H_{7.7}$. The inset shows the temperature dependence of a and c for Gd_2Co_7 over a wider temperature range. The appearance of the anomalies in case of $Gd_2Co_7H_{7.7}$ may be due not only to magnetic phase transitions but also to hydrogen ordering processes or its redistribution among the interstitial sites [85 A 13].

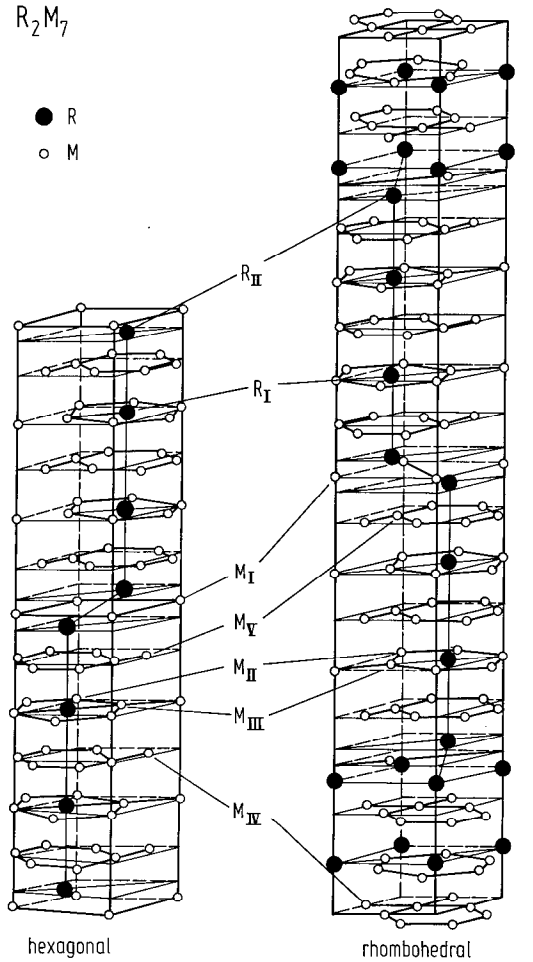

Fig. 274. Crystal structures of R_2M_7 compounds. These crystallize both in a hexagonal-type structure ($P6_3/mmc$-space group) or in a rhombohedral-type structure ($R\bar{3}m$-space group) [69 P 1].

Table 62a. Atomic sites in R_2M_7 compounds, hexagonal $P6_3/mmc$ space group [69 P 1].

Atom	Site	Coordinates
R_I	4f	$\pm(1/3, 2/3, z; 2/3, 1/3, 1/2+z)$, $z=0.040$
R_{II}	4f	$\pm(1/3, 2/3, z; 2/3, 1/3, 1/2+z)$, $z=0.166$
M_I	2a	$(0,0,0; 0,0,1/2)$
M_{II}	4e	$\pm(0,0,z; 0,0,1/2+z)$, $z=0.166$
M_{III}	4f	$\pm(1/3, 2/3, z; 2/3, 1/3, 1/2+z)$, $z=0.833$
M_{IV}	6h	$\pm(x, 2x, 1/4; 2\bar{x}, \bar{x}, 1/4; x, \bar{x}, 1/4)$, $x=0.833$
M_V	12k	$\pm(x, 2x, z; 2\bar{x}, \bar{x}, z; \bar{x}, 2\bar{x}, 1/2+z; 2x, x, 1/2+z, \bar{x}; x, 1/2+z)$

Table 62b. Atomic sites in R_2M_7 compounds, rhombohedral $R\bar{3}m$ space group [69 P 1].

Atom	Site	Coordinates
R_I	6c	$\pm(0,0,z)$, $z=0.055$
R_{II}	6c	$\pm(0,0,z)$, $z=0.149$
Ni_I	3b	$(0,0,1/2)$
Ni_{II}	6c	$\pm(0,0,z)$, $z=0.278$
Ni_{III}	6c	$\pm(0,0,z)$, $z=0.388$
Ni_{IV}	9e	$\pm(1/2, 0, 0; 0, 1/2, 0; 1/2, 1/2, 0)$
Ni_V	18h	$\pm(x, \bar{x}, z; x, 2x, z; 2\bar{x}, \bar{x}, z)$, $x=1/2$, $z=0.111$

The following translations are added (0, 0, 0; 2/3, 1/3, 1/3; 1/3, 2/3, 2/3).

Table 64. Lattice constants and volume expansion ($\Delta V/V$) of R_2M_7 hydrides [1].

	a Å	c_{hex} Å	c_{rh} Å	$\Delta V/V$ %	Ref.
$Ce_2Co_7H_6$	4.949	29.69			80 V 3
$Gd_2Co_7H_{7.7}$	5.234		38.57	15	85 A 13
$Y_2Co_7H_{1.5}$	4.988		37.72		80 V 3
$Y_2Co_7H_2(\beta_L)$ [2]	4.991		37.92		85 Y 6
$Y_2Co_7H_{3.1}(\beta_{II})$ [2]	5.002		38.71		85 Y 6
$Y_2Co_7H_6(\gamma_L)$ [2]	5.142		38.21		85 Y 6
$Y_2Co_7H_6$	5.160		38.18	12.6	83 B 3
$La_2Ni_7H_x$	5.100	31.00		16···23	83 B 10, 84 B 12
$La_2Ni_7H_{10}$	amorphous				76 O 5
$Ce_2Ni_7H_4$	4.920	29.63			80 V 3
$Y_2Ni_7H_x$	4.962		38.38	6.5	84 B 12

[1]) It has been suggested that hydrogen occupies interstitial sites in the lattice [85 Y 6].

[2]) The $\alpha \rightarrow \beta$ transformation involves $\Delta H = -48.5$ kJ/mol H_2 and the $\beta \rightarrow \gamma$ transformation $\Delta H = -38.0$ kJ/mol H_2.

Table 63a. Lattice constants of R_2Co_7 compounds (Å) for both hexagonal and rhombohedral structures.

	65 B 2		67 O 4		70 B 10			73 R 2		83 B 3		85 Y 6	
	a	c_{rh}	a	c_{rh}	a	c_{rh}	c_{hex}	a	c_{hex}	a	c_{rh}	a	c_{rh}
La_2Co_7					5.101	36.69	24.51						
Ce_2Co_7					4.940	36.52	24.46	4.949(2)	24.47(1)				
Pr_2Co_7					5.060	36.52	24.43	5.072(3)	24.51(1)				
Nd_2Co_7					5.059	36.42	24.39	5.063(2)	24.45(1)				
Sm_2Co_7					5.041	36.31	24.33						
Gd_2Co_7	5.024	36.32	5.023(2)	36.29(1)	5.022	36.24	24.19						
Tb_2Co_7	5.003	36.26	5.002(2)	36.21(1)	5.008	36.18							
Dy_2Co_7	4.998	36.22	4.995(2)	36.18(1)	4.992	36.13							
Ho_2Co_7	4.983	36.17	4.979(2)	36.12(1)	4.960	36.07							
Er_2Co_7			4.973(2)	36.11(1)									
Tm_2Co_7			4.965(2)	36.05(1)									
Lu_2Co_7			4.946(2)	35.98(1)									
Y_2Co_7	5.002	36.20	4.998(2)	36.18(1)	5.002	36.15				4.99	36.23	5.003	36.21

Table 63b. Lattice constants of R_2Ni_7 compounds (Å) for both hexagonal and rhombohedral structures.

	59 C 1		67 L 5, 69 P 1			70 B 11			80 V 3			84 B 12		
	a	c_{hex}	a	c_{hex}	c_{rh}	a	c_{hex}	c_{rh}	a	c_{hex}	c_{rh}	a	c_{hex}	c_{rh}
La_2Ni_7						5.058	24.71					5.058	24.71	
Ce_2Ni_7	4.98(2)	24.52(8)	4.93	24.19		4.927	24.45		4.927	24.45				
Pr_2Ni_7			5.01	24.23	36.36	5.015	24.44	36.64						
Nd_2Ni_7			5.00	24.20	36.31	4.983	24.40	36.60						
Sm_2Ni_7						4.969	24.35	36.53						
Gd_2Ni_7			4.96	24.09	36.14	4.953	24.21	36.41						
Tb_2Ni_7			4.94	24.06	36.10	4.948	24.12	36.23						
Dy_2Ni_7			4.93	24.05	36.08	4.928	24.10	36.18						
Ho_2Ni_7			4.92		36.04	4.921		36.09						
Er_2Ni_7			4.91		35.71	4.909		36.07						
Y_2Ni_7			4.94		36.12	4.949		36.23	4.949		36.23	4.947		36.25

For structure and lattice parameters see also

R_2Co_7 [65 B 1, 70 B 10, 71 B 15, 73 B 22]; R = Ce, Pr, Nd, Sm, Gd, Tb, Dy, Ho, Er, Tm, Lu [66 O 2]; R = Gd, Tb, Ho, Y [66 L 4]; R = Gd, Tb, Dy, Ho, Tm, Lu, Y [67 O 4]; R = La, Ce, Pr, Nd, Sm, Gd, Tb, Dy, Ho, Er, Th [70 B 11]; R = La [77 S 15]; R = Pr [77 S 15]; R = Nd [77 S 15]; R = Gd [65 B 2]; R = Y [69 K 5]

R_2Ni_7 [69 P 1, 69 V 1]; R = Ce, Pr, Nd, Gd, Tb, Dy, Ho, Er, Y [67 L 5]; R = La, Ce, Pr, Nd, Sm, Gd, Tb, Dy, Ho, Er, Y [70 B 12]; R = La [83 B 10]; R = Ce [59 C 1, 75 P 8]; R = Gd [75 P 8]; R = Zr [72 E 2]

$R_2M_7H_x$ $Gd_2Co_7H_x$ [85 A 13]; $Y_2Co_7H_x$ [84 B 3, 85 A 14]; $La_2Ni_7H_x$ [83 B 10]; $Y_2Ni_7H_x$ [84 B 12]

For thermal variation of lattice constants see

Th_2Co_7, $Th_2Co_7H_x$ [84 A 13]; $Y_2Co_7H_{6.7}$ [85 A 14]; Tb_2Co_7 [82 A 12]

For hydrogen absorption and desorption see

$R_2M_7H_x$ $R_2Co_7H_x$ [78 G 2, 87 I 3]; $Y_2Co_7H_x$ [85 Y 6]; $La_2Ni_7H_x$ [77 K 6]; $Ce_2Co_7H_x$ [80 B 16]

$(R'R'')_2M_7H_x$ $(YLa)_2Co_7H_x$, $(YGd)_2Co_7H_x$ [87 Y 6]

$R_2(M'M'')_7$ $Y_2(Co,Ni)_7H_x$ [87 Y 6]

Magnetization, Curie temperatures

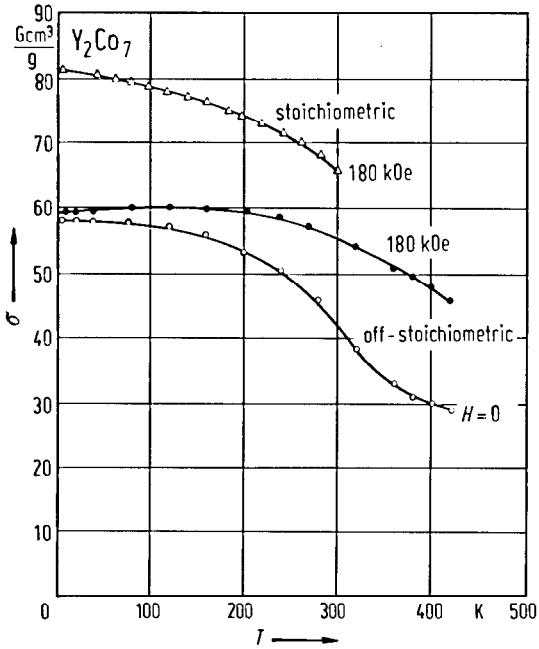

Fig. 277. Thermal variation of the spontaneous magnetization and of the magnetization in a magnetic field of 180 kOe of Y_2Co_7 having lower Co content than the stoichiometric one, as well as of the stoichiometric Y_2Co_7 alloy. In the first case, random substitutions of some Co by Y atoms take place. Consequently, some Co atoms have higher Y coordination. It results a decrease of the magnetic correlations and the Co atoms situated in the neighbourhood of these substitutions are unstable from the magnetic point of view [87 B 1].

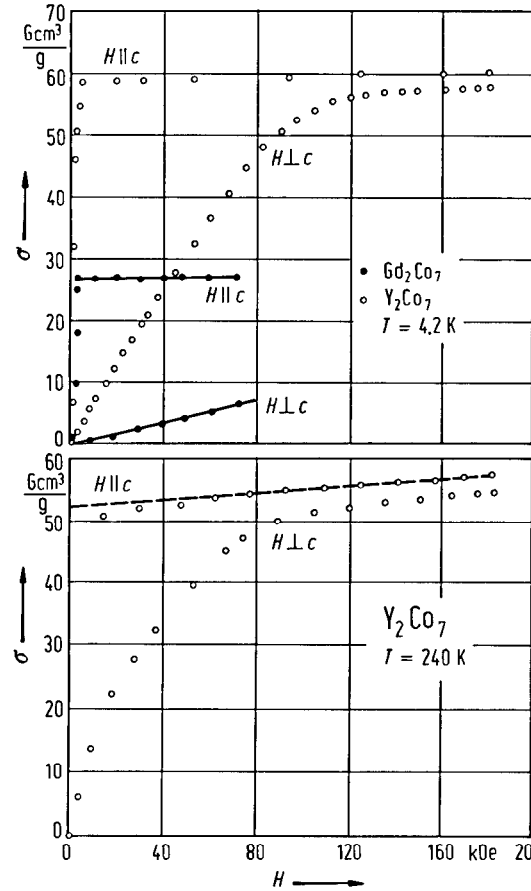

Fig. 276. Magnetization isotherms for Gd_2Co_7 at 4.2 K and Y_2Co_7 having lower Co content than the stoichiometric one, at 4.2 and 240 K, parallel and perpendicular to the *c* axis. For both compounds the *c* axis is the easy axes of magnetization. In case of Y_2Co_7, at 240 K, a field-induced transition to a state with higher magnetization is evidenced. Similar transitions have been observed in the temperature range 160···320 K. For temperatures higher than 320 K this transition is covered by the effects of thermal fluctuations of the magnetization [87 B 1]. For stoichiometric Y_2Co_7 compound a normal behaviour is found.

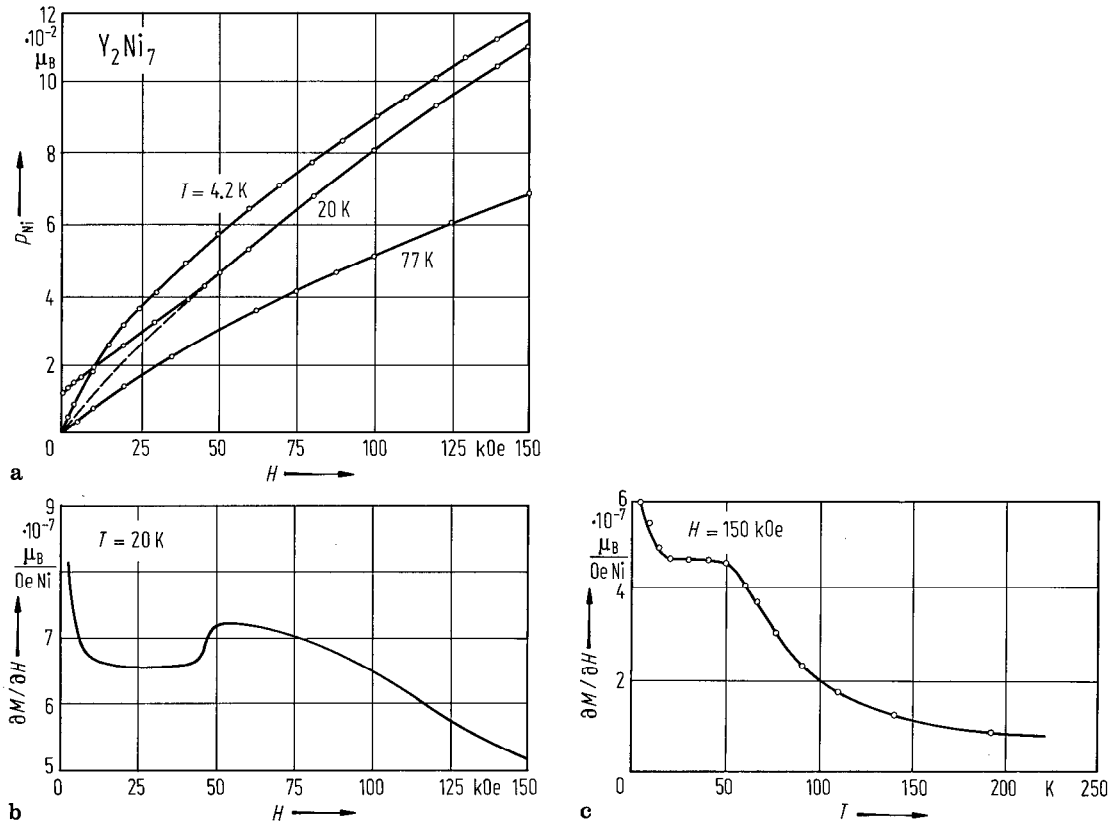

Fig. 278. (a) Magnetization isotherms of Y_2Ni_7 at 4.2, 20 and 77 K; (b) field dependence of the differential magnetic susceptibility at 20 K; (c) temperature dependence of the differential magnetic susceptibility at 150 kOe [83 G 3]. As shown in (b) the maximum in the differential susceptibility corresponds to a change of regime. The high-field susceptibility, which corresponds to the paramagnetic susceptibility of the 3d-band without spin fluctuations, shows a "plateau" between 20 and 50 K (c).

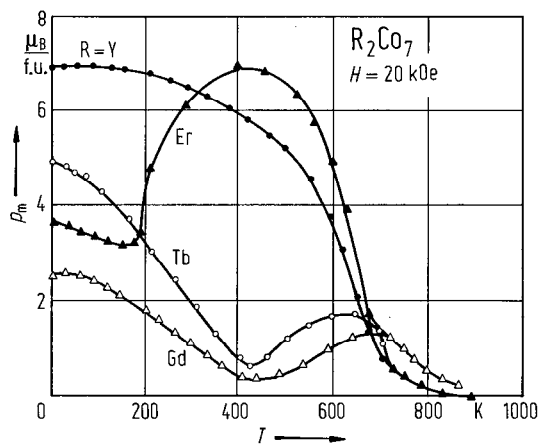

Fig. 279. Thermal variation of magnetizations in a magnetic field of 20 kOe for R_2Co_7 compounds with R = Gd, Tb and Y [66 L 4] and R = Er [68 B 7].

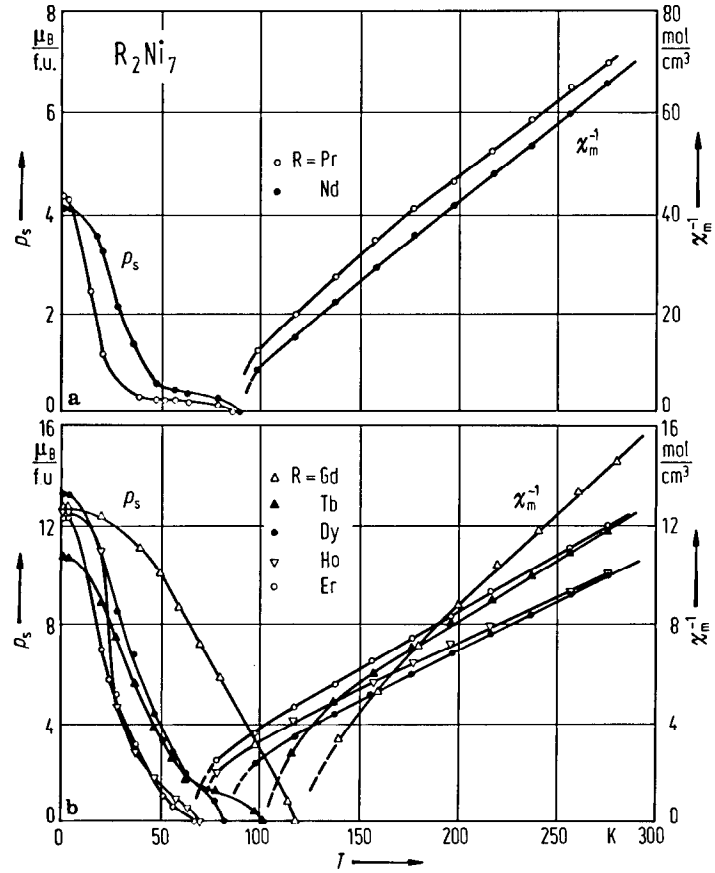

Fig. 280. Thermal variation of spontaneous magnetizations and reciprocal magnetic susceptibilities for (a) Pr_2Ni_7, Nd_2Ni_7; (b) Gd_2Ni_7, Tb_2Ni_7, Dy_2Ni_7, Ho_2Ni_7 and Er_2Ni_7 [69 P 1, 67 L 5].

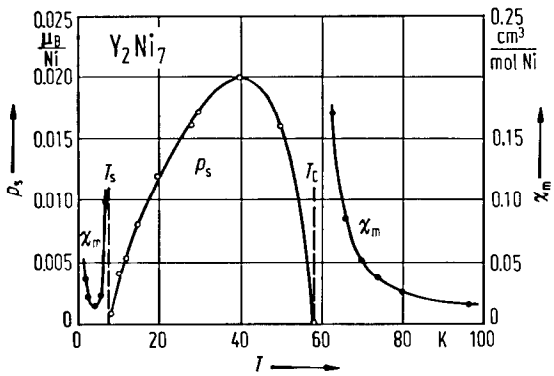

Fig. 281. Thermal variations of magnetic susceptibility and spontaneous magnetization of Y_2Ni_7. Above $T_C = 58$ K there is no spontaneous magnetization and Y_2Ni_7 is paramagnetic. As the temperature decreases, spontaneous magnetization appears at $T_C = 58$ K and the compound is weakly ferromagnetic. The spontaneous magnetization passes through a maximum at $\cong 40$ K and vanishes at the compensation temperature $T_s = 7$ K [83 G 3]. Initially, the experimental data were attributed to a thermally induced ferromagnetism. Later on [90 B 1] the above behaviour was shown to originate actually from the existence of Gd impurities in the studied sample and interpreted in terms of an inhomogeneous ferromagnetism. The Y_2Ni_{17} samples obtained in [67 L 5, 69 P 1, 84 B 12] show a common ferromagnetic behaviour.

Table 65a. Magnetic properties of R_2Co_7 compounds.

	T_C(K)							p_s(μ_B/f.u.)							Paramagnetic behaviour
	66 L 4	68 B 7	68 V 1	70 B 6, 72 B 11	70 S 6	83 B 3	77 b 1	66 L 4	68 B 7	68 V 1	70 B 6, 72 B 11	70 S 6 [1])	83 B 3	85 Y 6	
La_2Co_7			490							6.6					C-W see Fig. 284
Ce_2Co_7					123										
Pr_2Co_7					574							10.5			
Nd_2Co_7					609							13.1			
Sm_2Co_7					713							9.1			
Gd_2Co_7	775			771				2.4			2.5				nonlinear see Fig. 284
Tb_2Co_7	717							5.3							
Dy_2Co_7							640								
Ho_2Co_7	670				647			6.0							
Er_2Co_7		670			646				7.5						
Y_2Co_7	639					639		7.4					9.6	9.24	C-W see Fig. 284

[1]) At room temperature

Table 65b. Magnetic properties of R_2Ni_7 compounds.

	T_C, T_N (K)					p_s (μ_B/f.u.)			Paramagnetic [1] behaviour	
	67 L 5, 69 P 1	72 B 14	75 P 4	83 J 1	84 B 12	67 L 5, 69 P 1	72 B 14	84 B 12	Θ K	p_{eff} μ_B/Ni
La_2Ni_7					$T_N = 53$				C-W [5] 70	
Ce_2Ni_7	48					0.26				
Pr_2Ni_7	85					4.36			[4]	
Nd_2Ni_7	87			93		4.14			[4]	
Gd_2Ni_7	118	119	116	116		12.65	12.70		nonlinear [2] $C_m = 16.81\,cm^3\,K/mol$	
Tb_2Ni_7	101		98	98		10.72			[4]	
Dy_2Ni_7	81		80	80		13.30			[4]	
Ho_2Ni_7	70					12.57			[4]	
Er_2Ni_7	67					12.28				
Y_2Ni_7	58		58	59	54	0.41		0.56	54 [3]	0.87

[1]) See Figs. 278, 280, 281. [2]) [72 B 14]. [3]) [84 B 12]. [4]) See Fig. 280. [5]) [83 P 4].

Table 66. Pressure and volume dependences of the Curie temperatures.

	dT_C/dp K kbar^{-1}	$d \ln T_C/d \ln V$	Ref.
Y_2Co_7 [1])		5.5	77 B 23
Nd_2Ni_7 [2])	0.08	−1.2	75 P 4
Gd_2Ni_7	−0.11	1.3	75 P 4
Tb_2Ni_7	0.00	0.0	75 P 4
Dy_2Ni_7	0.03	−0.6	83 J 1
Y_2Ni_7	0.08	−1.9	83 J 1

[1]) The volume dependence of T_C values in R_xM_y compounds was analysed in [83 J 1].

[2]) The pressure dependence of the Curie temperatures of R_2Ni_7 compounds was analysed by using the s-d model [84 I 6].

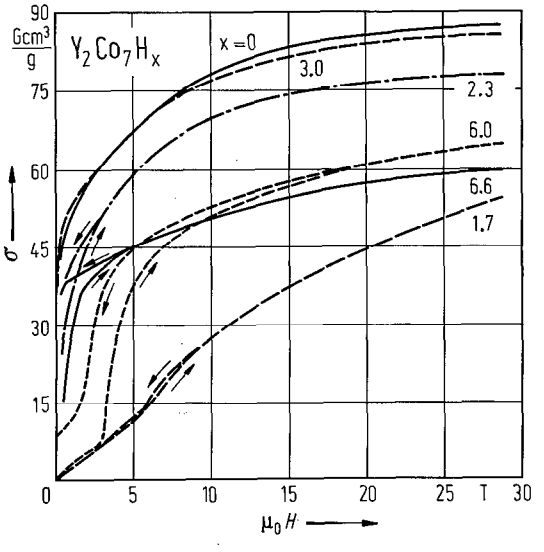

Fig. 282. Magnetization isotherms in $Y_2Co_7H_x$ hydrides [85 Y 5, 86 G 4]. The metamagnetic transition is observed in the β- and γ-hydrides except for $Y_2Co_7H_3$. This transition is attributed to the itinerant-electron metamagnetism of the strongly paramagnetic Co sites near the onset of the ferromagnetism. See also [83 B 3].

Table 67. Magnetic properties of R_2M_7 hydrides [1].

	T	$p_M(\mu_B)$			H_c [2]	H_c^* [2]	T_C	T_N	p_{eff}	Θ	Ref.
	K	Low-moment state ($H<H_c$)	High-moment state ($H=280$ kOe)	Normal behaviour	kOe		K		μ_B/M	K	
$Gd_2Co_7H_{7.7}$	4.2			0.90				420			85 A 13
Y_2Co_7 [3]	4.2			1.32							85 Y 6
$Y_2Co_7H_{1.7}$	4.2	0.19	0.81		56(4)	56(4)					85 Y 6
$Y_2Co_7H_{2.3}$	4.2	–	–	1.18	–	–					85 Y 6
$Y_2Co_7H_{3.0}$	4.2	–	–	1.27	–	–					85 Y 6
$Y_2Co_7H_{4.8}$	4.2	0.29	1.03	–	37(1)	24(4)					85 Y 6
$Y_2Co_7H_{6.0}$	4.2	0.09	0.98	–	31(1)	20(4)					85 Y 6
$Y_2Co_7H_{6.0}$					20···15 between 4.2···300 K			470			83 B 3
$Y_2Co_7H_{6.6}$	4.2	0.22	0.90		10(1)	–					85 Y 6
$La_2Ni_7H_x$	Pauli paramagnet										84 B 12
$Y_2Ni_7H_x$	4.2			0.046	–	–	98		0.95	99	84 B 12

[1]) See also Figs. 282, 286–290.
[2]) Critical field for increasing (H_c) and decreasing (H_c^*) the magnetic field.
[3]) Parent phase.

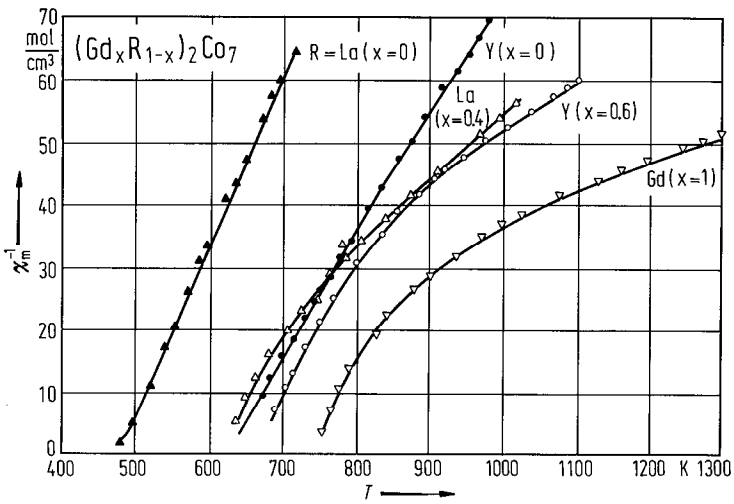

Fig. 284. Thermal variation of reciprocal magnetic susceptibilities for some $(Gd_xY_{1-x})_2Co_7$ [85 B 11] and $(Gd_xLa_{1-x})_2Co_7$ [85 B 13] compounds. For Y_2Co_7 and La_2Co_7 ferromagnetic compounds, χ^{-1} vs. T curves show a Curie-Weiss dependence. In case of ferrimagnetic compounds χ^{-1} vs. T is nonlinear.

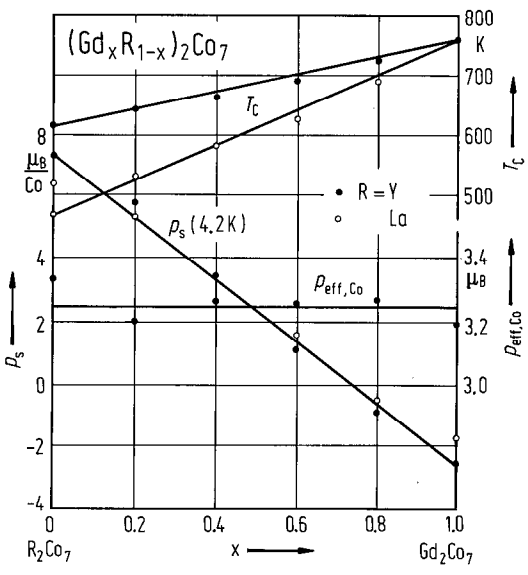

Fig. 283. Composition dependence of the saturation magnetizations at 4.2 K, Curie temperatures, and effective Co magnetic moments in $(Gd_xY_{1-x})_2Co_7$ [85 B 11] and $(Gd_xLa_{1-x})Co_7$ [85 B 13] compounds.

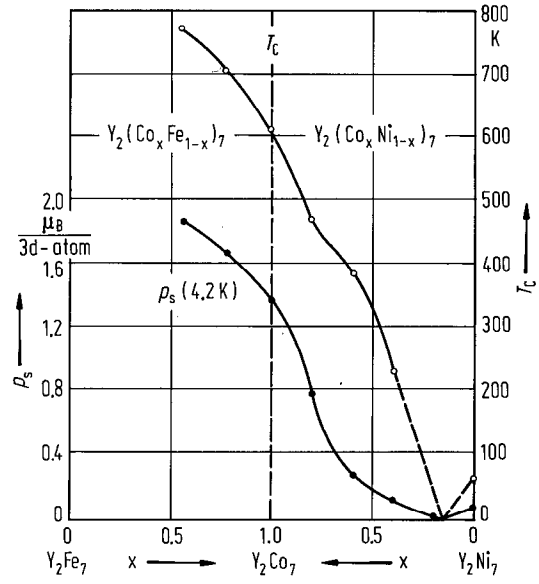

Fig. 285. Saturation magnetic moments at 4.2 K and ordering temperatures in $Y_2(Co_xM_{1-x})_7$ compounds as function of composition [72 P 2, 75 T 1]. No structural data were determined for these compounds. For $Y_2(Co_xNi_{1-x})_7$ with approximately composition $x \cong 0.2$, the magnetic moment passes through a minimum before increasing again to Y_2Ni_7 compound. The behaviour of the ordering temperatures is parallel to the magnetic moment behaviour. In $Y_2(Co_xFe_{1-x})_7$ compounds the ordering temperature is still rising with increasing Fe content when the limit of solubility is reached.

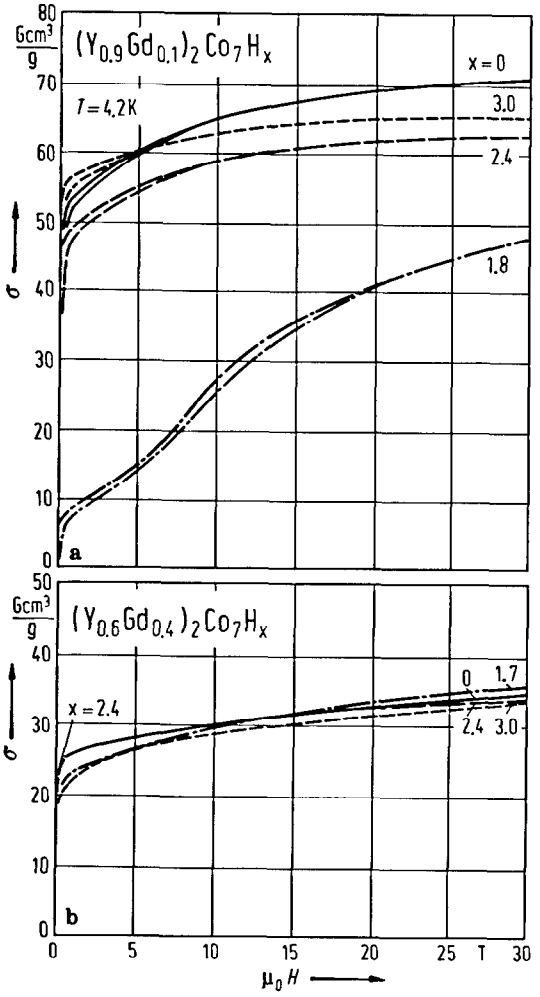

Fig. 286. Magnetization isotherms at 4.2 K for $(Y_{1-y}Gd_y)_2Co_7H_x$ system: (a) y = 0.1 (b) y = 0.4 [87 Y 7]. The metamagnetic transition shown by the β_L-hydrides at y = 0.1 and 0.2 is considered to be due to the itinerant metamagnetism of the Co magnetic moment. Some paramagnetic Co atoms achieve a spin-splitting state above the critical magnetic field as result of the applied and exchange fields.

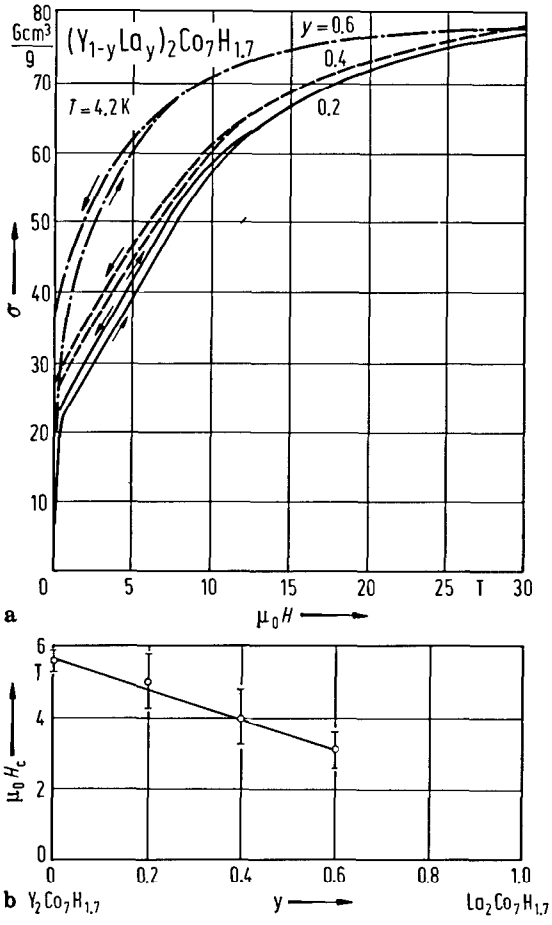

Fig. 287. (a) Magnetization isotherms at 4.2 K for $(Y_{1-y}La_y)_2Co_7H_{1.7}$ hydrides. (b) Dependence of the critical field H_c at 4.2 K on the La content [87 Y 6].

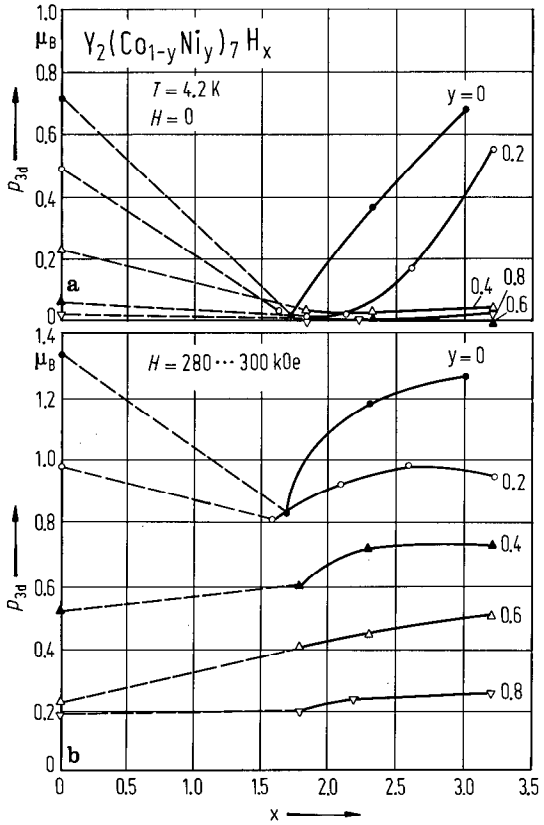

Fig. 289. Variation of the magnetic moment at 4.2 K for the $Y_2(Co_{1-y}Ni_y)_7H_x$ system: (a) in zero magnetic field and (b) in the maximum applied field (approximately 280···300 kOe) [86 G 4, 87 Y 7]. The partial substitution of Co in $Y_2Co_7H_x$ by Ni abruptly reduces the spontaneous magnetization. The β-hydride of the lowest hydrogen concentration, $Y_2Co_7H_{1.7}$, is a Pauli paramagnet. Further hydrogen absorption in this phase induces an abrupt increase in the spontaneous magnetization. The β-hydride of the highest hydrogen concentration, $Y_2Co_7H_{3.0}$, has almost the same value of the magnetization as that of uncharged material. In the γ-phase (x = 6.0···6.6), on the contrary, an increase in the hydrogen concentration reduces the spontaneous magnetization.

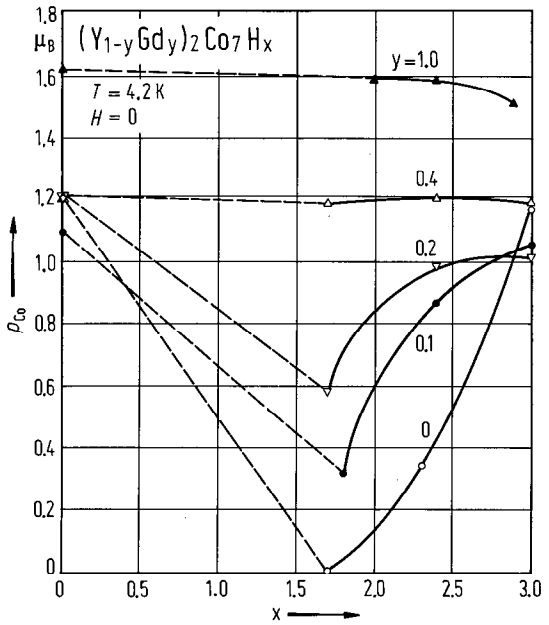

Fig. 288. Dependence of the Co magnetic moment on the hydrogen content, at 4.2 K in zero magnetic field for the $(Y_{1-y}Gd_y)_2Co_7H_x$ system [87 Y 6]. The Co magnetic moment depends strongly upon the magnetic field polarizing it. The exchange field produced by Gd spins assists the increase in the Co magnetic moment. The disappearance of ferromagnetism in the β_L-hydride (y = 0, x = 1.7) is attributed to the weakening in the exchange interactions upon hydrogen absorption.

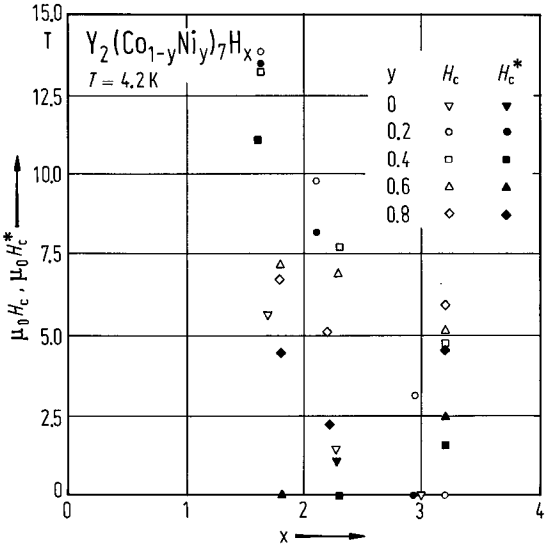

Fig. 290. Dependence of the critical magnetic field, H_c (in increasing field) and H_c^* (in decreasing field), at 4.2 K on Ni content and hydrogen composition for the $Y_2(Co_{1-y}Ni_y)_7H_x$ system [87 Y 6]. The critical field generally decreases with increasing hydrogen content.

For magnetic properties see also

R_2M_7	M = Co, Ni [83 G 3]
R_2Co_7	[72 B 8, 79 D 4]; R = Gd, Tb, Ho, Y [66 L 4]; R = Sm, Gd, Er, Tm, Y [74 D 7]; R = La, Pr, Nd [77 S 15]; R = Th [84 A 13]
R_2Ni_7	[69 P 1]; R = Ce, Pr, Nd, Gd, Tb, Dy, Ho, Er, Y [67 L 5]; R = Gd, Tb, Dy, Y [75 P 4]; R = La [83 B 10, 83 P 4]; R = Y [81 G 4, 81 G 5, 81 G 6, 83 G 3, 84 S 8(T), 86 M 3(T)]
$R_2M_7H_x$	$La_2Co_7H_x$ [80 B 18, 83 B 10]; Ce_2Co_7 [80 B 16]; $Gd_2Co_7H_x$ [85 A 13]; $Y_2Co_7H_x$ [82 B 14, 83 B 3, 84 B 3, 85 A 14, 85 Y 4, 85 Y 5, 85 Y 6, 86 A 5, 86 G 4]; $Th_2Co_7H_x$ [84 A 13] $La_2Ni_7H_x$ [83 B 10]; $Y_2Ni_7H_x$ [84 B 12]
$(R'R'')_2M_7$	$(GdLa)_2Co_7$ [85 B 12, 85 B 13]; $(GdY)_2Co_7$ [85 B 11, 85 B 12]
$R_2(M'M'')_7$	$R_2(FeCo)_7$ [73 H 4]; $R_2(FeNi)_7$ [73 H 4]; $Gd_2(CoNi)_7$ [85 B 12]; $Y_2(CoNi)_7$ [72 P 2]
$(R'R'')_2M_7H_x$	$(YLa)_2Co_7H_x$ [87 Y 6]; $(YGd)_2Co_7H_x$ [87 Y 6, 87 Y 7]
$R_2(M'M'')_7$	$Y_2(CoNi)_7H_x$ [87 Y 6]

Pressure effect on T_C

R_2Co_7, R_2Ni_7 [83 J 1]; R = Y [83 B 4]

T_C in R_2Co_7 and R_2Ni_7 [86 P 7]

Neutron diffraction

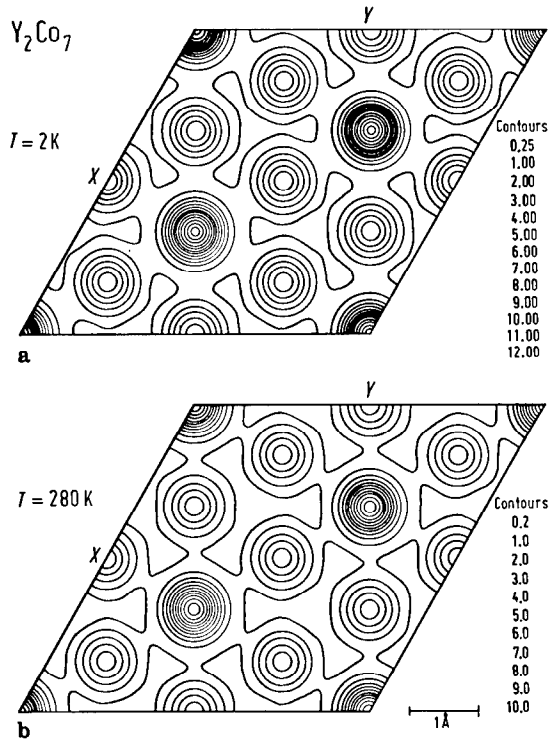

Fig. 291. Projection on the (001) plane of the magnetization density at (a) 2 K and (b) 280 K of Y_2Co_7 having lower Co content than the stoichiometric one (contours are in 0.1 μ_B Å^{-2}). As observed from Table 68 the magnetic moments of Co_I (3b site) and Co_V (18h site) atoms decrease by 27% and 23%, respectively, between 2 and 280 K, much stronger than for the other sites. The longitudinal fluctuations influence mainly the magnetic contribution of Co_I and Co_V atoms, their superimposed magnetic susceptibility having a maximum similar to that observed in YCo_2 compound [87 B 1].

Table 68. Magnetic moments determined by neutron diffraction in some R_2M_7 compounds.

	T K	p_R (μ_B)		p_M (μ_B)					Ref.
		R I	R II	3b	6c	6c	9e	18h	
Y_2Co_7	4.2	–	–	1.28(6)	1.45(5)	1.45(5)	1.37(3)	1.11(2)	69 K 5
Y_2Co_7 [1])	4.2	–	–	1.057(41)	1.255(14)	1.255(14)	1.179(12)	0.954(9)	87 B 1
	280	–	–	0.769(67)	1.033(26)	1.033(26)	0.991(18)	0.734(18)	
Er_2Ni_7	4.2	8.9(7)	5.5(13)			≅0			71 P 1
		10(10)° with c axis	55(8)° with c axis						74 Y 1

[1]) With Co content lower than the stoichiometric one.

EPR, FMR

For FMR measurements see
Y_2Co_7 [86 T 9]; Gd_2Ni_7 [80 B 15]

For EPR measurements Gd_2Ni_7 [80 B 15]

Mössbauer effect, perturbed angular correlations

For perturbed angular correlation
^{140}Ce in La_2Co_7 see [81 M 11]

NMR

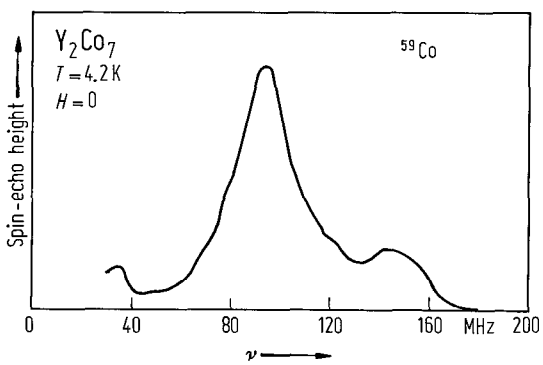

Fig. 292. Uncalibrated NMR zero-field spin-echo spectrum of ^{59}Co at 4.2 K in Y_2Co_7 compound [77 F 3]. In this compound there are five Co sites, but their anisotropy energies are comparable in magnitude (see [84 K 1]). That is reflected in the NMR spectrum where one intense broadened line at 96 MHz is observed.

For NMR studies see also
^1H in La_2Ni_7 [79 H 9, 80 H 10]
^{59}Co in Y_2Co_7 [76 F 1, 77 F 3, 77 Y 5]; Gd_2Co_7 [71 U 1]
89Y in Y_2Co_7 [76 F 1]; see also Table 61
^{155}Gd, ^{157}Gd in Gd_2Co_7 [71 U 1]

Anisotropy, magnetostriction

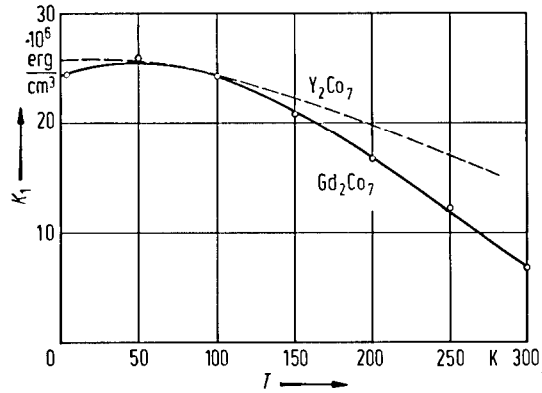

Fig. 293. Thermal variation of the anisotropy constants, K_1, of Gd_2Co_7 and stoichiometric Y_2Co_7 compounds. The stronger temperature dependence of K_1 in Gd_2Co_7 shows the increasing importance of the noncollinearity of the magnetic moment configuration reduced by the external field [87 B 1].

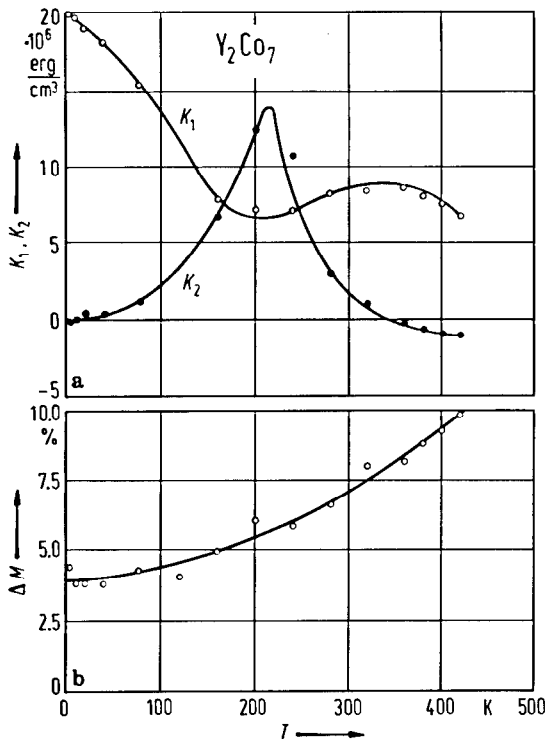

Fig. 294. Thermal variation of (a) the anisotropy constants K_1 and K_2 as well as (b) the magnetization anisotropy, ΔM, in Y_2Co_7 having lower Co-content than the stoichiometric one. The K_1 values have a minimum at 220 K, whereas K_2 values have a maximum. This behaviour is attributed to the gradual metamagnetic transition. The transition from the state with high magnetization towards the one with low magnetization when temperature increases, is due to the longitudinal fluctuations of the magnetization. These fluctuations enhance the decrease of K_1 values as compared with the situation when only transverse fluctuations are present. In high external magnetic fields, the state with high magnetization is gradually regenerated due to quenching of the longitudinal fluctuations of the magnetization. The anisotropy increases up to the value characteristic of the high-magnetization state. This fact is reflected in important and positive K_2 values. At 220 K, the longitudinal fluctuations have minimum amplitude. At higher temperatures, the effect of these fluctuations decrease since the K_1 values increase [87 B 1].

Table 69. Anisotropy fields determined in some R_2Co_7 compounds.

	T K	H_A kOe	Ref.
La_2Co_7	RT	> 50	73 B 21
Pr_2Co_7	RT	>100	73 B 21
Nd_2Co_7	RT	small	73 B 21
Sm_2Co_7	RT	>200	73 B 21
Gd_2Co_7	RT	>100	73 B 21
Gd_2Co_7	4.2	210	85 A 13
Y_2Co_7	RT	> 50	73 B 21
Y_2Co_7	4.2	105	85 A 14
Y_2Co_7	4.2···400	dependent on temperature	84 K 1

For anisotropy studies see also
R_2Co_7 [73 B 21, 78 K 12, 79 D 4]; R = Sm, Gd, Er, Tm, Y [74 D 7]; R = Sm, Y [74 K 6]; R = La, Pr, Nd [77 S 15]; R = Pr, Sm [84 W 1]; R = Tb [82 A 11]; R = Y [84 K 1, 85 T 7, 86 T 9]
$R_2Co_7H_x$ R = Gd [85 A 13]
$R_2(M'M'')_7$ [81 K 4]

For spin reorientation see
R_2Co_7 [79 D 4]

Table 70. Magnetostriction of $Y_2Co_7H_2$ hydride at room temperature.

	λ_s	Ref.
$Y_2Co_7H_6$	$-0.35 \cdot 10^{-3}$	83 B 3

For magnetostriction studies see
$Gd_2Co_7H_x$ [85 A 13]; $Y_2Co_7H_x$ [85 A 14]
Tb_2Co_7 [82 A 11]

Domain structure, magnetization processes

For magnetization processes see
Pr_2Co_7, Sm_2Co_7 [84 W 1]; $Gd_2Co_7H_x$ [85 A 13]

For domain structure
Ho_2Co_7 [79 K 6]; $Y_2Co_7H_x$ [84 B 3]

Transport properties

For thermopower studies in La_2Ni_7, Ce_2Ni_7 [85 G 17], Ce_2Ni_7 [84 L 7]

Electron spectroscopy

For electron spectroscopy see
L_{111} spectroscopy
Ce_2Co_7 [82 F 9]

2.4.2.15 R_5M_{19} compounds

Crystal structure, lattice parameters

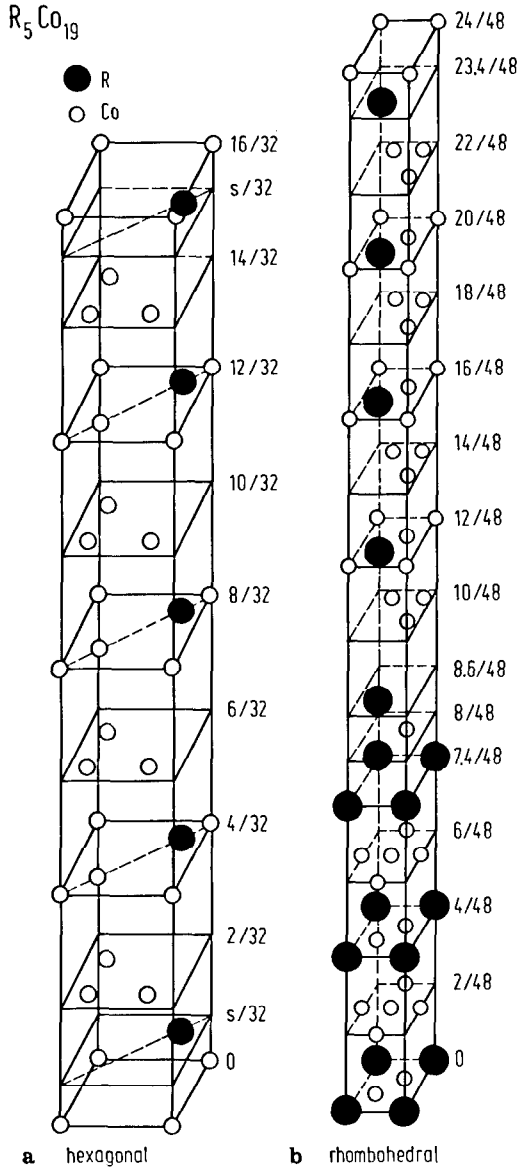

Fig. 295. (a) Half of unit cell of the R_5Co_{19} hexagonal compounds ($P6_3/mmc$-space group) [79 L 1]. The sets of atomic positions are given in Table 71(a). (b) Half of unit cell of the R_5Co_{19} rhombohedral compounds ($R\bar{3}m$-space group) [74 K 9]. The sets of atomic positions are given in Table 71(b). In both figures small circles are M atoms and large circles the R atoms.

Table 71a. Atomic positions in R_5M_{19} compounds, hexagonal structure having $P6_3/mmc$ space group [79 L 1].

Atom	Site	x	y	z
R_1	2c	1/3	2/3	1/4
R_2	4f	1/3	2/3	1/8
R_3	4f	1/3	2/3	s/32
M_1	2a	0	0	0
M_2	2b	0	0	1/4
M_3	2d	1/3	2/3	3/4
M_4	4e	0	0	1/8
M_5	4f	1/3	2/3	7/8
M_6	12k	5/6	2/3	1/16
M_7	12k	5/6	2/3	3/16

Table 71b. Atomic positions in R_5M_{19} compounds, rhombohedral structure having $R\bar{3}m$-space group [74 K 9].

Atom	Site	x	y	z
R	3a	0	0	0
R_1	6c	0	0	1/12
R_2	6c	0	0	0.154
M	3b	0	0	1/2
M_1	6c	0	0	1/4
M_2	6c	0	0	1/3
M_3	6c	0	0	5/12
M'_1	18h	1/2	$\overline{1/2}$	1/8
M'_2	18h	1/2	$\overline{1/2}$	1/24

To these are added the translations: (0, 0, 0), (1/3, 2/3, 2/3), (2/3, 1/3, 1/3).

Table 72. Structure and lattice constants (Å) of R_5Co_{19} compounds.

	Structure and space group	73 R 2		73 K 6		74 K 9	
		a	c	a	c	a	c
La_5Co_{19}	rhombohedral $R\bar{3}m$	5.123	48.74				
Ce_5Co_{19}	hexagonal $P6_3/mmc$					4.9446	32.460
	rhombohedral $R\bar{3}m$	4.939	48.71	4.9475	48.7434	4.9447	48.688
Pr_5Co_{19}	rhombohedral $R\bar{3}m$	5.053	48.71	5.065	49.144		
Nd_5Co_{19}	rhombohedral $R\bar{3}m$	5.054	46.66	5.052	48.666		
Sm_5Co_{19}	hexagonal $P6_3/mmc$					5.0312	32.265
	rhombohedral $R\bar{3}m$					5.0314	48.402
Y_5Co_{19}	hexagonal $P6_3/mmc$					5.0041	32.059
	rhombohedral $R\bar{3}m$					5.0039	48.087

For structure and lattice constants see also the reports of Schweizer (1972) and Ray and Strnat (1972) cited in [75 S 13] and [73 K 6, 75 P 8].

Magnetization, Curie temperatures

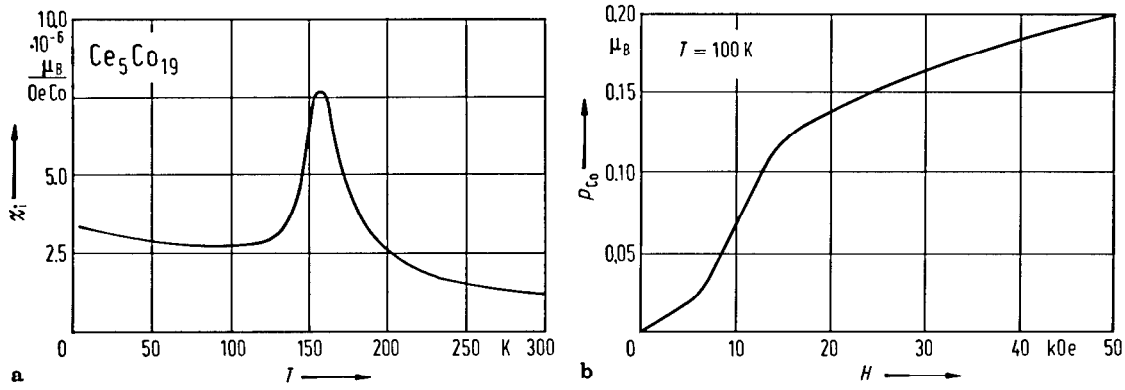

Fig. 296. (a) Thermal dependence of the initial magnetic susceptibility χ_i in Ce_5Co_{19} compound. (b) Field variation of the magnetization at 100 K [83 G 4]. A maximum in χ_i is observed at 160 K, which does not correspond to any anomaly in the temperature dependence of the electrical resistivity. Below 160 K, a transition towards a state of higher magnetization is induced by an applied magnetic field.

Table 73. Magnetic properties of R_5Co_{19} compounds.

	T_C (K)				σ_s (kG/f.u.) [1]
	75 R 1	75 K 3	75 S 13	82 R 2	75 R 1
La_5Co_{19}	616				6.250
Ce_5Co_{19}	293				0.579
Pr_5Co_{19}	690		698		9.630
Nd_5Co_{19}	714				10.030
Sm_5Co_{19}		783			
Y_5Co_{19}				721(2)	

[1]) At room temperature.

For magnetic properties see also
R_5Co_{19} R = Ce, CeLa, CeMM [73 F 2]; R = La, Ce, Pr, Nd [75 R 1]; R = Ce, La, Pr, Nd [75 S 13]; R = Ce [83 G 4]; R = Pr [84 W 1, 85 C 5]; R = Y [82 R 2]

2.4.2.16 R_6M_{23} compounds

Crystal structure, lattice parameters

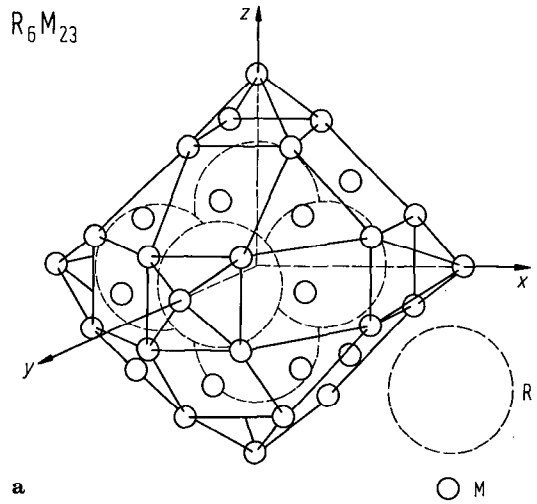

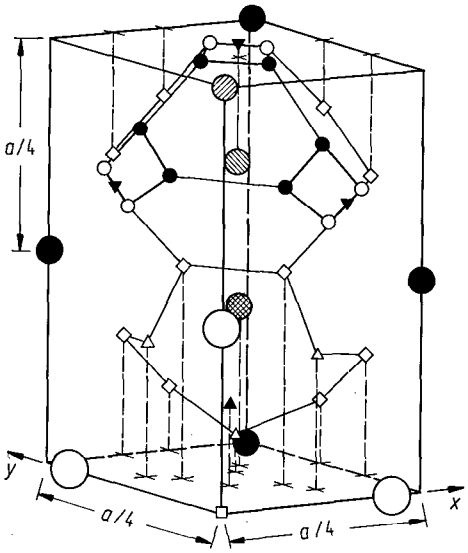

symbol	atom / interstice (I)	Wyckoff notation
○	R	24e
▨	M	4b
●	M	24d
▩	M	$32f_1$
▨	M	$32f_2$
□	I	4a
▲	I	$32f_3$
▼	I	48i
○	I	$96j_1$
●	I	$96j_2$
△	I	$96k_1$
◇	I	192l

b

Fig. 297. (a) Crystalline structure of R_6M_{23}-type compounds. These show a fcc-type lattice having the space group Fm3m. The R atoms are located in e-type sites and M atoms in b, d, f_1 and f_2 sites. The above structure may be also maintained upon hydrogenation (or deuteration). The equivalent positions of the atoms in the crystallographic space group Fm3m of $Y_6Mn_{23}H_{22}$ hydride are given in Table 74. Four type of sites are evidenced for D atoms. In (b) a model of the basic building block for R_6M_{23} intermetallic compound is shown. The volume shown is 1/32 of a unit cell. There are 4 octahedral a sites (R_6) per unit cell, $32f_3$ sites (R_3M), $96k_1$ sites (R_2M_2), $96j_1$ sites (RM_3), $96j_2$ sites (RM_3), and 192l sites (RM_3). The concept of minimum hole radius (0.04 nm) and minimum H–H distance (0.210 nm) were used to predict hydrogen site occupany [83 W 3]. The model suggests that in $Y_6Mn_{23}D_{18}$ and $Th_6Mn_{23}D_{16}$ (space group Fm3m), in addition to a and f_3 sites, j_1 sites should be also involved. In $Y_6Mn_{23}D_{22}$ system, the deuterium atoms fill the a site and partially fill the f_3, j_1 and k_1 sites [84 H 2], which is in relatively good agreement with the Westlake model [83 W 3]. There is a structural and accompanying magnetic transition occurring at ≅175 K. The crystal structure transforms into a primitive tetragonal structure of space group P4/mmm [84 H 2]. The equivalent positions of the atoms in P4/mmm-type structure are also given in Table 74. The $Ho_6Fe_{23}D_{12.1}$ hydride shows at low temperature a body-centred tetragonal structure of I4/mmm space group [83 R 5]. The equivalent positions of the atoms in this structure are given in Table 75. It was suggested [85 S 22], that the room-temperature tetragonal ($c > a$) hydride phase, $R_6M_{23}H_x$, results if $x > 9$ and the volume of the unit cell is less than a "cut-off" value of about $1.883(5) \cdot 10^3$ Å^3, Table 77. The tetragonal structure seems to be compatible with a hydrogen-induced distortion of the j_1 interstitial sites, which are otherwise too small to accomodate hydrogen atoms. The model [85 S 22] predicts that no Mn-rich tetragonal hydride phases will be found, while several Fe-rich tetragonal hydride phases should occur.

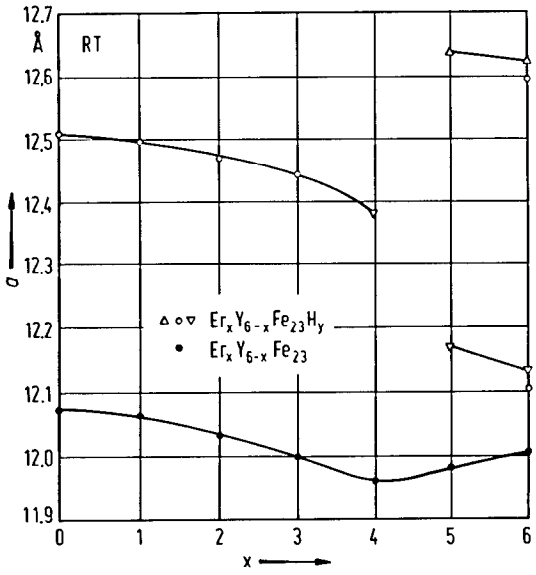

Fig. 298. Lattice parameters vs. composition determined at room temperature in $Y_{6-x}Er_xFe_{23}$ alloys and their hydrides: (open circles, triangles, inverted triangles) hydrides; (solid circles) parent compounds [83 P 9]. The parent alloys crystallize in a face-centred cubic structure. A pronounced minimum in the lattice parameter was evidenced for $Er_4Y_2Fe_{23}$. A similar minimum was also observed in the 1 atm hydrogen capacity of the alloys. The hydrides of the Y-rich compounds were found to retain the cubic structure of the parent compounds, whereas the hydrides of Er_5YFe_{23} and Er_6Fe_{23} adopt tetragonally distorted structures.

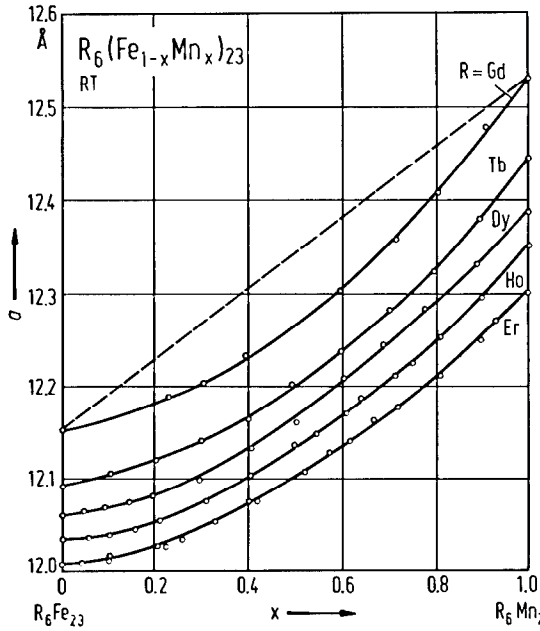

Fig. 299. Composition dependence of the lattice constants in $R_6(Fe_{1-x}Mn_x)_{23}$ (R = Gd, Tb, Dy, Ho and Er) compounds at room temperature [71 H 2].

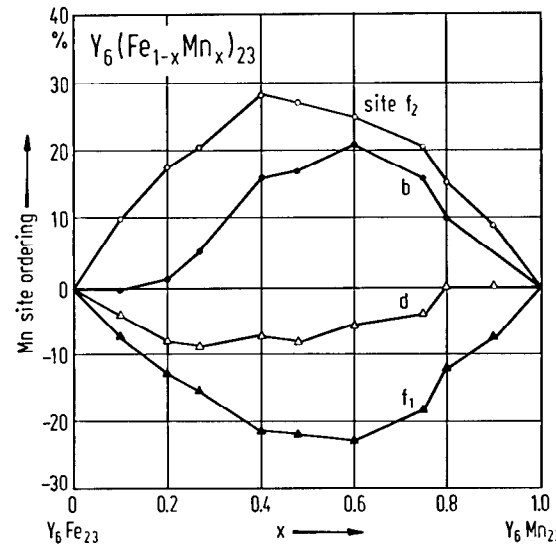

Fig. 300. Preferential site ordering of Fe and Mn atoms, expressed as a percentage departure of Mn atoms from a stoichiometric distribution, in $Y_6(Fe_{1-x}Mn_x)_{23}$ compounds. Throughout the entire compositional range of the ternary system, Mn atoms prefer to occupy the f_2 sites and Fe atoms the f_1 sites [80 H 2, 81 H 1].

Table 74. Equivalent positions in Fm3m and P4/mmm crystallographic space groups of $Y_6Mn_{23}D_{22}$, Z=4 for the Fm3m structure, and Z=2 for the P4/mmm structure [84 H 2].

	Face-centred cubic (Fm3m)			Primitive tetragonal (P4/mmm)					
Atom	Site	(x, y, z)	N/2 f.u.	Site	(x, y, z)	x	y	z	N/2 f.u.
Y	e	$(x, 0, 0)$	12	g	$(0, 0, z)$			0.205	2
	$x=0.205$			h	$(1/2, 1/2, z)$			0.295	2
				j	$(x, x, 0)$	0.205			4
				k	$(x, x, 1/2)$	0.295			4
Mn	b	(1/2, 1/2, 1/2)	2	b	(0, 0, 1/2)				1
				c	(1/2, 1/2, 0)				1
Mn	d	(0, 1/4, 1/4)	12	e	(0, 1/2, 1/2)				2
				f	(0, 1/2, 0)				2
				r_1	(x, x, z)	0.250		0.750	8
Mn	f_1	(x, x, x)	16	s_1	$(x, 0, z)$	0.358		0.179	8
	$x=0.179$			t_1	$(x, 1/2, z)$	0.142		0.321	8
Mn	f_2	(x, x, x)	16	s_2	$(x, 0, z)$	0.256		0.372	8
	$x=0.372$			t_2	$(x, 1/2, z)$	0.244		0.128	8
D	a	(0, 0, 0)	2	a	(0, 0, 0)				1
				d	(1/2, 1/2, 1/2)				1
D	f_3	(x, x, x)	16	s_3	$(x, 0, z)$	0.200		0.100	8
	$x=0.100$			t_3	$(x, 1/2, x)$	0.300		0.400	8
D	j_1	$(0, y, z)$	48	p	$(x, y, 0)$	0.204	0.458		8
	$y=0.169$			q	$(x, y, 1/2)$	0.296	0.042		8
	$z=0.373$			r_2	(x, x, z)	0.127		0.331	8
				r_3	(x, x, z)	0.169		0.373	8
				r_4	(x, x, z)	0.331		0.127	8
				r_5	(x, x, z)	0.373		0.169	8
D	k_1	(x, x, z)	48	s_4	$(x, 0, z)$	0.322		0.049	8
	$x=0.161$			t_4	$(x, 1/2, z)$	0.178		0.451	8
	$z=0.049$			u_1	(x, y, z)	0.112	0.210	0.161	16
				u_2	(x, y, z)	0.290	0.388	0.339	16

Table 75. Equivalent positions in lattice for the compounds $Ho_6Fe_{23}D_u$ (u = 0; 1.5; 8.2; 15.7) (space group Fm3m) and $Ho_6Fe_{23}D_{12.1}$ (space group I4/mmm) [83 R 5].

	$Ho_6Fe_{23}D_u$ (Fm3m)			$Ho_6Fe_{23}D_{12.1}$ (I4/mmm)		
Atom	Site	(x, y, z)	N/2 f.u.	Site	(x, y, z)	N/2 f.u.
Ho	e	(x, 0, 0)	12	e	(0, 0, z)	4
		x = 0.205, u = 0			z = 0.201	4
		x = 0.205, u = 1.5				
		x = 0.211, u = 8.2		h	(x, x, 0)	8
		x = 0.209, u = 15.7			x = 0.214	
Fe	b	(1/2, 1/2, 1/2)	2	b	(0, 0, 1/2)	2
Fe	d	(0, 1/4, 1/4)	12	c	(0, 1/2, 0)	4
				f	(1/4, 1/4, 1/4)	8
Fe	f_1	(x, x, x)	16	n_1	(0, y, z)	16
		x = 0.175, u = 0			y = 0.354	
		x = 0.176, u = 1.5			z = 0.175	
		x = 0.178, u = 8.2				
		x = 0.177, u = 15.7				
Fe	f_2	(x, x, x)	16	n_2	(0, y, z)	16
		x = 0.379, u = 0			y = 0.245	
		x = 0.379, u = 1.5			z = 0.363	
		x = 0.377, u = 8.2				
		x = 0.372, u = 15.7				
D	a	(0, 0, 0)	2	a	(0, 0, 0)	
D	f_3	(x, x, x)	16	n_3	(0, y, z)	16
		x = 0.110, u = 1.5			y = 0.200	
		x = 0.098, u = 8.2			z = 0.094	
		x = 0.096, u = 15.7				
D	j_1	(0, y, z)	48	l_1	(x, 1/2, 0)	12
		y = 0.135, u = 15.7			x = 0.290	
		z = 0.340, u = 15.7				
D	j_2	(0, y, z)	48	l_2	(x, 1/2, 0)	12
		y = 0.076, u = 15.7			x = 0.208	
		z = 0.385, u = 15.7				
D	k_1	(x, x, z)	48	0	(x, y, z)	32
		x = 0.155, u = 8.2			x = 0.132	
		z = 0.031, u = 8.2			y = 0.222	
		x = 0.159, u = 15.7			z = 0.166	
		z = 0.047, u = 15.7				

Table 76a. Lattice parameters of R_6Mn_{23} compounds (Å).

	65 K 1	65 K 2	65 W 1	67 K 1	77 B 19, 77 B 22, 81 B 15	80 P 8 80 P 9	82 P 1	83 C 8	83 T 7, 84 T 2	85 S 22
Nd_6Mn_{23}	12.657		12.657	12.663	12.671		12.670			
Sm_6Mn_{23}	12.670	12.670	12.558	12.572	12.563		12.560			
Gd_6Mn_{23}	12.670	12.580	12.532	12.519	12.515	12.592				
Tb_6Mn_{23}		12.440	12.396		12.396	12.484				
Dy_6Mn_{23}	12.380	12.380	12.361	12.358		12.439				
Ho_6Mn_{23}	12.340	12.340	12.324	12.337		12.383				
Er_6Mn_{23}	12.290	12.290	12.275	12.285		12.321	12.280			
Tm_6Mn_{23}		12.260	12.226					12.243		12.242(5)
Yb_6Mn_{23}									12.189(5)	
Lu_6Mn_{23}		12.200	12.187		12.199					
Y_6Mn_{23}	12.470	12.470	12.438	12.457	12.445	12.451				

Table 76b. Lattice parameters of R_6Fe_{23} compounds (Å).

	65 K 2	68 R 1	69 G 1	70 V 1	71 M 6	79 B 5	83 R 5	84 G 6	84 H 6	85 S 22
Gd_6Fe_{23}		12.134								
Tb_6Fe_{23}	12.070	12.081								
Dy_6Fe_{23}	12.060	12.052		12.062						
Ho_6Fe_{23}	12.040	12.034			12.032		12.029			
Er_6Fe_{23}	12.010	12.004							12.011	11.944(6)
Tm_6Fe_{23}	11.980	11.972						11.972		
Yb_6Fe_{23}		11.945								
Lu_6Fe_{23}	11.950	11.933	11.934							
Y_6Fe_{23}	12.120	12.082	12.086			12.095				

Table 77a. Lattice parameters and volume expansion of R_6Mn_{23}-hydrides (deuterides) [1]) at room temperature having Fm3m space group.

	a Å	$\Delta V/V$ %	Ref.
$Nd_6Mn_{23}H_x$	13.237	14	81 B 15
$Sm_6Mn_{23}H_x$	13.129	11.2	81 B 15
$Gd_6Mn_{23}H_x$	12.950	8.8	77 B 22, 81 B 15
$Gd_6Mn_{23}H_{22}$	12.970	10	80 P 8
$Tb_6Mn_{23}H_{23}$	13.017	12	80 P 9
$Dy_6Mn_{23}H_{23}$	12.892	11	80 P 9
$Ho_6Mn_{23}D_{22}$	12.773(1)	9.8	86 L 5
$Ho_6Mn_{23}H_{23}$	12.852	12	80 P 8
$Er_6Mn_{23}H_{23}$	12.706	9.7	80 P 8
$Tm_6Mn_{23}H_x$	12.691(3)	11.4(2)	85 S 22
$Tm_6Mn_{23}H_x$	12.492(4)	6.3(2)	85 S 22
$Tm_6Mn_{23}H_x$	12.467(3)	5.6(2)	85 S 22
$Tm_6Mn_{23}H_x$	12.449(4)	5.2(2)	85 S 22
$Tm_6Mn_{23}H_x$	12.422(6)	4.5(3)	85 S 22
$Lu_6Mn_{23}H_x$	12.462	6.7	77 B 22
$Y_6Mn_{23}D_{8.3}$	12.7853	8.3	79 C 5
$Y_6Mn_{23}D_{18}$	12.799	8.6	79 C 5
$Y_6Mn_{23}H_{21}$	12.780	8.0	77 B 19
$Y_6Mn_{23}D_{23}$	12.805	8.8	84 H 2
$Y_6Mn_{23}D_{23}$	12.840	9.7	79 C 5
$Y_6Mn_{23}H_{22}$	12.780	8.0	77 B 19, 77 B 22
$Y_6Mn_{23}H_{25}$	12.842	9.7	77 M 5, 77 O 4
$Y_6Mn_{23}H_{26}$	12.880	10.5	84 B 4
$Th_6Mn_{23}D_{16}$	12.922	10.0	80 H 4
$Th_6Mn_{23}D_{30}$	13.203	17.3	80 H 4
$Th_6Mn_{23}H_{30}$	13.259	18.8	77 M 5
$Th_6Mn_{23}H_x$	13.205	19.0	77 B 22

[1]) Hydrogenated R_6Mn_{23} forms three hydrides (β, γ and δ) in addition to a terminal solid solution. Enthalpies of formation for R_6Mn_{23} are in the range -32 to -34 kJ (mol H_2)$^{-1}$. See also footnote to Table 77b.

Table 77b. Lattice parameters and volume expansion of R_6Fe_{23}-hydrides (deuterides) [1]. (x) signifies that the hydrogen content was not measured.

	T K	Structure	a Å	c Å	$\Delta V/V$ %	Ref.
$Ho_6Fe_{23}D_{1.5}$	4.2	cubic	12.022	–	–	83 R 5
	295	cubic	11.906	–	–	
$Ho_6Fe_{23}D_{8.2}$	4.2	cubic	12.158	–	3.9	
	78	cubic	12.160	–	3.9	83 R 5
	295	cubic	12.187	–	3.9	
$Ho_6Fe_{23}D_{15.7}$	4.2	cubic	12.406	–	10.2	83 R 5
	295	cubic	12.423	–	9.8	
$Ho_6Fe_{23}D_{1.5}$	RT	cubic	12.050	–	0.03	83 P 8
$Ho_6Fe_{23}D_{8.2}$	RT	cubic	12.242	–	4.81	83 P 8
$Ho_6Fe_{23}D_{12.1}$	RT	tetragonal	12.209	12.577	7.1	83 P 8
$Ho_6Fe_{23}D_{15.7}$	RT	cubic	12.445	–	10.22	83 P 8
$Ho_6Fe_{23}H_{16}$	RT	cubic	12.399	–	9.0	81 B 9
$Er_6Fe_{23}H_{14}$	RT	tetragonal	12.131	12.601	7.6	81 B 9
$Er_6Fe_{23}H_{13.7}$	RT	tetragonal	12.135	12.625	7.5	83 P 9
$Er_6Y_1Fe_{23}D_{12.1}$	RT	tetragonal	12.209	12.577	7.1	83 P 9
$Er_6Fe_{23}H_{(17.8)}$	RT	cubic	12.390(5)	–	10.0(3)	85 S 22
$Er_6Fe_{23}H_{(17.6)}$	RT	cubic	12.384(5)	–	9.8(3)	85 S 22
$Er_6Fe_{23}H_{(13)}$	RT	tetragonal	12.105(3)	12.594(13)	6.7(3)	85 S 22
$Er_6Fe_{23}H_x$	RT	tetragonal	12.079(3)	12.594(15)	6.2(3)	85 S 22
$Er_6Fe_{23}H_x$	RT	cubic	12.163(3)	–	4.0(2)	85 S 22
$Tm_6Fe_{23}H_x$	RT	tetragonal	12.085	12.595	6.5	84 G 6
$Tm_6Fe_{23}H_{14.1}$	RT	tetragonal	12.070(5)	12.597(4)	7.2(2)	84 H 3
$Y_6Fe_{23}H_{20}$	RT	cubic	12.573	–	12.6	84 B 4
$Y_6Fe_{23}H_{20}$	RT	cubic	12.385	–	7.6	83 C 8

[1]) Hydrogenated R_6Fe_{23} systems exhibit four hydrides (β, γ, δ and ε) plus a terminal solid solution. All of these are rather stable with enthalpies of formation in the range of -19 to -52 kJ (mol H_2)$^{-1}$ absorbed. Hydride stability correlates with the size of the interstitial holes in which the hydrogen resides: the smaller the hole, the less stable the hydride. The $Ho_6Fe_{23}H_x(D_x)$ systems exhibit isotope effects, the hydride being more stable for the $\gamma \rightarrow \delta$ transformation and the deuteride for the $\delta \rightarrow \varepsilon$ transformation [87 S 20].

Table 77c. Lattice parameters (Å) of R_6M_{23}-deuterides having other types of structures.

	T K	Space group	a	c	Ref.
$Y_6Mn_{23}D_{23}$ [1])	4.2	P4/mmm	9.030	12.722	84 H 2
	78		9.031	12.723	
$Th_6Mn_{23}D_{16}$	4.2	P4/mmm	9.076	12.961	84 H 1
$Ho_6Mn_{23}D_{23}$	9	P4/mmm	8.981	12.636	86 L 5
$Ho_6Fe_{23}D_{12.1}$	4.2	I4/mmm	8.561	12.608	83 R 5
	295	I4/mmm	8.611	12.608	

[1]) A bct structure with space group I4/mmm has been initially suggested [82 C 14]. The high-resolution data [84 H 2] make the P4/mmm symmetry the better choice.

Table 77d. Lattice parameters and volume expansion of $Y_6(FeMn)_{23}$ alloys and their hydrides at room temperature.

	a Å	$\Delta V/V$ %	Ref.
$Y_6Fe_{22}Mn$	12.094		84 B 4
$Y_6Fe_{22}MnH_{20}$	12.584	12.7	84 B 4
$Y_6Fe_{20}Mn_3$	12.110		84 B 4
$Y_6Fe_{20}Mn_3H_{21}$	12.723	16.0	84 B 4
$Y_6Fe_{18}Mn_5$	12.138		84 B 4
$Y_6Fe_{18}Mn_5H_{22}$	12.788	16.9	84 B 4
$Y_6Fe_{17.25}Mn_{5.75}$	12.298		77 O 4
$Y_6Fe_{17.25}Mn_{5.75}H_{26}$	12.611	7.8	77 O 4
$Y_6Fe_{14.26}Mn_{8.74}$	12.219		77 O 4
$Y_6Fe_{14.26}Mn_{8.74}H_{22}$	12.549	8.3	77 O 4
$Y_6Fe_{11.5}Mn_{11.5}$	12.137		77 O 4
$Y_6Fe_{11.5}Mn_{11.5}H_{22}$	12.449	7.9	77 O 4
$Y_6Fe_9Mn_{14}$	12.265		84 B 4
$Y_6Fe_9Mn_{14}H_{24}$	12.814	14.0	84 B 4
$Y_6Fe_{5.75}Mn_{17.25}$	12.094		84 B 4
$Y_6Fe_{5.75}Mn_{17.25}H_{20}$	12.412	8.1	84 B 4
$Y_6Fe_5Mn_{18}$	12.331		84 B 4
$Y_6Fe_5Mn_{18}H_{25}$	12.855	13.3	84 B 4

For hydrogen absorption and desorption see

$R_6M_{23}H_x$ $R_6Mn_{23}H_x$, R = Gd, Dy, Ho, Er [87 S 20]; R = Nd, Sm, Gd, Y [81 B 15]; R = Y [76 B 18, 83 W 3, 84 M 1]; R = Th [77 M 5, 83 W 3, 84 M 1]; $R_6Fe_{23}H_x$ [83 S 22, 83 W 4, 87 S 20]; R = Ho, Er [81 B 9]; R = Ho, Er, Lu, Y [87 S 20]

$R_6(M'M'')_{23}$ $Er_6(FeMn)_{23}H_x$ [82 Z 3]; $Y_6(FeMn)_{23}H_x$ [84 B 4]

For structure and lattice parameters see also

R_6M_{23} R_6Mn_{23} [67 K 1, 67 K 2, 83 C 8]; R = Sm, Gd, Tb, Dy, Ho, Er, Tm, Lu [65 K 2]; R = Nd, Sm, Gd, Tb, Dy, Ho, Er, Tm, Lu, Y [65 W 1]; R = Nd, Sm, Gd, Er, $Er_{0.5}Y_{0.5}$ [82 P 1]; R = Gd [64 W 4]; R = Dy [70 D 1]; R = Yb [83 T 6, 83 T 7, 83 T 8]; R = Y [77 B 13, 77 B 19]; R = Th [52 F 1, 77 B 13]

R_6Fe_{23} [83 C 8]; R = Dy [82 B 1]; R = Y [76 B 18]

$R_6M_{23}H_x$ $R_6Mn_{23}H_x$ [77 B 21, 77 B 22]; R = Nd, Sm, Gd, Y [81 B 15]; R = Gd, Ho, Er [80 P 8]; R = Tb, Dy [80 P 9]; R = Tm, Er [85 S 22]; R = Tm [84 H 3]; R = Y [77 B 13, 77 B 19, 79 C 5, 82 C 14, 83 W 3]; R = Th [77 B 13, 80 H 4, 83 W 3]

$R_6Fe_{23}H_x$ [83 W 4]; R = Ho, Er [81 B 9]; R = Tm, Er [85 S 22]; R = Ho [83 P 8]; R = Y [76 B 18]

$(R'R'')_6M_{23}$ $(ThY)Mn_{23}$ [81 B 8, 82 B 10]; $(ErY)_6Fe_{23}$ [83 P 9]

$(R'R'')_6M_{23}H_x$ $(ThY)Mn_{23}H_x$ [82 B 10]

$R_6(M'M'')_{23}$ $R_6(FeMn)_{23}$, R = Dy, Ho, Er [71 H 2]; R = Gd [86 N 1]; R = Sm [80 Z 3]; R = Y [76 B 5, 80 H 2, 80 H 5]

$Tb_6(FeAl)_{23}$ [72 O 5]; $Y_6(FeAl)_{23}$ [79 B 5]

$R_6(M'M'')_{23}H_x$ $Y_6(FeMn)_{23}H_x$ [77 O 4, 84 B 4]

Single crystal growing: $Y_6(FeCo)_{23}$ [82 W 6]

For thermal expansion see also:

Er_6Fe_{23} [73 B 23]; R_6Mn_{23}, R = Gd, Tb, Y [80 J 1]

Magnetization, Curie temperatures

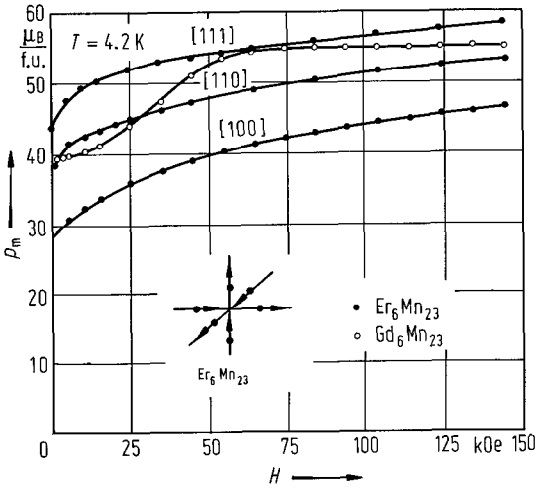

Fig. 301. Magnetization isotherms at 4.2 K for Gd_6Mn_{23} and Er_6Mn_{23} compounds. The magnetic field is applied along the [111], [110] and [100] crystallographic axes. In the insert, the arrangement of Er magnetic moments in Er_6Mn_{23} compound in zero applied field at 4.2 K is shown [79 D 3, 79 H 2].

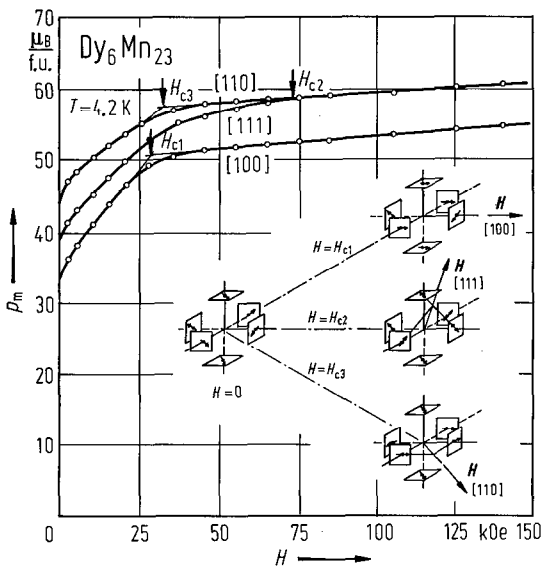

Fig. 302. Magnetization isotherms at 4.2 K for Dy_6Mn_{23} compounds. The magnetic field is applied along the [111], [110] and [100] crystallographic axes. In the insert the arrangements of Dy magnetic moments in zero field and for different fields as compared to critical values, H_c, are shown [79 D 3, 79 H 2].

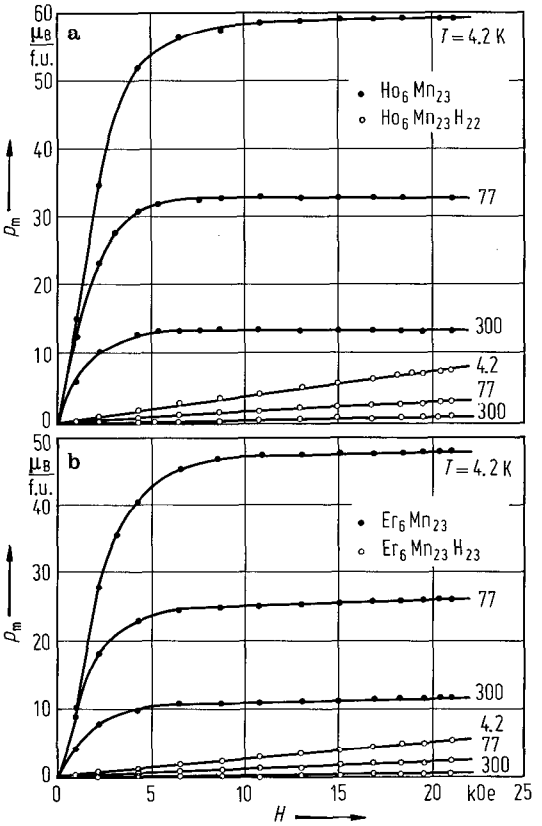

Fig. 303. Magnetization isotherms for (a) Ho_6Mn_{23} and its hydride and (b) Er_6Mn_{23} and its hydride measured at 4.2, 77 and 300 K [80 P 8]. A substantial weakening, by hydrogenation, of the magnetic coupling between the rare-earth and manganese sublattices is suggested.

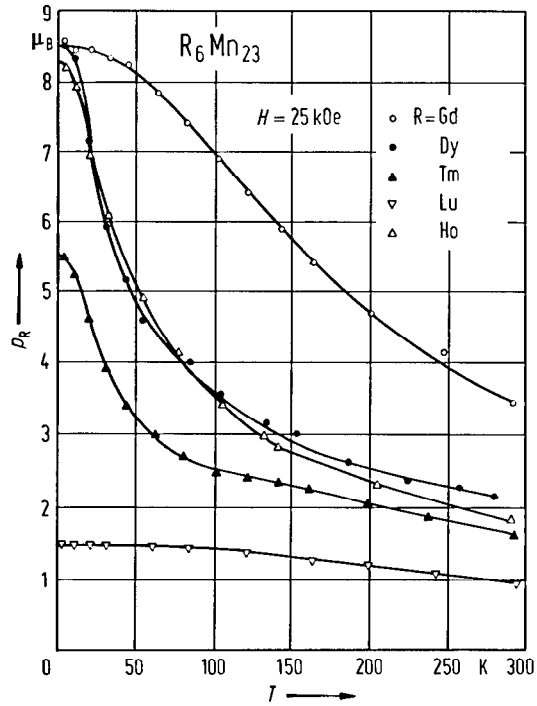

Fig. 304. Temperature dependence of the magnetization in R_6Mn_{23} (R=Gd, Dy, Ho, Tm, Lu) compounds [65 D 1]. The data were obtained in the temperature range 1.3···300 K and magnetic fields up to 25 kOe.

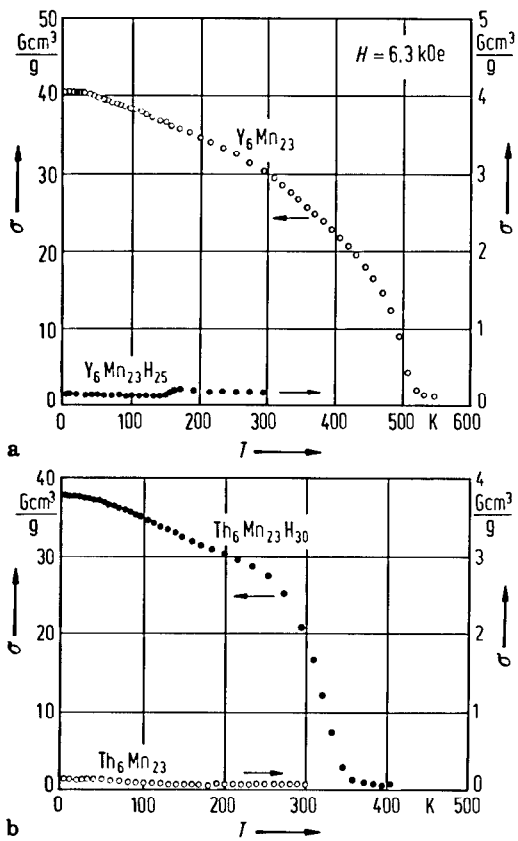

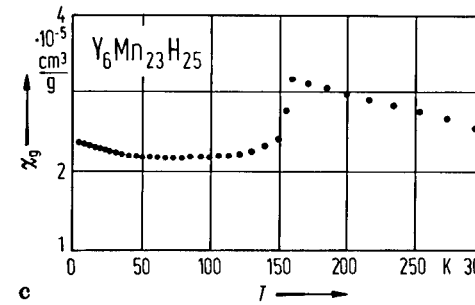

Fig. 305. Temperature dependence of the magnetizations in (a) Y_6Mn_{23} and (b) Th_6Mn_{23} in a magnetic field of 6.3 kOe before and after hydrogen absorption [77 M 5]. The temperature dependence of the magnetic susceptibility of $Y_6Mn_{23}H_{25}$ is given in (c).

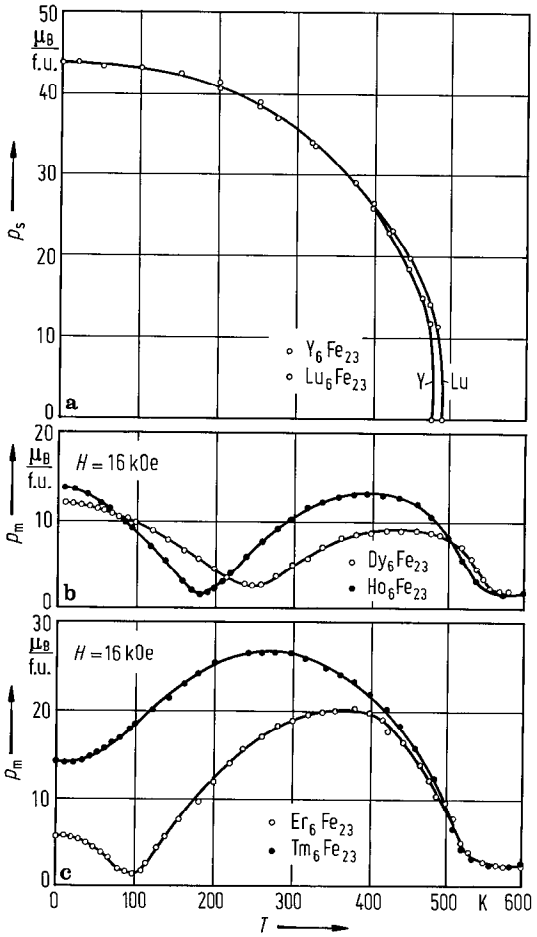

Fig. 306. Thermal variation of (a) spontaneous magnetization for Lu_6Fe_{23} and Y_6Fe_{23} [69 G 1], and magnetization at 16 kOe for (b) Dy_6Fe_{23}, Ho_6Fe_{23} and (c) Er_6Fe_{23} and Tm_6Fe_{23} compounds [84 H 5].

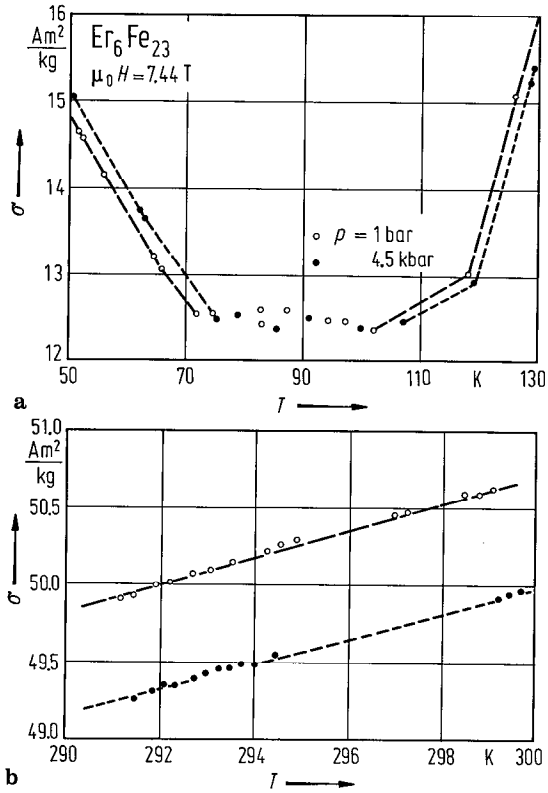

Fig. 307. (a) Magnetization versus temperature curves near the compensation temperature of Er_6Fe_{23} in $\mu_0 H = 7.44$ T for different pressures. (b) shows the corresponding data near room temperature. The Er–Fe interaction is independent of pressure, temperature and magnetic field, in the range of experimental facilities. The magnetic moment of the Fe sublattice at 4.2 K has a negative pressure dependence that is about twice as large as that for pure Fe. The volume dependence of the Fe magnetic moments, however, is of nearly equal magnitude in Er_6Fe_{23} as in iron [83 F 7].

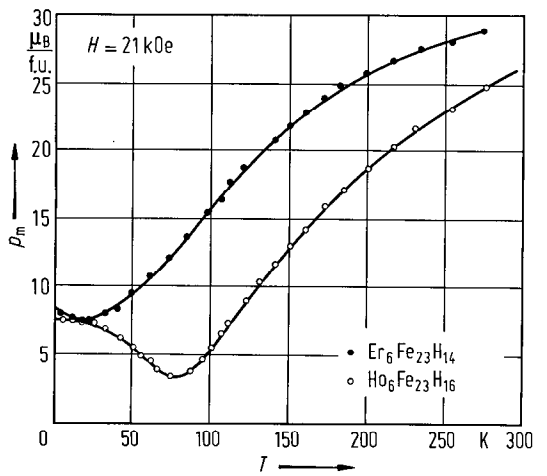

Fig. 308. Magnetization versus temperatures in an applied magnetic field of 21 kOe for $Ho_6Fe_{23}H_{16}$ and $Er_6Fe_{23}H_{14}$ hydrides [81 B 9].

Table 78a. Magnetic properties of R_6Mn_{23} compounds.

	T_C(K)						p_s at 4.2 K (μ_B/f.u.)								p_{eff} [4]) μ_B/R	Θ [4]) K
	69 K 4	77 B 22	80 P 8, 80 P 9	81 B 15	82 P 1	84 T 2	65 D 1	71 K 1	77 B 22	79 H 2	80 P 9, 80 P 8	81 B 15	82 P 1	84 T 2		
Nd_6Mn_{23}	416			438	445		9.6					4.8 [3])	10.1		5.23	60
Sm_6Mn_{23}	439			450	442		3.0					3.0 [3])	10.3		5.04	85
Gd_6Mn_{23}	468	461		461			50.4		49	54.5*	55 [1])				10.04	− 90
Tb_6Mn_{23}	455		455	455			44.4				49 [2])	49 [3])			15.3	−360
Dy_6Mn_{23}	443		443	443			49.8				49.6 [2])				11.47	25
Ho_6Mn_{23}	434		434				49.2				59.8 [2])				11.83	− 5
Er_6Mn_{23}	415		415		420		45.6			46*	38 [1])				10.56	30
Tm_6Mn_{23}							30.6									
Yb_6Mn_{23}						406								0.7		
Lu_6Mn_{23}		378							8.9			8.9 [3])				
Y_6Mn_{23}	486	486	486	486				13.6	13.2	13.8*		13.2 [3])			2.35	475
Th_6Mn_{23}							$\chi_g = 1.10^{-6}$ cm^3 g^{-1}			[77 B 22]						

[1]) K. Hardman, Ph. D. Thesis cited in [80 P 8], in a field of 50 kOe.
[2]) In a field of 21 kOe.
[3]) In a field of 18 kOe.
[4]) [69 K 4].

Table 78b. Magnetic properties of R_6Fe_{23} compounds.

	T_C(K)							p_s at 4.2 K (μ_B/f.u.)							
	68 S 1	69 G 1	70 V 1	80 b 1	77 b 1	81 B 9	84 H 5	68 S 1	69 G 1	70 V 1	80 b 1	77 b 1	77 O 5	81 B 9	84 H 5
Gd_6Fe_{23}	659 [1])							15.3							
Tb_6Fe_{23}				577							11.3				
Dy_6Fe_{23}			545				529			15.1			18.2		11.89
Ho_6Fe_{23}						501	509							13.8 [2])	13.79
Er_6Fe_{23}						493	489							8.2 [2])	6.03
Tm_6Fe_{23}				443			483				13.6				14.50
Yb_6Fe_{23}					481							43.9			
Lu_6Fe_{23}		491		494					44		44.7				
Y_6Fe_{23} [3])		478		464		485	484		44		41.5			38 [2])	42.84

[1]) As cited in [77 b 1].
[2]) In a field of 21 kOe.
[3]) Above T_C the reciprocal magnetic susceptibility follows a Curie-Weiss law, $p_{eff} = 3.73\,\mu_B$/Fe [70 B 8].

Table 79. Magnetic properties of some R_6M_{23} hydrides (deuterides).

	$T_C(T_N)$	T_{comp}	p_s	Ref.
	K		μ_B/f.u.	
$Nd_6Mn_{23}H_x$	220		20.8 [1])	81 B 15
$Sm_6Mn_{23}H_x$	230		15.3 [1])	81 B 15
$Gd_6Mn_{23}H_x$	260		14.2 [1])	81 B 15
$Gd_6Mn_{23}H_x$	166		14.2	77 B 22
$Gd_6Mn_{23}H_{22}$	≅180		8.4 [2])	80 P 9
$Tb_6Mn_{23}H_{23}$	≅220		17.7 [2])	80 P 9
$Dy_6Mn_{23}H_{23}$		paramagnetic		80 P 9
$Lu_6Mn_{23}H_x$	266		3.4	77 B 22
$Y_6Mn_{23}D_{23}$	(170)		(AF)	82 C 14, 84 H 2
$Y_6Mn_{23}H_{23}$		$\chi_g = 0.2 \cdot 10^{-5}$ cm^3 g^{-1}		77 B 22
$Y_6Mn_{23}H_{25}$		nonmagnetic		77 M 5, 78 B 21
$Th_6Mn_{23}H_x$	335		16.5	77 B 22
$Th_6Mn_{23}H_{30}$	329		18.4	77 M 5
$Ho_6Fe_{23}D_{1.5}$	575	170	15.9	83 P 8, 87 W 3
$Ho_6Fe_{23}D_{8.2}$	671	120	14.6	83 P 8, 87 W 3
$Ho_6Fe_{23}D_{12.1}$	696	98	11.4	83 P 8, 87 W 3
$Ho_6Fe_{23}D_{15.7}$	702	72	7.2	83 P 8, 87 W 3
$Ho_6Fe_{23}H_{16}$	>300	75	7.8	81 B 9
$Er_6Fe_{23}H_{14}$	>300	19.5	8.0	81 B 9
$Tm_6Fe_{23}H_{14}$	550		23.6	84 G 6

[1]) In a field of 18 kOe.
[2]) In a field of 21 kOe.

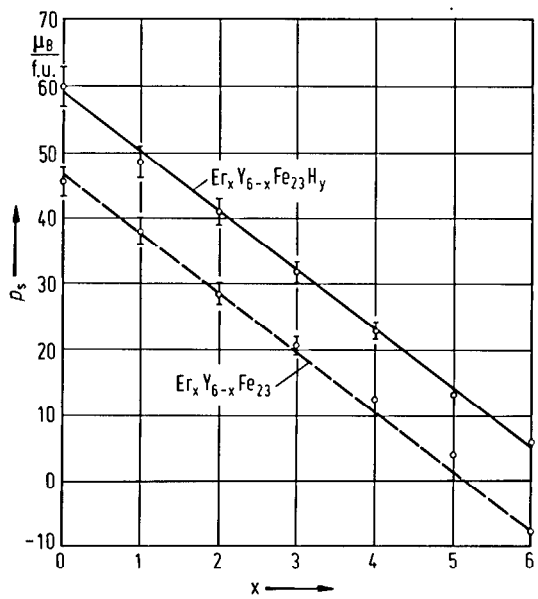

Fig. 309. Saturation magnetization at 4.2 K versus composition in $Y_{6-x}Er_xFe_{23}$ alloys and their hydrides [83 P 9]. The lines drawn through the points are those predicted assuming the Fe magnetic moment to be constant and $p_{Er} = 9\,\mu_B$ coupled antiparallel to the Fe moments. These data suggest that the Er moment is not significantly quenched by the crystal field effects.

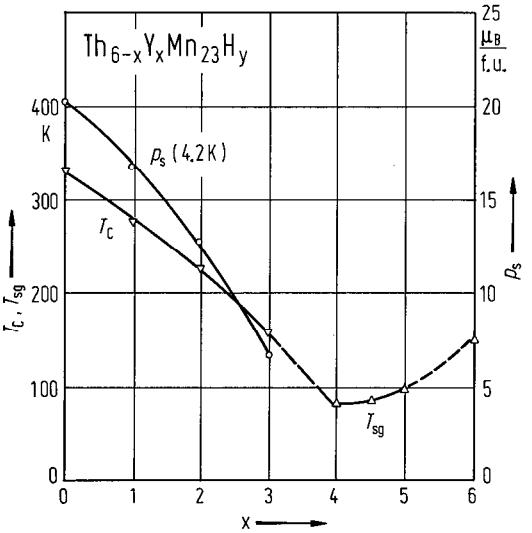

Fig. 310. Saturation magnetization at 4.2 K and ordering temperature of $Th_{6-x}Y_xMn_{23}$ hydrides, as function of composition [82 B 10]. T_C is the Curie temperature, T_{sg} the spin glass freezing temperature. The Th-rich ($x = 0 \cdots 3$) hydrides exhibit magnetic ordering. They resemble the Th_6Mn_{23} hydride. The Y-rich hydride ($x = 4.6$) behave as spin glass systems. The different magnetic behaviour is ascribed to the substantial difference in the Mn–Mn nearest-neighbour distance. The spin glass nature of the Y-rich hydrides is though to originate from fluctuations in the sign of the exchange interaction from point to point in the lattice. Hydrogen capacity varies linearly with x.

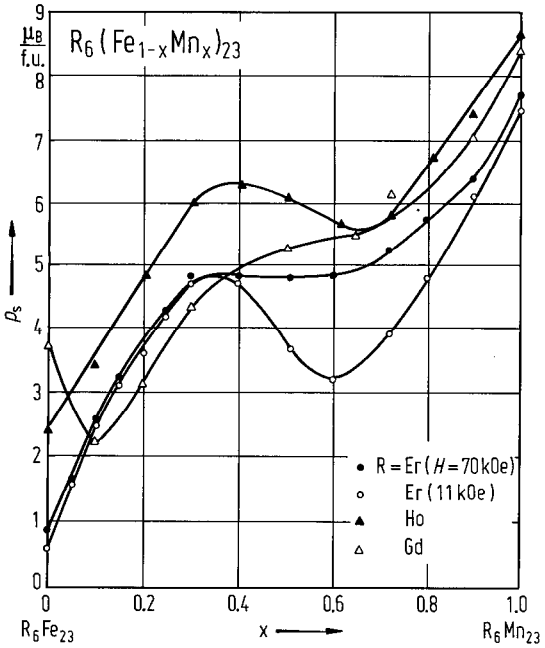

Fig. 311. Composition dependence of the saturation magnetization at 4.2 K in $Gd_6(Fe_{1-x}Mn_x)_{23}$ [71 K 1], $Ho_6(Fe_{1-x}Mn_x)_{23}$ [71 H 2, 73 K 11], and $Er_6(Fe_{1-x}Mn_x)_{23}$, [78 H 5] compounds.

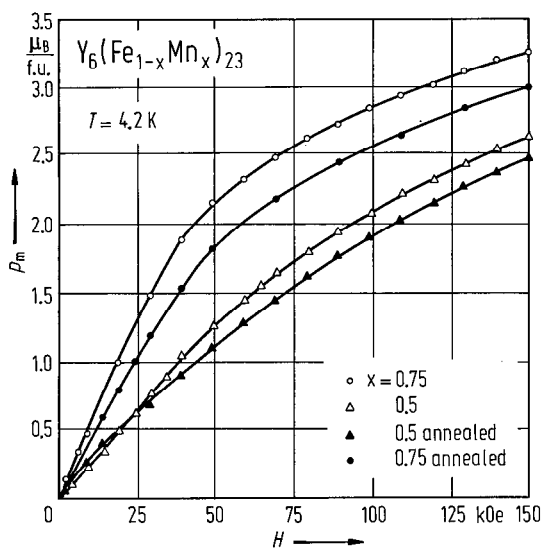

Fig. 313. Magnetization isotherms at 4.2 K for some $Y_6(Fe_{1-x}Mn_x)_{23}$ compounds [79 J 2]. These suggest a magnetic clustering or spin glass behaviour.

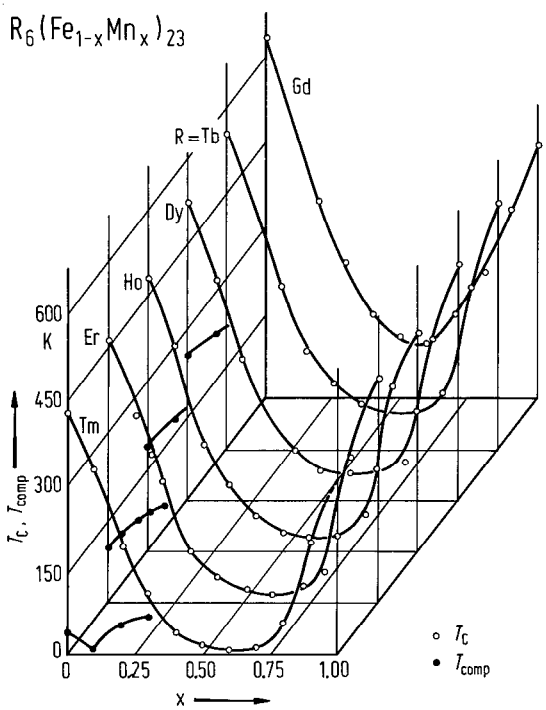

Fig. 312. Composition dependence of the Curie temperature T_C and compensation temperature T_{comp}, in $R_6(Fe_{1-x}Mn_x)_{23}$ (R = Gd, Tb, Dy, Ho, Er, Tm) compounds [78 H 5].

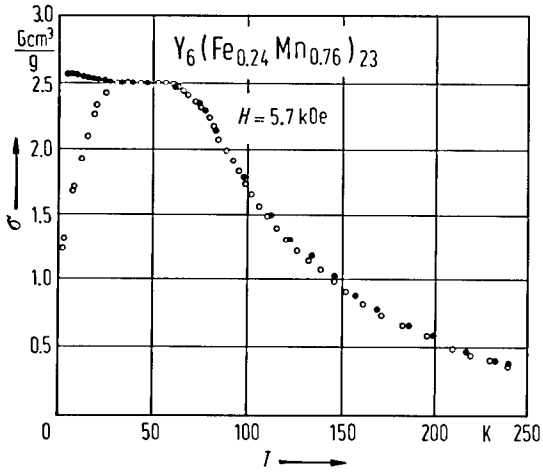

Fig. 314. Magnetization versus temperature at an applied magnetic field of $H = 5.7$ kOe for $Y_6(Fe_{0.24}Mn_{0.76})_{23}$. Results obtained after zero field cooling are indicated by open circles and after field cooling by solid circles. This behaviour may be understood in terms of spin glass behaviour [77 H 4].

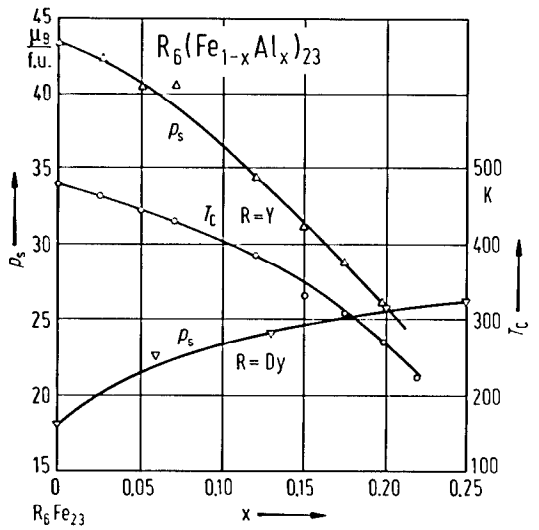

Fig. 316. Composition dependences of the saturation magnetizations at 4.2 K in $Y_6(Fe_{1-x}Al_x)_{23}$ [79 B 5] and $Dy_6(Fe_{1-x}Al_x)_{23}$ [77 O 5] compounds and of the Curie temperatures in $Y_6(Fe_{1-x}Al_x)_{23}$ compounds [79 B 5].

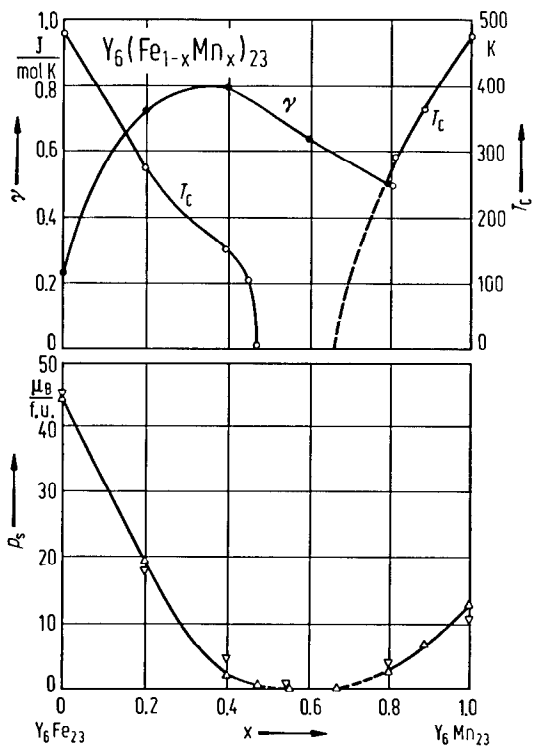

Fig. 315. Composition dependences of the Curie temperature; saturation magnetization at 4.2 K, inverted triangles [76 B 5], triangles [71 K 1]; as well as electronic specific heat coefficient [76 B 5] in $Y_6(Fe_{1-x}Mn_x)_{23}$ compounds.

For magnetic properties see also:

R_6M_{23} R_6Mn_{23} [65 K 1, 69 K 4, 83 C 8, 87 U 2(T)]; R = Gd, Dy, Er, Y [79 H 2]; R = Nd, Sm, Gd, Tb, Dy, Ho, Er, Tm, Lu [65 D 1]; R = Sm, Gd, Dy, Ho, Er, Y [66 K 1]; R = Nd, Sm, Gd, Er, $Er_{0.5}Y_{0.5}$ [82 P 1]; R = Gd, Dy, Er [79 D 3]; R = Tb, Dy [80 P 9]; R = Er [82 Z 3]; R = Yb [83 T 6, 83 T 7, 83 T 8, 84 T 2]; R = Y [77 B 13, 77 B 19, 82 Z 3, 84 M 1]; R = Th [77 B 13, 84 M 1]; R = Dy, Tm [82 B 15]

R_6Fe_{23} [69 K 4, 79 B 2, 83 C 8, 88 R 1]; R = Dy, Ho, Er, Tm, Lu, Y [84 H 5]; R = Dy [82 B 1]; R = Er [72 B 15, 79 G 11]; R = Tm [72 B 6, 84 G 5]; R = Y [70 B 8, 72 B 15, 74 M 8, 76 B 18]

$R_6M_{23}H_x$ $R_6Mn_{23}H_x$ [77 B 21, 77 B 22]; R = Gd, Dy, Ho [80 P 8]; R = Tb, Dy [80 P 9]; R = Nd, Sm, Gd, Y [81 B 15]; R = Y [77 B 13, 77 B 19, 77 B 22, 79 C 5, 84 M 1, 87 W 3]; R = Th [77 B 13, 77 M 5, 78 B 22, 78 W 3, 84 M 1, 87 W 3]; R = Dy, Tm [82 B 15]

$R_6Fe_{23}H_x$ [83 W 2]; R = Ho [81 B 9, 83 P 8, 87 W 3]; R = Er [81 B 9]; R = Tm [84 G 5]; R = Lu [81 G 18]; R = Y [76 B 18, 78 B 22]

$(R'R'')_6M_{23}$	$(ThY)_6Mn_{23}$ [81 B 8, 82 B 10]; $(YEr)_6Fe_{23}$ [83 P 9]; $(GdY)_6Fe_{23}$ [83 P 10]
$(R'R'')_6M_{23}H_x$	$(ThY)_6Mn_{23}H_x$ [82 B 10]; $(GdY)_6Fe_{23}H_x$ [83 P 10]
$R_6(M'M'')_{23}$	$R_6(FeMn)_{23}$ [69 K 4, 73 H 4]; R = Gd, Tb, Dy, Ho, Er, Tm [73 K 11]; R = Sm [80 Z 3, 82 B 3, 82 B 4, 82 Z 1, 83 Z 1]; R = Gd [71 K 1, 86 N 1, 87 N 1]; R = Dy [71 H 2]; R = Ho [71 H 2]; R = Er [71 H 1, 71 H 2, 78 H 5, 83 F 7]; R = Y [68 K 2, 71 K 1, 76 B 5, 76 O 4, 77 G 9, 77 F 5, 77 H 4, 79 J 2, 81 H 1, 83 C 8, 83 L 3]; $R_6(FeNi)_{23}$ [73 H 4], $Tb(FeAl)_{23}$ [72 O 5]; $Dy(FeAl)_{23}$ [77 O 1, 77 O 5]; $Y(FeAl)_{23}$ [79 B 5]
$R_6(M'M'')_{23}H_x$	$Y_6(FeMn)_{23}H_x$ [77 O 4]; $(GdY)_6Fe_{23}H_x$ [83 P 10]

Neutron diffraction

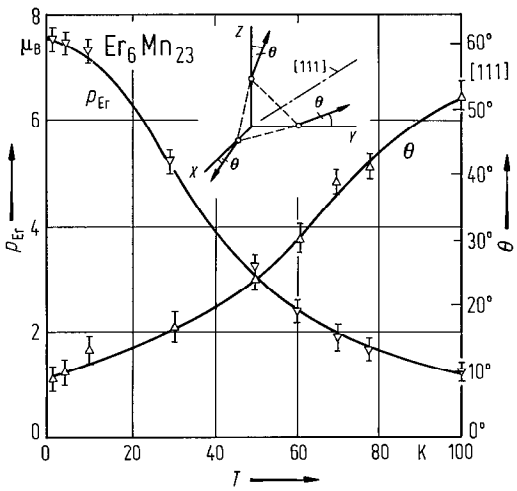

Fig. 317. Temperature dependence of the Er magnetic moment and the angle θ between p_{Er} and the [100] axis in Er_6Mn_{23} compound [82 K 1]. At low temperatures, the crystal field term favours the [100] direction. The Er atoms on the three different cube axes have easy directions normal, to each other and thus the magnetic structure is noncollinear.

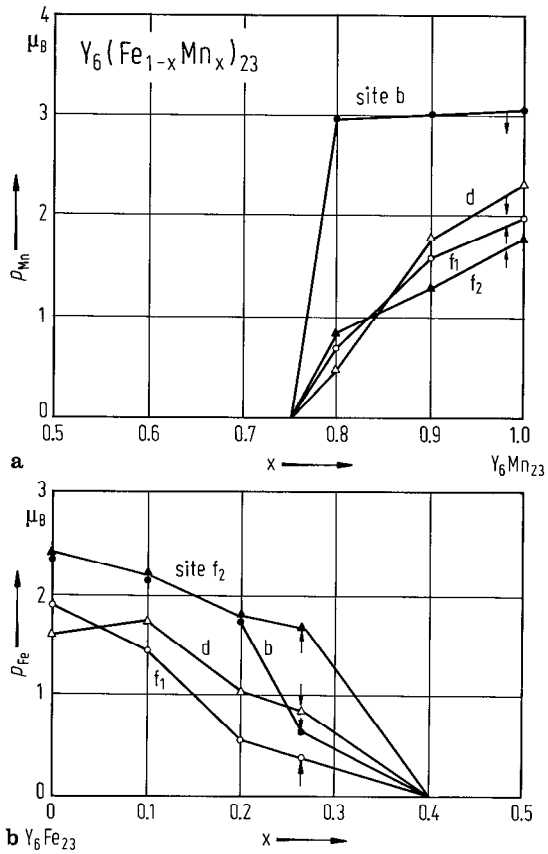

Fig. 318. (a) Composition dependence of the Mn magnetic moments of the four sublattices in $Y_6(Fe_{1-x}Mn_x)_{23}$ alloys at 4.2 K with $x > 0.7$. The magnetic moments of Fe atoms are not ordered in this composition range. The arrows indicate the relative spin directions on each site. (b) Fe sublattice magnetic moments as a function of Mn content for $x < 0.4$. The magnetic moments of Mn atoms are not ordered. All Fe moments are coupled parallel except for $x = 0.27$ which has the antiferromagnetic configuration [81 H 1]. In case of $Y_6(Fe_{0.4}Mn_{0.6})_{23}$ compound an antiferromagnetic short-range order with correlation length of $\cong 30$ Å coexists with ferrimagnetic short-range order with a correlation length of $\cong 200$ Å. A mean magnetic moment of 0.7 μ_B/3d atom was detected at low temperatures [83 L 3]. The neutron depolarization measurements on $Y_6(Fe_{1-x}Mn_x)_{23}$ having $x = 0.50$ and 0.55 show the absence of spontaneous order down to 30 mK [77 G 9].

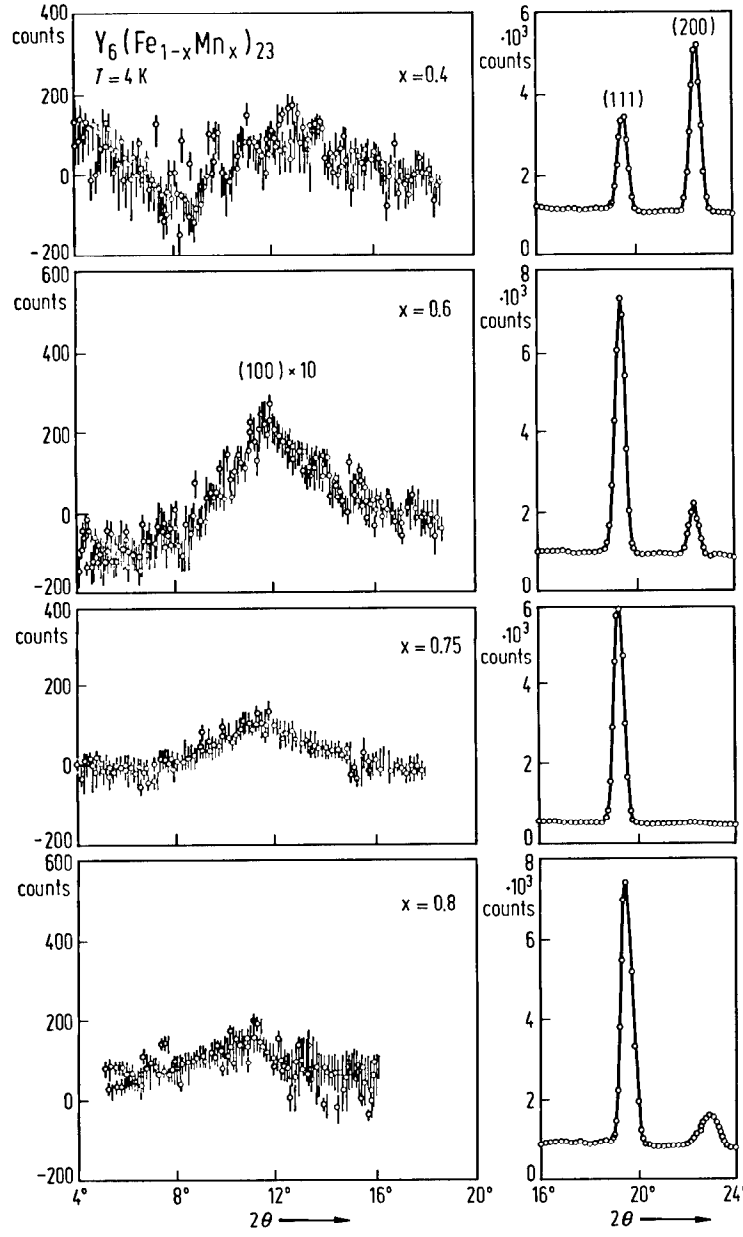

Fig. 319. Diffuse scattering peaks arising from short-range antiferromagnetic correlations observed at the forbidden lattice reflection point (100) in $Y_6(Fe_{1-x}Mn_x)_{23}$ alloys in the composition range $0.50 < x < 0.75$. This corresponds to the destruction of long-range order for these intermediate compositions by competing ferromagnetic (Fe) and antiferromagnetic (Mn) exchange interactions [87 R 8]. See also [83 L 3, 83 H 1]. The Q-width of the scattering reflects a cluster size of 30···45 Å with the average Mn magnetic moment largest for the $Y_6(Mn_{0.6}Fe_{0.4})_{23}$ compound, varying from 1.43 μ_B at 4.2 K to 1.1 μ_B at 100 K [83 H 1]. Other compositions studied showed similar short-range correlations but with smaller average magnetic moments, suggesting that the maximum exchange disorder occurs in the range $x = 0.5 \cdots 0.6$. The Fe magnetic moments in this range do not order in ferromagnetic clusters, as confirmed from both neutron small-angle scattering results and Mössbauer effect studies.

Table 80. Magnetic moments of rare-earth and transition metal atoms, determined by neutron diffraction in R_6M_{23} compounds.

	T K	$p_R(\mu_B)$	$p_M(\mu_B)$				Ref.
		24e	4b	24d	$32f_1$	$32f_2$	
Er_6Mn_{23} [1])	4.2	7.5(1)	−2.6(2)	−1.7(1)	1.6(1)	1.5(1)	82 K 1
	300	0.50(5)	−1.88(9)	−1.44(4)	1.21(4)	1.05(3)	82 K 1
Y_6Mn_{23}	4.2	0.01(3)	−2.81(12)	−2.07(4)	1.79(4)	1.77(4)	79 D 3, 82 K 1
	300	0.03(3)	−2.25(9)	−1.72(4)	1.52(3)	1.27(3)	79 D 3, 82 K 1
	4.2	–	−3.05	−2.34	1.99	1.80	84 H 2
$Y_6Mn_{19.7}$ [2])	80	–	−2.4(2)	−2.0(1)	2.4(1)	2.2(1)	83 J 2
$Y_6Mn_{21.1}$ [2])	80	–	−3.6(2)	−2.5(1)	1.9(1)	1.7(1)	83 J 2
$Y_6Mn_{21.7}$ [2])	80	–	−3.5(1)	−2.4(1)	1.9(1)	1.8(1)	83 J 2
$Y_6Mn_{22.5}$ [2])	80	–	−3.5(1)	−2.4(1)	1.8(1)	1.7(1)	83 J 2
$Y_6Mn_{23.7}$ [2])	80	–	−3.4(1)	−2.4(1)	1.7(1)	1.8(1)	83 J 2
$Y_6Mn_{24.6}$ [2])	80	–	−4.6(2)	−2.5(1)	1.9(1)	1.7(1)	83 J 2
Ho_6Fe_{23}	4.2	9.3		−2.25			70 R 3
	4.2	9.7	−2.2	−1.3	−1.6	−2.2	83 R 5
	78	9.3	−2.2	−1.1	−1.5	−1.9	83 R 5
	295	5.6	−2.2	−1.4	−1.5	−2.1	83 R 5
Er_6Fe_{23}	4.2 [3])	7.8(1)	−1.2(1)	−1.4(1)	−2.3(2)	−2.0(2)	84 H 6
	10 [4])	8.03(9)	−1.9(2)	−2.27(9)	−3.2(1)	−3.0(1)	84 H 6
	300 [3])	3.77(8)	−1.6(2)	−1.49(7)	−2.29(9)	−1.70(8)	84 H 6
	300 [4])	4.28(9)	−0.9(2)	−1.2(1)	−1.9(1)	−1.5(1)	84 H 6
Y_6Fe_{23}	4.2	−0.17	1.97	1.76	1.99	2.20	80 H 3

[1]) See also Fig. 317.

[2]) The compositions were determined in post-cast samples by absorption analysis. The extreme variations in stoichiometry cause little change in the magnetic moment magnitude. The different results obtained in the literature on Y_6Mn_{23} probably arise from the presence of a small amount of a second phase, YMn_2, in the Mn-deficient samples, and YMn_{12} in the Mn-rich samples [83 J 2].

[3]) Unconstrained data determined at University of Missouri Research Reactor.

[4]) Unconstrained data determined at Petten Reactor.

Table 81a. Magnetic moments of rare-earth and transition metal atoms determined by neutron diffraction studies in R_6M_{23}-deuterides, Fm3m structure. [1])

	T K	$p_R(\mu_B)$	$p_M(\mu_B)$				Ref.
		24e	4b	24d	$32f_1$	$32f_2$	
$Ho_6Fe_{23}D_{1.5}$	4.2	10.2	−2.2	−0.9	−1.3	−2.0	83 R 5
	295	5.7	−2.2	−1.2	−1.4	−1.9	83 R 5
$Ho_6Fe_{23}D_{8.2}$	4.2	9.1	−2.2	−1.8	−0.88	−2.1	83 R 5
	295	4.2	−2.2	−1.6	−0.83	−1.9	83 R 5
$Ho_6Fe_{23}D_{15.2}$	4.2	10.2	−2.2	−2.4	−2.0	−2.2	83 R 5
	295	4.3	−2.2	−2.3	−1.8	−1.9	83 R 5
$Ho_6Fe_{23}D_{22}$	4.2	9.1	−2.2	−1.8	−0.88	−2.1	83 R 5
	77	8.3	−2.2	−1.8	−0.83	−2.1	83 R 5
	295	4.2	−2.2	−1.6	−0.83	−1.9	83 R 5
$Th_6Mn_{23}D_{3.0}$	4.2	–	−3.5	0.80(10)	1.84(10)	1.50(10)	84 H 1

[1]) See also [79 C 5].

Table 81b. Magnetic moments of rare-earth and transition metal atoms determined by neutron diffraction studies in R_6Mn_{23}-deuterides, P4/mmm structure.

	T K	$p_R(\mu_B)$				$p_M(\mu_B)$									Ref.
		g	h	j	k	b	c	e	f	r_1	s_1	t_1	s_2	t_2	
$YMn_{23}D_{23}$	4.2	–	–	–	–	−3.68	+3.68	0	0	0	0	0	1.60	−1.60	84 H 2
	78	–	–	–	–	−3.60	+3.60	0	0	0	0	0	2.08	−2.08	84 H 2
$Ho_6Mn_{23}D_{23}$	9	3.4	3.4	3.5	3.5	3.5	3.5	2.3	2.3	0	2.8	2.8	1.5	1.5	86 L 5
		$\theta = 51.4°$	128.6°	100.1°	79.9°	89.5°	150.5°	67.7°	112.3°		47.5°	62.5°	30.3°	149.7°	

Table 81c. Magnetic moments of rare-earth and transition metal atoms determined by neutron diffraction studies in R_6Fe_{23}-deuterides, I4/mmm structure.

	T K	$p_R(\mu_B)$		$p_M(\mu_B)$					Ref.
		8e	16h	4b	8c	16f	$32n_1$	$32n_2$	
$Ho_6Fe_{23}D_{12.1}$	4.2	10.2	10.2	−2.0	−2.5	−2.5	−1.1	−2.5	83 R 5
	295	4.1	4.3	−2.2	−2.0	−2.3	−1.1	−2.0	83 R 5

For neutron diffraction studies see also

R_6M_{23} R_6Mn_{23}, R = Er [82 K 1]; R = Yb [83 T 6, 83 T 7, 83 T 8, 84 T 2]; R = Y [68 D 3, 78 H 2, 79 D 3, 82 K 1, 83 J 2]
R_6Fe_{23}, R = Ho [70 R 3]; R = Er [84 H 6]; R = Y [78 H 2]

$R_6M_{23}H_x$ $Ho_6Mn_{23}D_x$ [86 L 5]; $Y_6Mn_{23}D_x$ [82 C 14, 84 H 2]; $Th_6Mn_{23}D_x$ [84 H 1]; $Ho_6Fe_{23}H_x$ [83 R 5, 87 R 9]

$R_6(M'M'')_{23}$ $Y_6(FeMn)_{23}$ [80 H 5, 81 H 1, 83 H 1, 83 L 3, 87 R 8]; $Y_6(FeAl)_{23}$ [85 G 3]

Mössbauer effect

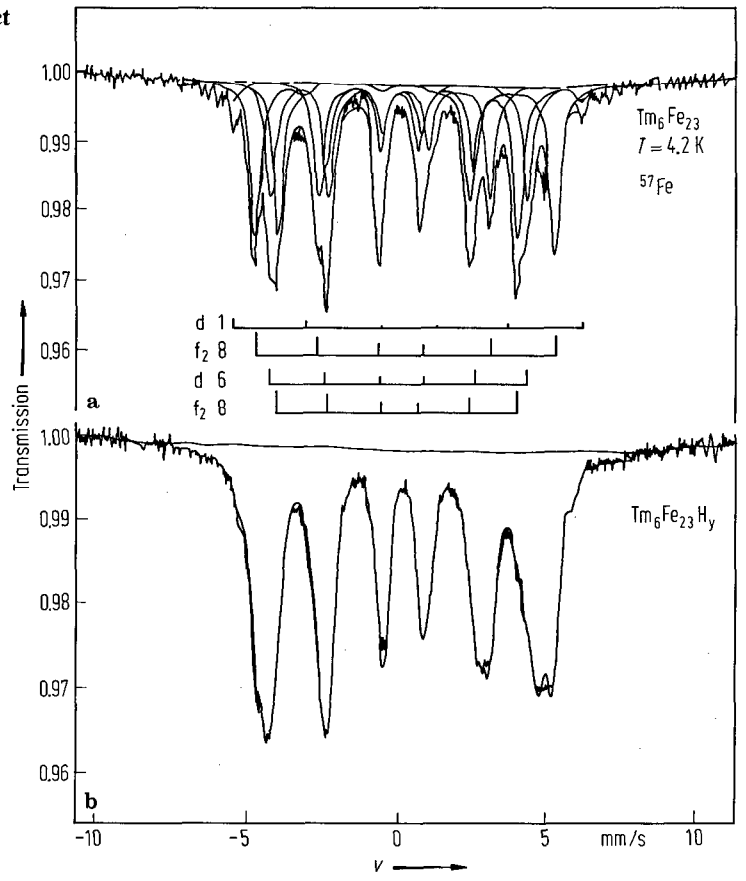

Fig. 320. ^{57}Fe Mössbauer spectra of (a) Tm_6Fe_{23} and (b) its hydride at 4.2 K. The decomposition of the Tm_6Fe_{23} spectrum into four subspectra corresponding to the four crystallographic Fe sites is shown schematically [84 G 6].

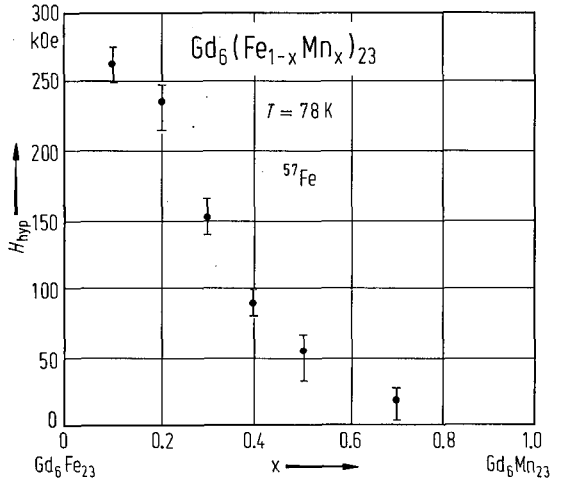

Fig. 321. Mean ^{57}Fe magnetic hyperfine fields at 78 K in $Gd_6(Fe_{1-x}Mn_x)_{23}$ alloys [86 N 1]. In $Er_6(^{57}Fe:Mn)_{23}H_{26}$ a sudden appearance below 85 K of a small hyperfine field is evidenced [81 S 14]. Similar, in $Y_6(^{57}Fe:Mn)_{23}H_{26}$, the small ^{57}Fe hyperfine field increases a abruptly below 110 K [81 S 15].

Table 82. ^{57}Fe magnetic hyperfine fields and easy direction of magnetization in several R_6Fe_{23} compounds.

	T K	H_{hyp}(kOe)					Easy axis of magnetization	Ref.
		1b	2d	4d	$8f_1$	$8f_2$		
Ho_6Fe_{23}	4.2	352		283	310	267	[111]	77 b 1
Er_6Fe_{23}	4.2	367		272	314	262	[111]	77 G 14, 78 G 5
Tm_6Fe_{23}	4.2	364		270	315	255		77 b 1, 84 G 5
Yb_6Fe_{23}	4.2	355		272	313	249		77 b 1
Y_6Fe_{23}	16	370	264	270	309	253	[100]	77 G 14, 78 G 5

Table 83. Hyperfine parameters obtained from ^{169}Tm Mössbauer spectroscopy, after extrapolation to 0 K. The $\mu_0 H^*_{hyp}$ values were obtained after correcting for the transferred field (3.2 T) due to the Fe sublattice. The last column lists the Tm magnetic moment corresponding to H^*_{hyp} [84 G 5].

	ΔQ cm/s	$\mu_0 H_{hyp}$ T	$\mu_0 H^*_{hyp}$ T	p_{Tm} μ_B
Tm_6Fe_{23}	15.2(3)	757	725	7.05
$Tm_6Fe_{23}H_x$	14.0(3)	727	695	6.75
Free Tm ion	15.7			7.00

For Mössbauer effect studies see also:

^{57}Fe $R_6(^{57}FeMn)_{23}$, R = Sm [83 Z 5]; R = Er [81 S 14]; R_6Fe_{23}, R = Dy [82 B 1]; R = Ho [87 W 3]; R = Er [77 G 14, 78 G 5, 85 W 4]; R = Tm [84 G 5, 84 G 6]; R = Y [69 K 4, 74 M 8, 74 M 9, 74 G 16, 78 G 5]
$R_6(^{57}FeMn)_{23}$, R = Er [81 S 14, 82 Z 3]; R = Y [81 S 15, 82 Z 3]
$R_6Fe_{23}D_x$, R = Ho [85 P 4, 87 W 3]; R = Tm [84 G 5, 84 G 6]; R = Lu [81 G 18]
$R_6(M'M'')_{23}$, $Gd(FeMn)_{23}$ [86 N 1, 87 N 1]; $Sm(FeMn)_{23}$ [82 B 3, 82 B 4]; $Y_6(FeMn)_{23}$ [80 L 5, 86 T 3]

^{155}Gd Gd_6Mn_{23} [77 T 6]; see also Table 60a

^{161}Dy Dy_6Mn_{23} [82 B 15, 83 G 14]; Dy_6Fe_{23} [82 B 1, 85 P 11]; $Dy_6Mn_{23}H_x$ [82 B 15, 83 G 14]

^{166}Er Er_6Mn_{23} [81 S 14]; Er_6Mn_{23} [81 S 14, 82 Z 3]

^{169}Tm Tm_6Mn_{23} [82 B 15, 82 G 16]; Tm_6Fe_{23} [84 G 5, 84 G 6]; $Tm_6Mn_{23}H_x$ [82 B 15, 82 G 16, 84 G 5]

NMR

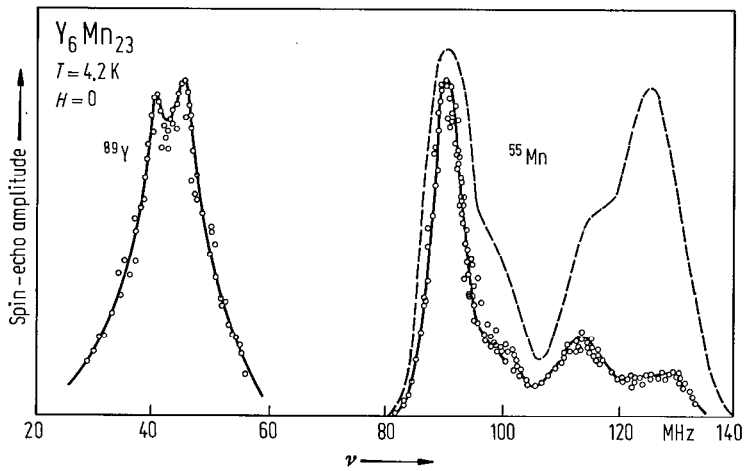

Fig. 322. ^{55}Mn and ^{89}Y zero-field spin-echo NMR spectra of Y_6Mn_{23} at 4.2 K. Solid lines and open circles indicate the spectra attribuable to ^{55}Mn and ^{89}Y nuclei in magnetic domains, where the pulse width was $t_e \cong 2.0\,\mu s$, The dotted line indicates that of the ^{55}Mn nuclei in domain walls, where $t_w = 0.2\,\mu s$ [83 Y 7]. The lowest-frequency (^{55}Mn) peak is attributed to the $32f_1$ and $32f_2$ sites, since their magnetic moments are almost the same. The peaks around 114 and 128 MHz are considered to be due to the 24d and 4b sites, respectively.

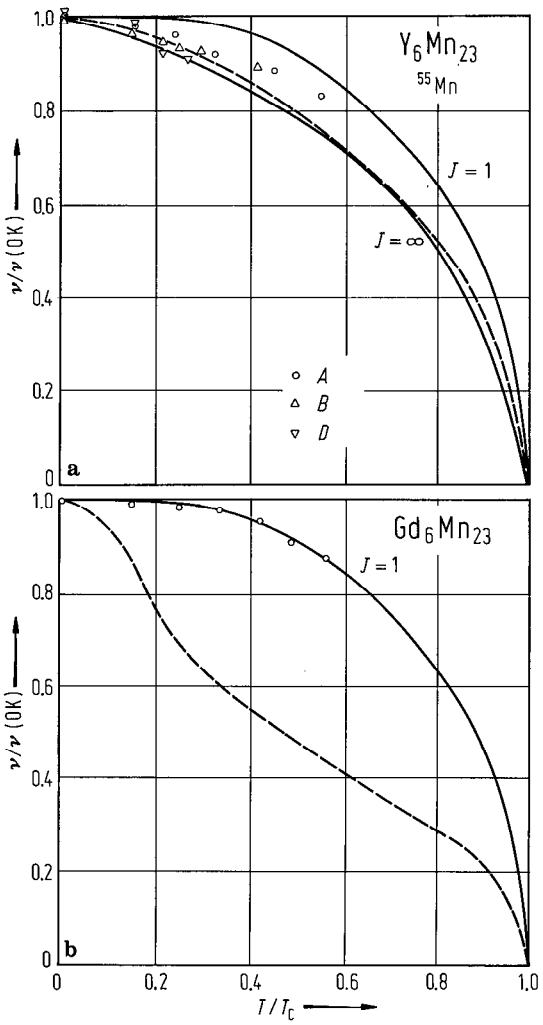

Fig. 323. (a) Normalized ^{55}Mn NMR frequencies, $\nu/\nu(0\,K)$, as a function of reduced temperature, T/T_C, in Y_6Mn_{23} compound [81 N 1]. The dashed line is the normalized magnetization curve [77 B 21]. The solid lines are the Brillouin functions for $J=1$ and $J=\infty$, respectively. The resonance frequencies extrapolated to 0 K, $\nu(0\,K)$, are A (122 MHz), B (108 MHz), D (88 MHz) for the three signals observed. The values $\nu/\nu(0\,K)$ decrease monotonically and change slower than those of the magnetization curve, which is in agreement with the Brillouin function for $J=\infty$. (b) Normalized ^{55}Mn NMR frequencies, $\nu/\nu(0\,K)$, as a function of T/T_C in Gd_6Mn_{23} compound. The dashed line is the normalized magnetization curve [77 B 21]. The solid line is the Brillouin function with $J=1$. The ν values for the peak A (ν (0 K) = 130 MHz) are only plotted. The other lines spread their widths as the temperature increased and their peaks were undistinguishable.

For NMR measurements see also:

^{55}Mn	Y_6Mn_{23} [83 Y 7]; $(YGd)_6Mn_{23}$ [81 N 1]; $Gd(FeMn)_{23}$ [87 N 1]
^{89}Y	Y_6Fe_{23} [83 Y 7]
^{152}Sm, ^{154}Sm	Sm_6Mn_{23} [71 R 6]
^{155}Gd, ^{157}Gd	$Gd_6(FeMn)_{23}$ [86 N 1]

Anisotropy, magnetostriction

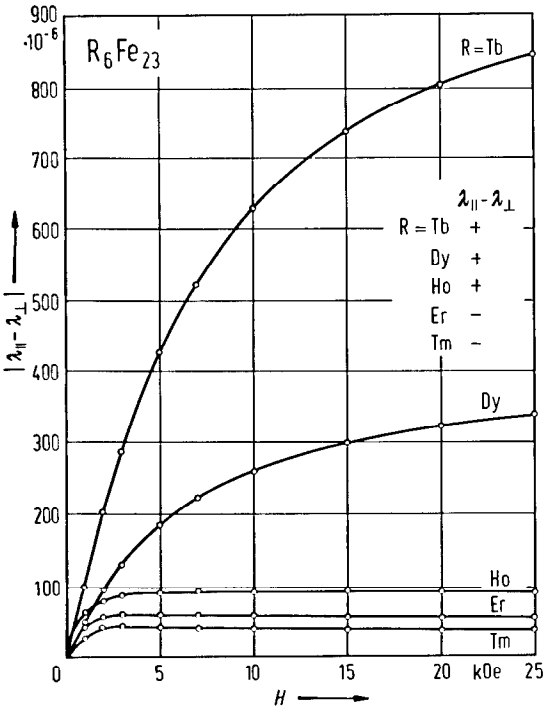

Fig. 324. Magnetic field dependence of the magnetostriction at room temperature in R_6Fe_{23} polycrystalline compounds [79 c 1, 80 c 1]. The Tb_6Fe_{23} and Dy_6Fe_{23} are not completely single-phase.

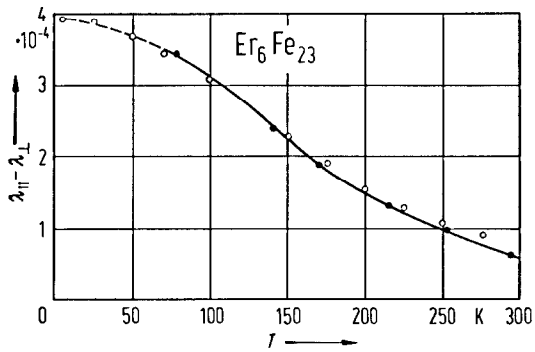

Fig. 325. Temperature dependence of the magnetostriction in Er_6Fe_{23} compound. The open circles are values calculated using the single-ion model. The solid curve is the best fit through the experimental data [80 P 7].

For anisotropy studies see

R_6Mn_{23} R = Gd, Dy, Er, Y [79 H 2]

For magnetostriction studies see also

R_6Fe_{23} R = Sm, Tb, Dy, Ho, Er, Tm, [79 c 1]; R = Tb, Dy, Ho, Er [80 P 7]; R = Ho, Er, Y [80 C 9]; R = Tb [72 C 6]; R = Tm [72 B 6]

$R_6(M'M'')_{23}$ $Y_6(FeMn)_{23}$ [77 F 5]

Transport properties

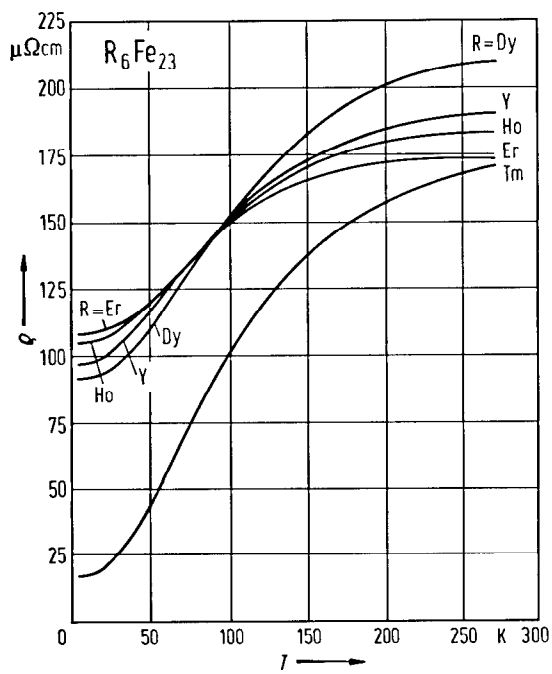

Fig. 326. Temperature dependence of the electrical resistivities in R_6Fe_{23} (R = Dy, Ho, Er, Tm, Y) compounds. The compounds exhibit a T^2 dependence at low temperatures, while above 100 K a negative curvature of ϱ vs. T is observed. The above behaviour is analysed on the basis of electron-spin wave scattering in the low-temperature range and on the basis of s–d scattering in the high-temperature range, taking explicitly into account the temperature dependence of the chemical potential [76 G 7].

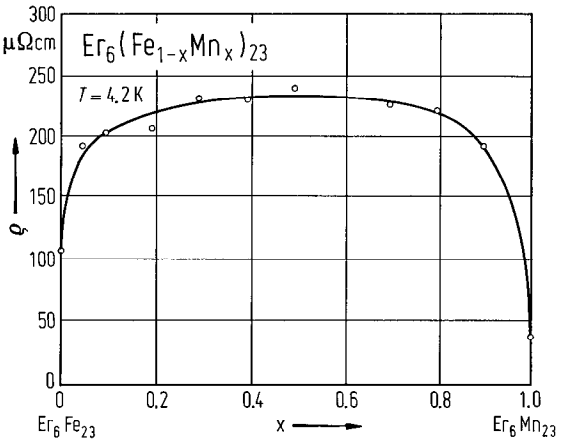

Fig. 327. Electrical resistivity values at 4.2 K in $Er_6(Fe_{1-x}Mn_x)_{23}$ compounds. The pseudobinary system shows a high residual resistivity. This system also exhibits a decreasing resistivity with increasing temperature. The above behaviour is explained by the strong scattering mechanism and the appearance of "quasi-localized" electron states [76 G 7].

For specific heat studies see also
R_6Mn_{23} R = Gd, Dy, Er, Lu [83 G 9]; R = Tb, Ho [83 G 10]; R = Y [80 B 7]
$Y_6(FeMn)_{23}$ [76 B 5] see Fig. 315

For electrical resistivity studies see also
R_6Mn_{23} R_2Fe_{23}, R = Dy, Ho, Er, Y [76 G 7]
$R_6(FeMn)_{23}$ R = Ho, Er, Y [76 G 7]; R = Er [82 G 7, 88 G 3]; R = Y [82 G 7]

Photoelectron spectroscopy

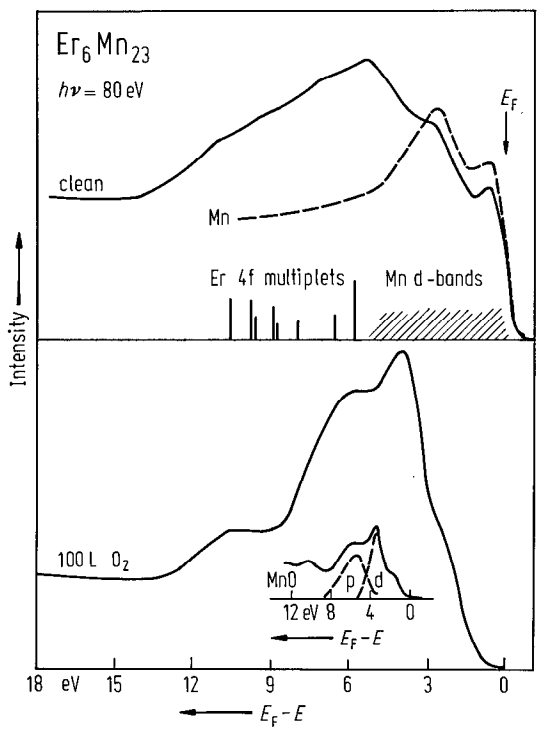

Fig. 328. Energy distribution curves for clean and oxidized Er_6Mn_{23} compound at $h\nu = 80$ eV, obtained by photoelectron spectroscopy using synchrotron radiation. By comparison to Mn metal, the Er_6Mn_{23} emission can be seen to be dominated by the Mn d-band. Additional structure at higher binding energy reflects the Er 4f multiplet states; these are localized states which do not participate in bonding [80 W 2]. Exposure to $\cong$ 100 L of O_2 (1 L = 10^{-6} Torr · s exposure) results in an emission spectrum similar to that of MnO as shown in insert.

2.4.2.17 RM_5 compounds

Crystal structure, lattice parameters

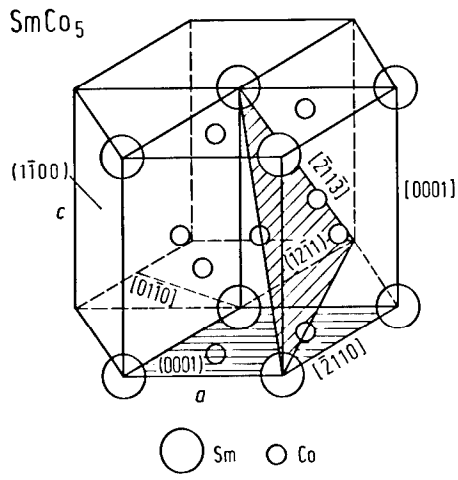

Fig. 329. Crystal structure of $SmCo_5$ ($CaCu_5$-type), where the positions of Co and Sm atoms are evidenced. In $SmCo_5$-single crystal with a low density of Sm_2Co_{17} precipitates, the predominant slip plane is the (0001) plane with a slip direction parallel to [$\bar{2}$110]. Most of the grow-in dislocations and stacking faults lie in the basal plane and have a Burgers vector of the type $\frac{1}{3}$ [$\bar{2}$110]. The second slip system is {11$\bar{2}$1} [$\bar{2}$113]. The dissociation of dislocations in the basal plane is energetically more favourable [78 F 3, 78 F 4].

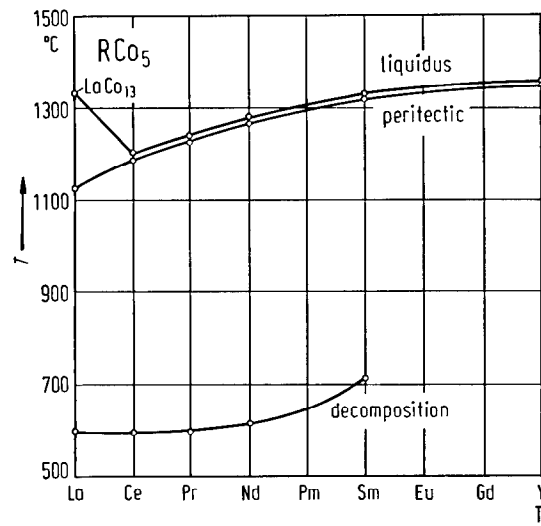

Fig. 330. Liquids and solidus (peritectic) temperatures and the temperatures of eutectoid decomposition for RCo_5-compounds with R = La to Sm [70 S 6, 72 D 2, 74 R 2, 75 H 2]. There are different view-points concerning the decomposition of RCo_5 compounds and the mechanism involved. Most investigators believe that RCo_5 decomposes eutectoidally to R_2Co_{17} and R_2Co_7 [72 B 15, 72 D 2, 73 B 22, 74 B 13, 74 M 2, 74 D 3, 74 S 8, 75 M 3, 76 P 5, 77 E 1, 80 B 17, 80 D 4]. Diffusion couple studies indicated that $SmCo_5$ does not exist at 800 °C in Sm–Co system [74 M 2] and $CeCo_5$ does not exist at 650 °C in the Ce–Co system [75 M 3]. Kumar et al. [78 K 13, 79 K 9, 80 K 17] rejected the idea of eutectoidal decomposition and instead suggested precipitation of Sm_2Co_{17}. Fidler et al. [80 F 3] observed precipitation of Sm_2Co_{17} and Sm_2Co_7 in $SmCo_5$ single crystal and suggested that $SmCo_5$ decomposes through homogeneous nucleation, as the precipitates were coherent and grew continuously. By prolonged heating $GdCo_5$ in the temperature range 720···850 °C local spinodal decomposition into Gd_2Co_{17} and Gd_2Co_7 occurs [82 C 10]. Single phase $PrCo_5$, after annealing decomposes into Pr_2Co_{17} and Pr_5Co_{19} [86 C 4]. Other studies do not support the suggestion for an unique stability of the $SmCo_5$ phase [74 L 1, 75 K 3]. Ray et al. [73 R 2, 74 R 2] were unable to detect the decomposition of RCo_5 (R = Ce, Pr, Nd) and did not regard these compounds as unstable in the studied temperature range. Some investigations also have not confirmed the eutectoid decomposition [74 K 10, 77 P 6]. See also [74 S 8, 75 H 2, 75 K 3]. The stability of RCo_5 may be reduced by adding a suitable amount of Fe, Mn, or Cr, or may be enhanced by adding an appropriate amount of Ga, Ge, Si, Cu or Al [73 B 20, 74 B 13, 74 D 3]. The decomposition temperature of YCo_5 is reduced by appropriate substitution of Co by Ni, Cu, Al [82 C 8]. The Ga and Cu increase the stability of the $GdCo_5$ phase [85 C 3].

For stability and decomposition see also

RCo_5 [74 B 13, 74 D 3]; R = Ce [75 M 3]; R = Sm [70 M 2, 72 D 2, 74 M 2, 74 S 8, 75 K 3, 77 E 1, 77 M 1, 80 D 4, 80 K 17]; R = Gd [72 D 2, 82 C 10]

$R(M'M'')_5$ $Ce(CoCu)_5$ [84 A 11, 85 G 12]; $Sm(CoCu)_5$ [76 P 5]

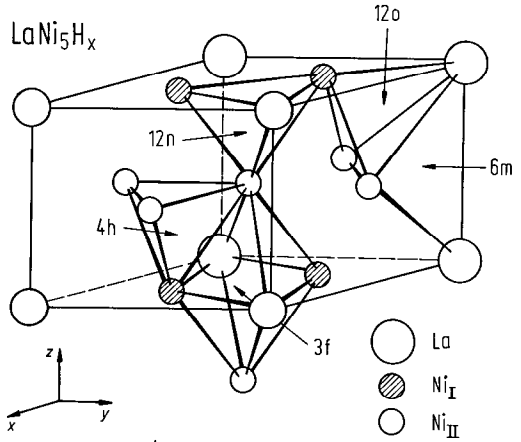

Fig. 331. Crystal structure of $LaNi_5$-hydrides having $CaCu_5$-type (P6/mmm) structure. In addition to R (one type of site) and M (two types of sites) atoms, there are five different types of interstitial sites, all of which are surrounded by a variety of atoms and different interatomic distances. See Table 85 [85 S 12]. The hydrogen occupies some interstitial sites. In α-phase $LaNi_5D_{0.4}$ a statistical distribution of deuterium atoms in the octahedral 3f sites was shown [78 F 6]. According to [78 S 12], the H atoms occupy the octahedral f site exclusively in $LaCu_5H_3$. For $LaNi_5$ and $CaNi_5$, the conclusions are more ambiguous: either they occupy the octahedral f site and the tetrahedral n (or o) site, or they occupy only the tetrahedral n site or only the tetrahedral o site [78 S 12]. In $LaNi_4FeD_{5.1}$, the D atoms are distributed over three interstitial sites (6m, 12n and 4h) [87 L 1]. The spectroscopic measurements on α-$LaNi_5H_{0.15}$ suggest that H(D) in α-$LaNi_5H_x$ occupies the octahedral 3f sites [77 F 4]. In addition has been proved that a second interstitial site (6m) is also occupied. In α-$LaNi_5D_x$ ($x = 0.1$ and 0.4) only the 3f or 12n sites gave a positive occupancy with a noticeable contribution on the reliability factor [87 S 21]. The occupancy of the 3f site is lower than that of the 12n site. In $LaNi_{5-x}M_x$ having $M_x = Al_{0.5}$, $Si_{0.5}$ or $Cu_{1.0}$, Al and Si substitute sites in the $z = 1/2$ plane and Cu in both $z = 0$ and $z = 1/2$ planes with a preference for $z = 0$ plane. The opportunity for 4h and 12o sites of being occupied by D atoms gradually disappears when the Al concentration increases. In $LaNi_4CuD_{5.07}$ the disappearance of the 12o sites is shown. $LaNi_{4.5}Si_{0.5}D_{4.3}$ seems to retain some deuterium in 4h site, a near neighbour of the Si site [82 A 2].

Table 84. Atomic positions in the ideal $CaCu_5$-type structure and the actual structure of $R_{1-s}Co_{5+2s}$ compounds [1]) (space group P6/mmm) [82 D 3].

Ideal structure type $CaCu_5$			Actual structure $R_{1-s}Co_{5+2s}$		
Atom	Occupation	Site	Atom	Occupation	Site
Ca	1	1a	R	1−s	1a
			Co_{III}	s	2e
Cu_I	1	2c	Co_I	1−3s	2c
			Co_{IV}	s	6l
Cu_{II}	1	3g	Co_{II}	1	3g

[1]) For heavy R atoms (having smaller atomic radius) the RCo_5 phase can be stabilized only in the presence of an excess of Co corresponding to a random replacement of R atoms by Co_{III} dumb-bells site (2e). The resulting local distributions require the introduction of Co_{IV} site (6l).

Table 85. Available interstitial (octahedral and tetrahedral) sites in $CaCu_5$-type lattice (space group P6/mmm) [78 S 12].

Interstitial	Symmetry of site	Number of sites in unit cell	x	y	z	Neighbouring atoms
f	octahedral	3	0.50	0.00	0.00	R_2; M_4; R_2M_4
h	tetrahedral	4	0.33	0.67	0.37	M_4; M_4
m	tetrahedral	6	0.13	0.25	0.50	R_2; M_2; R_2M_2
n	tetrahedral	12	0.40	0.00	0.11	R_1; M_3; RM_3
o	tetrahedral	12	0.20	0.40	0.27	R_1; M_3; RM_3

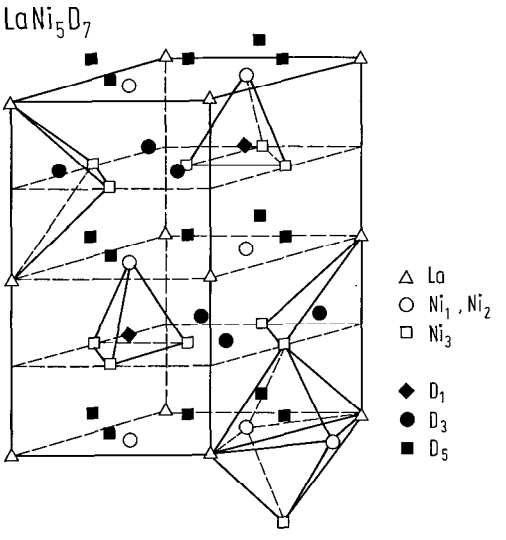

Fig. 332. Structure of the hypothetical fully ordered $LaNi_5D_7$ compound (space group $P6_3mc$) [87 L 2]. On 2b sites (D_1, D_2) deuterium atoms are found nearly at the center of the tetrahedron ($d_{D_1Ni_1}=1.62$ Å, $d_{D_1Ni_3}=1.68$ Å). On 6c sites, D_3, D_4 and D_5 atoms are displaced by about 0.4 Å from the center of both the tetrahedron and octahedron. There are only two d_{DD} distances shorter than 2.1 Å, minimum distance which is generally considered in hydrides ($d_{D_1D_4}=1.65$ Å and $d_{D_3D_4}=1.50$ Å). In the hypothetical ordered $LaNi_5D_7$ phase, the D_1, D_3 and D_5 sites would be nearly fully occupied, the D_2 and D_4 sites nearly empty and all the D–D distances would be in the range 2.5···2.9 Å. According to [86 T 4] the D atoms occupy three different sites: two tetrahedrally with Ni_4 and La_2Ni_2 neighbours and one octahedral site, La_2Ni_4. The crystal symmetry of $\beta(\gamma)RM_5$ deuterides (hydrides) is rather controversed. In addition to above structures some other models were also used to analyse the RM_5-hydrides: (a) Kuijpers [73 K 15] suggested a slight orthorhombic distortion of the hexagonal $CaCu_5$-type structure, which was supported later [81 I 3]. (b) A trigonal deformation of the $CaCu_5$ unit cell was reported [73 B 14], the space group symmetry being reduced from P6/mmm to P31m. The D atoms are found to occupy fully the 3g site ($z\cong0.1$) whereas the 6d site ($z\cong0.5$) is only partially filled. This structure has been adopted also by other authors [78 A 3, 78 B 10, 78 F 6, 83 N 8]. After [83 N 8] hydrogen is situated on two sites, one fully occupied (3c) and one partially occupied (6d). (c) In [82 Y 6] it has been suggested that the trigonal deformation is better described by the space group P321 with the deuterium atoms partially occupying the $6g_1$ ($z\cong0.1$) and $6g_2$ ($z\cong0.5$) sites. (d) Lartigue et al. [87 L 2] suggest the possibility of trigonal deformation with a structure having P31c space group. (e) In RCo_5H_4, the hydrogen atoms occupy positions in orthorhombic space group Cmmm, derived from 3f and 6m sites [74 K 19]. After [83 G 17], D atoms in $LaNi_4CoD_4$ are distributed in 4e and 4h sites. See also [84 Y 9, 87 T 5].

Table 86. Comparison between $LaNi_5$ sites and $LaNi_5D_7$ sites [86 T 4].

$LaNi_5$ – space group P6/mmm						$LaNi_5D_7$ – space group $P6_3mc$						
Atom	Site	Site symmetry	x	y	z	Atom	Site	Site symmetry	x	y	z	Environment
La	1a	6/mmm	0	0	0	La	2a	3m	0	0	0	
Ni	2c	6m2	1/3	2/3	0	Ni_1	2b	3m	1/3	2/3	Z_{Ni_1}	
						Ni_2	2b	3m	1/3	2/3	Z_{Ni_2}	
Ni	3g	mmm	1/2	1/2	1/2	Ni_3	6c	m	X	$-X$	Z_{Ni_3}	
Precursor D sites [1]												
D(T)	4h	3m	1/3	2/3	Z	D_1	2b	3m	1/3	2/3	Z_1	Ni_4(T)
						D_2	2b	3m	2/3	1/3	Z_2	Ni_4(T)
D(T)	6m	mm	X	$2X$	1/2	D_3	6c	m	X	$-X$	Z_3	Ni_2La_2(T)
						D_4	6c	m	X	$-X$	Z_4	Ni_2La_2(T)
D(O)	3f	mmm	1/2	1/2	0	D_5	6c	m	X	$-X$	Z_5	Ni_4La_2(O)

[1]) (T) tetrahedral; (O) octahedral.

Table 87a. Lattice parameters of RM_5 compounds [1]) (Å).

	86 S 20		87 K 3	
	a	*c*	*a*	*c*
$NdFe_5$	4.946	4.170	4.935	4.204
$SmFe_5$			4.955	4.054
$TbFe_5$			4.959	4.033

[1]) The compounds were obtained by rapid solidification. These crystallize in $CaCu_5$-type structure, as RCo_5 and RNi_5 compounds.

Table 87b. Lattice parameters of RCo_5 compounds (Å).

	59 W 1		60 N 1		66 L 3		68 V 1		73 K 9		74 G 10		73 R 2		77 O 9		82 D 3	
	a	*c*	*a*	*c*	*a*	*c*	*a*	*c*	*a*	*c*	*a*	*c*	*a*	*c*	*a*	*c*	*a*	*c*
$LaCo_5$							5.105	3.966										
$CeCo_5$	4.922	4.026	4.920	4.010	4.926	4.020	4.922	4.016			4.928	4.019	4.9282	4.0151				
$PrCo_5$	5.010	3.990			5.024	3.988	5.013	3.980					5.032	3.992				
$NdCo_5$	5.026	3.975			5.012	3.978	5.020	3.977					5.028	3.977				
$SmCo_5$			4.940	3.960	4.989	3.981	5.004	3.969	4.997	3.978	4.974	3.985						
$GdCo_5$	4.974	3.973	4.930	3.970	4.976	3.973	4.973	3.969			4.931 [5])	4.008 [5])						
$TbCo_5$					4.946	3.980	4.950 [1])	3.979 [1])										
$DyCo_5$	4.926	3.988	4.890	4.000	4.933	3.983	4.897 [2])	4.007 [2])							4.905	3.970		
$HoCo_5$			4.880	3.960	4.911	3.993	4.881 [3])	4.006 [3])									4.901 [6])	3.966 [6])
$ErCo_5$	4.885	4.002			4.883	4.007	4.870 [4])	4.002 [4])			4.889	4.004						
$TmCo_5$					4.863	4.017												
YCo_5	4.928	3.992	4.830	4.000	4.937	3.978	4.935	3.964			4.942	3.976						

The compositions of the samples are: [1]) $TbCo_{5.1}$; [2]) $DyCo_{5.2}$; [3]) $HoCo_{5.5}$; [4]) $ErCo_{5.9}$; [5]) $GdCo_6$; [6]) $HoCo_{5.6}$.

Table 87c. Lattice parameters of RNi_5 compounds (Å).

	59 W 1		60 N 1		64 M 2		68 B 5, 77 b 1		72 U 1		78 O 6		80 A 4		80 N 1		85 G 4	
	a	*c*	*a*	*c*	*a*	*c*	*a*	*c*	*a*	*c*	*a*	*c*	*a*	*c*	*a*	*c*	*a*	*c*
$LaNi_5$[1])	5.013	3.984	5.010	3.980	5.014	3.983							5.030(10)	3.960(10)				
$CeNi_5$	4.875	4.010	4.910	4.000	4.878	4.006												
$PrNi_5$	4.958	3.980			4.957	3.976							4.960(10)	3.980(10)				
$NdNi_5$	4.948	3.977			4.952	3.976												
$SmNi_5$			4.930	3.970	4.924	3.974												
$EuNi_5$							4.911	3.965			4.905	3.948					4.923(2)	3.963(1)
$GdNi_5$	4.899	3.973	4.900	3.960	4.906	3.968			4.904	3.967								
$TbNi_5$					4.894	3.966												
$DyNi_5$	4.869	3.969	4.880	3.990	4.872	3.968												
$HoNi_5$			4.880	3.990	4.872	3.966												
$ErNi_5$	4.856	3.966			4.858	3.965												
$TmNi_5$															4.853	3.960		
$YbNi_5$					4.841	3.965												
YNi_5	4.880	3.970	4.850	3.930														

[1]) For $LaNi_5$ see also Table 88.

Table 88. Lattice constants of some RNi_5-based hydrides and their parent compounds.

	a Å	c Å	$\Delta V/V$ %	Ref.
$LaNi_5$	5.011	3.911		87 S 21
$LaNi_5D_{0.1}$	5.022(2)	3.978(1)	0.1	87 S 21
$LaNi_5D_{0.4}$	5.025(3)	3.991(2)	0.55	87 S 21
$LaNi_5H_{6.7}$	5.440	4.310	27.3	77 T 5
$LaNi_5D_7$	5.387(1)	4.273(1)	23.7	73 B 14
$LaNi_4Cu$	5.033(1)	4.007(1)	–	82 A 2
$LaNi_4CuD_{5.07}$	5.374(1)	4.190(1)	19.2	82 A 2
$LaNi_4Al$	5.063(1)	4.063(1)	–	79 A 2
$LaNi_4AlD_4$	5.310(2)	4.249(2)	15	79 A 2
$LaNi_{4.5}Al_{0.5}$	5.040(1)	4.023(5)	–	82 A 2
$LaNi_{4.5}Al_{0.5}D_{5.4}$	5.353(1)	4.263(1)	19.5	82 A 2
$LaNi_{4.5}Al_{0.5}H_{4.5}$	5.340	4.201	17	79 M 10
$LaNi_{4.6}Al_{0.4}$	5.018	4.033		79 M 10
$LaNi_{4.6}Al_{0.4}H_5$	5.358	4.207	19	79 M 10
$LaNi_{4.5}Si_{0.5}$	5.007(1)	3.992(1)	–	82 A 2
$LaNi_{4.5}Si_{0.5}D_{4.9}$	5.328(1)	4.077(1)	15.6	82 A 2
$LaNi_4Mn$	5.096(1)	4.075(1)	–	79 A 2
$LaNi_4MnD_6$	5.437(1)	4.332(2)	21	79 A 2
$LaNi_4FeD_{5.1}$	5.376(3)	4.210(1)	16	87 L 1
$CeNi_{2.5}Cu_{2.3}Al_{0.2}$	5.038	4.055		84 S 12
$CeNi_{2.5}Cu_{2.3}Al_{0.2}H_{5.0}$	5.238	4.158	11	84 S 12
$CeNi_{2.5}Cu_{2.0}Al_{0.5}$	5.050	4.081		84 S 12
$CeNi_{2.5}Cu_{2.0}Al_{0.5}H_{4.7}$	5.259	4.176	11	84 S 12
$CeNi_2Cu_2Al$	5.106	4.126		84 S 12
$CeNi_2Cu_2AlH_{3.7}$	5.270	4.226	9.1	84 S 12
$EuNi_5$	4.905	3.948		78 O 6
$EuNi_5H_x$	5.340	4.170	8	78 O 6
$EuNi_5H_{5.5}$	5.4519(21)	4.8354(24)	5.2	78 O 6
$ThNi_3Al_2$	5.127	4.112	–	77 T 2
$ThNi_3Al_2H_{2.7}$	5.217	4.183	5.1	77 T 2

Table 89. Changes in the unit cell parameters with the phase transformation in $LaNi_5H_x$ system [85 O 2, 87 A 3] [1]).

Phase	a Å	$\Delta a/a$ %	c Å	$\Delta c/c$ %	V Å^3
α	5.01→5.06	1.0	4.00	0.3	86.9→ 88.5
α→β	5.06→5.27	4.2	4.00→4.05	1.2	88.5→ 97.5
β	5.27→5.31	0.8	4.05→4.10	1.3	97.5→100
β→γ	5.31→5.36	1.0	4.10→4.18	2.0	100 →104
γ	5.36→5.40	0.8	4.18→4.25	1.8	104 →107.4

[1]) According to [85 O 2, 87 A 3] in $LaNi_5H_x$ system, the presence of three phases are evidenced having the compositions: $LaNi_5H_{0...0.5}$; $LaNi_5H_{\cong 3}$ and $LaNi_5H_{\cong 6}$, respectively. Above 80 °C, the desorption isotherms show two plateaus corresponding to α→β and β→γ transformations. The lattice expansion accompanying these phase transformations are anisotropic. For α to β the a-axis expansion predominates, while for β to γ the c axis expansion predominates. The presence of the α, β and γ phases were also evidenced in $PrNi_5H_x$ system [87 M 1]. Some authors reported in $LaNi_5H_x$ system only the presence of α and β phases. See for example [80 B 4, 81 M 13, 86 M 1].

For hydrogen absorption and desorption see also

RM_5H_x [82 Y 7, 85 S 12]

RCo_5H_x [72 K 2, 72 K 3, 73 K 15, 74 B 17, 77 K 3, 77 K 4, 80 L 1]; R = La [72 K 4, 78 G 3, 82 Y 2, 84 F 3, 84 P 6]; R = Ce [72 K 4, 77 K 3]; R = Pr [82 Y 2]; R = Nd [78 G 3, 82 Y 2, 82 Y 3]; R = Sm [77 K 3, 80 L 2]; R = Y, Th [74 T 1]; R = Er [78 G 3]

RNi_5H_x [77 E 2, 83 L 4]; R = La, Ce, Pr, Sm, Gd, Tb, Ho, Er [87 A 9]; R = La [73 V 2, 74 V 3, 76 B 9, 76 B 10, 76 V 2, 76 V 5, 77 K 3, 77 T 3, 77 T 4, 77 T 5, 78 B 19, 78 L 5, 78 V 2, 79 A 2, 79 N 4, 79 W 2, 80 B 9, 80 C 7, 80 D 3, 80 J 3, 80 K 3, 80 M 13, 80 O 4, 80 S 6, 80 S 7, 81 M 13, 82 A 14, 82 L 6, 82 O 3, 83 B 7, 83 F 5, 83 G 6, 83 L 4, 83 M 4, 83 N 5, 83 T 3, 84 A 2, 84 G 4, 84 R 2, 84 U 1, 85 I 6, 85 N 5, 85 O 2, 85 P 14, 85 T 3, 86 M 1, 86 S 1, 87 A 3, 87 P 1, 87 R 5, 87 R 7, 87 U 1, 87 G 2]; R = Pr [87 M 1]; R = Eu [85 G 4]; R = Y, Th [74 T 1, 81 T 1]

$(R'R'')M_5H_x$ (LaR)Ni_5H_x [74 V 3]; R = Pr, Nd, Sm [82 U 1]; (LaYb)Ni_5H_x [78 A 2]; (LaCo)Ni_5H_x [78 S 12]; (CaEu)Ni_5H_x [84 S 7]; (CeNd)$(NiCu)_5H_x$ [84 S 12]

$R(M'M'')_5H_x$ La(NiM)$_5H_x$ [83 B 7]; M = Al, Mn [79 A 2]; M = Pd, Ag, Cu, Co, Fe, Cr [76 V 2]; M = Cu, Al, Fe [78 S 1]; M = Al, Mn [79 A 2]; M = Al, Cu, Ti [79 B 1]; M = Al, Cu, Fe, Mn [82 P 3]; M = Mn, Cu, Fe, Si, Al [85 P 5]; La$(NiFe)_5H_x$ [80 M 8, 87 L 1, 87 L 3]; La$(NiCo)_5H_x$ [73 V 3, 76 V 2]; La$(NiMn)_5H_x$ [82 L 3]; La$(NiCu)_5H_x$ [78 S 12, 80 B 4, 84 E 1]; La$(NiAl)_5H_x$ [77 A 2, 77 M 7, 77 S 1, 78 M 9, 79 M 10, 80 B 4, 81 B 4, 82 T 5, 84 G 4, 87 B 9, 87 B 11, 87 D 1, 87 P 1]; La(NiM)$_5$, M = In, Sn, Ga [78 M 9]; La$(NiTi)_5H_x$ [80 B 4]; La$(NiSn)_5H_x$ [85 O 1]; Ce$(NiCu)_5H_x$ [82 P 12, 85 M 5]; Ce$(NiCuAl)_5H_x$ [84 S 12]; Pr(NiM)$_5H_x$, M = Cu, Fe [86 P 5]; RNi_4AlH_x, R = La, Ce, Pr, Nd, Sm, Gd, Tb, Dy, Ho, Er, Tm [78 T 1]; MM$(NiMn)_5H_x$ [85 I 6]; Th$(NiAl)_5H_x$ [77 T 2]; (LaEu)$(NiMn)_5H_x$ [80 C 6, 80 C 7]

The diffusion process of hydrogen in intermetallic compounds was investigated by NMR [74 H 2, 76 H 1, 78 H 6, 79 B 9, 79 K 2, 80 K 3] and quasi-elastic neutron scattering (QNS) [77 F 4, 79 L 4, 79 N 4, 82 A 2, 82 A 3, 82 A 3, 83 N 8, 84 L 2] mostly in the $LaNi_5$-hydride. The first results were analysed in terms of a single jump diffusion process. The values of the diffusion coefficients ranged from $6 \cdot 10^{-6}$ cm^2 s^{-1} [78 H 6], to $6 \cdot 10^{-9}$ cm^2 s^{-1} [79 L 4] and the activation energies ranged from 110 meV [79 N 4] to 300 meV [79 B 9]. The NMR data in $LaNi_5$-hydrides [80 K 3] suggest that the diffusion involves two separate processes with activation energies of 415 and 208 meV, respectively. The QNS investigations in $LaNi_5H_{5.8}$ and $LaNi_4MH_x$ with M = Al, Mn [82 A 2, 82 A 3] provided the existence of a rapid localized motion of hydrogen. The QNS spectra [84 L 2] were decomposed into three components. These were attributed to two types of diffusion motion in addition to a rapid localized motion.

For hydrogen diffusion see also

$LaCo_5$–H_x [84 P 6]; $LaNi_5(H)D_x$ [85 P 14]

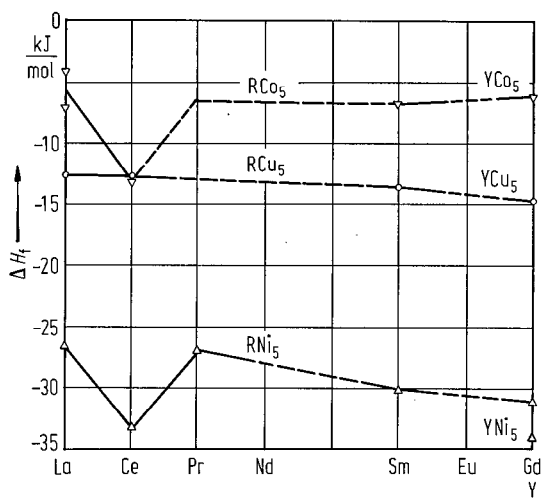

Fig. 333: Enthalpies of formation of RCo_5, RCu_5 and RNi_5 compounds [87 M 4]. The enthalpies of formation of RCo_5 compounds are much higher than those of RNi_5. The more negative value measured for $CeCo_5$ is related to the different valence state of Ce in $CeCo_5$. The composition dependences of the enthalpies of formation and lattice parameters indicate an ideal behaviour for mixing $SmCo_5$ and $SmCu_5$ on one hand and for YCo_5 and YCu_5 on the other hand. This result is consistent with the homogeneous state found for $Sm(Co_{1-x}Cu_x)_5$ and $Y(Co_{1-x}Cu_x)_5$ at 400 °C on the whole concentration range. For the mixtures of $CeCo_5$ and $CeCu_5$, the enthalpies of formation exhibit a slightly positive deviation, which predicts the solid state miscibility gap evidenced in the $CeCo_5$–$CeCu_5$ section below 800 °C.

For enthalpies of formation see also

RM_5 M = Fe, Co, Ni [86 L 1]

$R(M'M'')_5$ La$(NiFe)_5$ [79 M 14]; La$(NiCr)_5$ [79 M 14]; La$(NiCu)_5$ [84 P 5]; Ce$(NiCu)_5$ [85 M 5] La$(NiCo)_5H_x$ [87 C 5, 87 C 6]; La$(NiAl)_5H_x$ [79 D 7]; Ce$(NiCu)_5H_x$ [85 M 5]

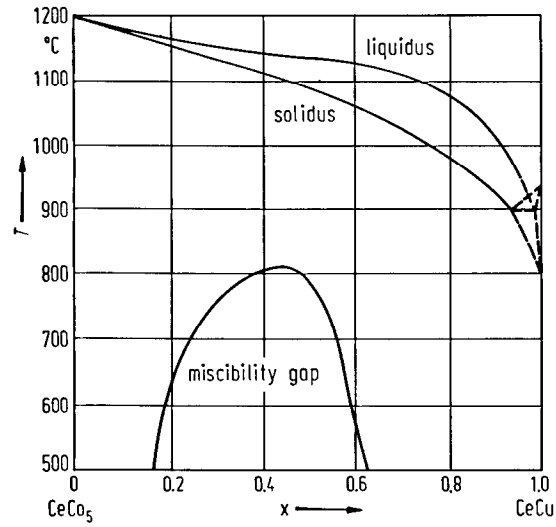

Fig. 334. Phase equilibria in the vertical section of $CeCo_5$–$CeCu_5$ system [85 G 12]. A solid state miscibility gap is present below about 800 °C.

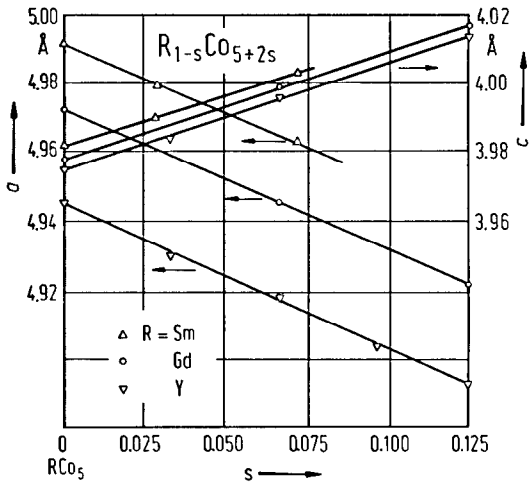

Fig. 335. Composition dependence of the room-temperature lattice parameters in $R_{1-s}Co_{5+2s}$ (R = Sm, Gd, Y) compounds [76 D 9].

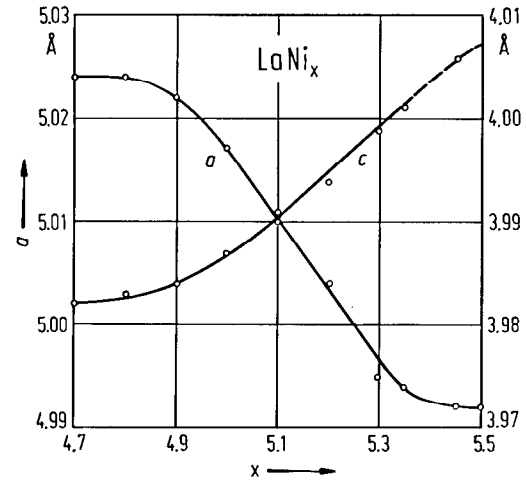

Fig. 336. Room-temperature lattice constants as function of composition for the compounds having the composition close to $LaNi_5$, annealed at 1200 °C and quenched [72 B 17]. A large homogeneity region was observed. The limit of homogeneity region is at 1200 °C (x = 4.85···5.40); at 1100 °C (x = 4.90···5.10); at 1000 °C (x = 4.95···5.05).

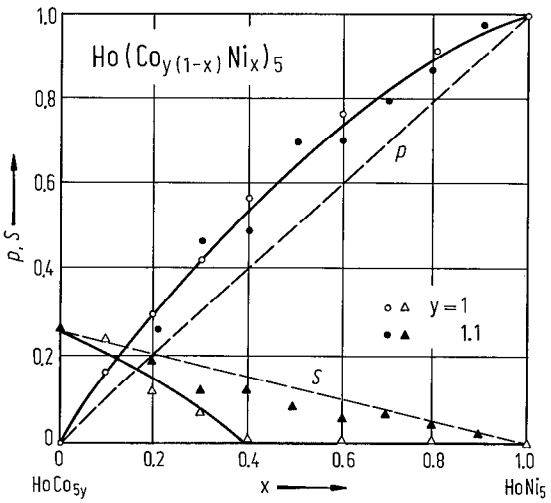

Fig. 338. Composition dependence of the probabilities (circles) $p(x)$ of occupation of 2c sites by the Ni atoms and (triangles), $S(x)$ for occupation by Co atoms of the 6l and 2e sites in the $TbCu_7$-type structure of (open symbols) $Ho(Co_{1-x}Ni_x)_5$ and (solid symbols) $Ho(Co_{1.1-1.1x}Ni_x)_5$ alloys. By dashed lines are plotted the relation $p(x)=x$, and the relation $S(x)=0.5(1-x)/2$ [83 C 3]. For the distribution of Co and Ni atoms in lattice sites of $Y(Co_{1-x}Ni_x)_5$ and $La(Co_{1-x}Ni_x)_5$ see also [80 P 4]. In $LaNi_xCo_{5-x}$ compounds Co atoms show a preference for 3g sites [80 P 4, 83 G 17]. The preference of atoms with greater atomic radius to occupy the 3g positions has been also observed in similar compounds, as for Mn in $LaNi_{5-x}Mn_x$, Al in $LaNi_{5-x}Al_x$ [80 L 3, 80 P 2], and Co in $Th(NiCo)_5$ [72 V 1, 73 A 4, 73 L 1, 76 E 1]. In $Pr(Co_{1-x}Al_x)_5$, Al atoms occupy randomly both Co(2c) and Co(3g) sites [73 O 5]. In the compounds based on $ThCo_5$ including Fe [73 L 1], Al [67 B 1], Ni [75 B 13] larger atoms than Co are likely to occupy preferentially the site Co(3g) and smaller atoms prefer to occupy the site Co(2c). For site occupancy in $R(CoCu)_5$ compounds see [81 Y 4].

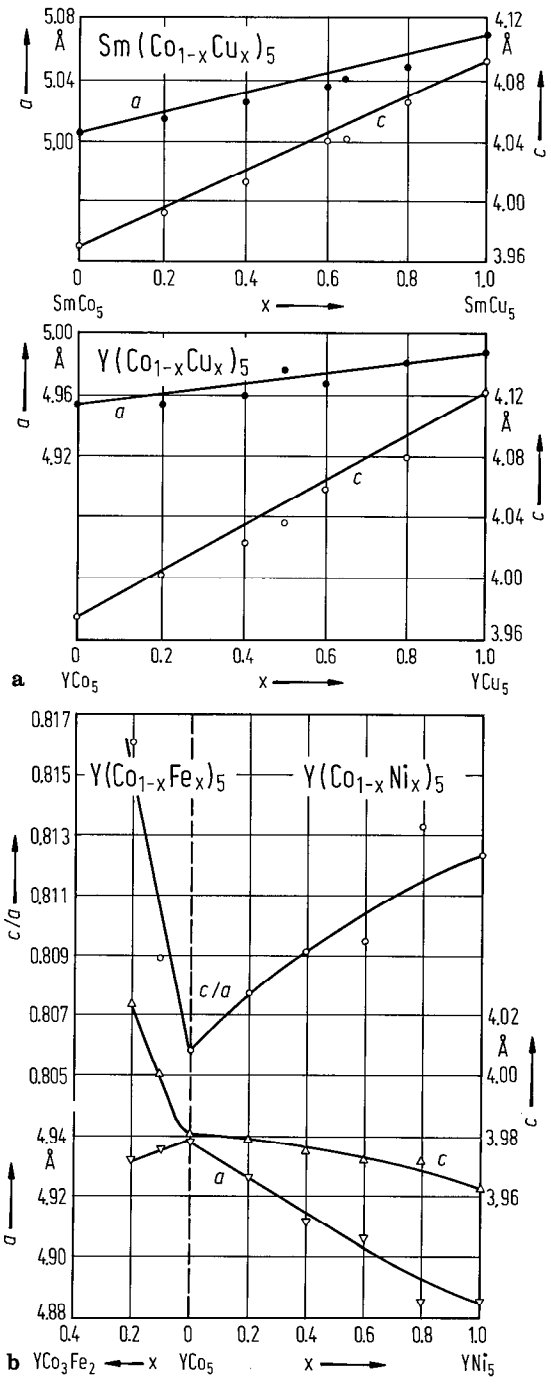

Fig. 337. Composition dependence of the room-temperature lattice parameters in (a) $Sm(Co_{1-x}Cu_x)_5$ and $Y(Co_{1-x}Cu_x)_5$ compounds [87 M 4] and (b) $Y(Co_{1-x}Ni_x)_5$ and $Y(Co_{1-x}Fe_x)_5$ systems [72 T 1]. Also shown in (b) is the axial ratio as function of composition.

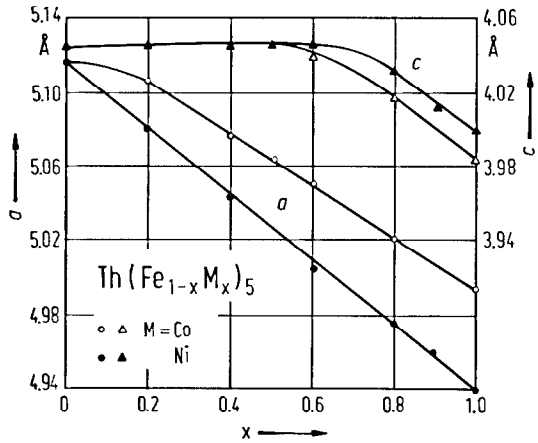

Fig. 339. Composition dependence of the room-temperature lattice constants in $ThFe_{5-5x}Co_{5x}$ (open symbols) and $ThFe_{5-5x}Ni_{5x}$ (full symbols). The triangles correspond to the *c* axis and the circles to the *a* axis [76 E 1]. For the series mentioned the preferential occupancy of the 2c site is consistently given as Ni > Co > Fe.

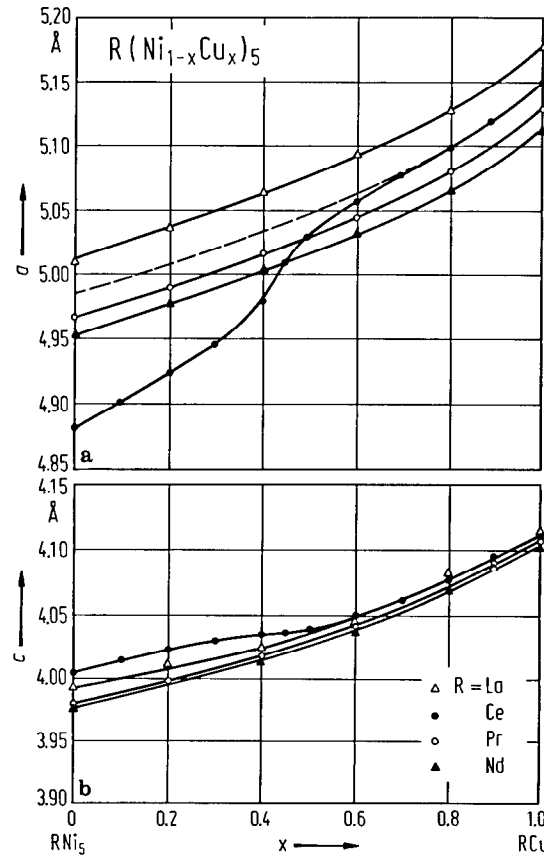

Fig. 340. Room-temperature lattice parameters versus Cu content in $R(Ni_{1-x}Cu_x)_5$ compounds for R = La, Ce, Pr and Nd; (a) lattice constants *a* (b) lattice constants *c*. The dashed line corresponds to a variation of the Ce *a* lattice parameter identical as for La, Pr and Nd compounds [82 G 5].

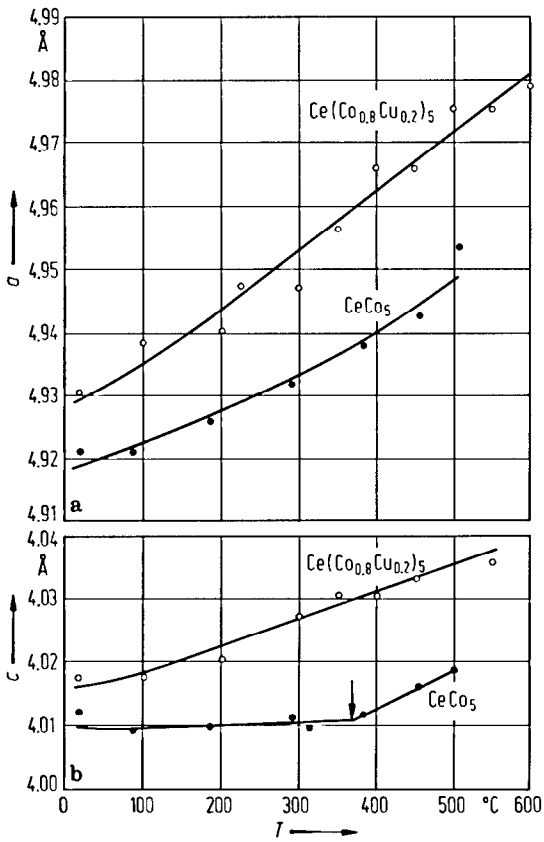

Fig. 341. Temperature dependence of the lattice constants *a* and *c* in $CeCo_5$ and $Ce(Co_{0.8}Cu_{0.2})_5$ compounds [81 Y 4]. The T_C value for $CeCo_5$ is indicated by an arrow. In $CeCo_5$ an invar-type thermal expansion anomaly in the *c* axis expansion is shown below T_C. Similar anomalies were observed in other RCo_5 compounds [74 B 14]. The anomalies are considerably reduced by partial substitution of the Co by Cu atoms.

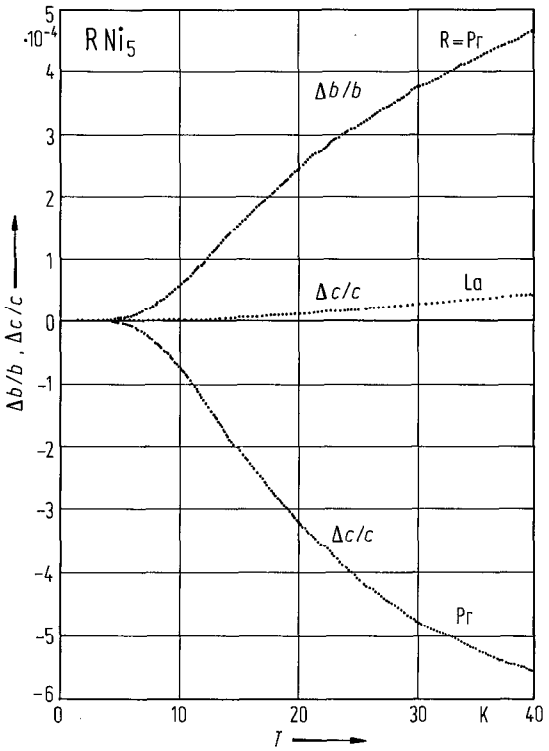

Fig. 342. Thermal dilatation of $PrNi_5$ and $LaNi_5$ measured along the *b* and *c* axis between 1.2 and 40 K. For $LaNi_5$ the thermal dilatation is isotrop. For $PrNi_5$ the thermal dilatation is isotrop in the basal plane but a high anisotropy is observed between *c* axis and basal plane [87 B 7].

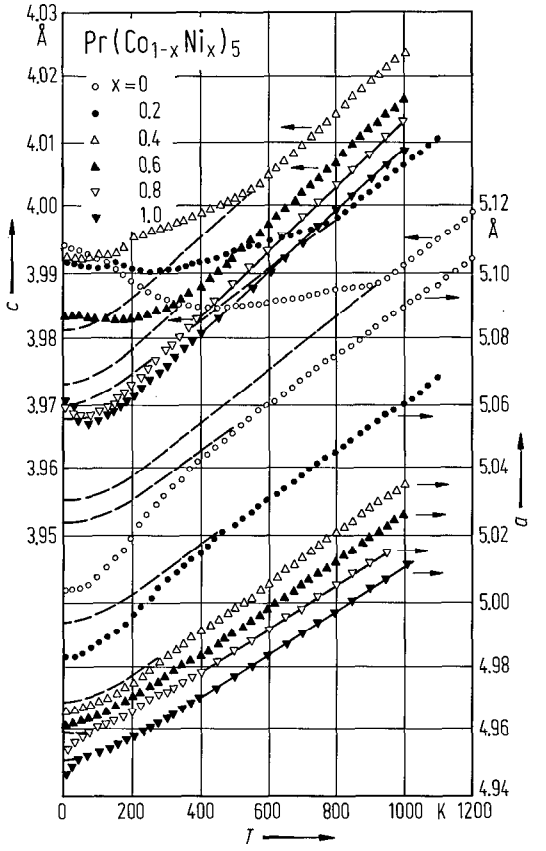

Fig. 343. Temperature dependence of the lattice constants in $Pr(Co_{1-x}Ni_x)_5$ compounds [85 A 10]. By broken line are plotted the phonon contribution to the thermal dilatation.

For crystal structure and lattice constants see also

RM_5	[75 D 3]
RFe_5	[87 K 3]; R = Nd [86 S 20]
RCo_5	[67 S 3, 69 U 1, 73 B 22, 74 K 8, 80 B 12, 82 P 4]; R = Ce, Pr, Nd, Gd, Dy, Y [59 W 1]; R = Sm, Tb, Ho [60 H 1]; R = Ce, Sm, Gd, Dy, Ho, Y [60 N 1]; R = Ce, Pr, Nd, Sm, Gd, Tb, Dy, Ho, Er, Tm, Y [66 L 3]; R = La, Ce, Pr, Nd, Sm, Gd, Tb, Dy, Ho, Er, Y, Th [68 V 1]; R = Ce, Sm, Er, Y [74 G 10]; R = Pr, Nd, Sm [79 M 11]; R = Ce [61 D 1, 74 D 12, 81 Y 4]; R = Pr [61 D 1, 71 K 3]; R = Sm [71 U 2, 73 K 5, 73 K 8, 73 K 9, 73 M 5, 75 K 5, 75 M 7, 76 D 9, 76 Y 2, 78 K 13, 85 G 13]; R = Gd [61 B 1, 61 N 2, 63 K 1]; R = Dy [61 B 1]; R = Er [69 S 1]; R = Y [69 K 5, 69 S 2*, 75 K 5, 76 D 9, 76 Y 2]
RNi_5	[60 H 2, 69 L 1, 82 P 4]; R = Ce, Pr, Nd, Gd, Dy, Er, Y [59 W 1]; R = La, Ce, Sm, Gd, Dy, Ho, Y [60 N 1]; R = La [79 A 2]; R = Ce [61 D 1]; R = Pr [61 D 1]; R = Gd [61 B 1, 61 N 2, 72 U 1]; R = Dy [61 B 1]; RCu_5, R = Gd, Tb, Dy, Y [71 B 22]
RM_5H_x	[82 Y 7]
RCo_5H_x	[74 K 18, 80 L 1]; R = Ce [74 K 19]; R = Pr [71 K 3, 74 K 19]
RNi_5H_x	[74 K 18]; R = La [73 B 14, 77 F 4, 78 A 3, 78 B 10, 78 F 9, 79 A 2, 80 P 1, 81 I 3, 82 A 3, 82 A 14, 82 O 3, 82 Y 6, 83 N 8, 84 H 4, 85 N 5, 85 O 2, 86 B 9, 86 M 1, 86 T 4, 87 L 2, 87 S 21, 87 T 5]; R = Pr [87 M 1]; R = Eu [85 G 4]

$(R'R'')M_5$ $(CeR)Co_5$, R = Zr, Hf [84 G 9]; $(PrSm)Co_5$ [71 S 3, 73 M 3]; $(PrTm)Co_5$ [74 N 2]; $(PrY)Co_5$ [88 P 1]; $(NdTm)Co_5$ [74 N 2]; $(NdY)Co_5$ [74 N 2]; $(NdU)Co_5$ [78 D 1]; $(SmGd)Co_5$ [79 M 5]; $(SmDy)Co_5$ [79 M 5]; $(SmGdDy)Co_5$ [79 M 5]; $(SmHo)Co_5$ [79 M 5]; $(SmEr)Co_5$ [79 M 5]; $(RTh)Co_5$, R = Gd, Ho, Er [73 W 1]; $(YU)Co_5$ [78 D 1]; $(YLa)(CoFe)_5$ [74 B 2]; $(ThY)Co_5$ [74 G 1, 79 W 3]; $(ThY)(FeCo)_5$ [74 G 1, 79 W 3]; $(SmZr)Fe_5$ [88 L 3]

$R(M'M'')_5$ $Ho(CoMn)_5$ [82 D 7]; $Th(CoMn)_5$ [77 M 10]; $R(MnNi)_5$ [83 P 3]; $La(NiMn)_5$ [80 L 3]; $Th(NiMn)_5$ [77 M 10]; $La(NiM)_5$, M = Mn, Al [79 A 2]; $La(NiM)_5$, M = Mn, Cu, Fe, Si, Al [85 P 5]; $Pr(CoM)_5$ [84 C 3]; $Pr(CoM)_5$, M = Fe, Ni, Mn, Cr, V, Ti [83 Z 4]; $Y(CoM)_5$ [82 C 7, 82 C 8]

$Ce(CoFe)_5$ [81 Y 4]; $Ho(CoFe)_5$ [82 D 7]; $Y(FeCo)_5$ [70 K 3, 72 T 1, 73 R 7]; $Th(FeCo)_5$ [72 V 1, 73 L 1, 73 R 7]; RNi_4Fe, R = La, Ce, Y [84 P 15]; $La(NiM)_5$, M = Mn, Fe, Ni, Cu, Al [82 P 3]; $La(NiFe)_5$ [84 L 1]; $Th(FeNi)_5$ [67 B 1, 72 V 1, 75 E 1, 76 E 1]; $Sm(CoM)_5$, M = Fe, Ni, Cu [76 E 6]

$La(CoNi)_5$ [73 V 3, 83 G 17]; $Ce(CoNi)_5$ [83 G 3]; $Pr(CoNi)_5$ [73 Z 1, 85 A 10]; $Nd(CoM)_5$, M = Ni, Cu, Al [87 C 3]; $Gd(CoNi)_5$ [81 C 1]; $Tb(CoNi)_5$ [82 P 9]; $Ho(CoNi)_5$ [79 D 9, 83 C 3]; $Er(CoNi)_5$ [85 D 12]; $Y(CoNi)_5$ [72 T 1, 75 T 1, 85 A 11]; $Th(CoNi)_5$ [73 A 4, 75 B 13, 75 N 3, 76 E 1]; $Ce(CoCu)_5$ [75 A 2, 79 L 1, 79 P 1, 81 Y 4, 86 L 2]; $Pr(CoCu)_5$ [73 Z 1]; $Pr(CoCuFe)_5$ [73 Z 1]; $Sm(CoCu)_5$ [74 N 11, 76 S 9, 78 P 3, 79 M 3, 79 O 2]; $Gd(CoCu)_5$ [70 S 4, 85 C 3, 85 C 4]; $Ho(CoCu)_5$ [79 D 9, 86 C 5]; $Y(CoCu)_5$ [81 Y 4]; $La(CoAl)_5$ [77 R 3]; $Ce(CoAl)_5$ [77 R 3, 78 A 6, 80 Z 2]; $Pr(CoAl)_5$ [73 O 4, 73 O 5]; $Sm(CoAl)_5$ [73 O 4, 73 O 5]; $Gd(CoAl)_5$ [70 S 4, 85 C 3, 85 C 4]; $Gd(CoGa)_5$ [85 C 3, 85 C 4]

$R(NiCu)_5$, R = La, Ce, Pr, Nd [82 G 5]; $La(NiCu)_5$ [84 P 5]; $Ce(NiCu)_5$ [77 B 24, 84 P 9]; $Yb(NiCu)_5$ [77 B 24]; $U(NiCu)_5$ [77 B 24, 82 R 3]; $La(NiAl)_5$ [79 D 7]; $Th(NiAl)_5$ [67 B 1]

$R(M'M'')_5H_x$ $La(NiM)_5H_x$, M = Mn, Fe, Cu, Si, Al [85 P 5]; M = Mn, Fe, Ni, Cu, Al [82 P 3]; M = Al, Ga, In, Sm [80 M 3]; M = Mn, Al [79 A 2]; $La(NiCo)_5H_x$ [83 G 17, 87 C 6]; $La(NiFe)_5H_x$ [82 D 2, 87 L 3]; $La(NiMn)_5H_x$ [80 P 2]; $La(NiCu)_5H_x$ [82 A 2]; $La(NiAl)_5H_x$ [78 M 10, 79 D 7, 79 M 10, 80 P 2, 82 A 2, 82 C 13, $La(NiSi)_5H_x$ [82 A 2]; $Ce(NiM)_5H_x$, M = Mn, Fe [86 P 6]; $Ce(NiCu)_5H_x$ [84 P 9]; $Ce(NiCuAl)_5H_x$ [84 S 12]; (CeNd)$(NiCu)_5H_x$ [84 S 12]; $Th(NiAl)_5H_x$ [77 T 2]

For thermal expansion see also

RCo_5 R = Pr, Tb, Dy, Ho [83 A 6*]; R = Nd [82 A 13]; R = Sm [74 J 2]

RNi_5 R = Ce [82 G 5]; R = Pr [76 O 11, 79 A 4, 80 L 6]

$R(M'M'')_2$ $Y(CoNi)_5$ [85 A 11, 85 A 12]; $Ce(CoCu)_5$ [81 Y 4]; $Y(CoCu)_5$ [79 Y 1, 81 Y 4]; $Ce(NiCu)_5$ [86 I 3]; $La(NiAl)_5$ [79 D 7]

For microstructure see also

RCo_5 [72 B 7, 73 N 1, 74 B 3, 78 F 3, 78 F 4, 79 K 9, 81 F 3, 81 L 3, 82 F 3, 86 T 1]

$(R'R'')M_5$ $(SmPr)Co_5$ [85 V 3]; $(SmPrNd)Co_5$ [85 V 3]

$R(M'M'')_5$ $Ce(CoCuFe)_5$ [73 L 2]; $Sm(FeCo)_5$ [73 B 20]; $Sm(CoCu)_5$ [73 J 1, 81 P 2]; $Sm(CoFeCuZr)_{6.85}$ [81 F 3]; $Y(CoM)_5$ [82 C 8]

For preparation see

RCo_5 [74 C 1]; $SmCo_5$ [73 M 8]; YCo_5 [82 W 6*]

For mechanical properties see

RM_5 $CeCo_5$ [74 R 5]; RNi_5, R = Sm, Gd, Pr, Nd, Tm [87 B 7*]

Magnetization, Curie temperatures

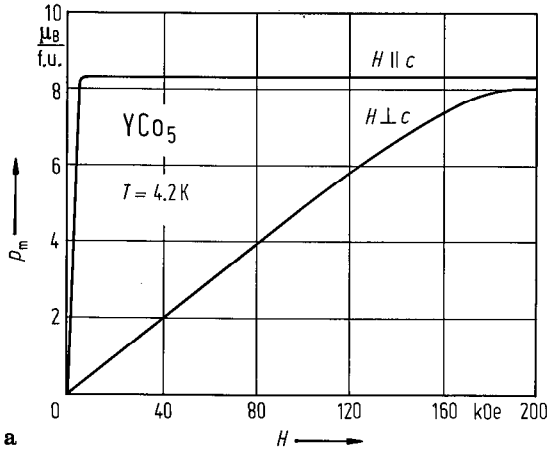

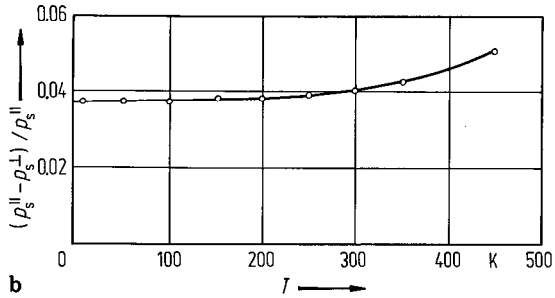

Fig. 344. (a) Magnetization isotherms of YCo_5 single crystal at 4.2 K. (b) Temperature dependence of the relative anisotropy of magnetization, $(p_s^{\parallel} - p_s^{\perp})/p_s^{\parallel}$, is plotted. The large anisotropy of the Co magnetization is associated with the Co magnetocrystalline anisotropy. At 4.2 K, the magnetization is reduced by 0.3 μ_B/f.u. when the applied magnetic field aligns in the basal plane. Between 4.2 and 450 K, the magnetization anisotropy increases by 20%, the disorder of the magnetic moments being larger along a hard direction than along the easy one [82 A 5].

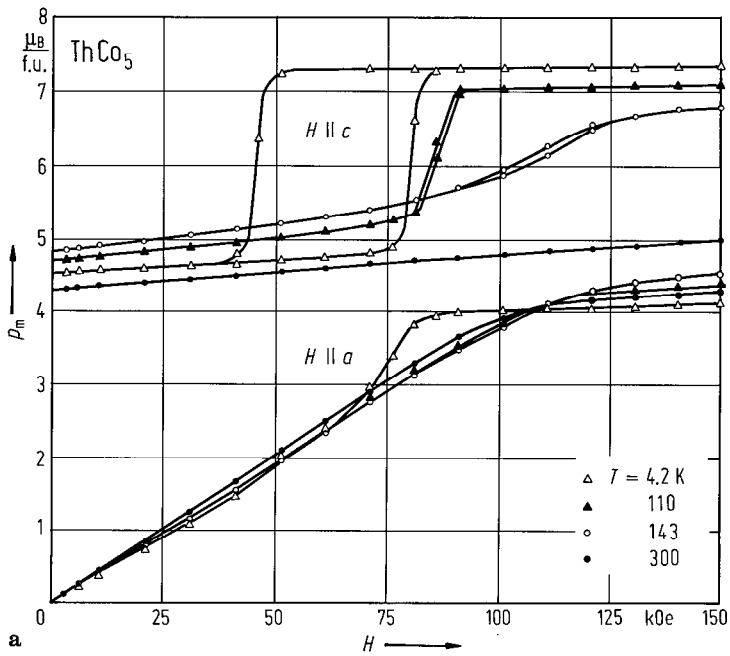

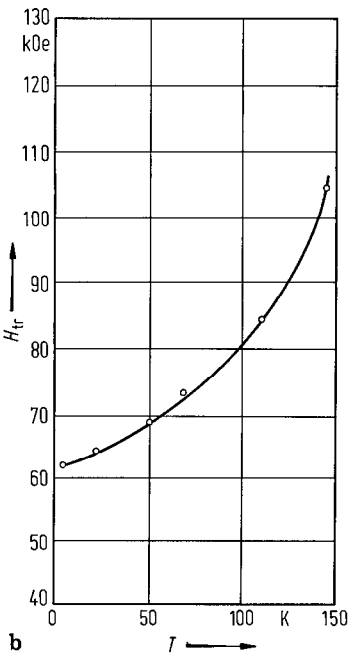

Fig. 345. Magnetization isotherms of $ThCo_5$ along the *c* and *a* axes as function of the applied magnetic field [79 G 6]. In fields lower than 20 kOe, the values of the magnetization have been obtained in decreasing field. A magnetic transition is observed, at 4.2 K, in 80 kOe, when the field applied along the *c* axis is increased. It exhibits a field hysteresis, the amplitude of which decreases when temperature increases. The thermal variation of the mean transition field appears in (b). See also [81 G 6, 83 G 4].

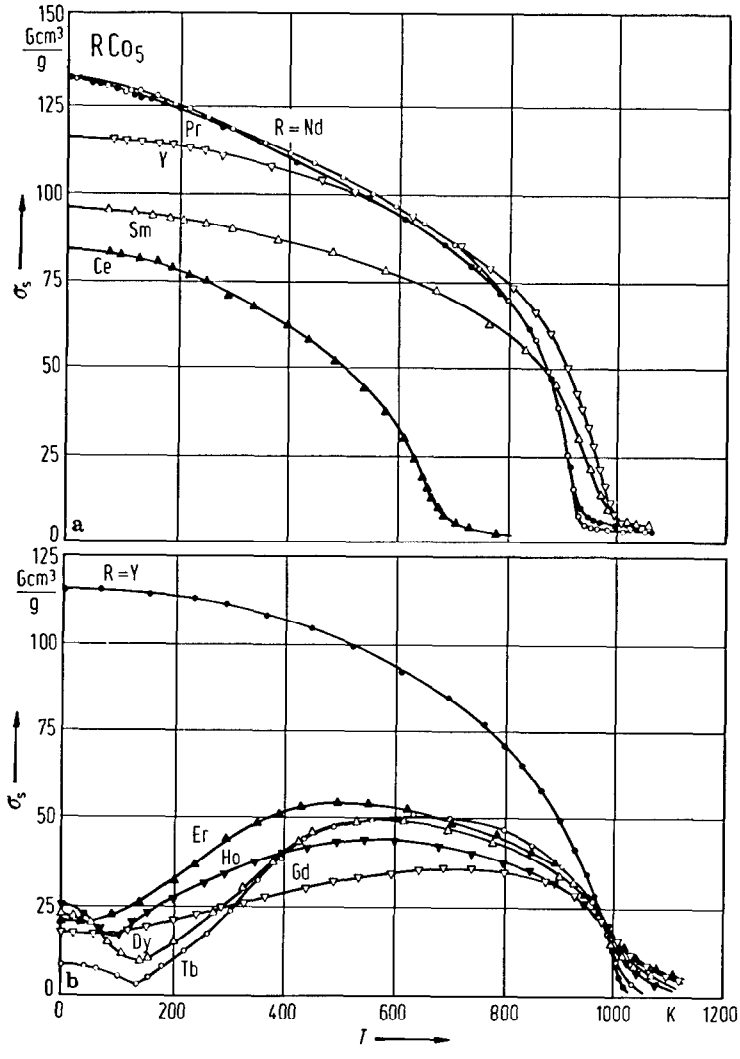

Fig. 346. Temperature dependence of the saturation magnetization in RCo_5 compounds: (a) R = Ce, Pr, Nd, Sm, Y [71 T 1]; (b) R = Gd, Tb, Dy, Ho, Er and Y [73 O 7].

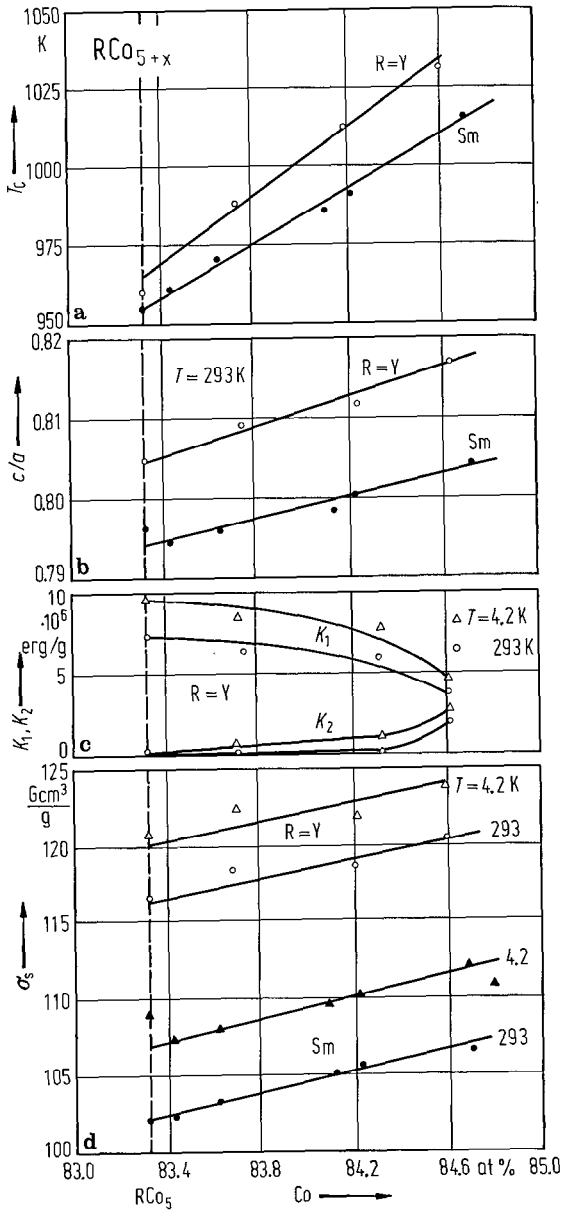

Fig. 347. Magnetic and crystallographic properties of RCo_{5+x} (R = Sm, and Y) compounds: (a) Curie temperature T_C, (b) c/a ratio of lattice constants, (c) anisotropy constants and (d) saturation magnetization [75 K 5].

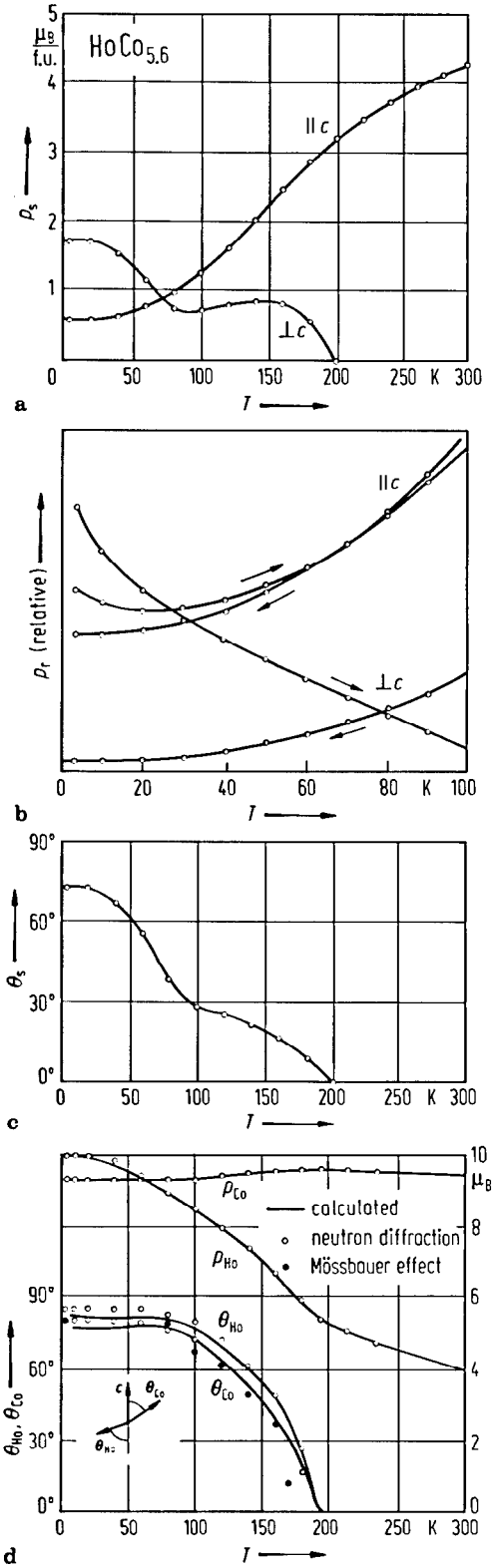

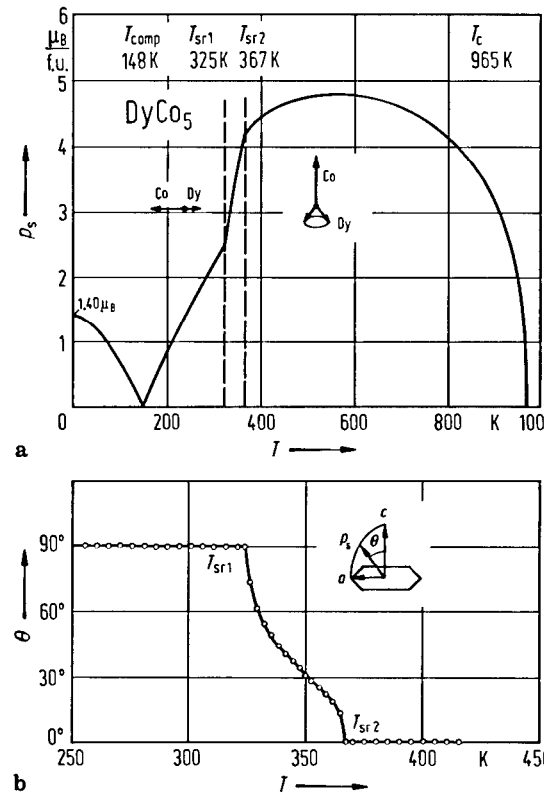

Fig. 349. (a) Temperature dependence of the spontaneous magnetization in $DyCo_5$ single crystal [83 T 5]. Between $T_{sr1} = 325$ K and $T_{sr2} = 367$ K, a very sharp change of p_s vs. T is observed. The direction of magnetization rotates continuously in the *ac* plane [77 O 9]. (b) Rotation angle θ of the spontaneous magnetization in the *ac* plane of $DyCo_5$ single crystal, induced by temperature [83 T 5]. $d\theta/dT$ is discontinuous at both T_{sr1} and T_{sr2}, but it is continuous between the two temperatures.

Fig. 348. Thermal variations of (a) the spontaneous magnetization components parallel and perpendicular to the *c* axis, (b) the remanent magnetization components, and (c) the angle θ_s (between p_s and *c* axis) in $HoCo_{5.6}$ compound [82 D 3]. At 4.2 K, $\theta_s = 72°$, while at room temperature, the spontaneous magnetization is parallel to *c* axis. (d) Temperature dependence of the Co and Ho magnetization in $HoCo_{5.6}$ compound determined by neutron diffraction studies [82 D 3]. The angles θ_{Co} and θ_{Ho} between *c* axis and Co and Ho magnetizations, respectively, are also given. Note that θ_s in (c) decreases between 30 and 80 K, the thermal variations of θ_{Co} and θ_{Ho} deduced from Mössbauer and neutron measurements take place mainly between 100 and 200 K. The deduced θ_{Ho} is slightly larger than θ_{Co}, suggesting a noncollinearity to occur during the spin reorientation process. The calculated values with the crystal field and exchange parameters given in Table 101 are plotted by solid lines.

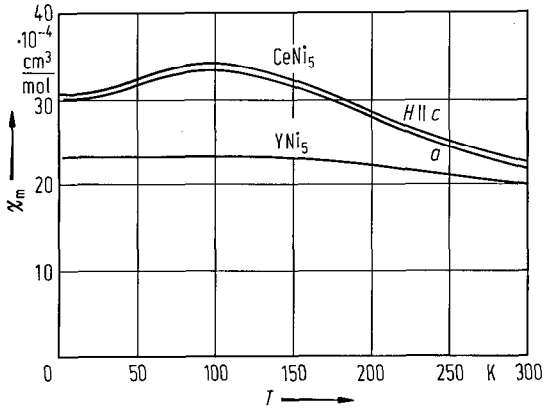

Fig. 350. Thermal variations of the magnetic susceptibilities of $CeNi_5$ and YNi_5 single crystals measured along the *a* and *c* directions [76 G 3, 82 G 3]. The anisotropy is nil in YNi_5 and very weak in $CeNi_5$. The $CeNi_5$ susceptibility presents a broad maximum at $\cong 100$ K.

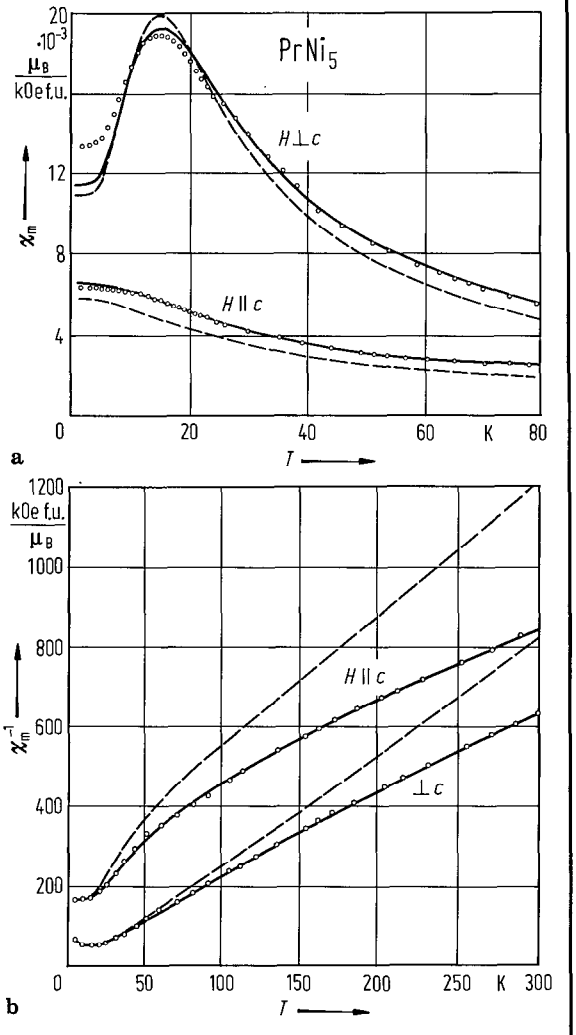

Fig. 351. (a) Thermal variations of the magnetic susceptibility χ of $PrNi_5$, parallel and perpendicular to the *c* axis. The open circles are the experimental data [87 B 7]. By solid and dashed lines are plotted the calculated variations with crystal field and exchange parameters obtained by [87 B 7, 88 B 3] and [79 A 4], respectively, see Table 94. A maximum in χ values is observed at 16 K when the external magnetic field is perpendicular to the *c* axis, while for external field along the *c* axis is susceptibility decreases continuously by increasing temperature. The observed maximum is due to the competition between the Curie and Van Vleck contributions in a system where the ground state in the crystal field is a nonmagnetic singlet. (b) Thermal variations of the reciprocal magnetic susceptibilities parallel and perpendicular to the *c* axis. The open circles are the experimental data. The solid lines are the calculated values with crystal field parameters [87 B 7] and the dashed lines represent the calculated contributions corrected for the Ni magnetic contributions. The negative curvature of χ vs. *T* values is attributed to the Ni contribution.

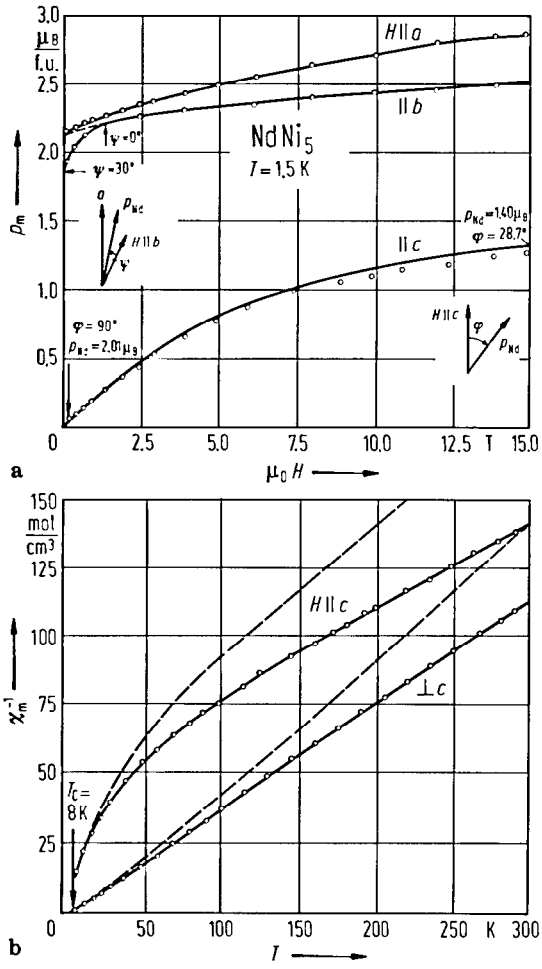

Fig. 352. (a) Magnetization isotherms of $NdNi_5$ single crystal at 1.5 K along the *a*, *b* and *c* axes of the orthohexagonal cell. In (b) the thermal variations of the reciprocal magnetic susceptibilities parallel and perpendicular to the *c* axis are plotted [80 N 1, 82 G 3, 84 A 11]. Circles are the experimental data and full lines represent the calculated variations considering crystal field, Zeeman and exchange interactions and applied magnetic field. The dotted lines represent the Nd contribution to the susceptibility. $NdNi_5$ orders ferromagnetically at $T_C = 8$ K along the easy *a* axis. In $NdNi_5$, the spontaneous magnetization is 2.14 μ_B/f.u. at 1.5 K. Application of a magnetic field results in a strong susceptibility response superposed on the spontaneous magnetization. Under 150 kOe the magnetization reaches 2.88 μ_B/f.u.

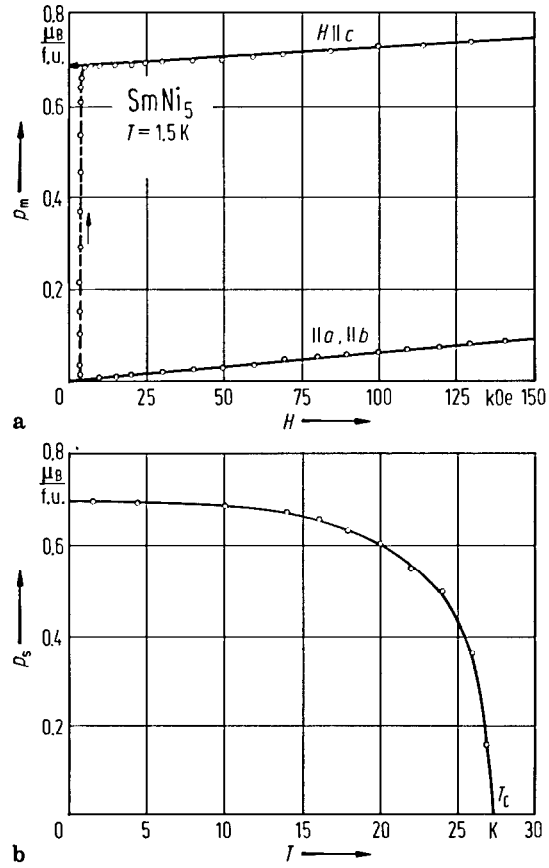

Fig. 353. (a) Magnetization isotherms in $SmNi_5$ at 1.5 K along the *a*, *b* and *c* axes. A very high uniaxial anisotropy is evidenced. The magnetization processes show the presence of thin walls between ferromagnetic domains [87 B 7, 88 B 1]. (b) Thermal variation of the spontaneous magnetization for $SmNi_5$ [87 B 7].

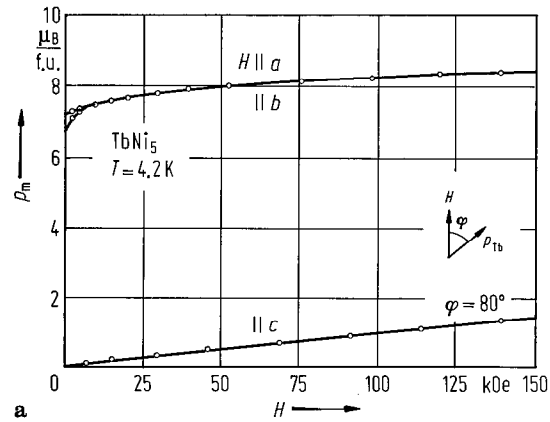

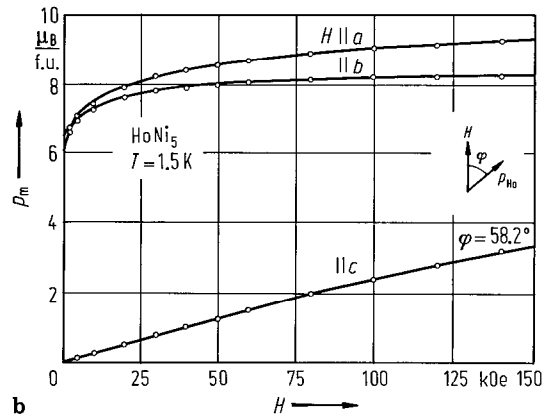

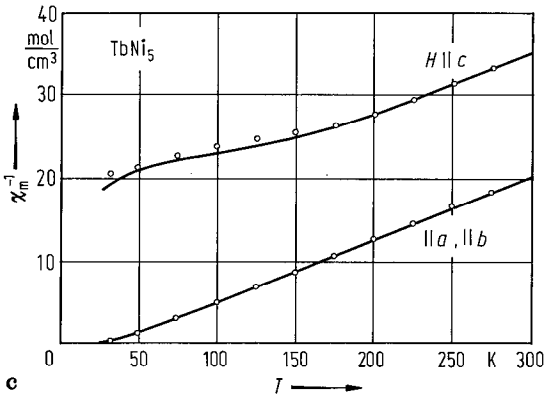

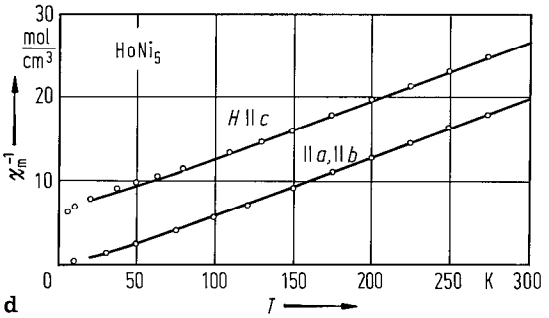

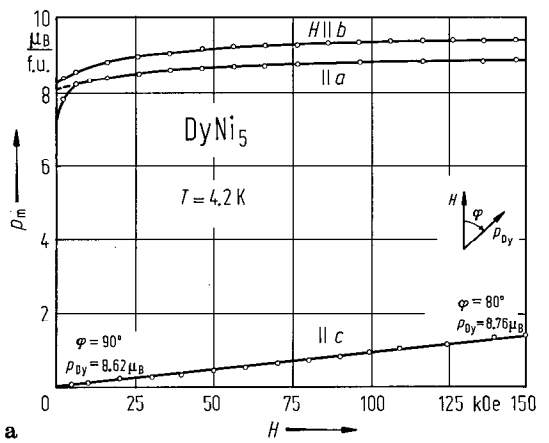

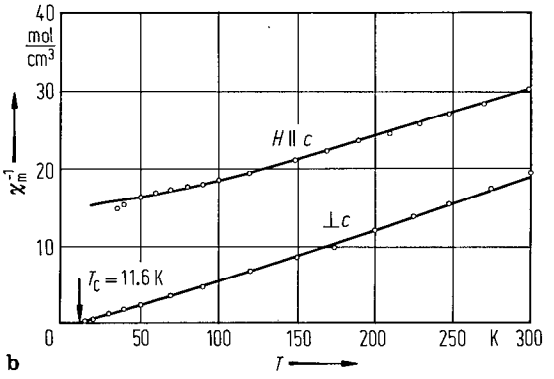

Fig. 355. (a) Magnetization isotherms of $DyNi_5$ single crystal at 4.2 K, along the *a*, *b* and *c* axes of the orthohexagonal cell. In (b) the thermal variations of the reciprocal magnetic susceptibilities along and perpendicular to the *c* axis are plotted. Circles are the experimental data and lines are the calculated variations with the parameters from Table 94 [81 A 4].

Fig. 354. Magnetization isotherms of (a) $TbNi_5$ and (b) $HoNi_5$ at low temperatures [79 G 3]. Due to strong anisotropy, a 150 kOe field applied along the *c* axis is not high enough to align the magnetization along the field. In $HoNi_5$ the magnetization measured along the *a* and *b* axes, which is almost zero in 3 kOe, increases with the field and reaches $\cong 9.2\ \mu_B$ and $\cong 8.2\ \mu_B$, respectively, in a field of 150 kOe. The difference observed in higher field originates from the large anisotropy of the magnetization. Thermal variations of the reciprocal magnetic susceptibilities are plotted in (c) and (d). The large uniaxial anisotropy is responsible for the difference between the paramagnetic Curie temperatures measured along the *c* axis and in the basal plane, respectively.

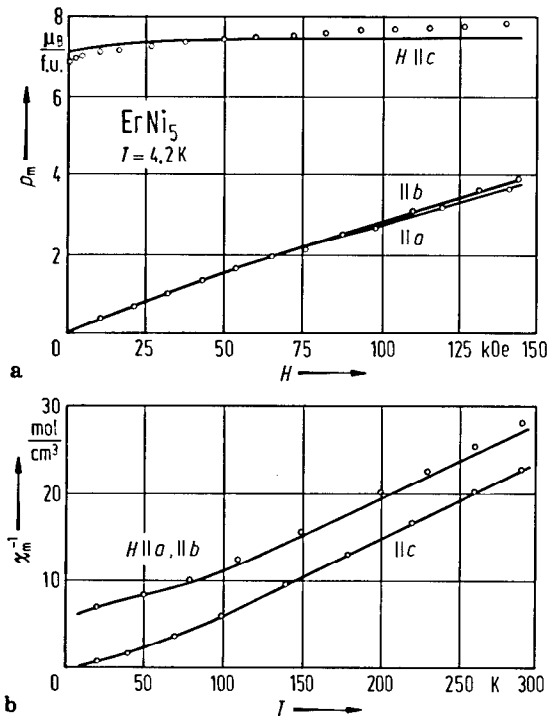

Fig. 356. (a) Magnetization isotherms of $ErNi_5$ single crystal at 4.2 K. Full lines represent the field dependence of magnetization calculated with crystal field and exchange parameters given in Table 94 [77 E 8]. A value of Ni magnetic moment, $p_{Ni}=0.07\,\mu_B$, is presumed. (b) Thermal variation of reciprocal magnetic susceptibility. Full lines represent the temperature dependence calculated by using the crystal field parameters from Table 94 [77 E 8].

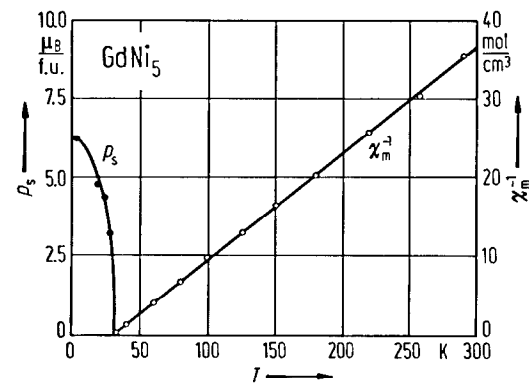

Fig. 358. Thermal variation of the spontaneous magnetization and reciprocal magnetic susceptibility for $GdNi_5$ compound [76 G 3]. The p_s vs. T curve agrees closely with that calculated for a Brillouin function with $J=7/2$.

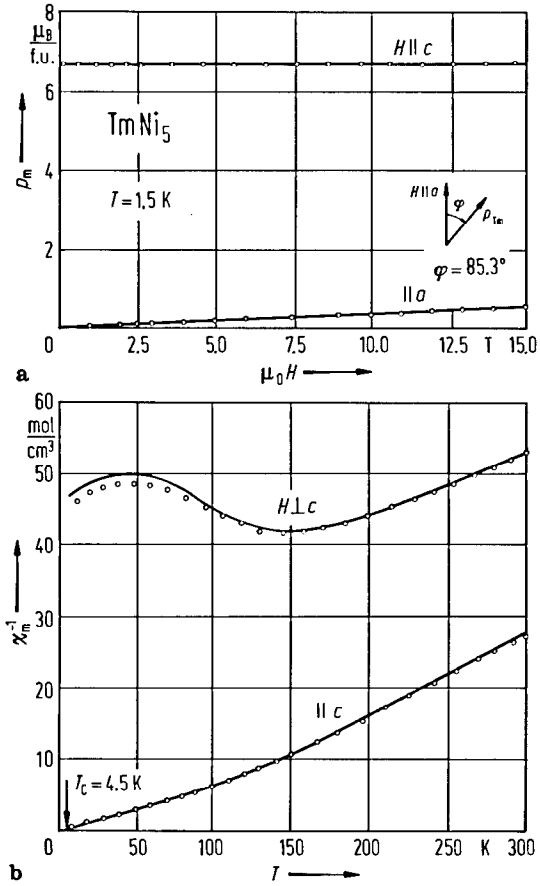

Fig. 357. (a) Magnetization isotherms of $TmNi_5$ at 1.5 K along the a, b and c axes of the orthohexagonal cell. In (b) the thermal variation of the reciprocal magnetic susceptibilities parallel and perpendicular to the c axis is plotted [80 N 1, 82 G 2]. Circles are the experimental data and lines represent the variations calculated with crystal field and exchange parameters given in Table 94. The superposed magnetic susceptibility at 1.5 K is weak, of the order of the $LaNi_5$ susceptibility. The spontaneous magnetization at 1.5 K reaches $6.73\,\mu_B$/f.u. In the paramagnetic regime a large anisotropy of the initial magnetic susceptibility is observed. Above 200 K, the thermal variation of the reciprocal susceptibilities, $\chi_{\parallel c}$ and $\chi_{\perp c}$, is linear and almost parallel.

Table 90a. Magnetic properties of RCo_5 compounds.

	T_C(K)							p_s(μ_B/f.u.)						
	66L3	71T1	73O7	77O9	79E3	83T5	83Y4	66L3	69B7 [1])	71T1	71W2	73O7	77O9	83Y4
$LaCo_5$					874				7.1					
$CeCo_5$	737	673			653			5.7	5.5	6.6				
$PrCo_5$	912	921						9.9	9.0	10.4				
$NdCo_5$	910	913			914			9.5	9.1	10.4	11.7			
$SmCo_5$	1020	984			959			6.0	7.2	7.7				
$GdCo_5$	1008		1013				953	1.2	2.6		1.3	1.42		1.7
$TbCo_5$	980		987					0.57	1.7			0.69		
$DyCo_5$	966		998	965		925		0.70	3.2		1.6	1.71	1.40	
$HoCo_5$	1000		1036					1.1	4.6		1.9	2.06		
$ErCo_5$	986		1066					0.46	5.6			1.71		
$TmCo_5$	1020							1.9						
YCo_5	977	978			970		978	6.8	7.5	7.9		8.30		7.76

[1]) At room temperature; the compositions are RCo_5 except $TbCo_{5.1}$, $DyCo_{5.3}$, $HoCo_{5.5}$, $ErCo_6$.

Table 90b. Magnetic properties of RNi_5 compounds [1].

	T_C(K)								p_s(μ_B/f.u.)							
	72 B 14	73 S 1	76 G 3	77 E 8	78 O 5	79 G 3	80 N 1, 85 G 20	88 B 1	63 B 1	70 L 3	71 W 1	72 B 14	76 G 3	80 A 8	78 O 5	80 N 1 [2]	88 B 1
$LaNi_5$	Pauli paramagnet $\chi_m = 2.0 \cdot 10^{-3}$ cm^3 mol^{-1} at 4.2 K [76 G 3] or $2.27 \cdot 10^{-3}$ cm^3 mol^{-1} [80 P 1]																
$CeNi_5$	Pauli paramagnet, see Fig. 350																
$PrNi_5$	Van Vleck paramagnet, see for example [72 C 8, 81 K 17]																
$NdNi_5$		6.4					8		2.2		2.27					2.14	
$SmNi_5$					41			27.5	0.7						0.442		0.756
$EuNi_5$	No evidence of magnetic ordering for $T \geqq 2.6$ K [78 O 6]																
$GdNi_5$	28	29.8	32						6.8		6.8	6.9	6.2				
$TbNi_5$						23			7.1	7.02(15)							
$DyNi_5$		12							7.7					8.62			
$HoNi_5$		4.1				4.5			7.2		7.8						
$ErNi_5$		8.0		10		10			7.8								
$TmNi_5$							4.5				6.7					6.73	
YNi_5	Pauli paramagnet $\chi_m = 2.3 \cdot 10^{-3}$ cm^3 mol^{-1} at 4.2 K [76 G 3], see Fig. 350																
$ThNi_5$	Pauli paramagnet $\chi_m = 1.9 \cdot 10^{-3}$ cm^3 mol^{-1} [75 E 1]																

[1]) For magnetic behaviour of RNi_5 single crystals see Figs. 350–358.
[2]) At 1.5 K.

Table 91. Magnetic properties of some RM_5 hydrides.

	x	T K	p_s μ_B/f.u.	p_{Co} μ_B	T_C K	Ref.
$GdCo_5H_x$	0	4.2	1.70	1.74	953	83 Y4
	0.4(1)	4.2	1.45	1.69		
	2.8(1)	4.2	0.44	1.49	480(50) [1]	
YCo_5H_x	0	4.2	7.76	1.55	978	83 Y4
	0.4(1)	4.2	7.21	1.44		
	2.8(1)	4.2	6.25	1.25	440(50)	
$LaNi_{4.5}Fe_{0.5}H_x$	5.6	4.2	0.77 [2]			87 L 1
$LaNi_{4.25}Fe_{0.75}H_x$	5.6	4.2	0.98 [2]			
$LaNi_4FeH_x$	5.3	4.2	1.30 [2]			
$LaNi_{3.8}Fe_{1.2}H_x$	5.2	4.2	1.48 [2]			

[1]) Tentatively evaluated.
[2]) Values obtained in field of 150 kOe.

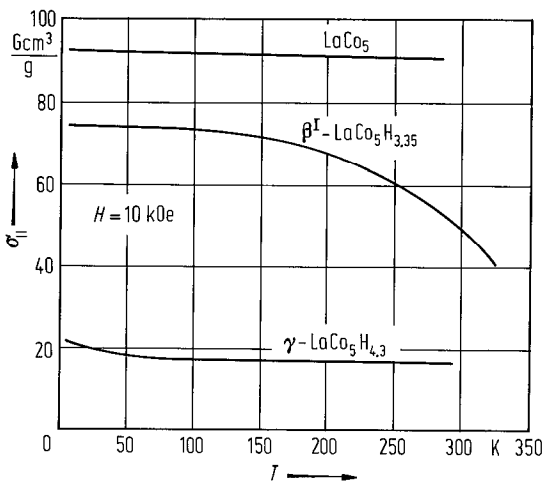

Fig. 359. Thermal variation of magnetization at 10 kOe in $LaCo_5$ and their hydrides [73 K 15]. The absorption of hydrogen leads to a reduction of the magnetic moment of Co atoms.

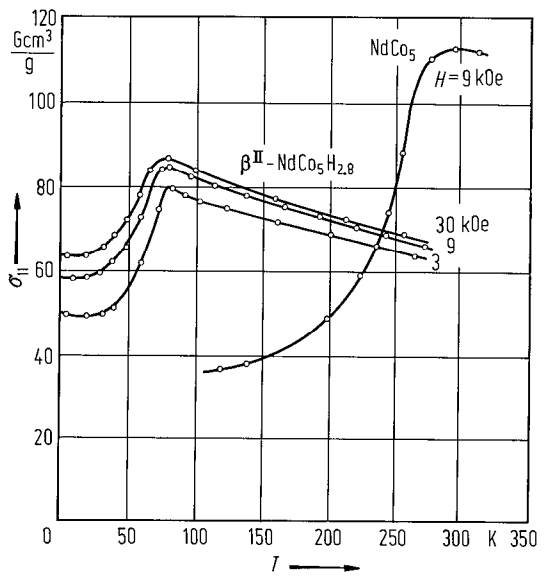

Fig. 360. Thermal variation of the magnetization in $NdCo_5$ compound and their hydrides [73 K 15]. The magnetization observed for hydrides at high temperatures is much reduced as compared to the pure compound. This effect is due probably to a reduction of Co magnetic moments. The temperature at which the direction of the magnetic moments departs from the *c* axis is shifted by about 200 K towards lower temperatures.

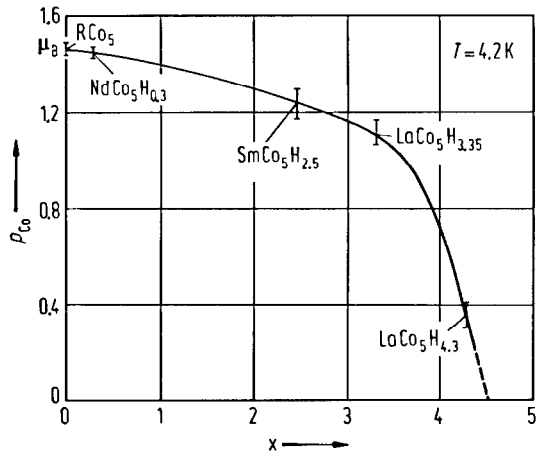

Fig. 361. Dependence of the Co magnetic moment at 4.2 K on the hydrogen content in some RCo_5 hydrides [73 K 15]. The presence of hydrogen as nearest neighbours of Co atoms leads probably to a reduced exchange interaction between 3d electrons, and consequently a decrease of Co magnetic moment is observed. The Co magnetic moment shown in RCo_5 is nearly the same for all R.

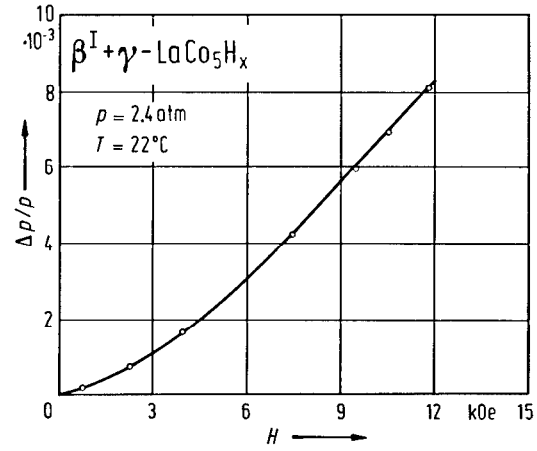

Fig. 362. Dependence of H_2 pressure in $LaCo_5H_x$ on the applied magnetic field [73 K 15, 74 B 17]. The hydrogen pressure rises almost simultaneously with the application of a magnetic field. Similar effects were observed in RCo_5 samples containing a mixture of the α-phase and β'-phase.

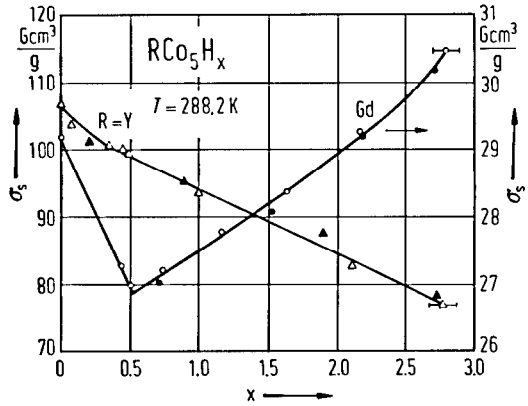

Fig. 363. Composition dependence of the saturation magnetization in (open symbols) the absorption and (solid symbols) the desorption processes for $GdCo_5H_x$ and YCo_5H_x at 288.2 K [83 Y 4].

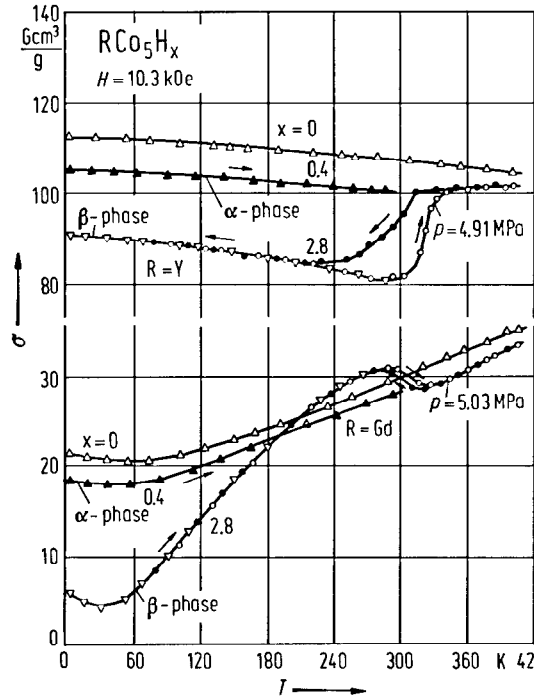

Fig. 364. Temperature dependence of the magnetization of YCo_5H_x and $GdCo_5H_x$ in a field of 10.3 kOe for the parent compound (x = 0) and the quenched α-(x = 0.4) and β-(x = 2.8) phases, the samples being under constant hydrogen pressure. The open and closed symbols indicate the data taken in the heating and cooling runs, respectively [83 Y 4].

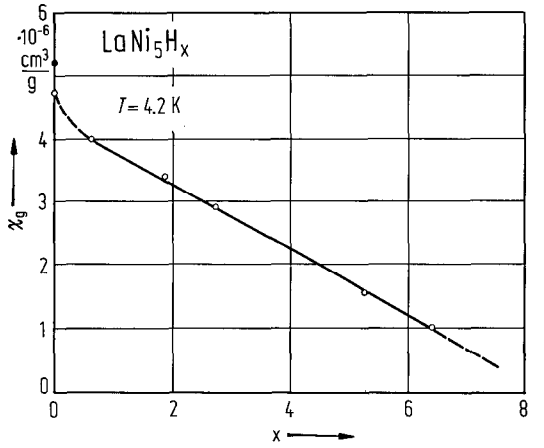

Fig. 365. Variation of the magnetic susceptibility, χ_g, of $LaNi_5H_x$ hydrides at 4.2 K with hydrogen content. The solid circle provides χ_g for a fresh sample [80 P 1]. The decrease of χ values with the hydrogen content is interpreted as a decrease of the density of states at the Fermi level. This implies, as shown by EPR measurements, a charge transfer from H_2 to Ni or an equivalent mechanism [76 W 1].

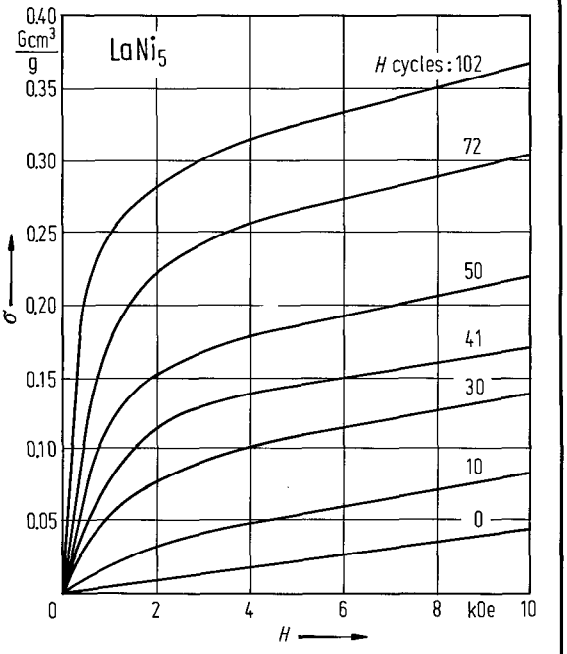

Fig. 366. Magnetization isotherms in $LaNi_5$ at 20 °C as function of the number of H cycles [80 S 5]. The $LaNi_5$ is an exchange-enhanced Pauli paramagnet with $\chi_g = 4.6 \cdot 10^{-6}\,cm^3\,g^{-1}$. Hydrogen absorption leads to a decrease of the magnetic susceptibility to $1.3 \cdot 10^{-6}\,cm^3\,g^{-1}$. This decrease is usually covered by a strong irreversible increase of surface magnetism where, through surface segregation and decomposition, superparamagnetic Ni precipitates are formed [78 S 15, 80 P 1].

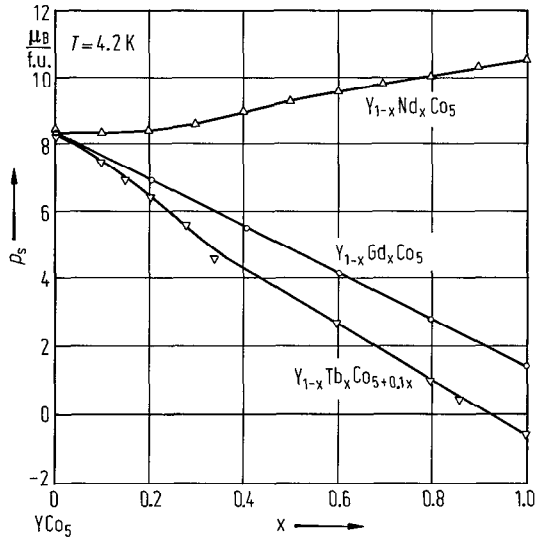

Fig. 367. Composition dependence of the saturation magnetic moment per formula unit of $Y_{1-x}R_xCo_5$ (R = Nd, Gd, Tb) at 4.2 K [80 E 1].

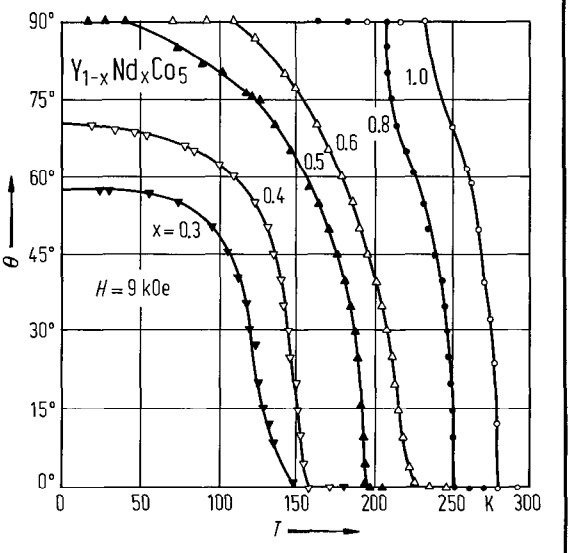

Fig. 368. Temperature dependence of the angle θ between the magnetization and the c axis in $Y_{1-x}Nd_xCo_5$ compounds in an external field $H = 9$ kOe [80 E 1]. The easy direction turns from the c axis to the c plane during cooling. By decreasing x, the spin reorientation temperature is lowered.

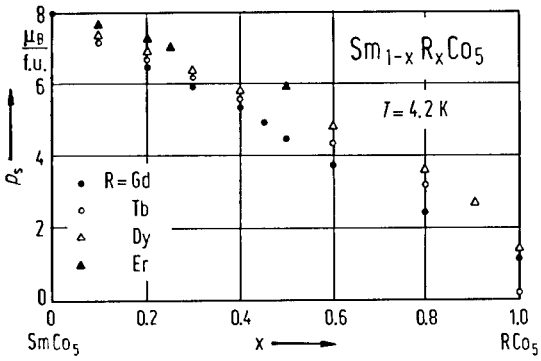

Fig. 369. Composition dependence of the saturation magnetization, at 4.2 K, in $Sm_{1-x}R_xCo_5$ (R = Gd, Tb, Dy and Er) compounds [75 D 7].

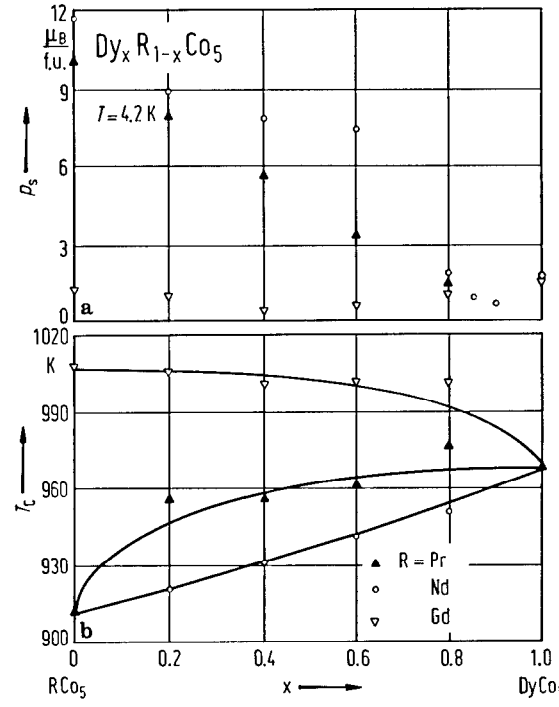

Fig. 370. Composition dependence of (a) the magnetizations at 4.2 K and (b) the Curie temperatures in $Dy_xR_{1-x}Co_5$ (R = Pr, Nd, Gd) compounds [71 W 2].

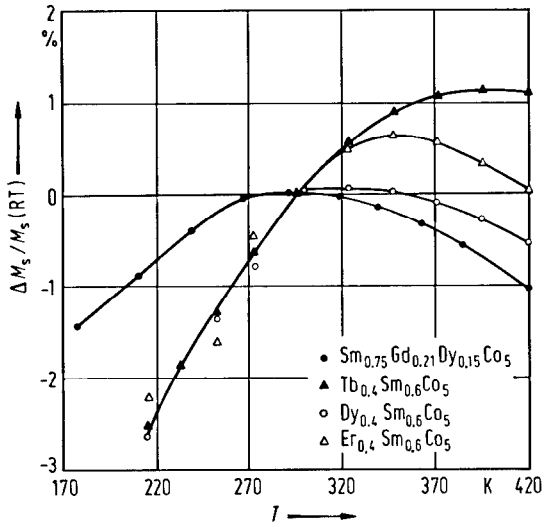

Fig. 371. Percentage changes of the saturation magnetization versus temperature (with respect to room temperature) in some $Sm_xR_{1-x}Co_5$ compounds. A small temperature dependence is obtained in ternary $Sm_xDy_{1-x}Co_5$ systems [78 M 6]. See also [74 B 6, 76 J 1, 78 N 3, 79 G 14].

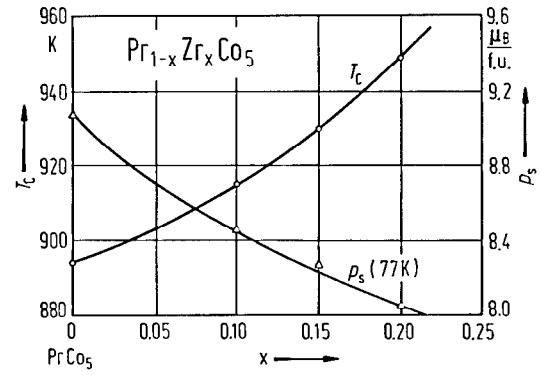

Fig. 372. Composition dependence of the saturation magnetization at 77 K and Curie temperature in $Pr_{1-x}Zr_xCo_5$ alloys [84 G 10].

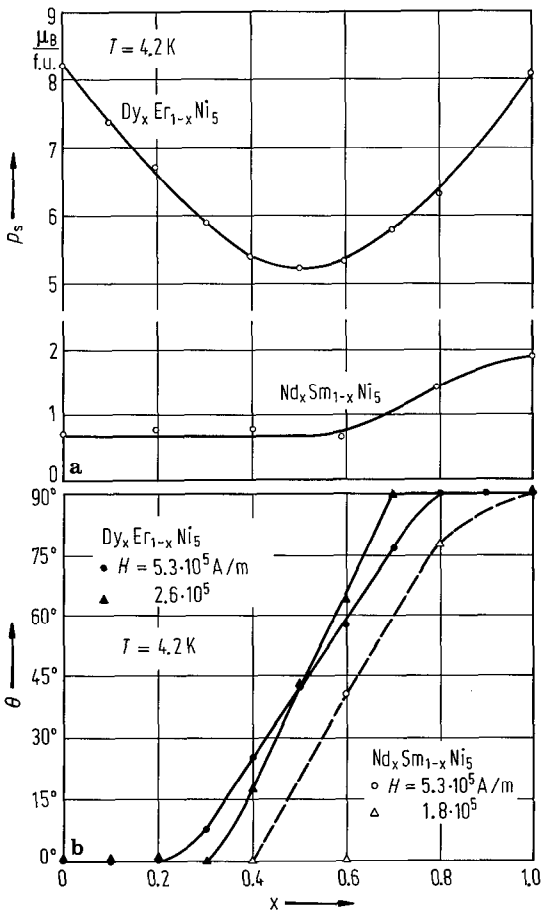

Fig. 373. Composition dependence of the saturation magnetization at 4.2 K in $Dy_xEr_{1-x}Ni_5$ and $Nd_xSm_{1-x}Ni_5$ [84 E 2]. (b) Composition dependence at 4.2 K of the angle θ between the easy axis of magnetization and the c axis in $Dy_xEr_{1-x}Ni_5$ and $Nd_xSm_{1-x}Ni_5$.

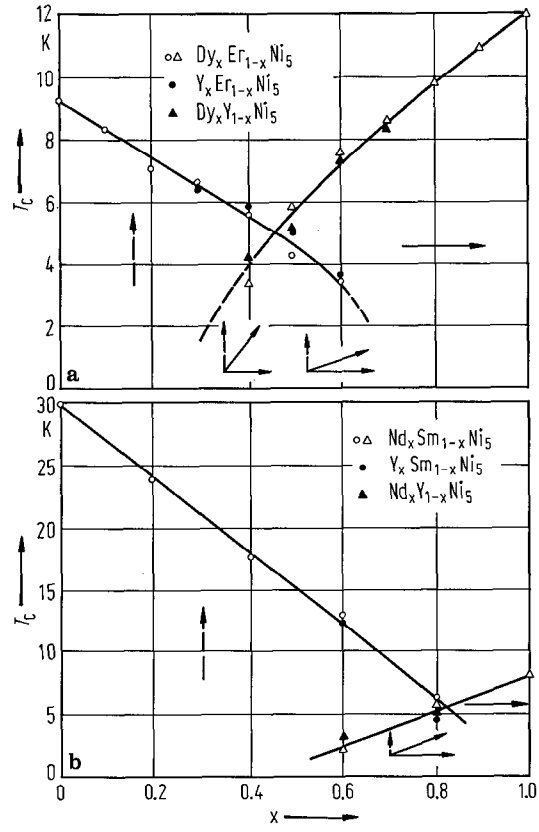

Fig. 374. Magnetic phase diagram of (a) $Dy_xEr_{1-x}Ni_5$, $Y_xEr_{1-x}Ni_5$, $Dy_xY_{1-x}Ni_5$, and (b) $Nd_xSm_{1-x}Ni_5$, $Y_xSm_{1-x}Ni_5$, $Nd_xY_{1-x}Ni_5$ systems. The Curie temperatures for magnetic ordering along and perpendicular to the c axis are denoted by circles and triangles, respectively. The directions of magnetization are also shown [85 K 14].

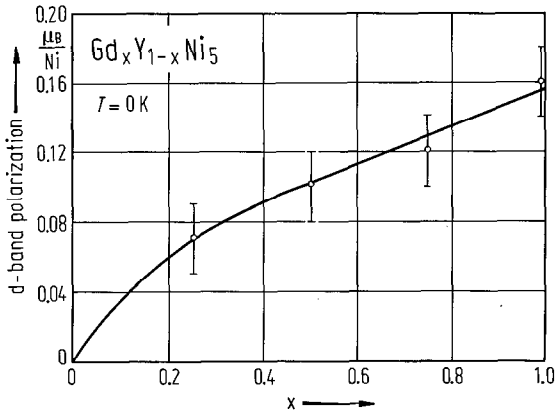

Fig. 375. Composition dependence of the d-band polarization at 0 K per Ni atom in $Gd_xY_{1-x}Ni_5$ alloys [76 G 3].

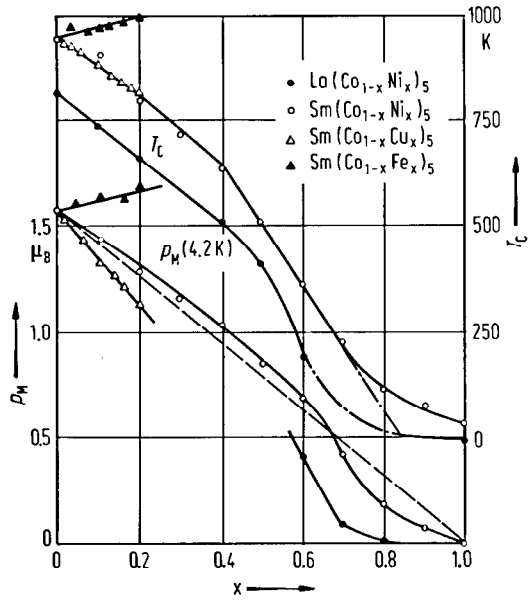

Fig. 376. Composition dependence of the Curie temperatures and mean magnetic moment of transition metal atoms at 4.2 K in $La(Co_{1-x}Ni_x)_5$ [75 B 8], $Sm(Co_{1-x}Ni_x)_5$ [76 E 6], $Sm(Co_{1-x}Cu_x)_5$ [76 E 6] and $Sm(Co_{1-x}Fe_x)_5$ [76 E 6]. When increasing the Ni and Cu content, both T_C and p_M values decrease, while in case of Fe an increase is shown. The $La(Co_{1-x}Ni_x)_5$ compounds having $x \leqq 0.4$ are ferromagnetic. In the concentration range $0.5 \leqq x \leqq 0.8$ a more complex behaviour is observed. Upon increasing the temperature from 4.2 K the magnetization first rises and after passing through a maximum decreases again. The observed magnetic behaviour is discussed in terms of mictomagnetism and narrow Bloch wall propagation.

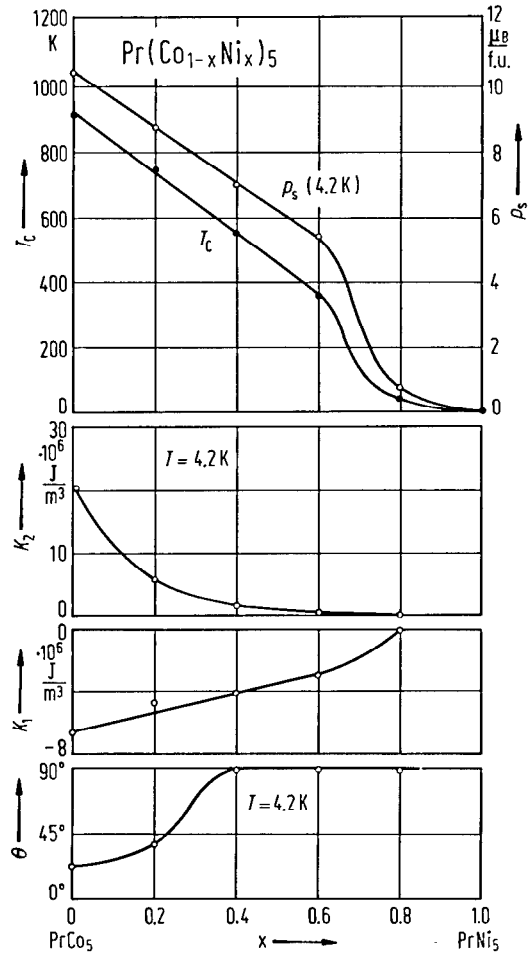

Fig. 377. Composition dependence of the spontaneous magnetic moment p_s, Curie temperature T_C, anisotropy constants K_1 and K_2, and the angle, θ, between c axis and easy direction of magnetization at 4.2 K for $Pr(Co_{1-x}Ni_x)_5$ compounds [85 A 10].

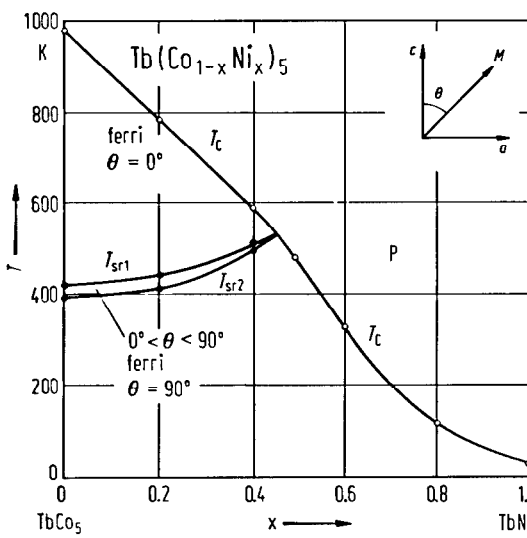

Fig. 378. Magnetic phase diagram of $Tb(Co_{1-x}Ni_x)_5$ compounds showing Curie temperatures (T_C) as well as start (T_{sr1}) and end (T_{sr2}) of spin reorientation [82 P 9]. See also [77 K 1].

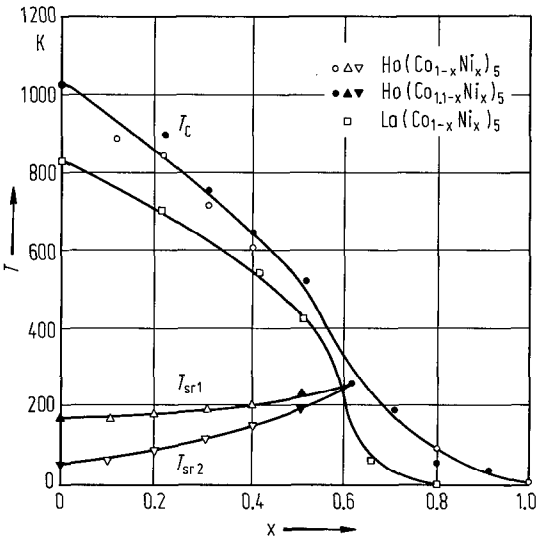

Fig. 379. Magnetic phase diagram of the $Ho(Co_{1-x}Ni_x)_5$ (open symbols) and $Ho(Co_{1.1-x}Ni_x)_5$ (solid symbols) systems [83 C 3]: Curie temperatures (T_C), start (T_{sr1}) and end (T_{sr2}) of spin reorientation. The Curie points of $La(Co_{1-x}Ni_x)_5$ compounds are also given [75 B 8].

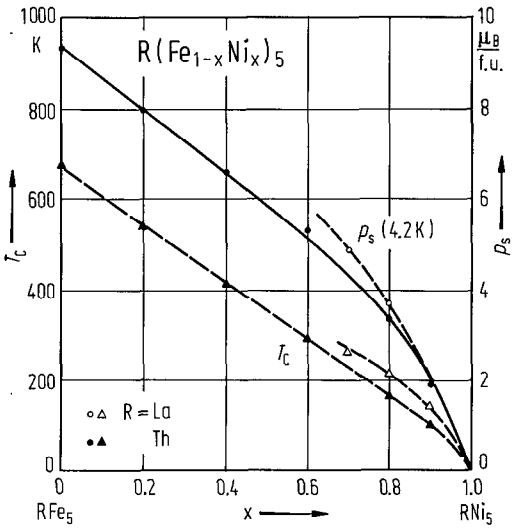

Fig. 380. Composition dependence of the saturation magnetic moment at 4.2 K (circles) and of the Curie temperatures (triangles) for the $La(Fe_{1-x}Ni_x)_5$ (open symbols) and $Th(Fe_{1-x}Ni_x)_5$ (full symbols) alloys [75 E 1].

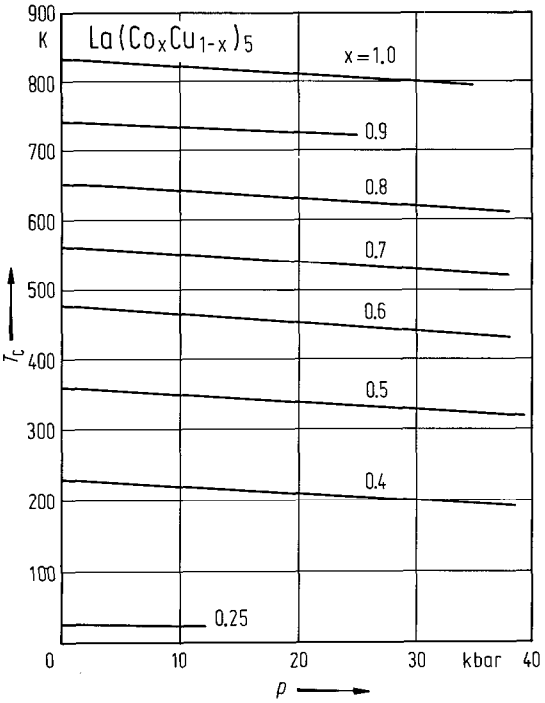

Fig. 381. Pressure dependence of the Curie temperature in $La(Co_xCu_{1-x})_5$ compounds [75 B 7]. In all cases the T_C values decrease with pressure.

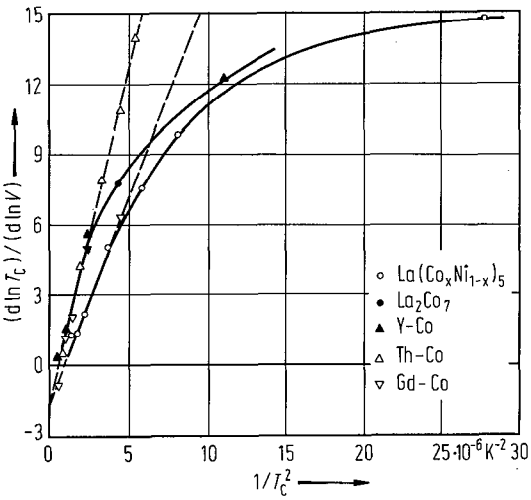

Fig. 382. Variation of $\Gamma = d \ln T_C / d \ln V$ for some $La(Co_xNi_{1-x})_5$ compounds as function of T_C^{-2} [75 B 6]. The data for Y–Co, Th–Co, Gd–Co and La_2Co_7 are also given. The values were corrected for thermal expansion accompanying the T_C shift under pressure. For compounds having $T_C > 500$ K ($x < 0.6$), the data fit the relation $\Gamma = a + bBT_C^{-2}$, predicted by the collective electron model.

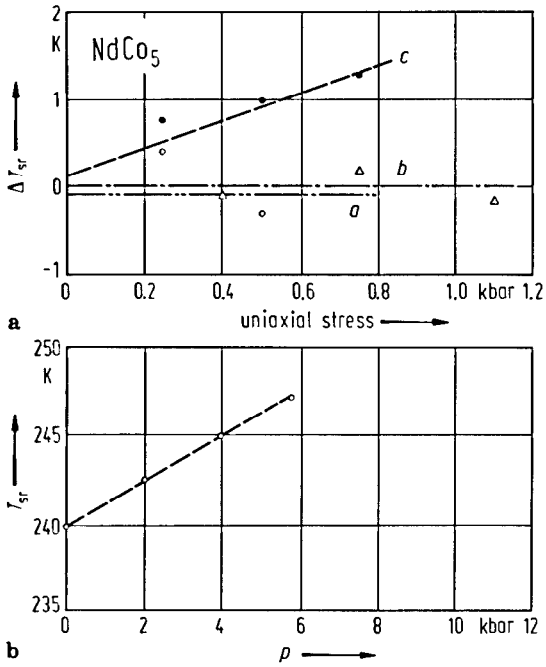

Fig. 383. (a) Variation of the spin reorientation temperature T_{sr} of $NdCo_5$ with uniaxial stress applied along the three crystallographic axes. T_{sr} is independent of stress in the basal plane but increases at a rate of 1.6 K/kbar parallel to the c axis. (b) shows the effect of hydrostatic pressure on the spin reorientation temperature [86 P 2].

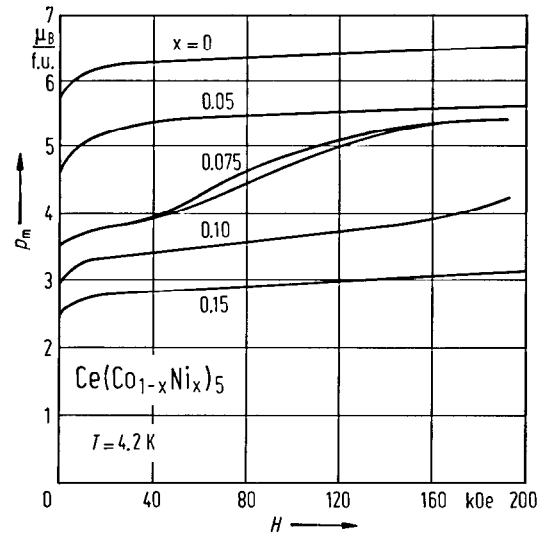

Fig. 384. Magnetic field dependence of the magnetizations in $Ce(Co_{1-x}Ni_x)_5$ compounds at 4.2 K [83 G 4]. In aligned powders, for $x = 0.075$, properties analogous to those of $ThCo_5$ are observed. The spontaneous magnetization exhibits a maximum near 200 K, and a transition towards a state of higher magnetization is induced by an applied magnetic field at low temperatures. The transition is not sharp because statistical site occupancy by Ni atoms leads to a distribution of exchange fields and consequently of the transition fields.

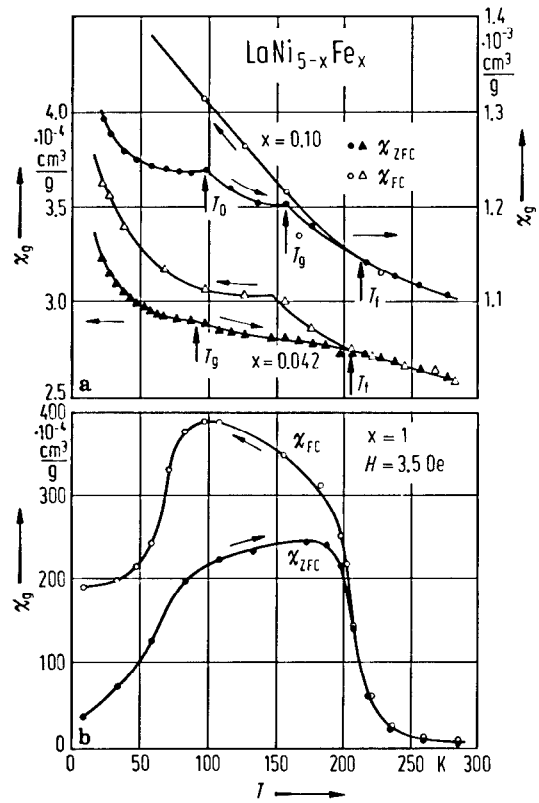

Fig. 385. (a) Magnetic susceptibility (zero-field-cooled, χ_{ZFC}, and field-cooled, χ_{FC}) for Fe concentrations, $x = 0.042$ and 0.10, smaller than the percolation threshold, $x_c = 0.30(5)$, in $LaNi_{5-x}Fe_x$ system. The temperatures T_f, T_g, T_o, which characterize the onset of irreversibilities, spin glass-like freezing and an extra peak in χ_{ZFC}, respectively, are marked by arrows [87 E 6]; (b) Magnetic susceptibility for a typical Fe concentration, $x = 1.0$ larger than x_c. For $x > x_c$, a sharp increase of $\chi_{FC} = \chi_{ZFC}$ at a Curie temperature T_C upon cooling gives evidence of the onset of a spontaneous magnetization in the ferromagnetic phase. At such Fe concentrations, T_C is roughly equal to the temperature T_f at which χ_{FC} and χ_{ZFC} split, within experimental uncertainty.

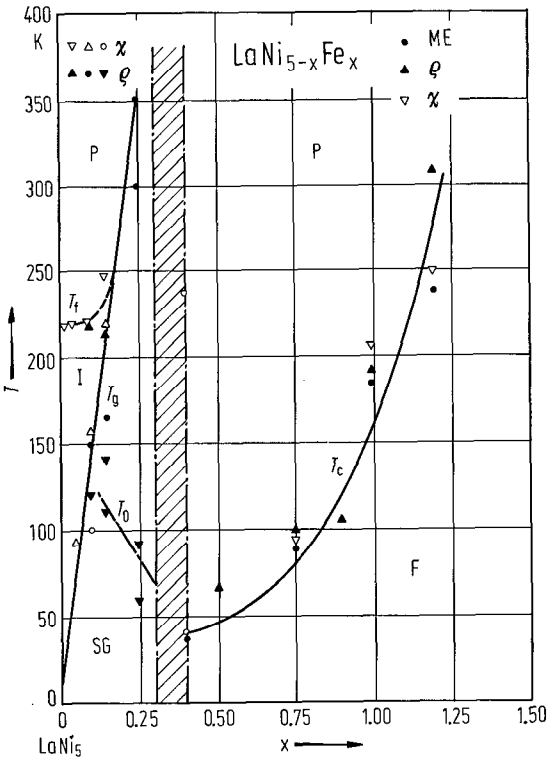

Fig. 386. Magnetic phase diagram of $LaNi_{5-x}Fe_x$ system [87 E 6]. P denotes the paramagnetic phase (with non-negligible local spin correlations). SG is a spin glass (or a cluster glass) state, separated from the P phase by a region of strong irreversibilities I, between the $T_f(x)$ (broken curve) and $T_g(x)$ curve (full curve) at $x < 0.4$. The broken-dotted curve represents the variation of T_0 with x. F is the ferromagnetic configuration at $x > 0.4$. The dashed area in the phase diagram is the region near $x \cong x_c$ which separates two different parts of the phase diagram, characterized by different magnetic properties. The symbols denote experimental determinations of the temperatures T_f, T_g, T_0 from magnetic susceptibility (χ) and electrical resistivity (ϱ) data. At $x > 0.4$, the $T_C(x)$ curve (full line) has been determined from Mössbauer effect (ME) [84 L 1], electrical resistivity (ϱ) and magnetic susceptibility (χ) data. Above a critical Fe concentration, $x_c \cong 0.3$, the system undergoes a superparamagnetic to long-range ferromagnetic ordering at a finite temperature T_C. At lower concentrations, no long-range spin ordering is observed, which suggests that x_c is the percolation threshold. Instead, a transition to a phase characterized by strong irreversibilities, is observed at temperature $T_f(x)$. Very strong ferromagnetic interactions between Fe atoms are observed at low concentrations ($x < x_c$), which contrast with small T_0 values observed for $x \geqq x_c$.

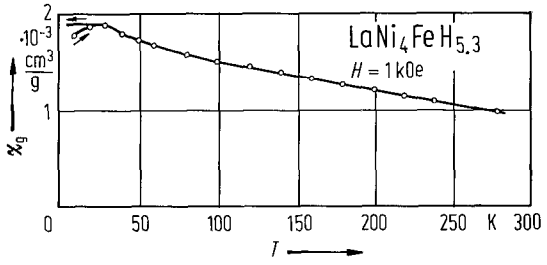

Fig. 387. Magnetic susceptibility in a constant magnetic field (1 kOe) by increasing and decreasing temperature for $LaNi_4FeH_{5.3}$. A maximum in χ values at 25 K and a hysteresis phenomenon at $T \cong 20$ K indicate a spin-glass-type behaviour [87 L 1].

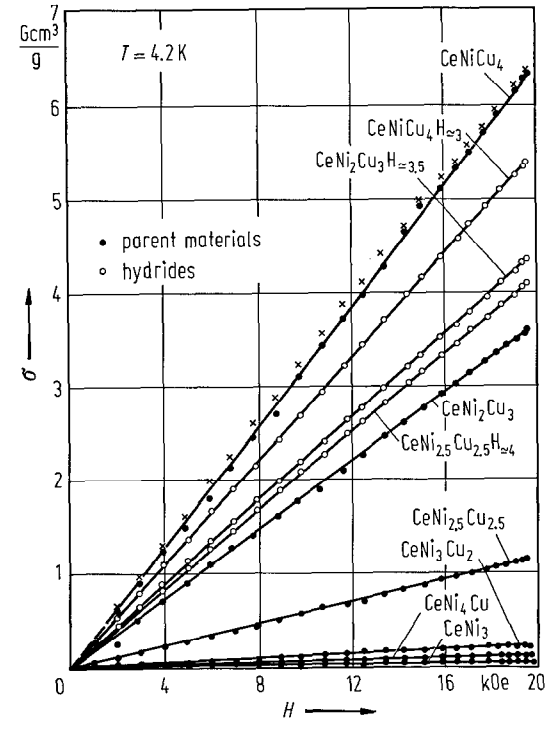

Fig. 388. Magnetization isotherms for $CeNi_{5-x}Cu_x$ system and their hydrides at 4.2 K. Two samples of $CeNiCu_4$ were examined. For $x < 2$ the compounds are Pauli paramagnets. For $x > 2$, the χ vs. T curve can be regarded as a sum of a Pauli-type contribution and Curie-Weiss paramagnetism associated with Ce^{3+} ion. Hydrogenation increased the unit cell volume by $\cong 15\%$ without a change of crystal structure. It also caused an increase in the effective magnetic moment for $x = 2.5$ and 3.0, but a small decrease was observed for $x \geqq 4.0$ [84 P 9].

For magnetic properties see also

RM_5 [85 K 5(T), 88 K 5]; R = Sm, Gd, Tb, Dy, Ho, Er, Y, M = Mn, Fe, Co, Ni [61 C 1]

RFe_5 [87 K 3]; R = Th [78 G 4]

RCo_5 [62 N 1, 67 S 3, 68 H 1, 68 S 1, 69 U 1, 70 S 5, 72 M 4, 73 M 9, 74 M 3, 74 H 6, 79 D 4, 82 E 1, 85 K 15, 85 Z 1, 86 R 2, 87 B 4, 87 U 2(T)]; R = Ce, Pr, Nd, Sm, Gd, Tb, Dy, Ho, Er, Tm, Y [61 N 1, 62 C 1, 66 L 3]; R = Ce, Sm, Gd, Dy, Ho, Y [60 N 2] (samples were oxidized during measurements); R = Ce, Pr, Sm, Y [67 S 4]; R = La, Ce, Pr, Nd, Sm, Gd, Tb, Dy, Ho, Er, Th, Y [68 B 6, 68 V 1, 69 B 7]; R = La, Ce, Pr, Sm, Y [70 S 6]; R = Ce, Pr, Sm, Y [71 B 2]; R = Ce, Pr, Nd, Sm, Y [71 T 1*]; R = Ce, Sm, Y [73 I 1]; R = Gd, Tb, Dy, Ho, Er, Y [73 O 7]; R = Nd, Sm, Y [73 S 3]; R = Pr, Nd, Sm, Gd, Y [74 K 3*]; R = Ce, Nd, Sm, CeMM, Y [74 K 15]; R = Pr, Nd, Tb, Dy, Ho [77 D 9]; R = Sm, Gd, Y [77 M 4(T)]; R = Pr, Tb, Dy, Ho [83 A 6*]; R = Tb, Dy, Ho [83 K 2]; R = Ce [67 L 4, 74 D 12, 76 A 4, 83 G 4]; R = Pr [71 K 3, 79 R 4(T), 80 A 7, 85 K 16, 88 X 1(T)]; R = Nd [66 B 2, 74 F 2*, 76 D 8, 76 O 8, 82 A 5, 82 A 13, 86 P 2]; R = Sm [69 B 8, 70 M 1, 72 M 2, 73 D 6, 74 D 6*, 74 G 2, 75 K 5, 75 P 1, 75 S 6, 76 A 4, 76 L 4, 76 M 4, 77 B 2, 77 C 7, 78 K 6, 82 A 4(T), 84 A 11, 84 B 6]; R = Gd [69 B 6, 83 G 3]; R = Tb [67 L 4, 75 E 2, 75 R 2, 85 E 1]; R = Dy [75 E 2, 75 E 3, 75 S 1, 77 O 9, 80 B 5, 80 B 6, 83 T 5]; R = Ho [82 D 3]; R = Y [67 H 2*, 74 F 1*, 75 K 5, 80 A 3, 81 A 1, 81 L 5, 82 A 5, 83 G 3, 84 A 11, 85 K 16, 85 S 25(T), 87 T 2(T)]; R = MM [75 N 1]; R = Th [77 G 7, 79 G 6, 81 G 6, 83 G 4, 84 A 11]

RNi_5 [63 B 1, 80 N 1*, 82 E 1]; R = Ce, Pr, Nd, Gd, Ho, Tm [71 W 1]; R = Tb, Ho, Er [84 G 2]; R = Pr, Nd, Sm, Gd, Tm [87 B 7]; R = Tb, Ho, Er [84 G 2]; R = La [80 S 17, 81 P 1, 82 M 1(T), 85 G 15, 87 G 11(T)]; R = Ce [82 G 3, 82 G 5, 85 G 6]; R = Pr [72 C 8, 75 A 1, 79 A 4, 79 R 5, 80 M 11, 81 F 5, 81 K 17, 83 B 6, 87 R 1, 86 F 1, 87 L 4, 87 L 5, 88 B 3]; R = Nd [84 A 11, 85 G 15]; R = Sm [87 B 2*, 87 E 3, 88 B 1*]; R = Gd [71 B 14, 78 R 3, 82 M 1(T), 83 G 3]; R = Tb [79 G 3*, 83 G 5, 84 G 3]; R = Dy [80 A 8*, 81 A 4*]; R = Ho [79 G 3*]; R = Er [77 E 8*, 83 G 5, 84 G 3]; R = Tm [82 G 2, 84 A 11]; R = Y [80 G 4, 81 G 6, 82 G 3, 82 G 5, 83 G 3, 85 G 6]

RCo_5H_x [72 K 2, 73 K 15, 74 B 17, 74 K 18]; R = La [72 K 4, 82 Y 2]; R = Ce [72 K 4]; R = Pr [71 K 3, 82 Y 2]; R = Nd [82 Y 2, 82 Y 3]; R = Sm [69 Z 2]; R = Gd [83 Y 4]; R = Y [83 Y 4]

RNi_5H_x [74 K 18]; R = La [78 B 17, 79 S 3, 80 P 1, 80 S 5, 80 S 7, 80 S 17, 81 S 9, 81 P 1, 87 G 11(T), 87 R 10(T)]

$(R'R'')Co_5$ $(LaSm)Co_5$ [69 B 7, 71 M 1, 76 L 5, 79 E 3]; $(LaHo)Co_5$ [69 B 7]; $(CeSm)Co_5$ [71 M 1, 79 E 3]; $(CeZr)Co_5$ [84 G 9]; $(CeHf)Co_5$ [84 G 9]; $(PrSm)Co_5$ [71 M 1, 71 S 3, 72 D 3, 73 D 4, 73 M 3, 75 B 5, 75 S 6, 77 E 5, 78 H 3, 83 E 2]; $(PrDy)Co_5$ [71 W 2]; $(PrTm)Co_5$ [74 N 2]; $(PrY)Co_5$ [82 A 8*, 83 E 2, 88 P 1]; $(PrTi)Co_5$, $(PrZr)Co_5$, $(PrHf)Co_5$ [84 G 10]; $(NdSm)Co_5$ [74 S 4, 75 F 3, 78 E 1, 79 E 3, 79 Z 1, 80 E 5, 82 E 2]; $(NdGd)Co_5$ [62 N 1, 71 W 2]; $(NdDy)Co_5$ [71 W 2, 77 O 8]; $(NdTm)Co_5$ [74 N 2]; $(NdY)Co_5$ [71 T 1, 74 N 2, 77 H 2, 79 E 1, 80 E 1, 80 E 4, 82 E 1, 82 E 3]; $(NdU)Co_5$ [78 D 1]; $(SmMM)Co_5$ [71 M 1, 73 D 4]; $(SmGd)Co_5$ [74 B 6, 75 D 7, 76 J 1, 78 M 6, 79 G 14, 79 M 5]; $(SmTb)Co_5$ [75 D 7, 78 M 6]; $(SmDy)Co_5$ [75 D 7, 78 N 3, 78 M 6, 79 G 14, 79 M 5, 83 E 3]; $(SmHo)Co_5$ [78 N 3, 79 M 5]; $(SmEr)Co_5$ [75 D 7, 78 M 6, 79 G 14, 79 M 5]; $(SmTm)Co_5$ [79 G 14]; $(SmY)Co_5$ [71 S 3, 79 E 3, 82 A 8*]; $(SmZr)Co_5$ [76 O 1]; $(SmGdR)Co_5$, R = Tb, Dy, Ho, Tm [83 P 15]; $(SmGdNd)Co_5$ [79 M 4]; $(SmGdDy)Co_5$ [79 G 14, 79 M 5]; $(SmGdHo)Co_5$ [79 G 14]; $(SmErHoDyGd)Co_5$ [78 N 3]; $(GdDy)Co_5$ [71 W 2]; $(GdHo)Co_5$ [71 W 2]; $(GdY)Co_5$ [79 E 1, 80 E 1]; $(GdTh)Co_5$ [73 W 1]; $(TbY)Co_5$ [79 E 1, 79 E 2, 80 E 1]; $(DyY)Co_5$ [83 D 5, 83 E 3]; $(HoY)Co_5$ [82 E 4]; $(HoTh)Co_5$ [73 W 1]; $(HoEr)(CoNi)_5$ [87 D 9]; $(ErY)Co_5$ [83 E 3]; $(ErTh)Co_5$ [73 W 1]; $(YU)Co_3$ [78 D 1]; $(YTh)Co_5$ [74 G 1, 79 W 3]; $(YTh)(FeCo)_5$ [74 G 1, 79 W 3]; $(SmZr)Fe_5$ [88 L 3]

$(R'R'')Ni_5$ $(NdSm)Ni_5$ [84 E 2, 85 K 14]; $(NdGd)Ni_5$ [69 W 1]; $(NdHo)Ni_5$ [69 W 1]; $(GdDy)Ni_5$ [69 W 1]; $(GdHo)Ni_5$ [69 W 1]; $(GdY)Ni_5$ [76 G 3*]; $(DyEr)Ni_5$ [84 E 2, 85 K 14]

$R(M'M'')_5$ $R(CoM)_5$, R = Gd, Tb, Y [76 O 1]; $Pr(CoM)_5$ [84 C 3]; $Pr(CoM)_5$, M = Mn, Fe, Ni, Cr, V, Ti [83 Z 4]

$Ho(MnCo)_5$ [80 D 8, 82 D 7]; $Th(CoMn)_5$ [77 M 10]; $R(MnNi)_5$ [83 P 3]; $La(MnNi)_5$ [82 L 3]; $Th(MnNi)_5$ [77 M 10]; $La(MnCu)_5$ [88 K 3]

$Sm(FeCo)_5$ [76 E 6]; $Ho(FeCo)_5$ [80 D 8, 82 D 7]; $Y(FeCo)_5$ [74 G 2]; $Th(FeCo)_5$ [72 V 1]; $R(FeNi)_5$ [73 H 4]; $R(FeNi)_5$, R = La, Ce, Y [84 P 15]; $La(FeNi)_5$ [82 L 1, 83 O 1, 84 L 1, 87 E 6, 88 E 1]; $Th(FeNi)_5$ [72 V 1, 75 E 1]

$R(CoNi)_5$, R = Ce, La, Gd, Sm, Y, Th [78 E 2]; $La(CoNi)_5$ [73 V 3, 75 B 6, 75 B 8, 75 B 15, 77 E 4, 77 E 7*]; $Ce(CoNi)_5$ [77 E 4, 77 E 7*]; $Pr(CoNi)_5$ [85 A 10]; $Sm(CoNi)_5$ [70 O 1, 75 E 4, 76 E 6, 76 O 3, 77 E 7*, 77 O 6, 78 O 3, 87 M 5]; $Gd(CoNi)_5$ [70 O 1, 77 E 3, 77 E 4, 77 E 7*, 80 O 3, 81 C 1]; $Tb(CoNi)_5$ [82 P 9]; $Ho(CoNi)_5$ [79 D 9, 80 D 8, 81 D 10, 83 C 4]; $Er(CoNi)_5$ [78 O 1, 85 D 12, 85 D 13]; $Y(CoNi)_5$ [75 T 1, 76 B 19, 76 B 20, 77 E 4, 77 E 7*, 79 E 4]; $Th(CoNi)_5$

[74 N 5, 75 B 8, 75 B 13, 75 B 15, 75 N 3]; $La(CoCu)_5$ [75 B 7]; $Ce(CoCu)_5$ [85 G 12, 86 L 2]; $Pr(CoCu)_5$ [70 S 1, 73 M 1, 78 M 2, 79 M 2]; $Sm(CoCu)_5$ [73 J 1, 73 K 1, 73 K 3, 74 M 3, 76 B 19, 76 E 6, 78 K 9, 86 M 2]; $Gd(CoCu)_5$ [70 S 4]; $Tb(CoCu)_5$ [62 N 1]; $Dy(CoCu)_5$ [62 N 1]; $Ho(CoCu)_5$ [79 D 9, 80 D 8, 81 D 10, 86 C 5]; $Er(CoCu)_5$ [83 D 7]; $Y(CoCu)_5$ [83 Y 5]; $Pr(CoAl)_5$ [73 O 5, 74 O 3]; $Sm(CoAl)_5$ [73 O 5, 75 O 2]; $Gd(CoAl)_5$ [70 S 4]; $R(CoZr)_5$ [78 Y 3]; $R(CoTi)_5$ [78 Y 3]; RCo_3B_2, R = Gd, Dy [85 M 1]

$La(NiM)_5$, M = Al, Ga, In, Sn [80 M 3]; $Ce(NiCu)_5$ [77 B 24, 82 G 5, 82 P 10, 84 B 7, 84 P 9, 85 G 16, 86 G 3]; $Sm(NiCu)_5$ [78 O 2]; $Yb(NiCu)_5$ [77 B 24]; $U(NiCu)_5$ [77 B 24, 82 R 3]; RNi_4Au [77 F 1]; $MM(NiAl)_5$ [86 R 4]

$R(M'M'')H_x$ $La(NiMn)_5H_x$ [82 L 3]; $Ce(NiM)_5H_x$, M = Mn, Fe [86 P 6]; $La(NiFe)_5H_x$ [83 O 1, 84 D 1, 87 L 1]; $Ce(NiCu)_5H_x$ [84 P 9]; $Ce(NiAl)_5H_x$ [84 P 10]; $MM(NiAl)_5H_x$ [86 R 4]

For mixed-valence compounds see
$Ce(CoCu)_5$ [81 S 6]; $Ce(NiCu)_5$ [81 S 6]; $Eu(NiCu)_5$ [78 R 5]

For nuclear demagnetizing see also
$PrNi_5$ [77 A 5, 78 A 5, 78 B 8, 81 F 5, 83 K 4, 86 S 19]

Neutron diffraction

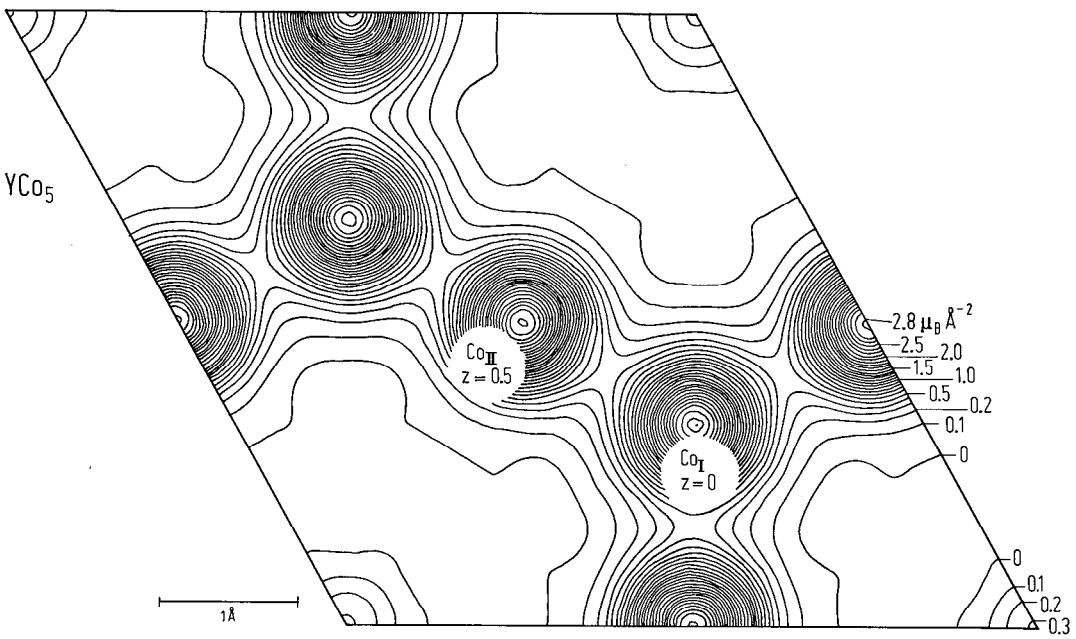

Fig. 389. Magnetization density projected along the *c* axis in YCo_5 compound. The magnetic densities on sites $Co_I(2c)$ and $Co_{II}(3g)$ slightly overlap while their centers are well separated. The distribution around the two sites is roughly the same. A weak magnetization can be seen at the origin of the unit cell, as expected from the projection of the substitution $Co_{IV}(6l)$ sites on the Y location. Around this site, the magnetization becomes negative [80 S 8].

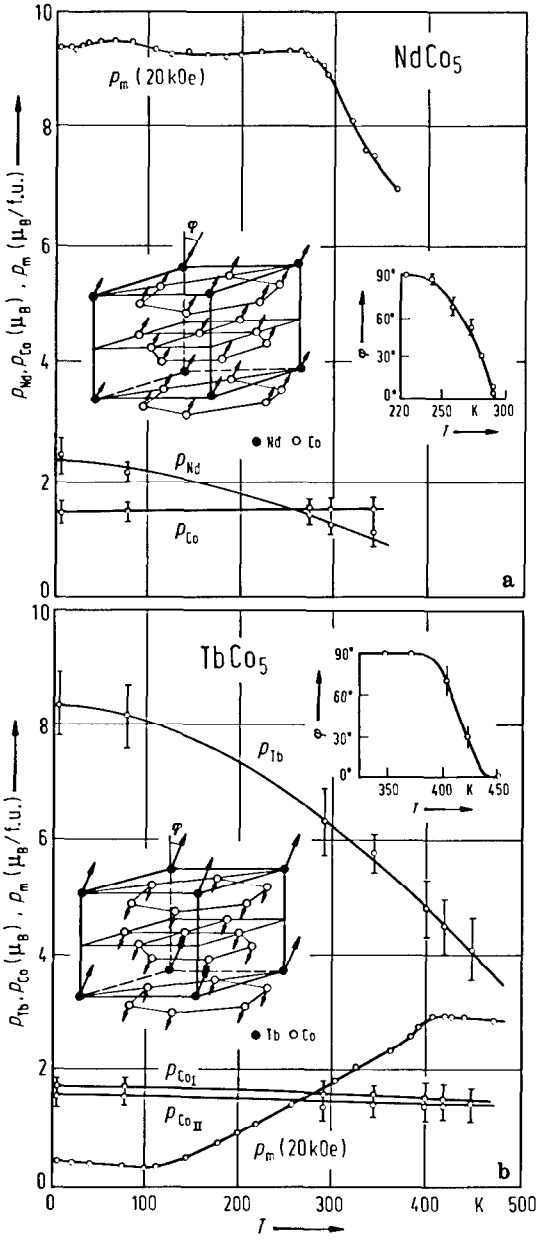

Fig. 391. Magnetic structures at low temperature, values of the atomic magnetic moments as function of temperature and temperature dependence of the angle φ between the direction of magnetic moment and c axis are given for (a) $NdCo_5$ and (b) $TbCo_5$ compounds. The thermal variation of the bulk magnetization in a magnetic field of 20 kOe is also plotted. In both compounds a spin reorientation from basal plane to c axis is evidenced as temperature increases [66 L 3].

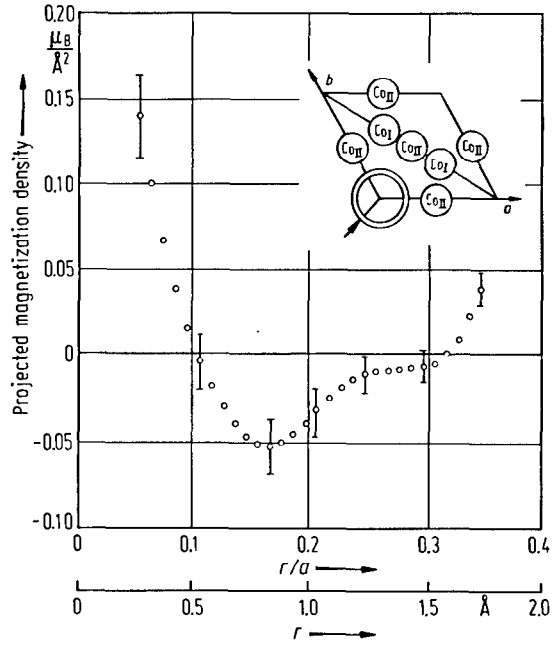

Fig. 390. Magnetization density projected along the c axis of YCo_5 vs. distance r in the ab-plane from the unit cell origin. It is positive for small distance, as result of the existence of substitution atoms $Co_{IV}(6l)$, decreases, becomes negative, presents a minimum at $r = 0.8$ Å, increases slightly, and, for $r > 1.5$ Å, increases rapidly as a part of the $Co_{II}(3g)$ magnetization density is included in the average [80 S 8].

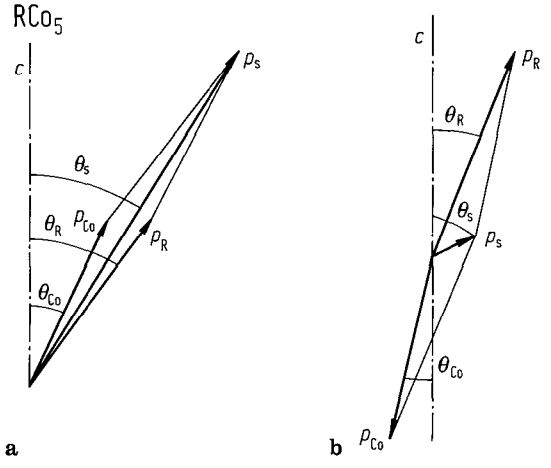

Fig. 392. Noncollinearity of the magnetic structure during reorientation process for (a) ferromagnetic RCo_5 compounds with light R and (b) ferrimagnetic RCo_5 with heavy R. In the ferromagnetic compounds the direction of M_s is so close to those of M_{co} and M_R that evidence for noncollinearity of the magnetic structure is very difficult to obtain experimentally. A more favourable situation is obtained in the ferrimagnetic compounds as seen in (b) [83 D 2].

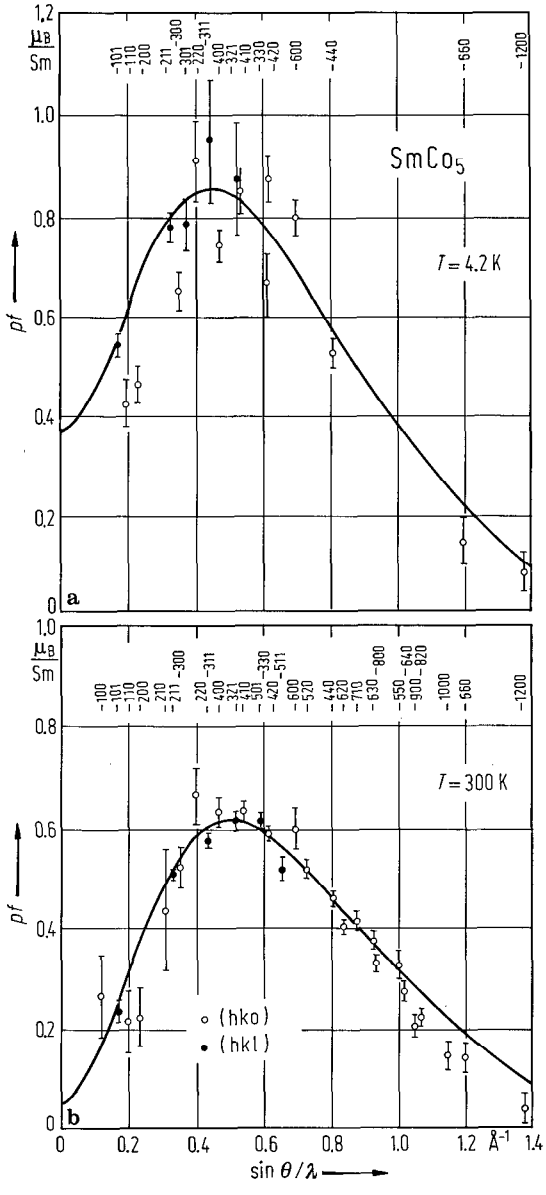

Fig. 393. Experimental values of the Sm magnetic neutron scattering amplitude for (hko) and (hkl), reflections and calculated form factor for the (hko) reflections at (a) 4.2 K and (b) 300 K, for $\mu_B H_{exch}/k_B = 175(25)$ K; $A_2^0\langle r^2\rangle = -200(50)$ K, $A_4^0\langle r^4\rangle = 0(50)$ K; $A_6^0\langle r^6\rangle = -50(50)$ K in $SmCo_5$. In (c) the level scheme of Sm^{3+} ion in the exchange and crystal field is plotted. The Sm form factor is very different at 4.2 and 300 K, giving direct evidence for the exchange and crystal field mixing of excited multiplets into the ground state multiplet. The Sm magnetic moment is smaller at 300 than at 4.2 K and its orbital character is less pronounced. The cross-over is calculated to occur at 350 K above which temperature the spin contribution exceeds the orbital one. The $SmCo_5$ compound is ferromagnetic below the cross-over and ferrimagnetic above [79 B 8, 79 G 7].

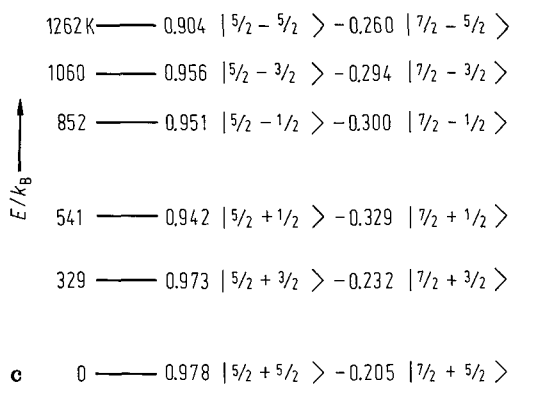

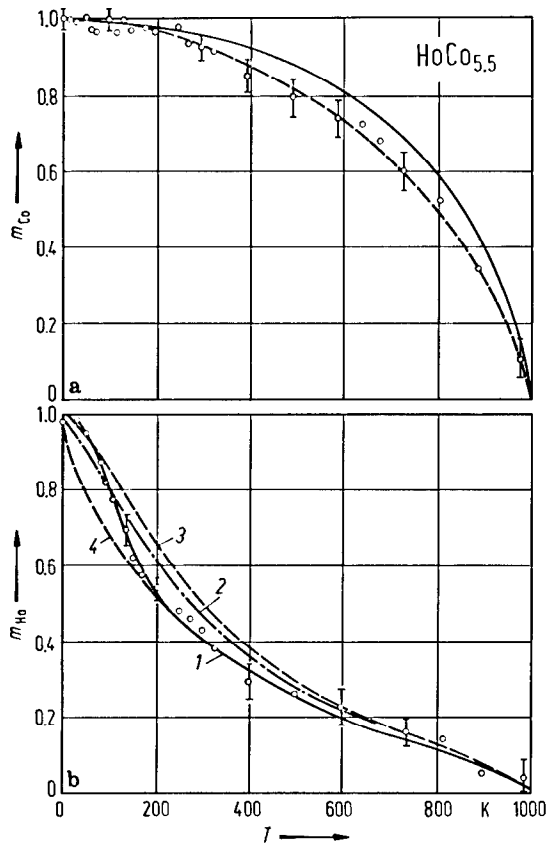

Fig. 394. Temperature dependence of (a) the reduced Co sublattice magnetization m_{Co} and (b) the reduced Ho sublattice magnetization m_{Ho} in $HoCo_{5.5}$ [81 C 3]. The solid line in (a) is the calculated curve according to [73 O 7], the dashed line after [81 C 3]. The lines in (b) are curves calculated according to the relation,

$$m_{Ho} = \sum_{n=-8}^{8} n \exp D \Big/ \sum_{n=-8}^{8} \exp D,$$

with

$$D = [Jn\cos(\theta_{Ho} - \theta_{Co}) + \tfrac{1}{2}K^0_{Ho} n^2 (1 - 3\cos^2\theta_{Ho})](k_B T)^{-1},$$

and $J = J^0_{Ho-Co} m_{Co}$, where J^0_{Ho-Co} is the exchange parameter between the sublattices, K^0_{Ho} is the anisotropy constant, and θ_{Ho} and θ_{Co} are the angles between c axis and respective sublattice magnetizations. The curves are calculated for $J^0_{Ho-Co} = 60$ K, and (*1*) $K^0_{Ho} = 3$ K and θ_{Ho} and θ_{Co} changing in the temperature range 45 to 170 K from 90° to 0°, (*2*) $K^0_{Ho} = 0$ K and $\theta_{Ho} \cong \theta_{Co}$ in all the temperature range, (*3*) $K^0_{Ho} = 3$ K and $\theta_{Ho} = 90°$ in all the temperature range, (*4*) $K^0_{Ho} = 3$ K and $\theta_{Ho} = 0$ in the temperature range 4.2···1000 K. In (*3*) and (*4*) θ_{Ho} and θ_{Co} behave similarly. The experimental data agree with curve (*3*) in the temperature range 4.2···45 K, and with curve (*4*) in the temperature range 170···500 K.

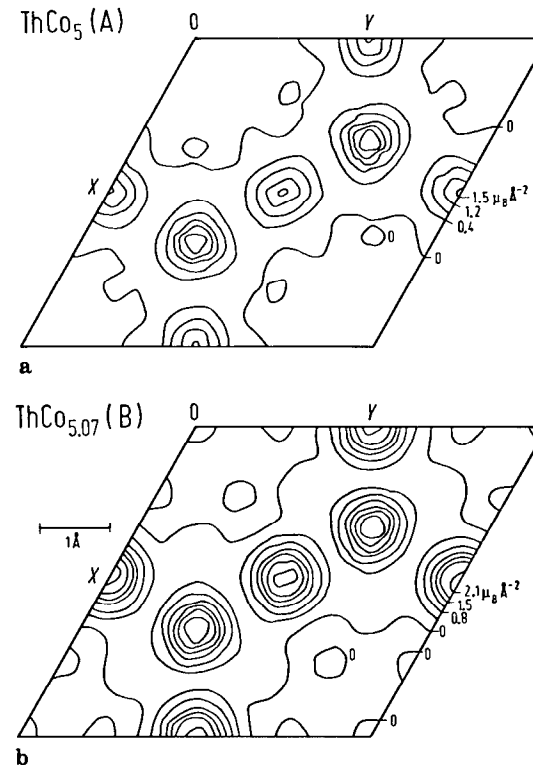

Fig. 395. Magnetization density projected onto the basal plane of $ThCo_5$(A) and $ThCo_{5.07}$(B) compounds. In crystal A, the Co magnetic moment on the 3g site, 0.90(8) μ_B, is lower than that on the 2c site, 1.20(8) μ_B. In crystal B, the magnetic moments of Co on 2c and 3g sites are equal, 1.63(8) μ_B [77 G 7].

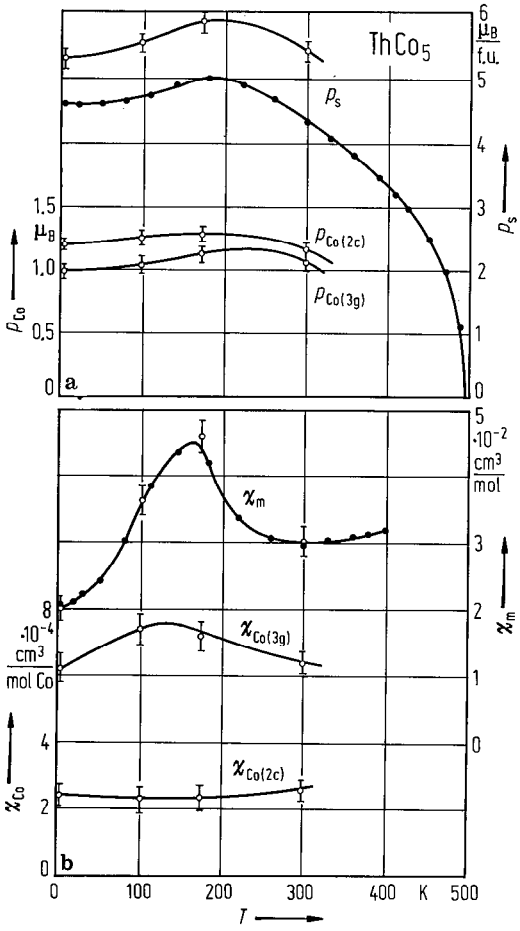

Fig. 396. (a) Thermal variations of the spontaneous magnetization of $ThCo_5$ and of Co 2c and 3g sites, $p_{Co(2c)}$, $p_{Co(3g)}$, obtained from magnetic measurements (solid circles) and polarized neutron diffraction (open circles) [79 G 6]. (b) Thermal variations of the superimposed magnetic susceptibility of $ThCo_5$ (χ_m) obtained from magnetic measurements (solid circles) and polarized neutron diffraction (open circles), the acting field being the applied magnetic field, and of the two Co sites ($\chi_{Co(2c)}$, $\chi_{Co(3g)}$), the acting field being the sum of the applied magnetic field and the molecular field resulting from the interaction between the two Co sites.

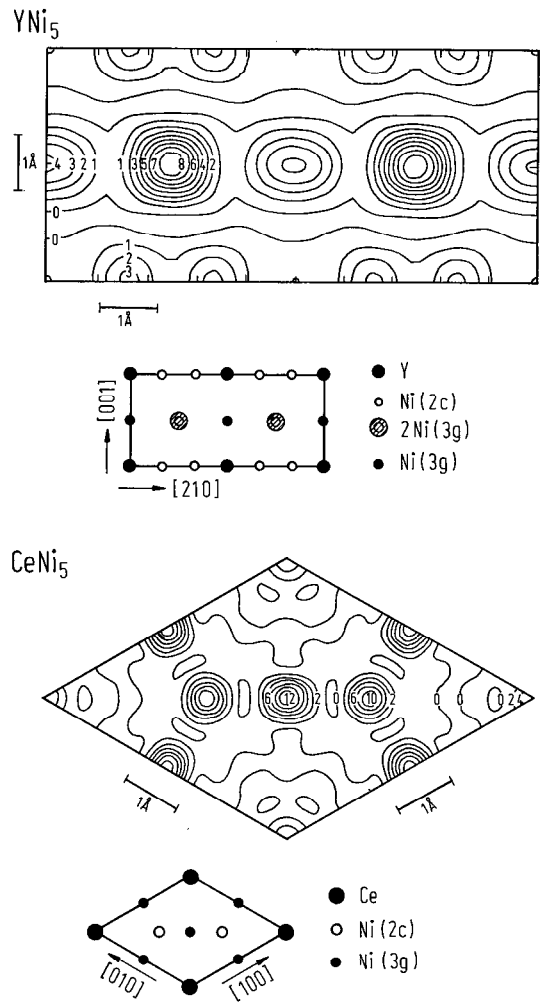

Fig. 397. Projections of the magnetic densities in YNi_5 and $CeNi_5$, averaged on a square of 0.4 Å on each side (contours are in $10^{-3}\,\mu_B/Å^2$) [82 G 3]. These evidence strong positive magnetic densities localized on Ni sites, those of the 3g sites being higher than those of the 2c sites. In YNi_5, these densities correspond to a form factor of 3d electrons at the top of the band, whereas in $CeNi_5$ they are observed much more localized. The observed localization results from the superposition of a contribution of 3d type, similar to that in YNi_5, and of a strong antiparallel polarization, more diffuse and nonuniform. No magnetic density is localized on Y and a weak one is found on Ce with 4f-type form factor.

Table 92a. Magnetic moments of Co, orbital proportion and occupation parameters in RCo_5 (R = Nd, Y) compounds [80S8, 82A5].

	T K	p_{Co} μ_B	Orbital proportion %	Occupation parameters	
YCo_5 [1])	4.2	(2c)1.77(2)	26(5)	dz^2	0.28(3)
				dxz; dyz	0.18(12)
				$d(x^2-y^2)$; dxy	0.58
		(3g)1.72(2)	16(4)	dz^2	0.15(2)
				dxz	0.24(4)
				dyz	0.19(3)
				$d(x^2-y^2)$	0.22(3)
				dxy	0.20
$NdCo_5$ [2])	260	(2c)1.95(3)	33(5)		
	($p \parallel c$)	(3g)1.90(3)	20(3)		
	260	(2c)1.84(3)	19(4)		
	($p \perp c$)	(3g)1.84(2)	12(2)		

[1]) Sum of the localized magnetic moments in one unit cell is 8.9(1) μ_B and the magnetization measured in one cell is 7.99(2) μ_B.

[2]) In $NdCo_5$ the anisotropy of Co atoms has sign opposite to that of Nd atoms. Above room temperature, the easy magnetization direction is determined by Co atoms to be along c. At low temperatures the anisotropy of Nd atoms is preponderant, the spontaneous magnetization is in the basal plane, parallel to the a axis. A rotation in spontaneous magnetization is observed between 240 and 290 K. In this range of temperatures the bulk anisotropy is small. A polarized neutron study has been performed at 260 K, the magnetization being successively aligned along a and c in $H_{ext} = 46$ kOe. A large orbital contribution to the Co magnetic moment is observed. This is reduced when the magnetization is perpendicular to c. The anisotropy of Co both in $NdCo_5$ and YCo_5 is nearly twice as large on the 2c site (of uniaxial symmetry), where the orbital contribution is largest, than on the 3g site. Such orbital contributions on a uniaxial site are difficult to reorient, and therefore, through spin-orbit coupling, are responsible for magnetic anisotropy.

Table 92b. Magnetic moments (μ_B) of R and M atoms determined by neutron diffraction studies in some RCo_5 and RNi_5 compounds.

	T (K)	p_R	$p_{Co(2c)}$	$p_{Co(3g)}$	Ref.
$CeCo_5$	4.2	–	1.30(30) $\parallel c$	1.30(30) $\parallel c$	67 L 4
	295	–	1.20(30) $\parallel c$	1.20(30) $\parallel c$	
$CeCo_5$	4.2	–	1.14(5)	1.14(5)	66 L 3
$PrCo_5$	4.2	1.58(8)	1.30(5)	1.30(5)	71 K 3
	RT	1.15(7)	1.50(5)	1.50(5)	
$NdCo_5$ [1])	4.2	2.45(30)	1.45(20)	1.45(20)	66 B 2, 66 L 3
	78	2.15(10)	1.50(20)	1.50(20)	
	295	1.20(10)	1.50(20)	1.50(20)	
$SmCo_5$	4.2	0.38	1.86	1.75	79 G 7
	300	0.04	1.86	1.75	
$TbCo_5$	4.2	8.35(55) $\parallel a$	1.55(20) $\parallel a$	1.70(10) $\parallel a$	67 L 4, 66 L 3
	78	8.15(55) $\parallel a$	1.55(25) $\parallel a$	1.67(25) $\parallel a$	
	295	6.30(55) $\parallel a$	1.35(25) $\parallel a$	1.55(25) $\parallel a$	
$TbCo_5$	4.2	8.50(40)	1.60(15)	1.72(15)	82 P 9
$TbCo_{5.1}$	4.2	8.35	1.55	1.67	75 E 2
$HoCo_{5.5}$ [2])	4.2	9.3(3) $\perp c$	1.68(10) $\perp c$	1.71(10) $\perp c$	81 C 3
	293	3.8(5) $\parallel c$	1.62(10) $\parallel c$	1.62(10) $\parallel c$	
$HoCo_{5.6}$	4.2	$\cong 10$	1.85	1.85	82 D 3
$HoCo_{5.5}$	4.2		1.57	1.72	83 C 3
$ErCo_{5.6}$	4.2	8.6 $\parallel c$	1.50 $\parallel c$	1.50 $\parallel c$	78 Y 2
$TmCo_5$	4.2	6.8 $\parallel c$	1.50 $\parallel c$	1.50 $\parallel c$	78 Y 2
YCo_5 [2])	4.2	–	1.66(4)	1.66(4)	69 K 5
YCo_5 [1])	4.2	–	1.77(2)	1.72(2)	80 S 8
$TbNi_5$	4.2	7.3(3)	$p_{Ni} = 0.0(2)$		82 P 9
$TbNi_5$	1.5	7.14(40) $\parallel a$	$p_{Ni} \cong 0$		70 L 3
$ErNi_5$	4.2	7.7 $\parallel c$	$p_{Ni} \cong 0$		64 C 2
$HoNi_5$	0	7.4(5)	$p_{Ni} \cong 0$		83 C 3

[1]) See also Table 92a.
[2]) See also [62 J 1].

Table 92c. Magnetic moments induced by a magnetic field of 48 kOe in RNi_5 (R = Y or Ce) compounds [82 G 3].

	$p_{Ni(2c)}$	$p_{Ni(3g)}$	p_R	p_m (10^{-3} μ_B/f.u.)		
	10^{-3} μ_B			localized	diffuse	bulk
YNi_5	2.4(4)	4.1(6)	–	17.1(12)	2.2(21)	19.3(9)
$CeNi_5$	7.0(7)	8.2(8)	2.4(6)	41.0(18)	−11.8(27)	29.2(9)

Table 93. Magnetic moments along the *c* axis at R and Co sites in $PrCo_5$ deuterides determined by neutron diffraction studies [71 K 3].

	T K	p_R μ_B	$p_{Co}(\mu_B)$		
			Co_I	Co_{II}	Co_{III}
$PrCo_5D_{3.7}$ [1])	4.2	1.64(13)	0.12(8)	0.79(6)	0.79(6)
	77	0.50(4)	0.98(6)	1.28(5)	1.28(5)
$PrCo_5D_{3.9}$	292	–	0.83(4)	0.83(4)	0.83(4)

[1]) The crystal structure was a Cmmm-type in which the Co atoms are located in: Co_I(0.366; 0; 0); Co_{II}(0; 0.5; 0.5) and Co_{III}(0.25; 0.25; 0.25).

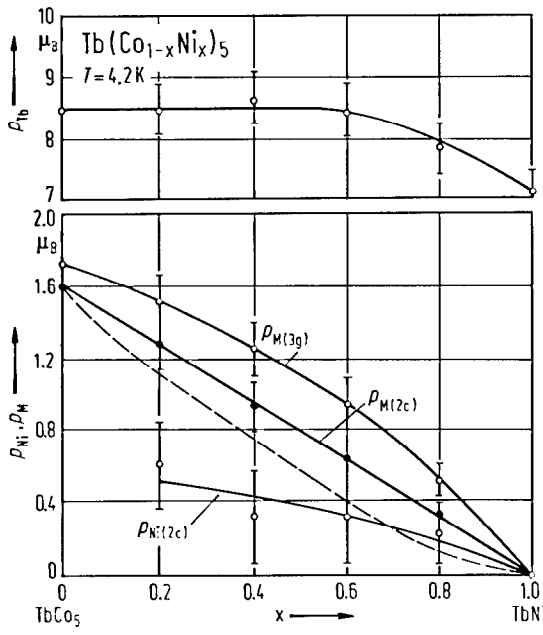

Fig. 398. Composition dependence of the Tb magnetic moment, p_{Tb}, and transition metal moments on sites 2c and 3g, $p_{M(2c)}$ and $p_{M(3g)}$, respectively, at 4.2 K in $Tb(Co_{1-x}Ni_x)_5$ compounds [82 P 9]. Assuming $p_{Co(2c)} = 1.60\,\mu_B$ and $p_{Co(3g)} = 1.72\,\mu_B$ at all x a good fit to the $p_{M(2c)}$ and $p_{M(3g)}$ data is obtained for $p_{Ni(3g)} = 0$ for all x and $p_{Ni(2c)}$ as shown in the figure. The dashed line provides $p_{M(2c)}$ calculated supposing $p_{Co(2c)} = 1.60\,\mu_B$ and $p_{Ni(2c)} = 0$ for all x.

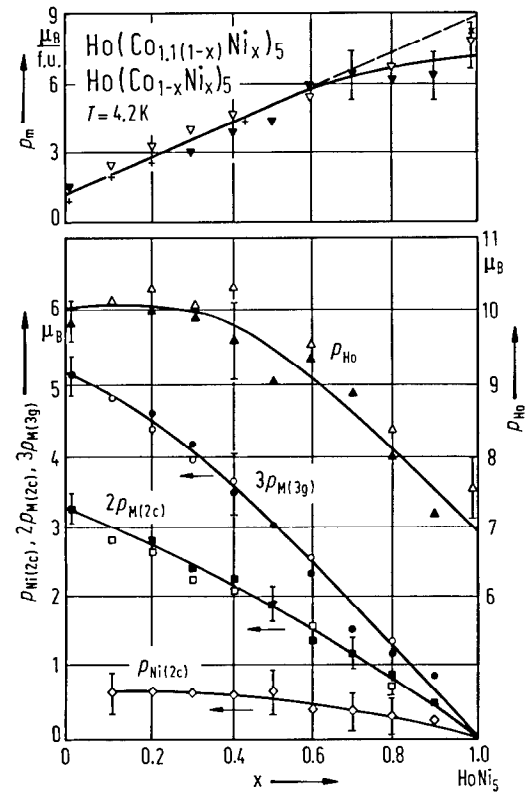

Fig. 399. Composition dependence of the resultant magnetization, p_m, Ho sublattice magnetization, p_{Ho}, transition metal magnetic moments in 2c and 3g sites, $p_{M(2c)}$, $p_{M(3g)}$, and Ni magnetic moment in 2c sites, $p_{Ni(2c)}$, at 4.2 K for (open symbols and crosses) $Ho(Co_{1-x}Ni_x)_5$ and (solid symbols) $Ho(Co_{1.1(1-x)}Ni_x)_5$ compounds [83 C 3]. (+) Data obtained from magnetization measurements [80 D 8]; (×) magnetization of $HoNi_5$ single crystal [79 G 3].

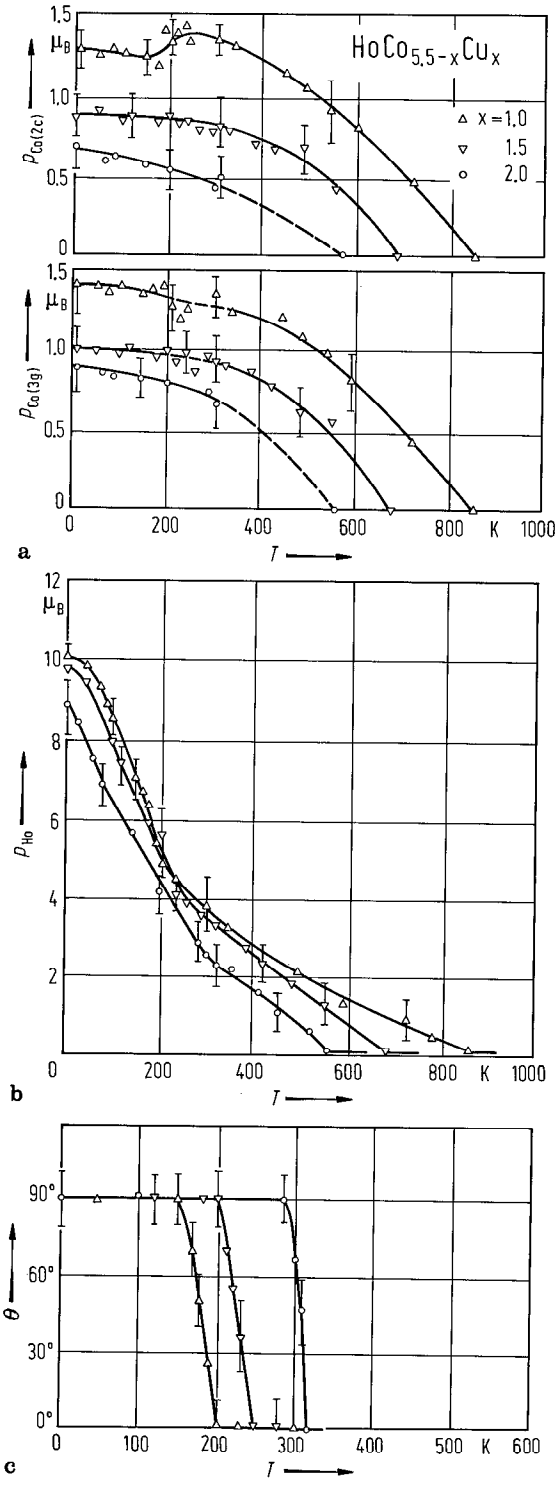

Fig. 400. Temperature dependence of (a) Co magnetic moments in 2c and 3g sites, (b) Ho magnetic moment, and (c) angle θ between the c axis and the direction of magnetization in $HoCo_{5.5-x}Cu_x$ compounds [86 C 5].

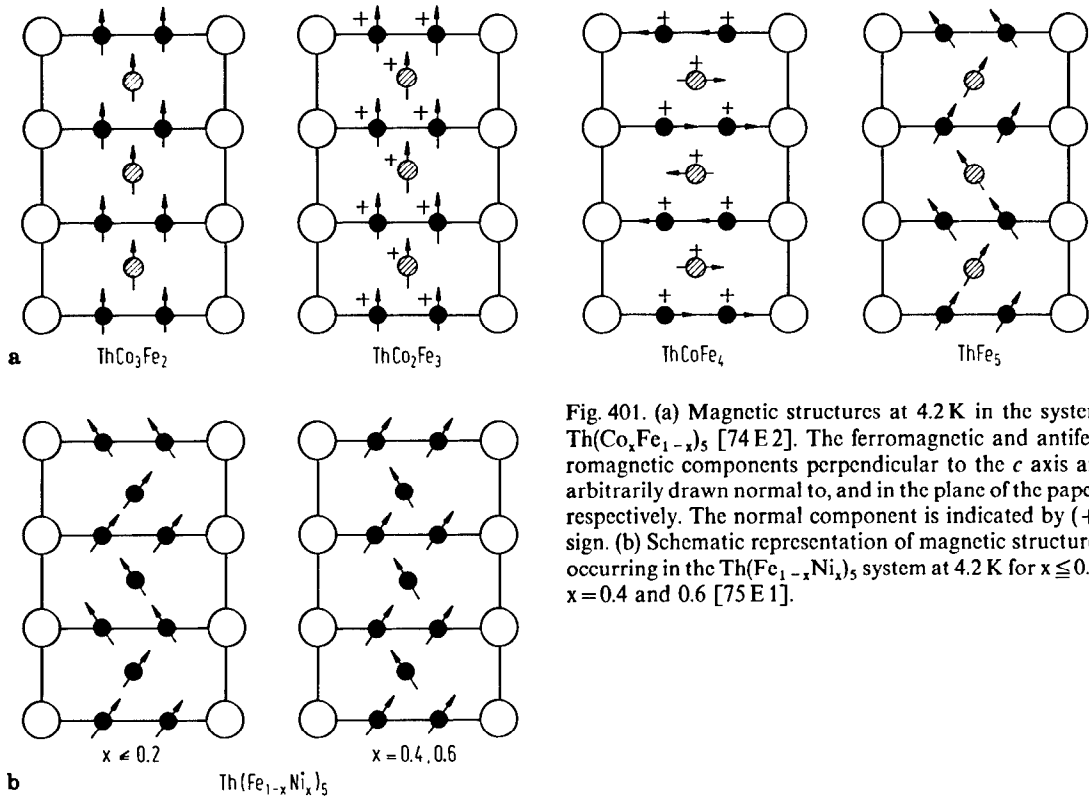

Fig. 401. (a) Magnetic structures at 4.2 K in the system $Th(Co_xFe_{1-x})_5$ [74 E 2]. The ferromagnetic and antiferromagnetic components perpendicular to the c axis are arbitrarily drawn normal to, and in the plane of the paper, respectively. The normal component is indicated by (+) sign. (b) Schematic representation of magnetic structures occurring in the $Th(Fe_{1-x}Ni_x)_5$ system at 4.2 K for $x \leqq 0.2$, $x = 0.4$ and 0.6 [75 E 1].

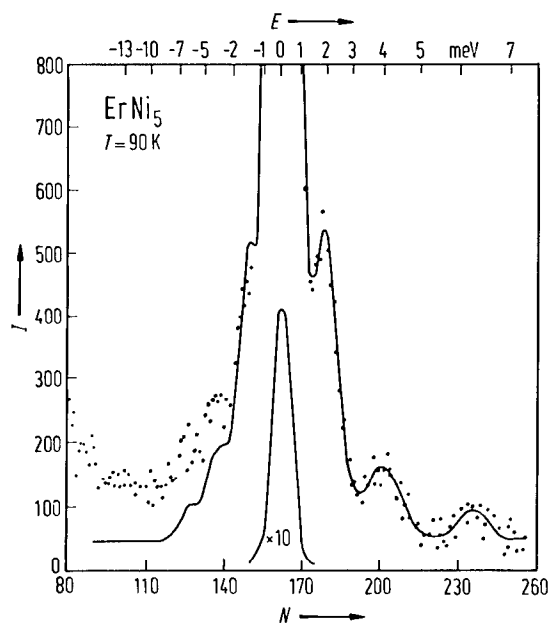

Fig. 402. Inelastic neutron scattering of $ErNi_5$ at temperature of 90 K obtained by the time-of-flight spectrometer in direct geometry with an input energy of 14.34 meV and a scattering angle of 55°. I is the number of events per channel, N is the channel number, and E is the energy loss by neutrons. Channel width is 8 μs and flight length of monochromatic neutrons is ≅ 3.5 m. The full line describes the calculated CEF spectrum [84 G 3].

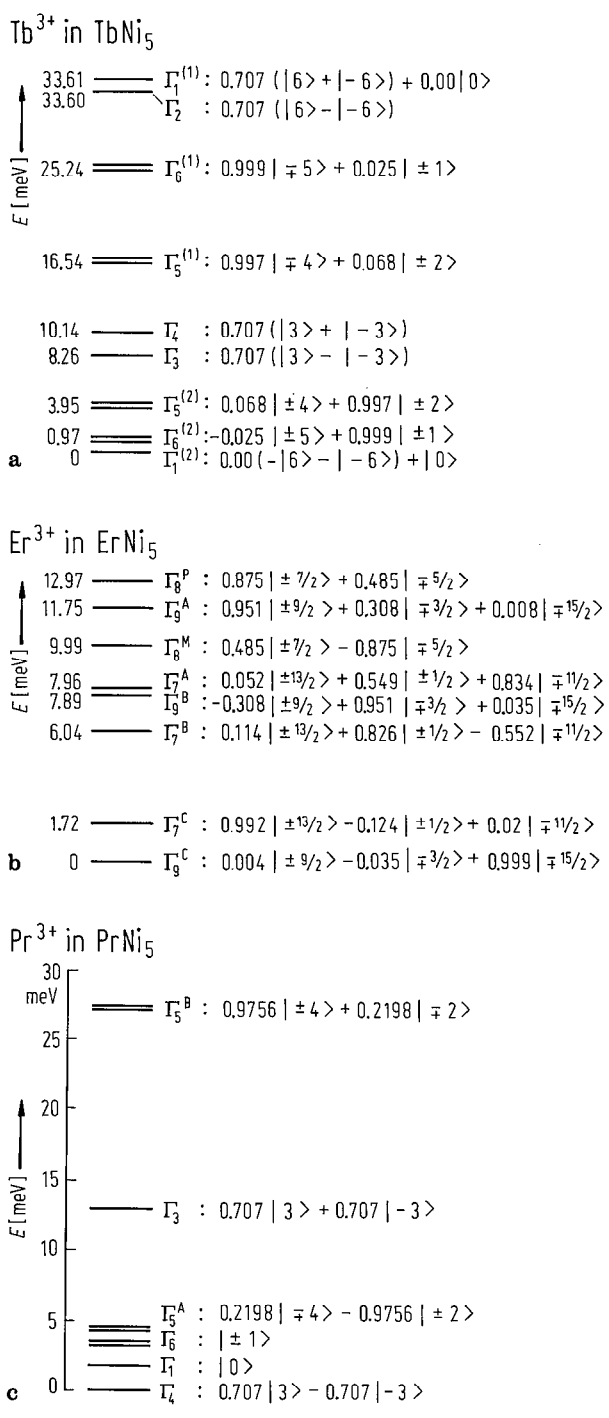

Fig. 403. Crystal electric field level scheme for (a) Tb^{3+} in $TbNi_5$ and (b) Er^{3+} in $ErNi_5$, as derived from inelastic neutron scattering experiments [84 G 3]. (c) Splitting energy level scheme of the ground-state multiplet $^3H_4$ of Pr^{3+} ion in $PrNi_5$ as determined by inelastic slow-neutron scattering [80 A 4].

Table 94. Crystal field parameters in RNi_5 compounds deduced from magnetic measurements on single crystals (MM) and neutron spectroscopy (NS).

	B_2^0	B_4^0	B_6^0	B_6^6	Type of analysis	Ref.
	K	10^{-2} K		10^{-4} K		
$PrNi_5$	5.82	4.49	8.77	310	NS	79 A 4
	5.57(46)	4.20(58)	9.40(35)	302(23)	NS	80 A 4
	5.68	4.43	6.51	360	MM	80 N 1
	5.84(20)	4.53(50)	8.86(80)	314	MM	88 B 3
$NdNi_5$	2.55	0.63	−3.80	−139	NS	85 G 15
	3.35	1.45	−3.50	−135	MM	80 N 1
$SmNi_5$	−18.9	−100	0	0	MM	88 B 1
$TbNi_5$	3.65	− 0.18	−0.12	− 3.65	NS	83 G 5, 84 G 3
	3.84	− 0.24	−0.06	− 3.67	NS	86 G 1
	3.84	− 0.04	−0.40	− 4.0	MM	80 N 1
	3.20	− 0.27	−0.45	− 1.0	MM	79 G 3
$DyNi_5$	2.03	0.22	0.11	2.40	MM	80 A 8, 81 A 4
	2.30	0.22	0.10	2.7	MM	84 A 11
$HoNi_5$	1.15	0.07	−0.09	− 2.7	NS	85 G 14
	1.15	0.19	−0.02	− 3.0	MM	80 N 1
	1.15	0.26	0	− 3.8	MM	79 G 3
$ErNi_5$	− 0.64	− 0.23	0.23	1.3	NS	84 G 3, 86 G 3
	− 0.69	0.0	0.53	3.5	MM	80 N 1
	− 0.70(10)	− 0.10(20)	0.5(2)	3(1)	MM	77 E 8
	− 0.83	− 0.02	0.37	1.0	MM	79 G 3
$TmNi_5$	− 3.80	− 1.26	1.13	− 7.5	NS	84 A 11, 82 G 2
	− 3.80	− 1.26	1.83	− 7.6	MM	82 G 2

For theoretical values of crystal field parameters calculated according to point charge model see also [77 E 8, 78 A 4, 80 A 8, 79 A 4, 79 G 3, 87 B 7].

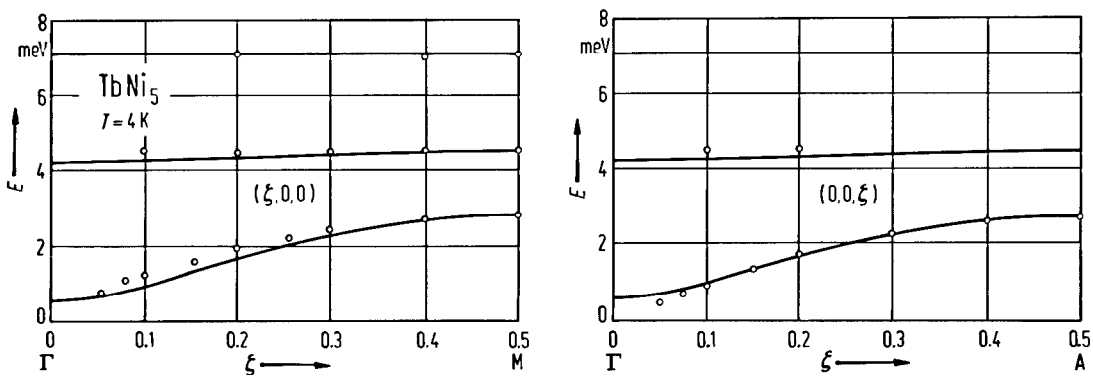

Fig. 404. Dispersion for excitations propagating along (ζ00) and (00ζ) in $TbNi_5$ at 4 K. The solid lines are results of a theoretical fit [86 G 1]. One dispersive acoustic mode and two nondispersive modes are evidenced.

For neutron diffraction studies see also

RCo_5	R = Ce [67 L 4]; R = Pr [71 K 3]; R = Nd [66 B 2, 66 L 3, 82 A 5]; R = Sm [79 B 8, 79 G 7]; R = Tb [66 L 3, 67 L 4, 75 E 2, 77 K 1, 77 K 2, 80 K 5, 81 S 16, 83 K 2]; R = Dy [75 E 2, 81 C 2, 83 K 2]; R = Ho [62 J 1, 81 C 3, 82 D 3, 83 D 2, 83 K 2]; R = Er [78 Y 2]; R = Tm [78 Y 2]; R = Y [62 J 1, 69 K 5, 74 S 3, 80 S 8, 82 A 5]; R = Th [74 E 2, 77 G 7, 79 G 6]
RNi_5	R = Ce [82 G 3]; R = Tb [70 L 3]; R = Er [64 C 2]; R = Y [81 G 5, 81 G 8, 82 G 3]
RM_5H_x	$PrCo_5D_{3.9}$ [71 K 3]
$(R'R'')M_5$	(TbY)Co_5 [82 P 8]; (YLa)$(FeCo)_5$ [74 B 2]
$R(M'M'')_5$	Th$(FeCo)_5$ [73 E 2, 74 E 2]; Th$(FeNi)_5$ [75 E 1, 76 E 1]
	La$(CoNi)_5$ [80 P 4]; Tb$(CoNi)_5$ [82 P 9, 83 K 5]; Ho$(CoNi)_5$ [83 C 3, 83 C 4, 83 K 5]; Y$(CoNi)_5$ [80 P 4]; Th$(CoNi)_5$ [73 A 4, 75 B 13, 76 E 1]; Ho$(CoCu)_5$ [86 C 5]
$R(M'M'')_5H_x$	La$(NiFe)_5H_x$ [87 L 1]

For inelastic neutron scattering see

RCo_5	R = La, Y, Th [75 H 1]
RNi_5	80 N 1*]; R = La [85 G 15]; R = Pr [78 A 4, 80 A 4, 80 A 5, 83 A 5, 86 S 19]; R = Nd [85 G 15]; R = Tb [83 G 5, 84 G 3, 86 G 1]; R = Ho [85 G 14]; R = Er [83 G 5, 84 G 3]; R = Tm [82 G 2]
RNi_5H_x	R = La [79 B 10, 83 N 8, 84 Y 9, 85 A 8, 85 L 1, 87 S 21]; R = Pr [84 A 10, 85 A 8]
$R(M'M'')_5$	Ce$(CuNi)_5$ [85 G 16, 86 G 3]
$R(M'M'')_5H_x$	La$(NiM)_5H_x$, M = Al, Cu, Mn [86 L 4]

EPR, FMR

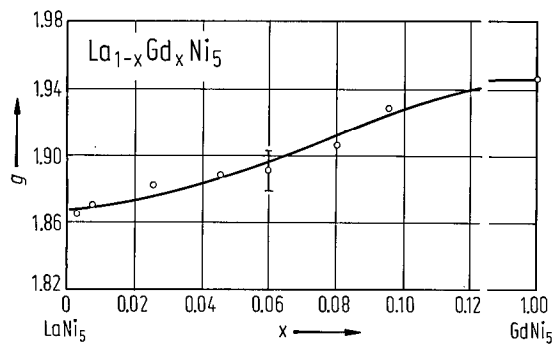

Fig. 405. Composition dependence of g values in $La_{1-x}Gd_xNi_5$ system [75 M 2]. The g value for $GdNi_5$ compound is taken from [71 B 14].

Table 95. g values and linewidth in some RNi_5 compounds. $\Delta g = g - 1.992$ [64 S 1].

	T(K)	g	Δg	ΔH(Oe)
$GdNi_5$	78	1.942(7)	−0.06	905
$GdCu_5$	65	2.009(7)	0.01	875
5% Gd in				
$LaNi_5$	20	1.877(7)	−0.12	550
YNi_5	20	1.900(7)	−0.10	525
$ThNi_5$	20	1.913(7)	−0.09	525
UNi_5	20	1.953(7)	−0.05	470

For EPR studies see
$GdNi_5$ [71 B 14, 72 U 1]
(GdLa)Ni_5 [64 S 1, 68 D 1, 75 M 2, 76 W 1, 79 L 6]; (GdPr)Ni_5 [80 L 4]; (GdLa)Ni_5H_x [76 W 1]

For FMR studies see
$LaNi_5H_x$ [81 S 8, 81 S 9]

Mössbauer effect, time-dependent perturbed angular correlation, muon spin rotation

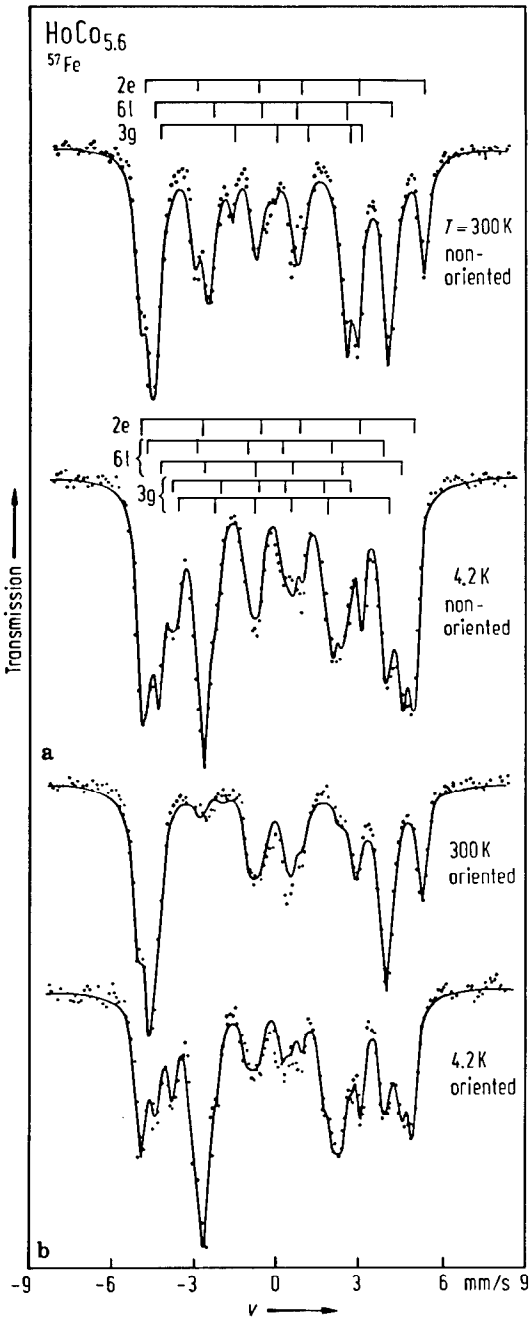

Fig. 406. ^{57}Fe Mössbauer spectra at 300 K and 4.2 K of (a) nonoriented powder and (b) oriented powder having *c* axis parallel to γ-ray for $HoCo_{5.6}$ sample having 6 at% Co replaced by Fe [82 D 3].

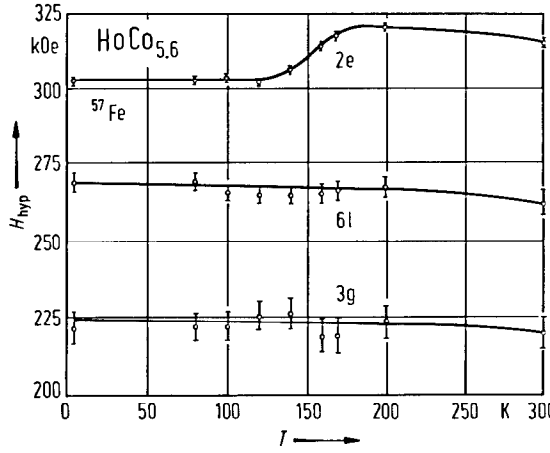

Fig. 407. Thermal variation of the average ^{57}Fe magnetic hyperfine field on 2e, 6l, and 3g sites in $HoCo_{5.6}$ doped with Fe [82 D 3].

Table 96a. Data obtained from the analysis of ^{57}Fe Mössbauer spectra of some RM_5-based compounds.

	T K	H_{hyp} (kOe)			IS [1]) (mm s^{-1})		ΔQ (mm s^{-1})		Ref.
		R(2e)	M(2c)	M(3g)	M(2c)	M(3g)	M(2c)	M(3g)	
$SmCo_{4.86}Fe_{0.33}$	80	328	245	200	−0.25	−1.13			74 P 3
	293	316	245	201	−0.29	−1.13			74 P 3
$SmCo_{4.8}Fe_{0.2}$	300	–	212	248	−0.07	−0.11	1.17	−0.22	73 B 7
$LaNi_4Fe$	4.2		216						84 L 1
$LaNi_4FeH_{5.3}$	4.2		210						87 L 1

[1]) Isomer shift relative to ^{57}Co in Cr.

Table 96b. Data obtained from the analysis of ^{57}Fe Mössbauer spectra of $HoCo_{5.6}$ [82 D 3].

	T K	H_{hyp} (kOe)					Angle between the moment and c axis
		R(2e)	M(6l)		M(3g)		
			intensity ratio		intensity ratio		
			2	4	1	2	
$HoCo_{5.6}$ ^{57}Fe doped	4.2	303(1)	266(3)	270(3)	204(10)	230(10)	80°

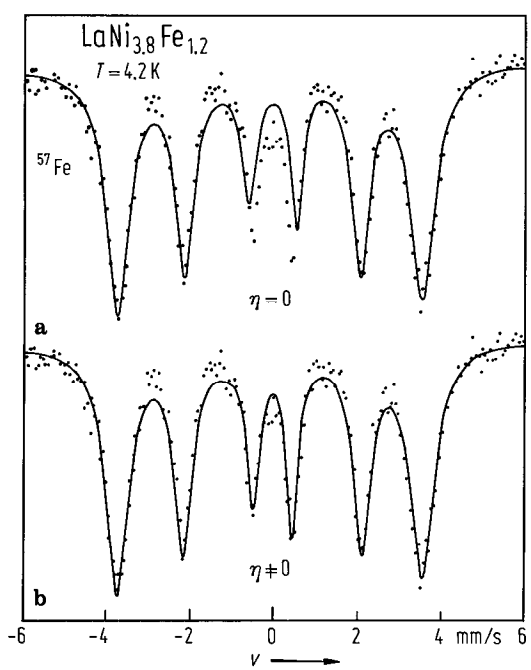

Fig. 408. Mössbauer spectra for ^{57}Fe in $LaNi_{3.8}Fe_{1.2}$ at $T=4.2$ K: (a) $\eta=0$ and (b) $\eta\neq0$ [84 L 1]. These favour a nonzero asymmetry parameter η. The data suggest that the majority (95%) of Fe atoms occupy 3g sites. Other studies [81 A 3, 81 N 2] evidence the presence of one doublet corresponding to a 3g site. After [83 C 1] evidence for the presence of Fe atoms both in 2c and 3g sites in $LaNi_{5-x}Fe_x$ ($x=0.035\cdots0.5$) system has been obtained. It seems that the site occupancy is influenced strongly by the metallurgical state.

Table 97. Data obtained by Mössbauer effect studies at ^{155}Gd and ^{151}Eu sites in RM_5-based compounds.

	IS [1] mm s^{-1}	e^2qQ/h MHz	H_{hyp} kOe	T K	Ref.
^{155}Gd					77 B 7
$Gd_{0.1}La_{0.9}Ni_5$	0.19(1)	328(3)	–	4.1	
$Gd_{0.1}La_{0.9}Ni_5H_{6.7}$	0.48(1)	159(3)	–	4.1	
$Gd_{0.1}La_{0.9}Co_5$	0.17(1)	300(2)	99(5) ($\theta=0°$)	4.1	
$Gd_{0.1}La_{0.9}Co_5H_{3.2}$	0.27(1)	100(3)	366(4) ($\theta=0°$)	4.1	
$Gd_{0.1}La_{0.9}Co_5H_{4.2}$	0.44(1)	97(5)	65(12) ($\theta=90°$) 40(20) ($\theta=0°$)	4.1	
^{151}Eu					78 O 6
$EuNi_5$	2.29(4)	–	0	2.6	
$EuNi_5H_x$	1.05(4)	170(20)	201(3)	2.6	

[1]) Relative to $SmPd_3$ source for ^{155}Gd and relative to EuF_3 for ^{151}Eu.

Table 98. ^{57}Fe hyperfine parameters at 4.2 K, angle θ between H_{hyp} and the principal axis of EFG, and the asymmetry parameter η of EFG in $LaNi_{5-x}Fe_x$ compounds [84 L 1]. See also [81 A 3, 83 C 1].

x	IS [1] mm s^{-1}	ΔQ mm s^{-1}	H_{hyp} kOe	θ	η
0.5	0.004	1.44	179	61°	0.74
0.75	0.024	0.88	205	60°	0.55
1.0	0.034	1.00	216	63°	0.59
1.2	0.034	1.16	220	78°	0.78

[1]) Relative to metallic iron.

For nuclear γ-resonance see also

^{57}Fe $R(^{57}FeCo)_5$, R = Pr, Nd, Tb, Dy, Ho, Er [77 A 9]; R = Ho [82 D 3]; R = Sm [82 N 5]
$ThFe_5$ [78 G 4, 78 G 5]; $ThFe_5H_x$ [84 G 7]
$Nd(CoFe)_5$ [85 A 5]; $Sm(CoFe)_5$ [73 B 7, 74 P 3]; $Th(FeCo)_5$ [72 V 1, 75 B 11]; $Th(FeNi)_5$ [72 V 1]
$La(FeNi)_5$ [81 N 2, 83 C 1, 83 O 1, 84 L 1, 87 L 1]
$La(FeNi)_5H_x$ [81 A 3, 81 N 2, 82 D 2, 82 L 1, 83 O 1, 87 L 1]

^{61}Ni $LaNi_5H_x$ [82 R 6]

^{119}Sn $LaNi_{4.7}Sn_{0.5}$ [85 O 1]; $SmCo_5$ [83 Z 3]

^{151}Eu EuM_5 [77 V 2, 78 B 1]; $EuNi_5$, $EuNi_5H_x$ [78 O 6]
$(La_{0.9}Eu_{0.1})Ni_{4.6}Mn_{0.4}$ [80 C 6, 80 C 7]

^{153}Eu $SmCo_5$ [82 N 5]

^{155}Gd $GdCo_5$, $GdNi_5$ [77 T 6]; $GdCo_3B_2$ [85 M 1]
(GdR)(CoM)$_5$, M = Cu, Ni, Pt [80 S 9]; (GdLa)Ni_5, (GdLa)Co_5 [77 B 7]

^{161}Dy DyM_5, M = Fe, Co, Ni [66 N 1]; $DyCo_5$ [65 N 1, 89 G 1]; $DyNi_5$ [65 N 1]

^{166}Er $ErCo_5$, $ErNi_5$ [89 G 1]

^{169}Tm $TmCo_5$ [89 G 1]; $TmNi_5$ [85 G 19, 85 G 20]

For nuclear γ-resonance on ^{61}Ni, ^{155}Gd and ^{161}Dy in RM_5 compounds see also Tables 60b, 60a, and 59.

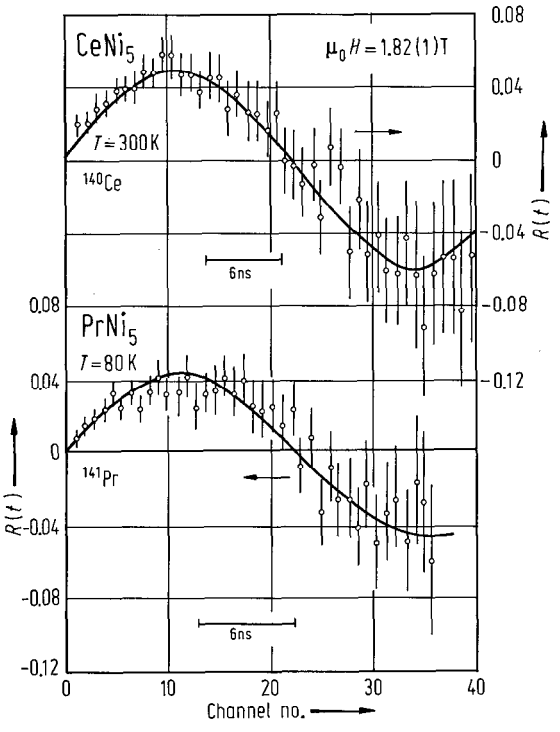

Fig. 409. Spin rotation spectra for ^{140}Ce in $CeNi_5$ at 300 K and ^{141}Pr in $PrNi_5$ at 80 K in a magnetic field of 1.82(1) T [87 D 8]. The paramagnetic enhancement factor determined is $\beta \cong 1.0$ in RNi_5 (R = La, Ce, Pr). This shows that Ce is nonmagnetic in these compounds as in the case of α-Ce.

For the perturbed angular coorelations see
^{111}Cd in RNi_5 [81 D 5, 81 D 6]; R = Nd, Sm, Eu, Gd, Dy, Er, Tm [84 P 11]
^{111}In in RNi_5 [80 D 7]
^{140}Ce in RNi_5 [87 D 8]
^{181}Ta in $DyNi_5$, $ErNi_5$ [82 K 4]

For μSR studies see also
$LaNi_5H_6$ [81 G 19, 84 G 11]

NMR

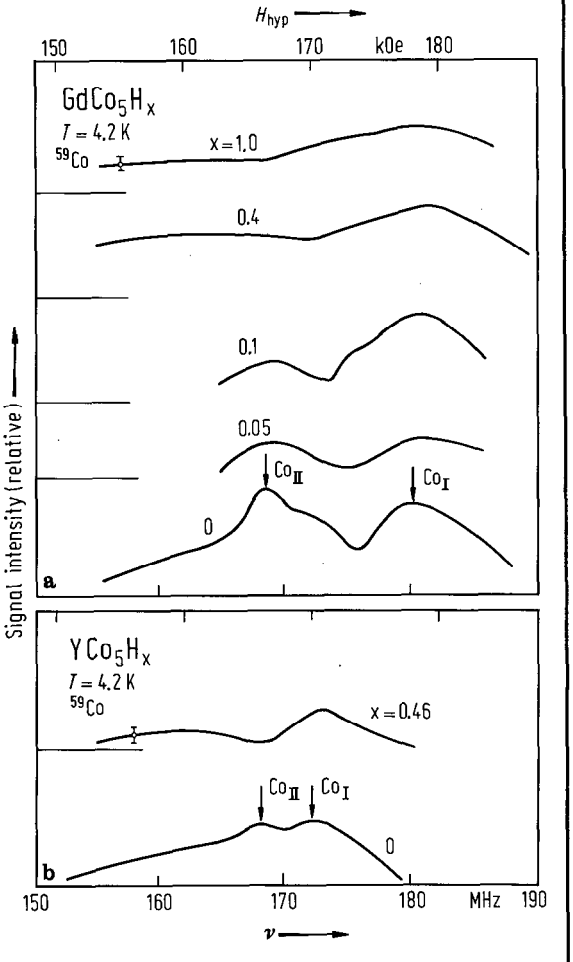

Fig. 410. Spectra of ^{59}Co NMR at 4.2 K in $GdCo_5H_x$ (a) and YCo_5H_x (b) [80 Y 2]. The hydrogen has a considerably greater effect on the $Co_{II}(3g)$ sites than on the $Co_I(2c)$ site. The intensity of the $Co_{II}(3g)$ signal decreases and becomes broader as the amount of adsorbed hydrogen increases. It is assumed that in RCo_5 (R = Y or Gd) hydrogen atoms are preferentially located in the Co-only layers and that they distribute the quadrupole interaction and/or cause the inhomogeneous magnetic hyperfine field at $Co_{II}(3g)$ site.

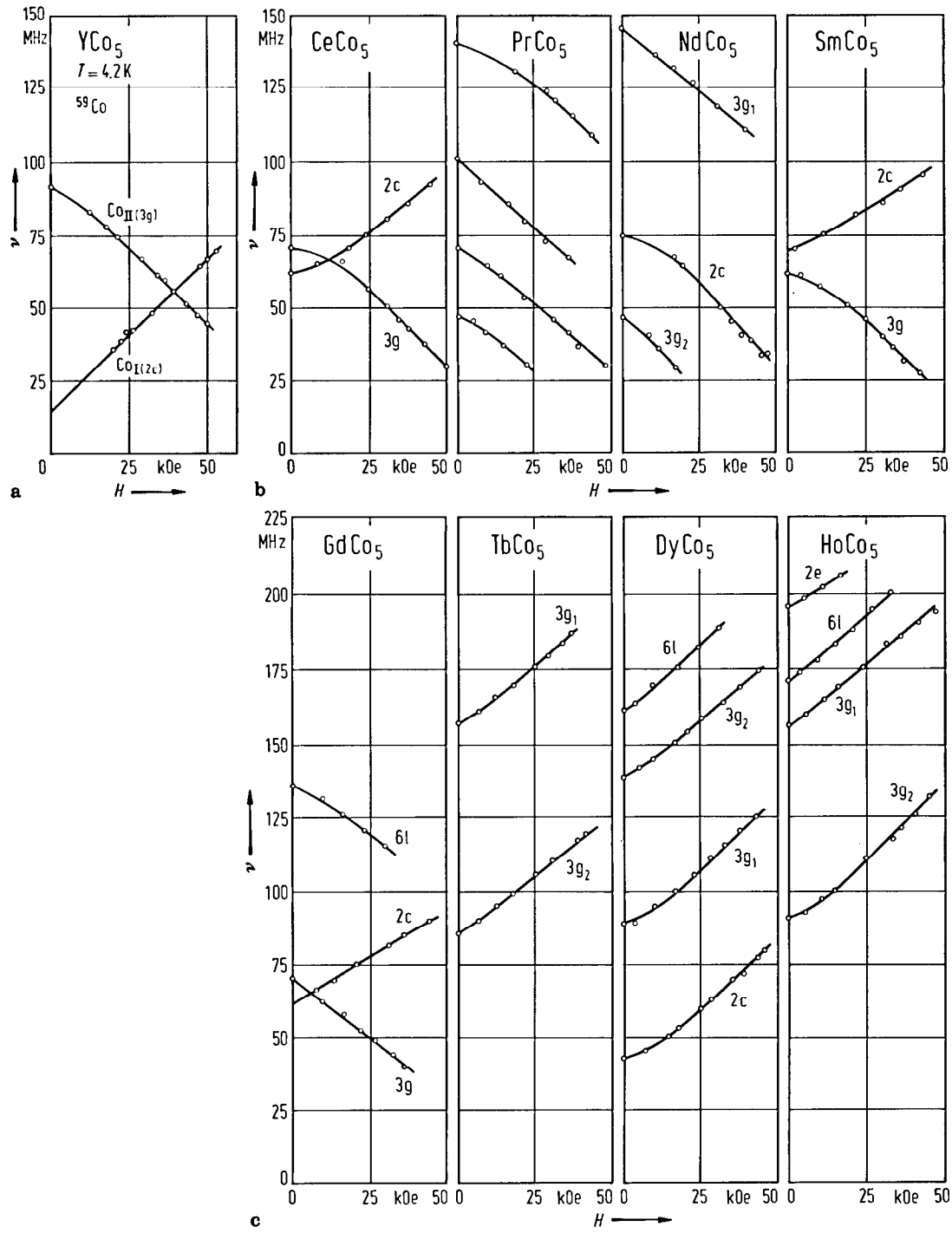

Fig. 411. Magnetic field dependence of the ^{59}Co resonance frequency at 4.2 K for (a) YCo_5, (b) RCo_5 (R = Ce, Pr, Nd, Sm), (c) RCo_5 (R = Gd, Tb, Dy, Ho) compounds [87 Y 8]. The magnetizations of RCo_5 (R = Nd, Tb and Dy) compounds are perpendicular to the *c* axis and those of R = Y, Ce, Sm and Gd are parallel to the *c* axis. For R = Pr and Ho, the magnetization makes angles of 21° and 72° with the *c* axis, respectively. In the case where the magnetization has an *ac* plane component, the 3g sites are divided into two sites, $3g_1$ and $3g_2$, with the population ratio 1:2. Then there are five sites, 2c, $3g_1$, $3g_2$, 6l and 2e, where the number of Co atoms at 6l and 2e sites are very small. Considering the actual structure of YCo_5, Table 84, there are the ratio of occupation numbers 1.7:3:0.3:0.1 for 2c, 3g, 6l and 2e sites. The NMR signals at the 6l and 2e sites in magnetic domains of YCo_5 were too weak to be detected. It should be noted that in YCo_5 the Co magnetic hyperfine field at the 2c site has a positive sign in contrast to the usual negative sign at the 3g site. This suggests that the Co atom at the 2c site in YCo_5 has a large orbital magnetic moment.

Table 99. ^{59}Co magnetic hyperfine field values at 4.2 K in RCo_5 compounds determined by NMR.

	Site	$H^{\parallel}_{hyp}$	$H^{\perp}_{hyp}$	$H^{\parallel}_{hyp}-H^{\perp}_{hyp}$	ΔH_{hyp} [1]) anisotrop	Δp_L [2]) μ_B	E_s [3]) cm^{-1}	Ref.
		kOe						
$SmCo_5$	2c	−114	−176	62		0.095	25	79 S 10
	3g	−159	−132	−27		−0.042	−10	79 S 10
YCo_5	2c	− 99	−159	60		0.092	24	79 S 10
	3g	−139	−121	−18		0.028	− 7	79 S 10
YCo_5	2c	− 87	−113	26	63			83 L 1
	3g	−141	−150	9	−28			83 L 1
$ThCo_5$	2c	− 76	−106	30	90			83 L 1
	3g	−144	170	26	−38			83 L 1
$GdCo_5$	2c		180					76 Y 3
	3g		167.5					76 Y 3
YCo_5	2c		171					76 Y 3
	3g		166					76 Y 3
$NdCo_5$	2c		−128					75 S 10
	3g		−106					75 S 10

[1]) ΔH_{hyp} anisotrop is the anisotropic hyperfine field estimated from the relations between the observed signals and the Co sites by using Streever's method [79 S 10].

[2]) Δp_L the orbital moment calculated from the anisotropic component of the orbital hyperfine field $(H^{\parallel}_{hyp}-H^{\perp}_{hyp})_L=2\Delta p_L\langle r^{-3}\rangle$ for $(H^{\parallel}_{hyp}-H^{\perp}_{hyp})_L\cong H^{\parallel}_{hyp}-H^{\perp}_{hyp}$ and $\langle r^{-3}\rangle=35\cdot10^{26}\,cm^{-3}$.

[3]) Local anisotropy energy per atom calculated from $E_s=|\lambda|\Delta p_L\langle p_s\rangle/2\mu_B^2$ where λ is the spin-orbit coupling. The positive E_s favours a moment alignment along the c axis.

For Fig. 412, see next page.

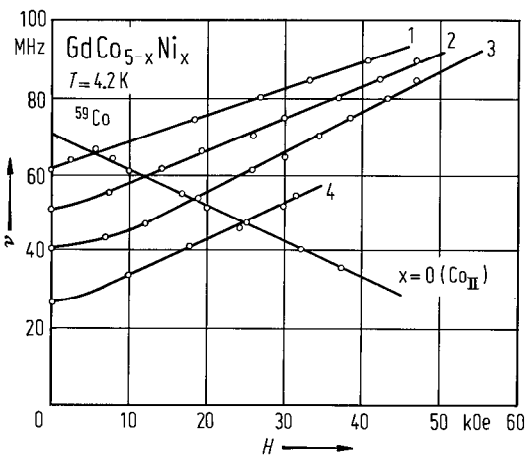

Fig. 413. Magnetic field dependence of the resonance frequencies of ^{59}Co in $GdCo_{5-x}Ni_x$ compounds [85 Y 9]. The change in the NMR signals between x = 0 and x = 1.0 suggests that the dominant sublattice magnetic moment changes from the Co sublattice to the Gd one at $x\cong1.0$, in agreement with the results of magnetic measurements. From the frequency shift due to substitution of Co by Ni, the effect of one Ni atom per formula unit on the Co magnetic hyperfine, field is estimated at ≅ 10 kOe. The disappearance of the signal from Co_I(2c) site by substituting Ni is in accordance with the trend of preferential site occupation of Ni at the site 2c. On the other hand Co_I(2c) signal is very unstable and difficult to be observed in most of the RCo_5 compounds.

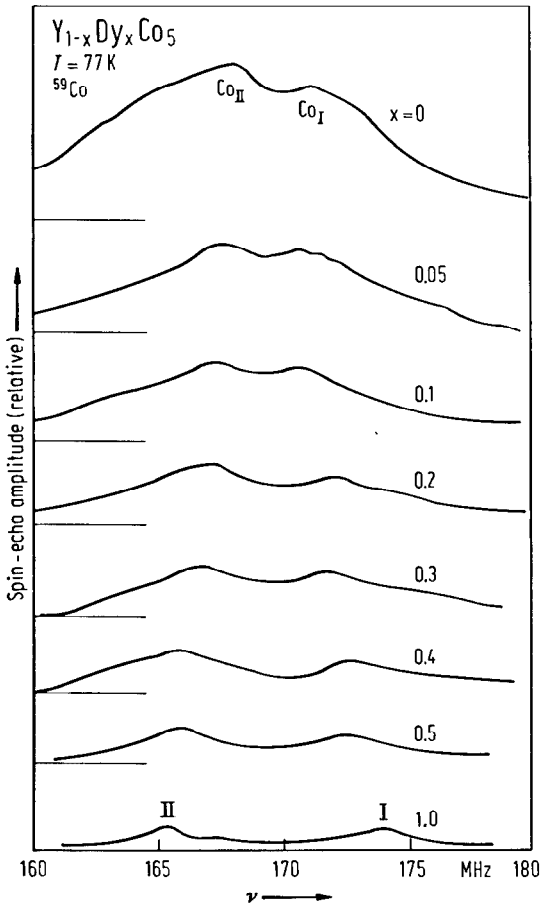

Fig. 412. Resonance line shape for ^{59}Co in $Y_{1-x}Dy_xCo_5$, at 77 K, having $0 \leqq x \leqq 0.5$ and $x = 1.0$. The peaks assigned by I and II, correspond to signal from Co(2c) and Co(3g) nuclei, respectively [77 Y 5].

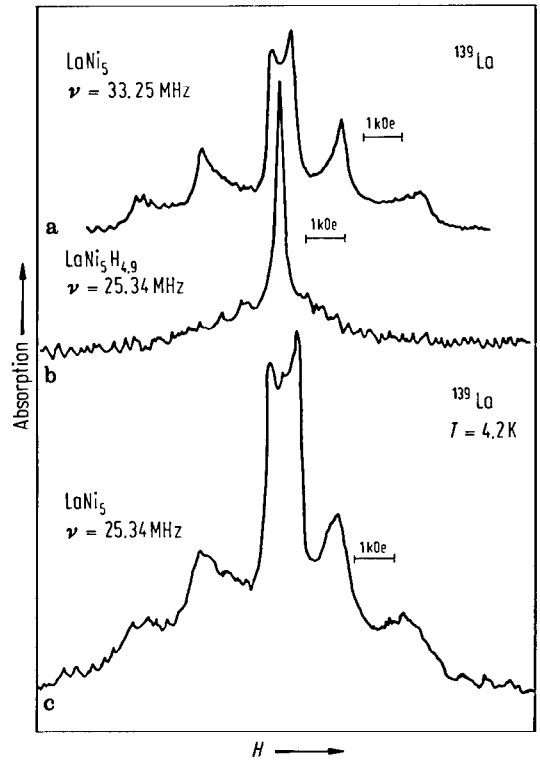

Fig. 414. ^{139}La NMR absorption lineshapes in (a) $LaNi_5$ before hydriding, (b) $LaNi_5H_{4.9}$, and (c) $LaNi_5$ after hydriding and allowing the hydrogen to escape [79 R 6]. The changes in NMR spectra are reversible. The original powder pattern has been restored with the same value of Knight shifts and quadrupole interaction [79 R 6]. Residual strains remain in the lattice which broaden the lines somewhat. With ternary addition (Co, Pt) the activation energy for proton diffusion remains unchanged.

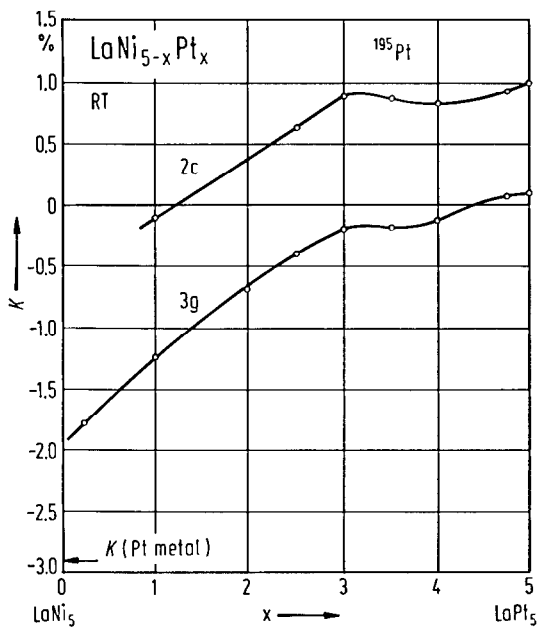

Fig. 415. Room-temperature Knight shift of ^{195}Pt in $LaNi_{5-x}Pt_x$ system, as function of x [75 W 2]. The upper curve is the Knight shift of the 2c sites and the lower curve is for the 3g site. The Knight shift of ^{195}Pt in Pt metal is indicated by an arrow. The Pt atoms prefer the 3g site and considerable ordering occurs for $x \leqq 4$.

Table 100. Magnetic hyperfine fields at ^{143}Nd nucleus and the derived Nd magnetic moments in NdM_x compounds by NMR studies at 4.2 K.

	H_{hyp} [1] MOe	p_{Nd} μ_B	Ref.
Free Nd^{3+} ion	4.30	3.27	72 b 1
Nd_2Co_{17}	3.91	3.00	75 S 10
$NdCo_3$, site I	3.53	2.70	75 S 10, 77 S 14
site II	3.21	2.40	
$NdCo_5$	3.44	2.60	75 S 10

[1]) The H_{hyp} values were calculated from NMR frequencies (taking $p_N(^{143}Nd) = -1.063\,\mu_N$) and $p_N(^{143}Nd)/p_N(^{145}Nd) = 1.608$. The Nd magnetic moments were derived from H_{hyp} values by assuming a proportionality between H_{hyp} and p_{Nd}. The estimated contributions to the Nd hyperfine field induced by magnetic moments on neighbouring atoms should be of the order of 0.1 MOe [72 b 1] and consequently were neglected.

For NMR studies see also

^{1}H $LaNi_5H_x$ [74 H 2, 76 B 3, 76 H 1, 77 H 5, 78 H 6, 79 K 2, 79 R 6, 80 K 3, 83 N 5]; $(LaCe)Ni_5H_x$, $(LaCe)(CoNi)_5H_x$ [78 H 6]
$La(NiCu)_5H_x$ [80 S 12]; $La(NiAl)_5H_x$ [79 B 9, 80 B 10]; $La(NiCr)H_x$ [79 H 8, 80 H 10]

^{59}Co RCo_5 [78 S 20]; R = Ce, Pr, Nd, Sm, Gd, Tb, Dy, Ho, Y [87 Y 8]; R = Nd [75 S 10]; R = Sm [79 S 10]; R = Gd [85 Y 9]; R = Y [76 E 3, 77 F 3, 77 S 6, 79 S 10, 81 K 19, 83 L 1, 85 Y 9]; R = Th [83 L 1]
RCo_5H_x, R = Gd, Y [80 Y 2, 82 F 6]
$(GdY)Co_5$ [76 Y 3, 85 Y 9]; $(DyY)Co_5$ [77 Y 5]; $(HoY)Co_5$ [77 Y 5]
$Y(FeCo)_5$ [76 I 4]; $Gd(CoNi)_5$ [85 Y 9]

^{63}Cu $Ce(CuNi)_5$ [82 P 10]
$CeCu_4Fe$ [83 C 7]

^{89}Y YCo_5 [76 F 1]; see also Table 61

^{139}La $LaNi_5$, $LaNi_5H_x$ [79 R 6]

^{141}Pr $PrNi_5$ [80 K 2, 80 Z 4]

^{143}Nd, ^{145}Nd $NdCo_5$ [75 S 10, 77 S 14]

^{147}Sm, ^{149}Sm $SmCo_5$ [75 S 11]

^{195}Pt $La(NiPt)_5$ [75 W 2]

Anisotropy, magnetostriction

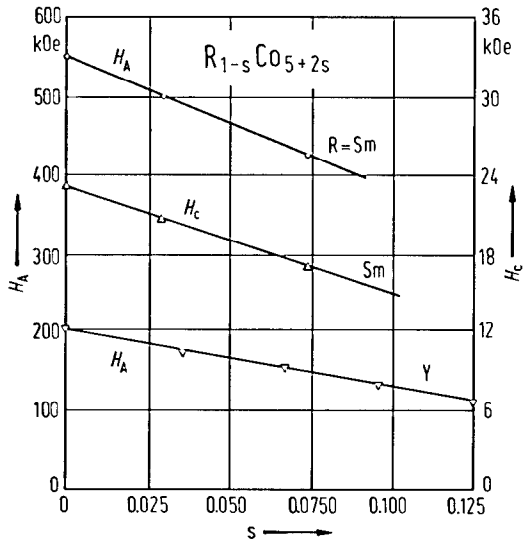

Fig. 416. Variation of anisotropy and coercive fields in the homogeneity range of $SmCo_5$ and YCo_5 phases, i.e. $R_{1-s}Co_{5+2s}$ compounds. For both type of compounds H_A decreases linearly when s increases. H_A would reach zero when s = 0.32 for Sm and 0.29 for Y compounds. This result is in agreement with the weak value of the anisotropy in R_2Co_{17} compounds, where s = 0.33. In the YCo_5 phase, where Y is nonmagnetic, the decrease of H_A is only induced by modification of the structure created by the pairs of atoms. The substitutions favour, locally, an easy magnetization direction which is perpendicular to the *c* axis. This effect induces the cancellation of the anisotropy in approximately three unit-cells. The main modifications of the environment affect the hexagonal arrangement of the six Co atoms which surround the replaced R atom. On the account of the hole due to the substitutions, these Co atoms leave the highly symmetrical, uniaxial position ($\bar{6}m2$) that they have in the $CaCu_5$ structure for a (mm) position on a two-fold axis perpendicular to the $\bar{6}$-axis. For the six Co atoms belonging to the three unit-cells which surround the substitution, the second-order anisotropy coefficients, which are generally the largest in value, must change their sign. In $SmCo_5$ the uniaxial anisotropy arises mainly from the large positive value of constant K_1 due to Sm atoms. When one of three atoms is replaced by a pair of Co atoms, the local changes in anisotropy results from two different effects: (1) the disappearance of the anisotropy related to the replaced Sm atom and (2) the modifications of the local surrounding by Co atoms (as in YCo_5). Moreover, the uniaxial character of the environment of Sm atoms close to the substitution disappears. This affects the crystalline potential and then amplifies the decrease of the anisotropy. Here, too, a substitution decreases the local anisotropy in a zone of three unit-cells [76 D 9].

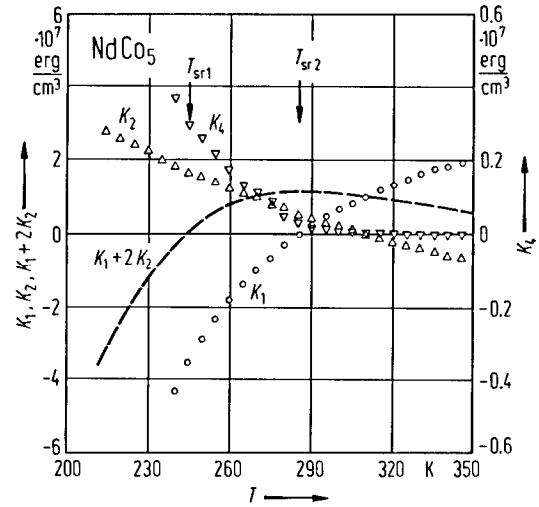

Fig. 418. Temperature dependence of the anisotropy constants K_1, K_2 and K_4 in $NdCo_5$ single crystal [76 O 8]. The easy direction of magnetization rotates continuously from the *b* axis [100] at the lower spin reorientation temperature ($T_{sr1} = 245$ K) to the *c* axis [001] at the upper spin reorientation temperature ($T_{sr2} = 285$ K) in the *bc* plane. K_1 changes the sign from negative to positive just at T_{sr2}, and K_2 from positive to negative at a temperature a little higher than T_{sr2}, but $K_1 + 2K_2$ reverses its sign exactly at T_{sr1}. The anisotropy constant in the basal plane, K_4, vanishes near T_{sr2}, though it is fairly large (10^7 erg cm^{-3}) at low temperatures. On account of this anisotropy change, the magnetization curve along the *a* axis [110] has a peak at a temperature slightly higher than T_{sr1}, when a field of more than 10 kOe is applied.

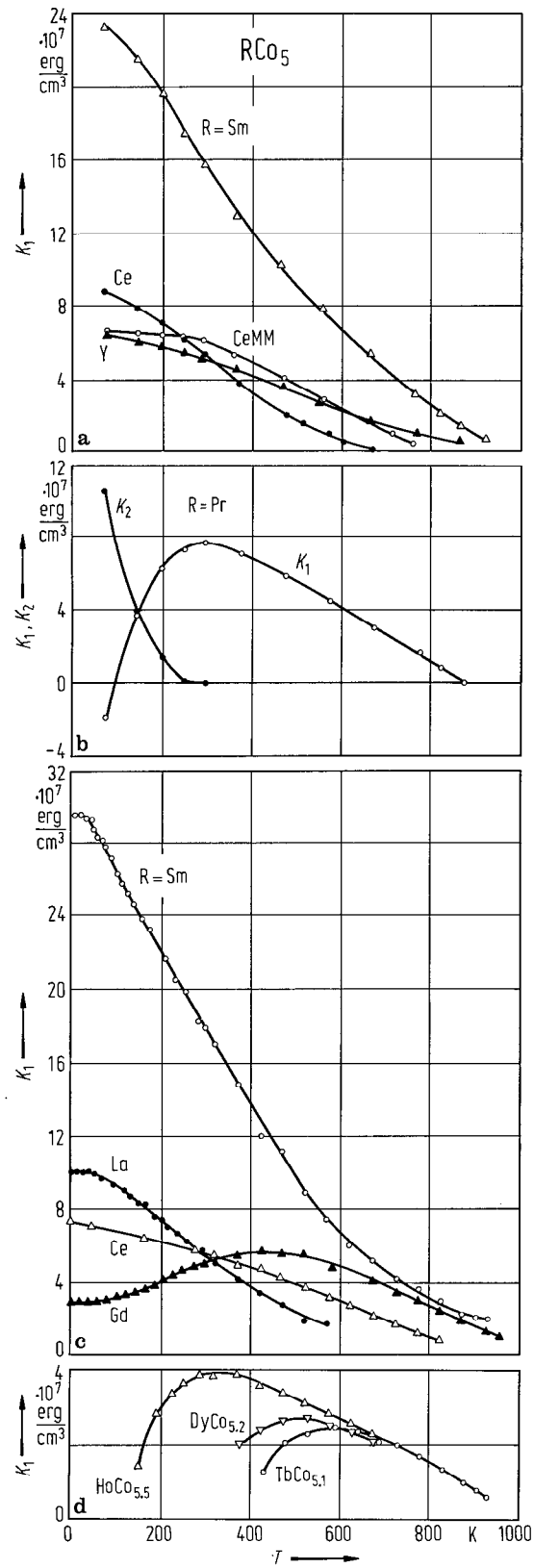

Fig. 417. Temperature dependence of the anisotropy constants (a) K_1 for RCo_5 (R = Y, Ce, Sm, and CeMM, a Ce-rich alloy of La, Pr, Nd); (b) K_1 and K_2 for $PrCo_5$ compound [74 K 15, 75 K 4]. (c) K_1 for RCo_5 (R = La, Ce, Sm and Gd), and (d) K_1 for $TbCo_{5.1}$, $DyCo_{5.2}$ and $HoCo_{5.5}$ [74 E 3]. The apparent anomalous thermal variation of the bulk anisotropy of ferrimagnetic compounds has essentially to deal with the induced-field noncollinearity of R and Co magnetic moments, the dipolar contribution being too small [86 B 3]. An anisotropy in the exchange energy of $GdCo_5$ is evidenced. The origin of this anisotropy results from spin-orbit coupling which introduces not only an anisotropic partial quenching of the 3d orbital contribution to the magnetization but also a nonnegligible spin anisotropy.

Table 101. Anisotropy constants of R atoms, exchange fields and crystal field parameters in RCo_5 compounds at 4.2 K.

	K_{1R}	K_{2R}	$g\mu_B H_{ex}/k_B$	B_2^0	B_4^0	B_6^0	B_6^6	Ref.
	10^{-14} erg/R		K	K	10^{-2} K	10^{-4} K		
$CeCo_5$	–	–	84	13.6	−28.6	–	–	74 K 5
$PrCo_5$	−2.24	3.22	70	− 2.7	0.66	–	–	82 E 1
	–	–	84	4.5	–	–	–	73 G 4
	–	–	118	6.26	2.7	–	–	74 K 5
$NdCo_5$	0	−2.0	98	3.5	− 0.22	–	−146	82 E 3
	–	–	115	1.3	–	–	–	73 G 4
	–	–	123	3.71	0.25	−5.0	−124	81 L 5
	–	–	160	1.78	0.9	–	–	74 K 5
	−4.0	+1.6	∞					71 T 1
	−6.5	+3.0	∞					75 F 3
	−7.1	+2.7	381					79 E 1
	−1.9	–	233					82 E 3
	0	−2.0	186					82 E 3
$SmCo_5$	2.39	–	750	−11.5	–	–		80 E 5
	–	–	–	− 7.9				73 G 4
	–	–	420	–	–	–	–	74 K 5
			240	−17	− 6.25	–	–	75 S 1
			200	− 7.43		–	–	74 B 15
			175(25)	− 8.25	0(12.5)	–	–	79 G 7
$GdCo_5$	–	–	588	–	–	–	–	74 K 5
	0	0	296	–	–	–	–	79 E 1
$TbCo_{5.1}$	−1.33	−0.91	117	1.7	− 0.26	–	− 2.1	79 E 1, 82 E 1
$TbCo_5$			210	1.4	–	–	–	73 G 4
$DyCo_{5.2}$	−2.92	0.14	70	1.3	0.013	–	1.1	82 E 1
$DyCo_5$			140	0.9	–	–	–	73 G 4
$HoCo_{5.5}$	−2.82	1.05	45	0.65	0.08	–	–	82 E 1
$HoCo_5$	–	–	140	0.3	–	–	–	73 G 4
$ErCo_5$	1.1	–	48	− 0.51	–	–	–	82 E 1
			84	− 0.4	–	–	–	73 G 4

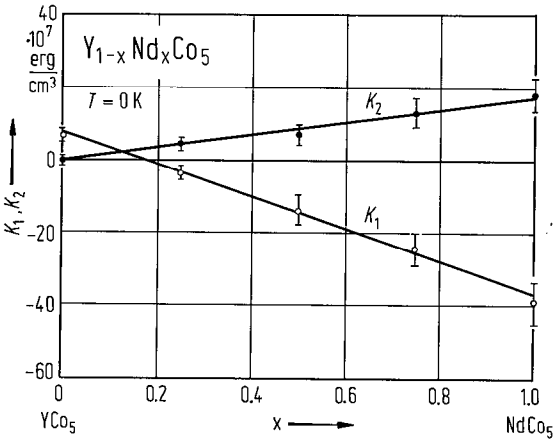

Fig. 419. Composition dependence of the anisotropy constants, K_1 and K_2, in $Y_{1-x}Nd_xCo_5$ compounds at 0 K [71 T 1]. These are linearly dependent on composition and support the single-ion model.

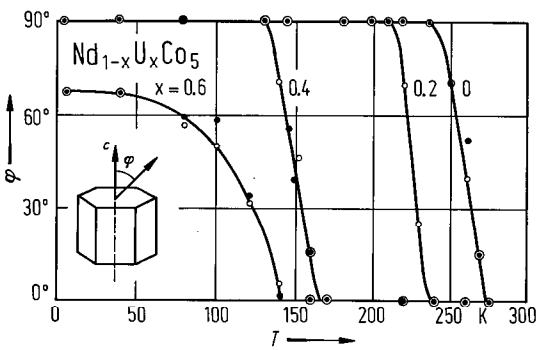

Fig. 420. Temperature dependence of the angle φ between c axis and direction of magnetization in $Nd_{1-x}U_xCo_5$ single crystals [79 D 4]. When the temperature increases from T_{sr1}, the angle φ gradually decreases, and for $T \geqq T_{sr2}$ the magnetization lies in the basal plane of the lattice. The angle φ determined by the equation $\varphi = \arcsin(-K_1/2K_2)^{1/2}$ is shown by solid circles, the torque measurements by open circles.

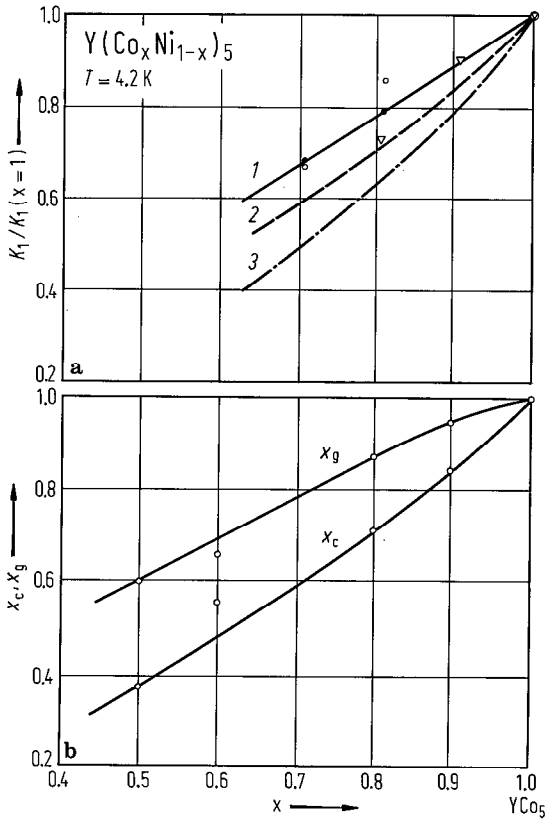

Fig. 421. (a) Composition dependence of the anisotropy constant K_1 in $Y(Co_xNi_{1-x})_5$ at 4.2 K [86 P 3]. Experimental data are from (triangles) [77 B 23], (open circles) [86 P 3], (solid circles) [77 E 4]. By lines are plotted the values calculated according to the relation $K_1/K_1(x=1) = (2K_1^c x_c + 3K_1^g x_g)/K_1(x=1)$ with (1) $K_1^c = 1.64 \cdot 10^{-22}$ J/Co, $K_1^g = 0.88 \cdot 10^{-22}$ J/Co; (2) $K_1^c = 4.64 \cdot 10^{-22}$ J/Co, $K_1^g = -1.35 \cdot 10^{-22}$ J/Co [79 S 10], and (3) $K_1^c = 3.33 \cdot 10^{-22}$ J/Co, $K_1^g = -0.18 \cdot 10^{-22}$ J/Co [84 K 1]. In (b) are given the distributions, x_c and x_g, considered for Co atoms in 2c and 3g sites, respectively [80 P 4].

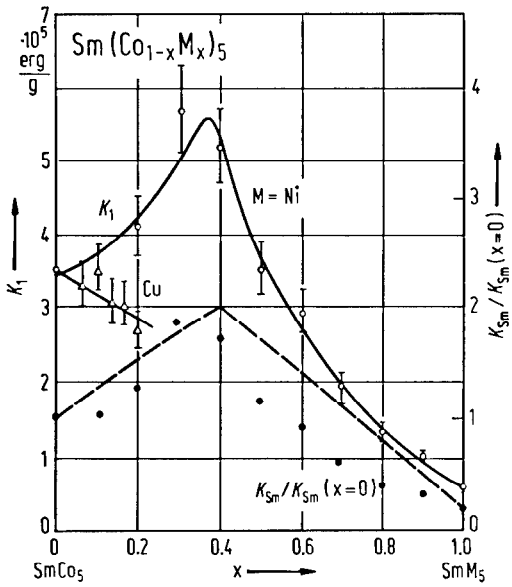

Fig. 4.22. Composition dependence of the anisotropy constants K_1 in $Sm(Co_{1-x}Ni_x)_5$ and $Sm(Co_{1-x}Cu_x)_5$ compounds, at 4.2 K [76 E 6]. By solid circles are denoted the $K_{Sm}/K_{Sm}(x=0)$ values and by broken line the prediction of the single-ion model of anisotropy.

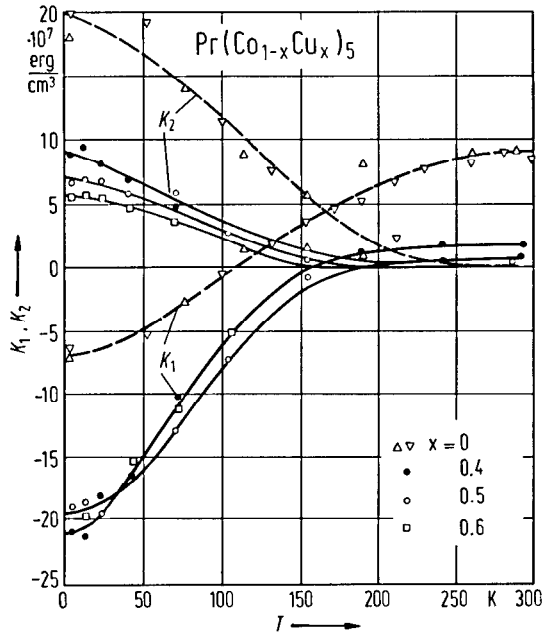

Fig. 423. (a) Anisotropy constants, K_1 and K_2, as a function of temperature for $Pr(Co_{1-x}Cu_x)_5$ compounds. The data for $PrCo_5$ are from (triangles upward) [71 T 1]; (triangles downward) [74 E 3, 76 E 4] and for x = 0.4 (solid circles); 0.5 (open circles) and 0.6 (squares) from [78 M 1]. From the above data the Pr sublattice anisotropy constants, $(K_1+K_2)_{Pr}$, were evaluated. The $(K_1+K_2)_{Pr}$ values are positive for x = 0 and negative for x = 0.4, 0.5, and 0.6. They are qualitatively in good agreement with stabilization energies calculated using a single-ion model in terms of the crystalline electric field and exchange field acting on Pr ion.

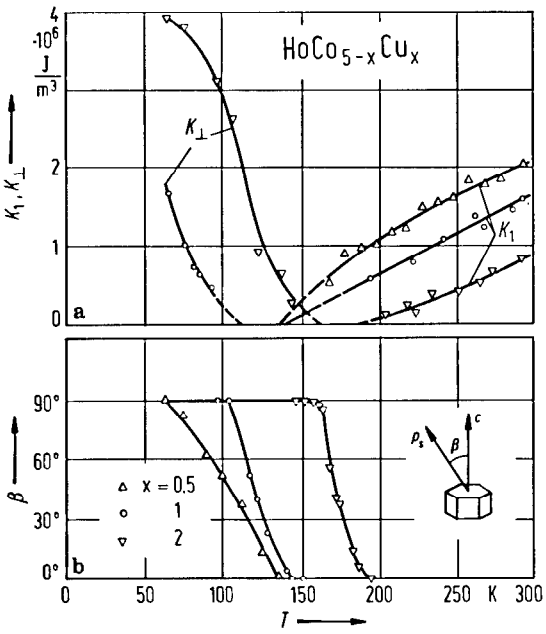

Fig. 424. Temperature and composition dependence of (a) the anisotropy constant, K_1 and $K_\perp = K_1 + 2K_2$, and (b) the angle of the easy direction of magnetization in $HoCo_{5-x}Cu_x$ compounds [81 D 10].

For anisotropy studies see also

RM_5 [70 S 3(T), 77 A 3, 88 K 5]

RCo_5 [70 S 5, 73 G 4, 73 G 5, 73 I 2, 74 I 2(T), 74 M 3, 76 E 4, 77 I 6, 79 D 4, 82 E 1, 86 R 1, 87 B 4, 88 T 1]; R = Ce, Pr, Sm, Y [67 S 4]; R = Ce, Pr, Nd, Sm, Y [71 T 1*]; R = Gd, Tb, Dy, Ho, Er [73 O 7]; R = La, Ce, Pr, Nd, Sm, Gd, Tb, Dy, Ho [74 E 3]; R = Ce, Nd, CeMM, Sm, Y [74 K 15*]; R = Ce, Pr, Y, Th [75 A 7]; R = Ce, Pr, Nd, Sm, CeMM, Y [75 K 4]; R = Sm, Gd, Y [79 S 12(T)]; R = Pr [80 A 7, 84 W 1, 85 K 16]; R = Nd [66 B 2, 74 F 2*, 76 D 8, 80 H 11, 82 A 5, 84 D 2]; R = Sm [73 K 13, 74 B 15, 74 D 6*, 74 K 6, 75 K 5, 75 S 1, 76 D 3, 76 D 9, 76 Y 2, 77 K 6, 79 T 2, 81 S 17(T), 82 B 6, 83 A 1(T), 83 J 3, 84 W 1]; R = Gd [86 B 3, 87 B 3]; R = Tb [75 E 2, 84 P 12]; R = Dy [75 E 2, 80 B 5]; R = Ho [68 K 1*]; R = Y [67 H 2*, 74 F 1*, 74 K 6, 75 K 5, 76 D 9, 76 Y 2, 80 A 3, 81 A 1, 81 L 5, 82 A 5, 84 K 1, 85 K 16, 85 S 25(T), 86 P 3, 87 B 3, 88 T 1]

$(R'R'')Co_5$ $(LaSm)Co_5$ [79 E 3]; $(CeSm)Co_5$ [79 E 3]; $(PrSm)Co_5$ [71 S 3, 77 E 6, 78 H 3]; $(PrY)Co_5$ [82 A 8*, 88 P 1]; $(NdSm)Co_5$ [75 F 3, 78 E 1, 79 E 3, 80 E 5, 81 K 6, 82 E 2]; $(NdY)Co_5$ [71 T 1, 76 M 12, 77 H 2, 80 E 1, 80 E 4, 82 E 1, 82 E 3]; $(NdU)Co_5$ [78 D 1]; $(SmDy)Co_5$ [83 E 3]; $(SmY)Co_5$ [71 S 3, 79 E 3, 82 A 8*]; $(GdY)Co_5$ [80 E 1, 80 E 2, 80 E 3, 82 A 16]; $(TbY)Co_5$ [80 E 1]; $(DyY)Co_5$ [83 D 5, 83 E 3]; $(HoY)Co_5$ [82 E 4]; $(ErY)Co_5$ [83 E 3]; $(YU)Co_5$ [78 D 1]

$R(M'M'')_5$ $R(CoM)_5$ [76 K 6]; $Sm(CoM)_5$, M = Fe, Ni, Cu [76 E 6]; $Y(FeCo)_5$ [73 R 7, 88 F 1]; $Th(FeCo)_5$ [73 R 7]; $R(CoNi)_5$ [77 I 6]; $Pr(CoNi)_5$ [85 A 10]; $Sm(CoNi)_5$ [75 E 4]; $Ho(CoNi)_5$ [81 D 10]; $Er(CoNi)_5$ [85 D 12, 87 D 10]; $Y(CoNi)_5$ [86 P 3]; $Pr(CoCu)_5$ [73 M 1, 78 M 1]; $Sm(CoCu)_5$ [73 K 2, 74 M 3, 76 B 2]; $Gd(CoCu)_5$ [70 S 4]; $Ho(CoCu)_5$ [81 D 10, 87 D 10]; $Er(CoCu)_5$ [83 D 6, 83 D 7]; $Gd(CoAl)_5$ [70 S 4]

For spin reorientation see also

RCo_5 RCo_5 [66 L 3, 79 D 4]; R = Tb, Dy, Ho [83 K 2]; R = Nd [76 O 8]; R = Tb [85 E 1]; R = Dy [77 O 9, 80 B 5]

$(R'R'')Co_5$ $(NdY)Co_5$ [77 D 8, 79 E 1]; $(NdDy)Co_5$ [77 O 8]; $(NdU)Co_5$ [78 D 1]; $(GdY)Co_5$ [79 E 1]; $(TbY)Co_5$ [79 E 1, 79 E 2]

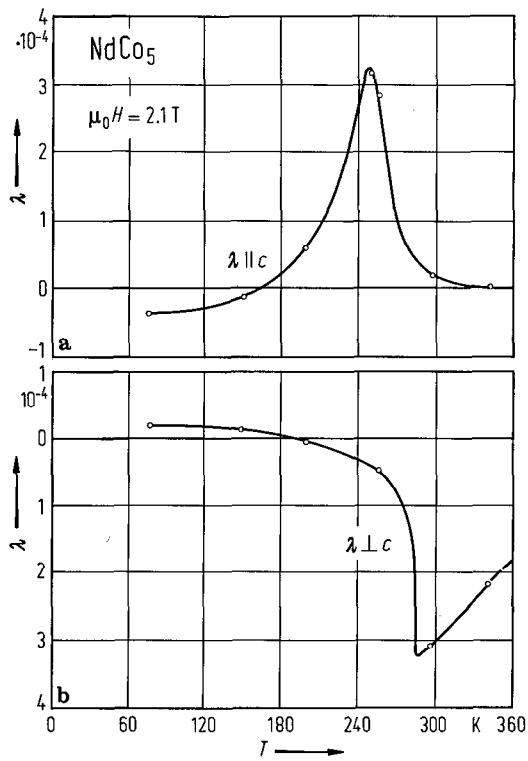

Fig. 425. Temperature dependence of the magnetostriction in a field of $\mu_0 H = 2.1$ T, (a) parallel and (b) perpendicular to the c axis in an oriented assembly of $NdCo_5$ particles [81 P 3]. The anomalous behaviour at 245 and 285 K is associated with the spin reorientation process.

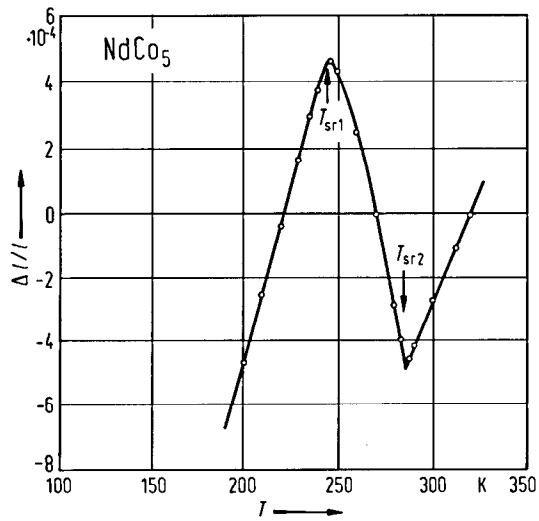

Fig. 426. Linear thermal expansion in the *c* direction on cooling $NdCo_5$ from 320 K to 200 K [81 P 3]. A pronounced anomaly in the thermal expansion is observed in the spin reorientation temperature range.

Table 102. Magnetostriction constants of RCo_5 compounds.

	T K	$\lambda_1^{\alpha,2}$ 10^{-3}	$\lambda_2^{\alpha,2}$ 10^{-3}	Ref.
$PrCo_5$ [1])	0	−1.10	−2.2	83 A 6, 85 A 10
$NdCo_5$	265	−3.5	8	82 A 13
$NdCo_5$ [1])	0	−0.80	1.7	83 A 6
$SmCo_5$ [1])	0	1.30	−2.6	83 A 6
$TbCo_{5.1}$	403.5	−3.0	6	83 A 6
$TbCo_{5.1}$ [1])	0	−1.80	3.5	83 A 6
$DyCo_{5.2}$	315	−4.0	8	83 A 6
$DyCo_{5.2}$ [1])	0	−1.90	3.8	83 A 6
$HoCo_{5.5}$	107.5	−2.5	5	83 A 6
$HoCo_{5.5}$ [1])	0	−0.60	1.2	83 A 6
$ErCo_{5.5}$ [1])	0	0.60	1.3	83 A 6
$TmCo_{5.5}$ [1])	0	0.60	−1.2	83 A 6

[1]) Calculated according to single-ion model.

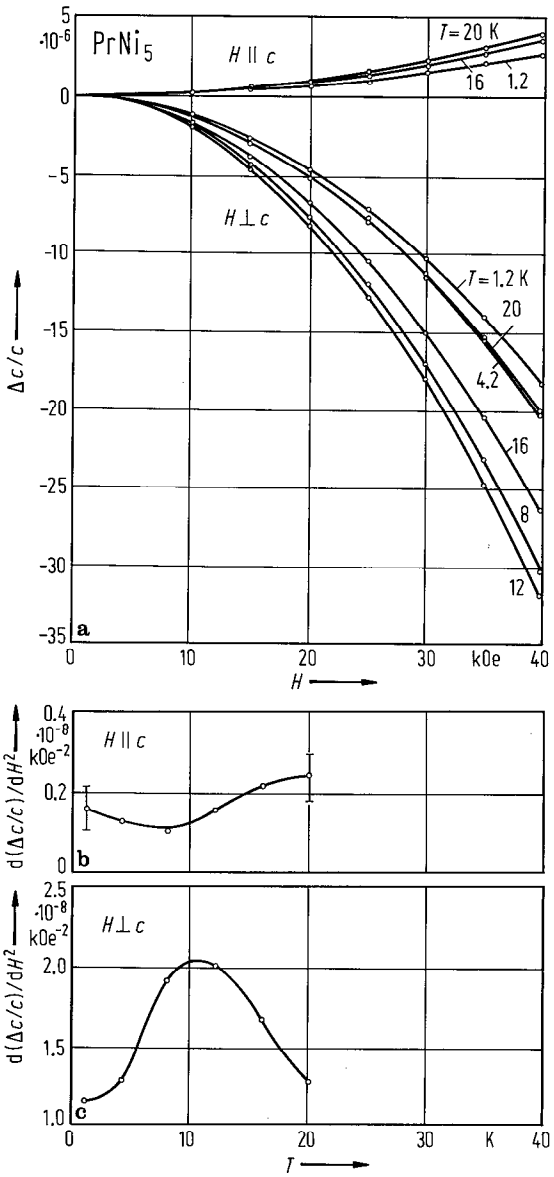

Fig. 427. (a) Magnetostriction of $PrNi_5$ for different temperatures along c axis, when the magnetic field is parallel and perpendicular to the c axis. In (b) and (c) the thermal variation of $d(\Delta c/c)/dH^2$ is shown. The maximum of $d(\Delta c/c)/dH^2$ around 15 K, as for the magnetic susceptibility, is due to the separation and the nature of the lowest crystal field levels [87 B 1].

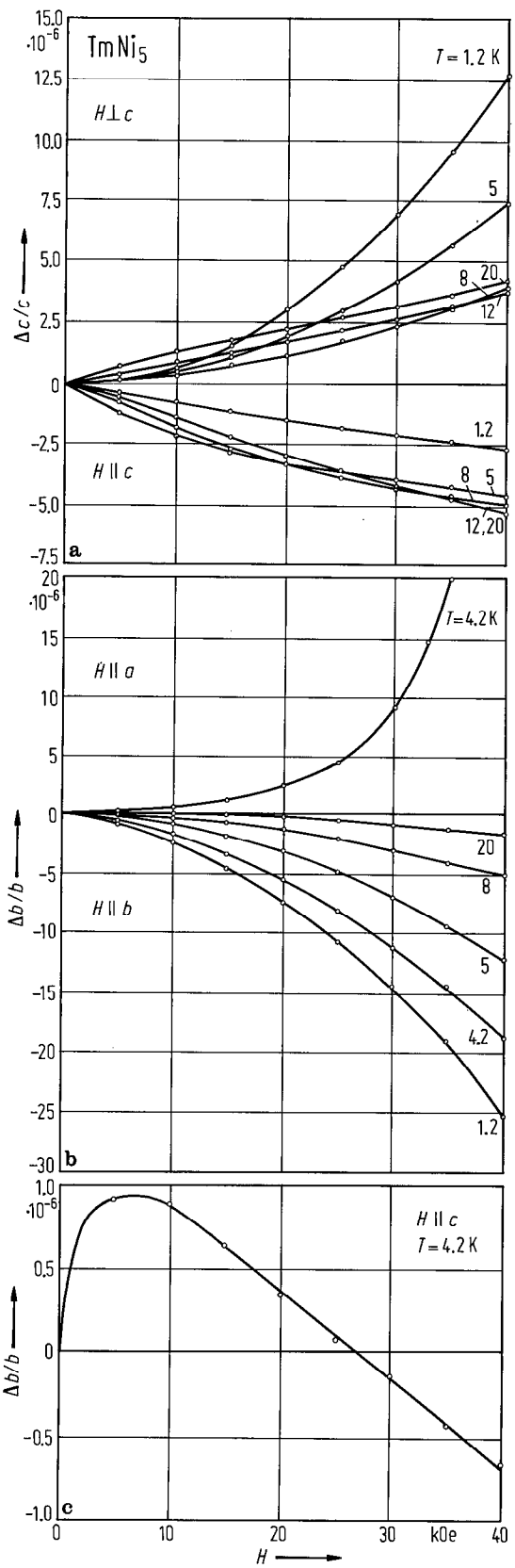

Fig. 428. Magnetostriction of $TmNi_5$ for different temperatures along (a) c axis when the magnetic field is parallel and perpendicular to the c axis, (b) b axis when the field is parallel and perpendicular to the b axis, and (c) b axis when the field is parallel to c axis. The observed magnetostriction along the c axis, for the external magnetic field parallel to c, and the change of sign for $(\Delta b/b)_{H \parallel c}$ at 4.2 K as function of the field, suggest a small contribution of the $(M_J=0)$-state to the ground-state [87 B 1].

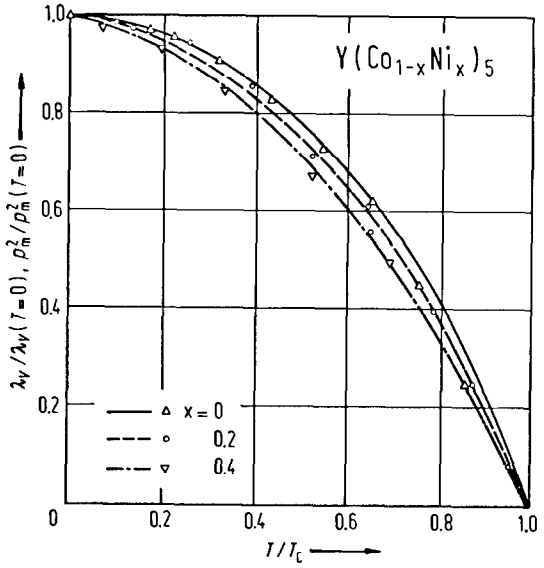

Fig. 429. Temperature dependence of (symbols) the reduced volume magnetostriction constant, $\lambda_V/\lambda_V(T=0)$, and (lines) the reduced square of magnetization, $p_m^2/p_m^2(T=0)$, in some $Y(Co_{1-x}Ni_x)_5$ compounds [85 A 11].

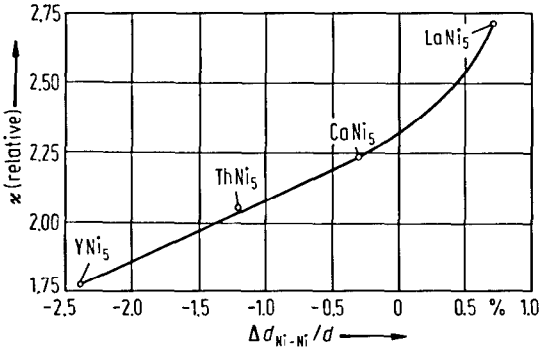

Fig. 431. Compressibility $\varkappa$ (in arbitrary units) for some RNi_5 compounds versus the percent change in the Ni–Ni distance in the midplane (3g sites) relative to the metallic diameter d in pure Ni. Where there is an expansion in the Ni–Ni distances, the compound is the most compressible ($LaNi_5$), whereas the compound which is least compressible is the one whose Ni–Ni distances have undergone the largest contraction (YNi_5) [80 T 2].

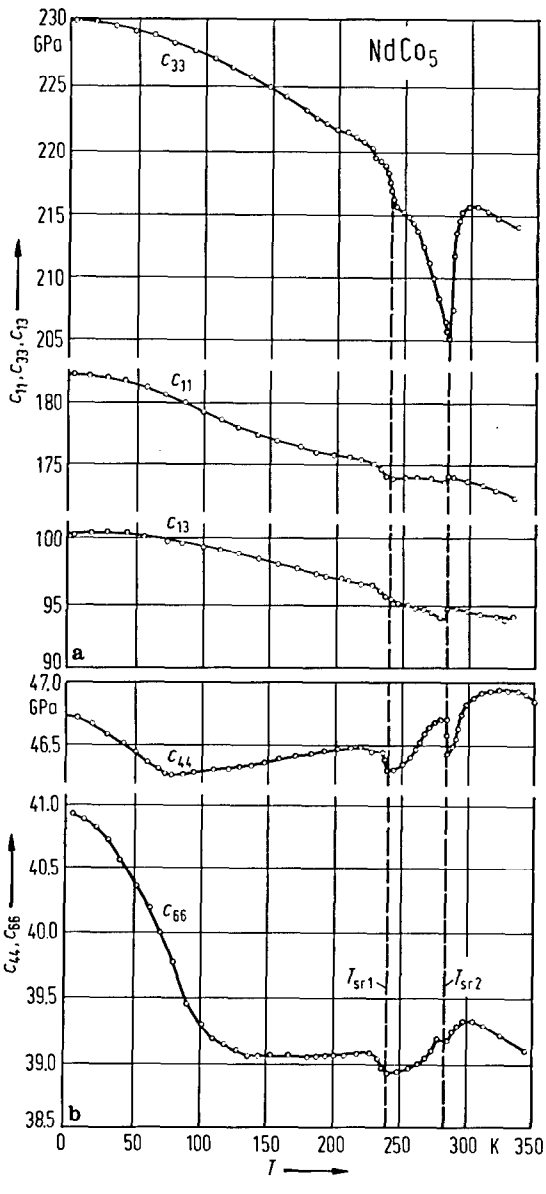

Fig. 430. Temperature dependence of the elastic constants, (a) c_{11}, c_{33} and c_{13}, (b) c_{44} and c_{66}, in $NdCo_5$-single crystal [84 D 2]. In the spontaneous spin reorientation range the elastic constants show an anomalous behaviour. See also [86 P 2].

For magnetostriction studies see also

RM_5	[88 K 5]
RCo_5	[74 K 13]; R = La, Ce, Sm, Y [74 H 9]; R = Pr, Tb, Dy, Ho [83 A 6*]; R = Nd [81 P 3, 82 A 13, 84 D 2, 87 A 4]; R = Sm [74 D 10, 77 D 6, 79 T 2]; R = Dy [80 B 6]; R = Th [75 B 14]
$R(M'M'')_5$	$Pr(CoNi)_5$ [85 A 10]; $Y(CoNi)_5$ [85 A 11, 85 A 12]

For elastic and magnetoelastic properties see

RCo_5	R = Nd, Tb, Dy [85 D 8]; R = Nd [83 P 1, 84 D 2, 86 P 2]; R = Sm [77 D 5]; R = Gd [78 U 3]
RNi_5	R = Ce [80 B 11]; R = Pr [88 B 3]
RNi_5H_x	R = La [87 R 10]
$(R'R'')Co_5$	$(NdY)Co_5$ [84 D 3]

Domain structure, magnetization processes

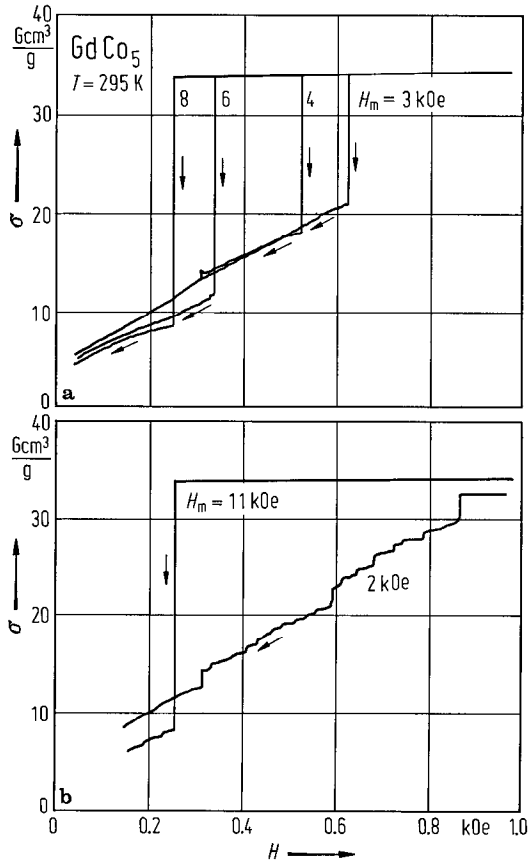

Fig. 432. (a) Magnetization reversal curves of $GdCo_5$ single crystal which was previously magnetized at various fields H_m. As the applied magnetic field decreases gradually from each value of H_m, magnetization reverses monotonically due to the demagnetizing field of the sample after the large jumps of magnetization at each nucleation field [80 U 1]. Dendritelike domains appear after reversal at the nucleation field. These patterns suggest that the first domain nucleates at one point and spreads out through the entire sample. The lifetime of moving walls of the dentritelike domain increases with the increasing diameter of the spheric or spheroidal samples along the easy axis of magnetization. The velocity of wall tips is estimated to be approximately 5m/s at room temperature except for extremely small samples. (b) Magnetization reversal curves of the same sample premagnetized at $H_m = 11$ and 2 kOe. These curves are obtained by decreasing the applied field in a sweep rate of 20 Oe/min.

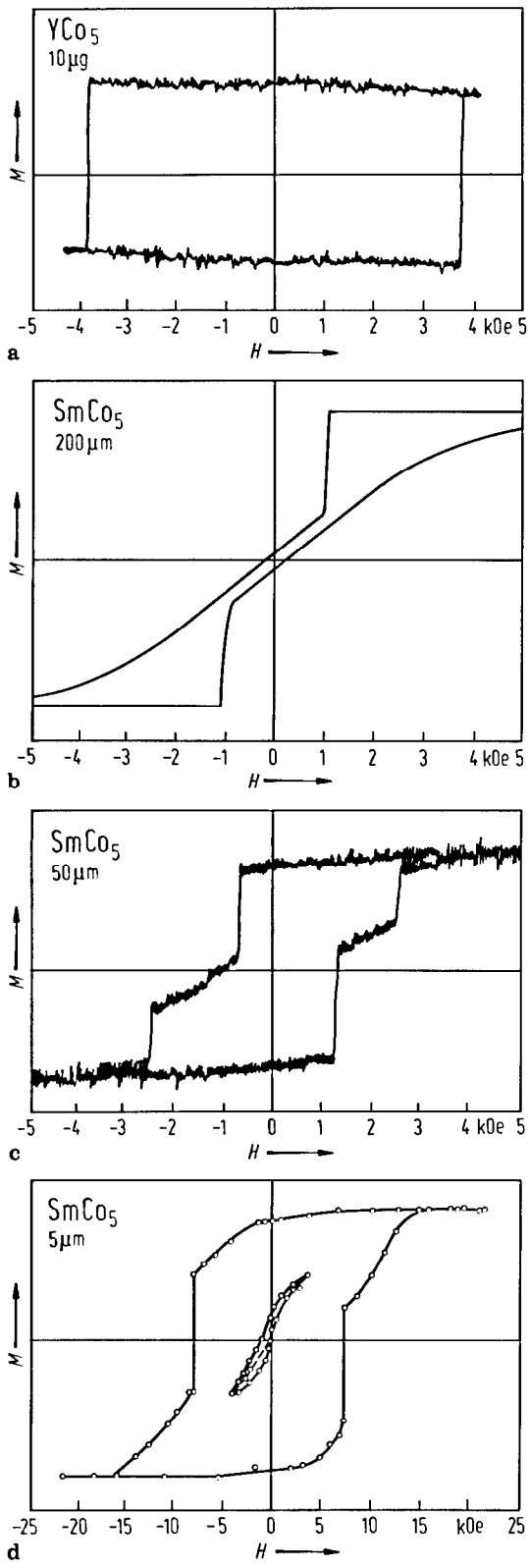

Fig. 433. Hysteresis loops of small particles of RCo_5 (R = Y or Sm) compounds: (a) YCo_5 having $\cong 10\,\mu g$ [71 B 8]; (b) $SmCo_5$ particle having 200 μm [71 B 7], (c) $SmCo_5$ particle of 50 μm [71 B 7] and (d) $SmCo_5$ particle of 5 μm [70 Z 2]. In (a) a rectangular loop behaviour is shown. Once the reverse domain was nucleated, it swept through and completely reversed the particle magnetization. The nucleation and coercive fields, respectively are identical. In (b) a domain nucleated and moved abruptly to a near-equilibrium position. It then moved to maintain zero internal field. In (c) are two distinct magnetization discontinuities separate by a region of gradual changes. It has been suggested [71 B 8] that a small-angle boundary divided the particle into two magnetically independent regions. The data from (d) were interpreted [70 Z 2, 71 Z 1] by the wall motion limited by pinning in parts of the crystal, but not in other parts. The minor loops shown for demagnetized particles, confirm that wall motion is easy over large portions of the particles. The relative importance of domain nucleation and local wall pinning varies greatly from particle to particle and the magnetization processes of particles may be influenced by both [73 L 4].

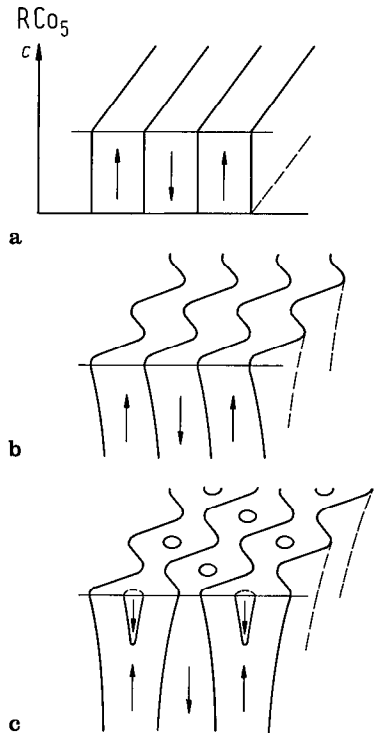

Fig. 434. Schematic representation of domain structures in platelets of hexagonal crystal having single direction of easy magnetization parallel to the *c* axis and large magnetic anisotropy, as RCo_5 (R = Y, Ce, Pr and Sm) compounds. Thickness of platelets increases from (a) to (c). The anisotropy is sufficiently large to inhibit closure domain formation and only 180° domain walls which are nearly parallel to the *c* axis occur. In thin crystal platelets the domains consist of parallel strips which are alternatively magnetized (a). Increasing the thickness causes the strips to become undular. The amplitude of waves decreases regularly with depth of penetration into the material (b). For still thicker crystals the surface structure illustrated in (c) appears. Cone-shaped surface domains of reverse magnetization penetrate as spikes partially through the crystal. Demagnetized particles even as small as 10 μm consist of a few domains. The demagnetization process of an initially fully magnetized particle thus proceeds by nucleation and subsequent growth of domains of reversed magnetization [71 B 1].

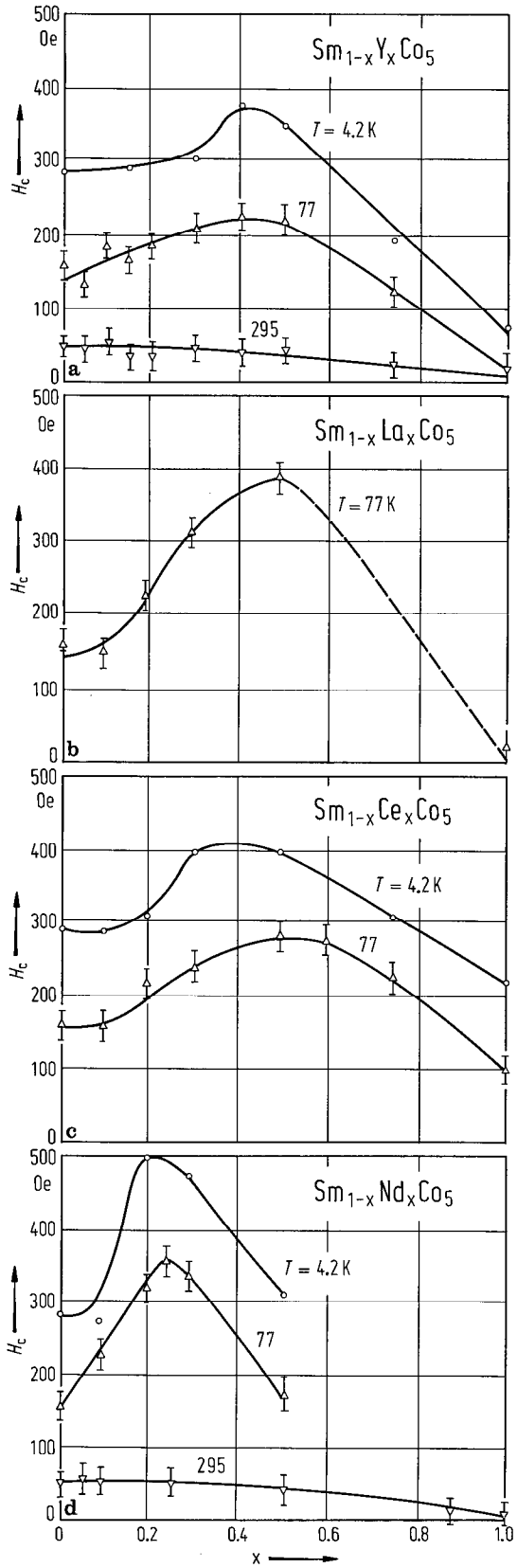

Fig. 435. Composition dependence of the coercive field for (a) $Sm_{1-x}Y_xCo_5$, (b) $Sm_{1-x}La_xCo_5$, (c) $Sm_{1-x}Ce_xCo_5$ and (d) $Sm_{1-x}Nd_xCo_5$ at 295, 77 and 4.2 K [79 E 3].

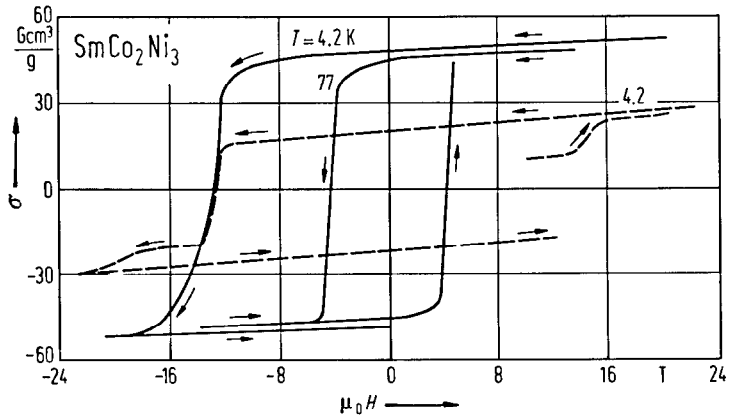

Fig. 436. Magnetic field dependence of the magnetization for $SmCo_2Ni_3$ in the form of aligned powders (parallel to field direction) at 77 K and 4.2 K. The dashed line represents the behaviour of bulk polycrystalline material at 4.2 K [78 F 8].

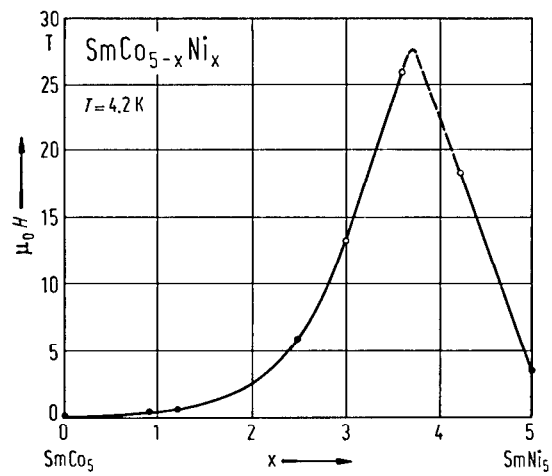

Fig. 437. Composition dependence of the coercive field in bulk $SmCo_{5-x}Ni_x$ compounds at 4.2 K [76 O 6, 77 O 6, 78 F 8]. Similar behaviour was observed in $SmCo_{5-x}Cu_x$ compounds [76 O 6, 77 E 5, 78 F 8]. The data were analysed in models involving local magnetic moments and thermal activation of domain wall motion [76 O 6]. The form of virgin magnetization curve, the presence of large intrinsic coercive forces and the observation of pronounced thermomagnetic history effects suggest the presence of narrow Bloch walls of only a few interatomic distances. It is argued that the presence of narrow Bloch walls is the primary reason for the high coercive forces observed usually in solid pieces of $RCo_{5-x}Cu_x$ compounds [76 B 19].

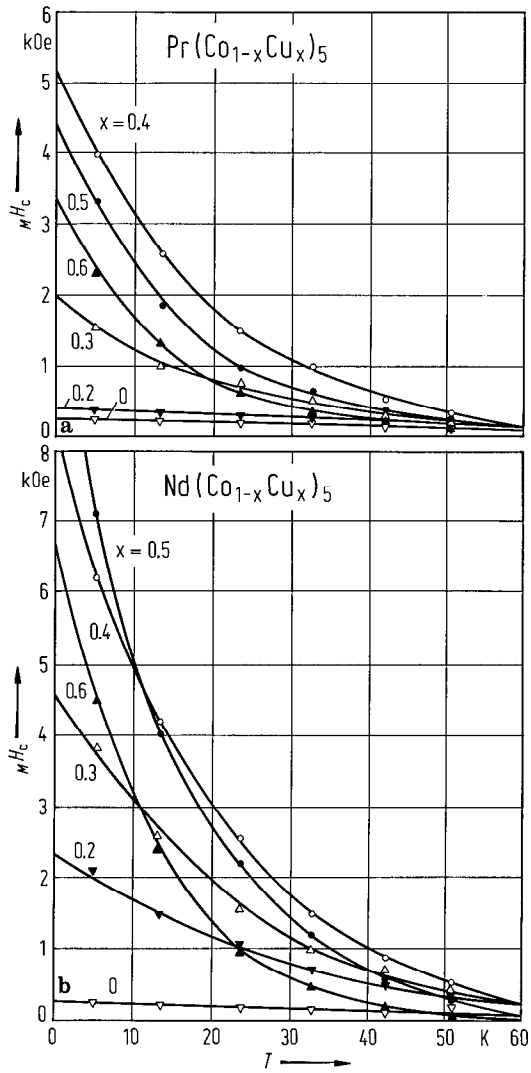

Fig. 438. Intrinsic coercive field, ${}_MH_c$, versus temperature in (a) $Pr(Co_{1-x}Cu_x)_5$ and (b) $Nd(Co_{1-x}Cu_x)_5$ compounds [79 M 1]. Compounds with $x \geqq 0.3$ have coercive fields greater than 5 kOe at low temperature, both in bulk single crystals and in powdered form. The coercive field increases steeply with decreasing temperature and the temperature dependence is stronger for larger x. The spin structure and energy of domain walls have been calculated using a discrete spin configuration model, and are found to be more sensitive to short-range fluctuations of the exchange interactions than to the anisotropy. Short-range exchange fluctuations can account for pinning fields of the same order of magnitude as the measured coercive fields. The exchange fluctuations may arise from fluctuations in the distributions of nonmagnetic Cu atoms in the compounds.

Table 103. Domain wall energy γ, exchange constant A, domain wall thickness δ, and single domain particle size d_c in some RCo_5 compounds at RT.

	γ erg cm^{-2}	A 10^{-6} erg cm^{-1}	δ Å	d_c µm	Ref.
$LaCo_5$	30				72 L 2
$CeCo_5$	25	1.3	65	0.92	72 L 2
	58				73 R 1
$PrCo_5$	40	1.1	35	0.61	72 L 2
	112				73 R 1
$NdCo_5$	30				72 L 2
$SmCo_5$	85	3.5	51	1.6	72 L 2
	150				73 R 1
	100 [1])				73 R 1
YCo_5	35	1.5	55	0.68	72 L 2

[1]) From basal-plane measurements.

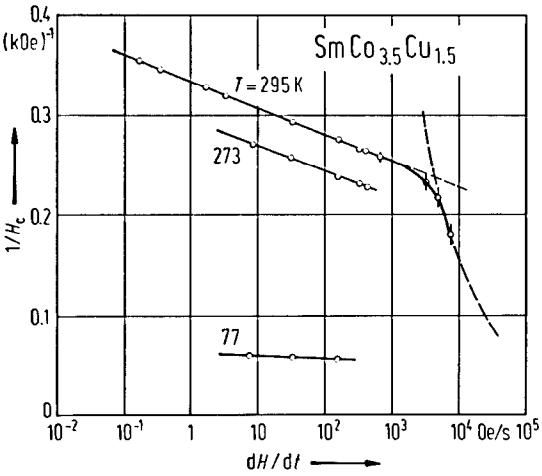

Fig. 439. Variation of reciprocal coercive field with logarithm of the sweep rate, in the range $10^{-2}\cdots10^{4}$ Oe/s, in $SmCo_{3.5}Cu_{1.5}$ single crystal at various temperatures. The reciprocal coercive field varies linearly with the logarithm of the sweep rate over a wide range, but lowers abruptly above a certain sweep rate. This suggests that the rate-controlling process of magnetization reversal changes from elementary nucleations on the parent domain walls to the domain growth resulting from wall motion [78 U 1].

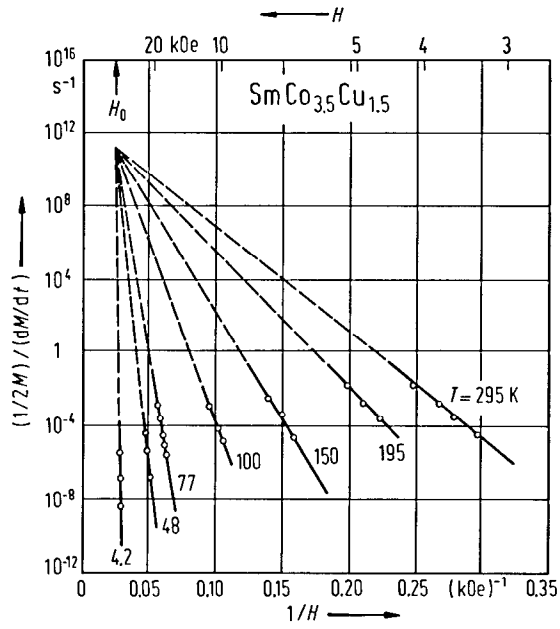

Fig. 440. Rate of magnetization variation in $SmCo_{3.5}Cu_{1.5}$ measured near the coercive field for several values of the applied magnetic field. The plot $\log(2M_s)^{-1}(dM/dt)$ vs. H^{-1} gives a convergent arrangement of straight lines. The intersection point is defined by $H_0 = 41.7$ kOe. The data suggest that the trapping effect of domain walls in Cu-rich regions is in competition with a kink creation mechanism [76 B 2].

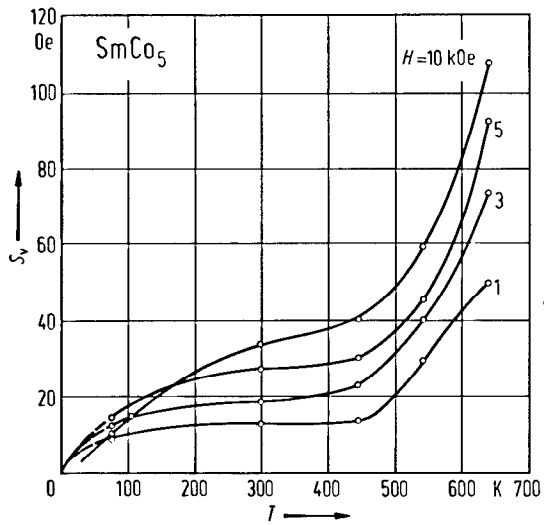

Fig. 441. Magnetic viscosity coefficient $S_v(T)$ for $SmCo_5$ powder samples (grain size 20···50 μm) measured at different external magnetic field strengths [74 H 1]. $S_v(T)$ is defined by the relation, $M(t) = M(0) + \chi_{irr} S_v(T) \ln t$, t in s, for the thermally activated magnetization relaxation, $M(t)$, after a sudden change of the external magnetic field. The irreversible susceptibility corresponding to the considered point on the hysteresis curve is denoted by χ_{irr}.

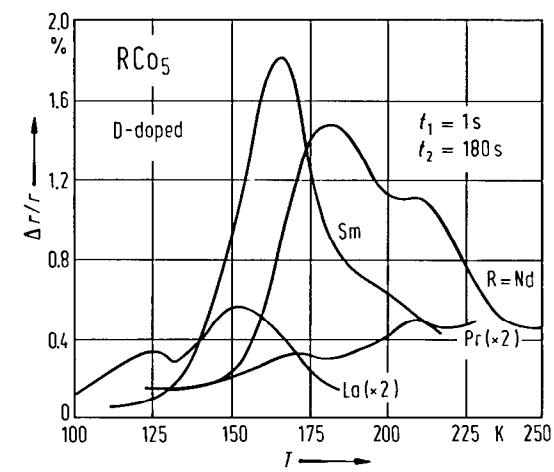

Fig. 442. Magnetic aftereffect spectra of some RCo_5 compounds (R = La, Pr, Nd, Sm) after deuterium charging [79 H 4]. $\Delta r/r$ denotes the relative change of the reciprocal initial magnetic susceptibility between times t_1 and t_2 of the relaxation process. The shape of the double peak relaxation spectrum can be quantitatively explained assuming that the hydrogen occupies two types of interstitial sites of orthorhombic symmetry. The relaxation process due to the transition within and between these configurations is described by two relaxation times which are related to the observed double peak spectrum.

For magnetization processes see

RM_5 [88 K 5]; R = Pr, Sm, M = Fe, Co [75 D 6]

RCo_5 [76 S 4, 70 S 5, 71 S 8, 72 H 2, 72 S 4, 73 B 5, 74 R 3, 74 S 5, 75 H 3, 76 E 3, 76 K 2, 76 N 6, 78 K 11]; R = Ce, Pr, Sm, Y [72 L 2]; R = Ce, Sm [76 A 4]; R = Pr, Nd, Sm [79 M 11]; R = Ce, Pr, Sm, Y [71 B 1]; R = La, Ce, Pr, Sm, Y [70 S 6]; R = Ce, Pr, Sm, Y [71 W 3]; R = Ce, Sm, Y [73 I 1]; R = Nd, Sm, Y [73 S 3]; R = Pr, Sm, Gd, Y [74 U 1]; R = Ce, Pr, Sm, Y [67 S 4]; R = La, Ce, Pr, Nd, Sm, Gd, Tb, Dy, Ho, Er, Th, Y [68 B 6]; R = Ce, Pr, Sm, Y [70 B 1]; R = La [70 M 4, 71 Z 1]; R = Ce [78 B 5]; R = Nd [70 L 5]; R = Pr [71 S 1, 71 T 4, 71 T 5, 73 L 4, 84 C 3, 84 W 1, 84 W 2]; R = Sm [68 B 2, 69 B 1, 69 B 8, 69 D 1, 69 W 2, 70 B 3, 70 M 1, 70 M 4, 70 S 7, 70 W 3, 70 Z 1, 70 Z 2, 71 B 7, 71 B 8, 71 M 3, 71 R 1, 71 U 2, 71 Z 1, 72 B 4, 72 B 7, 72 D 2, 72 J 1, 72 M 2, 72 M 3, 73 A 2, 73 D 6, 73 E 3*, 73 E 4, 73 G 3, 73 K 9, 73 K 14, 73 L 4, 73 M 5, 73 M 7, 73 S 4, 73 U 1, 74 D 2, 74 D 5*, 74 D 6*, 74 E 4, 74 G 2, 74 L 1, 75 M 4, 75 M 5, 75 E 5, 75 H 2, 75 K 2, 75 M 1, 75 P 1, 76 D 10, 76 H 3, 76 K 8, 76 T 3, 77 B 12, 77 G 1, 77 K 7, 77 N 2, 77 N 3, 78 B 5, 78 C 4, 78 K 5, 78 K 6, 78 K 13, 78 L 3, 78 S 21, 79 K 9, 79 M 6*, 79 S 4, 79 T 2, 80 B 17, 80 F 2, 80 S 2, 81 G 1, 81 I 4, 81 M 14, 82 B 6, 83 S 9, 84 B 6, 84 O 1, 84 S 18, 84 W 1, 85 A 3, 85 S 8, 86 T 1]; R = Gd [72 B 3, 72 D 2, 74 E 4, 73 E 3*, 75 K 2, 76 D 5, 76 K 5*, 78 U 3, 80 U 1*, 82 U 2*]; R = Tb [70 L 5]; R = Y [69 B 1, 71 B 8]; R = MM [75 N 1]

$(R'R'')Co_5$ $(LaSm)Co_5$ [71 M 1, 79 E 3]; $(CeSm)Co_5$ [71 M 1, 79 E 3]; (CeSm) $(CoCuFe)_5$ [71 N 4]; $(PrNd)Co_5$ [71 T 6]; $(PrSm)Co_5$ [71 M 1, 72 C 3, 73 C 2, 73 M 3, 77 E 6, 78 L 3, 85 G 5, 85 V 3]; $(NdSm)Co_5$ [73 S 4, 74 S 4, 75 F 3, 79 E 3, 79 Z 1]; $(NdY)Co_5$ [80 E 1]; $(SmGd)Co_5$ [75 D 7]; $(SmTb)Co_5$ [75 D 7]; $(SmDy)Co_5$ [75 D 7]; $(SmEr)Co_5$ [75 D 7]; $(SmY)Co_5$ [79 E 3]; $(SmMM)Co_5$ [71 M 1, 77 B 1]; $(SmPrNd)Co_5$ [85 V 3]; $(SmErGd)Co_5$ [82 S 16]; $(SmRGd)Co_5$, R = Tb, Dy, Ho, Tm [83 P 15]; $(GdY)Co_5$ [80 E 1]; $(TbY)Co_5$ [80 E 1]

$R(M'M'')_5$ $Sm(FeCo)_5$ [73 B 20, 86 C 3]; $Y(FeCo)_5$ [74 G 2]; $R(CoCuFe)_5$ [72 S 4]; $Ce(CoCuFe)_5$ [71 N 4]; $Sm(CoCuFe)_5$ [69 N 1, 71 R 5]; $R(FeNi)_5$ [78 O 5]

$R(CoM)_5$, R = La, Sm, M = Ni, Cu, Al [83 F 1, 83 F 2]; R = Ni, Al, Si [84 F 1]; $R(CoNi)_5$ [76 E 5]; R = Ce, La, Gd, Sm, Y, Th [78 E 2]; R = La, Ce, Gd, Y [77 E 4]; R = La, Ce, Sm, Gd, Y [77 E 7*]; $La(CoNi)_5$ [75 B 8, 75 B 15, 76 O 7, 83 P 5]; $Sm(CoNi)_5$ [70 O 1, 75 E 4, 75 P 2, 76 O 3, 77 O 6, 78 F 8, 78 O 3, 78 O 4, 83 P 5]; $Gd(CoNi)_5$ [70 O 1, 80 O 3]; $Er(CoNi)_5$ [78 O 1]; $Y(CoNi)_5$ [76 B 19, 76 B 20, 76 O 7]; $Th(CoNi)_5$ [75 B 8, 75 B 13, 75 B 15, 75 N 3]

$R(CoCu)_5$ [76 B 6]; R = Pr, Nd [79 M 1]; $La(CoCu)_5$ [77 B 23]; $Ce(CoCu)_5$ [69 N 1]; $Pr(CoCu)_5$ [73 M 2, 79 M 2]; $Sm(CoCu)_5$ [68 N 2, 69 N 1, 70 H 1, 70 U 1, 73 K 2, 73 K 3, 76 B 2, 76 B 19, 76 O 6, 77 P 6, 77 U 1, 78 F 8, 78 U 1, 78 U 2, 79 O 2, 83 A 7, 83 U 1, 86 U 1, 86 U 2]; $Er(CoCu)_5$ [83 D 7]; $Y(CoCu)_5$ [77 B 23]; $Pr(CoAl)_5$ [74 O 3]; $Sm(CoAl)_5$ [74 O 1, 75 O 2]

$SmNi_4M$, M = Fe, Cu, Al [77 O 7]; $Sm(NiCu)_5$ [78 O 2]

For domain structure see

RM_5 [88 K 5]

RCo_5 [72 H 2, 73 F 3, 74 R 3, 76 H 2, 76 W 2]; R = Ce, Pr, Sm, Y [71 B 1, 71 B 2, 71 W 3, 72 L 2]; R = La, Ce, Sm [70 M 3]; R = Ce, Pr, Sm [73 R 1]; R = Nd [73 E 5]; R = Sm [71 B 3, 72 K 1, 72 W 1, 73 E 3*, 73 G 3, 73 L 3, 73 R 4, 74 C 4, 74 K 1, 75 C 6, 75 K 2, 75 M 4, 77 B 12, 77 F 2, 79 F 4*, 80 F 2, 81 F 3, 81 G 1, 81 M 14, 84 O 1, 85 A 3, 85 S 8]; R = Gd [73 E 3*, 75 K 2]; R = Y [85 P 9]

$(R'R'')Co_5$ $(SmPr)Co_5$ [74 S 7, 75 S 5, 77 P 7]

$R(M'M'')_5$ $Sm(CoCu)_5$ [77 U 1, 78 K 9, 78 P 3, 78 S 14, 86 M 2]; $Sm(CoFeCuZr)_{6.95}$ [81 F 3]; $Sm(CoAl)_5$ [74 O 4]

For magnetic aftereffect see

RCo_5 R = La, Pr, Nd, Sm [79 H 4]; R = Ce [74 R 6]; R = Sm [73 E 1(T), 74 H 1, 79 H 5, 80 G 1, 84 S 17, 85 S 23]

RCo_5H_x R = La, Pr, Nd, Sm [79 H 4]; R = Nd [73 M 4]

$R(M'M'')_5$ $Sm(CoNi)_5$ [77 E 5]; $Sm(CoCu)_5$ [73 S 2]

For magnetic viscosity see

RCo_5 R = Ce [76 G 1]; R = Sm [73 H 1]

Transport properties

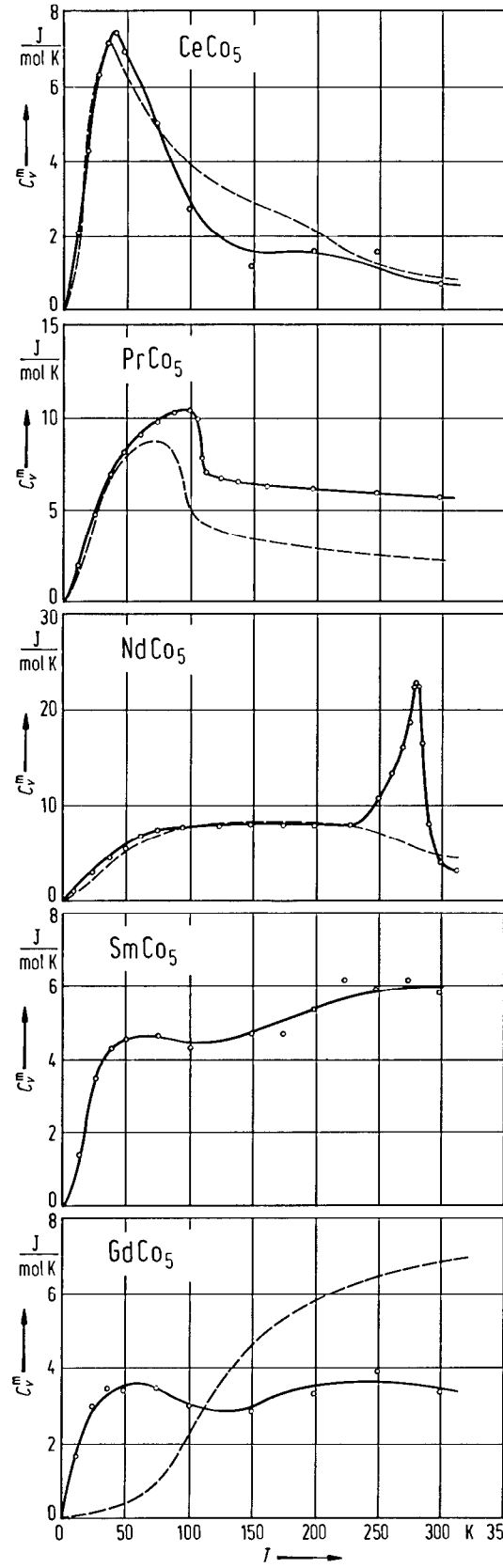

Fig. 443. Temperature dependence of the magnetic part of the specific heat, C_V^m, in some RCo_5 (R = Ce, Pr, Nd, Sm and Gd) compounds [74 K 5]. The C_V^m values were obtained by substracting from C_V the heat capacity of $LaNi_5$. From these data crystal field parameters were determined, Table 101. The calculated C_V^m values are plotted by dashed lines.

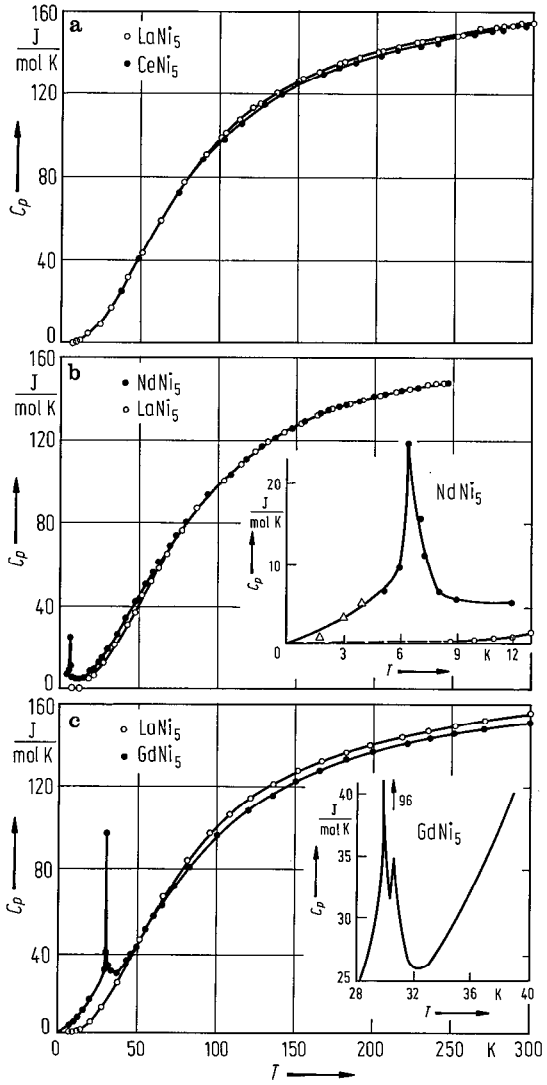

Fig. 444. Thermal variation of the heat capacity for (a) $LaNi_5$, $CeNi_5$, (b) $NdNi_5$, and (c) $GdNi_5$ [73 M 6]. The C_p values of $CeNi_5$ ($T \geqq 4$ K), close resemble those of the Pauli paramagnet $LaNi_5$. $NdNi_5$ exhibits a λ-type thermal anomaly peaking at 6.4 K, which is ascribed to the break-up of ferromagnetism. It also shows excess heat capacity at higher temperatures resulting from excitations in the crystal field spectrum. Results for $GdNi_5$ are unusual. Magnetic entropy is introduced over an anomalously wide range of temperatures. The process culminates in two λ-type thermal anomalies peaking at 29.8 and 30.6 K, suggesting that the development of the cooperative phase occurs in two stages. Magnetic entropies of $NdNi_5$ and $GdNi_5$ at 300 K are observed to be 95 and 86%, respectively, of $R \ln(2J+1)$. Triangles in the inset of (b) represent data of [71 N 3].

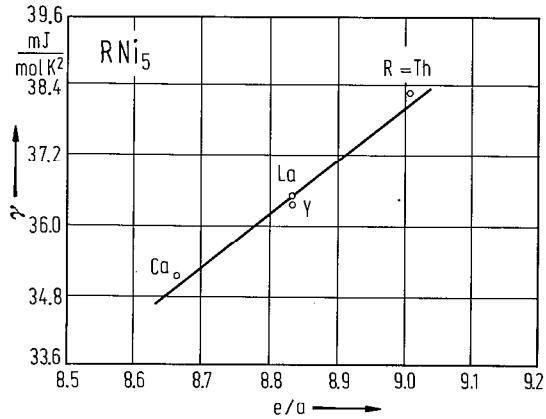

Fig. 446. Plot of electronic specific heat constant γ as function of electron concentration, e/a, for $CaNi_5$, YNi_5, $LaNi_5$ and $ThNi_5$ compounds [80 T 2]. The γ values are nearly the same (the difference between the lowest and largest value being smaller than 9%), but they show a linear variation with electron concentration.

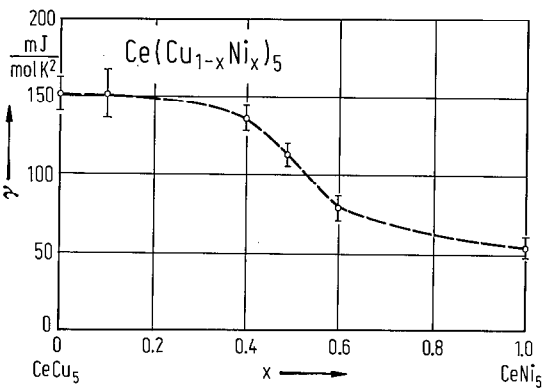

Fig. 447. Composition dependence of the electronic specific heat coefficient γ in $Ce(Cu_{1-x}Ni_x)_5$ compounds [85 G 16]. A decrease of the electron density of states at the Fermi level becomes relevant for the transition from concentrated Kondo system to intermediate valence state for $0.4 < x < 0.6$.

For Fig. 445, see next page.

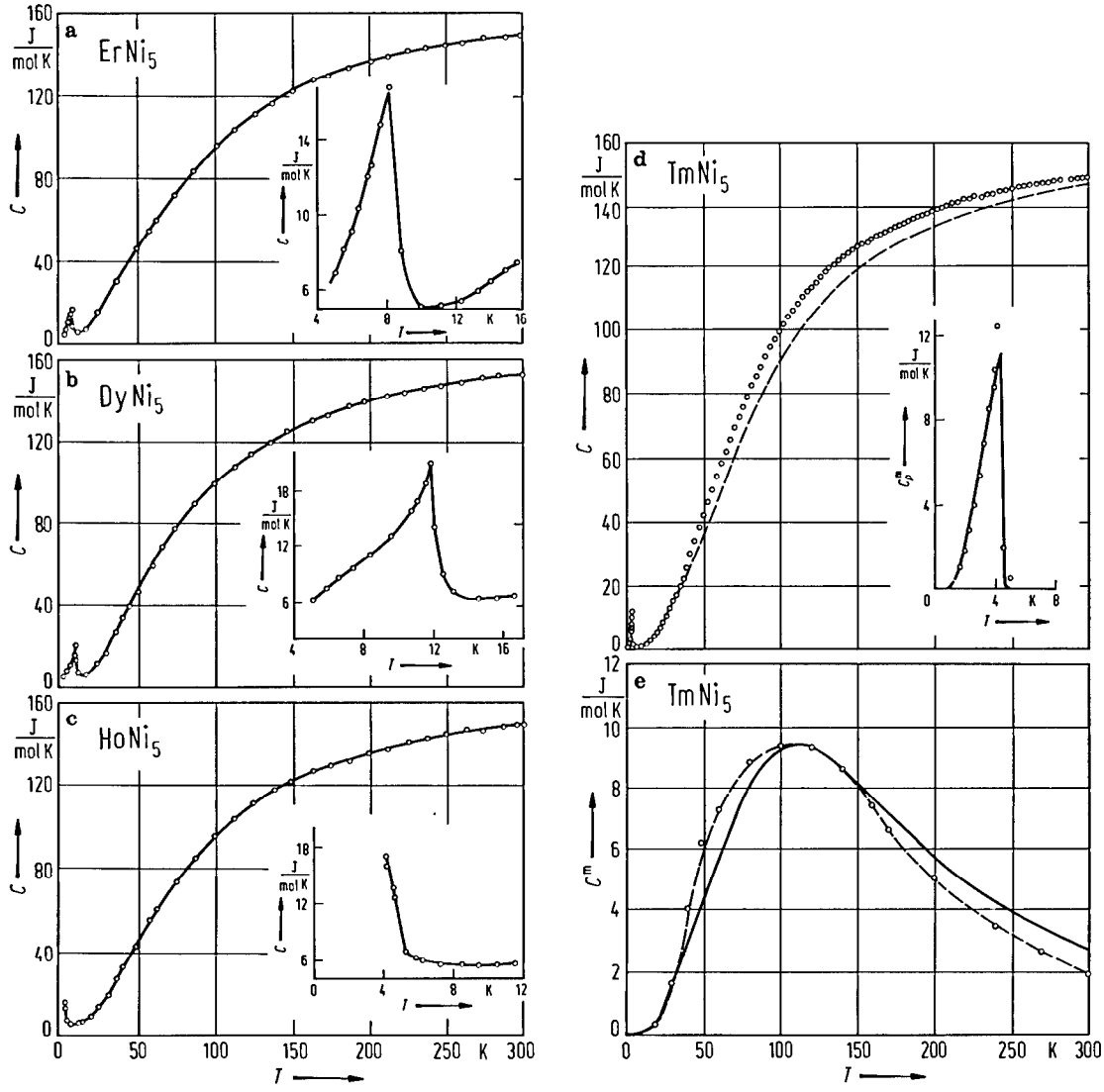

Fig. 445. Thermal variation of the heat capacity in (a) $ErNi_5$, (b) $DyNi_5$ and (c) $HoNi_5$ compounds [73 S 1]. Typical λ-type anomalies are shown at temperatures between 4 and 12 K. These are attributed to the onset of magnetic ordering. (d) $TmNi_5$ [82 G 2] showing experimental data (open circles) as well as lattice and electronic contributions (dashed line) to the heat capacity. As evidenced in the insert a λ-type anomaly is observed at T_C. A large magnetic contribution to the specific heat is evidenced above T_C. As shown in (e) this contribution corresponds to a strong Schottky anomaly [82 G 2]. Solid lines in (d) and (e) correspond to calculations.

Table 104. Data obtained from specific heat measurements on RNi_5 compounds [71 N 3].

	γ mJ K^{-2} mol^{-1}	β mJ K^{-4} mol^{-1}	$\eta(E_F)$ eV^{-1} atom^{-1}	Θ_D K
$LaNi_5$	34.33(13)	0.299(14)	2.43	340.9
$CeNi_5$	40.01(11)	0.279(12)	2.83	347.1
$PrNi_5$	37.02(16)	0.309(17)	2.64	333.5

See also [80 T 2].

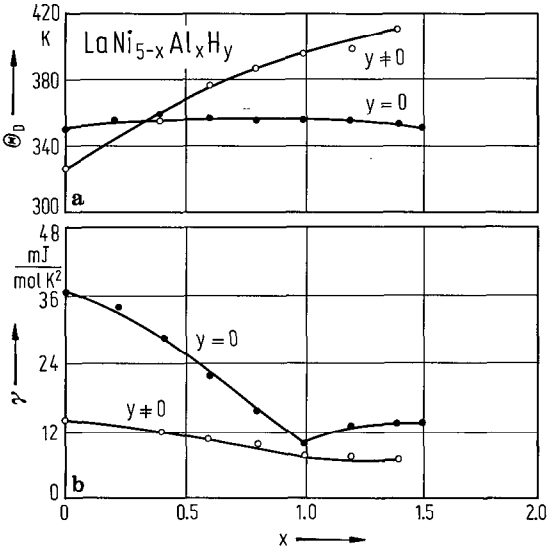

Fig. 448. Electronic specific heat coefficient γ and the Debye temperature Θ_D versus Al concentration in $LaNi_{5-x}Al_x$ system before (solid circles) and after (open circles) hydrogenation [80 C 4]. The γ values in the $LaNi_{5-x}Pt_x$ system decrease in a smooth fashion as the Ni content increases. The $La_{1-x}Th_xNi_5$ alloys only exhibit a slight change in the electronic specific heat coefficient [80 C 4].

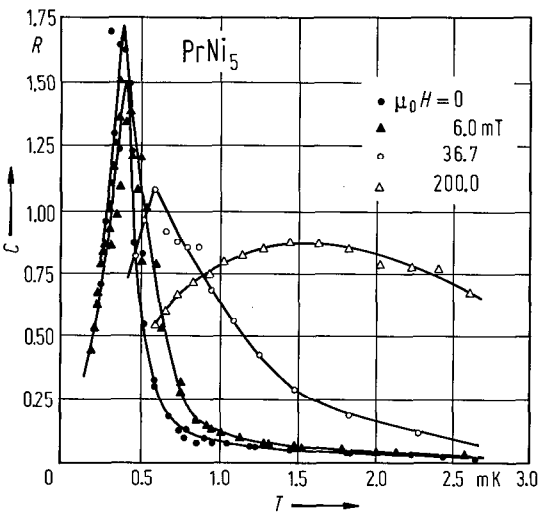

Fig. 449. Low-temperature part of the nuclear specific heat per mole of $PrNi_5$ measured in the indicated magnetic fields. A spontaneous nuclear ordering in zero field of ^{141}Pr occurs at 0.40(2) mK [75 A 1, 80 K 16].

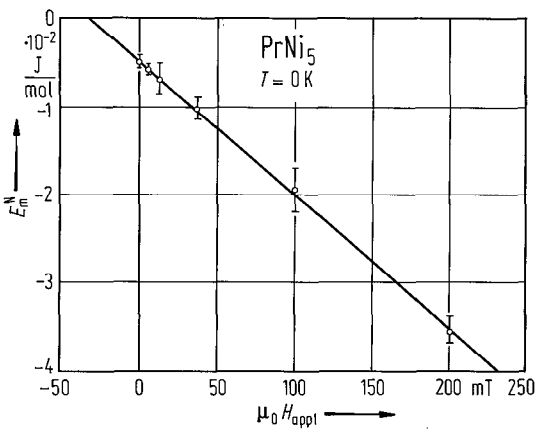

Fig. 450. Nuclear magnetic energy of $PrNi_5$ at $T=0$ K obtained by integrating its specific heat as a function of applied magnetic field [80 K 16]. The data indicate that an internal field of $\mu_0 H_i = 66(10)$ mT adds linearly to the applied field and that the order is ferromagnetic. The enhanced nuclear magnetic moment is 0.027(4) μ_B, and the nuclear exchange parameter is $\sum_j J_{ij}^N/k_B = 0.20(4)$ mK.

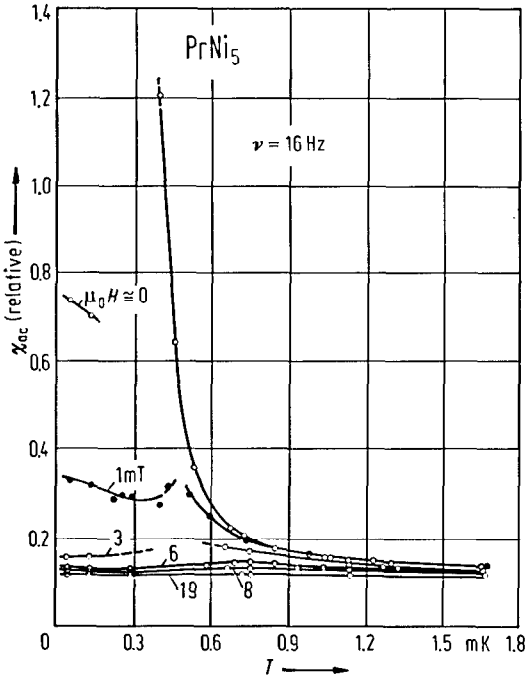

Fig. 451. ac susceptibility, χ, of $PrNi_5$ at 16 Hz as function of temperature in different static magnetic fields [83 K 4]. The lowest two lines are for 8 and 19 mT, respectively. The observed behaviour is similar to that expected for a nuclear ferromagnet with $T_C = 0.40$ mK. The ac susceptibility changes drastically even in fields which are much smaller than the exchange field of 65 mT for $T = 0$, or of 18 mT for $T \gg T_C$. The application of a field seems to shift the apparent paramagnetic Curie temperature, Θ_{ac}, to substantially lower values. For example, measurements at 16 Hz in zero field yield the same Θ value as dc measurements, $\Theta_{ac} = \Theta_{dc} = 0.42$ mK. In 6 mT, $\Theta_{ac} = -0.02(10)$ mK, whereas $\Theta_{dc} = 0.35(7)$ mK. See also [80 M 11, 81 K 17].

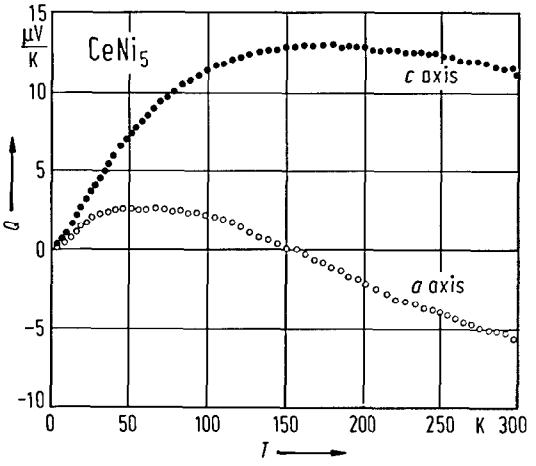

Fig. 452. Thermoelectric power, Q, of $CeNi_5$ single crystal along a and c axes [87 S 3]. The Q values along the a axis have a flat maximum of 3 μV/K at 40···80 K, change the sign at 150 K and keep decreasing up to 300 K, while Q along the c axis has a maximum of 13 μV/K at 150···200 K and stays positive up to 300 K. The average for the three main crystallographic axes is found to be near that of polycrystalline data [84 C 1].

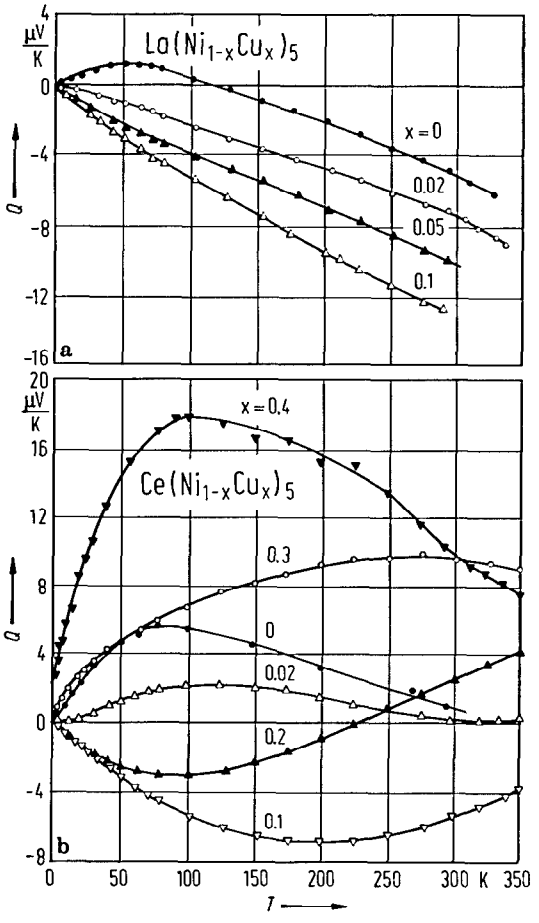

Fig. 453. Thermoelectric power (TEP) of (a) $La(Ni_{1-x}Cu_x)_5$ and (b) $Ce(Ni_{1-x}Cu_x)_5$ systems as function of temperature [84 C 1]. The thermopower anomaly observed in mixed-valent $CeNi_5$ is dominated by conduction-electron scattering from Ni-derived 3d states. The temperature shift of the anomaly by increasing La content in $(LaCe)Ni_5$ reflects composition-induced changes in the Ni-derived 3d-band structure and a giant mixed-valent TEP anomaly develops below 300 K as the 4f stability is increased by substituting Ni by Cu.

For specific heat measurements see

RCo_5 [78 T 3]; R = Ce, Pr, Nd, Sm, Gd [74 K 5]; R = Nd [77 O 8]; R = Sm [78 Z 2]; R = Dy [61 S 1]

RNi_5 R = La, Ce, Pr, Nd, Gd [71 N 3]; R = La, Ce, Nd, Gd [73 M 6]; R = La, Y, Th, Ca [80 T 2]; R = La [80 O 5, 82 S 1, 85 G 15]; R = Pr [72 C 8, 75 A 1, 79 R 5, 80 K 16, 81 K 17, 82 S 1, 87 R 1]; R = Nd [85 G 15]; R = Gd [70 W 2]; R = Dy [73 S 1, 74 B 4, 74 S 1]; R = Ho [73 S 1, 74 B 4, 74 S 1]; R = Er [73 S 1, 74 B 4, 74 S 1]; R = Tm [82 G 2]

RNi_5H_x R = La [80 O 4, 80 O 5]

$(R'R'')M_5$ $(LaTh)Ni_5$ [80 C 4]; $(LaTh)Ni_5H_x$ [80 C 4]

$R(M'M'')_5$ $La(NiCu)_5$ [80 T 1]; $Ce(NiCu)_5$ [85 A 7, 85 G 16, 86 G 3]; $La(NiAl)_5$ [80 C 4]; $Y(NiAl)_5$ [80 T 1]; $Th(NiAl)_5$ [79 G 12, 80 T 1]; $La(NiPt)_5$ [80 C 4]
$La(NiAl)_5H_x$ [80 C 4]

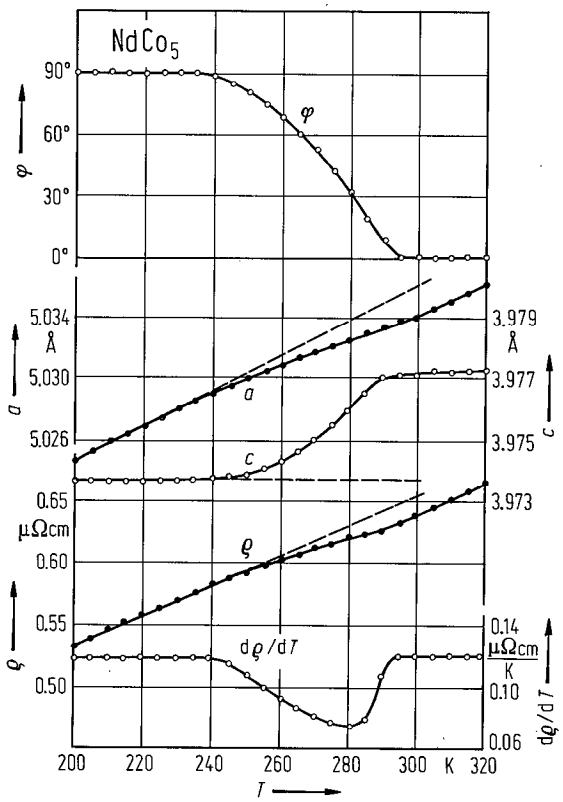

Fig. 454. Electrical resistivity along the c axis, ϱ, temperature coefficient of electrical resistivity, $d\varrho/dT$, angle φ between the easy axis of magnetization and the c axis, and lattice parameters a and c as function of temperature for $NdCo_5$ compound [82 A 13]. The magnetostrictive constants determined in the center of spin reorientation temperature range are $\lambda_2^{\varepsilon,2} = 8 \cdot 10^{-4}$ and $\lambda_1^{\varepsilon,2} = -3 \cdot 10^{-4}$. The lack of orthorhombic distortion of the $NdCo_5$ shows that $\lambda^{\gamma,2} < 10^{-4}$ at all temperatures. The temperature coefficient of the electrical resistivity ϱ along the c axis is constant below and above the spin reorientation temperature. This suggests that the anisotropy of the interaction between the conduction electrons and the magnetic moments is small.

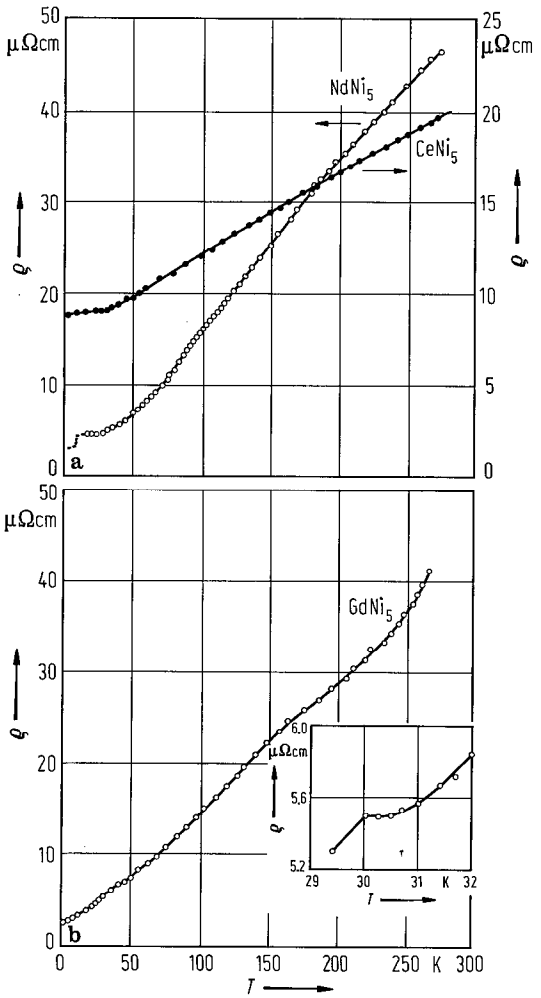

Fig. 455. Temperature dependence of the electrical resistivity in (a) $CeNi_5$, $NdNi_5$ and (b) $GdNi_5$ compounds [73 M 6]. The magnetic transitions are evidenced in $NdNi_5$ and $GdNi_5$, the loss of the spin-disorder resistivity being readily apparent in the former material.

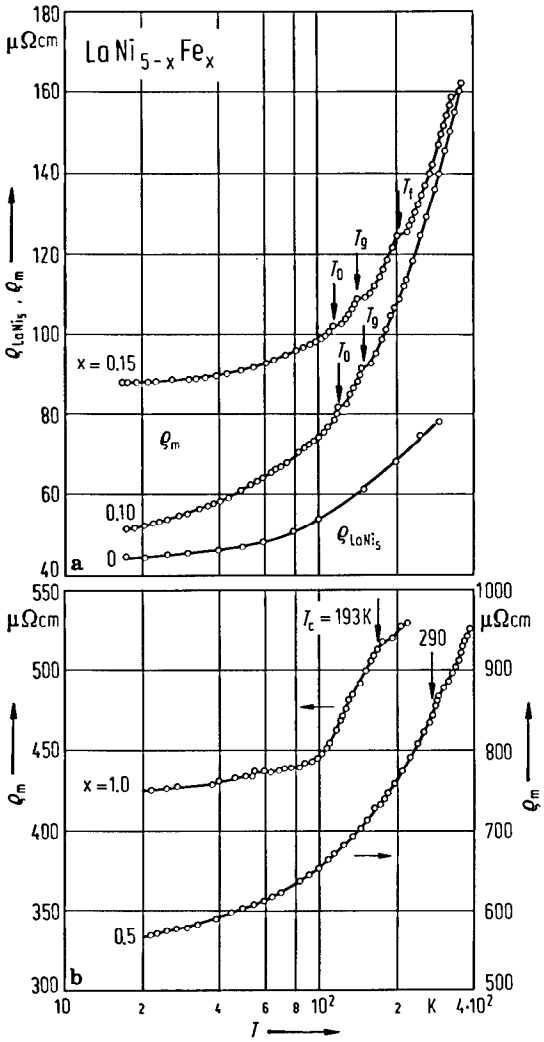

Fig. 457. (a) Electrical resistivities in $LaNi_{5-x}Fe_x$ compounds. x = 0: resistivity vs. T curve, ϱ_{LaNi_5}, of $LaNi_5$, which represents the phonon contribution to the variations of $\varrho(x \neq 0)$. For $x \neq 0$, $\varrho_m = \varrho - \varrho_{LaNi_5}$, has been plotted as function of temperature. This gives the magnetic contributions to the resistivities. The temperatures T_0, T_g and T_f (see Figs. 385 and 386) were indicated. (b) Magnetic part of the resistivity, ϱ_m, as function of temperature for large Fe content. The Curie temperatures, evidenced by a sharp drop of electrical resistivity, are marked by arrows [87 E 6].

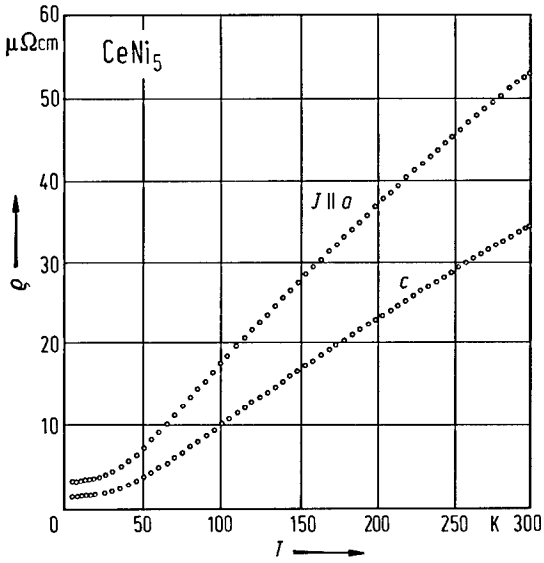

Fig. 456. Thermal variations of the electrical resistivity of $CeNi_5$ measured along the a and c directions. At very low temperatures it has a BT^2 dependence, the B coefficient being $7 \cdot 10^{-10}\,\Omega\,cm\,K^{-2}$ along c, and $11 \cdot 10^{-10}\,\Omega\,cm\,K^{-2}$ along a. The residual resistivities are $1.4 \cdot 10^{-6}$ and $3.2 \cdot 10^{-6}\,\Omega\,cm$, respectively [82 G 5].

For electrical resistivity see also
RCo_5 R = Nd [82 A 13]
RNi_5 R = La, Ce, Nd, Gd [73 M 6]; R = La [85 A 2]; R = Ce [82 G 5, 85 G 6, 87 S 3]; R = Pr [72 C 8, 84 R 1, 87 L 5]; R = Sm [88 B 1*]; R = Gd [78 R 3]; R = Y [85 G 6]
RM_5H_x $LaCo_5H_x$, $SmCo_5H_x$ [85 S 2]; $LaNi_5H_x$ [85 A 2, 85 S 2]
$(R'R'')M_5$ $(CeLa)Ni_5$ [84 C 1]
$R(M'M'')_5$ $La(NiFe)_5$ [87 E 6, 88 E 1]; $La(NiCu)_5$ [84 C 1]; $Ce(NiCu)_5$ [84 B 7, 84 C 1]; $Ce(NiGa)_5$ [87 K 10]

For thermopower studies see also
$CeNi_5$ [87 S 3]
$(CeLa)Ni_5$ [84 C 1]
$La(NiCu)_5$ [84 C 1]; $Ce(MnM)_5$, M = Ge, Al [88 K 4]; $Ce(NiCu)_5$ [84 B 7, 84 C 1, 84 L 8]; $Ce(NiGa)_5$ [87 K 10]

Spectroscopic studies

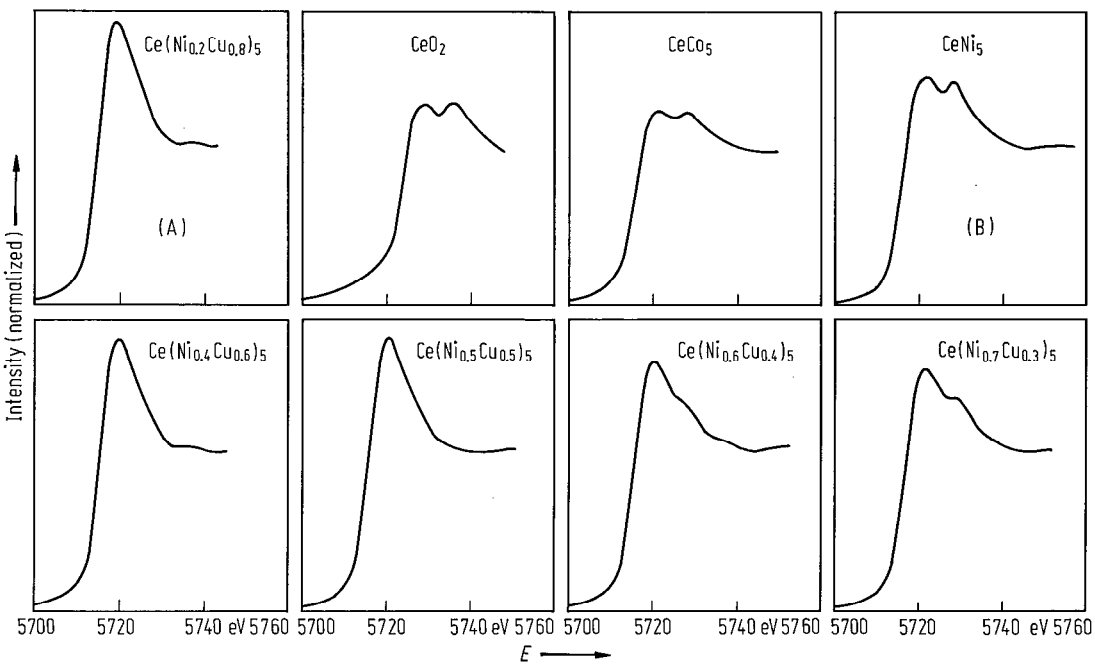

Fig. 458. L_{III} absorption edges for Ce in $CeNi_5$, $CeCo_5$, CeO_2 and some $Ce(Ni_{1-x}Cu_x)_5$ alloys at room temperature [82 G 5]. These show that in $CeCo_5$ and $CeNi_5$, Ce has the same valence state, close to 4+, as in the insulator CeO_2. In $Ce(Ni_{1-x}Cu_x)_5$ compounds for Cu content ranging from x = 0.8 to 0.3, the shape of the absorption edge changes gradually from that characteristic of the trivalent state (A) to that characteristic of the almost tetravalent state (B). For valence state of Ce and Yb in intermetallic compounds see also [79 D 2, 81 K 16].

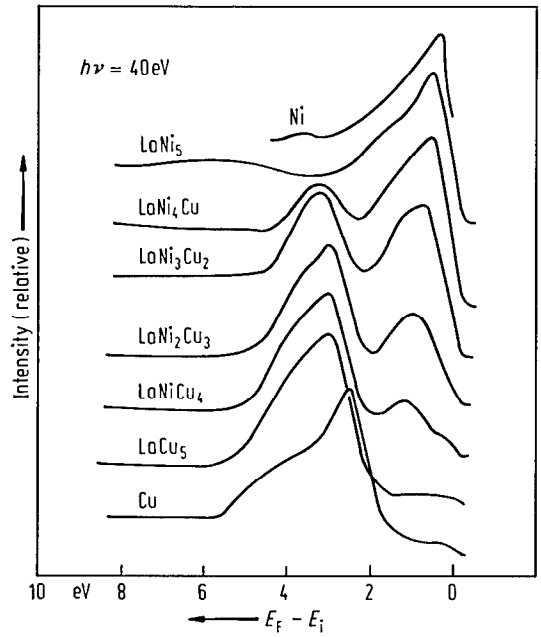

Fig. 459. Photoemission spectra for Ni, $LaNi_5$, $LaNi_{5-x}Cu_x$, $LaCu_5$ and Cu [82 W 2]. The band in $LaNi_5$ closely resembles that of elemental Ni and the d-band in $LaCu_5$ closely resembles that of elemental Cu. The APW calculations [82 M 1] for $LaNi_5$ revealed good agreement with the above data. The density of states in $LaNi_5$ and $LaNi_5H_7$ were analysed in [87 G 11]. E_i is the initial-state energy.

For spectroscopic studies see

L_{III} absorption spectra

RCo_5 R = Nd, Sm, Gd [76 S 5]; R = Tb, Dy, Ho, Er [76 S 6]; R = Pr, Sm [77 S 2]; R = Tm, Y [77 S 3]; R = Ce [82 F 9, 82 G 5, 83 F 4]; R = Pr [82 F 9]

RFe_5 R = Ce [83 F 4]

RNi_5 R = Ce [82 G 5, 83 F 4]

$(R'R'')Ni_5$ $R_{0.9}Ce_{0.1}Ni_5$, R = La, Pr, Gd, Er, Lu [83 R 1]

$R(M'M'')_5$ $Ce(NiCu)_5$ [82 G 5]

Photoemission spectroscopy

$CeCo_5$ [81 K 16]; $SmCo_5$ [77 S 7]; $LaNi_5$ [81 S 2]; $CeNi_5$ [81 K 16]

$LaNi_5H_x$ [78 S 15, 82 W 7]

$(CaEu)Ni_5H_x$ [84 S 7]; $La(NiMn)_5$ [87 L 3]; $La(NiCu)_5$ [82 W 2]

X-ray absorption spectroscopy

$DyCo_5$ [80 H 7]; $CeNi_5$ [86 H 4]

Electron energy loss spectra

$SmCo_5$ [87 C 2]

Photoelectron spectroscopy

$LaNi_5$, $LaNi_5Ti_{0.1}$, $LaNi_5Zr_{0.1}$ [80 W 2]; $LaNi_5H_x$, $La(NiAl)_5H_x$ [87 B 11]; $(CaEu)Ni_5H_x$ [84 S 7]

Auger electron spectroscopy

$(CaEu)Ni_5H_x$ [84 S 7]; $La(NiM)_5$ [87 L 3]

Microcontact spectra

$PrNi_5$ [84 A 3*, 84 A 4*, 84 A 5*]

2.4.2.18 R_2M_{17} compounds

Structure, lattice parameters

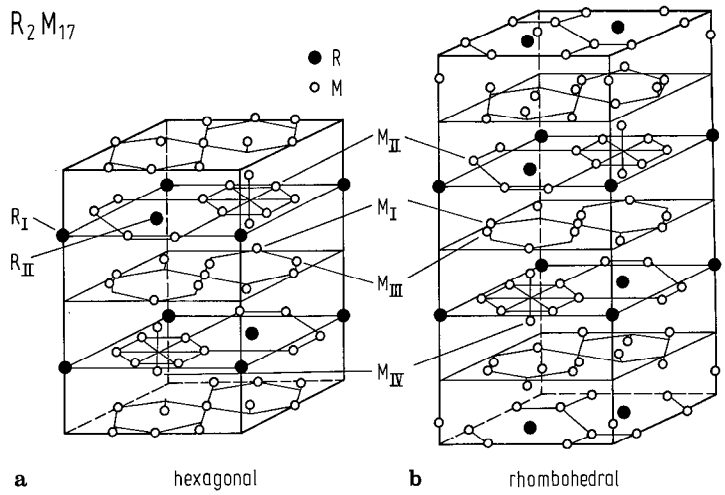

Fig. 460. Crystal structure of R_2M_{17} compounds: (a) hexagonal structure (Th_2Ni_{17}-type) having $P6_3/mmc$ space group (b) rhombohedral structure (Th_2Zn_{17}-type) having $R\bar{3}m$ space group. A $TbCu_7$-type structure was also evidenced, Table 105.

Table 105a. Atomic sites in R_2M_{17}-type compounds, hexagonal structure (Th_2Ni_{17}-type) having $P6_3/mmc$-space group [56 F 1, 56 M 1, 66 B 3].

Atom	Site	Coordinates
R_I	2b	$\pm(0,0,1/4)$
R_{II}	2d	$\pm(1/3, 2/3, 3/4)$
M_I	6g	$\pm(1/2, 0, 0; 0, 1/2, 0; 1/2, 1/2, 0; 1/2, 0, 1/2; 0, 1/2, 1/2; 1/2, 1/2, 1/2)$
M_{II}	12j	$\pm(x, y, 1/4; \bar{y}, x-y, 1/4; y-x, \bar{x}, 1/4; \bar{y}, \bar{x}, 1/4; x, x-y, 1/4; y-x, y, 1/4)$; $x=1/3$; $y=0.968$
M_{III}	12k	$\pm(x, 2x, z; 2\bar{x}, \bar{x}, z; x, \bar{x}, z; \bar{x}, 2\bar{x}, 1/2+z; 2x, x, 1/2+\bar{z}; \bar{x}, x, 1/2+z)$; $x=1/6$; $z=0.984$
M_{IV}	4f	$\pm(1/3, 2/3, z; 2/3, 1/3, 1/2+z)$; $z=0.109$

Table 105b. Atomic sites in R_2M_{17}-type compounds, rhombohedral structure (Th_2Zn_{17}-type) having $R\bar{3}m$-space group.

Atom	Site	Coordinates
R	6c	$\pm(0, 0, z)$; $z=1/3$
M_I	9d	$\pm(1/2, 0, 1/2; 0, 1/2, 1/2; 1/2, 1/2, 1/2)$
M_{II}	18f	$\pm(x, 0, 0; 0, x, 0; x, x, 0)$; $x=0.283$
M_{III}	18h	$\pm(x, x, z; x, 2x, z; 2\bar{x}, \bar{x}, z)$; $x=1/2$, $z=0.148$
M_{IV}	6c	$\pm(0, 0, z)$; $z=0.094$

In addition the following translations (0, 0, 0); (2/3, 1/3, 1/3), (1/3, 2/3, 2/3).

For $TbCu_7$-type structure having P6/mmm-space group [71 B 22] see subsect. 2.4.2.17, Table 84 ($s=2/9$).

Table 106a. Lattice parameters (Å) of R_2Fe_{17} compounds having Th_2Ni_{17}-type structure (hexagonal).

	66 B 4		68 R 1		69 G 1		70 B 14		71 M 6		72 B 16		72 G 7		77 O 5		86 S 17*	
	a	*c*	*a*	*c*	*a*	*c*	*a*	*c*	*a*	*c*	*a*	*c*	*a*	*c*	*a*	*c*	*a*	*c*
Ce_2Fe_{17}							8.490	8.281										
Gd_2Fe_{17}	8.486	8.349			8.496	8.343												
Tb_2Fe_{17}	8.467	8.309	8.473	8.323														
Dy_2Fe_{17}	8.444	8.310	8.467	8.312											8.455	8.309		
Ho_2Fe_{17}	8.434	8.284	8.460	8.277					8.438	8.310							8.44	8.31
Er_2Fe_{17}	8.423	8.284	8.435	8.281														
Tm_2Fe_{17}			8.406	8.291														
Yb_2Fe_{17}											8.414	8.249						
Lu_2Fe_{17}			8.401	8.272	8.386	8.279							8.401	8.266				
Y_2Fe_{17}	8.463	8.282	8.466	8.300	8.461	8.299												

Table 106b. Lattice parameters (Å) of R_2Fe_{17} compounds having Th_2Zn_{17}-type structure (rhombohedral).

	63 K 1		66 B 4		65 K 2		66 R 1		68 J 1		70 B 14	
	a	*c*	*a*	*c*	*a*	*c*	*a*	*c*	*a*	*c*	*a*	*c*
Ce_2Fe_{17}							8.488	12.402			8.490	12.416
Pr_2Fe_{17}					8.58	12.47	8.582	12.462	8.585	12.464		
Nd_2Fe_{17}							8.578	12.462				
Sm_2Fe_{17}							8.554	12.441				
Gd_2Fe_{17}	8.55	12.40	8.517	12.429			8.538	12.431				
Tb_2Fe_{17}			8.49	12.42	8.54	12.43						
Y_2Fe_{17}			8.46	12.41								

Table 106c. Lattice parameters (Å) of R_2Co_{17} compounds having Th_2Ni_{17}-type structure (hexagonal) [1]).

	66 B 4, 77 b 1		66 O 2		66 L 4		71 G 1, 71 G 2		72 B 16		73 K 4		81 M 8		86 S 18	
	a	*c*	*a*	*c*	*a*	*c*	*a*	*c*	*a*	*c*	*a*	*c*	*a*	*c*	*a*	*c*
Ce_2Co_{17}	8.371	8.136	8.335(2)	8.104(4)	8.3779	8.1339					8.3779	8.1339				
Sm_2Co_{17}	8.360	8.515			8.384	8.159										
Gd_2Co_{17}	8.351	8.125			8.373	8.134					8.378	8.139				
Tb_2Co_{17}	8.348	8.125			8.347	8.127										
Dy_2Co_{17}	8.328	8.125	8.335(2)	8.102(3)	8.356	8.113					8.3614	8.117			8.357	8.117
Ho_2Co_{17}	8.320	8.113	8.335(2)	8.101(3)	8.331	8.117					8.3315	8.1339			8.331	8.131
Er_2Co_{17}	8.310	8.113	8.301(2)	8.100(3)	8.317	8.125					8.3126	8.1306	8.302	8.103	8.310	8.135
Tm_2Co_{17}			8.285(2)	8.095(3)	8.298	8.131							8.285	8.095		
Yb_2Co_{17}									8.309	8.096			8.271	8.089		
Lu_2Co_{17}			8.247(2)	8.093(3)			8.29	8.12								
Y_2Co_{17}	8.341	8.125			8.356	8.123	8.25	8.14			8.355	8.128				

[1]) The hexagonal Th_2Ni_{17}-type intermetallic compounds close to R_2M_{17} stoichiometry in Er–Co and Y–Ni systems do not exist but in an ideal case. Substitutions must occur on all R rows parallel to the *c* axis with subsequent displacements of the M atoms. This leads to a nonstoichiometric composition, e.g. $RM_{9.5}$ [72 G 7]. In Lu–Fe system the stoichiometry shifts from $LuFe_{8.5}$ to $LuFe_{9.5}$ [72 G 8].

Table 106d. Lattice parameters (Å) of R_2Co_{17} compounds having Th_2Zn_{17}-type structure (rhombohedral).

	66 B 3		66 B 4		66 O 2		73 K 4		76 K 3		81 M 8		86 S 18	
	a	*c*	*a*	*c*	*a*	*c*	*a*	*c*	*a*	*c*	*a*	*c*	*a*	*c*
Ce_2Co_{17}	8.368	12.204	8.370	12.193	8.335(2)	12.153(4)	8.378	12.206						
Pr_2Co_{17}	8.438	12.253	8.427	12.265	8.415(2)	12.170(4)	8.4419	12.2605			8.432	12.333		
Nd_2Co_{17}	8.422	12.246	8.407	12.257	8.441(2)	12.181(4)	8.4279	12.2433						
Sm_2Co_{17}	8.385	12.214	8.379	12.212	8.402(2)	12.172(4)	8.4019	12.2308						
Gd_2Co_{17}	8.377	12.198	8.365	12.184	8.361(2)	12.159(4)	8.3787	12.2091	8.349	12.24				
Tb_2Co_{17}	8.357	12.186	8.344	12.190	8.341(2)	12.152(4)								
Dy_2Co_{17}	8.346	12.180	8.310	12.070	8.335(2)	12.135(3)	8.365	12.169						
Ho_2Co_{17}							8.332	12.201						
Y_2Co_{17}	8.355	12.183	8.344	12.190			8.355	12.192					8.35	12.27

Table 106e. Lattice parameters (Å) of R_2Co_{17} compounds having $TbCu_7$-type structure [73 K 4].

	a	*c*
Sm_2Co_{17}	4.8562	4.0813
Gd_2Co_{17}	4.837	4.066

The existence of RCo_z compounds with $z \cong 7$ for R = La, Ce, Pr and Nd has been suggested [83 G 16].

Table 106f. Lattice parameters of R_2Ni_{17} compounds (Å).

	66 B 4		67 L 1, 69 P 1		67 T 1		68 C 2		69 V 1		72 B 16		82 P 4		84 C 4	
	a	*c*	*a*	*c*	*a*	*c*	*a*	*c*	*a*	*c*	*a*	*c*	*a*	*c*	*a*	*c*
Nd_2Ni_{17}							8.44	8.12	8.402	8.048						
Sm_2Ni_{17}	8.471	8.049	8.47	8.06			8.38	8.105					8.367	8.061		
Eu_2Ni_{17}					8.35	8.06										
Gd_2Ni_{17}	8.431	8.049	8.43	8.04			8.33	8.06								
Tb_2Ni_{17}	8.315	8.041	8.31	8.04			8.30	8.04								
Dy_2Ni_{17}	8.299	8.037	8.29	8.03			8.29	8.02								
Ho_2Ni_{17}	8.298	8.027	8.29	8.02			8.28	8.02							8.295	8.034
Er_2Ni_{17}	8.287	8.017	8.28	8.01			8.25	8.00								
Tm_2Ni_{17}			8.25	8.01			8.25	8.00								
Yb_2Ni_{17}							8.25	8.005			8.28	8.024				
Lu_2Ni_{17}							8.21	7.995								
Y_2Ni_{17}	8.307	8.040	8.30	8.04			8.31	8.04								

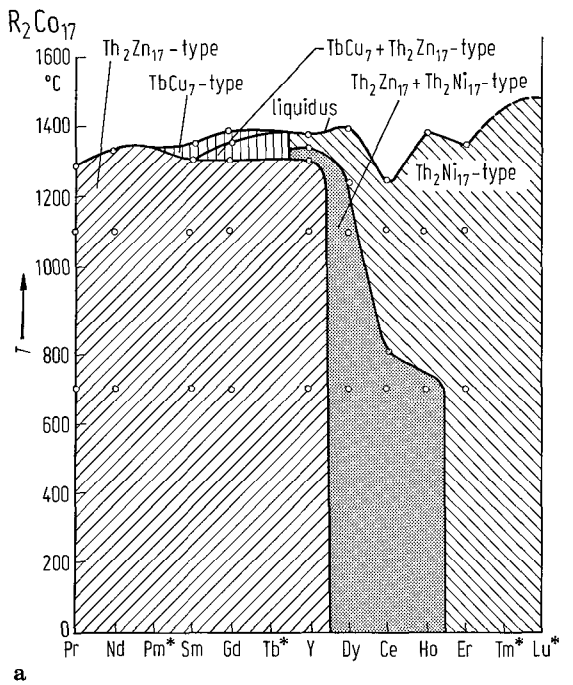

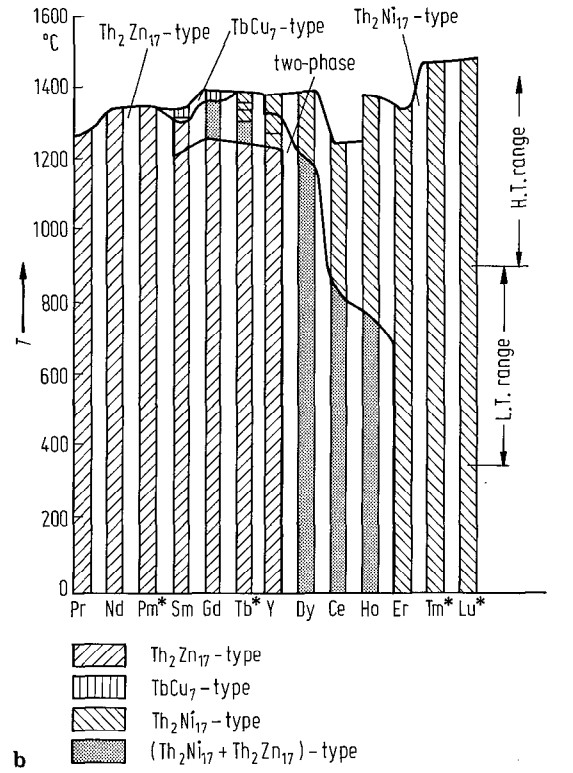

Fig. 461. Polymorphic forms of R_2Co_{17} compounds at different temperatures [73 K 4]. By asterisks are denoted alloys not investigated in the above work.

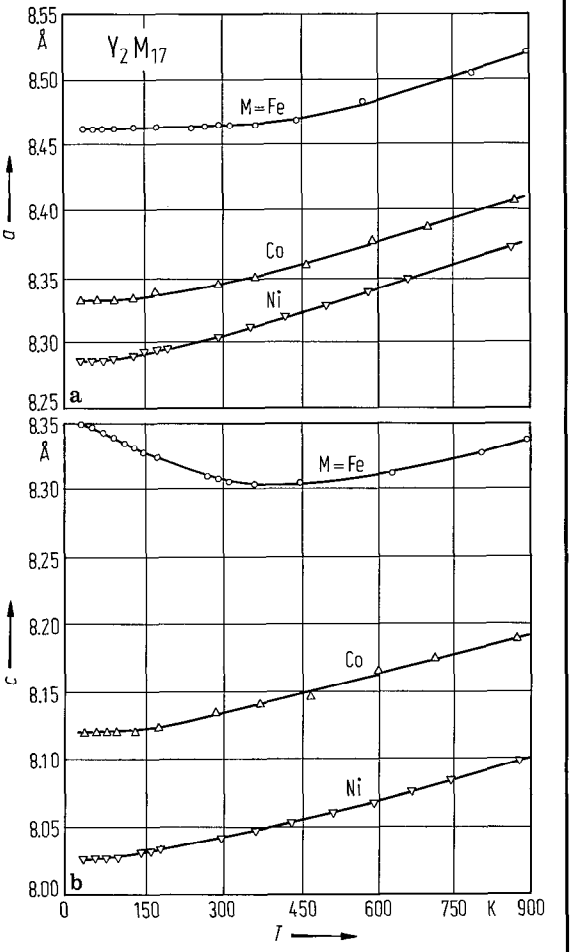

Fig. 462. Thermal variation of the lattice parameters for Y_2Ni_{17}, Y_2Co_{17} and Y_2Fe_{17} compounds. By full lines are plotted the lattice contribution to the thermal expansion [74 G 8]. The interactions between Fe atoms are dependent on the distances d between them, being negative for $d \lesssim 2.45$ Å. Thus, the magnetic interactions between $Fe_{IV}(4f)$–$Fe_{IV}(4f)$ are strongly negative while those between $Fe_I(6g)$–$Fe_{III}(12k)$, $Fe_I(6g)$–$Fe_{II}(12j)$, and $Fe_{III}(12k)$ –$Fe_{III}(12k)$ are weakly negative. The interactions associated with Fe atoms situated at distances larger than $\cong 2.45$ Å are positive. The negative interactions are not satisfied and consequently a large magnetic energy is stored. Competition between the temperature dependence of the magnetic and elastic energy provokes the observed expansion anomalies in R_2Fe_{17} compounds. See also [71 G 4].

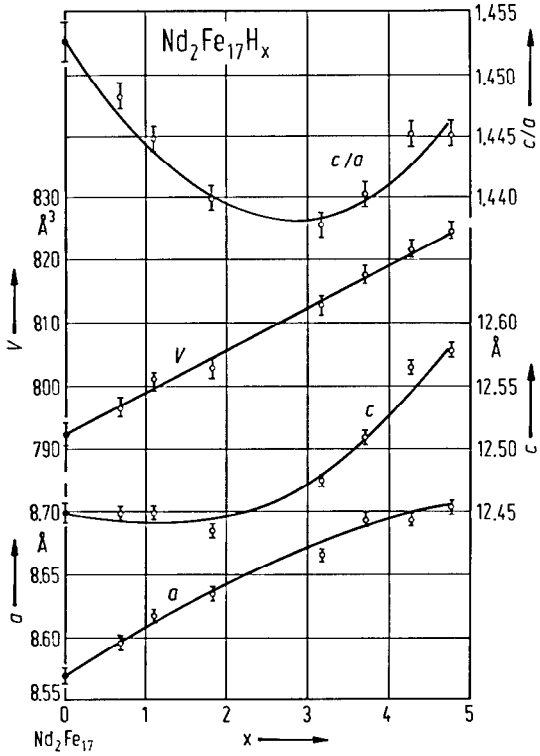

Fig. 463. Variation at room temperature of the *a* and *c* lattice constants, the volume cell, *V*, and *c/a* ratio as function of the hydrogen content for $Nd_2Fe_{17}H_x$ hydrides [88 R 4], including the data from [82 H 3] (full symbols). The lattice expansion is strongly anisotropic.

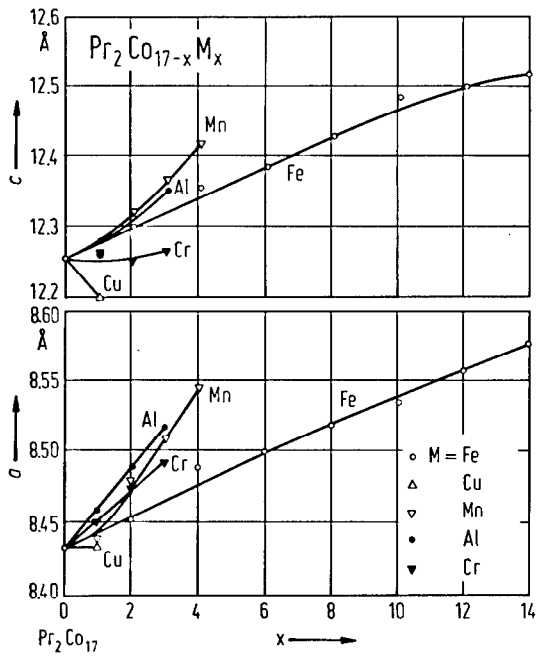

Fig. 464. Composition dependence of the room-temperature lattice constants in $Pr_2Co_{17-x}M_x$ compounds, where M = Fe, Mn, Cr, Cu and Al [83 S 4]. Single-phase materials were obtained with $x \leq 14$ for M = Fe, $x \leq 4$ for M = Mn, $x \leq 3$ for M = Cr or Al and $x \leq 1.0$ for M = Cu. The rhombohedral Th_2Zn_{17} structure was retained for these systems. Similar variations in lattice parameters were observed in related systems as $Ce_2Co_{17-x}M_x$ [82 F 12] and $Sm_2Co_{17-x}M_x$ [72 S 1].

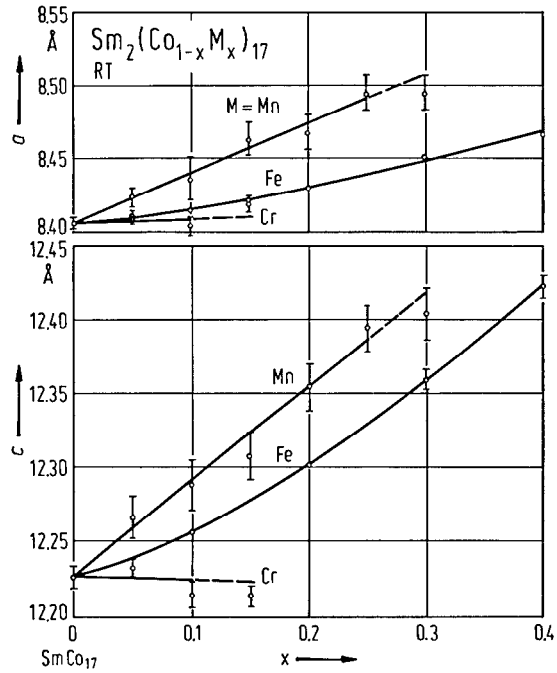

Fig. 465. Composition dependence of the lattice constants in $Sm_2(Co_{1-x}M_x)_{17}$ with M = Mn, Fe, Cr, at room temperature [77 P 3].

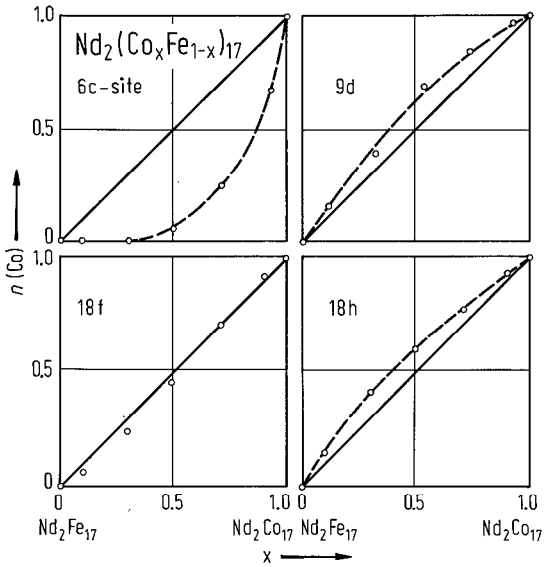

Fig. 466. Co occupancy fraction, n (Co)-normalized to unity – for the four transition metal sites (c, d, f, h) as function of Co concentration in $Nd_2(Co_xFe_{1-x})_{17}$ compounds [82 H 3]. The 6c-type transition metal sites are preferentially occupied by Fe ions. Concomitantly, the 9d and 18h sites have Co occupations larger than those predicted by stoichiometry (solid lines), while the 18f sites deviate only slightly from random occupation. In $Y_2(Co_{0.97}Fe_{0.03})_{17}$ appears to be a net preference of Fe for 6c and 18f sites ($R\bar{3}m$-type structure) [76 D 9]. After [76 P 2] in $Y_2(Co_{0.31}Fe_{0.69})_{19.6}$ alloy, Fe atoms show a preference for 6c sites at low substitution and relative preference for the 9d and 18h sites over the 18f sites. In hexagonal $Tm_2(Fe_{1-x}Co_x)_{17}$ compounds a slight preference of Fe for the 4f sites is shown [76 G 12]. The site occupation in $Sm_2(CoM)_{17}$ compounds has been analysed in [84 K 10].

For crystal structure and lattice parameters see also

R_2M_{17} [56 M 1]

R_2Mn_{17} R = Yb [83 T 7]

R_2Fe_{17} [64 W 5, 65 W 2, 66 R 1, 68 R 1] (initially considered as RFe_7); [66 B 4, 66 S 1, 82 P 4]; R = Pr, Tb, Ho [65 K 2]; R = Tb, Y, Th [72 G 8]; R = Gd [61 S 2, 63 K 1, 70 G 2]; R = Dy [82 B 1]; R = Ho [70 R 2]; R = Lu [72 G 7]; R = Y [74 G 8, 77 S 11]

R_2Co_{17} [66 B 4, 68 B 1, 73 B 22, 73 K 4, 78 B 5, 80 B 12, 82 P 4]; R = Ce, Pr, Nd, Sm, Gd, Tb, Dy, Ho, Er, Tm, Y [66 B 3]; R = Ce, Pr, Nd, Sm, Gd, Tb, Dy, Ho, Er, Tm, Y [66 L 4]; R = Pr, Er, Tm, Yb [81 M 8]; R = Sm [73 K 7]; R = Gd [76 K 3]; R = Er [69 S 1]; R = Y [65 O 2, 69 S 2*, 72 Y 1, 74 G 8]

R_2Ni_{17} [65 V 1, 66 B 4, 69 L 1, 69 P 1, 82 P 4]; R = Sm, Gd, Tb, Dy, Ho, Er, Tm, Y [67 L 1]; R = Nd, Sm, Gd, Tb, Dy, Ho, Er, Tm, Yb, Lu, Y [68 C 2]; R = Y [74 G 8]; R = Th [42 N 1, 75 D 3]

$R_2M_{17}H_x$ $Nd_2Fe_{17}H_x$ [88 R 4]

$(R'R'')_2M_{17}$ $(CeY)_2Co_{17}$ [83 P 7]; $(SmPr)_2Co_{17}$ [74 D 9]; $(SmGd)_2Co_{17}$ [74 D 9]; $(SmY)_2Co_{17}$ [74 D 9]; $(SmR)_2(CoZr)_{17}$, R = La, Ce, Y [85 F 4]; $(SmPr)_2(CoZr)_{17}$ [83 F 8]; $(ErPr)_2Co_{17}$ [81 M 8, 82 H 11]; $(ErZr)_2Co_{17}$ [82 H 11]; $(YbPr)_2Co_{17}$ [81 M 8, 82 H 11]; $(YbZr)_2Co_{17}$ [82 H 11]

$R_2(M'M'')_{17}$ $R_2(MnFe)_{17}$, R = La, Ce, Pr, Nd, Sm, Gd, Dy, Ho, Er, Tm, Yb, Lu, Y [76 F 2]; $Ce_2(MAl)_{17}$, M = Mn, Fe, Cu [63 Z 1]; M = Mn, Co, Cu [62 Z 1]; $Ce_2(CoM)_{17}$, M = Ti, V, Cr, Mn, Fe, Cu, Zr, Hf [82 F 12]; M = Cu, V, Ti, Zr, Hf [82 W 4]; $Pr_2(CoM)_{17}$, M = Fe, Mn, Cr [83 J 4]; M = Fe, Mn, Cr, Cu, Al [84 S 3]; $Sm_2(CoM)_{17}$, M = V, Ti, Zr, Hf [82 S 9]; $Ho_2(CoM)_{17}$, M = Fe, Ni, Mo, Cr, W, Ti, Cu, Al [84 C 4]; M = Mn, Fe, Ni, Cr, Ti, Al, Cu [82 C 9]; $Er_2(CoM)_{17}$, M = Mn, Fe, Ni [77 N 1]; $Pr_2(CoMn)_{17}$ [83 J 5]; $Er_2(CoMn)_{17}$ [82 W 4]; $Gd_2(CoMn)_{17}$ [86 K 1]; $Yb_2(CoMn)_{17}$ [81 M 8]; $Y_2(CoMn)_{17}$ [85 Y 8, 86 K 1]; $Er_2(FeCoMn)_{17}$ [81 M 8]; $(ErPr)_2(FeCoMn)_{17}$ [81 W 1]; $La_2(MnAl)_{17}$ [82 F 1]; $Ce_2(MnAl)_{17}$ [82 F 1]; $Er_2(MnGa)_{17}$ [85 M 4]

$R_2(FeCo)_{17}$ [77 S 10]; $Pr(FeCo)_{17}$ [83 J 5]; $Sm_2(FeCo)_{17}$ [74 D 9, 75 S 4]; $Gd_2(FeCo)_{17}$ [74 S 10]; $Dy_2(FeCo)_{17}$ [74 S 10, 82 R 1]; $Er_2(FeCo)_{17}$ [74 D 9, 81 M 8, 82 W 4]; $Tm_2(FeCo)_{17}$ [74 N 3]; $Yb_2(FeCo)_{17}$ [77 N 1]; $Y_2(FeCo)_{17}$ [71 R 2, 71 S 7, 72 H 1, 74 S 10, 75 T 1, 85 C 2]; $Gd_2(FeNi)_{17}$ [75 S 8]; $Dy_2(FeNi)_{17}$ [76 S 11]; $Y_2(FeNi)_{17}$ [76 S 11]; $La_2(FeAl)_{17}$ [82 F 1]; $Nd_2(FeAl)_{17}$ [70 V 3]; $Sm_2(FeAl)_{17}$ [76 M 5]; $Tb_2(FeAl)_{17}$ [75 O 1]; $Dy_2(FeAl)_{17}$ [77 O 5, 84 P 13]; $Tm_2(FeAl)_{17}$ [74 N 3]; $Y_2(FeAl)_{17}$ [86 P 4]; $Er_2(FeSi)_{17}$ [87 A 6]

$Sm_2(CoNi)_{17}$ [78 M 11]; $Er_2(CoNi)_{17}$ [74 D 9, 79 S 1]; $Y_2(CoNi)_{17}$ [75 T 1, 78 M 11]; $Pr_2(CoAl)_{17}$ [73 O 4, 73 O 5]; $Nd_2(CoAl)_{17}$ [77 N 1]; $Sm_2(CoAl)_{17}$ [73 O 4, 73 O 5, 77 N 1]; $Y_2(CoAl)_{17}$ [74 H 3*]; $(PrEr)_2(MnFeCo)_{17}$ [82 W 3]; $Pr_2(CoCr)_{17}$ [83 J 4, 83 J 5]; $Pr_2(CoCuM)_{17}$, M = Zr, Hf, Ti [86 H 5]; $Sm(CoCu)_z$ [76 M 6]; $Sm(CoCuFeTi)_z$ [83 S 1]; $Sm_2(CoCr)_{17}$ [79 S 1]; $Er_2(CoCr)_{17}$ [79 S 1]; $Sm_2(CoM)_{17}$, M = Ag, Ge [85 J 2]; $R_2(CoZr)_{17}$, R = Ce, Sm [82 F 11]; $Y_2(CoZr)_{17}$ [85 Y 8]; $R_2(NiAl)_{17}$ [85 P 10(T)]; $Y_2(NiCu)_{17}$ [70 C 1]

For thermal expansion of lattice parameters see
R_2Fe_{17} [79 G 4]; R = Pr, Tm [83 M 5]; R = Y, Lu [71 G 4]; R = Er [73 B 23]
Y_2Co_{17} [71 G 4]; Y_2Ni_{17} [71 G 4]; $Dy_2(FeCo)_{17}$ [82 R 1]

For microstructure see
R_2Co_{17} [74 A 1]; R = Sm [77 G 8]
$R_2(M'M'')_{17}$ $Sm(CoCu)_z$ [77 M 6]; $Sm_2(CoM)_{17}$, M = Mn, Fe, Ni, Sn [82 P 6]; $Ce(CoCuFeTi)_z$ [78 L 4]; $Sm(CoCuFe)_z$ [77 L 3, 78 L 4]; $Sm(CoFeMn)_z$ [78 M 14]

For single crystal growing see
R_2M_{17} [83 M 3]; Y_2Co_{17} [82 W 6]; $(YCe)_2Co_{17}$ [85 M 7]; $R_2(FeCo)_{17}$ [73 F 5]; $Y_2(CoFe)_{17}$, $Y_2(CoAl)_{17}$, $Y_2(CoFeCu)_z$ [82 W 6]; $Y_2(CoM)_{17}$, M = Fe, Al, Cu [83 S 19, 83 S 20]

For thermal decomposition see
$Ce_2(CoFe)_{17}$ [73 R 3]

For M site occupation see
$Y_2(FeCo)_{17}$ [76 P 2, 86 T 5]; $Y_2(CoMn)_{17}$, $Y_2(CoZr)_{17}$ [85 Y 8]; $Nd_2(FeCo)_{17}$ [82 H 3]; $Sm_2(CoFeMn)_{17}$ [84 K 10]

Magnetization, Curie temperatures

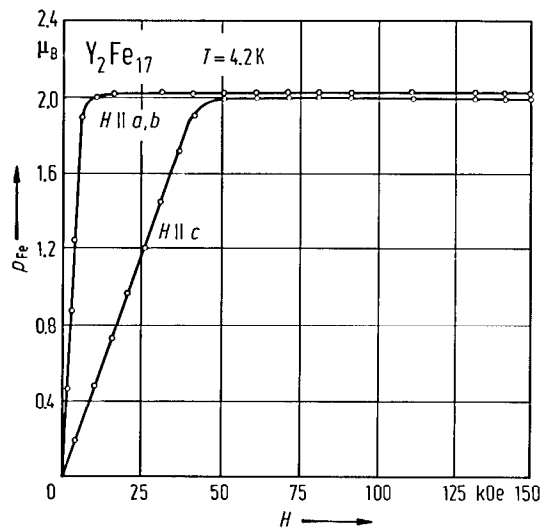

Fig. 467. Magnetization isotherms at 4.2 K in Y_2Fe_{17} single crystal. The magnetic field is applied parallel and perpendicular to the c axis. An anisotropy of magnetization, $\Delta p_s = 0.010\,\mu_B$/Fe atom, i.e. 0.8% of the spontaneous magnetization is evidenced [87 A 13]. The temperature dependence of Δp_s values is plotted in Fig. 501.

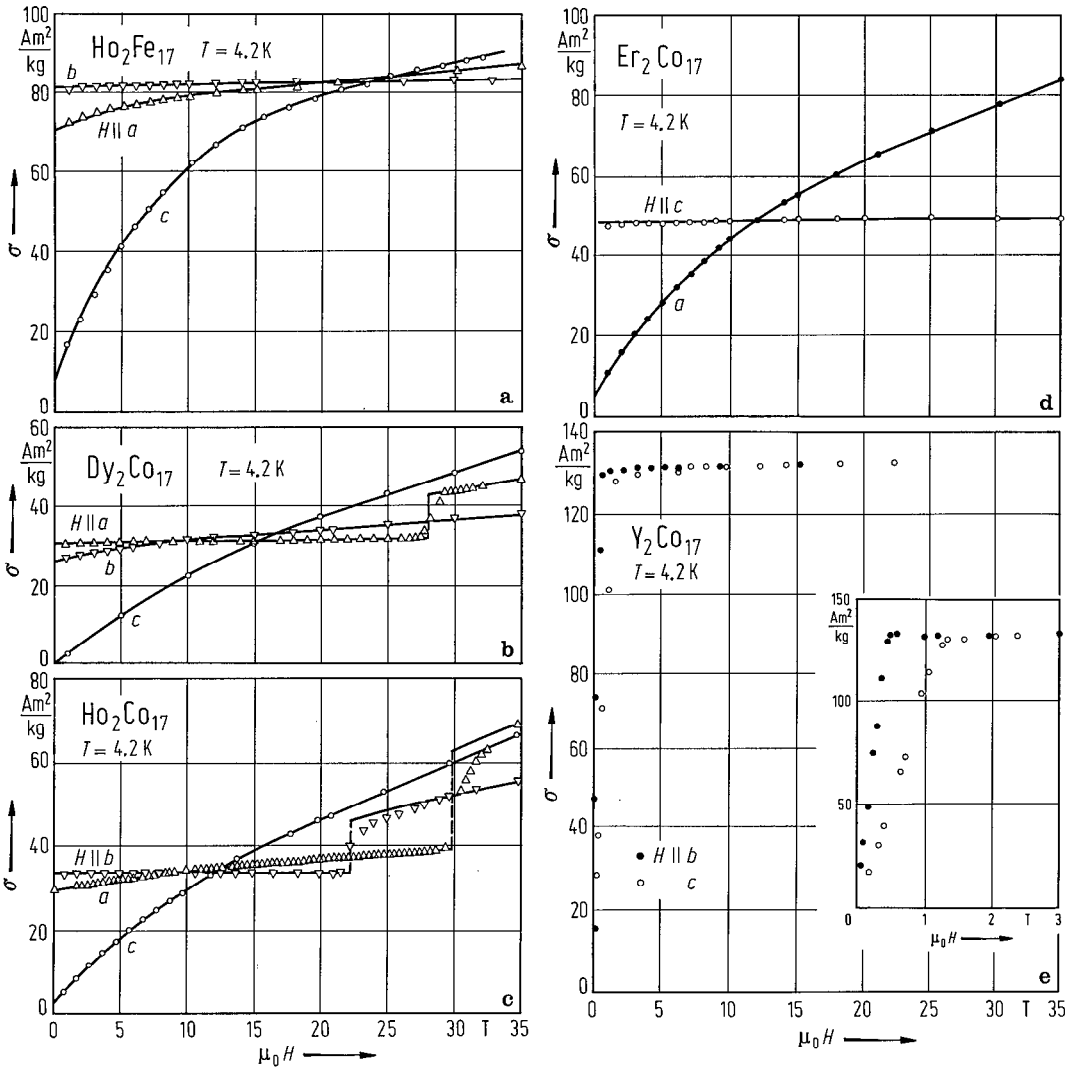

Fig. 468. Magnetization curves at 4.2 K, along different crystallographic directions in some R_2M_{17} single crystals: (a) Ho_2Fe_{17} compound having the *b* axis as easy axis of magnetization, (b) Dy_2Co_{17} compound having the *a* axis as easy axis of magnetization within the easy basal plane, (c) Ho_2Co_{17} compound having the *b* axis as easy axis of magnetization within the easy basal plane, (d) Er_2Co_{17} with the hexagonal *c* axis as easy axis of magnetization, and (e) Y_2Co_{17} compound. In (e) the inset shows the low-field behaviour of Y_2Co_{17}. The easy plane compounds Ho_2Co_{17}, Dy_2Co_{17} exhibit within the basal plane first order moment reorientation transitions. The magnetization isotherms for ferrimagnetic compounds were analysed in a two-sublattices model (solid lines) in order to determine the anisotropy constants as well as the exchange interactions coefficients [86 S 18].

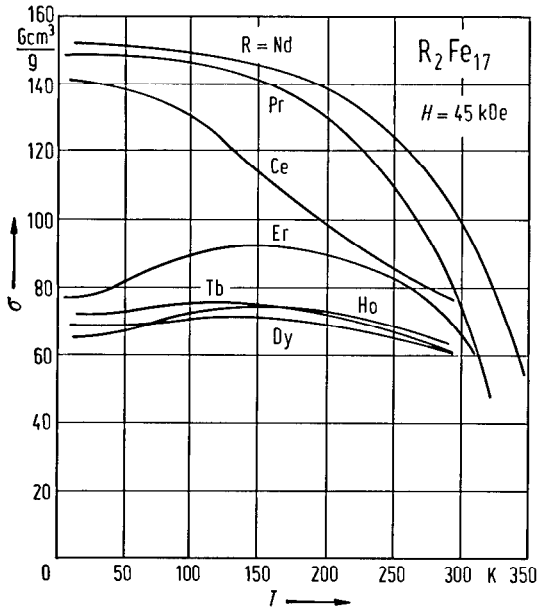

Fig. 469. Thermal variations of magnetization in R_2Fe_{17} (R = Ce, Nd, Pr, Tb, Dy, Ho, Er) compounds measured in a magnetic field of 45 kOe [66 S 2].

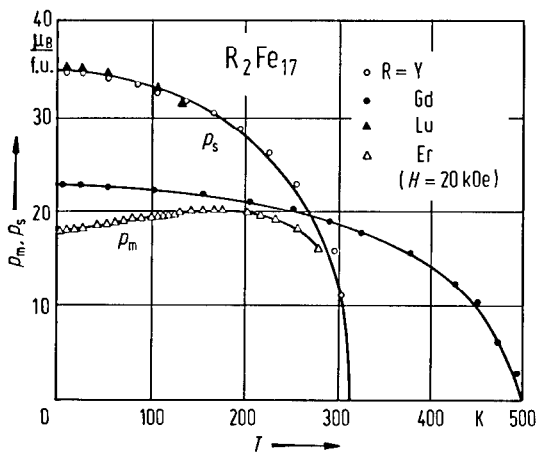

Fig. 470. Thermal variations of the spontaneous magnetization for Gd_2Fe_{17}, Lu_2Fe_{17}, Y_2Fe_{17} [69 G 1] and of the magnetization for Er_2Fe_{17} measured in a magnetic field of 20 kOe [87 A 6].

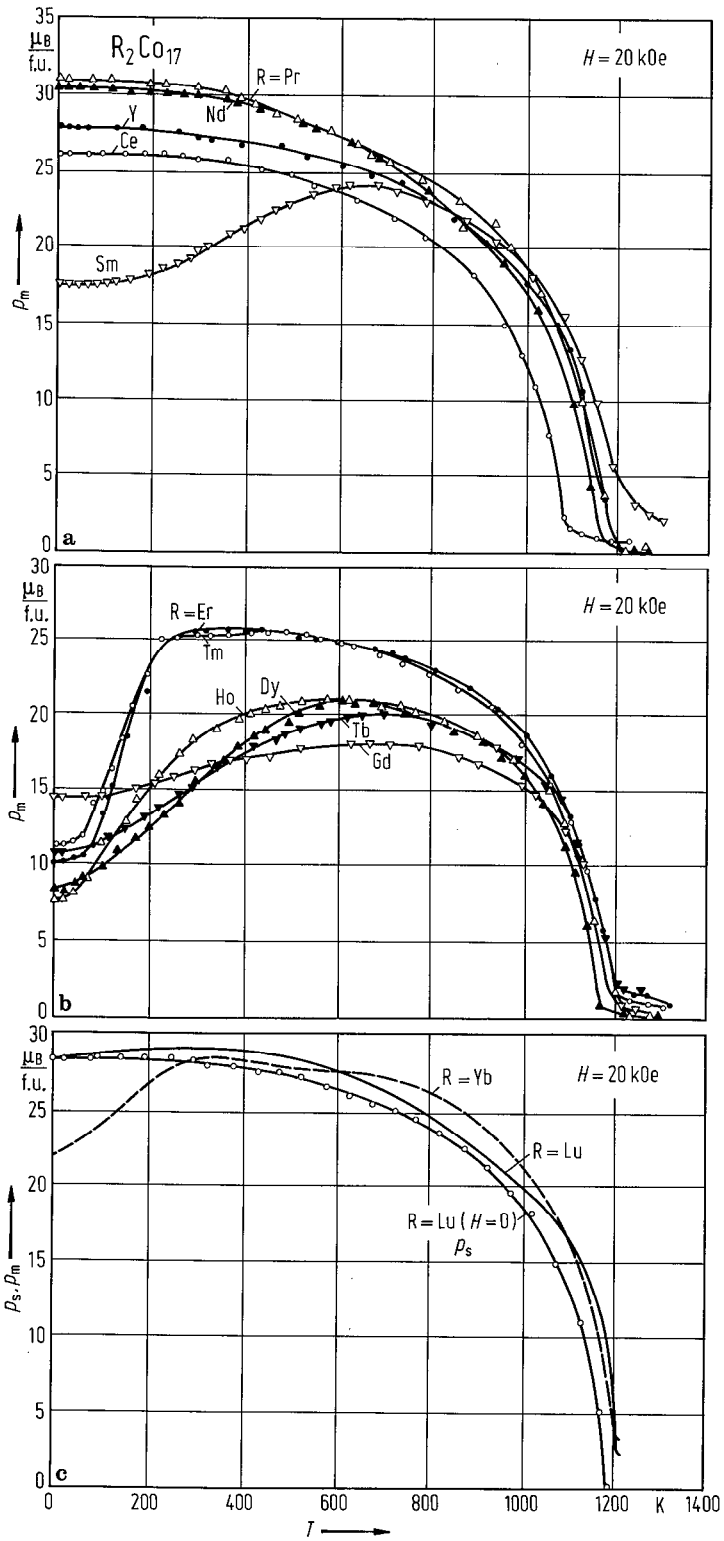

Fig. 471. Temperature dependence of the magnetization in R_2Co_{17} compounds in a magnetic field of 20 kOe: (a) R = Ce, Pr, Nd, Sm, Y (b) R = Gd, Tb, Dy, Ho, Er, Tm [66 L 1] and (c) R = Yb, Lu [74 N 6]. The thermal variation of the spontaneous magnetization for Lu_2Co_{17} is also plotted [71 G 1, 71 G 2].

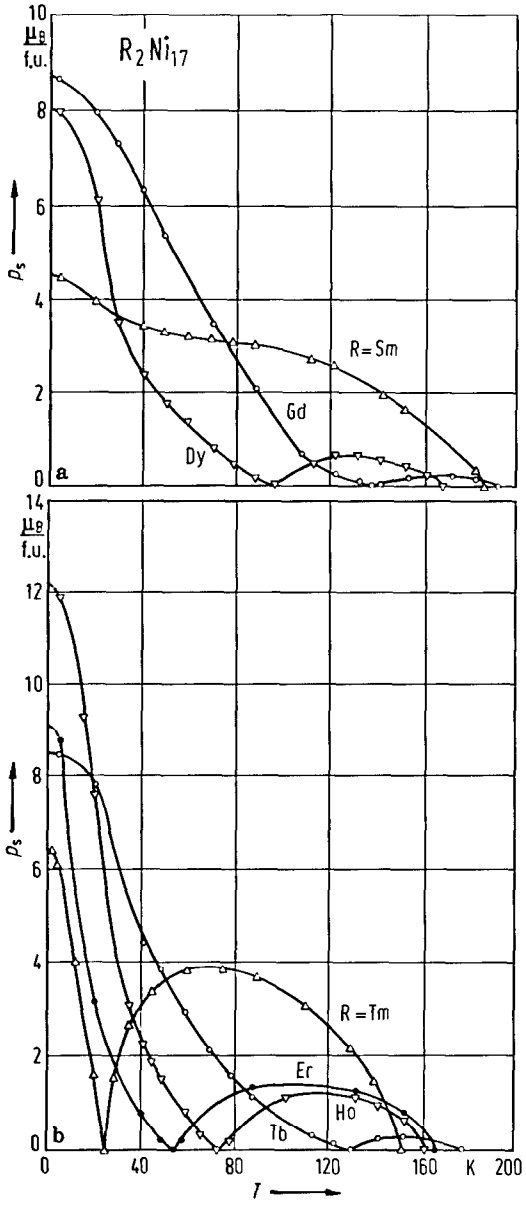

Fig. 472. Temperature dependence of the spontaneous magnetization in R_2Ni_{17} compounds: (a) R=Sm, Gd, Dy; (b) R=Tb, Ho, Er and Tm [67 L 1].

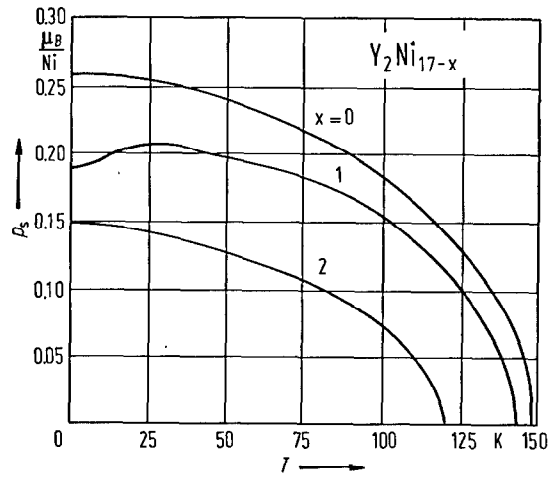

Fig. 473. Thermal variation of the spontaneous magnetization of Y_2Ni_{17}, Y_2Ni_{16} and Y_2Ni_{15} compounds [80 G 2]. The change in stoichiometry comes from the replacement of some of the Ni dumbell atoms by Y ones. The evolution of the magnetic properties results from the decrease of magnetic interactions as Y atoms replace Ni atoms. The variation of the interactions with the modification of the Ni surroundings allows the stabilization of the high- or low-magnetization states in Y_2Ni_{17} and Y_2Ni_{16} compounds, respectively. The very weak itinerant ferromagnetism in Y_2Ni_{15} must be associated with the intrinsic properties of some of the four Ni sites.

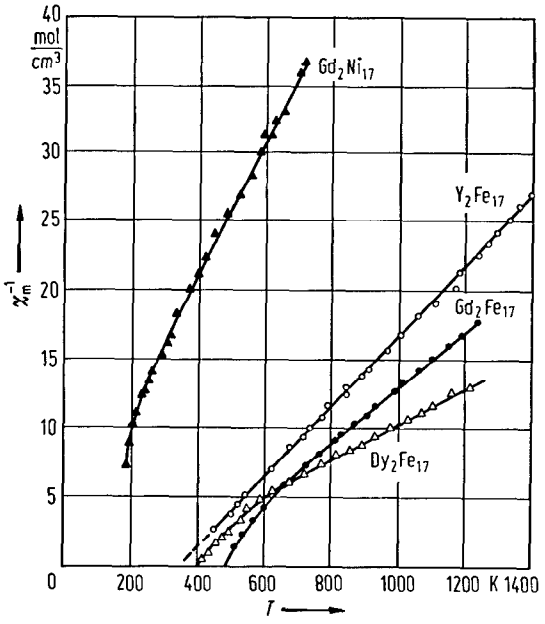

Fig. 474. Thermal variation of the reciprocal magnetic susceptibility for Gd_2Fe_{17} [82 b 1], Dy_2Fe_{17} [84 P 13], Y_2Fe_{17} [70 B 8] and Gd_2Ni_{17} [72 B 14]. In case of ferrimagnetic compounds the χ^{-1} vs. T curves show a nonlinear behaviour.

Table 107a. Magnetic properties of R_2Fe_{17} compounds.

	T_C(K)								
	66S1	69B5	69G1	70B14	70L8	74N1	77G14	77b1	84P13
Ce_2Fe_{17}				270			213		
Pr_2Fe_{17}	283				282(1)		286		
Nd_2Fe_{17}	327						325		
Sm_2Fe_{17}	389								
Gd_2Fe_{17}	460		479		472(1)				
Tb_2Fe_{17}	408						407		
Dy_2Fe_{17}	363						364		395
Ho_2Fe_{17}	325						335		
Er_2Fe_{17}		310					297		
Tm_2Fe_{17}	232.5				271(3)		275		
Yb_2Fe_{12}							255	280	
Lu_2Fe_{17}			270		263(2)				
Y_2Fe_{17}			310	332		302	358		

	p_s (μ_B)								Paramagnetic behaviour
	66S1	69B5	69G1, 71G3	70B14	74N1	77b1	81C4*	84P13	70B8, 82b1
Ce_2Fe_{17}				30.6		29.7			
Pr_2Fe_{17}	30.6								
Nd_2Fe_{17}	30.0								
Sm_2Fe_{17}									
Gd_2Fe_{17}			22.9			21.1			nonlinear χ^{-1} vs. T: Fig. 474
Tb_2Fe_{17}						17.9			
Dy_2Fe_{17}						16.1		17.1	
Ho_2Fe_{17}						14.8	16.36(16)		
Er_2Fe_{17}		16.2				17.1			
Tm_2Fe_{17}									
Yb_2Fe_{17}						25.6			
Lu_2Fe_{17}			34.9			34.2			
Y_2Fe_{17}			34.7	32.8	34.1	32.9			C-W χ^{-1} vs. T: Fig. 474

Table 107b. Magnetic properties of R_2Co_{17} compounds.

	T_C(K)						
	66 L 1, 66 L 3	68 B 7	71 G 1, 71 G 2	72 B 11	72 S 1	74 N 1	78 M 11
Ce_2Co_{17}	1083						
Pr_2Co_{17}	1171						
Nd_2Co_{17}	1150						
Sm_2Co_{17}	1190						1190
Gd_2Co_{17}	1209			1220			
Tb_2Co_{17}	1180						
Dy_2Co_{17}	1152						
Ho_2Co_{17}	1173				1173		
Er_2Co_{17}	1187	1160				1160	
Tm_2Co_{17}	1182					1175	
Yb_2Co_{17}						1180	
Lu_2Co_{17}			1192			1175	
Y_2Co_{17}	1167		1167		1167		1213

	p_s(μ_B)								
	66 L 1, 66 L 3	68 B 7	71 G 1, 71 G 2	72 B 11	72 S 1	74 N 1	78 K 11, 79 D 4	78 M 11	81 C 4*
Ce_2Co_{17}	26.1(2)						24.6		
Pr_2Co_{17}	31.0(4)						32.6		
Nd_2Co_{17}	30.5(4)						33.2		
Sm_2Co_{17}	20.1(2)						27.8	29.1	
Gd_2Co_{17}	14.4(2)			14.1			13.8		
Tb_2Co_{17}	10.70(15)						8.9		
Dy_2Co_{17}	8.30(15)						7.5		
Ho_2Co_{17}	7.7(1)				9.3		7.5		8.36(8)
Er_2Co_{17}	10.1(5)	10.6				10.56	9.8		
Tm_2Co_{17}	11.3(6)					13.80	13.4		
Yb_2Co_{17}						22.80			
Lu_2Co_{17}			26.9			28.50	26.9		
Y_2Co_{17}	27.8(3)		27.2		27.8		27.2	28.05	

Table 107c. Magnetic properties of R_2Ni_{17} compounds.

	T_C(K)						$p_s(\mu_B)$						Paramagnetic behaviour
	67 L 1	72 B 14	74 J 1, 75 J 1	75 S 8	77 Y 2	80 G 4	67 L 1	68 C 1	72 B 14	74 J 1, 75 J 1	75 S 8	80 G 4	72 B 14
Sm_2Ni_{17}	186						4.5	5.25					
Gd_2Ni_{17}	205	190		187			8.8	9.36	8.90		8.20		χ^{-1} vs. T nonlinear $C_m = 19.9\,cm^3\,K\,mol^{-1}$
Tb_2Ni_{17}	178				178		8.5	12.2					
Dy_2Ni_{17}	168		154				8.05	14.7					
Ho_2Ni_{17}	162		152				12.2	13.8		13.0(3)			
Er_2Ni_{17}	166		140		166		9.1	11.0		9.2(3)			
Tm_2Ni_{17}	152				152			7.31					
Lu_2Ni_{17}								5.00					
Y_2Ni_{17}	160		151			149	5.0	4.67				4.42	

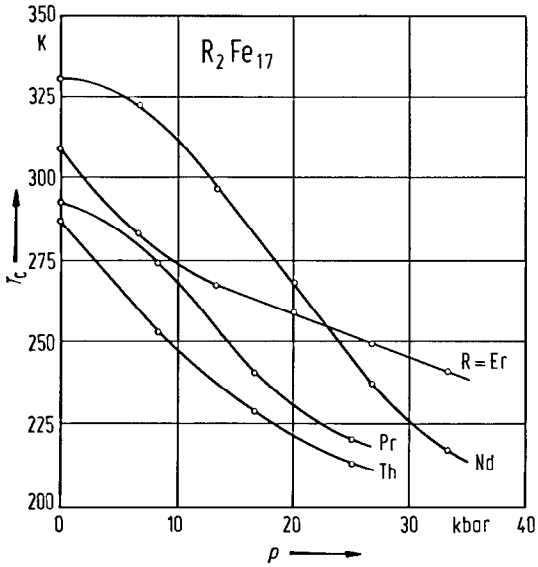

Fig. 475. Pressure dependence of the Curie temperature T_C in some R_2Fe_{17} compounds [73 B 25]. Rather great decrease of T_C values is evidenced as pressure increases, in agreement with the previous discussion (cf. caption to Fig. 462). See also [74 B 18, 85 R 2].

Table 108. Pressure dependence of the Curie temperatures in R_2M_{17} compounds. $\Gamma = d\log T_C / d\log V$.

	dT_C/dp K/kbar	Γ	Ref.
Er_2Fe_{17} [1])	−4.1	2.2	73 B 25
Y_2Fe_{17}	−9.8	5.3	71 G 3
Nd_2Co_{17}	+0.7	−1.0	73 B 25
Gd_2Co_{17}	+0.6	−0.8	73 B 25
Er_2Co_{17}	+1.1	−1.5	73 B 25
Y_2Co_{17}	−0.3	0.4	73 B 25
Dy_2Ni_{17}	−0.44(3)	4.4	75 J 1
Ho_2Ni_{17}	−0.44(3)	4.5	74 J 1
Er_2Ni_{17}	−0.48(3)	4.8	74 J 1
Y_2Ni_{17}	−0.44(3)	4.6	75 J 1

[1]) Deduced from Fig. 3 in [73 B 25] for $p \leqq 6$ kbar, see also Fig. 475.

▶

Fig. 476. Composition dependence of the lattice constants at room temperature (RT), a and c, Curie temperature T_C, specific magnetization at RT, σ, measured in an external magnetic field of 27 kOe on textured powders, and anisotropy constants at RT, K_1, for compounds having rhombohedral structure ($R\bar{3}m$): $(Sm_{1-x}Gd_x)_2Co_{17}$, $(Sm_{1-x}Pr_x)_2Co_{17}$, $(Sm_{1-x}Y_x)_2Co_{17}$, $Sm_2(Co_{1-x}Fe_x)_{17}$ and hexagonal structure ($P6_3/mmc$): $Er_2(Co_{1-x}Fe_x)_{17}$, $Er_2(Co_{1-x}Ni_x)_{17}$. Solid and open bars indicate easy-axis and easy-plane anisotropy, respectively [74 D 9]. The T_C values for $Sm_2(Co_{1-x}Fe_x)_{17}$ are from [73 M 10].

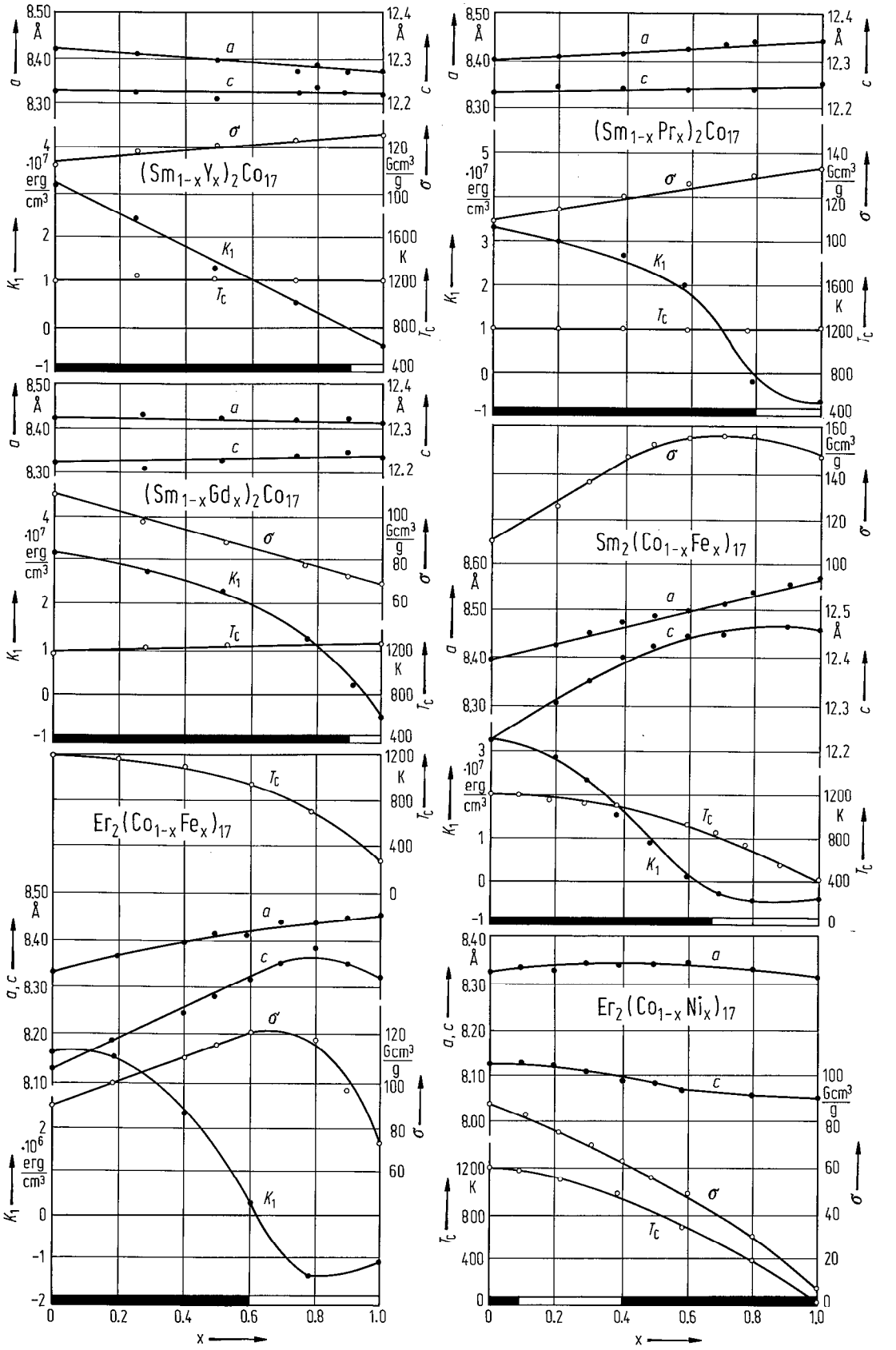
$(Sm_{1-x}Y_x)_2Co_{17}$
$(Sm_{1-x}Gd_x)_2Co_{17}$
$Er_2(Co_{1-x}Fe_x)_{17}$
$(Sm_{1-x}Pr_x)_2Co_{17}$
$Sm_2(Co_{1-x}Fe_x)_{17}$
$Er_2(Co_{1-x}Ni_x)_{17}$
a
c
σ
K_1
T_c
x

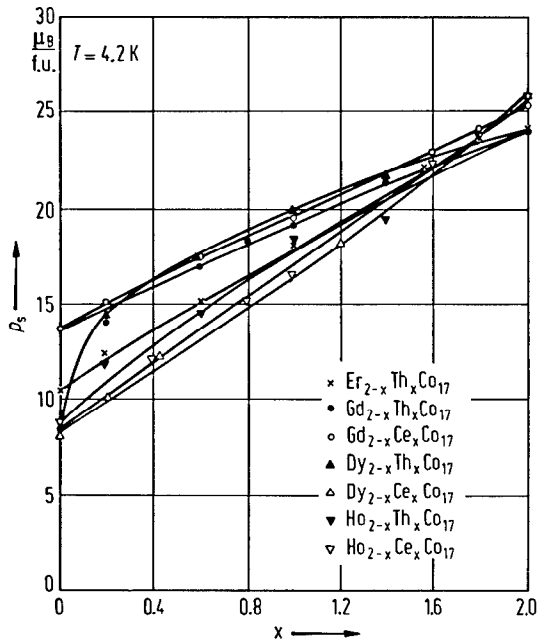

Fig. 477. Composition dependence of the saturation magnetization in $R_{2-x}R'_xCo_{17}$ compounds at 4.2 K with R = Gd, Dy, Ho or Er and R' = Th or Ce [73 N 4, 75 N 2].

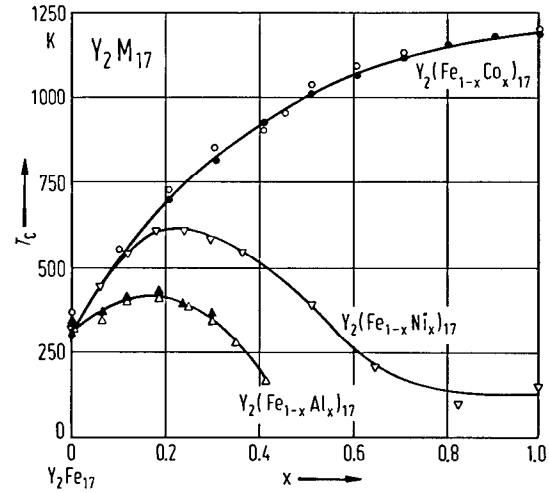

Fig. 478. Composition dependence of the Curie temperature in $Y_2(Fe_{1-x}Co_x)_{17}$, open symbols [75 P 5], solid symbols [73 M 11]; $Y_2(Fe_{1-x}Al_x)_{17}$, open symbols [74 N 1], solid symbols [86 P 4]; and $Y_2(Fe_{1-x}Ni_x)_{17}$ [74 N 1] compounds.

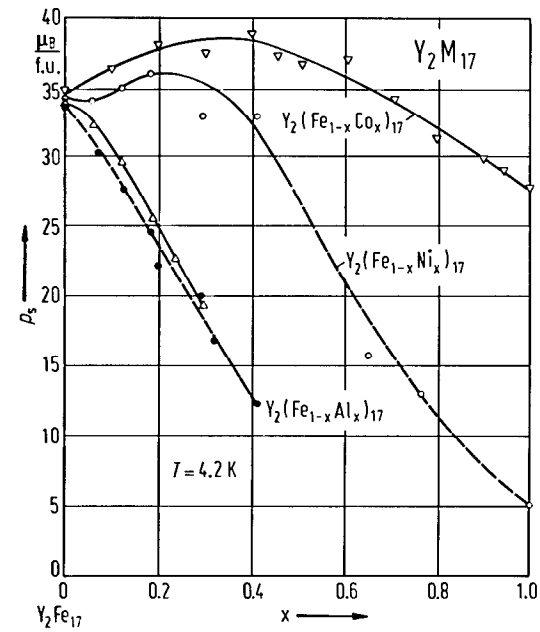

Fig. 479. Composition dependence of the saturation magnetic moment in $Y_2(Fe_{1-x}Co_x)_{17}$ [75 P 5]; $Y_2(Fe_{1-x}Al_x)_{17}$, solid symbols [86 P 4], open symbols [74 N 1]; and $Y_2(Fe_{1-x}Ni_x)_{17}$ [74 N 1] compounds at 4.2 K.

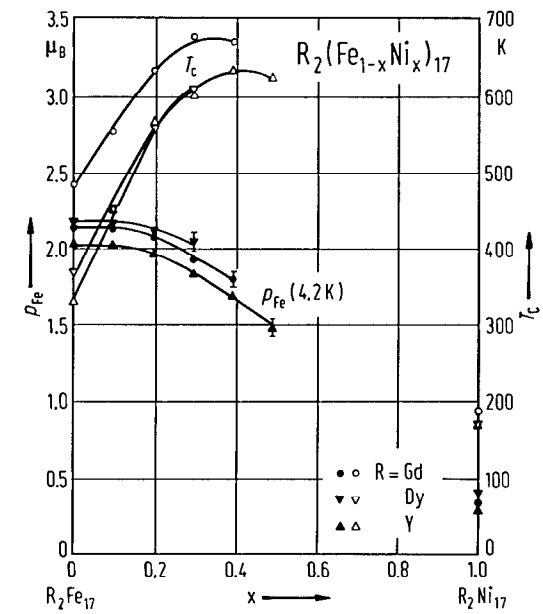

Fig. 480. Composition dependence of the mean Fe magnetic moment at 4.2 K and Curie temperatures in $R_2(Fe_{1-x}Ni_x)_{17}$ compounds with R = Gd, Dy, and Y [76 S 11].

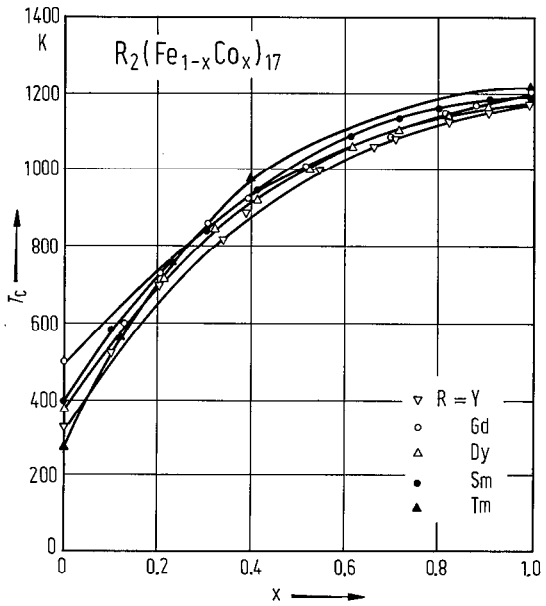

Fig. 481. Composition dependence of the Curie temperatures in $R_2(Fe_{1-x}Co_x)_{17}$ compounds with R = Gd, Dy, Y [74 S 10], R = Sm [73 M 11] and R = Tm [77 G 13].

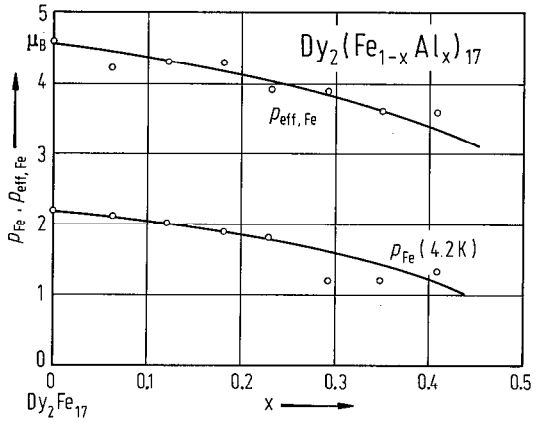

Fig. 482. Composition dependence of the mean Fe magnetic moments determined by saturation magnetization at 4.2 K and mean effective Fe magnetic moments in $Dy_2(Fe_{1-x}Al_x)_{17}$ compounds [84 P 13].

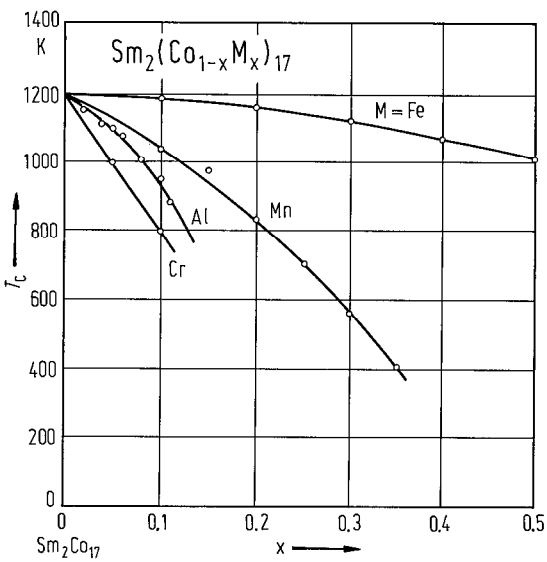

Fig. 483. Curie temperature of $Sm_2(Co_{1-x}M_x)_{17}$ alloys with M = Fe, Mn, Cr and Al. By Co substitution a decrease in T_C values is observed [77 P 4].

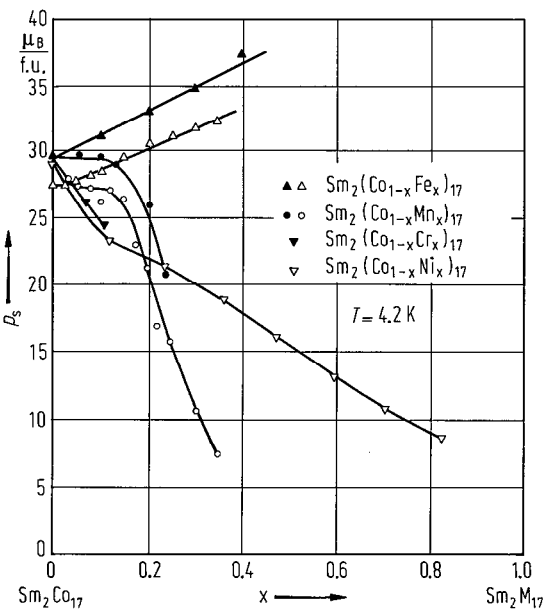

Fig. 484. Composition dependence of the saturation magnetization at 4.2 K in $Sm_2(Co_{1-x}M_x)_{17}$ compounds: M = Fe, open symbols [77 P 4], solid symbols [73 P 2, 75 T 1]; M = Mn, open symbols [77 P 4], solid symbols [73 P 2, 75 T 1], M = Ni [78 M 11], and M = Cr [73 P 2, 75 T 1, 77 P 4].

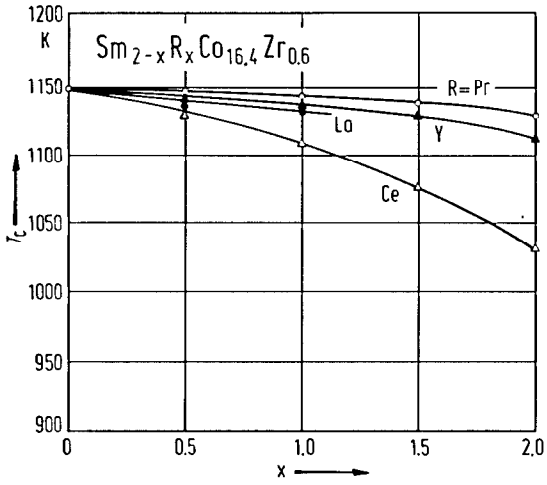

Fig. 485. Composition dependence of the Curie temperatures in the $Sm_{2-x}R_xCo_{16.4}Zr_{0.6}$ system, with R = La, Ce, Pr and Y [85 F 4].

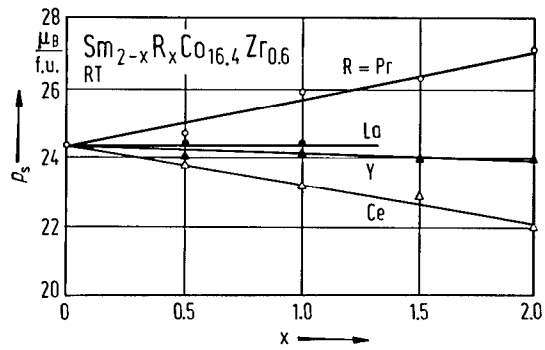

Fig. 486. Variation of the saturation magnetization with composition in the $Sm_{2-x}R_xCo_{16.4}Zr_{0.6}$ system at room temperature with R = La, Ce, Pr and Y [85 F 4].

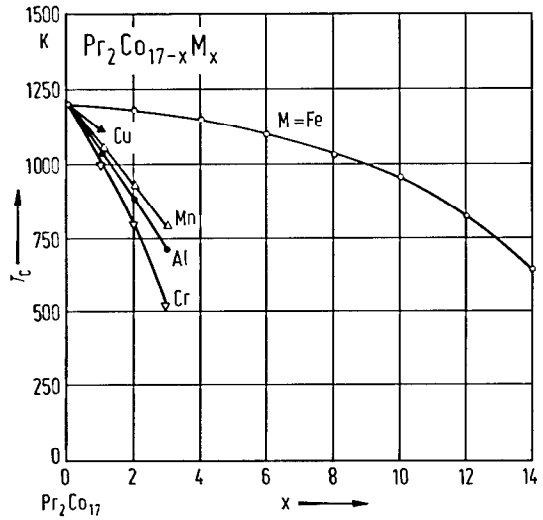

Fig. 487. Composition dependence of the Curie temperatures in $Pr_2Co_{17-x}M_x$ compounds, where M = Fe, Mn, Cr, Cu, or Al [83 S 4].

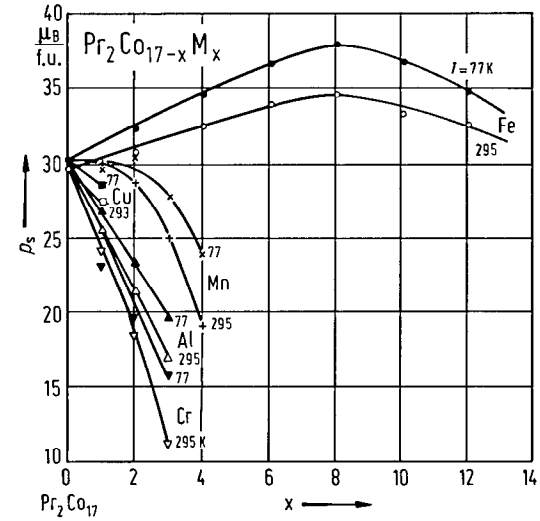

Fig. 488. Variation of the saturation magnetic moment as function of composition in $Pr_2Co_{17-x}M_x$ compounds at 77 and 295 K for M = Fe, Mn, Cr, Cu and Al [83 S 4].

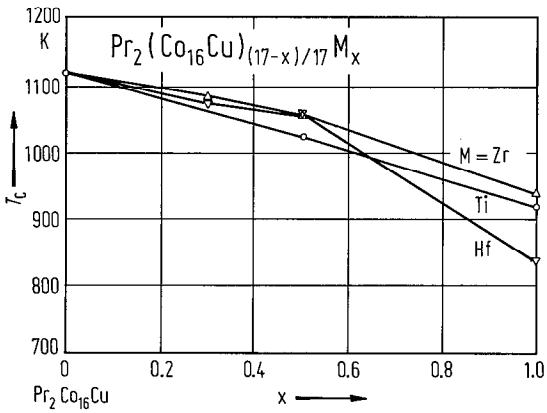

Fig. 489. Composition dependence of the Curie temperatures in $Pr_2(Co_{16}Cu)_{(17-x)/17}M_x$ alloys with M = Ti, Hf and Zr [86 H 5].

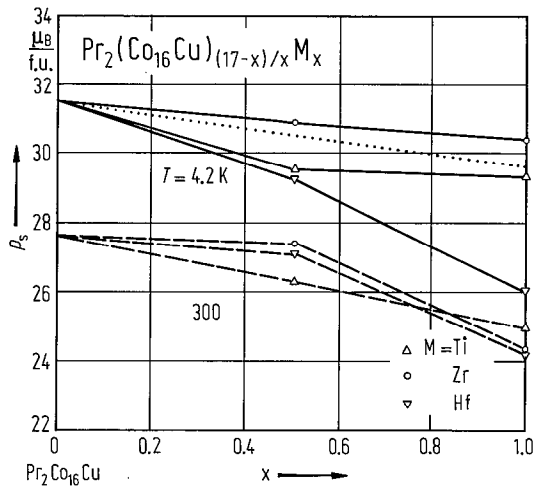

Fig. 490. Dependence of the saturation magnetization on the concentration of M = Ti, Zr and Hf in $Pr_2(Co_{16}Cu)_{(17-x)/17}M_x$ system, at 4.2 K (full lines) and at 300 K (dashed lines) [86 H 5]. The dotted line shows p_s expected for simple dilution in the transition metal lattice.

For magnetic measurements see also:

R_2M_{17} [85 R 2, 88 K 5]

R_2Fe_{17} [74 G 8, 85 R 3, 87 R 2, 88 R 1]; R = Pr, Nd, Er, Th [72 B 15]; R = Er, Tm, Yb [74 G 14]; R = Ce [70 B 14, 72 G 4, 74 G 7]; R = Pr [68 J 1]; R = Nd [88 W 3]; R = Tb [76 O 2]; R = Dy [82 B 1]; R = Ho [81 C 4*]; R = Er [75 J 1]; R = Tm [73 G 7, 74 G 7]; R = Lu [72 G 4, 74 G 7]; R = Y [70 B 8, 75 J 1, 77 S 11, 86 D 3, 87 A 13*]

R_2Co_{17} [67 S 3, 79 D 4, 78 B 5, 86 R 2, 87 U 2, 88 R 1]; R = Ce, Pr, Nd, Sm, Gd, Tb, Ho, Er, Tm, Lu, Y [66 L 1, 66 L 4, 66 S 2]; R = Ce, Pr, Nd, Y, Th [72 S 1]; R = Sm, Gd, Er, Tm, Y [74 D 8]; R = Er, Tm, Yb [74 N 6]; R = Tb, Dy, Ho [75 D 4*]; R = Pr, Er, Tm, Yb [81 M 8]; R = Ce, Pr, Nd, Sm, Gd, Tb, Dy, Ho, Er, Tm, Yb [85 R 4]; R = Dy, Ho, Er, Y [86 S 18]; R = Nd [87 R 3]; R = Sm [72 S 3, 79 D 6, 87 R 3]; R = Gd [76 K 3, 76 K 4]; R = Tb [76 M 13]; R = Dy [73 D 7, 86 S 17*]; R = Ho [76 M 13, 81 C 4*, 85 F 3*, 85 R 4, 87 S 17*]; R = Er [75 J 1, 76 M 13]; R = Tm [74 M 4]; R = Lu [74 M 4]; R = Y [67 H 2*, 73 D 7, 75 J 1, 77 M 9, 79 H 1, 85 S 25(T), 87 S 24(T)]

R_2Ni_{17} [68 C 1, 69 C 1 (reported T_C values exceed the correct ones), 69 P 1, 77 P 2]; R = Sm, Gd, Tb, Dy, Ho, Er, Tm, Y [67 L 1]; R = Nd, Sm, Gd, Tb, Dy, Ho, Er, Tm, Yb, Lu, Y [68 C 1]; R = Dy, Ho, Er, Y [75 J 1]; R = Dy, Ho, Er, Y [75 P 4]; R = Ho [74 J 1]; R = Er [74 J 1]; R = Y [80 G 2, 80 G 4, 81 G 5, 84 V 1, 85 R 9, 87 S 12(T)]

$R_2M_{17}H_x$ $Nd_2Fe_{17}H_x$ [88 R 4]

$(R'R'')M_{17}$ $(GdY)_2Fe_{17}$ [82 A 10]; $(DyY)_2Fe_{17}$ [82 P 7]

$(R'R'')_2M_{17}$ $(RCe)_2Co_{17}$, R = Gd, Dy, Ho, MM [73 N 4, 75 N 2]; $(RPr)_2Co_{17}$, R = Sm, Er, Tm, Yb [83 W 2]; $(RTh)_2Co_{17}$, R = Gd, Dy, Ho, Er, MM [73 N 4, 75 N 2]; $(SmPr)_2Co_{17}$ [74 D 9]; $(SmPr)_2(CoZr)_{17}$ [83 F 8]; $(SmGd)_2Co_{17}$ [74 D 9]; $(SmY)_2Co_{17}$ [74 D 9, 82 D 6]; $(SmGdDy)_2(CoCuZr)_{17}$, $(SmGdHo)_2(CoCuZr)_{17}$, $(SmErGd)_2(CoCuZr)_{17}$ [85 C 1]; $(SmR)_2(CoCuZr)_{17}$, R = Pr, Nd [85 W 5]; $(SmR)_2(CoM)_{17}$, R = Gd, Dy, Er [80 R 3]; $(SmPr)_2Co_{16.4}Zr_{0.6}$ [83 F 8]; $(SmR)_2Co_{16.4}Zr_{0.6}$, R = La, Ce, Y [85 F 4]; $(SmGd)_2(CoMn)_{17}$ [79 B 3]; $(SmNd)_2(CoFe)_{17}$ [79 L 5]; $(GdY)_2Co_{17}$ [82 A 15, 87 K 1]; $(DyY)_2Co_{17}$ [74 M 5, 77 M 9]; $(ErPr)_2Co_{17}$ [81 M 8, 82 H 11, 82 W 5]; $(ErPr)_2Co_{13}(FeMn)_4$ [78 M 10, 81 W 1, 82 W 3]; $(ErZr)_2Co_{17}$ [82 H 11]; $(YbPr)_2Co_{17}$ [81 M 8, 82 H 11]; $(YZr)_2Co_{17}$ [82 H 11]; $(LuTm)_2Co_{17}$ [74 M 4, 75 M 6]

$R_2(M'M'')_{17}$ $R_2(CoM)_{17}$, R = Ce, Pr, Sm, Er, Tm, Yb, M = Ti, V, Cr, Mn, Cu, Zr, Hf [83 W 2]; R = Sm, Er, M = Fe, Ni, Cu [85 Z 2]; $Ce_2(CoM)_{17}$, M = Ti, V, Cr, Mn, Fe, Cu, Zr, Hf [82 F 12]; R = Cu, V, Ti, Zr, Hf [82 W 4]; $Pr_2(CoM)_{17}$, M = Fe, Mn, Cr, Cu, Al [83 S 4, 84 S 3]; $Sm_2(CoM)_{17}$, M = V, Ti, Zr, Hf [82 S 9]; M = Ag, Ge [85 J 2]; $Ho_2(CoM)_{17}$, M = Fe, Ni, Mo, Cr, W, Ti, Cu, Al [84 C 4]; M = Mn, Fe, Ni, Cr, Ti, Al, Cu [82 C 9]; $Dy_2(FeM)_{17}$, M = Co, Al [83 R 2]

$R_2(MnCo)_{17}$, R = Ce, Pr, Nd, Y, Th [72 S 1]; $Pr_2(CoMn)_{17}$ [82 J 1, 83 J 4, 83 J 5, 83 Z 6]; $Sm_2(CoMn)_{17}$ [77 P 4, 77 P 5, 81 K 1, 84 J 1]; $Er_2(CoMn)_{17}$ [76 N 4, 77 N 1, 82 W 4]; $Er_2(FeCoMn)_{17}$ [78 M 10, 81 M 8]; $Yb_2(CoMn)_{17}$ [81 M 8]; $Yb_2(FeCoMn)_{17}$ [78 M 10, 81 M 8]; $Y_2(CoMn)_{17}$ [85 Y 8]; $La_2(MnAl)_{17}$ [82 F 1]; $Ce_2(MnAl)_{17}$ [82 F 1]

$R_2(FeCo)_{17}$ [71 R 3, 71 R 4, 74 H 4, 75 S 12, 85 R 6, 88 G 2]; R = Ce, Pr, Nd, Sm, Y, MM [72 R 1]; R = Ce, Pr, Nd, Y, Th [72 S 1]; R = Gd, Dy, Y [73 K 11]; R = Ce, Pr, Nd, Sm, Y, MM [73 M 11]; R = Pr, Nd, Sm, Gd, Y, MM [74 K 3*]; R = Gd, Dy, Y [74 S 10]; R = Ce, Sm, Y [84 O 2]; $Pr_2(FeCo)_{17}$ [74 S 6*, 76 M 7, 82 M 4, 82 S 24, 83 J 4, 83 J 5, 83 T 9, 83 Z 6]; $Sm_2(FeCo)_{17}$ [73 M 10, 74 D 9, 75 P 6, 75 S 4, 76 P 4, 77 P 4, 77 P 5]; $Dy_2(FeCo)_{17}$ [82 R 1]; $Ho_2(FeCo)_{17}$ [86 S 18, 87 S 16]; $Er_2(FeCo)_{17}$ [74 D 9, 76 N 4, 77 N 1, 81 M 8, 82 W 4]; $Tm_2(FeCo)_{17}$ [74 N 3]; $Yb_2(FeCo)_{17}$ [77 N 1]; $Y_2(FeCo)_{17}$ [71 S 7, 72 S 3, 73 P 2, 74 S 6*, 75 P 5, 75 T 1, 76 D 9, 83 S 19*, 83 S 20*, 85 C 2]

$R_2(FeNi)_{17}$, R = Gd [73 K 11]; R = Ho, Tm, Y [74 N 1]; R = Gd [75 S 8]; R = Dy [76 S 11]; R = Y [73 K 11, 76 S 11]

$R_2(FeAl)_{17}$, R = Ho, Tm, Y [74 N 1]; R = La [82 F 1]; R = Sm [76 M 5]; R = Tb [73 O 6]; R = Dy [77 O 1, 84 P 13, 85 R 5, 85 R 7, 88 R 1]; R = Tm [74 N 3]; R = Y [86 P 4]; $Er_2(FeSi)_{17}$ [87 A 6]

$Sm_2(CoNi)_{17}$ [78 M 11]; $Gd_2(CoNi)_{17}$ [77 E 3]; $Er_2(CoNi)_{17}$ [74 D 9, 76 N 4, 77 N 1, 79 S 1]; $Y_2(CoNi)_{17}$ [75 T 1, 78 M 11]; $Pr_2(CoCr)_{17}$ [83 J 4, 83 J 5, 83 Z 6]; $Sm_2(CoCr)_{17}$ [77 P 4, 77 P 5]; $Sm_2(CoCr)_{17}$ [79 S 1]; $Er_2(CoCr)_{17}$ [79 S 1]; $Y_2(CoCu)_{17}$ [77 H 1*, 83 S 19*, 83 S 20*]; $Pr_2(CoAl)_{17}$ [74 O 3]; $Nd_2(CoAl)_{17}$ [77 N 1]; $Sm_2(CoAl)_{17}$ [74 O 3, 77 N 1]; $Y_2(CoAl)_{17}$ [77 H 1*, 83 S 19*, 83 S 20*]; $Sm_2(CoAg)_{17}$ [84 J 2]; $Ce_2(CoZr)_{17}$ [82 F 11]; $Sm_2(CoZr)_{17}$ [81 K 1, 82 F 11]; $Y_2(CoZr)_{17}$ [85 Y 8]; $Pr_2(CoCuM)_{17}$, M = Zr, Hf, Ti [86 H 5]; $Ce(CoCuFeTi)_z$ [77 I 5]; $Sm(CoCuFeTi)_z$ [83 S 1]; $Sm(CoCu)_z$ [76 M 8]; $Sm(CoCuFe)_z$ [76 M 9, 79 A 5]; $Sm(CoZrFeCu)_z$ [79 B 4, 85 L 2]

$R_2(NiAl)_{17}$ [85 P 10(T)]; $Gd_2(CuNi)_{17}$ [79 P 2*); $Tb_2(NiAl)_{17}$ [86 H 1]; $Dy_2(NiAl)_{17}$ [83 C 6]; $Y_2(CuNi)_{17}$ [70 C 1 (reported T_C values exceed the real ones)]

Neutron diffraction

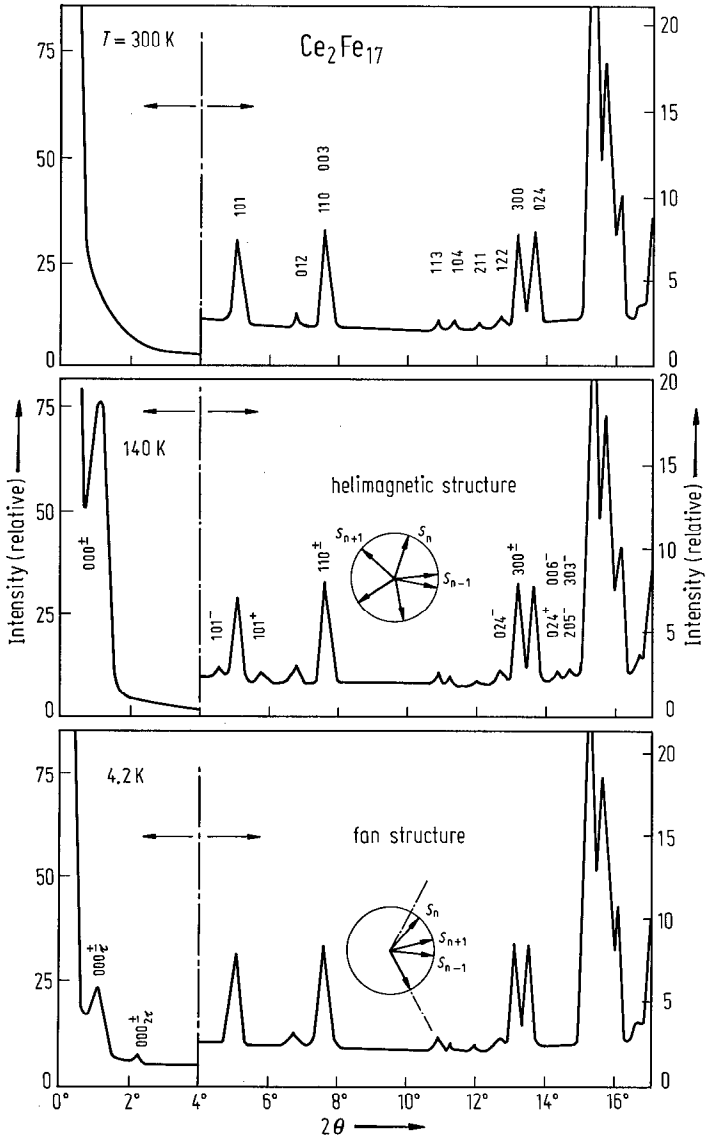

Fig. 491. Neutron diffraction pattern of Ce_2Fe_{17} compound at 300, 140, and 4.2 K. At low temperatures a transition from helimagnetic to fan structure is exhibited [74 G 8]. In compounds with R = Tm or Lu a transition from helimagnetic to ferrimagnetic (or ferromagnetic) ordering is shown. The observed spin structures are due to the competition between positive and negative exchange interactions between Fe atoms – see caption to Fig. 462. A complex magnetic structure was also suggested in Yb_2Fe_{17} compound by Mössbauer effect measurement [74 G 14].

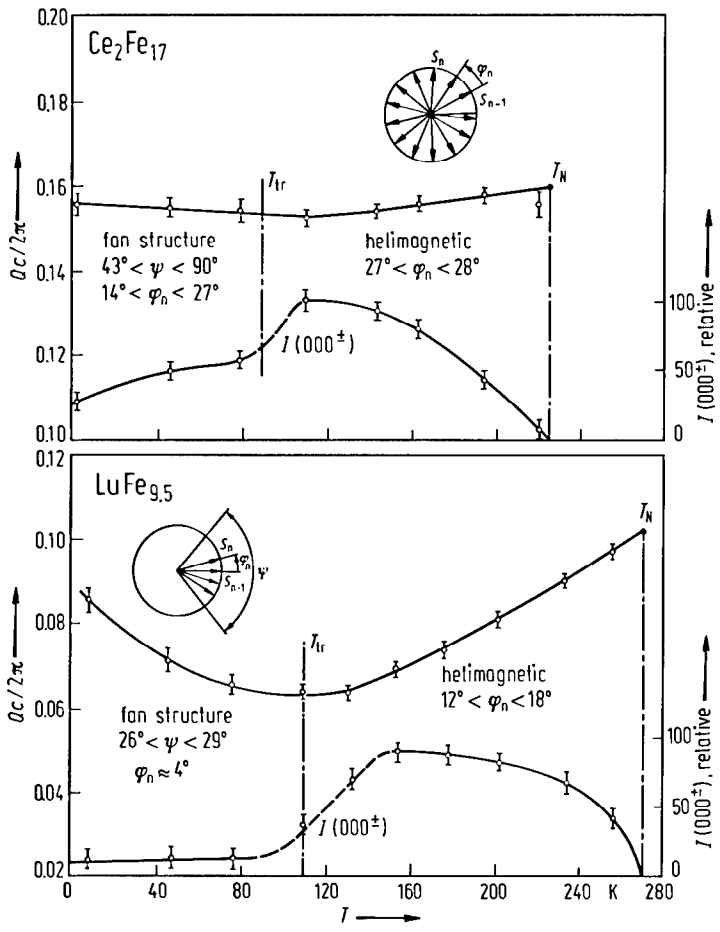

Fig. 492. Thermal variation of the propagation vector, Q, in c-units of the $CaCu_5$-type structure, and of the intensity of the $000\pm$ line in $LuFe_{9.5}$ and Ce_2Fe_{17} compounds [72 G 4]. In the transition region, both helimagnetic and fan structures may be observed due to the lack of homogeneity of the samples. The limiting angle of the fan structure is ψ.

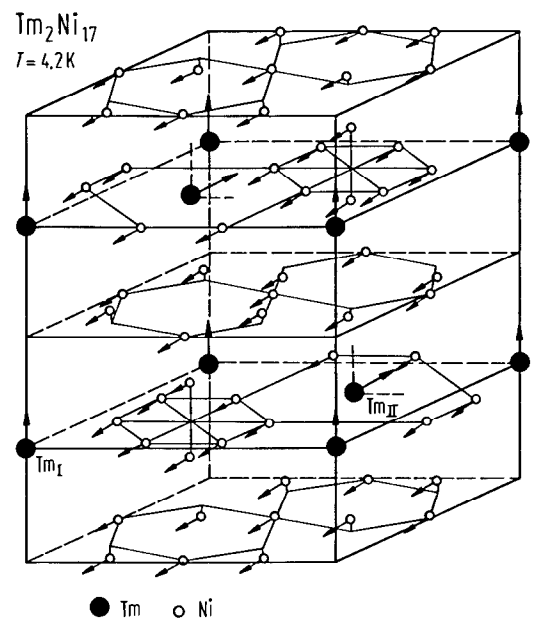

Fig. 493. Magnetic structure of Tm_2Ni_{17} at 4.2 K. A canted magnetic structure is evidenced, where the Tm moments of site I, $p_{Tm(I)}$, are parallel to the c axis, and the Tm moments of site II, $p_{Tm(II)}$, and of the Ni sublattice make an angle with the c axis. In case of Tb_2Ni_{17} and Er_2Ni_{17} collinear magnetic structures are evidenced with all moments perpendicular to the c axis [77 Y 2].

Table 109. Magnetic structures determined by neutron diffraction measurements in R_2M_{17} compounds.

	Magnetic structure	T K	$p_R(\mu_B)$		$p_M(\mu_B)$				Ref.
			p_{R1}	p_{R2}	p_c	p_d	p_f	p_h	
Ce_2Fe_{17}	fan	< 90							72 G 4,
	helimagnet	130		–			1.55		74 G 7,
	see Fig. 491								74 G 8
Ce_2Fe_{17}	helimagnet I	4.2···110							74 P 1
	helimagnet II	120···T_C							
Nd_2Fe_{17}	ferromagnet	300	1.20(17)	1.20(17)	1.85(28)	1.58(25)	1.56(18)	1.47(18)	82 H 3
Ho_2Fe_{17}	ferrimagnet	77		9.5(2)		−2.1			71 M 6
Tm_2Fe_{17}	ferrimagnet c axis	4.2		6.4(2)		−2.2(1)			74 E 1
	ferrimagnet (*ab*) plane	80		4.2(2)		−2.2(1)			
	ferrimagnet (*ab*) plane	231		0.0(3)		−1.5(3)			
Tm_2Fe_{17}	helimagnet	235···275							74 G 7
	ferrimagnet ⊥ c axis	80···235							
	ferrimagnet ∥ c axis	< 80							
Lu_2Fe_{17}	fan	<150							72 G 4,
	helicoidal	150···270							74 G 8
Nd_2Co_{17}	ferromagnet	300	1.74(17)	1.74(17)	3.22(16)	1.50(14)	1.04(9)	1.63(11)	82 H 3
Y_2Co_{17}	ferromagnet	300			2.12(5)	1.87(4)	1.89(4)	1.87(4)	74 S 3
Tb_2Ni_{17}	ferrimagnet ⊥ c axis	4.2	8.7(4)	8.5(5)			−0.3(4)		77 Y 2
Dy_2Ni_{17}	ferrimagnet ⊥ c axis	4.2	9.4(4)	8.5(4)			−0.2(2)		77 Y 3
Ho_2Ni_{17}	ferrimagnet ⊥ c axis	4.2	8.9	8.5			−0.3		77 Y 1
Er_2Ni_{17}	ferrimagnet ∥ c axis	4.2	8.4(5)	7.5(4)			−0.3(4)		77 Y 2
Tm_2Ni_{17}	canted structure	4.2	6.4(5)	5.6(5)			−0.3(4)		77 Y 2
Y_2Ni_{17}	ferrimagnet ⊥ c axis	4.2					0.35(10)		77 Y 1

For neutron diffraction studies see also
R_2Fe_{17} R=Ce [72G4, 74G7, 74G8, 74P1]; R=Nd [82H3]; R=Ho [71M6]; R=Tm [74E1]; R=Th [73E2]
R_2Co_{17} R=Ho [70M5]; R=Y [74S3]
R_2Ni_{17} R=Tb, Er, Tm [77Y2]; R=Ho, Y [77Y1]; R=Dy [77Y3]
$R_2(M'M'')_{17}$ $Nd_2(FeCo)_{17}$ [82H3]

For inelastic neutron scattering studies see
Ho_2Co_{17} [80C5*, 80N4, 82C12]; Ho_2Fe_{17} [82C12]

EPR, FMR

Ferromagnetic resonance measurements on Gd_2Ni_{17} may be analysed according to Wangsness' relation with $g_{Gd}=2.00$ and $g_{Ni}=2.10$ [80B15].

Mössbauer effect

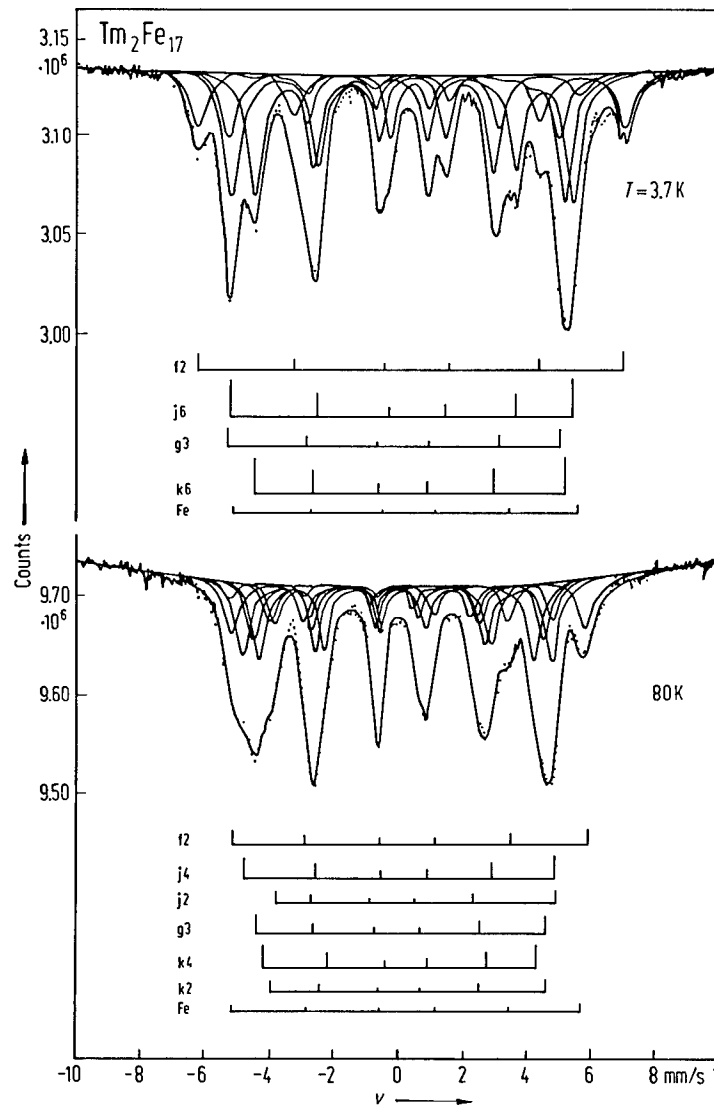

Fig. 494. Mössbauer spectra of Tm_2Fe_{17} obtained below and above the magnetic phase transition at 72K. The measured spectra, given by the data points, are fitted to a superposition of a number of hyperfine spectra, each of which has been associated with one of the crystallographic iron site as indicated underneath the spectra. The hyperfine spectrum due to a small contamination of metallic Fe is also indicated [74G15].

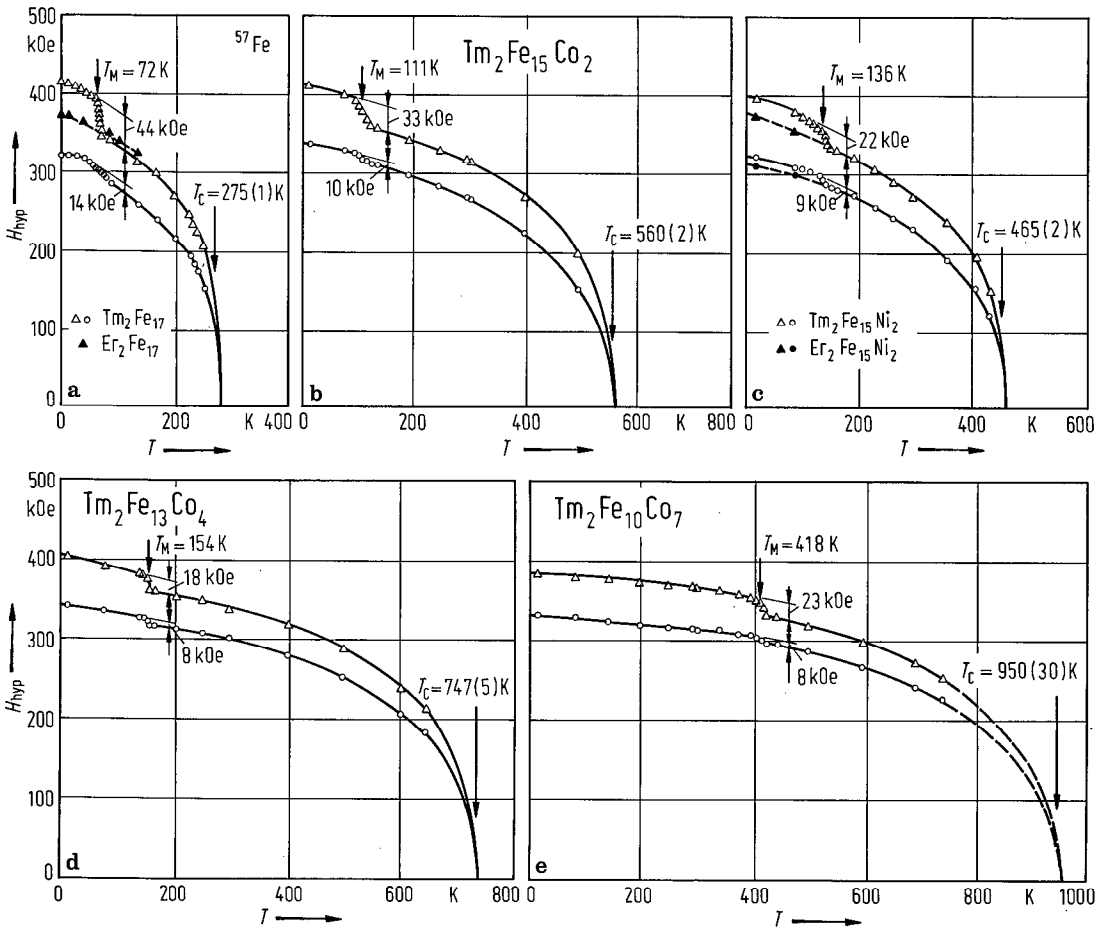

Fig. 495. Temperature dependence of the magnetic hyperfine field at ^{57}Fe observed in several compounds having Th_2Ni_{17} structure [76 G 11]: (a) Tm_2Fe_{17}, Er_2Fe_{17}, (b) $Tm_2Fe_{15}Co_2$; (c) $Tm_2Fe_{15}Ni_2$, $Er_2Fe_{15}Ni_2$, (d) $Tm_2Fe_{13}Co_4$; (e) $Tm_2Fe_{10}Co_7$. The temperature T_M marks the transition from a magnetization parallel to the c axis ($T < T_M$) to a magnetization parallel to the a axis ($T > T_M$). Triangles: H_{hyp} at f-site Fe nuclei; circles: H_{hyp} (average) at other-site nuclei.

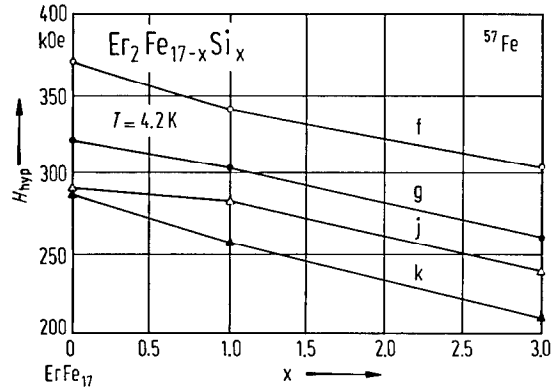

Fig. 496. Hyperfine magnetic field strength for four crystallographic inequivalent Fe sites obtained from ^{57}Fe Mössbauer effect measurements at 4.2 K in $Er_2Fe_{17-x}Si_x$ alloys [87 A 6].

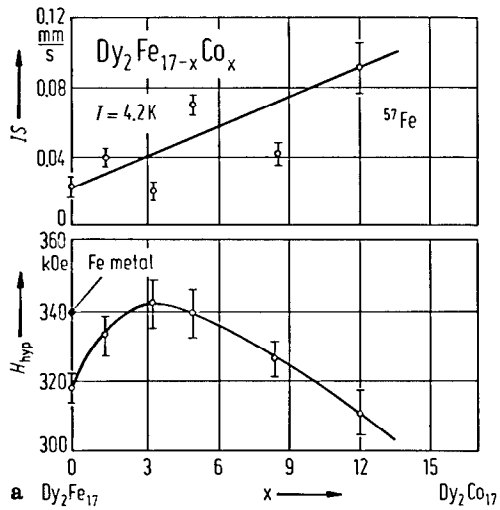

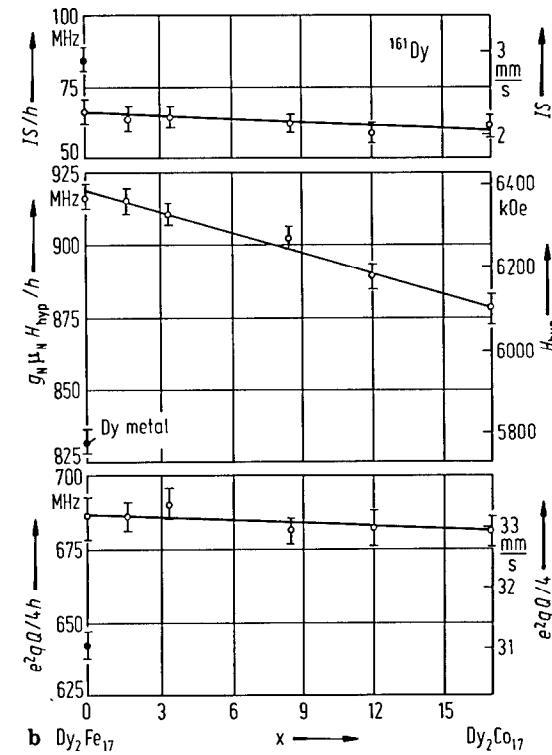

Fig. 497. Hyperfine interaction parameters at (a) ^{57}Fe and (b) ^{161}Dy nuclei in $Dy_2Fe_{17-x}Co_x$ compounds at 4.2 K [85 P 12]. The isomer shifts are relative to (a) pure iron and (b) a GdF_3 source at room temperature. The data for Dy metal are also given.

Table 110. Magnetic hyperfine field at ^{57}Fe in R_2Fe_{17} compounds.

	Structure	T	H_{hyp} (kOe) for sites hex: f rh: c	g d	k h	j f	Ref.
Ce_2Fe_{17}		4.2	329		257(20) [2]		74 G 15, 78 G 5
Pr_2Fe_{17}	rh	81	342	275	$(2h_1)$251 $(4h_2)$291	$(2f_1)$286 $(4f_2)$265	77 G 14
Nd_2Fe_{17}	rh	80	351	282	$(2h_1)$284 $(4h_2)$263	$(2f_1)$281 $(4f_2)$304	74 G 15, 77 G 14
	rh	77	332		275 [2]		74 G 14
Sm_2Fe_{17}	rh	15	368				74 G 15
Gd_2Fe_{17}	rh	15	381		306 [2]		74 G 15
	hex	15	379		315 [2]		74 G 14
	rh	77	359		291 [2]		74 G 14
Tb_2Fe_{17}	hex	84	367	303	$(2k_1)$293 $(4k_2)$262	$(2j_1)$291 $(4j_2)$317	74 G 15
Dy_2Fe_{17}	hex	80	364	291	$(2k_1)$276 $(4k_2)$313	$(2j_1)$317 $(4j_2)$283	74 G 15, 77 G 14
	hex	4.2	368	301	$(2k_1)$283 $(4k_2)$289	$(2j_1)$349 $(4j_2)$307	82 B 1
Ho_2Fe_{17}		15	372		312 [2]		74 G 15, 77 G 14
Er_2Fe_{17}	hex	4.2	371		314(20) [2]		78 G 5
Er_2Fe_{17} [1]	hex	4.2	370	320	290	290	87 A 6
Tm_2Fe_{17}	hex	3.7	419	322	302	334	77 G 14
Yb_2Fe_{17}	hex	15	362		316 [2]		74 G 15, 77 G 14
Y_2Fe_{17}	hex	4.2	357		294(20) [2]		78 G 5
	rh	15	364		299 [2]		74 G 15
	hex	300	299.92	299.99	208.54	265.7	85 C 2
Y_2Fe_{17} [1]	hex	4.2		(Fe_I) 361(3) in the occupancy ratio $Fe_I:Fe_{II}:Fe_{III}=2.3:9:6$	(Fe_{II}) 321(4)	(Fe_{III}) 290(4)	87 A 13

[1] From Fig. 5 in [87 A 6].
[2] Average hyperfine field for g(d), k(h), j(f) sites.

Table 111. Magnetic hyperfine field at ^{169}Tm, quadrupole splitting and crystal field terms in Tm_2M_{17} compounds at $T = 4.2$ K [87 G 8].

	Tm site	$\mu_0 H_{hyp}$ T	$e^2qQ/2$ cm/s	$(e^2qQ/2)_{latt.}$ cm/s	B_2^0, V_2^0 K
Tm_2Fe_{17}	I	755(3)	15.2(3)	−0.5(3)	$B_2^0 = -0.5(3)$
	II	739(3)	16.2(3)	0.5(3)	$B_2^0 = 0.5(3)$
Tm_2Co_{17}	I	737(2)	14.8(2)	−0.9(2)	$B_2^0 = -0.9(2)$
	II	724(2)	15.4(2)	−0.3(2)	$B_2^0 = -0.3(2)$
Tm_2Ni_{17}	I, II	720(6)	14.0(5)	−1.7(5)	$B_2^0 = -1.7(5)$
Tm_2Ni_{17} [1])	I	720(6)	14.1(5)		$V_2^0 = -2.1(4)$
	II	720(6)			$V_2^0 = -1.9(3)$
Tm^{3+} free ion		720	15.7		

[1]) The crystal field parameter V_2^0 negative for both Tm sites and is the same within the accuracy of analysis. The negative V_2^0 implies an easy direction of magnetization parallel to the c axis at low temperatures and a crystal field split ground state corresponding to $|J = \pm 6\rangle$ for both Tm sites [86 G 7].

For nuclear γ resonance studies see also

^{57}Fe R_2Fe_{17} [73 A 1, 74 G 15, 76 E 2]; R = Pr, Gd, Tm, Lu [70 L 8]; R = Ce, Pr, Nd, Tb, Dy, Tm, Yb [77 G 14]; R = Ce, Er, Y, Th [78 G 5]; R = Ce [70 B 14]; R = Nd [71 A 1]; R = Gd [71 A 1]; R = Dy [82 B 1, 82 G 13]; R = Tm [73 G 7]; R = Y [74 M 9, 77 S 11, 86 D 3, 87 A 13]; $Nd_2Fe_{17}H_x$ [88 R 4]; $(DyY)_2Fe_{17}$ [85 P 12, 85 P 13]

$R_2(FeCo)_{17}$ [77 S 10, 82 N 5]; $Tm_2(FeCo)_{17}$ [76 G 11, 76 G 12, 77 G 13]; $Y_2(FeCo)_{17}$ [71 S 7, 73 S 8, 85 C 2]; $R_2(FeNi)_{17}$, R = Gd, Dy, Y [77 S 12]; $Er_2(FeNi)_{17}$ [76 G 11]; $Tm_2(FeNi)_{17}$ [76 G 11]; $La_2(FeAl)_{17}$ [82 F 1]; $Dy_2(FeAl)_{17}$ [83 P 19]; $Er_2(FeSi)_{17}$ [87 A 6]; $Er_2(FeMn)_{17}$ [88 T 3]

^{153}Eu $Sm_2(CoFe)_{17}$, Sm_2Co_xMy, M = Fe, Cu, Zn, Zr [82 N 5]

^{155}Gd Gd_2Co_{17} [77 T 6, 85 D 5]; Gd_2Fe_{17} [85 D 5]

^{161}Dy Dy_2Fe_{17} [74 B 7, 79 B 7, 82 B 1, 82 G 13, 84 P 16, 85 P 11]; Dy_2Co_{17} [74 B 7, 79 B 7]; Dy_2Ni_{17} [79 B 7] $(DyY)_2Fe_{17}$ [85 P 12, 85 P 13]; $Dy_2(FeAl)_{17}$ [83 P 19]; see also Table 59

^{166}Er $(ErPr)_2Co_{17}$ [82 W 5]

^{169}Tm Tm_2Fe_{17} [86 G 7, 87 G 8, 89 G 1]; Tm_2Co_{17} [87 G 8, 89 G 1]

NMR

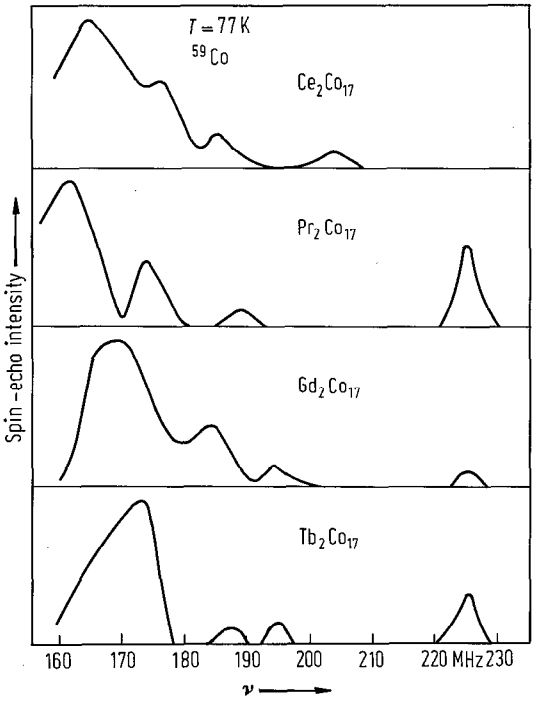

Fig. 498. NMR spectra of R_2Co_{17} (R = Ce, Pr, Gd and Tb) compounds at 77 K [76I5]. The ^{59}Co spectra have four peaks corresponding to crystallographically inequivalent sites.

Table 112. Magnetic hyperfine field determined by NMR on ^{59}Co in R_2Co_{17} compounds.

	T K	H_{hyp}(kOe)				Ref.
		18f	18h	6c	9d	
Ce_2Co_{17}	77	−182	−161	−200	−173	76I5
Pr_2Co_{17}	77	−186	−158	−221	−170	76I5
Nd_2Co_{17}	77	−187	−161	−221	−171	75S10
Sm_2Co_{17}	4.2	161	132	176	150	82P11
Gd_2Co_{17}	77	−191	−167	−221	−180	76I5
Tb_2Co_{17}	77	−191	−170	−221	−184	76I5
Dy_2Co_{17}	77	−192	−165	−221	−179	76I5
Ho_2Co_{17}	77	−192	−165	−220	−179	76I5
Y_2Co_{17}	77	−175(1)	−168(2)	−198(1)	−168(2)	76N1
Y_2Co_{17}	77	−195	−165	−215	−178	73D5
Y_2Co_{17}	4.2	171	174 179	200.8 199.8	96	82F5

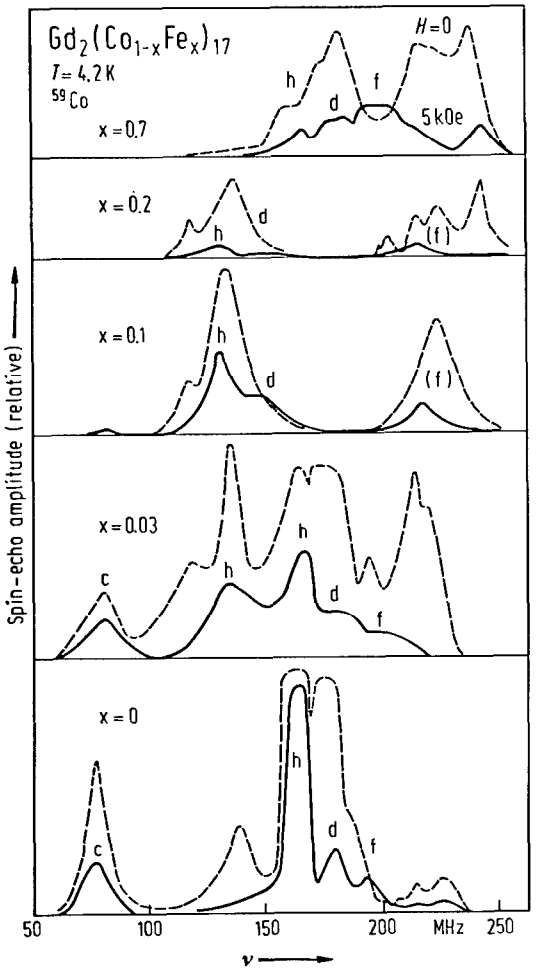

Fig. 499. ^{59}Co spin-echo spectra of $Gd_2(Co_{1-x}Fe_x)_{17}$ compounds for x = 0, 0.03, 0.1, 0.2 and 0.7, at 4.2 K. Broken curves show the results in zero external field and full curves show the results at 5 kOe. The assignments to the lattice sites are also shown [81 K 3].

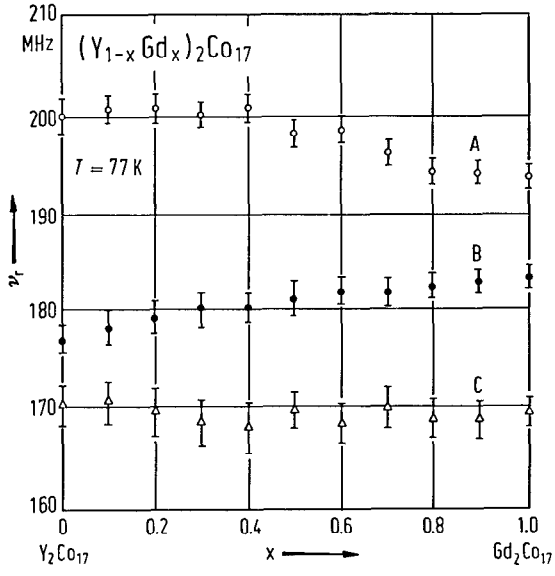

Fig. 500. Variation of the ^{59}Co resonance frequency as a function of Gd concentration in $(Gd_xY_{1-x})_2Co_{17}$ compounds at 77 K [76 N 1]. This dependence is attributed to the contribution of Gd 4f electrons to the hyperfine field. The resonance frequencies were ascribed to: A – 6c(Co_{IV}); B – 18f(Co_{II}), C – 18h + 9d(Co_{III} + Co_I).

For NMR studies see also

^{27}Al	$Tb_2(NiAl)_{17}$ [86 H 1]
^{59}Co	R_2Co_{17}, R = Ce, Pr, Nd, Gd, Tb, Dy, Ho, Y [76 I 5]; R = Nd [75 S 10]; R = Sm [82 P 11]; R = Gd [73 D 5, 80 F 5]; R = Y [73 D 5, 77 F 3, 77 Y 5, 78 F 5, 79 S 10, 80 F 5]
	$(YNd)_2Co_{17}$ [87 K 6]; $(YGd)_2Co_{17}$ [76 N 1, 82 F 5]
	$R_2(CoMn)_{17}$ [82 F 4]; $R_2(CoFe)_{17}$, R = Ce, Pr, Nd, Gd, Tb, Dy, Ho, Y [76 I 5]; $Gd_2(FeCo)_{17}$ [81 K 3]; $Y_2(FeCo)_{17}$ [76 I 4, 79 S 10]; $Gd_2(CoMn)_{17}$ [82 F 7, 82 F 8]; $Y_2(CoMn)_{17}$ [82 F 7, 82 F 8]; $Y_2(CoCu)_{17}$ [81 I 1, 81 I 2]; $Y_2(CoAl)_{17}$ [81 I 1, 81 I 2];
^{89}Y	Y_2Fe_{17} [73 O 9, 83 V 2, 85 V 2]; Y_2Co_{17} [76 F 1, 85 R 9]; $(YGd)_2Co_{17}$ [82 F 5]; see also Table 61
^{143}Nd, ^{145}Nd	Nd_2Co_{17} [75 S 10, 77 S 14]
^{147}Sm, ^{149}Sm	Sm_2Co_{17} [82 P 11]

Anisotropy, magnetostriction

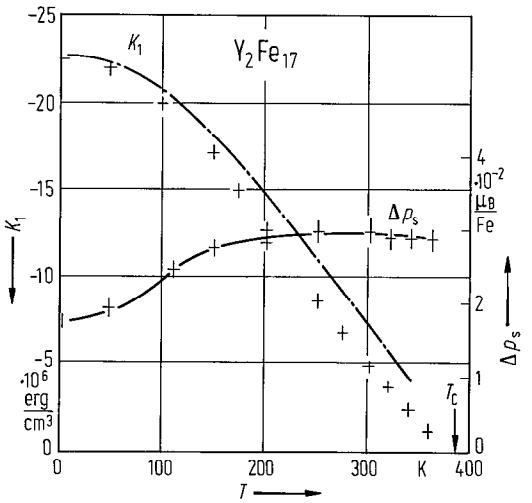

Fig. 501. Thermal variation of the anisotropy constant K_1 and the anisotropy in the magnetization, Δp_s, in Y_2Fe_{17} compound [87 A 13]. The decrease with temperature of K_1 is slightly faster than that theoretically predicted for a localized magnetic moment, $K_1(T)=K_1(0)(M(T)/M(0))^2$-dot-dashed line [86 D 3]. The large anisotropy of the magnetization is associated with the large magnetocrystalline anisotropy, see Fig. 467.

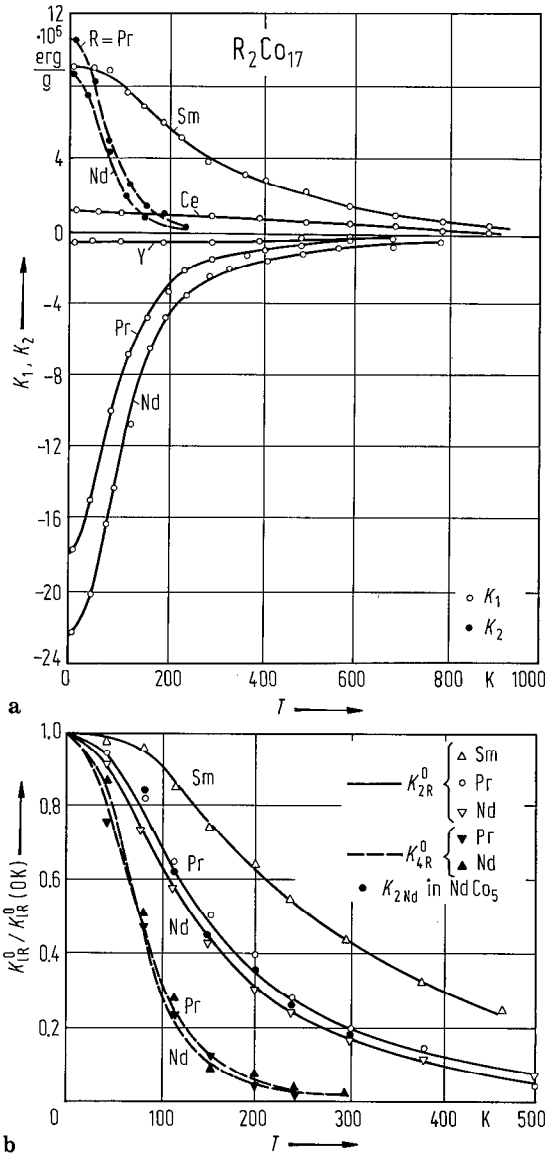

Fig. 502. (a) Temperature dependence of the anisotropy constants K_1 and K_2 in R_2Co_{17} compounds with R = Ce, Pr, Nd, Sm and Y [79 D 4]. In (b) are plotted the $K^0_{lR}/K^0_{lR}(0\,K)$ values, l = 2 and 4, compared with the prediction of the one-ion model $K^0_{lR}(T)/K^0_{lR}(0) = \hat{I}_{l+1/2}[\mathscr{L}^{-1}(m_R)]$ (solid lines).

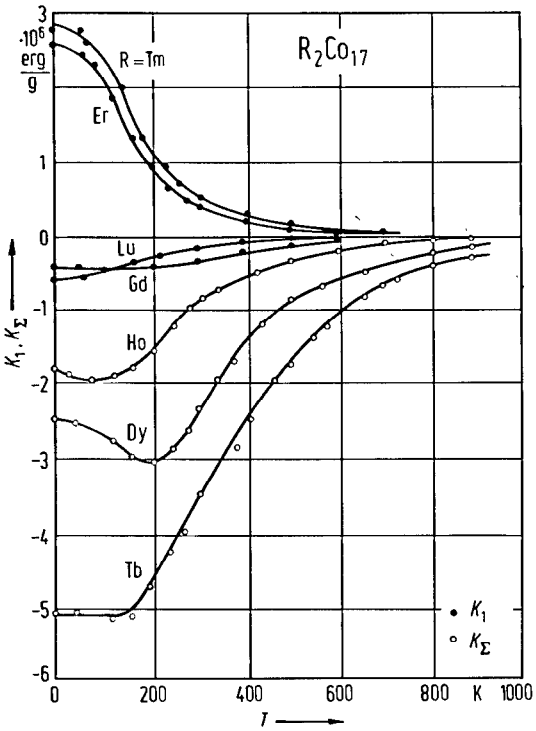

Fig. 503. Temperature dependence of the anisotropy constant K_1 in R_2Co_{17} compounds with R = Gd, Er, Tm, Lu (full circles) and of the effective anisotropy constants, $K_\Sigma = K_1 + 2K_2 + \ldots$, in R_2Co_{17} compounds with R = Tb, Dy and Ho (open circles). The shape of the K vs. T curves is more complex than in light rare-earth compounds, especially for Tb_2Co_{17}, Dy_2Co_{17} and Ho_2Co_{17}. This may be connected with the fact that under the action of an external magnetic field a noncollinear magnetization can appear along the hard direction and give an additional increase of the magnetization [75 D 4, 79 D 4].

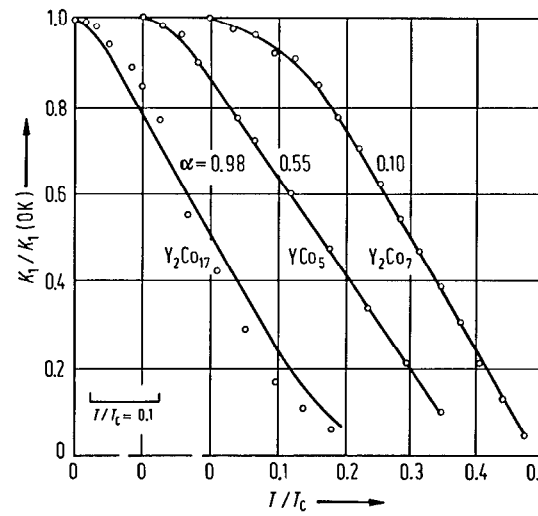

Fig. 504. Temperature dependence of K_1 for the Co sublattice in Y_2Co_{17}, YCo_5 and Y_2Co_7 compounds and the values calculated according to the relation $K_1/K_1(0\,K) = (1 - \alpha T/T_C)\,[M/M(0\,K)]^2$ [79 D 4]. The experimental data seem to be satisfactory described by the Akulov-Zener-Carr law mentioned above.

Table 113. Anisotropy constants of some R_2M_{17} compounds.

	T	K_1	K_2	Ref.
	K	10^6 erg cm^{-3}		
Ho_2Fe_{17}	4.2	−56.5(5)	17.5(5) K_4: 0.85(3)	81 C 4
Y_2Fe_{17}	4.2	−23(1)	− 0.11	86 D 3, 87 A 13
Sm_2Co_{17}	77	67	14	74 D 7
	293	32	3.5	74 D 7
Gd_2Co_{17}	77	− 4.7	0.50	74 D 7
	293	− 3.0	0.35	74 D 7
	293	− 2.7	3	76 K 3
Tb_2Co_{17}	77	–	–	75 D 4
	293	−40	2.5	75 D 4
Dy_2Co_{17}	77	−28	2.0	75 D 4
	293	−31	3.0	75 D 4
Ho_2Co_{17}	4.2	−14.8(4)	K_4: 0.66(2)	81 C 4
	77	−20	1.5	75 D 4
	293	−11	0.7	75 D 4
Er_2Co_{17}	4.2	5.0	1.6	74 N 6
	77	17	4.00	74 D 7
	293	3.5	0.23	74 D 7
	RT	2.7	1.6	74 N 6
Tm_2Co_{17}	4.2	18.9	1.6	74 N 6
	77	27	4.00	74 D 7
	293	3.9	0.23	74 D 7
	RT	4.3	1.3	74 N 6
Yb_2Co_{17}	4.2	3.4	4.3	74 N 6
	RT	3.8	0	
Lu_2Co_{17}	77	− 5.8	0.90	75 D 4
	293	− 2.0	0.20	
Y_2Co_{17}	77	− 5.8	0.50	74 D 7
	293	− 4.0	0.30	
	RT	− 2.9	0.03	66 H 1
	RT	− 2.1	− 0.10	

For Fig. 505, see next page.

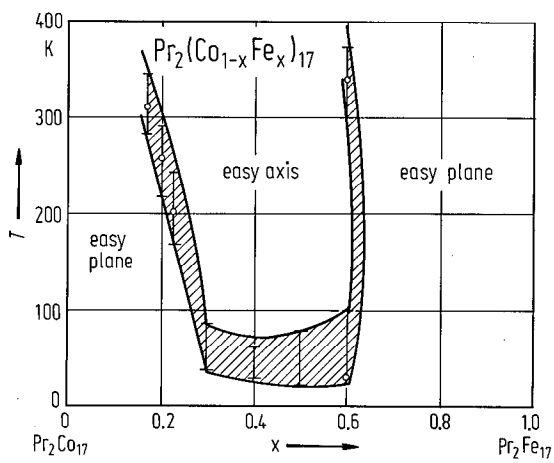

Fig. 506. Magnetization orientation phase diagram in $Pr_2(Co_{1-x}Fe_x)_{17}$ compounds [82 M 4]. The shaded region represents the region over which the easy axis rotates. The experimental data are consistent with the theoretical analysis [82 C 1, 82 C 2].

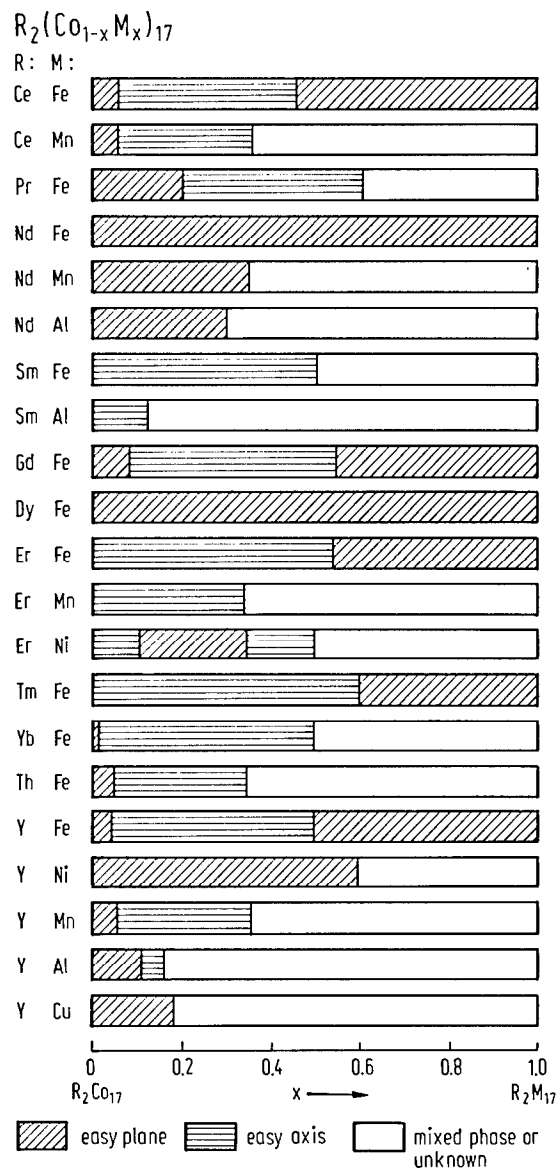

Fig. 505. Dependence of the easy direction of magnetization on the composition in some $R_2(Co_{1-x}M_x)_{17}$ compounds [74 A 1, 78 H 1, 79 E 5].

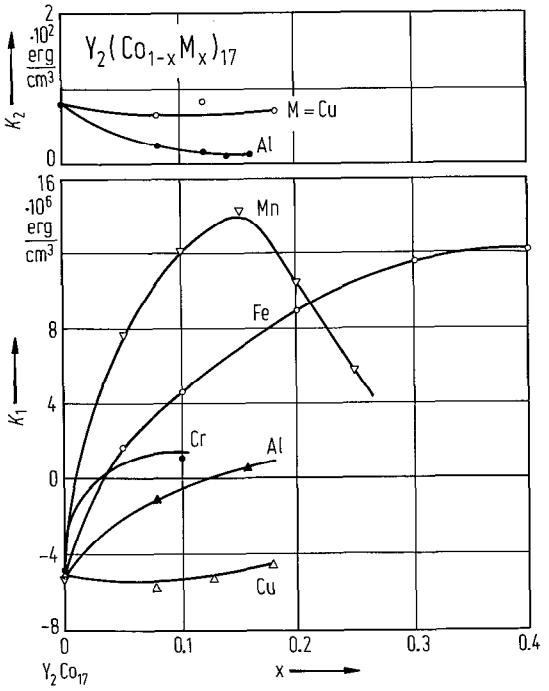

Fig. 507. Composition dependence of the anisotropy constants K_1 and K_2 for $Y_2(Co_{1-x}M_x)_{17}$ compound with M = Fe, Mn, Cr extrapolated at 0 K [77 P 3] (K_1) and with M = Cu and Al, at 77 K [72 H 1, 74 H 3, 77 H 1] (K_1, K_2).

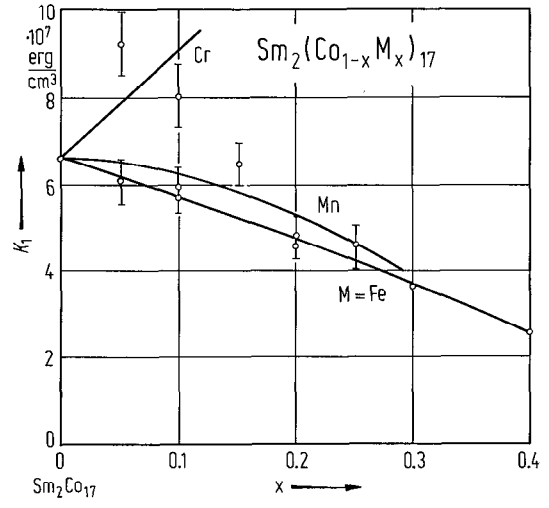

Fig. 509. Anisotropy constant K_1 at 0 K for the $Sm_2(Co_{1-x}M_x)_{17}$ compounds with M = Cr, Mn and Fe [77 P 3].

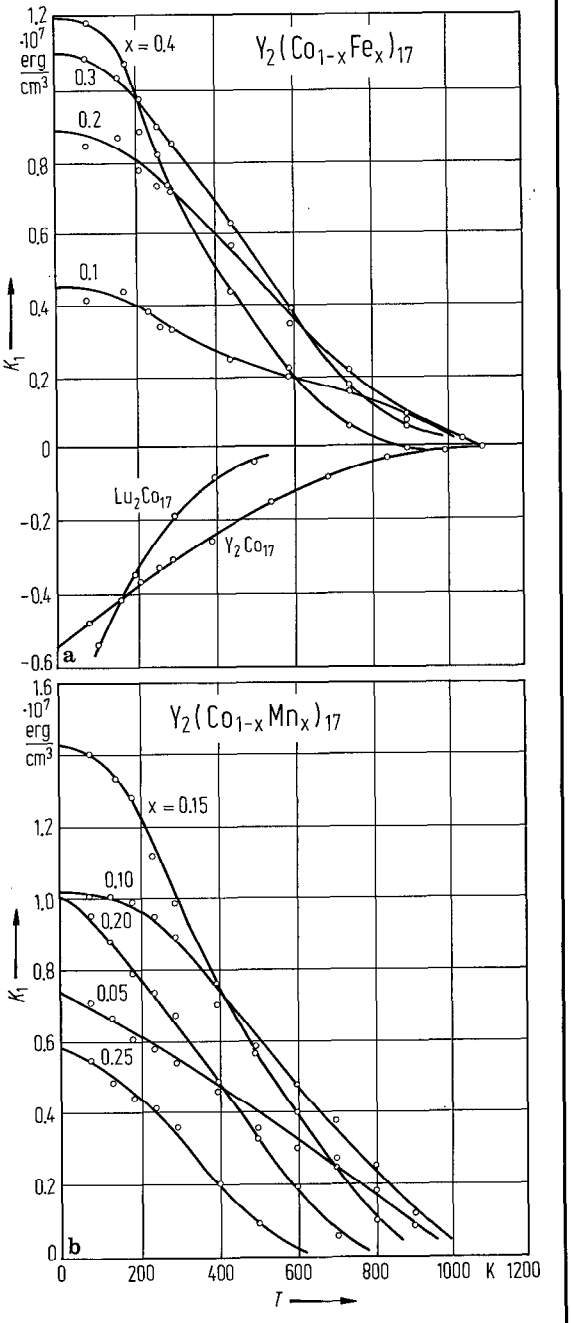

Fig. 508. Temperature dependence of the magnetocrystalline anisotropy constant K_1, for some $Y_2(Co_{1-x}M_x)_{17}$ compounds with: (a) M = Fe and (b) M = Mn [75 P 5, 77 P 3].

For anisotropy studies see also:

R_2M_{17} [88 K 5]

R_2Fe_{17} [87 R 2]; R = Ho [81 C 4*, 82 S 2]; R = Tm [78 W 2]; R = Y [86 D 3, 87 A 13]; Er_2Fe_{17} [78 I*]

R_2Co_{17} [73 G 4, 73 G 5, 74 A 1, 74 K 4, 78 W 2, 78 B 5, 79 D 4, 87 R 1, 88 T 1]; R = Sm, Gd, Er, Tm, Y [74 D 8]; R = Sm, Y [74 K 6]; R = Er, Tm, Yb [74 N 6]; R = Sm, Er, Tm [74 G 11]; R = Tb, Dy, Ho [75 D 4*]; R = Tb, Ho, Er [76 M 13]; R = Pr, Nd, Sm, Gd [77 T 1]; R = Sm, Er, Tm [78 K 1]; R = Ce, Pr, Nd, Sm, Gd, Tb, Dy, Ho, Er, Tm, Yb [85 R 4]; R = Pr [84 W 1]; R = Nd [87 R 3]; R = Sm [76 K 7, 82 B 6, 83 J 3, 84 W 1, 87 R 3]; R = Gd [76 K 3, 76 K 4]; R = Ho [81 C 4*, 82 S 2, 85 R 4]; R = Y [66 H 1, 67 H 2*, 77 M 9, 78 H 1, 78 K 3, 79 H 1, 79 S 12(T), 84 K 1]

$(R'R'')_2M_{17}$ $(NdY)_2Co_{17}$ [85 K 2]; $(SmPr_2Co_{17}$ [74 D 9, 81 L 1]; $(SmNd)_2Co_{17}$ [81 L 1]; $(SmGd)_2Co_{17}$ [74 D 9]; $(SmGd)_2(CoMn)_{17}$ [79 B 3]; $(SmY)_2Co_{17}$ [74 D 9, 81 L 1, 82 D 6]; $(SmR)_2Co_{16.4}Zr_{0.6}$, R = La, Ce, Y [85 F 4]; $(GdY)_2Co_{17}$ [87 K 1, 87 K 2]; $(DyY)_2Co_{17}$ [74 M 5, 77 M 9]; $(NdSm)_2(FeCo)_{17}$ [79 L 5]

$R_2(M'M'')_{17}$ $R_2(CoM)_{17}$ [76 K 6]; $Ce_2(CoM)_{17}$, M = Cu, V, Ti, Zr, Hf [82 W 4]; $Pr_2(CoM)_{17}$, M = Mn, Fe, Cr [83 J 4, 83 J 5]; $Sm_2(CoM)_{17}$, M = Fe, Mn, Cr [77 P 3, 77 P 5, 78 D 3, 81 L 1]; $Er_2(CoM)_{17}$, M = Fe, Mn, Ni [76 N 4, 77 N 1]; $Y_2(CoM)_{17}$, M = Mn, Fe, Cr [77 P 3, 81 L 1]

$Pr_2(CoMn)_{17}$ [83 J 5]; $Sm_2(CoMn)_{17}$ [81 K 1]; $Gd_2(CoMn)_{17}$ [82 F 7, 86 K 1]; $Y_2(CoMn)_{17}$ [82 F 7, 84 K 1, 86 K 1]; $Er_2(CoMn)_{17}$ [82 W 4]

$R_2(FeCo)_{17}$ [82 C 1(T), 82 C 2(T)]; R = Gd, Dy, Y [77 G 11, 78 M 8]; R = Pr [74 S 6*]; R = Sm [73 M 10, 74 D 9, 76 P 4]; R = Er [74 D 9, 82 W 4]; R = Tm [88 F 1]; R = Yb [77 N 1]; R = Y [72 H 1, 74 S 6*, 75 P 5, 78 K 2, 83 S 19*, 86 T 5, 88 F 1]

$Sm_2(CoNi)_{17}$ [78 M 11]; $Er_2(CoNi)_{17}$ [74 D 9]; $Y_2(CoNi)_{17}$ [78 M 11]; $Pr_2(CoCr)_{17}$ [83 J 5]; $Y_2(CoCu)_{17}$ [77 H 1*, 81 I 2, 83 S 19*]; $Nd_2(CoAl)_{17}$ [77 N 1]; $Sm_2(CoAl)_{17}$ [77 N 1]; $Y_2(CoAl)_{17}$ [74 H 3*, 77 H 1*, 81 I 2, 83 S 19*]; $Sm_2(CoAg)_{17}$ [85 J 2]; $Sm_2(CoGe)_{17}$ [85 J 2]; $R_2(CoZr)_{17}$, R = Ce, Sm [82 F 11]; $Sm_2(CoZr)_{17}$ [81 K 1]

For spin reorientation see

R_2Co_{17} [79 D 4]

$R_2(M'M'')_{17}$ M', M'' = Fe, Co, Mn, Al, Ni, Cu [79 E 5]

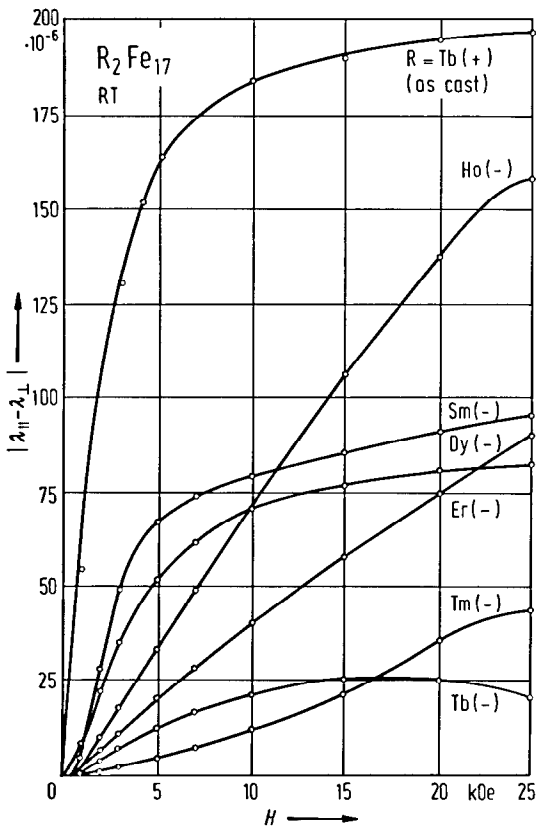

Fig. 510. Room-temperature magnetostriction of some R_2Fe_{17} polycrystals [80 A 2, 80 c 1]. The sign of $\lambda_{\parallel} - \lambda_{\perp}$ is indicated in parentheses. Tb_2Fe_{17} and Dy_2Fe_{17} compounds contain both rhombohedral and hexagonal phases. With the exception of Tb_2Fe_{17} (as cast), all samples were thermally treated at 1000 °C.

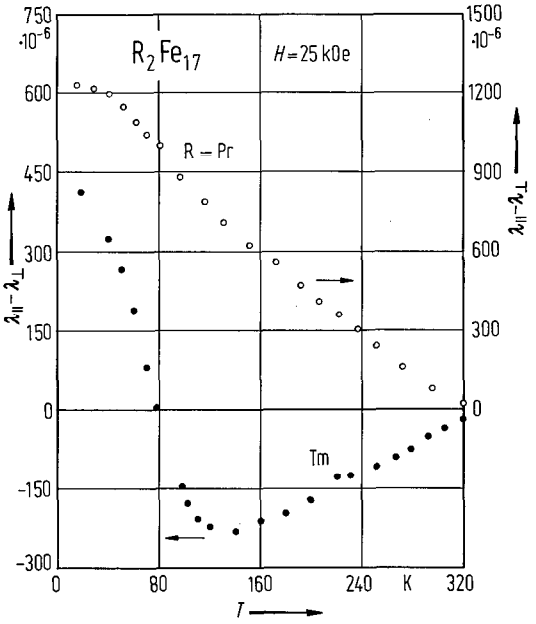

Fig. 511. Temperature dependence of the magnetostriction, $\lambda_{\parallel}-\lambda_{\perp}$, at $H=25$ kOe in R_2Fe_{17} (R = Pr and Tm) compounds [83 M 5]. In case of Tm_2Fe_{17} compound the sign of $\lambda_{\parallel}-\lambda_{\perp}$ is negative at high temperatures. Near $T\cong80$ K it becomes positive and the magnetostriction increases with decreasing temperature. Near $T\cong220$ K the magnetostriction is nearly temperature independent. This behaviour may be correlated with the start of spin reorientation from easy plane to easy axis (c axis) at $T\cong90$ K, and the fact that below $T\cong235$ K the easy direction of magnetization becomes the a axis in the basal plane.

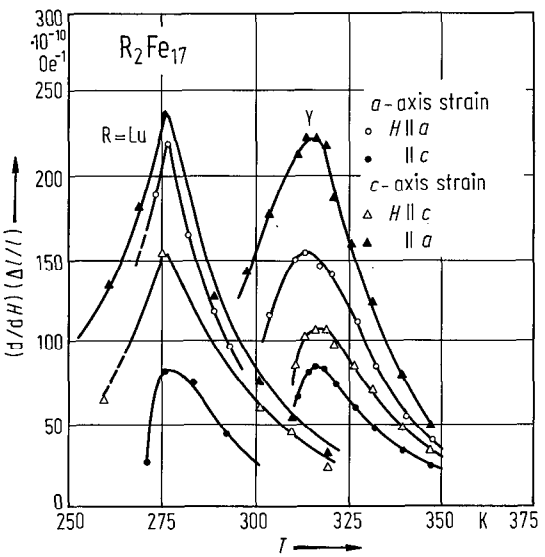

Fig. 512. Forced magnetostriction of Y_2Fe_{17} and Lu_2Fe_{17} single crystals. Strains are measured along the a axis and c axis [76 G 5]. The largest magnetostriction is measured along the c axis and a positive sign is observed for $\Delta(c/a)/(c/a)$, see Fig. 513. These results are associated with the strong dependence of the negative interactions occurring in the substitution zone on the interatomic distances.

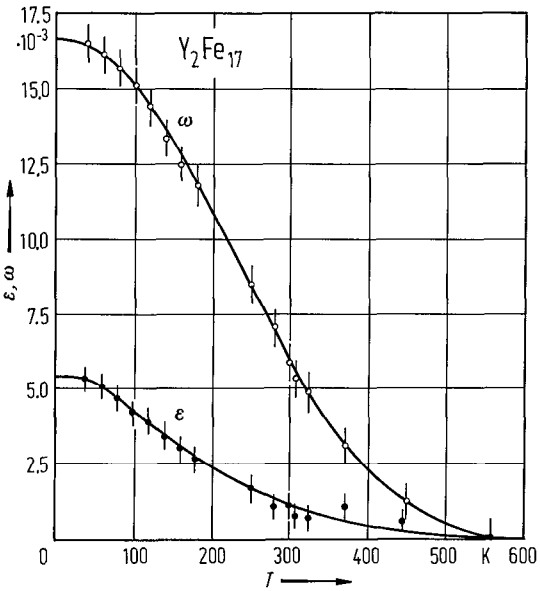

Fig. 513. Temperature dependence of the volume, $\omega=\Delta V/V$, and the c/a ratio, $\varepsilon=\Delta(c/a)/(c/a)$, anomalies in Y_2Fe_{17} single crystal [76 G 5].

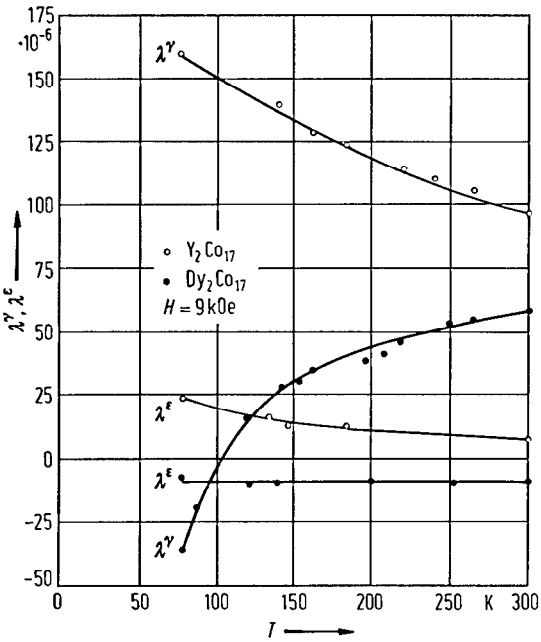

Fig. 514. Temperature dependence of the magnetostriction coefficients λ^γ and λ^ε in Y_2Co_{17} and Dy_2Co_{17} for an applied magnetic field of 9 kOe [73 D 7].

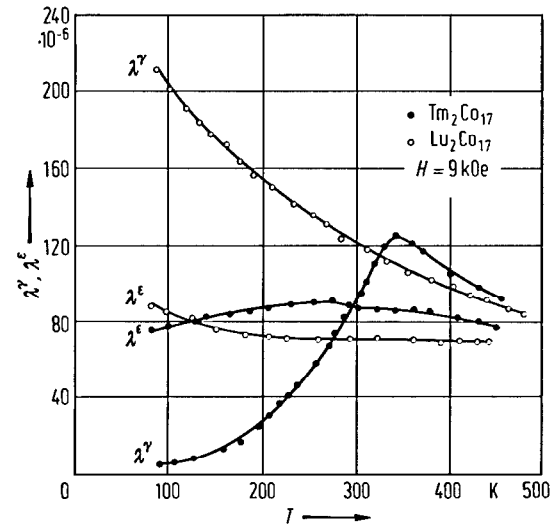

Fig. 515. Temperature dependence of the magnetostriction coefficients λ^γ and λ^ε in Tm_2Co_{17} and Lu_2Co_{17} for a magnetic field of 9 kOe [74 M 4].

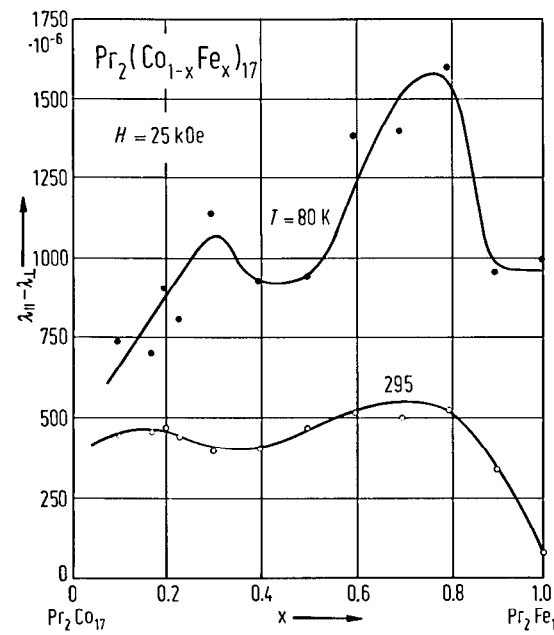

Fig. 516. Composition dependence of the magnetostriction, $\lambda_\parallel - \lambda_\perp$, at $H = 25$ kOe as function of the Fe content in $Pr_2(Co_{1-x}Fe_x)_{17}$ compounds at $T = 80$ and 295 K [82 M 4].

For magnetostriction studies see also:

R_2Fe_{17} [80A2, 85R3]; R=Pr [83M5]; R=Tb [72C6, 74C2, 74C3]; R=Tm [83M5]; R=Lu [76G5]; R=Y [76G5]

R_2Co_{17} [74A1]; R=Gd [75D5]; R=Tb [72C5, 76M13]; R=Dy [73D7, 74M6*]; R=Ho [76M13, 79D5*]; R=Er [76M13, 79D5*]; R=Tm [74M4, 79D5*]; R=Lu [74M4, 79D5*]; R=Y [73D7, 74M6*, 75D5]

R_2Ni_{17} R=Tb [72C5]

$(R'R'')_2M_{17}$ $(SmY)_2Co_{17}$ [84K11]; $(DyY)_2Co_{17}$ [74M6*]; $(LuTm)_2Co_{17}$ [74M4]

$R(M'M'')_{17}$ $Pr_2(FeCo)_{17}$ [82M4, 83T9, 84R4]; $Dy_2(FeCo)_{17}$ [82R1, 83R2, 87H2]; $Dy_2(FeAl)_{17}$ [83R2, 85R1, 87H2, 88R1]; $Er_2(FeCo)_{17}$ [86K6]

For elastic and magnetoelastic properties see also:

$Er_2(FeCo)_{17}$ [86A6]

Transport properties

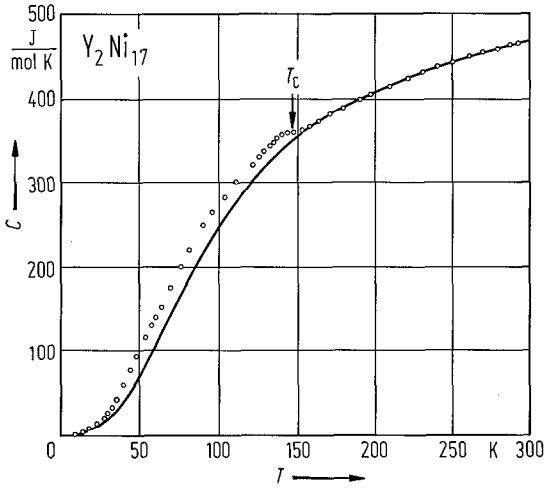

Fig. 517. Thermal variation of the specific heat of Y_2Ni_{17}. The circles are the experimental values, the line corresponds to the lattice and electronic contributions with Debye temperature $\Theta_D = 404$ K and electronic coefficient $\gamma = 0.17\,J\,mol^{-1}\,K^{-2}$ [80G2]. A magnetic contribution is evidenced between 30 and 160 K. The magnetic entropy at T_C is determined as $S_m = 30(10)\,J\,mol^{-1}\,K^{-1}$. For $p_{Ni} = 0.26\,\mu_B$ deduced from magnetization measurements, a maximum magnetic entropy, $S_m = 25\,J\,mol^{-1}\,K^{-1}$, is obtained.

For specific heat measurements see also

R_2M_{17} Y_2Ni_{17} [80G2]

$R_2(M'M'')_{17}$ $Pr_2(CoFe)_{17}$ [84G8]

For magnetocaloric effect see also

$R_2(M'M'')_{17}$ $Ce_2(CoFe)_{17}$ [84O2]; $Sm_2(FeCo)_{17}$ [84O2]; $Y_2(FeCo)_{17}$ [84O2]

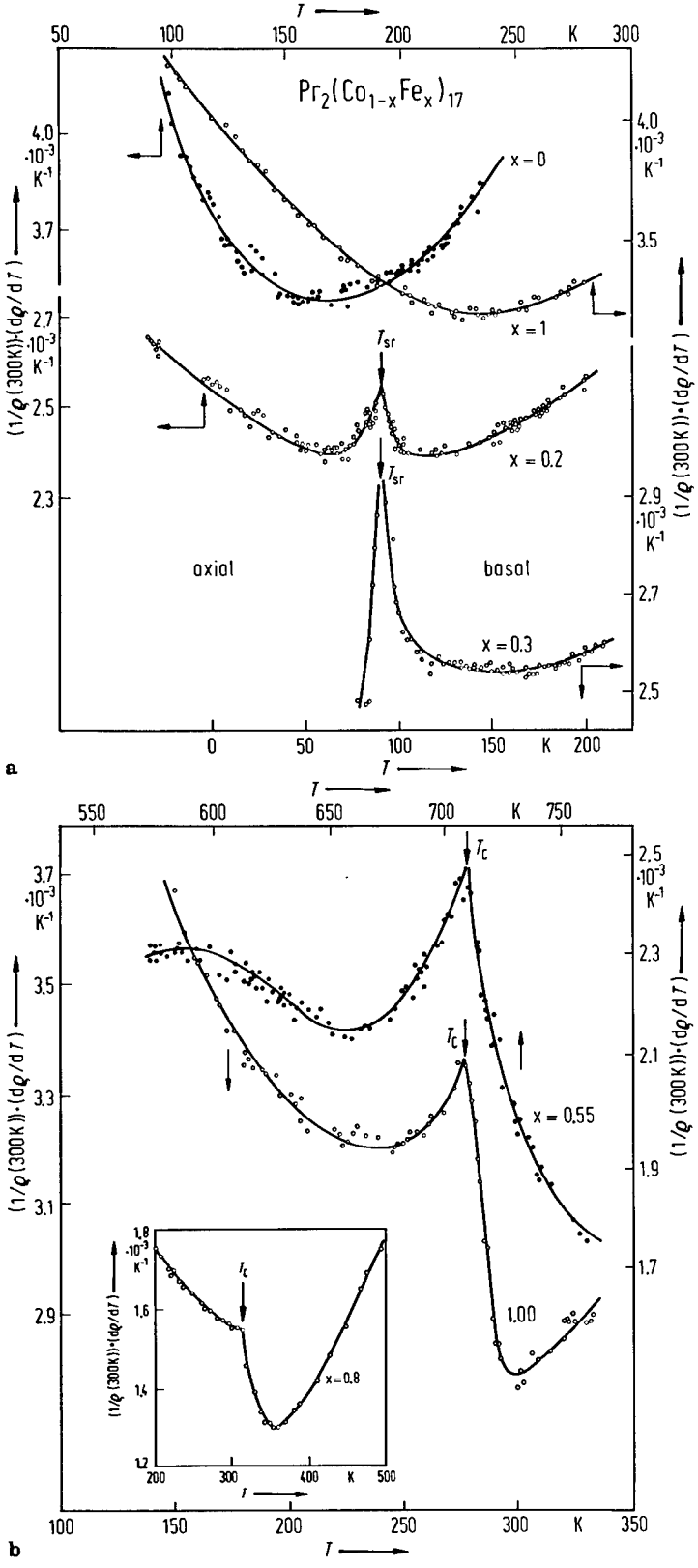

Fig. 518. Temperature derivative of the electrical resistivity, $d\varrho/dT$, in $Pr_2(Co_{1-x}Fe_x)_{17}$ compounds. (a) Anomalous behaviour is observed near the spin reorientation temperature for the samples having $x=0.2$ and 0.3. No anomalies have been found for the samples with $x=0$ and $x=1.0$. (b) Behaviour of the temperature derivative, $d\varrho/dT$, near the Curie point for $x=0.55$, $x=0.80$ and $x=1.00$ [85 M 9].

For electrical resistivity and magnetoresistivity studies see also
R_2M_{17} Y_2Ni_{17} [80 G 2]
$R_2(M'M'')_{17}$ $Pr_2(CoFe)_{17}$ [82 S 24, 85 M 9]

Domain structure, magnetization processes

Fig. 519. Magnetic domains in Sm_2Co_{17}. Rosette structure in grain at right is characteristic of easy-axis magnetic symmetry. Characteristic easy-axis domain patterns were seen in Sm_2Co_{17}, Gd_2Co_{17} and $R_2(FeCo)_{17}$. Domains were not seen in Pr_2Co_{17}, Ce_2Co_{17}, Y_2Co_{17} and Nd_2Co_{17} [72 L 1].

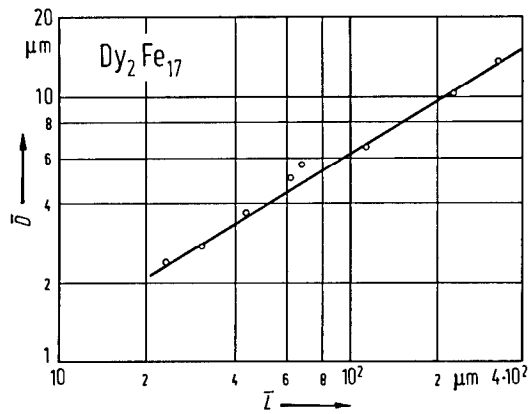

Fig. 520. Dependence of the mean domain width $\bar{D}$ on the mean grain thickness $\bar{L}$ in polycrystalline Dy_2Fe_{17} compound. The points record the experimental results and the line is the theoretical relation described by the equation $\bar{D}=0.32\,\bar{L}^{2/3}$. From these data are estimated the Bloch wall energy $\gamma=16.6\cdot10^{-3}\,J\,m^{-3}$, the Bloch wall width $\delta=1.8\cdot10^{-9}\,m$, and $K_1=6.9\cdot10^{6}\,J\,m^{-3}$ [80 P 3].

For magnetization processes see also:

R_2M_{17} [88 K 5]; Sm_2M_{17} [85 B 1]

R_2Fe_{17} [66 S 1]

R_2Co_{17} [67 S 3, 76 N 3]; R = Sm, Er, Tm [74 U 1]; R = Pr [84 W 1, 85 C 5]; R = Sm [70 B 1, 72 S 3, 73 C 3, 77 G 8, 82 B 6, 84 O 1, 84 W 1, 85 B 6]; R = Y [78 K 3]

$R_2(M'M'')_{17}$ $Sm_2(CoM)_{17}$ [85 S 23]; M = Mn, Fe, Cu [79 E 5]

$R_2(FeCo)_{17}$ [71 R 3, 75 S 12]; $Pr_2(CoFe)_{17}$ [76 M 7]; $Sm_2(CoFe)_{17}$ [70 N 2, 74 H 5, 75 P 6, 81 J 1]; $Y_2(FeCo)_{17}$ [72 S 3]; $MM_2(FeCo)_{17}$ [73 T 3]

$Pr_2(CoAl)_{17}$ [74 O 3]; $Sm_2(CoAl)_{17}$ [74 O 3]; $Sm(CoCu)_z$ [75 P 7, 76 M 6, 76 M 8, 76 N 3, 76 P 3, 77 M 6, 78 N 1, 79 N 1, 86 C 1]

$R(CoCuFe)_z$, R = Ce, Sm [75 M 5]; $Ce(CoCuFeTi)_z$ [77 I 5]; $Sm(CoCuFe)_z$ [75 L 1, 76 M 9, 76 S 7, 77 L 3]; $Sm(CoFeMn)_z$ [76 N 2, 79 E 5]; $Sm(CoCuFeZr)_z$ [77 O 10, 81 F 3, 82 P 5]; $Sm(CoCuFeTi)_z$ [83 U 1]; $Sm(FeNiCoM)_z$ [85 L 2]; $(SmR)(CoCuFeZr)_z$ R = Pr, Nd [85 W 5]

For domain structure see

R_2M_{17} [88 K 5]; R_2Fe_{17} [86 S 11]; Dy_2Fe_{17} [80 P 3]; R_2Co_{17}, R = Pr, Nd, Sm, Gd, Y [72 L 1]; Sm_2Co_{17} [73 R 1, 84 O 1]; Dy_2Co_{17} [76 A 3]; R = Ho [79 K 6]; R = Er [79 K 5]

$R_2(M'M'')_{17}$ $Sm_2(CoMn)_{17}$ [81 D 8]; $R_2(FeCo)_{17}$, R = Ce, Pr, Sm, Gd, Y [72 L 1]; $Sm(CoCu)_z$ [79 M 8, 79 N 1]; $Er_2Fe_3Co_{14}$ [79 K 5]; $Ho_2Fe_3Co_{14}$ [79 K 6]

For magnetic aftereffect see also

$R_2(M'M'')_{17}$ $Sm_2(CoM)_{17}$ [85 S 23]

Spectroscopic studies

For spectroscopic studies see

Valence band spectra Gd_2Fe_{17} [79 A 6]

L_{III} spectra Ce_2Co_{17} [82 F 9]

2.4.2.19 RM_{12} compounds

Crystal structure, lattice parameters

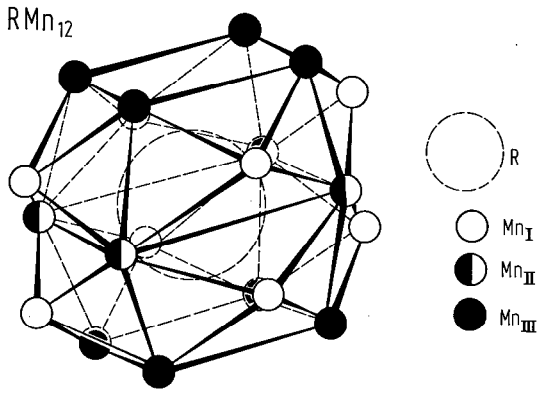

Fig. 521. Packing of Mn atoms about R atom in RMn_{12} compounds. These compounds crystallize in a body-centred tetragonal structure having I4/mm-space group, each unit cell containing two formula units [52 F 1]. The positions of the atoms in lattice are given in Table 114.

Table 114. Positions of the atoms in RM_{12}-type structure (space group I4/mmm) [52 F 1].

Atom	Site	Coordinates
R	2a	0, 0, 0
Mn_I	8f	1/4, 1/4, 1/4; 3/4, 3/4, 1/4; 1/4, 1/4, 3/4; 3/4, 1/4, 1/4
Mn_{II}	8i	x, 0, 0; $\bar{x}$, 0, 0; 0, x, 0; 0, $\bar{x}$, 0; $x=0.361$
Mn_{III}	8j	x, 1/2, 0; $\bar{x}$, 1/2, 0; 1/2, x, 0; 1/2, $\bar{x}$, 0; $x=0.277$

Adding also (0, 0, 0); (1/2, 1/2, 1/2) to all positions.

Table 115. Lattice parameters (Å) of RMn_{12} compounds.

	66 W 1		67 K 1		76 D 7		81 Y 3	
	a	*c*	*a*	*c*	*a*	*c*	*a*	*c*
$NdMn_{12}$			8.660	4.810				
$GdMn_{12}$	8.720	4.780	8.624	4.782				
$TbMn_{12}$	8.680	4.780	8.573	4.760				
$DyMn_{12}$	8.670	4.760	8.579	4.763				
$HoMn_{12}$	8.620	4.750	8.570	4.747				
$ErMn_{12}$	8.560	4.740	8.540	4.740				
$TmMn_{12}$	8.540	4.730						
YMn_{12}	8.530	4.780	8.595	4.773	8.59	4.79	8.579	4.760

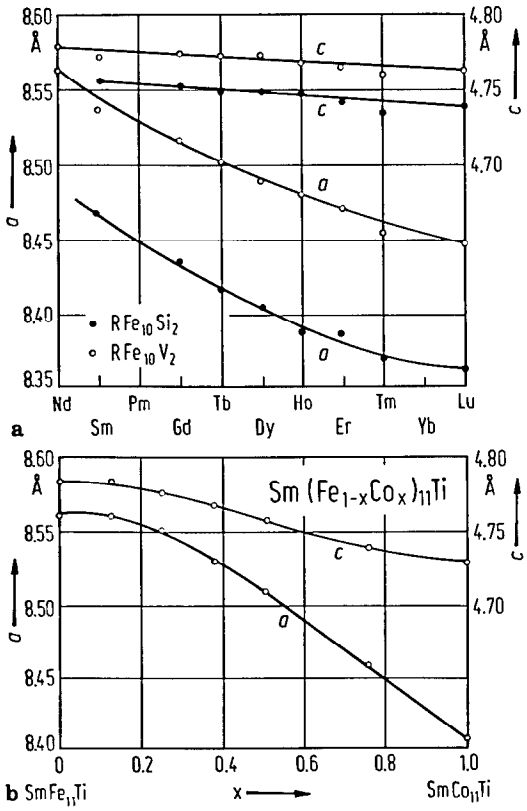

Fig. 522. Lattice parameters of (a) $R_2Fe_{10}V_2$ [87 D 2] and $RFe_{10}Si_2$ [88 B 5] compounds at room temperature. The occurrence of the $ThMn_{12}$-type structure is not limited to the composition $RFe_{10}M_2$. The most extensive solid solution ranges of $RFe_{12-x}M_x$ alloys are observed in the $RFe_{12-x}V_x$ system, where $1.4 \leqq x \leqq 3.5$. For M = Si and Mo compounds the solid solution ranges are much smaller, and for M = Ti and W the $ThMn_{12}$-type structure is not observed for x = 2, but for slightly smaller x values [88 B 5, 88 D 1]. (b) $Sm(Fe_{1-x}Co_x)_{11}Ti$ solid solutions [88 O 1].

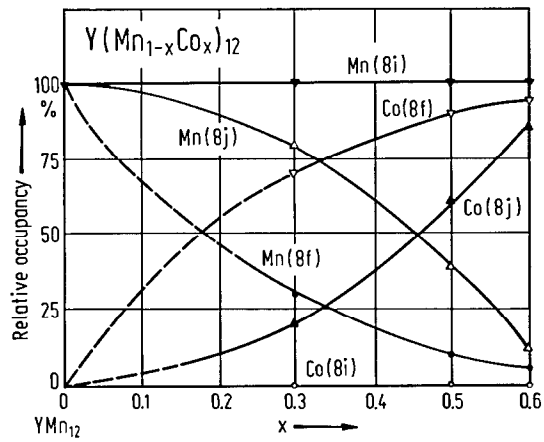

Fig. 523. Composition dependence of the occupation of crystallographic sites by Mn and Co in $Y(Mn_{1-x}Co_x)_{12}$ compounds at room temperature determined by neutron diffraction studies [83 Z 2]. At room temperature, the Co atoms tend to occupy the 8f sites primarily and then the 8j sites. They avoid the 8i sites when x is lower than 0.67. In $YFe_{11}Ti$ the 8f and 8j sites are virtually fully occupied by Fe whilst the 8i sites are partially occupied by Fe and Ti atoms [88 M 2].

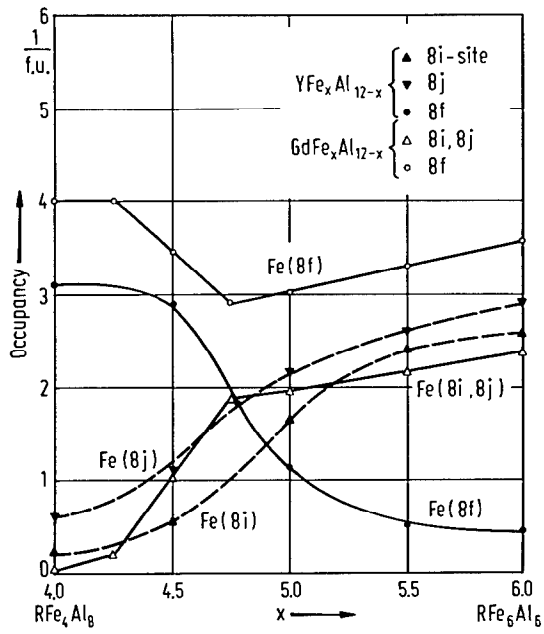

Fig. 524. Composition dependence of the occupation of crystallographic sites by Fe in RFe_xAl_{12-x} ($4 \leqq x \leqq 6$) compounds with R = Y [86 F 3] and Gd [87 L 7] determined by Mössbauer effect studies at room temperature. The data for $GdFe_6Al_6$ are from [81 F 2]. The RFe_xAl_{12-x} with $4 \leqq x \leqq 6$ crystallize in a body-centred tetragonal structure of $ThMn_{12}$-type [77 V 3, 78 B 23, 78 F 2, 81 F 2, 82 F 2, 83 F 3, 84 P 7]. In RFe_4Al_8 mainly the 8f site is populated by Fe. With increasing Fe content, the Fe spills from the 8f site into the other two, 8j and 8i, sites. The $ThMn_{12}$-type structure was also observed in compounds with x = 8 and 10 obtained by melt-spinning and annealing at 450 K [88 W 2].

Table 116a. Lattice constants of RM_6Al_6 (M = Cr, Mn, Fe, Cu) compounds (Å) having $ThMn_{12}$-type structure [80 F 1].

	a	*c*
$GdCr_6Al_6$	8.893	5.186
$DyCr_6Al_6$	8.890	5.132
$ErCr_6Al_6$	8.878	5.126
$TmCr_6Al_6$	8.872	5.122
$LuCr_6Al_6$	8.866	5.119
$GdMn_6Al_6$	8.845	5.108
$TbMn_6Al_6$	8.820	5.092
$DyMn_6Al_6$	8.800	5.080
$HoMn_6Al_6$ [1])	8.777	5.067
$ErMn_6Al_6$	8.768	5.062
$TmMn_6Al_6$	8.765	5.060
$YbMn_6Al_6$	8.751	5.053
$LuMn_6Al_6$ [1])	8.760	5.057
YMn_6Al_6	8.796	5.079
$PrFe_6Al_6$ [1])	8.845	5.106
$EuFe_6Al_6$ [1])	8.937	5.160
$GdFe_6Al_6$	8.687	5.015
$TbFe_6Al_6$	8.651	5.029
$DyFe_6Al_6$	8.650	5.001
$HoFe_6Al_6$	8.636	4.985
$ErFe_6Al_6$	8.619	5.016
$TmFe_6Al_6$	8.605	5.005
$YbFe_6Al_6$ [1])	8.662	5.001
YFe_6Al_6	8.646	4.992
$GdCu_6Al_6$	8.691	5.062
$TbCu_6Al_6$	8.657	5.053
$DyCu_6Al_6$	8.662	5.042
$HoCu_6Al_6$	8.651	5.039
$ErCu_6Al_6$	8.630	5.029
$TmCu_6Al_6$	8.624	5.040
$YbCu_6Al_6$	8.643	5.043
$LuCu_6Al_6$	8.605	5.050
YCu_6Al_6	8.662	5.058

Table 116b. Lattice constants of RM_6Al_6 (M = Mn, Cu) compounds (Å) having $NaZn_{13}$- and Th_2Zn_{17}-type structures [80 F 1].

	Structure	*a*	*c*
$LaCu_6Al_6$	$NaZn_{13}$	11.90	
$CeCu_6Al_6$	$NaZn_{13}$	11.87	
$PrCu_6Al_6$	$NaZn_{13}$	11.86	
$NdCu_6Al_6$	$NaZn_{13}$	11.84	
$SmCu_6Al_6$	$NaZn_{13}$	11.81	
$EuCu_6Al_6$	$NaZn_{13}$	11.92	
$LaMn_6Al_6$	Th_2Zn_{17}	9.225	13.14
$CeMn_6Al_6$	Th_2Zn_{17}	8.999	13.11
$PrMn_6Al_6$	Th_2Zn_{17}	9.005	13.13
$NdMn_6Al_6$	Th_2Zn_{17}	8.996	13.14
$SmMn_6Al_6$	Th_2Zn_{17}	8.951	13.09

[1]) Indicates some impurities in the sample.

For crystal structure and lattice parameters see

RMn_{12} [84 P 8]; R = Gd, Tb, Dy, Ho [87 O 4]; R = Th [52 F 1, 75 D 3]

$R(M'M'')_{12}$ $R(MnM)_{12}$, M = Fe, Co, Ni [84 P 8]; $Y(MnFe)_{12}$ [81 Y 2, 81 Y 3]; $Er(MnGa)_{12}$ [85 M 4]

RM_4Al_8, M = V, Cr, Mn, Fe, Co, Ni, Cu [76 B 22], M = Cu, Cr, Mn [79 F 3]; R = Mn, Cr [84 P 7]; CeM_4Al_8, M = Mn, Fe, Cu [62 Z 1, 63 Z 1]; RFe_4Al_8 [78 F 2, 83 N 11]; RFe_5Al_7 [83 N 11]; RM_6Al_6, M = Fe, Cu, Mn, Cr [80 F 1, 84 P 7]; M = Mn, Cu, R = La, Ce, Pr, Nd, Sm [82 F 1]; RFe_6Al_6 [83 N 11]

$R(FeTi)_{12}$, R = Nd, Sm [88 L 4]; $RFe_{10}V_2$ [87 D 2, 87 D 3]; $RFe_{10}M_2$, M = Cr, V, Ti, Mo, W, Si [88 B 5]; $NdFe_{10}Mo_2$ [87 D 4, 88 D 1]; $YFe_{10}M_2$, $GdFe_{10}M_2$, M = Si, Ti, V, Cr, Co, W [87 D 4, 88 D 1]; $Sm(FeTi)_{12}$ [87 S 22, 88 L 4]; $Y(FeV)_{12}$ [87 D 4, 88 D 1]; $Y(Fe_{11}Ti)$ [88 M 2]; $YFe_{10}Ti$ [88 M 2]; $SmFe_{10}Ti$ [88 Y 2] (later identified as $Sm(FeTi)_{12}$ [88 O 1]; $Ce(MnNi)_{11}$ [75 K 1]; $U(NiSi)_{11}$ [75 K 1]

For thermal expansion see: $TmFe_{10}V_2$ [88 B 5]

Magnetization, Curie temperatures

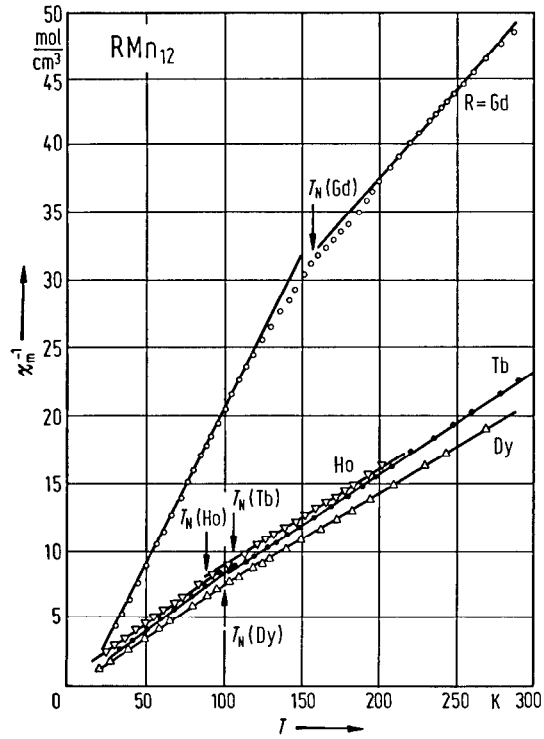

Fig. 525. Temperature dependence of the reciprocal magnetic susceptibility for RMn_{12} (R = Gd, Tb, Dy and Ho) compounds. The arrows indicate the Néel temperature [87O4].

Table 117. Magnetic properties of RMn_{12} compounds.

	T_N(K)			T_R [1](K)		T_{R1} [1](K)	p_s(μ_B/f.u.)		p_{eff}(μ_B/R)		Θ(K)
	69K4	77D3	87O4	77D3	87O4	87O4	77D3	87O4	77D3	87O4	87O4
$NdMn_{12}$	135										
$GdMn_{12}$			160	4.6	5.0	3.6		4.2	8.0	7.92	−80
$TbMn_{12}$		110	108	4.4	4.7	3.0	6.5 $\perp c$	4.4	9.7	10.26	− 7
$DyMn_{12}$	110		100	2.2	2.2		5.0 $\perp c$	5.05	10.4	10.50	−11
$HoMn_{12}$		95	90	1.6	1.7		5.0 $\parallel c$	6.4	10.5	10.40	− 8
$ErMn_{12}$		87		1.9			6.5 $\parallel c$		9.8		
$TmMn_{12}$				1.2					7.6		
YMn_{12}		110									

[1]) T_R is the ordering temperature of R sublattice. The T_{R1} value is obtained from ac-susceptibility.

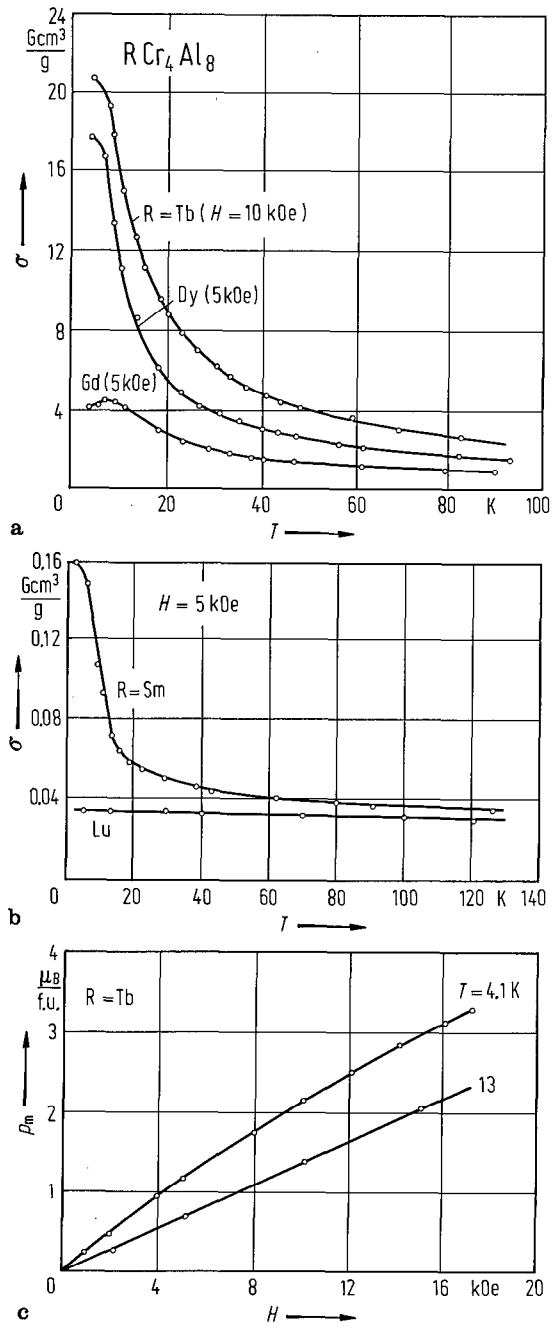

Fig. 526. Temperature dependences of the magnetizations in RCr_4Al_8 compounds with (a) R = Gd, Tb, Dy and (b) R = Sm, Lu. In (c) the magnetization isotherms at 4.1 and 13 K for $TbCr_4Al_8$ are plotted [79 F 3].

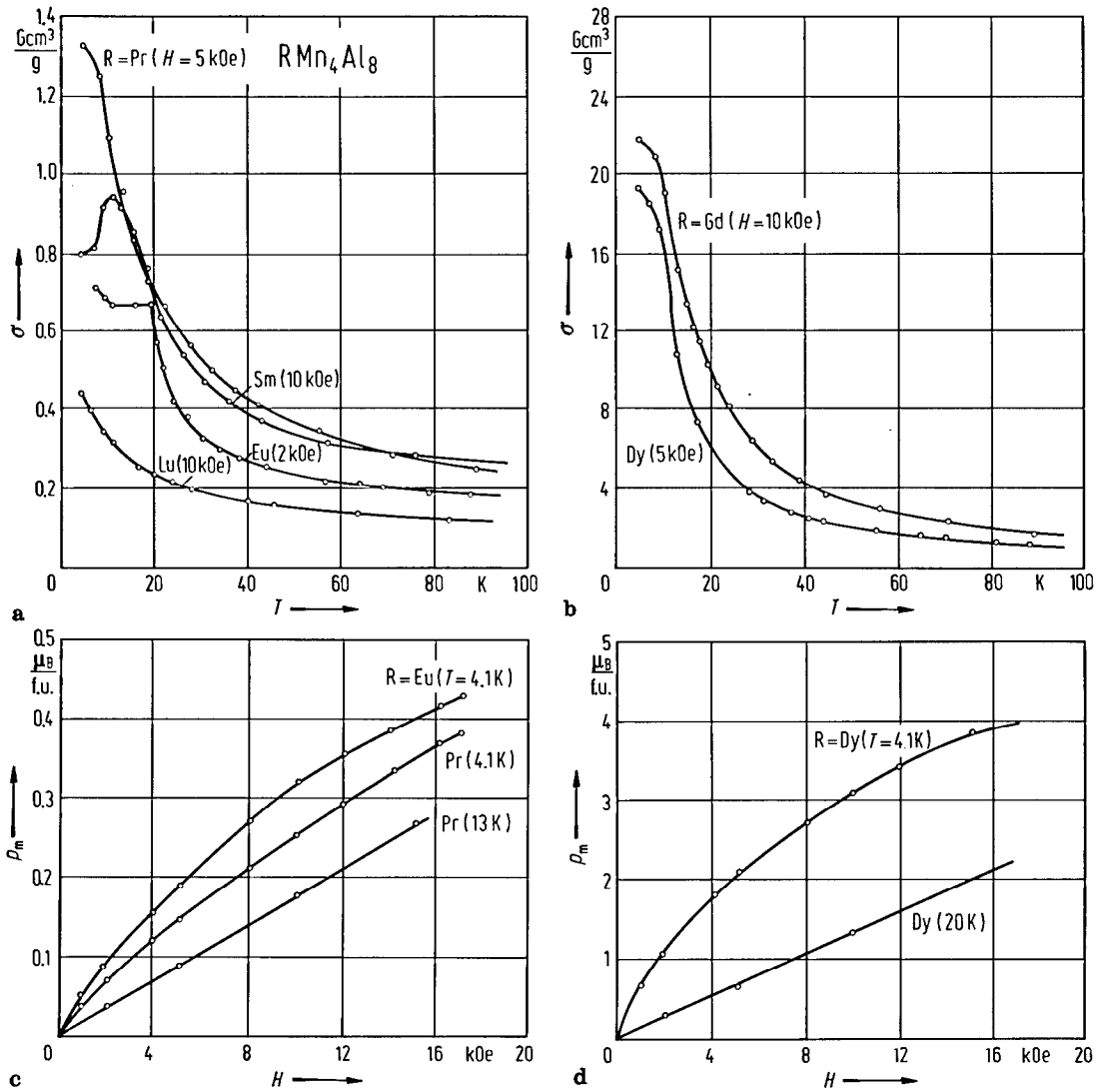

Fig. 527. Temperature dependence of the magnetization in RMn_4Al_8 compounds: (a) R = Pr, Sm, Eu and Lu; (b) Gd and Dy. In (c) and (d) the magnetization isotherms at low temperatures are given for some of these alloys [79 F 3].

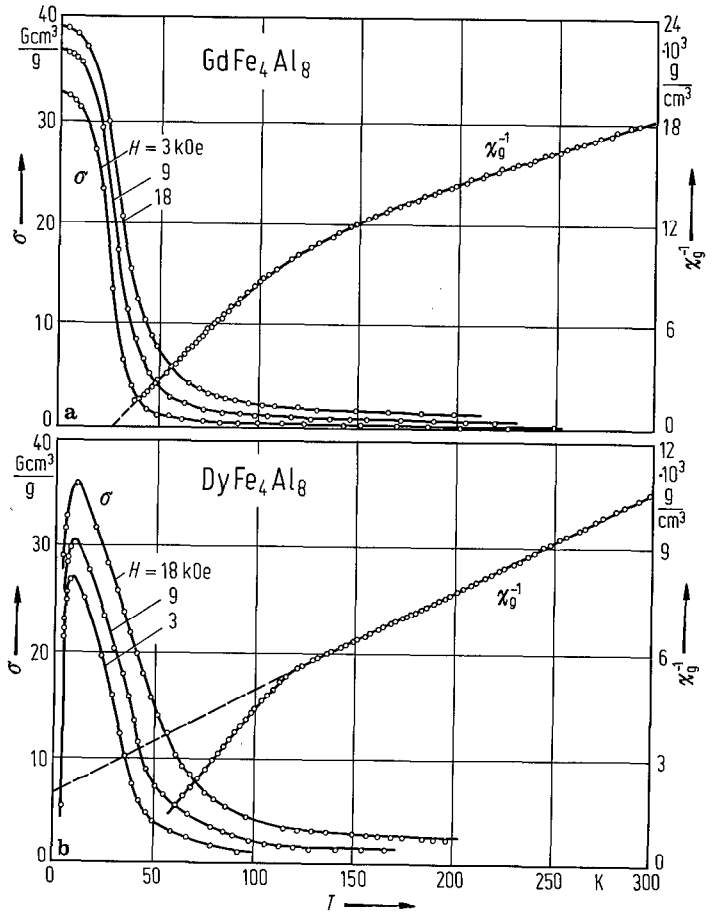

Fig. 528. Temperature dependence of the magnetization and reciprocal magnetic susceptibility for (a) $GdFe_4Al_8$ and (b) $DyFe_4Al_8$ compounds. The ordering of R magnetic moments becomes manifest only at very low temperatures, T_R. This fact is attributed to the small R–Fe interaction strength and the particular crystal structure of the compounds, leading to vanishing molecular field at the R sites once the antiferromagnetic ordering of Fe magnetic moments has been established [78 B 23].

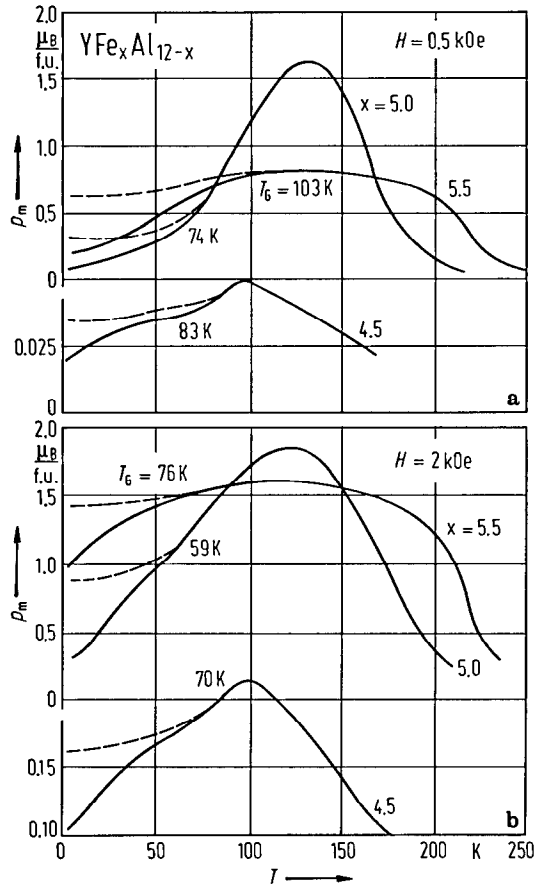

Fig. 529. Field-cooled (dashed lines) and zero-field-cooled (solid lines) temperature dependences of the magnetizations of YFe_xAl_{12-x} compounds at (a) 0.5 kOe and (b) 2 kOe. Only for systems, with x = 4.5, 5.0 and 5.5 differences are observed between zero-field-cooled and field-cooled magnetizations. The temperature at which the two curves separate is defined as the spin glass temperature, T_G [86 F 2, 86 F 3].

For magnetic properties see also

RMn_{12} [69 K 4]; R = Gd, Dy, Er [66 K 1]; R = Gd, Tb, Dy, Ho, Tm, Y [77 D 3]; R = Th [88 W 3]

$R(M'M'')_{12}$ RFe_4Al_8 [77 V 3, 78 F 2, 83 N 11]; R = Nd, Gd, Tm [78 B 23]; RM_4Al_8, M = Cu, Cr, Mn [79 F 3]; $GdFe_4Al_8$ [87 F 9]; RFe_5Al_7 [82 F 2, 83 F 3, 83 N 11]; RM_6Al_6, M = Cr, Mn, Cu [81 F 2]; RFe_6Al_6 [81 F 1, 83 N 11]; RM_6Al_6, M = Mn, Cu, R = La, Ce, Pr, Nd, Sm [82 F 1]; $Gd(FeAl)_{12}$ [87 L 6, 87 L 7, 88 W 2]; $R(MAl)_{12}$, M = Cr, Mn [80 N 5]; $Y(FeAl)_{12}$ [82 Y 4, 86 F 2, 86 F 3]; $Y(FeMn)_{12}$ [81 Y 2, 82 Y 5]; $R(FeAl)_{12}$ [87 M 2]

$RFe_{10}V_2$ [87 D 2]; $RFe_{10}M_2$, M = Ti, V, Cr, Mo, W, Si [87 D 4, 88 B 5, 88 B 6, 88 D 1]; $GdFe_{10}M_2$, M = Si, Ti, V, Cr, Co, W [87 D 4, 87 M 2]; $NdFe_{10}Mo_2$ [87 D 4, 88 D 1]; $Y(FeV)_{12}$ [87 D 4, 88 D 1]; $YFe_{10}M_2$, M = Si, Ti, V, Cr, Co, W [87 D 4, 88 D 1]; $RFe_{10}Ti$, R = Gd, Dy, Y [87 O 1, 88 Z 1]; $RFe_{10}M$, M = Ti, V, Mo, R = Gd, Dy, Y [88 Z 1]; $SmFe_{10}Ti$ [88 Y 2]; $SmFe_{10}M$, M = Ti, V, Mo [88 Z 1]; $Nd(FeTi)_{12}$, $Sm(FeTi)_{12}$ [88 K 1]; $RFe_{11}Ti$ [88 O 1]; $SmFe_{11}Ti$ [88 O 1, 88 L 4]; $DyFe_{11}Ti$ [88 L 2]; $SmTi(FeCo)_{11}$ [87 O 1, 88 O 1]; $YSi_2(FeCo)_{10}$ [88 B 5]; $CeMn_6Ni_5$ [88 W 3]; $(NdDy)Fe_{10}Ti$ [88 Z 1]

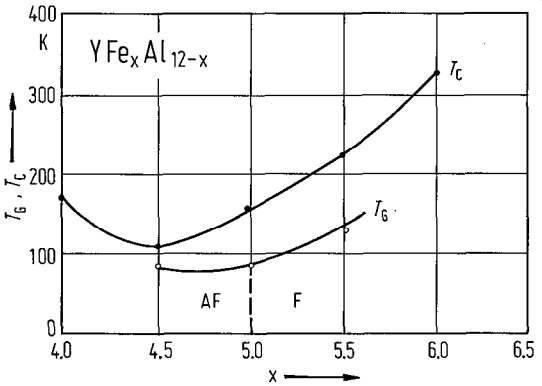

Fig. 530. Composition dependence of the ordering temperature T_C and spin glass temperature T_G determined by extrapolation to zero magnetic field in YFe_xAl_{12-x} compounds [86 F 3].

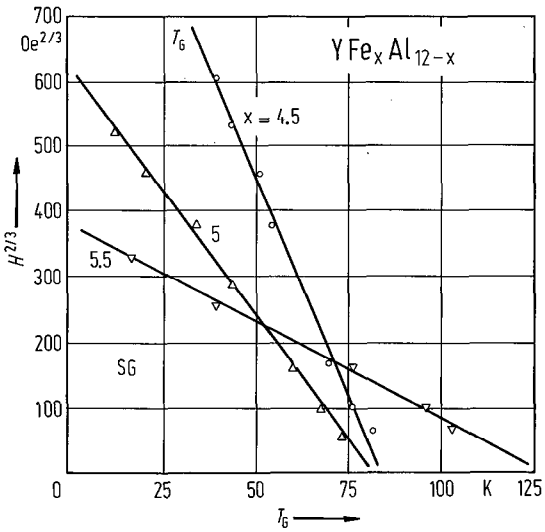

Fig. 531. Dependence of the spin glass temperature T_G in YFe_xAl_{12-x} compounds, on the applied magnetic field to the power 2/3. The lines plotted, in the $H^{2/3}-T$ diagram represent the lines of phase transitions from spin glass behaviour to a magnetically ordered state [86 F 3].

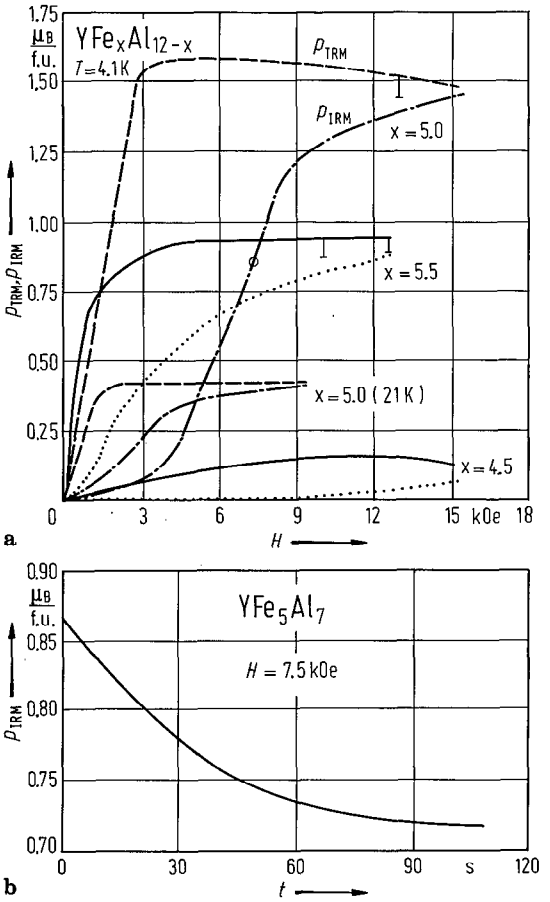

Fig. 532. Thermoremanent (p_{TRM}) and isothermal remanent (p_{IRM}) magnetizations of some YFe_xAl_{12-x} compounds at 4.1 K as function of the applied magnetic field [86 F 2, 86 F 3]. These are typical of all spin glasses. The remanent magnetization values are time-dependent; they decay quite slowly after field removal, as evidenced by vertical bars. (b) Exhibits this behaviour for p_{IRM} in YFe_5Al_7 at 7.5 kOe (open circle in (a)). The magnetic field at which p_{IRM} and p_{TRM} approach a common value is close to the field obtained by extrapolating T_G to 0 K in Fig. 531.

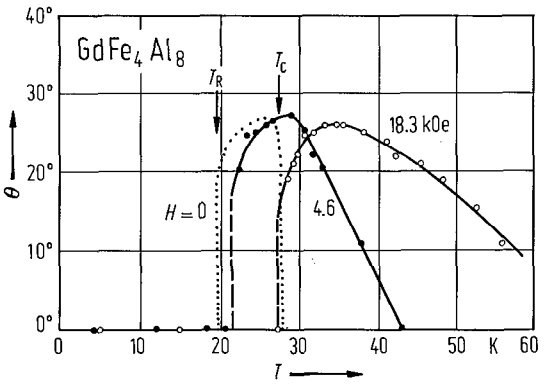

Fig. 533. Temperature dependence of the tilting angle θ of the easy axis with respect to the a axis in the (ac) plane in $GdFe_4Al_8$. Closed and open circles are the θ values at the applied field H of 4.6 and 18.3 kOe, respectively [87 F 9]. Besides $T_N = 170$ K defined by a cusp, two magnetic phase transitions were defined in the $\chi-T$ curve at 28 and 20 K by a sharp peak and by an inflection point in the rapidly increasing part, respectively. These are denoted by T_C, the Curie temperature, and by T_R, a spin reorientation temperature. The dotted curve represents the curve at $H=0$ between T_R and T_C by plotting the T-value at a given θ estimated from the experimental $T-H$ dependences.

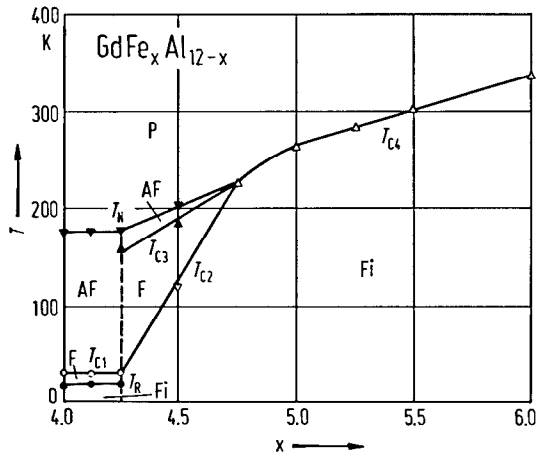

Fig. 534. Magnetic phase diagram of $GdFe_xAl_{12-x}$ compounds. The symbols P, AF, F, and Fi signify paramagnetic, antiferromagnetic, ferromagnetic, and ferrimagnetic states, respectively [87 L 7]. The various types of magnetic ordering may be correlated with the site occupancy by Fe atoms.

Table 118a. Lattice parameters and magnetic properties of RM_4Al_8 compounds (M = Cr, Mn) [79 F 3].

	a Å	c Å	T_N K	p_s [1] μ_B/f.u.	C_m $cm^3 K mol^{-1}$	Θ K	p_{eff}(R) μ_B	p_{eff}(M) μ_B
$LaCr_4Al_8$	9.131	5.127						
$CeCr_4Al_8$	9.042	5.128						
$PrCr_4Al_8$	9.023	5.135	6(2)	0.38	2.2	−16(2)	3.58	0.16
$NdCr_4Al_8$	9.000	5.136			2.1	−11(2)	3.62	0.12
$SmCr_4Al_8$	8.973	5.136	19(2)	0.03	1.4	−24(2)	0.86	0.61
$GdCr_4Al_8$	8.950	5.133	8(2)	1.5	9.1	− 9(2)	7.94	0.15
$TbCr_4Al_8$	8.925	5.130	12(2)	3.3	12.6	− 5(2)	9.72	0.08
$DyCr_4Al_8$	8.926	5.132	16(2)	4.2	15.5	− 5(2)	10.63	0.12
$HoCr_4Al_8$	8.910	5.126	8(2)	4.1	13.8	− 5(2)	10.6	–
$ErCr_4Al_8$	8.903	5.124	14(2)	3.8	12.3	− 4(2)	9.59	0.08
$TmCr_4Al_8$	8.903	5.131	11(2)	2.4	7.7	−11(2)	7.57	0.07
$YbCr_4Al_8$	8.945	5.132	–	–	0.43	7(2)	1.45	0.10
$LuCr_4Al_8$	8.884	5.119						
YCr_4Al_8	8.920	5.130						
$LaMn_4Al_8$ [1]	9.057	5.167						
$CeMn_4Al_8$	8.910	5.150	–	–	0.40	8(2)	–	0.9
$PrMn_4Al_8$	8.952	5.142	11(2)	0.38	2.90	− 1(2)	3.58	1.6
$NdMn_4Al_8$	8.925	5.133	7(2)	0.48	3.05	− 8(2)	3.62	1.7
$SmMn_4Al_8$	8.902	5.120	12(2)	0.14	1.04	−18(2)	0.86	1.4
$EuMn_4Al_8$	8.982	5.161	20(2)	0.46	–	–	–	–
$GdMn_4Al_8$	8.911	5.116	28(2)	3.1	9.23	4(2)	7.94	1.6
$TbMn_4Al_8$	8.865	5.108	21(2)	4.3	13.3	7(2)	9.72	1.7
$DyMn_4Al_8$	8.849	5.112	19(2)	4.0	16.0	−26(2)	10.63	1.9
$HoMn_4Al_8$	8.845	5.097	14(2)	4.8	15.7	− 2(2)	10.60	1.5
$ErMn_4Al_8$	8.837	5.093	15(2)	4.1	12.0	− 2	9.59	1.0
$TmMn_4Al_8$	8.848	5.080	13(2)	3.7	8.26	5(2)	7.57	1.5
$YbMn_4Al_8$ [1]	8.875	5.111	–	–	–	–	–	–
$LuMn_4Al_8$	8.814	5.083	–	–	0.39	10	–	0.9
YMn_4Al_8	8.857	5.101	–	–	0.34	5(2)	–	0.8

[1]) At 4.2 K and 17 kOe.

For lattice parameters of RM_4Al_8 (M = Mn, Fe, Cr) compounds see also [76 B 22].

Table 118b. Lattice parameters and magnetic properties of RFe_4Al_8 compounds.

	a Å	c Å	T_R K	T_{ord} K		Θ K	C_m $cm^3\,K\,mol^{-1}$		p_s [1] μ_B/f.u.	p_{eff}(R) μ_B	p_{eff}(Fe) μ_B	
	78 F 2		78 F 2		78 B 23	78 F 2	78 F 2	78 B 23	78 F 2	78 F 2	78 F 2	78 B 23 [2]
$LaFe_4Al_8$	8.900	5.075	–	103	135.4(2)	– 68	9.7	7.1	0.36	–	4.4	3.77
$CeFe_4Al_8$	8.793	5.047	–	115	159.7(2)	23	8.7	6.3	0.26	–	4.2	3.55
$PrFe_4Al_8$	8.824	5.054	12	107	–	35	10.5	8.9	1.06	3.58	4.2	3.82
$NdFe_4Al_8$	8.804	5.054	19	137	142.0(2)	44	11.4	8.6	0.18	3.62	4.4	3.73
$SmFe_4Al_8$	8.770	5.053	44	108	–	68	8.2	6.8	0.46	0.86	4.0	3.66
$EuFe_4Al_8$	8.784	5.051		137	–	–148	11.3		0.27	3.52	4.5	–
$GdFe_4Al_8$	8.743	5.052	11	130	172.3(2)	–151	18.0	15.0	2.40	7.92	4.5	3.78
$TbFe_4Al_8$	8.740	5.036	20	126	165.3(2)	–105	21.4	18.5	2.10	9.72	4.4	3.65
$DyFe_4Al_8$	8.728	5.050	25	122	–	– 80	22.6	22.3	2.30	10.60	4.2	3.92
$HoFe_4Al_8$	8.720	5.038	22	137	–	– 66	23.9	20.5	1.65	10.60	4.4	3.43
$ErFe_4Al_8$	8.700	5.028	25	111	183.0(2)	– 38	20.6	18.3	2.80	9.56	4.3	3.70
$TmFe_4Al_8$	8.688	5.037	20	109	186.6(2)	7	16.3	13.6	2.00	7.60	4.3	3.40
$YbFe_4Al_8$	8.691	5.017(7)	8	103	–	62	13.3	6.7	2.80	4.54	4.6	2.87
$LuFe_4Al_8$	8.687	5.030	–	97	197.3(2)	79	9.5	13.6	0.60	–	4.3	5.17
YFe_4Al_8	8.750	5.060	–	94	184.7(2)	– 16	10.6	7.1	0.28	–	4.6	3.77

[1]) At 4.1 K and 16 kOe.
[2]) Deduced from C values according to addition law of susceptibilities.

Table 118c. Lattice parameters and magnetic properties of RCu_4Al_8 [79 F 3].

	a Å	c Å	T_N K	Θ K	$p_{eff}(R)$ calc. μ_B	$p_{eff}(R)$ exp. μ_B
$CeCu_4Al_8$	8.839(3)	5.153(3)		−17(1)	2.54	2.62
$PrCu_4Al_8$	8.817(3)	5.150(3)	15(1)	−15(1)	3.58	3.56
$NdCu_4Al_8$	8.789(3)	5.143(3)	20(1)	−18(1)	3.64	3.58
$SmCu_4Al_8$	8.797(3)	5.143(3)	≅25	−40(5)	0.86	1.00
$EuCu_4Al_8$ [1]	8.886(3)	5.156(3)	–	–	–	–
$GdCu_4Al_8$	8.746(3)	5.146(3)	32(1)	−16(1)	7.94	7.89
$TbCu_4Al_8$	8.752(3)	5.134(3)	22(1)	−14(1)	9.72	9.50
$DyCu_4Al_8$	8.725(3)	5.137(3)	17(1)	− 5(1)	10.60	10.60
$HoCu_4Al_8$	8.720(3)	5.122(3)	7(1)	− 7(1)	10.60	10.90
$ErCu_4Al_8$	8.712(3)	5.130(3)	6(1)	−10(1)	9.60	9.80
$TmCu_4Al_8$	8.674(3)	5.114(3)	5(1)	− 6(1)	7.57	7.76
$YbCu_4Al_8$	8.746(3)	5.122(3)	flat χ vs. T curve			
$LuCu_4Al_8$	8.670(3)	5.098(3)	flat χ vs. T curve			

[1]) Contained an additional phase.

Table 120. Magnetic properties of RM_6Al_6 (M = Fe, Cu) compounds [81 F 2].

	T_{ord} [1]) K	T_{max} K	Θ K	C_m $cm^3\,K\,mol^{-1}$	$p_{eff}(Fe)$ μ_B
$EuFe_6Al_6$ [2])	135(5)				
$GdFe_6Al_6$	345(5)	220(10)	328(5)	16.0(2)	3.3(2)
$TbFe_6Al_6$	335(5)	260(10)	328(5)	19.0(2)	3.1(2)
$DyFe_6Al_6$	325(5)	250(10)	320(5)	19.5(2)	3.0(2)
$HoFe_6Al_6$	310(5)	215(10)	311(5)	19.4(2)	2.7(2)
$ErFe_6Al_6$	320(5)	210(10)	328(5)	19.0(2)	3.1(2)
$TmFe_6Al_6$ [3])	320(5)	150(10)	345(5)	14.3(2)	3.1(2)
$YbFe_6Al_6$	210(5)	120(10)	327(5)	16.8(2)	3.0(2) (4.7)
YFe_6Al_6	345(5)	250(10)			

	T_N K	Θ K	C_m $cm^3\,K\,mol^{-1}$	$p_{eff}(R)$ μ_B
$GdCu_6Al_6$	21(2)	− 22(1)	7.8	7.9(1)
$DyCu_6Al_6$	3.9(1)	− 14(1)	14.8	10.9(1)
$ErCu_6Al_6$	2.6(1)	− 12(1)	12.4	9.9(1)
$TmCu_6Al_6$		− 5(1)	6.6	7.3(1)

[1]) Derived from ^{57}Fe Mössbauer effect studies.
[2]) Contained $EuAl_2$.
[3]) Contained $YbAl_2$.

Table 119. Lattice parameters and magnetic properties of RFe_5Al_7 compounds [83 F 3].

	a Å	c Å	T_{ord}(K) magnetic study	T_{ord}(K) Mössbauer data	T_{comp} K	H_c kOe	p_s [1] 4.1 K μ_B/f.u.	T_{max} [2] K	C_m $cm^3\,K\,mol^{-1}$	Θ K	p_{eff}(R) theory μ_B	p_{eff}(Fe) μ_B
$SmFe_5Al_7$	8.763(1)	5.056(1)	220(10)		185(5) [3]	13.6(3)	5.1	205(10)	9.7(3)	265	0.84	3.9
$GdFe_5Al_7$	8.709(1)	5.025(1)	268(10)	260(10)		0.4(3)	0.4	193(10)	16.8(3)	241	7.94	3.8
$TbFe_5Al_7$	8.706(1)	5.026(1)	248(10)	240(10)	90(5)	6.3(3)	0.6	185(10)	15.7(3)	174	9.72	2.5
$DyFe_5Al_7$	8.701(1)	5.020(1)	227(10)	225(10)	93(5)	24.3(3)	1.8	192(10)	21.3(3)	177	10.63	3.4
$HoFe_5Al_7$	8.685(1)	5.014(1)	227(10)	210(10)	67(5)	9.5(3)	2.3	160(10)	21.6(3)	186	10.60	3.5
$ErFe_5Al_7$	8.675(1)	5.009(1)	218(10)	215(10)	29(5)	18.5(3)	1.7	140(10)	19.5(3)	192	9.59	3.6
$TmFe_5Al_7$ [4]	8.680(1)	5.001(1)					0.5	100(10)		109	7.57	
$YbFe_5Al_7$	8.678(1)	5.008(1)	207(10)	180(10)		2.0(3)	3.6	110(10)	9.7(3)	224	0	3.9
$LuFe_5Al_7$	8.662(1)	4.988(1)	212(10)	165(10)		2.0(3)	5.4	140(10)	11.3(3)	224	0	4.2
YFe_5Al_7	8.706(1)	5.026(1)	215(10)	165(10)		2.0(3)	5.8	135(10)	12.3(3)	230	0	4.4

[1]) Magnetic moment at 4.1 K and in field of 50 kOe (18 kOe for R = Gd and Tm).
[2]) Maximum point of magnetization in low fields.
[3]) Only when cooled within seconds in small field.
[4]) Contained an appreciable amount of a second phase.

For Mössbauer effect study on RFe_5Al_7 see [82 F 2, 83 F 3].

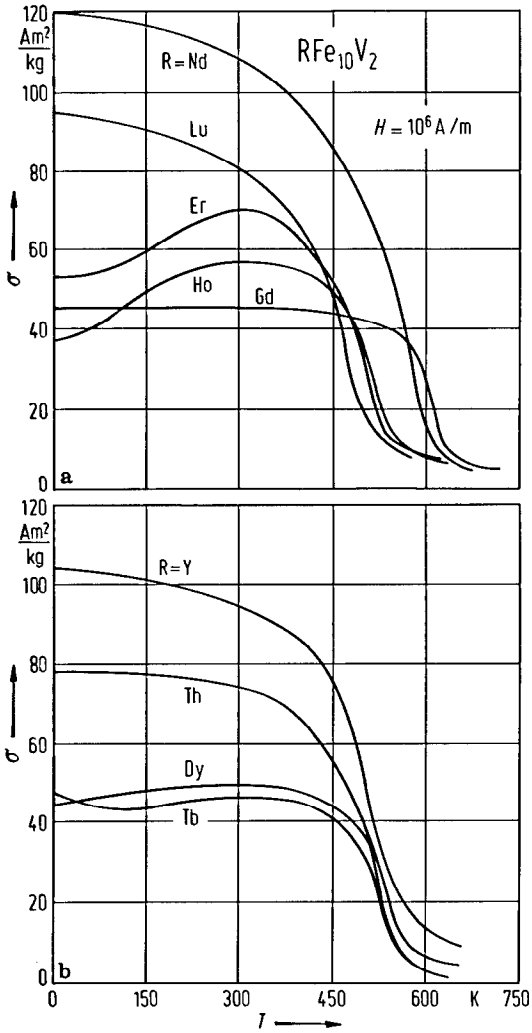

Fig. 535. Thermal variations of the magnetizations in $RFe_{10}V_2$ compounds: (a) R = Nd, Gd, Ho, Er, Lu and (b) R = Tb, Dy, Th, Y in a magnetic field of 1000 kAm^{-1} (12.5 kOe). As in binary systems the R and Fe magnetizations couple parallel or antiparallel, when R is a light or heavy rare-earth element, respectively [87 D 2].

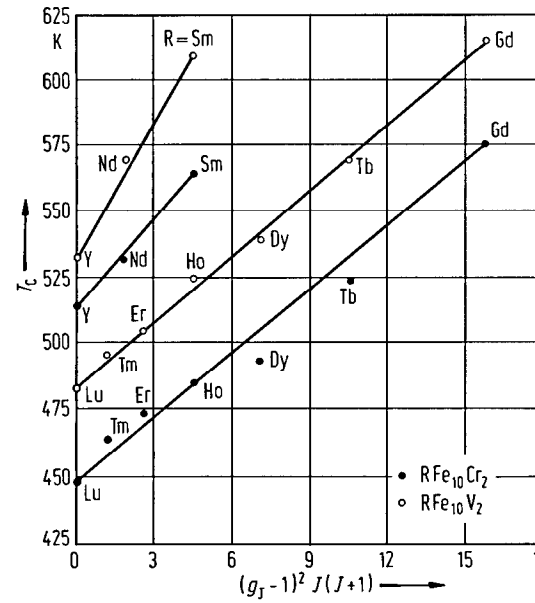

Fig. 536. Curie temperatures of $RFe_{10}V_2$ [87 D 2] and $RFe_{10}Cr_2$ [88 B 5] compounds as a function of the De Gennes factor, $G=(g_J-1)^2J(J+1)$.

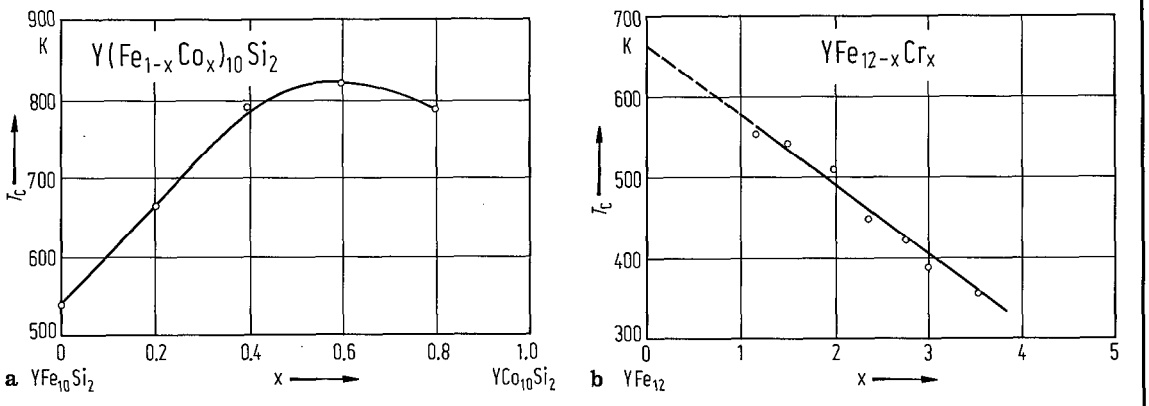

Fig. 537. Curie temperatures of (a) $Y(Fe_{1-x}Co_x)_{10}Si_2$ and (b) $YFe_{12-x}Cr_x$ compounds [88 B 5].

Neutron diffraction

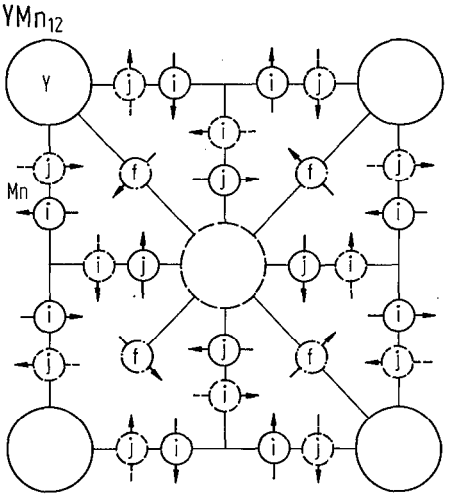

Fig. 538. Magnetic structure of YMn_{12}. Y atoms are represented by large circles and Mn atoms by small circles; the atoms drawn with full lines lie in the plane $z=0$, those drawn with dashed lines lie in the plane $z=1/2$. The Mn atoms on the f site (dashed dotted lines) lie in the planes $z=1/4$ and $z=3/4$ [76 D 7, 77 D 3]. In the YMn_{12} crystallographic structure, each Mn atom lies in a mirror plane which contains the c axis. In the magnetic structure, each magnetic moment is perpendicular to this mirror plane. The Shubnikov group of the magnetic structure is $I_p4/m'mm$. Although the magnetic structure is non-collinear, the arrangements of magnetic moments between first neighbouring atoms are nearly collinear. The structure is justified considering the large negative exchange interactions associated with the short interatomic Mn–Mn distances (2.4···2.5 Å). The perpendicular couplings which appear between atoms belonging to two neighbouring arrangements are associated with interatomic Mn–Mn distances close to 2.7 Å, when the exchange interactions vanish.

Table 121a. Magnetic moments of Fe and Mn determined by neutron diffraction studies in some compounds having I4/mmm tetragonal body-centred structure.

	T K	$p_{Mn}(\mu_B)$			$p_{Fe}(\mu_B)$			Ref.
		8i	8j	8f	8i	8j	8f	
YMn_{12}	4.2	0.42(4)	0.42(4)	0.14(4)	–	–	–	76 D 7
$Y(Mn_{0.7}Fe_{0.3})_{12}$	4.2	1.30(5)	1.36(6)	0.04(5)	1.30(5)	1.36(6)	0.04(5)	81 Y 3
$Y(Mn_{0.4}Fe_{0.6})_{12}$	4.2	0.98(10)	1.07(10)	0.1(1)	0.98(10)	1.07(8)	0.1(1)	81 Y 3
$Y(Fe_{0.417}Al_{0.583})_{12}$	4.1	no long-range magnetic order						[1]
$YFe_{10}V_2$	4.2				1.95	1.52	1.83	88 H 1

[1]) Shaked, H. and Melamud, M., unpublished data cited in [86 F 3].

Table 121b. Magnetic moments of 3d transition metal atoms in $Y(Mn_{1-x}Co_x)_{12}$ compounds [1]) [84 Z 1].

	T K	$p_{3d}(\mu_B)$		
		8i	8j	8f
YMn_{12}	77	0.66	0.66	0.22
$Y(Mn_{0.7}Co_{0.3})_{12}$	77	2.00	2.10	2.10
$Y(Mn_{0.6}Co_{0.4})_{12}$	77	1.80	1.84	1.84
$Y(Mn_{0.5}Co_{0.5})_{12}$	77	1.40	1.50	1.50
$Y(Mn_{0.4}Co_{0.6})_{12}$	77	1.20	1.20	1.20

[1]) The $Y(Mn_{1-x}Co_x)_{12}$ compounds show an antiferromagnetic structure of noncollinear type for $x = 0$, 0.3, and 0.4. The arrangement of some magnetic moments on 8f and 8j sites change into parallel to each other for $x = 0.5$, 0.6, and 0.67, whereas the magnetic moments of 8i sites remain in antiparallel configuration. Moreover, the ratio of the ferromagnetic component increases with the increase of Co content. All magnetic moments on 8i, 8j and 8f sites are parallel to each other in the basal plane of the tetragonal structure for $x = 0.8$. The sample exhibits ferromagnetism in this case. As compared with YMn_{12}, the substitution of Mn with Co leads to an increase of the mean magnetic moment on 8i, 8j and 8f sites.

Table 122. Magnetic structures of some RFe_4Al_8 compounds determined by neutron diffraction studies at 4.2 K.

	Fe sublattice	R sublattice	Ref.
YFe_4Al_8	Antiferromagnetic G_x [2]); 0.65 μ_B $p_{Fe}=0.65\,\mu_B$	–	79 S 5
$TbFe_4Al_8$	Antiferromagnetic along $\pm$ [100] G_x [2]); 0.75 μ_B Ferromagnetic along [010] G_y [2]); 0.75 μ_B $p_{Fe}=1.02\,\mu_B$	A ferromagnetic moment is induced in Tb sublattice along [110] direction. This moment serves as a spiral axis for a spiral having a propagation vector 0.1315 [110]. The magnetic moment of the conical spiral thus formed increases sharply to saturation at $\cong$20 K. F_x [2])$=2.91\,\mu_B$; F_y [2])$=-2.91\,\mu_B$; spiral: 6.27 μ_B; $p_{Tb}=7.50\,\mu_B$	79 S 5
$DyFe_4Al_8$ [1])	Conical spiral structure. The propagation vector of the spiral is along [110], and the rotation angle of the Fe moments is about 45°. $p_{Fe}=3.6\,\mu_B$	No indication of the magnetic ordering of rare-earth sublattice.	83 S 6
$HoFe_4Al_8$ [1])	Conical spiral structure. The propagation vector of the spiral is along [110], and the rotation angle of the Fe moments is about 35°. $p_{Fe}=3.6\,\mu_B$	No indication of the magnetic ordering of rare-earth sublattice.	83 S 6

[1]) These results contradict a previous interpretation [77 B 5]. The Fe magnetic moments seem to be greater than these supposed by comparing to data given by [79 S 5].

[2]) The significations of F_x, G_x and G_y are: $F_x=p_{1x}+p_{2x}+p_{3x}+p_{4x}$; $F_y=p_{1y}+p_{2y}+p_{3y}+p_{4y}$; $G_x=p_{1x}-p_{2x}+p_{3x}-p_{4x}$; $G_y=p_{1y}-p_{2y}+p_{3y}-p_{4y}$.

For neutron diffraction studies see also
YMn_2 [76 D 7, 77 D 3]
$Y(MnFe)_{12}$ [81 Y 3, 82 Y 5]; $Y(MnCo)_{12}$ [83 Z 2, 84 Z 1, 85 H 1]; $YFe_{11}Ti$ [88 M 2]
RFe_4Al_4, R = Tb [79 S 5]; R = Dy, Ho [83 S 6]; R = Tb, Er [77 B 5]

Mössbauer effect

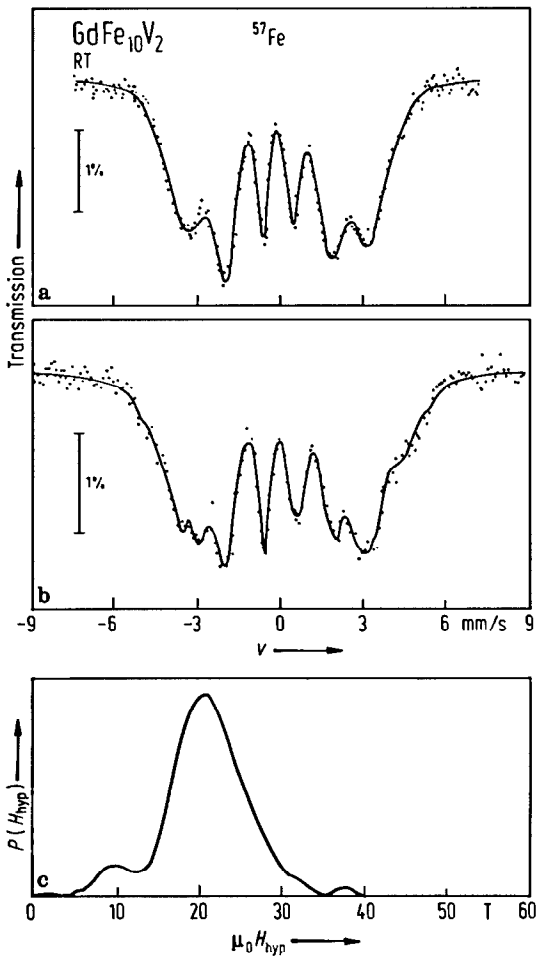

Fig. 539. Room-temperature ^{57}Fe Mössbauer spectra of the melt-spin $GdFe_{10}V_2$ (a) before annealing and (b) after annealing at 450 °C. (c) shows the magnetic hyperfine field distribution for the pre-annealed sample [88 W 2].

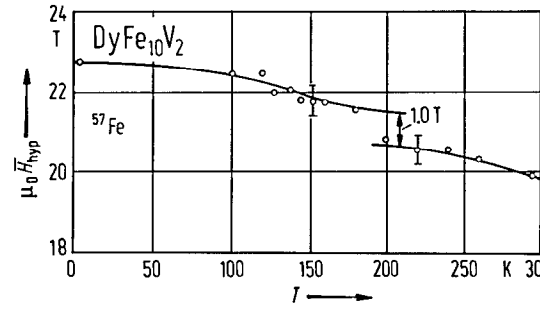

Fig. 540. Temperature dependence of the average ^{57}Fe hyperfine field in $DyFe_{10}V_2$. A drop of 1 T in H_{hyp} values is evidenced at about 190 K, indicating a magnetic phase transition, where the magnetization turns to the c axis at higher temperatures [88 G 5].

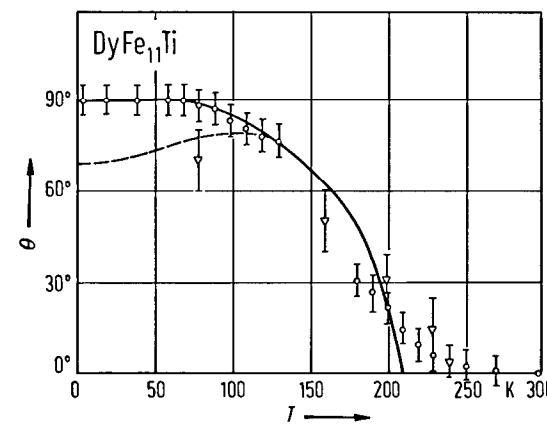

Fig. 541. Thermal variation of the angle θ between the magnetization and c axis in $DyFe_{11}Ti$. The reorientation has its onset at 80 K and is complete at 200 K. The solid and dashed lines are calculated values in a crystal field model with $B_2^0 = 0.30$ K, $B_4^0 = 0.53 \cdot 10^{-3}$ K, $B_6^0 = 1.5 \cdot 10^{-6}$ K and $B_6^0 = 0$, respectively. The circles are the data determined from magnetic measurements and triangles are obtained from Mössbauer effect measurements [88 L 2].

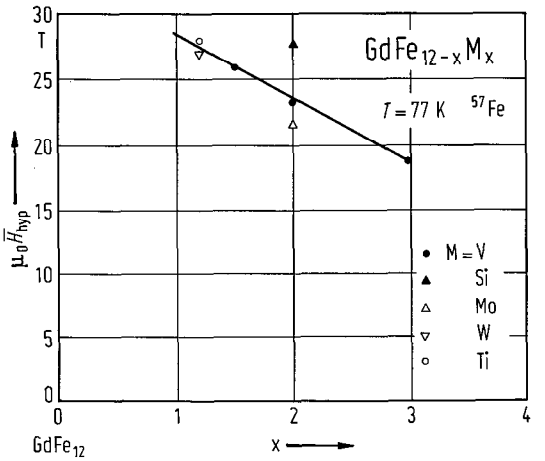

Fig. 542. Average ^{57}Fe hyperfine fields $\bar{H}_{hyp}$, at 77 K in some $GdFe_{12-x}M_x$ alloys. The samples containing M = V, Ti, Mo, W have comparable $\bar{H}_{hyp}$ values for the same concentration, x, whereas for Si $\bar{H}_{hyp}$ drastically increases. The above behaviour was connected with the site preference of the Si atoms which share the 8j and 8f positions, while V, Ti and Mo substitute Fe in 8i sites, which carries the highest magnetic moment [89 S 1].

Table 123. Magnetic hyperfine field, H_{hyp}, and quadrupole splitting, $e^2qQ/2$, of $RFe_{10}V_2$ compounds measured at 4.2 K [88 G 5].

	$\mu_0 H_{hyp}$ T	$e^2qQ/2$ cm s^{-1}
^{161}Dy		
$DyFe_{10}V_2$	547(3)	6.3(3)
Dy^{3+} free ion	565	7.0
^{166}Er		
$ErFe_{10}V_2$	740(10)	0.80(10)
Er^{3+} free ion	765	0.81
^{169}Tm		
$TmFe_{10}V_2$	702(4)	15.8(3)
Tm^{3+} free ion	720	15.7

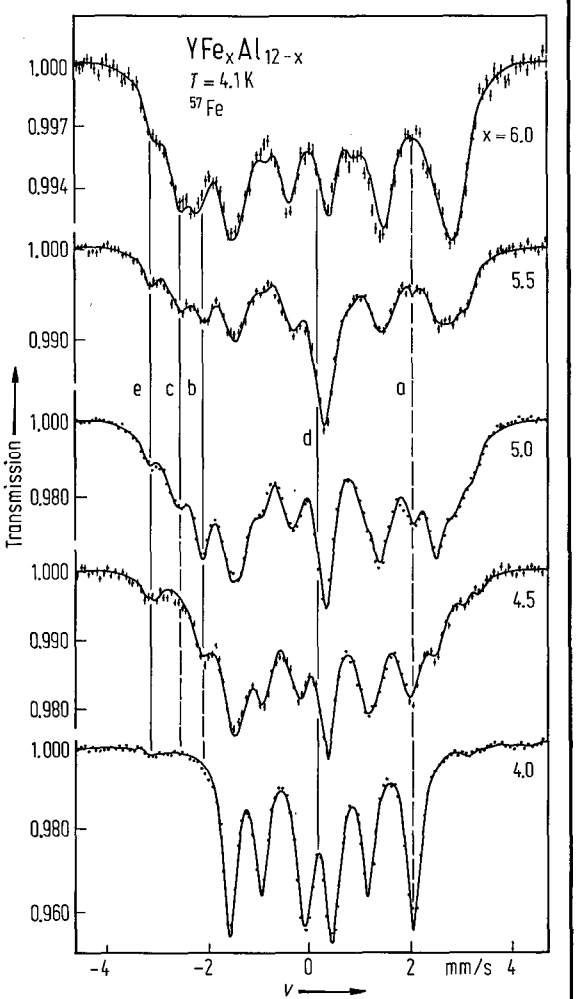

Fig. 543. Mössbauer spectra of ^{57}Fe in YFe_xAl_{12-x} compounds at 4.1 K. The solid curves are theoretical least-squares fit spectra composed of spectra in the f site (vertical a line), j site (b line) and i site (c line). The assignment to j and i sites may also be reversed. Line d shows the contribution to the spectra from very small hyperfine fields, large only for the spin glass systems, while the e line arises from pure metallic iron [86 F 3].

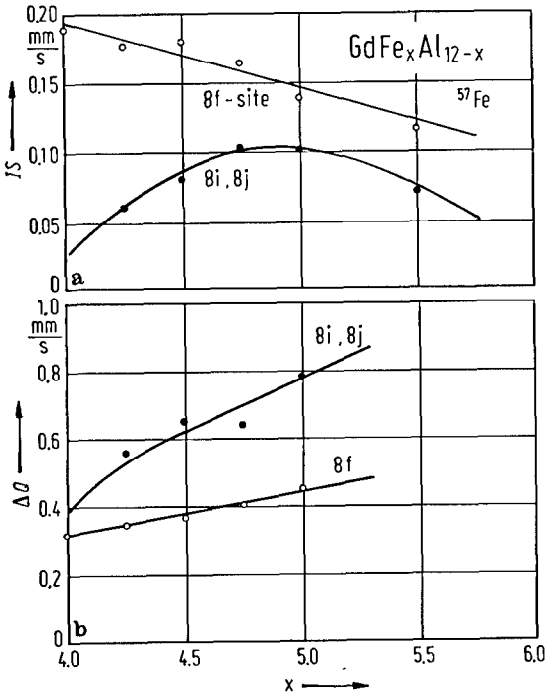

Fig. 544. Composition dependence of (a) the isomer shift (relative to α-Fe standard) and (b) quadrupole splitting of 8f and 8i, 8j sites in $GdFe_xAl_{12-x}$ compounds [87 L 7].

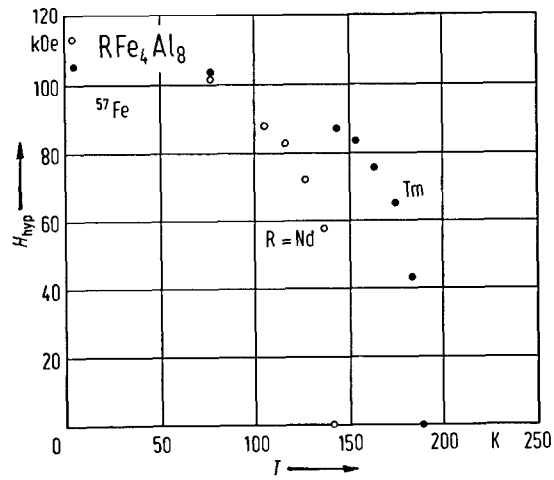

Fig. 546. Temperature dependence of the magnetic hyperfine fields at ^{57}Fe in $TmFe_4Al_8$ and $NdFe_4Al_8$ compounds [78 B 23].

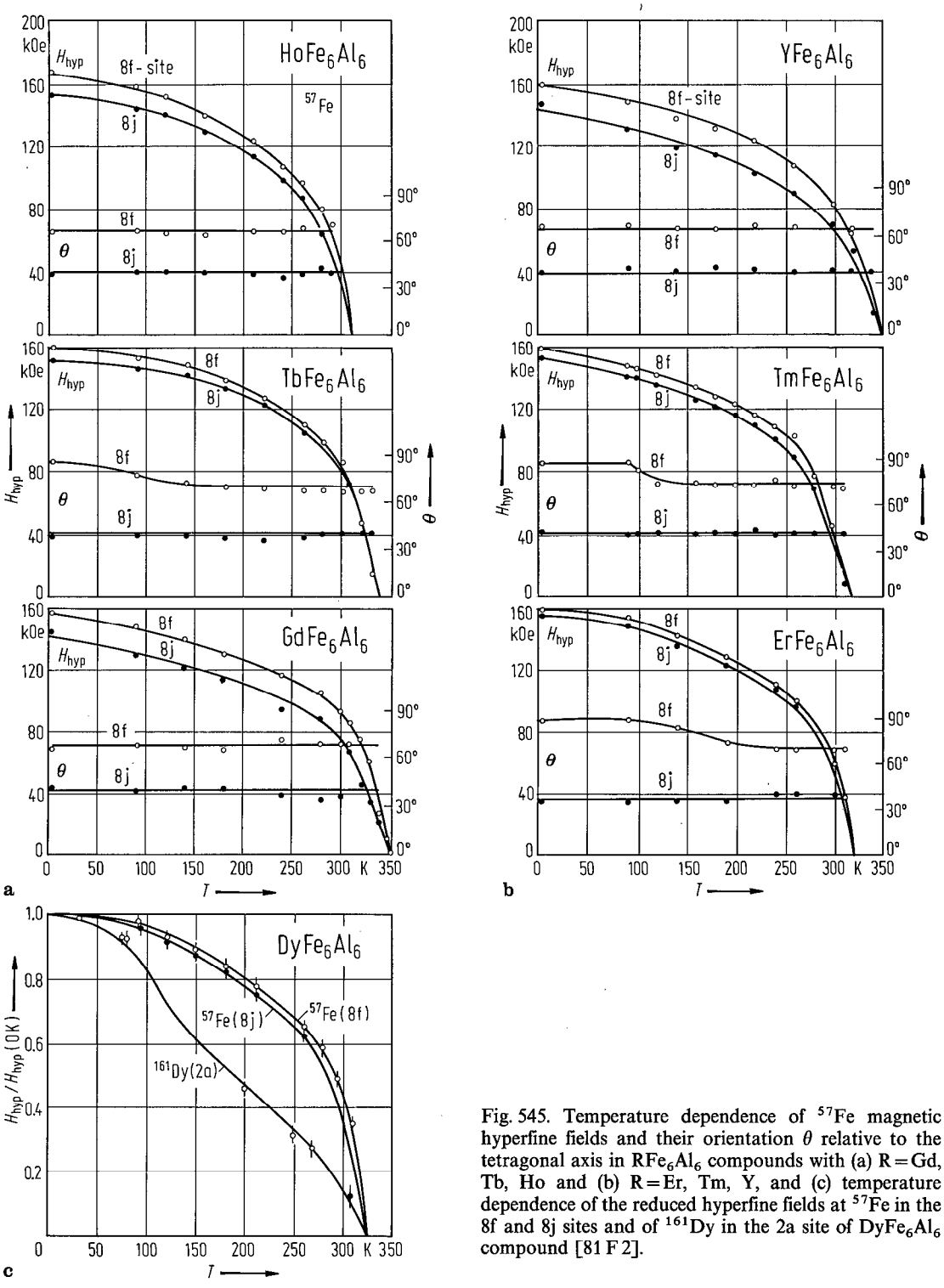

Fig. 545. Temperature dependence of ^{57}Fe magnetic hyperfine fields and their orientation θ relative to the tetragonal axis in RFe_6Al_6 compounds with (a) R = Gd, Tb, Ho and (b) R = Er, Tm, Y, and (c) temperature dependence of the reduced hyperfine fields at ^{57}Fe in the 8f and 8j sites and of ^{161}Dy in the 2a site of $DyFe_6Al_6$ compound [81 F 2].

Table 124. Hyperfine interaction parameters at ^{57}Fe in YFe_xAl_{12-x} compounds. The parameters assigned to the j and i sites may be reversed [86 F 3]. ΔH_{hyp}: relative spread in magnetic hyperfine field.

	Site	YFe_4Al_8	$YFe_{4.5}Al_{7.5}$	YFe_5Al_7	$YFe_{5.5}Al_{6.5}$	YFe_6Al_6
H_{hyp} (kOe) at 4.2 K	f	113	109	111	111	70
	j	0	144	144	145	145
	i	0	172	172	172	166
ΔH_{hyp} (%)	f	3	14	6	2	2 [1]
	j	–	4	6	6	16
	i	–	16	10	8	4
$e^2qQ/4$ (mm s^{-1})	f	0.07	0.07	0.09	0.13	0.15 [1]
	j	0.30	0.09	0.08	0.10	0.11
	i	0.17 [2]	0.08	0.05	0.09	0.09
IS (mm s^{-1}) [3]	f	0.18	0.18	0.20	0.18	0.19 [1]
	j	0.23	0.12	0.14	0.13	0.14
	i	0.22	0.07	0.06	0.07	0.07

[1]) Was not a free parameter in fitting the spectrum.
[2]) These values agree with those measured above T_C.
[3]) IS relative to $^{57}CoRh$ source.

Table 125a. Hyperfine interaction parameters of Mössbauer isotopes (^{155}Gd, ^{161}Dy, ^{166}Er) in RM_4Al_8 compounds (M = Cr, Mn, Fe, Cu).

	T K	IS mm s^{-1}	$g\mu_N H_{hyp}/h$ MHz	e^2qQ/h MHz	θ [1]	Ref.
Isotope ^{155}Gd		IS relative to $SmPd_3$ source				78 F 2
$GdCr_4Al_8$	4.1	0.44(5)	172(4)	301(4)	80(7)°	
	77	0.40(5)		295(4)		
$GdMn_4Al_8$	4.1	0.43(5)	102(5)	217(4)	46(6)°	
	77	0.39(5)		218(4)		
$GdFe_4Al_8$	4.1	0.4(1)	188(5)	– 238(5)	44(4)°	
	77	0.4(1)	24(20)	– 228(5)		
$GdCu_4Al_8$	4.1	0.4(1)	166(4)	– 83	60(6)°	
	77	0.4(1)		– 83(1)		
Isotope ^{161}Dy		IS relative to GdF_3 source				79 F 3
$DyCr_4Al_8$	4.1	1.3(1)	– 835(30)	2360(120)		
$DyMn_4Al_8$	4.1	1.5(1)	– 835(30)	2485(120)		
$DyFe_4Al_8$	4.1	1.5(1)	– 845(30)	2545(120)		
$DyCu_4Al_8$	4.1	1.5(1)	– 750(30)	1880(120)		
Free ion			– 840	2560		
Isotope ^{166}Er		IS relative to $Ho_{0.4}Y_{0.6}H_2$ source				79 F 3
$ErCr_4Al_8$	4.1	–0.05	1790(50)	690(60)		
$ErMn_4Al_8$	4.1		1735(50)	570(60)		
$ErFe_4Al_8$	4.1		1610(50)	560(60)		
$ErCu_4Al_8$	4.1		1350(150)	490(60)		
Free ion			1840	1100		

[1]) Angle between hyperfine field and c axis.

Table 125b. Hyperfine interaction parameters of Mössbauer isotopes (^{170}Yb, ^{151}Eu, ^{57}Fe) in RM_4Al_8 compounds (M = Cr, Mn, Fe, Cu).

	T K	IS mm s^{-1}	H_{hyp} kOe	e^2qQ/h MHz	θ [1]	Ref.
Isotope ^{170}Yb		IS relative to $TmAl_2$ source				79 F 3
$YbCr_4Al_8$	4.1	− 0.2	–	385(10)	40(5)°	
$YbMn_4Al_8$	4.1	− 0.2	–	− 340(10)		
$YbFe_4Al_8$	4.1	–	550(30)	2280(30)		
$YbCu_4Al_8$	4.1	− 0.1	–	210(10)		
Isotope ^{151}Eu		IS relative to SmF_3 source				78 F 2
$EuMn_4Al_8$	4.1	− 3.90				
	300	− 6.95				
	505	− 7.20				
$EuFe_4Al_8$	4.1	− 0.1	148(4)	− 30(15)		
	273	− 1.38		137(7)		
	513	− 3.05		155(7)		
$EuCu_4Al_8$	300	−10.8				
Isotope ^{57}Fe		IS relative to Fe metal				79 F 3
YCr_4Al_8	4.1	0.21(3)		9.7(2)		
$TbCr_4Al_8$	4.1	0.21(3)		10.0(2)		
	77	0.23(3)		9.2(2)		
$TbMn_4Al_8$	4.1	0.26(3)	59(5)	17.0	48(5)°	
	77	0.29(3)		17.4(3)		
YMn_4Al_8	4.1	0.21(4)		13.2(2)		
	77	0.21(3)		11.9(2)		
$CeCu_4Al_8$	4.1	0.23(4)		4.3(2)		
	295	0.23(4)		4.1(2)		
$NdCu_4Al_8$	4.1	0.25(3)		3.6(2)		
$TbCu_4Al_8$	4.1	0.22(3)		3.8(2)		
	295	0.24(3)		3.2(2)		
$ErCu_4Al_8$	4.1	0.25(3)		3.1(2)		
Isotope ^{57}Fe		IS relative to ^{57}Co–Rh source				78 B 23
$LaFe_4Al_8$	4.2	0.59	114			
$CeFe_4Al_8$	4.2	0.57	118			
$NdFe_4Al_8$	4.2	0.58	113			
$GdFe_4Al_8$	4.2	0.58	101			
$TbFe_4Al_8$	4.2	0.58	106			
$ErFe_4Al_8$	4.2	0.57	112			
$TmFe_4Al_8$	4.2	0.58	111			
$LuFe_4Al_8$	4.2	0.56	108			
YFe_4Al_8	4.2	0.57	116			
$ThFe_4Al_8$	4.2	0.56	112			

[1]) Angle between hyperfine field and c axis.

For Mössbauer effect studies on ^{169}Tm and ^{161}Dy in RFe_4Al_8 compounds see also [82 G 15]. The Tm sublattice orders below 4(1) K and the Dy sublattice below $T_C = 35$ K. For ^{57}Fe studies see also [77 V 3].

Table 126a. Hyperfine interaction parameters at ^{57}Fe in RFe_6Al_6 compounds at 4.1 K and relative population of sites [80 N 5, 81 F 2].

	H_{hyp} [1] kOe		e^2qQ/h MHz		IS [2] cm s^{-1}			Relative population of sites %			θ [3]	
	f	j	f	j	f	j	i	f	j	i	f	j
$GdFe_6Al_6$	153(2)	142(2)	−24(3)	22(3)	0.00(3)	0.20(3)	0.18(3)	60(2)	26(2)	14(2)	68(2)°	45(2)°
$TbFe_6Al_6$	158(2)	151(2)	−20(3)	26(2)	0.00(3)	0.24(3)	0.25(3)	60(2)	30(2)	10(2)	81(4)°	40(1)°
$DyFe_6Al_6$	169(2)	153(2)	−17(1)	16(1)	0.04(3)	0.18(3)	0.18(3)	63(2)	32(2)	5(2)	60(2)°	34(2)°
$HoFe_6Al_6$	166(2)	152(2)	−22(1)	23(1)	0.02(3)	0.20(3)	0.17(3)	61(2)	35(2)	3(2)	65(2)°	40(2)°
$ErFe_6Al_6$	163(2)	159(2)	−16(1)	18(2)	0.05(3)	0.30(3)	0.25(3)	66(2)	30(2)	1(2)	90(5)°	39(2)°
$TmFe_6Al_6$					0.06(3)	0.17(3)	0.26(3)	62(2)	30(2)	7(2)		
$YbFe_6Al_6$					0.16(3)	0.18(3)	0.13(3)	61(2)	31(2)	9(2)		
YFe_6Al_6	154(2)	144(2)	−19(2)	17(2)	0.06(3)	0.24(3)	0.19(3)	67(2)	17(2)	16(2)	67(2)°	38(2)°

[1]) Besides the high T_C, the Fe in 8i sites is not ordered magnetically even at 90 K, though ordered at 4.2 K.
[2]) Isomer shift relative to Co–Rh source.
[3]) Orientation of the hyperfine field relative to the principal axis of the EFG tensor.

Table 126b. Hyperfine interaction parameters of ^{155}Gd, ^{161}Dy, ^{166}Er, ^{170}Yb and ^{151}Eu in RM_6Al_6 compounds [81 F 2].

	T K	H_{hyp} kOe	e^2qQ/h MHz	IS cm s^{-1}	θ [1]
$^{155}GdFe_6Al_6$	4.1	209(2)	− 108(4)	0.38(2)	43(4)°
	77	209(2)	− 108(4)	0.38(2)	43(4)°
$^{155}GdMn_6Al_6$	4.1	198(7)	160(12)	0.45(3)	90(5)°
	77		190(10)	0.41(3)	
$^{155}GdCu_6Al_6$	4.1	246(2)	− 60(4)	0.53(2)	48(3)° or 61(3)°
	77			0.55(2)	
$^{155}GdRh_6Al_6$	4.1	186(4)	264(4)	0.10(3)	60(2)°
	77		264(4)	0.15(3)	
$^{161}DyFe_6Al_6$	4.1	5880(20)		0.91(3)	
$^{166}ErFe_6Al_6$	4.1	8240(20)	1370(20)	0.0(1)	
$^{170}YbFe_6Al_6$	4.1	990(30)	3900(600)		44(2)°
$^{151}EuFe_6Al_6$	4.1	240(5)		0.2(2)	
	77	137(4)		0.19(4)	

[1]) Orientation of the hyperfine field relative to the tetragonal axis.

For Mössbauer effect studies see also

^{57}Fe $Y(^{57}FeMn)_{12}$ [83 S 24]; $Gd(FeAl)_{12}$ [87 L 7, 88 W 2]; $R(FeAl)_{12}$ [80 N 5]; $Y(FeAl)_{12}$ [82 Y 4, 86 F 2, 86 F 3]; RFe_4Al_8 [77 V 3, 78 F 2]; R = Nd, Gd, Tm [78 B 23]; $EuFe_4Al_8$ [78 F 1]; RFe_5Al_7 [83 F 3]; R = Gd, Tb, Dy, Ho [83 N 11]; RFe_6Al_6 [81 F 1]; $RFe_{10}V_2$ [88 G 5]; $DyFe_{11}Ti$ [88 L 2]; $R(FeM)_{12}$, M = V, Mo, Ti, W, Si, R = Sm, Gd, Er, Y [89 S 1]

^{151}Eu EuM_4Al_8 [79 F 3]; $EuFe_4Al_8$ [78 F 1, 78 F 2]; $EuFe_6Al_6$ [81 F 2]

^{155}Gd GdM_4Al_8 [79 F 3]; $GdFe_4Al_8$ [78 F 2]; $GdFe_5Al_7$ [83 F 3]; GdM_6Al_6, M = Fe, Cu, Mn, Rh [81 F 2]; $GdFe_{10}M_2$, M = Ti, V, Cr, Mo, Si, W [88 B 6]

^{161}Dy DyM_4Al_8 [79 F 3]; $DyFe_4Al_8$ [82 G 15]; $DyFe_6Al_6$ [81 F 1, 81 F 2]; $DyFe_{10}V_2$ [88 G 5]

^{166}Er ErM_4Al_8 [79 F 3]; $ErFe_6Al_6$ [81 F 1, 81 F 2]; $ErFe_{10}V_2$ [88 G 5]

^{169}Tm $TmFe_4Al_8$ [82 G 15, 85 G 19]; $TmFe_{10}V_2$ [88 G 5]

^{170}Yb YbM_4Al_8 [79 F 3]; $YbFe_4Al_8$ [78 F 2]; $YbFe_6Al_6$ [81 F 1, 81 F 2]

NMR

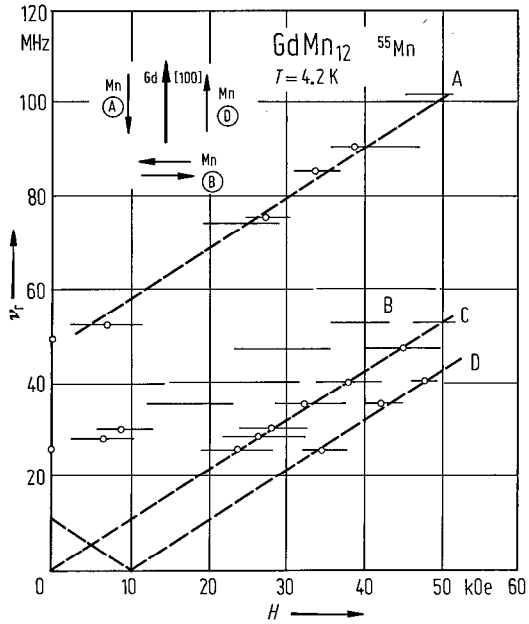

Fig. 547. External magnetic field dependence of the resonance frequency of ^{55}Mn in $GdMn_{12}$. The magnetic structure is shown in the inset. The signals A and D are due to the Mn atoms at i and j sites whose magnetic moments are collinear with the Gd magnetic moments. The broad signal B is due to Mn atoms at i and j sites whose magnetic moments are perpendicular to the Gd magnetic moments. The signal C is due to Mn atoms at f sites, whose magnetic moments are very small as in case of YMn_{12} [87 O 4].

For NMR studies see also
^{55}Mn YMn_{12} [83 Y 7]; ^{95}Mo, ^{97}Mo, $R(FeMo)_{12}$ [89 S 1]

Anisotropy, magnetostriction

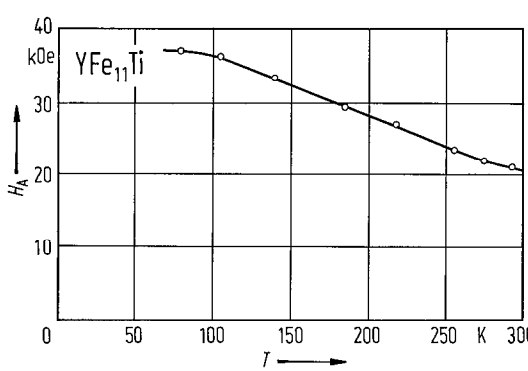

Fig. 548. Temperature dependence of the anisotropy field in $YFe_{11}Ti$ compound [88 M 2].

For anisotropy see also
$Sm(FeTi)_{12}$ [88 Y 2]; $Dy(FeTi)_{12}$ [88 L 2]; $Y(FeTi)_{12}$ [88 M 2]

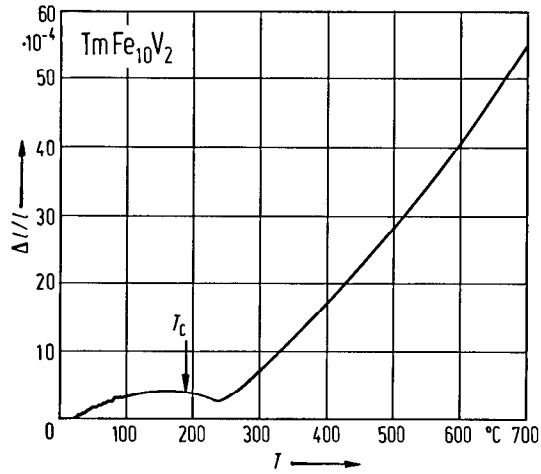

Fig. 549. Thermal expansion behaviour of $TmFe_{10}V_2$. An invar-type anomaly is evidenced. The Curie temperature is indicated by arrow [88 B 5].

Magnetization processes

For magnetization processes see also
$Y(FeAl)_{12}$ [86 F 2, 86 F 3]; RFe_5Al_7 [82 F 2, 83 F 3]; $Sm(FeTi)_{12}$, $Nd(FeTi)_{12}$ [88 K 1]

Transport properties

For electrical resistivity and thermopower studies see
$Y(MnAl)_{12}$ [87 K 4]

Photoemission study

For X-ray photoemission study see
$EuFe_4Al_8$ [81 M 4]

2.4.2.20 RM_{13}-type compounds

Crystalline structure, lattice parameters

$La(FeSi)_{13}$, $La(NiSi)_{13}$,
$Ce(CoSi)_{13}$, $Pr(CoSi)_{13}$,
$Nd(CoSi)_{13}$ [68 K 3]

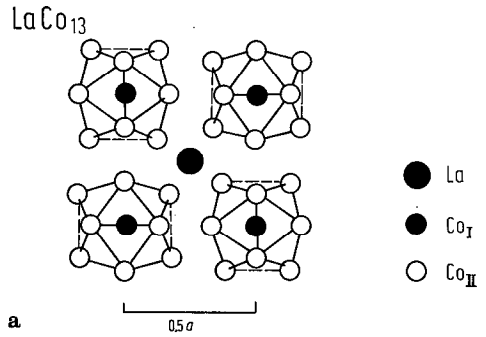

Fig. 550. (a) Projection along the *c* axis for a part of the $NaZn_{13}$-type unit cell in which the $LaCo_{13}$ compound crystallizes. The Co atoms occupy two different sites in a ratio $Co_I:Co_{II}=1:12$, Table 127. Each Co_I atom is surrounded by an icosahedron of $12Co_{II}$ atoms and thus has a fcc-like local symmetry. The icosahedra are packed in alternate directions so that each unit cell contains 8 icosahedra and therefore 104 spins. Each Co_{II} atom has $1Co_I$ and $9Co_{II}$ nearest neighbours [67 Z 1]. (b) Dependence of the lattice constant *a* on Fe concentration in $La(Fe_xAl_{1-x})_{13}$ compounds. The scale on the right-hand side refers to the distance, d, between the Fe_I and Fe_{II} atoms [84 P 3]. In $La(Fe_xAl_{1-x})_{13}$ system single-phase samples were obtained in the concentration range $0.46 \leqq x \leqq 0.92$; for $La(Fe_xSi_{1-x})_{13}$ in the range $0.81 \leqq x \leqq 0.88$, and $x \geqq 0.81$ for $La(Co_xSi_{1-x})_{13}$ system. In case of $La(Ni_{1-x}Si_x)_{13}$ only the sample with $x=0.154$ was studied [83 P 2, 84 P 3]. For the crystal structure of $La(FeSi)_{13}$, $R(CoSi)_{13}$ with R = Ce, Nd and $La(NiSi)_{13}$ see also [68 K 3] and for $La(FeCoM)_{13}$, M = Si, Al see [85 B 14] and for $La(FeAl)_{13}$ see [83 Y 1, 85 P 2].

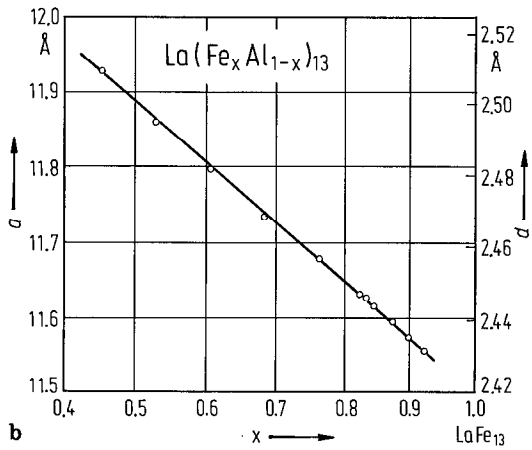

Table 127. Positions of the atoms in the $NaZn_{13}$-type structure of $LaCo_{13}$ [67 Z 1].

Atom	Site
8La	$\pm(1/4, 1/4, 1/4)$
$8Co_I$	(0, 0, 0); (1/2, 1/2, 1/2)
$96Co_{II}$	$\pm(0, y, z)$; $\pm(1/2, \bar{z}, y)$ $y=0.112$, $z=0.178$

Magnetization, Curie temperature

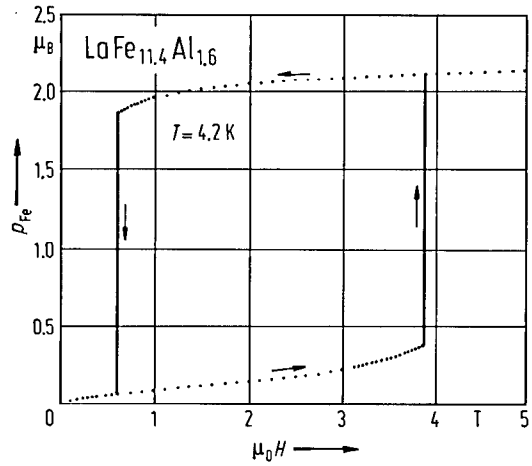

Fig. 551. Magnetization isotherm at 4.2 K for $La(Fe_{0.877}Al_{0.123})_{13}$ sample [84 P 3]. The sample was cooled in zero field to helium temperature and then the magnetic field was increased. The spin-flip field at 4.2 K, measured in increasing field is 3.88 T, but only 0.61 T with decreasing field. The transition takes place within a field change of 1 mT. Analogous behaviour was found for other samples with $x > 0.877$.

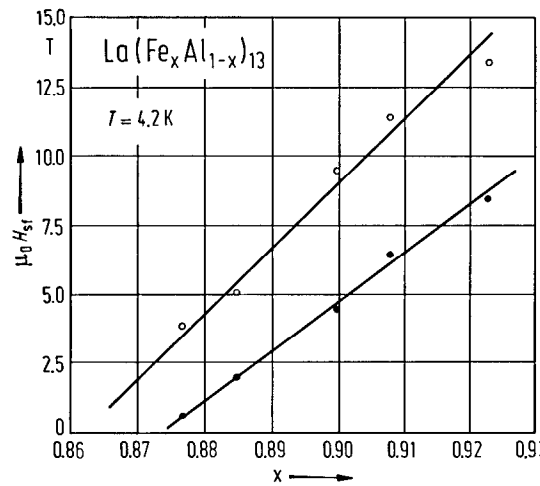

Fig. 552. Composition dependence of the spin-flip fields observed in some $La(Fe_xAl_{1-x})_{13}$ compounds at 4.2 K, for increasing (open circles) and decreasing field (full circles) [84 P 3].

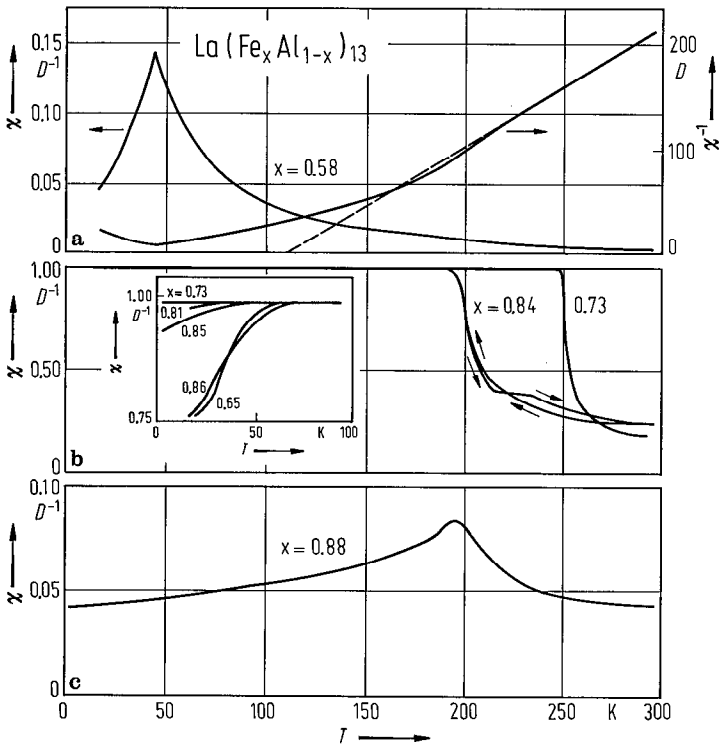

Fig. 553. Temperature dependence of the low-field magnetic susceptibilities for the three typical regimes of $La(Fe_xAl_{1-x})_{13}$ system [84 P 2]. In (a) a mictomagnetic behaviour is shown, in (b) a ferromagnetic transition and in (c) an antiferromagnetic one. The insert in (b) shows the low-temperature deviations from the soft ferromagnetic state. Note the different χ scales. The susceptibilities were plotted in units of inverse demagnetizing factor D^{-1}. $D = 4\pi/3$ for the spherical samples. The full ferromagnetic state is indicated by a susceptibility of $1.00D^{-1}$.

Fig. 554. Magnetic phase diagram of $La(Fe_xAl_{1-x})_{13}$ system [84 P 2, 86 P 1]. In the first regime, $0.46 \leqq x \leqq 0.62$, the magnetic susceptibility has a distinct mictomagnetic cusp at about 50 K. The large positive paramagnetic Curie temperature indicates the predominantly ferromagnetic exchange interactions, i.e. mictomagnetism. The effective Fe magnetic moment determined at high temperatures (where a Curie-Weiss law is evidenced) is 3.5 μ_B/Fe. In the second regime, $0.62 \leqq x \leqq 0.86$ a ferromagnetic behaviour is shown. In the concentration range, $0.84 \leqq x \leqq 0.86$, a hysteresis has been observed where the susceptibility above T_C behaves differently on heating and cooling, but both curves yield the same T_C, Fig. 553(b). In the third regime, $0.86 \leqq x \leqq 0.92$, an antiferromagnetic order is suggested. The cusp temperature, Curie temperature, and Néel temperature are indicated for the respective regimes. The $La(M_xSi_{1-x})_{13}$ compounds with M = Fe or Co are ferromagnetic [83 P 2], while $LaNi_{11}Si_2$ is a Pauli paramagnet [83 P 2].

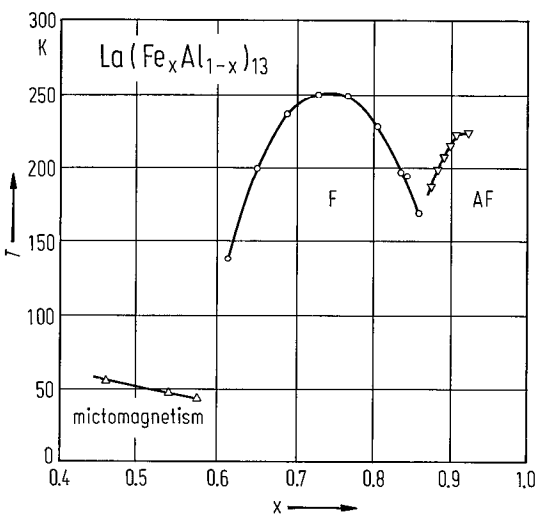

Table 128. Physical properties of $LaCo_{13}$ compound.

	a		T_C	p_s (μ_B/f.u.)
	Å		K	
$LaCo_{13}$	11.344	11.330	1290	20.5
Ref.	67 B 3	67 Z 1	68 V 1	68 V 1, 75 H 1

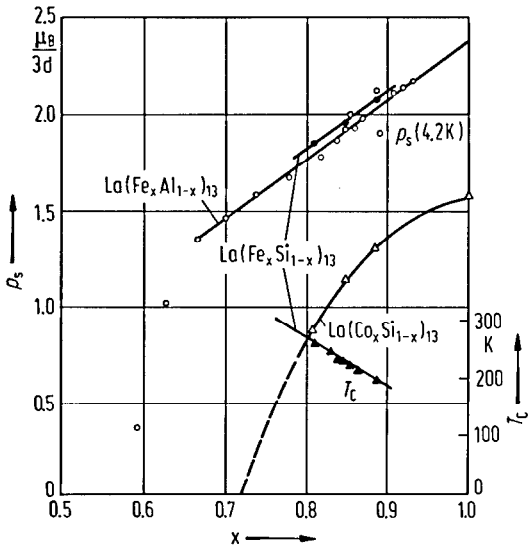

Fig. 555. Composition dependence of the saturation magnetization at 4.2 K in $La(Fe_xAl_{1-x})_{13}$ [84 P 2], $La(Fe_xSi_{1-x})_{13}$ [83 P 2] and $La(Co_xSi_{1-x})_{13}$ [83 P 2] compounds. In case of $La(Fe_xAl_{1-x})_{13}$ system the magnetic moment increases linearly with x having a slope of 0.24 μ_B/Fe per substituted Fe atom. In the mictomagnetic regime there are deviations from this line; probably, the field of 5.0 T is not enough to saturate the magnetization. The saturation magnetic moment in the antiferromagnetic regime has been measured in high field where metamagnetic transitions to the full saturated magnetic moment were found. A linear dependence of the mean Fe moment is also seen in $La(Fe_xSi_{1-x})_{13}$. A rapid decrease of the Co magnetic moment in $La(Co_xSi_{1-x})_{13}$ compounds is shown. The Curie temperatures T_C of $La(Fe_xSi_{1-x})_{13}$ are linearly dependent on composition.

For magnetic properties see also
$La(FeCoM)_{13}$, M = Si, Al [85 B 14]
$La(FeAl)_3$ [83 V 1, 83 Y 1, 84 P 2, 84 P 3, 85 P 2, 87 A 1]

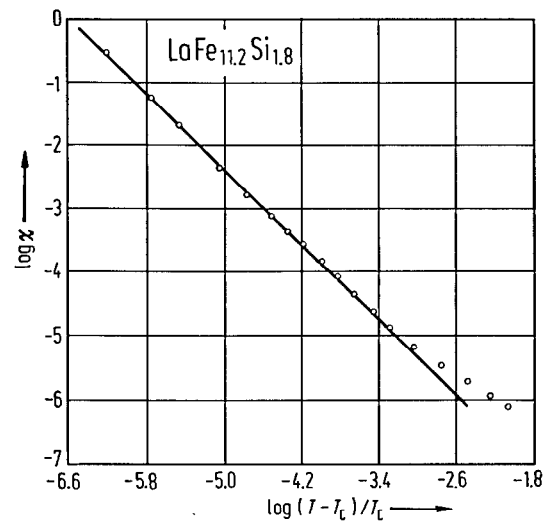

Fig. 556. Temperature dependence of the magnetic susceptibility at $T > T_C$ close to the Curie point in $LaFe_{11.2}Si_{1.8}$ compound [83 P 2]. χ follows a relation of the form $\chi \propto \left(\frac{T-T_C}{T_C}\right)^{\gamma}$ where $\gamma = 1.38$. A value $\gamma = 1.37$ was obtained in $LaFe_{10.8}Fe_{2.2}$ compound.

Neutron diffraction

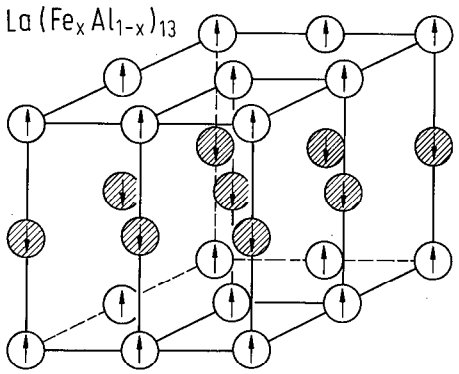

Fig. 557. Model for the antiferromagnetic structure of $La(Fe_xAl_{1-x})_{13}$ compound – as for x = 0.91 [86 H 2, 86 P 1]. Each "spin" represents a cluster of thirteen atoms by considering the icosahedron of Fe_{II} atoms and the central Fe_I atom. The Fe_I sites are predominantly (> 97%) occupied by Fe. The Al atoms are statistically distributed only over the Fe_{II} sites, thereby favouring the fcc-like coordination of the Fe atoms. The occurrence of the small magnetic moment on Fe_I site, $p_{Fe_I} \cong 1.10\,\mu_B$ cf. Table 129, reflects the instability of the Fe magnetic moment in a fcc local environment. The magnetic unit cell coincides with the nuclear unit cell, which forms the basis of cluster model.

Table 129. Magnetic moments of Fe determined by neutron diffractions in $La(Fe_xAl_{1-x})_{13}$ compounds at 4.2 K.

x	T_{ord} K	Magnetic structure	$p_{Fe}(\mu_B)$		Ref.
			Fe_I	Fe_{II}	
0.91	218	AF	1.10(7)	2.14(3)	86 H 2, 86 P 1
0.69	237	F	1.41(8)		86 H 2, 86 P 1

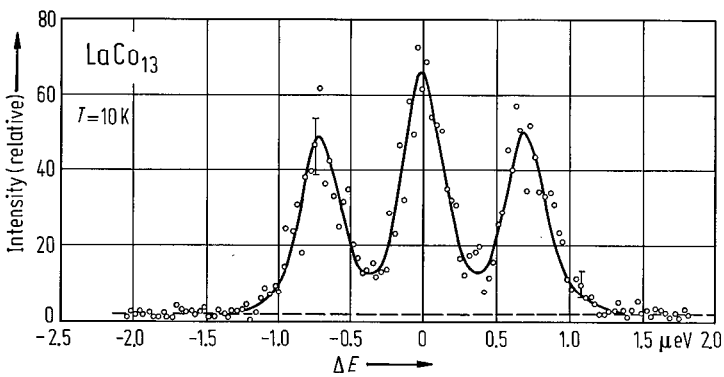

Fig. 558. Energy spectra obtained by means of inelastic spin-flip scattering of neutrons in $LaCo_{13}$ compound at 10 K [75 H 1]. The mean Co magnetic hyperfine field determined from these data is $H_{hyp} = -173$ kOe.

Mössbauer effect

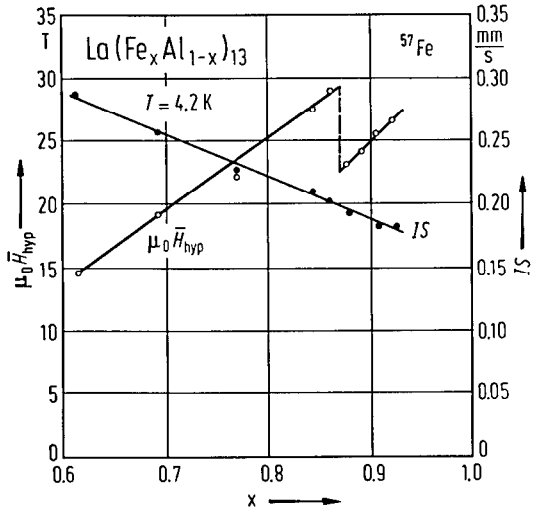

Fig. 559. Fe concentration dependence of the average magnetic hyperfine field, $\bar{H}_{hyp}$, and the isomer shift, *IS*, for ^{57}Fe, in La(Fe$_x$Al$_{1-x}$)$_{13}$ compounds at 4.2 K [86 H 2]. The $\bar{H}_{hyp}$ values increase with x, the ferromagnetic-antiferromagnetic phase boundary being revealed by a substantial drop of $\bar{H}_{hyp}$ close to the composition x = 0.87. See also [83 V 1].

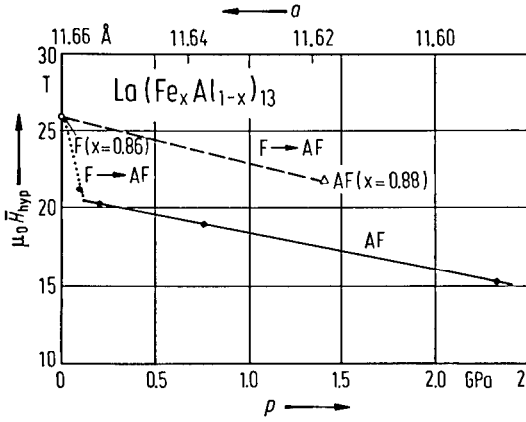

Fig. 560. Average magnetic hyperfine field $\bar{H}_{hyp}$ at 4.2 K, of La(Fe$_x$Al$_{1-x}$)$_{13}$ as function of pressure and lattice parameter for x = 0.86 and 0.88 at ambient pressure and for x = 0.86 at p = 0.1; 0.2; 0.8 and 2.4 GPa. The dashed line shows the F→AF phase transition due to change in the chemical composition, the dotted line denotes the F→AF phase transition due to external pressure. The solid line indicates the pressure dependence of $\bar{H}_{hyp}$ in the pressure-induced AF phase [87 A 1].

For Mössbauer effect see also
La(FeSi)$_{13}$ [83 P 2], La(FeAl)$_{13}$ [83 V 1, 83 Y 1, 86 H 2]

Anisotropy, magnetostriction

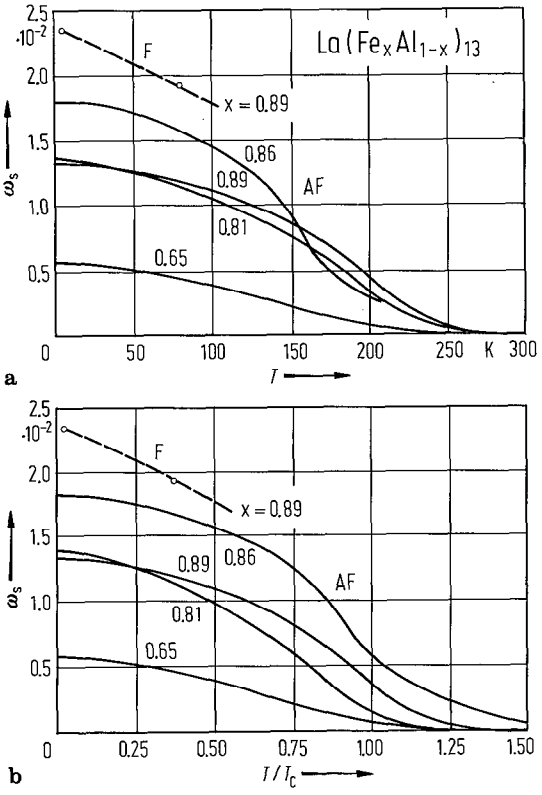

Fig. 561. Spontaneous volume magnetostriction, ω_s, as function of temperature and reduced temperature T/T_C in $La(Fe_xAl_{1-x})_{13}$. The thermal expansion exhibits a strong Invar-type character and is described by a combined band and local-moment model which allows calculations of corresponding magneto-volume coupling constants [85 P 2, 86 P 1].

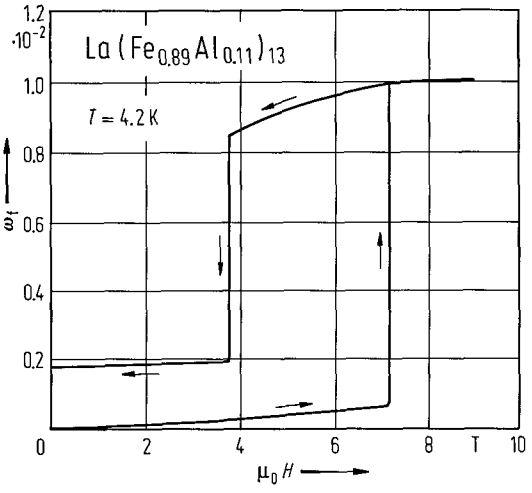

Fig. 562. Forced volume magnetostriction, $\omega_f = \Delta V/V$, as a function of magnetic field for the antiferromagnetic $La(Fe_{0.89}Al_{0.11})_{13}$ sample at 4.2 K. The behaviour of the other samples in the antiferromagnetic regime is analogous. Up to the spin-flip transition the relative volume change, $\omega_f \cong 6 \cdot 10^{-4}$, is rather small. At the spin-flip transition there is a huge magnetic expansion, $\omega_f = 1 \cdot 10^{-2}$. Upon decreasing the field the same hysteresis loop is followed as has been observed with magnetization [85 P 2], see Fig. 551. For $La(FeCoAl)_3$ see [84 B 13].

Transport properties

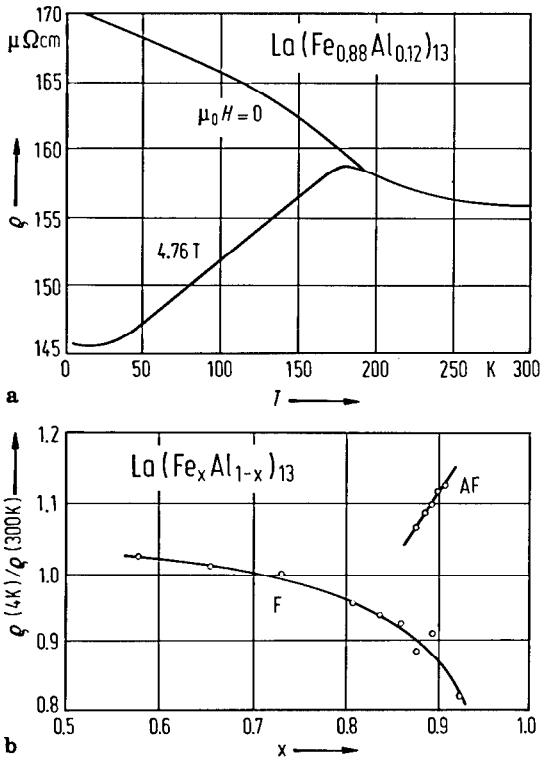

Fig. 563. (a) Temperature dependence of the electrical resistivity ϱ for the $La(Fe_{0.88}Al_{0.12})_{13}$ sample in a field of 4.76 T along with the zero-field resistance as a typical example of the antiferromagnetic regime. (b) shows the ratio $\varrho(4\,K)/\varrho(300\,K)$ versus Fe concentration in $La(Fe_xAl_{1-x})_{13}$ compounds. By F is denoted the ferromagnetic or induced ferromagnetic state and AF the antiferromagnetic ground state [85 P 2]. Upon applying a field at 4.2 K, the resistivity $\varrho(H)$ first decreases at a rate 1 μΩ cm/T and at the spin-flip transition there is a $\Delta\varrho$ of 20 μΩ cm. Thus, there is a total decrease of the resistivity in a field of 4.76 T of about 17%. The negative $d\varrho/dT$ in zero field becomes positive beyond the spin-flip field. Above T_N there is no observable field dependence of the resistivity. The magnetoresistance of the spin-flipped antiferromagnetic samples is quite similar to the zero-field resistance of the ferromagnetic samples. Samples in the ferromagnetic regime do not show pronounced changes in electrical resistivity upon applying a magnetic field.

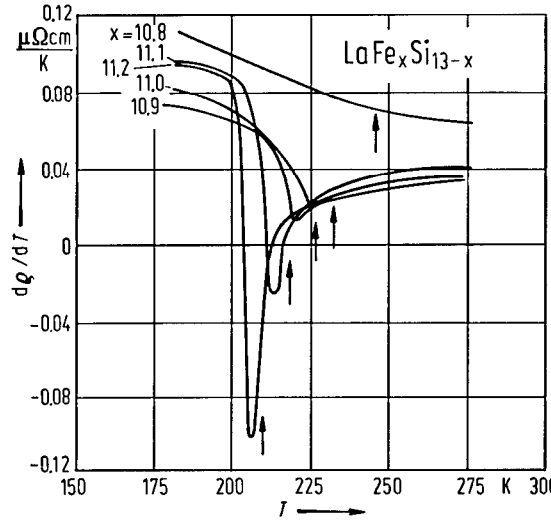

Fig. 564. Temperature dependence of the electrical resistivity derivative $d\varrho/dT$ in several $LaFe_xSi_{13-x}$ compounds near T_C. The position of T_C is indicated by means of arrows [83 P 2]. The anomalous critical behaviour of the resistivity was explained in terms of lattice softening near the Curie temperatures associated with the Invar-type anomaly.

For electrical resistivity studies see
$La(CoSi)_{13}$, $La(NiSi)_{13}$, $La(FeSi)_{13}$, $La(FeAl)_{13}$ [83 P 2, 85 P 2]

Magnetization processes

For magnetization processes see
$La(FeAl)_{13}$ [84 P 3]

2.4.3 References for 2.4

General References

58 h 1 Hansen, M., Anderko, K.: Constitution of Binary Alloys, McGraw Hill Book Co. **1958**.

61 g 1 Gschneidner, H.A.: Rare Earth Alloys, New York: Van Nostrand **1961**.

62 s 1 Savitski, E.M., Terekhova, V.F., Burov, I.V. Markova, I., Numkin, D.: Rare Earth Alloys, Academy of Sci. of the USSR, Moscow **1962**.

63 n 1 Nevitt, M.V.: Electronic Structure and Alloy Chemistry of the Transition Elements (Beck, P.A., ed.), New York: John Wiley and Sons, Inc. **1963**.

64 s 1 Schubert, K.: Kristallstruckturen zweikomponentiger Phasen, Berlin, Heidelberg, New York: Springer **1964**

65 e 1 Elliot, R.P.: Constitution of Binary Alloys, First Supplement, McGraw-Hill Book Co. **1965**.

68 o 1 Ofer, S., Nowik, I., Cohen, S.G.: Chemical Applications of Mössbauer Spectroscopy. New York: Academic Press **1968**, ch. 8.

68 w 1 Wallace, W.E.: Progr. Rare Earth Science and Technology **3** (1968) 1.

69 s 1 Shunk, F.A.: Constitution of Binary Alloys. Second Supplement, McGraw-Hill Book Co. **1969**.

71 t 1 Taylor, K.N.R.: Adv. Phys. **20** (1971) 551.

71 w 1 Wallace, W.E.: Progr. Rare Earth Science and Technology (Eyring, L., ed.), Oxford: Pergamon Press **3** (1971) 1.

72 b 1 Bleaney, B.: Magnetic Properties of Rare Earth, London: Plenum Press **1972**, ch. 8.

72 r 1 Rhyne, J.J., McGuire, T.R.: IEEE Trans. Magn. MAG-**8** (1972) 105.

73 n 1 Nesbitt, E.A., Wernick, J.H.: Rare Earth Permanent Magnets, New York: Academic Press **1973**.

73 t 1 Taylor, R.H.: Adv. Phys. **22** (1973) 681.

73 w 1 Wallace, W.E.: Rare Earth Intermetallics, New York: Academic Press **1973**.

75 b 1 Burzo, E.: Lecture at Symposium on Physics of Metals, Zloty-Potok, Poland **1975**, Preprint SR-14-1975.

75 s 1 Savitski, E.M., Terekhova, V.F.: Metallography of Rare Earth Metals, Moscow: Publ. House Nauka **1975**.

77 b 1 Buschow, K.H.J.: Rep. Progr. Phys. **40** (1977) 1179.

78 k 1 Kirchmayr, H.R., Poldy, C.A.: J. Magn. Magn. Mater. **8** (1978) 1.

78 m 1 Moffatt, W.G.: The Handbook of Binary Phase Diagrams, General Electric **1978**.

78 w 1 Wallace, W.E., in: Hydrogen in Metals, Berlin, Heidelberg, New York: Springer **1978**, p. 169.

79 b 1 Barnes, R.G.: NMR, EPR and Mössbauer Effect: Metals, Alloys and Compounds. Handbook on Physics and Chemistry of Rare Earths, vol. 2, Amsterdam, New York: North Holland Publ. Co. **1979**, p. 387.

79 b 2 Burzo, E.: Fizica Fenomenelor Magnetice, vol. 1, Ed. Academiei RSR, Bucuresti **1979**.

79 c 1 Clark, A.E.: Magnetostrictive RFe_2 Compounds. Handbook on Physics and Chemistry of Rare Earths, vol. 2, Amsterdam, New York: North Holland Publ. Co. **1979**, p. 231.

79 i 1 Iandelli, A., Palenzona, A.: Crystal Chemistry of Intermetallic Compounds. Handbook on Physics and Chemistry of Rare Earths, vol. 2, Amsterdam, New York: North Holland Publ. Co. **1979**, p. 1.

79 k 1 Kirchmayr, H.R., Poldy, C.A.: Magnetic Properties of Intermetallic Compounds. Handbook on Physics and Chemistry of Rare Earths, vol. 2, Amsterdam, New York: North Holland Publ. Co. **1979**, p. 55.

79 l 1 Libowitz, G.G., Maeland, A.J.: Hydrides. Handbook on Physics and Chemistry of Rare Earths, vol. 3, Amsterdam, New York: North Holland Publ. Co. **1979**, p. 299.

79 s 1 Steiner, W.: J. Magn. Magn. Mater. **14** (1979) 47.

80 b 1 Belov, K.P.: Redkozemelnye Magnetiki i ikh Primenenye, Moskwa: Publ. House Nauka **1980**.

80 b 2 Buschow, K.H.J., in: Ferromagnetic Materials (Wohlfarth, E.P., ed.), Amsterdam, New York: North Holland Publ. Co. **1980**, p. 229.

80 c 1 Clark, A.E., in: Ferromagnetic Materials (Wohlfarth, E.P., ed.), Amsterdam, New York: North Holland Publ. Co. **1980**, p. 531.

81 b 1 Burzo, E.: Fizica Fenomenelor Magnetice, vol. 2, Ed. Academiei RSR, Bucuresti **1981**.

82 b 1 Burzo, E.: Lecture at Internat. Symposium on Magnetic Properties of Rare Earth Alloys, Oct. **1982**, Varna Preprint GS-6, 1982.

82 b 2 Buschow, K.H.J., Bounten, P.C.P., Miedema, A.R.: Rep. Progr. Phys. **45** (1982) 937.

82 g 1 Gratz, E., Zuckermann, M.J.: Transport Properties of Rare Earth Intermetallic Compounds. Handbook on Physics and Chemistry of Rare Earths, vol. 5, Amsterdam, New York: North Holland Publ. Co. **1982**, p. 117.

83 b 1 Burzo, E.: Fizica Fenomenelor Magnetice, vol. 3., Ed. Academiei RSR, Bucuresti **1984**.

84 b 1 Buschow, K.H.J.: Hydrogen Absorption in Intermetallic Compounds. Handbook on Physics and Chemistry of Rare Earths, vol. 6, Amsterdam, New York: North Holland Publ. Co. **1984**, p. 1.

84 m 1 Moffatt, W.G.: The Handbook of Binary Phase Diagrams, Genium Publ. Co., New York **1984**.

86 b 1 Burzo, E.: Magneti Permanenti, vol. 1, Ed. Academiei RSR, Bucuresti **1986**.

88 d 1 De Boer, F.R., Boom, R., Mattens, W.C.M., Miedema, A.R., Niessen, A.K.: Cohesion in Metals, Transition Metal Alloys, Amsterdam, Oxford, New York, Tokyo: North Holland **1988**.

88 f 1 Flanagan, T.B., Oates, W.A.: Thermodynamics of Intermetallic Compound-Hydrogen Systems. Hydrogen in Intermetallic Compounds (Schlapbach, L., ed.), Berlin, Heidelberg, New York, Tokyo: Springer **1988**, p. 49.

88 g 1 Griessen, R., Riesterer, T.: Heat of Formation. Hydrogen in Intermetallic Compounds (Schlapbach, L., ed.), Berlin, Heidelberg, New York, Tokyo: Springer **1988**, p. 219.

88 g 2 Gupta, M., Schlapbach, L.: Electronic Properties in Hydrogen. Intermetallic Compounds (Schlapbach, L., ed.), Berlin, Heidelberg, New York, Tokyo: Springer **1988**, p. 139.

88 k 1 Kumar, K.: J. Appl. Phys. **63** (1988) R 13.

88 p 1 Percheron-Guegan, A., Elter, J.M.: Preparation of Intermetallics and Hydrides. Hydrogen in Intermetallic Compounds (Schlapbach, L., ed.), Berlin, Heidelberg, New York, Tokyo: Springer **1988**, p. 11.

88 w 1 Wiesinger, G., Hilscher, G.: Magnetic Properties, Mössbauer Effect and Superconductivity. Hydrogen in Intermetallic Compounds (Schlapbach, L., ed.), Berlin, Heidelberg, New York, Tokyo: Springer **1988**, p. 285.

88 y 1 Yvon, K., Fischer, P.: Crystal and Magnetic Structures of Ternary Hydrogen. Hydrides in Intermetallic Compounds (Schlapbach, L., ed.), Berlin, Heidelberg, New York, Tokyo: Springer **1988**, p. 87.

Special References

36 N 1 Néel, L.: Ann. Phys. **4** (1936) 232.

37 N 1 Néel, L.: Ann. Phys. **8** (1937) 237.

42 N 1 Nowotny, H.: Z. Metallkd. **34** (1942) 247.

47 V 1 Vogel, R.: Z. Metallkd. **38** (1947) 97.

48 N 1 Néel, L.: Ann. Phys. **3** (1948) 137.

52 F 1 Florio, J.V., Rundle, R.E., Snow, A.I.: Acta Crystallogr. **5** (1952) 449.

52 W 1 Wucher, J.: J. Phys. Radium **13** (1952) 278.

53 B 1 Berry, R.L., Raynor, G.V.: Acta Crystallogr. **6** (1953) 178.

54 R 1 Ruderman, M.A., Kittel, C.: Phys. Rev. **96** (1954) 99.

55 J 1 Jepson, J.O., Duwez, P.: Trans. Am. Soc. Met. **47** (1955) 543.

56 F 1 Florio, J.V., Baenzinger, N.C., Rundle, R.E.: Acta Crystallogr. **9** (1956) 367.

56 K 1 Kasuya, T.: Prog. Theor. Phys. **16** (1956) 45.

56 M 1 Makarov, E.S., Vinogradov, S.P.: Kristallografiya **1** (1956) 634.

56 W 1 Wangsness, R.K.: Am. J. Phys. **24** (1956) 60.

57 Y 1 Yoshida, K.: Phys. Rev. **106** (1957) 893.

58 D 1 De Gennes, P.G.: C.R. Acad. Sci. **247** (1958) 1936.

59 C 1 Cromer, D.T., Larson, A.C.: Acta Crystallogr. **12** (1959) 855.

59 C 2 Cromer, D.T., Olsen, C.E.: Acta Crystallogr. **12** (1959) 689.

59 N 1 Nesbitt, E.A., Wernick, J.H., Corenzwit, E.: J. Appl. Phys. **30** (1959) 365.

59 W 1 Wernick, J.H., Geller, S.: Acta Crystallogr. **12** (1959) 662.

60 H 1 Haszko, S.E.: Trans. AIME **218** (1960) 958.

60 H 2 Haszko, S.E.: Trans. AIME **218** (1960) 763.

60 H 3 Hubbard, W.M., Adams, E., Gilfrich, J.V.: J. Appl. Phys. **31** (1960) 368.

60 N 1 Nassau, K., Cherry, L.V., Wallace, W.E.: J. Phys. Chem. Solids **16** (1960) 123.

60 N 2 Nassau, K., Cherry, L.V., Wallace, W.E.: J. Phys. Chem. Solids **16** (1960) 131.

60 W 1 Wernick, J.H., Geller, S.: Trans. AIME **218** (1960) 866.

61 B 1 Baenzinger, N.C., Moriarty, J.L.: Acta Crystallogr. **14** (1961) 948.
61 C 1 Cherry, L.V., Wallace, W.E.: J. Appl. Phys. **32** (1961) 3405.
61 C 2 Copeland, M., Kato, H.: Proc. 2nd Conf. on Rare Earth Res., New York: Gordon and Breach **1961**, p. 137.
61 C 3 Cromer, D.T., Larson, A.C.: Acta Crystallogr. **14** (1961) 1226.
61 D 1 Dwigth, A.E.: Trans. Am. Soc. Met. **53** (1961) 479.
61 F 1 Finney, J.J., Rosenzweig, A.: Acta Crystallogr. **14** (1961) 69.
61 F 2 Friedel, J., Leman, G., Olszewski, S.: J. Appl. Phys. **32** (1961) 325 S.
61 N 1 Nesbitt, E.A., Williams, H.J., Wernick, J.H., Sherwood, R.C.: J. Appl. Phys. **32** (1961) 342 S.
61 N 2 Novy, V.F., Vickery, R.C., Kleber, E.V.: Trans. AIME **221** (1961) 588.
61 R 1 Roof Jr., R.B., Larson, A.C., Cromer, D.T.: Acta Crystallogr. **14** (1961) 1084.
61 S 1 Saba, W.G., Wallace, W.E., Craig, R.S.: J. Chem. Phys. **35** (1961) 689.
61 S 2 Savitski, E.M., Terekhova, V.F., Burov, I.V., Chistyakov, O.D.: Zh. Neorg. Khim. **6** (1961) 1732.
61 W 1 Wallace, W.E., Epstein, L.S.: J. Chem. Phys. **35** (1961) 2238.
61 W 2 Wernick, J.H., Haszko, S.E.: J. Phys. Chem. Solids **18** (1961) 207.

62 C 1 Cherry, L.V., Wallace, W.E.: J. Appl. Phys. **33** (1962) 1515.
62 D 1 De Gennes, P.G.: J. Phys. (Paris) **23** (1962) 510.
62 F 1 Friedel, J.:. J. Phys. (Paris) **23** (1962) 501.
62 H 1 Hubbard, W., Adams, E.: J. Phys. Soc. Jpn. **17** Suppl. B 1 (1962) 143.
62 J 1 James, W., Lemaire, R., Bertaut, F.: C.R. Acad. Sci. **255** (1962) 896.
62 L 1 Larson, A.C., Cromer, D.T.: Acta Crystallogr. **15** (1962) 1224.
62 N 1 Nesbitt, E.A., Williams, H.J., Wernick, J.H., Sherwood, R.C.: J. Appl. Phys. **33** (1962) 1674.
62 S 1 Savitski, E.M., Terekhova, V.F., Burov, I.V.: Zh. Neorg. Khim. **7** (1962) 2572.
62 S 2 Shull, C.G., Yamada, Y.: J. Phys. Soc. Jpn. **17** (1962) B III.
62 W 1 Wernick, J.H., Haszko, S.E., Dorsi, D.: J. Phys. Chem. Solids **23** (1962) 567.
62 W 2 Wertheim, G.K., Wernick, J.H.: Phys. Rev. **125** (1962) 1937.
62 W 3 Wohlfarth, E.P., Rhodes, P.: Philos. Mag. **7** (1962) 1817.
62 Z 1 Zarechnyuk, O.S., Kripyakevich, P.I.: Kristallografiya **7** (1962) 543.

63 B 1 Bleaney, B.: Proc. R. Soc. London Ser. A **276** (1963) 28.
63 K 1 Kripyakevich, P.I., Terekhova, V.F., Zarechnyuk, C., Burov, I.V.: Kristallografiya **8** (1963) 268.
63 N 1 Nesbitt, E.A., Williams, H.J., Wernick, J.H., Sherwood, R.C.: J. Appl. Phys. **34** (1963) 1347.
63 S 1 Skrabek, E.A., Wallace, W.E.: J. Appl. Phys. **34** (1963) 1356.
63 W 1 Wallace, W.E., Skrabek, E.A.: Proc. 3rd Conf. on Rare Earth Res., Purdue Univ., Florida **1963**, p. 431.
63 Z 1 Zarechnyuk, O.S., Kripyakevich, P.I.: Kristallografiya **7** (1963) 543.

64 A 1 Abrahams, S.C., Bernstein, J.L., Sherwood, R.C., Wernick, J.H., Williams, H.J.: J. Phys. Chem. Solids **25** (1964) 1069.
64 B 1 Bleaney, B.: Proc. 4th Conf. on Rare Earth Res., New York: Gordon and Breach **1964**, vol. 2, p. 499.
64 C 1 Cohen, R.L.: Phys. Rev. A **134** (1964) 94.
64 C 2 Corliss, L.M., Hastings, J.M.: J. Phys. **25** (1964) 557.
64 C 3 Corliss, L.M., Hastings, J.M.: J. Appl. Phys. **35** (1964) 1051.
64 C 4 Crangle, J., Ross, J.W.: Proc. Int. Conf. Magnetism, Nottingham **1964**, p. 241.
64 F 1 Farrell, J., Wallace, W.E.: J. Chem. Phys. **41** (1964) 1524.
64 M 1 Mansmann, M., Wallace, W.E.: J. Chem. Phys. **40** (1964) 1167.
64 M 2 McMasters, O.D., Gschneidner, K.A.: Nucl. Metall. Ser. **10** (1964) 93.
64 N 1 Nevitt, M.V., Kimball, C.W., Preston, R.S.: Proc. Int. Conf. Magnetism, Nottingham **1964**, p. 137.
64 R 1 Ross, N., Crangle, J.: Phys. Rev. A **133** (1964) 509.
64 S 1 Shaltiel, D., Wernick, J.H., Williams, H.J., Peter, M.: Phys. Rev. A **135** (1964) 1346.
64 T 1 Teslyuk, M.J., Kripyakevich, P.I., Frankevich, D.P.: Kristallografiya **9** (1964) 558.
64 W 1 Wallace, W.E.: J. Chem. Phys. **41** (1964) 3857.
64 W 2 Wallace, W.E., Skrabek, A.E.: Proc. 4th Conf. on Rare Earth Res., New York: Gordon and Breach **1964**, vol. 2, p. 431.
64 W 3 Walline, R.E., Wallace, W.E.: J. Chem. Phys. **41** (1964) 1587.
64 W 4 Wang, F.E., Gilfrich, J.V., Ernst, D.W., Hubbard, W.H.: Acta Crystallogr. **17** (1964) 931.

64 W 5 Weik, H., Fischer, P., Halg, W., Stoll, E.: Proc. 4th Conf. on Rare Earth Res., New York: Gordon and Breach **1964**, p. 20.
64 W 6 Wertheim, G.K., Jaccarino, V., Wernick, J.H.: Phys. Rev. A **135** (1964) 151.
64 W 7 Wood, J.D., Conard, G.P.: Proc. 4th Conf. on Rare Earth Res., New York: Gordon and Breach **1964**, vol. 2, p. 209.

65 B 1 Bertaut, E.F., Lemaire, R., Schweizer, J.: Bull. Soc. Fr. Mineral. Crystallogr. **88** (1965) 580.
65 B 2 Bertaut, E.F., Lemaire, R., Schweizer, J.: C.R. Acad. Sci. **260** (1965) 3595.
65 D 1 De Savage, B.F., Bozorth, R.M., Wang, F.E., Callen, E.R.: J. Appl. Phys. **36** (1965) 992.
65 D 2 Dwigth, A.E., Cronner, R.A., Downey, J.W.: Acta Crystallogr. **18** (1965) 835.
65 F 1 Felcher, G.P., Corliss, L.M., Hastings, J.M.: J. Appl. Phys. **36** (1965) 1001.
65 H 1 Harris, I.R., Mansey, R.C., Raynor, G.V.: J. Less Common Met. **9** (1965) 270.
65 J 1 Jaccarino, V., Walker, L.R.: Phys. Rev. Lett. **15** (1965) 259.
65 K 1 Kirchmayr, H.R., Schindl, K.H.: Z. Angew. Phys. **19** (1965) 517.
65 K 2 Kripyakevich, P.I., Frankevich, D.P.: Kristallografiya **10** (1965) 560.
65 K 3 Kripyakevich, P.I., Teslyuk, M.Yu., Frankevich, D.M.: Kristallografiya **10** (1965) 422.
65 M 1 Moon, R.M., Koehler, W.C., Farrell, J.: J. Appl. Phys. **36** (1965) 978.
65 N 1 Nowik, I., Wernick, J.H.: Phys. Rev. A **140** (1965) 131.
65 O 1 Ofer, S., Rakavy, M., Segal, E., Khurgin, B.: Phys. Rev. A **138** (1965) 241.
65 O 2 Ostertag, W.: Acta Crystallogr. **19** (1965) 150.
65 P 1 Pelleg, J., Carlson, O.N.: J. Less Common Met. **9** (1965) 281.
65 S 1 Smith, J.F., Hansen, D.A.: Acta Crystallogr. **18** (1965) 60.
65 V 1 Van Vucht, J.H.N.: J. Less Common. Met. **10** (1965) 146.
65 W 1 Wang, F.E., Holden, J.R.: Trans AIME **233** (1965) 731.
65 W 2 Weik, H., Fisher, P., Halg, W., Stell, E.: Rare Earth Research, New York: Gordon and Breach **1965**, vol. 3, p. 19.

66 B 1 Barnes, R.G., Beaudry, B.J., Lecander, R.G.: J. Appl. Phys. **37** (1966) 1248.
66 B 2 Bartholin, H., Van Laar, B., Lemaire, R., Schweizer, J.: J. Phys. Chem. Solids **27** (1966) 1287.
66 B 3 Bouchet, G., Laforest, J., Lemaire, R., Schweizer, J.: C.R. Acad. Sci. B **262** (1966) 1227.
66 B 4 Buschow, K.H.J.: J. Less Common Met. **11** (1966) 204.
66 B 5 Buschow, K.H.J.: Z. Metallkd. **57** (1966) 728.
66 C 1 Callen, H.B., Callen, E.: J. Phys. Chem. Solids **27** (1966) 1271.
66 E 1 Ellinger, F.H., Land, C.C., Johnson, K.A., Struebing, V.O.: Trans. AIME **236** (1966) 1577.
66 F 1 Farrell, J., Wallace, W.E.: Inorg. Chem. **5** (1966) 105.
66 G 1 Gossard, A.C., Wernick, J.H.: Phys. Rev. Lett. **16** (1966) 995.
66 H 1 Hoffer, G., Strnat, K.J.: IEEE Trans. Magn. MAG-**2** (1966) 487.
66 K 1 Kirchmayr, H.R.: IEEE Trans. Magn. MAG-**2** (1966) 493.
66 K 2 Kissel, F., Tsuchida, T., Wallace, W.E.: J. Chem. Phys. **44** (1966) 4651.
66 L 1 Laforest, J.R., Lemaire, R., Pauthenet, R., Schweizer, J.: C.R. Acad. Sci. B **262** (1966) 1260.
66 L 2 Lederer, P., Blandin, A.: Philos. Mag. **14** (1966) 363.
66 L 3 Lemaire, R.: Cobalt **32** (1966) 132.
66 L 4 Lemaire, R.: Cobalt **33** (1966) 201.
66 L 5 Lemaire, R., Schweizer, J.: Phys. Lett. **21** (1966) 366.
66 N 1 Nowik, I., Ofer, S., Wernick, J.H.: Phys. Lett. **20** (1966) 232.
66 O 1 Ofer, S., Segal, E.: Phys. Rev. **141** (1966) 448.
66 O 2 Ostertag, W., Strnat, K.J.: Acta Crystallogr. **21** (1966) 560.
66 R 1 Ray, A.E.: Acta Crystallogr. **21** (1966) 426.
66 S 1 Strnat, K., Hoffer, G., Ray, A.E.: IEEE Trans. Magn. MAG-**2** (1966) 489.
66 S 2 Strnat, K., Hoffer, G., Ostertag, W., Olson, J.C.: J. Appl. Phys. **37** (1966) 1252.
66 T 1 Taylor, K.N.R., Ellis, H.D., Darby, M.T.: Phys. Lett. **20** (1966) 327.
66 W 1 Wang, F.E., Gilfrich, J.: Acta Crystallogr. **21** (1966) 476.

67 B 1 Ban, Z., Sikirica, M., Raseta, R.: J. Less Common Met. **12** (1967) 478.
67 B 2 Barnes, R.G., Lecander, R.G.: J. Phys. Soc. Jpn. **22** (1967) 930.
67 B 3 Buschow, K.H.J., Velge, W.A.J.J.: J. Less Common Met. **13** (1967) 11.

67 D 1 Dixon, M., Aoyagi, M., Craig, R.S., Wallace, W.E.: Proc. 6th Conf. on Rare Earth Res., Gathlingburg, Tennessee **1967**, p. 548.
67 G 1 Gegenwarth, R.E., Budnick, J.I., Skalski, S., Wernick, J.H.: Phys. Rev. Lett. **18** (1967) 9.
67 H 1 Harris, I.R., Mansey, R.C.: J. Less Common Met. **13** (1967) 591.
67 H 2 Hoffer, G., Strnat, K.J.: J. Appl. Phys. **38** (1967) 1377.
67 K 1 Kirchmayr, H.R.: Z. Kristallogr. **124** (1967) 152.
67 K 2 Kirchmayr, H.R., Lugscheider, W.: Z. Metallkd. **58** (1967) 185.
67 L 1 Laforest, J., Lemaire, R., Paccard, D., Pauthenet, R.: C.R. Acad. Sci. **264** (1967) 676.
67 L 2 Lemaire, R., Paccard, D.: Bull. Soc. Fr. Mineral. Crystallogr. **90** (1967) 311.
67 L 3 Lemaire, R., Schweizer, J.: C.R. Acad. Sci. **264** (1967) 642.
67 L 4 Lemaire, R., Schweizer, J.: J. Phys. (Paris) **28** (1967) 216.
67 L 5 Lemaire, R., Paccard, D., Pauthenet, R.: C.R. Acad. Sci. B **265** (1967) 1280.
67 L 6 Lemaire, R., Pauthenet, R., Schweizer, J., Silvera, I.S.: J. Phys. Chem. Solids **28** (1967) 2471.
67 M 1 Marei, S.A., Craig, R.S., Wallace, W.E., Tsuchida, T.: J. Less Common Met. **13** (1967) 391.
67 O 1 Oesterreicher, H., Wallace, W.E.: J. Less Common Met. **13** (1967) 91.
67 O 2 Oesterreicher, H., Wallace, W.E.: J. Less Common Met. **13** (1967) 475.
67 O 3 Ostertag, W.: Trans. AIME **239** (1967) 690.
67 O 4 Ostertag, W.: J. Less Common Met. **13** (1967) 385.
67 P 1 Paccard, D., Pauthenet, R.: C.R. Acad. Sci. **264** (1967) 1056.
67 P 2 Peter, M., Dupraz, J., Cottet, H.: Helv. Phys. Acta **40** (1967) 301.
67 S 1 Schweizer, J.: Phys. Lett. A **24** (1967) 739.
67 S 2 Smith, T.F., Harris, I.R.: J. Phys. Chem. Solids **28** (1967) 1846.
67 S 3 Strnat, K.J.: Cobalt **36** (1967) 33.
67 S 4 Strnat, K.J., Hoffer, G.I., Olson, J.C., Ostertag, W., Becker, J.J.: J. Appl. Phys. **28** (1967) 1001.
67 T 1 Terekhova, V.F., Kripyakevich, P.I., Frankevich, D.P., Torchinova, R.S.: Russ. Metall. **1** (1967) 107.
67 V 1 Van Vucht, J.H.N.: J. Less Common Met. **10** (1967) 146.
67 Z 1 Zarechnyuk, O.S., Kripyakevich, P.I.: Kristallografiya **12** (1967) 512.

68 A 1 Abel, A.W., Craig, R.S.: J. Less Common Met. **16** (1968) 77.
68 B 1 Bartholin, H., Laforest, J., Lemaire, R., Schweizer, J., Silvera, I.S.: Acta Crystallogr. **21** (1968) Suppl. A 94.
68 B 2 Becker, J.: J. Appl. Phys. **39** (1968) 1270.
68 B 3 Berthet-Colominas, C., Laforest, J., Lemaire, R., Pauthenet, R., Schweizer, J.: Cobalt **39** (1968) 97.
68 B 4 Bowden, G.J., Bunbury, D.St.P., Guimaraes, A.P., Snyder, R.E.: J. Phys. C **1** (1968) 1376.
68 B 5 Buschow, K.H.J.: J. Less Common Met. **16** (1968) 45.
68 B 6 Buschow, K.H.J., Van der Goot, A.S.: J. Less Common Met. **14** (1968) 323.
68 B 7 Buschow, K.H.J., Fast, J.F., Van der Goot, A.S.: Phys. Status Solidi (a) **29** (1968) 825.
68 C 1 Carfagna, P., Wallace, W.E.: Proc. 7th. Conf. on Rare Earth Res., Coronado, California **1968**, p. 105.
68 C 2 Carfagna, P.D., Wallace, W.E.: J. Appl. Phys. **39** (1968) 5259.
68 D 1 Davidov, D., Shaltiel, D.: Phys. Rev. Lett. **21** (1968) 1752.
68 D 2 Dwight, A.E.: Proc. 7th Conf. on Rare Earth Res., Coronado, California **1968**, p. 273.
68 D 3 Dworak, A., Kirchmayr, H.R., Rauch, H.: Z. Angew. Phys. **24** (1968) 318.
68 F 1 Feron, J.L., Lemaire, R., Paccard, D., Pauthenet, R.: C.R. Acad. Sci. B **267** (1968) 371.
68 F 2 Fisher, M.E., Langer, J.S.: Phys. Rev. Lett. **20** (1968) 665.
68 G 1 Gignoux, D.: Thesis, Univ. Grenoble, **1968**.
68 H 1 Hoffer, G.L., Salmans, L.R.: Proc. 7th Conf. on Rare Earth Res., Coronado, California **1968**, p. 337.
68 J 1 Johnson, Qu., Wood, D.H., Smith, G.S., Ray, A.E.: Acta Crystallogr. B **24** (1968) 274.
68 J 2 Joseph, R.R., Gschneidner Jr., K.A.: Scr. Metall. **2** (1968) 631.
68 K 1 Katsuraki, H., Yoshii, S.: J. Phys. Soc. Jpn. **24** (1968) 1171.
68 K 2 Kirchmayr, H.R.: J. Appl. Phys. **39** (1968) 1088.
68 K 3 Kripyakevich, P.I., Zarechnyuk, O.S., Gladyshevski, E.I., Bodak, O.I.: Z. Anorg. Allg. Chem. **358** (1968) 90.
68 L 1 Lemaire, R., Paccard, D., Pauthenet, R., Schweizer, J.: J. Appl. Phys. **39** (1968) 1092.
68 M 1 Mansey, R.C., Raynor, G.V., Harris, I.R.: J. Less Common Met. **14** (1968) 329.
68 M 2 Mansey, R.C., Raynor, G.V., Harris, I.R.: J. Less Common Met. **14** (1968) 337.
68 N 1 Nakamichi, T.: J. Phys. Soc. Jpn. **25** (1968) 1189.

68 N 2 Nesbitt, E.A., Williams, R.H., Sherwood, R.C., Buehler, E., Wernick, J.H.: Appl. Phys. Lett. **12** (1968) 361.
68 P 1 Petrich, G., Mössbauer, R.L.: Phys. Lett. **26** A (1968) 403.
68 P 2 Piercy, A.R., Taylor, K.N.R.: J. Phys. C **1** (1968) 1112.
68 P 3 Piercy, A.R., Taylor, K.N.R.: J. Appl. Phys. **39** (1968) 1096.
68 R 1 Ray, A.E.: Proc. 7th Conf. on Rare Earth Res., Coronado, California **1968**, p. 473.
68 S 1 Salmans, L.R., Strnat, K., Hoffer, G.I.: Tech. Rep. **1968**, AFML-CF-68-159.
68 V 1 Velge, W.A.J.J., Buschow, K.H.J.: J. Appl. Phys. **39** (1968) 1717.
68 W 1 Wallace, W.E., Mader, K.H.: Inorg. Chem. **7** (1968) 1627.

69 B 1 Becker, J.J.: IEEE Trans. Magn. MAG-**5** (1969) 211.
69 B 2 Bloch, D., Chaisse, F.: C.R. Acad. Sci. **268** (1969) 660.
69 B 3 Buschow, K.H.J., Van der Goot, A.S.: J. Less Common Met. **17** (1969) 249.
69 B 4 Buschow, K.H.J., Van der Goot, A.S.: J. Less Common Met. **18** (1969) 309.
69 B 5 Buschow, K.H.J., Van der Goot, A.S.: Phys. Status Solidi **35** (1969) 515.
69 B 6 Buschow, K.H.J., Van der Goot, A.S.: J. Less Common Met. **19** (1969) 153.
69 B 7 Buschow, K.H.J., Velge, W.A.J.J.: Z. Angew. Phys. **26** (1969) 157.
69 B 8 Buschow, K.H.J., Naastepad, P.A., Westendorp, F.F.: J. Appl. Phys. **40** (1969) 4029.
69 C 1 Carfagna, P.D., Wallace, W.E.: J. Appl. Phys. **39** (1969) 5259.
69 D 1 Das, D.K.: IEEE Trans. Magn. MAG-**5** (1969) 214.
69 G 1 Givord, F.: Thèse de 3-ème Cycle, Université de Grenoble **1969**.
69 H 1 Harris, I.R., Mansey, R.C., Slanicka, M., Taylor, K.N.R.: J. Less Common Met. **19** (1969) 437.
69 K 1 Kawatra, M.P., Skalski, S., Mydosh, J.A., Budnick, J.I.: Phys. Rev. Lett. **23** (1969) 83.
69 K 2 Kirchmayr, H.R.: Z. Metallkd. **60** (1969) 778.
69 K 3 Kirchmayr, H.R.: Z. Metallkd. **60** (1969) 699.
69 K 4 Kirchmayr, H.R.: Z. Angew. Phys. **27** (1969) 18.
69 K 5 Kren, E., Schweizer, J., Tasset, F.: Phys. Rev. **186** (1969) 479.
69 L 1 Lemaire, R., Paccard, D.: Bull. Soc. Fr. Mineral. Crystallogr. **92** (1969) 9.
69 L 2 Lemaire, R., Schweizer, J., Yakinthos, J.: Acta Crystallogr. B **25** (1969) 710.
69 L 3 Lihl, F., Ehold, J.R., Kirchmayr, H.R., Wolf, H.D.: Acta Phys. Austriaca **30** (1969) 164.
69 M 1 McDermott, M.J., Marklund, K.K.: J. Appl. Phys. **40** (1969) 1007.
69 N 1 Nesbitt, E.A.: J. Appl. Phys. **40** (1969) 1259.
69 P 1 Paccard, D.: Ph.D. Thesis, University of Grenoble, **1969**.
69 P 2 Petrich, G.: Z. Phys. **221** (1969) 431.
69 S 1 Schweizer, J., Tasset, F.: J. Less Common Met. **18** (1969) 245.
69 S 2 Schweizer, J., Tasset, F.: Mater. Res. Bull. **4** (1969) 369.
69 T 1 Taylor, K.N.R.: Phys. Lett. **29** A (1969) 372.
69 T 2 Taylor, K.N.R., Christopher, J.T.: J. Phys. C **2** (1969) 2237.
69 U 1 Umebayashi, H.: Solid State Phys. Jpn. **4** (1969) 583.
69 V 1 Virkar, A.V., Raman, A.: J. Less Common Met. **18** (1969) 59.
69 W 1 Wallace, W.E., Hopkins Jr., H.P., Lehman, K.: J. Solid State Chem. **1** (1969) 39.
69 W 2 Westendorp, F.F., Buschow, K.H.J.: Solid State Commun. **7** (1969) 639.
69 Z 1 Zarechnyuk, O.S., Myskiv, M.G., Ryabov, V.R.: Russ. Metall. **10** (1969) 133.
69 Z 2 Zijlstra, H., Westendorp, F.F.: Solid State Commun. **7** (1969) 857.

70 B 1 Becker, J.J.: J. Appl. Phys. **41** (1970) 1055.
70 B 2 Becle, C., Lemaire, R., Paccard, D.: J. Appl. Phys. **41** (1970) 855.
70 B 3 Benz, M.G., Martin, D.L.: Appl. Phys. Lett. **17** (1970) 176.
70 B 4 Bloch, D., Lemaire, R.: Phys. Rev. B **2** (1970) 2648.
70 B 5 Blow, S.: J. Phys. C **3** (1970) 835.
70 B 6 Burzo, E.: Rev. Roum. Phys. **15** (1970) 573.
70 B 7 Burzo, E.: Rev. Roum. Phys. **15** (1970) 689.
70 B 8 Burzo, E., Givord, F.: C.R. Acad. Sci. B **271** (1970) 1159.
70 B 9 Burzo, E., Pop, I., Chechernikov, V.I.: Colloq. Int. CNRS, Les Elements des Terres Rares, 1969, Ed. CNRS **1970**, vol. II, p. 87.
70 B 10 Buschow, K.H.J.: Colloq. Int. CNRS, Les Elements de Terres Rares, 1969, Ed. CNRS **1970**, vol. I, p. 101.

70B11 Buschow, K.H.J.: Acta Crystallogr. B **26** (1970) 1389.
70B12 Buschow, K.H.J., Van der Goot, A.S.: J. Less Common Met. **22** (1970) 419.
70B13 Buschow, K.H.J., Van Stapele, R.P.: J. Appl. Phys. **41** (1970) 4066.
70B14 Buschow, K.H.J., Van Wieringen, J.S.: Phys. Status Solidi **42** (1970) 231.
70C1 Carfagna, P.D., Wallace, W.E., Craig, R.S.: J. Solid State Chem. **2** (1970) 1.
70C2 Christopher, J.T., Taylor, K.N.R.: Colloq. Int. CNRS, Les Elementes des Terres Rares, 1969, Ed. CNRS **1970**, vol. II, p. 66.
70D1 Dariel, M.P., Erez, G.: J. Less Common Met. **22** (1970) 360.
70F1 Feron, J.L., Gignoux, D., Lemaire, R., Paccard, D.: Colloq. Int. CNRS, Les Elements des Terres Rares, 1969, Ed. CNRS **1970**, vol. II, p. 75.
70G1 Gignoux, D.R., Lemaire, R., Paccard, D.: Solid State Commun. **8** (1970) 391.
70G2 Givord, F., Lemaire, R.: J. Less Common Met. **21** (1970) 463.
70H1 Hoffer, F.: IEEE Trans. Magn. MAG-**6** (1970) 211.
70K1 Kawatra, M.P., Mydosh, J.A., Budnick, J.I.: Phys. Rev. B **2** (1970) 665.
70K2 Khurgin, B., Nowik, I., Rakavy, M., Ofer, S.: J. Phys. Chem. Solids **31** (1970) 49.
70K3 Kirchmayr, H.R.: Proc. 8th Conf. on Rare Earth Res., Reno, Nevada **1970**, p. 11.
70K4 Kirchmayr, H.R., Lugscheider, W.: Z. Metallkd. **61** (1970) 22.
70L1 Lemaire, R., Paccard, D.: J. Less Common Met. **21** (1970) 403.
70L2 Lemaire, R., Paccard, D.: C.R. Acad. Sci. **270** (1970) 1131.
70L3 Lemaire, R., Paccard, D.: C.R. Acad. Sci. B **270** (1970) 18.
70L4 Lemaire, R., Paccard, D.: Colloq. Int. CNRS, Les Elements des Terres Rares, 1969, Ed. CNRS **1970**, vol. II, p. 231.
70L5 Lemaire, R., Pauthenet, R., Schweizer, J.: IEEE Trans. Magn. MAG-**6** (1970) 153.
70L6 Leon, B., Wallace, W.E.: J. Less Common Met. **22** (1970) 1.
70L7 Leon, B., Wallace, W.E.: Proc. 8th Conf. on Rare Earth Res., Reno, Nevada **1970**, p. 41.
70L8 Levinson, L.M., Rosenberg, E., Shaulov, A., Shtrikman, S., Strnat, K.: J. Appl. Phys. **41** (1970) 910.
70M1 McCaig, M.: IEEE Trans. Magn. MAG-**6** (1970) 198.
70M2 McCurrie, R.A.: Philos. Mag. **22** (1970) 1013.
70M3 McCurrie, R.A., Carswell, G.P.: J. Mater. Sci. **5** (1970) 825.
70M4 McCurrie, R.A., Carswell, G.P., O'Neill, J.B.: J. Mater. Sci. **6** (1970) 164.
70M5 Moreau, J.M., Michel, C., Simmons, M., O'Keefe, T., James, W.J.: Proc. 8th Conf. on Rare Earth Res., Reno, Nevada, **1970**, p. 34.
70N1 Nakamichi, T., Kai, K., Aoki, Y., Ikeda, K., Yamamoto, M.: J. Phys. Soc. Jpn. **29** (1970) 794.
70N2 Nesbitt, E.A., Chin, G.Y., Gallagher, P.K., Sherwood, R.C., Wernick, J.H.: J. Appl. Phys. **41** (1970) 1107.
70O1 Oesterreicher, H., Parker, F.T.: Phys. Status Solidi (a) **58** (1970) 585.
70O2 Oesterreicher, H., Corlliss, L.M., Hastings, J.M.: J. Appl. Phys. **41** (1970) 2326.
70R1 Ray, A.E., Hofer, G.I.: Proc. 8th Conf. Rare Earth Res., Reno, Nevada **1970**, p. 524.
70R2 Roe, G.J., O'Keefe, T.J.: Metall. Trans. **1** (1970) 2565.
70R3 Roe, G.J., O'Keefe, T.J., Moreau, J.M., Michael, C., James, W.J.: Colloq. Int. CNRS, Les Elements des Terres Rares, 1969, Ed. CNRS, **1970**, vol. II, p. 251.
70S1 Samarin, B.A.: Appl. Phys. Lett. **17** (1970) 196.
70S2 Schweizer, J., Yakinthos, J.: Colloq. Int. CNRS, Les Elements des Terres Rares, 1969, Ed. CNRS, **1970**, vol. II, p. 239.
70S3 Segal, E., Wallace, W.E.: J. Solid State Chem. **2** (1970) 347.
70S4 Shidlovsky, I., Wallace, W.E.: J. Solid State Chem. **2** (1970) 193.
70S5 Strnat, K.J.: IEEE Trans. Magn. MAG-**6** (1970) 182.
70S6 Strnat, K.J., Ray, A.E.: Z. Metallkd. **61** (1970) 461.
70S7 Strnat, K.J., Tsui, J.B.Y.: Proc. 8th Conf. on Rare Earth Res., Reno, Nevada **1970**, vol. 1, p. 3.
70S8 Strydom, A., Alberts, L.: J. Less Common Met. **22** (1970) 503.
70U1 Uehara, M., Morimoto, I.: Jpn. J. Appl.: Phys. **9** (1970) 226.
70V1 Van der Goot, A.S., Buschow, K.H.J.: J. Less Common Met. **21** (1970) 151.
70V2 Van Vucht, J.H.N., Kujpers, F.A., Bruning, H.C.A.M.: Philips Res. Rep. **25** (1970) 133.
70V3 Vivchard, O.I., Zarechnyuk, O.S., Ryabov, V.R.: Russ. Metall. **11** (1970) 140.
70W1 Wallace, W.E., Volkmann, T.V., Craig, R.S.: J. Phys. Chem. Solids **31** (1970) 2185.
70W2 Wallace, W.E., Craig, R.S., Thompson, A., Deenadas, C., Dixon, M., Aoyagi, M., Marzouk, N.: Colloq. Int. CNRS, Les Elements des Terres Rares, 1969, Ed. CNRS, **1970**, vol. II, p. 427.
70W3 Westendorp, F.F.: Solid State Commun. **8** (1970) 139.

70Y1 Yamada, T., Kunetomi, N., Nagai, Y., Cox, D.E., Shirane, D.: J. Phys. Soc. Jpn. **23** (1970) 615.
70Z1 Zijlstra, H.: IEEE Trans. Magn. MAG-6 (1970) 179.
70Z2 Zijlstra, H.: J. Appl. Phys. **41** (1970) 4881.

71A1 Agarval, V.K., Kuzmin, R.N.: Kristallografiya **16** (1971) 774.
71B1 Bachmann, K.: IEEE Trans. Magn. MAG-7 (1971) 647.
71B2 Bachmann, K., Hofer, F.: Z. Angew. Phys. **32** (1971) 41.
71B3 Bachmann, K., Bischofberger, A., Hofer, G.: J. Mater. Sci. **6** (1971) 169.
71B4 Barbara, B., Becle, C., Lemaire, R., Paccard, D.: IEEE Trans. Magn. MAG-7 (1971) 654.
71B5 Barbara, B., Becle, C., Lemaire, R., Paccard, D.: J. Phys. (Paris) **32** (1971) C1-299.
71B6 Bargouth, M.O., Will, G.: J. Phys (Paris) **32** (1971) C1-675.
71B7 Becker, J.J.: IEEE Trans. Magn. MAG-7 (1971) 644.
71B8 Becker, J.J.: J. Appl. Phys. **42** (1971) 1537.
71B9 Bloch, D., Chaisse, F., Givord, F., Voiron, J., Burzo, E.: J. Phys. (Paris) **32** (1971) C1-659.
71B10 Brown, G., Issa, M.A., Taylor, K.N.R.: J. Phys. F **1** (1971) L10.
71B11 Burzo, E.: Proc. 17th Congress AMPERE, Bucharest, 1970, Publ. House Roumanian Acad. Sci. **1971**, p. 876.
71B12 Burzo, E.: Z. Angew. Phys. **32** (1971) 127.
71B13 Burzo, E.: J. Less Common Met. **23** (1971) 123.
71B14 Burzo, E., Ursu, I.: Solid State Commun. **9** (1971) 2289.
71B15 Buschow, K.H.J.: Philips Res. Rep. **26** (1971) 49.
71B16 Buschow, K.H.J.: J. Appl. Phys. **42** (1971) 3433.
71B17 Buschow, K.H.J.: J. Less Common Met. **25** (1971) 131.
71B18 Buschow, K.H.J.: Phys. Status Solidi (a) **7** (1971) 199.
71B19 Buschow, K.H.J.: Proc. Int. Conf. Magnetism of Rare Earths and Actinides, Durham, England **1971**, p. 140.
71B20 Buschow, K.H.J., Van Stapele, R.P.: J. Phys. (Paris) **32** (1971) C1-672.
71B21 Buschow, K.H.J., Van Diepen, A.M., De Wijn, H.W.: J. Appl. Phys. **42** (1971) 4315.
71B22 Buschow, K.H.J., Van der Goot, A.S.: Acta Crystallogr. B **27** (1971) 1085.
71C1 Cannon, A., Budnick, J.I., Kawatra, M.P., Mydosh, J.A., Kalshi, S.: Phys. Lett. **35** A (1971) 247.
71C2 Chatterjee, D., Taylor, K.N.R.: J. Less Common Met. **25** (1971) 423.
71C3 Cooper, J.R., Rizzuto, C., Olcese, G.: Proc. Int. Conf. Magnetism of Rare Earths and Actinides, Durham, England **1971**, p. 183.
71G1 Givord, F., Lemaire, R.: Cobalt **50** (1971) 16.
71G2 Givord, F., Lemaire, R.: Solid State Commun. **9** (1971) 341.
71G3 Givord, D., Givord, F., Lemaire, R.: J. Phys. (Paris) **32** (1971) C1-668.
71G4 Givord, D., Lemaire, R., James, W.J., Moreau, J.M., Shah, J.S.: IEEE Trans. Magn. MAG-7 (1971) 657.
71G5 Greedan, J.E.: Proc. 9th Conf. on Rare Earth Res., Blacksburg, Virginia **1971**, p. 208.
71G6 Guimaraes, A.P.: Ph.D. Thesis, University of Manchester, **1971**.
71H1 Hilscher, G., Kirchmayr, H.R., Steiner, W.: Z. Angew. Phys. **32** (1971) 203.
71H2 Hilscher, G., Kirchmayr, H.R., Wiesinger, G.: Proc. Int. Conf. Magnetism of Rare Earths and Actinides, Durham, England **1971**, p. 152.
71K1 Kirchmayr, H.R., Steiner, W.: J. Phys. (Paris) **32** (1971) C1-665.
71K2 Koon, N., Schindler, A., Carter, F.: Phys. Lett. **37** A (1971) 413.
71K3 Kuijpers, F.A., Loopstra, B.O.: J. Phys. (Paris) **32** (1971) C1-656.
71L1 Leon, B., Rao, V.U.S., Wallace, W.E.: J. Less Common Met. **24** (1971) 247.
71M1 Martin, D.L., Benz, M.G.: Cobalt **50** (1971) 11.
71M2 Mackenzie, I.S., McCausland, M.A.H., Wagg, A.R., Guimaraes, A.P., Holden, E., Beiley, S.: Proc. 16th Congress AMPERE, Bucharest, 1970, Publ. House Romanian Acad. Sci. **1971**, p. 480.
71M3 McCurrie, R.A., Carswell, G.P.: Philos. Mag. **23** (1971) 333.
71M4 Melville, D., Taylor, K.N.R.: Proc. Int. Conf. Magnetism of Rare Earths and Actinides, Durham, England **1971**, p. 150.
71M5 Miura, S., Kaneko, T., Ohoshi, M., Kamigaki, K.: J. Phys. (Paris) **32** (1971) C1-1124.
71M6 Moreau, J.M., Michel, C., Simmons, M., O'Keefe, T.J., James, W.J.: J. Phys. (Paris) **32** (1971) C1-670.
71N1 Nair, C., Oesterreicher, H.: J. Less Common Met. **24** (1971) 237.
71N2 Narasimhan, K.S.V.L., Butera, R.A., Craig, R.S.: Proc. 9th Conf on Rare Earth Res., Blacksburg, Virginia, **1971**, p. 218.

71 N 3 Nasu, S., Neumann, H.H., Marzouk, N., Craig, R.S., Wallace, W.E.: J. Phys. Chem. Solids **32** (1971) 2779.
71 N 4 Nesbitt, E.A., Chin, G.Y., Gallanger, P.K., Sherwood, R.C., Wernick, J.H.: J. Appl. Phys. **42** (1971) 1530.
71 N 5 Neumann, H.H., Nasu, S., Craig, R.S., Marzouk, N., Wallace, W.E.: J. Phys. Chem. Solids **32** (1971) 2788.
71 O 1 Oesterreicher, H.: J. Less Common Met. **23** (1971) 7.
71 O 2 Oesterreicher, H.: J. Phys. Chem. Solids **32** (1971) 1403.
71 O 3 Oesterreicher, H.: J. Less Common Met. **25** (1971) 341.
71 O 4 Oesterreicher, H.: Phys. Status Solidi (a) **7** (1971) K 55.
71 O 5 Oesterreicher, H.: J. Appl. Phys. **42**, (1971) 5137.
71 O 6 Oesterreicher, H.: J. Phys. (Paris) **32**, (1971) C1–1141.
71 P 1 Paccard. D., Schweizer, J., Yakinthos, J.: J. Phys. (Paris) **32** (1971) C 1–663.
71 P 2 Poldy, C.A., Taylor, K.N.R.: Proc. Int. Conf. Magnetism of Rare Earth and Actinides, Durham, England, **1971**, p. 156.
71 P 3 Primavesi, G.J., Taylor, K.N.R.: Proc. 9th Conf. on Rare Earth Res., Blacksburg, Virginia **1971**, p. 229.
71 P 4 Primavesi, G.J., Taylor, K.N.R., Harris, I.R.: J. Phys. (Paris) **32** (1971) C 1–661.
71 R 1 Raichlen, J.S., Doremus, H.: J. Appl. Phys. **42** (1971) 3166.
71 R 2 Ray, A.E., Harmer, R.S.: Proc. 9th Conf. on Rare Earth Res., Blacksburg, Virginia **1971**, vol. 1, p. 368.
71 R 3 Ray, A.E., Strnat, K.J.: Air Force Materials Laboratory, Wright Patterson Air Force Base, Ohio, Tech. Rep. AFML-TR-71-210, **1971**.
71 R 4 Ray, A.E., Strnat, K.J., Biermann, A.T.: IEEE Trans. Magn. MAG-7 (1971) 656.
71 R 5 Ray, A.E., Mildrum, H., Strnat, K.J., Harmer, R.: J. Phys. (Paris) **32** (1971) C 1–554.
71 R 6 Richter, F.W., Schitt, J.: Z. Naturforsch. A **26** (1971) 1563.
71 R 7 Robinson, L.B., Ferguson, L.M., Milstein, F.: Phys. Rev. B **3** (1971) 1025.
71 R 8 Rossat-Mignod, J., Yakinthos, J.: Phys. Status Solidi (b) **47** (1971) 239.
71 S 1 Schweizer, J., Strnat, K.J., Tsui, J.B.Y.: IEEE Trans. Magn. MAG-7 (1971) 429.
71 S 2 Schweizer, J., Strnat, K.J., Tsui, J.B.Y.: Proc. 9th Conf. on Rare Earth Res., Blacksburg, Virginia **1971**, vol. 1, p. 96.
71 S 3 Shibata, T., Katayama, T., Mizuhara, T.: Jpn. J. Appl. Phys. **10** (1971) 163.
71 S 4 Slanicka, M.E., Taylor, K.N.R., Primavesi, G.J.: J. Phys. F **1** (1971) 679.
71 S 5 Smith, T.F., Luo, H.L., Maple, M.P., Harris, I.R.: J. Phys. F **1** (1971) 896.
71 S 6 Stearns, M.B.: Phys. Rev. B **4** (1971) 1081.
71 S 7 Steiner, W., Kirchmayr, H.R., Springs, W.: Z. Angew. Phys. **32** (1971) 146.
71 S 8 Strnat, K.J., Ray, A.E.: Cobalt **61** (1971) 461.
71 T 1 Tatsumoto, E., Okamoto, T., Fujii, H., Inoue, J.: J. Phys. (Paris) **32** (1971) C 1–550.
71 T 2 Taylor, K.N.R.: Phys. Lett. **35** A (1971) 153.
71 T 3 Taylor, K.N.R., Primavesi, G.J.: J. Phys. F **1** (1971) L 7.
71 T 4 Tsui, J.B.Y., Strnat, K.J.: Appl. Phys. Lett. **18** (1971) 107.
71 T 5 Tsui, J.B.Y., Strnat, K.J.: IEEE Trans. Magn. MAG-7 (1971) 427.
71 T 6 Tsui, J.B.Y., Strnat, K.J., Harmer, R.S.: J. Appl. Phys. **42** (1971) 1539.
71 U 1 Ueno, N., Nagai, H., Tsujimura, A.: J. Phys. Soc. Jpn. **31** (1971) 1275.
71 U 2 Umebayashi, H., Fujimura, Y.: Jpn. J. Appl. Phys. **10** (1971) 1585.
71 V 1 Voiron, J., Bloch, D.: J. Phys. (Paris) **32** (1971) 949.
71 W 1 Wallace, W.E., Aoyagi, M.: Monatsh. Chem. **102** (1971) 1455.
71 W 2 Wallace, W.E., Volkmann, T.V., Hopkins, H.P.: J. Solid State Chem. **3** (1971) 510.
71 W 3 Westendorp, F.F.: J. Appl. Phys. **42** (1971) 5727.
71 W 4 Will, G.: Z. Angew. Phys. **32** (1971) 1.
71 W 5 Will, G., Bargouth, M.O.: Phys. Kondens. Mater. **13** (1971) 137.
71 Y 1 Yakinthos, J., Rossat-Mignod, J., Belakhovsky, M.: Phys. Status Solidi (b) **47** (1971) 247.
71 Z 1 Zijlstra, H.: J. Appl. Phys. **42** (1971) 1510.
71 Z 2 Zinn, W.: J. Phys. (Paris) **32** (1971) C 1–724.
71 Z 3 Zumsteg, F.C., Parks, R.D.: J. Phys. (Paris) **32** (1971) C 1–534.

72 A 1 Atzmony, U., Dariel, M.P., Bauminger, E.R., Lebenbaum, D., Nowik, J., Ofer, S.: Phys. Rev. Lett. **28** (1972) 244.
72 B 1 Barbara, B., Gignoux, D.: C.R. Acad. Sci. **274** (1972) 319.

72 B 2 Barbara, B., Fillion, G., Gignoux, D., Lemaire, R.: Solid State Commun. **10** (1972) 1149.
72 B 3 Becker, J.J.: AIP Conf. Proc. **5** (1972) 1067.
72 B 4 Becker, J.J.: IEEE Trans. Magn. MAG-**8** (1972) 520.
72 B 5 Belov, K.P., Bisliev, A.M., Nikitin, S.A., Kolesnichenko, V.E.: Fiz. Met. Metalloved **34** (1972) 470.
72 B 6 Belov, K.P., Nikitin, S.A., Vasiliev, A.M., Savitski, E.M., Terekhova, V.F., Kolesnichenko, V.E.: J. Eksp. Teor. Fiz. Pisma **16** (1972) 448.
72 B 7 Benz, M.G., Martin, D.L.: J. Appl. Phys. **43** (1972) 4733.
72 B 8 Bloch, D., Chaisse, F.: C.R. Acad. Sci. **274** (1972) 221.
72 B 9 Bloch, D., Camphausen, D.L., Voiron, J., Ayasse, J.B., Berton, A., Chaussy, J.: C.R. Acad. Sci. **275** (1972) 601.
72 B 10 Burzo, E.: Int. J. Magn. **3** (1972) 161.
72 B 11 Burzo, E.: Phys. Rev. B **6** (1972) 2882.
72 B 12 Burzo, E., Domsa, F.: Phys. Status Solidi (b) **51** (1972) K 89.
72 B 13 Burzo, E., Laforest, J.: Int. J. Magn. **3** (1972) 171.
72 B 14 Burzo, E., Laforest, J.: C.R. Acad. Sci. B **274** (1972) 114.
72 B 15 Buschow, K.H.J.: J. Less Common Met. **29** (1972) 283.
72 B 16 Buschow, K.H.J.: J. Less Common Met. **26** (1972) 329.
72 B 17 Buschow, K.H.J., Van Mal, H.H.: J. Less Common Met. **29** (1972) 203.
72 C 1 Campbell, I.A.: J. Phys. F **2** (1972) L 47.
72 C 2 Cannon, J.F., Robertson, D.L., Hall, H.T.: Mater. Res. Bull. **7** (1972) 5.
72 C 3 Charles, R.J., Martin, D.L., Valentine, L., Cech, R.E.: AIP Conf. Proc. **5** (1972) 1072.
72 C 4 Clark, A.E., Belson, H.S.: Phys. Rev. B **5** (1972) 3642.
72 C 5 Clark, A.E., Belson, H.S.: AIP Conf. Proc. **5** (1972) 1498.
72 C 6 Clark, A.E., Belson, H.S.: IEEE Trans. Magn. MAG-**8** (1972) 477.
72 C 7 Clark, A.E., Belson, H.S., Tamagawa, N.: Phys. Lett. **42** A (1972) 160.
72 C 8 Craig, R.S., Sankar, S.G., Marzouk, N., Rao, V.U.S., Wallace, W.E., Segal, E.: J. Phys. Chem. Solids **33** (1972) 2267.
72 D 1 Deenadas, C., Craig, R.S., Marzouk, N., Wallace, W.E.: J. Solid State Chem. **4** (1972) 1.
72 D 2 Den Broeder, F.J.A., Buschow, K.H.J.: J. Less Common Met. **29** (1972) 65.
72 D 3 Deryagin, A.V., Scherbakova, E.V., Shur, Ya.S.: Ivz. Akad. Nauk SSSR: Ser. Fiz. **36** (1972) 1606.
72 E 1 Eatough, N.L., Hall, H.T.: Inorg. Chem. **11** (1972) 2608.
72 E 2 Eshelman, F.R., Smith, J.F.: Acta Crystallogr. B **28** (1972) 1594.
72 F 1 Felner, I., Mayer, I., Grill, A., Schieber, M.: Solid State Commun. **11** (1972) 1231.
72 G 1 Gignoux, D., Shah, J.S.: Solid State Commun. **11** (1972) 1709.
72 G 2 Gignoux, D., Lemaire, R., Paccard, D.: Phys. Lett. **41** A (1972) 187.
72 G 3 Gignoux, D., Rossat-Mignod, J., Tcheu, F.: Phys. Status Solidi (a) **14** (1972) 483.
72 G 4 Givord, D., Lemaire, R.: C.R. Acad. Sci. B **274** (1972) 1166.
72 G 5 Givord, F., Shah, J.S.: C.R. Acad. Sci. B **274** (1972) 923.
72 G 6 Givord, F., Lemaire, R., Shah, J.S.: C.R. Acad. Sci. **274** (1972) 161.
72 G 7 Givord, D., Lemaire, R., Roudaut, E., Moreau, J.M.: J. Less Common Met. **29** (1972) 361.
72 G 8 Givord, D., Givord, F., Lemaire, R., James, W.J., Shah, J.S.: J. Less Common Met. **29** (1972) 389.
72 G 9 Gomes, A.A.: Phys. Lett. **39** A (1972) 139.
72 G 10 Greedan, J.E.: AIP Conf. Proc. **5** (1972) 1425.
72 H 1 Hamano, M., Yajima, S., Umebayashi, H.: IEEE Trans. Magn. MAG-**8** (1972) 518.
72 H 2 Hilzinger, H.R., Kronmüller, H.: Phys. Status Solidi (b) **54** (1972) 593.
72 J 1 Jones, F.G., Lehman, H.E., Smeggil, J.G.: IEEE Trans. Magn. MAG-**8** (1972) 555.
72 K 1 Kandaurova, G.S., Shur, Y.S., Deryagin, A.V.: Izv. Akad. Nauk SSSR: Ser. Fiz. **36** (1972) 1591.
72 K 2 Kuijpers, F.A.: Phys. Lett. **39** A (1972) 240.
72 K 3 Kuijpers, F.A.: Ber. Bunsenges. Phys. Chem. **76** (1972) 1220.
72 K 4 Kuijpers, F.A.: J. Less Common Met. **27** (1972) 27.
72 L 1 Livingston, J.D.: J. Mater. Sci. **7** (1972) 1472.
72 L 2 Livingston, J.D., McConnell, M.D.: J. Appl. Phys. **43** (1972) 4756.
72 M 1 Machado da Silva, J.M., McDermott, J.M., Hill, R.W.: J. Phys. C **5** (1972) 1573.
72 M 2 Martin, D.L., Benz, M.G.: IEEE Trans. Magn. MAG-**8** (1972) 35.
72 M 3 Martin, D.L., Benz, M.G.: IEEE Trans. Magn. MAG-**8** (1972) 562.
72 M 4 Martin, D.L., Benz, M.G.: AIP Conf. Proc. **5** (1972) 970.
72 N 1 Narasimhan, K.S.V.L., Butera, R.A., Craig, R.S.: Phys. Lett. **40** A (1972) 381.
72 O 1 Oesterreicher, H.: Phys. Status Solidi (a) **12** (1972) K 109.

72O2 Oesterreicher, H.: Solid State Commun. **10** (1972) 525.
72O3 Oesterreicher, H.: J. Phys. Chem. Solids **33** (1972) 1031.
72O4 Oesterreicher, H., Pitts, R.: J. Appl. Phys. **43** (1972) 5174.
72O5 Oesterreicher, H., Pitts, R.: J. Less Common Met. **29** (1972) 100.
72O6 Oesterreicher, H., Stanley, J., Pitts, R.: Phys. Status Solidi (a) **12** (1972) K 65.
72P1 Poldy, C.A., Taylor, K.N.R.: J. Less Common Met. **27** (1972) 95.
72P2 Poldy, C.A., Taylor, K.N.R.: J. Phys. F **2** (1972) L 105.
72P3 Primavesi, G.J., Taylor, K.N.R.: J. Phys. F **2** (1972) 761.
72R1 Ray, A.E., Strnat, K.J.: IEEE Trans. Magn. MAG-**8** (1972) 516.
72R2 Robertson, D.L., Cannon, J.F., Hall, H.T.: Mater. Res. Bull. **7** (1972) 977.
72S1 Schaller, H.J., Craig, R.S., Wallace, W.E.: J. Appl. Phys. **43** (1972) 3161.
72S2 Stewart, A.M.: Phys. Rev. B **6** (1972) 1985.
72S3 Strnat, K.: IEEE Trans. Magn. MAG-**8** (1972) 511.
72S4 Strnat, K.: AIP Conf. Proc. **5** (1972) 1047.
72T1 Taylor, K.N.R., Poldy, C.A.: J. Less Common Met. **27** (1972) 255.
72T2 Taylor, K.N.R., Primavesi, G.J.: J. Phys. F **2** (1972) L 32.
72T3 Taylor, K.N.R., Primavesi, G.J.: J. Less Common Met. **29** (1972) 97.
72T4 Taylor, K.N.R., Melville, D., Primavesi, G.J.: J. Phys. F **2** (1972) 584.
72T5 Titcomb, C., Craig, R.S., Wallace, W.E., Rao, V.U.S.: Phys. Lett. **39** A (1972) 157.
72U1 Ursu, I., Burzo, E.: J. Magn. Res. **8** (1972) 274.
72V1 Van Diepen, A.M., Buschow, K.H.J., Van Wieringen, J.S.: J. Appl. Phys. **43** (1972) 645.
72V2 Voiron, J.: C.R. Acad. Sci. **274** (1972) 589.
72W1 Westendorp, F.F.: Appl. Phys. Lett. **20** (1972) 441.
72W2 Williamson, D.L., Bukshpan, S., Ingalls, R.: Phys. Rev. B **6** (1972) 4194.
72Y1 Yajima, S., Hamano, M.: J. Phys. Soc. Jpn. **32** (1972) 861.
72Y2 Yakinthos, J.K., Paccard, D.: Solid State Commun. **10** (1972) 989.
72Y3 Yakinthos, J., Rossat-Mignod, J.: Phys. Status Solidi (b) **50** (1972) 747.

73A1 Agarval, V.K., Kuzmin, R.N.: Dokl. Akad. Nauk SSSR **209** (1973) 328.
73A2 Alff, E., Givord, D., Haberer, J.P.: IEEE Trans. Magn. MAG-**9** (1973) 631.
73A3 Aoki, Y., Nakamichi, T., Yamamoto, M.: Phys. Status Solidi (b) **56** (1973) K 17.
73A4 Atoji, M., Atoji, I., Do-Dinh, C., Wallace, W.E.: J. Appl. Phys. **44** (1973) 5096.
73A5 Atzmony, U., Dariel, M.P., Bauminger, E.R., Lebenbaum, D., Nowik, I., Ofer, S.: Proc. 10th Conf. on Rare Earth Res., Carefree, Arizona **1973**, p. 605.
73A6 Atzmony, U., Dariel, M.P., Bauminger, E.R., Lebenbaum, D., Nowik, I., Ofer, S.: Phys. Rev. B **7** (1973) 4220.
73B1 Barb, D., Burzo, E., Morariu, M.: Proc. 5th Int. Conf. Mössbauer Spectr., Bratislava, Czechoslovakia **1973**, vol. 1, p. 37.
73B2 Barb, D., Burzo, E., Morariu, M.: C.R. Acad. Sci. B **277** (1973) 131.
73B3 Barbara, B., Gignoux, D., Givord, D., Givord, F., Lemaire, R.: Int. J. Magn. **4** (1973) 77.
73B4 Bauminger, E.R., Lebenbaum, D., Nowik, I., Ofer, S.: Proc. 10th Conf. on Rare Earth Res., Carefree, Arizona **1973**, p. 605.
73B5 Becker, J.J.: IEEE Trans. Magn. MAG-**9** (1973) 161.
73B6 Belov, K.P., Nikitin, S.A., Bisliev, A.M., Savitski, E.M., Terekhova, V.F., Kolesnichenko, V.E.: J. Eksp. Teor. Fiz. **64** (1973) 2154.
73B7 Belozerski, G.I., Belyanina, N.V., Ivanova, I.N., Shaturian, S.A., Shapiro, A.I.: Fiz. Tverd. Tela **15** (1973) 305.
73B8 Bhat, N.V.: Proc. Nucl. Phys. and Solid State Physics, Bangalore, India **1973**, p. 114.
73B9 Bisliev, A.M., Zvezdin, A.K., Kim, D., Nikitin, S.A., Popkov, A.F.: J. Eksp. Teor. Fiz. Pisma **17** (1973) 484.
73B10 Bisliev, A.M., Nikitin, S.A., Savitski, Ye.N., Terekhova, V.F., Kolesnichenko, V.Ye.: Fiz. Met. Metalloved. **36** (1973) 965.
73B11 Bloch, D., Voiron, J., Berton, A., Chaussy, J.: Solid State Commun. **12** (1973) 685.
73B12 Bodak, O.I., Gladyshevski, E.I., Koshel, O.S., Kharchenko, O.I.: Metallofizika **46** (1973) 94.
73B13 Bowden, G.J.: J. Phys. F **3** (1973) 2206.
73B14 Bowman, A.L., Anderson, J.L., Nereson, N.G.: Proc. 10th Conf. on Rare Earth Res., Carefree, Arizona **1973**, p. 485.
73B15 Brouha, M., Buschow, K.H.J.: J. Phys. F **3** (1973) 2218.

73 B 16 Burzo, E.: Stud. Cercet. Fiz. **25** (1973) 425.
73 B 17 Burzo, E., Stud. Cercet. Fiz. **25** (1973) 509.
73 B 18 Burzo, E.: Proc. X-th Rare Earth Research Conf. Arizona **1973**, p. 96.
73 B 19 Burzo, E., Lazar, D.P.: C.R. Acad. Sci. B **276** (1973) 239.
73 B 20 Buschow, K.H.J.: J. Less Common Met. **31** (1973) 359.
73 B 21 Buschow, K.H.J.: J. Less Common Met. **33** (1973) 311.
73 B 22 Buschow, K.H.J., Den Broeder, F.A.J.: J. Less Common Met. **33** (1973) 191.
73 B 23 Buschow, K.H.J., Miedema, A.R.: Solid State Commun. **13** (1973) 367.
73 B 24 Buschow, K.H.J., Van Diepen, A.M., De Wijn, H.W.: Phys. Rev. B **8** (1973) 5134.
73 B 25 Brouha, M., Buschow, K.H.J.: J. Appl. Phys. **44** (1973) 1813.
73 C 1 Cannon, J.A., Budnick, J.F., Craig, R.S., Sankar, S.G., Keller, D.A.: AIP Conf. Proc. **10** (1973) 905.
73 C 2 Carriker, R.C.: Appl. Phys. Lett. **22** (1973) 160.
73 C 3 Carriker, R.C., Rashidi, A.S.: AIP Proc. Conf. **10** (1973) 608.
73 C 4 Clark, A.E.: Appl. Phys. Lett. **23** (1973) 642.
73 C 5 Clark, A.E., Belson, H.S., Strakna, R.C.: J. Appl. Phys. **44** (1973) 2913.
73 C 6 Clark, A.E., Belson, H.S., Tamagawa, N.: AIP Conf. Proc. **10** (1973) 749.
73 D 1 Dariel, M.P., Atzmony, U.: Int. J. Magn. **4** (1973) 213.
73 D 2 Dariel, M.P., Atzmony, U., Lebenbaum, D.: Proc. 10th Conf. on Rare Earth Res., Carefree, Arizona **1973**, p. 439.
73 D 3 Dariel, M.P., Atzmony, U., Lebenbaum, D.: Phys. Status Solidi (b) **59** (1973) 615.
73 D 4 Das, D.K.: AIP Conf. Proc. **10** (1973) 628.
73 D 5 Deportes, J., Tsujimura, A.: C.R. Acad. Sci. B **277** (1973) 333.
73 D 6 Doser, M., Smeggil, J.G.: IEEE Trans. Magn. MAG-**9** (1973) 168.
73 D 7 D'Silva, T., Igarashi, H., Miller, A.E.: Proc. 10th Conf. on Rare Earth Res., Carefree, Arizona **1973**, p. 458.
73 D 8 Dwight, A.E., Kimball, C.W., Preston, R.S., Taneja, S.P., Weber, L.: Proc. 10th Conf. on Rare Earth Res., Carefree, Arizona **1973**, p. 1027.
73 E 1 Egami, T.: Phys. Status Solidi (a) **19** (1973) 747.
73 E 2 Elemans, J.B.A.A., Buschow, K.H.J.: Phys. Status Solidi (b) **57** (1973) K 155.
73 E 3 Ermolenko, A.S., Korolev, A.V.: Fiz. Met. Metalloved. **36** (1973) 52.
73 E 4 Ermolenko, A.S., Korolev, A.V., Shur, Ya.S.: J. Eksp. Teor. Fiz. Pisma **17** (1973) 499.
73 E 5 Evans, D.J., Garret, H.J.: IEEE Trans. Magn. MAG-**9** (1973) 197.
73 F 1 Farmar, P.D., Lawson, A.C.: Phys. Lett. **44** A (1973) 1.
73 F 2 Feldman, D., Khan, Y.: Appl. Phys. **2** (1973) 177.
73 F 3 Feldman, D., Schultz, I.: Prakt. Metallogr. **10** (1973) 462.
73 F 4 Felner, I., Schieber, M.: Solid State Commun. **13** (1973) 457.
73 F 5 Field, W.G., Sampson, J.L.: AIP Conf. Proc. **10** (1973) 603.
73 F 6 Fischer, W.G., Kuzmin, R.V., Vardapetyan, R.P.: Proc. 5th Int. Conf. Mössbauer Spectr., Bratislava, Czechoslovakia **1973**, p. 41.
73 G 1 Gignoux, D.: Ph.D. Thesis, University of Grenoble, **1973**.
73 G 2 Gignoux, D., Paccard, D., Rossat-Mignod, J., Tcheou, F.: Proc. 10th Conf. on Rare Earth Res., Carefree, Arizona **1973**, p. 596.
73 G 3 Goto, K., Sakurai, T., Yazaki, T.: Appl. Phys. Lett. **22** (1973) 686.
73 G 4 Greedan, J.E., Rao, V.U.S.: J. Solid State Chem. **6** (1973) 387.
73 G 5 Greedan, J.E., Rao, V.U.S.: Proc. 10th Conf. on Rare Earth Res, Carefree, Arizona **1973**, p. 466.
73 G 6 Grössinger, R., Steiner, W., Wiesinger, G., Kirchmayr, H.: Proc. 5th Int. Conf. Mössbauer Spectr., Bratislava, Czechoslovakia **1973**, p. 46.
73 G 7 Gubbens, P.C.M., Buschow, K.H.J.: J. Appl. Phys. **44** (1973) 3739.
73 G 8 Guimaraes, A.P., Bunbury, D.St.P.: J. Phys. F **3** (1973) 885.
73 H 1 Hahn, A., Paulus, M.: Phys. Lett. **44** A (1973) 219.
73 H 2 Hidaka, M., Sakai, M., Hosokawa, H., Sakurai, J.: J. Phys. Soc. Jpn. **35** (1973) 452.
73 H 3 Hilscher, G., Rais, H., Kirchmayr, H.R.: Phys. Status Solidi (b) **59** (1973) K 5.
73 H 4 Hilscher, G., Kirchmayr, H.R., Steiner, W., Wiesinger, G.: Proc. 10th Conf. on Rare Earth Res., Carefree, Arizona **1973**, vol. 1, p. 301.
73 H 5 Horn, P.M., Bass, R., Parks, R.D.: Phys. Rev. B **7** (1973) 332.
73 I 1 Inomata, K., Shikanai, S., Horie, H., Fukui, K.: Jpn. J. Appl. Phys. **12** (1973) 565.
73 I 2 Irkhin, Yu.P., Zabolotzki, E.I., Rozenfeld, E.V., Karpenko, V.P.: Fiz. Tverd. Tela **15** (1973) 2963.
73 J 1 Jin, T.S.: J. Korean Inst. Met. **11** (1973) 231.

73 K 1 Kamino, K., Kimura, Y., Suzuki, T., Hayama, Y., Nesbitt, E.A., Wernick, J.H., Corenzwitt, E., Buschow, K.H.J., Luiter, W., Naastepad, P.A., Westendorp, F.F., Das, D.K.: Trans. Jpn. Inst. Met. **14** (1973) 135.
73 K 2 Katayama, T., Shibata, T.: Jpn. J. Appl. Phys. **12** (1973) 762.
73 K 3 Katayama, T., Shibata, T.: Jpn. J. Appl. Phys. **12** (1973) 319.
73 K 4 Khan, Y.: Acta Crystallogr. B **29** (1973) 2502.
73 K 5 Khan, Y., Feldman, D.: J. Less Common Met. **31** (1973) 211.
73 K 6 Khan, Y., Feldman, D.: J. Less Common Met. **33** (1973) 305.
73 K 7 Khan, Y., Müller, B.: J. Less Common Met. **32** (1973) 39.
73 K 8 Khan, Y., Quershi, A.H.: IEEE Trans. Magn. MAG-**9** (1973) 156.
73 K 9 Khan, Y., Quershi, A.H.: J. Less Common Met. **32** (1973) 307.
73 K 10 Kirchmayr, H.R.: Appl. Phys. **1** (1973) 187.
73 K 11 Kirchmayr, H.R., Hilscher, G., Steiner, W., Wiesinger, G.: IEEE Trans. Magn. MAG-**9** (1973) 214.
73 K 12 Koon, N.C., Schindler, A.I., Carter, F.L.: Proc. 10th Conf. on Rare Earth Res., Carefree, Arizona **1973**, p. 449.
73 K 13 Korolev, A.V., Ermolenko, A.S.: Fiz. Met. Metalloved. **36** (1973) 957.
73 K 14 Kronmüller, H., Hilzinger, H.R.: Int. J. Magn. **5** (1973) 27.
73 K 15 Kuijpers, F.A.: Philips Res. Rep. Suppl. **2** (1973) 1.
73 K 16 Kunesh, C.J., Narasimhan, K.S.V.L., Butera, R.A.: AIP Conf. Proc. **10** (1973) 1065.
73 K 17 Kunesh, C.J., Narasimhan, K.S.V.L., Butera, R.A.: J. Phys. Chem. Solids **34** (1973) 817.
73 K 18 Kunesh, C.J., Narasimhan, K.S.V.L., Butera, R.A.: J. Phys. Chem. Solids **34** (1973) 2003.
73 K 19 Kunesh, C.J., Narasimhan, K.S.V.L., Butera, R.A.: Proc. 10th Conf. on Rare Earth Res., Carefree, Arizona **1973**, p. 292.
73 L 1 Laforest, J., Shah, J.: IEEE Trans. Magn. MAG-**9** (1973) 217.
73 L 2 Leamy, H.J., Green, L.M.: IEEE Trans. Magn. MAG-**9** (1973) 205.
73 L 3 Livingston, J.D.: Phys. Status Solidi (a) **18** (1973) 579.
73 L 4 Livingston, J.D.: AIP Conf. Proc. **10** (1973) 643.
73 M 1 Maeda, H.: Jpn. J. Appl. Phys. **12** (1973) 1825.
73 M 2 Maeda, H.: Jpn. J. Appl. Phys. **12** (1973) 1959.
73 M 3 Magat, L.M., Korotkova, M.N., Shcherbakova, Ye.V., Ermolenko, A.S.: Fiz. Met. Metalloved. **36** (1973) 1308.
73 M 4 Martense, I.: Can. J. Phys. **51** (1973) 2407.
73 M 5 Martin, D.L., Benz, M.G., Rockwood, A.C.: AIP Conf. Proc. **10** (1973) 583.
73 M 6 Marzouk, N., Craig, R.S., Wallace, W.E.: J. Phys. Chem. Solids **34** (1973) 15.
73 M 7 McCurrie, R.A., Carswell, G.P.: Philos. Mag. **28** (1973) 611.
73 M 8 McFarland, C.M.: Proc. 10th Conf. on Rare Earth Res., Carefree, Arizona **1973**, p. 692.
73 M 9 Menth, A., Klein, H.P.: Helv. Phys. Acta **46** (1973) 416.
73 M 10 Mildrum, H.F., Hartings, M.S., Strnat, K.J., Trout, J.G.: AIP Conf. Proc. **10** (1973) 618.
73 M 11 Mildrum, H.F., Trout, J., Hartings, M., Strnat, K.: Proc. 10th Conf. on Rare Earth Res., Carefree, Arizona **1973**, vol. 1, p. 476.
73 M 12 Misknis, R.T., Narasimhan, K.S.V.L., Wallace, W.E., Craig, R.S.: Proc. 10th Conf. on Rare Earth Res., Carefree, Arizona **1973**, p. 429.
73 M 13 Misknis, R.T., Narasimhan, K.S.V.L., Wallace, W.E., Craig, R.S.: Proc. 10th Conf. on Rare Earth Res., Carefree, Arizona **1973**, p. 439.
73 N 1 Naastepad, P.A., Den Broeder, F.J.A., Klein Wassink, R.J.: Powder Metall. Int. **5** (1973) 61.
73 N 2 Narasimhan, K.S.V.L., Butera, R.A., Craig, R.S.: J. Phys. Chem. Solids **34** (1973) 1075.
73 N 3 Narasimhan, K.S.V.L., Butera, R.A., Craig, R.S.: J. Appl. Phys. **44** (1973) 879.
73 N 4 Narasimhan, K.S.V.L., Wallace, W.E.: Proc. 10th Conf. on Rare Earth Res., Carefree, Arizona **1973**, p. 282.
73 N 5 Nikitin, S.A., Bisliev, A.M.: Fiz. Tverd. Tela **15** (1973) 3681.
73 N 6 Nikitin, S.A., Talalaeva, E.B., Chernikova, L.A., Andreenko, A.S.: J. Eksp. Teor. Fiz. **65** (1973) 2058.
73 N 7 Nowik, I., Dunlap, B.D.: J. Phys. Chem. Solids **34** (1973) 465.
73 O 1 Oesterreicher, H.: J. Phys. Chem. Solids **34** (1973) 1267.
73 O 2 Oesterreicher, H.: J. Appl. Phys. **44** (1973) 2350.
73 O 3 Oesterreicher, H.: J. Less Common Met. **30** (1973) 225.
73 O 4 Oesterreicher, H.: J. Less Common Met. **32** (1973) 385.
73 O 5 Oesterreicher, H.: J. Less Common Met. **33** (1973) 25.
73 O 6 Oesterreicher, H., Pitts, R.: J. Appl. Phys. **44** (1973) 5570.

73 O 7 Okamoto, T., Fujii, H., Inoue, C., Tatsumoto, E.: J. Phys. Soc. Jpn. **34** (1973) 835.
73 O 8 Olcese, G.L.: J. Less Common Met. **33** (1973) 71.
73 O 9 Oppelt, A., Buschow, K.H.J.: J. Phys. F **3** (1973) L 212.
73 P 1 Palenzona, A., Cirafici, S.: J. Less Common Met. **33** (1973) 361.
73 P 2 Poldy, C.A., Taylor, K.N.R.: Phys. Status Solidi (a) **18** (1973) 123.
73 P 3 Poldy, C.A., Taylor, K.N.R.: J. Phys. F **3** (1973) 145.
73 R 1 Ratnam, D.V., Wells, R.G.: AIP Conf. Proc. **10** (1973) 568.
73 R 2 Ray, A.E., Biermann, A.T., Harmer, R.S., Davison, J.E.: Cobalt **4** (1973) 103.
73 R 3 Ray, A.E., Strnat, K.J., Harmer, R.S., Hartings, M.S.: AIP Conf. Proc. **10** (1973) 613.
73 R 4 Riley, A., Jones, G.A.: IEEE Trans. Magn. MAG-**9** (1973) 201.
73 R 5 Rosen, M., Klimker, H., Atzmony, U., Dariel, M.P.: Phys. Rev. B **8** (1973) 2336.
73 R 6 Rosen, M., Klimker, H., Atzmony, U., Dariel, M.P.: Proc. 10th Conf. on Rare Earth Res., Carefree, Arizona **1973**, p. 728.
73 R 7 Rothwarf, F., Leupold, H.A., Greedan, J., Wallace, W.E., Das, D.K.: Int. J. Magn. **4** (1973) 267.
73 S 1 Sankar, S.G., Keller, D.A., Craig, R.S., Wallace, W.E., Rao, V.U.S.: Proc. 10th Conf. on Rare Earth Res., Carefree, Arizona, **1973**, p. 273.
73 S 2 Savina, E.A., Mishin, D.D., Grechishkin, P.M.: Izv. Vyssh. Uchebn. Zaved. Fiz. **9** (1973) 125.
73 S 3 Searle, C.W., Frederick, G.D., Garret, H.J.: IEEE Trans. Magn. MAG-**9** (1973) 164.
73 S 4 Searle, G.W., Frederick, W.G.D., Garrett, H.J.: AIP Conf. Proc. **10** (1973) 573.
73 S 5 Simmons, M., Moreau, J.M., James, W.J., Givord, F., Lemaire, R.: J. Less Common Met. **30** (1973) 75.
73 S 6 Southern, B.W.: Can. J. Phys. **51** (1973) 1646.
73 S 7 Stearns, M.B.: Phys. Rev. B **8** (1973) 4383.
73 S 8 Steiner, W., Haferl, R.: Proc. 5th Int. Conf. Mössbauer Spectr., Bratislavia, Czechoslovakia **1973**, p. 49.
73 T 1 Taneja, S.P.: Proc. Nucl. Phys. and Solid State Phys. Symp., Bangalore, India **1973**, p. 313.
73 T 2 Tsai, S.C., Narasimhan, K.S.V.L., Kunesh, C.J., Butera, R.A.: Proc. 10th Conf. on Rare Earth Res., Carefree, Arizona, **1973**, p. 1017.
73 T 3 Tsui, J.B.Y., Mildrum, H.F., Strnat, K.J., Shanley, C.W.: AIP Conf. Proc. **10** (1973) 623.
73 U 1 Ulyanov, A.I., Deryagin, A.V., Mishin, D.D.: Fiz. Met. Metalloved. **35** (1973) 1094.
73 V 1 Van Diepen, A.M., De Wijn, H.W., Buschow, K.H.J.: Phys. Rev. B **8** (1973) 1125.
73 V 2 Van Mal, H.H.: Chem. Ing. Tech. **2** (1973) 80.
73 V 3 Van Mal, H.H., Buschow, K.H.J., Kuijpers, A.F.: J. Less Common Met. **32** (1973) 289.
73 V 4 Vasilkovski, V.A., Kovtun, N.M., Kupryanov, A.K., Nikitin, S.A., Ostrovski, V.F.: J. Eksp. Teor. Fiz. **65** (1973) 693.
73 V 5 Voiron, J.: Thesis, University of Grenoble, **1973**.
73 V 6 Voiron, J., Beille, J., Bloch, D., Vettier, C.: Solid State Commun. **13** (1973) 201.
73 W 1 Wallace, W.E., Swearingen, J.T.: J. Solid State Chem. **8** (1973) 37.
73 Z 1 Zaharova, M.I., Fuentes, Kh.: Fiz. Met. Metalloved. **36** (1973) 662.
73 Z 2 Zarechnyuk, O.S., Rykhal, R.M., Virchar, O.I.: Metallofizika **46** (1973) 92.
73 Z 3 Zoric, I., Thomas, G.A., Parks, R.D.: Phys. Rev. Lett. **30** (1973) 22.

74 A 1 Allen, C.W., Kuruzar, D.I., Miller, A.E.: IEEE Trans. Magn. MAG-**10** (1974) 716.
74 A 2 Arif, S.K., Bowden, G.J., Bunbury, D.St.P., Proc. 18th Congress AMPERE, Nottingham **1974**, vol. 1, p. 85.
74 A 3 Atzmony, U., Dariel, M.P.: Phys. Rev. B **10** (1974) 2060.
74 B 1 Barb, D., Burzo, E., Morariu, M.: J. Phys (Paris) **35** (1974) C 6-625.
74 B 2 Barrick, J.C., Simmons, M., James, J., Laforest, J., Shah, J.S.: J. Less Common Met. **37** (1974) 379.
74 B 3 Bartram, S.F., Smeggil, J.G., Davis, A.M., Gochner, R.P.: J. Less. Common Met. **35** (1974) 355.
74 B 4 Bechman, C.A., Wallace, W.E., Craig, R.S.: J. Phys. Chem. Solids **35** (1974) 463.
74 B 5 Belov, K.P., Vasilkovski, V.A., Kovtun, N.M., Kupryanov, A.K., Nikitin, S.A.: J. Eksp. Teor. Fiz. Pisma **20** (1974) 662.
74 B 6 Benz, M.G., Laforce, R.P., Martin, D.L.: AIP Conf. Proc. **18** (1974) 1173.
74 B 7 Bowden, G.J., Day, R.K., Sarwar, M.: Proc. Int. Conf. Magnetism, 1973, Moscow, Publ. House Nauka **1974**, vol. IV, p. 475.
74 B 8 Brouha, M., Buschow, K.H.J., Miedema, A.R.: IEEE Trans. Magn. MAG-**10** (1974) 182.
74 B 9 Burzo, E.: Solid State Commun. **14** (1974) 1295.
74 B 10 Burzo, E., Lazar, D.P.: Proc. Int. Conf. Magnetism, 1973, Moscow, Publ. House Nauka **1974**, vol. V, p. 344.

74 B 11 Burzo, E., Bodea, M., Barb, D.: Proc. 18th Congress AMPERE, Nottingham **1974**, vol. 1, p. 71.
74 B 12 Burzo, E., Lazar, D.P., Ciorascu, M.: Phys. Status Solidi (b) **65** (1974) K 145.
74 B 13 Buschow, K.H.J.: J. Less Common Met. **37** (1974) 91.
74 B 14 Buschow, K.H.J., Miedema, A.R., Brouha, M.: J. Less Common Met. **38** (1974) 9.
74 B 15 Buschow, K.H.J., Van Diepen, A.M., De Wijn, H.W.: Solid State Commun. **15** (1974) 903.
74 B 16 Buschow, K.H.J., Van Diepen, A.M., De Wijn, H.W.: Proc. Int. Conf. Magnetism, 1973, Moscow, Publ. House Nauka **1974**, vol. IV, p. 41.
74 B 17 Buschow, K.H.J., Kuijpers, F.A., Miedema, A.R., Van Maal, H.H.: Proc. 11th Conf. on Rare Earth Res., Transverse City, Michigan **1974**, p. 417.
74 C 1 Cech, R.E.: J. Met. **26** (1974) 32.
74 C 2 Clark, A.E.: AIP Conf. Proc. **18** (1974) 1015.
74 C 3 Clark, A.E., Belson, H.S., Tamagawa, N., Callen, E.: Proc. Int. Conf. Magnetism, 1973, Moscow, Publ. House Nauka **1974**, vol. 4, p. 335.
74 C 4 Craik, D.J., Hill, E.: Phys. Lett. **48** A (1974) 157.
74 D 1 Dariel, M.P., Atzmony, U., Guiser, R.: J. Less Common Met. **34** (1974) 315.
74 D 2 Den Broeder, F.A.J., Zijlstra, H.: Proc. 3rd Europ. Conf. on Hard Magnetic Materials, Amsterdam, Netherlands, **1974**, p. 118.
74 D 3 Den Broeder, F.A.J., Westerhout, G.D., Buschow, K.H.J.: Z. Metallkd. **65** (1974) 501.
74 D 4 Deportes, J., Gignoux, D., Givord, F.: Phys. Status Solidi (b) **64** (1974) 29.
74 D 5 Deryagin, A., Ulyanov, A.: Phys. Status Solidi (a) **25** (1974) K 129.
74 D 6 Deryagin, A., Ulyanov, A.: Phys. Status Solidi (a) **24** (1974) K 11.
74 D 7 Deryagin, A.V., Kudrevatykh, N.V., Baskhov, Y.F.: Proc. Int. Conf. Magnetism, 1973, Moscow, Publ. House, Nauka **1974**, vol. I(2), p. 222.
74 D 8 Deryagin, A., Ulyanov, A., Barabanova, E., Bashkov, Y.: Phys. Status Solidi (a) **23** (1974) K 199.
74 D 9 Deryagin, A., Ulyanov, A., Kudrevatykh, N., Barabanova, E., Bashkov, Y., Andreev, A., Tarasov, E.: Phys. Status Solidi (a) **23** (1974) K 15.
74 D 10 Doane, D.A., Graham, C.D.: AIP Conf. Proc. **18** (1974) 1192.
74 D 11 Dwight, A.E., Kimball, C.W.: Acta Crystallogr. B **30** (1974) 2791.
74 D 12 Dworschak, G., Khan, Y.: J. Phys. Chem. Solids **35** (1974) 1021.
74 E 1 Elemans, J.B.A.A., Buschow, K.H.J.: Phys. Status Solidi (a) **24** (1974) K 125.
74 E 2 Elemans, J.B.A.A., Buschow, K.H.J.: Phys. Status Solidi (a) **24** (1974) 393.
74 E 3 Ermolenko, A.S.: Proc. Int. Conf. Magnetism, 1973, Moscow, Publ. House Nauka **1974**, vol. I(1), p. 231.
74 E 4 Ermolenko, A.S., Korolev, A.V., Lagunova, V.I., Scherbakova, E.V.: Fiz. Met. Metalloved. **38** (1974) 1001.
74 F 1 Frederick, W.G.D., Hoch, M.: IEEE Trans. Magn. MAG-**10** (1974) 733.
74 F 2 Frederick, W.G.D., Searle, C.W., Hoch, M.: AIP Conf. Proc. **18** (1974) 1197.
74 G 1 Ganapathy, E.V., Wallace, W.E., Craig, R.S.: Proc. 11th Conf. on Rare Earth Res., Transverse City, Michigan **1974**, p. 417.
74 G 2 Gass, V.G., Shur, Ya.S., Glaser, A.A.: Fiz. Tverd. Tela **16** (1974) 1704.
74 G 3 Gignoux, D.: J. Phys. (Paris) **35** (1974) 455.
74 G 4 Gignoux, D., Gomez-Sal, J.C.: Phys. Lett. **50** A (1974) 63.
74 G 5 Gignoux, D., Lemaire, R.: Solid State Commun. **14** (1974) 877.
74 G 6 Gignoux, D., Lemaire, R., Chaussy, J.: Proc. Int. Conf. Magnetism, 1973, Moscow, Publ. House Nauka **1974**, vol. V, p. 361.
74 G 7 Givord, D., Lemaire, R.: Proc. Int. Conf. Magnetism, 1973, Moscow, Publ. House Nauka **1974**, vol. III, p. 492.
74 G 8 Givord, F., Lemaire, R.: IEEE Trans. Magn. MAG-**10** (1974) 109.
74 G 9 Gomes, A.A., Guimaraes, A.P.: J. Phys. F **4** (1974) 1454.
74 G 10 Gorbunov, V.I., Grunau, L.M., Potapov, N.N.: Fiz. Met. Metalloved. **37** (1974) 119.
74 G 11 Greedan, J.E., Hutchens, R.D., Narasimhan, K.S.V.L., Wallace, W.E.: Proc. 11th Conf. on Rare Earth Res., Transverse City, Michigan **1974**, p. 449.
74 G 12 Green, M.L.: J. Less Common Met. **37** (1974) 169.
74 G 13 Gschneidner Jr., K.A., Verkade, M.E.: Selected Cerium Phase Diagrams, Rare Earth Information Center Publication IS-RIC 7, Iowa State University, Ames, Iowa **1974**.
74 G 14 Gubbens, P.C.M., Buschow, K.H.J.: Proc. Int. Conf. Magnetism, 1973, Moscow, Publ. House Nauka, **1974**, vol. V, p. 60.
74 G 15 Gubbens, P.C.M., Van Loef, J.J., Buschow, K.H.J.: J. Phys. (Paris) **35** (1974) C 6-617.

74 G 16 Gubbens, P.C.M., Van Apeldoorn, J.H.F., Van der Kraan, A.M., Buschow, K.H.J.: J. Phys. F **4** (1974) 921.
74 H 1 Hahn, A., Paulus, M., Steigenberger, N., Stierstadt, K.: Int. J. Magn. **6** (1974) 167.
74 H 2 Halstead, T.K.: J. Solid State Chem. **11** (1974) 114.
74 H 3 Hamano, M., Yajima, S., Umebayashi, H.: Proc. 11th Conf. on Rare Earth Res. Transverse City, Michigan **1974**, p. 477.
74 H 4 Hamano, M., Yajima, S., Umebayashi, H.: Trans. Jpn. Inst. Met. **15** (1974) 273.
74 H 5 Heinrich, J.P., Garret, H., Allen, R.P.: J. Appl. Phys. **45** (1974) 1873.
74 H 6 Hinz, I.D.: Hermsdorfer Tech. Mitt. **14** (1974) 1272.
74 H 7 Hirst, L.L., Stohr, J., Zech, E., Shenoy, G.K., Kalvius, G.M.: Proc. 18th Congress AMPERE, Nottingham **1974**, vol. 1, p. 67.
74 H 8 Horn, P.M., Parks, R.D., Lambeth, D.N., Stanley, H.E.: Phys. Rev. B **9** (1974) 316.
74 H 9 Hrabrov, V.I., Shur, Ya.S.: J. Eksp. Teor. Fiz. Pisma **20** (1974) 468.
74 I 1 Ikeda, K., Nakamichi, F., Yamada, T., Yamamoto, M.: J. Phys. Soc. Jpn. **36** (1974) 611.
74 I 2 Irkhin, Yu.P., Rosenfeld, E.V.: Fiz. Tverd. Tela **16** (1974) 485.
74 J 1 Jaakkola, S., Parviainen, S.: Phys. Status Solidi (a) **21** (1974) K 53.
74 J 2 Jennings, L.D., Chipman, D.R.: AIP Conf. Proc. **18** (1974) 1187.
74 K 1 Kandaurova, G.S., Beketov, V.N.: Fiz. Tverd. Tela **16** (1974) 1857.
74 K 2 Kandaurova, G.S., Deryagin, A.V., Lagutin, A.E.: Dokl. Akad. Nauk SSSR **219** (1974) 320.
74 K 3 Katayama, T., Shibata, T.: J. Cryst. Growth **24/25** (1974) 396.
74 K 4 Kazakov, A.A., Deryagin, A.V., Kudrevatykh, N.V., Reymer, V.A.: Fiz. Tverd. Tela **16** (1974) 3732.
74 K 5 Keller, D.A., Sankar, S.G., Craig, R.S., Wallace, W.E.: AIP Conf. Proc. **18** (1974) 1207.
74 K 6 Khan, Y.: Phys. Status Solidi (a) **23** (1974) K 151.
74 K 7 Khan, Y.: Acta Crystallogr. B **30** (1974) 861.
74 K 8 Khan, Y.: Phys. Status Solidi (a) **21** (1974) 69.
74 K 9 Khan, Y.: Phys. Status Solidi (a) **23** (1974) 425.
74 K 10 Khan, Y.: J. Less Common Met. **34** (1974) 191.
74 K 11 Khan, Y.: Z. Metallkd. **65** (1974) 489.
74 K 12 Kharchenko, O.I., Kashel, O.S., Bodak, O.I.: Metallofizika **52** (1974) 101.
74 K 13 Khrabrov, V.I., Shur, Ya.S.: J. Eksp. Teor. Fiz. Pisma **20** (1974) 468.
74 K 14 Kimball, C.W., Dwight, A.R., Preston, R.S., Taneja, S.P.: AIP Conf. Proc. **18** (1974) 1242.
74 K 15 Klein, H.P., Menth, A.: AIP Conf. Proc. **18** (1974) 1177.
74 K 16 Klimker, H., Rosen, M., Dariel, M.P., Atzmony, U.: Phys. Rev. B **10** (1974) 2968.
74 K 17 Koon, N.C., Schindler, A., Williams, C., Carter, F.: J. Appl. Phys. **45** (1974) 5389.
74 K 18 Kuijpers, F.A.: Delft Prog. Rep. Ser. A **1** (1974) 92.
74 K 19 Kuijpers, F.A., Loopstra, B.O.: J. Phys. Chem. Solids **35** (1974) 301.
74 L 1 Lee, R.W., Croat, J.J.: IEEE Trans. Magn. MAG-**10** (1974) 708.
74 M 1 Maletta, H., Crecelius, G., Zinn, W.: J. Phys. (Paris) **35** (1974) C 6–279.
74 M 2 Martin, D.L., Smeggil, J.G.: IEEE Trans. Magn. MAG-**10** (1974) 704.
74 M 3 Menth, A., Klein, H.P., Bernasconi, J., Strassler, J.: AIP Conf. Proc. **18** (1974) 1182.
74 M 4 Miller, A.E., D'Silva, T, Miura, K.: Proc. 11th Conf. on Rare Earth Res. Transverse City, Michigan **1974**, p. 461.
74 M 5 Miller, A.E., Shanley, J.F., D'Silva, T.: Proc. 11th Conf. on Rare Earth Res., Transverse City, Michigan **1974**, p. 469.
74 M 6 Miller, A.E., D'Silva, T., Igarashi, H., Shanley, J.: AIP Conf. Proc. **18** (1974) 1253.
74 M 7 Milstein, J.B., Koon, N.C., Johnson, I.R., Williams, C.M.: Mater. Res. Bull. **9** (1974) 1617.
74 M 8 Morariu, M., Burzo, E., Barb, D.: Phys. Status Solidi (b) **62** (1974) K 55.
74 M 9 Morariu, M., Burzo, E., Barb, D.: Proc. Int. Conf. Magnetism, 1973, Moscow, Publ. House, Nauka **1974**, vol. IV, p. 491.
74 M 10 Moreau, J.M., Paccard, D., Gignoux, D.: Acta Crystallogr. B **30** (1974) 2122.
74 M 11 Moreau, J.M., Paccard, D., Parthé, E.: Acta Crystallogr. B **30** (1974) 2583.
74 N 1 Narasimhan, K.S.V.L., Wallace, W.E.: AIP Conf. Proc. **18** (1974) 1248.
74 N 2 Narasimhan, K.S.V.L., Wallace, W.E., Hutchens, R.D.: Proc. 11th Conf. on Rare Earth Res., Transverse City, Michigan **1974**, p. 487.
74 N 3 Narasimhan, K.S.V.L., Wallace, W.E., Hutchens, R.D.: IEEE Trans. Magn. MAG-**10** (1974) 729.
74 N 4 Narasimhan, K.S.V.L., Butera, R.A., Craig, R.S., Wallace, W.E.: J. Solid State Chem. **9** (1974) 267.
74 N 5 Narasimhan, K.S.V.L., Do-Dinh, C., Wallace, W.E., Hutchens, R.D.: Proc. 11th Conf. on Rare Earth Res., Transverse City, Michigan **1974**, p. 451.

74 N 6 Narasimhan, K.S.V.L., Wallace, W.E., Hutchens, R.D., Greedan, J.E.: AIP Conf. Proc. **18** (1974) 1212.
74 N 8 Nikitin, S.A., Bisliev, A.M.: Fiz. Met. Metalloved. **37** (1974) 81.
74 N 9 Nikitin, S.A., Talalaeva, E.Y., Tchernikova, L.A., Andreenko, A.S., Bisliev, A.M.: Proc. Int. Conf. Magnetism, 1973, Moscow, Publ. House Nauka **1974**, vol. V, p. 339.
74 N 10 Nikitin, S.A., Vasilkovski, V.A., Kovtun, N.M., Kupryanov, A.K., Ostrovski, V.F.: Fiz. Tverd. Tela **16** (1974) 3137.
74 N 11 Nishida, I., Uehara, M.: J. Less Common Met. **34** (1974) 285.
74 O 1 Oesterreicher, H.: Solid State Commun. **14** (1974) 571.
74 O 2 Oesterreicher, H.: Inorg. Chem. **13** (1974) 2807.
74 O 3 Oesterreicher, H.: Proc. Int. Conf. Magnetism, 1973, Moscow, Publ. House, Nauka **1974**, vol. I(2), p. 217.
74 O 4 Oesterreicher, H.: Phys. Status Solidi (a) **26** (1974) K 117.
74 P 1 Plumier, R., Sougi, M.: Proc. Int. Conf. Magnetism, 1973, Moscow, Publ. House, Nauka **1974**, vol. III, p. 487.
74 P 2 Poldy, C.A., Kirchmayr, H.R.: Phys. Status Solidi (b) **65** (1974) 553.
74 P 3 Povitzki, V.A., Grahovski, E.B., Makarov, E.F., Malahov, G.V.: Fiz. Met. Metalloved. **38** (1974) 1095.
74 R 1 Raevskaya, M.B., Sokolovskaya, E.M., Tokunova, E.F., Burnasheva, V.V.: Metallofizika **52** (1974) 109.
74 R 2 Ray, A.E.: Cobalt **1** (1974) 13.
74 R 3 Riley, A.: J. Less Common Met. **35** (1974) 305.
74 R 4 Rosen, M., Klimker, H., Atzmony, U., Dariel, M.P.: Phys. Rev. B **9** (1974) 254.
74 R 5 Roy, G.J., Gaunt, P.: Phys. Lett. **47** A (1974) 175.
74 R 6 Roy, G.J., Gaunt, P.: AIP Conf. Proc. **18** (1974) 1202.
74 S 1 Sankar, S.G., Keller, D.A., Craig, R.S., Wallace, W.E., Rao, V.V.S.: J. Solid State Chem. **9** (1974) 78.
74 S 2 Sarkar, D., Segnan, R., Cornell, R., Callen, E., Harris, R., Plischke, M., Zuckerman, M.J.: Phys. Rev. Lett. **32** (1974) 542.
74 S 3 Schweizer, J., Tasset, F.: Proc. Int. Conf. Magnetism, 1973, Moscow, Publ. House Nauka **1974**, vol. IV, p. 257.
74 S 4 Searle, C.W.: Appl. Phys. Lett. **24** (1974) 30.
74 S 5 Searle, C.W.: J. Appl. Phys. **45** (1974) 4581.
74 S 6 Shanley, C.W., Harmer, R.S.: AIP Conf. Proc. **18** (1974) 1217.
74 S 7 Shur, Ya.S., Puzanova, T.Z., Glazer, A.A.: Fiz. Met. Metalloved. **37** (1974) 1116.
74 S 8 Smeggil, J.E., Rao, P., Livingston, J.D., Koch, E.F.: AIP Conf. Proc. **18** (1974) 1144.
74 S 9 Steiner, W., Ortbauer, H.: Phys. Status Solidi (a) **26** (1974) 451.
74 S 10 Steiner, W., Choi, B.K., Hilscher, G., Wiesinger, G., Kirchmayr, H.: Proc. Int. Conf. Magnetism, 1973, Moscow, Publ. House, Nauka **1974**, vol. IV, p. 63.
74 T 1 Takeshita, T., Wallace, W.E., Craig, R.S.: Inorg. Chem. **13** (1974) 2282.
74 T 2 Tsai, S.C., Narasimhan, K.S.V.L., Kunesh, C.J., Butera, R.A.: J. Appl. Phys. **45** (1974) 3582.
74 U 1 Ulyanov, A.I., Deryagin, A.V., Kandaurova, G.S.: Phys. Status Solidi (a) **26** (1974) K 167.
74 V 1 Van Diepen, A.M., De Wijn, H.W., Buschow, K.H.J.: Proc. Int. Conf. Magnetism, 1973, Moscow, Publ. House Nauka **1974**, vol. I(1), p. 227.
74 V 2 Van der Kraan, A.M., Gubbens, P.C.M.: J. Phys. (Paris) **35** (1974) C 6–469.
74 V 3 Van Mal, H.H., Buschow, K.H.J., Miedema, A.R.: J. Less Common Met. **35** (1974) 65.
74 V 4 Voiron, J., Berton, A., Chaussy, J.: Phys. Lett. **50** A (1974) 17.
74 W 1 Williams, C.M., Koon, N.C.: AIP Conf. Proc. **18** (1974) 1247.
74 W 2 Williams, K.L., Bartlett, R.W., Jorgensen, P.J.: J. Less Common Met. **37** (1974) 174.
74 Y 1 Yakinthos, J.K.: Phys. Status Solidi (b) **64** (1974) 643.
74 Z 1 Zuckermann, M.I.: J. Phys. F **4** (1974) 1800.

75 A 1 Andres, K., Schmidt, P.H., Darack, S.: AIP Conf. Proc. **24** (1975) 238.
75 A 2 Arbuzov, M.P., Pavlyukov, A.A., Pogorilyi, A.G.: Fiz. Met. Metalloved. **40** (1975) 848.
75 A 3 Arif, S.K., McCausland, M.A.H.: J. Phys. F **5** (1975) L 247.
75 A 4 Arif, S.K., Bunbury, D.St.P., Bowden, G.J.: J. Phys. F **5** (1975) 1785.
75 A 5 Arif, S.K., Bunbury, D.St.P., Bowden, G.J.: J. Phys. F **5** (1975) 1792.
75 A 6 Arif, S.K., Bunbury, D.St.P., Bowden, G.J., Day, R.K.: J. Phys. F **5** (1975) 1048.
75 A 7 Asti, G., Bolzoni, F., Melville, D., Rinaldi, S.: IEEE Trans. Magn. MAG-**11** (1975) 1437.
75 A 8 Atzmony, U., Dariel, M.P.: AIP Conf. Proc. **24** (1975) 662.
75 B 1 Barnea, G.: J. Phys. C **8** (1975) L 216.

75 B 2 Barnes, R.G., Lunde, B.K.: AIP Conf. Proc. **24** (1975) 217.
75 B 3 Belov, K.P., Elyutin, O.P., Kataev, G.I., Kim, D., Nikitin, S.A., Pshechenkova, G.V., Solntseva, L.I., Surovaya, G.N., Taratynov, V.P.: Fiz. Met. Metalloved. **39** (1975) 284.
75 B 4 Bloch, D., Edwards, D.M., Shimizu, M., Voiron, J.: J. Phys. F **5** (1975) 1217.
75 B 5 Boidenko, V.S.: Izv. Vyssh. Uchebn. Zaved. Fiz. **3** (1975) 35.
75 B 6 Brouha, M., Buschow, K.H.J.: J. Phys. F **5** (1975) 543.
75 B 7 Brouha, M., Buschow, K.H.J.: J. Appl. Phys. **46** (1975) 1355.
75 B 8 Brouha, M., Buschow, K.H.J.: IEEE Trans. Magn. MAG-**11** (1975) 1358.
75 B 9 Burzo, E.: Solid State Commun. **16** (1975) 759.
75 B 10 Burzo, E., Bodea, M., Barb, D.: C.R. Acad. Sci. B **280** (1975) 345.
75 B 11 Burzo, E., Bodea, M., Barb, D., Laforest, J.: Proc. Int. Conf. Mössbauer Spetr., Cracow, Poland **1975**, vol. 1, p. 171.
75 B 12 Buschow, K.H.J.: J. Less Common Met. **40** (1975) 361.
75 B 13 Buschow, K.H.J., Brouha, M., Elemans, J.B.A.A.: Phys. Status Solidi (a) **30** (1975) 177.
75 B 14 Buschow, K.H.J., Brouha, M., Langereis, C.: Solid State Commun. **16** (1975) 789.
75 B 15 Buschow, K.H.J., Brouha, M., Rijnbeck, A.G.: Solid State Commun. **16** (1975) 31.
75 B 16 Buschow, K.H.J., Van Mal, H.H., Miedema, A.R.: J. Less Common Met. **42** (1975) 163.
75 C 1 Cannon, J.A., Budnick, J.I., Burch, T.J.: Solid State Commun. **17** (1975) 1385.
75 C 2 Clark, A.E., Savage, H.T.: IEEE Trans. Sonics Ultrason. SU-**22** (1975) 50.
75 C 3 Clark, A.E., Cullen, J.R., Sato, K.: AIP Conf. Proc. **24** (1975) 670.
75 C 4 Clinton, J., Bittner, H., Oesterreicher, H.: J. Less Common Met. **41** (1975) 187.
75 C 5 Colley, M.G., Chaplin, D.H., Swan, D.E., Wilson, G.V.H.: J. Phys. F **5** (1975) L 80.
75 C 6 Craik, D.J., Hill, E.W., Harrison, A.J.: IEEE Trans. Magn. MAG-**11** (1975) 1379.
75 C 7 Crecelius, G., Maletta, H.: Proc. Int. Conf. Mössbauer Spectr., Cracow, Poland **1975**, vol. I, p. 149.
75 D 1 Dejonqueres, M.C., Cyrot-Lackmann, F.: J. Phys. F **5** (1975) 1368.
75 D 2 Del Moral, A., Melville, D.: J. Phys. F **5** (1975) 767.
75 D 3 Deportes, J., Givord, D., Lemaire, R., Nagai, H.: J. Less Common Met. **40** (1975) 299.
75 D 4 Deryagin, A.V., Kudrevatykh, N.V.: Phys. Status Solidi (a) **30** (1975) K 129.
75 D 5 Deryagin, A.V., Kudrevatykh, N.: Phys. Status Solidi (b) **68** (1975) K 163.
75 D 6 Deryagin, A.V., Barabanova, E.A., Ulyanov, A.I.: Phys. Status Solidi (a) **31** (1975) 391.
75 D 7 Deryagin, A.V., Bashkov, Yu.F., Andreev, A.V.: Dokl. Akad. Nauk SSSR **22** (1975) 584.
75 D 8 Dublon, G., Dariel, M.P., Atzmony, U.: Phys. Lett. **51** A (1975) 262.
75 D 9 Dublon, G., Atzmony, U., Dariel, M.P., Shaked, H.: Phys. Rev. B **12** (1975) 4628.
75 D 10 Dwight, A.E.: J. Less Common Met. **43** (1975) 117.
75 D 11 Dwight, A.E., Kimball, C.W., Preston, R.S., Taneja, S.P., Weber, L.: J. Less Common Met. **40** (1975) 285.
75 E 1 Elemans, J.B.A.A., Buschow, K.H.J., Zandbergen, H.W., De Jong, J.P.: Phys. Status Solidi (a) **29** (1975) 595.
75 E 2 Ermolenko, A.S., Rosenfeld, E.V., Irkhin, Yu.P., Kelarev, V.V., Rozhda, A.F., Sidorov, S.K., Pirogov, A.N., Vohmianin, A.P.: J. Eksp. Teor. Fiz. **69** (1975) 1743.
75 E 4 Ermolenko, A.S., Korolev, A.V.: J. Eksp. Teor. Fiz. Pisma **21** (1975) 34.
75 E 5 Ermolenko, A.S., Scherbakova, E.V., Efremova, N.N., Finkelstein, L.D.: Fiz. Met. Metalloved. **40** (1975) 289.
75 F 1 Fischer, G., Meyer, A.: Solid State Commun. **16** (1975) 355.
75 F 2 Fischer, W., Kuzmin, R.N.: Proc. Int. Conf. Mössbauer Spectr., Cracow, Poland **1975**, vol. I, p. 65.
75 F 3 Frederick, W.G.D., Hoch, M.: IEEE Trans. Magn. MAG-**11** (1975) 1434.
75 G 1 Georges, R., Schweizer, J., Yakinthos, J.: J. Phys. Chem. Solids **36** (1975) 415.
75 G 2 Gignoux, D., Givord, F., Lemaire, R.: Phys. Rev. B **12** (1975) 3878.
75 G 3 Grössinger, R., Steiner, W.: Phys. Status Solidi (a) **28** (1975) K 135.
75 H 1 Heidemann, A., Richter, D., Buschow, K.H.J.: Z. Phys. B **22** (1975) 367.
75 H 2 Herget, C., Domazer, H.G.: Goldschmidt Informiert **4** (1975) 3.
75 H 3 Hilzinger, H.R., Kronmüller, H.: Phys. Lett. **51** A (1975) 59.
75 I 1 Ikeda, K., Nakamichi, T.: J. Phys. Soc. Jpn. **39** (1975) 963.
75 J 1 Jaakkola, S., Parviainen, S., Stenholm, H.: Z. Phys. B **20** (1975) 109.
75 K 1 Kalychak, Ya.M., Akselrod, L.G., Yarmolyuk, Ya.P., Bodak, O.I., Gladyshevski, E.I.: Kristallografiya **20** (1975) 1045.
75 K 2 Kandaurova, G.S., Deryagin, A.V., Lagutin, A.E.: Phys. Status Solidi (a) **27** (1975) 429.
75 K 3 Khan, Y., Qureshi, A.H.: Phys. Status Solidi (a) **28** (1975) 169.

75K4 Klein, H.P., Menth, A., Perkins, R.S.: Physica **80** B (1975) 153.
75K5 Korolev, A.V., Ermolenko, A.S., Emakov, A.E., Antonov, A.V., Magat, L.M., Makarova, G.M.: Fiz. Met. Metalloved. **39** (1975) 1107.
75K6 Kuhn, K., Perry, A.J.: J. Met. Sci. **9** (1975) 339.
75K7 Kunesh, C.J., Narasimhan, K.S.V.L., Butera, R.A.: J. Appl. Phys. **46** (1975) 1349.
75L1 Livingston, J.D.: J. Appl. Phys. **46** (1975) 5259.
75L2 Longworth, G., Harris, I.R.: J. Less Common Met. **41** (1975) 175.
75M1 Magat, L.M., Makarova, G.M., Solina, L.V., Ermolenko, A.S., Scherbakova, E.V., Shur, Ya.S.: Fiz. Met. Metalloved. **39** (1975) 295.
75M2 Male, S.E., Taylor, R.H.: J. Phys. F **5** (1975) 126.
75M3 Martin, D.L., Smeggil, J.G., Hatfield, W., Bolon, R.: IEEE Trans. Magn. MAG-**11** (1975) 1420.
75M4 McCurrie, R.A., Mitchell, R.K.: IEEE Trans. Magn. MAG-**11** (1975) 1408.
75M5 Mildrum, H.F., Iden, D.J.: Goldschmidt Informiert **4** (1975) 54.
75M6 Miller, A.M., Miura, K., Rodrigues, H., D'Silva, T.: AIP Conf. Proc. **24** (1975) 672.
75M7 Mirkin, L.I., Smyslov, E.F.: Izv. Vyssh. Uchebn. Zaved. Fiz. **7** (1975) 127.
75M8 Misknis, E.T., Narasimhan, K.S.V.L., Wallace, W.E., Craig R.S.: J. Solid State Chem. **13** (1975) 311.
75M9 Moreau, J.M., Parthé, E., Paccard, D.: Acta Crystallogr. B **31** (1975) 747.
75M10 Miedema, A.R., Boom, R., De Boer, F.R.: J. Less Common Met. **41** (1975) 283.
75N1 Nagel, H., Menth, A.: Goldschmidt Informiert **4** (1975) 42.
75N2 Narasimhan, K.S.V.L., Wallace, W.E.: J. Solid State Chem. **13** (1975) 315.
75N3 Narasimhan, K.S.V.L., Dinh, C.D., Wallace, W.E., Hutchens, R.D.: J. Appl. Phys. **46** (1975) 4961.
75N4 Nicklow, R.M., Koon, N.C., Williams, C.M., Milstein, J.B.: AIP Conf. Proc. **24** (1975) 165.
75N5 Nikitin, S.A., Bisliev, A.M.: Vestn. Mosk. Univ. Fiz. Astronomiya **16** (1975) 195.
75N6 Nikitin, S.A., Kim, D., Popkov, A.F., Zvezdin, A.K., Popkov, A.F.: Fiz. Tverd. Tela **17** (1975) 2659.
75N7 Nikitin, S.A., Kim, D., Zvezdin, A.K., Popkov, A.F.: J. Eksp. Teor. Fiz. Pisma **22** (1975) 297.
75N8 Nikitin, S.A., Vasilkovski, V.A., Kovtun, N.M., Kupriyanov, A.K.: J. Eksp. Teor. Fiz. **69** (1975) 2212.
75N9 Nikitin, S.A., Talalaeva, E.V., Chernikova, L.A., Andreenko, A.S.: Fiz. Met. Metalloved. **40** (1975) 967.
75N10 Nikitin, S.A., Vasilkovski, V.A., Kovtun, N.M., Kupriyanov, A.K., Ostrovski, V.F.: J. Eksp. Teor. Fiz. **68** (1975) 577.
75O1 Oesterreicher, H.: J. Less Common Met. **40** (1975) 207.
75O2 Oesterreicher, H.: J. Phys. F **5** (1975) 1607.
75P1 Paladino, A.E., Dionne, N.J., Weihrauch, P.F., Wettstein, E.C.: Goldschmidt Informiert **4** (1975) 63.
75P2 Parker, F.T., Misroch, M., Oesterreicher, H.: Mater. Res. Bull. **10** (1975) 1075.
75P3 Parthé, E., Lemaire, R.: Acta Crystallogr. B **31** (1975) 1879.
75P4 Parviainen, S., Jaakkola, S.: EPS Conf. Abstr. **1** A (1975) 33.
75P5 Perkins, R.S., Nagel, H.: Physica B **80** (1975) 143.
75P6 Perkins, R.S., Gaiffi, S., Menth, A.: IEEE Trans. Magn. MAG-**11** (1975) 1431.
75P7 Perkins, R.S., Perry, A.J., Nagel, H., Menth, A.: AIP Conf. Proc. **24** (1975) 693.
75P8 Pfeiffer, J.: Z. Metallkd. **66** (1975) 93.
75P9 Preston, R.S., Dwight, A.E., Fedro, A.J., Kimball, C.W.: AIP Conf. Proc. **24** (1975) 660.
75R1 Ray, A.E., Strnat, J.: IEEE Trans. Magn. MAG-**11** (1975) 1429.
75S1 Sankar, S.G., Rao, V.U.S., Segal, E., Wallace, W.E., Frederick, W.G.D., Garret, H.J.: Phys. Rev. B **11** (1975) 435.
75S2 Savage, H.T., Clark, A.E., Powers, J.M.: IEEE Trans. Magn. MAG-**11** (1975) 1355.
75S3 Schelleng, J.H., Koon, N.C.: AIP Conf. Proc. **24** (1975) 668.
75S4 Shibata, T., Katayama, T., Yoneyama, J., Nakamura, S.: Bull. Electrotech. Lab. Jpn. **39** (1975) 254.
75S5 Shur, Ya.S., Puzanova, T.Z., Glazer, A.A.: Fiz. Met. Metalloved. **39** (1975) 746.
75S6 Shur, Ya.S., Shirayeva, O.I., Maikov, Y.G.: Fiz. Met. Metalloved. **39** (1975) 1118.
75S8 Steiner, W., Hrubec, J.: J. Less Common Met. **41** (1975) 165.
75S9 Steiner, W., Ortbauer, H.: Phys. Status Solidi (a) **31** (1975) K 119.
75S10 Streever, R.L.: AIP Conf. Proc. **24** (1975) 462.
75S11 Streever, R.L.: Phys. Rev. B **12** (1975) 4653.
75S12 Strnat, K.J., Ray, A.E.: Goldschmidt Informiert **35** (1975) 47.
75S13 Strnat, K.J., Ray, A.E.: AIP Conf. Proc. **24** (1975) 680.
75T1 Taylor, K.N.R., Poldy, C.A.: J. Phys. F **5** (1975) 1593.
75T2 Tsuchida, T., Sugaki, S., Nakamura, Y.: J. Phys. Soc. Jpn. **39** (1975) 495.
75V1 Van der Kraan, A.M., Gubbens, P.C.M., Buschow, K.H.J.: Phys. Status Solidi (a) **31** (1975) 495.

75 V 2 Van der Kraan, A.M., Van der Velden, K.N.J., Gubbens, P.C.M., Buschow, K.H.J.: Proc. Int. Conf. Mössbauer Spectr., Cracow, Poland **1975**, p. 179.
75 V 3 Van der Velden, K.N.J., Van der Kraan, A.M., Gubbens, P.C.M., Buschow, K.H.J.: Proc. Int. Conf. Mössbauer Spectr., Cracow, Poland **1975**, p. 181.
75 W 1 Wallace, W.E., Ilyushin, A.S., Lopez, D.: Proc. Int. Conf. Mössbauer Spectr., Cracow, Poland **1975**, p. 97.
75 W 2 Weisman, I.D., Bennett, L.H., McAlister, A.J., Watson, R.E.: Phys. Rev. B **11** (1975) 82.
75 W 3 Williams, C.M., Koon, N.C.: Phys. Rev. B **11** (1975) 4360.
75 Y 1 Yakinthos, J.K., Chappert, J.: Solid State Commun. **17** (1975) 979.
75 Y 2 Yakinthos, J.K., Mentzafos, D.E.: Phys. Rev. B **12** (1975) 1928.
75 Y 3 Yanovsky, R., Bauminger, E.R., Levron, D., Nowik, I., Ofer, S.: Solid State Commun. **17** (1975) 1511.

76 A 1 Adams, W., Moreau, J.M., Parthé, E. Schweizer, J.: Acta Crystallogr. B **32** (1976) 2697.
76 A 2 Allen, C.E.W., Liao, K.C., Miller, A.E.: Proc. 12th Conf. on Rare Earth Res., Vail, Colorado **1976**, p. 274.
76 A 3 Allen, C.W., Miller, A.E., Culity, B.D.: AIP Conf. Proc. **29** (1976) 655.
76 A 4 Apostolov, A., Mikhov, M., Yordanova, M., Hristov, V.: C.R. Acad. Bulg. Sci. **29** (1976) 1589.
76 A 5 Arif, S.K., Bunbury, D.S.P.: Phys. Status Solidi (a) **33** (1976) 91.
76 A 6 Atzmony, U., Dariel, M.P.: Phys. Rev. B **13** (1976) 4006.
76 A 7 Atzmony, U., Dublon, G.: J. Phys. (Paris) **37** (1976) C 6-625.
76 A 8 Atzmony, U., Dariel, M.P., Dublon, G.: Phys. Rev. B **14** (1976) 3713.
76 B 1 Bailey, L.J., Richter, E.: Proc. 2nd Int. Workshop on Rare Earth-Cobalt Permanent Magnets and their Applications, Dayton, Ohio **1976**, p. 235.
76 B 2 Barbara, B., Uehara, M.: IEEE Trans. Magn. MAG-**12** (1976) 997.
76 B 3 Barnes, R.G., Harper, W.C., Nelson, S.O., Thome, D.K., Torgeson, D.R.: J. Less Common. Met. **49** (1976) 483.
76 B 4 Bechman, C.A., Goudy, A., Takeshita, T., Wallace, W.E., Craig, R.S.: Inorg. Chem. **15** (1976) 2184.
76 B 5 Bechman, C.A., Narasimhan, K.S.V.L., Wallace, W.E., Craig, R.S., Butera, R.A.: J. Phys. Chem. Solids **37** (1976) 245.
76 B 6 Becker, J.J.: IEEE Trans. Magn. MAG-**12** (1976) 965.
76 B 7 Belov, K.P., Kataev, G.I., Nikitin, S.A., Chuprikov, G.E.: Sov. Phys. Acoust. **22** (1976) 431.
76 B 8 Belov, K.P., Vasilkovski, V.A., Kovtun, N.M., Kupriyanov, A.K., Nikitin, S.A.: Fiz. Tverd. Tela **18** (1976) 2244.
76 B 9 Biris, A., Bucur, R.U., Ghete, P., Indrea, E., Lupu, D.: J. Less Common. Met. **49** (1976) 477.
76 B 10 Boser, O.: J. Less Common Met. **46** (1976) 91.
76 B 11 Burzo, E.: Solid State Commun. **20** (1976) 565.
76 B 12 Burzo, E.: Solid State Commun. **18** (1976) 1431.
76 B 13 Burzo, E.: Solid State Commun. **20** (1976) 569.
76 B 14 Burzo, E., Baican, R.: Solid State Commun. **18** (1976) 1475.
76 B 15 Burzo, E., Lazar, D.P.: Solid State Commun. **18** (1976) 381.
76 B 16 Burzo, E., Lazar, D.P.: J. Solid State Chem. **16** (1976) 257.
76 B 17 Burzo, E., Lazar, D.P., Valeanu, M.: Rev. Roum. Phys. **21** (1976) 569.
76 B 18 Buschow, K.H.J.: Solid State Commun. **19** (1976) 421.
76 B 19 Buschow, K.H.J., Brouha, M.: AIP Conf. Proc. **29** (1976) 618.
76 B 20 Buschow, K.H.J., Brouha, M.: J. Appl. Phys. **47** (1976) 1653.
76 B 21 Buschow, K.H.J., Van Diepen, A.M.: Solid State Commun. **19** (1976) 79.
76 B 22 Buschow, K.H.J., Van Vucht, J.H.N., Van den Hoogenhof, W.W.: J. Less Common Met. **50** (1976) 145.
76 C 1 Cannon, J.A., Budnick, J.I., Burch, T.J., Ray, K., Wang, I.: J. Magn. Magn. Mater. **3** (1976) 255.
76 C 2 Chappert, J., Yakinthos, J.K.: Hyp. Int. **2** (1976) 251.
76 C 3 Clark A.E.: AIP Conf. Proc. **34** (1976) 13.
76 C 4 Clark, A.E., Cullen, J.R., McMasters, O.D., Callen, E.R.: AIP Conf. Proc. **29** (1976) 192.
76 D 1 Dariel, M.P., Holthuis, J.T., Pickus, M.R.: J. Less Common Met. **45** (1976) 91.
76 D 2 Dariel, M.P., Malekzadeh, M., Pikus, M.: AIP Conf. Proc. **29** (1976) 583.
76 D 3 De Wijn, H.W., Van Diepen, A.M., Buschow, K.H.J.: Phys. Status Solidi (b) **76** (1976) 11.
76 D 4 Del Moral, A.: An. Fis. **72** (1976) 265.
76 D 5 Den Broeder, F.J.A., Zijlstra, H.: J. Appl. Phys. **47** (1976) 2688.
76 D 6 Deodhar, S.S., Ficalora, P.J.: High Temp. Sci. **8** (1976) 185.
76 D 7 Deportes, J., Givord, D.: Solid State Commun. **19** (1976) 845.

76 D 8 Deportes, J., Givord, D., Schweizer, J., Tasset, F.: IEEE Trans. Magn. MAG-**12** (1976) 1000.
76 D 9 Deportes, J., Givord, D., Lemaire, R., Nagai, H., Yang, Y.T.: J. Less Common Met. **44** (1976) 273.
76 D 10 Deribas, A.A., Ermolenko, A.S., Kiselyov, A.N., Shcherbakova, Ye.V.: Fiz. Met. Metalloved. **41** (1976) 892.
76 D 11 Deryagin, A.V.: Usp. Fiz. Nauk **20** (1976) 392.
76 D 12 Dublon, G., Kroupp, M., Dariel, M.P., Atzmony, U.: Phys. Status Solidi (b) **76** (1976) 669.
76 E 1 Elemans, J.B.A.A., Buschow, K.H.J.: Phys. Status Solidi (a) **34** (1976) 355.
76 E 2 Elemans, J.B.A.A., Gubbens, P.C.M., Buschow, K.H.J.: J. Less Common Met. **44** (1976) 51.
76 E 3 Ermakov, A.E., Serikov, V.V., Barihov, V.A., Schur, Ya.S.: Fiz. Met. Metalloved. **42** (1976) 408.
76 E 4 Ermolenko, A.S.: IEEE Trans. Magn. MAG-**12** (1976) 992.
76 E 5 Ermolenko, A.S., Korolev, A.V., Rozhda, A.F.: Fiz. Met. Metalloved. **42** (1976) 518.
76 E 6 Ermolenko, A.S., Zabolotzki, E.I., Korolev, A.V.: Fiz. Met. Metalloved. **41** (1976) 960.
76 F 1 Figiel, H., Oppelt, A., Dormann, E., Buschow, K.H.J.: Phys. Status Solidi (a) **36** (1976) 275.
76 F 2 Frankevich, D.P., Kirchiv, G.I.: Ivz. Akad. Nauk SSSR Met. **4** (1976) 233.
76 G 1 Gaunt, P., Roy, G.J.: Philos. Mag. **34** (1976) 781.
76 G 2 Gignoux, D., Gomez-Sal, J.C.: J. Magn. Magn. Mater. **1** (1976) 203.
76 G 3 Gignoux, D., Givord, D., Del Moral, A.: Solid State Commun. **19** (1976) 891.
76 G 4 Gignoux, D., Givord, D., Givord, F., Koehler, W.C., Moon, R.M.: Phys. Rev. B **14** (1976) 162.
76 G 5 Givord, D., du Tremolet de Lacheisserie, E.: IEEE Trans. Magn. MAG-**12** (1976) 31.
76 G 6 Givord, D., Givord, F., Gignoux, D., Koehler, W.C., Moon, R.M.: J. Phys. Chem. Solids **37** (1976) 567.
76 G 7 Gratz, E., Kirchmayr, H.R.: J. Magn. Magn. Mater. **2** (1976) 187.
76 G 8 Grössinger, R., Steiner, W., Krec, K.: J. Magn. Magn. Mater. **2** (1976) 196.
76 G 9 Gualtieri, D.M., Narasimhan, K.S.V.L., Takeshita, T.: J. Appl. Phys. **47** (1976) 3432.
76 G 10 Gualtieri, D.M., Narasimhan, K.S.V.L., Wallace, W.E.: AIP Conf. Proc. **34** (1976) 219.
76 G 11 Gubbens, P.C.M., Buschow, K.H.J.: Phys. Status Solidi (a) **34** (1976) 729.
76 G 12 Gubbens, P.C.M., Van der Kraan, A.M., Buschow, K.H.J.: Solid State Commun. **19** (1976) 355.
76 G 13 Güntherodt, G., Schevchik, N.J.: AIP Conf. Proc. **29** (1976) 174.
76 H 1 Halstead, T.K., Abood, N.A., Buschow, K.H.J.: Solid State Commun. **19** (1976) 425.
76 H 2 Hilzinger, H.R.: Phys. Status Solidi (a) **38** (1976) 487.
76 H 3 Hilzinger, H.R., Kronmüller, H.: J. Magn. Magn. Mater. **2** (1976) 11.
76 I 1 Ikonomous, P.F., Yakinthos, J.K.: Z. Phys. B **24** (1976) 77.
76 I 2 Ilyushin, A.S., Wallace, W.E.: J. Solid State Chem. **17** (1976) 131.
76 I 3 Ilyushin, A.S., Wallace, W.E.: J. Solid State Chem. **17** (1976) 373.
76 I 4 Inomata, K.: Jpn. J. Appl. Phys. **15** (1976) 821.
76 I 5 Inomata, K.: J. Phys. Soc. Jpn. **41** (1976) 1890.
76 J 1 Jones, F.G., Tokunaga, M.: IEEE Trans. Magn. MAG-**12** (1976) 968.
76 K 1 Kalychak, Ya.M., Bodak, O.I., Gladyshevski, E.I.: Izv. Akad. Nauk SSSR: Neorg. Mater. **12** (1976) 1149.
76 K 2 Kamino, K., Yamane, T.: Proc. 2nd Int. Workshop on Rare Earth-Cobalt Permanent Magnets and their Applications, Dayton, Ohio, **1976**, p. 377.
76 K 3 Katayama, T., Koizumi, Y., Kawanishi, K., Shibata, T., Tsushima, T.: AIP Conf. Proc. **29** (1976) 606.
76 K 4 Katayama, T., Koizumi, Y., Kawanishi, K., Shibata, T., Tsushima, T.: Bull. Electrotech. Lab. **40** (1976) 1.
76 K 5 Katayama, T., Ohkoshi, M., Koizumi, Y., Shibata, T., Tsushima, T.: Appl. Phys. Lett. **28** (1976) 635.
76 K 6 Kazakov, A.A., Reimer, V.A.: Fiz. Met. Metalloved. **41** (1976) 28.
76 K 7 Kazakov, A.A., Reimer, V.A., Deryagin, A.V., Kudrevatykh, L.: Fiz. Tverd. Tela **18** (1976) 284.
76 K 8 Kronmüller, H., Hilzinger, H.R.: J. Magn. Magn. Mater. **2** (1976) 3.
76 L 1 Lee, E.W., Choudhury, G.M.: J. Less Common Met. **46** (1976) 305.
76 L 2 Lee, E.W., Pourarian, F.: Phys. Status Solidi (a) **33** (1976) 483.
76 L 3 Lee, E.W., Pourarian, F.: Phys. Status Solidi (a) **34** (1976) 383.
76 L 4 Livshits, B.G., Lileev, A.S., Menushenkov, V.P.: Ivz. Akad. Nauk SSSR Met. **4** (1976) 161.
76 L 5 Livshits, B.G., Linetski, Ya.L., Savich, A.N.: Izv. Akad. Nauk SSSR Met. **1** (1976) 139.
76 M 1 Maeland, A.J., Andersen, A.F., Videm, K.: J. Less Common Met. **45** (1976) 347.
76 M 2 Malekzadeh, M., Dariel, M.P., Pickus, M.R.: Mater. Res. Bull. **11** (1976) 1419.
76 M 3 Malik, S.K., Takeshita, T., Wallace, W.E.: Magn. Lett. **1** (1976–1977) 33.
76 M 4 Malik, S.K., Sankar, S.G., Rao, V.U.S., Wallace, W.E.: IEEE Trans. Magn. MAG-**12** (1976) 1003.
76 M 5 McNeely, D., Oesterreicher, H.: J. Less Common Met. **44** (1976) 183.
76 M 6 Melton, K.H., Perkins, R.S.: J. Appl. Phys. **47** (1976) 2671.

76 M 7 Melville, D., Khan, W.I., Rinaldi, S.: IEEE Trans. Magn. MAG-**12** (1976) 1012.
76 M 8 Menth, A.: AIP Conf. Proc. **29** (1976) 600.
76 M 9 Menth, A., Nagel, H.: Appl. Phys. Lett. **29** (1976) 270.
76 M 10 Merches, M., Narasimhan, K.S.V.L., Wallace, W.E., Ilyushin, A.: AIP Conf. Proc. **34** (1976) 233.
76 M 11 Miedema, A.R.: J. Less Common Met. **46** (1976) 67.
76 M 12 Miller, A.E., D'Silva, T., Heinrich, J.P.: AIP Conf. Proc. **29** (1976) 605.
76 M 13 Miller, A.E., D'Silva, T., Rodrigues, H.: IEEE Trans. Magn. MAG-**12** (1976) 1006.
76 M 14 Milstein, J.P.: AIP Conf. Proc. **29** (1976) 592.
76 M 15 Minakata, R., Shiga, M., Nakamura, Y.: J. Phys. Soc. Jpn. **41** (1976) 1435.
76 M 16 Misawa, S., Kanematsu, K.: J. Phys. F **6** (1976) 2119.
76 M 17 Morariu, M., Burzo, E., Barb, D.: J. Phys. (Paris) **37** (1976) C 6-615.
76 M 18 Moreau, J.M., Paccard, D.: Acta Crystallogr. B **32** (1976) 1654
76 M 19 Moreau, J.M., Paccard, D., Parthé, E.: Acta Crystallogr. B **32** (1976) 496.
76 M 20 Muraoka, Y., Shiga, M., Nakamura, Y.: J. Phys. Soc. Jpn. **40** (1976) 905.
76 N 1 Nagai, H., Yoshie, H., Unate, T., Tsujimura, A., Deportes, J.: J. Phys. Soc. Jpn. **41** (1976) 1907.
76 N 2 Nagel, H.: AIP Conf. Proc. **29** (1976) 603.
76 N 3 Nagel, H., Perry, A.J., Menth, A.: J. Appl. Phys. **47** (1976) 2662.
76 N 4 Narasimhan, K.S.V.L.: IEEE Trans. Magn. MAG-**12** (1976) 1009.
76 N 5 Narasimhan, K.S.V.L., Butera, R.A., Kunesh, C.J.: AIP Conf. Proc. **29** (1976) 588.
76 N 6 Narita, K.: Proc. 2nd Int. Workshop on Rare Earth-Cobalt Permanent Magnets and their Applications, Dayton, Ohio, **1976**, p. 55.
76 N 7 Nicklow, R.M., Koon, N.C., Williams, C.M., Milstein, J.B.: Phys. Rev. Lett. **36** (1976) 532.
76 O 1 Oesterreicher, H.: J. Less Common Met. **45** (1976) 111.
76 O 2 Oesterreicher, H.: J. Less Common Met. **46** (1976) 127.
76 O 3 Oesterreicher, H., Parker, F.T.: Magn. Lett. **1** (1976-1978) 77.
76 O 4 Oesterreicher, H., Bittner, H.F., Parker, I.T.: Magn. Lett. **1** (1976-1978) 89.
76 O 5 Oesterreicher, H., Clinton, J., Bittner, H.: Mater. Res. Bull. **11** (1976) 1241.
76 O 6 Oesterreicher, H., Parker, F.T., Misroch, M.: Magn. Lett. **1** (1976) 41.
76 O 7 Oesterreicher, H., Parker, F.T., Misroch, M.: Solid State Commun. **19** (1976) 539.
76 O 8 Okhoshi, M., Kobayashi, H., Katayama, T., Hirana, M., Tsushima, T.: AIP Conf. Proc. **29** (1976) 616.
76 O 9 Oppelt, A., Buschow, K.H.J.: Phys. Rev. B **13** (1976) 4698.
76 O 10 Oppelt, A., Merkel, A., Buschow, K.H.J.: Phys. Status Solidi (a) **37** (1976) K 205.
76 O 11 Ott, H.R., Andres, E., Buher, E., Maita, J.P.: Solid State Commun. **18** (1976) 1303.
76 P 1 Parthé, E.: Acta Crystallogr. B **32** (1976) 2813.
76 P 2 Perkins, R.S., Fischer, P.: Solid State Commun. **20** (1976) 1013.
76 P 3 Perkins, R.S., Bernasconi, J., Wiesmann, H.J.: J. Appl. Phys. **47** (1976) 2679.
76 P 4 Perkins, R.S., Strässler, S., Menth, A.: AIP Conf. Proc. **29** (1976) 610.
76 P 5 Perry, A.J.: IEEE Trans. Magn. MAG-**12** (1976) 962.
76 P 6 Preston, R.S., Taneja, S.P., Drensky, S.M., Dwight, A.E., Kimbal, C.W., Sill, L.R.: AIP Conf. Proc. **29** (1976) 194.
76 R 1 Rhyne, J.J.: AIP Conf. Proc. **29** (1976) 182.
76 R 2 Rosen, M., Klimker, H., Atzmony, U., Dariel, M.P.: J. Phys. Chem. Solids **37** (1976) 513.
76 S 1 Sankar, S.G., Wallace, W.E.: Magn. Lett. **1** (1976) 3.
76 S 2 Sankar, S.G., Wallace, W.E.: AIP Conf. Proc. **29** (1976) 334.
76 S 3 Sankar, S.G., Keller, D.A., Craig, R.S.: Proc. 12th Conf. on Rare Earth Res., Vail, Colorado **1976**, p. 284.
76 S 4 Sankar, S.G., Keller, D.A., Craig, R.S.: J. Magn. Magn. Mater. **1** (1976) 333.
76 S 5 Sarode, P.R., Chetal, A.R.: J. Phys. F **6** (1976) L 163.
76 S 6 Sarode, P.R., Chetal, A.R.: J. Phys. Soc. Jpn. **40** (1976) 1637.
76 S 7 Senno, H., Tawara, Y., Hirota, E.: Appl. Phys. Lett. **29** (1976) 514.
76 S 8 Shechter, H., Bukshpan-Ash, D.: Phys. Rev. B **14** (1976) 3087.
76 S 9 Song Jim Tae: J. Korean Inst. Met. **14** (1976) 117.
76 S 10 Stearns, M.B.: Phys. Rev. B **13** (1976) 1183.
76 S 11 Steiner, W., Planck, A., Weiss, G.: J. Less Common Met. **45** (1976) 143.
76 T 1 Tauber, A., Finnegau, R.D., Schwartz, A., Rothwarf, F.: Proc. 12th Conf. on Rare Earth Res. Vail, Colorado, **1976**, p. 1073.
76 T 2 Timme, R.W.: J. Acoust. Soc. Am. **59** (1976) 459.
76 T 3 Trout, S.R., Graham Jr., C.D.: IEEE Trans. Magn. MAG-**12** (1976) 1015.

76 V 1 Van der Kraan, A.M., Van der Velden, K.N.J., Van Apeldoorn, J.H.F., Gubbens, P.C.M., Buschow, K.H.J.: Phys. Status Solidi (a) **35** (1976) 137.
76 V 2 Van Mal, H.H.: Phys. Res. Repts. Suppl. **1** (1976) 1.
76 V 3 Van Mal, H.H., Buschow, K.H.J., Miedema, A.R.: J. Less Common Met. **49** (1976) 473.
76 V 4 Van Steenwijk, F.J., Huiskamp, W.J., Lefever, H.Th., Thiel, R.C., Buschow, K.H.J.: Proc. Int. Conf. Appl. Mössbauer Effect, **1976**, p. 204.
76 V 5 Van Vucht, J.H.N.: Philips Tech. Rev. **36** (1976) 136.
76 V 6 Van Vucht, J.H.N., Buschow, K.H.J.: J. Less Common Met. **46** (1976) 133.
76 W 1 Walsh, W.M., Rupp, L.W., Schmidt, P.H., Longinotti, L.D.: AIP Conf. Proc. **29** (1976) 686.
76 W 2 Wells, R.G., Ratnam, D.V.: IEEE Trans. Magn. MAG-**12** (1976) 971.
76 W 3 Wiesinger, G.: J. Phys. (Paris) **37** (1976) C 6–585.
76 W 4 Williams, C.M., Koon, N.C., Millstein, J.B.: AIP Conf. Proc. **29** (1976) 191.
76 Y 1 Yakinthos, J.K., Rentzperis, P.J.: Solid State Commun. **18** (1976) 1235.
76 Y 2 Yang, Y.O.: Acta Phys. Sinica **25** (1976) 327.
76 Y 3 Yoshie, H., Matsushima, M., Miyagi, N., Unate, T., Nagai, H., Tsujimura, A.: J. Phys. Soc. Jpn. **41** (1976) 481.

77 A 1 Abbundi, R., Clark, A.E.: IEEE Trans. Magn. MAG-**13** (1977) 1519.
77 A 2 Achard, J.C., Percheron-Guegan, A., Diaz, H., Briancourt, F.: Proc. 2nd Int. Conf. on Hydrogen in Metals, Paris, **1977**, vol. 3, Oxford: Pergamon Press **1978**, Paper 1E12.
77 A 3 Adam, S., Adam, Gh.: Rev. Roum. Phys. **22** (1977) 1063.
77 A 4 Allen, C.W., Liao, K.C., Miller, A.E.: J. Less Common Met. **52** (1977) 109.
77 A 5 Andres, K., Darack, S.: Physica B + C **86–88** (1977) 1071.
77 A 6 Arif, S.K., Ross, J.W., McCausland, M.A.H.: Physica B + C **86–88** (1977) 158.
77 A 7 Arif, S.K., Sigalas, I., Bunbury, D.St.P.: Phys. Status Solidi (a) **41** (1977) 585.
77 A 8 Atzmony, U.: Crystal Field Effects in Metals and Alloys, New York: Plenum Press **1977**, p. 133.
77 A 9 Atzmony, U., Dublon, G.: Physica B + C **86–88** (1977) 167.
77 A 10 Atzmony, U., Dariel, M.P., Dublon, G.: Phys. Rev. **15** (1977) 3565.
77 B 1 Bachmann, K.: J. Magn. Magn. Mater. **4** (1977) 8.
77 B 2 Barabanov, V.A., Gurenko, V.A., Plekhanov, A.F., Sitas, N.I.: Probl. Tekh. Elektrodin. **62** (1977) 31.
77 B 3 Barbara, B., Uehara, M.: Physica B + C **86–88** (1977) 1481.
77 B 4 Barbara, B., Giraud, J.P., Laforest, J., Lemaire, R., Siaud, E., Schweizer, J.: Physica B + C **86–88** (1977) 155.
77 B 5 Bargouth, M.O., Will, G., Buschow, K.H.J.: J. Magn. Magn. Mater. **6** (1977) 129.
77 B 6 Barnea, G.: J. Phys. F **7** (1977) 315.
77 B 7 Bauminger, E.R., Davidov, D., Felner, I., Nowik, I., Ofer, S., Shaltiel, D.: Physica B + C **86–88** (1977) 201.
77 B 8 Belov, K.P., Bocharev, E.P., Epifanova, K.I., Kataev, G.I., Kim, D., Nikitin, S.A., Popov, Yu.F., Chuprikov, G.E.: Fiz. Met. Metalloved. **43** (1977) 295.
77 B 9 Berthier, Y., Devine, R.A.B., Barbara, B.: Phys. Rev. B **16** (1977) 1025.
77 B 10 Besnus, M.J., Bouton, J.M., Clad, R., Herr, A.: Physica B + C **86–88** (1977) 85.
77 B 11 Bodea, M., Barb, D., Burzo, E.: Proc. Int. Conf. Mössbauer Spectr., Bucharest, Romania **1977**, vol. I, p. 413.
77 B 12 Bodenberger, R., Aubert, A.: Phys. Status Solidi (a) **44** (1977) K 7.
77 B 13 Boltich, E.B., Pourarian, F., Wallace, W.E., Smith, H.K., Malik, S.K.: Solid State Commun. **23** (1977) 599.
77 B 14 Bowden, G.J., Day, R.K.: J. Phys. F **7** (1977) 191.
77 B 15 Burzo, E.: Rev. Roum. Phys. **22** (1977) 207.
77 B 16 Burzo, E., Baican, R., Ursu, I.: Solid State Commun. **21** (1977) 263.
77 B 17 Busch, G., Schlapbach, L., Von Waldkirch, Th.: Helv. Phys. Acta **50** (1977) 149.
77 B 18 Buschow, K.H.J.: Physica B + C **86–88** (1977) 79.
77 B 19 Buschow, K.H.J.: Solid State Commun. **21** (1977) 1031.
77 B 20 Buschow, K.H.J.: J. Less Common Met. **51** (1977) 173.
77 B 21 Buschow, K.H.J., Sherwood, R.C.: J. Appl. Phys. **48** (1977) 4643.
77 B 22 Buschow, K.H.J., Sherwood, R.C.: IEEE Trans. Magn. MAG-**13** (1977) 1571.
77 B 23 Buschow, K.H.J., Brouha, M., Biesterbos, J.W.M., Dirks, A.G.: Physica B + C **91** (1977) 261.
77 B 24 Buschow, K.H.J., Brouha, M., Van Daal, H.J., Miedema, R.: Valence Instabilities and Related Narrow Band Phenomena, New York: Plenum Press **1977**, p. 125.

77C1 Carneiro, G.M., Pethick, C.J.: Phys. Rev. B **16** (1977) 1933.
77C2 Chamberlain, J.R.: Physica B+C **86–88** (1977) 138.
77C3 Chappert, J., Yakinthos, J.K.: Crystal Field Effects in Metals and Alloys, New York: Plenum Press **1977**.
77C4 Clark, A.E., Abbundi, R., Savage, H.T., McMasters, O.D.: Physica B+C **86–88** (1977) 73.
77C5 Contardi, V., Feuro, R., Marazza, R., Rossi, R.: J. Less Common Met. **51** (1977) 277.
77C6 Corson, M.R., Kolk, B., Hoy, G., Zimmerman, G.O., Van der Kraan, A.M., Gubbens, P.C.M.: Proc. 4th Conf. Hyperfine Interactions, Madison, New Jersey, **1977.**
77C7 Craik, D.J., Hill, E.W.: Physica B+C **86–88** (1977) 1486.
77C8 Crecelius, G., Maletta, H., Hauck, J.: J. Magn. Magn. Mater. **4** (1977) 40.
77C9 Cullen, J.R., Clark, A.E.: Phys. Rev. B **15** (1977) 4510.
77D1 Davis, R.L., Day, R.K., Dunlop, J.B.: J. Phys. F **7** (1977) 1885.
77D2 Day, R.K.: Physica B+C **86–88** (1977) 71.
77D3 Deportes, J., Givord, D., Lemaire, R., Nagai, H.: Physica B+C **86–88** (1977) 69.
77D4 Deryagin, A.V., Baranov, I.V., Reimer, V.A.: J. Eksp. Teor. Fiz. **73** (1977) 1389.
77D5 Doane, D.A.: J. Appl. Phys. **48** (1977) 2591.
77D6 Doane, D.A.: J. Appl. Phys. **48** (1977) 2062.
77D7 Dormann, E., Buschow, K.H.J.: Physica B+C **86–88** (1977) 75.
77D8 Druzhinin, V.V., Zapasski, S.P.: Fiz. Met. Metalloved. **44** (1977) 929.
77D9 Druzhinin, V.V., Zapasski, S.P., Povyshev, V.M.: Fiz. Tverd. Tela **19** (1977) 159.
77D10 Dublon, G., Atzmony, U.: J. Phys. F **7** (1977) 1069.
77E1 Egorov, V.A., Sidorenko, L.M., Domyshev, V.A.: Fiz. Met. Metalloved. **43** (1977) 885.
77E2 Elattar, A., Takeshita, T., Wallace, W.E., Craig, R.S.: Science **196** (1977) 1093.
77E3 Engkagul, C., Kalceff, W., Miles, P., Stewart, A.M., Taylor, K.N.R.: Physica B+C **86–88** (1977) 171.
77E4 Ermolenko, A.S., Rozhda, A.F.: Fiz. Met. Metalloved. **43** (1977) 312.
77E5 Ermolenko, A.S., Rozhda, A.F.: Fiz. Met. Metalloved. **44** (1977) 535.
77E6 Ermolenko, A.S., Scherbakova, E.V., Rozhda, A.F.: Fiz. Met. Metalloved. **43** (1977) 753.
77E7 Ermolenko, A.S., Korolyov, A.V., Rozhda, A.F.: IEEE Trans. Magn. MAG-**13** (1977) 1339.
77E8 Escudier, P., Gignoux, D., Givord, D., Lemaire, R., Murani, A.P.: Physica B+C **86–88** (1977) 197.
77F1 Felner, I.: Solid State Commun. **21** (1977) 267.
77F2 Fidler, J., Kirchmayr, H.R., Skalicky, P.: Philos. Mag. **35** (1977) 1125.
77F3 Figiel, H., Oppelt, A., Dormann, E., Buschow, K.H.J.: Physica B+C **86–88** (1977) 77.
77F4 Fischer, P., Furrer, A., Busch, G., Schlapbach, L.: Helv. Phys. Acta **50** (1977) 421.
77F5 Franse, J.J.M.: Physica B+C **86–88** (1977) 283.
77G1 Gaunt, P., Mylvaganam, C.K.: J. Appl. Phys. **48** (1977) 2587.
77G2 Gignoux, D., Givord, F.: Solid State Commun. **21** (1977) 499.
77G3 Gignoux, D., Givord, F., Koehler, W.C.: Physica B+C **86–88** (1977) 165.
77G4 Gignoux, D., Givord, F., Lemaire, R.: Crystal Field Effects in Metals and Alloys, New York: Plenum Press **1977**, p. 335.
77G5 Gignoux, D., Givord, F., Schweizer, J.: J. Phys. F **7** (1977) 1823.
77G6 Gignoux, D., Gomez-Sal, J.C., Lemaire, R., De Combarieu, A.: Solid State Commun. **21** (1977) 637.
77G7 Givord, D., Laforest, J., Lemaire, R.: Physica B+C **86–88** (1977) 204.
77G8 Glardon, R., Kurz, W.: J. Mater. Sci. **12** (1977) 658.
77G9 Goldbirsch, R., Weber, H.W., Hilscher, G., Grössinger, R., Steiner W.: Phys. Status Solidi (a) **44** (1977) 593.
77G10 Gratz, E., Poldy, C.A.: Phys. Status Solidi (b) **82** (1977) 159.
77G11 Grössinger, R., Steiner, W., Culetto, F., Kirchmayr, H.R.: Physica B+C **86–88** (1977) 210.
77G12 Gualtieri, D.M., Wallace, W.E.: J. Less Common Met. **55** (1977) 53.
77G13 Gubbens, P.C.M., Van der Kraan, A.M., Buschow, K.H.J.: Physica B+C **86–88** (1977) 199.
77G14 Gubbens, P.C.M.: Ph.D. Thesis, University of Delft, **1977**.
77G15 Guidotti, R.A., Atkinson, G.B., Wong, M.M.: J. Less Common Met. **52** (1977) 13.
77H1 Hamano, M., Yajima, S.: Trans. Jpn. Inst. Met. **18** (1977) 185.
77H2 Heinrich, J.P., Miller, A.E.: IEEE Trans. Magn. MAG-**13** (1977) 1336.
77H3 Hendy, P., Lee, E.W.: J. Phys. F **7** (1977) 1835.
77H4 Hilscher, G., Buis, N., Franse, J.J.M.: Physica B+C **91** (1977) 170.
77H5 Hodosov, E.F., Linnik, A.I., Kobzenko, G.F., Ivanchenko, V.G.: Fiz. Met. Metalloved. **44** (1977) 433.
77H6 Hunter, J., Taylor, K.N.R.: Physica B+C **86–88** (1977) 161.
77I1 Ikeda, K.: J. Less Common Met. **52** (1977) 101.

77I2 Ikeda, K.: J. Phys. Soc. Jpn. **42** (1977) 1541.
77I3 Ilyushin, A.S.: Fiz. Met. Metalloved. **43** (1977) 1249.
77I4 Ilyushin, A.S., Terenkov, Yu.V.: Vestn. Mosk. Univ. Fiz. Astronomiya **18** (1977) 139.
77I5 Inomata, K., Oshima, T., Ido, T., Yamada, M.: Appl. Phys. Lett. **30** (1977) 669.
77I6 Irkhin, Yu.P.: Physica B+C **86–88** (1977) 1434.
77K1 Kelarev, V.V., Sidorov, S.K., Pirogov, A.N., Vohmianin, A.P.: J. Eksp. Teor. Fiz. Pisma **26** (1977) 330.
77K2 Kelarev, V.V., Pirogov, A.N., Vohmianin, A.P., Turkhan, A.P., Sidorov, S.K.: Fiz. Met. Metalloved. **43** (1977) 1181.
77K3 Kitada, M.: J. Jpn. Inst. Met. **41** (1977) 412.
77K4 Kitada, M.: J. Mater. Sci. **12** (1977) 2134.
77K5 Koon, N.C., Williams, C.M.: US Navy J. Underwater Acoustics **27** (1977) 127.
77K6 Koot, M.E., Milheava, V.I.: Russ. J. Inorg. Chem. **22** (1977) 1581.
77K7 Kütterer, R., Hilzinger, H.R., Kronmüller, H.: J. Magn. Magn. Mater. **4** (1977) 1.
77L1 Le Roy, J., Moreau, J.M., Paccard, D., Parthé, E.: Acta Crystallogr. B **33** (1977) 3406.
77L2 Lee, E.W., Hendy, P.: Physica B+C **86–88** (1977) 163.
77L3 Livingston, J.D., Martin, D.L.: J. Appl. Phys. **48** (1977) 1350.
77L4 Luijpen, M.G., Gubbens, P.C.M., Van der Kraan, A.M., Buschow, K.H.J.: Physica B+C **86–88** (1977) 141.
77M1 Makarova, G.M., Magat, L.M.: Fiz. Met. Metalloved. **43** (1977) 1003.
77M2 Malik, S.K., Wallace, W.E.: Solid State Commun. **24** (1977) 283.
77M3 Malik, S.K., Wallace, W.E.: Solid State Commun. **24** (1977) 417.
77M4 Malik, S.K., Arlinghaus, K.J., Wallace, W.E.: Phys. Rev. B **16** (1977) 1242.
77M5 Malik, S.K., Takeshita, T., Wallace, W.E.: Solid State Commun. **23** (1977) 599.
77M6 Melton, K.N., Nagel, H.: J. Appl. Phys. **48** (1977) 2608.
77M7 Mendelsohn, M.G., Gruen, D.M., Dwight, A.E.: Nature **269** (1977) 45.
77M8 Meyer, C., Srour, B., Gros, Y., Hartman-Boutron, F.: J. Phys. (Paris) **38** (1977) 1449.
77M9 Miller, A.E., D'Silva, T., Shanley, J.: J. Appl. Phys. **48** (1977) 3466.
77M10 Moldovan, A.G., Malik, S.K., Wallace, W.E.: Phys. Status Solidi (a) **43** (1977) 317.
77M11 Moriya, T.: Physica B+C **86–88** (1977) 356.
77M12 Muraoka, Y., Shiga, M., Nakamura, Y.: Phys. Status Solidi (a) **42** (1977) 369.
77M13 Muraoka, Y., Shiga, M., Nakamura, Y.: J. Phys. Soc. Jpn. **42** (1977) 2067.
77N1 Narasimhan, K.S.V.L., Wallace, W.E.: IEEE Trans. Magn. MAG-**13** (1977) 1333.
77N2 Nesterin, V.A., Vasilev, V.V., Mikhailov, Yu.A.: Elektrotechnika **48** (1977) 46.
77N3 Nikiforov, A.K., Adadvorov, G.A., Kuznetsov, A.A., Mishin, D.D.: Izv. Vyssh. Uchebn. Zaved. Fiz. **5** (1977) 137.
77O1 Oesterreicher, H.: J. Less Common Met. **53** (1977) 245.
77O2 Oesterreicher, H.: Phys. Status Solidi (a) **39** (1977) K 41.
77O3 Oesterreicher, H.: Phys. Status Solidi (a) **40** (1977) K 139.
77O4 Oesterreicher, H., Bittner, H.: Phys. Status Solidi (a) **41** (1977) K 101.
77O5 Oesterreicher, H., McNeely, D.: J. Less Common Met **53** (1977) 235.
77O6 Oesterreicher, H., Parker, F.T., Misroch, M.: Physica B+C **86–88** (1977) 1475.
77O7 Oesterreicher, H., Parker, F.T., Misroch, M.: IEEE Trans. Magn. MAG-**13** (1977) 1331.
77O8 Ohkoshi, M., Kobayashi, H.: IEEE Trans. Magn. MAG-**13** (1977) 1158.
77O9 Ohkoshi, M., Kobayashi, H., Katayama, T., Hirano, M., Tsushima, T.: Physica B+C **86–88** (1977) 195.
77O10 Ojima, T., Tomizawa, S., Toneyama, T., Hori, T.: IEEE Trans. Magn. MAG-**13** (1977) 1317.
77O11 Olcese, G.L.: J. Phys. Chem. Solids **38** (1977) 1239.
77O12 Oppelt, A., Schäfer, J., Wiesinger, G., Buschow, K.H.J.: J. Magn. Magn. Mater. **6** (1977) 163.
77O13 Ortbauer, H., Steiner, W., Haferl, R.: Phys. Status Solidi (a) **39** (1977) 157.
77P1 Parthé, E., Moreau, J.M.: J. Less Common Met. **53** (1977) 1.
77P2 Parviainen, S., Jaakkola, J.: Proc. Int. Conf. Properties of Solid under High Pressure, Leuwen **1977**, p. 33.
77P3 Perkins, R.S., Strässler, S.: Phys. Rev. B **15** (1977) 477.
77P4 Perkins, R.S., Strässler, S.: Phys. Rev. B **15** (1977) 490.
77P5 Perkins, R.S., Strässler, S.: Physica B+C **86–88** (1977) 1479.
77P6 Perry, A.J.: J. Less Common Met. **51** (1977) 153.
77P7 Puzanova, T.Z., Shur, Ya.S.: Fiz. Met. Metalloved. **43** (1977) 743.
77R1 Rhyne, J.J., Koon, N.C., Milstein, J.B., Alperin, H.A.: Physica B+C **86–88** (1977) 149.
77R2 Rinaldi, S., Cullen, J.R., Blessing, G.V.: Phys. Lett. **61** A (1977) 465.

77R3 Rykhal, R.M., Zarechnyuk, O.S., Jarmolyuk, Ya.P.: Dopov. Akad. Nauk Ukr. SSR Ser. A **3** (1977) 265.
77S1 Sandrock, G.D.: Proc. 12th Intersociety Energy Conversion Engineering Conf., American Nuclear Soc. **1977**, vol. 1, p. 951.
77S2 Sarode, P.R., Chetal, A.R.: J. Phys. C **10** (1977) 153.
77S3 Sarode, P.R., Chetal, A.R.: J. Phys. F **7** (1977) 1103.
77S4 Sarynin, V.K., Burnasheva, V.V., Semenko, K.H.: Izv. Akad. Nauk SSSR Met. **4** (1977) 69.
77S5 Savage, H., Clark, A., Koon, N., Williams, C.: IEEE Trans. Magn. MAG-**13** (1977) 1517.
77S6 Searle, C.W., Kunkel, H.P., Kupca, S., Maartense, I.: Phys. Rev. B **15** (1977) 3305.
77S7 Shabanova, I.N., Efimenko, A.I., Trapeznikov, V.A.: J. Electron Spectrosc. Relat. Phenom. **10** (1977) 197.
77S8 Shaltiel, D., Jacob, I., Davidov, D.: J. Less Common Met. **53** (1977) 117.
77S9 Shiga, M., Minakata, R., Tsuchida, T., Nakamura, Y.: J. Phys. Soc. Jpn. **42** (1977) 814.
77S10 Steiner, W., Choi, B.K.: Phys. Status Solidi (a) **43** (1977) 111.
77S11 Steiner, W., Haferl, R.: Phys. Status Solidi (a) **42** (1977) 739.
77S12 Steiner, W., Hilscher, H., Haferl, R.: Phys. Status Solidi (a) **43** (1977) 437.
77S13 Steiner, W., Mayerhofer, J., Grössinger, R.: Physica B+C **86–88** (1977) 192.
77S14 Streever, R.L.: Phys. Rev. B **16** (1977) 1796.
77S15 Strnat, K.J., Ray, A.E., Mildrum, H.F.: IEEE Trans. Magn. MAG-**13** (1977) 1323.
77S16 Szpunar, B., Kozarewski, B.: Acta Phys. Pol. A **51** (1977) 125.
77S17 Szpunar, B., Kozarewski, B.: Phys. Status Solidi (b) **82** (1977) 205.
77S18 Szpunar, B., Lindgard, P.A.: Phys. Status Solidi (b) **82** (1977) 449.
77T1 Takahashi, M., Kanaya, M., Kadowaki, S., Wakiyama, T., Anayama, T.: Jpn. J. Appl. Phys. **16** (1977) 1285.
77T2 Takeshita, T., Wallace, W.E.: J. Less Common Met. **55** (1977) 61.
77T3 Tanaka, S., Flanagan, T.B.: J. Less Common Met. **51** (1977) 79.
77T4 Tanaka, S., Clewley, J.D., Flanagan, T.B.: J. Less Common Met. **56** (1977) 137.
77T5 Tanaka, S., Clewley, J.D., Flanagan, T.B.: J. Phys. Chem. **81** (1977) 1684.
77T6 Tomala, K., Czjzek, G., Fink, J., Schmidt, H.: Solid State Commun. **24** (1977) 857.
77U1 Uehara, M.: J. Appl. Phys. **48** (1977) 5197.
77V1 Van Diepen, A.M., Buschow, K.H.J.: Solid State Commun. **22** (1977) 113.
77V2 Van Steenwijk, F.J., Huiskamp, W.J., Lefever, H.Th., Thiel, R.C., Buschow, K.H.J.: Physica B+C **86–88** (1977) 89.
77V3 Van der Kraan, A.M., Buschow, K.H.J.: Physica B+C **86–88** (1977) 93.
77V4 Van der Kraan, A.M., Gubbens, P.C.M., Buschow, K.H.J.: Proc. Int. Conf. Mössbauer Spectr., Bucharest, Romania **1977**, vol. I, p. 121.
77W1 Webb, D.C., Davis, K.I., Koon, N.C., Ganguly, A.K.: Appl. Phys. Lett. **31** (1977) 245.
77W2 Williams, C.M., Koon, N.C.: Physica B+C **86–88** (1977) 147.
77Y1 Yakinthos, J.K.: Physica B+C **86–88** (1977) 207.
77Y2 Yakinthos, J.K.: Phys. Status Solidi (b) **82** (1977) 349.
77Y3 Yakinthos, J.K., Roudat, E.: Phys. Status Solidi (a) **39** (1977) K 151.
77Y4 Yanovsky, R., Bauminger, E.R., Nowik, I., Ofer, S.: Physica B+C **86–88** (1977) 145.
77Y5 Yoshie, H.: J. Phys. Soc. Jpn. **43** (1977) 862.

78A1 Abbundi, R., Clark, A.E.: J. Appl. Phys. **49** (1978) 1969.
78A2 Achard, J.C., Percheron-Guegan, A., Sarradin, J., Bronoel, C.: Proc. Int. Symp. on Hydrides for Energy Storage, Geilo, Norway, 1977, Oxford: Pergamon Press **1978**, p. 485.
78A3 Andersen, A.F.: Proc. Int. Symp. on Hydrides for Energy Storage, Geilo, Norway, 1977, Oxford: Pergamon Press **1978**, p. 61.
78A4 Andreef, A., Valter, K., Grissmann, Kh., Kaun, L.P., Lippold, B., Mats, V., Frandkhaim, T.: Joint Institute for Nuclear Research Dubna, USSR **1978**, Comm. P 14-11324.
78A5 Andres, K.: Cryogenics **18** (1978) 473.
78A6 Arbuzov, M.P., Pavlyukov, A.A., Opanasenko, O.S., Gikhman, Ye.I.: Fiz. Met. Metalloved. **46** (1978) 441.
78A7 Atzmony, U., Dariel, M.P.: Phys. Rev. B **17** (1978) 396.
78A8 Aubert, G., Gignoux, D., Givord, F., Lemaire, R., Michelutti, B.: Solid State Commun. **25** (1978) 85.
78B1 Bauminger, E.R., Felner, I., Ofer, S.: J. Magn. Magn. Mater. **7** (1978) 317.
78B2 Belov, K.P., Vasilkovski, V.A., Kovtun, A.K., Kupriyanov, A.K., Nikitin, S.A., Ostrovski, V.F.: Fiz. Tverd. Tela **20** (1978) 600.
78B3 Berry, B.S., Pritchet, W.C., Savage, H.T.: J. Appl. Phys. **49** (1978) 6075.

78 B 4 Besnus, M.J., Bauer, P., Genin, J.M.: J. Phys. F **8** (1978) 191.
78 B 5 Blaettner, H.E., Strnat, K.J., Ray, A.E.: The Rare Earth in Modern Science and Technology, New York: Plenum Press **1978**, p. 421.
78 B 6 Blessing, G.V., Cullen, J.R., Rinaldi, S.: Phys. Lett. **66** A (1978) 498.
78 B 7 Bowden, G.J., Day, R.K.: J. Phys. F **8** (1978) 533.
78 B 8 Buchal, C., Fischer, K.J., Kubota, M., Mueller, R.M., Pobell, F.: J. Phys. Lett. **39** (1978) L 457.
78 B 9 Bukshpan, D., Shechter, H., Nowik, I.: J. Magn. Magn. Mater **7** (1978) 212.
78 B 10 Burnasheva, V.V., Yartis, V.A., Fadeeva, N.V., Solovev, P., Semenenko, K.N.: Dokl. Akad. Nauk SSSR **238** (1978) 844.
78 B 11 Burzo, E.: Rev. Roum. Phys. **23** (1978) 689.
78 B 12 Burzo, E.: Phys. Rev. B **17** (1978) 1414.
78 B 13 Burzo, E.: Solid State Commun. **25** (1978) 525.
78 B 14 Burzo, E., Baican, R.: J. Less Common Met. **60** (1978) 315.
78 B 15 Burzo, E., Balanescu, M.: Solid State Commun. **28** (1978) 693.
78 B 16 Burzo, E., Lazar, D.P., Palii, I.: Phys. Status Solidi (a) **45** (1978) K 145.
78 B 17 Busch, G., Schlapbach, L.: Helv. Phys. Acta **51** (1978) 5.
78 B 18 Busch, G., Schlapbach, L., Von Waldkirch, T.: J. Less Common Met. **60** (1978) 83.
78 B 19 Busch, G., Schlapbach, L., Von Waldkirch, T.: Proc. Int. Symp. on Hydrides for Energy Storage, Geilo, Norway, 1977, Oxford: Pergamon Press **1978**, p. 287.
78 B 20 Buschow, K.H.J.: Proc. Int. Symp. on Hydrides for Energy Storage, Geilo, Norway, 1977, Pergamon Oxford **1978**, p. 273.
78 B 21 Buschow, K.H.J., Miedema, A.R.: Proc. Int. Symp. on Hydrides for Energy Storage, Geilo, Norway, 1977, Oxford: Pergamon Press **1978**, p. 15.
78 B 22 Buschow, K.H.J., Sherwood, R.C.: J. Appl. Phys. **49** (1978) 1480.
78 B 23 Buschow, K.H.J., Van der Kraan, A.M.: J. Phys. F **8** (1978) 921.
78 C 1 Careiron, M., Gignoux, D.: Solid State Commun. **25** (1978) 735.
78 C 2 Carstens, D.H.W.: J. Nucl. Mater. **73** (1978) 50.
78 C 3 Carstens, D.H.W.: J. Less Common Met. **61** (1978) 253.
78 C 4 Chi, M.C., Gyorgy, E.M., Alben, R.: J. Appl. Phys. **49** (1978) 2016.
78 C 5 Clark, A.E., Abbundi, R., Gillmor, W.R.: IEEE Trans. Magn. MAG-**14** (1978) 542.
78 C 6 Corson, M.R., Kolk, B., Hoy, G., Zimmerman, G.O., Van der Kraan, A.M., Gubbens, P.C.M.: Hyp. Int. **4** (1978) 411.
78 C 7 Creagh, D.C., Ayling, S.H.: J. Mater. Sci. **13** (1978) 113.
78 C 8 Croat, J.J.: J. Appl. Phys. **49** (1978) 1972.
78 C 9 Cullen, J.R., Rinaldi, S., Blessing, G.V.: J. Appl. Phys. **49** (1978) 1960.
78 C 10 Cullen, J.R., Rinaldi, S., Blessing, G.: Inst. Phys. Conf. Ser. **37** (1978) 79.
78 C 11 Cullen, J.R., Blessing, G., Rinaldi, S., Callen, E.: J. Magn. Magn. Mater. **7** (1978) 160.
78 D 1 Deryagin, A.V., Andreev, A.V., Reimer, V.A.: J. Eksp. Teor. Fiz. **74** (1978) 1789.
78 D 2 Deryagin, A.V., Kudrevatykh, N.V., Moskalev, V.N.: Phys. Status Solidi (a) **45** (1978) 71.
78 D 3 Deryagin, A.V., Kudrevatykh, N.V., Moskalev, V.N.: Fiz. Met. Metalloved. **45** (1978) 718.
78 E 1 Ermolenko, A.S., Rozhda, A.F.: IEEE Trans. Magn. MAG-**14** (1978) 676.
78 E 2 Ermolenko, A.S., Korolev, A.V., Rozhda, A.F.: Izv. Akad. Nauk SSSR Ser. Fiz. **42** (1978) 1762.
78 F 1 Felner, I., Nowik, I.: Solid State Commun. **28** (1978) 67.
78 F 2 Felner, I., Nowik, I.: J. Phys. Chem. Solids **39** (1978) 951.
78 F 3 Fidler, J., Skalicky, P.: Proc. 19th Int. Conf. on Electron Microscopy, Toronto, Canada **1978**, vol. I, p. 470.
78 F 4 Fidler, J., Skalicky, P.: Phys. Status Solidi (a) **50** (1978) 73.
78 F 5 Figiel, H., Dormann, E., Oppelt, A.: Proc. 10th Polish NMR Seminar, Crakow, Poland **1978**, p. 243.
78 F 6 Fischer, P., Hälg, W., Schlapbach, L., Von Waldkirch, Th.: Helv. Phys. Acta **51** (1978) 4.
78 F 7 Fischer, P., Hälg, W., Schlapbach, L., Yvon, K.: J. Less Common Met. **60** (1978) 1.
78 F 8 Foner, S., McNiff Jr., E.J., Oesterreicher, H., Parker, F.T., Misroch, M.: J. Appl. Phys. **49** (1978) 2061.
78 F 9 Furrer, A., Fischer, P., Hälg, W., Schlapbach, L.: Proc. Int. Symp. on Hydrides for Energy Storage, Geilo, Norway, 1977, Oxford: Pergamon Press **1978**, p. 73.
78 G 1 Gignoux, D., Givord, F., Lemaire, R., Nguyen Van Tinh, N.: Inst. Phys. Conf. Ser. **37** (1978) 300.
78 G 2 Goudy, A., Wallace, W.E., Craig, R.S., Takeshita, T.: Adv. Chem. Ser. **167** (1978) 312.
78 G 3 Gualtieri, D.M., Wallace, W.E.: J. Less Common Met. **61** (1978) 261.
78 G 4 Gubbens, P.C.M., Van der Kraan, A.M.: J. Magn. Magn. Mater. **9** (1978) 349.
78 G 5 Gubbens, P.C.M., Van der Kraan, A.M., Buschow, K.H.J.: Solid State Commun. **26** (1978) 107.

78 H 1 Hamano, M., Yajima, S.: Proc. 2nd Int. Symp. Magnetic Anisotropy and Coercivity in Rare-Earth-Transition Metal Alloys, California **1978**, p. 102.
78 H 2 Hardman, K., James, W.J., Yelon, W.: The Rare Earths in Modern Science and Technology, New York: Plenum Press **1978**, p. 403.
78 H 3 Heinrick, J.P., Miller, A.E.: J. Appl. Phys. **49** (1978) 1943.
78 H 4 Hendy, P., Lee, E.W.: Phys. Status Solidi (a) **50** (1978) 101.
78 H 5 Hilscher, G., Rais, H.: J. Phys. F **8** (1978) 511.
78 H 6 Hodosov, Ye.F., Linnik, A.I., Kobzenko, G., Ivanchenko, V.G.: Fiz. Met. Metalloved. **44** (1978) 178.
78 I 1 Inoue, T., Sparlin, D.M., James, W.J.: The Rare Earth in Modern Science and Technology, New York: Plenum Press **1978**, p. 415.
78 K 1 Khan, W.I., Melville, D.: Int. Phys. Conf. Ser. **37** (1978) 305.
78 K 2 Khan, W.I., Melville, D.: Phys. Status Solidi (a) **48** (1978) 209.
78 K 3 Khan, W.I., Melville, D., Montenegro, J.F.D.: IEEE Trans. Magn. MAG-**14** (1978) 674.
78 K 4 Klimker, H., Rosen, M.: J. Magn. Magn. Mater. **7** (1978) 361.
78 K 5 Kononenko, A.S., Sergeev, V.V., Spidchenko, V.K.: Fiz. Met. Metalloved. **46** (1978) 496.
78 K 6 Kononenko, A.S., Sergeev, V.V., Malakhov, G.V., Altman, V.A., Nikolaeva, G.I., Pashkov, P.P.: Izv. Akad. Nauk SSSR Met. **5** (1978) 184.
78 K 7 Koon, N.C., Rhyne, J.J.: Solid State Commun. **26** (1978) 537.
78 K 8 Koon, N.C., Williams, C.M.: J. Appl. Phys. **49** (1978) 1948.
78 K 9 Korolev, A.V., Ermolenko, A.S., Lagunova, V.I.: Fiz. Met. Metalloved. **46** (1978) 656.
78 K 10 Kost, M.E., Shilov, A.L.: Izv. Akad. Nauk SSSR Neorg. Mater. **14** (1978) 1629.
78 K 11 Kronmüller, H.: J. Magn. Magn. Mater. **7** (1978) 341.
78 K 12 Kudrevatykh, N.V., Deryagin, A.V., Kazakov, A.A., Reimer, A.V., Moskalev, N.V.: Fiz. Met. Metalloved. **45** (1978) 1169.
78 K 13 Kumar, K., Das, D., Wettstein, E.: J. Appl. Phys. **49** (1978) 2052.
78 K 14 Kupriyanov, A.K., Nikitin, S.A., Torchinova, R.S.: Fiz. Met. Metalloved. **45** (1978) 945.
78 L 1 Lemaire, R.: Proc. Symp. on Physical Properties of Solids in High Magnetic Fields, Wroclaw, Poland **1978**, p. 101.
78 L 2 Lindgard, P.A., Szpunar, B.: J. Magn. Magn. Mater. **7** (1978) 124.
78 L 3 Linetski, Ya.L., Knizhnik, Ye.G., Volski, A.A.: Fiz. Met. Metalloved. **46** (1978) 1197.
78 L 4 Livingston, J.D.: IEEE Trans. Magn. MAG-**14** (1978) 668.
78 L 5 Lundin, C.E., Lynch, F.E.: Proc. Int. Symp. on Hydrides for Energy Storage, Geilo, Norway, 1977, Oxford: Pergamon Press **1978**, p. 395.
78 M 1 Maeda, H.: Phys. Status Solidi (a) **45** (1978) 445.
78 M 2 Maeda, H.: Phys. Status Solidi (a) **46** (1978) 233.
78 M 3 Malekzadeh, M., Pickus, M.R.: Appl. Phys. Lett. **33** (1978) 108.
78 M 4 Malik, S.K., Wallace, W.E., Takeshita, T.: Solid State Commun. **28** (1978) 359.
78 M 5 Malik, S.K., Wallace, W.E., Takeshita, T.: Solid State Commun. **28** (1978) 977.
78 M 6 Martis, R.J.J., Gupta, N., Sankar, S.G., Rao, V.U.S.: J. Appl. Phys. **49** (1978) 2070.
78 M 7 Melville, D., Al-Rabl, K.M.: Inst. Phys. Conf. Ser. **37** (1978) 293.
78 M 8 Melville, D., Asti, G.: Physica B+C **95** (1978) 395.
78 M 9 Mendelsohn, M.H., Gruen, D.M.: Mater. Res. Bull. **13** (1978) 1221.
78 M 10 Merches, M., Narasimhan, K.S.V.L., Wallace, W.E.: The Rare Earth in Modern Science and Technology, New York: Plenum Press **1978**, p. 409.
78 M 11 Merches, M., Sankar, S.G., Wallace, W.E.: J. Appl. Phys. **49** (1978) 2055.
78 M 12 Misawa, S.: J. Phys. F **8** (1978) L 263.
78 M 13 Mishra, S.G., Ramakrishnan, T.V.: Phys. Rev. B **18** (1978) 2308.
78 M 14 Mishra, R.C., Thomas, G.: J. Appl. Phys. **49** (1978) 2067.
78 M 15 Mook, A., Koon, N.C.: J. Appl. Phys. **49** (1978) 2133.
78 M 16 Moskaitis, R.J., Butera, R.A.: J. Appl. Phys. **49** (1978) 1443.
78 N 1 Nagel, H., Menth, A.: IEEE Trans. Magn. MAG-**14** (1978) 671.
78 N 2 Narasimhan, K.S.V.L.: The Rare Earth in Modern Science and Technology, New York: Plenum Press, **1978**, p. 81.
78 N 3 Narasimhan, K.S.V.L., Wells, M.G.H., Ratnam, D.V.: J. Appl. Phys. **49** (1978) 2072.
78 O 1 Oesterreicher, H., Misroch, M., Parker, F.T.: IEEE Trans. Magn. MAG-**14** (1978) 665.
78 O 2 Oesterreicher, H., Parker, F.T., Misroch, M.: J. Appl. Phys. **49** (1978) 2058.
78 O 3 Oesterreicher, H., Parker, F.T., Misroch, M.: Phys. Rev. B **18** (1978) 480.
78 O 4 Oesterreicher, H., Parker, F.T., Misroch, M.: J. Appl. Phys. **16** (1978) 67.

78 O 5 Oesterreicher, H., Parker, F.T., Misroch, M.: Appl. Phys. **16** (1978) 185.
78 O 6 Oliver, F.W., West, K.W., Cohen, R.L., Buschow, K.H.J.: J. Phys. F **8** (1978) 701.
78 P 1 Poldy, C.A., Gratz, E.: J. Magn. Magn. Mater. **8** (1978) 223.
78 P 2 Pourarian, F.: Phys. Lett. **67** A (1978) 407.
78 P 3 Puzanova, T.Z., Shura, Ya.S.: Fiz. Met. Metalloved. **46** (1978) 283.
78 R 1 Rhyne, J.J., Koon, N.C.: J. Appl. Phys. **49** (1978) 2133.
78 R 2 Rhyne, J.J., Sankar, S.G., Wallace, W.E.: The Rare Earth in Modern Science and Technology, New York: Plenum Press **1978**, p. 63.
78 R 3 Riedi, P.C.: Solid State Commun. **27** (1978) 673.
78 R 4 Rinaldi, S., Cullen, J.: Phys. Rev. B **18** (1978) 3677.
78 R 5 Ross, J.W., Walley, S.P.: Inst. Phys. Conf. Ser. **37** (1978) 155.
78 S 1 Sandrock, G.D.: Proc. 2nd World Hydrogen Energy Conf., Zürich, Pergamon Press **1978**, p. 1625.
78 S 2 Sankar, S.G., Gualtieri, D.M., Wallace, W.E.: The Rare Earth in Modern Science and Technology, New York: Plenum Press **1978**, p. 69.
78 S 3 Savage, H.T., Abbundi, R.: IEEE Trans. Magn. MAG-**14** (1978) 545.
78 S 4 Savage, H.T., Clark, A.E.: Inst. Phys. Conf. Ser. **37** (1978) 310.
78 S 5 Savage, H.T., Abbundi, R., Clark, A.E., Cullen, J.R., Rinaldi, S.: J. Appl. Phys. **49** (1978) 1995.
78 S 6 Schinkel, C.J.: J. Phys. F **8** (1978) L 87.
78 S 7 Sery, R.S., Savage, H.T., Tanner, B.K., Clark, G.F.: J. Appl. Phys. **49** (1978) 2010.
78 S 8 Shaltiel, D.: J. Less Common Met. **62** (1978) 407.
78 S 9 Shibata, T., Katayama, T., Tsushima, T.: J. Appl. Phys. **49** (1978) 2075.
78 S 10 Shiga, M., Nakamura, Y.: Inst. Phys. Conf. Ser. **39** (1978) 540.
78 S 11 Shimizu, M., Yamada, H.: J. Phys. Soc. Jpn. **44** (1978) 1521.
78 S 12 Shinar, J., Shaltiel, D., Davidov, D., Grayevsky, A.: J. Less Common Met. **60** (1978) 209.
78 S 14 Shur, Ya.S., Glazer, A.A., Gan, V.G., Puzanova, T.Z.: Izv. Akad. Nauk SSSR Ser. Fiz. **42** (1978) 1738.
78 S 15 Siegman, H.C., Schlapbach, L., Brundle, C.R.: Phys. Rev. Lett. **40** (1978) 972.
78 S 16 Slebarski, A.: J. Less Common Met. **59** (1978) 1.
78 S 17 Slebarski, A., Chelkovski, A.: J. Less Common Met. **57** (1978) 125.
78 S 18 Steiner, W., Ortbauer, H., Gratz, E.: Proc. Int. Conf. Magnetism of Rare Earth and Actinides, Durham 1977, UK, London Inst. Phys. **1978**, p. 299.
78 S 19 Steiner, W., Gratz, G., Ortbauer, H., Camen, H.W.: J. Phys. F **8** (1978) 1525.
78 S 20 Streever, R.L.: Phys. Lett. **65** A (1978) 360.
78 S 21 Sukhorukov, R.Yu., Turov, V.D.: Izv. Vyssh. Uchebn. Zaved. Priborostr. **21** (1978) 54.
78 S 22 Sylvester, J.G., Ambrosio, A., Blackstead, H.A., Miller, A.E.: J. Appl. Phys. **49** (1978) 1564.
78 T 1 Takeshita, T., Malik, S.K., Wallace, W.E.: J. Solid State Chem. **23** (1978) 271.
78 T 2 Tari, A.: Phys. Status Solidi (a) **46** (1978) 173.
78 T 3 Tsushima, T., Okhoshi, M., Hirano, M., Katayama, T.: Bull. Electrotech. Lab. Jpn. **42** (1978) 41.
78 U 1 Uehara, M.: J. Appl. Phys. **49** (1978) 4155.
78 U 2 Uehara, M.: Trans. Nat. Res. Inst. Met. **20** (1978) 366.
78 U 3 Ulyanov, A.I., Novikov, V.F., Deryagin, A.V.: Fiz. Met. Metalloved. **45** (1978) 212.
78 V 1 Vittoria, C., Lubitz, P., Ritz, V.: J. Appl. Phys. **49** (1978) 4908.
78 V 2 Von Waldkirch, T., Zürcher, P.: Appl. Phys. Lett. **33** (1978) 689.
78 W 1 Wallace, W.E.: Topics in Applied Physics, Berlin: Springer **1978**, vol. 28, p. 182.
78 W 2 Wallace, W.E., Rao, V.U.S., Sankar, S.G., Merches, M.: Proc. 2nd Int. Symp. Magnetic Anisotropy and Coercivity in Rare-Earth-Transition Metal Alloys, California **1978**, p. 118.
78 W 3 Wallace, W.E., Malik, S.K., Takeshita, T., Sankar, S.G., Gualtieri, D.M.: J. Appl. Phys. **49** (1978) 1486.
78 W 4 Williams, C.M., Koon, N.C.: Solid State Commun. **27** (1978) 81.
78 W 5 Williams, C.M., Koon, N.C.: Proc. Int. Conf. Magnetism of Rare Earth and Actinides, Durham England, 1977, UK, London, Inst. Phys. **1978**, p. 284.
78 W 6 Williams, C.M., Koon, N.C., Milstein, J.B.: J. Phys. Chem. Solids **39** (1978) 823.
78 Y 1 Yakinthos, J.K.: J. Phys. Chem. Solids **39** (1978) 485.
78 Y 2 Yakinthos, J.K.: Inst. Phys. Conf. Ser. **37** (1978) 315.
78 Y 3 Yoneyama, T., Tomizawa, S., Hori, T., Ojima, T.: Proc. 3rd Int. Workshop on Rare Earth Permanent Magnets and Their Appl., Univ. of Dyton, Ohio **1978**, p. 406.
78 Y 4 Yoshie, H.: J. Phys. Soc. Jpn. **44** (1978) 1158.
78 Z 1 Zarek, W., Winiarska, A., Ogrodnik, A., Chelkowski, A.: Acta Phys. Pol. A **53** (1978) 397.
78 Z 2 Zinovyev, V.Ye., Sperelup, V.I., Petrova, L.N., Plekhanov, A.F., Alyoshin, A.P.: Fiz. Met. Metalloved. **46** (1978) 1306.

79 A 1 Abbundi, R., Clark, A.E., Koon, N.C.: J. Appl. Phys. **50** (1979) 1671.
79 A 2 Achard, J.C., Givord, F., Percheron-Guegan, A., Soubeyroux, J.L., Tasset, F.: J. Phys. (Paris) **40** (1979) C 5-218.
79 A 3 Alberdi, J.M., Barandiaran, J.M., Ilarraz, M.: Phys. Status Solidi (a) **52** (1979) K 101.
79 A 4 Andres, K., Darak, S., Otto, H.R.: Phys. Rev. B **19** (1979) 5475.
79 A 5 Arbuzov, M.P., Pavlyukov, A.A., Opanasenko, O.S., Krakovich, E.V.: Poroshk. Metall. **18** (1979) 41.
79 A 6 Azoulay, J., Ley, L.: Solid State Commun. **31** (1979) 131.
79 B 1 Belkbir, L., Gerard, N., Percheron-Guegan, N., Achard, J.C.: Int. J. Hydrogen Energy **4** (1979) 541.
79 B 2 Belov, K.P., Nikitin, S.A., in: Fizika i Khimia Magnitnyk Poluprovodnikov i Dielektrikov, Belov, K.P. Tret'jakov, Yu.D. (eds.), Moskva: Izd. Univ. **1979**, p. 40.
79 B 3 Bergner, R.L., Leupold, H.A., Breslin, J.T., Rothwarf, F., Tauber, A.: J. Appl. Phys. **50** (1979) 2349.
79 B 4 Bergner, R.L., Leupold, H.A., Breslin, J.T., Shappirio, J.R., Tauber, A., Rothwarf, F.: J. Appl. Phys. **50** (1979) 2352.
79 B 5 Besnus, M.J., Bouton, J.M., Clad, R.: Phys. Status Solidi (a) **53** (1979) 351.
79 B 6 Besnus, M.J., Herr, A., Fischer, G.: J. Phys. F **9** (1979) 745.
79 B 7 Bogé, M., Chappert, J., Yaounc, A., Coey, J.M.D.: Solid State Commun. **31** (1979) 987.
79 B 8 Boucherle, J.X., Givord, D., Laforest, J., Schweizer, J., Tasset, F.: J. Phys. (Paris) **40** (1979) C 5-180.
79 B 9 Bowman Jr., R.C., Gruen, D.M., Mendelsohn, M.H.: Solid State Commun. **32** (1979) 501.
79 B 10 Buhrer, W., Furrer, A., Halg, W., Schlapbach, L.: J. Phys. F **9** (1979) L 141.
79 B 11 Burnasheva, N.V., Klimeshin, V.V., Semenenko, K.N.: Izv. Akad. Nauk SSSR Neorg. Mat. **15** (1979) 251.
79 B 12 Burzo, E.: J. Phys. (Paris) **40** (1979) C 5-184.
79 B 13 Burzo, E., Ursu, I.: J. Appl. Phys. **50** (1979) 1471.
79 B 14 Burzo, E., Ursu, I.: Rev. Roum. Phys. **14** (1979) 265.
79 B 15 Burzo, E., Vadeanu, St.: J. Less Common Met. **66** (1979) 111.
79 B 16 Burzo, E., Baican, R., Armas, P.: J. Phys. F **9** (1979) L 47.
79 B 17 Burzo, E., Baican, R., Ursu, I.: Proc. 20th Congress AMPERE, Tallin 1978, Berlin, Heidelberg, New York: Springer Verlag **1979**, p. 376.
79 B 18 Buschow, K.H.J., De Chatel, P.F.: Pure Appl. Chem. **52** (1979) 135.
79 B 19 Buschow, K.H.J., Van Essen, R.M.: Solid State Commun. **32** (1979) 1241.
79 B 20 Butera, R.A., Clinton, T.J., Moldovan, A.G., Sankar, S.G., Gschneidner Jr., K.A.: J. Appl. Phys. **50** (1979) 7492.
79 C 1 Capellman, H.: Z. Phys. B **35** (1979) 269.
79 C 2 Chiu, L.B., Elliston, P.R., Stewart, A.M., Taylor, K.N.R.: J. Less Common Met. **65** (1979) P 59.
79 C 3 Chiu, L.B., Elliston, P.R., Stewart, A.M., Taylor, K.N.R.: J. Phys. F **9** (1979) 955.
79 C 4 Clark, G.F., Tanner, B.K., Sery, R.S., Savage, H.T.: J. Phys. (Paris) **40** (1979) C 5-183.
79 C 5 Commandre, M., Fruchart, D., Rouault, A., Sauvage, D., Shoemaker, C.B., Shoemaker, D.P.: J. Phys. Lett. **40** (1979) L 639.
79 C 7 Corson, M.R., Hoy, G.R., Kolk, B.: J. Phys. (Paris) **40** (1979) C 2-159.
79 C 8 Cyrot, M., Lavagna, M.: J. Phys. (Paris) **40** (1979) 763.
79 C 9 Cyrot, M., Lavagna, M.: J. Appl. Phys. **50** (1979) 2333.
79 C 10 Cyrot, M., Gignoux, D., Givord, F., Lavagna, M.: J. Phys. (Paris) **40** (1979) C 5-171.
79 D 1 Dariel, M.P., Mintz, M.H., Hadari, Z.: J. Phys. (Paris) **40** (1979) C 5-213.
79 D 2 De Boer, F.R., Dijkman, W.H., Mattens, W.C.M.: J. Less Common Met. **64** (1979) 241.
79 D 3 Delapalme, A., Deportes, J., Lemaire, R. Hardman, K., James, W.J.: J. Appl. Phys. **50** (1979) 1987.
79 D 4 Deryagin, A.V.: J. Phys. (Paris) **40** (1979) C 5-165.
79 D 5 Deryagin, A.V., Kudrevatykh, N.V., Levitin, R.Z., Popov, V.F.: Phys. Status Solidi (a) **51** (1979) K 125.
79 D 6 Deryagin, A.V., Urabanova, E.A., Kudrevatykh, N.V., Moskalev, V.N.: Izv. Vyssh. Uchebn. Zaved. Fiz. **22** (1979) 108.
79 D 7 Diaz, H., Percheron-Guegan, A., Achard, J.C., Chatillon, C., Mathieu, J.C.: Int. J. Hydrogen Energy **4** (1979) 445.
79 D 8 Didisheim, J.J., Yvon, K., Shaltiel, D., Fischer, P.: Solid State Commun. **31** (1979) 47.
79 D 9 Drzazga, Z., Kroh, J., Broda, H., Chelkowski, A.: Acta Phys. Pol. A **55** (1979) 849.
79 D 10 Dunlap, B.D., Shenoy, G.K., Friedt, J.M., Viccaro, P.J., Niarchos, D., Kierstead, H., Aldred, A.T., Westlake, D.G.: J. Appl. Phys. **50** (1979) 7682.
79 E 1 Ermolenko, A.S.: IEEE Trans. Magn. MAG-**15** (1979) 1765.
79 E 2 Ermolenko, A.S., Rozenfeld, Ye.V.: Fiz. Met. Metalloved. **48** (1979) 505.
79 E 3 Ermolenko, A.S., Shcherbakova, Ye.V.: Fiz. Met. Metalloved. **48** (1979) 275.

79 E 4 Ermolenko, A.S., Menchikov, A.Z., Dorofeev, Y.A.: Phys. Status Solidi (a) **54** (1979) K 113.
79 E 5 Ervens, W.: Goldschmidt Informiert **48** (1979) 3.
79 F 1 Feder, D., Nowik, I.: J. Magn. Magn. Mater. **12** (1979) 149.
79 F 2 Feder, D., Nowik, I.: J. Magn. Magn. Mater. **12** (1979) 162.
79 F 3 Felner, I., Nowik, I.: J. Phys. Chem. Solids **40** (1979) 1035.
79 F 4 Fidler, J., Kronmüller, H.: Phys. Status Solidi (a) **56** (1979) 545.
79 F 5 Fish, G.E., Rhyne, J.J., Sankar, S.G., Wallace, W.E.: J. Appl. Phys. **50** (1979) 2003.
79 F 6 Fuess, H., Givord, D., Gregory, A.R., Schweizer, J.: J. Appl. Phys. **50** (1979) 2000.
79 G 1 Germano, D.J., Butera, R.A., Sankar, S.G., Gschneidner, Jr., K.A.: J. Appl. Phys. **50** (1979) 7495.
79 G 2 Gignoux, D., Givord, F.: J. Phys. F **9** (1979) 1409.
79 G 3 Gignoux, D., Nait-Saada, A., Perrier de la Báthie, R.: J. Phys. (Paris) **40** (1979) C 5–188.
79 G 4 Gignoux, D., Givord, D., Givord, F., Lemaire, R.: J. Magn. Magn. Mater. **10** (1979) 288.
79 G 5 Gignoux, D., Givord, F., Perrier de la Báthie, R., Sayetat, F.: J. Phys. F **9** (1979) 763.
79 G 6 Givord, D., Laforest, J., Lemaire, R.: J. Appl. Phys. **50** (1979) 7489.
79 G 7 Givord, D., Laforest, J., Schweizer, J., Tasset, F.: J. Appl. Phys. **50** (1979) 2008.
79 G 8 Gomez-Sal, J.C.: An. Fis. **73** (1979) 169.
79 G 9 Gomez-Sal, J.G., Gignoux, C.: An. Fis. **73** (1979) 137.
76 G 10 Gratz, E., Sassik, H., Nowotny, H., Steiner, W., Mair, G.: J. Phys. (Paris) **40** (1979) C 5–186.
79 G 11 Grössinger, R., Hilscher, G.: J. Phys (Paris) **40** (1979) C 5–202.
79 G 12 Gschneidner, K.A., Takeshita, R., Beaudry, B.J., McMasters, O.D., Taner, S.M.A., Ho, J.C., King, G.B., Gruber, J.B.: J. Phys. (Paris) **40** (1979) C 5–114.
79 G 13 Gubbens, P.C.M., Van der Kraan, A.M., Buschow, K.H.J.: J. Phys. (Paris) **40** (1979) C 5–200.
79 G 14 Gupta, N., Martis, R.J.J., Sankar, S.G., Rao, V.U.S.: J. Appl. Phys. **50** (1979) 2343.
79 H 1 Hamano, M., Yajima, S.: Trans. Jpn. Inst. Met. **20** (1979) 57.
79 H 2 Hardman, K., James, W.J., Deportes, J., Lemaire, R., Perrier de la Báthie, R.: J. Phys. (Paris) **40** (1979) C 5–204.
79 H 3 Heiman, N., Kazama, N.: Phys. Rev. B **19** (1979) 1623.
79 H 4 Herbst, G., Kronmüller, H.: Z. Phys. Chem. N.F. **116** (1979) S 31.
79 H 5 Herbst, G., Kronmüller, H.: Phys. Lett. **70** A (1979) 341.
79 H 6 Hilscher, G., Kirchmayr, H.: J. Phys. (Paris) **40** (1979) C 5–196.
79 H 7 Hirosawa, T., Tsuchida, T., Nakamura, Y.: J. Phys. Soc. Jpn. **47** (1979) 804.
79 H 8 Hodosov, E.F., Linnik, A.I., Kobzenko, G.F., Ivanchenko, V.G.: Fiz. Met. Metalloved. **48** (1979) 1104.
79 H 9 Hodosov, E.F., Linnik, A.I., Kobzenko, G.F., Ivanchenko, V.G.: Fiz. Met. Metalloved. **47** (1979) 863.
79 H 10 Hrubec, J., Steiner, W.: J. Phys. (Paris) **40** (1979) C 5–198.
79 I 1 Iandelli, A., Palenzona, A.: Rev. Chim. Miner. **16** (1979) 230.
79 I 2 Ilarraz, J., Del Moral, A.: Phys. Status Solidi (a) **51** (1979) K 41.
79 J 1 Jacob, I., Shaltiel, D.: J. Less Common Met. **65** (1979) 117.
79 J 2 James, W.J., Hardman, K., Yelon, W., Kebe, B.: J. Phys. (Paris) **40** (1979) C 5–206.
79 J 3 James, W.J., Hardman, K., Yelon, W., Keem, J., Croat, J.: J. Appl. Phys. **50** (1979) 2006.
79 J 4 Japa, S., Krop, K., Radwanski, R., Nolinnski, J.: J. Phys. (Paris) **40** (1979) C 2–193.
79 K 1 Kandaurova, G.S., Lagutin, A.E.: Fiz. Met. Metalloved. **48** (1979) 46.
79 K 2 Karlicek, R.F., Lowe, I.J.: Solid State Commun. **31** (1979) 163.
79 K 3 Kierstead, H.A., Viccaro, P.J., Shenoy, G.K., Dunlap, B.D.: J. Less Common Met. **66** (1979) 219.
79 K 4 Klimker, H., Dariel, M.P., Rosen, M.: J. Phys. Chem. Solids **40** (1979) 195.
79 K 5 Koczorowska, L., Wrzeciono, A.: Bull. Acad. Pol. Sci. Ser. Phys. Astron. **27** (1979) 117.
79 K 6 Koczorowska, L., Wrzeciono, A.: Bull. Acad. Pol. Sci. Ser. Phys. Astron. **27** (1979) 121.
79 K 7 Koon, N.C., Williams, C.M.: J. Phys. (Paris) **40** (1979) C 5–194.
79 K 8 Koon, H.C., Das, B.N., Rhyne, J.J.: J. Appl. Phys. **50** (1979) 1969.
79 K 9 Kumar, K., Das, D.: J. Appl. Phys. **50** (1979) 2940.
79 K 10 Kaczmarska, K., Kwapulinska, E., Chelkowski, A.: Acta Phys. Pol. A **55** (1979) 67.
79 L 1 Labulle, B., Petipas, C.: J. Less Common Met. **66** (1979) 183.
79 L 2 Lagutin, A.Ye.: Fiz. Met. Metalloved. **47** (1979) 72.
79 L 3 Landolt, M., Meier, F., Zurcher, P., Oesterreicher, H., Ensslov, K., Hoenigschmid, J., Bucher, E.: Solid State Commun. **32** (1979) 1009.
79 L 4 Lebsanft, E., Richter, D., Töpler, J.: Z. Phys. Chem. N.F. **116** (1979) 175.
79 L 5 Lee, R.W.: IEEE Trans. Magn. MAG-**15** (1979) 1762.
79 L 6 Levin, R., Grayevskey, A., Shaltiel, D., Zevin, V., Davidov, D.: Phys. Rev. B **20** (1979) 2624.

79 L 7 Levin, R., Grayevsky, A., Shaltiel, D., Zevin, V., Davidov, D., Williams, D.L., Kaplan, N.: Solid State Commun. **32** (1979) 855.
79 L 8 Linetski, Ya.L., Knizhnik, E.G.: Izv. Akad. Nauk SSSR Met. **5** (1979) 233.
79 M 1 Maeda, H.: J. Appl. Phys. **50** (1979) 2346.
79 M 2 Maeda, H.: Jpn. J. Appl. Phys. **18** (1979) 2163.
79 M 3 Magat, L.M., Hrabov, V.I.: Fiz. Met. Metalloved. **48** (1979) 1323.
79 M 4 Martis, R.J.J.: IEEE Trans. Magn. MAG-**15** (1979) 1760.
79 M 5 Martis, R.J.J., Gupta, N., Sankar, S.G., Rao, V.U.S.: IEEE Trans. Magn. MAG-**15** (1979) 948.
79 M 6 McCurrie, R.A., Willmore, L.E.: J. Appl. Phys. **50** (1979) 3560.
79 M 7 Melamud, M., Hathaway, K., Cullen, J.: J. Appl. Phys. **50** (1979) 7498.
79 M 8 Melnikov, S.A., Sein, V.A., Lileev, A.S., Menushenkova, N.V.: Izv. Akad. Nauk SSSR Met. **4** (1979) 126.
79 M 9 Melville, D., Al-rawi, K.M., Khan, W.I.: J. Appl. Phys. **50** (1979) 7725.
79 M 10 Mendelsohn, M.H., Gruen, D.M., Dwigth, A.E.: J. Less Common Met. **63** (1979) 193.
79 M 11 Merkulova, G.Ya.: Izv. Akad. Nauk SSSR Met. **5** (1979) 173.
79 M 12 Meyer, C., Gros, Y., Hartmann-Boutron, F., Capponi, J.J.: J. Phys. (Paris) **40** (1979) 403.
79 M 13 Meyer, C., Hartmann-Boutron, F., Gros, Y., Srour, B., Capponi, J.J.: J. Phys. (Paris) **40** (1979) C 5–191.
79 M 14 Misawa, T., Nomachi, A.P., Yajima, S., Sugawara, H.: J. Jpn. Inst. Met. **43** (1979) 104.
79 M 15 Mizoguchi, T., Tanaka, Y., Tsuchida, T., Nakamura, Y.: J. Phys. (Paris) **40** (1979) C 2–221.
79 M 16 Morariu, M., Burzo, E., Barb, D.: Rev. Roum. Phys. **24** (1979) 637.
79 M 17 Moriya, T.: J. Magn. Magn. Mater. **14** (1979) 1.
79 M 18 Muraoka, Y., Shiga, M., Nakamura, Y.: J. Phys. F **9** (1979) 1889.
79 N 1 Nagel, H.: J. Appl. Phys. **50** (1979) 1026.
79 N 2 Nelepa, P.J., Butera, R.A.: J. Appl. Phys. **50** (1979) 7539.
79 N 3 Niarchos, D., Viccaro, P.J., Dunlap, B.D., Shenoy, G.K.: J. Appl. Phys. **50** (1979) 7690.
79 N 4 Noreous, D., Olson, L.G., Dahlborg, U.: J. Chem. Phys. Lett. **67** (1979) 432.
79 N 5 Novikov, V.F., Dolgykh, E.V.: Fiz. Met. Metalloved. **49** (1979) 292.
79 N 6 Novikov, V.F., Dolgykh, E.V., Ulyanov, A.I., Deryagin, A.V.: Fiz. Met. Metalloved. **48** (1979) 1093.
79 O 1 Oesterreicher, H., Parker, F.T.: Phys. Lett. **73** A (1979) 71.
79 O 2 Oesterreicher, H., Parker, F.T., Misroch, M.: J. Appl. Phys. **50** (1979) 4273.
79 P 1 Pavlyukova, A.A., Gikhman, E.I.: Fiz. Met. Metalloved. **47** (1979) 210.
79 P 2 Pop, I., Dihoiu, N., Coldea, M.: Philos. Mag. B **39** (1979) 245.
79 P 3 Pourarian, F.: Phys. Lett. **72** A (1979) 175.
79 P 4 Prange, R.E., Korenman, V.: Phys. Rev. B **19** (1979) 4691.
79 R 1 Ramos-Bernal, S.: J. Phys. (Paris) **40** (1979) C 2–683.
79 R 2 Rhyne, J.J., Koon, N.C., Das, B.N.: J. Magn. Magn. Mater. **14** (1979) 273.
79 R 3 Rhyne, J.J., Fish, G.E., Sankar, S.G., Wallace, W.E.: J. Phys. (Paris) **40** (1979) C 5–209.
79 R 4 Rinaldi, S., Paretti, L.: J. Appl. Phys. **50** (1979) 7719.
79 R 5 Roach, P.R., Xebb, R.A., Ketterson, J.B.: J. Low Temp. Phys. **34** (1979) 439.
79 R 6 Rubinstein, M., Swartzendruber, L.J., Bennett, L.H.: J. Appl. Phys. **50** (1979) 2046.
79 S 1 Satyanarayana, M.V., Wallace, W.E., Craig, R.S.: J. Appl. Phys. **50** (1979) 2324.
79 S 2 Savage, H.T., Abbundi, R., Clark, A.E., McMasters, O.D.: J. Appl. Phys. **50** (1979) 1674.
79 S 3 Schlapbach, L., Seiler, A., Siegman, H.C., Von Waldkirch, T., Zurcher, P., Brundle, C.R.: Int. J. Hydrogen Energy **4** (1979) 21.
79 S 4 Searle, C.W., Maartensee, I.: J. Appl. Phys. **50** (1979) 1039.
79 S 5 Shaked, H., Pinto, H., Felner, I.: AIP Conf. Proc. on Modulated Structure **53** (1979) 295.
79 S 6 Shoemaker, D.P., Shoemaker, C.B.: J. Less Common Met. **68** (1979) 43.
79 S 7 Slebarski, A., Lawniczak, K., Auleytner, J.: Phys. Statuts Solid (a) **54** (1979) 79.
79 S 8 Steiner, W.: J. Magn. Magn. Mater. **14** (1979) 47.
79 S 9 Stetsenko, P.N., Antipov, S.D., Mostafa, M.A.: Pis'ma Zh. Eksp. Teor. Fiz. **29** (1979) 684.
79 S 10 Streever, R.L.: Phys. Rev. B **19** (1979) 2704.
79 S 11 Szpunar, B.: Acta Phys. Pol. A **55** (1979) 791.
79 S 12 Szpunar, B., Lindgard, P.A.: J. Phys. F **9** (1979) L 55.
79 T 1 Tari, A.: Phys. Rev. B **19** (1979) 3462.
79 T 2 Trout, S.R., Graham Jr., C.D.: J. Appl. Phys. **50** (1979) 2361.
79 V 2 Van der Kraan, A.M., Gubbens, P.C.M., Buschow, K.H.J.: J. Phys. (Paris) **40** (1979) C 2–190.
79 V 3 Viccaro, P.J., Friedt, J.M., Niarchos, D., Dunlap, B.D., Shenoy, G.K., Aldred, A.T., Westlake, D.G.: J. Appl. Phys. **50** (1979) 2051.

79 V 4 Viccaro, P.J., Shenoy, G.K., Dunlap, B.D., Westlake, D.G., Miller, J.F.: J. Phys. (Paris) **40** (1979) C 2-198.
79 W 1 Wallace, W.E.: Z. Phys. Chem. N.F. **115** (1979) 219.
79 W 2 Wallace, W.E., Karlicek, R.F., Imamura, H.: J. Phys. Chem. **83** (1979) 1708.
79 W 3 Wallace, W.E., Ganapathy, E.V., Craig, R.S.: J. Appl. Phys. **50** (1979) 2327.
79 W 4 Wohlfarth, E.P.: J. Phys. F **9** (1979) L 123.
79 Y 1 Yang, Y.T., Ho, W.W., Yang, K.L., Tchou, T.S., Tseng, S.S., Kin, L.: J. Phys. (Paris) **40** (1979) C 5-177.
79 Z 1 Zvereva, V.I., Ivanova, O.A., Schetnikov, A.E.: Fiz. Met. Metalloved. **47** (1979) 300.

80 A 1 Abbundi, R., Clark, A.E., McMasters, O.D.: IEEE Trans. Magn. MAG-**16** (1980) 1074.
80 A 2 Abbundi, R., Clark, A.E., Savage, H.T., McMasters, O.D.: J. Magn. Magn. Mater. **15-18** (1980) 595.
80 A 3 Alameda, J.M., Deportes, J., Givord, D., Lemaire, R., Lu, Q.: J. Magn. Magn. Mater. **15-18** (1980) 1257.
80 A 4 Alekseev, P.A., Andreef, A., Griesmann, H., Kaun, L.P., Lippold, B., Matz, W., Sadikov, I.P., Chistyakov, O.D., Markova, I.A., Savitski, E.M.: Phys. Status Solidi (b) **97** (1980) 87.
80 A 5 Andreef, A., Griesmann, H., Kaun, L.P., Matz, W., Alekseev, P.A., Sadikov, I.P., Chestyakov, O.D., Markova, I.A., Savitski, E.M.: Crystalline Electric Field and Structural Effects in f-Electron Systems, Plenum Press, New York **1980**, p. 205.
80 A 6 Araujo, S.I., Guimaraes, A.P.: J. Phys. F **10** (1980) 1313.
80 A 7 Asti, G., Bolzoni, F.: J. Magn. Magn. Mater. **15-18** (1980) 561.
80 A 8 Aubert, G., Gignoux, D., Michelutti, B., Nait Saada, N.: J. Magn. Magn. Mater. **15-18** (1980) 551.
80 B 1 Baranov, N.V., Deryagin, A.V.: Ukr. Fiz. Zh. **25** (1980) 1635.
80 B 2 Barberis, G.E., Donoso, J.P., Rettori, C., Davidov, D.: J. Less Common Met. **70** (1980) 69.
80 B 3 Béal-Monod, M.T., Lawrence, J.M.: Phys. Rev. B **21** (1980) 5400.
80 B 4 Belkbir, L., Joly, E., Gerard, N., Achard, J.C., Percheron-Guegan, A.: J. Less Common Met. **73** (1980) 69.
80 B 5 Berezin, A.G., Levitin, R.Z.: J. Eksp. Teor. Fiz. **79** (1980) 1109.
80 B 6 Berezin, A.G., Levitin, R.Z., Popov, Yu.F.: J. Eksp. Teor. Fiz. **79** (1980) 268.
80 B 7 Blacklock, K., White, H.V., Hardman, K., James, W.J.: J. Chem. Phys. **72** (1980) 2883.
80 B 8 Blasius, A., Gonser, U.: Appl. Phys. **22** (1980) 331.
80 B 9 Bowerman, B.S., Wulff, C.A., Biehl, G.E., Flanagan, T.B.: J. Less Common Met. **73** (1980) 1.
80 B 10 Bowman, R.C., Craft, B.D., Attalla, A.: J. Less Common Met. **73** (1980) 227.
80 B 11 Butler, B., Givord, D., Givord, F., Palmer, S.B.: J. Phys. C **13** (1980) L 743.
80 B 12 Buravikhin, V.A., Sidorenko, L.M., Pigorov, V.A., Aphkanov, V.B.: Izv. Akad. Nauk SSSR Met. **2** (1980) 235.
80 B 13 Burzo, E.: J. Phys. F **10** (1980) 2025.
80 B 14 Burzo, E.: Invited Lecture 5th School of Theoretical Physics, Silesian University, Wisla, Poland, **1980**.
80 B 15 Burzo, E., Balanescu, M.: Phys. Status Solidi (b) **100** (1980) K 33.
80 B 16 Buschow, K.H.J.: J. Less Common Met. **72** (1980) 257.
80 B 17 Buschow, K.H.J., Den Broeder, F.J.A.: J. Appl. Phys. **51** (1980) 1839.
80 B 18 Buschow, K.H.J., Smit, P.H., Van Essen, R.M.: J. Magn. Magn. Mater. **15-18** (1980) 1261.
80 C 1 Carmichael, C.M., Paul, G.L., Taylor, K.N.R.: J. Magn. Magn. Mater. **15-18** (1980) 1483.
80 C 2 Castets, A., Gignoux, D., Hennion, B.: J. Magn. Magn. Mater. **15-18** (1980) 375.
80 C 3 Chiu, L.B., Elliston, P.R., Stewart, A.M., Taylor, K.N.R., Issa, M.A.A.: J. Phys. F **10** (1980) 2297.
80 C 4 Chung, Y., Takeshita, T., McMasters, C.D., Gschneidner Jr., K.A.: J. Less Common Met. **74** (1980) 217.
80 C 5 Clausen, K.N., Lebech, B.: J. Magn. Magn. Mater. **15-18** (1980) 347.
80 C 6 Cohen, R.L., West, K.W., Wernick, J.H.: J. Less Common Met. **70** (1980) 229.
80 C 7 Cohen, R.L., West, K.W., Wernick, J.H.: J. Less Common Met. **73** (1980) 273.
80 C 8 Cohen, R.L., West, K.W., Oliver, F., Buschow, K.H.J.: Phys. Rev. B **21** (1980) 941.
80 C 9 Croat, J.J.: J. Magn. Magn. Mater. **15-18** (1980) 597.
80 D 1 Da Cunha, S.F., Guimaraes, A.P.: J. Phys. Chem. Solids **41** (1980) 761.
80 D 2 Day, R.K., Dunlop, J.B.: J. Magn. Magn. Mater. **15-18** (1980) 651.
80 D 3 Dayan, D., Minz, M.H., Dariel, M.P.: J. Less Common Met. **73** (1980) 15.
80 D 4 Den Broeder, F.J.A., Buschow, K.H.J.: J. Less Common Met. **70** (1980) 289.
80 D 5 Deryagin, A.V., Baranov, I.V.: Fiz. Met. Metalloved. **49** (1980) 1245.
80 D 6 Deryagin, A.V., Baranov, N.V.: Pisma J. Techn. Fiz. **6** (1980) 645.
80 D 7 Devare, S.H., Pillay, R.G., Malik, S.K., Dhar, S.K., Devare, H.G.: Phys. Lett. **79** A (1980) 237.
80 D 8 Drzazga, Z., Chelkowski, A., Kubiak, S., Broda, H., Kroh, J., Mydlarz, T.: J. Magn. Magn. Mater. **15-18** (1980) 1241.

80 E 1 Ermolenko, A.S.: Phys. Status Solidi (a) **59** (1980) 331.
80 E 2 Ermolenko, A.S.: Fiz. Met. Metalloved. **50** (1980) 741.
80 E 3 Ermolenko, A.S.: Fiz. Met. Metalloved. **50** (1980) 747.
80 E 4 Ermolenko, A.S.: Fiz. Met. Metalloved. **50** (1980) 962.
80 E 5 Ermolenko, A.S., Rozhda, A.F.: Fiz. Met. Metalloved. **50** (1980) 1186.
80 F 1 Felner, I.: J. Less Common Met. **72** (1980) 241.
80 F 2 Fidler, J., Kronmüller, H.: J. Magn. Magn. Mater. **15–18** (1980) 1461.
80 F 3 Fidler, J., Kirchmayr, H., Wernisch, J.: J. Less Common Met. **71** (1980) 245.
80 F 4 Figiel, H., Gratz, E.: Proc. ISMAR-AMPERE Conf. on Magnetic Resonance, Delft **1980**, p. 275.
80 F 5 Figiel, H., Jaszczewski, M.: J. Magn. Magn. Mater. **15–18** (1980) 673.
80 F 6 Fisch, G.E., Rhyne, J.J., Brun, T., Viccaro, P.J., Niarchos, D., Dunlap, B.D., Shenoy, G.K., Sankar, S.G., Wallace, W.E.: The Rare Earth in Modern Science and Technology, New York: Plenum Press **1978**, vol. 2, p. 569.
80 G 1 Gaunt, P., Mylvaganam, C.K.: J. Magn. Magn. Mater. **15–18** (1980) 1449.
80 G 2 Gignoux, D., Lemaire, R., Molho, P.: J. Magn. Magn. Mater. **21** (1980) 119.
80 G 3 Gignoux, D., Givord, F., Sayetat, F.: J. Magn. Magn. Mater. **15–18** (1980) 1235.
80 G 4 Gignoux, D., Lemaire, R., Molho, P., Tasset, F.: J. Magn. Magn. Mater. **15–18** (1980) 289.
80 G 5 Gignoux, D., Lemaire, R., Molho, P., Tasset, F.: J. Magn. Magn. Mater. **21** (1980) 307.
80 G 6 Givord, D., Gregory, A.E., Schweitzer, J.: J. Magn. Magn. Mater. **15–18** (1980) 293.
80 G 7 Goldberg-Murmis, V., Atzmony, V.S., Dariel, M.P.: J. Mater. Sci. **15** (1980) 127.
80 G 8 Gratz, E., Wohlfarth, E.P.: J. Magn. Magn. Mater. **15–18** (1980) 903.
80 G 9 Gratz, E., Kirchmayr, H.R., Sechovsky, V., Wohlfarth, E.P.: J. Magn. Magn. Mater. **21** (1980) 191.
80 G 10 Gratz, E., Hilscher, G., Kirchmayr, H.R., Sassik, H.: The Rare Earth in Modern Science and Technology, New York: Plenum Press **1980**, vol. 2, p. 327.
80 G 11 Gratz, E., Sechovsky, V., Wohlfarth, E.P., Kirchmayr, H.R.: J. Phys. F **10** (1980) 2819.
80 G 12 Gratz, E., Sassik, H., Nowotny, H., Steiner, W., Mair, G.: J. Phys. (Paris) **40** (1980) C 5–186.
80 G 13 Grin, Yu.N., Yarmolyuk, Ya.P., Gladishevski, E.I.: Dopov. Akad. Nauk Ukr. SSR Ser. A **1** (1980) 78.
80 H 1 Haferl, R., Steiner, W., Ortbauer, H.: J. Phys. (Paris) **41** (1980) C 1–195.
80 H 2 Hardmann, K., James, W.J., Yelon, W.B.: J. Phys. Chem. Solids **41** (1980) 1105.
80 H 3 Hardmann, K., James, W.J., Yelon, W.: The Rare Earth in Modern Science and Technology, New York: Plenum Press **1980**, vol. 2, p. 403.
80 H 4 Hardmann, K., Rhyne, J.J., Smith, K., Wallace, W.E.: J. Less Common Met. **74** (1980) 97.
80 H 5 Hardmann, K., James, W.J., Long, G.J., Yelon, W.B., Kebe, B.: The Rare Earth in Modern Science and Technology, New York: Plenum Press **1980**, vol. 2, p. 315.
80 H 6 Hartmann-Boutron, F., Meyer, C.: J. Phys. (Paris) **41** (1980) 1075.
80 H 7 Hatwan, T.K., Maoli, S.K., Ghatkav, M.N., Padalia, B.D.: Phys. Status Solidi (b) **95**, (1980) 621.
80 H 8 Hilscher, G., Gratz, E., Sassik, H., Kirchmayr, H.: Inst. Phys. Conf. Ser. **55** (1980) 291.
80 H 9 Hiraoka, T.: J. Phys. Soc. Jpn. **49** (1980) 2159.
80 H 10 Hodosov, E.F., Linnik, A.I.: Fiz. Tverd. Tela **22** (1980) 2491.
80 H 11 Hug, M.: Phys. Status Solidi (a) **60** (1980) 573.
80 I 1 Ikeda, K., Gschneidner Jr., K.A.: Phys. Rev. Lett. **45** (1980) 1341.
80 I 2 Ilarraz, J., Del Moral, A.: Phys. Status Solidi (a) **57** (1980) 89.
80 I 3 Inoue, J., Shimizu, M.: J. Phys. F **10** (1980) 721.
80 J 1 Jaakola, S., Korventausta, I., Hovi, V., Lakkisto, M.: Ann. Acad. Sci. Tenn. Ser. AVI **1980**, 3.
80 J 2 Jacob, I., Davidov, D., Shaltiel, D.: J. Magn. Magn. Mater. **20** (1980) 226.
80 J 3 Jacob, I., Bloch, J.M., Shaltiel, D., Davidov, D.: Solid States Commun. **35** (1980) 155.
80 J 4 Japa, St., Krop, K., Przybylski, M.: J. Phys. (Paris) **41** (1980) C 1–199.
80 K 1 Kandaurova, G.S., Lagutin, A.E., Keilin, V.I.: Fiz. Tverd. Tela **22** (1980) 1894.
80 K 2 Kaplan, N., Williams, D.I., Grayevski, A.: Phys. Rev. B **21** (1980) 899.
80 K 3 Karlicek, R.F., Lowe, I.J.: J. Less Common Met. **73** (1980) 29.
80 K 4 Kataev, G.I., Shubin, V.V.: Akust. Zh. **26** (1980) 142.
80 K 5 Kelarev, V.V., Pirogov, A.N., Chuev, V.V., Vohmyanin, A.P., Sidorov, S.K.: Fiz. Met. Metalloved. **50** (1980) 59.
80 K 6 Kitano, Y., Komura, Y., Kajiwara, H.K., Watanabe, K.: Acta Crystallogr. A **36** (1980) 16.
80 K 7 Kierstead, H.A.: J. Less Common Met. **70** (1980) 199.
80 K 8 Kierstead, H.A.: J. Less Common Met. **71** (1980) 303.
80 K 9 Kierstead, H.A.: J. Less Common Met. **73** (1980) 61.
80 K 10 Kierstead, H.A.: J. Less Common Met. **71** (1980) 311.

80K11 Klepp, K., Parthé, E.: Acta Crystallogr. B **36** (1980) 774.
80K12 Klimker, H., Dariel, M.P., Rosen, M.: J. Phys. Chem. Solids **41** (1980) 215.
80K13 Kolodziejczyk, A., Sarkissian, B.V.B., Coles, B.R.: J. Phys. F **10** (1980) L 333.
80K14 Koon, N.C., Rhyne, J.J.: J. Magn. Magn. Mater. **15–18** (1980) 349.
80K15 Koon, N.C., Rhyne, J.J.: Crystalline Electric Field and Structural Effects in f-Electron Systems, New York: Plenum Press **1980**, p. 125.
80K16 Kubota, M., Folle, H.R., Buchal, Ch., Mueller, R.M., Pobell, F.: Phys. Rev. Lett. **45** (1980) 1812.
80K17 Kumar, K., Das, D.: J. Appl. Phys. **51** (1980) 1841.
80L1 Lakner, J.F., Uribe, F.S., Stewart, S.A.: J. Less Common Met. **72** (1980) 87.
80L2 Larsen, J.W., Livesay, B.R.: J. Less Common Met. **73** (1980) 79.
80L3 Lartique, C., Percheron-Guegan, A., Achard, J.C., Tasset, F.: J. Less Common Met. **75** (1980) 23.
80L4 Levin, R., Davidov, D., Grayevsky, A., Shaltiel, D., Zevin, V.: J. Phys. F **10** (1980) 1285.
80L5 Long, G.J., Hardmann, K., James, W.J.: Solid State Commun. **34** (1980) 253.
80L6 Lüthi, B., Ott, H.R.: Solid State Commun. **33** (1980) 717.
80M1 Malik, S.K., Boltich, E.B., Wallace, W.E.: Solid State Commun. **33** (1980) 921.
80M2 Markosyan, A.S.: Fiz. Tverd. Tela **22** (1980) 3454.
80M3 Mendelsohn, M.H., Gruen, D.M.: The Rare Earth in Modern Science and Technology, New York: Plenum Press **1980**, p. 593.
80M4 Meyer, C., Hartmann-Boutron, F., Capponi, J.J., Chappert, J., McMassenet, O.: J. Magn. Magn. Mater. **15–18** (1980) 1229.
80M5 Meyer, C., Hartmann-Boutron, F., Gros, Y., Capponi, J.J.: J. Phys. (Paris) **41** (1980) C 1–191.
80M6 Miravat, Abdel Aal, Chechernikov, N.I.: Fiz. Met. Metalloved. **49** (1980) 658.
80M7 Misawa, S.: J. Phys. F **10** (1980) L 115.
80M8 Misawa, T., Kikuchi, M., Sugawara, H.: J. Jpn. Inst. Met. **44** (1980) 387.
80M9 Mori, K., Sato, K.: J. Phys. Soc. Jpn. **49** (1980) 246.
80M10 Mori, H., Fujita, T., Satoh, T., Ohtsuka, T.: Phys. Lett. **79** A (1980) 121.
80M11 Mueller, R.M., Buchal, Ch., Folle, H.R., Kubota, M., Probell, F.: Cryogenics **20** (1980) 395.
80M12 Muraoka, Y., Shiga, M., Nakamura, Y.: J. Phys. F **10** (1980) 127.
80M13 Murray, J.J., Post, M.L., Taylor, J.B.: J. Less Common Met. **73** (1980) 33.
80N1 Nait-Saada, A.: These, Inst. Nat. Polytechnique, Grenoble **1980**.
80N2 Newns, D.M., Henson, A.C.: J. Phys. F **10** (1980) 2429.
80N3 Niarchos, D., Viccaro, P.J., Dunlap, A.D., Shenoy, G.K., Aldred, A.T.: J. Less Common Met. **73** (1980) 283.
80N4 Norgaard-Clausen, E., Lebech, B.: J. Magn. Magn. Mater. **15–18** (1980) 347.
80N5 Nowik, I., Felner, I., Seh, M.: J. Magn. Magn. Mater. **15–18** (1980) 1215.
80O1 Oesterreicher, H., Bittner, H.: J. Less Common Met. **73** (1980) 339.
80O2 Oesterreicher, H., Bittner, H.: J. Magn. Magn. Mater. **15–18** (1980) 1264.
80O3 Oesterreicher, H., Parker, F.T.: Phys. Status Solidi (a) **58** (1980) 585.
80O4 Ohlendorf, D., Flotow, H.E.: J. Less Common Met. **73–74** (1980) 25.
80O5 Ohlendorf, D., Flotow, H.E.: J. Chem. Phys. **73** (1980) 2937.
80O6 Okamoto, T., Fujii, H., Matsushita, T., Kido, Y.: Trans. J. Inst. Met. **21** (1980) 389.
80O7 Olcese, G.L.: Solid State Commun. **35** (1980) 87.
80P1 Palleau, J., Chouteau, G.: J. Phys. Lett. **41** (1980) L 227.
80P2 Percheron-Guegan, A., Lartigue, C., Achard, J.C.: J. Less Common Met. **74** (1980) 1.
80P3 Pfranger, R., Plusa, D., Szymura, S., Wyslocki, B.: J. Magn. Magn. Mater. **21** (1980) 43.
80P4 Pirogov, A.N., Ermolenko, A.S., Dvinyaninov, V.N., Chuyev V.V., Kelarev, V.V.: Fiz. Met. Metalloved. **49** (1980) 585.
80P5 Pourarian, F., Tajabor, N.: Phys. Status Solidi (a) **61** (1980) 537.
80P6 Pourarian, F., Lakner, J.F., Wallace, W.E., Elalter, A.: J. Less Common Met. **74** (1980) 161.
80P7 Pourarian, F., Wallace, W.E., Sankar, S.G., Obermayer, R.: The Rare Earth in Modern Science and Technology, New York: Plenum Press **1980**, p. 321.
80P8 Pourarian, F., Boltich, E.B., Wallace, W.E., Craig, R.S., Malik, S.K.: J. Magn. Magn. Mater. **21** (1980) 128.
80P9 Pourarian, F., Boltich, E.B., Wallace, W.E., Malik, S.K.: J. Less Common Met. **74** (1980) 153.
80R1 Raj, P., Kulshreshtha, S.K.: J. Phys. (Paris) **41** (1980) 1487.
80R2 Rhyne, J.J., Koon, N.C., Alperin, H.A.: The Rare Earth in Modern Science and Technology, New York: Plenum Press **1980**, p. 313.

80R3 Rothwarf, F., Leupold, H.A., Breslin, J.T., Bergner, R.L., Winter, J.J.: The Rare Earth in Modern Science and Technology, New York: Plenum Press **1980**, vol. 2, p. 355.
80S1 Sato, K.: Trans. Jpn. Inst. Met. **21** (1980) 336.
80S2 Sattler, W., Adler, E.: J. Magn. Magn. Mater. **15–18** (1980) 1447.
80S3 Savage, H.T., Abbundi, R., Clark, A.E., McMasters, O.D.: J. Magn. Magn. Mater. **15–18** (1980) 609.
80S4 Schaafsma, A.S., Besnus, M.J., Vincze, I., Van der Woode, F.: J. Magn. Magn. Mater. **15–18** (1980) 1149.
80S5 Schlapbach, L.: J. Phys. F **10** (1980) 2477.
80S6 Schlapbach, L., Seiler, A., Stucki, F., Siegmann, H.C.: J. Less Common Met. **73** (1980) 145.
80S7 Schlapbach, L., Stucki, F., Seiler, A., Siegmann, H.C.: J. Magn. Magn. Mater. **15–18** (1980) 1271.
80S8 Schweizer, J., Tasset, F.: J. Phys. F **10** (1980) 2799.
80S9 Seh, M., Cohen, S., Nowik, I.: J. Phys. (Paris) **41** (1980) C 1–201.
80S10 Shimizu, M.: J. Magn. Magn. Mater. **20** (1980) 47.
80S11 Shimotomai, M., Miyake, H., Doyama, M.: J. Phys. F **10** (1980) 707.
80S12 Shinar, J., Malchin, A., Davidov, D., Kaplan, M.: J. Less Common Met. **73** (1980) 255.
80S13 Slebarski, A.: J. Less Common Met. **72** (1980) 231.
80S14 Smit, P.H., Buschow, K.H.J.: Phys. Rev. B **21** (1980) 3839.
80S15 Steiner, W., Haferl, R., Grössinger, R.: J. Phys. (Paris) **41** (1980) C 1–193.
80S16 Steiner, W., Haferl, R., Ortbauer, H., Wolfram, S.: J. Magn. Magn. Mater. **15–18** (1980) 1185.
80S17 Stucki, F., Schlapbach, L.: J. Less Common Met. **74** (1980) 143.
80T1 Takeshita, T., Dublon, G., McMasters, O.D., Gschneidner, Jr., K.A.: The Rare Earths in Modern Science and Technology, New York: Plenum Press **1980**, vol. 2, p. 563.
80T2 Takeshita, T., Gschneidner Jr., K.A., Thome, D.K., McMasters, O.D.: Phys. Rev. B **21** (1980) 5636.
80T3 Tanaka, Y., Tsuchida, T., Nakamura, Y.: J. Phys. Soc. Jpn. **48** (1980) 1092.
80T4 Tari, A., Larica, C.: J. Phys (Paris) **41** (1980) 35.
80U1 Uehara, M.: J. Appl. Phys. **51** (1980) 5495.
80V1 Van der Kraan, A.M., Gubbens, P.C.M., Buschow, K.H.J.: J. Phys. (Paris) **41** (1980) C 1–197.
80V2 Van Dongen, J.C.M., Nieuwenhuys, G.J., Mydosh, J.A., Van der Kraan, A.M., Buschow, K.H.J.: Inst. Phys. Conf. Ser. **55** (1980) 275.
80V3 Van Essen, R.H., Buschow, K.H.J.: J. Less Common Met. **70** (1980) 189.
80V4 Viccaro, P.J., Shenoy, G.K., Niarchos, D., Dunlap, B.D.: J. Less Common Met. **73** (1980) 265.
80V5 Vittoria, C., Lubitz, P., Koon, N.C., Schelleng, J.: J. Magn. Magn. Mater. **15–18** (1980) 567.
80W1 Wallace, W.E.: The Rare Earth in Modern Science and Technology, New York: Plenum Press **1980**, p. 559.
80W2 Weaver, J.H., Franciosi, A., Wallace, W.E., Smith, H.K.: J. Appl. Phys. **51** (1980) 5847.
80W3 Williams, C.M., Koon, N.C., Das, B.N.: J. Magn. Magn. Mater. **15–18** (1980) 553.
80W4 Wohlfarth, E.P.: J. Magn. Magn. Mater. **20** (1980) 77.
80W5 Wohlfarth, E.P.: J. Phys. Lett. **41** (1980) L 563.
80Y1 Yamada, Y., Ohmae, H.: J. Phys. Soc. Jpn. **48** (1980) 1513.
80Y2 Yamaguchi, M., Sasaki, S., Ohta, T.: J. Less Common Met. **73** (1980) 201.
80Y3 Yousif, A.A., Hamilton, W.D.: Hyp. Int. **8** (1980) 29.
80Z1 Zakharov, S.A.: Fiz. Met. Metalloved. **50** (1980) 1103.
80Z2 Zarechnyuk, O.S., Richal, R.M., Korin, V.V.: Dopov. Akad. Nauk Ukr. SSR Ser. A **1** (1980) 84.
80Z3 Zarek, W., Pardavi-Horvath, M., Obuszko, Z.: J. Magn. Magn. Mater. **21** (1980) 47.
80Z4 Zevin, V., Barboy, E.: Z. Phys. B **39** (1980) 173.

81A1 Alameda, J.M., Givord, D., Lemaire, R., Lu, Q.: J. Appl. Phys. **52** (1981) 2079.
81A2 Andreev, A.V., Deryagin, A.V., Zadvorkin, S.M., Moskalev, V.N.: Fiz. Met. Metalloved. **51** (1981) 975.
81A3 Atzmony, U., Dayan, D., Dariel, M.P.: Mater. Res. Bull. **16** (1981) 793.
81A4 Aubert, G., Gignoux, D., Hennion, B., Michelutti, B., Nait-Saada, A.: Solid State Commun. **37** (1981) 741.
81B1 Bauchspiess, K.R., Boksch, W., Holland-Moritz, E., Launois, H., Pott, R., Wohlleben, D.: Valence Fluctuations in Solids, Amsterdam: North Holland **1981**, p. 417.
81B2 Bauminger, E.R., Savage, H.T.: J. Appl. Phys. **52** (1981) 2055.
81B3 Béal-Monod, M.T.: Phys. Rev. B **24** (1981) 261.
81B4 Belkbir, L., Joly, E., Gerard, N.: J. Less Common Met. **81** (1981) 199.
81B5 Belov, K.P., Vasilkovski, V.A., Kovtun, N.M., Kupriyanov, A.R., Nikitin, S.A., Ostrovski, V.F.: Pis'ma Zh. Eksp. Teor. Fiz. **33** (1981) 597.

81 B 6 Berthier, Y., Devine, R.A.B.: J. Appl. Phys. **52** (1981) 2071.
81 B 7 Berthier, Y., Devine, R.A.B., Butera, R.A.: Proc. NMR and RES Spectroscopies Applied to Mat. Sci., Amsterdam: North-Holland **1981**, p. 449.
81 B 8 Boltich, E.B., Wallace, W.E., Pourarian, F., Malik, S.K.: J. Magn. Magn. Mater. **25** (1981) 295.
81 B 9 Boltich, E.B., Pourarian, F., Wallace, W.E., Smith, H.K., Malik, S.K.: Solid State Commun. **40** (1981) 117.
81 B 10 Burzo, E.: J. Less Common Met. **77** (1981) 251.
81 B 11 Burzo, E.: Bull. Magn. Res. **2** (1981) 239.
81 B 12 Burzo, E., Seitabla, D.: J. Phys. F **11** (1981) L 255.
81 B 13 Burzo, E., Seitabla, D.: Solid State Commun. **37** (1981) 663.
81 B 14 Burzo, E., Balanescu, M., Chipara, M.: J. Solid State Chem. **21** (1981) 755.
81 B 15 Buschow, K.H.J.: Solid State Commun. **40** (1981) 207.
81 C 1 Chuang, Y.C., Wu, C.H., Li, T.C., Chang, S.C., Wang, M.S.: J. Less Common Met. **78** (1981) 219.
81 C 2 Chuev, V.V., Kelarev, V.V., Pirogov, A.N., Sidorov, S.K., Lieberman, A.A.: Fiz. Met. Metalloved. **52** (1981) 80.
81 C 3 Chuev, V.V., Kelarev, V.V., Sidorov, S.K., Pirogov, A.N., Vohmianin, A.P.: Fiz. Tverd. Tela **23** (1981) 1760.
81 C 4 Clausen, K., Nielsen, O.V.: J. Magn. Magn. Mater. **23** (1981) 237.
81 C 5 Cullen, J.R.: J. Appl. Phys. **52** (1981) 2038.
81 D 1 Da Cunha, J.B.M., Vasquez, A.: Hyp. Int. **9** (1981) 547.
81 D 2 Da Cunha, J.B.M., Viccaro, P.J., Vasquez, A.: Hyp. Int. **12** (1981) 119.
81 D 3 De Jongh, L.J., Bartolome, J., Greidanus, F.J.A.M., De Groot, H.J.M., Stipdonk, H.L., Buschow, K.H.J.: J. Magn. Magn. Mater. **25** (1981) 207.
81 D 4 Deportes, J., Givord, D., Ziebeck, K.R.A.: J. Appl. Phys. **52** (1981) 2074.
81 D 5 Devare, S.H., Pillay, R.G., Malik, S.K., Ghar, S.K., Devare, H.G.: Hyp. Int. **10** (1981) 949.
81 D 6 Devare, S.H., Pillay, R.G., Malik, S.K., Ghar, S.K., Devare, H.G.: Hyp. Int. **10** (1981) 935.
81 D 7 Devine, R.A.B., Berthier, Y.: J. Magn. Magn. Mater. **25** (1981) 135.
81 D 8 Diko, P., Miskuf, J., Mihalik, M., Juranek, Z., Karel, V.: Acta Phys. Slovaca **31** (1981) 309.
81 D 9 Donoso, J.P., Rettori, C., Barberis, G.E., Davidov, D.: Solid State Commun. **39** (1981) 203.
81 D 10 Drzazga, Z.: J. Magn. Magn. Mater. **25** (1981) 11.
81 F 1 Felner, I., Seh, M., Nowik, I.: J. Phys. Chem. Solids **42** (1981) 1091.
81 F 2 Felner, I., Seh, M., Rakavy, M., Nowik, I.: J. Phys. Chem. Solids **42** (1981) 369.
81 F 3 Fidler, J.: Proc. 5th Int. Workshop on Rare Earth-Cobalt Permanent Magnets and their Applications, Roanoke, Virginia **1981**, p. 407.
81 F 4 Figiel, H., Gratz, E., Kapusta, Cz.: J. Magn. Magn. Mater. **23** (1981) 123.
81 F 5 Folle, H.R., Kubota, M., Buchal, C., Mueller, R.M., Pobell, F.: Z. Phys. B **41** (1981) 223.
81 F 6 Fujii, H., Sinha, V.K., Pourarian, F., Wallace, W.E.: J. Phys. Chem. **85** (1981) 3112.
81 G 1 Gaunt, P., Mylvaganam, C.K.: Philos. Mag. B **44** (1981) 569.
81 G 2 Genin, J.M., Bauer, Ph., Besnus, M.J.: Phys. Status Solidi (a) **64** (1981) 325.
81 G 3 Germano, D.J., Butera, R.A.: Phys. Rev. B **24** (1981) 2640.
81 G 4 Gignoux, D., Lemaire, R., Molho, P.: Recent Developm. Condensed Matt. Physics, Eur. Phys. Soc. Conf., New York: Plenum Press **1981**, vol. 4, p. 464.
81 G 5 Gignoux, D., Lemaire, R., Molho, P., Tasset, F.: J. Appl. Phys. **52** (1981) 2087.
81 G 6 Gignoux, D., Givord, D., Laforest, J., Lemaire, R., Molho, P.: Proc. 1st Int. Conf. Phys. of Magnetic Materials, Jaszowiec, Poland, 1980, Ossolineum **1981**, p. 96.
81 G 7 Gignoux, D., Givord, D., Laforest, J., Lemaire, R., Molho, P.: Inst. Phys. Conf. Ser. **55** (1981) 287.
81 G 8 Gignoux, D., Givord, D., Lemaire, R., Nait-Saada, A., Del Moral, A.: J. Magn. Magn. Mater. **23** (1981) 274.
81 G 9 Graf, H., Balzer, G., Möslang, A., Recknagel, E., Weidinger, A.: Hyp. Int. **8** (1981) 605.
81 G 10 Gratz, E.: J. Magn. Magn. Mater. **24** (1981) 1.
81 G 11 Gratz, E., Sassik, H., Nowotny, H.: J. Phys. F **11** (1981) 429.
81 G 12 Gratz, E., Strom-Olsen, J.C., Zuckermann, M.J.: Solid State Commun. **40** (1981) 833.
81 G 13 Gratz, E., Grössinger, R., Oesterreicher, H., Parker, F.T.: Phys. Rev. B **23** (1981) 2542.
81 G 14 Gratz, E., Hilscher, G., Kirchmayr, H., Sassik, H.: Proc. 15th Conf. on Rare Earth Res., La Rolla, Missouri **1981**, p. 367.
81 G 15 Gregory, A., Mueller, R., Fuess, H.: Z. Kristallogr. **154** (1981) 279.
81 G 16 Grössinger, R., Haferl, R., Hilscher, G., Wiesinger, G., Buschow, K.H.J., Smit, P.H.: Inst. Phys. Conf. Ser. **55** (1981) 295.

81 G 17 Gubbens, P.C.M., Van der Kraan, A.M., Buschow, K.H.J.: Phys. Status Solidi (a) **64** (1981) 657.
81 G 18 Gubbens, P.C.M., Van der Kraan, A.M., Buschow, K.H.J.: Solid State Commun. **37** (1981) 635.
81 G 19 Gygax, F.N., Hintermann, A., Ruegg, W., Schenck, A., Studer, A., Schlapbach, L., Stucki, F.: Recent Developm. Condensed Matt. Physics, Eur. Phys. Soc. Conf., New York: Plenum Press **1981**, vol. 2, p. 1.
81 H 1 Hardmann, K., Rhyne, J.J., James, W.J.: J. Appl. Phys. **52** (1981) 2049.
81 H 2 Hathaway, K., Cullen, J.: J. Appl. Phys. **52** (1981) 2282.
81 H 3 Hilscher, G.: J. Magn. Magn. Mater. **25** (1981) 229.
81 H 4 Hirosawa, S., Nakamura, Y.: J. Magn. Magn. Mater. **25** (1981) 284.
81 H 5 Hug, M.: Phys. Status Solidi (a) **65** (1981) K 29.
81 I 1 Inomata, K.: Phys. Rev. B **23** (1981) 2076.
81 I 2 Inomata, K.: J. Jpn. Inst. Met. **45** (1981) 547.
81 I 3 Irodova, A.V., Kost, M.E., Padurets, L.N., Somenkov, V.A., Sokolova, E.I., Shilshtein, S.Sh.: Zh. Neorg. Khim. **26** (1981) 307.
81 I 4 Iwama, Y., Nishio, T.: Proc. 5th Int. Workshop on Rare Earth-Cobalt Permanent Magnets and their Applications, Roanoke, Virginia **1981**, p. 443.
81 J 1 Juranek, Z., Safarika, P.J., Kovac, J., Potocky, L.: Acta Phys. Slovaca **31** (1981) 305.
81 K 1 Kavecansky, V., Diko, P., Miskuf, J., Karel, V., Jahn, L.: Acta Phys. Slovaca **31** (1981) 327.
81 K 2 Katayama, T., Shibata, T.: J. Magn. Magn. Mater. **23** (1981) 172.
81 K 3 Kawakami, M.: J. Phys. F **11** (1981) 267.
81 K 4 Kazakov, A.A., Reimer, V.A.: Fiz. Met. Metalloved. **51** (1981) 5301.
81 K 5 Kebe, B., James, W.J., Deportes, J., Lemaire, R., Yelon, W., Day, R.K.: J. Appl. Phys. **52** (1981) 2052.
81 K 6 Khan, W.F., Melville, D.: J. Magn. Magn. Mater. **23** (1981) 117.
81 K 7 Kierstead, H.A.: J. Less Common Met. **77** (1981) 281.
81 K 8 Kierstead, H.A.: J. Less Common Met. **80** (1981) 115.
81 K 9 Kierstead, H.A.: J. Less Common Met. **78** (1981) 61.
81 K 10 Kierstead, H.A.: J. Less Common Met. **81** (1981) 221.
81 K 11 Kierstead, H.A.: J. Less Common Met. **78** (1981) 29.
81 K 12 Kirilicheva, L.A., Ilyushin, A.S., Perov, A.P.: Fiz. Met. Metalloved. **52** (1981) 430.
81 K 13 Konopka, D., Zarek, W.: J. Less Common Met. **81** (1981) 5.
81 K 14 Koon, N.C., Rhyne, J.J.: Phys. Rev. B **23** (1981) 207.
81 K 15 Krill, G., Kappler, J.P.: J. Phys. C **14** (1981) 1515.
81 K 16 Krill, G., Kappler, J.P., Mayer, A., Abadli, L., Ravet, M.F.: J. Phys. F **11** (1981) 1713.
81 K 17 Kubota, M., Folle, H.R., Buchal, Ch., Mueller, R.M., Pobell, F.: Physica B **108** (1981) 1093.
81 K 18 Kudrevatykh, N.V., Moskalev, V.N., Deryagin, A.Y., Andreev, A.V., Zadvorkin, S.M.: Ukr. Fiz. Zh. **26** (1981) 1734.
81 K 19 Kunkel, H.P., Searle, C.W.: Phys. Rev. B **23** (1981) 65.
81 L 1 Lee, R.W.: J. Appl. Phys. **52** (1981) 2549.
81 L 2 Lee, R.W.: J. Appl. Phys. **52** (1981) 2058.
81 L 3 Linetzki, Ya.L., Skakov, Yu.A., Yagodin, Yu.D.: Fiz. Met. Metalloved. **51** (1981) 296.
81 L 4 Liu, Z.B., Tai, L.C.: J. Appl. Phys. **52** (1981) 2064.
81 L 5 Lu, Q.: Ph.D. Thesis, Grenoble **1981**, p. 82.
81 M 1 Malik, S.K., Wallace, W.E.: J. Magn. Magn. Mater. **24** (1981) 23.
81 M 2 Malik, S.K., Boltich, E.B., Wallace, W.E.: Solid State Commun. **37** (1981) 329.
81 M 3 Malik S.K., Dhar, S.K., Vijayaraghavan, R.: The Rare Earth in Modern Science and Technology, New York: Plenum Press **1981**, vol. 3, p. 385.
81 M 4 Malik, S.K., Dhar, S.K., Vijayaraghavan, R., Manohar, A., Padalia, B.D., Prabhawalkar, P.D.: Proc. Valence Fluctuations in Solids, Amsterdam: North-Holland **1981**, p. 245.
81 M 5 Markosyan, A.S.: Fiz. Tverd. Tela **23** (1981) 1153.
81 M 6 Markosyan, A.S.: Fiz. Tverd. Tela **23** (1981) 1656.
81 M 7 Melville, D., Al Rawi, K.M., Khan, W.I.: Phys. Status Solidi (a) **66** (1981) 133.
81 M 8 Merches, M., Wallace, W.E., Craig, R.S.: J. Magn. Magn. Mater. **24** (1981) 97.
81 M 9 Meyer, C., Hartmann-Boutron, F., Gros, Y.: Proc. NMR and RES Spectroscopies Applied to Mat. Sci., North Holland **1981**, p. 455.
81 M 10 Meyer, C., Hartmann-Boutron, G., Gros, Y., Berthier, Y., Buevoz, J.L.: J. Phys. (Paris) **42** (1981) 605.
81 M 11 Misheva, M., Tumbev, G.: Bulgarian J. Phys. **8** (1981) 572.
81 M 12 Mori, K., Sato, K.: Proc. 3rd Int. Conf. on Ferrites CAPJ, Japan, **1981**, p. 932.
81 M 13 Murray, J.J., Post, M.L., Taylor, J.B.: J. Less Common Met. **80** (1981) 211.

81 M 14 Mylvaganam, C.K., Gaunt, P.: Philos, Mag. B **44** (1981) 581.
81 N 1 Nagai, H., Ikami, Y., Yoshie, H., Tsujimura, A.: J. Phys. Soc. Jpn. **50** (1981) 1873.
81 N 2 Niarchos, D., Viccaro, P.J., Shenoy, G.K., Dunlap, B.D., Aldred, A.T.: Hyp. Int. **9** (1981) 563.
81 N 3 Novikov, V.F., Dolgykh, E.V.: Fiz. Met. Metalloved. **51** (1981) 977.
81 P 1 Parker, F.T., Oesterreicher, H.: J. Less Common Met. **79** (1981) 297.
81 P 2 Pavlyukov, A.A.: Fiz. Met. Metalloved. **51** (1981) 666.
81 P 3 Pourarian, F., Satyanarayana, M.V., Wallace, W.E.: J. Magn. Magn. Mater. **25** (1981) 113.
81 P 4 Pourarian, F., Wallace, W.E., Malik, S.K.: J. Magn. Magn. Mater. **25** (1981) 299.
81 P 5 Pourarian, F., Fuji, H., Wallace, W.E., Sinha, V.K., Smith, H.K.: J. Phys. Chem. **85** (1981) 3105.
81 R 1 Rubinstein, M., Lubitz, P., Koon, N.C.: J. Magn. Magn. Mater. **24** (1981) 288.
81 S 1 Sato, K., Koyachi, K., Mori, K.: J. Appl. Phys. **52** (1981) 2084.
81 S 2 Schlapbach, L.: Solid State Commun. **38** (1981) 117.
81 S 3 Sebek, J., Stehno, J., Sechovsky, V., Gratz, E.: Solid State Commun. **40** (1981) 457.
81 S 4 Seh, M., Nowik, I.: J. Magn. Magn. Mater. **22** (1981) 239.
81 S 5 Seitabla, D., Burzo, E., Ionescu, T.: Rev. Roum. Phys. **26** (1981) 689.
81 S 6 Shaburov, V.L., Sovestnov, A.E., Markova, I.A., Savitzki, E.M., Chistyakov, O.D., Schkatova, T.M.: Fiz. Tverd. Tela **23** (1981) 2455.
81 S 8 Shaltiel, D., Von Waldkirch, T., Stucki, F., Schlapbach, L.: Recent Developm. in Condensed Matt. Physics, Eur. Phys. Soc. Conf., New York: Plenum Press **1981**, vol. 4, p. 383.
81 S 9 Shaltiel, D., Von Waldkirch, T., Stucki, F., Schlapbach, L.: J. Phys. F **11** (1981) 471.
81 S 10 Shimizu, K., Dhar, S.K., Vijayaraghavan, R., Malik, S.K.: J. Phys. Soc. Jpn. **50** (1981) 1200.
81 S 11 Shimotomai, M., Miyake, H., Komatsu, S., Doyama, M.: Hyp. Int. **11** (1981) 223.
81 S 12 Sidzimov, B.S., Nikortin, S.A., Yakovlev, A.A., Neov. S.D., Krezhov, K.A.: Bulgarian J. Phys. **8** (1981) 370.
81 S 13 Sovetsnov, A.K., Shaburova, V.A., Markova, L.A., Savitski, E.M., Chistyakov, O.D., Schkatova, T.M.: Fiz. Tverd. Tela **23** (1981) 2827.
81 S 14 Stewart, G.A., Zukrowski, J., Wortmann, G.: Solid State Commun. **39** (1981) 1017.
81 S 15 Stewart, G.A., Zukrowski, J., Wortmann, G.: J. Magn. Magn. Mater. **25** (1981) 77.
81 S 16 Syromiatnikov, V.N., Pirogov, A.V., Chuev, V.V., Kelarev, V.V.: Fiz. Met. Metalloved. **52** (1981) 323.
81 S 17 Szpunar, B.: Acta Phys. Pol. A **60** (1981) 791.
81 T 1 Takeshita, T., Gschneidner, K.A., Lakner, J.F.: J. Less Common Met. **78** (1981) P 43.
81 T 2 Takeuchi, A.Y., Da Cunha, S.F.: J. Phys. F **11** (1981) L 241.
81 T 3 Tari, A., Larica, C., Popplewell, J.: J. Less Common Met. **78** (1981) P 7.
81 V 1 Vasilkovski, V.A., Kovtun, N.M., Ostrovski, V.F.: Fiz. Tverd. Tela **23** (1981) 3001.
81 V 2 Vasilkovski, V.A., Kovtun, N.M., Kupriyanov, A.K., Nikitin, S.A., Ostrovski, V.F.: Zh. Eksp. Teor. Fiz. **80** (1981) 364.
81 V 3 Vasilkovski, V.A., Kovtun, N.M., Kupriyanov, A.K., Nikitin, S.A., Ostrovski, V.F.: Fiz. Tverd. Tela **23** (1981) 2467.
81 V 4 Viccaro, P.J., Niarchos, D., Shenoy, G.K., Dunlap, B.D.: Proc. NMR and RES Spectroscopies Applied to Mat. Sci., North Holland, **1981**, p. 327.
81 W 1 Wallace, W.E., Merches, M., Craig, R.S.: The Rare Earth in Modern Science and Technology, New York: Plenum Press **1981**, vol. 3, p. 373.
81 Y 1 Yamada, Y., Ohira, K.: J. Phys. Soc. Jpn. **50** (1981) 3569.
81 Y 2 Yang, Y.C.: Acta Met. Sinica **17** (1981) 355.
81 Y 3 Yang, Y.C., Kebe, B., James, W.J., Deportes, J., Yelon, W.: J. Appl. Phys. **52** (1981) 2077.
81 Y 4 Yang, Y.C., Ho, W.W., Lin, C., Yang, J.L., Jin, L., Zhu, J.X., Zeng, X.X.: J. Appl. Phys. **52** (1981) 2082.

82 A 1 Abbundi, R., Clark, A.E., McMasters, O.D.: J. Appl. Phys. **53** (1982) 2664.
82 A 2 Achard, J.C., Dianoux, A.J., Lartigue, C., Percheron-Guegan, A., Tasset, F.: The Rare Earth in Modern Science and Technology, New York: Plenum Press **1982**, vol. 3, p. 481.
82 A 3 Achard, J.C., Lartigue, C., Percheron-Guegan, A., Dianoux, A.J., Tasset, F.: J. Less Common Met. **88** (1982) 89.
82 A 4 Adam, S., Adam, G., Corciovei, A.: Phys. Status Solidi (b) **114** (1982) 85.
82 A 5 Alameda, J.M., Givord, D., Lu, Q.: The Rare Earth in Modern Science and Technology, New York: Plenum Press **1981**, vol. 3, p. 399.
82 A 6 Allen, J.W., Oh, S.J., Lindau, I., Maple, M.P., Suassuna, J.F., Hagström, S.B.: Phys. Rev. B **26** (1982) 445.
82 A 7 Amaral, L., Livi, F.P., Gomes, A.: J. Phys. F **12** (1982) 2091.

82 A 8 Andoh, Y., Fujii, H., Fujiwara, H., Okamoto, T.: J. Phys. Soc. Jpn. **51** (1982) 435.
82 A 9 Andreef, A., Frauenheim, T., Goremychkin, E.A., Griesmann, H., Lippold, A., Matz, W., Chistyakov, O.D., Savitski, E.M.: Phys. Status Solidi (b) **111** (1982) 507.
82 A 10 Andreenko, A.S., Apostolov, A., Mikhov, M., Nikitin, S.A., Shedulko, N., Stanev, N.: Phys. Status Solidi (a) **74** (1982) K 105.
82 A 11 Andreev, A.V., Deryagin, A.V., Moskalev, V.N., Mishnikov, N.V.: Phys. Status Solidi (a) **73** (1982) K 69.
82 A 12 Andreev, A.V., Tarasov, E.N., Deryagin, A.Y., Zadvorkin, S.M.: Phys. Status Solidi (a) **71** (1982) K 245.
82 A 13 Andreev, A.V., Deryagin, A.V., Zadvorkin, S.M.: Phys. Status Solidi (a) **70** (1982) K 113.
82 A 14 Andresen, A.F.: J. Less Common Met. **88** (1982) 1.
82 A 15 Apostolov, A., Stanev, N., Sheludko, N., Mikhov, M., Ogojska, T., Cholakov, P.: Bulgarian J. Phys. **9** (1982) 619.
82 A 16 Asti, G., Deriu, A.: Proc. 6th Int. Workshop on Rare Earth-Cobalt Permanent Magnets and their Applications, Baden, Wien **1982**, p. 525.
82 B 1 Bara, J.J., Pedziwiatr, A.T., Zarek, W.: J. Magn. Magn. Mater. **27** (1982) 168.
82 B 2 Bara, J.J., Pedziwiatr, A.T., Zarek, W., Konopka, D., Gacek, U.: J. Magn. Magn. Mater. **27** (1982) 159.
82 B 3 Bara, J.J., Pedziwiatr, A.T., Pardavi-Horvath, M., Kucharski, Z., Suwalski, J.: J. Magn. Magn. Mater. **27** (1982) 32.
82 B 4 Bara, J.J., Pedziwiatr, A.T., Zarek, W., Pardavi-Horvath, M., Kucharski, Z., Suwalski, J.: Proc. Indian Nat. Sci. Acad., Part A **1982**, p. 521.
82 B 5 Bara, J.J., Pedziwiatr, A.T., Zarek, W., Konopka, D., Gacek, U.: Proc. Indian Nat. Sci. Acad., Part A **1982**, p. 944.
82 B 6 Barabanov, Y.A.: Fiz. Met. Metalloved. **54** (1982) 97.
82 B 7 Bauer, P., Genin, J.M.: Phys. Status Solidi (a) **71** (1982) K 149.
82 B 8 Besnus, M.J., Herr, A., Le Dang, K., Veillet, P., Schaafsma, A.S., Van Der Woude, F., Vincze, I., Mezei, F., Galis, G.H.M.: J. Phys. F **12** (1982) 2393.
82 B 9 Bleaney, B., Bowden, G.J., Cadogan, J.M., Day, R.K., Dunlap, J.S.: J. Phys. F **12** (1982) 795.
82 B 10 Boltich, E.B., Wallace, W.E., Pourarian, F., Malik, S.K.: J. Phys. Chem. **86** (1982) 524.
82 B 11 Boucherle, J.X., Schweizer, J., Givord, D., Gregory, A.: J. Appl. Phys. **53** (1982) 1950.
82 B 12 Burzo, E., Seitabla, D.: J. Phys. F **12** (1982) 2675.
82 B 13 Burzo, E., Seitabla, D., Chipara, M.: Phys. Status Solidi (b) **113** (1982) 87.
82 B 14 Buschow, K.H.J.: J. Magn. Magn. Mater. **29** (1982) 91.
82 B 15 Buschow, K.H.J., Gubbens, P.C.M., Ras, W., Van der Kraan, A.M.: J. Appl. Phys. **53** (1982) 8329.
82 B 16 Butler, B., Palmer, S.B., Givord, D., Givord, F.: J. Phys. F **12** (1982) 2813.
82 C 1 Callen, B.: J. Appl. Phys. **53** (1982) 2367.
82 C 2 Callen, E.: Physica **114** B (1982) 71.
82 C 3 Castets, A., Gignoux, D., Hennion, B.: Phys. Rev. B **25** (1982) 337.
82 C 4 Castets, A., Gignoux, D., Hennion, B., Nicklow, R.M.: J. Appl. Phys. **53** (1982) 1979.
82 C 5 Chachkhiani, Z.B., Aal, M.M., Chechernikov, V.I., Chachkhiani, L.G.: Izv. Vyssh. Uchebn. Zaved. Fiz. **25** (1982) 27.
82 C 6 Cheng, W., Creuzet, G., Garoche, P., Campbell, I.A., Gratz, E.: J. Phys. F **12** (1982) 475.
82 C 7 Chuang, Y.C., Wu, C.H., Chang, Y.C.: J. Less Common Met. **84** (1982) 201.
82 C 8 Chuang, Y.C., Wu, C.H., Chang, Y.C.: J. Less Common Met. **83** (1982) 235.
82 C 9 Chuang, Y.C., Wu, C.H., Li, T.C., Chang, S.C., Kao, L.: Proc. 6th Int. Workshop on Rare Earth-Cobalt Permanent Magnets and their Applications, Baden, Wien **1982**, p. 721.
82 C 10 Chuang, Y.C., Wu, C.H., Li, T.C., Chang, S.C., Kao, L.: Prakt. Metallogr. **19** (1982) 495.
82 C 11 Clark, G.R., Tanner, B.K., Savage, H.T.: Philos. Mag. B **46** (1982) 331.
82 C 12 Clausen, K., Lebech, B.: J. Phys. C **15** (1982) 5092.
82 C 13 Crowder, C., James, W.J., Yelon, W.B.: J. Appl. Phys. **53** (1982) 2637.
82 C 14 Crowder, C., Kebe, B., James, W.J., Yelon, W.B.: The Rare Earth in Modern Science and Technology, New York: Plenum Press **1982**, vol. 3, p. 473.
82 D 1 Da Cunha, S.F., Franceschini, D.F., Takeuchi, A.Y.: J. Phys. F **12** (1982) 3083.
82 D 2 Dai, S., Wang, C., Teng, C., Xiao, N., Qi, S.: Acta Met. Sinica **18** (1982) 599.
82 D 3 Decrop, B., Deportes, J., Givord, D., Lemaire, R., Chapert, J.: J. Appl. Phys. **53** (1982) 1953.
82 D 4 Decrop, B., Deportes, J., James, W.J., Yelon, W.: The Rare Earth in Modern Science and Technology, New York: Plenum Press **1982**, p. 361.
82 D 5 Deryagin, A.V., Baranov, N.V.: Metallofizica **4** (1982) 26.

82D6 Deryagin, A.V., Kudrevatykh, N.V., Moskalev, V.N.: Fiz. Met. Metalloved. **54** (1982) 473.
82D7 Drzazga, Z.: Phys. Status Solidi (a) **72** (1982) 771.
82E1 Ermolenko, A.S.: Proc. 6th Workshop on Rare Earth-Cobalt Permanent Magnets and their Applications, Baden, Wien **1982**, p. 771.
82E2 Ermolenko, A.S.: Fiz. Met. Metalloved. **53** (1982) 620.
82E3 Ermolenko, A.S.: Fiz. Met. Metalloved. **53** (1982) 706.
82E4 Ermolenko, A.S., Rozhda, A.I.: Fiz. Met. Metalloved. **54** (1982) 697.
82F1 Felner, I., Nowik, I.: J. Phys. Chem. Solids **43** (1982) 463.
82F2 Felner, I., Nowik, I., Baberschke, K., Nieuwenhuys, G.J.: Solid State Commun. **44** (1982) 691.
82F3 Fidler, J.: Philos. Mag. B **46** (1982) 565.
82F4 Figiel, H.: J. Magn. Magn. Mater. **27** (1982) 303.
82F5 Figiel, H.: J. Magn. Magn. Mater. **29** (1982) 117.
82F6 Figiel, H.: J. Less Common Met. **83** (1982) L 27.
82F7 Figiel, H., Kakol, Z.: Proc. 6th Int. Workshop on Rare Earth Cobalt Permanent Magnets and Their Applications, Baden, Wien **1982**, p. 757.
82F8 Figiel, H., Lemanska, K., Lemanski, A.: Acta Phys. Pol. A **61** (1982) 99.
82F9 Finkelstein, L.D., Samsonova, I.D.: Fiz. Met. Metalloved. **53** (1982) 718.
82F10 Fujii, F., Pourarian, F., Wallace, W.E.: J. Magn. Magn. Mater. **27** (1982) 215.
82F11 Fujii, H., Satyanarayana, M.V., Wallace, W.E.: Solid State Commun. **41** (1982) 445.
82F12 Fujii, H., Satyanarayana, M.V., Wallace, W.E.: J. Appl. Phys. **53** (1982) 2371.
82F13 Fujii, H., Sinha, V.K., Pourarian, F., Wallace, W.E.: J. Less Common Met. **88** (1982) 44.
82G1 Gaidukova, I.Yu., Markosyan, A.S.: Fiz. Met. Metalloved. **54** (1982) 184.
82G2 Gignoux, D., Hennion, B., Nait-Saada, A.: Crystalline Electric Field Effects in f-Electron Systems, Wroclaw, Poland 1981, New York: Plenum Press **1982**, p. 485.
82G3 Gignoux, D., Givord, D., Givord, F., Lemaire, R.: The Rare Earth in Modern Science and Technology, New York: Plenum Press **1982**, vol. 3, p. 393.
82G4 Gignoux, D., Gomez-Sal, J.C., Paccard, D.: Solid State Commun. **44** (1982) 695.
82G5 Gignoux, D., Givord, F., Lemaire, R., Launois, H., Sayetat, F.: J. Phys. (Paris) **43** (1982) 173.
82G6 Gratz, E., Nowotny, H.: J. Magn. Magn. Mater. **29** (1982) 127.
82G7 Gratz, E., Zuckermann, M.J.: J. Magn. Magn. Mater. **29** (1982) 181.
82G8 Gratz, E., Hilscher, G., Kirchmayr, H., Sassik, H.: The Rare Earth in Modern Science and Technology, New York: Plenum Press **1982**, vol. 3, p. 367.
82G9 Greidanus, F.J.A.M., De Jongh, L.J., Huiskamp, W.J., Buschow, K.H.J.: Physica B **112** (1982) 92.
82G10 Greidanus, F.J.A., De Jongh, L.J., Huiskamp, W.J., Furrer, A., Buschow, K.H.J.: Crystalline Electric Field Effects in f-Electron Systems, Wroclaw, Poland, 1981, New York: Plenum Press **1982**, p. 602.
82G11 Grover, A.K., Coles, B.R., Sarkissian, B.V.B., Stone, H.E.N.: J. Less Common Met. **86** (1982) 29.
82G12 Gschneidner, K.A., McMasters, O.D.: The Rare Earth in Modern Science and Technology, New York: Plenum Press **1982**, p. 299.
82G13 Gubbens, P.C.M., Buschow, K.H.J.: J. Phys. F **12** (1982) 2715.
82G14 Gubbens, P.C.M., Van der Kraan, A.M., Buschow, K.H.J.: J. Magn. Magn. Mater. **29** (1982) 113.
82G15 Gubbens, P.C.M., Van der Kraan, A.M., Buschow, K.H.J.: J. Magn. Magn. Mater. **27** (1982) 61.
82G16 Gubbens, P.C.M., Van der Kraan, A.M., Buschow, K.H.J.: J. Magn. Magn. Mater. **30** (1982) 383.
82H1 Hardman, K., Rhyne, J.J., Malik, S.K., Wallace, W.E.: J. Appl. Phys. **53** (1982) 1944.
82H2 Herbst, J.F., Croat, J.J.: J. Appl. Phys. **53** (1982) 4304.
82H3 Herbst, J.F., Croat, J.J., Lee, R.W., Yelon, W.B.: J. Appl. Phys. **53** (1982) 250.
82H4 Hilscher, G.: J. Magn. Magn. Mater. **27** (1981) 1.
82H5 Hilscher, G., Grössinger, R., Sechovsky, V., Nozar, P.: J. Phys. F **12** (1982) 1209.
82H6 Hirosawa, S., Nakamura, Y.: J. Phys. Soc. Jpn. **51** (1982) 2819.
82H7 Hirosawa, S., Nakamura, Y.: J. Phys. Soc. Jpn. **51** (1982) 1162.
82H8 Hirosawa, S., Nakamura, Y.: J. Appl. Phys. **53** (1982) 2069.
82H9 Hirosawa, S., Nakamura, Y.: J. Phys. Soc. Jpn. **51** (1982) 2464.
82H10 Hirosawa, S., Nakamura, Y.: J. Magn. Magn. Mater. **25** (1982) 284.
82H11 Hirosawa, S., Nakamura, Y.: J. Magn. Magn. Mater. **30** (1982) 238.
82H12 Hrubec, J., Steiner, W., Reissner, M.: J. Magn. Magn. Mater. **29** (1982) 100.
82H13 Huq, M.: Phys. Status Solidi (a) **74** (1982) 667.
82I1 Iannarella, L., Guimaraes, A.P., Da Silva, X.A.: Phys. Status Solidi (b) **114** (1982) 255.
82I2 Ichinose, K., Fujiwara, K., Yoshie, H., Nagai, H., Tsujimura, A.: J. Phys. Soc. Jpn. **51** (1982) 3853.

82I3 Inoue, J., Shimizu, M.: J. Phys. F **12** (1982) 1811.
82J1 Jurczyk, M., Wrzeciono, A.: Proc. 6th Int. Workshop on Rare Earth-Cobalt Permanent Magnets and Their Applications, Baden, Wien **1982**, p. 733.
82K1 Kebe, B., Crowder, C., James, W.J., Deportes, J., Lemaire, R., Yelon, W.: The Rare Earth in Modern Science and Technology, New York: Plenum Press **1982**, vol. 3, p. 377.
82K2 Kierstead, H.A.: J. Less Common Met. **86** (1982) L 5.
82K3 Krasinova, G.N., Livintzev, V.V.: Fiz. Met. Metalloved. **53** (1982) 1032.
82K4 Krup, M.B., Prasad, K.G., Raghunathan, K., Sharma, R.P.: Phys. Lett. **90** A (1982) 59.
82L1 Lamloumi, J., Lartigue, C., Percheron-Guegan, A., Achard, J.: The Rare Earth in Modern Science and Technology, New York: Plenum Press **1982**, p. 487.
82L2 Landolt, M., Niedermann, P., Mauri, D., Meier, F., Zurcher, P.: J. Appl. Phys. **53** (1982) 2014.
82L3 Lartigue, C., Percheron-Guegan, A., Gschneidner, K.A.: J. Less Common Met. **88** (1982) 211.
82L4 Levitin, R.Z., Markosyan, A.S., Snegirev, V.V.: JETP Pisma **36** (1982) 367.
82L5 Lord, D.G., Savage, H.T., Rosemeier, R.G.: J. Magn. Magn. Mater. **29** (1982) 137.
82L6 Lynch, J.F., Reilly, J.J.: J. Less Common Met. **87** (1982) 225.
82M1 Malik, S.K., Arlinghaus, F., Wallace, W.E.: Phys. Rev. B **25** (1982) 6488.
82M2 Markosyan, A.S.: Fiz. Met. Metalloved. **54** (1982) 1109.
82M3 Matz, W., Lippold, B., Goremychkin, E.A., Andreev, A., Greissman, H., Frauenheim, T.: Crystalline Electric Field Effects in f-Electron Systems, Wroclaw, Poland 1981, New York: Plenum Press **1982**, p. 69.
82M4 Mori, K., Hathaway, K., Clark, A.E.: J. Appl. Phys. **53** (1982) 8110.
82M5 Mori, H., Satoh, T., Fujita, T., Ohtsuka, T.: J. Low. Temp. Phys. **49** (1982) 397.
82M6 Mori, H., Satoh, T., Suzuki, H., Ohtsuka, T.: J. Phys. Soc. Jpn. **51** (1982) 1785.
82M7 Moskalev, V.N., Deryagin, A.B., Kudrevatykh, N.V., Terentiev, S.V.: Fiz. Met. Metalloved. **54** (1982) 61.
82N1 Nakanishi, H., Machida, K., Matsubara, T.: Solid State Commun. **43** (1982) 899.
82N2 Niarchos, D., Meyer, C., Schuttler, B., Shenoy, G.K., Dunlap, B.D., Aldred, A.T.: Proc. Int. Conf. Appl. Mössbauer Effect, Jaipur 1981, New Delhi: Indian Acad. Sci. Publ. **1982**, p. 331.
82N3 Nishihara, Y., Yamaguchi, Y.: J. Phys. Soc. Jpn. **51** (1982) 1333.
82N4 Nishihara, Y., Katayama, T., Ogawa, S.: J. Phys. Soc. Jpn. **51** (1982) 2487.
82N5 Nowik, I., Felner, I., Seh, M., Rakavay, M.: J. Magn. Magn. Mater. **30** (1982) 295.
82O1 Oesterreicher, H., Parker, F.T.: J. Phys. F **12** (1982) 1027.
82O2 Okamoto, T., Fuji, H., Takeda, S., Hihara, T.: J. Less Common Met. **88** (1982) 181.
82O3 Ono, S., Ishido, Y., Imanari, K., Tabata, T.: J. Less Common Met. **88** (1982) 57.
82P1 Parker, F.T., Oesterreicher, H.: Appl. Phys. A **27** (1982) 65.
82P2 Parviainen, S., Lehtinen, M.: J. Magn. Magn. Mater. **30** (1982) 87.
82P3 Pasturel, A., Chatillon, C., Percheron-Guegan, A., Achard, J.C.: The Rare Earth in Modern Science and Technology, New York: Plenum Press **1982**, vol. 3, p. 489.
82P4 Paszkowicz, W. Poziewska, M., Slepowronski, S., Warchol, S., Modrzejewski, A.: Reprint INR 1938/XIV/IS/A, Institut of Nuclear Research **1982**.
82P5 Paul, D.I.: J. Appl. Phys. **53** (1982) 2362.
82P6 Pfeiffer, I.: Z. Metallkd. **73** (1982) 174.
82P7 Pfranger, R., Plusa, D., Szymura, S., Wyslocki, B.: Physica B+C **114** (1982) 212.
82P8 Pirogov, A.N., Dvinianiov, V.N., Kelarev, V.V., Chuev, V.V., Sidorov, S.K.: Fiz. Met. Metalloved. **54** (1982) 830.
82P9 Pirogov, A.N., Kelarev, V.V., Ermolenko, A.S., Chuev, V.V., Sidorov,S.K., Artamonova, A.M.: Zh. Eksp. Teor. Fiz. **83** (1982) 1398.
82P10 Pop, I., Pop, R., Coldea, M.: J. Phys. Chem. Solids **43** (1982) 199.
82P11 Potentziani, E., Paul, D.I., Tauber, A.: Phys. Rev. B **25** (1982) 47.
82P12 Pourarian, F., Wallace, W.E.: J. Less Common Met. **87** (1982) 275.
82P13 Pourarian, F., Wallace, W.E., Malik, S.K.: J. Less Common Met. **83** (1982) 95.
82P14 Pourarian, F., Wallace, W.E., Malik, S.K.: J. Magn. Magn. Mater. **25** (1982) 299.
82R1 Radwanski, R.J., Figiel, H., Krop, K., Warchol, S.: Solid State Commun. **41** (1982) 921.
82R2 Rahman, I.Z., Melville, D., Khan, W.I.: Phys. Status Solidi (a) **70** (1982) K 175.
82R3 Razafimandimby, H.A., Erdols, P.: Z. Phys. B **46** (1982) 193.
82R4 Richter, D., Hempermann, R., Vinhas, L.A.: J. Less Common Met. **88** (1982) 353.
82R5 Romaka, V.L., Zarechnyuk, D.S., Rykhal, R.M., Yarmolyuk, Ya.P., Skolozdra, R.V.: Fiz. Met. Metalloved. **54** (1982) 410.

82R6 Rummel, H., Cohen, R.L., Gütlich, P., West, K.W.: Appl. Phys. Lett. **40** (1982) 477.
82S1 Sahling, A., Frach, P., Hegenbarth, E.: Phys. Status Solidi (b) **112** (1982) 243.
82S2 Sarkis, A., Callen, E.: J. Appl. Phys. **53** (1982) 2365.
82S3 Sarkissian, B.V.B.: J. Appl. Phys. **53** (1982) 8070.
82S4 Sarkissian, B.V.B.: Proc. 4th Conf. on Supercond. in d and f Band Metals, Karlsruhe **1982**, p. 311.
82S5 Sarkissian, B.V.B., Grover, A.K.: J. Phys. F **12** (1982) L 107.
82S6 Sarkissian, B.V.B., Grover, A.K., Coles, B.R.: Physica B+C **109–110** (1982) 2041.
82S7 Sato, K., Isikawa, Y., Mori, K.: J. Appl. Phys. **53** (1982) 8222.
82S8 Sato, K., Iwasaki, S., Ishikawa, Y., Mori, K.: J. Appl. Phys. **53** (1982) 1938.
82S9 Satyanarayana, M.V., Fujii, H., Wallace, W.E.: J. Appl. Phys. **53** (1982) 2374.
82S10 Scherbakova, E.V., Ermolenko, A.S.: Fiz. Met. Metalloved. **54** (1982) 1103.
82S11 Schlapbach, L., Pina-Perez, C., Siegrist, T.: Solid State Commun. **41** (1982) 135.
82S12 Seiler, A., Schlapbach, L., Scherrer, H.: Surf. Sci. **12** (1982) 98.
82S13 Sharma, D.K., Govil, J.C., Tyagi, R.K., Gupta, D.K.: Indian J. Pure Appl. Phys. **20** (1982) 174.
82S14 Shimizu, K.: J. Phys. Soc. Jpn. **51** (1982) 2703.
82S15 Shimotomai, M., Komatsu, S., Doyama, M.: Proc. Int. Conf. Appl. Mössbauer Effect, Jaipur 1981, New Delhi: Indian Acad. Sci. Publ. **1982**, p. 586.
82S16 Shur, Y.S., Ponovareva, O.I., Maykov, V.S., Popov, A.G.: Fiz. Met. Metalloved. **53** (1982) 727.
82S17 Sidzhimov, B.S., Neov, S.D., Nikitin, S.A.: Bulgarian J. Phys. **9** (1982) 34.
82S18 Sinha, V.K., Pourarian, F., Wallace, W.E.: J. Less Common Met. **87** (1982) 283.
82S19 Skolozdra, R.V., Koretskaya, O.Eh., Gorelenko, Yu.K.: Ukr. Fiz. Zh. **27** (1982) 263.
82S20 Slebarski, A., Auleytner, J.: Phys. Status Solidi (b) **109** (1982) 125.
82S21 Slebarski, A., Auleytner, J.: J. Phys. F **12** (1982) 2591.
82S22 Slebarski, A., Byszewski, P.: J. Magn. Magn. Mater. **27** (1982) 182.
82S23 Smit, P.H., Donkersloot, H.C., Buschow, K.H.J.: J. Appl. Phys. **53** (1982) 2640.
82S24 Sousa, J.B., Montenegro, J.F.D., Moreira, J.M., Braga, M.E.: J. Phys. F **12** (1982) 351.
82S25 Szpunar, B.: J. Phys. F **12** (1982) 759.
82T1 Takeuchi, A.Y., Da Cunha, S.F.: J. Magn. Magn. Mater. **30** (1982) 135.
82T2 Tari, A.: J. Magn. Magn. Mater. **29** (1982) 133.
82T3 Tari, A.: J. Magn. Magn. Mater. **30** (1982) 209.
82T4 Tari, A.: J. Appl. Phys. **53** (1982) 1941.
82T5 Tauber, A., Finnigan, R.D.: The Rare Earth in Modern Science and Technology, New York: Plenum Press **1982**, vol. 3, p. 493.
82U1 Uchida, H., Tada, M., Huang, Y.: J. Less Common Met. **88** (1982) 81.
82U2 Uehara, M.: J. Appl. Phys. **53** (1982) 3730.
82V1 Van der Kraan, A.M., Gubbens, P.C.M., Buschow, K.H.J.: Proc. Indian Nat. Sci. Acad., Part A **1982**, p. 518.
82V2 Van der Liet, A., Frings, P.H., Menovsky, A., Franse, J.J., Mydosh, J.A., Nieuwenhuys, G.J.: J. Phys. F **12** (1982) L 153.
82W1 Wallace, W.E.: J. Less Common Met. **88** (1982) 141.
82W2 Wallace, W.E., Pourarian, F.: J. Phys. Chem. **86** (1982) 4958.
82W3 Wallace, W.E., Merches, M., Craig, R.S.: The Rare Earth in Modern Science and Technology, New York: Plenum Press **1982**, vol. 3, p. 373.
82W4 Wallace, W.E., Fujii, H., Satyanarayana, M.V., Hirosawa, S.: Proc. 6th Int. Workshop on Rare Earth-Cobalt Permanent Magnets and their Applications, Baden, Wien **1982**, p. 537.
82W5 Wallace, W.E., Merches, M., Shenoy, G.K., Viccaro, P.J.: J. Phys. Chem. Solids **43** (1982) 55.
82W6 Warchol, S., Modrzejewski, A.: Cryst. Res. Techn. **17** (1982) 1347.
82W7 Weaver, J.H., Franciosi, A., Peterman, D.J., Takeshita, T., Gschneidner, K.A.: J. Less Common Met. **86** (1982) 195.
82W8 Winter, C., Arrott, A.S.: J. Appl. Phys. **53** (1982) 2733.
82Y1 Yamada, H., Shimizu, M.: J. Phys. F **12** (1982) 2413.
82Y2 Yamaguchi, M., Katume, T., Ohta, T.: J. Less Common Met. **88** (1982) 195.
82Y3 Yamaguchi, M., Katume, T., Ohta, T.: J. Appl. Phys. **53** (1982) 2787.
82Y4 Yang, Y.C., Long, G.J., James, W.J., Yeh, R.: J. Appl. Phys. **53** (1982) 1958.
82Y5 Yang, Y.C., Long, G.J., Kebe, S., James, W.J., Deportes, J.: The Rare Earth in Modern Science and Technology, New York: Plenum Press **1982**, p. 403.
82Y6 Yartis, V.A., Burnasheva, V.V., Semenenkov, K.N., Fadeeva, N.V., Solovev, S.P.: Int. J. Hydrogen Energy 7 (1982) 957.

82Y7 Yoshikawa, A., Matsumoto, T., Yagisawa, K.: J. Less Common Met. **88** (1982) 73.
82Z1 Zarek, W.: J. Less Common Met. **87** (1982) 185.
82Z2 Zarek, W., Bara, J.J., Pedziwiatr, A.T., Pardavi-Horvath, M., Kucharski, Z., Suwalski, J.: Proc. Int. Conf. Appl. Mössbauer Effect, Jaipur 1981, New Delhi: Indian Acad. Sci. Publ. **1982**, p. 542.
82Z3 Zukrowski, J., Stewart, G.A., Kalkowski, G., Wortmann, G., Wiesinger, G.: Crystalline Electric Field and Structural Effects in f-Electron Systems, Wroclaw, Poland, 1981, New York: Plenum Press **1982**, p. 149.

83A1 Adam, S., Adam, G.: Proc. Int. Conf. Magnetism of Rare-Earth and Actinides, Bucharest, Romania **1983**, vol. 1, p. 253.
83A2 Akselrod, Z.Z., Budzynski, M., Komissarova, B.A., Kryukova, L.N., Ryasny, G.K., Sorokin, A.A.: Phys. Status Solidi (b) **119** (1983) 667.
83A3 Aksenov, L.V., Goremychkin, Ye.A., Frauenheim, T.: Fiz. Met. Metalloved. **55** (1983) 496.
83A4 Aksenov, V.L., Goremychkin, E.A., Frauenheim, T.: Physica B+C **120** (1983) 176.
83A5 Aksenov, V.L., Goremychkin, E.A., Mühle, E., Buehrer, W.: Physica B+C **120** (1983) 310.
83A6 Andreev, A.V., Deryagin, A.V., Zadvorkin, S.M.: J. Eksp. Teor. Fiz. **85** (1983) 974.
83A7 Arbuzov, M.P., Pavlyukov, A.A.: Fiz. Met. Metalloved. **56** (1983) 918.
83B1 Baranov, N., Gratz, E., Nowotny, H., Steiner, W.: J. Magn. Magn. Mater. **37** (1983) 206.
83B2 Baranov, N.V., Vokhmyanin, A.P., Deryagin, A.V., Kelarev, V.V., Pirogov, A.N., Rymner, V.A., Syromyatnikov, V.N.: Fiz. Met. Metalloved. **56** (1983) 261.
83B3 Bartashevich, M.N., Deryagin, A.V., Kudrevatykh, I.V., Tarasov, E.N.: Zh. Eksp. Teor. Fiz. **84** (1983) 1140.
83B4 Beille, J., Gignoux, D., Lemaire, R., Voiron, J., Shimizu, M.: Physica B+C **119** (1983) 133.
83B5 Belov, K.P.: Proc. Int. Conf. Magnetism of Rare-Earth and Actinides, Bucharest, Romania **1983**, vol. 2, p. 33.
83B6 Bowden, G.J., Clark, R.G.: J. Phys. C **16** (1983) 1089.
83B7 Bucur, R.V., Lupu, D.: J. Less Common Met. **90** (1983) 203.
83B8 Burzo, E.: J. Magn. Magn. Mater. **31–34** (1983) 213.
83B9 Burzo, E.: Proc. Int. Conf. Magnetism of Rare-Earth and Actinides, Bucharest, Romania **1983**, vol. 2, p. 115.
83B10 Buschow, K.H.J.: J. Magn. Magn. Mater. **40** (1983) 224.
83B11 Buschow, K.H.J., Van der Kraan, A.M.: J. Less Common Met. **91** (1983) 203.
83C1 Campbell, S.J., Day, R.K., Dunlop, J.B., Stewart, A.M.: J. Magn. Magn. Mater. **31–34** (1983) 167.
83C2 Carmichael, C.M., Paul, G.L., Taylor, K.N.R.: J. Magn. Magn. Mater. **31–34** (1983) 1025.
83C3 Chuev, V.V., Kelarev, V.V., Pirogov, A.N., Sidorov, S.K., Koriakova, V.S.: Fiz. Met. Metalloved. **55** (1983) 510.
83C4 Chuev, V.V., Scherbakova, E.V., Kelarev, V.V., Pirogov, A.N., Sidorov, S.K.: Fiz. Met. Metalloved. **56** (1983) 929.
83C5 Clark, A.E., Savage, H.T.: J. Magn. Magn. Mater. **31–34** (1983) 849.
83C6 Coldea, M., Pop, I., Dihoiu, N.: J. Magn. Magn. Mater. **31–34** (1983) 204.
83C7 Coldea, M., Pop, I., Tulai, I.: Proc. Int. Conf. Magnetism of Rare Earth and Actinides, Bucharest, Romania, **1983**, vol. 1, p. 104.
83C8 Crowder, C.E., James, W.J.: J. Less Common Met. **95** (1983) 1.
83D1 Da C. Brochado Oliveira, J.M., Harris, I.R.: J. Mater. Sci. **18** (1983) 3649.
83D2 Decrop, B., Deportes, J., Lemaire, R.: J. Less Common Met. **94** (1983) 199.
83D3 Da Cunha, J.B.M., Vasquez, A.: Hyp. Int. **9** (1981) 547.
83D4 Dolgykh, E.V., Novikov, V.F.: Fiz. Met. Metalloved. **56** (1983) 924.
83D5 Druzhinin, V.V., Ermolenko, A.S., Shkarubskii, V.V.: Fiz. Tverd. Tela **25** (1983) 300.
83D6 Drzazga, Z.: Phys. Status Solidi (a) **76** (1983) 647.
83D7 Drzazga, Z., Mydlarz, T.: Phys. Status Solidi (a) **80** (1983) 403.
83D8 Dwight, A.E.: J. Less Common Met. **93** (1983) 411.
83E1 Ensslen, K., Bucher, E., Oesterreicher, H.: J. Less Common Met. **92** (1983) 343.
83E2 Ermolenko, A.S.: Fiz. Met. Metalloved. **55** (1983) 503.
83E3 Ermolenko, A.S., Rozhda, A.F.: Fiz. Met. Metalloved. **55** (1983) 267.
83F1 Fahnle, M., Oesterreicher, H.: J. Magn. Magn. Mater. **38** (1983) 331.
83F2 Fahnle, M., Oesterreicher, H.: Phys. Rev. B **27** (1983) 5586.
83F3 Felner, I., Nowik, I., Seh, M.: J. Magn. Magn. Mater. **38** (1983) 172.
83F4 Finkelstein, L.D., Samsonova, N.D.: Fiz. Met. Metalloved. **56** (1983) 466.

83 F 5 Flanagan, T.B., Mason, N.B., Biehl, G.E.: J. Less Common Met. **91** (1983) 107.
83 F 6 Franse, J.J.M., Hien, T.D., Ngan, N.H.K., Duc, N.H.: J. Magn. Magn. Mater. **39** (1983) 275.
83 F 7 Frings, P.H., Franse, J.J.M., Hilscher, G.: J. Phys. F **13** (1983) 175.
83 F 8 Fujii, H., Wallace, W.E.: J. Less Common Met. **94** (1983) 257.
83 F 9 Fujii, H., Fujimoto, J., Takeda, S., Hihara, T., Okamoto, T.: J. Magn. Magn. Mater. **31–34** (1983) 223.
83 F 10 Fujiwara, K., Ichinose, K., Nagai, H., Tsujimura, A.: J. Magn. Magn. Mater **31–34** (1983) 707.
83 G 1 Gaidukova, I.Yu., Kuglyashov, S.B., Markosyan, A.S., Levitin, R.Z., Pastushenkov, Yu.G., Snegirev, VV.: Zh. Eksp. Teor. Fiz. **84** (1983) 1858.
83 G 2 Gignoux, D., Givord, F.: J. Magn. Magn. Mater. **31–34** (1983) 217.
83 G 3 Gignoux, D., Givord, F., Lemaire, R., Tasset, F.: J. Less Common Met. **94** (1983) 1.
83 G 4 Givord, D., Laforest, J., Lemaire, R., Lu, Q.: J. Magn. Magn. Mater. **31–34** (1983) 191.
83 G 5 Goremychkin, E.A., Muhle, E., Popescu, M.: Proc. Int. Conf. Magnetism of Rare-Earth and Actinides, Bucharest, Romania **1983**, vol. 1, p. 87.
83 G 6 Goudy, A.J., Stokes, D.G., Gazzillo, J.A.: J. Less Common Met. **91** (1983) 149.
83 G 7 Gratz, E.: Solid State Commun. **48** (1983) 825.
83 G 8 Gratz, E., Nowotny, H., Steiner, W.: Proc. Int. Conf. Magnetism of Rare-Earths and Actinides, Bucharest, Romania, **1983**, vol. 1, p. 116.
83 G 9 Graves-Tompson, R.J., White, H.W., Hardmann, K., James, W.J.: J. Appl. Phys. **54** (1983) 2836.
83 G 10 Graves-Tompson, R.J., White, H.W., Kebe, B., James, W.J.: J. Chem. Phys. **78** (1983) 7502.
83 G 11 Greidanus, F.J.A., De Jongh, L.J., Huiskamp, W.J., Furrer, A., Buschow, K.H.J.: Physica B+C **115** (1983) 137.
83 G 12 Grössinger, R.: Proc. Int. Conf. Magnetism of Rare-Earths and Actinides, Bucharest, Romania **1983**, vol. 1, p. 1.
83 G 13 Grover, A.K., Sarkissian, B.V.B.: J. Magn. Magn. Mater. **31–34** (1983) 515.
83 G 14 Gubbens, P.C.M., Ras, W., Van der Kraan, A.M., Buschow, K.H.J.: Phys. Status Solidi (b) **117** (1983) 277.
83 G 15 Guimaraes, A.P., Alves, N., Alves, K.M.B.: Proc. Int. Conf. Magnetism of Rare-Earths and Actinides, Bucharest, Romania **1983**, vol. 1, p. 74.
83 G 16 Gupta, H.C., Wallace, W.E., Craig, R.S.: J. Magn. Magn. Mater. **36** (1983) 95.
83 G 17 Gurewitz, E., Pinto, H., Dariel, M.P., Shaked, H.: J. Phys. F **13** (1983) 545.
83 G 18 Gignoux, D., Givord, F., Lemaire, R., Tasset, F.: J. Less Common Met. **94** (1983) 165.
83 H 1 Hardmann-Rhyne, K., Rhyne, J.J.: J. Less Common Met. **94** (1983) 23.
83 H 2 Hirosawa, S., Pourarian, F., Sinha, V.K., Wallace, W.E.: J. Magn. Magn. Mater. **38** (1983) 159.
83 H 3 Houard, J., Bisch, P.M., Gomes, A.A.: J. Phys. F **13** (1983) 2629.
83 H 4 Hrubec, J., Steiner, W., Reissner, M.: J. Magn. Magn. Mater. **37** (1983) 93.
83 H 5 Huang, C.Y., Olsen, C.E., Fuller, W.W., Huang, J.H., Wolf, S.A.: Solid State Commun. **45** (1983) 795.
83 I 1 Ibarra, M.R., Del Moral, A.: Proc. Int. Conf. Magnetism of Rare-Earths and Actinides, Bucharest, Romania **1983**, vol. 1, p. 92.
83 I 2 Ichinose, K., Fujiwara, K., Yoshie, H., Nagai, H., Tsujimura, A.: J. Phys. Soc. Jpn. **52** (1983) 4318.
83 I 3 Ilyushin, A.S., Tebenkov, Yu.V., Perov, A.P., Nalgiyev, A.G.M.: Fiz. Met. Metalloved. **56** (1983) 1127.
83 I 4 Isikawa, Y., Higashi, K., Miyazaki, T., Sato, K.: J. Magn. Magn. Mater. **31–34** (1983) 1057.
83 J 1 Jaakkola, S., Parviainen, S., Penttila, S.: J. Phys. F **13** (1983) 491.
83 J 2 James, W.F., Van Schalkwyk, T.G.D., Crowder, C.E.: J. Less Common Met. **94** (1983) 221.
83 J 3 Jin, H.M., Chen, H.N., Tang, D.S., Han, J.F., Shi, Y.: J. Magn. Magn. Mater. **31–34** (1983) 857.
83 J 4 Jurczyk, M.: Phys. Status Solidi (a) **80** (1983) 657.
83 J 5 Jurczyk, M.: Proc. 7th Int. Workshop on Rare Earth-Cobalt Permanent Magnets and their Applications, Beijing, China, **1983**, p. 307.
83 K 1 Kapusta, Cz., Figiel, H., Lalowicz, Z.T.: Proc. Int. Conf. Magnetism of Rare-Earths and Actinides, Bucharest, Romania, **1983**, vol. 1, p. 167.
83 K 2 Kelarev, V.V., Chuev, V.V., Pirogov, A.N., Sidorov, S.K.: Phys. Status Solidi (a) **79** (1983) 57.
83 K 3 Kolodziejczyk, A.: Proc. Int. Conf. Magnetism of Rare-Earth and Actinides, Bucharest, Romania **1983**, vol. 1, p. 171.
83 K 4 Kubota, M., Buchal, C., Mueller, R.M., Pobell, F.: J. Magn. Magn. Mater. **31–34** (1983) 739.
83 K 5 Kelarev, V.V., Chuev, V.V., Pirogov, A.N., Sidorov, S.K.: Phys. Stat. Solidi (b) **118** (1983) K75.
83 L 1 Laforest, J., Lemaire, R., Nagai, H., Tsujimura, A.: Solid State Commun. **48** (1983) 941.
83 L 2 Lewicki, A., Tarnawski, Z., Kapusta, Cz., Kolodziejczyk, A., Figiel, H., Chmist, J., Lalowicz, Z., Sniadower, L.: J. Magn. Magn. Mater. **36** (1983) 297.
83 L 3 Lin, C., Blanckenhagen, P.V., Hilscher, G., Wiesinger, G.: J. Magn. Magn. Mater. **31–34** (1983) 199.

83 L 4 Liu, J., Huston, E.L.: J. Less Common Met. **90** (1983) 11.
83 M 1 Makihara, Y., Andoch, Y., Hashimoto, Y., Fujii, H., Hasuo, M., Okamoto, T.: J. Phys. Soc. Jpn. **52** (1983) 629.
83 M 2 Malik, S.K., Pourarian, F., Wallace, W.E.: J. Magn. Magn. Mater. **40** (1983) 27.
83 M 3 Menovsky, A., Franse, J.J.M.: J. Cryst. Growth **65** (1983) 286.
83 M 4 Miyamoto, M., Yamaji, K., Nataki, Y.: J. Less Common Met. **89** (1983) 117.
83 M 5 Mori, K., Clark, A.E., McMasters, O.D.: J. Magn. Magn. Mater. **31–34** (1983) 855.
83 M 6 Moruzzi, V.L., Williams, A.R., Malozemoff, A.P., Gambino, R.J.: Phys. Rev. B **28** (1983) 5511.
83 M 7 Muraoka, Y., Shiga, M., Nakamura, Y.: J. Magn. Magn. Mater. **31–34** (1983) 121.
83 M 8 Muraoka, Y., Wada, H., Shiga, M., Nakamura, Y.: Physica B+C **119** (1983) 174.
83 N 1 Nagai, H., Yoshie, H., Tsujimura, A.: J. Phys. Soc. Jpn. **52** (1983) 1122.
83 N 2 Nakamura, Y.: J. Magn. Magn. Mater. **31–34** (1983) 829.
83 N 3 Nakamura, Y.: Proc. Int. Conf. Magnetism of Rare-Earths and Actinides, Bucharest, Romania **1983**, vol. 2, p. 47.
83 N 4 Nakamura, Y., Shiga, M., Kawano, S.: Physica B **120** (1983) 212.
83 N 5 Ngai, K.L., Rendell, R.W., Rajagopal, A.K.: Proc. Int. Symp. Electronic Structure and Properties of Hydrogen in Metals, New York: Plenum Press **1983**, p. 473.
83 N 6 Niarchos, D., Viccaro, P.J., Shenoy, G.K., Dunlap, B.D., Yakinthos, J.K.: J. Phys. Chem. Solids **44** (1983) 307.
83 N 7 Nishihara, Y., Yamaguchi, Y.: J. Phys. Soc. Jpn. **52** (1983) 3630.
83 N 8 Noreus, D., Olsson, L.G., Werner, P.E.: J. Phys. F **13** (1983) 715.
83 N 9 Novikov, V.F., Dolgykh, E.V., Gatullin, A.F.: Zh. Tekh. Fiz. **53** (1983) 1877.
83 N 10 Novikov, V.F., Apsiti, L.V., Gamderov, A.F.: Fiz. Met. Metalloved. **56** (1983) 77.
83 N 11 Nowik, I., Felner, I.: Proc. Int. Conf. Magnetism of Rare-Earths and Actinides, Bucharest, Romania **1983**, vol. 1, p. 24.
83 O 1 Oliver, F.W., Kebede, T., Thompson, K., Gilchrist, J.: Solid State Commun. **46** (1983) 837.
83 P 1 Palmer, S.B.: Physica B+C **119** (1983) 130.
83 P 2 Palstra, T.T.M., Mydosh, J.A., Nieuwenhuys, G.J., Van der Kraan, A.M., Buschow, K.H.J.: J. Magn. Magn. Mater. **36** (1983) 290.
83 P 3 Parker, F.T., Oesterreicher, H.: J. Magn. Magn. Mater. **36** (1983) 195.
83 P 4 Parker, F.T., Oesterreicher, H.: J. Less Common Met. **90** (1983) 127.
83 P 5 Parker, F.T., Oesterreicher, H.: Phys. Status Solidi (a) **75** (1983) 273.
83 P 6 Parpia, D.Y., Tanner, B.K., Lord, D.G.: Nature **303** (1983) 684.
83 P 7 Paszkowicz, W., Modrzejewski, A., Rozbiewska, M.: Proc. Int. Conf. Magnetism Rare-Earths and Actinides, Bucharest, Romania **1983**, vol. 1, p. 96.
83 P 8 Pedziwiatr, A.T., Smith, H.K., Wallace, W.E.: J. Solid State Chem. **47** (1983) 41.
83 P 9 Pedziwiatr, A.T., Boltich, E.B., Wallace, W.E., Craig, R.S.: J. Solid State Chem. **46** (1983) 342.
83 P 10 Pedziwiatr, A.T., Boltich, E.B., Wallace, W.E., Craig, R.S.: Proc. Int. Symp. Electronic Structure and Properties of Hydrogen in Metals, New York: Plenum Press **1983**, p. 367.
83 P 11 Pfranger, R., Plusa, D., Wyslocki, B.: Proc. Int. Conf. Magnetism of Rare-Earths and Actinides, Bucharest, Romania **1983**, vol. 1, p. 76.
83 P 12 Pfranger, R., Plusa, D., Wyslocki, B.: Phys. Status Solidi (a) **80** (1983) 73.
83 P 13 Plusa, D., Pfranger, R., Wyslocki, B.: Proc. Int. Conf. Magnetism of Rare-Earths and Actinides, Bucharest, Romania **1983**, vol. 1, p. 84.
83 P 14 Plusa, D., Pfranger, R., Wyslocki, B.: J. Magn. Magn. Mater. **40** (1983) 271.
83 P 15 Ponomareva, O.I., Shur, Y.S., Maykov, V.G., Popov, A.G.: Fiz. Met. Metalloved. **55** (1983) 1101.
83 P 16 Pourarian, F., Wallace, W.E.: J. Less Common Met. **91** (1983) 223.
83 P 17 Prakash, O., Chaudhry, M.A., Ross, J.W., McCausland, M.A.H.: J. Magn. Magn. Mater. **36** (1983) 271.
83 P 18 Pszczola, J., Zukrowski, J., Suwalski, J.: Proc. Int. Conf. Magnetism of Rare-Earths and Actinides, Bucharest, Romania **1983**, vol. 1, p. 80.
83 P 19 Pszczola, J., Zukrowski, J., Suwalski, J., Kucharski, Z., Lukasiak, M.: J. Magn. Magn. Mater. **40** (1983) 197.
83 R 1 Raaen, S., Parks, R.D.: Solid State Commun. **48** (1983) 199.
83 R 2 Radwanski, R.J., Krop, K.: Physica B+C **119** (1983) 180.
83 R 3 Rambabu, D., Nagarajan, R., Malik, S.K., Vijayaraghavan, R., Pourarian, F., Wallace, W.E.: J. Magn. Magn. Mater. **31–34** (1983) 759.
83 R 4 Rhyne, J.J., Koon, N.C.: Proc. Int. Conf. Magnetism of Rare-Earths and Actinides, Bucharest, Romania **1983**, vol. 1, p. 9.

83 R 5 Rhyne, J.J., Hardmann-Rhyne, K., Kevin Smith, H., Wallace, W.E.: J. Less Common Met. **94** (1983) 95.
83 R 6 Riedi, P.C., Webber, G.D.: J. Phys. F **13** (1983) 1057.
83 R 7 Romaka, V.A., Schevich, O.M., Gladyshevskiy, R.Y., Yarmolyuk, Y.P., Grin, Y.N.: Fiz. Met. Metalloved. **56** (1983) 479.
83 R 8 Ross, J.W., Chaudhry, M.A.: Hyp. Int. **14** (1983) 233.
83 S 1 Sahashi, M., Mizoguchi, M., Inomata, K.: J. Magn. Magn. Mater. **31–34** (1983) 225.
83 S 2 Sato, K., Higachi, K., Miyazaki, T., Isikawa, Y.: J. Colloque of Liberal Arts, Toyama University, Japan **16** (1983) 1.
83 S 3 Sato, K., Iwasaki, S., Mori, K., Isikawa, Y.: J. Magn. Magn. Mater. **31–34** (1983) 207.
83 S 4 Satyanarayana, M.V., Fujii, H., Wallace, W.E.: J. Magn. Magn. Mater. **40** (1983) 241.
83 S 5 Savitski, E.M., Torchinova, R.S., Ilyushin, A.S.: Proc. 34th Int. Astronautical Federation, Budapest **1983**, p. 155.
83 S 6 Schäfer, W., Will, G.: J. Less Common Met. **94** (1983) 205.
83 S 7 Shenoy, G.K., Schuttler, B., Viccaro, P.J., Niarchos, D.: J. Less Common Met. **94** (1983) 37.
83 S 8 Shevchenko, V.I., Pogorelyi, A.N., Perepelitza, A.V.: Fiz. Tverd. Tela **25** (1983) 2203.
83 S 9 Shibata, T., Katayama, T.: J. Magn. Magn. Mater. **31–34** (1983) 1029.
83 S 10 Shiga, M., Nakamura, Y.: J. Magn. Magn. Mater. **31–34** (1983) 1411.
83 S 11 Shiga, M., Wada, H., Nakamura, Y.: J. Magn. Magn. Mater. **31–34** (1983) 119.
83 S 12 Shimotomai, M., Doyama, J.: J. Magn. Magn. Mater. **31–34** (1983) 215.
83 S 13 Sidzhimov, B.S., Neov, S.D., Nikitin, S.A.: Bulgarian J. Phys. **10** (1983) 203.
83 S 14 Sidzhimov, B., Neov, S., Stanev, N., Bozukov, L.: Bulgarian J. Phys. **10** (1983) 328.
83 S 15 Sima, V., Smetana, T., Sechovsky, V., Grössinger, R., Franse, J.J.M.: J. Magn. Magn. Mater. **31–34** (1983) 201.
83 S 16 Sinha, V.K., Wallace, W.E.: J. Less Common Met. **91** (1983) 239.
83 S 17 Sinha, V.K., Pourarian, F., Wallace, W.E.: J. Less Common Met. **91** (1983) 229.
83 S 18 Slebarski, A., Kaczmarska, K., Kwapulinska, E.: J. Magn. Magn. Mater. **38** (1983) 51.
83 S 19 Slepowronski, M., Warchol, S., Modrzejewski, A.: Proc. Int. Conf. Magnetism of Rare-Earths and Actinides, Bucharest, Romania **1983**, vol. 1, p. 100.
83 S 20 Slepowronski, M., Warchol, S., Modrzejewski, A.: J. Cryst. Growth **65** (1983) 293.
83 S 21 Smetana, Z., Sima, V., Gratz, E., Franse, J.J.M.: J. Magn. Magn. Mater. **31–34** (1983) 633.
83 S 22 Smith, H.K., Wallace, W.E., Craig, R.S.: J. Less Common Met. **94** (1983) 89.
83 S 23 Stetsenko, P.N.: Proc. Int. Conf. Magnetism of Rare-Earths and Actinides, Bucharest, Romania **1983**, vol. 2, p. 55.
83 S 24 Stewart, G.A., Whittle, G.L., Campbell, S.J.: Hyp. Int. **16** (1983) 681.
83 S 25 Sulkowski, C., Rogacki, K., Kolodziejczyk, A., Kozlowski, G., Chmist, J.: J. Phys. F **13** (1983) 2147.
83 T 1 Takeda, S.: J. Sci. Hiroshima Univ. Ser. A **46** (1983) 149.
83 T 2 Takigawa, M., Yasuoka, H., Yamaguchi, Y., Ogawa, S.: J. Phys. Soc. Jpn. **52** (1983) 3318.
83 T 3 Tanaka, S.: J. Less Common Met. **89** (1983) 169.
83 T 4 Terao, K., Shimizu, M.: Phys. Lett. **95** A (1983) 111.
83 T 5 Tsushima, T., Ohokashi, M.: J. Magn. Magn. Mater. **31–34** (1983) 197.
83 T 6 Tsvyashchenko, A.V., Popova, S.V., Makhotkin, V.E., Frandkov, V.A., Zaritski, V.N.: Proc. Int. Conf. Magnetism of Rare-Earths and Actinides. Bucharest, Romania, **1983**, vol. 2, p. 85.
83 T 7 Tsvyashchenko, A.V., Popova, S.V.: J. Less Common Met. **90** (1983) 211.
83 T 8 Tsvyashchenko, A.V., Popova, S.V., Makhotkin, V.E., Fradkov, V.A., Zaritski, V.N.: Proc. Int. Conf. Magnetism of Rare-Earths and Actinides, Bucharest, Romania **1983**, vol. 1, p. 135.
83 T 9 Turilli, G., Rinaldi, S., Leccabue, F.: Proc. Int. Conf. Magnetism of Rare-Earths and Actinides, Bucharest, Romania **1983**, vol. 1, p. 104.
83 U 1 Uehara, M.: J. Magn. Magn. Mater. **31–34** (1983) 1017.
83 U 2 Ursu, I., Burzo, E., Seitabla, D.: Proc. Int. Conf. Magnetism of Rare-Earths and Actinides, Bucharest, Romania **1983**, vol. 1, p. 126.
83 V 1 Van der Kraan, A.M., Buschow, K.H.J., Palstra, T.T.M.: Hyp. Int. **15–16** (1983) 717.
83 V 2 Vasilkovski, V.A., Gorlenko, A.A., Kovtun, N.M., Siryuk, V.M.: J. Eksp. Teor. Fiz. **85** (1983) 1349.
83 V 3 Vasilkovski, V.A., Gorlenko, A.A., Kovtun, N.M., Siryuk, V.M.: Fiz. Tverd. Tela **25** (1983) 3157.
83 W 1 Wada, S., Kohara, T., Asayama, K., Kitaoka, Y., Kohori, Y., Ishikawa, N.: Solid State Commun. **48** (1983) 5.
83 W 2 Wallace, W.E., Fujii, H., Boltich, E., Hirosawa, S., Pourarian, F., Merches, M., Oswald, E., Schwab, E., Satyanarayana, M.V.: Proc. Int. Conf. Magnetism of Rare-Earths and Actinides. Bucharest, Romania **1983**, vol. 2, p. 1.

83 W 3 Westlake, D.G.: J. Mater. Sci. **18** (1983) 605.
83 W 4 Westlake, D.G.: J. Less Common Met. **91** (1983) 275.
83 W 5 Westlake, D.G.: J. Less Common Met. **90** (1983) 251.
83 Y 1 Yamada, Y., Ohira, K.: J. Phys. Soc. Jpn. **52** (1983) 3646.
83 Y 2 Yamada, H., Shimizu, M.: J. Magn. Magn. Mater. **31–34** (1983) 211.
83 Y 3 Yamaguchi, Y., Nishihara, Y., Ogawa, S.: J. Magn. Magn. Mater. **31–34** (1983) 513.
83 Y 4 Yamaguchi, M., Ohta, T., Katayama, T.: J. Magn. Magn. Mater. **31–34** (1983) 221.
83 Y 5 Yang, Y., Ho, W., Lu, Z.: Proc. 7th Int. Workshop on Rare Earth-Cobalt Permanent Magnets and their Applications, Beijing, China **1983**, p. 247.
83 Y 6 Yoshimoto, N., Sakurai, J., Komura, Y.: J. Magn. Magn. Mater. **31–34** (1983) 137.
83 Y 7 Yoshimura, K., Nakamura, Y.: J. Magn. Magn. Mater. **40** (1983) 55.
83 Y 8 Yvon, K., Braun, H.F., Gratz, E.: J. Phys. F **13** (1983) L 131.
83 Z 1 Zarek, W., Kasprzyk, A., Kozubek, E.: Phys. Status Solidi (a) **75** (1983) 359.
83 Z 2 Zeng, X.X., Zhu, J.X., Jin, L., Zhou, H.M., Zhang, B.S., Yang, J.L., Yang, Y.C., He, W.W., Lin, C., Luo, S., Pei, X.D.: Acta Phys. Sinica **32** (1983) 1608.
83 Z 3 Zhao, J., Lu, Q., Chen, X., Chen, J., Zhang, J., Xia, Y.: Proc. 7th Int. Workshop on Rare Earth-Cobalt Permanent Magnets, Beijing, China **1983**, p. 287.
83 Z 4 Zhuang, Y., Wu, C., Zhang, S., Li, Z.: Proc. 7th Int. Workshop on Rare Earth-Cobalt Permanent Magnets, Beijing, China **1983**, p. 255.
83 Z 5 Zukrowski, J., Stewart, G.A., Kalkowski, G., Wortmann, G., Wiesinger, G.: Crystalline Electric Field Effects in f-Electron Systems, New York: Plenum Press **1983**, p. 149.
83 Z 6 Zurczik, M.: Phys. Status Solidi (a) **80** (1983) 657.

84 A 1 Abe, T.: J. Phys. Soc. Jpn. **53** (1984) 1837.
84 A 2 Adachi, G.Y., Nagai, H., Shiokawa, J.: J. Less Common Met. **97** (1984) L 9.
84 A 3 Akimenko, A.I., Yanson, I.K.: Fiz. Nizk. Temp. **10** (1984) 889.
84 A 4 Akimenko, A.I., Ponomarenko, N.M., Yanson, I.K.: Proc. Int. Conf. Low Temp. Phys. **17** (1984) 1394.
84 A 5 Akimenko, A.I., Ponomarenko, N.M., Yanson, I.K., Ianos, Sh., Raiffers, M.: Fiz. Tverd. Tela **26** (1984) 2264.
84 A 6 Akselrod, Z.Z., Bondarkov, M.D., Budzynski, M., Komissarova, B.A., Kryukova, L.N., Serrano, U.A.P., Ryasny, G.K., Sorokin, A.A., Shpinkova, L.G.: Fiz. Tverd. Tela **26** (1984) 2175.
84 A 7 Al-Assadi, K.F., Mackenzie, F.S., McCausland, M.A.: J. Phys. F **14** (1984) 525.
84 A 8 Aleksandryan, V.V., Levitin, R.Z., Markosyan, A.S.: Fiz. Tverd. Tela **26** (1984) 1921.
84 A 9 Aleksandryan, V.V., Belov, K.P., Levitin, R.Z., Markosyan, A.S., Snegirev, V.V.: Pis'ma Zh. Eksp. Teor. Fiz. **40** (1984) 815.
84 A 10 Alekseev, P.A., Orlov, V.G., Sadikov, I.P., Kjems, J.K.: J. Less Common Met. **101** (1984) 419.
84 A 11 Allibert, C., Ballou, R., Bley, F., Deportes, J., Gignoux, D., Givord, D., Laforest, J., Lemaire, R.: Proc. 2nd Int. Conf. Phys. of Magnetic Materials, Jadwisin, Poland **1984**, p. 283.
84 A 12 Andreev, A.V., Deryagin, A.V., Ezov, A.A., Mushinkov, N.V.: Fiz. Met. Metalloved. **58** (1984) 1179.
84 A 13 Andreev, A.V., Bartashevich, M.I., Deryagin, A.V.: Zh. Eksp. Teor. Fiz. **87** (1984) 623.
84 A 14 Apsitis, L.V., Novikov, V.F.: Fiz. Met. Metalloved. **58** (1984) 699.
84 B 1 Baranov, N.V., Deryagin, A.V., Kvashnin, G.M.: Pis'ma Zh. Eksp. Teor. Fiz. **10** (1984) 598.
84 B 2 Baranov, N.V., Deryagin, A.V., Kozlov, A.I., Sinitzki, E.V.: Fiz. Met. Metalloved. **61** (1984) 733.
84 B 3 Bartaschevich, M.I., Deryagin, A.V., Kudrevatykh, R.V., Tarasov, E.N.: Zh. Eksp. Teor. Fiz. **26** (1984) 1505.
84 B 4 Bayer, G., Wallace, W.E.: J. Phys. Chem. **88** (1984) 3220.
84 B 5 Belov, K.P., Borombayev, N.K., Markosyan, A.S., Snegirev, V.V.: Fiz. Met. Metalloved. **57** (1984) 506.
84 B 6 Bogatin, Ya.G., Zemchenkov, V.S., Povolotski, E.G.: Poroshk. Met. **23** (1984) 37.
84 B 7 Brandt, N.B., Moschalkov, V., Sluchanko, N.E., Savitzki, E., Schkatova, T.M.: Fiz. Tverd. Tela **26** (1984) 2110.
84 B 8 Brown, P.J., Ziebeck, K.R.A., Deportes, J., Givord, D.: J. Appl. Phys. **55** (1984) 1881.
84 B 9 Burzo, E.: Proc. 2nd Int. Conf. Phys. of Magnetic Materials, Jadwisin, Poland, **1984**, p. 304.
84 B 10 Burzo, E.: Proc. 11th Congress AMPERE, Zürich, Switzerland **1984**, p. 295.
84 B 11 Burzo, E., Balanescu, M.: J. Phys. C **17** (1984) 3247.
84 B 12 Buschow, K.H.J.: J. Less Common Met. **97** (1984) 185.
84 B 13 Buschow, K.H.J.: J. Less Common Met. **100** (1984) 29.
84 C 1 Cabus, S., Gloss, K., Gottwick, V., Horn, S., Klemm, M., Kübler, J., Steglich, F.: Solid State Commun. **51** (1984) 909.

84C2 Chaudry, R., Jha, S.S.: Pramana **22** (1984) 431.
84C3 Chuang, Y.C., Wu, C.H., Chang, S.C., Li, T.C.: J. Less Common Met. **97** (1984) 245.
84C4 Chuang, Y.C., Wu, C.H., Li, T.C., Chang, S.C., Kao, L.: J. Less Common Met. **96** (1984) 183.
84C5 Clark, A.E., Savage, H.T., Spano, M.L.: IEEE Trans. Magn. MAG-**20** (1984) 1443.
84D1 Dai, S.Y., Wang, J.L., Wang, C.G.: Kexue Tongbao **29** (1984) 1452.
84D2 Deryagin, A.V., Kvashnin, G.M., Kapitonov, A.M.: Fiz. Met. Metalloved. **57** (1984) 686.
84D3 Deryagin, A.V., Kvashnin, G.M., Kapitonov, A.M.: Fiz. Tverd. Tela **26** (1984) 3106.
84D4 Deryagin, A.V., Moskalev, V.N., Mushinkov, N.V., Terentiev, S.V.: Fiz. Met. Metalloved. **57** (1984) 1086.
84D5 Deryagin, A.V., Kudrevatykh, N.V., Moskalev, V.N., Mushinkov, N.V.: Fiz. Met. Metalloved. **58** (1984) 1148.
84D6 Dolgyh, E.V., Novikov, V.F.: Fiz. Met. Metalloved. **57** (1984) 692.
84D7 Drulis, H., Petrynski, W., Stalinski, B.: J. Less Common Met. **101** (1984) 229.
84E1 Endrzheevskaya, S.N., Lukyanchikov, V.S., Shablina, A.G., Skorkhod, V.V., Denbnovetskaya, E.N.: Poroshk. Metall. **23** (1984) 62.
84E2 Ermolenko, A.S., Korolev, A.V., Kuchin, A.G.: Fiz. Met. Metalloved. **57** (1984) 914.
84F1 Fahnle, M., Oesterreicher, H.: Phys. Rev. B **29** (1984) 2793.
84F2 Fillion, G., Gignoux, D., Givord, F., Lemaire, R.: J. Magn. Magn. Mater. **44** (1984) 173.
84F3 Flanagan, T.B., Majorowski, S., Clewley, J.D., Park, C.: J. Less Common Met. **103** (1984) 93.
84F4 Fujii, H., Pourarian, F., Wallace, W.E.: J. Less Common Met. **103** (1984) 267.
84G1 Gignoux, D., Gomez-Sal, J.C.: Phys. Rev. B **30** (1984) 3967.
84G2 Goremychkin, E.A., Mühle, E.: Pis'ma Zh. Eksp. Teor. Fiz. **39** (1984) 469.
84G3 Goremychkin, E.A., Mühle, E., Ivanutski, P.G., Krotenko, V.T., Pasechnik, M.U., Slisenko, V.V., Vasiklevich, A.A., Lippold, E., Chistyakov, O.D., Savitski, E.M.: Phys. Status Solidi (b) **121** (1984) 623.
84G4 Goudy, A.J., Wallingford, R.A.: J. Less Common Met. **99** (1984) 249.
84G5 Gubbens, P.C.M., Van der Kraan, A.M., Buschow, K.H.J.: J. Phys. F **14** (1984) 235.
84G6 Gubbens, P.C.M., Van der Kraan, A.M., Buschow, K.H.J.: J. Phys. F **14** (1984) 2195.
84G7 Gubbens, P.C.M., Van der Kraan, A.M., Buschow, K.H.J.: J. Appl. Phys. **56** (1984) 2547.
84G8 Guedes de Sousa, E.B., Sa, M.A., Montenegro, J.F.D., Machado da Silva, J.M., Melville, D.: Solid State Commun. **49** (1984) 853.
84G9 Gupta, H.O., Malik, S.K., Wallace, W.E.: J. Magn. Magn. Mater. **42** (1984) 339.
84G10 Gupta, H.O., Wallace, W.E., Oswald, E.: J. Magn. Magn. Mater. **50** (1984) 339.
84G11 Gygax, F.N., Hintermann, A., Ruegg, W., Schenck, A., Studer, W., Van Der Wal, A.J., Stucki, F., Schlapbach, L.: J. Less Common Met. **101** (1984) 327.
84H1 Hardman-Rhyne, K., Kevin-Smith, H., Wallace, W.E.: J. Less Common Met. **96** (1984) 201.
84H2 Hardman-Rhyne, K., Rhyne, J.J., Prince, E., Crowder, C., James, W.J.: Phys. Rev. B **29** (1984) 416.
84H3 Harris, M.B., Stewart, G.A., Creagh, D.C.: Proc. 8th Int. Phys. Condensed Matter Meeting, February **1984**.
84H4 Hempelmann, R., Richter, D., Eckold, G., Rush, J.J., Rowe, J.M., Montoya, M.: J. Less Common Met. **104** (1984) 1.
84H5 Herbst, J.F., Croat, J.J.: J. Appl. Phys. **55** (1984) 3023.
84H6 Herbst, J.F., Croat, J.J., Van Laar, B., Yelon, W.B.: J. Appl. Phys. **56** (1984) 1224.
84H7 Hirosawa, S., Pourarian, F., Wallace, W.E.: J. Magn. Magn. Mater. **43** (1984) 187.
84H8 Houard, J., Bisch, P.M., Gomes, A.A.: J. Phys. F **14** (1984) 2729.
84I1 Ibarra, M.R., Del Moral, A., Abell, J.S.: J. Magn. Magn. Mater. **46** (1984) 157.
84I2 Ibarra, M.R., Del Moral, A., Abell, J.S.: J. Phys. Chem. Solids **45** (1984) 789.
84I3 Ibarra, M.R., Arnaudas, J.I., Algarabel, P.A., Del Moral, A.: J. Magn. Magn. Mater. **46** (1984) 167.
84I4 Ikeda, K., Gschneidner, K.A., Stierman, R.J., Tsang, T.W.E., McMasters, O.D.: Phys. Rev. B **29** (1984) 5039.
84I5 Ilyushin, A.S., Makhmud, I.A.: Izv. Vyssh. Uchebn. Zaved. Fiz. **27** (1984) 52.
84I6 Inoue, J., Shimizu, M.: Phys. Lett. **104** A (1984) 166.
84I7 Ishikawa, Y., Mori, K., Sato, K., Chashi, M., Yamaguchi, Y.: J. Appl. Phys. **55** (1984) 2031.
84I8 Ishiyama, K., Shinogi, A., Endo, K.: J. Phys. Soc. Jpn. **53** (1984) 2456.
84J1 Juranek, Z., Potocky, L.: Czech. J. Phys. B **34** (1984) 1079.
84J2 Jurczyk, W., Wrzeciono, A.: IEEE Trans. Magn. MAG-**20** (1984) 1578.
84K1 Kakol, Z., Figiel, H., Turek, K.: IEEE Trans. Magn. MAG-**20** (1984) 1605.

84 K 2 Kataev, G.I., Leontev, P.I., Nikitin, S.A., Talalaeva, E.V., Shubin, V.V.: Fiz. Met. Metalloved. **58** (1984) 613.
84 K 3 Kavaman, I.D., Savchenkova, S.F., Kelarev, V.V., Sidorov, S.K., Liberman, A.A.: Fiz. Met. Metalloved. **57** (1984) 808.
84 K 4 Kierstead, H.A.: J. Less Common Met. **96** (1984) 133.
84 K 5 Kirchmayr, H.: Proc. 2nd Int. Conf. Phys. of Magnetic Materials, Jadwisin, Poland **1984**, p. 338.
84 K 6 Kirchmayr, H.R.: IEEE Trans. Magn. MAG-**20** (1984) 1645.
84 K 7 Kolodziejczyk, A., Sulkowski, C.: Proc. Int. Conf. Low Temp. Phys. **17** (1984) BN 14.
84 K 8 Kolodziejczyk, A., Spalek, J.: J. Phys. F **14** (1984) 1277.
84 K 9 Krasnikova, G.N., Litvintsev, V.V., Bodak, O.I., Koshel, O.D., Kolotun, V.F.: Izv. Vyssh. Uchebn. Zaved. Fiz. **27** (1984) 50.
84 K 10 Krishnan, K.M., Rabenberg, L., Mishra, R.K., Thomas, G.: J. Appl. Phys. **55** (1984) 2058.
84 K 11 Kudrevatykh, N.V., Li, Y.V., Melville, D.: Fiz. Met. Metalloved. **58** (1984) 709.
84 L 1 Lamloumi, J., Percheron-Guegan, A., Achard, J.C., Jehano, G., Givord, D.: J. Phys. (Paris) **45** (1984) 1643.
84 L 2 Lartigue, G., Percheron-Guegan, A., Achard, J.C., Bee, M., Dianoux, A.J.: J. Less Common Met. **101** (1984) 391.
84 L 3 Lawrence, J.M., De Boer, M.L., Parks, R.D., Smith, J.L.: Phys. Rev. B **29** (1984) 568.
84 L 4 Lehtinen, M., Parviainen, S., Stenholm, H.: Ann. Acad. Sci. Fenn. Ser. AVI **1984**, 430.
84 L 5 Levitin, R.Z., Markosyan, A.S., Snegirev, V.V.: Fiz. Tverd. Tela **26** (1984) 29.
84 L 6 Levitin, R.Z., Markosyan, A.S., Snegirev, V.V.: Fiz. Met. Metalloved. **57** (1984) 274.
84 L 7 Lutziv, P.B., Koterlin, M.D., Babich, O.I.: Fiz. Tverd. Tela **26** (1984) 1781.
84 L 8 Lutziv, R.V., Koterlin, M.D., Babich, O.I., Bodak, O.I.: Fiz. Tverd. Tela **26** (1984) 1182.
84 M 1 Malik, S.K., Bayer, G.T., Boltich, E.B., Wallace, W.E.: J. Less Common Met. **98** (1984) 109.
84 M 2 Monterroso, R.E.M.: Thesis, Univ. Grenoble **1984**.
84 M 3 Mori, K., Ishikawa, Y., Sato, K.: J. Phys. Soc. Jpn. **53** (1984) 664.
84 M 4 Muraoka, Y., Okuda, H., Shiga, M., Nakamura, Y.: J. Phys. Soc. Jpn. **53** (1984) 331.
84 M 5 Muraoka, Y., Okuda, H., Shiga, M., Nakamura, Y.: J. Phys. Soc. Jpn. **53** (1984) 1453.
84 N 1 Nakanishi, H.: J. Phys. Soc. Jpn. **53** (1984) 4332.
84 N 2 Nishihara, Y., Yamaguchi, Y.: J. Phys. Soc. Jpn. **53** (1984) 2201.
84 N 3 Nishihara, H., Kido, G., Nishihara, Y., Itoh, M., Yasuoka, H.: Solid State Commun. **49** (1984) 1113.
84 N 4 Novikov, V.F., Dolgykh, E.V.: Fiz. Tverd. Tela **26** (1984) 214.
84 O 1 Oesterreicher, H.: J. Less Common Met. **99** (1984) L 17.
84 O 2 Oesterreicher, H., Parker, F.T.: J. Appl. Phys. **55** (1984) 4334.
84 O 3 Olcese, G.L., Canepa, F., Costa, G.A.: Solid State Commun. **51** (1984) 825.
84 O 4 Oraltay, R.G., Franse, J.J.M., Brommer, P.E., Menovsky, A.: J. Phys. F **14** (1984) 737.
84 P 1 Palerno, L., Da Silva, X.A.: J. Magn. Magn. Mater. **43** (1984) 308.
84 P 2 Palstra, T.T.M., Nieuwenhuys, G.J., Mydosh, J.A., Buschow, K.H.J.: J. Appl. Phys. **55** (1984) 2367.
84 P 3 Palstra, T.T.M., Werij, H.C.C., Nieuwenhuys, G.J., Mydosh, J.A., De Boer, F.R., Buschow, K.H.J.: J. Phys. F **14** (1984) 1961.
84 P 4 Parker, F.T.: Solid State Commun. **50** (1984) 637.
84 P 5 Pasturel, A., Liautaud, F., Colinet, C., Allibert, C., Percheron-Guegan, A., Achard, J.C.: J. Less Common Met. **96** (1984) 93.
84 P 6 Patrikeev, Yu.B., Levinski, Yu.V., Badovski, V.V., Filyand, Yu.M.: Izv. Akad. Nauk SSSR Neorg. Mater. **20** (1984) 1503.
84 P 7 Pearson, W.B.: J. Less Common Met. **96** (1984) 103.
84 P 8 Pearson, W.B.: J. Less Common Met. **96** (1984) 115.
84 P 9 Pedziwiatr, A.T., Pourarian, F., Wallace, W.E.: J. Appl. Phys. **55** (1984) 1987.
84 P 10 Pedziwiatr, A.T., Pourarian, F., Wallace, W.E.: J. Solid State Chem. **33** (1984) 263.
84 P 11 Pillay, R.G., Devare, S.H., Pleiter, F., Devare, H.G.: Phys. Status Solidi (b) **121** (1984) K 141.
84 P 12 Pirogov, A.N., Kelarev, V.V., Chuev, V.V.: Fiz. Met. Metalloved. **58** (1984) 615.
84 P 13 Plusa, D., Pfranger, R., Wyslocki, B.: J. Less Common Met. **99** (1984) 87.
84 P 14 Plusa, D., Pfranger, R., Wyslocki, B.: J. Magn. Magn. Mater. **40** (1984) 271.
84 P 15 Pourarian, F., Pedziwiatr, A.T., Wallace, W.E.: J. Appl. Phys. **55** (1984) 1981.
84 P 16 Pszczola, J., Zukrowski, J., Krop, K., Suwalski, J.: J. Magn. Magn. Mater. **44** (1984) 223.
84 R 1 Reiffers, M., Flachbart, K., Beznosov, A.B.: Proc. Int. Conf. Low. Temp. Phys. **17** (1984) 1087.
84 R 2 Reilly, J.J., Johnson, J.R.: J. Less Common Met. **104** (1984) 175.
84 R 3 Reissner, M., Steiner, W., Kappler, J.P., Bauer, P., Besnus, M.J.: J. Phys. F **14** (1984) 1249.

84 R 4 Rinaldi, S.: Proc. 2nd Int. Conf. Phys. of Magnetic Materials, Jadwisin, Poland **1984**, p. 392.
84 S 1 Sarkissian, B.V.B., Tholence, J.L.: J. Appl. Phys. **55** (1984) 2025.
84 S 2 Sarkissian, B.V.B., Beille, J.: J. Appl. Phys. **55** (1984) 2004.
84 S 3 Satyanarayana, M.V., Fujii, H., Wallace, W.E.: J. Magn. Magn. Mater. **40** (1984) 241.
84 S 4 Savitski, E.M., Torchinova, R.S., Ilyushin, A.S.: Proc. 35th Int. Astronautical Federation, Lausanne **1984**, p. 1.
84 S 5 Schwarz, K., Mohn, P.: J. Phys. F **14** (1984) L 129.
84 S 6 Scoboria, P., Harris, A., Andraka, B., Mihalisin, T., Raaen, S., Parks, R.D.: J. Appl. Phys. **55** (1984) 1969.
84 S 7 Shamir, N., Atzmony, U., Gavara, Z., Mintz, M.H.: J. Less Common Met. **103** (1984) 367.
84 S 8 Shimizu, M., Inoue, J., Nagasawa, S.: J. Phys. F **14** (1984) 2673.
84 S 9 Shimotomai, M., Fujisawa, H., Doyama, M.: J. Jpn. Inst. Metals **48** (1984) 233.
84 S 10 Sima, V., Smetana, Z.: Solid State Commun. **49** (1984) 981.
84 S 11 Sima, V., Grössinger, R., Sechovsky, V., Smetana, Z., Sassik, H.: J. Phys. F **14** (1984) 981.
84 S 12 Sinha, V.K., Wallace, W.E.: J. Less Common Met. **96** (1984) 283.
84 S 13 Skolozdra, R.V., Koretskaya, D.E., Gorelenkov, Y.K.: Izv. Akad. Nauk SSSR Neorg. Mater. **20** (1984) 604.
84 S 14 Slebarski, A., Zahorowski, W.: J. Phys. F **14** (1984) 1553.
84 S 15 Sokolovskaya, E.M., Raevskaya, M.V., Efremenko, N.E.: Izv. Akad. Nauk SSSR Met. **4** (1984) 231.
84 S 16 Stewart, A.M.: J. Phys. C **17** (1984) 1557.
84 S 17 Stieler, S., Heiden, C., Kuntze, K., Kohake, D.: IEEE Trans. Magn. MAG-**20** (1984) 1581.
84 S 18 Strnat, K.J., Li, D., Mildrum, H.F.: J. Appl. Phys. **55** (1984) 2100.
84 T 1 Tai, L.C.: J. Appl. Phys. **55** (1984) 300.
84 T 2 Tsvyashchenko, A.V., Popova, S.V., Makhotkin, V.E., Fradkov, V.A., Zaritski, V.N.: J. Less Common Met. **96** (1984) 99.
84 U 1 Uchida, H., Huang, Y.C.: J. Less Common Met. **101** (1984) 459.
84 V 1 Vasilkovski, V.A., Gorelenko, A.A., Kovtun, H.M., Siryuk, V.M.: Fiz. Tverd. Tela **26** (1984) 267.
84 V 2 Vittoria, C., Schelleng, J.H., Lubitz, P., Forester, D.W.: J. Appl. Phys. **55** (1984) 2450.
84 W 1 Wallace, W.E.: J. Less Common Met. **100** (1984) 85.
84 W 2 Wallace, W.E., Craig, R.S., Gupta, H.D., Hirosawa, S., Pedziwiatr, A., Oswald, E., Schwab, E.: IEEE Trans. Magn. MAG-**20** (1984) 1599.
84 Y 1 Yamada, H., Inoue, J., Terao, K., Kanda, S., Shimizu, M.: J. Phys. F **14** (1984) 1943.
84 Y 2 Yamada, Y., Kitaoka, Y., Asayama, K., Sakata, A.: J. Phys. Soc. Jpn. **53** (1984) 3198.
84 Y 3 Yamada, Y., Kitaoka, Y., Asayama, K., Sakata, A.: J. Phys. Soc. Jpn. **53** (1984) 3634.
84 Y 4 Yamaguchi, Y., Nishihara, Y.: Solid State Commun. **50** (1984) 785.
84 Y 5 Yamaguchi, Y., Nishihara, Y., Ogawa, S.: J. Phys. Soc. Jpn. **53** (1984) 3985.
84 Y 6 Yoshimura, K., Nakamura, Y.: J. Phys. Soc. Jpn. **53** (1984) 3611.
84 Y 7 Yoshimura, K., Hirowasa, S., Nakamura, Y.: J. Phys. Soc. Jpn. **53** (1984) 2120.
84 Y 8 Yoshimura, K., Shimizu, T., Takigawa, M., Yasuoke, H., Nakamura, Y.: J. Phys. Soc. Jpn. **53** (1984) 503.
84 Y 9 Yvon, K.: J. Less Common Met. **103** (1984) 53.
84 Z 1 Zeng, X.X., Zhou, H.M., Zhang, B.S., Jin, L., Yang, J.L., Yang, Y.C., He, W.W., Lin, C., Luo, S., Pei, X.D.: Acta Phys. Sinica **33** (1984) 850.

85 A 1 Abbati, I., Braicovich, L., Michelis, B., Fasana, A., Olcese, G.L., Canepa, F., Costa, G.A.: Solid State Commun. **55** (1985) 1081.
85 A 2 Adachi, G., Sakaguchi, H., Niki, K., Nagai, N., Shinokawa, J.: J. Less Common Met. **108** (1985) 107.
85 A 3 Adler, E., Hamann, P.: Proc. 8th Int. Workshop on Rare Earth-Cobalt Permanent Magnets and their Applications, Dayton, Ohio **1985**, p. 747.
85 A 4 Ait-Bahammou, A., Hartmann-Boutron, F., Meyer, C., Gros, Y., Berthier, Y.: Proc. Int. Conf. Appl. Mössbauer Effect, Leuwen, Holland **1985**.
85 A 5 Alameda, J.M., Givord, D., Jeandey, C., Li, H.S., Oddou, J.L.: J. Phys. (Paris) **46** (1985) 1581.
85 A 6 Aleksandryan, V.V., Lagutin, A.S., Levitin, R.Z., Markosyan, A.S., Snegirev, V.V.: Zh. Eksp. Teor. Fiz. **89** (1985) 271.
85 A 7 Alekseev, P.A., Lazukov, V.N., Sadikov, I.P., Sergeeva, I.A., Khlopkin, M.N.: Pis'ma Zh. Eksp. Teor. Fiz. **41** (1985) 492.
85 A 8 Alekseev, P.A., Ivanitski, P.G., Kost, M.E., Maistrenko, A.N., Pasechnik, M.V., Sadikov, I.P., Shilov, A.L.: Fiz. Tverd. Tela **27** (1985) 3173.

85A9 Andraka, B., Timlin, J., Mihalisin, T.: J. Magn. Magn. Mater. **47–48** (1985) 93.
85A10 Andreev, A.V., Deryagin, A.V., Zadvorkin, S.M.: Fiz. Met. Metalloved. **60** (1985) 730.
85A11 Andreev, A.V., Deryagin, A.V., Zadvorkin, S.M.: Fiz. Met. Metalloved. **59** (1985) 339.
85A12 Andreev, A.V., Bartashevich, M.I., Deryagin, A.V., Tarasov, E.N.: Zh. Eksp. Teor. Fiz. **89** (1985) 959.
85A13 Andreev, A.V., Deryagin, A.V., Zadvorkin, S.M., Kvashinin, G.M.: Fiz. Tverd. Tela **27** (1985) 3164.
85A14 Andreev, A.V., Bartashevich, M.I., Deryagin, A.V., Kudrevatyh, N.V., Tarasov, E.N.: Fiz. Met. Metalloved. **60** (1985) 864.
85A15 Andreev, A.V., Deryagin, A.V., Zadvorkin, S.M., Moskalev, V.N., Sinitsin, Y.V.: Fiz. Met. Metalloved. **59** (1985) 481.
85A16 Ansaldo, E.J., Noakes, D.R., Brewer, J.H., Harshman, D.R., Keitel, R., Senba, M., Huang, C.Y., Sarkissian, B.V.B.: Solid State Commun. **55** (1985) 193.
85B1 Bach, T.C.: Phys. Status Solidi (b) **128** (1985) 503.
85B2 Barata, A.C., Guimaraes, A.P.: Physica B **130** (1985) 484.
85B3 Belorizky, E., Berthier, Y.: Physica B **130** (1985) 474.
85B4 Berthier, V., De Saxce, T., Fruchart, D., Vuillet, P.: Physica B **130** (1985) 520.
85B5 Besnus, M.J., Bauer, P., Kappler, J.P., Reissner, M., Steiner, W.: Physica B **130** (1985) 423.
85B6 Bohlmann, M.A.: Proc. 8th Int. Workshop on Rare Earth-Cobalt Permenant Magnets and their Applications, Dayton, Ohio **1985**, p. 321.
85B7 Bondarkov, M.D., Budzinski, M., Sorokin, A.A., Shpinkova, L.G.: Vestn. Mosk. Univ. Ser. 3, **40** (1985) 92.
85B8 Brandt, N.B., Moshchalkov, V.V., Sluchanko, N.E., Gippins, A.A., Shkatova, T.M.: Fiz. Tverd. Tela **27** (1985) 2484.
85B9 Burzo, E.: J. Appl. Phys. **57** (1985) 3232.
85B10 Burzo, E.: New Frontiers in Rare Earth Science and Applications, Beijing, China **1985**, vol. 2, p. 948.
85B11 Burzo, E., Pop, V., Plugaru, N.: J. Less Common Met. **111** (1985) 97.
85B12 Burzo, E., Pop, V., Plugaru, N.: New Frontiers in Rare Earth Science and Applications, Beijing, China **1985**, vol. 2, p. 904.
85B13 Burzo, E., Plugaru, N., Pop, V.: Acta Phys. Pol. A **68** (1985) 479.
85B14 Buschow, K.H.J.: Philips J. Res. **40** (1985) 305.
85C1 Camp, F.E., Narasimhan, K.S.V.L., Hurt, J.C.: IEEE Trans. Magn. MAG-**21** (1985) 1970.
85C2 Chang, Y.C., Jiang, J., Chuang, Y.C.: J. Less Common Met. **107** (1985) 1.
85C3 Chuang, Y.C., Wu, C.H., Chen, H.B.: J. Less Common Met. **106** (1985) 219.
85C4 Chuang, Y.C., Wu, C.H., Chen, H.B.: J. Less Common Met. **106** (1985) 41.
85C5 Chuang, Y.C., Wu, C.H., Chang, S.C., Li, T.C., Wang, Y.C.: Proc. 8th Int. Workshop on Rare Earth-Cobalt Permanent Magnets and their Applications, Dayton, Ohio **1985**, p. 243.
85C6 Clark, A.E., Crowder, D.N.: IEEE Trans. Magn. MAG-**21** (1985) 1945.
85C7 Creuzet, G., Fert, A., Gaonach, C., Gignoux, D.: Physica B **130** (1985) 138.
85D1 Da C. Brochado-Oliviera, J.M., Harris, I.R.: J. Less Common Met. **105** (1985) L 9.
85D2 Da Cunha, J.B.M., Viccaro, P.J., Vasquez, A.: J. Phys. F **15** (1985) 709.
85D3 De Azevedo, W.M., Mackenzie, I.S., Berthier, Y.: J. Phys. F **15** (1985) L 243.
85D4 De Saxce, T., Berthier, Y., Fruchart, D.: J. Less Common Met. **107** (1985) 35.
85D5 De Vries, J.W.C., Thiel, R.C., Buschow, K.H.J.: J. Phys. F **15** (1985) 1413.
85D6 De Vries, J.W.C., Thiel, R.C., Buschow, K.H.J.: J. Less Common Met. **111** (1985) 313.
85D7 Del Moral, A., Ibarra, M.R.: J. Phys. Chem. Solids **46** (1985) 127.
85D8 Deryagin, A.V., Kvashnin, G.M., Kapitonov, A.M.: Fiz. Tverd. Tela **27** (1985) 255.
85D9 Deryagin, N.N., Mudzhiri, G.T., Nestorov, V.I., Churakov, A.K.: Zh. Eksp. Teor. Fiz. **89** (1985) 2149.
85D10 Deryagin, N.N., Krylov, V.I., Mujiri, G.T., Nesterov, V.I., Reiman, S.I.: Phys. Status Solidi (b) **131** (1985) 555.
85D11 Deryagin, A.V., Kazakov, A.A., Kudrevatykh, N.V., Moskalev, V.N., Mushinkov, N.V., Terentiev, S.V.: Fiz. Met. Metalloved. **60** (1985) 295.
85D12 Drzazga, Z.: Physica B **130** (1985) 305.
85D13 Drzazga, Z., Mydlarz, T., Klistala, C.: Acta Phys. Pol. A **68** (1985) 489.
85D14 Duc, N.H., Hien, T.D., Franse, J.J.M.: Acta Phys. Pol. A **68** (1985) 127.
85E1 Ermolenko, A.S.: Fiz. Tverd. Tela **27** (1985) 246.
85F1 Figiel, H., Kapusta, C.Z., Gratz, E.: Physica B **130** (1985) 481.
85F2 Franceschini, D.F., Da Cunha, S.F.: J. Magn. Magn. Mater. **52** (1985) 280.
85F3 Franse, J.J.M., De Boer, F.R., Frings, P.H., Gersdorf, R., Menovsky, A., Müller, F.A., Radwanski, R.J., Sinnema, S.: Phys. Rev. B **31** (1985) 4347.

85F4 Fujii, H., Wallace, W.E.: J. Magn. Magn. Mater. **50** (1985) 64.
85F5 Fujii, H., Okamoto, T., Wallace, W.E., Pourarian, F., Morisaki, T.: J. Magn. Magn. Mater. **46** (1985) 245.
85G1 Gaidukova, I.Y., Dubenko, I.S., Markosyan, A.S.: Fiz. Met. Metalloved. **59** (1985) 300.
85G2 Gaidukova, I.Y., Dubenko, I.S., Markosyan, A.S.: Fiz. Met. Metalloved. **60** (1985) 515.
85G3 Gan, R.J., Littlewood, N.T., James, W.J.: IEEE Trans. Magn. MAG-**21** (1985) 1984.
85G4 Gavra, Z., Muray, J.J., Calvert, L.D., Taylor, J.B.: J. Less Common Met. **105** (1985) 291.
85G5 Ghandehari, M.H., Fidler, J.: IEEE Trans. Magn. MAG-**21** (1985) 1973.
85G6 Gignoux, D., Gomez-Sal, J.C.: J. Appl. Phys. **57** (1985) 3125.
85G7 Gignoux, D., Voiron, J.: Phys. Rev. B **32** (1985) 4822.
85G8 Gignoux, D., Voiron, J.: Phys. Lett. **108** (1985) 473.
85G9 Gignoux, D., Givord, F., Lemaire, R., Tasset, F.: J. Magn. Magn. Mater. **50** (1985) 53.
85G10 Gignoux, D., Lemaire, R., Mendia-Monterroso, R., Moreau, J.M., Schweizer, J.: Physica B **130** (1985) 376.
85G11 Gignoux, D., Givord, F., Hennion, B., Ishikawa, Y., Lemaire, R.: J. Magn. Magn. Mater. **52** (1985) 421.
85G12 Girodin, D., Allibert, C.H., Givord, F., Lemaire, R.: J. Less Common Met. **110** (1985) 149.
85G13 Givord, D., Lienard, A., Perrier de la Bathie, R., Tenaud, P., Viadieu, T.: J. Phys. (Paris) **46** (1985) C-313.
85G14 Goremychkin, E.A., Muhle, E., Lippold, B., Chistyakov, O.D., Savitski, E.M.: Phys. Status Solidi (b) **127** (1985) 371.
85G15 Goremychkin, E.A., Muhle, E., Natkaniec, I., Popescu, M., Chistyakov, O.D.: Fiz. Tverd. Tela **27** (1985) 1989.
85G16 Goremychkin, E.A., Kolchugina, N.B., Muhle, E., Popescu, M., Sahling, A.L., Sahling, S., Chistyakov, O.D.: Preprint, Joint Institute for Nuclear Research, Dubna, USSR **1985**, E14-85-789.
85G17 Gottwick, U., Gloos, K., Horr, S., Steglich, F., Grewe, N.: J. Magn. Magn. Mater. **47–48** (1985) 536.
85G18 Gschneidner Jr., K.A., Ikeda, K., Tsang, T.W.E., McMasters, O.D., Stierman, R.J., Eucker, S.S., Lambert, S.E., Maple, M.B., Buchal, C.: Physica B **130** (1985) 202.
85G19 Gubbens, P.C.M., Van der Kraan, A.M., Buschow, K.H.J.: J. Less Common Met. **111** (1985) 301.
85G20 Gubbens, P.C.M., Van der Kraan, A.M., Buschow, K.H.J.: J. Magn. Magn. Mater. **50** (1985) 199.
85H1 Ho, W.W., Pei, X.D., Luo, S., Yang, Y.Ch., Lin, C., Zeng, X.X., Zhou, H.M., Zhang, B.S., Jin, L., Yang, J.L.: Proc. 8th Int. Workshop on Rare Earth-Cobalt Permanent Magnets and their Applications, Dayton, Ohio **1985**, p. 671.
85H2 Höchst, H., Covalita, E., Buschow, K.H.J.: Phys. Rev. B **31** (1985) 6167.
85I1 Ichinose, K., Fujiwara, K., Yoshie, H., Nagai, H., Tsujimura, A.: J. Phys. Soc. Jpn. **54** (1985) 1103.
85I2 Inoue, T., Goto, K.: IEEE Transl. J. Magn. Jpn. TJMJ-**1** (1985) 992.
85I3 Inoue, J., Shimizu, M.: J. Phys. F **15** (1985) 1511.
85I4 Ishida, S., Asano, S., Ishida, J.: J. Phys. Soc. Jpn. **54** (1985) 4695.
85I5 Ishida, S., Asano, S.: J. Phys. Soc. Jpn. **54** (1985) 4688.
85I6 Ishikawa, H., Oguro, K., Kato, A., Suzuki, H., Ishii, E.: New Frontiers in Rare Earth Science and Applications, Beijing, China **1985**, vol. 2, p. 1058.
85I7 Isikawa, Y., Mori, K., Ueno, K., Sato, K., Malzawa, K.: J. Magn. Magn. Mater. **52** (1985) 434.
85J1 Jin, L.H., James, W.J., Rhyne, J., Lemaire, R.: Chinese Phys. Lett. **2** (1985) 253.
85J2 Jurczyk, M., Koczorowska, L., Wrzeciono, A.: Proc. 8th Int. Workshop on Rare Earth-Cobalt Permanent Magnets and their Applications, Dayton, Ohio **1985**, p. 761.
85K1 Kaczmarska, K., Kwapulinska, E., Slebarski, A., Zipper, E., Chelkowski, A.: J. Magn. Magn. Mater. **50** (1985) 101.
85K2 Kakol, Z., Figiel, H.: Physica B **130** (1985) 312.
85K3 Kasprzyk, A., Zarek, W., Slebarski, A.: J. Less Common Met. **105** (1985) 231.
85K4 Kataev, G.I., Nikolaev, V.I., Rusakov, V.S., Fedorenko, I.V., Shubin, V.V.: Vestn. Mosk. Univ. Ser. 3, **40** (1985) 89.
85K5 Keller, J., Amador, C., De Teresa, C.: Physica B **130** (1985) 37.
85K6 Kirchmayr, H.R.: New Frontiers in Rare Earth Science and Applications, Beijing, China **1985**, vol. 2, p. 879.
85K7 Klimker, H., Gefen, Y., Rosen, M.: J. Phys. Chem. Solids **46** (1986) 157.
85K8 Kolodziejczyk, A.: Physica B **130** (1985) 189.
85K9 Kolodziejczyk, A., Sulkowski, C.: J. Phys. F **15** (1985) 1151.
85K10 Kolodziejczyk, A., Zukrowski, J.: J. Phys. F **15** (1985) L 131.
85K11 Kolodziejczyk, A., Rauluszkievicz, J., Reich, A., Sarkissian, B.V.B.: Acta Phys. Pol. A **68** (1985) 543.

85 K 12 Koon, N.C., Williams, C.M.: J. Appl. Phys. **57** (1985) 3227.
85 K 13 Korenman, V.: J. Appl. Phys. **57** (1985) 3000.
85 K 14 Kuchin, A.G., Korolev, A.V., Ermolenko, A.S.: Fiz. Met. Metalloved. **59** (1985) 498.
85 K 15 Kurihara, K., Ohtsuka, S., Ukai, T., Mori, N.: Physica B **130** (1985) 47.
85 K 16 Kurihara, K., Ohtsuka, S., Ukai, T., Mori, N.: Physica B **130** (1985) 317.
85 L 1 Lartigue, C., Percheron-Guegan, A., Achard, J.C.: J. Less Common Met. **113** (1985) 127.
85 L 2 Lin, H., Zhong, W.D.: Acta Phys. Sinica **34** (1985) 1385.
85 L 3 Lonzarich, G.G., Taillefer, L.: J. Phys. C **18** (1985) 4339.
85 M 1 Malik, S.K., Umarji, A.M., Shenoy, G.K.: J. Appl. Phys. **57** (1985) 3252.
85 M 2 Maezawa, K., Wakabayashi, S., Sato, K.: J. Appl. Phys. **57** (1985) 3219.
85 M 3 Markosyan, A.S., Snegirev, V.V.: Fiz. Met. Metalloved. **59** (1985) 1151.
85 M 4 Markov, V.Ya., Belyavina, N.N., Karpenko, V.A., Karpenko, A.A.: Dopov. Akad. Nauk Ukr. SSR Ser. A **9** (1985) 76.
85 M 5 Meyer-Liautaud, F., Pasturel, A., Allibert, C.H., Colinet, C.: J. Less Common Met. **110** (1985) 119.
85 M 6 Mizutani, V., Fukamichi, K., Goto, T.: Technical Report of ISSP Ser. A **1985**, p. 1609.
85 M 7 Modrzejewski, N., Slepowronski, M., Warchol, S.: Acta Phys. Pol. A **68** (1985) 503.
85 M 8 Mohn, P., Schwarz, K.: Physica B **130** (1985) 26.
85 M 9 Moreira, J.M., Sousa, J.B., Montenegro, J.D., Braga, M.E., Melville, D.: Physica B **130** (1985) 88.
85 M 10 Mukimov, K.M., Sharijsov, Sh.M., Ernazarova, L.A.: Phys. Status Solidi (b) **127** (1985) K 129.
85 M 11 Müller, H., Kirchmayr, H.R., Szasz, A., Kojnok, J.: Physica B **130** (1985) 59.
85 N 1 Nagai, H., Oguro, I.: J. Phys. Soc. Jpn. **54** (1985) 466.
85 N 2 Nakamura, Y.: IEEE Transl. J. Magn. Jpn. TJMJ-**1** (1985) 58.
85 N 3 Nishihara, Y., Yamaguchi, Y.: J. Phys. Soc. Jpn. **54** (1985) 1122.
85 N 4 Nishihara, Y., Yamaguchi, Y.: J. Phys. Soc. Jpn. **54** (1985) 1689.
85 N 5 Nomura, K., Uruno, H., Ono, S., Shinozuka, H., Suda, S.: J. Less Common Met. **107** (1985) 221.
85 O 1 Oliver, F.W., Morgan, W., Hammond, E.C., Wood, S., May, L.: J. Appl. Phys. **57** (1985) 3250.
85 O 2 Ono, S., Nomura, K., Akiba, E., Urono, H.: J. Less Common Met. **113** (1985) 113.
85 P 1 Padalia, B.D., Prabhawalkar, V.: J. Less Common Met. **105** (1985) 321.
85 P 2 Palstra, T.T.M., Nieuwenhuys, G.J., Mydosh, J.A., Buschow, K.H.J.: Phys. Rev. B **31** (1985) 4622.
85 P 3 Paszkowicz, W.: Acta Phys. Pol. A **68** (1985) 505.
85 P 4 Pedziwiatr, A.T., Stadnik, Z.M., Zukrowski, J., Smith, H.K., Wallace W.E.: Solid State Commun **55** (1985) 455.
85 P 5 Percheron-Guegan, A., Lartigue, C., Achard, J.C.: J. Less Common Met. **109** (1985) 287.
85 P 6 Pfranger, R., Plusa, D., Wyslocki, B., Mydlarz, T.: Acta Phys. Pol. A **68** (1985) 31.
85 P 7 Pfranger, R., Plusa, D., Wyslocki, B., Mydlarz, T.: Physica B+C **133** (1985) 10.
85 P 8 Plusa, D.: J. Magn. Magn. Mater. **51** (1985) 331.
85 P 9 Plusa, D., Pfranger, R., Wyslocki, B.: Phys. Status Solidi (a) **92** (1985) 533.
85 P 10 Pop, I., Crisan, V., Coldea, M., Hagan, C., Borodi, G.: Physica B+C **130** (1985) 504.
85 P 11 Pszczola, J., Zukrowski, J., Krop, K., Suwalski, J.: Physica B **130** (1985) 439.
85 P 12 Pszczola, J., Zukrowski, J., Krop, K., Suwalski, J., Kucharski, Z., Lukasiak, M.: Physica B **130** (1985) 436.
85 P 13 Pszczola, J., Zukrowski, J., Krop, K., Suwalski, J., Kucharski, Z., Lukasiak, M.: Physica B **130** (1985) 446.
85 P 14 Ptashnik, V.B., Stepanov, Yu.P., Baikov, Yu.M., Dunaeva, T.Yu.: Izv. Akad. Nauk SSSR Neorg. Mater. **21** (1985) 1344.
85 R 1 Radwanski, R.J.: J. Phys. F **15** (1985) 459.
85 R 2 Radwanski, R.J., Franse, J.J.M.: Acta Phys. Pol. A **68** (1985) 401.
85 R 3 Radwanski, R.J., Franse, J.J.M., Krop, K.: Acta Phys. Pol. A **68** (1985) 373.
85 R 4 Radwanski, R.J., Franse, J.J.M., Sinnema, S.: J. Magn. Magn. Mater. **51** (1985) 175.
85 R 5 Radwanski, R.J., Franse, J.J.M.: J. Magn. Magn. Mater. **46** (1985) 289.
85 R 6 Radwanski, R.J., Franse, J.J.M., Sinnema, S.: J. Phys. F **15** (1985) 969.
85 R 7 Radwanski, R.J., Franse, J.J.M., Krop, K., Duraj, R., Zach, R.: Physica B **130** (1985) 286.
85 R 8 Rastogi, A.K., Coles, B.R.: J. Phys. F **15** (1985) 1165.
85 R 9 Riedi, P.C., Dumelow, T., Abell, J.S.: Physica B **130** (1985) 449.
85 R 10 Rossi, D., Marazza, R., Ferro, R.: J. Less Common Met. **107** (1985) 99.
85 S 1 Sa, M.A., Oliveira, J.B., Machado da Silva, J.M., Harris, I.R.: J. Less Common Met. **108** (1985) 263.
85 S 2 Sakaguchi, H., Taniguchi, N., Adachi, G., Shiokawa, I.: New Frontiers in Rare Earth Science and Applications, Beijing, China **1985**, vol. 2, p. 1076.

85 S 3 Sakurai, J., Tagawa, Y., Komura, Y.: J. Magn. Magn. Mater. **52** (1985) 205.
85 S 4 Sarkissian, B.V.B.: J. Appl. Phys. **57** (1985) 3203.
85 S 5 Sarkissian, B.V.B.: J. Appl. Phys. **57** (1985) 3771.
85 S 6 Savage, H.T., Clark, A.E., Lord, D.L., McMasters, O.D.: J. Appl. Phys. **57** (1985) 3747.
85 S 7 Scherbakova, E.V., Ermolenko, A.S.: Fiz. Met. Metalloved. **59** (1985) 344.
85 S 8 Searle, C.W.: J. Appl. Phys. **57** (1985) 481.
85 S 9 Sechovsky, V., Hilscher, G.: Physica B+C **130** (1985) 207.
85 S 10 Sechovsky, V., Nozar, P.: Acta Phys. Pol. A **68** (1985) 235.
85 S 11 Seitabla, D.: Stud. Cercet. Fiz. **37** (1985) 27.
85 S 12 Semenenko, K.N., Burnasheva, V.V.: J. Less Common Met. **105** (1985) 1.
85 S 13 Shimizu, K.: J. Phys. Soc. Jpn. **54** (1985) 1155.
85 S 14 Shimizu, K.: J. Phys. Soc. Jpn. **54** (1985) 2009.
85 S 15 Shimotomai, M., Doyama, M., Fujisawa, H.: J. Magn. Magn. Mater. **47–48** (1985) 102.
85 S 16 Shimotomai, M., Mekhrabov, D., Doyama, M., Fujisawa, H.: Physica B **130** (1985) 283.
85 S 17 Shirakawa, K., Fukamichi, K., Aoki, K., Masumoto, T., Kaneko, T.: J. Phys. F **15** (1985) 961.
85 S 18 Smetana, Z., Sima, V.: Czech. J. Phys. B **35** (1985) 1232.
85 S 19 Smetana, Z., Sima, V., Borombajev, M.K., Markosyan, A.S., Levitin, R.Z.: Acta Phys. Slovaca **35** (1985) 300.
85 S 20 Sokolovskaya, E.M., Raevskaya, M.V., Kazakova, E.F., Ilias, A.I., Pastushenkova, M.A., Bodak, O.I.: Izv. Akad. Nauk SSSR Met. **5** (1985) 197.
85 S 21 Steiner, W., Reissner, M., Schäfer, W., Will, G.: Physica B **130** (1985) 426.
85 S 22 Stewart, G.A., Creagh, D.C.: J. Phys. F **15** (1985) 1639.
85 S 23 Stieler, S., Kuntze, K., Kohake, D.: Proc. 8th Int. Workshop on Rare Earth-Cobalt Permanent Magnets and their Applications, Dayton, Ohio **1985**, p. 179.
85 S 24 Subramanian, P.R., Smith, J.F.: Metall. Trans. **816** (1985) 577.
85 S 25 Szpunar, B.: Physica B **130** (1985) 29.
85 T 1 Tagawa, Y., Sakurai, K., Komura, Y., Wada, H., Shiga, M., Nakamura, Y.: J. Phys. Soc. Jpn. **54** (1985) 591.
85 T 2 Takeuchi, A.Y., Da Cunha, S.F.: J. Magn. Magn. Mater. **49** (1985) 257.
85 T 3 Tao, H.: New Frontiers in Rare Earth Science and Applications, Beijing, China **1985**, vol. 2, p. 1070.
85 T 4 Tsvyashchenko, A.V., Fomicheva, L.N.: J. Less Common Met. **105** (1985) L 1.
85 T 5 Tsvyashchenko, A.V., Popova, S.V.: J. Less Common Met. **108** (1985) 115.
85 T 6 Turecki, Z.: Acta Phys. Pol. A **67** (1985) 1043.
85 T 7 Turek, K., Kakol, Z., Kolodziejczyk, A., Krop, K.: Physica B **130** (1985) 314.
85 V 1 Vasilkovski, V.A.: Fiz. Tverd. Tela **27** (1985) 1069.
85 V 2 Vasilkovski, V.A., Gorlenko, A.A., Kovtun, N.M., Siryuk, V.M.: Zh. Eksp. Teor. Fiz. **85** (1985) 1349.
85 V 3 Velicescu, M.: J. Less Common Met. **111** (1985) 71.
85 W 1 Wada, H., Yoshimura, K., Shiga, M., Goto, T., Nakamura, Y.: J. Phys. Soc. Jpn. **54** (1985) 3543.
85 W 2 Wallace, W.E.: Prog. Solid State Chem. **16** (1985) 127.
85 W 3 Wang, H.W., Pei, X.D., Sheng, L., Chang, Y.Y., Lin, C., Zeng, X.X., Zhou, H.M., Zhang, B.S., Jin, L., Yang, J.L.: Proc. 8th Int. Workshop on Rare Earth-Cobalt Permanent Magnets and their Applications, Dayton, Ohio **1985**, p. 671.
85 W 4 Wiesinger, G.: Physica B **130** (1985) 418.
85 W 5 Willman, C.J., Narasimhan, K.S.V.L.: IEEE Trans. Magn. MAG-**21** (1985) 1976.
85 Y 1 Yamada, H., Shimizu, M.: J. Phys. F **15** (1985) L 175.
85 Y 2 Yamada, H., Sakata, A.: J. Phys. Soc. Jpn. **54** (1985) 4321.
85 Y 3 Yamada, H., Inoue, J., Shimizu, M.: J. Phys. F **15** (1985) 169.
85 Y 4 Yamaguchi, M., Ross, D.K., Goto, T., Ohta, T.: Z. Phys. Chem. N.F. **145** (1985) S 101.
85 Y 5 Yamaguchi, M., Ikeda, H., Ohta, T., Goto, T., Katayama, T.: Solid State Commun. **53** (1985) 383.
85 Y 6 Yamaguchi, M., Ikeda, H., Ohta, T., Katayama, T., Goto, T.: J. Less Common Met. **106** (1985) 165.
85 Y 7 Yanase, A.: J. Magn. Magn. Mater. **52** (1985) 403.
85 Y 8 Yang, Y.C., Chen, H.Y., Xing, F., Ho, W.E., Wu, P., Yang, J.L., Zhang, B.S., Zhou, H.M., Jui, L., Xu, Z.J., Zeng, X.X.: IEEE Trans. Magn. MAG-**21** (1985) 1987.
85 Y 9 Yoshie, H., Shiga, M., Nakamura, Y.: J. Phys. Soc. Jpn. **54** (1985) 1116.
85 Y 10 Yoshie, H., Fujii, T., Nagai, H., Tsujimura, A.: J. Phys. Soc. Jpn. **54** (1985) 2725.
85 Y 11 Yoshimura, K., Nakamura, Y.: Solid State Commun. **56** (1985) 767.
85 Y 12 Yumaguzhin, R.Yu., Levitin, R.Z., Popov, Yu.F.: Fiz. Tverd. Tela **27** (1985) 179.
85 Z 1 Zhong, W.D.: Res. Met. Mat. (China) **11** (1985) 1.

85 Z 2 Zhuang, Y., Wu, C., Wang, Y., Li, Z., Gao, L.: New Frontiers in Rare Earth Science and Applications, Beijing, China **1985**, vol. 2, p. 960.

86 A 1 Abd, El Al, M., Ilyushin, A.S., Pechennikov, A.V., Chechernikov, V.I.: Fiz. Met. Metalloved. **62** (1986) 1224.

86 A 2 Abe, T.: J. Phys. Soc. Jpn. **55** (1986) 4003.

86 A 3 Abell, J.S., Butler, D., Greenough, R.D., Joyce, V., Pitman, K.C.: J. Magn. Magn. Mater. **62** (1986) 6.

86 A 4 Alves, K.M.B., Alves, N., Guimaraes, A.P., Mackenzie, I.S., Ross, J.W.: J. Magn. Magn. Mater. **54–57** (1986) 501.

86 A 5 Andreev, A.V., Bartashevich, M.I., Deryagin, A.V., Tarasov, Y.N.: Fiz. Met. Metalloved. **62** (1986) 905.

86 A 6 Andreev, A.V., Deryagin, A.V., Zadvorkin, S.M., Kvashnin, G.M., Kudrevatykh, N.V.: Fiz. Met. Metalloved. **61** (1986) 744.

86 A 7 Andreev, A.V., Baranov, I.V., Vokhmyanin, A.P., Deryagin, A.V., Zadvorkin, S.M., Kvashnin, G.M., Kelarev, V.V., Sinitsyn, E.V.: Fiz. Met. Metalloved. **62** (1986) 482.

86 A 8 Armitage, J.G.M., Dumelow, T., Mitchell, R.H., Riedi, P.C., Abell, J.S., Mohn, P., Schwarz, K.: J. Phys. F **16** (1986) L 141.

86 B 1 Ballou, R., Deportes, J., Kebe, B., Lemaire, R.: J. Magn. Magn. Mater. **54–57** (1986) 494.

86 B 2 Ballou, R., Gignoux, D., Gorges, B., Lemaire, R.: J. Magn. Magn. Mater. **54–57** (1986) 497.

86 B 3 Ballou, R., Deportes, J., Gorges, B., Lemaire, R., Ousset, J.C.: J. Magn. Magn. Mater. **54–57** (1986) 465.

86 B 4 Ballou, R., Gignoux, D., Lemaire, R., Mendia-Monterroso, R., Schweizer, J.: J. Magn. Magn. Mater. **54–57** (1986) 499.

86 B 5 Baranov, N.V., Deryagin, A.V., Kozlov, A.I., Sinitzyn, B.: Fiz. Met. Metalloved. **61** (1986) 733.

86 B 6 Barth, S., Albert, E., Heiduk, G., Möslang, A., Weidinger, A., Recknagel, E., Buschow, K.H.J.: Phys. Rev. B **33** (1986) 430.

86 B 7 Berthier, Y., Gignoux, D., Tari, A.: J. Magn. Magn. Mater. **58** (1986) 265.

86 B 8 Berthier, Y., Gignoux, D., Kuentzler, R., Tari, A.: J. Magn. Magn. Mater. **54–57** (1986) 479.

86 B 9 Benham, M.J., Ross, D.K., Lartigue, C., Percheron-Guegan, A.: Z. Phys. Chem. N.F. **147** (1986) 219.

86 B 10 Bondarkov, M.D., Shpinkova, L.G., Akselrod, Z.Z., Komissarova, B.A., Kryukova, L.N., Ryasnyi, G.K., Sorokin, A.A.: Izv. Akad. Nauk SSSR Ser. Fiz. **50** (1986) 1002.

86 B 11 Borombaev, M.K., Levitin, R.Z., Markosyan, A.S., Smetana, Z., Snegirev, V.V., Svoboda, P.: Phys. Status Solidi (a) **97** (1986) 501.

86 B 12 Borombaev, M.K., Levitin, R.Z., Markosyan, A.S., Smetana, Z., Svoboda, P., Sima, V.: Phys. Status Solidi (a) **98** (1986) 221.

86 C 1 Chang, L.: Metallography **19** (1986) 327.

86 C 2 Chappert, J., Yaouanc, A., Hartmann, O., Karlsson, E., Wackelgard, E., Wappling, R., Asch, L., Kalvius, G.M.: Hyp. Int. **31** (1986) 331.

86 C 3 Cheung, T.D., Wickramasekara, L., Cadieu, F.J.: J. Magn. Magn. Mater. **54–57** (1986) 1641.

86 C 4 Chuang, Y.C., Wu, C.H., Chang, S.C., Li, T.C., Wang, Y.C.: J. Less Common Met. **125** (1986) 25.

86 C 5 Chuev, V.V., Kelarev, V.V., Sidorov, S.K., Syromiatnikov, V.N., Pirogov, A.N.: Fiz. Met. Metalloved. **61** (1986) 510.

86 C 6 Coles, B.R., Chhabra, A.K.: J. Magn. Magn. Mater. **54–57** (1986) 1039.

86 C 7 Colinet, C., Pasturel, A.: J. Less Common Met. **119** (1986) 167.

86 C 8 Colinet, C., Pasturel, A., Buschow, K.H.J.: Metall. Trans. A **17** (1986) 777.

86 C 9 Cook, D.C., McGhee, A.: Nucl. Instr. Meth. Phys. Res. B **18** (1986) 80.

86 C 10 Creuzet, G., Gignoux, D.: Phys. Rev. B **33** (1986) 515.

86 D 1 Da Cunha, S.F., Franceschini, D.F., Gomes, A.A., Takeuchi, A.Y.: J. Magn. Magn. Mater. **62** (1986) 47.

86 D 2 Deutz, A.F., Brom, H.B., Deelen, H., De Jongh, L.J., Huiskamp, W.J., Buschow, K.H.J.: Solid State Commun. **60** (1986) 917.

86 D 3 Deportes, J., Kebe, B., Lemaire, R.: J. Magn. Magn. Mater. **54–57** (1986) 1089.

86 D 4 Dumelow, T., Riedi, P.C., Mohn, P., Schwarz, K., Yamada, Y.: J. Magn. Magn. Mater. **54–57** (1986) 1089.

86 F 1 Fedorov, Ya.V., Shender, E.F.: Zh. Eksp. Teor. Fiz. **90** (1986) 2152.

86 F 2 Felner, I., Nowik, I.: J. Magn. Magn. Mater. **54–57** (1986) 163.

86 F 3 Felner, I., Nowik, I.: J. Magn. Magn. Mater. **58** (1986) 169.

86 G 1 Gignoux, D., Rhyne, J.J.: J. Magn. Magn. Mater. **54–57** (1986) 1179.

86 G 2 Gignoux, D., Voiron, J.: J. Magn. Magn. Mater. **54–57** (1986) 363.

86 G 3 Goremychkin, E.A., Kolchugina, N.B., Muhle, E., Popescu, M., Sahling, A.L., Sahling, S., Chistyakov, D.: Fiz. Tverd. Tela **28** (1986) 3642.

86G4 Goto, T., Sakakibara, T., Yamaguchi, M.: J. Magn. Magn. Mater. **54–57** (1986) 1085.
86G5 Gratz, E., Bauer, E., Sechovsky, V., Chmist, J.: J. Magn. Magn. Mater. **54–57** (1986) 517.
86G6 Gratz, E., Hilscher, G., Sassik, H., Sechovsky, V.: J. Magn. Magn. Mater. **54–57** (1986) 459.
86G7 Gubbens, P.C.M., Van der Kraan, A.M., Buschow, K.H.J.: J. Magn. Magn. Mater. **54–57** (1986) 483.
86G8 Guimaraes, A.P., Alves, K.M.B., Alves, N., Gratz, E.: Notas de Fisica **1986**, ISSN 0029-3865.
86H1 Hagan, C., Pop, I.: J. Magn. Magn. Mater. **58** (1986) 78.
86H2 Helmholdt, R.B., Palstra, T.T., Nieuwenhuys, G.J., Mydosh, J.A., Van der Kraan, A.M., Buschow, K.H.J.: Phys. Rev. B **34** (1986) 169.
86H3 Hien, T.D., Duc, N.H., Franse, J.J.M.: J. Magn. Magn. Mater. **54–57** (1986) 471.
86H4 Hillebrecht, F.U., Strasser, G., Natzer, F.P.: J. Phys. F **16** (1986) 937.
86H5 Hirosawa, S., Oswald, E., Wallace, W.E.: J. Magn. Magn. Mater. **59** (1986) 185.
86I1 Ilyushin, A.S., Castro, D.A., Mahmud, I.A.: Vestn. Mosk. Univ. Ser. A **41** (1986) 83.
86I2 Ilyushin, A.S., Castro, D.A., Zasimov, V.S.: Fiz. Met. Metalloved. **61** (1986) 622.
86I3 Ilyushin, A.S., Moshchalkov, V.V., Nikolaev, A.A., Perov, A.P., Slushanko, N.E., Burchanov, G.S., Shkatova, T.M.: Fiz. Tverd. Tela **28** (1986) 3423.
86I4 Inoue, J., Shimizu, M.: J. Magn. Magn. Mater. **54–57** (1986) 991.
86I5 Isikawa, Y., Mori, K., Fujii, A., Sato, K.: J. Phys. Soc. Jpn. **55** (1986) 3165.
86I6 Ishiyama, K., Endo, K.: J. Phys. Soc. Jpn. **55** (1986) 2535.
86I7 Ivey, D.G., Northwood, D.O.: J. Less Common Met. **115** (1986) 295.
86J1 Jesser, R., Clad, R.: J. Magn. Magn. Mater. **54–57** (1986) 710.
86J2 Jin, L., James, W.J., Lemaire, R., Rhyne, J.: J. Less Common Met. **118** (1986) 269.
86J3 Jiuxin, Q., Xiaoping, D., Chaogui, Z., Yupu, Y.: Int. J. Hydrogen Energy **11** (1986) 129.
86J4 Joyce, V., Abell, J.S., Greenough, R.D., Pitman, K.C.: J. Magn. Magn. Mater. **54–57** (1986) 877.
86K1 Kakol, Z., Figiel, H.: Phys. Status Solidi (b) **138** (1986) 151.
86K2 Karnachev, A.S., Maksimchuk, T.V., Reymer, V.A., Sihitsyn, Y.V., Solovyev, Y.: Fiz. Met. Metalloved. **61** (1986) 910.
86K3 Kido, G., Tadakuma, Y., Nakagawa, Y., Nishihara, Y., Yamaguchi, Y.: J. Magn. Magn. Mater. **54–57** (1986) 885.
86K4 Kobayashi, K., Kanematsu, K.: J. Phys. Soc. Jpn. **55** (1986) 1336.
86K5 Kobayashi, K., Kanematsu, K.: J. Phys. Soc. Jpn. **55** (1986) 4435.
86K6 Kudrevatykh, N.V., Li, Y.V., Melville, D.: Fiz. Met. Metalloved. **61** (1986) 898.
86K7 Kuentzler, R., Tari, A.: J. Magn. Magn. Mater. **61** (1986) 29.
86L1 Labulle, B., Petipas, C.: Phys. Status Solidi (a) **93** (1986) 419.
86L2 Labulle, B., Dufraux, G., Petipas, C., Vigier, P.: J. Less Common Met. **115** (1986) 103.
86L3 Laha, S., Ursekar, R.M., Pandian, S., Gupta, K.P., Mazumdar, A.K., Pedmavati Sankar, T.A., Ramakrishna, U., Subbarao, E.C., Velu, M.T.: J. Less Common Met. **124** (1986) 211.
86L4 Lartigue, C., Dianoux, A.J., Percheron-Guegan, A., Acchard, J.C.: Hydrogen in Disordered and Amorphous Solids, Rhodes, Greece 1985, New York: Plenum Press **1986**, p. 327.
86L5 Littlewood, N.T., James, W.J., Yelon, W.B.: J. Magn. Magn. Mater. **54–57** (1986) 491.
86M1 Matsumoto, T., Matsushita, A.: J. Less Common Met. **123** (1986) 135.
86M2 Mitchell, R.K., McCurrie, R.A.: J. Appl. Phys. **59** (1986) 4113.
86M3 Moriya, T.: J. Phys. Soc. Jpn. **55** (1986) 357.
86M4 Motoya, K.: J. Phys. Soc. Jpn. **55** (1986) 3733.
86N1 Nagai, H., Oyama, N., Ikami, Y., Yoshie, H., Tsujimura, A.: J. Phys. Soc. Jpn. **55** (1986) 177.
86N2 Nishihara, Y., Yamaguchi, Y.: J. Phys. Soc. Jpn. **55** (1986) 920.
86N3 Nishihara, Y., Yamaguchi, Y., Negishi, A.: J. Magn. Magn. Mater. **54–57** (1986) 945.
86O1 Okamoto, T., Fujii, H., Makihara, Y., Hihara, T., Hashimoto, Y.: J. Magn. Magn. Mater. **54–57** (1986) 1087.
86O2 Ouladdiaf, B.: Thesis, Univ. Grenoble, France **1986**.
86P1 Palstra, T.M.M., Nieuwenhuys, G.J., Mydosh, J.A., Helmholdt, R.B., Buschow, K.H.J.: J. Magn. Magn. Mater. **54–57** (1986) 995.
86P2 Patterson, C., Givord, D., Votron, J., Palmer, S.B.: J. Magn. Magn. Mater. **54–57** (1986) 891.
86P3 Pirogov, A.N., Ermolenko, A.S., Kelarev, V.V., Sidorov, S.K.: Fiz. Met. Metalloved. **62** (1986) 1035.
86P4 Plusa, D., Pfranger, R., Wyslocki, B., Mydlarz, T.: J. Less Common Met. **120** (1986) 1.
86P5 Pourarian, F., Wallace, W.E.: Int. J. Hydrogen Energy **11** (1986) 789.
86P6 Pourarian, F., Liu, M.Z., Lu, B.Z., Huang, M.Q., Wallace, W.E.: J. Solid State Chem. **65** (1986) 111.
86P7 Pszczola, J., Krop, K.: J. Magn. Magn. Mater. **59** (1986) 95.

86R1 Radwanski, R.J.: J. Magn. Magn. Mater. **62** (1986) 120.
86R2 Radwanski, R.J.: Phys. Status Solidi (b) **137** (1986) 487.
86R3 Radwanski, R.J.: Z. Phys. B **65** (1986) 65.
86R4 Rai, K.N., Rani, R., Srikanth, V., Kumar, J.: J. Less Common Met. **118** (1986) 285.
86R5 Rastogi, A.K., Coles, B.R.: J. Magn. Magn. Mater. **54–57** (1986) 117.
86R6 Reissner, M., Steiner, W.: Hyp. Int. **28** (1986) 1017.
86S1 Sakaguchi, H., Nagai, H., Adachi, G., Shiokawa, J.: J. Less Common Met. **126** (1986) 83.
86S2 Sakakibara, T., Goto, T., Yoshimura, K., Shiga, M., Nakamura, Y.: Phys. Lett. A **117** (1986) 243.
86S3 Sarkissian, B.V.B.: J. Phys. F **16** (1986) 755.
86S4 Sarkissian, B.V.B., Tholence, J.L.: J. Magn. Magn. Mater. **54–57** (1986) 1525.
86S5 Sarkissian, B.V.B., Salce, B., Khoder, A.F.: J. Magn. Magn. Mater. **54–57** (1986) 1531.
86S6 Sato, K., Yosida, Y., Isikawa, Y., Mori, K.: J. Magn. Magn. Mater. **54–57** (1986) 467.
86S7 Sato, K., Isikawa, Y., Mori, K., Clark, A.E., Callen, E.: J. Magn. Magn. Mater. **54–57** (1986) 875.
86S8 Scherbakova, E.B., Ermolenko, A.S., Korolev, A.V.: Fiz. Met. Metalloved. **62** (1986) 89.
86S9 Schott, J., Sommer, F.: J. Less Common Met. **119** (1986) 307.
86S10 Sharapov, Y.R., Chechernikov, V.I., Pechenikov, A.V., Ilyushin, A.S., Torchinova, R.S.: Fiz. Met. Metalloved. **61** (1986) 1024.
86S11 Sharipov, S.M., Mukimov, K.M., Ernazarova, L.A.: Phys. Status Solidi (b) **134** (1986) K 59.
86S12 Shiga, M., Wada, H., Yoshimura, K., Nakamura, Y.: J. Magn. Magn. Mater. **54–57** (1986) 1073.
86S13 Shimizu, M., Inoue, J.: J. Magn. Magn. Mater. **54–57** (1986) 963.
86S14 Shimizu, M., Okeya, S.: J. Phys. Soc. Jpn. **55** (1986) 1062.
86S15 Shimizu, M., Kunihara, K., Inoue, J.: J. Phys. F **16** (1986) 1263.
86S16 Sidzhimov, B., Neov, S., Stanev, N., Tscholakov, P.: Phys. Status Solidi (a) **93** (1986) K 37.
86S17 Sinnema, S., Franse, J.J.M., Menovsky, A., Radwanski, R.J.: J. Magn. Magn. Mater. **54–57** (1986) 1639.
86S18 Sinnema, S., Franse, J.J.M., Menovsky, A., De Boer, F.R., Radwanski, R.: Proc. 3rd Int. Conf. Phys. of Magnetic Materials, Szcyrk-Bila, Poland **1986**, p. 324.
86S19 Skrbek, L., Tintera, J., Prusak, J., Safrata, S.: Cesk. Cas. Fyz. Sek. A **36** (1986) 479.
86S20 Stadelmaier, H.H., Schneider, G., Ellner, M.: J. Less Common Met. **115** (1986) L 11.
86S21 Steiner, W., Reissner, M., Buschow, K.H.J.: J. Magn. Magn. Mater. **54–57** (1986) 1079.
86T1 Tang, X., Zhang, Y.: J. Magn. Magn. Mater. **54–57** (1986) 1643.
86T2 Tari, A., Kuentzler, R.: J. Magn. Magn. Mater. **53** (1986) 359.
86T3 Tharp, D.E., Long, G.J., James, W.J.: Hyp. Int. **28** (1986) 593.
86T4 Thompson, P., Reilly, J.J., Corliss, L.M., Hastings, J.M., Hempelmann, R.: J. Phys. F **16** (1986) 675.
86T5 Thuy, N.P., Franse, J.J.M.: J. Magn. Magn. Mater. **54–57** (1986) 915.
86T6 Tsvyashchenko, A.V.: J. Less Common Met. **118** (1986) 103.
86T7 Tsvyashchenko, A.V., Makhotkin, V.E., Fradkov, V.A., Kuznetsov, V.N.: J. Less Common Met. **118** (1986) 173.
86T8 Tsvyashchenko, A.V., Alikhanov, R.A., Smirnov, L.S., Buzin, V.I., Makhotin, V.E., Fradkov, V.A.: Fiz. Tverd. Tela **28** (1986) 2832.
86T9 Turek, K., Kolodziejczyk, A.: J. Magn. Magn. Mater. **62** (1986) 205.
86U1 Uehara, M., Barbara, B.: J. Phys. (Paris) **47** (1986) 235.
86U2 Uehara, M., Barbara, B., Dieny, B., Stamp, P.C.E.: Phys. Lett. A **114** (1986) 23.
86V1 Vasil'kovskii, V.A., Gorlenko, A.A., Derkachenko, V.N., Deryagin, A.V., Kovtun, N.M., Mushnikov, N.V., Ostrovskii, V.F.: Fiz. Tverd. Tela **28** (1986) 2896.
86W1 Wickramasekara, L., Cheung, T.D., Cadieu, F.J.: J. Magn. Magn. Mater. **54–57** (1986) 1679.
86W2 Wiesinger, G.: Hyp. Int. **28** (1986) 545.
86W3 Wise, K.M., Butera, R.A.: J. Solid State Chem. **62** (1986) 47.
86Y1 Yamada, H., Shimizu, M.: J. Phys. F **16** (1986) 1039.
86Y2 Yamada, H., Inoue, J., Shimizu, M.: J. Magn. Magn. Mater. **54–57** (1986) 961.
86Y3 Yamaguchi, Y., Nishihara, Y.: J. Magn. Magn. Mater. **54–57** (1986) 1521.
86Y4 Yanase, A.: J. Phys. F **16** (1986) 1501.
86Y5 Yarmolyuk, Ya.P., Grin, Yu.N., Vasilechko, L.O., Belski, V.K.: Kristallografiya **31** (1986) 181.
86Y6 Yoshimura, K., Shiga, M., Nakamura, Y.: J. Phys. Soc. Jpn. **55** (1986) 3585.
86Y7 Yoshimura, K., Takigawa, M., Yasuoka, H., Shiga, M., Nakamura, Y.: J. Magn. Magn. Mater. **54–57** (1986) 1075.

87 A 1 Abd-Elmeguid, M.M., Schleede, B., Micklitz, H., Palstra, T.T., Nieuwenhuys, G.J., Buschow, K.H.J.: Solid State Commun. **63** (1987) 177.

87 A 2 Abd-el' Aal, M.M., Ilyushin, A.S., Pechennikov, A.V., Chechernikov, V.I.: Fiz. Met. Metalloved **63** (1987) 1224.

87 A 3 Akiba, E., Nomura, K., Ono, S.: J. Less Common Met. **129** (1987) 159.

87 A 4 Algarabel, P.A., Del Moral, A., Ibarra, M.R., Sousa, J.B., Moreira, J.M., Montenegro, J.F.: J. Magn. Magn. Mater. **68** (1987) 177.

87 A 5 Ali, N., Datars, W.R., Kozlowski, G., Wood, S.B.: J. Phys. F **17** (1987) 143.

87 A 6 Alp, E.E., Umarji, A.M., Malik, S.K., Shenoy, G.K., Huang, M.Q., Boltich, E.B., Wallace, W.E.: J. Magn. Magn. Mater. **68** (1987) 305.

87 A 7 Amado, M.M., Montenegro, J.D., Moreira, J.M., Braga, M.E., Sousa, J.B.: Phys. Status Solidi (a) **99** (1987) 625.

87 A 8 Andoh, Y., Hashimoto, T., Fujii, H., Okamoto, T., Fujiwara, H.: J. Magn. Magn. Mater. **70** (1987) 168.

87 A 9 Aoki, K., Yamamoto, T., Masumoto, T.: Scr. Metall. **21** (1987) 27.

87 A 10 Aoki, K., Yamamoto, T., Satoh, Y., Fukamichi, K., Masumoto, T.: Acta Metall. **35** (1987) 2465.

87 A 11 Asano, S., Ishida, S.: J. Magn. Magn. Mater. **70** (1987) 39.

87 A 12 Asano, S., Ishida, S.: J. Magn. Magn. Mater. **70** (1987) 187.

87 A 13 Averbuch Pouchot, M.T., Chevalier, R., Deportes, J., Kebe, B., Lemaire, R.: J. Magn. Magn. Mater. **68** (1987) 190.

87 B 1 Ballou, R.: Thesis, Univ. Grenoble **1987**.

87 B 2 Ballou, R., Barthem, V.M.T.S., Gignoux, D.: Acta Phys. Pol. A **72** (1987) 17.

87 B 3 Ballou, R., Deportes, J., Lemaire, R.: J. Magn. Magn. Mater. **70** (1987) 306.

87 B 4 Ballou, R., Deportes, J., Lemaire, R.: Acta Phys. Pol. A **72** (1987) 21.

87 B 5 Ballou, R., Gignoux, D., Lemaire, R., Schweizer, J.: Acta Phys. Pol. A **72** (1987) 25.

87 B 6 Ballou, R., Deportes, J., Lemaire, R., Nakamura, Y., Ouladdiaf, B.: J. Magn. Magn. Mater. **70** (1987) 129.

87 B 7 Barthem, V.M.T.S.: Thesis, Univ. Grenoble **1987**.

87 B 8 Belorizky, E., Fremy, M.A., Gavigan, J.P., Givord, D., Li, H.S.: J. Appl. Phys. **61** (1987) 3971.

87 B 9 Bjurström, H., Suda, S.: J. Less Common Met. **131** (1987) 61.

87 B 10 Bomken, K., Weber, D., Yoshizawa, M., Aesmus, W., Lüthi, L., Walker, J.: J. Magn. Magn. Mater. **63–64** (1987) 315.

87 B 11 Bonnet, J.E., Dantzer, P., Dexpert, H., Esteva, J.M., Karnatak, R.: J. Less Common Met. **130** (1987) 491.

87 B 12 Borombaev, M.K., Markosyan, A.S.: Fiz. Met. Metalloved. **63** (1987) 714.

87 B 13 Broda, H.: Acta Phys. Pol. A **72** (1987) 29.

87 B 14 Branwood, A., Janio, A.L., Piercy, A.R.: J. Appl. Phys. **61** (1987) 3796.

87 B 15 Budzynski, M., Kochetov, O.I., Subotowicz, M., Niezgoda, H., Spustek, H., Tanska-Krupa, W.: Phys. Status Solidi (b) **140** (1987) 589.

87 C 1 Chechernikov, V.I., Pechenikov, A.V., Torchinova, R.S., Sharapov, Yu.R., Ilyushin, A.S., Chekushin, V.A.: Fiz. Met. Metalloved. **63** (1987) 610.

87 C 2 Cheung, T.D., Guo, X., Cadieu, F.J.: J. Appl. Phys. **61** (1987) 3979.

87 C 3 Chuang, Y.C., Wu, H.C., Fong, J.: J. Less Common Met. **133** (1987) 215.

87 C 4 Colinet, C., Pasturel, A., Buschow, K.H.J.: J. Appl. Phys. **62** (1987) 3712.

87 C 5 Colinet, C., Pasturel, A., Percheron-Guegan, A., Achard, J.C.: J. Less Common Met. **130** (1987) 542.

87 C 6 Colinet, C., Pasturel, A., Percheron-Guegan, A., Achard, J.C.: J. Less Common Met. **134** (1987) 109.

87 D 1 Dantzer, P.: J. Less Common Met. **131** (1987) 349.

87 D 2 De Boer, F.R., Kai, H.Y., De Mooij, D.B., Buschow, K.H.J.: J. Less Common Met. **135** (1987) 199.

87 D 3 De Mooij, D.B., Buschow, K.H.J.: Philips Res. Repts. **42** Suppl. No. 2 (1987) 246.

87 D 4 De Mooij, D.B., Buschow, K.H.J.: J. Less Common Met. **136** (1987) 207.

87 D 5 Deportes, J., Ouladdiaf, B., Ziebeck, K.R.A.: J. Phys. (Paris) **48** (1987) 1029.

87 D 6 Deportes, J., Ouladdiaf, B., Ziebek, K.R.A.: J. Magn. Magn. Mater. **70** (1987) 14.

87 D 7 Deportes, J., Lemaire, R., Ouladdiaf, B., Roudaut, F.: J. Magn. Magn. Mater. **70** (1987) 191.

87 D 8 Devare, S.H., Devare, H.G.: J. Magn. Magn. Mater. **63–64** (1987) 584.

87 D 9 Drzazga, Z.: Acta Phys. Pol. A **72** (1987) 41.

87 D 10 Drzazga, Z., Drzazga, M.: J. Magn. Magn. Mater. **65** (1987) 21.

87 D 11 Dumelow, T., Fowler, D.K., Prakash, O., Riedi, P.C.: Hyp. Int. **34** (1987) 411.

87 E 1 Abd-El Aal, M.M., Ilyushin, A.S., Chechernikov, V.I., Pechenikov, A.V.: Acta Phys. Hung. **62** (1987) 69.

87 E 2 Abd-El Aal, M.M., Chechernikov, V.I., Kazakova, L.I., Cheremushkina, A.V.: Acta Phys. Hung. **62** (1987) 73.
87 E 3 El-Masry, N.A., Stadelmaier, H.H.: J. Appl. Phys. **61** (1987) 3589.
87 E 4 Endo, E., Iijima, M., Shinogi, A., Ishiyama, K.: J. Phys. Soc. Jpn. **56** (1987) 1316.
87 E 5 Endo, K., Ishiyama, K., Shinogi, A.: J. Magn. Magn. Mater. **70** (1987) 157.
87 E 6 Escorne, M., Lamloumi, J., Percheron-Guegan, A., Achard, J.C., Mauger, A.: J. Magn. Magn. Mater. **65** (1987) 63.
87 F 1 Figiel, H., Barata, A.C., Guimaraes, A.P.: Phys. Status Solidi (b) **139** (1987) 311.
87 F 2 Fillion, G., Fremy, M.A., Gignoux, D., Gomez-Sal, J.C., Gorges, B.: J. Magn. Magn. Mater. **63–64** (1987) 117.
87 F 3 Flanagan, T.B., Clowley, J.D., Mason, N.B., Chung, H.S.: J. Less Common Met. **130** (1987) 309.
87 F 4 Fruchart, D., Berthier,Y., De Saxce, T., Vuillet, P.: J. Less Common Met. **130** (1987) 89.
87 F 5 Fruchart, D., Berthier, Y., De Saxce, T., Vuillet, P.: J. Solid State Chem. **67** (1987) 197.
87 F 6 Fujii, H., Saga, M., Okamoto, T.: J. Less Common Met. **130** (1987) 25.
87 F 7 Fujiwara, K., Ichinose, K., Tsujimura, A.: J. Phys. Soc. Jpn. **56** (1987) 2149.
87 F 8 Fujiwara, E., Ichinose, K., Nagai, H., Tsujimura, A.: J. Magn. Magn. Mater. **70** (1987) 184.
87 F 9 Fujiwara, H., Liu, W.L., Kadomatsu, H., Tokunaga, T.: J. Magn. Magn. Mater. **70** (1987) 301.
87 G 1 Gaidukova, I.Yu., Markosyan, A.S., Tsvyashchenko, A.V.: Fiz. Met. Metalloved. **64** (1987) 186.
87 G 2 Gamo, T., Johnson, J.R., Reilly, J.J.: J. Less Common Met. **131** (1987) 81.
87 G 3 Gignoux, D.: J. Magn. Magn. Mater. **70** (1987) 81.
87 G 4 Gignoux, D., Gomez-Sal, J.C., Rodriguez-Fernandez, J.: J. Magn. Magn. Mater. **66** (1987) 101.
87 G 5 Gignoux, D., Vettier, C., Voiron, J.: J. Magn. Magn. Mater. **70** (1987) 388.
87 G 6 Gratz, E., Bauer, E., Nowotny, H.: J. Magn. Magn. Mater. **70** (1987) 118.
87 G 7 Gratz, E., Pillmayr, N., Bauer, E., Hilscher, G.: J. Magn. Magn. Mater. **70** (1987) 159.
87 G 8 Gubbens, P.C.M.,Van der Kraan, A.M., Van Loef, J.J., Buschow, K.H.J.: J. Magn. Magn. Mater. **67** (1987) 255.
87 G 9 Gubkyn, M.K., Kataev, G.I., Mamatova, T.A., Prokoshev, V.G., Schubin, V.V.: Fiz. Met. Metalloved. **64** (1987) 480.
87 G 10 Guimaraes, A.P., Alves, K.M.B., Alves, N., Gratz, E.: J. Appl. Phys. **61** (1987) 3985.
87 G 11 Gupta, M.: J. Less Common Met. **130** (1987) 219.
87 H 1 Hashimoto, Y., Fujii, H., Okamoto, T., Makihara, Y.: J. Magn. Magn. Mater. **70** (1987) 291.
87 H 2 Hong, N.M., Thy, N.P.: Acta Phys. Pol. A **72** (1987) 49.
87 I 1 Ichinose, K.: J. Phys. Soc. Jpn. **56** (1987) 2908.
87 I 2 Ichinose, K., Fujiwara, K., Nakamura, M., Oyasato, M., Tsujimura, A.: J. Magn. Magn. Mater. **70** (1987) 154.
87 I 3 Imamura, H., Fujiwara, K., Tsuchiya, S.: J. Less Common Met. **134** (1987) L 1.
87 I 4 Inoue, J., Shimizu, M.: J. Magn. Magn. Mater. **70** (1987) 49.
87 I 5 Ishiyama, K., Endo, K., Sakakibara, T., Goto, T., Sugiyama, K., Dato, M.: J. Phys. Soc. Jpn. **56** (1987) 29.
87 I 6 Isikawa, Y., Mori, K., Mizushima, T., Fujii, A.,Takeda, H., Sato, K.: J. Magn. Magn. Mater. **70** (1987) 385.
87 J 1 Janio, A.L., Branwood, A., Dudley, R., Piercy, A.R.: J. Phys. D **20** (1987) 24.
87 J 2 Jin, L., James, W.J., Lemaire, R., Rhyne, J.: J. Less Common Met. **130** (1987) 259.
87 K 1 Kakol, Z., Figiel, H.: J. Magn. Magn. Mater. **70** (1987) 309.
87 K 2 Kakol, Z., Figiel, H., Kapusta, G.: Phys. Status Solidi (b) **143** (1987) 255.
87 K 3 Kametkar, S.M., Hadjipanayis, G.C., Nazareth, A., Cheng, S.C.: Proc. Int. Symposium on Physics of Magnetic Materials, World Scientific **1987**, p. 391.
87 K 4 Kamimura, H., Sakurai, J., Ramura, Y., Nakamura, H., Shiga, M.: J. Magn. Magn. Mater. **70** (1987) 145.
87 K 5 Kanematsu, K., Kobayashi, K.I.: J. Magn. Magn. Mater. **70** (1987) 271.
87 K 6 Kapusta, Cz., Figiel, H., Guzdek, B.: Acta Phys. Pol. A **72** (1987) 61.
87 K 7 Kido, G., Nakagawa, Y., Nishihara, Y., Yamaguchi, F.: J. Magn. Magn. Mater. **70** (1987) 181.
87 K 8 Kolodziejczyk, A.: J. Magn. Magn. Mater. **70** (1987) 8.
87 K 9 Kolodziejczyk, A., Leciejewicz, J., Szytula, A., Chmist, J., Wegrzyn, J.: Acta Phys. Pol. A **72** (1987) 319.
87 K 10 Koterlin, M.D., Babich, O.I., Morohivskii, B.C., Len, G.Y., Lutziv, R.V., Grin, Y.N.: Fiz. Tverd. Tela **29** (1987) 943.
87 L 1 Lamloumi, J., Percheron-Guegan, A., Lartigue, C., Achard, J.C., Jehanno, G.: J. Less Common Met. **130** (1987) 111.

87 L 2 Lartigue, C., Le Bail, A., Percheron-Guegan, A.: J. Less Common Met. **129** (1987) 65.
87 L 3 Lartigue, C., Yu, X.N., Jiang, Z.X., Lin, Z.D., Percheron-Guegan, A., Achard, J.C.: J. Less Common Met. **130** (1987) 517.
87 L 4 Leyarovski, E., Mrachkov, J., Gilevski, A., Mydlarz, T.: Phys. Rev. B **35** (1987) 8668.
87 L 5 Lippold, B., Muller, H., Mahmoud, S.: Phys. Status Solidi (b) **141** (1987) 247.
87 L 6 Liu, W.L.: J. Sci. Hiroshima Univ. **51** (1987) 221.
87 L 7 Liu, W.L., Kadomatsu, H., Fujiwara, H., Kanamori, T., Goto, M.: Solid State Commun. **63** (1987) 947.
87 L 8 Lukasiak, M., Pszczola, J., Opeta, J., Krop, K., Suwalski, J.: Acta Phys. Pol. A **72** (1987) 81.
87 M 1 Matsumoto, T., Matsushita, A.: J. Less Common Met. **132** (1987) 115.
87 M 2 Melamud, M., Bennet, L.H., Watson, R.E.: J. Appl. Phys. **61** (1987) 4246.
87 M 3 Methasiri, T., Tang, I.M.: J. Magn. Magn. Mater. **67** (1987) 190.
87 M 4 Meyer-Liautaud, F., Derkaoui, B., Allibert, C.H., Castanet, R.: J. Less Common Met. **127** (1987) 231.
87 M 5 Mikhov, M.T., Gong, W., Hadjipanayis, G.C.: J. Appl. Phys. **61** (1987) 3460.
87 M 6 Mizutani, U., Fukamichi, K., Goto, T.: J. Phys. F **17** (1987) 257.
87 M 7 Motoya, K., Freltoft, T., Böni, P., Shirane, G.: J. Phys. Soc. Jpn. **56** (1987) 885.
87 N 1 Nagai, H., Ohyama, N., Yoshie, H., Tsujimura, A.: J. Magn. Magn. Mater. **70** (1987) 171.
87 N 2 Narasimha Rao, C., Wada, H., Shiga, N., Nakamura, Y.: J. Magn. Magn. Mater. **70** (1987) 151.
87 N 3 Nishihara, Y.: J. Magn. Magn. Mater. **70** (1987) 75.
87 N 4 Nishihara, Y., Tatsumoto, M., Yamaguchi, Y., Kido, G.: J. Magn. Magn. Mater. **70** (1987) 173.
87 O 1 Ohashi, K., Yokoyama, T., Osugi, R., Tawara, Y.: IEEE Trans. Magn. MAG-**23** (1987) 3101.
87 O 2 Ohyama, T., Sakurai, J., Komura, Y.: J. Magn. Magn. Mater. **63–64** (1987) 581.
87 O 3 Okamoto, T., Nagata, H., Fujii, H., Makihara, Y.: J. Magn. Magn. Mater. **70** (1987) 139.
87 O 4 Okamoto, N., Nagai, H., Yoshie, H., Tsujimura, A., Hihara, T.: J. Magn. Magn. Mater. **70** (1987) 299.
87 O 5 Oomi, G., Terada, T., Shiga, M., Nakamura, Y.: J. Magn. Magn. Mater. **70** (1987) 137.
87 O 6 Oyasato, M., Ichinose, K., Fujiwara, K., Tsujimura, A.: J. Magn. Magn. Mater. **70** (1987) 233.
87 P 1 Park, J.M., Lee, J.Y.: Mater. Res. Bull. **22** (1987) 455.
87 P 2 Paul-Boncour, V., Percheron-Guegan, A., Diaj, M., Achard, J.C.: J. Less Common Met. **131** (1987) 201.
87 P 3 Paul-Boncour, V., Diaf, M., Percheron-Guegan, A., Achard, J.C.: J. Phys. (Paris) **47** (1986) C 8–1093.
87 P 4 Petrii, O.A., Semenenko, K.N., Korobov, I.I., Vasina, S.Ya., Kovrigina, I.V., Burnasheva, V.V.: J. Less Common Met. **36** (1987) 121.
87 P 5 Pillmayr, N., Schmitzer, C., Gratz, E., Hilscher, G., Sechovsky, V.: J. Magn. Magn. Mater. **70** (1987) 162.
87 R 1 Radwanski, R.J.: J. Phys. F **17** (1987) 267.
87 R 2 Radwanski, R.J., Krop, K.: Acta Phys. Pol. A **72** (1987) 105.
87 R 3 Radwanski, R.J., Franse, J.J., Sinnema, S.: J. Magn. Magn. Mater. **70** (1987) 313.
87 R 4 Rastogi, A.K., Murani, A.P.: Proc. 5th Conf. on Valence Fluctuations in Solids, Bangalore, India, New York: Plenum Press **1987**.
87 R 5 Reilly, J.J., Johnson, J.R., Gamo, T.: J. Less Common Met. **131** (1987) 41.
87 R 6 Reissner, M., Grösinger, A., Steiner, W.: J. Magn. Magn. Mater. **70** (1987) 165.
87 R 7 Resnik, A., Stiouti, M., Crayevsky, A., Shaltiel, D.: J. Less Common Met. **131** (1987) 117.
87 R 8 Rhyne, J.J.: J. Magn. Magn. Mater. **70** (1987) 88.
87 R 9 Rhyne, J.J., Hardman-Rhyne, K.A., Smith, H.K., Wallace, W.E.: J. Less Common Met. **129** (1987) 207.
87 R 10 Riesterer, T.: J. Less Common Met. **130** (1987) 541.
87 R 11 Roy, S.B., Coles, B.: J. Phys. F **17** (1987) L 215.
87 S 1 Sakakibara, T., Goto, T., Yoshimura, K., Shiga, M., Nakamura, Y., Fukamichi, K.: J. Magn. Magn. Mater. **70** (1987) 126.
87 S 2 Sakurai, J., Ohyama, T., Komura, Y.: J. Magn. Magn. Mater. **63–64** (1987) 578.
87 S 3 Sakurai, J., Kamimura, H., Ohyama, T., Komura, Y., Gignoux, D.: J. Magn. Magn. Mater. **70** (1987) 383.
87 S 4 Sarkissian, B.V.B.: J. Phys. F **17** (1987) 1569.
87 S 5 Shevchenko, V.I., Pogorelyi, A.N., Perepelitza, V.I.: Metallofizika **9** (1987) 104.
87 S 6 Shevchenko, V.I., Pogorelyi, A.N., Perepelitza, V.I.: Fiz. Met. Metalloved. **64** (1987) 1018.
87 S 7 Shields, T.C., Mayers, J., Harris, I.R.: J. Magn. Magn. Mater. **63–64** (1987) 587.
87 S 8 Shiga, M., Wada, H., Nakamura, H., Yoshimura, K., Nakamura, Y.: J. Phys. F **17** (1987) 1781.
87 S 9 Shilov, A.L., Kost, M.E., Kuznetsov, N.T.: J. Less Common Met. **128** (1987) 1.
87 S 10 Shimizu, K.: J. Magn. Magn. Mater. **70** (1987) 178.
87 S 11 Shimizu, A., Inoue, J.: J. Magn. Magn. Mater. **70** (1987) 61.

87 S 12 Shimizu, M., Inoue, J.: J. Phys. F **17** (1987) 1221.
87 S 13 Shinogi, A., Saito, T., Endo, K.: J. Phys. Soc. Jpn. **56** (1987) 2633.
87 S 14 Shinohara, T., Furusawa, A., Hayashiba, S., Kanazawa, M., Sato, M.: Hyperfine Interactions **36** (1987) 243.
87 S 15 Shinohara, T., Furusawa, A., Hayashiba, S., Kanazawa, M., Sato, M.: J. Magn. Magn. Mater. **70** (1987) 282.
87 S 16 Sinnema, S., Franse, J.J.M., Radwanski, R.J., Menovsky, A., De Boer, F.R.: J. Phys. F **17** (1987) 233.
87 S 17 Sinnema, S., Franse, J.J.M., Radwanski, R.J., Menovsky, A., De Boer, F.R.: J. Less Common Met. **127** (1987) 105.
87 S 18 Slebarski, A.: J. Magn. Magn. Mater. **66** (1987) 107.
87 S 19 Slebarski, A., Jelonek, J., Wohleben, D.: Z. Phys. B **66** (1987) 47.
87 S 20 Smith, H.K., Rhync, J.J., Hardman-Rhyne, K.A., Wallace, W.E.: J. Less Common Met. **130** (1987) 421.
87 S 21 Soubeyroux, J.L., Percheron-Guegan, A., Achard, J.C.: J. Less Common Met. **129** (1987) 181.
87 S 22 Stadelmair, H.H., Cadieu, F.J., Lui, N.C.: Matt. Lett. **6** (1987) 80.
87 S 23 Steiner, W., Reissner, M.: J. Magn. Magn. Mater. **70** (1987) 105.
87 S 24 Szpunar, B., Wallace, W.E.: Phys. Rev. B **35** (1987) 1988.
87 T 1 Takahashi, H., Ukai, T., Mori, N.: J. Magn. Magn. Mater. **70** (1987) 149.
87 T 2 Takahashi, H., Ohatsuka, S., Ukai, T., Mori, N.: J. Magn. Magn. Mater. **70** (1987) 189.
87 T 3 Teter, J.P., Clark, A.E., McMasters, O.D.: J. Appl. Phys. **61** (1987) 3787.
87 T 4 Tharp, D., Yang, Y., James, W., Yelon, W., Xie, D., Yang, J.: J. Appl. Phys. **61** (1987) 4249.
87 T 5 Thompson, P., Reilly, J.J., Hastings, J.M.: J. Less Common Met. **129** (1987) 105.
87 T 6 Tsvyashchenko, A.V., Fomicheva, L.N.: J. Less Common Met. **135** (1987) L 9.
87 T 7 Turek, K., Kakol, Z., Kolodziejczyk, A.: J. Magn. Magn. Mater. **66** (1987) 337.
87 U 1 Uchida, H., Ebisawa, T., Terao, K., Hosoda, N., Huang, Y.C.: J. Less Common Met. **131** (1987) 365.
87 U 2 Ukyo, M., Koizumik, K., Takahashi, H.: J. Appl. Phys. **61** (1987) 3987.
87 V 1 Vettier, C., Burlet, P., Rossat-Mignot, J.: J. Magn. Magn. Mater. **63–64** (1987) 18.
87 W 1 Wada, H., Nakamura, H., Yoshimura, K., Shiga, M., Nakamura, Y.: J. Magn. Magn. Mater. **70** (1987) 134.
87 W 2 Wada, H., Nakamura, H., Fukami, E., Yoshimura, K., Shiga, M., Nakamura, Y.: J. Magn. Magn. Mater. **70** (1987) 17.
87 W 3 Wallace, W.E., Pourarian, F., Pedziwiatr, A.T., Boltich, E.B.: J. Less Common Met. **130** (1987) 33.
87 W 4 Wiesinger, G.: J. Less Common Met. **130** (1987) 181.
87 Y 1 Yamada, H., Shimizu, M.: J. Magn. Magn. Mater. **70** (1987) 47.
87 Y 2 Yamada, H., Tohyama, T., Shimizu, M.: J. Magn. Magn. Mater. **70** (1987) 44.
87 Y 3 Yamada, H., Tohyama, T., Shimizu, M.: J. Magn. Magn. Mater. **66** (1987) 409.
87 Y 4 Yamada, H., Tohyama, T., Shimizu, M.: J. Phys. F **17** (1987) L 163.
87 Y 5 Yamada, H., Hitaoka, Y., Asayama, K., Sakata, A.: J. Magn. Magn. Mater. **70** (1987) 175.
87 Y 6 Yamaguchi, M., Ohta, T., Goto, T., Sakakibara, T., Katayama, T.: J. Less Common Met. **130** (1987) 47.
87 Y 7 Yamaguchi, M., Ohta, T., Goto, T., Sakakibara, T., Katayama, T.: Solid State Commun. **63** (1987) 285.
87 Y 8 Yoshie, H., Ogino, K., Nagai, H., Tsujimura, A., Nakamura, Y.: J. Magn. Magn. Mater. **70** (1987) 303.
87 Y 9 Yoshimura, K., Fukamichi, K., Yasuoka, H., Mekata, M.: J. Phys. Soc. Jpn. **56** (1987) 3652.
87 Y 10 Yoshimura, K., Nakamura, H., Takigawa, M., Yasuko, H., Shiga, M., Nakamura, Y.: J. Magn. Magn. Mater. **70** (1987) 142.
87 Y 11 Yoshimura, K., Takigawa, M., Takahashi, Y., Yasuoka, H., Mekata, M.: J. Magn. Magn. Mater. **70** (1987) 11.
87 Y 12 Yoshimura, K., Takigawa, M., Takahashi, Y., Yasuoka, H., Nakamura, Y.: J. Phys. Soc. Jpn. **56** (1987) 1138.
87 Y 13 Yoshimura, K., Yoshimoto, Y., Mekata, M., Sakakibara, T., Goto, T.: J. Magn. Magn. Mater. **70** (1987) 147.
87 Z 1 Zhong, W.D., Lan, J., Liu, Z.X.: J. Magn. Magn. Mater. **68** (1987) 197.

88 A 1 Asano, S., Ishida, S.: J. Phys. F **18** (1988) 501.
88 B 1 Ballou, R., Barthem, V.M.T.S., Gignoux, D.: Physica B **149** (1988) 340.
88 B 2 Ballou, R., Deportes, J., Lemaire, R., Ouladdiaf, B.: J. Appl. Phys. **63** (1988) 3487.
88 B 3 Barthem, V.M.T.S., Gignoux, D., Nait-Saada, A., Schmitt, D., Creuzet, G.: Phys. Rev. B **37** (1988) 1733.
88 B 4 Budzynski, M., Subotovicz, M., Niezgoda, H., Spustek, H., Tanska-Krupa, W., Wasiewicz, R.: Phys. Status Solidi (b) **147** (1988) 685.
88 B 5 Buschow, K.H.J.: J. Appl. Phys. **63** (1988) 3130.

88 B 6 Buschow, K.H.J., De Mooij, D.B., Brouha, M., Smit, H.H., Thiel, R.C.: IEEE Trans. Magn. MAG-**24** (1988) 1616.
88 C 1 Clark, A.E., Teter, J.P., McMasters, O.D.: J. Appl. Phys. **63** (1988) 3910.
88 D 1 De Mooij, D.B., Buschow, K.H.J.: J. Less Common Met. **136** (1988) 207.
88 D 2 Deportes, J., Ouladdiaf, B., Ziebeck, K.R.A.: J. Magn. Magn. Mater. **78** (1988) 14.
88 D 3 Duc, N.H., Hien, T.D., Brommer, P.E., Franse, J.J.M.: Physica B **149** (1988) 352.
88 D 4 Duc, N.H., Hien, T.D., Brommer, P.E., Franse, J.J.M.: J. Phys. F **18** (1988) 275.
88 E 1 Escorne, M., Lamloumi, J., Percheron-Guegan, A., Achard, J.C., Mauger, A., Jehanno, G.: J. Appl. Phys. **63** (1988) 4121.
88 F 1 Franse, J.J.M., Thui, N.P., Hong, N.M.: J. Magn. Magn. Mater. **72** (1988) 361.
88 F 2 Freltoft, T., Böni, P., Shirane, G., Motoya, K.: Phys. Rev. B **37** (1988) 3454.
88 F 3 Fujiwara, K.: J. Phys. Soc. Jpn. **57** (1988) 2133.
88 G 1 Gaidukova, I.Yu., Kelarev, V.V., Markosian, A.S., Menshikov, A.Z., Pirogov, A.N.: J. Magn. Magn. Mater. **72** (1988) 357.
88 G 2 Gavigan, J.P., Givord, D., Li, H.S., Voiron, J.: Physica B **149** (1988) 345.
88 G 3 Gratz, E.: Physica B **149** (1988) 283.
88 G 4 Gratz, E., Bauer, E., Nowotny, H., Burkov, A.T., Vedernikov, M.V.: Solid State Commun. **69** (1988) 1007.
88 G 5 Gubbens, P.C.M., Van der Kraan, A.M., Buschow, K.H.J.: Hyperfine Interactions **40** (1988) 389.
88 H 1 Helmholdt, R.B., Vleggar, J.J.M., Buschow, K.H.J.: J. Less Common Met. **138** (1988) L 11.
88 H 2 Hilscher, G., Pillmayr, N., Schmitzer, C., Gratz, E.: Phys. Rev. B **37** (1988) 3480.
88 H 3 Horikoshi, H.: J. Sci. Hiroshima Univ. A **52** (1988) 179.
88 I 1 Inoue, J.: Physica B **149** (1988) 376.
88 K 1 Kamprath, N., Wickramasekara, L., Hegde, H., Liu, N.C., Jayanetti, J.K.D., Cadieu, F.J.: J. Appl. Phys. **63** (1988) 3696.
88 K 2 Kaneko, T., Marumo, K., Miura, S., Kido, K., Abe, S., Yoshida, H., Kamigaki, K., Nakagawa, Y.: Physica B **149** (1988) 334.
88 K 3 Kasiorowska, J., Van Noort, D., Bajorek, A., Van Duyneveldt, A.J.: Physica B+C **147** (1988) 316.
88 K 4 Koterlin, M.D., Babich, O.N., Morokhivski, B.S., Konyuk, M.B., Lutsiv, R.V.: Fiz. Tverd. Tela **30** (1988) 1512.
88 K 5 Kumar, K.: J. Appl. Phys. **63** (1988) R 13.
88 L 1 Leont'ev, P.I., Markosian, A.S., Nikitin, S.A., Snegirev, V.V.: Fiz. Tverd. Tela **30** (1988) 3700.
88 L 2 Li, H.S., Hu, B.P., Coey, J.M.D.: Solid State Commun. **66** (1988) 133.
88 L 3 Liu, N.C., Kamprath, N., Wickramasekara, L., Cadieu, F.J., Stadelmaier, H.H.: J. Appl. Phys. **63** (1988) 3589.
88 M 1 Motoya, K., Freltoft, T., Boni, P., Shirane, G.: Phys. Rev. B **38** (1988) 4796.
88 M 2 Moze, O., Pareti, L., Solzi, M., David, W.I.F.: Solid State Commun. **66** (1988) 465.
88 N 1 Nakamura, H., Wada, H., Yoshimura, K., Shiga, M., Nakamura, Y., Sakurai, J., Komura, Y.: J. Phys. F **18** (1988) 981.
88 N 2 Nieva, G.L., Sereni, J.G., Afyouni, M., Schmerber, G., Kappler, J.P.: Z. Phys. B **70** (1988) 181.
88 O 1 Ohashi, K., Tawara, Y., Osugi, R., Sakurai, J., Komura, Y.: J. Less Common Met. **139** (1988) L 1.
88 P 1 Pareti, L., Moze, O., Solzi, M., Bolzoni, F.: J. Appl. Phys. **63** (1988) 172.
88 P 2 Pillay, R.G., Grover, A.K., Balasubramian, V., Rostogi, A.K., Tandor, P.N.: J. Phys. F **18** (1988) L 63
88 P 3 Pillay, R.G., Rastogi, A.K., Grover, A.K., Balasubramanian, V., Tandor, P.N.: Hyperfine Interactions **40** (1988) 413.
88 P 4 Pillmayr, N., Hilscher, G., Gratz, E., Sechowsky, V.: J. Phys. (Paris) **49** (1988) C8-273.
88 R 1 Radwanski, R.J., Franse, J.J.M., Krop, K.: Physica B **149** (1988) 306.
88 R 2 Rastogi, A.K., Hilscher, G., Gratz, E., Pillmayr, N.: J. Phys. (Paris) **49** (1988) C8-277.
88 R 3 Roy, S.B., Coles, B.R.: J. Appl. Phys. **63** (1988) 4094.
88 R 4 Rupp, B., Wiesinger, G.: J. Magn. Magn. Mater. **71** (1988) 269.
88 S 1 Shiga, L.: Physica B **149** (1988) 293.
88 S 2 Shimizu, K., Sato, K., Nagano, N.: Physica B **149** (1988) 319.
88 S 3 Shinogi, A., Iijima, M., Saito, T., Endo, K.: Physica B **149** (1988) 323.
88 S 4 Shpinkova, L.G., Sorokin, A.A.: Phys. Status Solidi (b) **147** (1988) K 75.
88 S 5 Steiner, W., Reissner, M., Moser, J., Will, G.: Physica B **149** (1988) 329.
88 T 1 Takahashi, H., Hikosaka, K., Ohtouka, S., Seo, A., Ukai, T., Mori, N.: J. Appl. Phys. **63** (1988) 3595.
88 T 2 Talik, E., Szade, J., Heimann, J., Winiarska, A., Winiarski, A., Chelkowski, A.: J. Less Common Met. **138** (1988) 129.

88 T 3 Thuy, N.P., Zukrowski, J., Fiegiel, H., Przewoznik, J., Krop, K.: Hyperfine Interactions **40** (1988) 441.
88 W 1 Wada, H., Yoshimura, K., Kido, G., Shiga, M., Mekata, M., Nakamura, Y.: Solid State Commun. **65** (1988) 23.
88 W 2 Wang, X.Z., Chevalier, B., Berlureau, T., Etourneau, J., Coey, J.M.D., Cadogan, J.M.: J. Less Common. Met. **138** (1988) 235.
88 W 3 Watson, R.E., Bennet, L.M., Melamud, M.: J. Appl. Phys. **63** (1988) 3136.
88 W 4 Wiesinger, G., Hilscher, G., Forsthuber, M.: Z. Phys. Chem. N. F. **163** (1989) 655.
88 X 1 Xu, Y., Chu, D.P., Yang, G.L., Zhai, H.R.: Physica B **149** (1988) 363.
88 Y 1 Yamada, H.: Physica B **149** (1988) 390.
88 Y 2 Yang, Y.C., Kong, L.S., Sun, S.H., Gu, D.M., Cheng, B.P.: J. Appl. Phys. **63** (1988) 3702.
88 Y 3 Yoshimura, K., Mekata, M., Takigawa, M., Takahoshi, Y., Yasuoka, H.: Phys. Rev. B **37** (1988) 3593.
88 Z 1 Zhao, Z.R., Ren, Y.G., Aylesworth, K.D., Sellmyer, D.J., Singleton, E., Strzeszewski, J., Hadjipanayis, G.C.: J. Appl. Phys. **63** (1988) 3699.
88 Z 2 Zhong, W.D., Lau, J., Liu, Z.X.: Acta Phys. Sinica **37** (1988) 645.

89 G 1 Gubbens, P.C.M., Van der Kraan, A.M., Buschow, K.H.J.: Hyperfine Interactions **49** (1989) 685.
89 S 1 Sinneman, T., Erdmann, K., Rosenberg, M., Buschow, K.H.J.: Hyperfine Interactions **49** (1989) 675.

90 B 1 Ballou, R., Gorges, B., Molho, P., Rouault, P.: J. Magn. Magn. Mat. **87** (1990) L 1.

2.5 Compounds of rare earth elements and 4d or 5d elements

2.5.1 Introduction

The tables and figures in this section contain magnetic data on metallic or pseudometallic compounds of the rare earth group of elements which contain besides the rare earth element at least one 4d (Ru, Rh, Pd) element or/and one 5d (Os, Ir, Pt) element. The compounds are summarized in two tables in subsect. 2.5.2. Table 1 is devoted to binary and pseudobinary compounds of the rare earth elements and 4d elements. It contains also pseudobinary compounds of the rare earth elements which contain besides a 4d element also 5d element. Table 2 is devoted to binary and pseudobinary compounds which contain besides the rare earth element at least one 5d element.

The compounds listed in the tables are designated by their chemical formula. The compounds are arranged in the order as their elements appear in the periodic system. Thus the rare earth elements are listed in following order

Sc, Y, La, Ce, Pr, Nd, Pm, Sm, Eu, Gd, Tb, Dy, Ho, Er, Tm, Yb, Lu,

the 4d elements in the order

Ru, Rh, Pd,

and the 5d elements in the order

Os, Ir, Pt.

The compounds are listed in the tables according to the decreasing atomic ratio of the rare earth to the 4d or/and 5d elements. Consequently, the rare-earth-rich compounds appear in the beginning of each table.

The tables provide information on paramagnetic Curie temperature Θ, ferromagnetic Curie temperature T_C, Néel temperature T_N, magnetic susceptibility χ, saturation or spontaneous magnetic moment p_s, and effective paramagnetic moment p_{eff}. The column "Remarks" may provide further data.

The observed effective paramagnetic moments as well as the saturation magnetic moments depend on the crystal electric field (CEF) splitting, which depends on the electron configuration and on the local symmetry of the particular element. This splitting is characterized by the CEF Hamiltonian which can be expressed in different ways, in terms of the CEF parameters B_n [64 h 1], or in the case of cubic symmetry by the so-called Lea Leask and Wolf parameters W and x [6211]. All these parameters are used in this compilation.

2.5.2 Survey of compounds and properties

Table 1. Rare earth compounds with 4d elements Ru, Rh, Pd. p_s refers to 4.2 K and χ to RT, unless stated otherwise. R: rare earth element, M: 4d element.

	Θ K	T_C K	T_N K	χ	p_s μ_B/R	p_{eff} μ_B/R	Remarks	Ref.
$R_{1-x}M_x$								
$Gd_{1-x}Ru_x$				Fig. 1			$\sigma(T)$: Fig. 1	80 A 1
x=0.15	80	78			6.1	8.5		
0.30	79	77			7.1	8.8		
0.40	56	57			6.0	8.1		
$Gd_{0.82}Rh_{0.18}$		111			5.6			80 A 1
$Gd_{0.76}Pd_{0.24}$		145			5.7			80 A 1
R_3M								
Y_3Ru				0.57			χ_g in 10^{-6} cm^3/g, Pauli paramagnet, crystal structure not known	76 L 1
Y_3Rh				440			χ_m in 10^{-6} cm^3/mol	75 L 2
Gd_3Ru	105					8.05	crystal strcture not known	76 L1
Gd_3Rh	150		115			8.05		75 L 2
Dy_3Ru	8					10.6	crystal structure not known	76 L 1
Dy_3Rh	72					10.6		75 L 2
$Y_{73}Ru_{27}$				0.78			χ_g in 10^{-6} cm^3/g, Pauli paramagnet, crystal structure not known	76 L 1
$Gd_{73}Ru_{27}$	75					8.1	crystal structure not known	76 L 1
$Dy_{73}Ru_{27}$	18					10.6	crystal structure not known	76 L 1
$Tb_{5.10}Pd_{1.90}$	50	$\cong$30	62		6.05	9.7		64 B 1
$Dy_{5.07}Pd_{1.93}$	45	~25	41		5.9	10.7	p_s at 55 kOe, H_c=9.7 kOe at 4.2 K	64 B 1
$Ho_{5.04}Pd_{1.96}$	33	~10	27		8.27	10.6	p_s at 55 kOe, H_c=1.3 kOe at 4.2 K	64 B 1
R_5M_2								
Y_5Pd_2				Fig. 2				77 Y 1
Gd_5Pd_2	333	335			6.89	7.6	p_s at 5.5 T	64 B 1
	335					7.8		73 L 2

Tb_5Pd_2	65.3		63.5	Fig. 3	10.63		77 Y 1
Dy_5Pd_2	44				11.0		73 L 2
	39		38	Fig. 3	11.38		77 Y 1
Ho_5Pd_2	63				10.6		73 L 2
	31		22.5	Fig. 3	11.48		77 Y 1
Er_5Pd_2	17		15	Fig. 4	9.77		77 Y 1
Tm_5Pd_2	4.5		7	Fig. 4	7.46		77 Y 1
R_7M_3							
Y_7Rh_3				650		χ_m in 10^{-6} cm^3/mol, Pauli paramagnet	75 L 2
La_7Rh_3				Fig. 5		Pauli paramagnet	73 O 1, 75 L 2
La_7Pd_3				Fig. 6			73 O 1
Ce_7Rh_3	13			Fig. 5	2.31	Ce valency 3.17 suggested	73 O 1
Ce_7Pd_3	29			Fig. 6	2.31	Ce valency 3.1 suggested	73 O 1
	−33		5.4		2.52	Ce trivalent	85 K 1
Pr_7Rh_3	37			Fig. 5	3.39		73 O 1
Pr_7Pd_3	30			Fig. 6	3.39		73 O 1
Nd_7Rh_3	58			Fig. 5	3.43		73 O 1
Nd_7Pd_3	49			Fig. 6	3.34		73 O 1
Sm_7Rh_3				Fig. 5	1.5	no Curie-Weiss behaviour	73 O 1
Sm_7Pd_3				8.34 Fig. 7		χ_g at RT in 10^{-6} cm^3/g, below 183 K susceptibility field-dependent, magnetization anisotropic with preferred direction along c axis, $\sigma(T)$ at 9.6 kOe along c axis: Fig. 8	75 J 1
Gd_7Rh_3	134	170		Fig. 9	8.35		73 O 1
	175		142	Fig. 10	7.9	above 470 K Curie-Weiss behaviour, $\sigma(T)$ at 10 kOe: Fig. 10, $\sigma(H, T)$: Fig. 11	75 L 1, 75 L 2
Tb_7Rh_3	55			Fig. 9	10.16		73 O 1
Dy_7Rh_3	41			Fig. 9	10.55		73 O 1
Ho_7Rh_3	34			Fig. 9	10.30		73 O 1
Er_7Rh_3	26			Fig. 9	9.22		73 O 1

continued

Table 1 (continued)

	Θ K	T_C K	T_N K	χ	p_s μ_B/R	p_{eff} μ_B/R	Remarks	Ref.
R_2M								
Y_2Ru				0.64			χ_g in 10^{-6} cm^3/g, Pauli paramagnet, crystal structure not known	76 L 1
Eu_2Pd	33					8.2		71 H 1
Gd_2Ru	48					7.95	crystal structure not known	76 L 1
Dy_2Ru	15					10.5	crystal structure not known	76 L 1
R_5M_3								
Y_5Rh_3				520			χ_m in 10^{-6} cm^3/mol	75 L 2
Gd_5Rh_3	98					7.98		75 L 2
R_3M_2								
Y_3Rh_2				300			χ_m in 10^{-6} cm^3/mol	75 L 2
Ce_3Pd_2	−26		3.3			2.52	Ce estimated to be trivalent	85 K 1
Sm_3Pd_2							no Curie-Weiss behaviour	73 L 2
				4.97			χ_g at RT in 10^{-6} cm^3/g	75 J 1
				Figs. 12, 7				
Gd_3Rh_2	73					7.9	high-temperature phase	75 L 2
	56	51		Fig. 13	6.85	8.35	p_s at 1.5 K and 60 kOe, $p_{Gd}(H)$ at 1.5 K: Fig. 14	84 G 1
Gd_3Pd_2	265					7.7		73 L 2
				Fig. 15	18.4		p_s at 20 kOe in μ_B/f.u., $\sigma(H)$ at 4.2 K: Fig. 15, at low temperatures ferromagnetic	80 Y 1
Tb_3Rh_2	34		24	Fig. 13	6.59	10.01	p_s at 1.5 K and 60 kOe, $p_{Tb}(H, T)$: Fig. 16	84 G 1
Tb_3Pd_2	28	40		Fig. 17	5.2	11.0	p_s at 20 kOe in μ_B/f.u.	80 Y 1
Dy_3Rh_2	15	18		Fig. 13	5.87	10.77	p_s at 1.5 K and 60 kOe, $p_{Dy}(H, T)$: Fig. 18	84 G 1
Dy_3Pd_2	22					10.8		73 L 2
	20	27		Fig. 19	8.2	11.0	p_s at 20 kOe in μ_B/f.u., $\sigma(H)$ at 4.2 K: Fig. 19	80 Y 1

Ho_3Rh_2	11	19		Fig. 13	7.07	10.63	p_s at 1.5 K and 60 kOe, $p_{Ho}(H)$ at 1.5 K: Fig. 14	84 G 1
Ho_3Pd_2	2					10.6		73 L 2
	14	20		Fig. 19	16.4	12.0	p_s at 20 kOe in μ_B/f.u., $\sigma(H)$ at 4.2 K: Fig. 19	80 Y 1
Er_3Rh_2	3	8		Fig. 13	5.78	9.59	p_s at 1.5 K and 60 kOe, $p_{Er}(H)$ at 1.5 K: Fig. 14	84 G 1
Er_3Pd_2	4	18		Fig. 19	9.5	9.8	p_s at 20 kOe in μ_B/f.u., $\sigma(H)$ at 4.2 K: Fig. 19	80 Y 1
Tm_3Pd_2	−10			Fig. 20	6.5	8.3	p_s at 20 kOe in μ_B/f.u., $\sigma(H)$ at 4.2 K: Fig. 20, ordering temperature below 4.2 K	80 Y 1
R_4M_3								
Gd_4Rh_3	33					7.92		75 L 2
RM								
ScRu	0			1.10			χ_g in 10^{-6} cm^3/g, Pauli paramagnet	73 T 1
YRh				0.15			χ_g in 10^{-6} cm^3/g	75 L 2
CePd	−22	6.5				2.50	Ce estimated to be trivalent	85 K 1
SmPd				4.39 Figs. 12, 7			χ_g at RT in 10^{-6} cm^3/g	75 J 1
EuPd			48			8.2	Eu divalent suggested	73 L 1
GdRh	25					7.95		75 L 2
	28	29			6.6	7.7		85 D 2
GdPd	29	32			6.27	9.83		85 D 2
TbRh	22	19.2		Fig. 21	4.9	9.4	p_s at 1.5 K and 27 kOe, $\sigma(H)$ at 1.5 K: Fig. 22, CEF effects	72 C 1
DyRh	2	4.8		Fig. 21	6.4	10.4	p_s at 2.3 K and 27 kOe, $\sigma(H)$ at 2.3 K: Fig. 22, p_{Dy} from neutron diffraction 7.1 μ_B, CEF effects	72 C 1
	8					10.6		75 L 2
DyPd	29					10.5		73 L 2
HoRh	−3		3.2	Figs. 21, 22	5.5	10.3	p_s at 1.7 K and 27 kOe, $\sigma(H)$ at 1.7 K: Fig. 22, CEF effects	72 C 1
HoRh	3					10.5		75 L 2
HoPd	20					10.4		73 L 2

continued

Table 1 (continued)

	Θ K	T_C K	T_N K	χ	p_s μ_B/R	p_{eff} μ_B/R	Remarks	Ref.
ErRh	−4		3.3	Figs. 21, 22	5.4	9.4	p_s at 1.6 K and 27 kOe, $\sigma(H)$ at 1.6 K: Fig. 22, CEF effects	72 C 1
TmRh	−7		2.7		3.90	7.1		80 B 1
YbPd	−92			Fig. 23		3.81	Yb in a mixed valent state	80 I 2
	160					4.3		77 K 1
				Fig. 24			magnetic transition at 0.5 K, magnetic order occurs at a fractional Yb valency of 2.8 suggested, orders probably antiferromagnetic	85 P 1
R_4M_5								
Gd_4Pd_5	2					8		73 L 2
Dy_4Pd_5	16					10.5		73 L 2
Ho_4Pd_5	10					10.3		73 L 2
R_3M_4								
Ce_3Pd_4	−27		3.1			2.59	Ce estimated to be trivalent	85 K 1
Pr_3Pd_4	−17			Fig. 25		3.46	$\sigma(T)$: Fig. 26	77 Y 2
Nd_3Pd_4	8		9.5	Fig. 25		3.42	$\sigma(H)$ at 4.2 K: Fig. 25, $\sigma(T)$: Fig. 26	77 Y 2
	8		9.5					79 G 1
Sm_3Pd_4				3.54			χ_g at RT in 10^{-6} cm^3/g	75 J 1
				Figs. 12, 7				
Gd_3Pd_4	−11			Fig. 25		8.09		77 Y 2
	−11							79 G 1
$Gd_3Pd_{4-x}Pt_x$							T_{M1}, T_{M2} susceptibility maxima, below T_{M1} long-range ordering, below T_{M2} spin glass phase suggested, $\sigma(H, T)$: Figs. 32, 33, $T_{M1}(x)$ and $\chi_{max}(x)$: Fig. 31	80 G 1
x = 0	−11			Fig. 27		8.10	T_{M1} = 17 K, T_{M2} = 6 K	
= 0.5	55			Figs. 27, 28		9.64	T_{M1} = 20 K, T_{M2} = 7.8 K	
= 1	80			Figs. 27, 28		9.70	T_{M1} = 20 K, T_{M2} = 7.5 K	
= 2	30			Figs. 27, 29		8.39	T_{M1} = 22 K, T_{M2} = 7.5 K	

x = 3	28			Fig. 30	8.17	T_{M1} = 20 K	
= 4	26			Fig. 30	8.14	T_{M1} = 23 K	
Tb_3Pd_4	−12		20	Figs. 25, 34	10.0		77 Y 2
	−12		20				79 G 1
Dy_3Pd_4	−6		14	Figs. 25, 34	10.4		77 Y 2
	−6		14				79 G 1
Ho_3Pd_4	−2		12	Figs. 25, 34	10.4		77 Y 2
	−2		12				79 G 1
Er_3Pd_4	−4			Fig. 25	9.71		77 Y 2
	−4						79 G 1
Tm_3Pd_4	−2			Fig. 25	7.39		77 Y 2
	−2						79 G 1
Yb_3Pd_4			3	Fig. 35	4.42	p_{eff} leads to Yb valency of 2.95	85 P 2
R_3M_5							
Ce_3Pd_5	−35	1.5			2.59	Ce estimated to be trivalent	85 K 1
RM_2							
$ScRu_2$				3.3		χ_m at RT in 10^{-4} cm^3/mol, superconductor at 1.52 K	64 S 1
YRu_2				4.0		χ_m at RT in 10^{-4} cm^3/mol, superconductor at 1.67 K	64 S 1
				1.3		χ_g in 10^{-6} cm^3/g, structure type $MgZn_2$	76 L 1
				Fig. 36			83 W 1
$Y_xHo_{1-x}Ru_2$	Fig. 37	Fig. 37			Fig. 37	for x = 0.8 the system is paramagnetic even at 4.2 K	85 O 1
YRh_2				0.47		χ_g in 10^{-6} cm^3/g, Pauli paramagnet	75 L 2
				206		χ_m in 10^{-6} cm^3/mol at 4.2 K, Pauli paramagnet, $\sigma(H)$ at 4.2 K and 274 K: Fig. 38	83 H 1
				Fig. 38			
$LaRu_2$				3.3		χ_m at RT in 10^{-4} cm^3/mol, superconductor at 1.6 K	64 S 1
				Fig. 36			83 W 1
$La_{1-x}Gd_xRu_2$		Fig. 39			7.6	p_{eff} in μ_B/Gd, below x ≃ 0.05 superconductor: Fig. 39	72 H 1
LaRuRh				Fig. 36			83 W 1

continued

Table 1 (continued)

	Θ K	T_C K	T_N K	χ	p_s μ_B/R	p_{eff} μ_B/R	Remarks	Ref.
$LaRh_2$				0.73			χ_m at RT in 10^{-4} cm^3/mol	64 S 1
				Fig. 36				83 W 1
$La_{1-x}Ce_xRh_2$				Fig. 40			χ_m for x = 0.2 and 0.4	84 H 1
$CeRu_2$				7.2			χ_m at RT in 10^{-4} cm^3/mol, superconductor at 4.9 K	64 S 1
				Figs. 41, 42		0.33	Ce valency 3.87 suggested	71 H 3
				Fig. 43			Ce tetravalent suggested	70 V 1
				Fig. 44				83 W 1
$Ce_{1-x}Pr_xRu_2$		Fig. 45					below x ≃ 0.32 superconductor: Fig. 45	58 M 1
		Fig. 46						71 W 1
	Fig. 47	Fig. 47		Fig. 48			$\sigma(H)$ at 2.7, 4.5 and 12 K: Fig. 49, Curie constant vs. x: Fig. 50, for x < 0.35 superconductor: Fig. 47, for all alloys $p_{eff} = 3.57\,\mu_B$/Pr	76 A 1
$Ce_{1-x}Nd_xRu_2$		Fig. 46						71 W 1
$Ce_{1-x}Gd_xRu_2$		Fig. 51					below x ≃ 0.08 superconductor: Fig. 51	58 M 1
		Fig. 52					superconductor for x < 0.11: Fig. 52	70 W 1, 71 W 1, 73 R 1, 77 R 1
		Fig. 53						
		Fig. 54					for x < 0.110 superconductor, ferromagnetically ordered Gd atoms down to x = 0.105 in $H = 0$ and to x = 0.095 with $H \neq 0$	78 K 1
				Fig. 55			high-field $\sigma(H)$ at 1.5 and 4.2 K: Fig. 56, low-field $\sigma(H)$ at 1.5 K: Fig. 57, coexistence of ferromagnetism and superconductivity suggested	85 K 2
$Ce_{1-x}Tb_xRu_2$		Figs. 52, 58					superconductor for x < 0.2, T_C(x) and T_s(x): Figs. 52 and 58	70 H 1, 71 W 1, 73 R 1, 81 F 1

$Ce_{1-x}Dy_xRu_2$		Fig. 52					71 W 1
	Fig. 59	Fig. 59				below x = 0.24 superconductor: Fig. 59, hysteresis loops at 1.5 and 4.2 K for x = 0.18: Fig. 60	78 A 1
			Figs. 61, 63			$\sigma(H, T)$: Fig. 62, $\sigma(T)$: Fig. 63, hysteresis loops at 4.2 K: Fig. 64	79 A 1
$Ce_{1-x}Ho_xRu_2$		Fig. 46					71 W 1
$Ce_{1-x}Er_xRu_2$		Fig. 46					71 W 1
$Ce(Ru_xRh_{1-x})_2$			Fig. 65			for x > 0.6 superconductor	84 H 2
$CeRu_{2-x}Os_x$			Fig. 66			complete solid solution, below x = 0.8 superconductor	85 H 1
$CeRh_2$			Fig. 43			Ce tetravalent suggested	70 V 1
			880			χ_m in 10^{-6} cm^3/mol	80 B 1
			Fig. 67				82 B 1
$Ce(Rh_xPt_{1-x})_2$			Fig. 68				82 B 1
$PrRu_2$		Fig. 69		Fig. 70			59 B 1
		40					59 C 1
		33.9					80 G 3
	23	33.9			3.96		80 V 1
		35.3		2.6		from neutron diffraction: p_{Pr}, simple ferromagnetic ordering suggested, $p_{Pr}(T)$: Fig. 71	82 F 1
		33.9		1.73		$p_{Pr}(H)$ at 4.2 K: Fig. 72, $p_{Pr}(H)$ at 77 K: Fig. 73 strong CEF effects	83 G 1
$PrRh_2$		8		2.2			64 C 1, 80 B 1
		7.9		1.16		$p_{Pr}(H)$ at 4.2 K: Fig. 72, $p_{Pr}(H)$ at 77 K: Fig. 73, strong CEF effects	83 G 1
	−5	7.9			3.67		80 V 1
		7.9					80 G 3
				2.1		from neutron diffraction: p_{Pr} at 4.2 K, simple ferromagnetic ordering suggested	82 F 1
$NdRu_2$		Fig. 69					59 B 1
		35					59 C 1
$NdRh_2$		7		1.7			64 C 1, 80 B 1

continued

Table 1 (continued)

	Θ K	T_C K	T_N K	χ	p_s μ_B/R	p_{eff} μ_B/R	Remarks	Ref.
$SmRh_2$		20			0.6			64 C 1, 80 B 1
		22			0.53			73 B 1
$SmPd_2$				2.70 Figs. 12, 7			χ_g in 10^{-6} cm^3/g	75 J 1
$EuRh_2$							no Curie-Weiss behaviour	64 C 1, 74 B 1
							Eu divalent	68 W 1
$EuPd_2$	80					7.8	Eu divalent	68 W 1
$GdRu_2$		Fig. 69			Fig. 70			59 B 1
		83						59 C 1
	100					7.95	structure type $MgZn_2$	76 L 1
$GdRh_2$		73			6.9			64 C 1, 80 B 1
		75			6.8			73 B 1
	75···80					7.9		75 L 2
		66			7.1	7.95	p_s at 6.5 kOe	79 H 1
				Fig. 74	7.0			80 T 1
		71			7.03			82 T 1
$GdPd_2$	−12					8.1		73 L 2
$TbRh_2$		39			7.1			64 C 1, 80 B 1
$DyRu_2$	35						structure type $MgZn_2$	76 L 1
$DyRh_2$		27			8.1	10.5		64 C 1, 80 B 1
	30···35					10.5		75 L 2
		25			8.0	10.37	p_s at 6.5 kOe	79 H 1
$DyPd_2$	6					10.3		73 L 2
$HoRu_2$		13		Fig. 75	8.0		$\sigma(T)$ at 5 kOe: Fig. 75, $p_{Ho}(H)$ at 4.2 K: Fig. 76	85 O 1
$HoRh_2$		16			7.7			64 C 1
	20···23					10.6		75 L 2
		16			8.3	10.52	p_s at 6.5 kOe	79 H 1

$HoPd_2$	3			10.3		73 L 2
$ErRu_2$		Fig. 69		Fig. 70		59 B 1
		13				59 C 1
$ErRh_2$		7		7.2		64 C 1, 80 B 1
$TmRh_2$	−6		Fig. 77	7.58	no magnetic ordering down to 2 K	84 G 2
$YbRh_2$	−6			4.50		80 B 1
$LuRu_2$				Fig. 70		59 B 1
RM_3						
$ScPd_3$			Fig. 78			72 G 1
$Sc_xCe_{1-x}Pd_3$			Fig. 79		transition from Ce tetravalent for $x > 0.5$ to an intermediate-valent state for $x < 0.3$ suggested from $\chi(T, x)$ and ESR experiments	80 G 5
YRh_3			287		χ_m in 10^{-6} cm^3/mol, Pauli paramagnet	75 L 2
YPd_3					diamagnetic at room temperature, paramagnetic below 50 K	71 G 1
				4.3		71 H 2
			Fig. 78			72 G 1
			Fig. 36			83 W 1
$Y_xCe_{1-x}Pd_3$			Fig. 80			81 G 1
			Fig. 81			82 K 1
$Y_{0.94}Pr_{0.06}Pd_3$					$\sigma(H)$ at 1.64 and 4.2 K: Fig. 82, $\sigma_s = 2.606$ G cm^3/g	81 H 1
$Y_{0.94}Nd_{0.06}Pd_3$					$\sigma(H)$ at 1.53 and 4.2 K: Fig. 82, $\sigma_s = 2.664$ G cm^3/g	81 H 1
$Y_{0.94}Sm_{0.06}Pd_3$					$\sigma(H)$ at 1.57 and 4.2 K: Fig. 82, $\sigma_s = 0.581$ G cm^3/g	81 H 1
YPd_3:Gd				7	p_s in μ_B/Gd, $p_{Gd}(H/T)$ at 15 mK: Fig. 83	81 B 1
$Y_{0.93}Gd_{0.07}Pd_3$					$\sigma(H)$ at 1.57 and 4.2 K: Fig. 82, $\sigma_s = 6.625$ G cm^3/g	81 H 1
$Y_{0.95}Tb_{0.05}Pd_3$					$\sigma(H)$ at 1.6 and 4.2 K: Fig. 82, $\sigma_s = 6.103$ G cm^3/g	81 H 1
			Fig. 84		$\sigma(H, T)$: Fig. 85	80 L 1

continued

Table 1 (continued)

	Θ K	T_C K	T_N K	χ	p_s μ_B/R	p_{eff} μ_B/R	Remarks	Ref.
$Y_{0.958}Dy_{0.042}Pd_3$							$\sigma(H)$ at 1.55 and 4.2 K: Fig. 82, $\sigma_s = 5.432\,G\,cm^3/g$	81 H 1
$Y_{0.955}Ho_{0.045}Pd_3$							$\sigma(H)$ at 1.54 and 4.2 K: Fig. 82, $\sigma_s = 6.104\,G\,cm^3/g$	81 H 1
YPd_3:^{166}Er							$p_{Er}(H/T)$ at 15 and 27 mK: Fig. 86	81 B 1
$Y_{0.94}Er_{0.06}Pd_3$							$\sigma(H)$ at 1.55 and 4.2 K: Fig. 82, $\sigma_s = 7.302\,G\,cm^3/g$	81 H 1
$Y_{0.98}Tm_{0.02}Pd_3$							$\sigma(H)$ at 1.52 and 4.2 K: Fig. 82, $\sigma_s = 1.907\,G\,cm^3/g$	81 H 1
$Y_{0.954}Yb_{0.046}Pd_3$							$\sigma(H)$ at 1.54 and 4.2 K: Fig. 82, $\sigma_s = 2.486\,G\,cm^3/g$	81 H 1
$LaPd_3$							diamagnetic at room temperature, paramagnetic below 50 K	71 G 1
				-0.242			χ_g in $10^{-6}\,cm^3/g$ at 295 K	72 G 1
				Fig. 87				
$La_xCe_{1-x}Pd_3$				Fig. 80				81 G 1
$CeRh_3$				Fig. 88				84 M 1
$CeRh_{3-x}Pd_x$				Fig. 89				77 T 1, 78 P 1
				Fig. 80				81 G 1
				Fig. 90				81 M 1
$CePd_3$				2.76			χ_g in $10^{-6}\,cm^3/g$ at 295 K, Ce tetravalent suggested, Pauli paramagnet	72 G 1
				Fig. 91				
				Fig. 90				81 M 1
				Fig. 92				82 T 2
				Fig. 44				83 W 1
				1.2			χ_0 in $10^{-3}\,cm^3/mol$, at $T \to 0$ Ce in intermediate-valent state, temperature of χ_{max}: $T_M \simeq 140$ K no magnetic ordering observed	85 K 1
				Fig. 94			$p_{Ce}(H, T)$: Fig. 94, $p_{Ce}(H)$ at 4.2 and 20 K: Fig. 95	85 A 1

			Fig. 93		intrinsic increase of the high-field susceptibility at low temperature established: Fig. 93, $p_{Ce}(H, T)$: Fig. 96	86 V 1
$CePd_3$:Gd				7	p_s in μ_B/Gd, $p_{Gd}(H/T)$ at 12 and 15 mK: Fig. 83	81 B 1
$CePd_3$:^{166}Er					$p_{Er}(H/T)$ at 15 and 27 mK: Fig. 86	81 B 1
	0		Figs. 97, 98		susceptibility of $CePd_3$ with <2000 ppm of ^{166}Er shows Curie behaviour from 3 to 10 mK, natural Er contains 22.9 at% of ^{167}Er, the samples with ^{166}Er still contained 3.3 at% of ^{167}Er	80 M 1
$CePd_{3-x}Pt_x$			Fig. 99			82 R 1
x = 0					structure type $AuCu_3$	
= 0.5	−229.7			2.10	structure type $AuCu_3$	
= 1.0	−296.4			1.96	structure type $AuCu_3$	
= 2	−40.6			2.50	structure type C15	
= 2.5	−54.3			2.50	structure type C15	
= 3	−58.3			2.54	structure type C15	
$PrPd_3$	−7			3.4		71 H 2
	0	1.05	10.90	3.69	χ_g in 10^{-6} cm^3/g at 295 K	72 G 1
			Fig. 100			
					$p_{Pr}(H)$: Fig. 101	85 D 1
$NdPd_3$	1			3.4		71 H 2
	−5		10.91	3.50	χ_g in 10^{-6} cm^3/g	72 G 1
			Fig. 102			
					$p_{Nd}(H)$ at different temperatures: Fig. 103	86 D 1
$SmPd_3$			Fig. 104		no Curie-Weiss behaviour	72 G 1, 71 G 1
			1.94		χ_g in 10^{-6} cm^3/g	75 J 1
			Figs. 12, 7			
$EuPd_3$					Eu trivalent	68 W 1
			Fig. 105			71 G 1, 72 G 1
			Fig. 106		Eu trivalent, addition of Si induced valency fluctuation, see $EuPd_3Si_{0.2}$, and $EuPd_3Si_{0.25}$	83 D 1, 84 M 1

continued

Table 1 (continued)

	Θ K	T_C K	T_N K	χ	p_s μ_B/R	p_{eff} μ_B/R	Remarks	Ref.
$GdRh_3$	53					7.85		75 L 2
$GdPd_3$			7.5					71 G 1
	3					8.0		71 H 2
	1.5		7.5	56.7		8.03	χ_g in 10^{-6} cm^3/g at 295 K,	72 G 1
				Fig. 107			$p_{Gd}(H)$ at 1.5 and 4.2 K: Fig. 107	
$TbPd_3$			2					71 G 1
	3					9.3		71 H 2
	1		2.5	83.0		9.61	χ_g in 10^{-6} cm^3/g at 295 K	72 G 1
				Fig. 108				
							from heat capacity: orders magnetically at 3.75 K	79 M 1
$DyPd_3$	2					10.1		71 H 2
	0			96.7		10.51	χ_g in 10^{-6} cm^3/g at 295 K	72 G 1
				Fig. 109				
$HoPd_3$	4					9.3		71 H 2
	0			93.4		10.38	χ_g in 10^{-6} cm^3/g at 295 K	72 G 1
				Fig. 109				
$ErPd_3$	0					9.5		71 H 2
	0			76.1		9.40	χ_g in 10^{-6} cm^3/g at 295 K	72 G 1
				Fig. 109				
$TmPd_3$	−1					7.5		71 H 2
			0.20					72 G 1
$YbPd_3$						4.3		71 H 2
	0							72 G 1
$LuPd_3$				−0.128			χ_g in 10^{-6} cm^3/g at 295 K	72 G 1
				Fig. 87				
							diamagnetic at room temperature, paramagnetic below 50 K	71 G 1
RM_4								
$ScPd_4$				Fig. 78				72 G 1
YPd_4				Fig. 78				72 G 1

RM_5					
YRh_5		754		χ_m in 10^{-6} cm^3/mol, Pauli paramagnet, high-temperature phase	75 L 2
$SmPd_5$		1.70 Figs. 12, 7		χ_g in 10^{-6} cm^3/g	75 J 1
$GdRh_5$	38		7.95	high-temperature phase	75 L 2
RM_7					
$CePd_7$		1.5		χ_m in 10^{-4} cm^3/mol at 300 K, Ce nearly trivalent ($\simeq$3.1) suggested, $\chi_g = 0.17 \cdot 10^{-6}$ cm^3/g, no magnetic ordering observed	85 K 1
R_xM_{1-x}					
$Y_{0.015}Pd_{0.985}$		Fig. 110			73 G 1
Ce_xPd_{1-x}		Fig. 111			80 H 1
x = 0.011		Fig. 112			
x = 0.065		Fig. 113			
$Ce_{0.01}Pd_{0.99}$		Fig. 110			73 G 1
Pr_xPd_{1-x}				$\sigma(H)$ at 4.2 K: Fig. 114	73 G 1
Nd_xPd_{1-x}				$\sigma(H)$ at 4.2 K: Fig. 114	73 G 1
Sm_xPd_{1-x}				$\sigma(H)$ at 4.2 K: Fig. 114	73 G 1
$Eu_{0.013}Pd_{0.987}$		Fig. 110			73 G 1
$Gd_{0.01}Pd_{0.99}$		Fig. 115	7.9	p_{eff} in μ_B/Gd, $\sigma(H)$ at 4.2 K: Fig. 116	73 G 1
$Tb_{0.01}Pd_{0.99}$		Fig. 115	9.2	p_{eff} in μ_B/Tb	73 G 1
$Dy_{0.01}Pd_{0.99}$		Fig. 115	10.3	p_{eff} in μ_B/Dy, $\sigma(H)$ at 4.2 K: Fig. 116	73 G 1
$Ho_{0.01}Pd_{0.99}$		Fig. 115	10.1	p_{eff} in μ_B/Ho, $\sigma(H)$ at 4.2 K: Fig. 116	73 G 1
$Er_{0.01}Pd_{0.99}$		Fig. 117	9.3	p_{eff} in μ_B/Er, $\sigma(H)$ at 4.2 K: Fig. 116	73 G 1
$Tm_{0.015}Pd_{0.985}$		Fig. 117	7.2	p_{eff} in μ_B/Tm, $\sigma(H)$ at 4.2 K: Fig. 116	73 G 1
$Yb_{0.0085}Pd_{0.9915}$		Fig. 117	4.0	p_{eff} in μ_B/Yb, $\sigma(H)$ at 4.2 K: Fig. 114	73 G 1
Lu_xPd_{1-x}		Fig. 110		$\sigma(H)$ at 4.2 K: Fig. 114	73 G 1

Table 2. Rare earth compounds with 5d elements Os, Ir, Pt. p_s refers to 4.2 K and χ to RT, unless stated otherwise. R: rare earth element, M: 5d element.

	Θ K	T_C K	T_N K	χ	p_s μ_B/R	p_{eff} μ_B/R	Remarks	Ref.
R_7M_3								
La_7Ir_3				Fig. 118			Pauli paramagnet	73 O 1
La_7Pt_3				Fig. 119			Pauli paramagnet	73 O 1
				Fig. 120				80 G 2
Ce_7Ir_3	−32			Fig. 118		2.35	Ce valency suggested 3.18 and 3.15 from ionic radius and magnetic moment measurements, respectively	73 O 1
Ce_7Pt_3	33			Fig. 119		2.30	Ce valency 3.1 suggested	73 O 1
	−12	7		Fig. 121		2.71	no saturation achieved at 20 kOe, $\sigma(H, T)$: Fig. 122, ferrimagnetic or noncollinear moment arrangement suggested	80 G 2
Pr_7Ir_3	34			Fig. 118		3.46		73 O 1
Pr_7Pt_3	23			Fig. 119		3.53		73 O 1
	6	16		Fig. 123		3.61	$\sigma(H, T)$: Fig. 122, ferrimagnetic or noncollinear moment arrangement suggested	80 G 2
Nd_7Pt_3	55			Fig. 119		3.40		73 O 1
Gd_7Pt_3		>300			6.9		$\sigma(H, T)$: Fig. 124	80 G 2
R_2M								
Gd_2Pt		165		Fig. 125			$\sigma(H, T)$: Fig. 127	80 G 4
		155		Fig. 126	6.95		p_s at 150 kOe, $p_{Gd}(H)$ at 4.2 K: Fig. 128	83 C 1
Tb_2Pt	70			Figs. 129, 130		9.90	hysteresis: Fig. 132, a second phase transition observed at 50 K, which is smeared out at higher magnetic fields	80 G 4
		95						
	99	98		Fig. 131	7.3	9.56	p_s at 20 K and 150 kOe $p_{Tb}(H, T)$: Fig. 133, strong magnetocrystalline anisotropy	82 C 2
	99	98		Fig. 126	7.41	9.66	p_s at 150 kOe, $p_{Tb}(H)$ at 4.2 K: Fig. 128	83 C 1

Dy_2Pt	50	75		Figs. 129, 130		10.65	$\sigma(H, T)$: Fig. 134, a second phase transition at 45 K observed, which is smeared out at higher magnetic fields	80 G 4
	60	66		Fig. 126	7.25	10.28	p_s at 150 kOe, $p_{Dy}(H)$ at 4.2 K: Fig. 128	83 C 1
Ho_2Pt	10	40		Figs. 129, 130		10.58	a second phase transition at 8 K observed, which is smeared out at higher magnetic fields	80 G 4
	22	17		Fig. 126	8.23	10.58	p_s at 150 kOe, $p_{Ho}(H)$ at 4.2 K: Fig. 128	83 C 1
Er_2Pt	4	35		Figs. 129, 130		9.62	a second phase transition at 6 K observed, which is smeared out at higher magnetic fields	80 G 4
	5		9	Fig. 126	6.95	9.04	p_s at 150 kOe, $p_{Er}(H)$ at 4.2 K: Fig. 128	83 C 1
Tm_2Pt	0		5	Fig. 126	4.5	7.34	p_s at 2 K and 150 kOe, $p_{Tm}(H)$ at 2 K: Fig. 128	83 C 1
R_5M_3								
Gd_5Pt_3		176		Fig. 135	7.2		no Curie-Weiss behaviour, p_s at 20 kOe $\sigma_m(H)$ at 4.2 K: Fig. 136	83 G 3
Tb_5Pt_3	78			Fig. 137	5.4	9.72	$\sigma(H, T)$: Fig. 138, nonlinear magnetic structure suggested, ferromagnetic, strong anisotropy effects at low temperatures	83 G 3
Dy_5Pt_3	50			Fig. 139	4.5	10.56	p_s at 20 kOe, $\sigma_m(H)$ at 4.2 K: Fig. 140, nonlinear magnetic structure suggested, ferromagnetic, strong anisotropy effects at low temperatures	83 G 3
Ho_5Pt_3	28			Fig. 141		10.25	$\sigma_m(H)$ at 4.2 and 36.8 K: Fig. 142, spontaneous magnetization in high field far below the saturation, nonlinear magnetic structure suggested, ferromagnetic, strong anisotropy effects at low temperatures	83 G 3

continued

Table 2 (continued)

	Θ K	T_C K	T_N K	χ	p_s μ_B/R	p_{eff} μ_B/R	Remarks	Ref.
RM								
CePt		5.81					T_C from specific heat Fig. 143	81 H 2
		5.8			0.73		T_C from temperature dependence of the electrical resistivity: Fig. 145, p_s at 1.5 K, $p_{Ce}(H, T)$: Fig. 144	83 G 2
PrPt	5	15		Fig. 146	1.02	3.46	T_C from ac susceptibility, CEF effects observed, $p_{Pr}(H)$ at 4.2 K: Fig. 147, from neutron diffraction: magnetic structure collinear with magnetic moments parallel to c axis, $p_{Pr} = 2.2(2)\,\mu_B$	82 C 1
		13.4					T_C from electrical resistivity: Figs. 148 and 149	86 G 1
NdPt	8	23		Fig. 146	1.44	3.68	T_C from ac susceptibility, $p_{Nd}(H)$ at 4.2 K: Fig. 147, from neutron diffraction: magnetic structure collinear with magnetic moments in the (a, c) plane, $p_{Nd} = 2.34(20)\,\mu_B$, angle between Nd moments and a axis 22(5)°; CEF effects observed	82 C 1
		22.5					T_C from electrical resistivity: Figs. 148 and 149	86 G 1
GdPt	66	66		Fig. 150	6.7	8.29	$\sigma_s(T)$: Fig. 150, $p_{Gd}(H)$ at 4.2 K: Fig. 151	80 C 1
		67.7					T_C from electrical resistivity Figs. 148 and 152	86 G 1
TbPt	44	56			8.1	9.71	$p_{Tb}(H)$: Fig. 151, p_{Tb} from neutron diffraction, magnetic space group Pn′m′a	80 C 1
		58.7					T_C from electrical resistivity: Figs. 148 and 152	86 G 1

DyPt	25	23			7.1	10.45	$p_{Dy}(H)$ at 4.2 K: Fig. 151, p_{Dy} from neutron diffraction, magnetic space group Pn′m′a	80 C 1
		22.2					T_C from electrical resistivity: Figs. 148 and 152	86 G 1
HoPt	15	16			8.2	10.24	$p_{Ho}(H)$ at 4.2 K: Fig. 151, p_{Ho} from neutron diffraction, magnetic space group Pnm′a′	80 C 1
		18.2					T_C from electrical resistivity: Figs. 148 and 152	86 G 1
ErPt	14	16			8.1	9.13	$p_{Er}(H)$ at 4.2 K: Fig. 151, p_{Er} from neutron diffraction, magnetic space group Pnm′a′	80 C 1
		18.4					T_C from electrical resistivity: Figs. 148 and 152	86 G 1
TmPt	2	6			7.0	7.36	$p_{Tm}(H)$ at 4.2 K: Fig. 151, p_{Tm} from neutron diffraction, magnetic space group Pnm′a′	80 C 1
YbPt	0					4.0		77 K 1
R_3M_4								
Nd_3Pt_4	9			Figs. 153, 154		3.9	$\sigma_m(H)$ at 4.2 K: Fig. 156, Θ and de Gennes factor: Fig. 155	79 G 1
Gd_3Pt_4	27			Figs. 153, 154		8.13	$\sigma_m(H)$ at 4.2 K: Fig. 156, Θ and de Gennes factor: Fig. 155	79 G 1
	26		23	Fig. 30		8.14	$\sigma(H)$ at 4.2 K: Fig. 32	80 G 1
Tb_3Pt_4	16			Figs. 153, 154		8.87	specimen contained a second phase, $\sigma_m(H)$ at 4.2 K: Fig. 156, Θ and de Gennes factor: Fig. 155	79 G 1
Dy_3Pt_4	9			Figs. 153, 154		10.5	$\sigma_m(H)$ at 4.2 K: Fig. 156, Θ and de Gennes factor: Fig. 155	79 G 1
Ho_3Pt_4	3			Figs. 153, 154		10.3	$\sigma_m(H)$ at 4.2 K: Fig. 156, Θ and de Gennes factor: Fig. 155	79 G 1

continued

Table 2 (continued)

	Θ K	T_C K	T_N K	χ	p_s μ_B/R	p_{eff} μ_B/R	Remarks	Ref.
Er_3Pt_4	−5			Figs. 153, 154		9.3	$\sigma_m(H)$ at 4.2 K: Fig. 156, Θ and de Gennes factor: Fig. 155	79 G 1
Tm_3Pt_4	−1			Figs. 153, 154		7.77	$\sigma_m(H)$ at 4.2 K: Fig. 156, Θ and de Gennes factor: Fig. 155	79 G 1
RM_2								
YIr_2				13.5			χ_m in 10^{-6} cm^3/mol	80 B 1
YPt_2				6.47			χ_m in 10^{-6} cm^3/mol	80 B 1
$LaOs_2$				Fig. 36				83 W 1
$La_{1-x}Ce_xOs_2$				Fig. 157				86 S 1
$LaIr_2$				60			χ_m at RT in 10^{-6} cm^3/mol	64 S 1
				Fig. 36				83 W 1
$LaPt_2$				−29			χ_m at RT in 10^{-6} cm^3/mol	64 S 1
				−32			χ_m in 10^{-6} cm^3/mol	82 B 1
				Fig. 36				83 W 1
$La_xGd_{1-x}Pt_2$								77 D 1
x = 0	31	30			6.98	8.40		
= 0.1	27	28			7.04	8.35		
= 0.2	24	26			6.88	7.86		
= 0.3	22	23			6.94	7.88		
$CeOs_2$					Fig. 70			59 B 1
				Fig. 44				83 W 1
$CeIr_2$					Fig. 70			59 B 1
				Fig. 43			Ce tetravalent suggested	70 V 1
				Fig. 44				83 W 1
$CePt_2$		7		Fig. 43		2.50	Ce trivalent suggested	70 V 1
	5		1.6			2.33	heat capacity gives T_N = 1.7 K: Fig. 158	72 J 1
	−78			Fig. 159		2.49		80 O 1
				22.9			χ_m at 300 K in 10^{-4} cm^3/mol	82 B 1
				Fig. 44				83 W 1

$PrOs_2$		Fig. 69		Fig. 70			59 B 1
$PrIr_2$		Fig. 69		Fig. 70			59 B 1
		11.2					80 G 3
	−4	11.2			3.72		80 V 1
				2.5		from neutron diffraction: p_{Pr},	82 F 1
				Fig. 71		simple ferromagnetic ordering suggested	
		11.2		2.08		$p_{Pr}(H)$ at 4.2 K: Fig. 72, $p_{Pr}(H)$ at 77 K: Fig. 73, strong CEF effects	83 G 1
$PrPt_2$		6		1.67			64 C 1, 80 B 1
	0	13.5	Fig. 160	1.60	3.45	$\sigma_m(H)$ at 4.2 and 300 K: Fig. 161	67 W 1
		7.7				$p_{Pr}(H)$ at 4.2 K: Fig. 162	80 G 3
	−6	7.7			3.70		80 V 1
				0.9		from neutron diffraction: p_{Pr}, simple ferromagnetic ordering suggested	82 F 1
		7.7		1.52		$p_{Pr}(H)$ at 4.2 K: Fig. 72, $p_{Pr}(H)$ at 77 K: Fig. 73, strong CEF effects	83 G 1
$NdOs_2$		Fig. 69		Fig. 70			59 B 1
$NdIr_2$		Fig. 69		Fig. 70		$\sigma_m(T,H)$: Fig. 163	59 B 1
$NdPt_2$		4		1.60			64 C 1, 80 B 1
	0	10		2.11	3.60		67 W 1
$SmOs_2$		Fig. 69		Fig. 70			59 B 1
$SmIr_2$		Fig. 69		Fig. 70			59 B 1
$SmPt_2$		6		0.19		strong CEF effect influence on p_s	73 B 1
$EuIr_2$		Fig. 69		Fig. 70			59 B 1
$EuPt_2$	105				7.9	Eu divalent	68 W 1
$GdOs_2$		Fig. 69		Fig. 70			59 B 1
$GdIr_2$		Fig. 69		Fig. 70			59 B 1
		84		6.8			79 C 1
	84	82.5		6.6	7.8		80 S 1

continued

Table 2 (continued)

	Θ K	T_C K	T_N K	χ	p_s μ_B/R	p_{eff} μ_B/R	Remarks	Ref.
$GdPt_2$		36			6.77			64 C 1, 80 B 1
	32	46.5		Fig. 160	6.28	8.10	$\sigma_m(H)$ at 4.2 and 300 K: Fig. 164	67 W 1
		37			6.77			73 B 1
	31	30			6.98	8.40	$\sigma(H)$ at 4.2 K: Fig. 165	77 D 1
$GdPt_x$		Fig. 166					T_C from electrical resistivity measurements for $2<x<3.5$	76 T 1
$TbOs_2$		Fig. 69			Fig. 70			59 B 1
$TbIr_2$		Fig. 69			Fig. 70		$\sigma_m(T,H)$: Fig. 163	59 B 1
		46			7.48		from neutron diffraction	63 F 1
$TbPt_2$		16			6.67			64 C 1, 80 B 1
	17	26			7.08	9.61		67 W 1
$DyOs_2$		Fig. 69			Fig. 70			59 B 1
$DyIr_2$		Fig. 69			Fig. 70			59 B 1
$DyPt_2$		14			7.34			64 C 1, 80 B 1
	7	25			6.40	10.58		67 W 1
$HoOs_2$		Fig. 69			Fig. 70			59 B 1
$HoIr_2$		Fig. 69			Fig. 70			59 B 1
		13			7.2		from neutron diffraction	63 F 1
$HoPt_2$		9			7.65			64 C 1, 80 B 1
	2	19		Fig. 160	8.88	10.60	$\sigma_m(H)$ at 4.2 and 300 K: Fig. 167	67 W 1
$ErOs_2$		Fig. 69			Fig. 70			59 B 1
$ErIr_2$		Fig. 69			Fig. 70			59 B 1
$ErPt_2$		3			7.26			64 C 1
	1	15			7.48	9.50		67 W 1
$TmIr_2$		Fig. 69			Fig. 70			59 B 1
	−4		0.4	Fig. 168		7.57	at low temperatures $\Theta=1.4$ K: Fig. 168	85 W 1

$YbIr_2$		Fig. 69			Fig. 70			59 B 1
	−4			Fig. 169		4.49		85 W 1
RM_3								
$LaPt_3$				376			χ_m at 80 K in 10^{-6} cm^3/mol	77 G 1
				298			χ_m at 300 K in 10^{-6} cm^3/mol feebly paramagnetic, Knight shift temperature-independent suggests that the d-band of Pt is full	
$CePt_3$	−108					2.92		77 G 1
	−58.3			Fig. 99		2.54		82 R 1
$PrPt_3$	−22					3.84		77 G 1
$TbPt_3$			20.5		8.4		from neutron diffraction	70 N 1
$DyPt_3$			13.2		9.0		from neutron diffraction: Dy magnetic moments are aligned in opposite directions in adjacent (111) magnetic planes	69 A 1
RM_5								
$CePt_5$						2.52	Ce trivalent	70 V 1
				Fig. 170				79 L 1
$PrPt_5$	−20				0.4		p_s at 19 kOe	80 I 1
$NdPt_5$	−7			Fig. 171	1.0	4.0	p_s at 19 kOe, $\sigma(H)$ at 4.2 K: Fig. 172	80 I 1
$GdPt_5$	13.5			Fig. 173	6.3	8.1	p_s at 19 kOe, $\sigma(H)$ at 4.2 K: Fig. 172, weak ferromagnet suggested	80 I 1
$TbPt_5$	5.5	≈8		Fig. 174	4.7	9.9	p_s at 19 kOe, $\sigma(H)$ at 4.2 K: Fig. 172	80 I 1
$DyPt_5$	2			Fig. 175	5.0	10.6	p_s at 19 kOe, $\sigma(H)$ at 4.2 K: Fig. 172	80 I 1
$HoPt_5$	2			Fig. 174	4.9	10.5	p_s at 19 kOe, $\sigma(H)$ at 4.2 K: Fig. 172	80 I 1
$ErPt_5$					4.3		p_s at 19 kOe, no paramagnetic behaviour, no ordering observed	80 I 1
$TmPt_5$	−14			Fig. 175	2.2	7.7	p_s at 19 kOe, $\sigma(H)$ at 4.2 K: Fig. 172	80 I 1

continued

Table 2 (continued)

	Θ K	T_C K	T_N K	χ	p_s μ_B/R	p_{eff} μ_B/R	Remarks	Ref.
R_xM_{1-x}								
Gd_xIr_{1-x}							solubility of Gd in Ir about 600 ppm, T_C and $\Theta \simeq 40$ K for all $x < 0.086$, T_C in the eutectics at $\simeq 32$ K, $\sigma(H, T)$ Fig. 176, $p_{Gd}(x)$: Fig. 177	80 S 1
x = 0.33	84	8.25			6.6	7.8		
= 0.22	58	72			6.4	7.4		
= 0.086	40				7.2	8.3		
= 0.010	40				6.9	8.1		

2.5.3 Figures

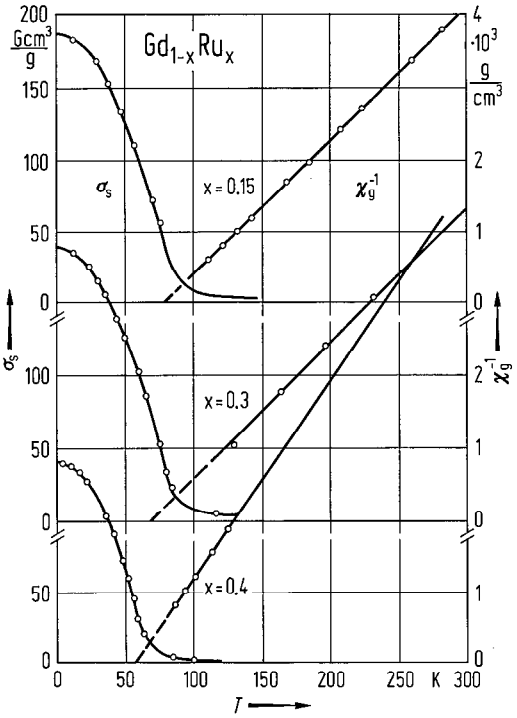

Fig. 1. $Gd_{1-x}Ru_x$. Temperature dependence of σ_s and χ_g^{-1} [80 A 1].

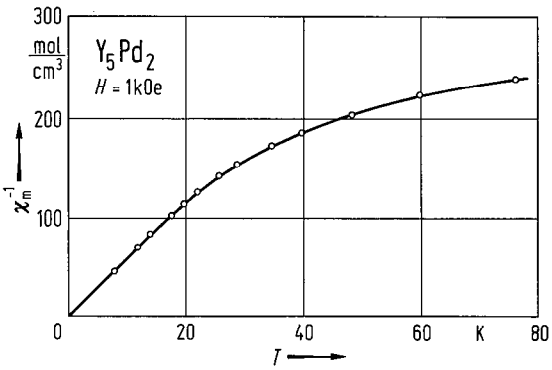

Fig. 2. Y_5Pd_2. Temperature dependence of χ_m^{-1} at 1 kOe [77 Y 1].

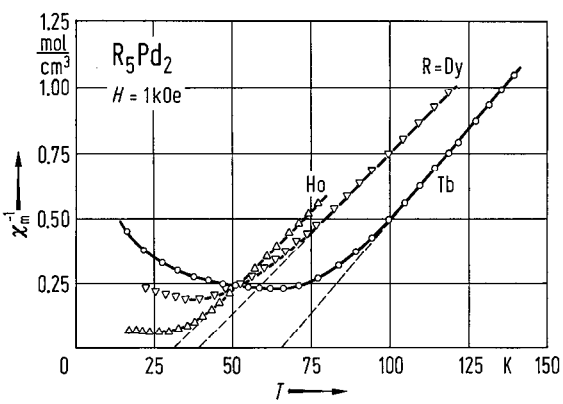

Fig. 3 R_5Pd_2, R = Tb, Dy, Ho. Temperature dependence of χ_m^{-1} at 1 kOe [77 Y 1].

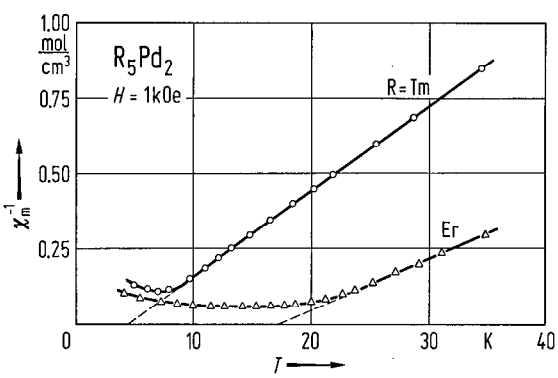

Fig. 4. R_5Pd_2, R = Er, Tm. Temperature dependence of χ_m^{-1} at 1 kOe [77 Y 1].

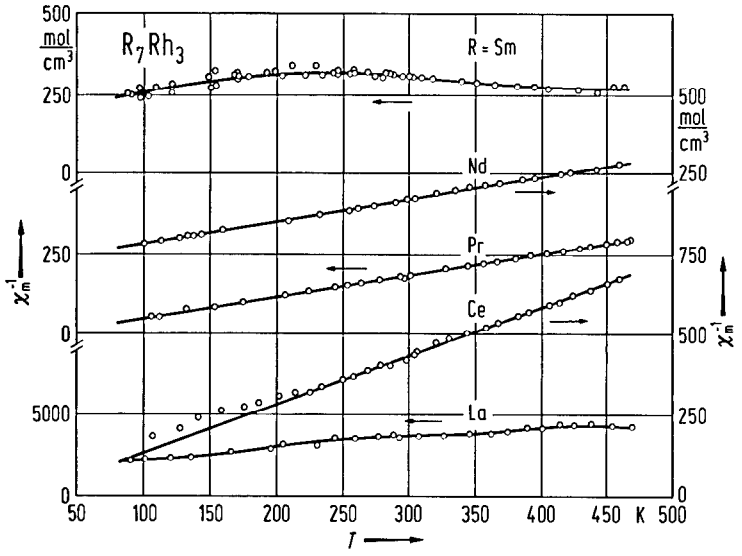

Fig. 5. R_7Rh_3, R = La, Ce, Pr, Nd, Sm. Temperature dependence of χ_m^{-1} [73 O 1].

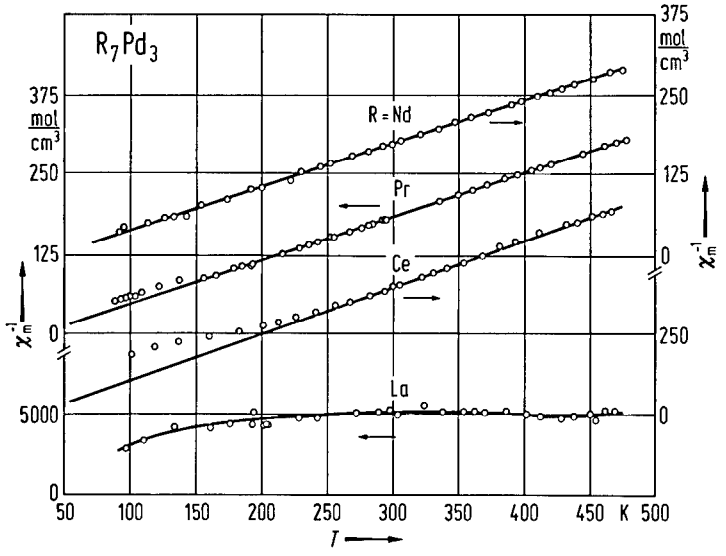

Fig. 6. R_7Pd_3, R = La, Ce, Pr, Nd. Temperature dependence of χ_m^{-1} [73 O 1].

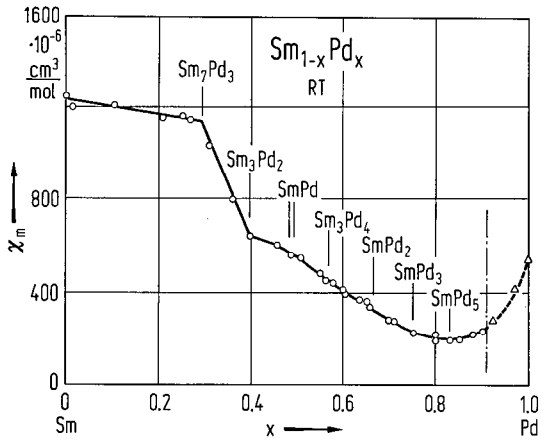

Fig. 7. $Sm_{1-x}Pd_x$. Room-temperature values of the molar susceptibilities vs. Pd atomic concentration [75 J 1]. The vertical line indicates the limit of solubility of Sm in Pd; triangles: data of [68 H 1].

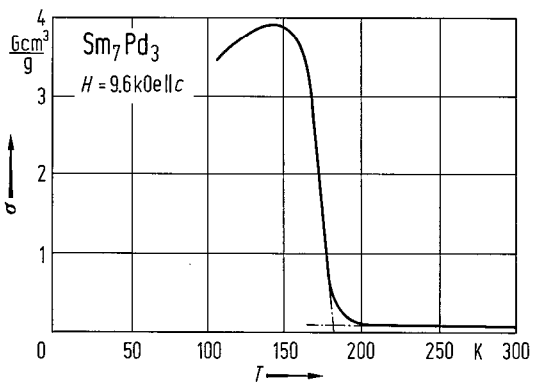

Fig. 8. Sm_7Pd_3. Interpolated temperature dependence of σ at 9.6 kOe along the preferred direction (hexagonal c axis) [75 J 1].

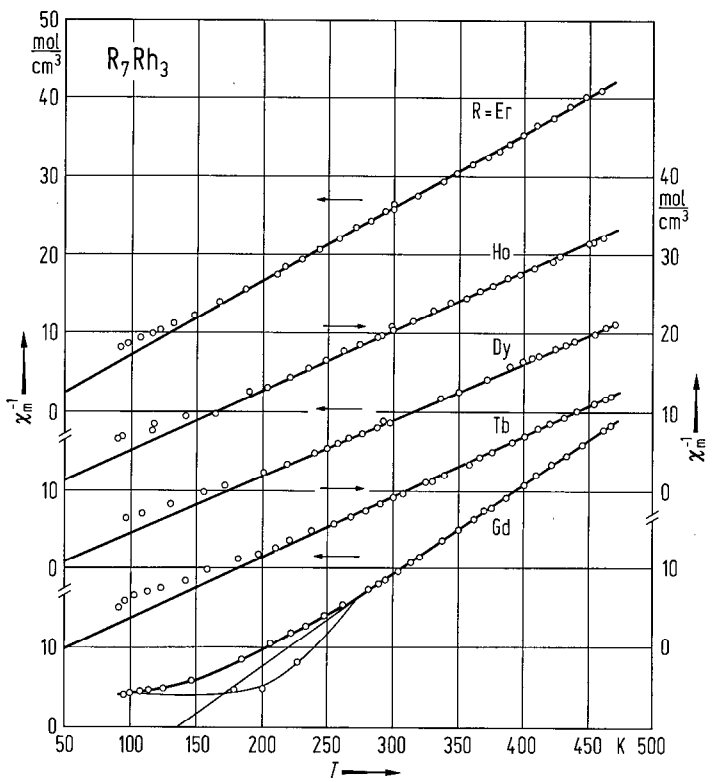

Fig. 9. R_7Rh_3, R = Gd, Tb, Dy, Ho, Er. Temperature dependence of χ_m^{-1} [73 O 1].

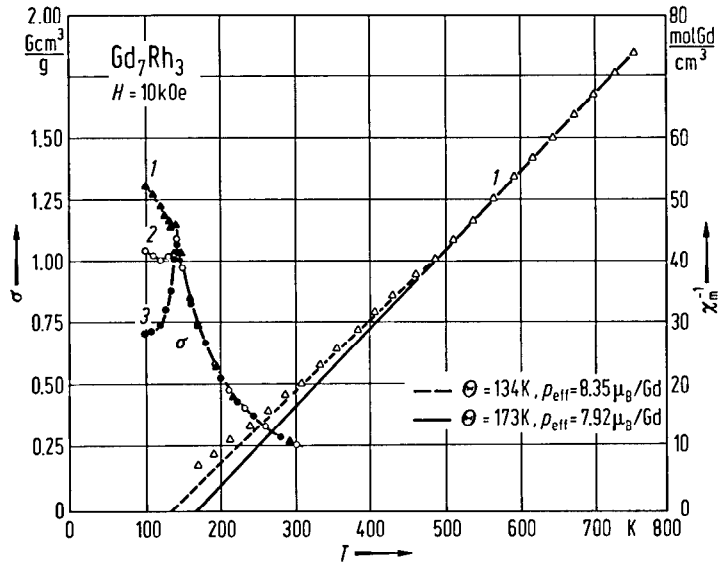

Fig. 10. Gd_7Rh_3. Temperature dependence of χ_m^{-1} (per mole of Gd) and σ at 10 kOe for (*1*) powder sample, (*2*) bulk sample, "free orientation" (easy magnetization direction in field direction), (*3*) bulk sample, easy direction approximately perpendicular to magnetic field [75 L 1].

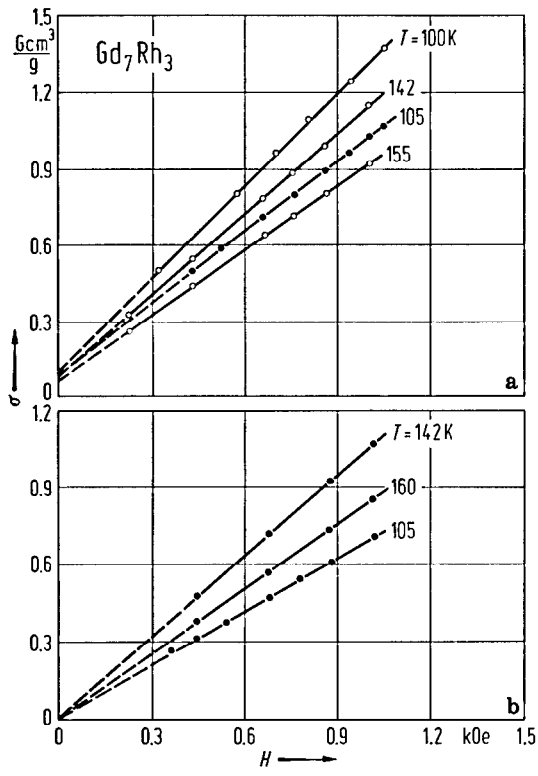

Fig. 11. Gd_7Rh_3. Magnetic field dependence of σ at different temperatures (a) for powder sample (open circles) and bulk sample (solid circles) with easy direction approximately in the magnetic field direction, and (b) for bulk sample with easy direction approximately perpendicular to the magnetic field [75 L 1].

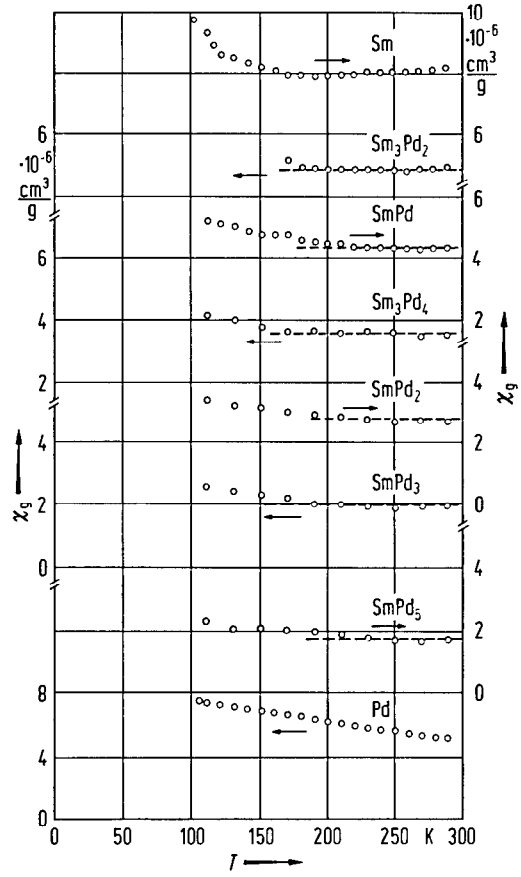

Fig. 12. Sm–Pd compounds. Temperature dependence of χ_g [75 J 1]. The broken lines indicate a Pauli-type paramagnetic behaviour.

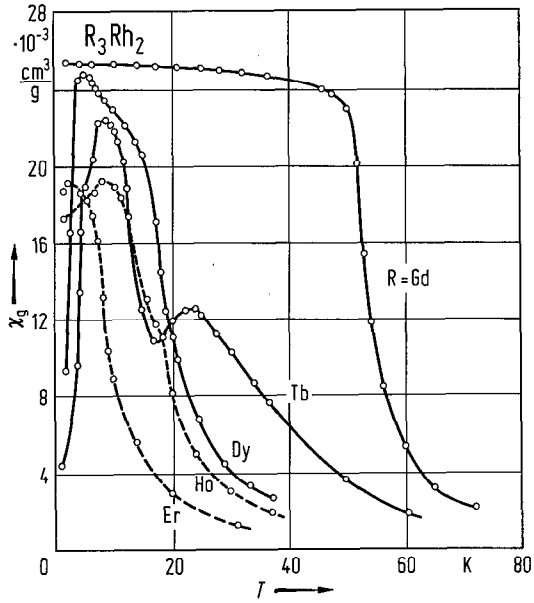

Fig. 13. R_3Rh_2, R = Gd, Tb, Dy, Ho, Er. Temperature dependence of χ_g (samples cooled in zero magnetic field) [84 G 1].

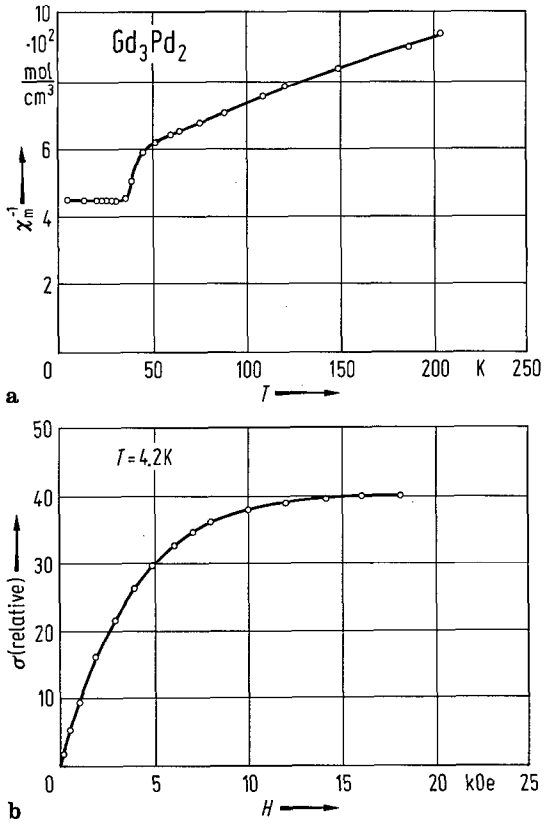

Fig. 15. Gd_3Pd_2. (a) Temperature dependence of χ_m^{-1} and (b) magnetic field dependence of σ (in arbitrary units) at 4.2 K [80 Y 1].

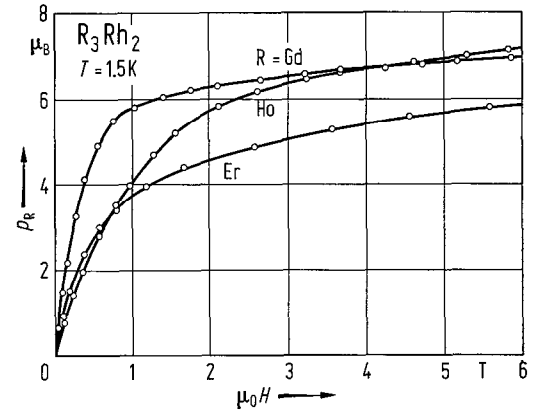

Fig. 14. R_3Rh_2, R = Gd, Ho, Er. Magnetic field dependence of p_R at 1.5 K [84 G 1].

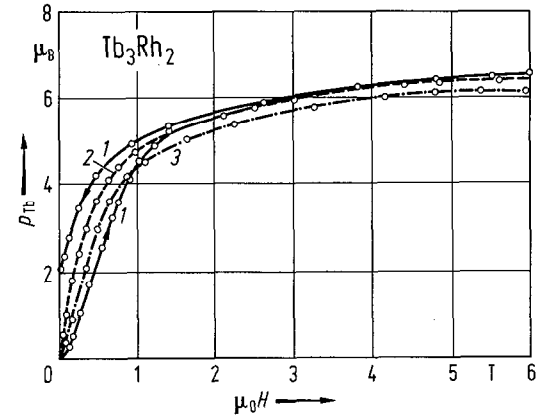

Fig. 16. Tb_3Rh_2. Magnetic field dependence of p_{Tb} at 1.5 K (*1*), 8 K (*2*), and 17 K (*3*) [84 G 1].

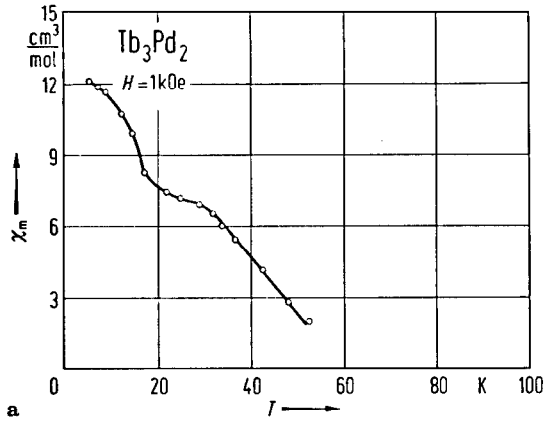

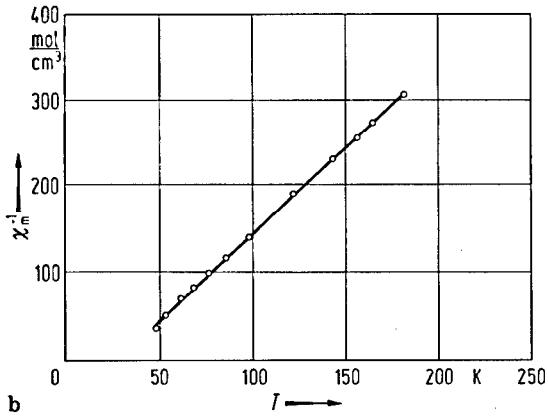

Fig. 17. Tb_3Pd_2. Temperature dependence of (a) χ_m and (b) χ_m^{-1} at 1 kOe [80 Y 1].

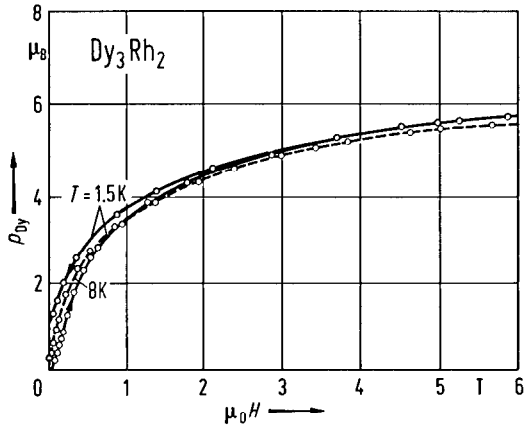

Fig. 18. Dy_3Rh_2. Magnetic field dependence of p_{Dy} at 1.5 K and 8 K [84 G 1].

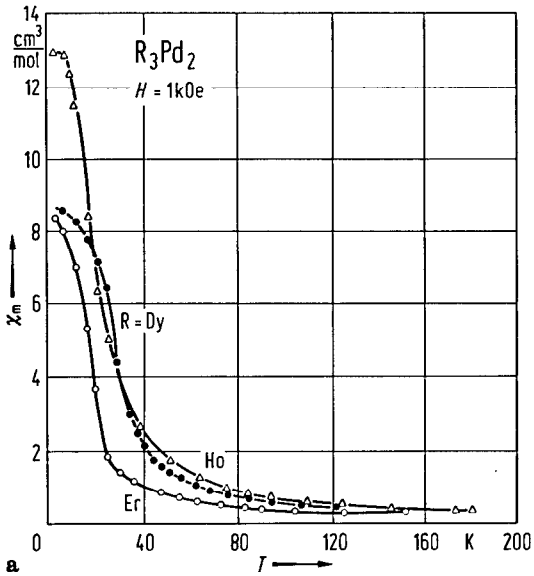

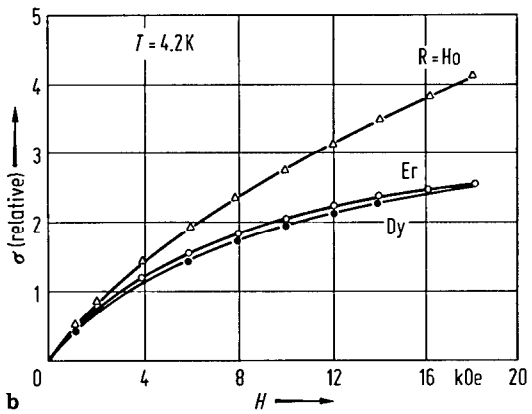

Fig. 19. R_3Pd_2, R = Dy, Ho, Er. (a) Temperature dependence of χ_m at 1 kOe and (b) magnetic field dependence of σ (in arbitrary units) at 4.2 K [80 Y 1].

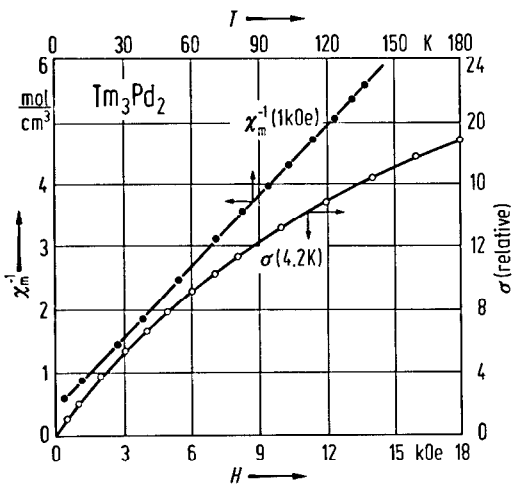

Fig. 20. Tm_3Pd_2. Temperature dependence of χ_m^{-1} at 1 kOe and magnetic field dependence of σ (in arbitrary units) at 4.2 K [80 Y 1].

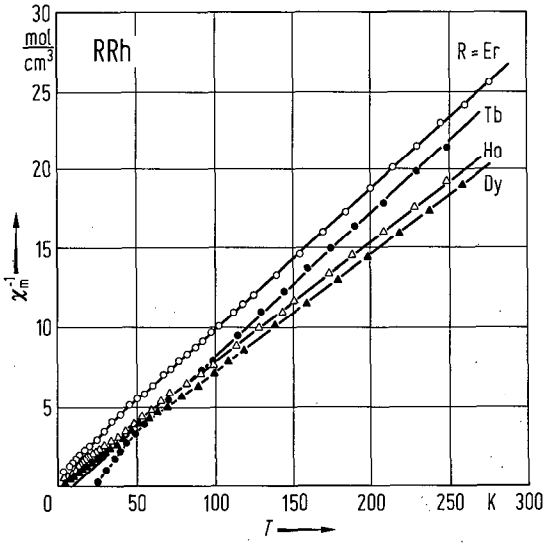

Fig. 21. RRh, R = Tb, Dy, Ho, Er. Temperature dependence of χ_m^{-1} [72 C 1].

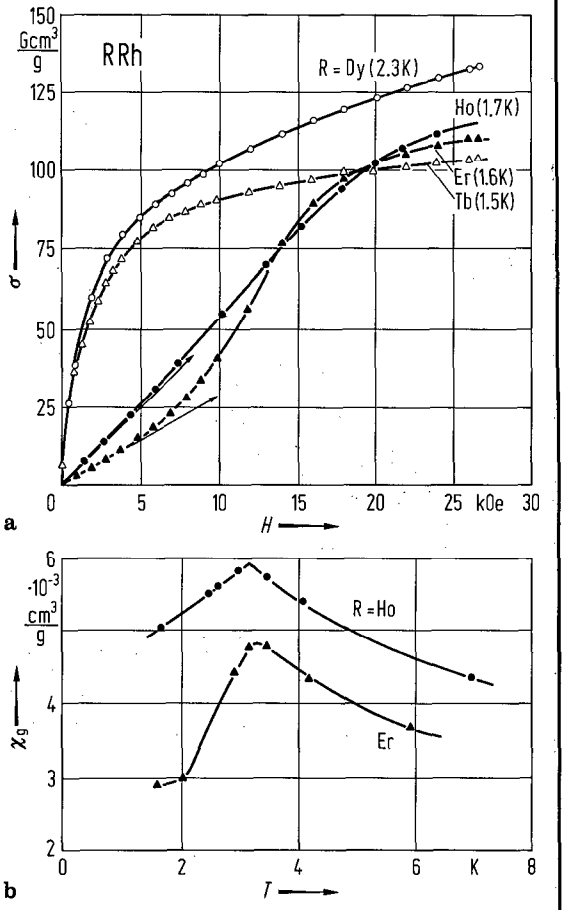

Fig. 22. RRh, R = Tb, Dy, Ho, Er. (a) Magnetic field dependence of σ and (b) temperature dependence of χ_g for HoRh and ErRh [72 C 1].

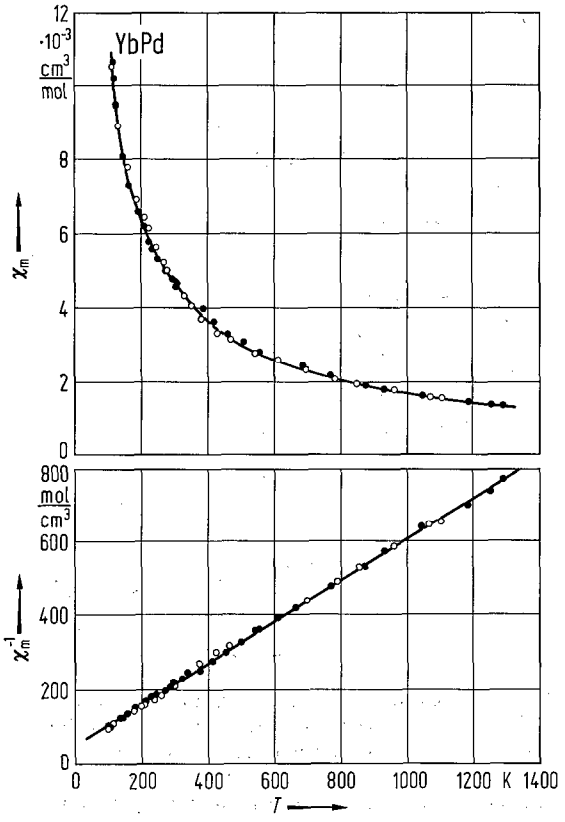

Fig. 23. YbPd. Temperature dependence of (a) χ_m and (b) χ_m^{-1}. Open and full circles indicate data for two samples of different preparation [80 I 2].

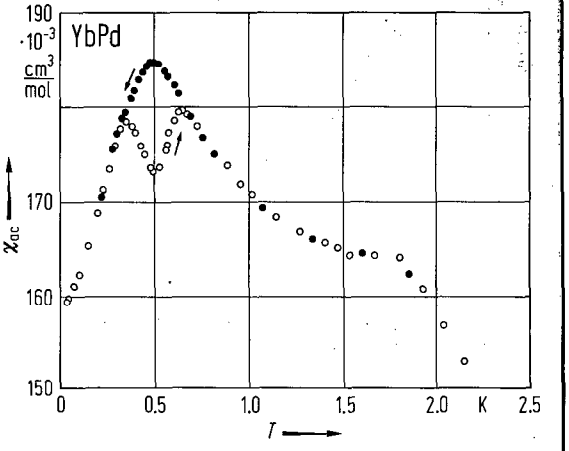

Fig. 24. YbPd. Temperature dependence of the ac susceptibility χ_{ac} at 0.172 mT [85 P 1].

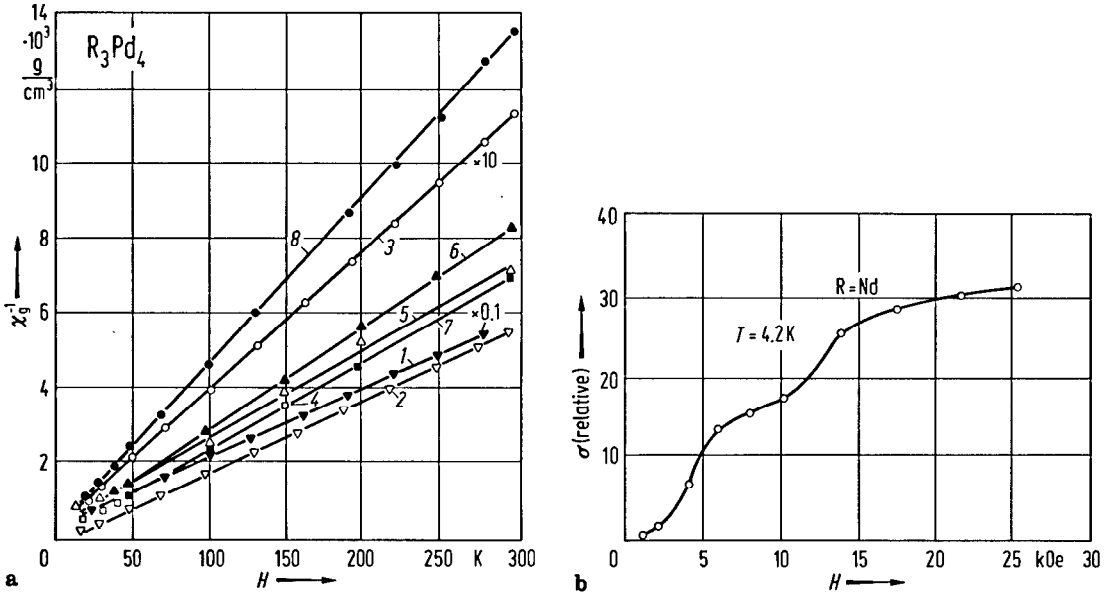

Fig. 25. R_3Pd_4, R = Pr (*1*), Nd (*2*), Gd (*3*), Tb (*4*), Ho (*5*), Er (*6*), Dy (*7*), Tm (*8*). (a) Temperature dependence of χ_g^{-1} and (b) magnetic field dependence of σ at 4.2 K (in arbitrary units) for Nd_3Pd_4 [77 Y 2].

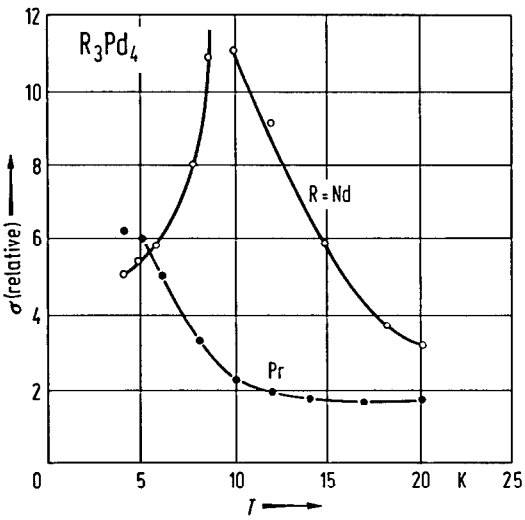

Fig. 26. R_3Pd_4, R = Pr, Nd. Temperature dependence of σ (in arbitrary units) [77 Y 2].

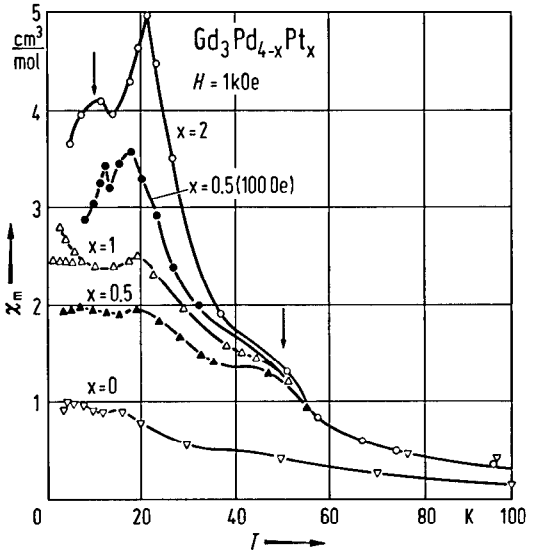

Fig. 27. $Gd_3Pd_{4-x}Pt_x$. Temperature dependence of χ_m at 1 kOe for $x \leqq 2$. The branches for the sample with x = 1 show the temperature dependence of χ_m after being cooled in 1 and 2 kOe, respectively. Arrows indicate a low-temperature maximum and an anomaly in $\chi_m(T)$ [80 G 1].

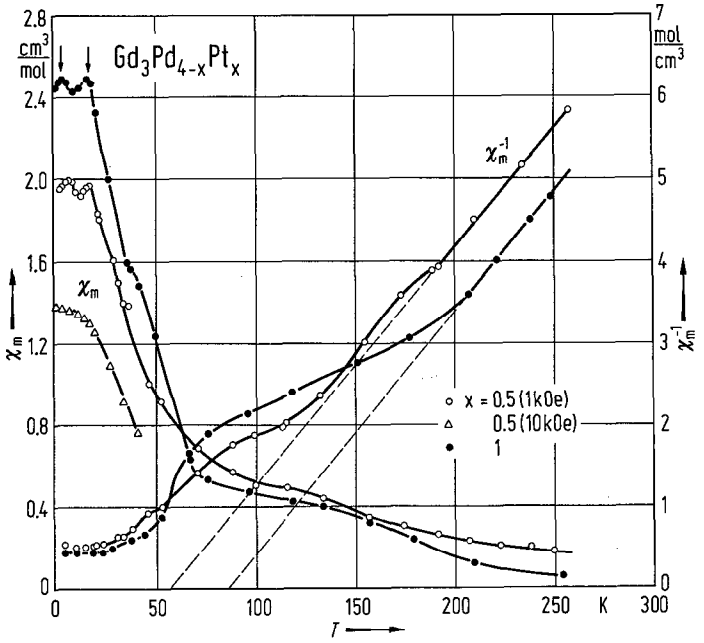

Fig. 28. $Gd_3Pd_{4-x}Pt_x$. Temperature dependence of χ_m and χ_m^{-1} for $x = 0.5$ at (open circles) 1 kOe and (triangles) 10 kOe, and $x = 1$. Arrows indicate low-temperature maxima [80 G 1].

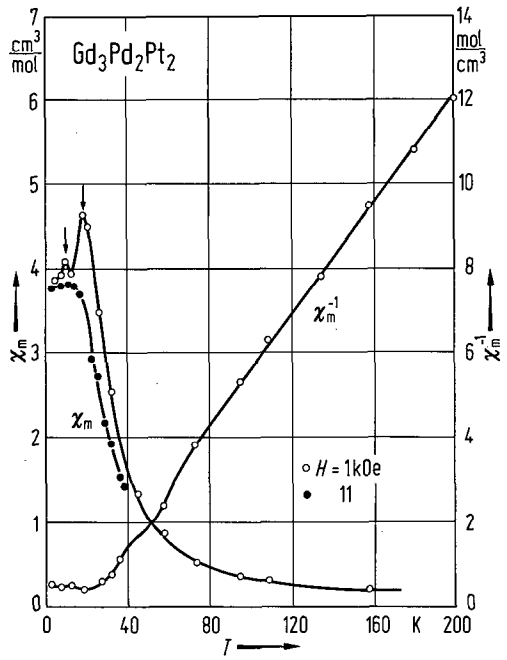

Fig. 29. $Gd_3Pd_2Pt_2$. Temperature dependence of χ_m and χ_m^{-1} at 1 and 11 kOe. Arrows indicate low-temperature maxima [80 G 1].

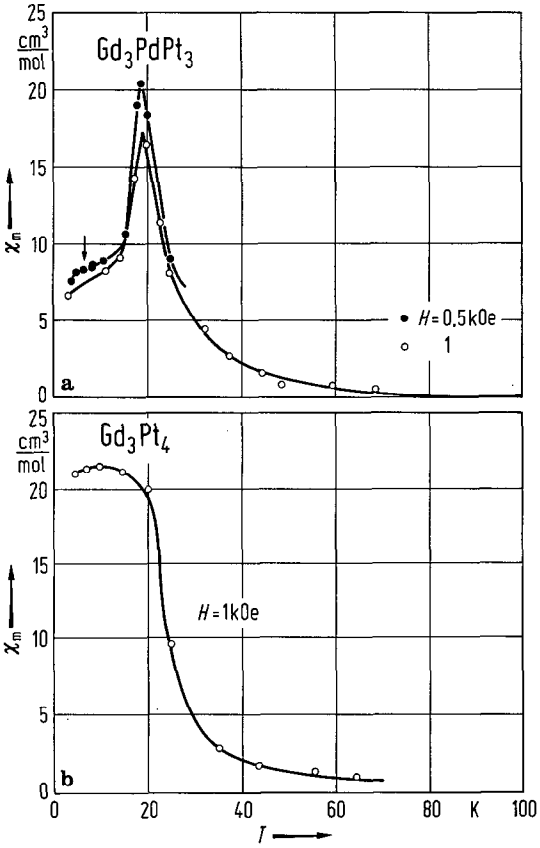

Fig. 30. Gd_3PdPt_3, Gd_3Pt_4. Temperature dependence of χ_m for (a) Gd_3PdPt_3 at 0.5 and 1 kOe and (b) Gd_3Pt_4 at 1 kOe. The arrow indicates a structure in $\chi_m(T)$ [80 G 1].

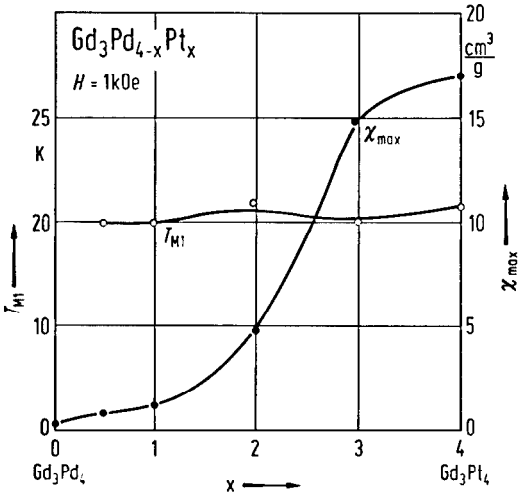

Fig. 31. $Gd_3Pd_{4-x}Pt_x$. Composition dependence of T_{M1} (onset of long-range order) and the maximum susceptibility at 1 kOe [80 G 1].

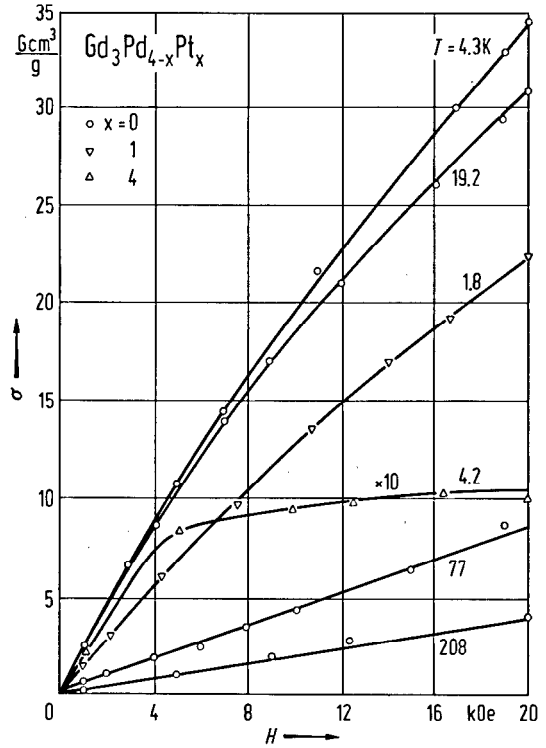

Fig. 32. $Gd_3Pd_{4-x}Pt_x$, x = 0, 1, 4. Magnetic field dependence of σ at different temperatures. The curves for x = 0.5 and 1 are identical [80 G 1].

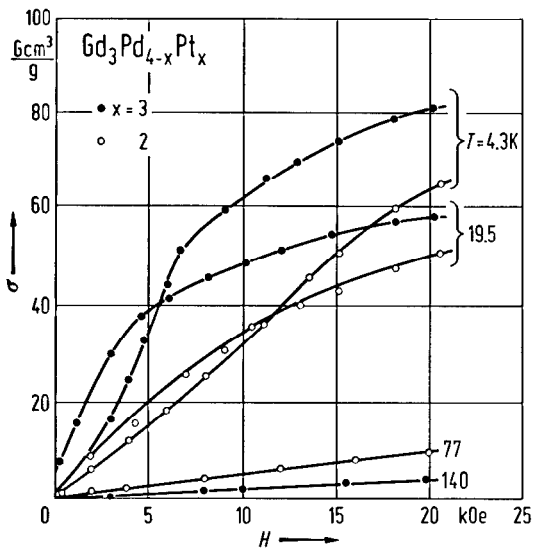

Fig. 33. $Gd_3Pd_{4-x}Pt_x$, x = 2, 3. Magnetic field dependence of σ at different temperatures [80 G 1].

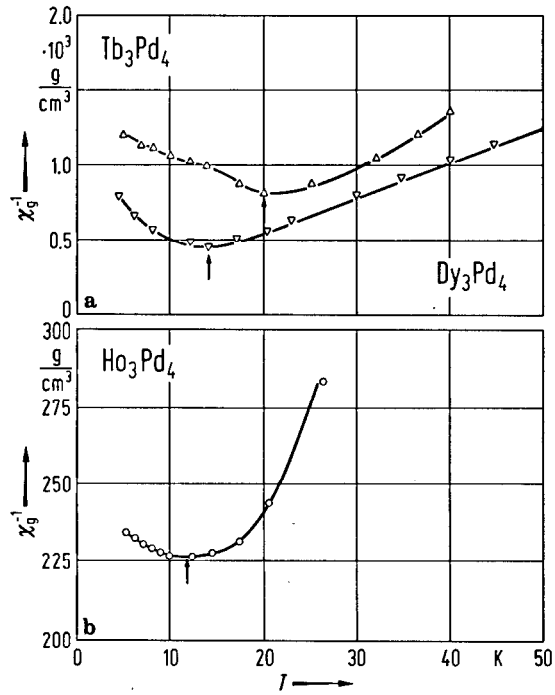

Fig. 34. R_3Pd_4, R = Tb, Dy, Ho. Temperature dependence of χ_g^{-1} for (a) R = Tb, Dy and (b) R = Ho. The arrows indicate T_N [77 Y 2].

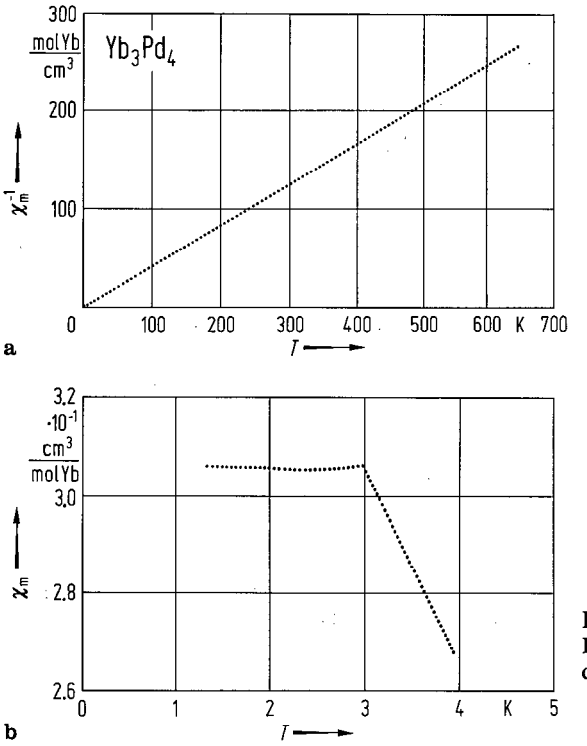

Fig. 35. Yb_3Pd_4. Temperature dependence of (a) χ_m^{-1} and (b) χ_m between 1.3 and 3 K [85 P 2].

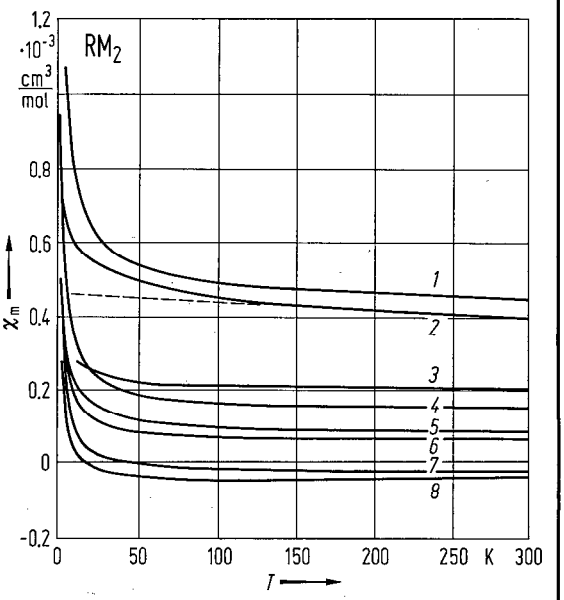

Fig. 36. YRu_2 (*1*), $LaRu_2$ (*2*), $LaOs_2$ (*3*), LaRuRh (*4*), $LaIr_2$ (*5*), $LaRh_2$ (*6*), $LaPt_2$ (*7*), YPd_3 (*8*). Temperature dependence of χ_m [83 W 1].

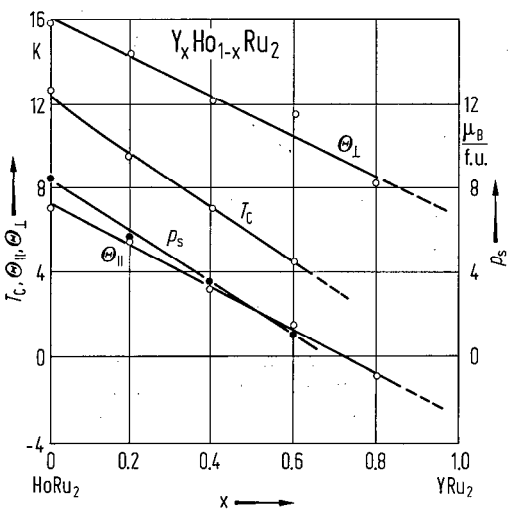

Fig. 37. $Y_xHo_{1-x}Ru_2$. Spontaneous magnetization p_s, Curie temperature T_C, paramagnetic Curie temperatures Θ, parallel, $\Theta_{\parallel}$, and perpendicular, $\Theta_{\perp}$, to the *c* axis, respectively, vs. Y concentration x [85 O 1].

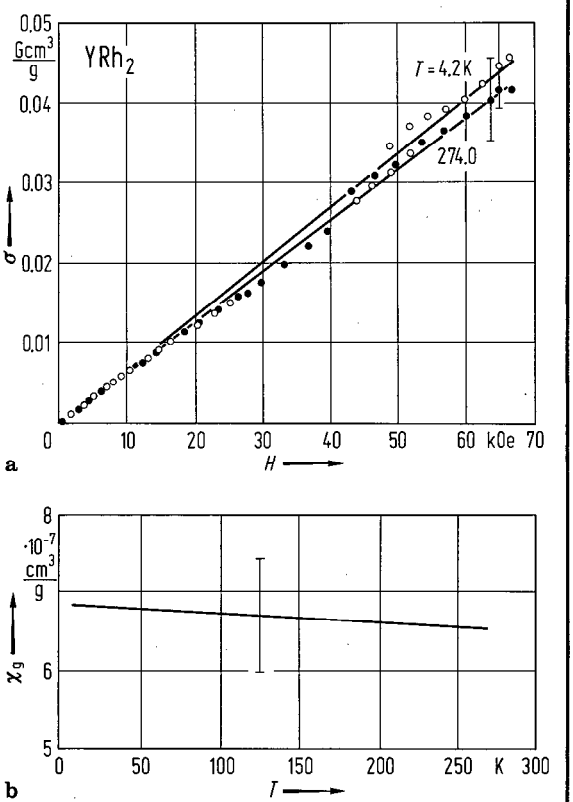

Fig. 38. YRh_2. (a) Magnetic field dependence of σ and (b) temperature dependence of χ_g [83 H 1].

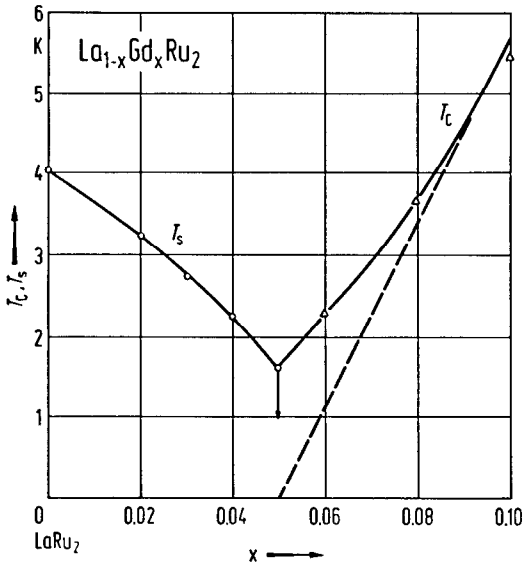

Fig. 39. $La_{1-x}Gd_xRu_2$. Composition dependence of T_C and the superconducting transition temperature T_s. The straight line in the upper part of the T_C curve is fitted to some further points at higher x which have been omitted for scaling reasons. The circle with arrow means that there is no superconductivity down to this temperature [72 H 1].

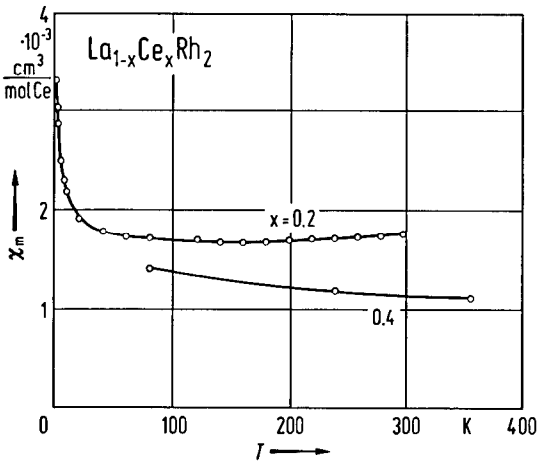

Fig. 40. $La_{1-x}Ce_xRh_2$. Temperature dependence of χ_m for x = 0.2 and 0.4 [84 H 1].

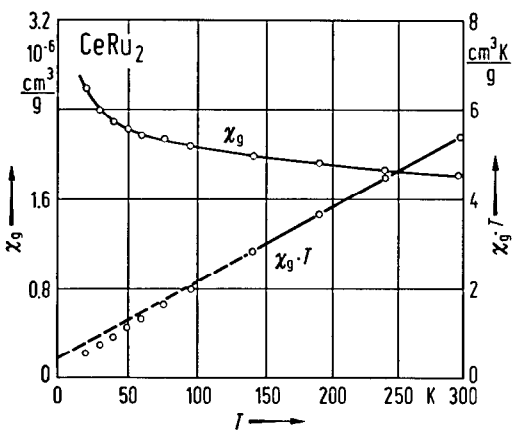

Fig. 41. $CeRu_2$. Temperature dependence of χ_g and $\chi_g T$ [71 H 3].

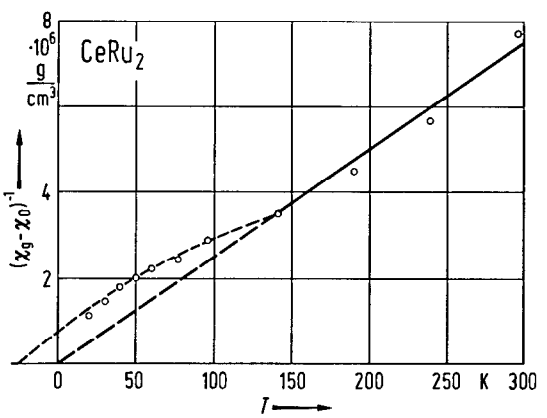

Fig. 42. $CeRu_2$. Temperature dependence of $(\chi_g - \chi_0)^{-1}$. χ_0 is the temperature-independent magnetic susceptibility, $\chi_0 = 1.70 \cdot 10^{-6}$ cm³/g [71 H 3].

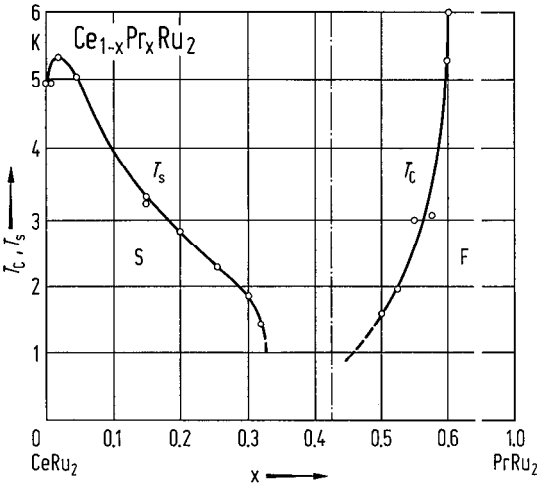

Fig. 45. $Ce_{1-x}Pr_xRu_2$. Composition dependence of T_C and superconducting transition temperature T_s [58 M 1].

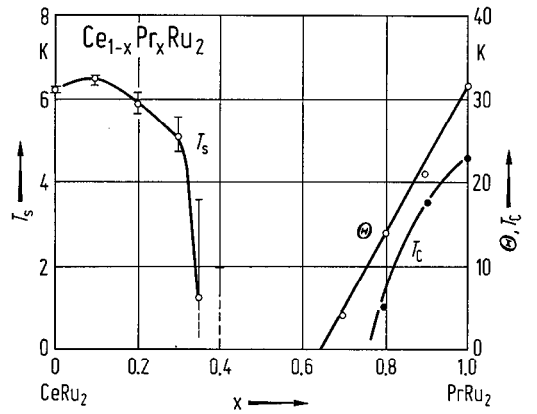

Fig. 47. $Ce_{1-x}Pr_xRu_2$. Composition dependence of T_C, Θ and the superconducting transition temperature T_s [76 A 1].

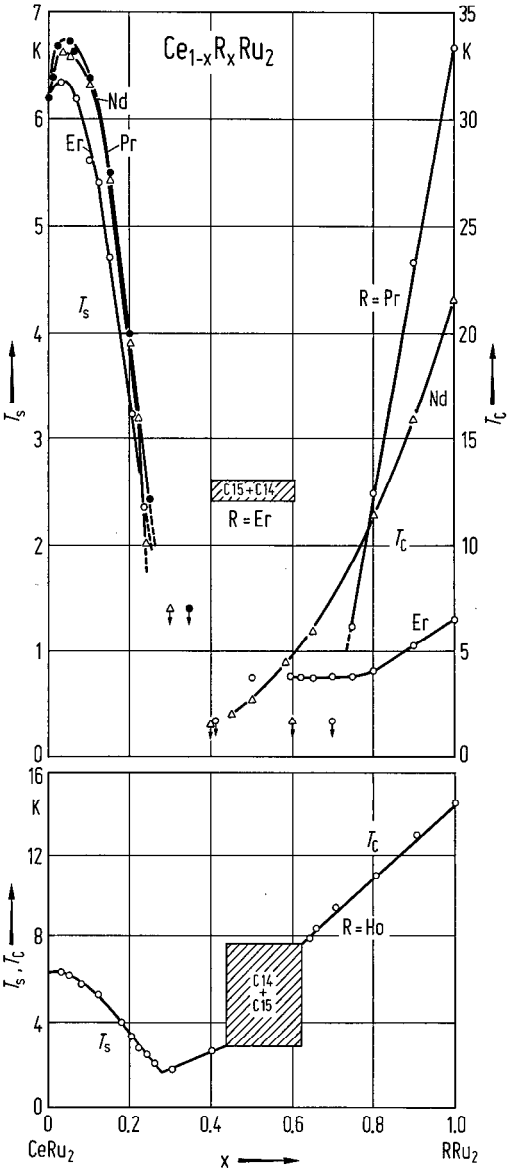

Fig. 46. $Ce_{1-x}R_xRu_2$, R = Pr, Nd, Ho, Er. Composition dependence of the magnetic spin ordering temperature T_C and superconducting transition temperature T_s. T_C is given by a maximum of the ac susceptibility. The shaded areas indicate two-phase regions of C15 and C14 structure types. (a) R = Pr, Nd, Er and (b) R = Ho [71 W 1].

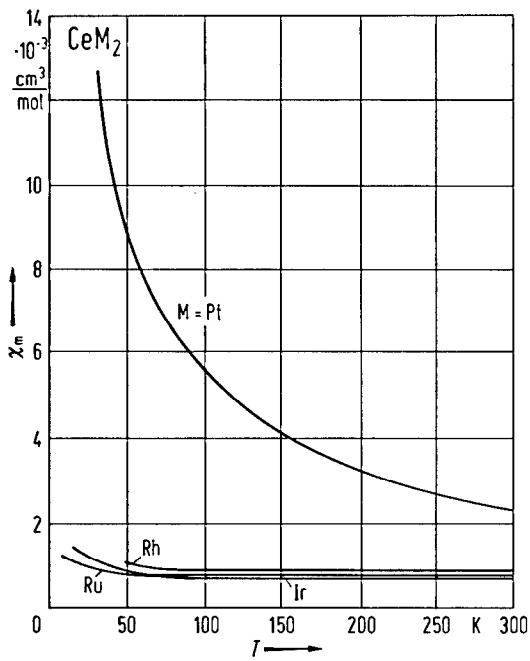

Fig. 43. CeM_2, M = Ru, Rh, Ir, Pt. Temperature dependence of χ_m [70 V 1].

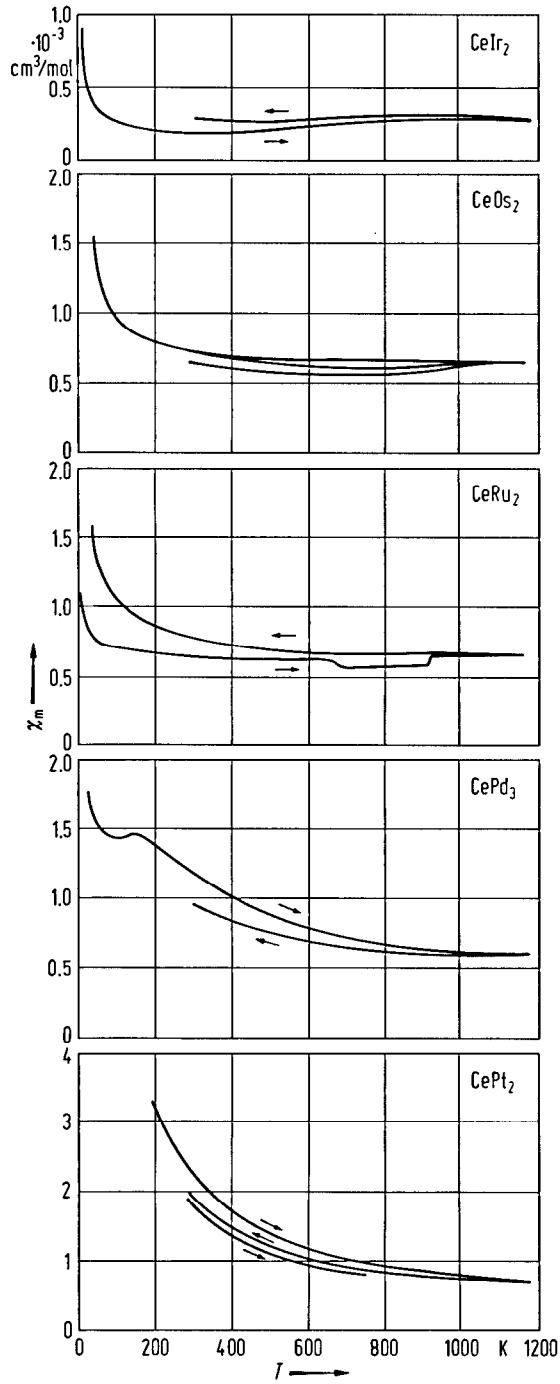

Fig. 44. $CeIr_2$, $CeOs_2$, $CeRu_2$, $CePd_3$, $CePt_2$. Temperature dependence of χ_m. First a low-temperature measurement was made, the following heating and cooling is indicated by arrows [83 W 1].

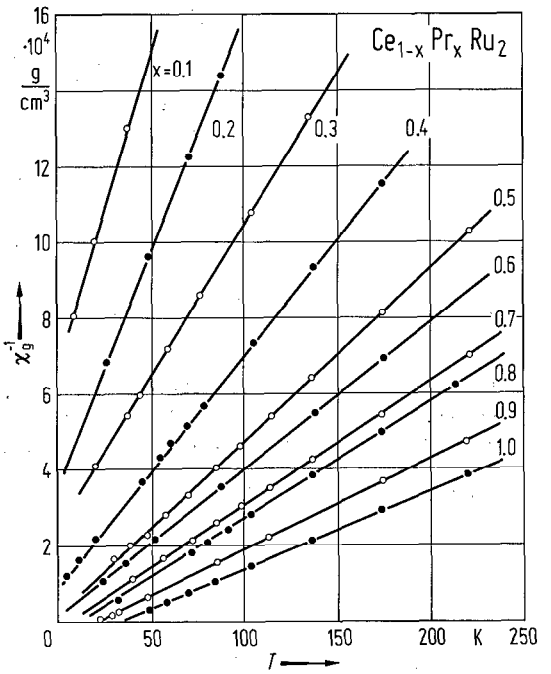

Fig. 48. $Ce_{1-x}Pr_xRu_2$. Temperature dependence of χ_g^{-1} for different x [76 A 1].

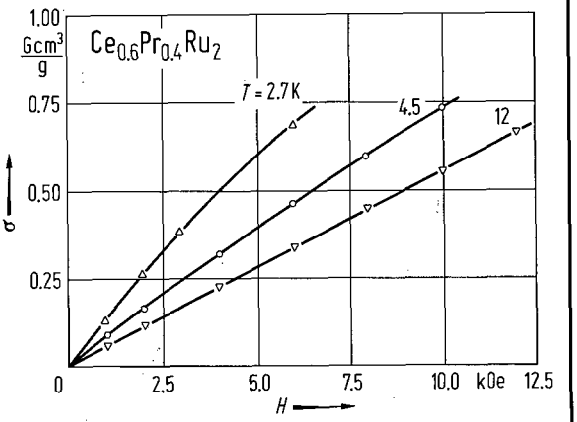

Fig. 49. $Ce_{0.6}Pr_{0.4}Ru_2$. Magnetic field dependence of σ at 2.7, 4.5 and 12 K [76 A 1].

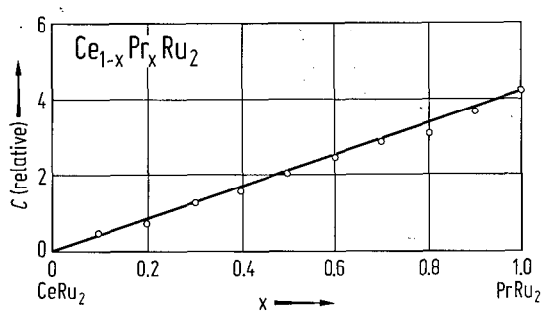

Fig. 50. $Ce_{1-x}Pr_xRu_2$. Composition dependence of the Curie constant C (in arbitrary units) [76 A 1].

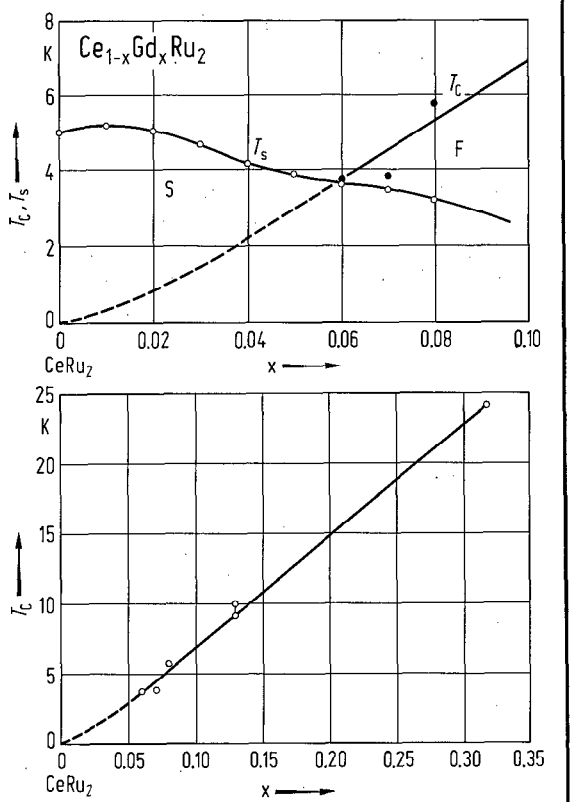

Fig. 51. $Ce_{1-x}Gd_xRu_2$. Composition dependence of T_C and superconducting transition temperature T_s [58 M 1].

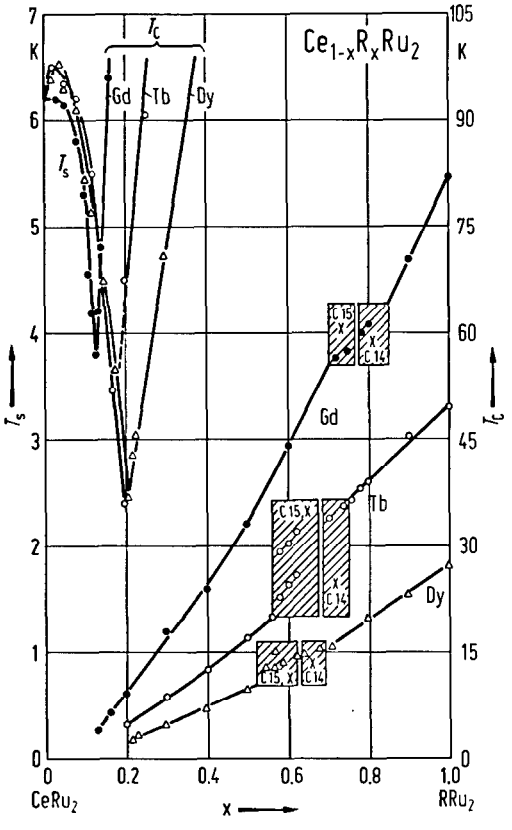

Fig. 52. $Ce_{1-x}R_xRu_2$, R = Gd, Tb, Dy. Composition dependence of T_C and T_s. The shaded areas indicate two-phase regions of C15 and C14 structure types and an unidentified phase X. See also Fig. 46 [71 W 1].

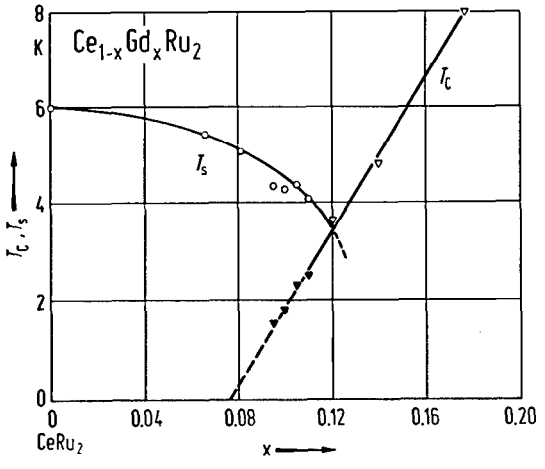

Fig. 54. $Ce_{1-x}Gd_xRu_2$. Composition dependence of T_C and the superconducting transition temperature T_s determined from magnetic susceptibility measurement. Solid triangles correspond to the temperature at which a small dip in the susceptibility appears [78 K 1].

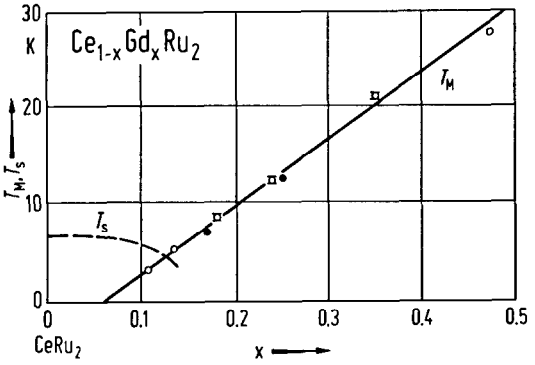

Fig. 53. $Ce_{1-x}Gd_xRu_2$. Composition dependence of the magnetic transition temperature T_M from (open circles) Mössbauer experiment and (solid circles) magnetic susceptibility maximum, and superconducting transition temperatures T_s [77 R 1, 77 D 2].

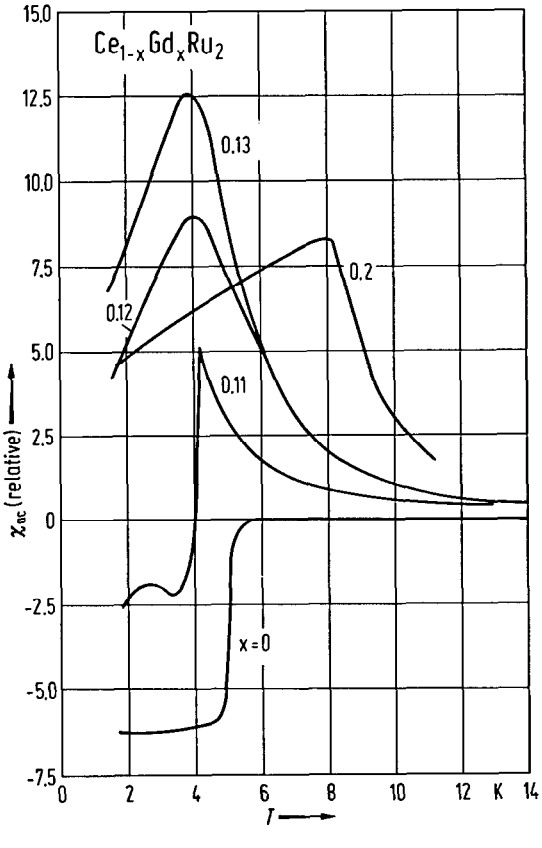

Fig. 55. $Ce_{1-x}Gd_xRu_2$. Temperature dependence of the ac susceptibility χ_{ac} (in arbitrary units) for different x [85 K 2].

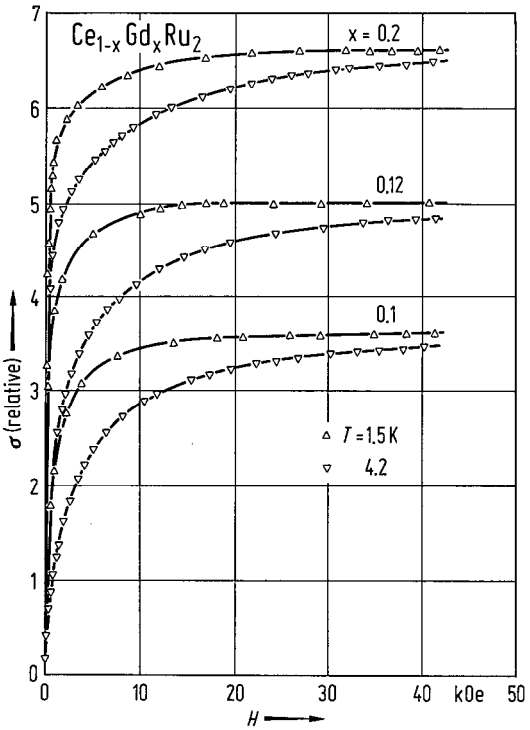

Fig. 56. $Ce_{1-x}Gd_xRu_2$. Magnetic field dependence of σ (in arbitrary units) at 1.5 and 4.2 K for different x [85 K 2].

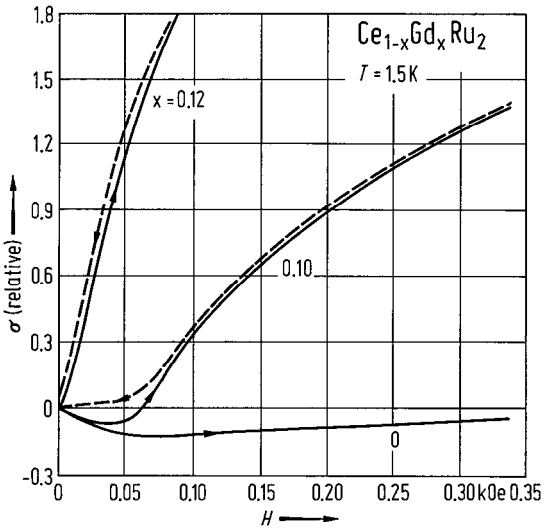

Fig. 57. $Ce_{1-x}Gd_xRu_2$. Low-field magnetization vs. H. The solid and dashed curves correspond to the virgin increasing and decreasing field-sweeps, respectively [85 K 2].

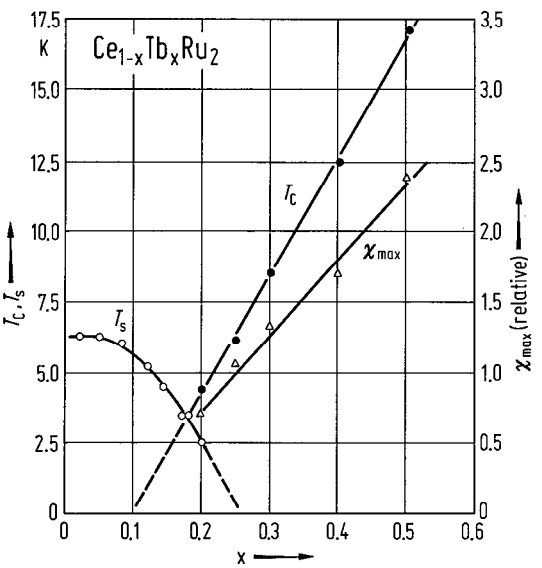

Fig. 58. $Ce_{1-x}Tb_xRu_2$. Composition dependence of T_C, susceptibility maximum χ_{max} (in arbitrary units) and superconducting transition temperature T_s [70 H 1].

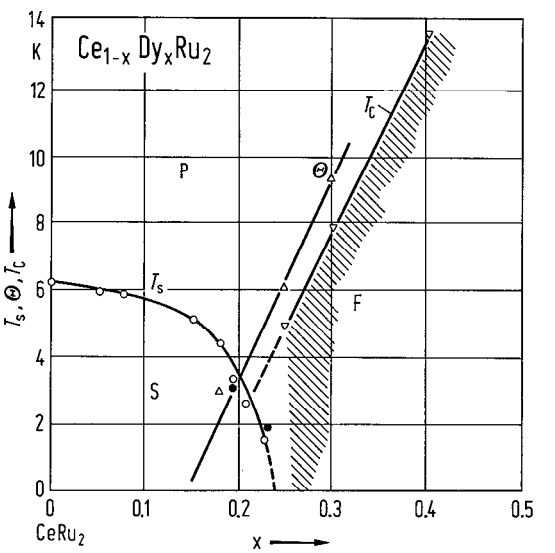

Fig. 59. $Ce_{1-x}Dy_xRu_2$. Composition dependence of Θ, T_C and the superconducting transition temperature T_s [78 A 1].

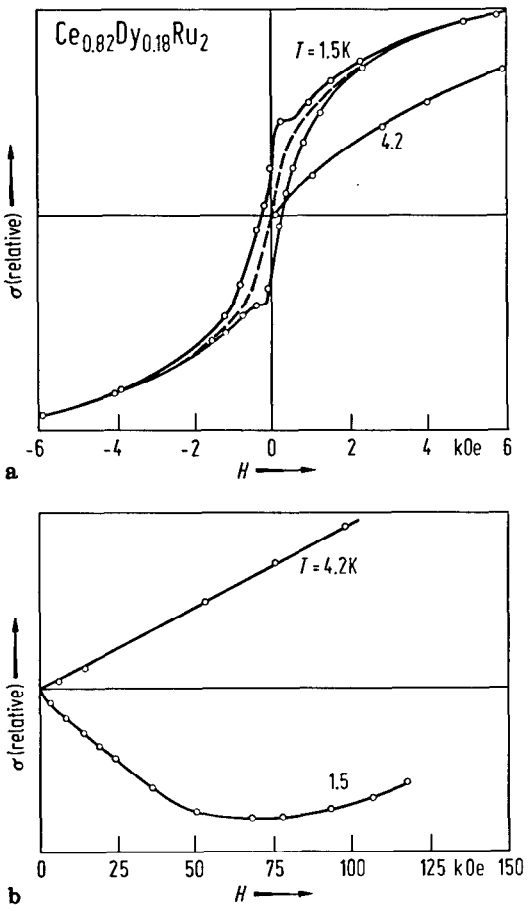

Fig. 60. $Ce_{0.82}Dy_{0.18}Ru_2$. (a) Hysteresis loops (in arbitrary units) and (b) initial magnetization curves [78 A 1].

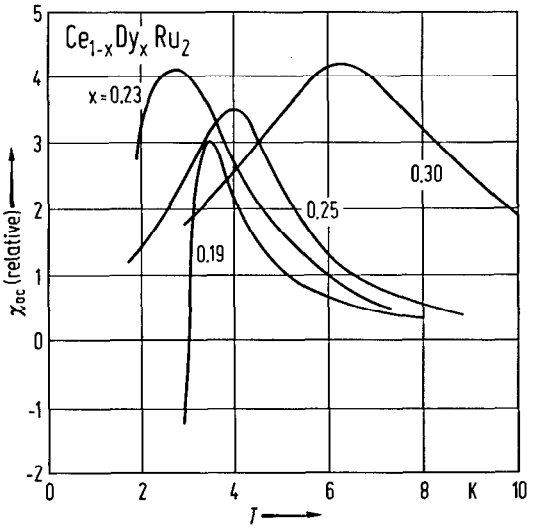

Fig. 61. $Ce_{1-x}Dy_xRu_2$. Temperature dependence of the ac susceptibility (in arbitrary units) for different x [79 A 1].

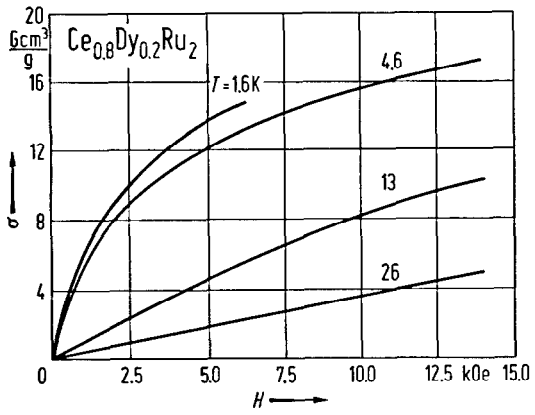

Fig. 62. $Ce_{0.8}Dy_{0.2}Ru_2$. Magnetic field dependence of σ at 1.6, 4.6, 13 and 26 K [79 A 1].

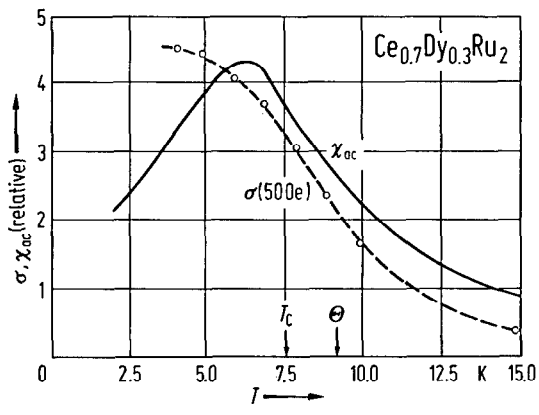

Fig. 63. $Ce_{0.7}Dy_{0.3}Ru_2$. Temperature dependence of the ac susceptibility χ_{ac} and σ at 50 Oe (in arbitrary units), Θ and T_C are the paramagnetic and ferromagnetic Curie temperatures [79 A 1].

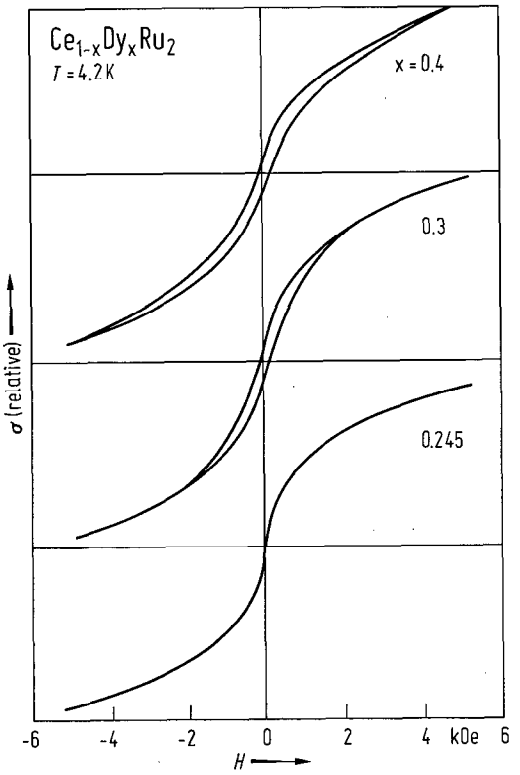

Fig. 64. $Ce_{1-x}Dy_xRu_2$. Hysteresis loops at 4.2 K (σ in arbitrary units) [79 A 1].

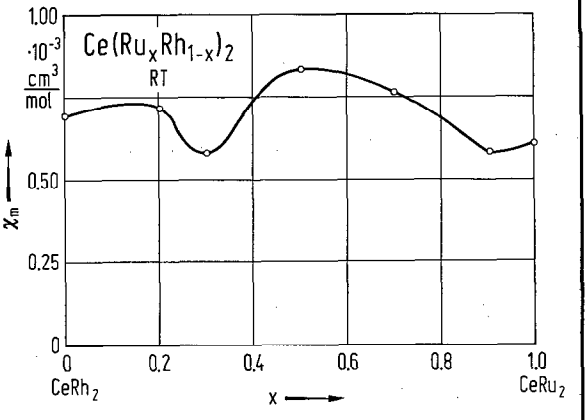

Fig. 65. $Ce(Ru_xRh_{1-x})_2$. Composition dependence of χ_m at room temperature [84 H 2].

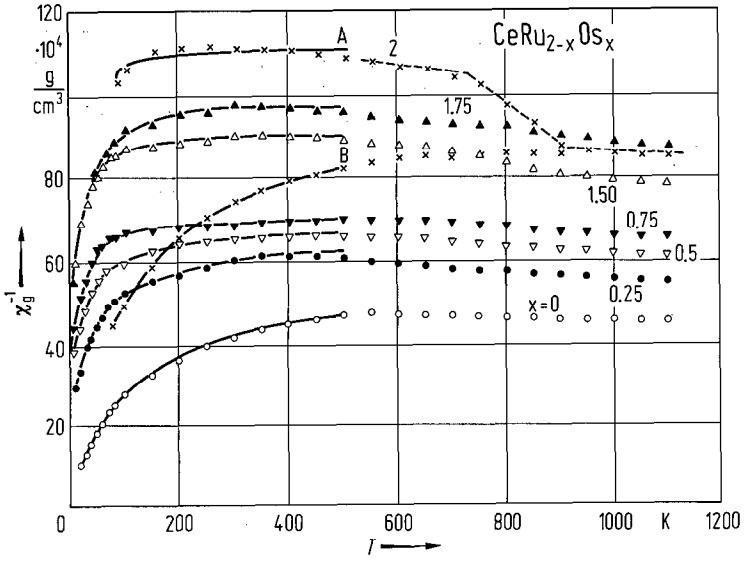

Fig. 66. $CeRu_{2-x}Os_x$. Temperature dependence of χ_g^{-1}. Susceptibility data for $CeOs_2$ during heating (A) and cooling (B) [85 H 1].

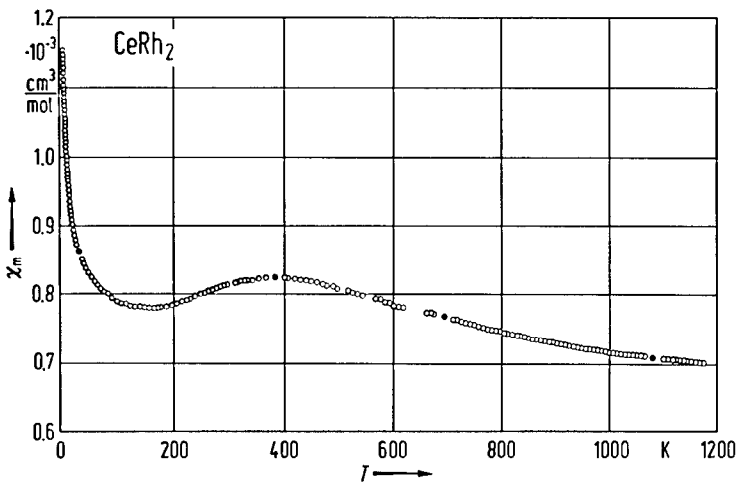

Fig. 67. $CeRh_2$. Temperature dependence of χ_m [82 B 1].

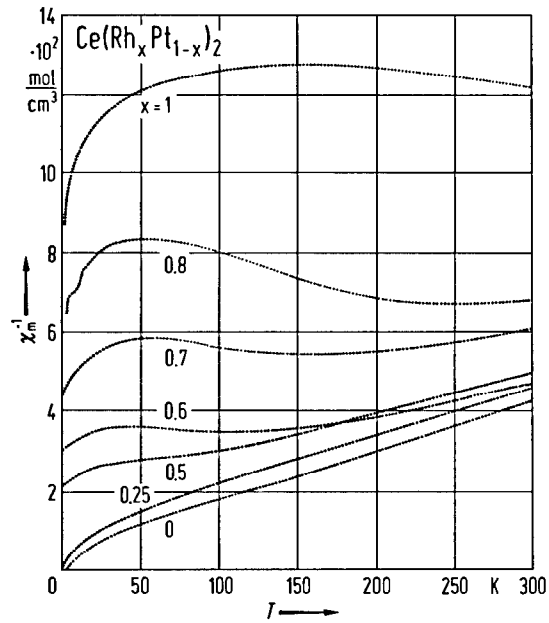

Fig. 68. $Ce(Rh_xPt_{1-x})_2$. Temperature dependence of χ_m^{-1} [82 B 1].

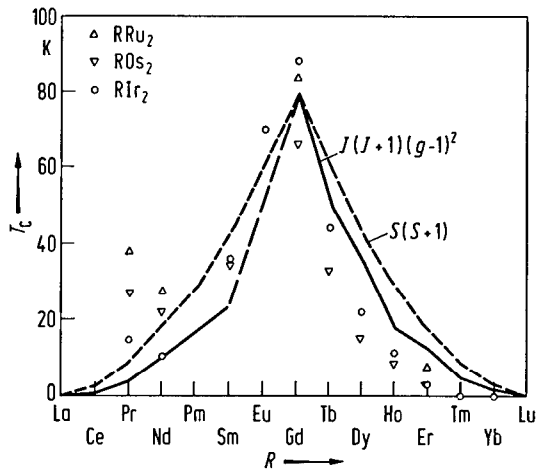

Fig. 69. RRu_2, ROs_2, RIr_2. Experimental values of T_C for three series of compounds and theoretical values of $S(S+1)$ and $J(J+1)(g-1)^2$ [59 B 1].

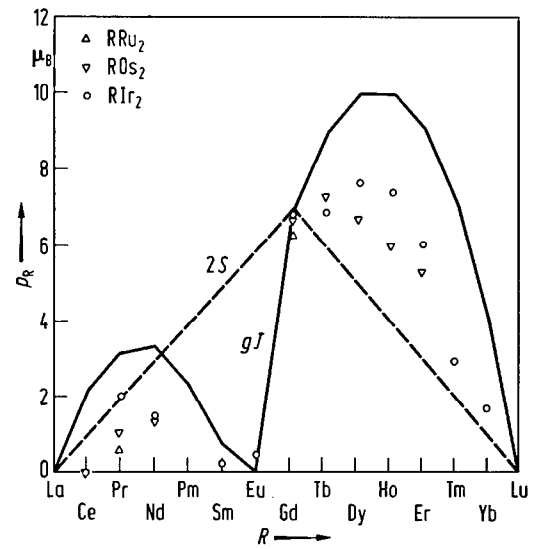

Fig. 70. RRu_2, ROs_2, RIr_2. Magnetic moment per R atom of three series of compounds, compared with theoretical values for R^{3+} ions for total moment (gJ) and for spin only [59 B 1].

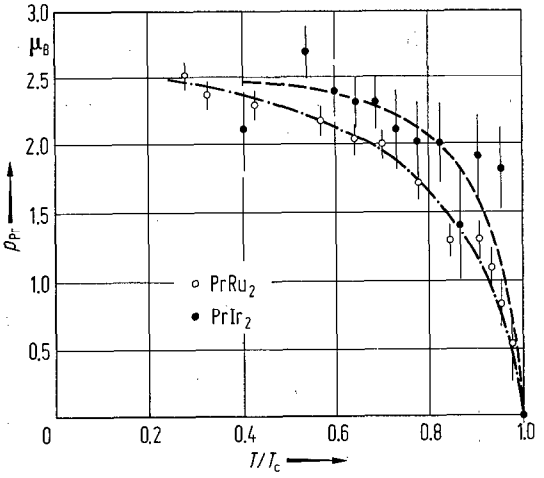

Fig. 71. $PrRu_2$, $PrIr_2$. Temperature dependence of the ordered magnetic moment p_{Pr} obtained from neutron diffraction [82 F 1].

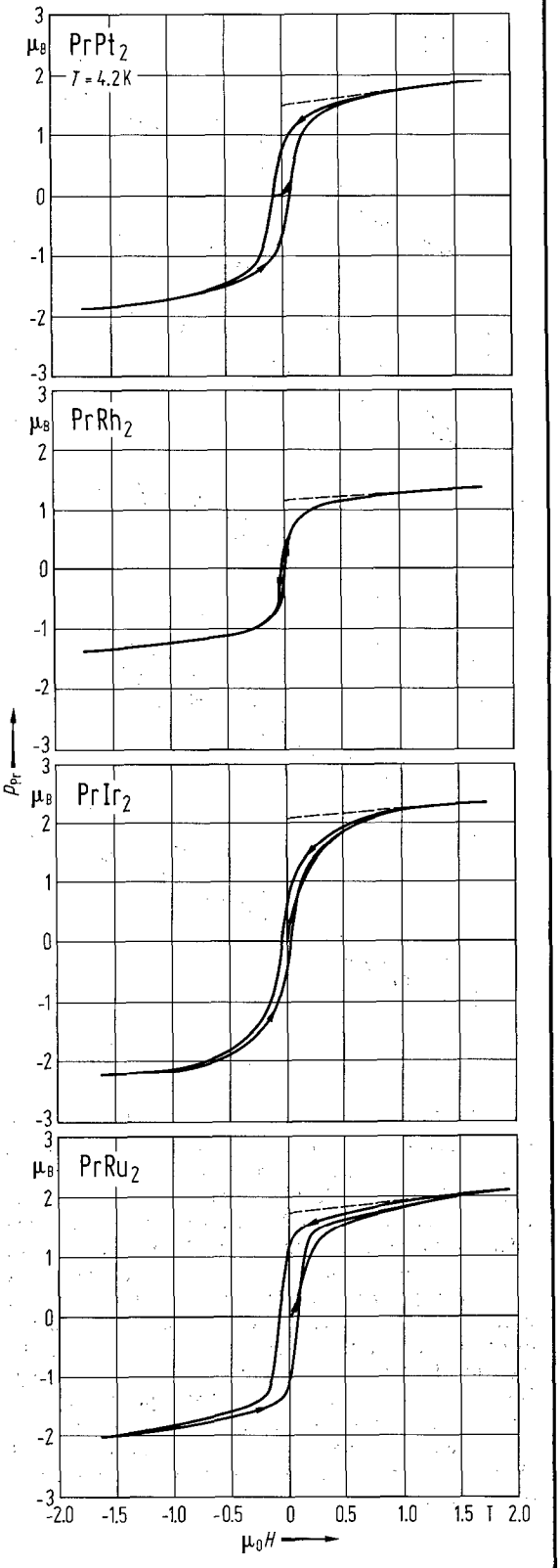

Fig. 72. PrM_2, M = Ru, Rh, Ir, Pt. Magnetic isotherms at 4.2 K [83 G 1].

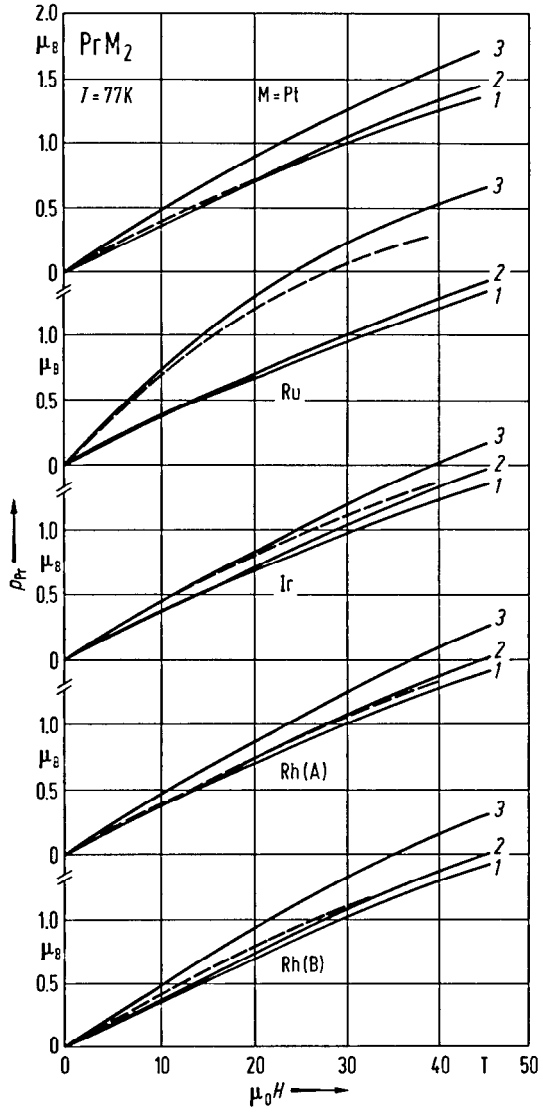

Fig. 73. PrM_2, M = Ru, Rh, Ir, Pt. Magnetic field dependence of p_{Pr} at 77 K. The pulsed-field magnetization measurements are indicated by the dashed line. The solid lines are theoretical calculations. The curves (*1*) and (*2*) are calculated on the basis of the CEF Hamiltonian ignoring interactions between magnetic ions. In the curves (*2*) the external magnetic field is assumed to be pointing along the cube edge. The curves (*1*) are obtained by averaging over all possible angles between quantization axis and external field direction. The curves (*3*) are obtained by including both the CEF Hamiltonian and the exchange Hamiltonian in the calculations. The experimental data on $PrRh_2$ are indicated twice. The theoretical calculations are based on different CEF parameters: $x = 0.93$, $W = -0.35$ meV for (A), and $x = 0.75$. $W = -0.33$ meV for (B) [83 G 1].

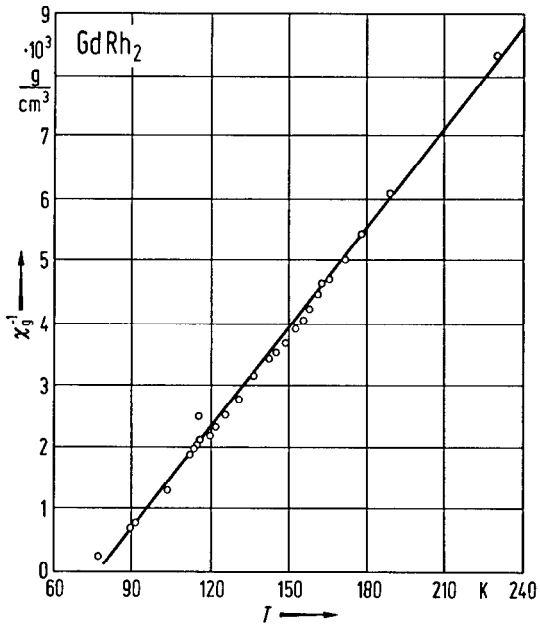

Fig. 74. $GdRh_2$. Temperature dependence of χ_g^{-1} [80 T 1].

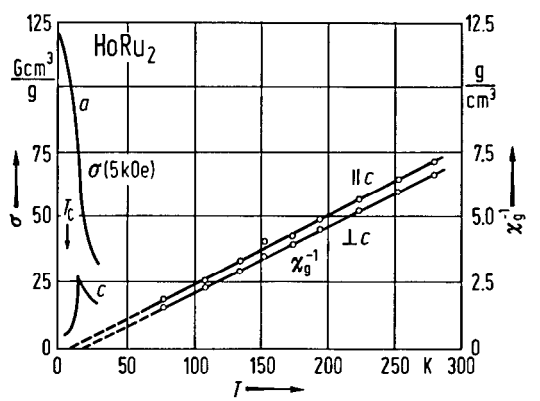

Fig. 75. $HoRu_2$. Single crystal. Temperature dependence of χ_g^{-1} in the directions parallel and perpendicular to the *c* axis, and temperature dependence of σ at 5 kOe along *a* and *c* axes [85 O 1].

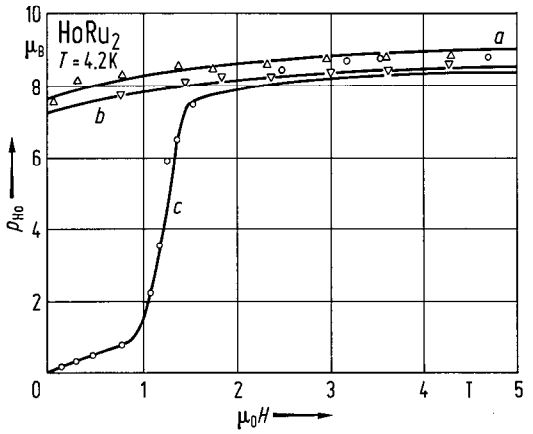

Fig. 76. $HoRu_2$. Single crystal. Magnetic field dependence of p_{Ho} at 4.2 K in the a axis ($11\bar{2}0$), b axis ($10\bar{1}0$), and c axis (0001). The full lines are calculated with CEF parameters $B_2^0 = 0.11$ K, $B_4^0 = 0$ K, $B_6^0 = 1.9 \cdot 10^{-5}$ K, $B_6^6 = 1.5 \cdot 10^{-4}$ K and $\lambda = 0.55\,T/\mu_B$, where λ is the molecular field parameter [85 O 1].

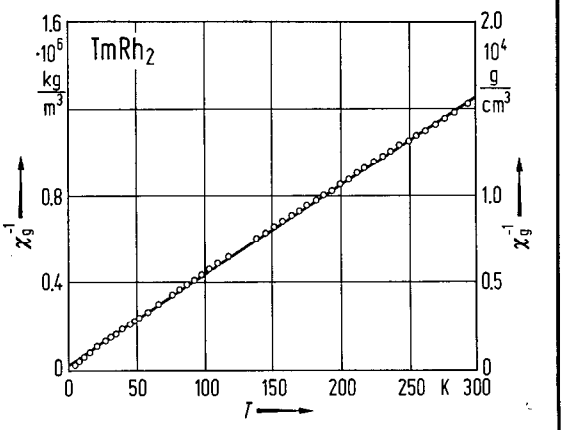

Fig. 77. $TmRh_2$. Temperature dependence of χ_g^{-1} [84 G 2].

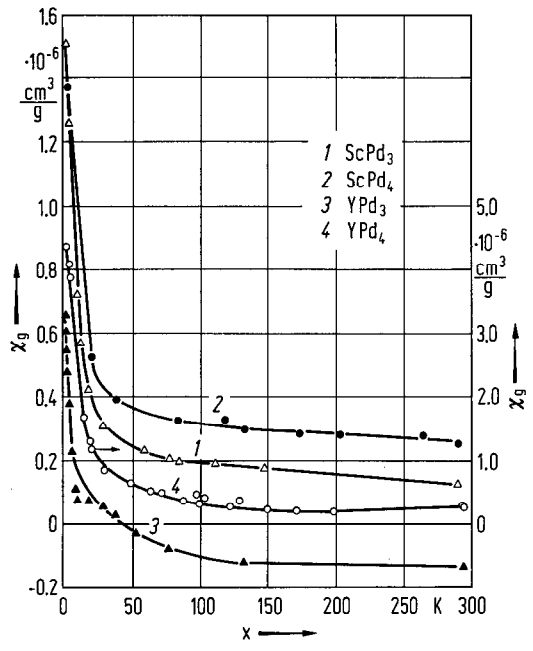

Fig. 78. RPd_3, RPd_4, R = Sc, Y. Temperature dependence of χ_g [72 G 1].

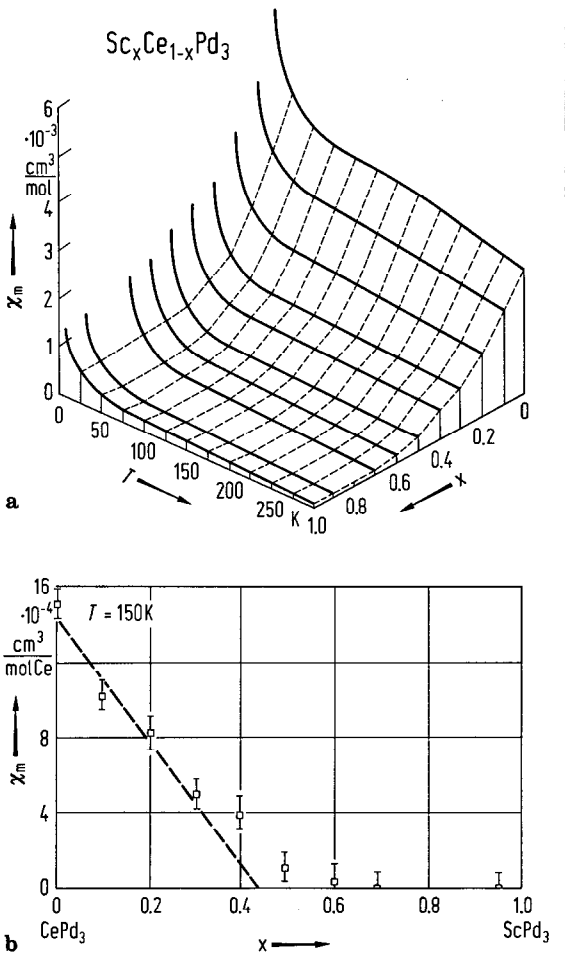

Fig. 79. $Sc_xCe_{1-x}Pd_3$. (a) Temperature and (b) composition dependence of χ_m [80 G 5].

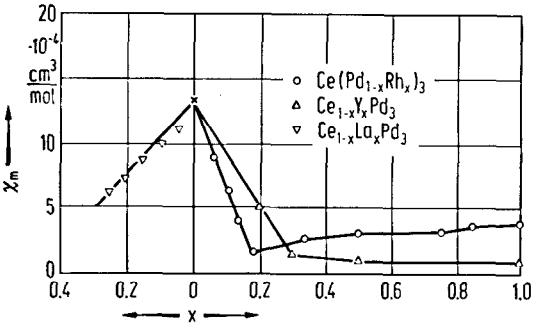

Fig. 80. $Ce(Pd_{1-x}Rh_x)_3$, $Ce_{1-x}Y_xPd_3$, $Ce_{1-x}La_xPd_3$. Magnetic susceptibility χ_m, vs. x [81 G 1].

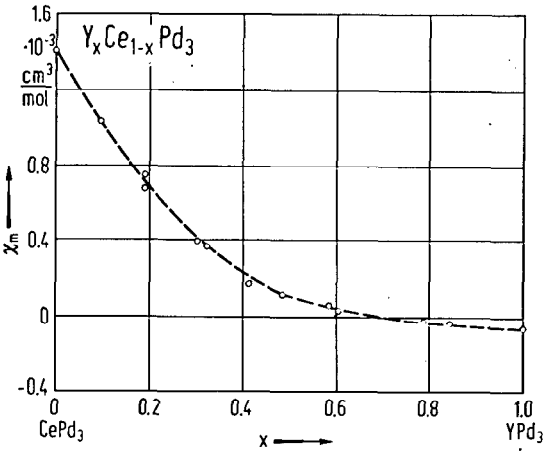

Fig. 81. $Y_xCe_{1-x}Pd_3$. Composition dependence of the low-temperature susceptibility χ_m. For $x \geqq 0.5$ the samples show a nearly temperature-independent susceptibility ($T \leqq 1000$ K) [82 K 1].

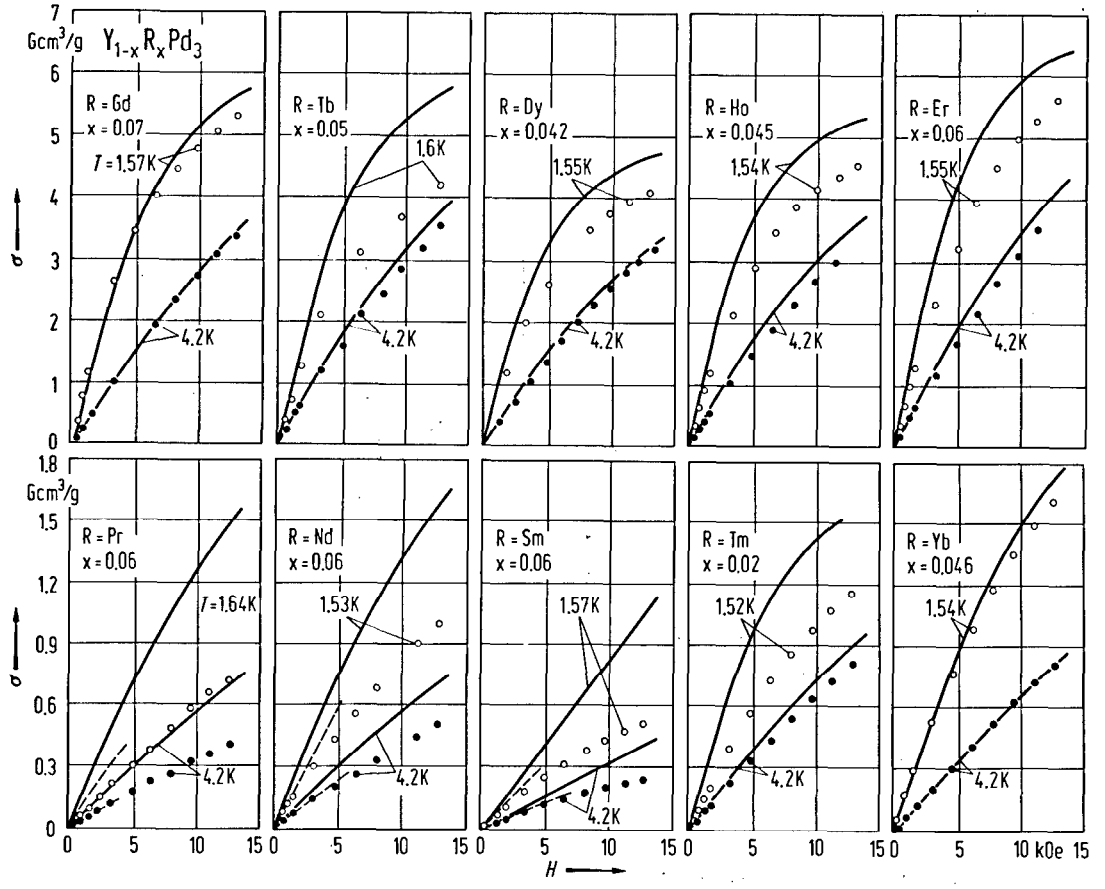

Fig. 82. $Y_{1-x}R_xPd_3$, R = Pr, Nd, Sm, Gd, Tb, Dy, Ho, Er, Tm, Yb. Magnetic field dependence of σ for x = 0.06 (R = Pr), 0.06 (Nd), 0.06 (Sm), 0.07 (Gd), 0.05 (Tb), 0.042 (Dy), 0.045 (Ho), 0.06 (Er), 0.02 (Tm), 0.046 (Yb). The solid lines are free-ion Brillouin functions. The dashed lines correspond to the initial magnetic susceptibilities for the CEF ground state Γ_5, $\Gamma_8^{(2)}$ and Γ_8 for Pr, Nd and Sm, respectively [81 H 1].

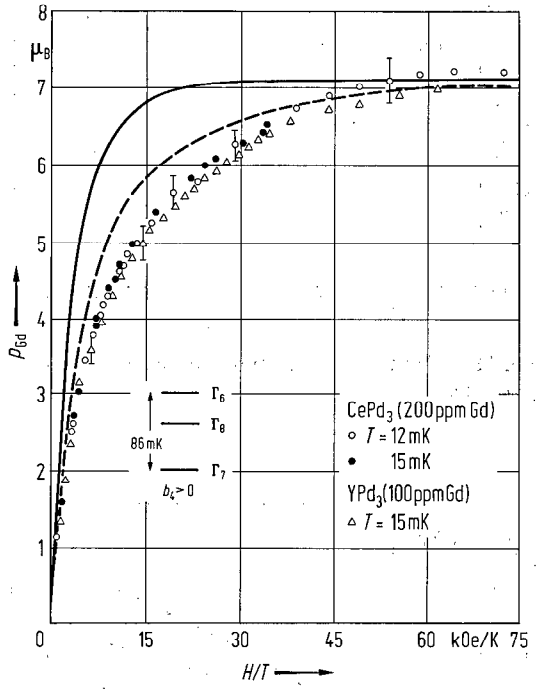

Fig. 83. YPd_3:Gd (100 ppm at $T=15$ mK), $CePd_3$:Gd (200 ppm at $T=12$ and 15 mK). Magnetic moment per Gd ion vs. H/T. The solid line is the theoretical free-ion magnetization $B_{7/2}(H/T)$, and the dashed line is the magnetization calculated with zero magnetic field CEF scheme ($b_4=2.7$ mK) at $T=12$ mK [81 B 1].

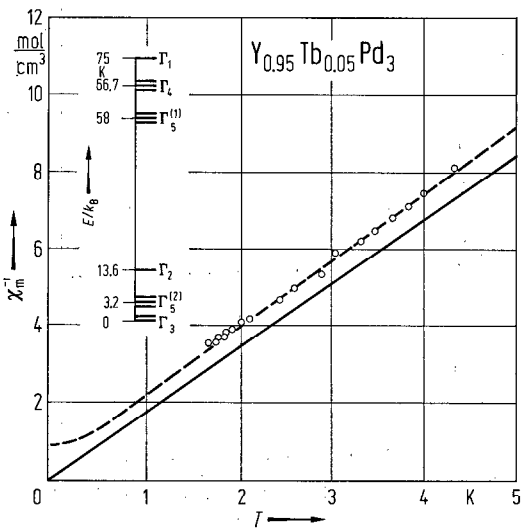

Fig. 84. $Y_{0.95}Tb_{0.05}Pd_3$. Temperature dependence of χ_m^{-1} (open circles) compared with the prediction from neutron crystal field spectrum (dashed line) with CEF parameters $W=-0.25$ meV and $x=0.97$. The solid line represents the Curie law [80 L 1].

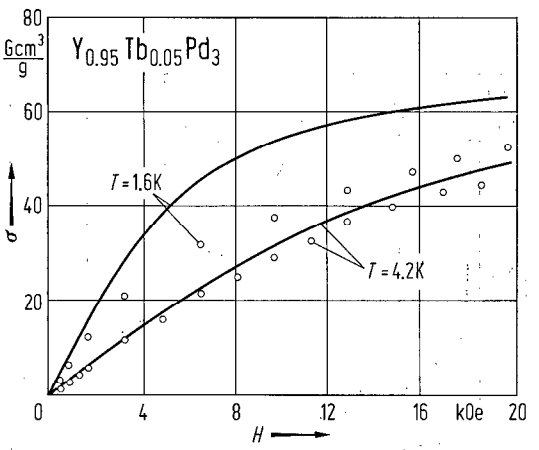

Fig. 85. $Y_{0.95}Tb_{0.05}Pd_3$. Magnetic field dependence of σ at 1.6 and 4.2 K. Solid lines are free-ion Brillouin functions [80 L 1].

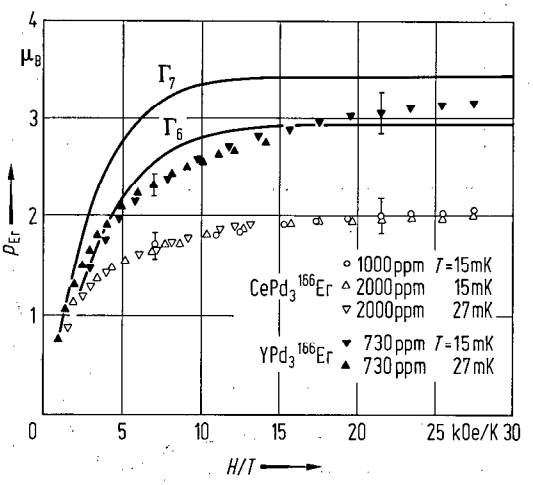

Fig. 86. YPd_3:Er (730 ppm at $T=15$ and 27 mK), $CePd_3$:Er (2000 ppm at $T=15$ and 27 mK and for 1000 ppm at $T=15$ mK). Magnetic moment per Er ion vs. H/T. Inelastic neutron scattering and ESR measurements indicate a Γ_6 ground state and a Γ_8 excited state for Er in YPd_3. For Er in $CePd_3$ ESR measurements indicate a Γ_7 ground state. The solid lines are calculated magnetization curves for these ground states [81 B 1].

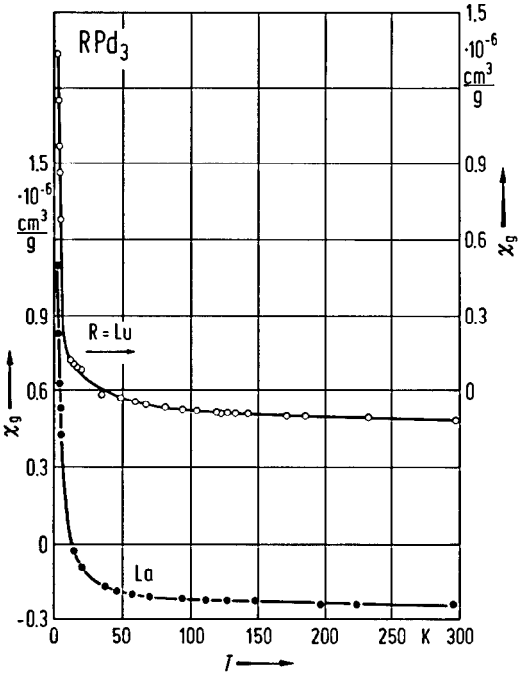

Fig. 87. RPd_3, R = La, Lu. Temperature dependence of χ_g [72 G 1].

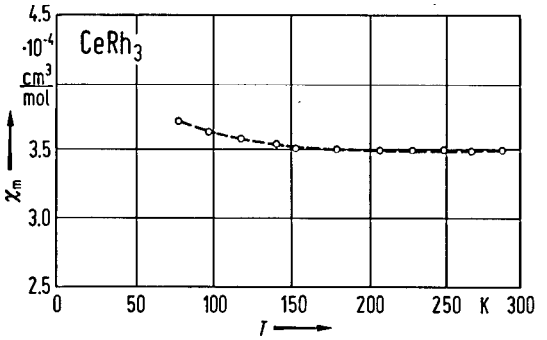

Fig. 88. $CeRh_3$. Temperature dependence of χ_m [84 M 1].

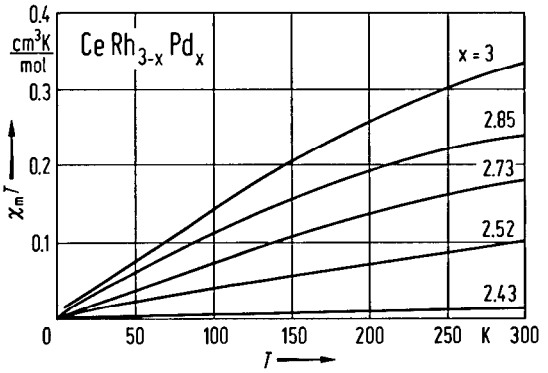

Fig. 90. $CeRh_{3-x}Pd_x$. Temperature dependence of $\chi_m T$ for different x [81 M 1].

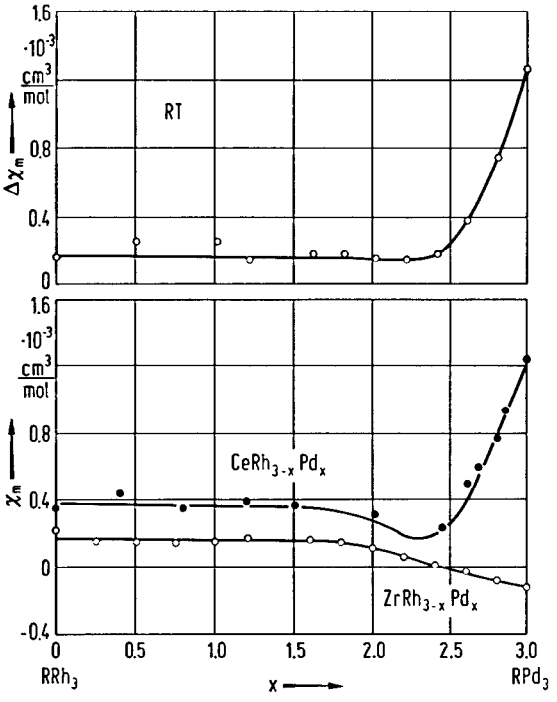

Fig. 89. $CeRh_{3-x}Pd_x$, $ZrRh_{3-x}Pd_x$. Composition dependence of χ_m and of $\Delta\chi_m = \chi_m(CeRh_{3-x}Pd_x) - \chi_m(ZrRh_{3-x}Pd_x)$, at room temperature [78 P 1, 77 T 1].

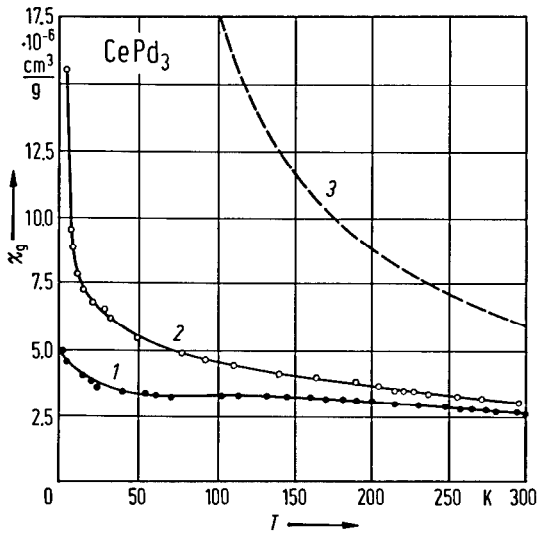

Fig. 91. $CePd_3$. Temperature dependence of χ_g. Jonson-Matthey cerium (*1*), 99.95% pure Koch-Light cerium (*2*), Ce^{3+} free-ion values (*3*) [72 G 1].

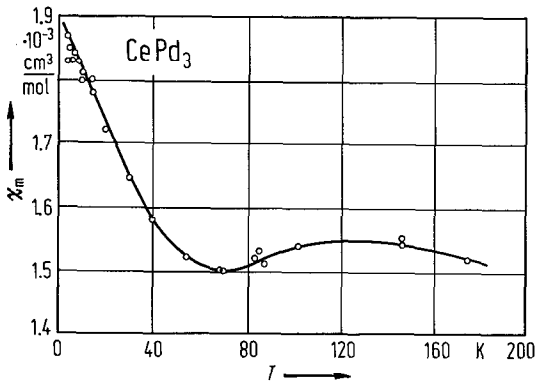

Fig. 92. $CePd_3$. Single crystal. Temperature dependence of χ_m [82 T 2].

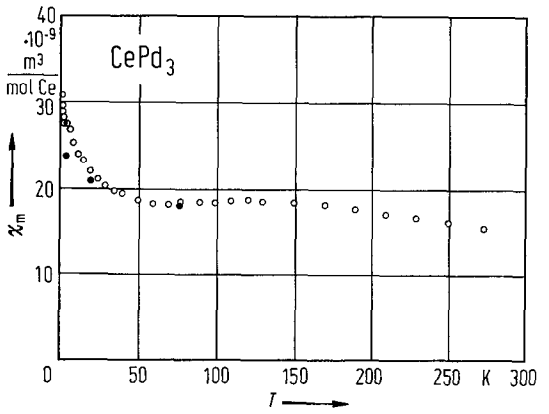

Fig. 93. $CePd_3$. Temperature dependence of χ_m. The filled symbols correspond to the intrinsic susceptibility values derived from high-field magnetization measurements [86 V 1].

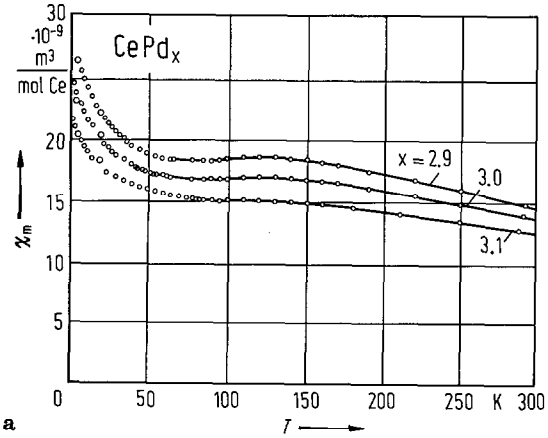

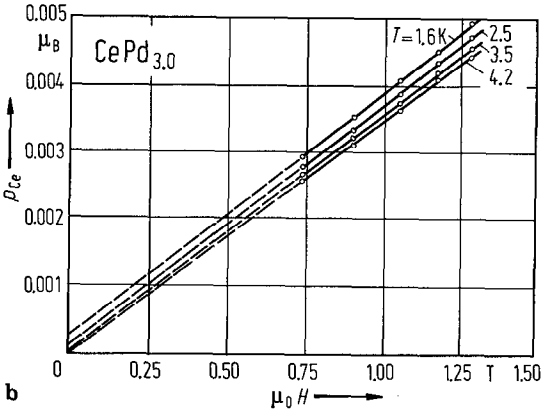

Fig. 94. $CePd_x$. (a) Temperature dependence of χ_m for x = 2.9, 3.0, and 3.1. The symbols correspond to the intrinsic susceptibility values derived from high-field magnetization measurements. (b) shows the low-field p_{Ce} vs. $\mu_0 H$ for $CePd_{3.0}$ at different temperatures [85 A 1].

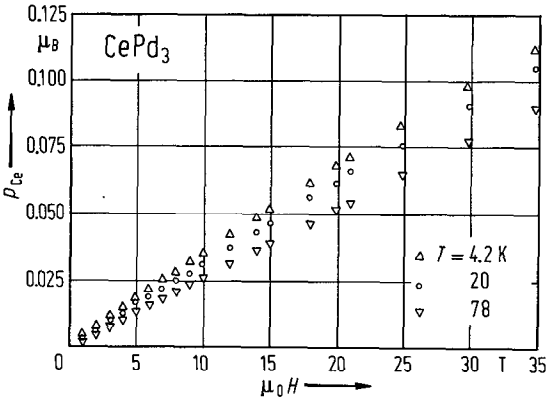

Fig. 96. $CePd_3$. Magnetic field dependence of p_{Ce} at 4.2, 20 and 78 K [86 V 1].

For Fig. 95 see next page

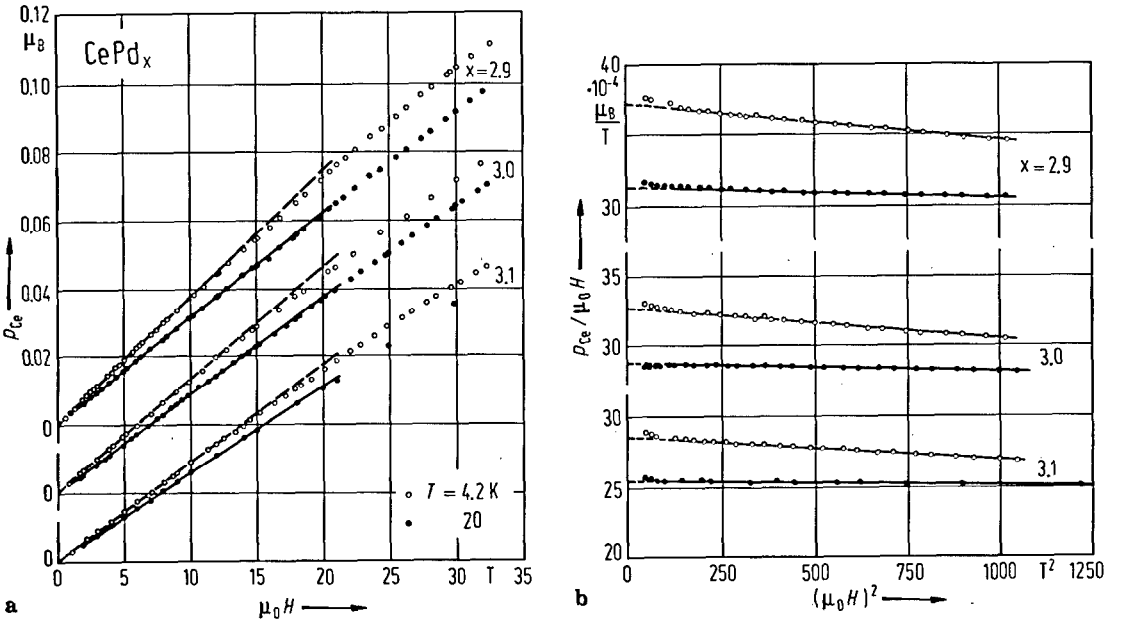

Fig. 95. $CePd_x$. (a) Magnetic field dependence of p_{Ce} and (b) $p_{Ce}/\mu_0 H$ vs. $(\mu_0 H)^2$ for x = 2.9, 3.0 and 3.1, at 4.2 and 20 K. The dashed lines correspond to the intrinsic magnetic susceptibility [85 A 1].

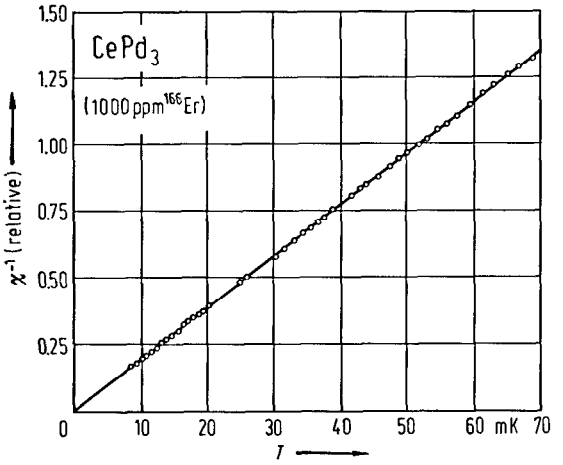

Fig. 97. $CePd_3$ (1000 ppm ^{166}Er). Temperature dependence of χ^{-1} (arbitrary units) [80 M 1].

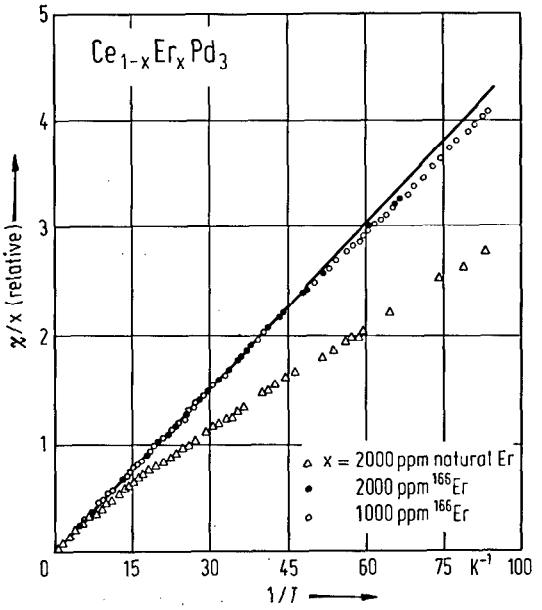

Fig. 98. $Ce_{1-x}Er_xPd_3$. Normalized susceptibility, χ/x, of natural Er and ^{166}Er impurities in $CePd_3$ vs. T^{-1} for x = 2000 ppm of natural Er, 2000 ppm of ^{166}Er and 1000 ppm of ^{166}Er [80 M 1].

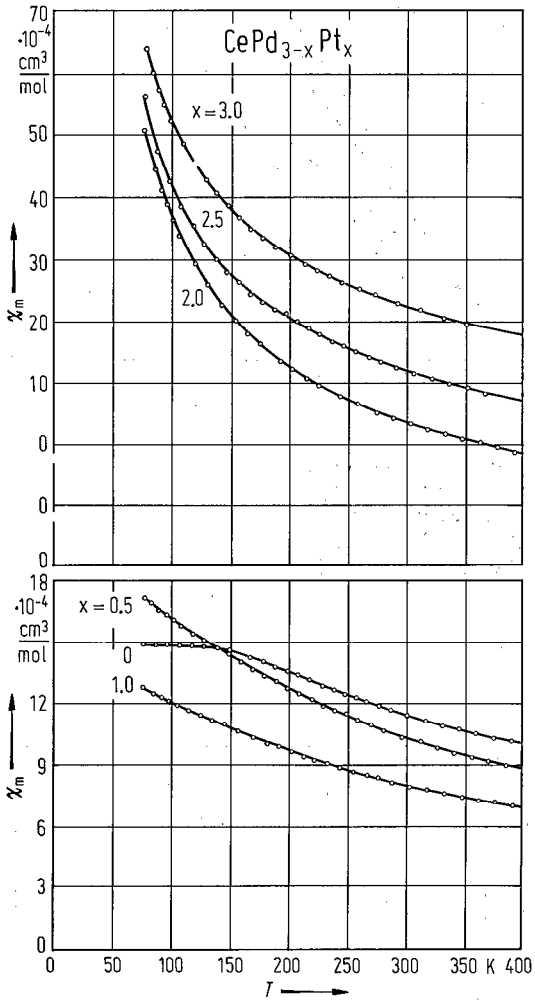

Fig. 99. $CePd_{3-x}Pt_x$. Temperature dependence of χ_m for different x [82 R 1].

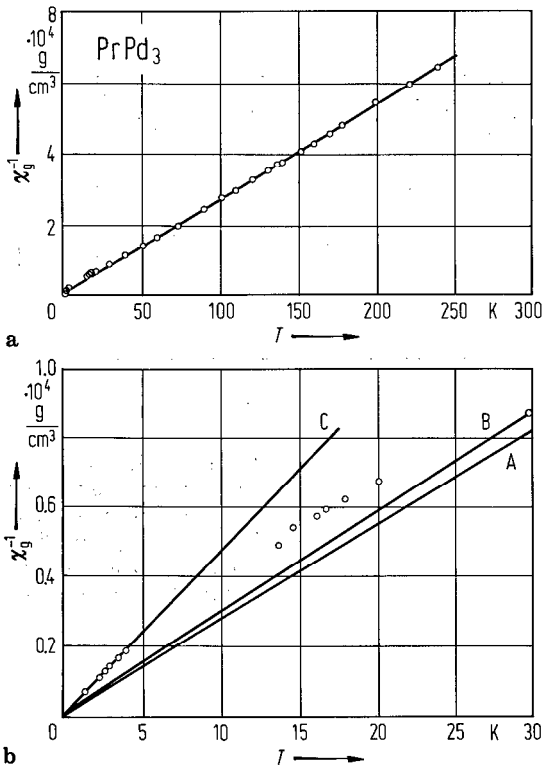

Fig. 100. $PrPd_3$. (a) Temperature dependence of χ_g^{-1} corrected by $-0.15 \cdot 10^{-6}$ cm^3/g for matrix diamagnetism. (b) shows on an expanded scale the data below 30 K in relation to (A) the line through the high-temperature data, (B) the free-ion slope and (C) the line corresponding to Γ_5 ground state [72 G 1].

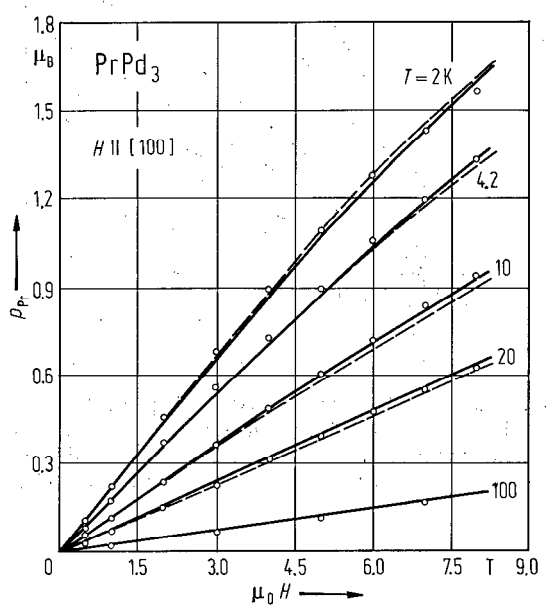

Fig. 101. $PrPd_3$. Magnetic field dependence of p_{Pr} at different temperatures. H is corrected for demagnetization field and is directed parallel to the [100] direction. Calculations with the set of CEF parameters: (i) $B_4 = 0.54 \cdot 10^{-2}$ meV, $B_6 = 0.45 \cdot 10^{-4}$ meV (dashed lines); and (ii) $B_4 = 0.45 \cdot 10^{-2}$ meV, $B_6 = -0.714 \cdot 10^{-4}$ meV (solid lines). In the Leask and Wolf notation [62 I 1] these parameters are (i) $x = 0.85$, $W = 0.38$ meV; and (ii) $x = 0.75$, $W = 0.36$ meV, respectively [85 D 1].

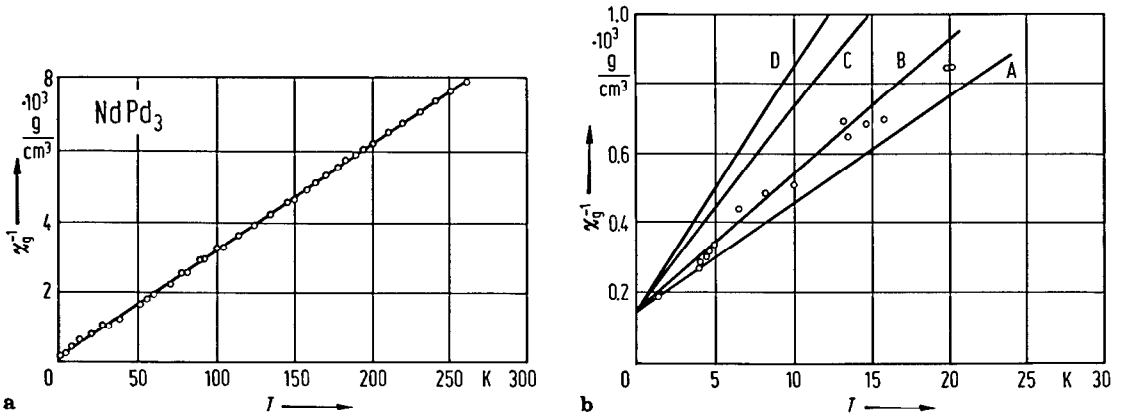

Fig. 102. $NdPd_3$. (a) Temperature dependence of χ_g^{-1} corrected by $-0.15 \cdot 10^{-6}$ cm³/g for matrix diamagnetism. (b) shows on an expanded scale the data below 20 K in relation to (A) the line through the high-temperature data, and the lines for the ground states (B) $\Gamma_8^{(1)}$, (C) $\Gamma_8^{(2)}$ and (D) Γ_6 covering at $T=0$ K [72 G 1].

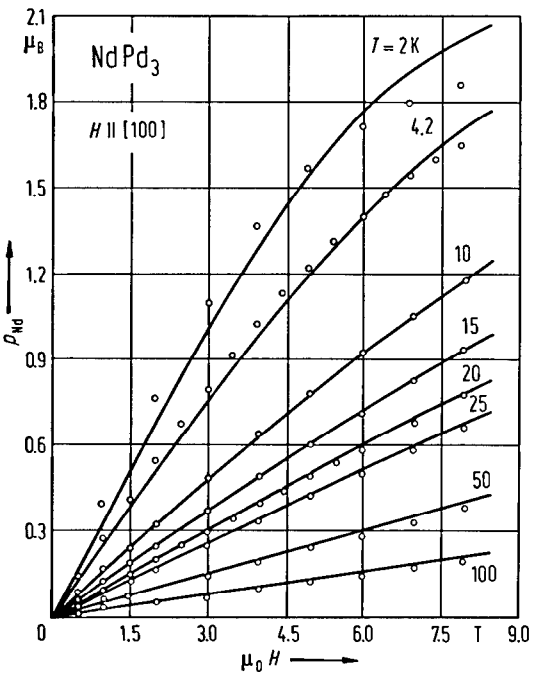

Fig. 103. $NdPd_3$. Single crystal. Magnetic field dependence of p_{Nd} at different temperatures with magnetic field along [100] axis. The lines are calculated with CEF parameters $x=-0.905$ and $W=-0.131$ meV [86 D 1].

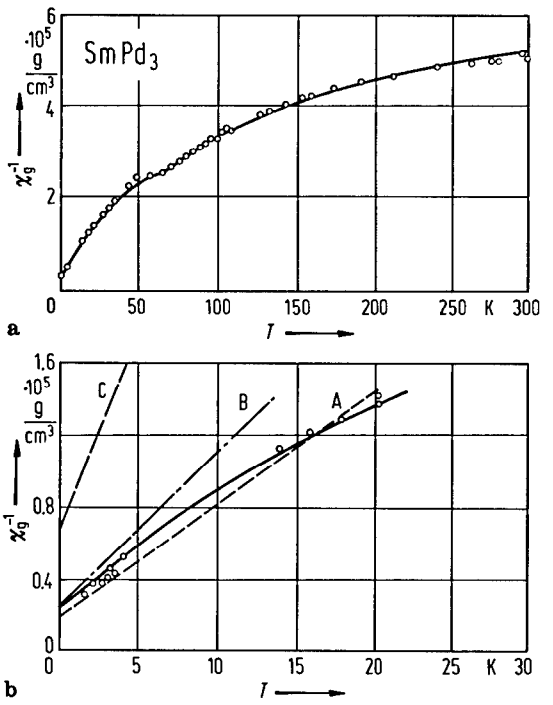

Fig. 104. $SmPd_3$. (a) Temperature dependence of χ_g^{-1} corrected for matrix diamagnetism. The solid line is calculated for the free-ion state. (b) shows on an expanded scale the data below 20 K in relation to the calculated curve (solid line) and the Curie-Weiss ($\Theta=-3$ K) lines for (A) the free-ion; (B) a Γ_8 ground state; (C) a Γ_7 ground state [72 G 1, 71 G 1].

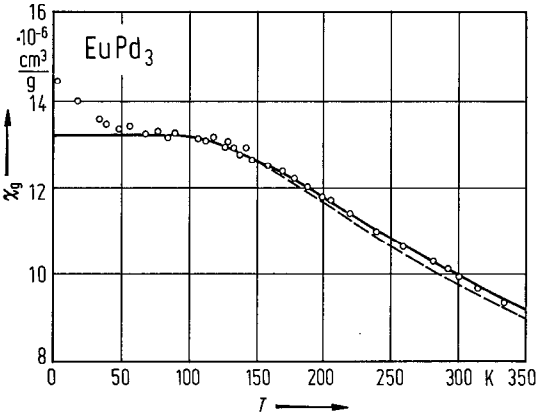

Fig. 105. $EuPd_3$. Temperature dependence of χ_g corrected for matrix diamagnetism. The solid line is calculated for the free-ion state from the CEF level scheme [71 G 1, 72 G 1].

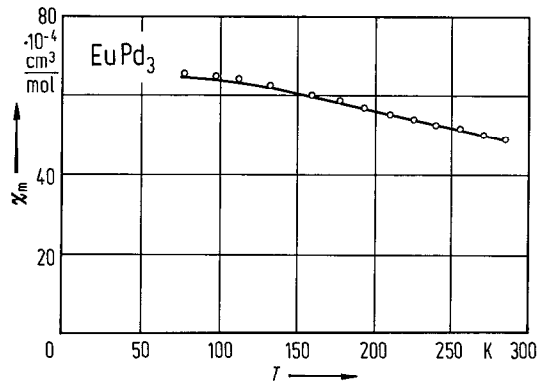

Fig. 106. $EuPd_3$. Temperature dependence of χ_m [83 D 1, 84 M 1].

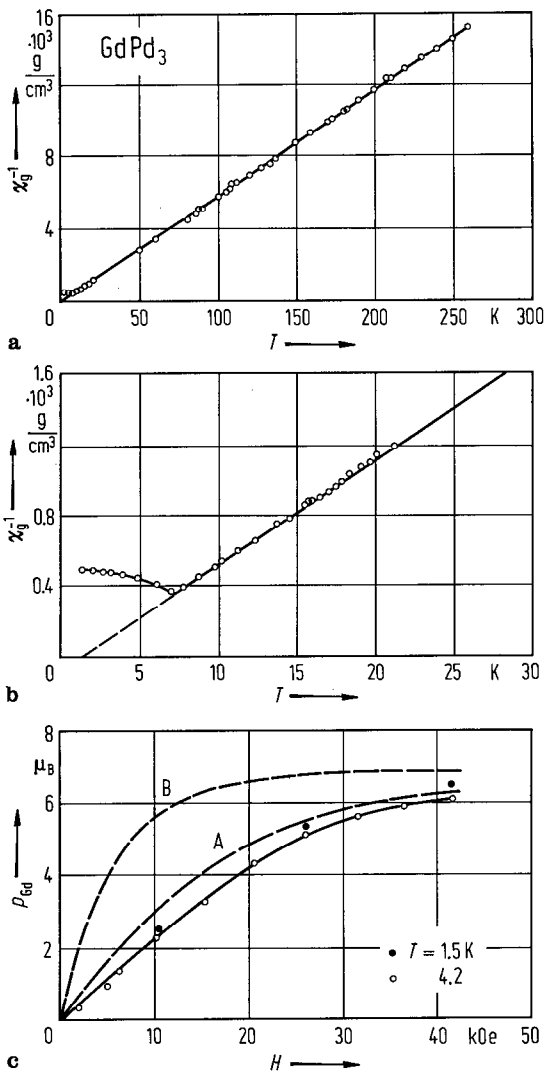

Fig. 107. $GdPd_3$. (a) Temperature dependence of χ_g^{-1} corrected for matrix diamagnetism. (b) shows the behaviour below 30 K on an expanded scale. (c) shows magnetic field dependence of p_{Gd} at 4.2, 1.5 K. Curves A and B represent the Brillouin function at 4.2 and 1.5 K, respectively [72 G 1].

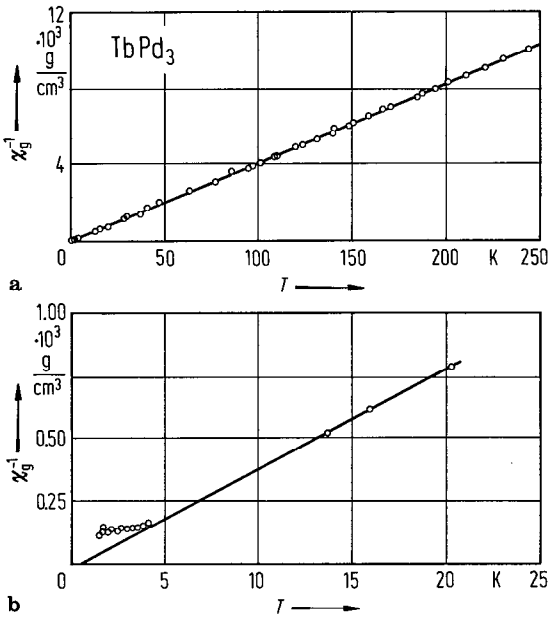

Fig. 108. $TbPd_3$. (a) Temperature dependence of χ_g^{-1} corrected for matrix diamagnetism. (b) shows the behaviour below 20 K on an expanded scale [72 G 1].

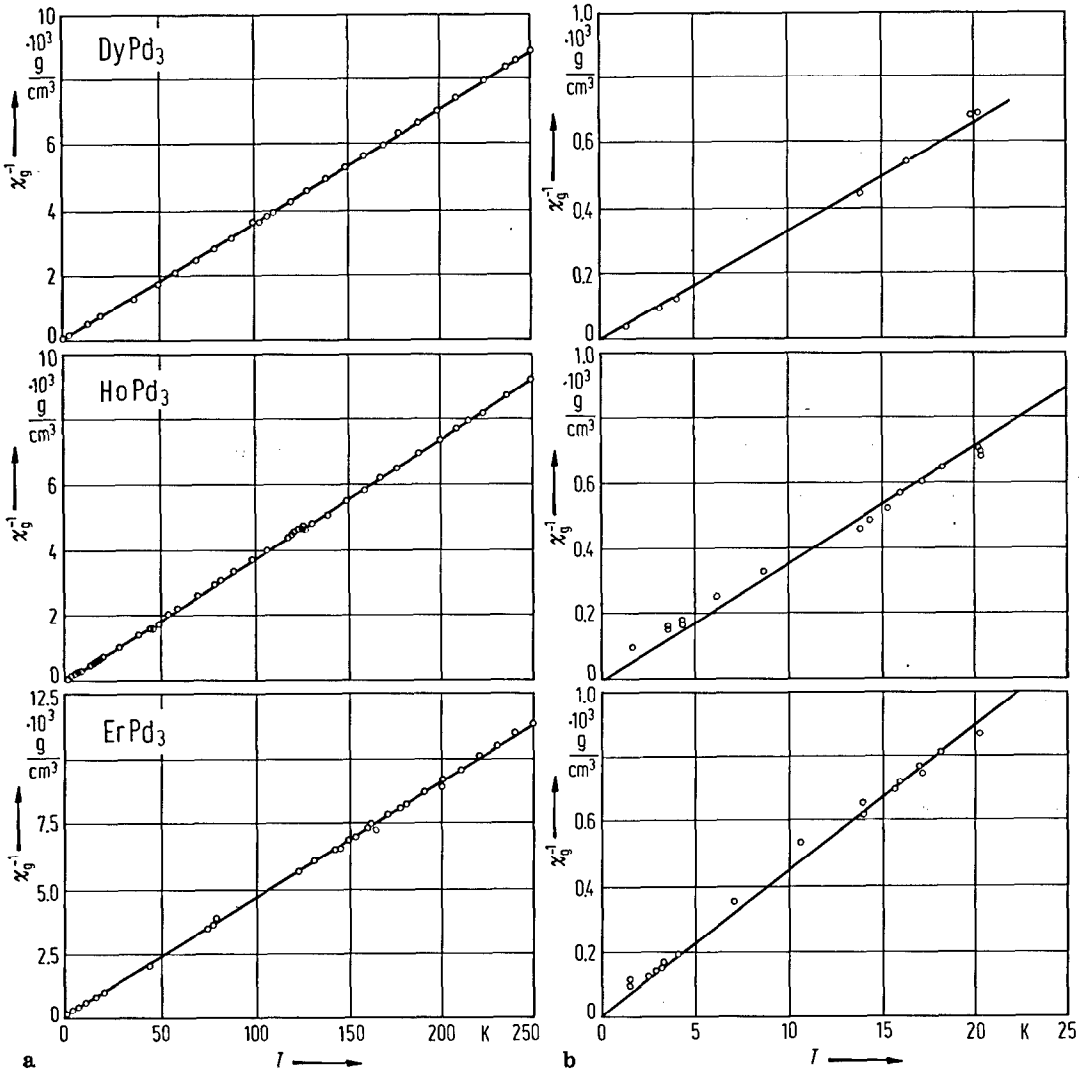

Fig. 109. RPd_3, R = Dy, Ho, Er. (a) Temperature dependence of χ_g^{-1} corrected for matrix diamagnetism. (b) shows the behaviour on an expanded scale [72 G 1].

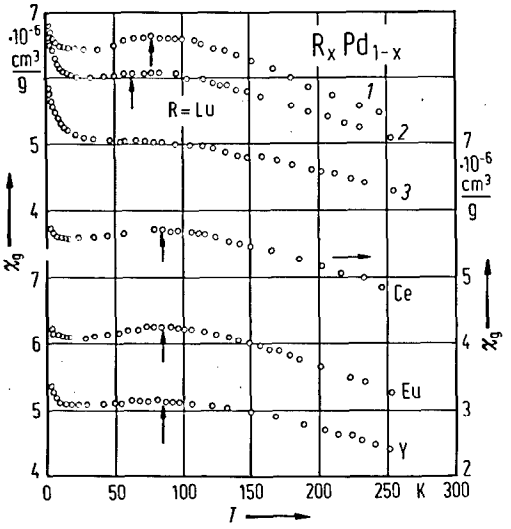

Fig. 110. R_xPd_{1-x}, R = Y, Ce, Eu, Lu. Temperature dependence of χ_g for R = Lu: (*1*) x = 0.005, (*2*) 0.01, (*3*) 0.02; Ce: x = 0.01; Eu: x = 0.013; Y: x = 0.015 (all these R have no magnetic moment in Pd). The arrows indicate the positions of the $\chi(T)$ maxima. The low-temperature increases in $\chi(T)$ are due to the rare-earth and/or iron-group impurities [73 G 1].

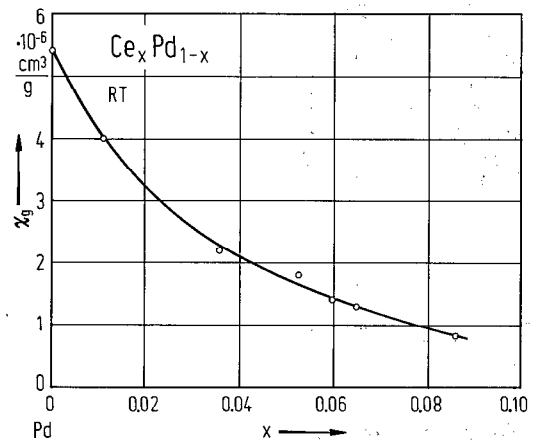

Fig. 111. Ce_xPd_{1-x}. Concentration dependence of χ_g at room temperature [80 H 1].

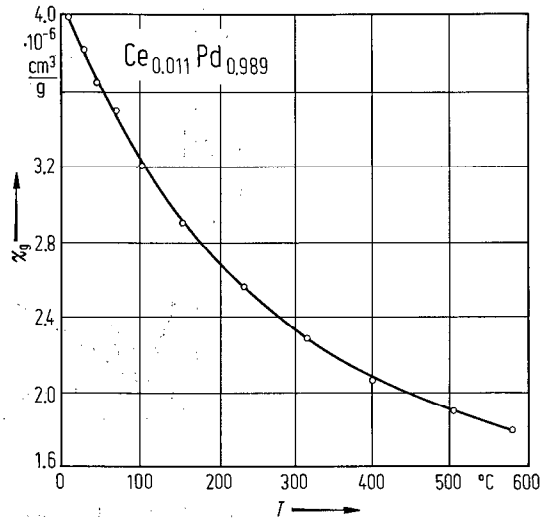

Fig. 112. $Ce_{0.011}Pd_{0.989}$. Temperature dependence of χ_g [80 H 1].

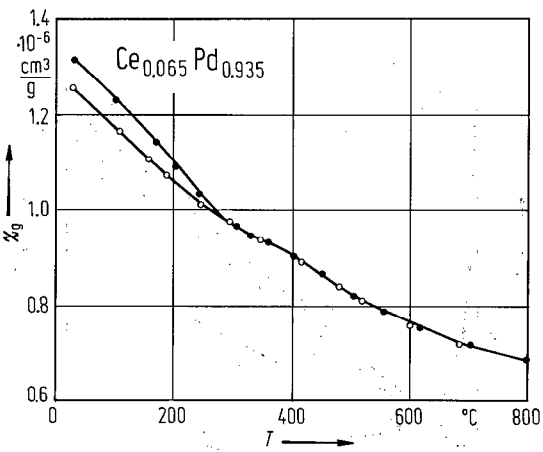

Fig. 113. $Ce_{0.065}Pd_{0.935}$. Temperature dependence of χ_g, of a quenched alloy, solid circles: during heating; open circles: during cooling [80 H 1].

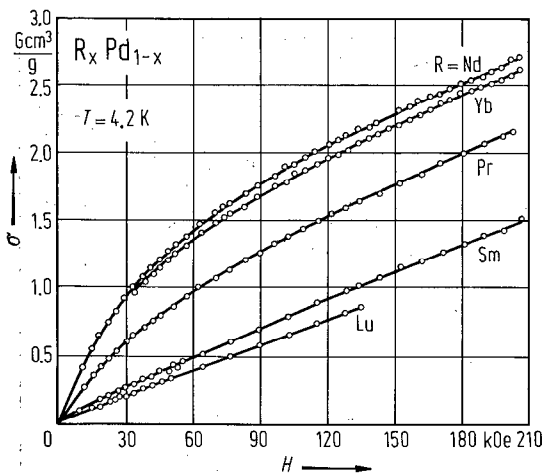

Fig. 114. R_xPd_{1-x}, R = Pr, Nd, Sm, Yb, Lu. Magnetic field dependence of σ at 4.2 K for dilute alloys (generally x = 0.01 or less). The solid lines represent the fit to the data by equation $\sigma(H) = \frac{aH}{1+b|H|} + cH$. In the limit of large H, $\sigma(H) = \frac{a}{b} + cH$, so that c is the matrix susceptibility and $\frac{a}{b}$ is proportional to the saturation moment per R atom, p_R [73 G 1].

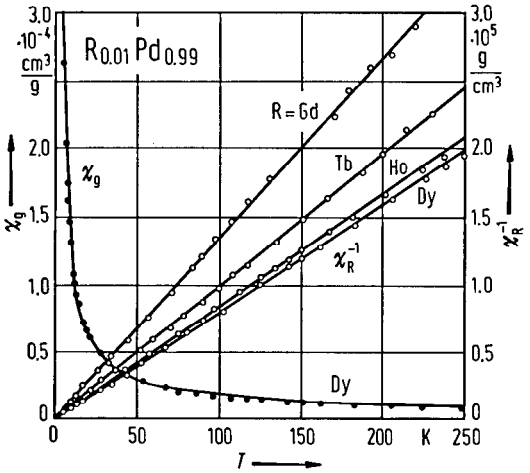

Fig. 115. $R_{0.01}Pd_{0.99}$, R = Gd, Tb, Dy, Ho. Inverse of the rare-earth contribution to the magnetic susceptibility, $\chi_R^{-1}(T)$, and $\chi_g(T)$ for $Dy_{0.01}Pd_{0.99}$, where $\chi_R(T) = \chi_g(T) - \chi_{mat}(T)$. $\chi_{mat}(T)$ is the susceptibility of $Lu_{0.01}Pd_{0.99}$ (see Fig. 110) [73 G 1].

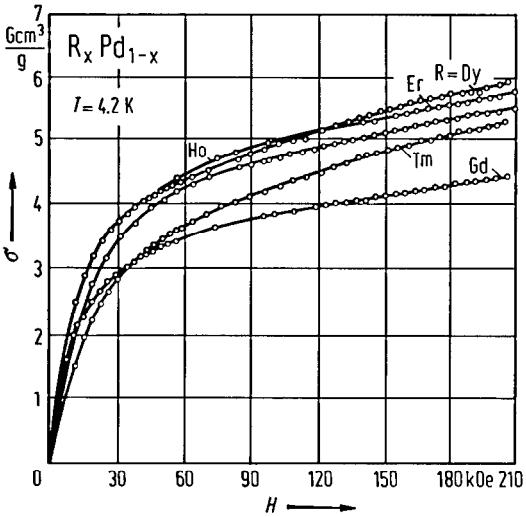

Fig. 116. R_xPd_{1-x}, R = Gd, Dy, Ho, Er, Tm. Magnetic field dependence of σ at 4.2 K. For explanation see the caption to Fig. 114 [73 G 1].

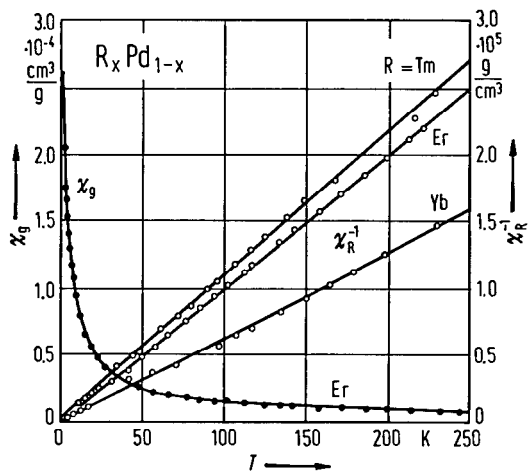

Fig. 117. R_xPd_{1-x}, R = Tm (x = 0.015), Er (x = 0.01), Yb (x = 0.0085). Inverse of the rare-earth contribution to the susceptibility χ_R^{-1}, and $\chi_g(T)$ for $Er_{0.01}Pd_{0.99}$. χ_R is defined in the caption to Fig. 115 [73 G 1].

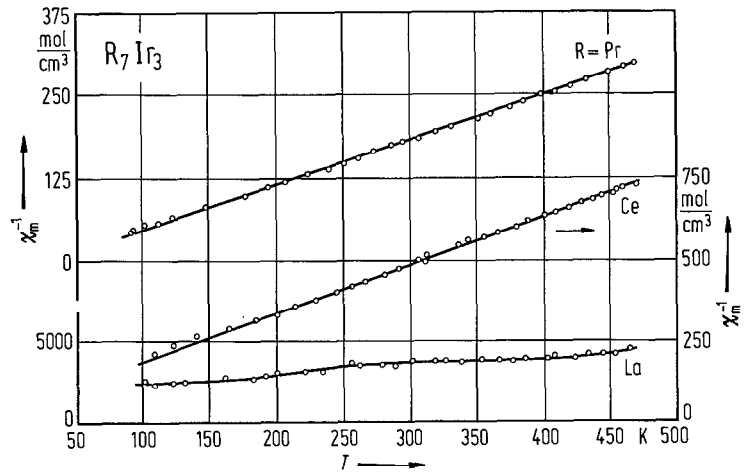

Fig. 118. R_7Ir_3, R = La, Ce, Pr. Temperature dependence of χ_m^{-1} [73 O 1].

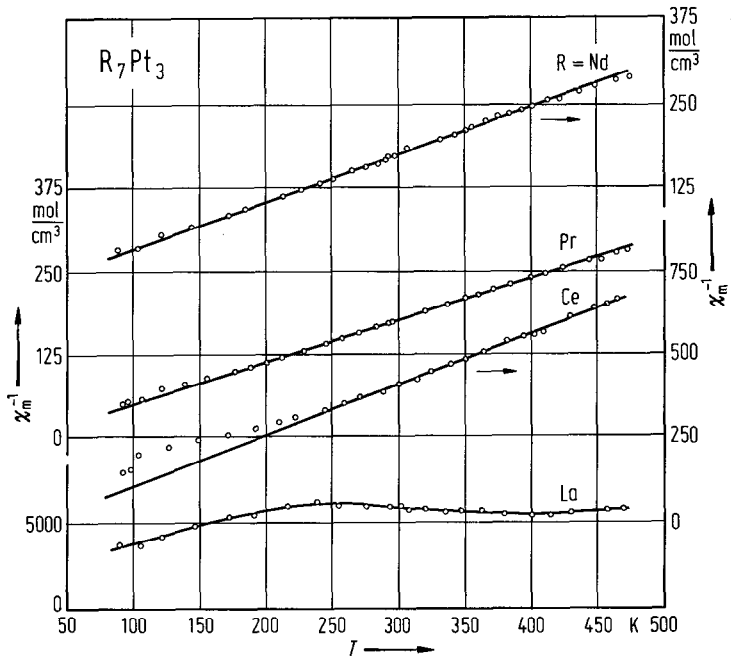

Fig. 119. R_7Pt_3, R = La, Ce, Pr, Nd. Temperature dependence of χ_m^{-1} [73 O 1].

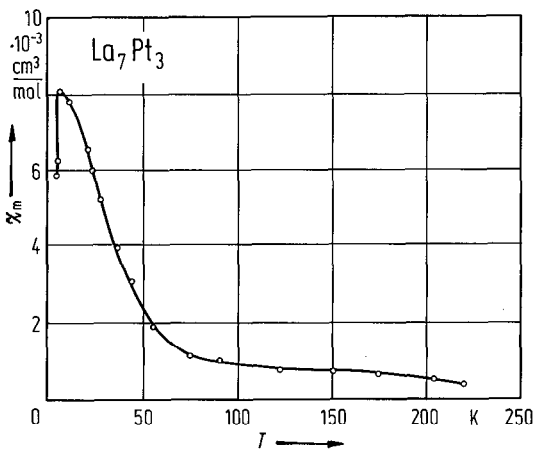

Fig. 120. La_7Pt_3. Temperature dependence of χ_m [80 G 2].

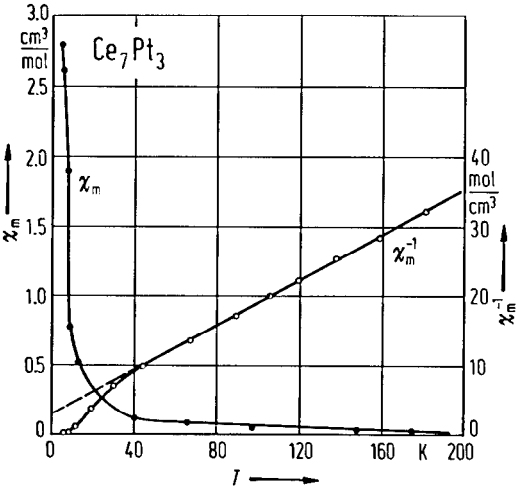

Fig. 121. Ce_7Pt_3. Temperature dependence of χ_m and χ_m^{-1} [80 G 2].

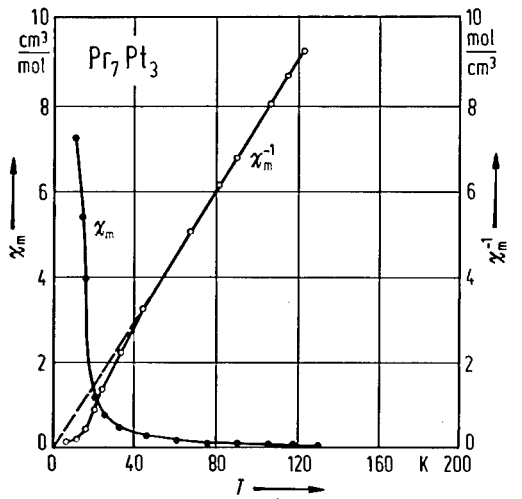

Fig. 123. Pr_7Pt_3. Temperature dependence of χ_m and χ_m^{-1} [80 G 2].

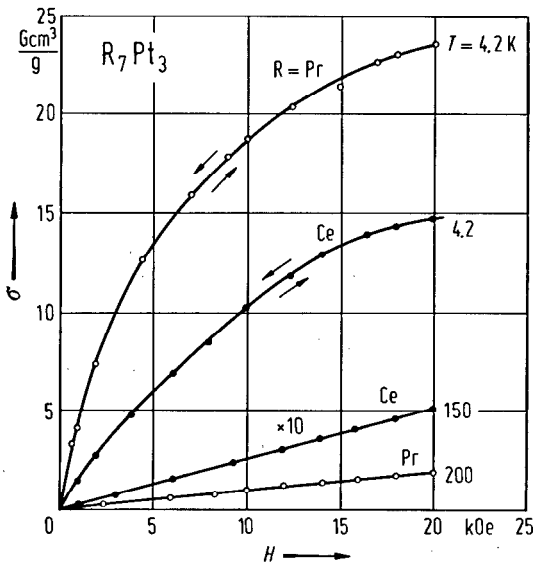

Fig. 122. R_7Pt_3, R = Ce, Pr. Magnetic field dependence of σ at different temperatures [80 G 2].

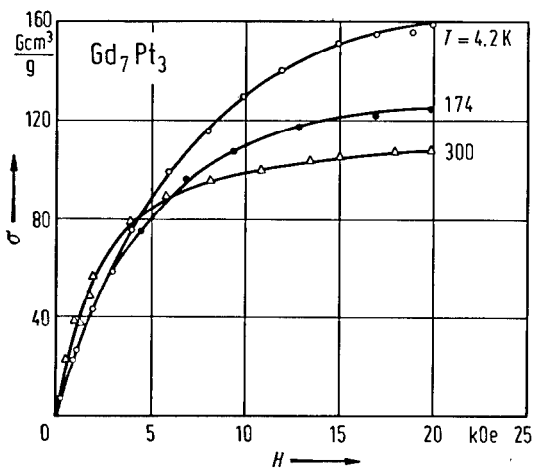

Fig. 124. Gd_7Pt_3. Magnetic field dependence of σ at different temperatures [80 G 2].

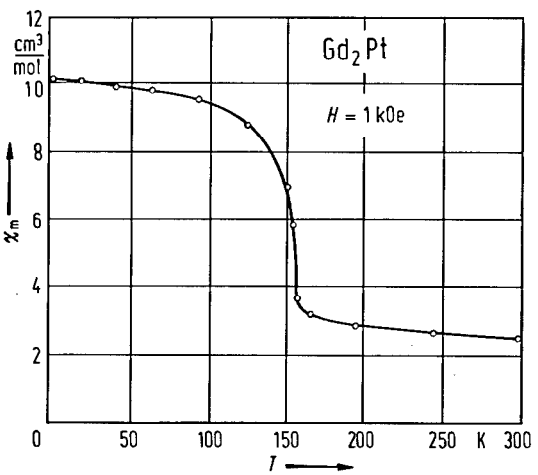

Fig. 125. Gd_2Pt. Temperature dependence of χ_m at 1 kOe [80 G 4].

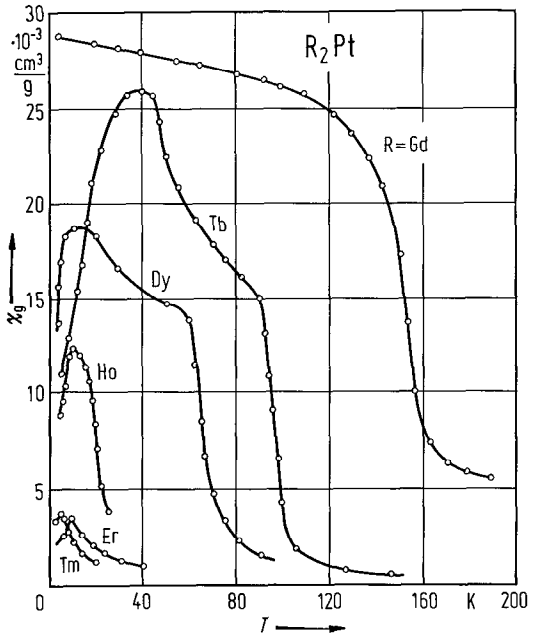

Fig. 126. R_2Pt, R = Gd, Tb, Dy, Ho, Er, Tm. Temperature dependence of χ_g (samples were cooled in zero magnetic field) [83 C 1].

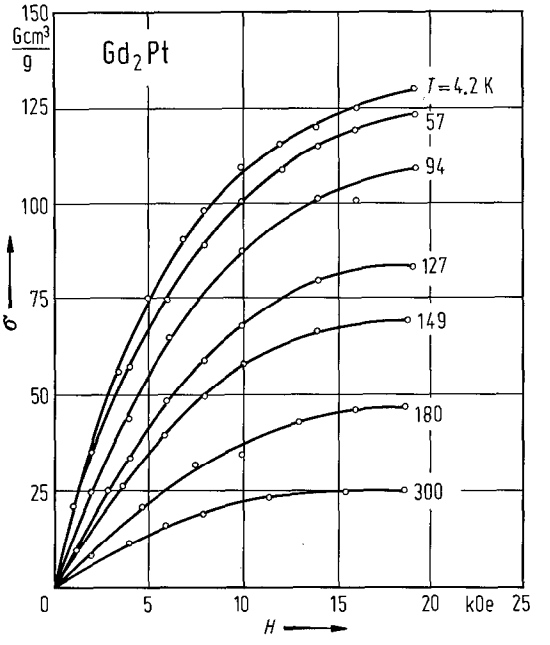

Fig. 127. Gd_2Pt. Magnetic field dependence of σ at different temperatures [80 G 4].

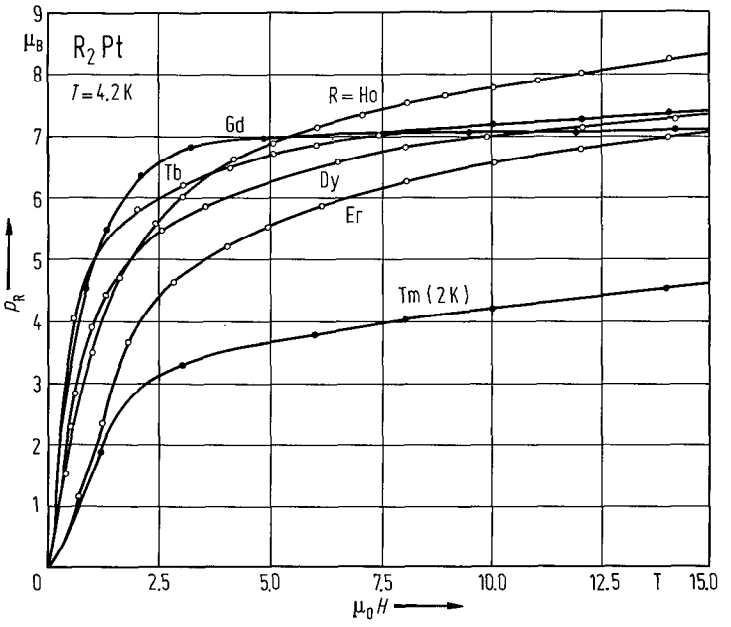

Fig. 128. R_2Pt, R = Gd, Tb, Dy, Ho, Er, Tm. Magnetic field dependence of p_R at 4.2 K (Tm: 2 K) [83 C 1].

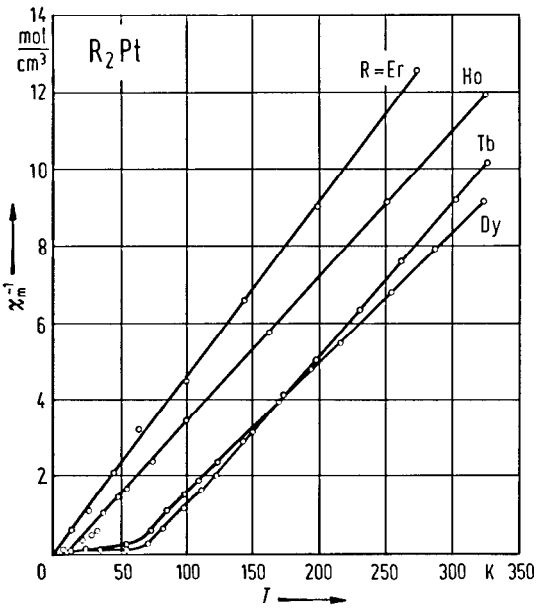

Fig. 129. R_2Pt, R = Tb, Dy, Ho, Er. Temperature dependence of χ_m^{-1} [80 G 4].

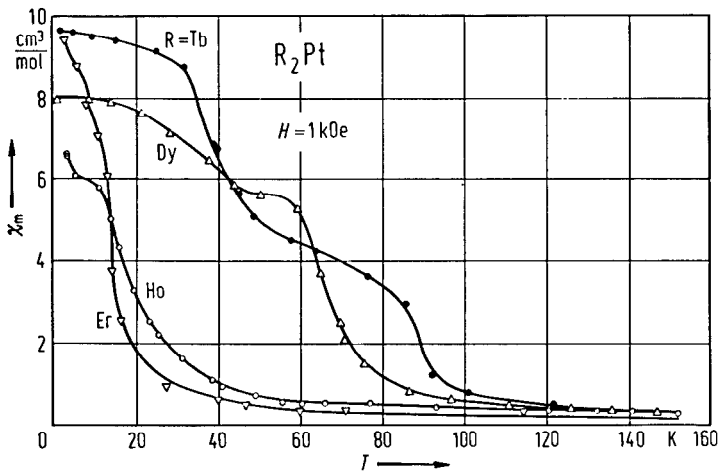

Fig. 130. R_2Pt, R = Tb, Dy, Ho, Er. Temperature dependence of the initial low-field χ_m at 1 kOe [80 G 4].

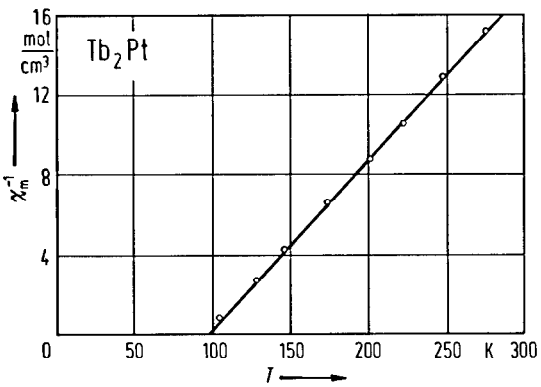

Fig. 131. Tb_2Pt. Temperature dependence of χ_m^{-1} [82 C 2].

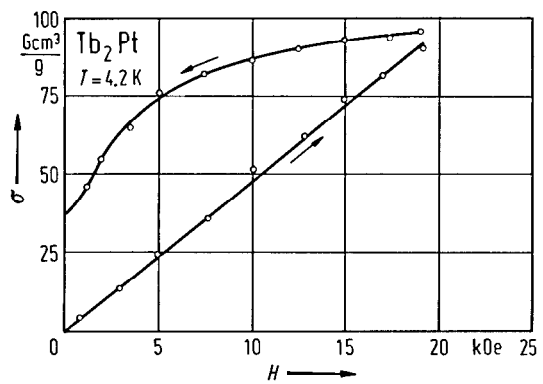

Fig. 132. Tb_2Pt. Hysteresis loop at 4.2 K [80 G 4].

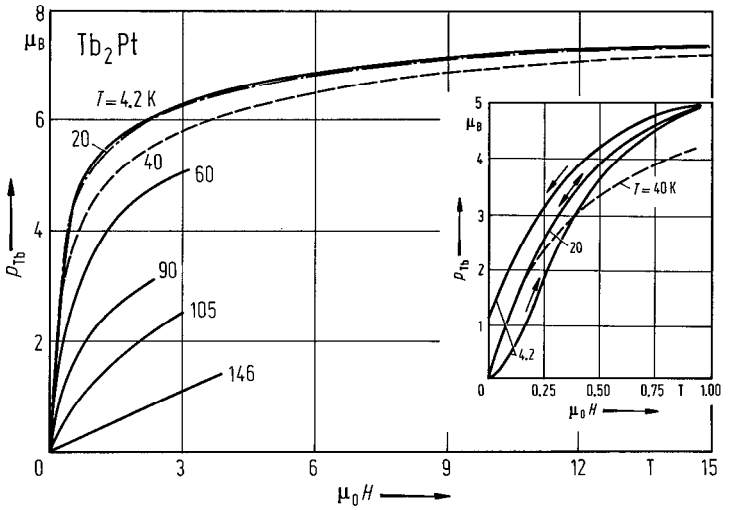

Fig. 133. Tb_2Pt. First magnetization curves, p_{Tb}, at different temperatures [82 C 2].

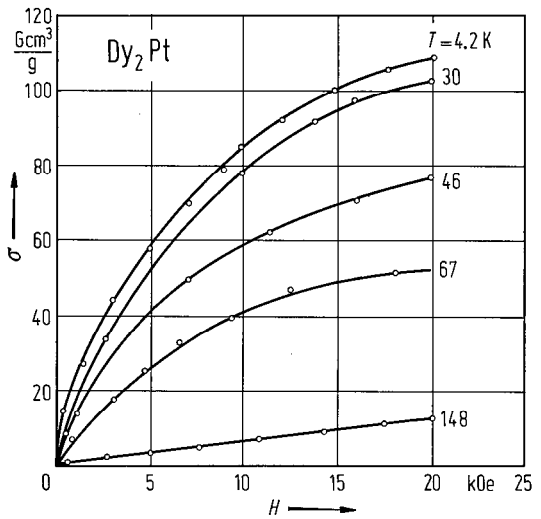

Fig. 134. Dy_2Pt. Magnetic field dependence of σ at different temperatures. These curves are typical of the R_2Pt compounds [80 G 4].

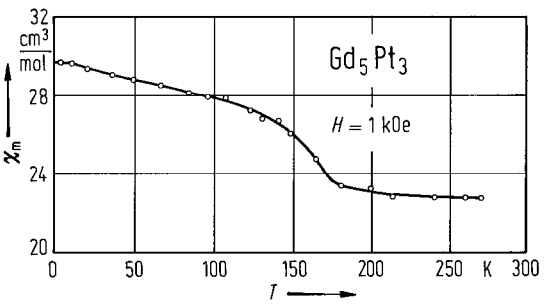

Fig. 135. Gd_5Pt_3. Temperature dependence of χ_m at 1 kOe [83 G 3].

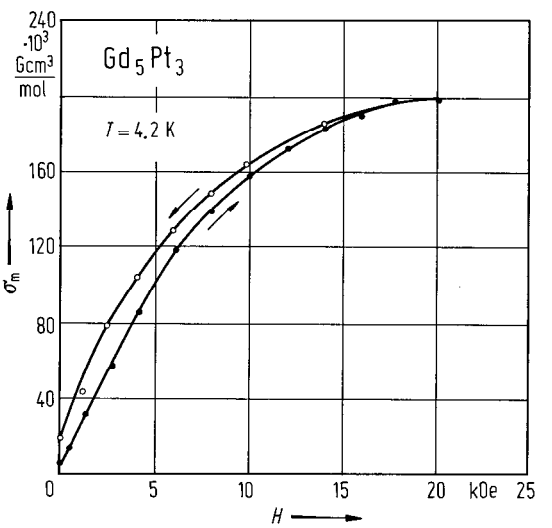

Fig. 136. Gd_5Pt_3. Magnetic field dependence of σ_m at 4.2 K [83 G 3].

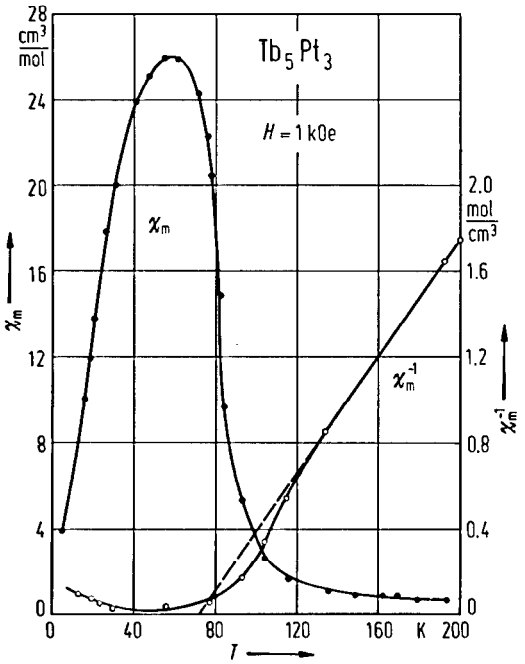

Fig. 137. Tb_5Pt_3. Temperature dependence of χ_m and χ_m^{-1} at 1 kOe [83 G 3].

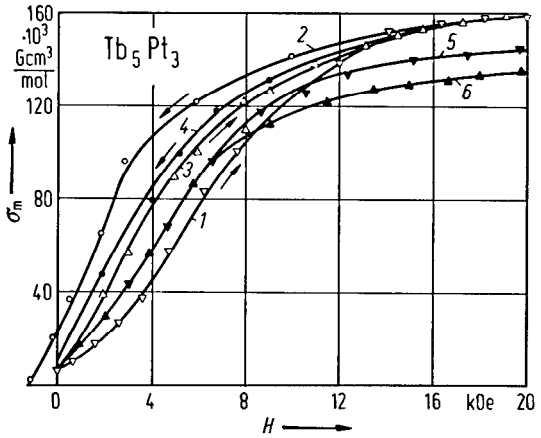

Fig. 138. Tb_5Pt_3. Isotherms. (*1*) Initial curve at 4.2 K after the sample was cooled down in zero field. (*2*) Decreasing field at 4.2 K. Increasing (*3*) and decreasing (*4*) field at 23 K. Increasing field at 44 K (*5*) and 80 K (*6*) [83 G 3].

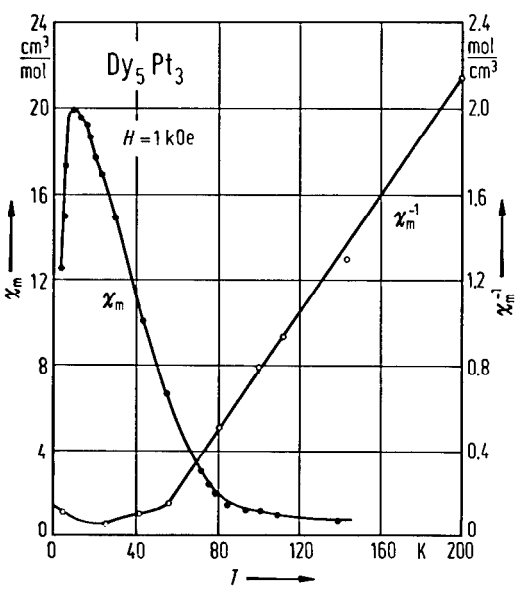

Fig. 139. Dy_5Pt_3. Temperature dependence of χ_m and χ_m^{-1} at 1 kOe [83 G 3].

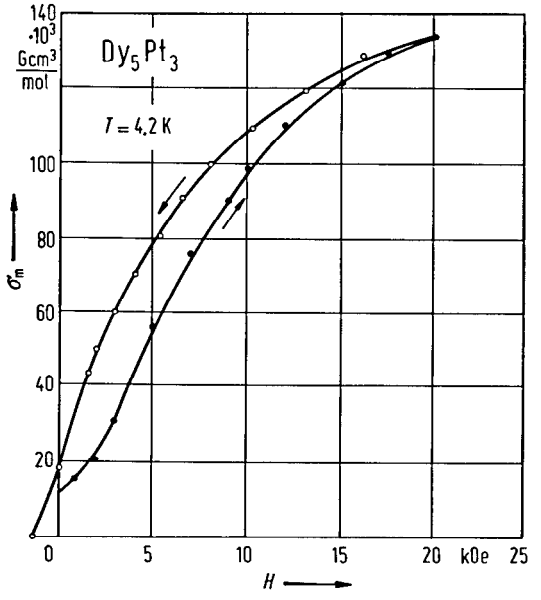

Fig. 140. Dy_5Pt_3. Magnetic field dependence of σ_m at 4.2 K [83 G 3].

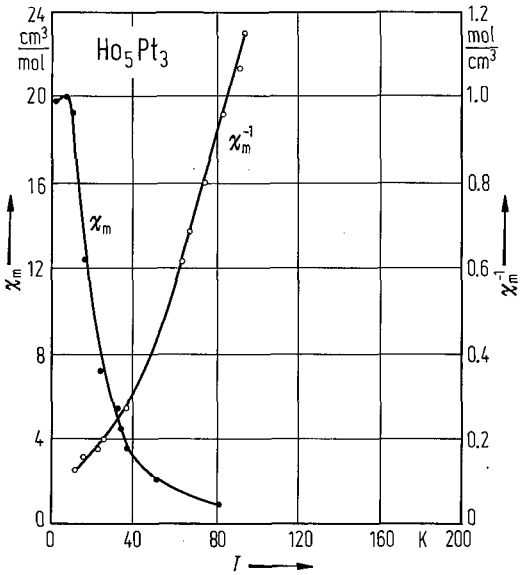

Fig. 141. Ho_5Pt_3. Temperature dependence of χ_m and χ_m^{-1} [83 G 3].

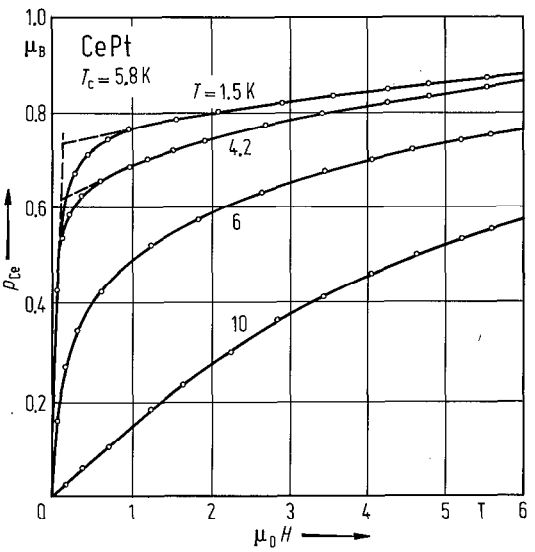

Fig. 144. CePt. Magnetic field dependence of p_{Ce} at different temperatures [83 G 2].

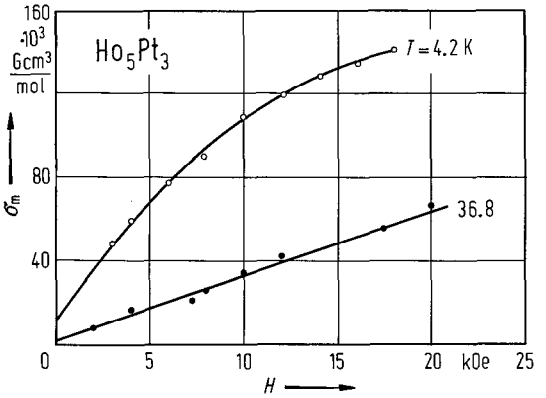

Fig. 142. Ho_5Pt_3. Magnetic field dependence of σ_m at 4.2 and 36.8 K [83 G 3].

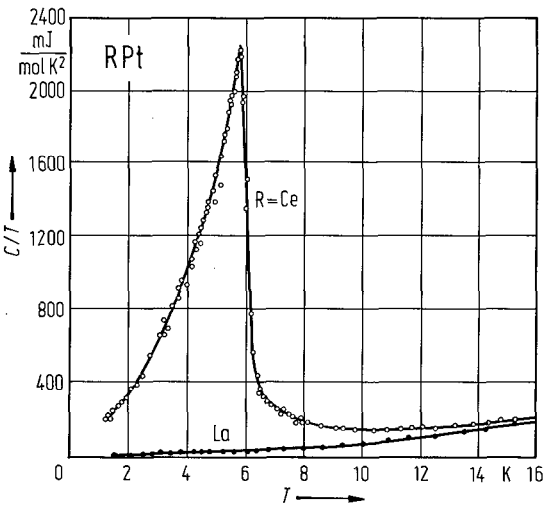

Fig. 143. CePt. Temperature dependence of the specific heat. LaPt is given for comparison [81 H 2].

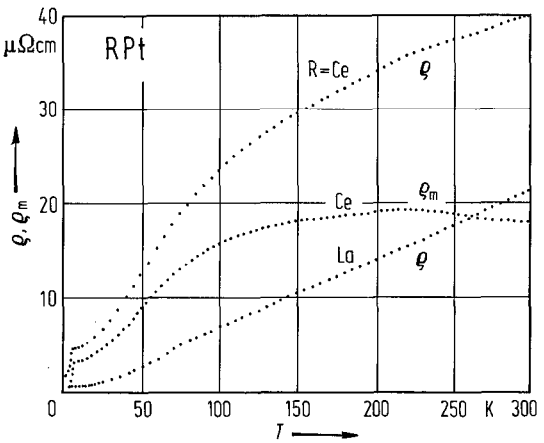

Fig. 145. CePt. Temperature dependence of the electrical resistivity ϱ and of the magnetic contribution to the electrical resistivity, ϱ_m, of CePt. The magnetic phase transition is accompanied by a change in the temperature dependence of ϱ. LaPt is given for comparison [83 G 2].

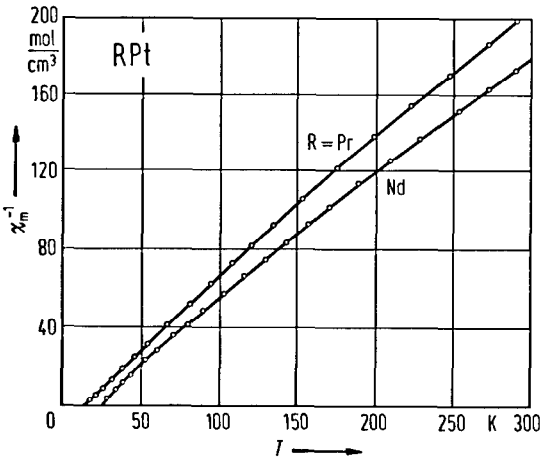

Fig. 146. RPt, R = Pr, Nd. Temperature dependence of χ_m^{-1} [82C1].

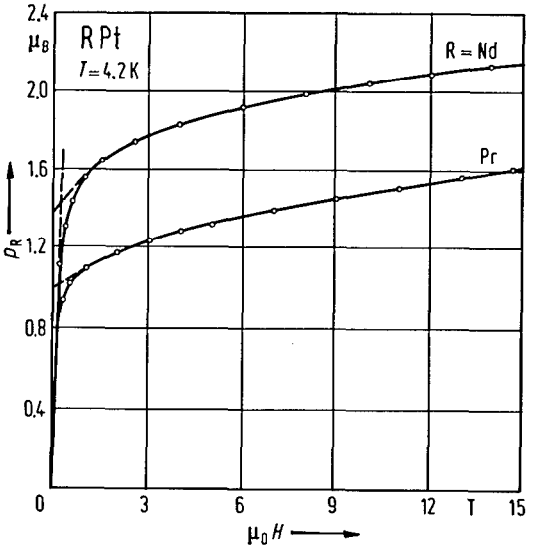

Fig. 147. RPt, R = Pr, Nd. Magnetic field dependence of p_R at 4.2 K [82C1].

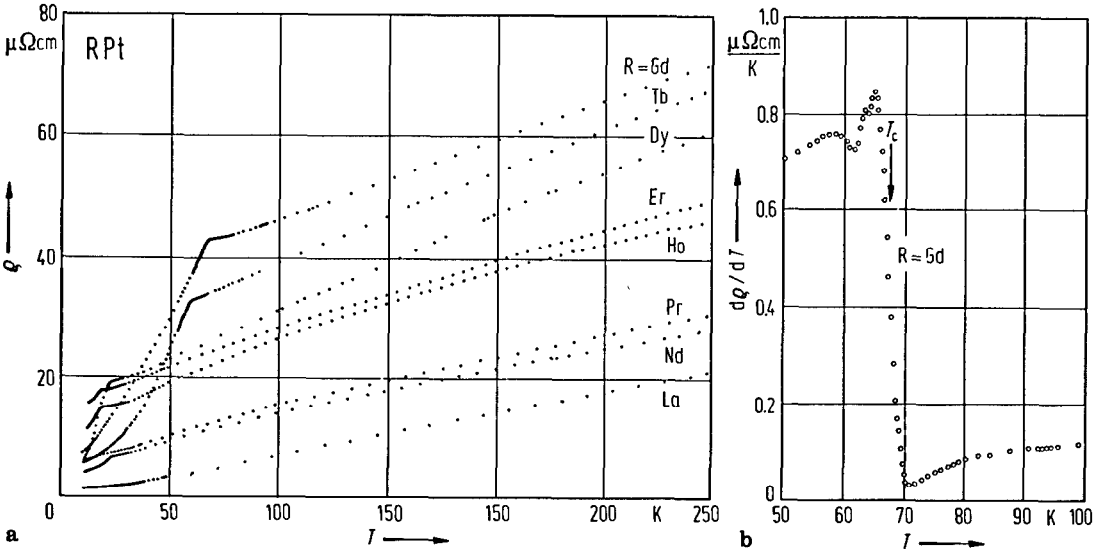

Fig. 148. RPt, R = La, Pr, Nd, Gd, Tb, Dy, Ho, Er. (a) Temperature dependence of the electrical resistivity ϱ. (b) shows $d\varrho/dT$ vs. T for GdPt [86G1].

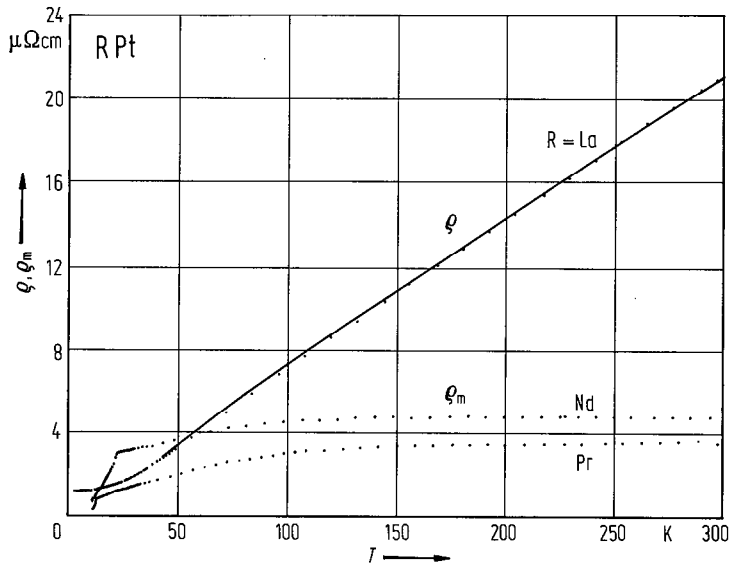

Fig. 149. RPt, R = La, Pr, Nd. Temperature dependence of the magnetic contribution to the electrical resistivity, ϱ_m, for PrPt and NdPt (after subtraction of the phonon, ϱ_p, and residual, ϱ_r, part), and temperature dependence of the electrical resistivity ϱ for LaPt. Solid line is calculated [86 G 1].

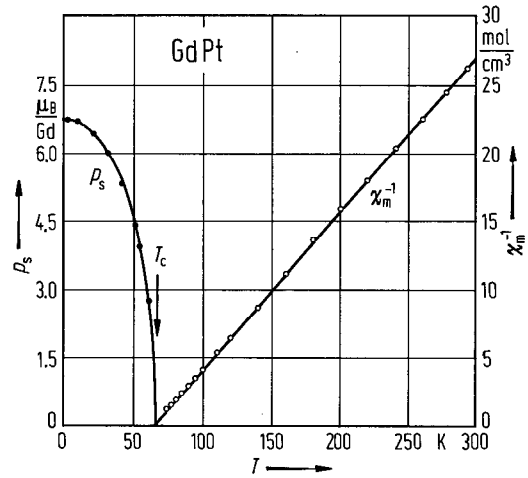

Fig. 150. GdPt. Temperature dependence of χ_m^{-1} and p_s. The solid line represents the $B_{7/2}$ Brillouin function, circles are the experimental points [80 C 1].

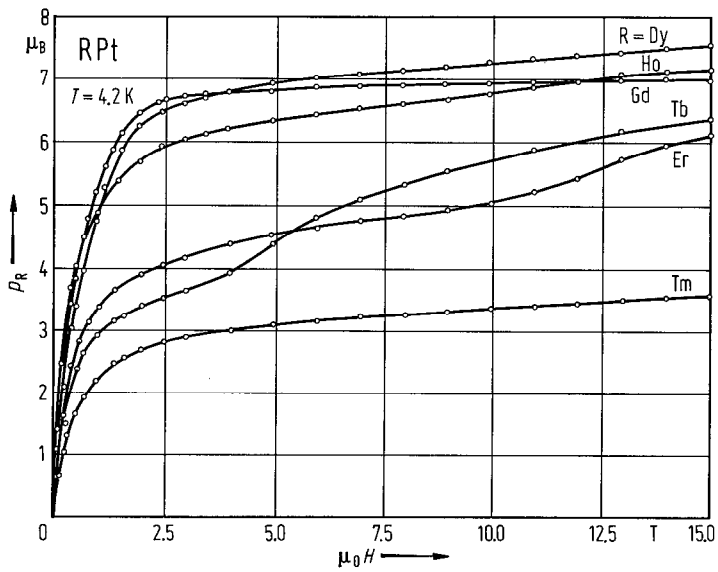

Fig. 151. RPt, R = Gd, Tb, Dy, Ho, Er, Tm. Magnetic field dependence of p_R at 4.2 K [80 C 1].

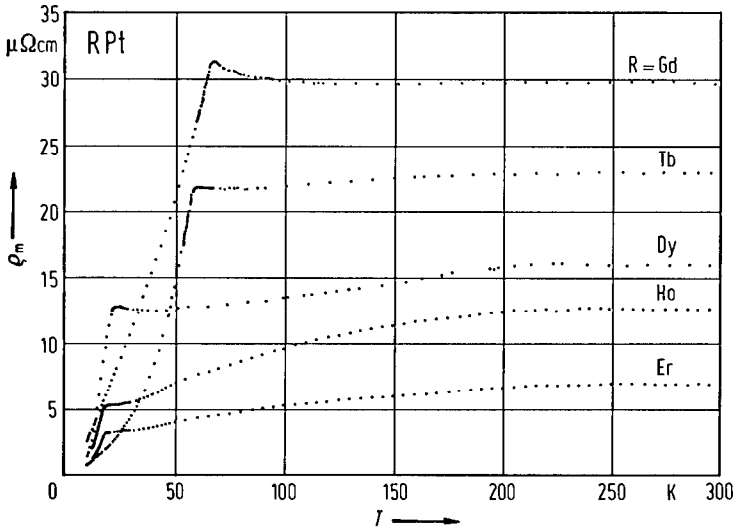

Fig. 152. RPt, R = Gd, Tb, Dy, Ho. Er. Temperature dependence of the magnetic contribution to the electrical resistivity, ϱ_m, after subtraction of the phonon, ϱ_p, and residual, ϱ_r, resistivities ($\varrho_m = \varrho - \varrho_p - \varrho_r$) [86 G 1].

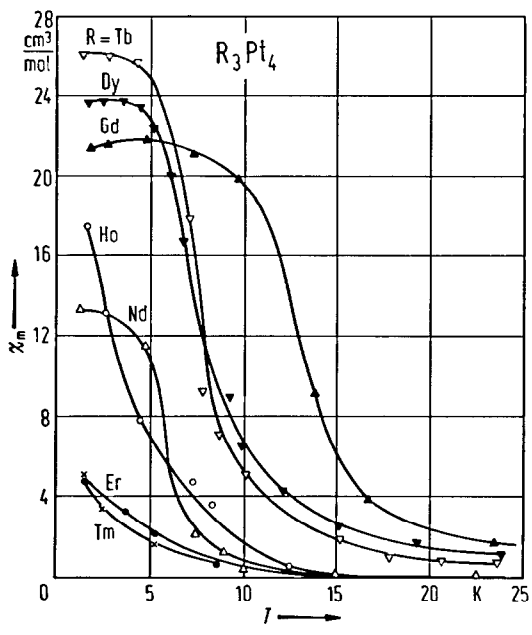

Fig. 153. R_3Pt_4, R = Nd, Gd, Tb, Dy, Ho, Er, Tm. Temperature dependence of χ_m [79 G 1].

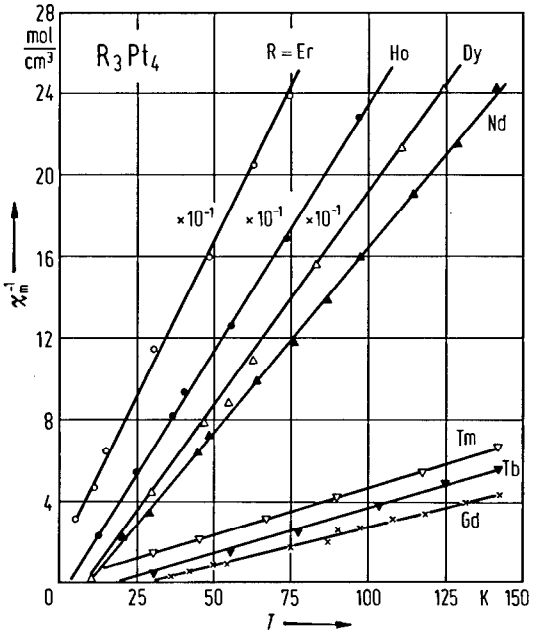

Fig. 154. R_3Pt_4, R = Nd, Gd, Tb, Dy, Ho, Er, Tm. Temperature dependence of χ_m^{-1} [79 G 1].

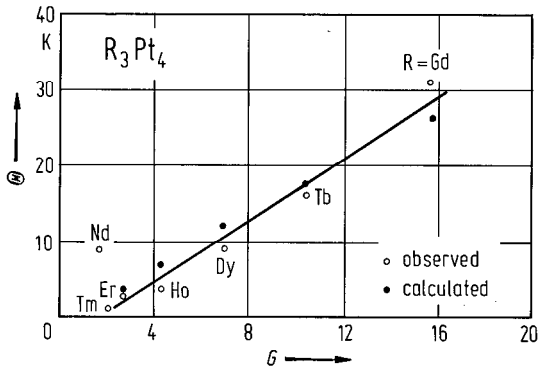

Fig. 155. R_3Pt_4, R=Nd, Gd, Tb, Dy, Ho, Er, Tm. Observed paramagnetic Curie temperatures Θ and calculated Θ for R^{3+} ions by Hund's rule vs. de Gennes factor $G=(g-1)^2J(J+1)$ [79 G 1].

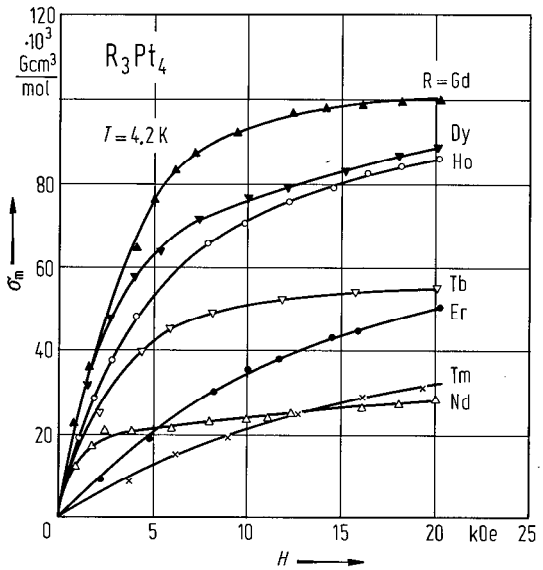

Fig. 156. R_3Pt_4, R=Nd, Gd, Tb, Dy, Ho, Er, Tm. Magnetic field dependence of σ_m at 4.2 K [79 G 1].

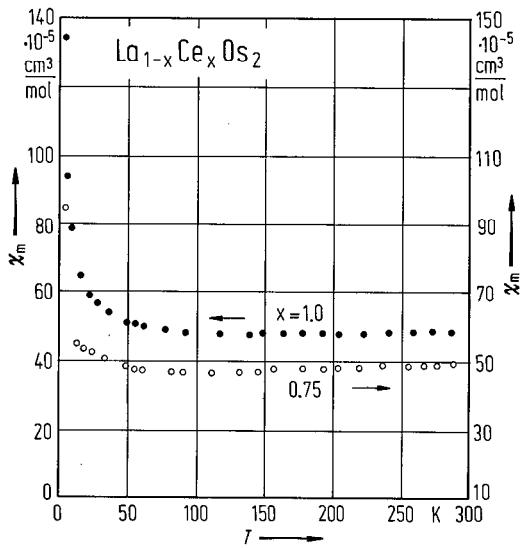

Fig. 157. $La_{1-x}Ce_xOs_2$. Temperature dependence of χ_m for x=0.75 and 1.0 [86 S 1].

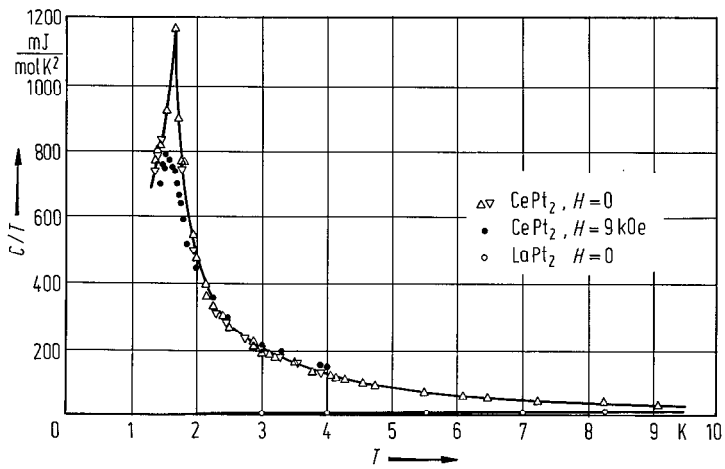

Fig. 158. $CePt_2$. Temperature dependence of the heat capacity C. For comparison the heat capacity of $LaPt_2$ is shown [72 J 1].

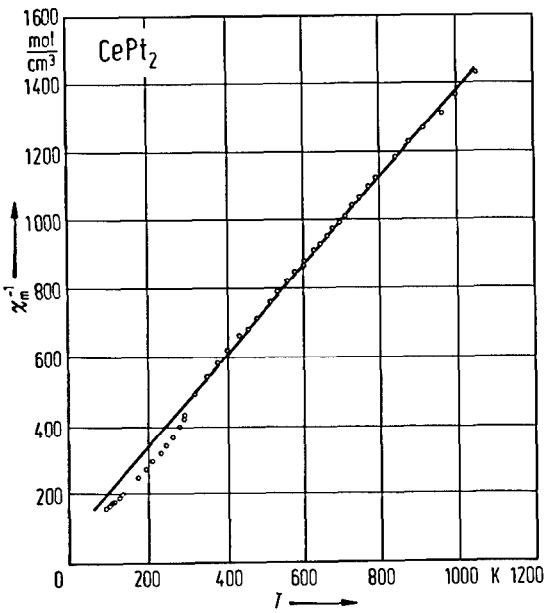

Fig. 159. $CePt_2$. Temperature dependence of χ_m^{-1} [80 O 1].

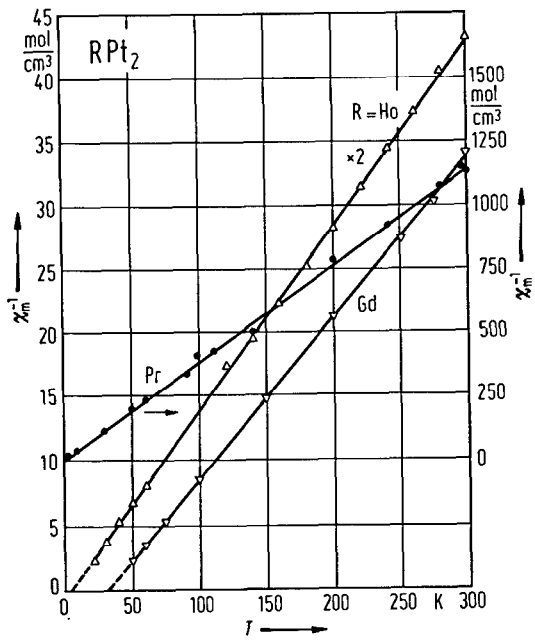

Fig. 160. RPt_2, R = Pr, Gd, Ho. Temperature dependence of χ_m^{-1} [67 W 1].

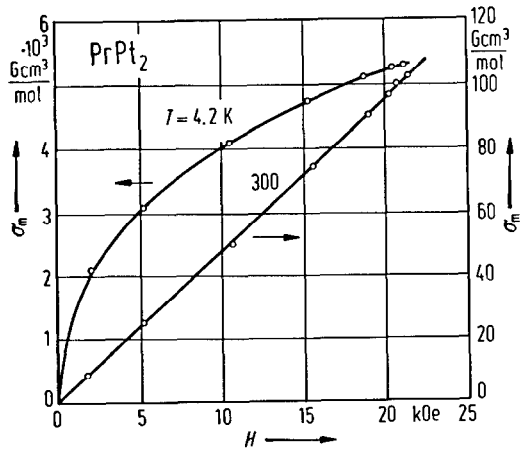

Fig. 161. $PrPt_2$. Magnetic field dependence of σ_m at 4.2 and 300 K [67 W 1].

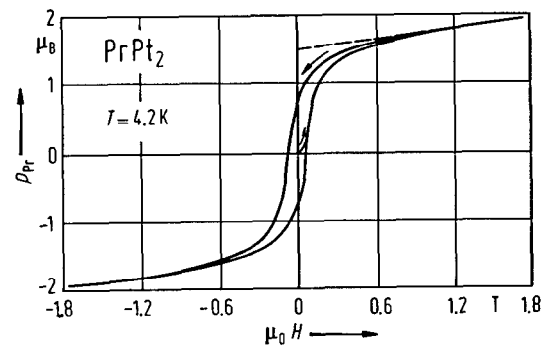

Fig. 162. $PrPt_2$. Magnetization curves at 4.2 K [80 G 3].

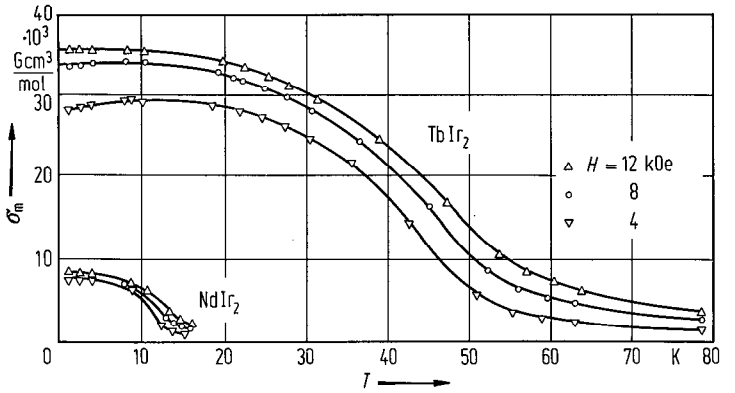

Fig. 163. RIr_2, R = Nd, Tb. Temperature dependence of σ_m at 12, 8 and 4 kOe [59 B 1].

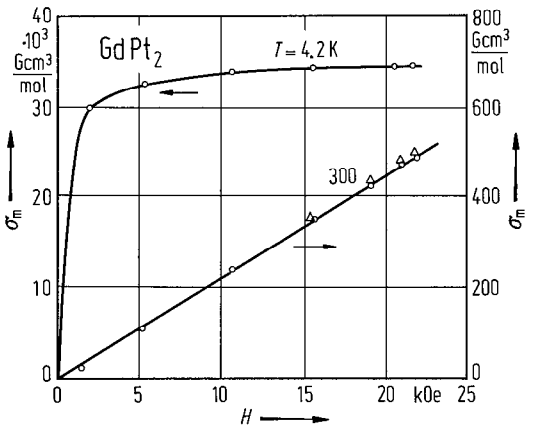

Fig. 164. $GdPt_2$. Magnetic field dependence of σ_m at 4.2 and 300 K [67 W 1].

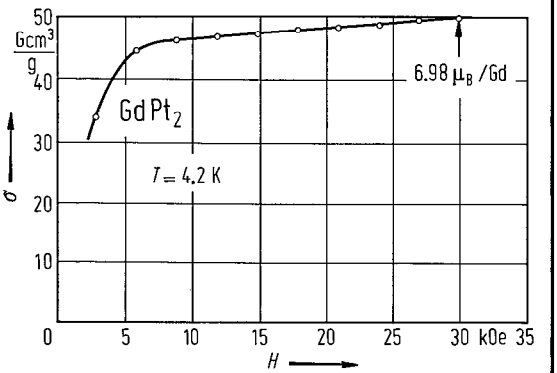

Fig. 165. $GdPt_2$. Magnetic field dependence of σ at 4.2 K [77 D 1].

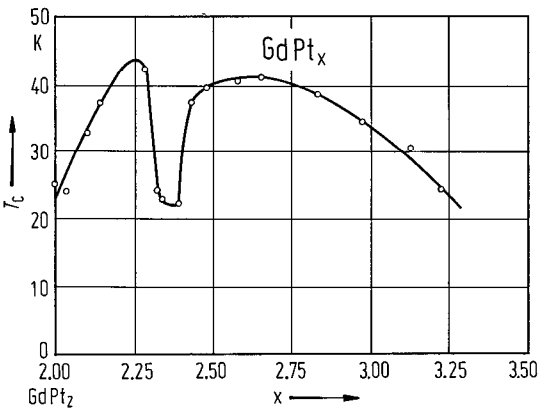

Fig. 166. $GdPt_x$. Variation of T_C indicated by electrical resistivity measurements as a function of x [76 T 1].

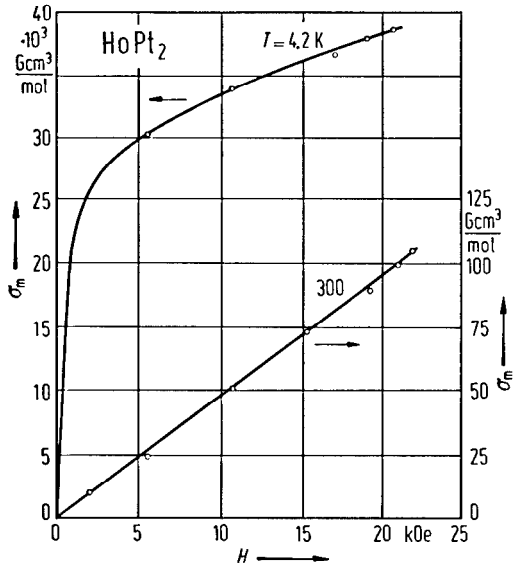

Fig. 167. $HoPt_2$. Magnetic field dependence of σ_m at 4.2 and 300 K [67 W 1].

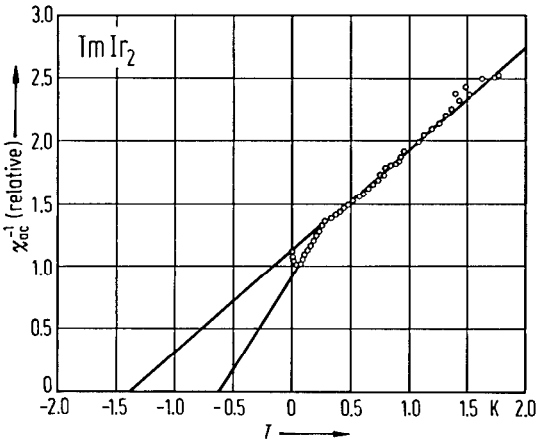

Fig. 168. $TmIr_2$. Low-temperature dependence of ac reciprocal susceptibility, χ_{ac}^{-1}, (in arbitrary units) [85 W 1].

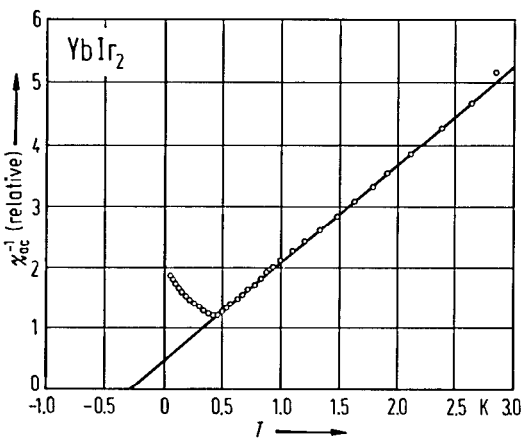

Fig. 169. $YbIr_2$. Low-temperature dependence of ac reciprocal susceptibility, χ_{ac}^{-1}, (in arbitrary units) [85 W 1].

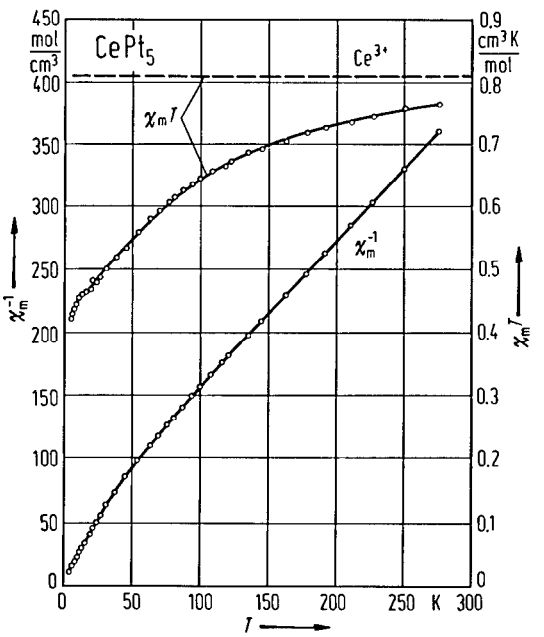

Fig. 170. $CePt_5$. Temperature dependence of $\chi_m T$ and χ_m^{-1}, and $\chi_m T$ for Ce^{3+} free ion. The solid lines are theoretical with CEF parameters $B_2^0 = 33.8\,cm^{-1}$, $B_4^0 = -0.0828\,cm^{-1}$, $\lambda = -0.54\,cm^3/mol$ and $\chi_0 = 50 \cdot 10^{-6}\,cm^3/mol$, where $(\chi_m - \chi_0)^{-1} = (\chi_m^{CEF})^{-1} - \lambda$ [79 L 1].

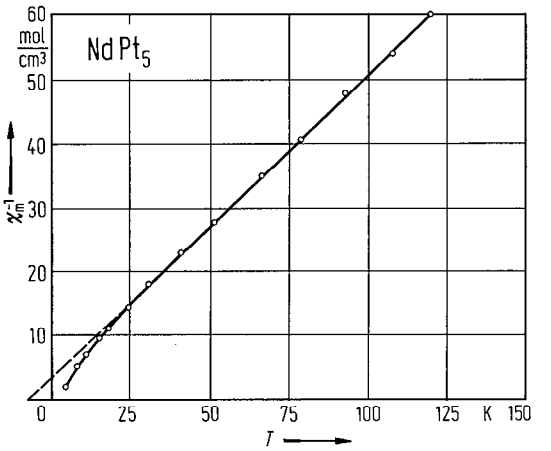

Fig. 171. $NdPt_5$. Temperature dependence of χ_m^{-1} [80I1].

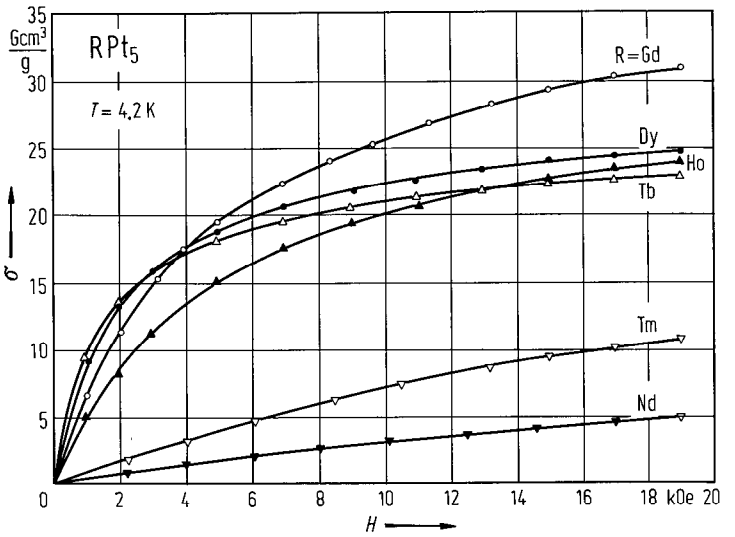

Fig. 172. RPt_5, R = Nd, Gd, Tb, Dy, Ho, Tm. Magnetic field dependence of σ at 4.2 K [80I1].

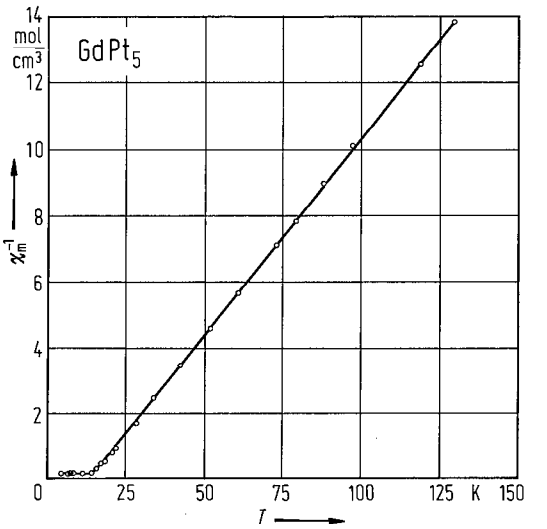

Fig. 173. $GdPt_5$. Temperature dependence of χ_m^{-1} [80I1].

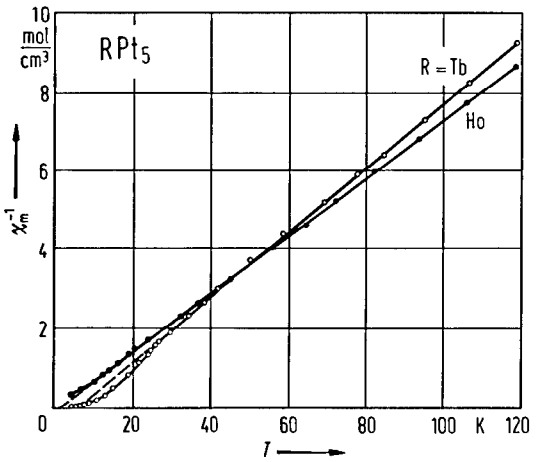

Fig. 174. RPt_5, R = Tb, Ho. Temperature dependence of χ_m^{-1} [80 I 1].

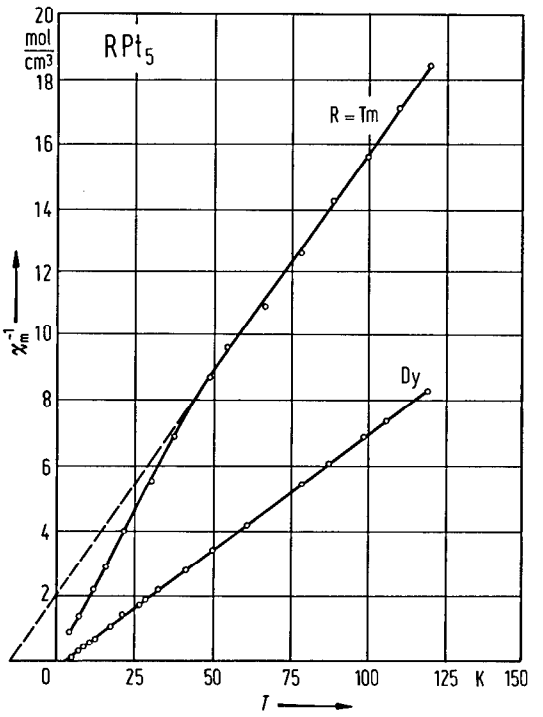

Fig. 175. RPt_5, R = Dy, Tm. Temperature dependence of χ_m^{-1} [80 I 1].

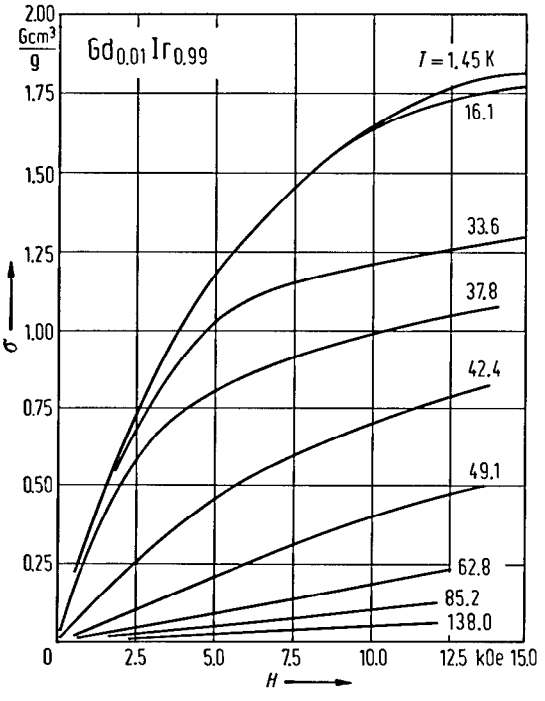

Fig. 176. $Gd_{0.01}Ir_{0.99}$. Magnetic field dependence of σ at different temperatures [80 S 1].

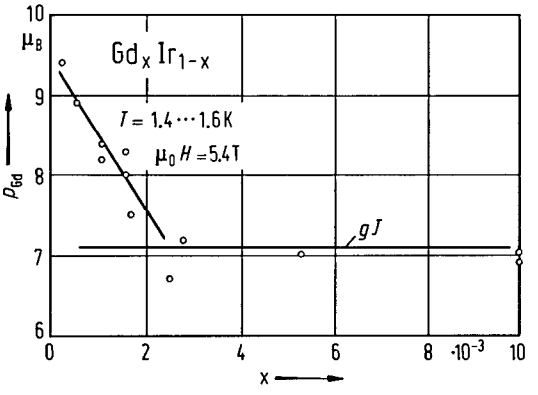

Fig. 177. Composition dependence of p_{Gd} at 1.4···1.6 K and 54 kOe after cooling the samples in a magnetic field from above T_C [80 S 1].

2.5.4 References for 2.5

General references

62l1 Lea, K.R., Leask, M.J.M., Wolf, P.W.: The Raising of Angular Momentum Degeneracy of f-Electron Terms by Cubic Crystal Fields. J. Phys. Chem. Solids **23** (1962) 1381.

64h1 Hutchings, M.T.: Point-Charge Calculations of Energy Levels of Magnetic Ions in Crystalline Electric Fields. Solid State Physics, Advances in Research and Applications (Seitz, F., Turnbull, D., eds.), New York, London: Academic Press, Vol. 16, **1964**, p. 227.

71t1 Taylor, K.N.R.: Intermetallic Rare-Earth Compounds. Adv. Phys. **20** (1971) 551.

72t1 Taylor, K.N.R., Darby, M.I.: Physics of Rare Earth Solids, Chapman and Hall Ltd. London **1972**.

73w1 Wallace, W.E.: Rare Earth Intermetallics. New York, London: Academic Press Inc. **1973**.

79b1 Buschow, K.H.J.: Intermetallic Compounds of Rare-Earth and Non-magnetic Metals. Rep. Progr. Phys. **42** (1979) 1373.

79i1 Iandelli, A., Palenzona, A.: Crystal Chemistry of Intermetallic Compounds. Handbook on the Physics and Chemistry of Rare Earths (Gschneidner, Jr., K.A. Eyring, L., eds.), Amsterdam: North-Holland Publ. Co., Vol. 2, **1979**, p. 1.

79k1 Kirchmayr, H.R., Poldy, C.A.: Magnetic Properties of Intermetallic Compounds of Rare Earth Metals. Handbook on the Physics and Chemistry of Rare Earths (Gschneidner, Jr., K.A., Eyring, L., eds.), Amsterdam: North-Holland Publ. Co. Vol. 2, **1979**, p. 55.

80b1 Buschow, K.H.J.: Rare Earth Compounds in Ferromagnetic Materials. A Handbook on the Properties of Magnetically Ordered Substances (Wohlfahrt, E.P., ed.), Amsterdam: North-Holland Publ. Co., Vol. 1, **1980**, p. 297.

Special references

58M1 Matthias, B.T., Suhl, H., Corenzwit, E.: Phys. Rev. Lett. **1** (1958) 449.

59B1 Bozorth, R.M., Matthias, B.T., Suhl, H., Corenzwit, E., Davis, D.D.: Phys. Rev. **115** (1959) 1595.

59C1 Compton, V.B., Matthias, B.T.: Acta Crystallogr. **12** (1959) 651.

63F1 Felcher, G.P., Koehler, W.C.: Phys. Rev. **131** (1963) 1518.

64B1 Berkowitz, A.E., Holtzberg, F., Methfessel, S.: J. Appl. Phys. **35** (1964) 1030.

64C1 Crangle, J., Ross, J.W.: Proc. Int. Conf. Mag. Nottingham **1964** p. 240.

64S1 Shaltiel, D., Wernick, J.H., Jaccarino, V.: J. Appl. Phys. **35** (1964) 978.

67W1 Wallace, W.E., Vlasov, Y.G.: Inorg. Chem. **6** (1967) 2216.

68H1 Harris, I.R., Norman, M.: J. Less Common Met. **15** (1968) 285.

68W1 Wickman, H.H., Wernick, J.H., Sherwood, R.C., Wagner, C.F.: J. Phys. Chem. Solids **29** (1968) 181.

69A1 Arnold, G., Nereson, N.: J. Chem. Phys. **51** (1969) 1495.

70H1 Hillenbrand, B., Wilhelm, M.: Phys. Lett. A **31** (1970) 448.

70N1 Nereson, N., Arnold, G.: J. Chem. Phys. **53** (1970) 2818.

70V1 van Daal, H.J., Buschow, K.H.J.: Phys. Status Solidi (a) **3** (1970) 853.

70W1 Wilhelm, M., Hillenbrand, B.: J. Phys. Chem. Solids **31** (1970) 559.

71G1 Gardner, W.E., Penfold, J., Harris, I.R.: J. Phys. (Paris) **32** (1971) C 1–1139.

71H1 Harris, J.R., Longworth, G.: J. Less Common Met. **23** (1971) 281.

71H2 Hutchens, R.D., Rao, V.U.S., Greedon, J.E., Wallace, W.E., Craig, R.S.: J. Appl. Phys. **42** (1971) 293.

71H3 Hillenbrand, B., Schuster, K., Wilhelm, M.: Z. Naturforsch. A **26** (1971) 1684.

71W1 Wilhelm, M., Hillenbrand, B.: Z. Naturforsch. A **26** (1971) 141.

72C1 Chamard-Bois, R., Nguyen, v.N., Pierre, J.: Phys. Status Solidi (b) **49** (1972) 161.

72G1 Gardner, W.E., Penfold, J., Smith, T.F., Harris, I.R.: J. Phys. F **2** (1972) 133.

72H1 Hillenbrand, B., Wilhelm, M.: Phys. Lett. A **40** (1972) 387.

72J1 Joseph, R.R., Gschneidner, Jr., K.A., Hungsberg, R.E.: Phys. Rev. B **5** (1972) 1878.

73B1 Buschow, K.H.J., van Diepen, A.M., de Wijn, H.W.: Phys. Rev. B **8** (1973) 5134.

73G1 Guertin, R.P., Praddaude, H.C., Foner, S., McNiff, Jr., E.J., Barsoumian, B.: Phys. Rev. B **7** (1973) 274.

73L1 Longworth, G., Harris, I.R.: J. Less Common Met. **33** (1973) 83.

73L2 Loebich, O., Raub, E.: J. Less Common Met. **31** (1973) 111.

73O1 Olcese, G.L.: J. Less Common Met. **33** (1973) 71.

73R1 Rupp, G.: J. Phys. F **3** (1973) 1403.

73 T 1 Tamminga, Y., Barkman, B., de Boer, F.R.: Solid State Commun. **12** (1973) 731.
74 B 1 Bauminger, E.R., Felner, J., Froindlich, D., Levron, D., Nowik, J., Ofer, S., Yanovsky, R.: J. Phys. (Paris) **35** (1974) C6–61.
75 J 1 Jordan, R.G., Loebich, Jr., O.: J. Less Common Met. **39** (1975) 55.
75 L 1 Loebich, Jr., O., Raman, A.: J. Less Common Met. **43** (1975) 89.
75 L 2 Loebich, Jr., O., Raub, E.: Mater. Res. Bull. **10** (1975) 1017.
76 A 1 Asada, Y.: J. Phys. Soc. Jpn. **41** (1976) 26.
76 L 1 Loebich, Jr., O., Raub, E.: J. Less Common Met. **46** (1976) 7.
76 T 1 Taylor, R.H., Harris, I.R., Gardner, W.E.: J. Phys. F **6** (1976) 1125.
77 D 1 Dormann, E., Huck, M., Buschow, K.H.J.: Z. Phys. B **27** (1977) 141.
77 D 2 Davidov, D., Baberschke, K., Mydosh, J.A., Nieuwenhuys, G.J.: J. Phys. F **7** (1977) L 47.
77 G 1 Grover, A.K., Gupta, L.C., Vijayaraghavan, R.: Physica B **86–88** (1977) 81.
77 K 1 Klaasse, J.C.P., Mattens, W.C.M., de Boer, F.R., de Chatel, P.F.: Physica B **86–88** (1977) 234.
77 R 1 Ruebenhauer, K., Fink, J., Schmidt, H., Czjzek, G., Tomala, K.: Phys. Status Solidi (b) **84** (1977) 611.
77 T 1 Tay, C.Y., Harris, I.R.: J. Less Common Met. **53** (1977) 177.
77 Y 1 Yakinthos, J.K., Anagnostopoulos, T., Ikonomou, P.F.: J. Less Common Met. **51** (1977) 113.
77 Y 2 Yakinthos, J.K., Gamari-Seale, H., Laforest, J. Physica Status Solidi (a) **40** (1977) K 105.
78 A 1 Asada, Y.: J. Phys. F **8** (1978) 2381.
78 K 1 Kumagai, Ken-ichi, Matsushira, T., Asayama, K.: J. Phys. Soc. Jpn. **45** (1978) 422.
78 P 1 Pountney, J.M., Winterbottom, J.M., Harris, J.R.: Inst. Phys. Conf. Ser. **37** (1978) 85.
79 A 1 Asada, Y.: J. Low. Temp. Phys. **36** (1979) 301.
79 C 1 Chiu, L.B., Elliston, P.R., Stewart, A.M., Taylor, K.N.R.: J. Less Common Met. **65** (1979) P 59.
79 G 1 Gamari-Seale, H., Yakinthos, J.K.: J. Appl. Phys. **50** (1979) 2315.
79 H 1 Hrubec, J., Steiner, W.: J. Phys. (Paris) **40** (1979) C 5–198.
79 L 1 Lueken, H., Meier, M., Klessen, G., Bronger, W., Fleischhauer, J.: J. Less Common Met. **63** (1979) P 35.
79 M 1 Machado da Silva, J.M.: J. Phys. (Paris) **40** (1979) C 5–152.
80 A 1 Algra, H.A., Buschow, K.H.J., Henskens, R.A.: J. Magn. Magn. Mater. **15–18** (1980) 1395.
80 B 1 Buschow, K.H.J.: Ferromagnetic Materials Vol. 1, (Wohlfahrt, E.P., ed.), North-Holland **1980**, 297.
80 C 1 Castets, A., Gignoux, D., Gomez-Sal, J.C.: J. Solid State Chem. **31** (1980) 197.
80 G 1 Gamari-Seale, H.: J. Magn. Magn. Mater. **22** (1980) 87.
80 G 2 Gamari-Seale, H.: J. Less Common Met. **75** (1980) P 43.
80 G 3 Greidanus, F.J.A.M., de Jongh, L.J., Husikamp, W.J., Buschow, K.H.J.: J. Magn. Magn. Mater. **15–18** (1980) 1231.
80 G 4 Gamari-Seale, H.: J. Magn. Magn. Mater. **20** (1980) 67.
80 G 5 Gambke, T., Elschner, B., Schaafhausen, J.: Phys. Lett. A **78** (1980) 413.
80 H 1 Hughes, D.T., Evans, J., Harris, I.R.: J. Less Common Met. **76** (1980) 119.
80 I 1 Ikonomou, P.F., Marcopoulos, V.G., Yakinthos, J.K.: J. Less Common Met. **71** (1980) P 13.
80 I 2 Iandelli, A., Olcese, G.L., Palenzona, A.: J. Less Common Met. **76** (1980) 317.
80 L 1 Ludwigs, H.-W., Häfner, U., Holland-Moritz, E., Zell, W., Roden, B., Wohlleben, D.: J. Magn. Magn. Mater. **15–18** (1980) 607.
80 M 1 Mota, A.C., Wohlleben, D., Hoyt, R.F., Borchardt, H.: J. Magn. Magn. Mater. **15–18** (1980) 95.
80 O 1 Olcese, G.L.: Solid State Commun. **35** (1980) 87.
80 S 1 Smith, J.L., Matthias, B.T.: J. Magn. Magn. Mater. **21** (1980) L 203.
80 T 1 Tari, A., Larica, C.: J. Phys. (Paris) **41** (1980) 35.
80 V 1 van Dongen, J.C.M., van der Linden, H.W.M., Greidanus, F.J.A.M., Nieuwenhuys, G.J., Mydosh, J.A., Buschow, K.H.J.: J. Magn. Magn. Mater. **15–18** (1980) 1245.
80 Y 1 Yakinthos, J.K., Kotsanidis, P.A., Gamari-Seale, E.: J. Less Common Met. **75** (1980) P 37.
81 B 1 Borchardt, H., Hoyt, R.F., Mota, A.C., Wohlleben, D.: Physica B **108** (1981) 1353.
81 F 1 Fernandez-Baca, J.A., Lynn, J.W.: J. Appl. Phys. **52** (1981) 2183.
81 G 1 Gambke, T., Elschner, B., Schaafhausen, J., Schaeffer, H.: Valence Fluctuation in Solids (Falicov, L.M., Hanke, H., Maple, M.B., eds.), North Holland Publ. Co. **1981**, 447.
81 H 1 Häfner, H.U., Ludwigs, H.-W., Nicholson, K., Wohlleben, D.: Z. Phys. B **42** (1981) 219.
81 H 2 Holt, B.J., Ramsden, J.D., Sample, H.H., Huber, J.G.: Physica B **107** (1981) 255.
81 M 1 Mihalisin, T., Scoboria, P., Ward, J.A.: Valence Fluctuation in Solids (Falicov, L.M., Hanke, H., Maple, M.B., eds.), North Holland Publ. Co. **1981**, 61.
82 B 1 Barberis, G.E., Roden, B., Weidner, P., Gupta, L.C., Davidov, D., Felner, I.: Solid State Commun. **42** (1982) 659.
82 C 1 Castets, A., Gignoux, D., Gomez-Sal, J.C., Roudaut, E.: Solid State Commun. **44** (1982) 1329.

82 C 2 Castets, A., Gignoux, D., Gomez-Sal, J.C., Rodriguez-Gonzalez, F., Roudaut, E.: Phys. Status Solidi (a) **73** (1982) 475.

82 F 1 Fischer, P., Hälg, W., Kaldis, E., Greidanus, F.J.A.M., Buschow, K.H.J.: AIP Conf. Proc. **89** (1982) 321.

82 K 1 Kappler, J.P., Krill, G., Besnus, M.J., Ravet, M.F., Hamdaoui, N., Meyer, A.: J. Appl. Phys. **53** (1982) 2152.

82 R 1 Rambabu, D., Dhar, S.K., Malik, S.K., Vijayaraghavan, R.: Phys. Lett. A **87** (1982) 294.

82 T 1 Tari, A.: J. Magn. Magn. Mater. **29** (1982) 133.

82 T 2 Thompson, J.R., Sekula, S.T., Loong, C.-K., Stassis, C.: J. Appl. Phys. **53** (1982) 7893.

83 C 1 Castets, A., Gignoux, D., Gomez-Sal, J.C., Rodriguez-Gonzalez, F.: Solid State Commun. **45** (1983) 993.

83 D 1 Dhar, S.K., Nagarajan, R., Malik, S.K., Rambabu, D., Vijayaraghavan, R.: J. Magn. Magn. Mater. **31–34** (1983) 393.

83 G 1 Greidanus, F.J.A.M., de Jongh, L.J., Huiskamp, W.J., Fischer, P., Furrer, A., Buschow, K.H.J.: Physica B **119** (1983) 215.

83 G 2 Gignoux, D., Gomez-Sal, J.C.: Solid State Commun. **45** (1983) 779.

83 G 3 Gamari-Seale, H., Yazdani, A.: J. Magn. Magn. Mater. **38** (1983) 57.

83 H 1 Hrubec, J., Steiner, W., Reissner, M.: J. Magn. Magn. Mater. **37** (1983) 93.

83 W 1 Weidner, P., Wittershagen, B., Roden, B., Wohlleben, D.: Solid State Commun. **48** (1983) 915.

84 G 1 Gignoux, D., Gomez-Sal, J.C., Paccard, D., Aramburu-Zabala, J.A.: Solid State Commun. **50** (1984) 43.

84 G 2 Gubbens, P.C.M., van der Kraan, A.M., Buschow, K.H.J.: J. Phys. F **14** (1984) 2195.

84 H 1 Harrus, A., Mihalisin, T., Batlogg, B.: J. Appl. Phys. **55** (1984) 1993.

84 H 2 Harrus, A., Timlin, J., Mihalisin, T., Batlogg, B.: J. Appl. Phys. **55** (1984) 1990.

84 M 1 Malik, S.K., Dhar, S.K., Vijayaraghavan, R.: Pramana **22** (1984) 329.

85 A 1 Aarts, J., de Boer, F.R., de Chatel, P.F., Menovsky, A.: Solid State Commun. **56** (1985) 623.

85 D 1 Drewes, W., Leson, A., Schelp, W., Bömken, K., Purwins, H.G.: Physica B **130** (1985) 213.

85 D 2 de Vries, J.W.C., Thiel, R.C., Buschow, K.H.J.: Physica B **128** (1985) 183.

85 H 1 Hiebl, K., Horvath, C., Rogl, P.: Physica B **130** (1985) 129.

85 K 1 Kappler, J.P., Besnus, M.J., Lehmann, P., Meyer, A., Sereni, J.: J. Less Common Met. **111** (1985) 261.

85 K 2 Kitaoka, Y., Chang, N.-S., Ebisu, T., Matsumura, M., Asayama, K., Kumagi, K.-I.: J. Phys. Soc. Jpn. **54** (1985) 1543.

85 O 1 Okamoto, T., Fujii, H., Andoh, Y., Fujiwara, H.: J. Magn. Magn. Mater. **52** (1985) 208.

85 P 1 Pott, R., Boksch, W., Leson, G., Politt, B., Schmidt, H., Freimuth, A., Keulerz, K., Langen, J., Neumann, G., Oster, F., Rohler, J., Walter, U., Weidner, P., Wohlleben, D.: Phys. Rev. Lett. **54** (1985) 481.

85 P 2 Politt, B., Dürkop, D., Weidner, P.: J. Magn. Magn. Mater. **47–48** (1985) 583.

85 W 1 Willis, J.O., Smith, J.L., Fisk, Z.: J. Magn. Magn. Mater. **47–48** (1985) 581.

86 D 1 Drewes, W., Schelp, W., Leson, A., Purwins, H.-G.: J. Magn. Magn. Mater. **54–57** (1986) 475.

86 G 1 Gomez-Sal, J.C., Rodriguez Fernandez, J., Lopez Sanchez, R.J., Gignoux, D.: Solid State Commun. **59** (1986) 771.

86 S 1 Schlott, M., Schaeffer, H., Elschner, B.: Z. Phys. B **63** (1986) 427.

86 V 1 Veenhuizen, P.A., van Kalkeren, G., Klaasse, J.C.P., Menovsky, A., Moleman, A.C., de Boer, F.R.: J. Magn. Magn. Mater. **54–57** (1986) 425.